SPK
-47.

NASA Conference Publication 2341

Twentieth Annual Conference on Manual Control

June 12-14, 1984 Ames Research Center, Moffett Field, California

Compiled by: Sandra G. Hart and Earl J. Hartzell

Volume I

(NASA-CP-2341-Vol-1) TWENTIETH ANNUAL CONFERENCE ON MANUAL CONTROL, VOLUME 1 (NASA) 653 p HC A99/MF A01 CSCL 05H

N85-14467 THRU N85-14534 Unclas G3/54 20591

National Aeronautics and Space Administration

NASA Conference Publication 2341

Twentieth Annual Conference on Manual Control

June 12-14, 1984 Ames Research Center, Moffett Field, California

Compiled by: Sandra G. Hart and Earl J. Hartzell
Ames Research Center
Moffett Field, California

Volume I

National Aeronautics and
Space Administration

Ames Research Center
Moffett Field, California 94035

FORWARD

Volumes I and II contain the Proceedings of the Twentieth Annual Conference on Manual Control. The proceedings were published with the support of the National Aeronautics and Space Administration and the Army Aeromechanics Laboratory, both located at Ames Research Center. The meeting was held at the Sheraton-Sunnyvale Hotel in Sunnyvale, California from June twelfth through fourteenth, 1984. Both formal papers that represented completed work and informal papers that represented work in progress were presented. The two volumes include all of the papers accepted for presentation at the meeting; seventy six complete manuscripts and nine abstracts. The papers are divided into two volumes that represent the two general classes of topics that were covered. Volume I covers more traditional "Annual Manual" topics such as time series modeling, flying qualities, and supervisory control models. Volume II contains papers that are more focused on psychological and physiological issues, such as evoked potential and workload measurement, that were included in the program of the concurrent "Annual Mental"

This was the twentieth in a series of conferences dating back to December 1964. These earlier meetings and their proceedings are listed below:

First Annual NASA-University Conference on Manual Control, the University of Michigan, December 1964. (Proceedings not printed.)

Second Annual NASA-University Conference on Manual Control, University of Southern California, February 28 to March 3, 1967. (NASA-SP-128)

Third Annual NASA-University Conference on Manual Control, University of Southern California, March 1-3, 1968. (NASA-SP-144)

Fourth Annual NASA-University Conference on Manual Control, University of Michigan, March 21-23, 1968. (NASA-SP-192)

Fifth Annual NASA-University Conference on Manual Control, Massachusetts Institute of Technology, March 27-29, 1969. (NASA-SP-215)

Sixth Annual Conference on Manual Control, Wright-Patterson AFB, Ohio, April 7-9, 1970. (AFIT/AFFDL Report, no number)

Seventh Annual Conference on Manual Control, Univeristy of Southern California, June 2-4, 1971. (NASA-SP-281)

Eighth Annual Conference on Manual Control, University of Michigan, May 17-19, 1972. (AFFDL-TR-72-92).

Ninth Annual Conference on Manual Control, Massachusetts Institute of Technology, May 23-25, 1973. (Proceedings published by MIT, no number)

Tenth Annual Conference on Manual Control, Wright-Patterson AFB, Ohio, April 9-11, 1974. (AFIT/AFFDL Report, no number)

Eleventh Annual Conference on Manual Control, NASA-Ames Research Center, May 21-23, 1975. (NASA TM X-62,464)

Twelfth Annual Conference on Manual Control, University of Illinois, May 25-27, 1976 (NASA TM X-73,170)

Thirteenth Annual Conference on Manual Control, Massachusetts Institute of Technology, June 15-17, 1977. (Proceedings published by MIT, no number)

Fourteenth Annual Conference on Manual Control, University of Southern California, April 25-27, 1978 (NASA CP-2060)

Fifteenth Annual Conference on Manual Control, Wright State University, Ohio, March 20-22, 1979. (AFFDL-TR-79,3134)

Sixteenth Annual Conference on Manual Control, Massachusetts Institute of Technology, May 5-7, 1980. (Proceedings published by MIT, no number)

Seventeenth Annual Conference on Manual Control, University of California at Los Angeles, June 16-18, 1981. (JPL Publications 81-95)

Eighteenth Annual Conference on Manual Control, Wright-Patterson AFB, Ohio, June 8-10, 1982. (AFWAL-TR-83-3021)

Nineteenth Annual Conference on Manual Control, Massachusetts Institute of Technolgy, May 23-25, 1983. (MIT publication, no number)

ACKNOWLEDGEMENTS

We would like to thank the following people for the many hours of help that they gave in planning, organizing and running the meeting itself and preparing the proceedings for publication: Michael Bortolussi, Roberta Cortilla, Carl Decker, Sherry Dunbar, Gary Guthart, Robin Karl, Patrick Lester, Dave Marcarian, Ronald Miller, and Richard Rothchild.

Sandra G. Hart

Sandra G. Hart, Conference Publications

E. James Hartzell

E. James Hartzell, General Chairman

CONTENTS
VOLUME ONE

FOREWARD i

TIME SERIES MODELING
Chairman: Dr. Greg Zacharias

Biezad, D. & Schmidt, D. K. Time series modeling of human operator dynamics in manual control tasks. 1

Altschul, R. E., Nagel, P. M. & Oliver, F. Statistical time series models of pilot control with applications to instrument discrimination. 41

Bosser, T. Utilization of historic information in an optimisation task. 77

MANUAL CONTROL
Chairman: Mr. Frank George

Jewell, W. & Citurs, K.D. Quantification of cross-coupling and motion feedthrough for multiaxis controllers used in an aircombat flying task. 79

King, M. Six degree of freedom control with each hand? 91

Hess, R. A. & Myers, A. A. A nonlinear filter for compensating for time delays in manual control systems. 93

Schmidt, D. K. & Yuan, P.-J. Model estimation and identification of manual controller objectives in complex tracking tasks. 117

Bekey, G. & Hadaegh, F. Y. Structure errors in system identification. 149

Repperger, D. W. & Levison, W. H. Effects of control stick parameters on human controller response. 157

EFFECTS OF TRANSPORT DELAYS IN SIMULATOR PERFORMANCE
Chairman: Mr. Henry Jex

Jewell, W. & Clement, W.F. A method for measuring the effective throughput time delay in simulated displays involving manual control. 173

Allen, R. W. & DiMarco, R. J. Effects of transport delays on manual control system performance. 185

Sanders, K. E., Anderson, D. C., & Watson, J. H. STOL Simulation requirements for development of integrated flight/propulsion control systems. 201

Privoznik, C. M., Berry, D. T., & Bartoli, A. G. Measurements of pilot time delay as influenced by controller characteristics and vehicle time delays. 209

Kruk, R. V. & Longridge, T. M. Psychophysiological research in development of a fibre-optic helmet mounted display. 221

FLYING QUALITIES
Chairman: Professor Ronald Hess

Heffley, R. K. , Bourne, S.M. & Hindson, W. S. Helicopter pilot performance for discrete-maneuver flight tasks. 223

Onstott, E. D., Warner, J. S. & Hodgkinson, J. Maximum normalized rate as a flying qualities parameter. 233

Sorenson, J. A. & Goka, T. Predictions of cockpit simulator experimental outcome using system models. 259

Hess, R. A. & McNally, B. D. Multi loop manual control of dynamic systems. 281

FAULT DIAGNOSIS/MODELING
Chairman: Dr. William Rouse

Curry, R. & Neu, J. E. A model for the effectiveness of aircraft alerting and warning systems. 299

Gersten, W. M. & Hawkins, J. D. Development and certification of a new stall warning and avoidance system. 301

Laritz, F. & Sheridan, T. Evaluation of fuzzy rulemaking for expert systems for failure detection. 327

Smith, P.J., Giffin, W. C. & Rockwell, T. H. The role of knowledge structure in fault diagnosis. 337

TELEOPERATORS
Chairman: Professor Thomas B. Sheridan

Corker, K. & Bejczy, A. The effect of part-simulation of weightlessness on human control of bilateral teleoperation: Neuromotor considerations. 339

Sheridan, T. B. Review of teleoperator research. 361

Rezek, T. Visual systems for remotely controlled vehicles. 367

SUPERVISORY CONTROL MODELS/TASKS
Chairman: Dr. Azad Madni

Berg, S. & Sheridan, T. B. Measuring workload differences between short-term memory and long-term memory scenarios in a simulated flight environment. 397

Moray, N., Richards, M. & Brophy, C. Visual attention to radar displays. 417

Hart, S. G., Battiste, V. & Lester, P. POPCORN: A supervisory control simulation for workload and performance research. 431

Morris, N. M., Rouse, W. B., Ward, S. L. & Frey, P.R. Psychological issues in online adaptive task allocation. 455

PERCEPTION AND ACTION IN SIMULATOR DISPLAYS
Chairman: Dr. Stanley Roscoe

Levison, W. H. & Warren, R. Use of linear perspective scene cues in a simulated height regulation task. 467

Haines, R. F. Cockpit window edge proximity effects on judgements of horizon vertical displacement. 491

van der Vaart, J. C. & Hosman, R. J. A. W. Mean and random errors of visual roll rate perception from central and peripheral visual displays. 515

McGreevy, M. W. & Ellis, S. R. Direction judgement errors in perspective displays. 531

Stoffregen, T. The interaction of focused attention with flow-field sensitivity. 551

Hosman, R. J. A. W. & van der Vaart, J.C. Accuracy of step response roll magnitude estimation from central and peripheral visual displays and simulator cockpit motion. 559

MODELS OF TARGET ACQUISITION
Chairman: Dr. Carroll Day

Zaleski, M. & Sanderson, P. Hitts' Law? A test of the relationship between information load and movement precision. 575

Jagacinski, R. J., Plamondon, B. D. & Miller, R. A. A production system model of capturing reactive moving targets. 585

Kim, W. S. , Lee, S. H., Hannaford, B., & Stark, L. Inverse modeling to obtain head movement controller signals. 601

Connelly, E. M. A control model: Interpretation of Fitts' Law. 621

Miller, R. A., Messing, L. J. & Jagacinski, R. J. The impact of pictorial display on operator learning and performance. 643

BIODYNAMIC FACTORS

Chairman: Professor John Lyman

Jex-Courter, B. & Jex, H. R. Does McRuer's Law hold for heart rate control via biofeedback display. 663

Winters, J. M. & Stark, L. New uses for sensitivity analysis: How different movement tasks effect limb model parameter sensitivity. 671

Velger, M., Merhav, S. J., & Grunwald, A. J. Suppression of biodynamic interference by adaptive filtering. 699

Repperger, D. W. & Mc Collor Active sticks - A new dimension in controller design. 719

Levison, W. H., McMillan, G. R., & Martin, E. A. Models for the effects of G-seat cueing on roll- axis tracking performance. 735

Hancock, P. A., Carlton, L. G. & Newell, K. M. An analysis of kinetic response variability. 753

Nam, M. -H., & Choi, O. -M. Effects of external loads on human head movement control systems. 761

CONTENTS
VOLUME TWO

EVOKED POTENTIALS
Chairman: Dr. Al Fregly

Donchin, E. The use of ERPs to monitor non-conscious mentation. 1

Kramer, A. F., Wickens, C. D. & Donchin, E. Performance enhancements under dual task conditions. 21

Junker, A. M. & Peio, K. J. In search of a visual-cortical describing function. A summary of work in progress. 37

SUBJECTIVE EVALUATION OF WORKLOAD
Chairman: Mrs. Sandra G. Hart

Gopher, D. Measurement of workload: Physics, psychophysics, and metaphysics. 55

Vidulich, M. A. & Wickens, C. D. Subjective workload assessment and voluntary control of effort in a tracking task. 57

Wierwille, W. W., Skipper, J. H. & Rieger, C. A. Decision tree rating scales for workload estimation. Theme and variations. 73

Miller, R. C. & Hart, S. G. Assessing the subjective workload of directional orientation tasks. 85

Damos, D. Classification schemes for individual differences in multiple-task performance and subjective estimates of workload. 97

MENTAL MODELS
Chairman: Professor Neville Moray

Sanderson, P.M. Mental models of invisible logical networks. 105

Gopher, D., Fussfeld, N., Koenig, W. & Karis, D. The representation of action plans in long term memory. 121

Rouse, W. B. & Morris, N. M. On looking inside the black box: Prospects and limits in the search for mental models. 123

Serfaty, D. & Kleinman, D. L. Issues in developing a normative descriptive model for dydactic decision making. 125

Sheridan, T. B., Roseborough, J., Charney, L, & Mendel, M. Getting mental models and computer models to cooperate. 127

OTHER ISSUES
Chairman: Professor Larry Stark

Williams, D. H., Simpson, C. A. & Barker, M. A comparative study of alternative controls and displays for the severely physically handicapped. 129

Stein, A. C., Allen, R. W. & Jex, H. R. A manual control test for the detection and deterrence of impaired drivers. 143

Agarwal, G. C., Corcos, D. & Gottlieb, G. L. Electromylographic patterns associated with discrete ankle movements. 157

Kraiss, K. F. & Kuttelwesch, K. H. Color and grey scale in sonar displays. 175

Wingrove, R. C. Manual control analysis applied to the money supply control task. 181

CREW FACTORS
Chairman: Cmdr. Kent Hull

Curry, R. E. What pilots like (and don't like) about the new cockpit technology. 199

Goguen, J. A. , Linde, C. A., & Murphy, M. R. Crew communication as a factor in aviation accidents. 217

Murphy, M. R., Randle, R. J., Tanner, T. A., Frankel. R. M., Goguen, J. A., & Linde, C. A full mission simulator study of aircrew performance: The measurement of crew coordination and decisionmaking factors and their relationships to flight task performance. 249

Siesfeld, A., Curley, R. & Calfee, R. Communication on the flight deck. 263

TRAINING
Chairman: Dr. Robert Hennessy

Poumade, M. L. Determining training device requirements in Army aviation systems. 273

Mane, A. M., Coles, M. G. H., Karis, D., Strayer, D. & Donchin, E. The design and use of subtasks in part training and their relationship to the whole task. 283

MULTIPLE TASK PERFORMANCE
Chairman: Professor Stuart Klapp

Casey, E. J., Kramer, A. F. & Wickens, C. D. Representing multidimensional systems using visual displays. 291

Klapp, S. T. , Kelly, P. A. , Battiste, V. & Dunbar, S. Types of tracking errors induced by concurrent secondary manual task. 299

Tsang, P. S. & Wickens, C. D. The effects of task structures or time-sharing efficiency and resource allocation optimality. 305

Soulsby, E. P. On choosing between two probabilistic choice sub-models in a dynamic multi task environment. 319

MEASUREMENT OF WORKLOAD AND PERFORMANCE IN SIMULATION
Chairman: Dr. Anil Phatak

Kim, W., Zangemeister, W. & Stark, L. No fatigue effect on blink rate. 337

Connelly, E. M. Performance measures for aircraft landings as a function of aircrat dynamics. 349

Kantowitz, B. H., Hart, S. G., Bortolussi, M. R., Shively, R. J., & Kantowitz, S. C. Measuring pilot workload in a moving-base simulator: II. Building levels of workload. 359

Milgram, P., van der Wijngaart, R., Veerbeek, H., Fokkerweg, A. Bleeker, O. & Fokker, O. F. Multi-crew model analytic assesment of decision-making demand and landing performance. 373

Hemmingway, J. C. An experimental evaluation of the Sternberg Task as a workload metric for helicopter flight handling qualities. 397

Time Series Modeling

N85 14488

Time Series Modeling of Human Operator Dynamics in Manual Control Tasks

Daniel J. Biezad* and David K. Schmidt**

School of Aeronautics and Astronautics
Purdue University
West Lafayette, Indiana

ABSTRACT

A time-series technique is presented for identifying the dynamic characteristics of the human operator in manual control tasks from relatively short records of experimental data. Control of system excitation signals used in the identification is not required. The approach is a multi-channel identification technique for modeling multi-input/multi-output situations. The method presented includes statistical tests for validity, is designed for digital computation, and yields estimates for the frequency responses of the human operator. A comprehensive relative power analysis may also be performed for validated models. This method is applied to several sets of experimental data; the results are discussed and shown to compare favorably with previous research findings. New results are also presented for a multi-input task that has not been previously modeled to demonstrate the strengths of the method.

NOMENCLATURE

channel	one of the physical variables used to describe system behavior in the time domain (observed state)
e(t)	vehicle subsystem output vector at time "t"
f(t)	manual control vector at time "t" for pilot subsystem

* Doctoral Candidate
** Professor

$G(z)$	discrete transfer function matrix
$G_{ij}(z)$	transfer function matrix relating subsystems "i" and "j"
$G_{M,k}$	predictor matrix at lag "k", $k \leq M$
$G(M,z)$	$\sum_{k=1}^{M} G_{M,k}\, z^{-k}$
$G_{ij,k}$	element i,j in $G_{M,k}$
$G_{ij}(M,z)$	$\sum_{k=1}^{M} G_{ij,k}\, z^{-k}$
i.i.d.	independent and identically distributed random variables
k	index for lag
M	maximum order for model
m	current order in identification process
N	number of vector samples
n	number of channels
T	matrix transpose (* conjugate transpose)
T(m)	Toeplitz autocorrelation matrix for order "m" process
X(t)	joint process vector
z^{-1}	backward shift operator
$\delta(t)$	control surface command vector at time "t"
Δ	uniform sample interval in seconds
ω	frequency (rad per sec)

1. INTRODUCTION

A pilot model is a mathematical expression which balances simplicity of mathematical structure with observed empirical reality according to the purpose for which it is used. A key question always facing the aviation community has been how to develop and use these models in order to specify, design, and evaluate piloted systems[1] so that they provide efficient, proven performance while admitting the pilot "symbiotically" into the control loop[2]. The successes of describing function and optimal control models in meeting this objective are well known[3], but the identification of these models is hindered by an dependence on long data records, a priori parameter knowledge, and a precisely controlled experimental environment.

A time series approach to pilot modeling, introduced ten years ago[4], initially appeared as just another "technique"; but recent applications of time series analysis to complex multi-channel tasks[5] indicate that this

approach may work well on relatively short data records with little or no a priori parameter knowledge. Moreover, the process of modeling provides a unifying mathematical "framework" relating recent research in closed-loop multi-channel identification theory to actual laboratory or flight test data records of relatively short duration. The "framework" includes establishing model existence, applying a proven identification technique, validating the resulting model, and analyzing model properties relative to model purpose.

Early researchers using time series to model manual control behavior recognized that obtaining single or multi-channel pilot models is a doubly formidable task because of the adaptive nature of the pilot and because of the inherent loop closures in the overall system[6]. Shinners[4] and Agarwal[7], in their pioneering work for single-input,single-output (dual-channel) systems, found that simple discrete transfer functions adequately described pilot manual control output in compensatory and pursuit tasks but did not consider the theoretical question of model existence or stability. The work of Goto, based on the theoretical methods of Akaike[8] and Whittle[9], considered model "existence" questions for a two subsystem closed-loop structure[10], but these methods assume that the autocorrelation statistics for the process are known a priori.

The purpose of this paper is to provide a unifying framework for time series modeling by deriving the specific theoretical and experimental conditions required for model existence and uniqueness, to apply an identification algorithm which guarantees stability and does not require a priori statistical information, and to demonstrate the application of this identification process in case studies. The derivation of existence conditions is applicable to a three subsystem closed-loop structure which contains the two subsystem results of Goto as a special case. The derived identification algorithm is called "Normalized Predictive Deconvolution", NPD, and is a generalization of the Levinson-Wiggins-Robinson algorithm[11] and the multi- channel Maximum Entropy Spectral Estimation algorithm[12].

2. THE MODEL

The pilot-as-controller discrete linear model is shown as part of a three subsystem structure in Figure 1. The double lines represent vector

precesses from three subsystems: the vehicle, the pilot, and the flight control system. Autoregressive (Markov) noise is added to each subsystem to represent a physical disturbance[13]; that is, injected noise is a linear sum of past values plus an i.i.d. discrete "shock" or "pulse". Mathematically this representation may be concisely represented by

$$X(t) = G(z)X(t) + \Psi(t) \tag{1}$$

where X(t) is a joint process vector partitioned into subsystems as

$$X(t) = \left| f^T(t), \delta^T(t), e^T(t) \right| \tag{2}$$

G(z) is a matrix of transfer functions in terms of the shift operator "z" which may also be partitioned into a general form given by

$$G(z) = \begin{vmatrix} 0 & G_{12}(z) & G_{13}(z)=G_p(z) \\ G_{21}(z)=G_f(z) & 0 & G_{23}(z) \\ G_{31}(z) & G_{32}(z)=G_a(z) & 0 \end{vmatrix} \tag{3}$$

The injected noise, $\Psi(t)$, is assumed both autoregressive of finite order "L" and uncorrelated between subsystems. Thus, it may be represented by the block diagonal form

$$\Psi(t) = C(L,z)\Psi(t) + \rho(t) \tag{4}$$

$$C(L,z) = \begin{vmatrix} \sum_{k=1}^{L} C_{11,k} z^{-k} & 0 & 0 \\ 0 & \sum_{k=1}^{L} C_{22,k} z^{-k} & 0 \\ 0 & 0 & \sum_{k=1}^{L} C_{33,k} z^{-k} \end{vmatrix} \tag{5}$$

$$\Psi(t) = \left| R^T(t) \ , \ V^T(t) \ , \ W^T(t) \right| \tag{6}$$

$$\rho(t) = \left| r^T(t) \ , \ v^T(t) \ , \ w^T(t) \right|_{i.i.d.} \tag{7}$$

The individual elements in Equation (3), in contrast to the finite order assumption for the noise representation, are expressible either as a ratio of discrete polynomials (transfer function) or as an infinite sequence in the delay operator z^{-1} (pulse response). Thus, between subsystems "i" and "j",

$$G_{ij}(z) = \sum_{k=1}^{\infty} G_{ij,k} \, z^{-k} \tag{8}$$

If the infinite sequence of Equation (8) is truncated at order "M", an approximation to the mathematical system of Equation (1) results which will be referred to as the joint autoregressive representation (JAR). The truncated elements of G(z) are given by

$$G_{ij}(M,z) = \sum_{k=1}^{M} G_{ij,k} \, z^{-k} \qquad \text{JAR} \tag{9}$$

By combining Equations (1), (4), and (9) the JAR may be written as

$$X(t) = G(M,z) \, X(t) + \Omega(z) \, \rho(t) \tag{10}$$

$$\Omega^{-1}(z) = \left| I - C(L,z) \right| \tag{11}$$

$$C_{ii}(L,z) = \sum_{k=1}^{L} C_{ii,k} \, z^{-k} \tag{12}$$

The joint innovations representation[14], JIR, is obtained by multiplying Equation (10) by Equation (11) and solving for X(t):

$$X(t) = A(M,z) \, X(t) + \rho(t) \tag{13}$$

$$A(M,z) = \sum_{k=1}^{M} A_{M,k} \, z^{-k} = \left| C(L,z) + G(M,z) - C(L,z)G(M,z) \right| \tag{14}$$

The block diagonal form of Equations (2) and (5) is now taken into account in the relationship between the JAR and JIR. Denoting each

subsystem of X(t) by subscript "i", Equations (13) and (14) are equivalent to

$$X_i(t) = C_{ii}(L,z)\, X_i(t) + \sum_{j=1}^{3} \left| I - C_{ii}(L,z) \right| G_{ij}(M,z)\, X_j(t) + \rho_i(t) \quad (15)$$

By comparing Equations (14) and (15) one obtains

$$C_{ii}(L,z) = A_{ii}(L,z) \quad (16)$$

$$G_{ij}(M,z) = C_{ii}(L,z)\, G_{ij}(M,z) + A_{ij}(M,z) \quad ; \; i \neq j \quad (17)$$

The JIR described by Equation (13) may also be put into the form

$$X(t) = \Gamma(M,z)\, \rho(t) \quad (18)$$

$$\Gamma(M,z) = \left| I - \sum_{k=1}^{M} A_{M,k}\, z^{-k} \right|^{-1} \quad (19)$$

The autocovariance matrix is found by post multiplying Equation (18) by the transpose of X(t) and taking the expected value:

$$R_{xx}(0) = E\left| X(t) X^T(t) \right| = \Gamma(M,z)\, P(0)\, \Gamma^*(M,z) \quad (20)$$

where

$$P(0) = E\left| \rho(t)\, \rho^T(t) \right| \quad (21)$$

The power spectral density of this process[5] is

$$\Phi_{xx}(\omega) = \left| \Gamma(M,z)\, \Delta\, P(0) \Gamma^*(M,z) \right|_{z = e^{j\omega\Delta}} \quad (22)$$

which has the property

$$\Phi_{xx}(z) = \Phi_{xx}^T(z^{-1}) = \Phi_{xx}^*(z) \quad (23)$$

An approximation to the frequency response between variables "i" and "j" may be found using

$$G_{ij}(\omega) \simeq \left| G_{ij}(M,z) \right|_{z = e^{j\omega\Delta}} \quad (24)$$

If P(0) is diagonal, the relative power in state "i" is defined as

$$P_{ii}(\omega) = \sum_{j=1}^{n} \Gamma_{ij}(\omega)\ \Delta\ P_{jj}(0)\Gamma^{*}_{ij}(\omega) \tag{25}$$

and the noise power contribution to channel "i" from the noise source in channel "j" is

$$q_{ij}(\omega) = \Gamma_{ij}(\omega)\ \Delta\ P_{jj}(0)\Gamma^{*}_{ij}(\omega)\frac{1.0}{P_{ii(\omega)}} \tag{26}$$

Thus it is shown how the JIR representation of Equation (13) may be transformed into the JAR representation of Equations (9) through (12) using the recursions of Equations (16) and (17). Once validated, the properties of the identified model may be analyzed using Equations (20) through (26). There must be assurance, however, that these modal representations exist in theory, and this topic is addressed in the next section.

3. THE EXISTENCE QUESTION

The primary factors in the determination of an acceptable pilot model are suitable experimental conditions, the assumed model structure, and the identification technique. Since the harm done by a faulty experiment, simulation, or flight test permanently voids the data, the conditions required for a unique and valid model are very important.

THEOREM 1: The JIR of Eqn.(18) is unique, and there is a unique mapping between the JAR of Eqn. (10) and the JIR of Eqn.(13) providing Eqn.(23) holds for the spectral density and providing there is a delay in every path of Figure 1.

For proof see the Appendix.

THEOREM 2: Given that the transfer matrix $\Gamma(z)$ has been identified from realization set $\{X(t) \mid t<N\}$ generated by $\Gamma(z)$, necessary conditions for

$$\lim_{M,N\to\infty} \Gamma(z)=\Gamma(z) \tag{27}$$

are

(1) The joint process X(t) is full rank

(2) There is a unique factorization

$$\Phi_{xx}(\omega) = \left| \Gamma(z) U \Lambda^{1/2} (U\Lambda^{1/2})^T \Gamma^*(z) \right|_{z=e^{j\omega\Delta}} \tag{28}$$

$$\Lambda > 0 \quad \text{and} \quad U \quad \text{Unitary} \tag{29}$$

For proof see the Appendix.

The practical implications of these theorems for flight simulations and flight tests are that sufficient noise sources be used to excite the vector process X(t), that there should be no feedforward paths which violate the requirement for a delay in each loop, and that no anticipatory loops are closed by the pilot for the same reason. Although some identification schemes allow correlated noise inputs[15], there is no way to distinguish them from feedforwards and/or anticipation. If validation tests, however, indicate a positive definite and diagonal autocorrelation matrix for the noise inputs, then there is evidence that a sufficient condition has been met for uniqueness.

To summarize, the design or test engineer should assure

(1) sufficient noise excitation in measured channels;

(2) pilot anticipation negligible (implies random or random appearing inputs;

(3) physical delays exist in each channel, including feedforward, which are significant relative to sample time;

(4) data realizations are not predominantly unstable or nonstationary;

(5) validation checks include a whiteness test for the estimated noise realizations.

4. MODEL IDENTIFICATION AND VALIDATION

Given the conditions are met for model existence, an identification scheme is desired which identifies the JIR of Equation (13) from data realization set $\{X(t) \mid t<N\}$. It is especially important that the scheme be stable (identified parameters are bounded) and not be dependent on a priori knowledge of autocorrelation statistics. The identification technique

presented here is called Normalized Predictive Deconvolution (NPD), which acts directly on the data sets and results in a stable and parsimonious JIR.

The basic principle of the NPD scheme follows that established by Wiggins and Robinson[11] who generalized Burg's[16] recursion for single-channel systems by hypothesizing a set of backward predictors given by

$$X(t) = B(M,z)\, X(t)+\rho'(t) \tag{30}$$

$$B(M,z) = \sum_{k=1}^{M} B_{M,k}\, z^{k} \tag{31}$$

$$\rho'(t) = \left| r'^{T}(t) \;,\; v'^{T}(t) \;,\; w'^{T}(t) \right|_{i.i.d.} \tag{32}$$

By post multiplying Equation (13) by $X^{T}(t-k)$ and Equation (30) by $X^{T}(t+k)$, taking expected value, and expressing the result in a block matrix form, the "normal equations" of Reference (17) result:

$$\begin{vmatrix} I & -A_{m,1} & \cdots & -A_{m,m-1} & -A_{m,m} \\ -B_{m,m} & -B_{m,m-1} & \cdots & -B_{m,1} & I \end{vmatrix} \quad T(m) = \begin{vmatrix} Q_F(m) & \cdots & 0 \\ 0 & \cdots & Q_B(m) \end{vmatrix} \tag{33}$$

where

$$T(m) = \begin{vmatrix} R_{xx}(0) & \cdots & R_{xx}(m) \\ \cdot & \cdots & \cdot \\ \cdot & \cdots & \cdot \\ \cdot & \cdots & \cdot \\ R_{xx}(-m) & \cdots & R_{xx}(0) \end{vmatrix} \tag{34}$$

$$Q_F(m) = R_{xx}(0) - \sum_{k=1}^{m} A_{m,k}\, R_{xx}(-k) \tag{35}$$

$$Q_B(m) = R_{xx}(0) - \sum_{k=1}^{m} B_{m,k}\, R_{xx}(k) \tag{36}$$

In the NPD scheme the solution to the "normal equations" is recursively generated as order "m" is incremented without knowing the autocorrelation matrices a priori. The top and bottom rows of Equation (33) are each

weighted with invertible forward and backward prediction scaling matrices $S_A(m)$ and $S_B(m)$ so that

$$\bar{A}_{m+1,i} = S_A^{-1}(m+1)\, A_{m+1,i} \quad ; \; 0 \leq i \leq m+1 \tag{37}$$

$$-\bar{K}_{m+1,0} = S_A^{-1}(m+1) \tag{38}$$

$$\bar{B}_{m+1,i} = S_B^{-1}(m+1)\, B_{m+1,i} \quad ; \; 0 \leq i \leq m+1 \tag{39}$$

$$-\bar{B}_{m+1,0} = S_B^{-1}(m+1) \tag{40}$$

To derive the forward recursion formula (the backward recursion follows analagously), the scaled bottom row of the "normal equations" is multiplied by an arbitrary but invertible matrix and added to the top row of Equation (33). Next, the order is incremented from "m" to "m+1" and the scaled results are expressed in the form

$$\begin{vmatrix} I & -\bar{K}_{m+1,1} & \cdots & -\bar{K}_{m+1,m+1} \\ -\bar{B}_{m+1,m+1} & -\bar{B}_{m+1,m} & \cdots & I \end{vmatrix} T(m) = \begin{vmatrix} Q_F(m+1) & \cdots & 0 \\ 0 & \cdots & Q_B(m+1) \end{vmatrix} \tag{41}$$

By matching the terms of Equation (41) with the previously obtained linear combination of rows the following recursion results:

$$\bar{A}_{m+1,i} = S_A^{-1}(m+1)\, S_A(m) \left| \bar{A}_{m,i} - S_A^{-1}(m)\varepsilon_F(m+1)Q_B^{-1}(m)\bar{B}_{m,m+1-i} \right| \tag{42}$$

$$Q_F(m+1) = S_A^{-1}(m+1)\, S_A(m) \left| Q_F(m) - S_A(m)\varepsilon_F(m+1)Q_B^{-1}(m)\varepsilon_B(m+1) \right| \tag{43}$$

$$\bar{B}_{m+1,i} = S_B^{-1}(m+1)\, S_B(m) \left| \bar{B}_{m,i} - S_B^{-1}(m)\varepsilon_B(m+1)Q_f^{-1}(m)S_A(m)\bar{A}_{m,m+1-i} \right| \tag{44}$$

$$Q_R(m+1) = S_B^{-1}\, S_B(m)\left|Q_B(m)-S_B^{-1}(m)\varepsilon_B(m+1)Q_F^{-1}(m)\varepsilon_F(m+1)\right| \tag{45}$$

where $0 < i < m+1$ in the above expressions, and where the forward and backward prediction error matrices are given by

$$\varepsilon_F(m+1) = R_{xx}(m+1)- \sum_{k=1}^{m} A_{m,m+1-k}\, R_{xx}(k) \tag{46}$$

$$\varepsilon_B(m+1) = R_{xx}(-m-1)- \sum_{k=1}^{m} B_{m,m+1-k}\, R_{xx}(-k) \tag{47}$$

By defining

$$p(m+1) = S_A^{-1}(m)\varepsilon_F(m+1)S_B^{-T}(m) \tag{48}$$
$$P_A(m+1) = I - p(m+1)p^T(m+1) \tag{49}$$
$$P_B(m+1) = I - p^T(m+1)p(m+1) \tag{50}$$
$$S_A(m+1) = S_A(m)-\varepsilon_F(m+1)S_{B_1}^{-1}(m)\varepsilon_B(m+1) \tag{51}$$
$$S_B(m+1) = S_B(m)-\varepsilon_B(m+1)S_A^{-1}(m)\varepsilon_F(m+1) \tag{52}$$

it may be shown using matrix algebra that

$$\left|P_A^{1/2}(m+1)\right|^{-1} = S_A^{-1}(m+1)\, S_A(m) \tag{53}$$

$$\left|P_B^{1/2}(m+1)\right|^{-1} = S_B^{-1}(m+1)\, S_B(m) \tag{54}$$

$$A_{m+1,i} = \left|P_a^{1/2}(m+1)\right|^{-1}\left|A_{m,i} - p(m+1)S_B^T(m)Q_B^T(m)S_B(m)B_{m,m+1-i}\right| \tag{55}$$

$$B_{m+1,i} = \left|P_B^{1/2}(m+1)\right|^{-1}\left|B_{m,i}-p^T(m+1)S_A^T(m)Q_F^{-1}(m)S_A(m)A_{m,m+1-i}\right| \tag{56}$$

If the scaling matrices of Equations (37) and (39) are chosen to be the "identity" matrix, then the classical Levinson-Wiggins-Robinson (LWR) algorithm of Reference (11) results in a normalized form. If the scaling matrices are chosen so that

$$S_A^{-1}(m) = \left| Q_F^{1/2}(m) \right|^{-1} \tag{57}$$

$$S_B^{-1}(m) = \left| Q_B^{1/2}(m) \right|^{-1} \tag{58}$$

then Equation (48) defines the Partial Autocorrelation Coefficient (PAC)[12] matrix. In addition, if the following approximations are used:

$$\hat{\beta}(m+1) = \left| R_F^{1/2}(m) \right|^{-1} R_{FB}(m) \left| R_B^{1/2}(m) \right|^{-T} \tag{59}$$

where

$$R_F(m) = \sum_{t=m+1}^{N} \Upsilon_F(m,t)\, \Upsilon_F^T(m,t) \tag{60}$$

$$R_{FB}(m) = \sum_{t=m+1}^{N} \Upsilon_F(m,t)\, \Upsilon_B(m,t-1) \tag{61}$$

$$R_B(m) = \sum_{t=m+1}^{N} \Upsilon_B(m,t-1)\, \Upsilon_B(m,t-1) \tag{62}$$

$$i_F(m,t) = S_A(m)\Upsilon_F(m,t) = X(t) - \sum_{k=1}^{m} A_{m,k} X(t-k) \tag{63}$$

$$i_R(m,t) = S_B(m)\Upsilon_B(m,t) = X(t) - \sum_{k=1}^{m} B_{m,m-k} X(t-k) \tag{64}$$

then the multi-channel Maximum Entropy Spectral Estimation algorithm of Reference (12) is obtained.

Morf, Vieira, and Kailath[18] have shown that there is a one-to-one correspondence between the PAC matrices defined above and the autocorrelation matrices for a joint stationary process; moreover, they show that the characterization theorem of stochastic processes assures PAC matrices with singular values less that unity.

To determine the order "M" at which the above recursion is stopped, a variation of the multi-channel Akaike rule[19], as modified by the recommendations of Kashyap[20], is presented here as the PAC selection criterion. This criterion assumes that, as the estimates for the PAC matrix elements becomes smaller, they become more random, thus causing the determinant to also become random. To balance this effect with a term sensitive to both order "m" and number of channels "n" , the following expression was chosen as the PAC selection rule:

$$J_p(m) = N \log |\det p(m)| + m(n)^2 \log N \qquad (65)$$

The order resulting in the "first" minimum value as order "m" is incremented is chosen for the JIR.

Validation is accomplished by testing the forward innovations for whiteness. These residuals are estimated using Equation (62) and the matrix set

$$E\left|i_F(M,t)i_F^T(M,t-k)\right| \quad ; \; t < N \quad ; \; 0 < k \qquad (66)$$

which is visually tested for whiteness over a reasonable number of lags "k". Plots of JIR statistics vs actual statistics (if available) and time histories of actual vs predicted JIR data may also be used.

Summarizing, a technique called Normalized Predictive Deconvolution has been presented to identify a stable JIR of Equation (13) without a priori knowledge of the process autocorrelation matrices shown in Equation (34). The algorithm is initialized at m=0 with

$$Q_B(0) = Q_F(0) = R_{xx}(0)$$

where Equations (60) and (63) are used to approximate $R_{xx}(0)$. The scaling matrices are then chosen, as in Equations (57) and (58) for example, then

by definition

$$\left|P_A^{1/2}(0)\right|^{-1} = S_A(0) \tag{67}$$

$$\left|P_B^{1/2}(0)\right|^{-1} = S_B(0) \tag{68}$$

and Equations (38) and (40) are used to find $X_{m,0}$ and $B_{m,0}$.

The PAC matrix p(1) is then computed from Equations (59) through (64), from which $P_A(1)$ and $P_B(1)$ are found using Equations (49) and (50). The new forward and backward predictors are determined from Equations (55) and (56) for m=1 and finally the value of the PAC selectic rule using Equation (65) is found. If desired the order is incremented and the process repeated.

Once the JIR is identified the JAR may be determined using Equations (16) and (17). The model characteristics are then calculated using Equations (22) through (26). Case studies which demonstrate the application of this identification process and analysis are presented next.

5. MODEL ANALYSIS: CASE STUDIES

In order to demonstrate the application of the JIR identification process on actual data sets a multi-channel "piloted" simulation was accomplished in the Flight Simulation Laboratory at Purdue University. Three pilots performed lateral bank angle tracking tasks using aileron deflection inputs with and without rudder deflection inputs for assistance.

In addition to obtaining the data sets, the goal of the simulation was to obtain subjective pilot ratings and comments for three vehicle configurations. The configurations were representative of large aircraft with the dutch roll modes selected to yield level 1, 2, or 3 handling qualities as currently in military specifications[21]. Table 1 summarizes the dutch roll characteristics and the corresponding pilot ratings and comments obtained during the simulation. Approximately 25 seconds (500 points at a 20 Hz sample rate) were used for modeling from each data run which was typically 60 seconds long.

The pursuit display shown to the pilot for the three-channel simulation (channels were aileron error, aileron deflection, and rudder deflection) is shown in Figure 2. For the two-channel simulation the "ball in the window" portion of the display was masked and no rudder inputs were allowed. Note from the ratings and comments in Table 1 that there is a considerable degradation for each configuration between the two-channel and the three-channel cases. This degradation is most severe for the level 3 configuration where a lateral pilot induced oscillation (PIO) resulted when the pilots were allowed to use rudder inputs.

The commanded bank angle disturbance was a second order autoregressive process given by

$$W(t) = 1.975\ W(t-1) - 0.977\ W(t-2) + .003\ w(t) \tag{69}$$

$$w(t) = \text{ i.i.d. normal } (0,1) \tag{70}$$

The parameters of this process were experimentally determined before taking tracking data to provide a realistic and unpredictable tracking signal to the pilots.

The JIR pilot model was identified using the NPD algorithm set up to provide the special case of the multi-channel Maximum Entropy Spectral Estimation algorithm[12]. The PAC order selection rule of Equation (65) consistently resulted in M=4 in Equation (13) except for the three-channel Configuration 3 where the order was M=7. Figure 3 illustrates the behavior of the PAC selection rule versus order for this case.

A typical experimental versus identified-model time history for the rudder deflection signal is shown in Figure 4 for models identified from 100, 200, and 500 points. The 100 point model used every fourth point of the data set between points 1 and 400; the 200 point model used every other point between points 1 and 400. Thus the final five seconds of the time history shows actual and predicted time histories which are independent of the modeling process. The 500 point model shows the best visual agreement between actual and predicted time histories.

The top row of the "normal equations" from Equation (33) may be used to define the predicted autocorrelation matrix as a function of lag for the identified JIR. With aileron deflection and aileron error as channels 1 and 2, respectively, the actual versus predicted autocorrelation matrix is shown in Figure 5 for the two-channel Configuration 3 , where the actual

value was estimated from the data sets using

$$R_{xx}(k) = E\left|X(t)X^{T}(t-k)\right| \tag{71}$$

The normalized residual matrix from Equations (63) and (66) is shown in Figure 6. Normalization implies that each element is divided by the square root of the products of the respective diagonal element magnitudes, or

$$\text{NORMALIZED}(i,j) = \frac{\text{ELEMENT}(i,j)}{\sqrt{\left|\text{ELEMENT}(i,i)\right|\left|\text{ELEMENT}(j,j)\right|}} \tag{72}$$

The prediction capability demonstrated in Figures 4 through 6 was typical for all identified models and was used as a validation check for all configurations. From these results it was assumed that the models passed the validation checks using experimental data.

If a model passes a validation check, the relative power analysis described by Goto[5] may be accomplished. The total power (variance) in the pilot's aileron deflection signal, computed from Equation (25), versus frequency for each two-channel configuration may be seen in Figure 7. Note that the power spectral density peak magnitude, in general, increases for configurations with higher (worse) pilot rating. Thus there is an indication that pilot workload (as evidenced by power spectral density) increases across a portion of pilot bandwidth as pilot rating increases for different configurations. This is consistent with workload being correlated with deflection rate[22].

Using Equation (26) it is possible to calculate the amount of power due to the noise source in each channel. The noise contribution versus frequency for the aileron channel is shown in Figure 8 for the two-channel Configuration 3 (the other configurations showed similar results). Note that the command disturbance noise is the primary contributor to pilot aileron deflection at low frequencies (below 3 rad/sec) and pilot injected noise (remnant) is the primary contributor to pilot aileron deflection at the higher frequencies (above 6 rad/sec). The two-channel results are summarized in Table 2 and the three-channel results are summarized in Table 3. As expected, the error variance, or element (2,2) in columns 2 and 5 of

Table 3, increases both with pilot rating and with the added workload of the three-channel task (as measured by the spectral density).

For the three-channel case studies, the total power in the pilot's aileron deflection signal for each configuration is shown in Figure 9. As in the two-channel ease study, the power spectral density peak magnitude increases for configurations with the higher (worse) rating, suggesting a proportional increase in pilot workload.

It is noted that the peak power tends to occur at the dutch roll frequency for each configuration, indicating that this mode is clearly present if not dominant in the pilot's output. If this is the case this mode may be a contributing cause to the lateral PIO occurring for Configuration 3 (refer to Table 1 for comments).

The plots depicting noise contributions into the aileron and rudder deflection signals are shown in Figures 10 and 11. In addition to the large increase in peak spectral density of Configuration 3 over the other configurations, note that command disturbance noise is not dominant in the frequency range of maximum power as in the two-channel case (Figure 8). In the aileron deflection channel, pilot injected noise contribution exceeds the command disturbance noise contribution. This same trend is even more noticeable in the noise contribution plots for the rudder channel in Figure 11, where the primary noise source is clearly pilot injected noise into the rudder channel.

To summarize the data analysis of the identified models, there is evidence that the cause of the PIO and resultant poor pilot rating is self-induced coupling caused by rudder excitation of a dutch roll mode with level 3 flying qualities. Recall in the two-channel case study for Configuration 3 that no lateral PIO occurred when the rudder input was denied the pilot. The command disturbance in each case was identically provided using Equation (69).

The frequency response of the pilot model, obtained from the approximation of Equation (24), is shown for each configuration for the three-channel cases in Figures 12 and 13. Note that for for poorly rated Configuration 3 that pilot aileron deflection is out of phase at low frequencies with displayed bank angle error.

As seen from the JIR analysis, the amount of information from the identification, validation, and analysis of models obtained from actual

data sets is very large. Thus selectivity in analysis is essential, and the purpose of the modeling effort is paramount in this selection process.

6. CONCLUSIONS

The fundamental conclusion from this research effort is that time series models and the analytical analysis tools they provide have the ability to quantitatively evaluate pilot-in-the-loop situations by displaying key relationships affecting the stability and response of a multi-channel "piloted" dynamic system. The NPD algorithm, in conjunction with the PAC selection rule, results in a parsimonious and stable multi-channel time series JIR model. This representation is unique if the existence conditions of Theorems 1 and 2 are met. Experimentally this requires sufficient and random-appearing excitation, physical delays in each path, and data realization sets which are stable.

Analysis of case studies illustrated the application of the modeling process, and demonstrated how the dominant source of a lateral PIO may be identified using analysis tools presented in this paper. It is important to remember that the case study results were primarily intended to illustrate the "application" of the identification process as opposed to a comprehensive evaluation of particular vehicle configurations.

It is recommended that the joint innovations identification process be applied to a more varied data base, including actual flight test data and flight control system variations. Multi-channel applications which study manual control response of operators in training status may also be accomplished.

7. ACKNOWLEDGMENT

The authors express their gratitude to Mr. Yuan Pin-Jar and to Capt William Smith, USAF, who are responsible for the laboratory computer programs and display setup used in the simulations, and to Mr. Chuck Malmsten for assistance in computer operation, maintenance, and data retrieval. This research was partially supported by NASA Dryden Flight Research Facility/Ames Research Center under grant no. NAG4-1. This support is appreciated.

8. APPENDIX

PROOF OF THEOREM 1. From Equation (10) we have

$$X(t) = \left|I - G(M,z)\right|^{-1} \Omega(z)\rho(t) \tag{A.1}$$

First the unique mapping between Equations (A.1) and (13) and (18) will be given, then the uniqueness conditions for the identified $\Gamma(z)$ will be derived. Referring to Figure 1 and temporarily eliminating notation for arguments let

$$K_1 = (I - G_p G_a G_f) \tag{A.2}$$
$$K_2 = (I - G_f G_p G_a) \tag{A.3}$$
$$K_3 = (I - G_a G_f G_p) \tag{A.4}$$

Expand the subsystem blocks in Equation (18) to obtain

$$X(t) = \begin{vmatrix} \Gamma_{11}(z) & \Gamma_{12}(z) & \Gamma_{13}(z) \\ \Gamma_{21}(z) & \Gamma_{22}(z) & \Gamma_{23}(z) \\ \Gamma_{31}(z) & \Gamma_{32}(z) & \Gamma_{33}(z) \end{vmatrix} \rho(t) \tag{A.5}$$

Use direct substitution from Equation (A.1) and match entries with Equation (A.5) to obtain

$$\Gamma_{11} = K_1^{-1}\Omega_{11} \tag{A.6}$$
$$\Gamma_{12} = K_1^{-1}G_p G_a \Omega_{22} \tag{A.7}$$
$$\Gamma_{13} = K_1^{-1}G_p \Omega_{33} \tag{A.8}$$
$$\Gamma_{21} = K_2^{-1}G_f \Omega_{11} \tag{A.9}$$
$$\Gamma_{22} = K_2^{-1}\Omega_{22} \tag{A.10}$$
$$\Gamma_{23} = K_2^{-1}G_f G_p \Omega_{33} \tag{A.11}$$
$$\Gamma_{31} = K_3^{-1}G_a G_f \Omega_{11} \tag{A.12}$$
$$\Gamma_{32} = K_3^{-1}G_a \Omega_{22} \tag{A.13}$$
$$\Gamma_{33} = K_3^{-1}\Omega_{33} \tag{A.14}$$

Since Ω_{ii} are non-singular prewhitening filters, K_i singular implies $\Phi_{xx}(\omega)$ singular from Equation (22). The reverse mapping is provided by the recursive relations in Equations (16) through (17). Note that if only two subsystems are present that Equations (A.6) through (A.14) yield the same

relationships given by Anderson[10] and Goto[5].

The final step in the proof is to show the uniqueness of $\Gamma(z)$ and this will be done using the following result from Popov as communicated by Anderson[10]:

For a nonsingular

$$\Phi_{xx}(z) = \Phi_{xx}^{*}(z) \tag{A.15}$$

there exists $D(z)$ such that

$$D^{*}(z)D(z) = \Phi_{xx}(z) \tag{A.16}$$

$$\det \left| D \right| \Big|_{z} = 1 \quad > \quad 0 \tag{A.17}$$

and there exists

$$\Phi_{xx}(\omega) = \left| \Gamma(z) \; \Delta \; P(0)\Gamma^{*}(z) \right|_{z \, = \, e^{j\omega\Delta}} \tag{A.18}$$

with $\Gamma(z)$ and $P(0)$ unique

$$\Gamma(z=\infty) = I \qquad \text{and} \qquad P(0) > 0 \tag{A.19}$$

To apply this result to the JAR use the condition that there is a delay in every path, thus

$$\left| G_{ij} \right|_{z=\infty} = 0 \tag{A.20}$$

$$\left| C_{ii} \right|_{z=\infty} = 0 \tag{A.21}$$

Substituting Equation (A.20) into Equations (A.6) through (A.14), and substituting Equation (A.21) into Equations (11) and (12), we obtain

$$\left| \Gamma_{ij} \right|_{z=\infty} = 0 \tag{A.22}$$

$$\left| \Gamma_{ii} \right|_{z=\infty} = I \tag{A.23}$$

$$\left| \Omega_{ii} \right|_{z=\infty} = I \qquad \text{(A.24)}$$

Thus Equation (A.19) is satisfied for the JAR. By the i.i.d. properties of $\rho(t)$, P(0) is positive definite; and by the properties of a Toeplitz Autocorrelation[17] matrix

$$\Phi_{xx}(z) = \Phi^{*}_{xx}(z)$$

satisfying Equation (A.15). Therefore Popov's result applies and $\Gamma(z)$ and P(0) are unique. Note that Anderson[10] has also shown that the block diagonals of $\Gamma_{ii}(z)$ must be nonsingular.

PROOF OF THEOREM 2. To prove that the joint process must be full rank for unique identification use Equation (28)

$$\Phi_{xx} = \left| \Gamma(z) \; \Delta \; P(0) \Gamma^{*}(z) \right|_{z=e^{j\omega\Delta}}$$

together with

$$R_{xx}(0) = E\left| X(t) X^{T}(t) \right| = \Gamma(z) \; \Delta \; P(0) \Gamma^{*}(z) \Big|_{z=1}$$

If X(t) is less than full rank then a singular P(0) is implied. A singular P(0) makes one or more blocks of $\Gamma(z)$ arbitrary.

To prove the unique factorization is a necessary condition for unique identification use Equation (22) and the fact that P(0) is positive definite. Then there is a unitary transformation[23] such that for some diagonal $\Lambda(0)$

$$P(0) = U\Lambda(0)U^{T} \quad , \quad \Lambda(0) > 0 \qquad \text{(A.25)}$$

Therefore

$$\Phi_{xx}(\omega) = \left| \Gamma(z) U \Delta \Lambda(0) U^{T} \Gamma^{*}(z) \right|_{z=e^{j\omega\Delta}} \qquad \text{(A.26)}$$

If P(0) is not diagonal, then the identified $\Gamma(z)$ is

$$\Gamma(z) = \Gamma(z) \; U \qquad \text{(A.27)}$$

where unitary matrix "U" depends on the correlation in P(0), and thus may not be unique. If P(0), however, is diagonal then $P(0) = \Lambda(0)$, $U = I$, and

$$\lim_{M,N\to\infty} \hat{\Gamma} = \Gamma(z)\, U = \Gamma(z) \qquad \text{(A.28)}$$

Thus if the unitary matrix "U" is identity then a sufficient condition exists for the factorization to be unique. The "physically realizable" normalized minimum phase stable factor results as defined by Anderson[10].

9. REFERENCES

1. Onstott E., Faulkner,"Prediction,Evaluation, and Specification of Closed Loop and Multiaxis Flying Qualities",AFFDL-TR-78-3, Wright-Patterson AFB,Ohio, Feb 1978.
2. Frosch, R.,"Robots and People", Aeronautics and Astronautics, Vol 21, No. 7, pp. 34-36, Aug. 1983.
3. Rouse W.,Systems Engineering Models of Human-Machine Interaction, North Holland,1980.
4. Shinners S.,"Modeling of Human Operator Performance Utilizing Time Series Analysis",IEEE Tansactions on SMC,Vol SMC-4,No 5, pp 446-458,Sept 74.
5. Goto N.,"A Statistical Method Applied to Pilot Behavior Analysis in Multiloop Systems,"AIAA Journal of Guidance and Control, Vol 3, No 1, Jan-Feb 80, pp 62-68.
6. Willsky A.,"Relationships Between Digital Signal Processing and Control and Estimation Theory",Proceedings of the IEEE,Vol 66, No 9,Sept 78.
7. Agarwal G., Gottlieb G., Osafo-Charles F., O'Niell W., "Application of Time-Series Modeling to Human Operator Dynamics",IEEE Transactions on Systems,Man, and Cybernetics,Vol SMC-10,No 12,pp849-860, Dec 1980.
8. Akaike, H.,"On the Use of a Linear Model for the Identification of Feedback Systems",Ann. Inst. Statist. Math.,,Vol.20, 1968,pp 425-439.
9. Whittle P.,"On the Fitting of Multivariate Regressions,and the Approximate Canonical Factorization of the Spectral Density Matrix", Biometrika,Vol 50,pp129-134,1963.
10. Anderson B.D.O., Ng T.S., Goodwin G.C., "Identifiability of MIMO Linear Dynamic Systems Operating in the Closed Loop", Automatica, Vol 13, 1977, pp477-485.
11. Wiggins R.,Robinson E.,"Recursive Solution to the Multichannel Filtering Problem", Journal of Geophysical Research, Vol. 70, 1965, pp.

1885-1891.

12. Morf M.,Vieira A.,Lee D.,Kailath T.,"Recursive Multi Channel Maximum Entropy Spectral Estimation",IEEE Transactions on Geo Electronics,Vol GE-16,pp 85-94,Apr 78.
13. Gelb A.,Applied Optimal Estimation,MIT Press,Cambridge,Mass.,1974.
14. Caines P.,Chan C.,"Feedback Between Stationary Stochastic Processes", IEEE Transactions on Automatic Control, Vol AC-20, Aug 75, pp 498-508.
15. Vorchik V.,Fetisov V.,Shteinberg E.,"Identification of a Closed-loop Stochastic System",Automatika,No 7,pp41-52,July73.
16. Anderson N.,"On the Calculation of Filter Coefficients for Maximum Entropy Spectral Analysis", Geophysics, Vol. 39, No. 1, Feb 74, pp 69-72.
17. Kailath T.,"A View of Three Decades of Linear Filtering Theory", IEEE Transactions on Information Theory,Vol IT-20,pp145-181, Mar 1974.
18. Morf M.,Vieira A.,Kailath T.,"Covariance Characterization by Partial Autocorrelation Matrices", Annals of Statistics, Vol 6, No 3, pp 643-648,May 1978.
19. Akaike, H.,"Canonical Correlation Analysis of Time Series and the Use of an Information Criterion", System Identification: Advances and Case Studies, Mehra ed., Academic Press, 1976.
20. Kashyap,"Inconsistency of Akaike Rule",IEEE Transactions on Automatic Control,Vol AC-25,No 5, Oct 1980,pp 997.
21. "Military Specification-Flying Qualities of Piloted Airplanes", MIL-F-8785C, 1980.
22. Schmidt D.K., "On the Use of the OCM Objective Function as a Pilot Rating Metric", 17th Annual Conference on Manual Control, UCLA, Los Angeles, June, 1981.
23. Strang G.,Linear Algebra, Academic Press, 1978.

Table I. Three-channel case study configurations

Configuration (Level)	Dutch Roll Parameters		PR	Comments
	ξ	ω_N		
1: two-ch	0.4	2.02	2	"Responsive and predictable"
1: three-ch	--	--	4	"Some coupling from rudder in to aileron axis, but mostly well behaved"
2: two-ch	0.1	2.02	4-5	"Some oscillations and overshoots when aggressive"
2: three-ch	--	--	7	"Coupled overshoots between rudder and aileron and bank angle when aggressive; unpredictable and oscillatory bank angle made worse when aggressive on rudder."
3: two-ch	.02	4.0*	6	"Overshoots and residual oscillations;" "unpredictable;" complex aileron inputs required for control"
3: three-ch	--	--	9	"Closed loop unstable for task;" "excessive lateral PIO."

*This is the frequency of the lateral PIO

Table 2 Two-channel case study results summary

Configuration (Level)	PR	Bank Angle Error Variance deg^2	Ail. Def. Variance deg^2	Cross Covariance Bank Angle to Aileron Deflection deg^2	Maximum PSD Value of Aileron Deflection $deg^2/rad/sec$
1	2	20.9	5.3	8.2	2.2
2	4-5	32.1	6.6	11.4	2.9
3	6	77.1	11.4	20.8	3.8

Table 3 Covariance matrix summary and comparison

Configuration (Level)	2-ch Covariance Matrix $R_{xx}(0)$	* Order M	Pilot Rating PR	Three-channel Covariance Matrix $R_{xx}(0)$ [equation (4.43)]	Normalized P(0) Matrix [equation (4.44)]
1	$\begin{matrix}\delta_a & e_a\end{matrix}$ $\begin{bmatrix}5.3, & 8.2\\ 8.2, & 20.9\end{bmatrix}$	4	4	$\begin{matrix}\delta_a & e_a & \delta_r\end{matrix}$ $\begin{bmatrix}4.93, & 8.55, & 8.83\\ 8.55, & 53.44, & 23.96\\ 8.83, & 23.96, & 25.0\end{bmatrix}$	$\begin{matrix}\delta_a & e_a & \delta_r\end{matrix}$ $\begin{bmatrix}1.0, & -0.10, & 0.15\\ -0.10, & 1.0 & 0.08\\ 0.15. & 0.08, & 1.0\end{bmatrix}$
2	$\begin{matrix}\delta_a & e_a\end{matrix}$ $\begin{bmatrix}6.6, & 11.4\\ 11.4, & 32.1\end{bmatrix}$	4	7	$\begin{matrix}\delta_a & e_a & \delta_r\end{matrix}$ $\begin{bmatrix}19.71, & 24.3\ , & 22.46\\ 24.3\ , & 138.1\ , & 43.87\\ 22.46, & 43.87, & 34.17\end{bmatrix}$	$\begin{bmatrix}1.0\ , & 0.11, & 0.15\\ 0.11, & 1.0\ , & 0.11\\ 0.15, & 0.11, & 1.0\end{bmatrix}$
3	$\begin{matrix}\delta_a & e_a\end{matrix}$ $\begin{bmatrix}11.4, & 20.8\\ 20.8, & 77.1\end{bmatrix}$	7	9	$\begin{matrix}\delta_a & e_a & \delta_r\end{matrix}$ $\begin{bmatrix}11.69, & 15.62, & 8.21\\ 15.62, & 541.1\ , & 41.78\\ 8.21, & 41.78, & 30.5\end{bmatrix}$	$\begin{bmatrix}1.0 & -.19\ , & .017\\ -.19\ , & 1.0\ , & .011\\ .017, & .011, & 1.0\end{bmatrix}$

*order obtained for FAC selection rule

Figure 1 Multi-channel piloted closed-loop system model

Figure 2 Multi-channel lateral axis tracking display

Figure 3 Order selection rule

Figure 4 Rudder channel actual vs. model output: 3-ch case study configuration 3

Figure 5 Autocorrelation matrix vs. lag: 2-ch case study configuration 3

Figure 6 Residual autocorrelation matrix vs. lag: 2-ch case study configuration 3

Figure 7 Total aileron deflection power: 2-ch case study

Figure 8 Noise contribution to aileron deflection PSC: 2-ch case study configuration 3

Figure 9 Total aileron deflection power: 3-ch case study

Figure 10 Noise contribution to aileron deflection PSD: 3-ch case study configuration 3

Figure 11 Noise contribution to rudder deflection PSD: 3-ch case study configuration 3

Figure 12 Frequency response magnitude δ_a/e_a: 3-ch case study

Figure 13 Frequency response phase δ_a/e_a: 3-ch case study

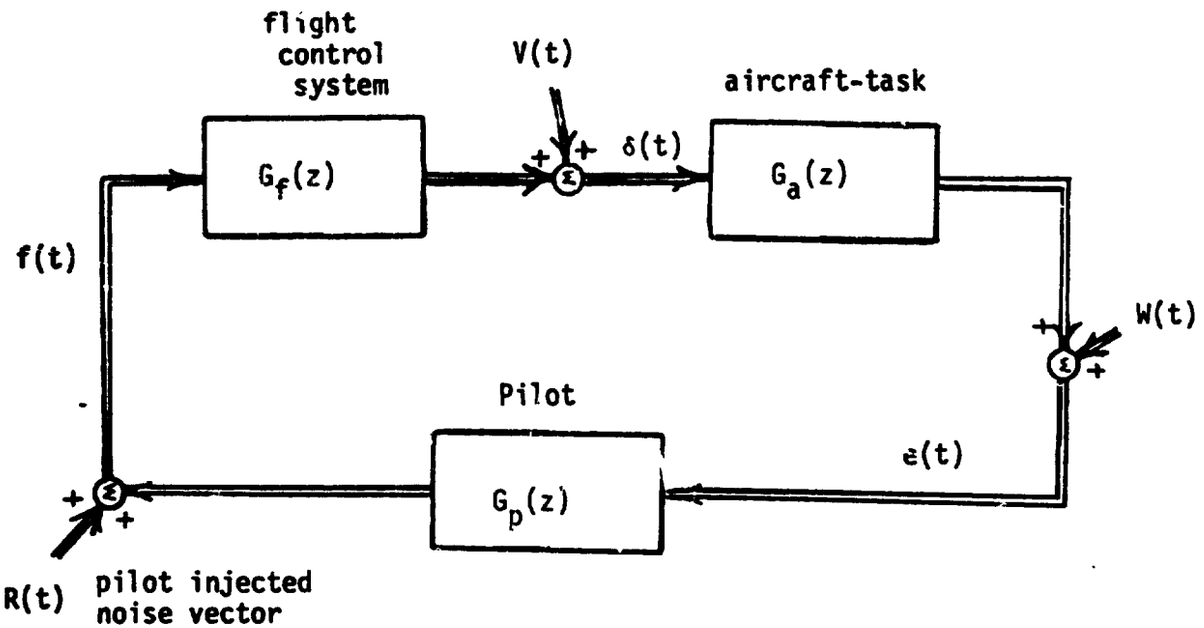
flight
control
system
V(t)
aircraft-task
δ(t)
$G_f(z)$
$G_a(z)$
f(t)
W(t)
Pilot
e(t)
$G_p(z)$
R(t)
pilot injected
noise vector

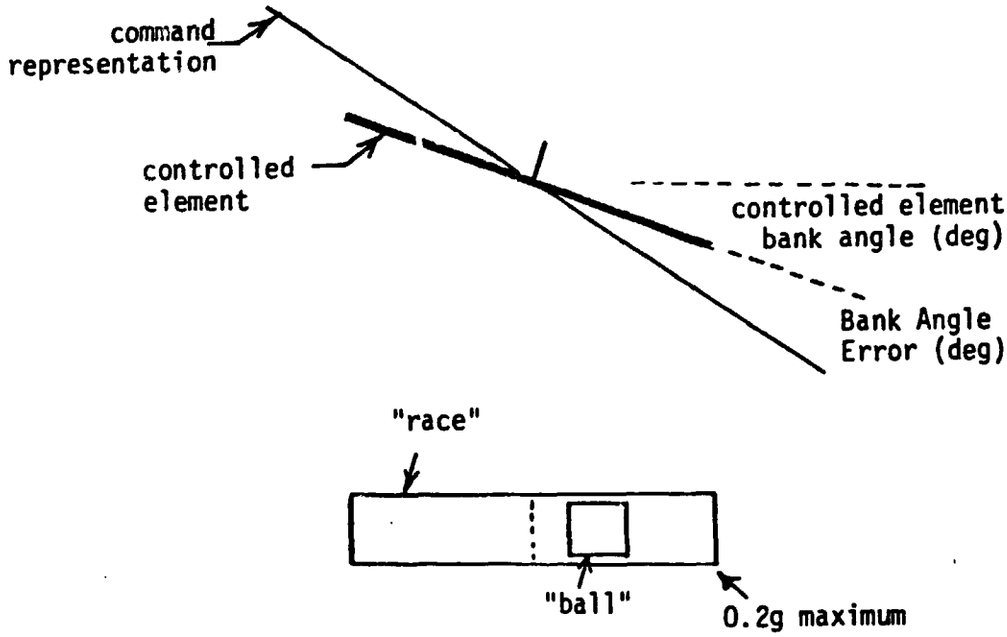
command
representation
controlled
element
controlled element
bank angle (deg)
Bank Angle
Error (deg)
"race"
"ball"
0.2g maximum

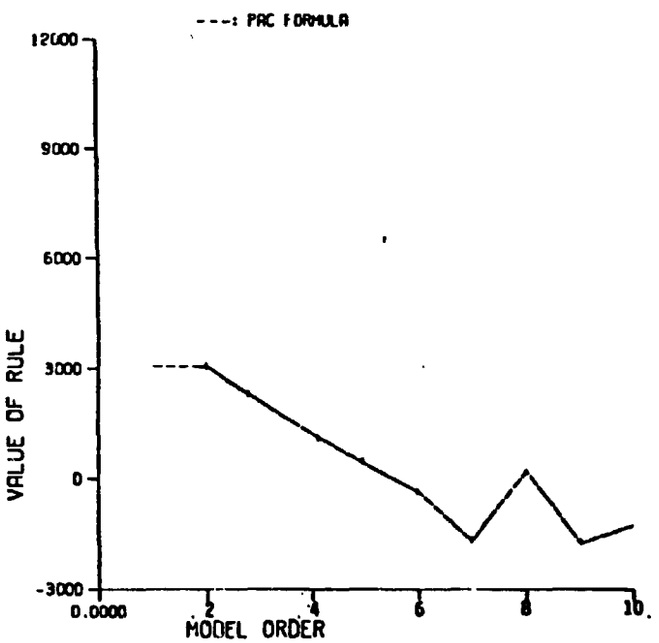
---: PRC FORMULA
12000
9000
6000
3000
0
-3000
VALUE OF RULE
0.0000
2
4
6
8
10.
MODEL ORDER

ORIGINAL PAGE IS
OF POOR QUALITY

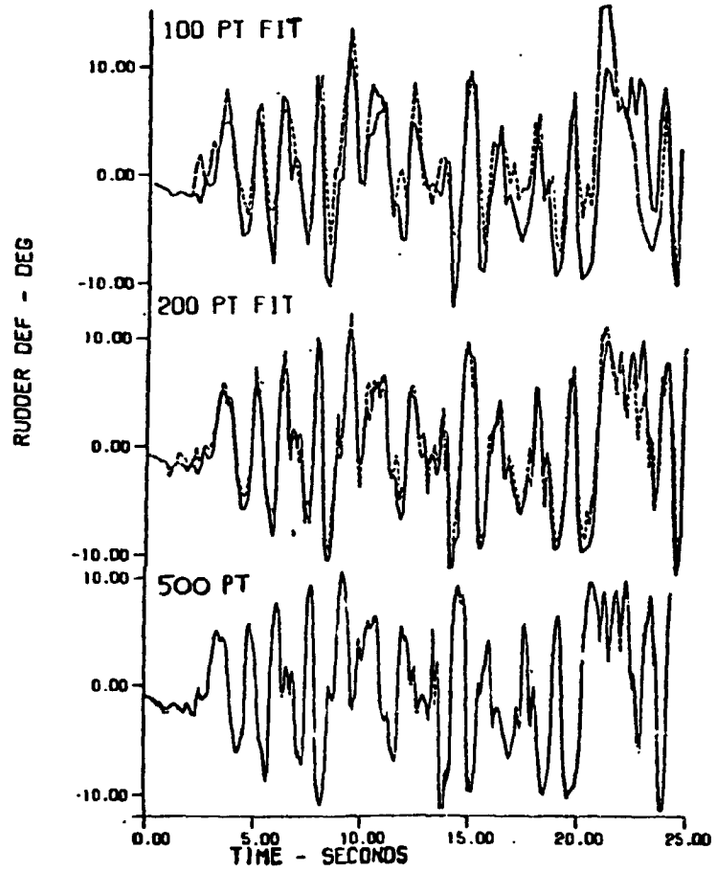

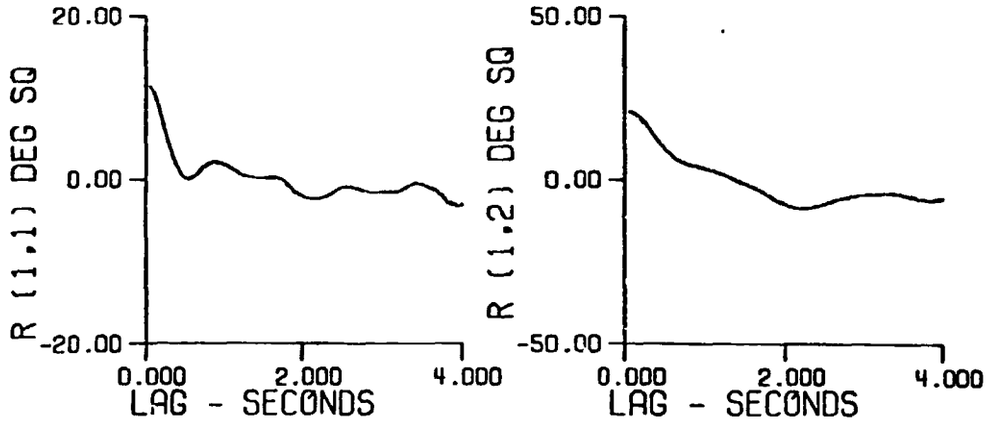

ACTUAL VALUE SOLID LINE
PREDICTED VALUE DASHED

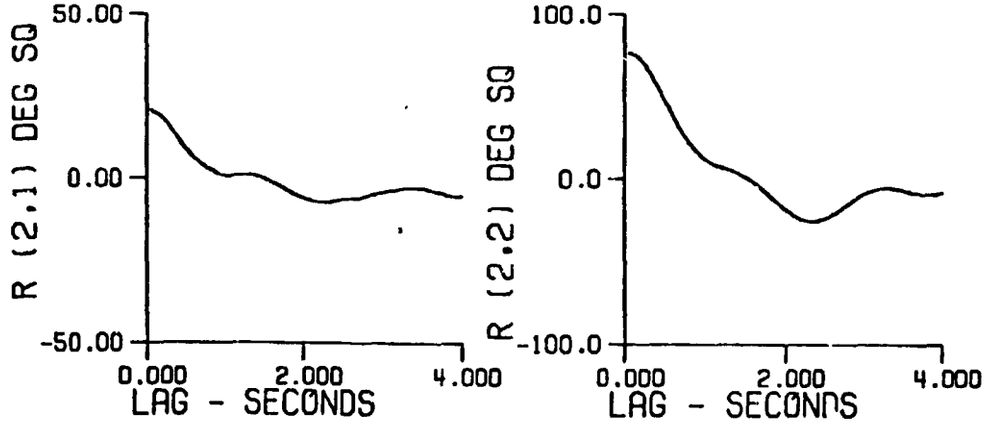

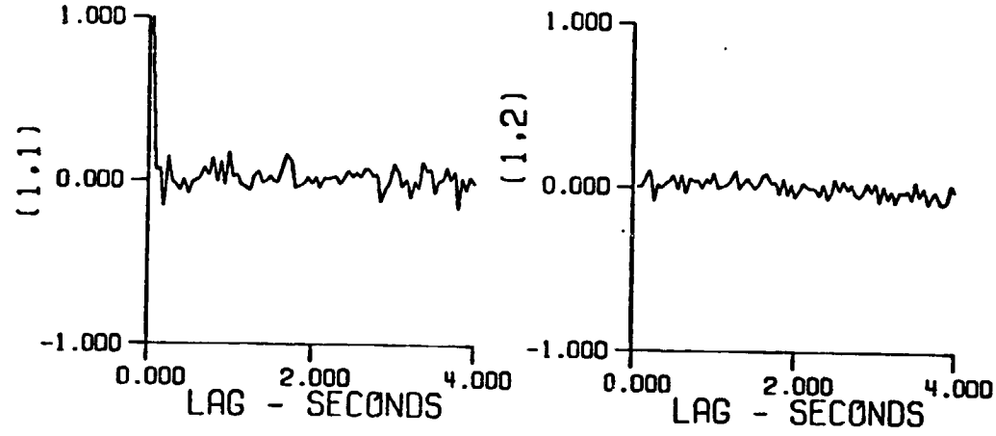
1.000
0.000
-1.000
(1,1)
0.000
2.000
4.000
LAG - SECONDS
1.000
0.000
-1.000
(1,2)
0.000
2.000
4.000
LAG - SECONDS

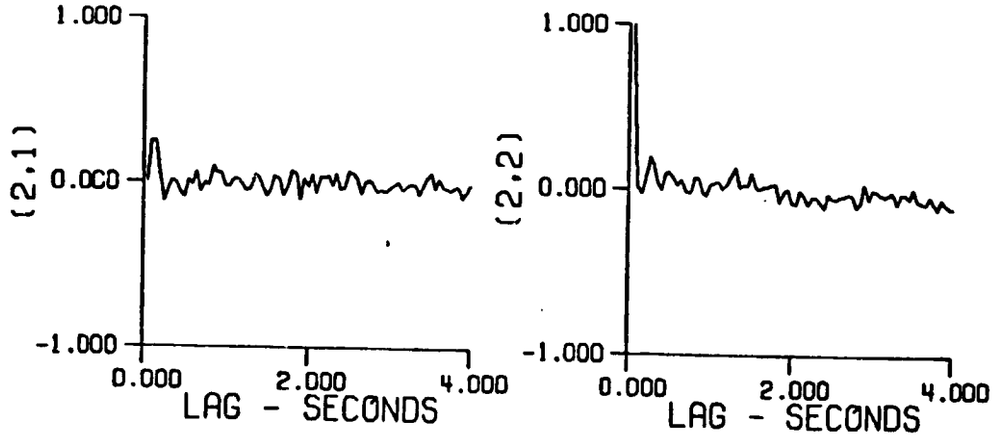
1.000
0.000
-1.000
(2,1)
0.000
2.000
4.000
LAG - SECONDS
1.000
0.000
-1.000
(2,2)
0.000
2.000
4.000
LAG - SECONDS

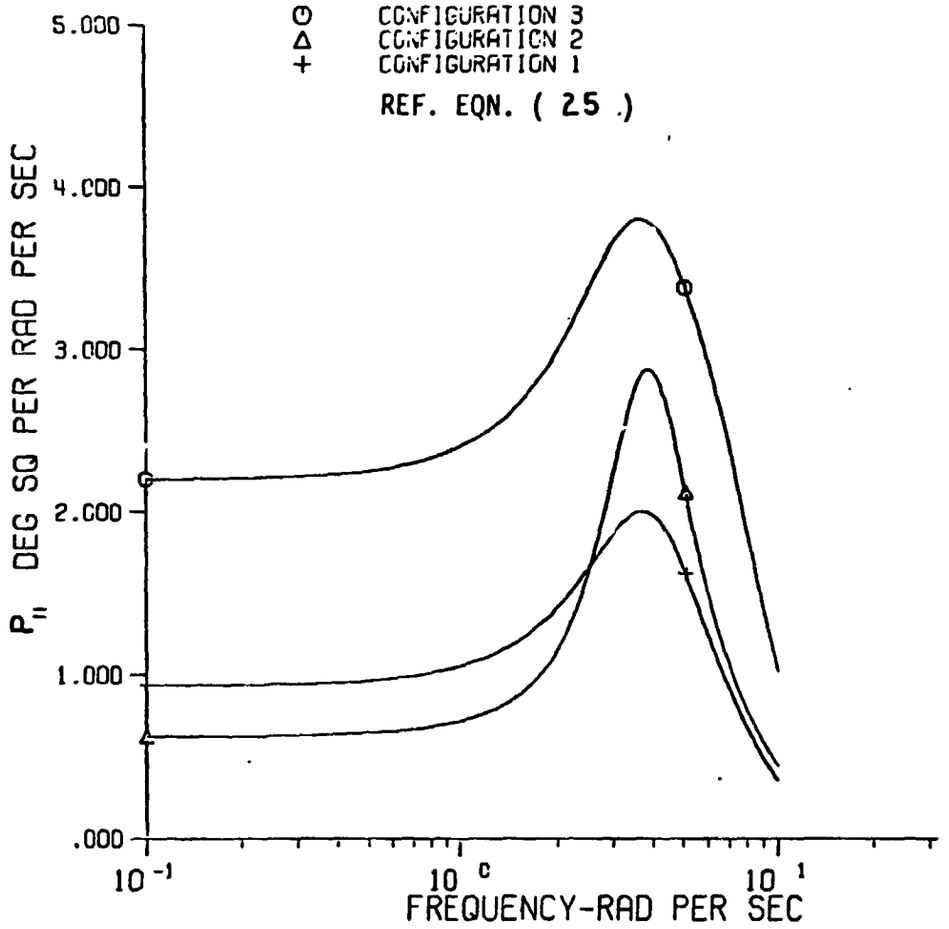
CONFIGURATION 3
CONFIGURATION 2
CONFIGURATION 1
REF. EQN. (25 .)
5.000
4.000
3.000
2.000
1.000
.000
$P_{\eta\eta}$ DEG SQ PER RAD PER SEC
10^{-1}
10^{0}
10^{1}
FREQUENCY-RAD PER SEC

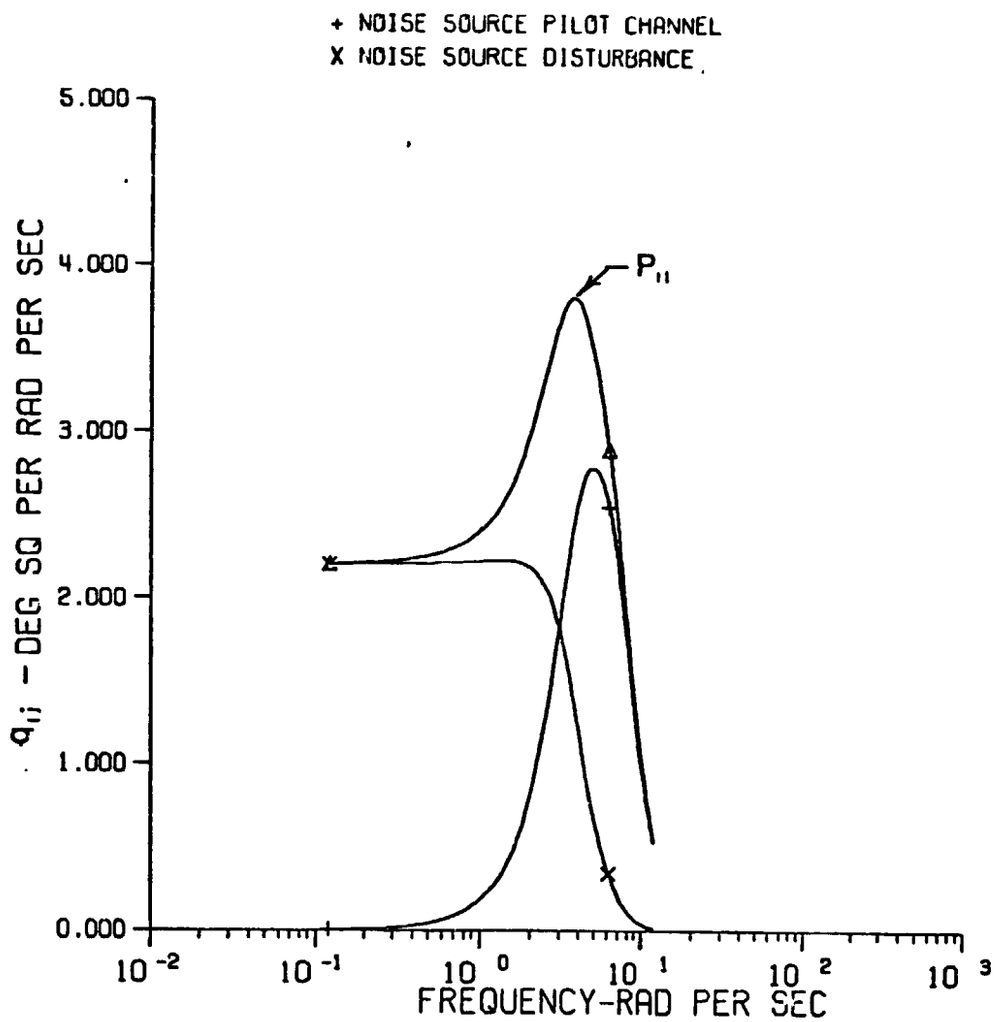
+ NOISE SOURCE PILOT CHANNEL
X NOISE SOURCE DISTURBANCE
5.000
4.000
3.000
2.000
1.000
0.000
q_{ij} - DEG SQ PER RAD PER SEC
P_{11}
10^{-2}
10^{-1}
10^{0}
10^{1}
10^{2}
10^{3}
FREQUENCY-RAD PER SEC

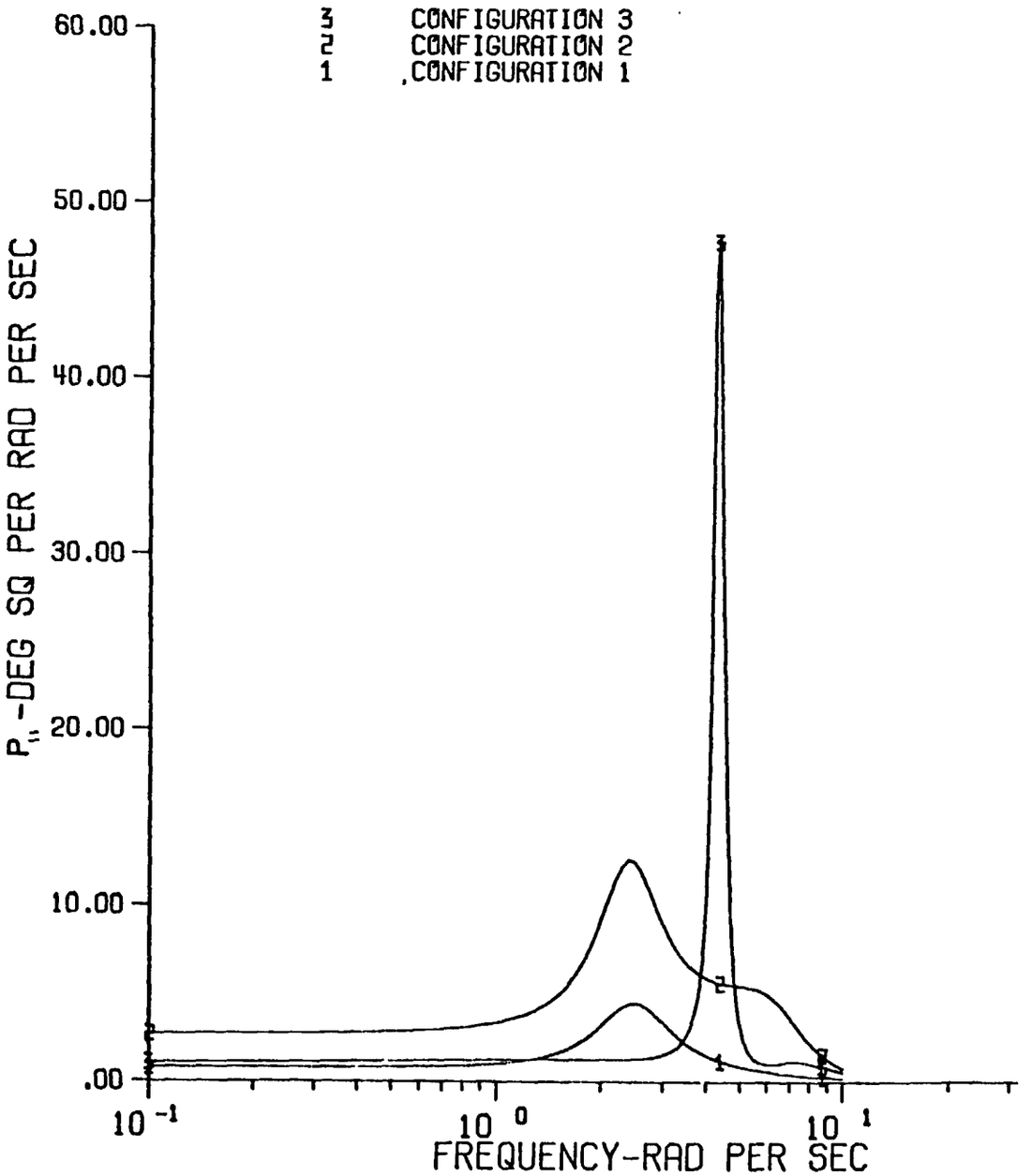
3 CONFIGURATION 3
2 CONFIGURATION 2
1 CONFIGURATION 1
60.00
50.00
40.00
30.00
20.00
10.00
.00
$P_{\dot{\gamma}_1}$-DEG SQ PER RAD PER SEC
10^{-1}
10^{0}
10^{1}
FREQUENCY-RAD PER SEC

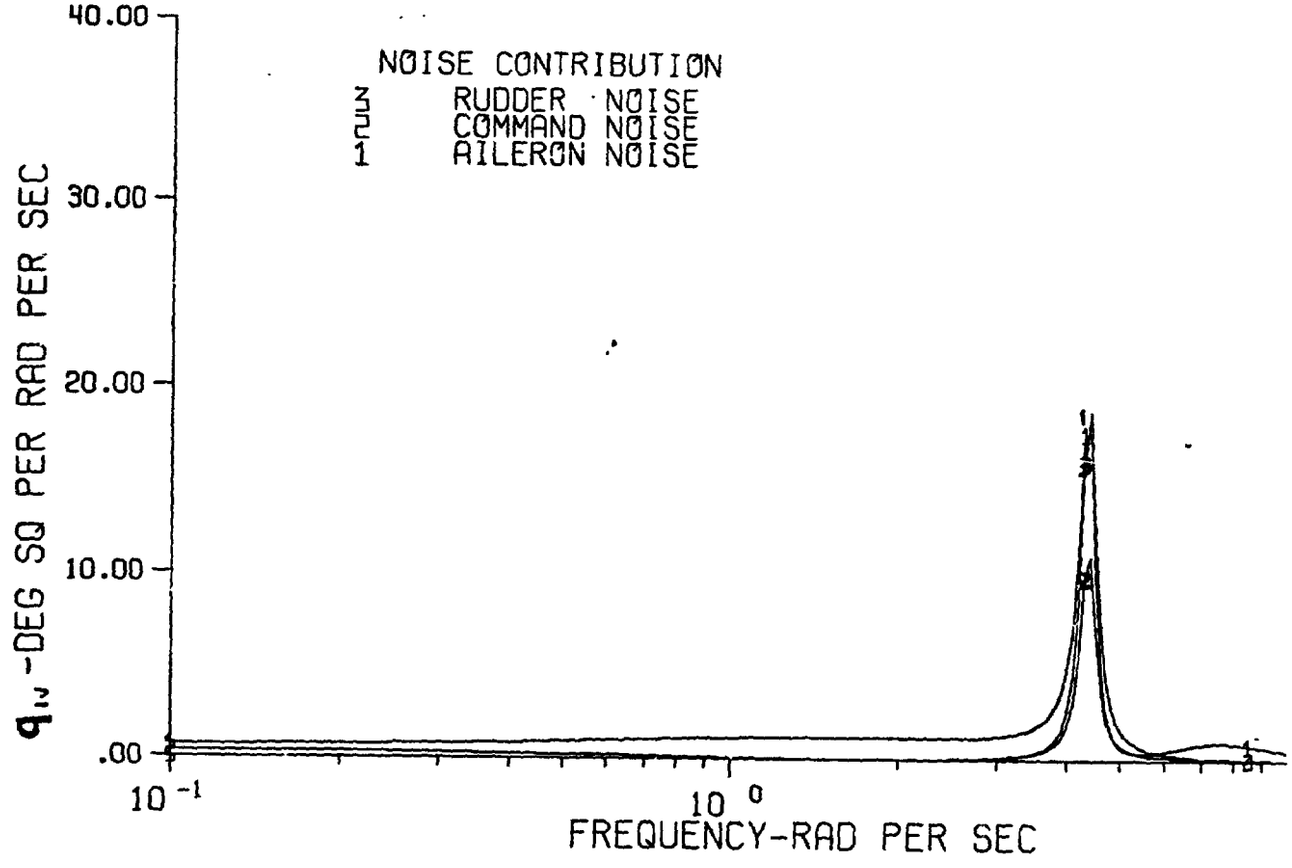
NOISE CONTRIBUTION
3 RUDDER NOISE
2 COMMAND NOISE
1 AILERON NOISE
40.00
30.00
20.00
10.00
.00
q_{ν} -DEG SQ PER RAD PER SEC
10^{-1}
10^{0}
FREQUENCY-RAD PER SEC

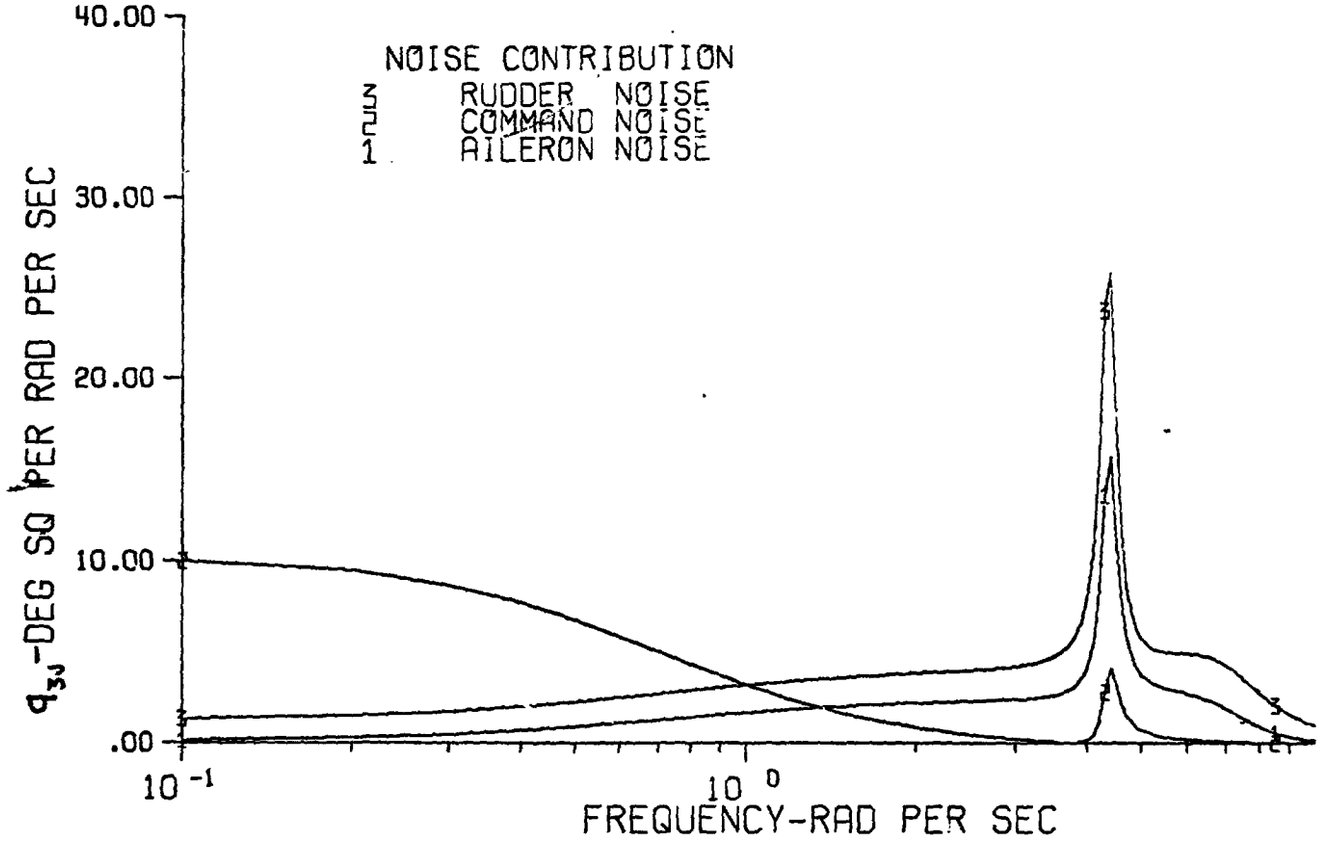
NOISE CONTRIBUTION
RUDDER NOISE
COMMAND NOISE
AILERON NOISE
40.00
30.00
20.00
10.00
.00
q_{3J}-DEG SQ PER RAD PER SEC
10^{-1}
10^{0}
FREQUENCY-RAD PER SEC

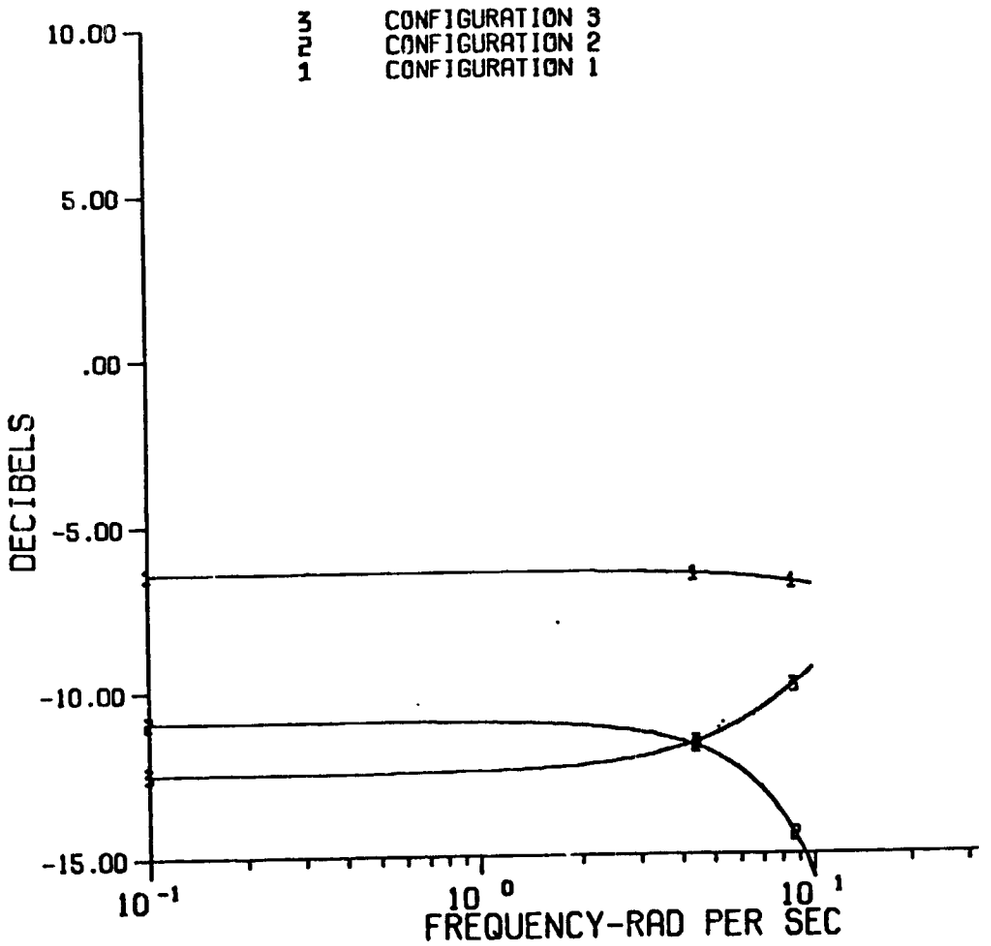
RUN
3 CONFIGURATION 3
2 CONFIGURATION 2
1 CONFIGURATION 1
10.00
5.00
.00
-5.00
-10.00
-15.00
DECIBELS
10 -1
10 0
10 1
FREQUENCY-RAD PER SEC

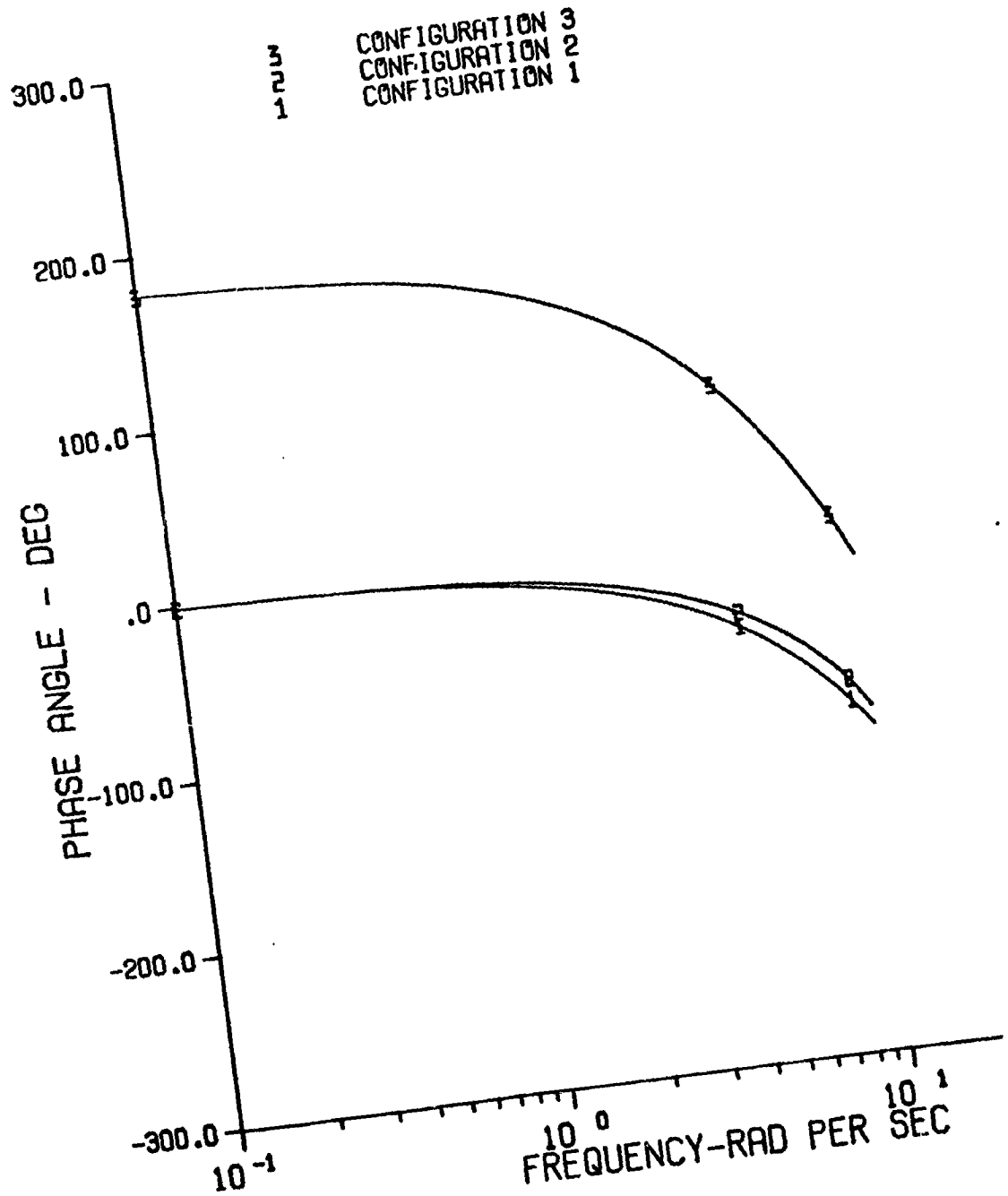
CONFIGURATION 3
CONFIGURATION 2
CONFIGURATION 1
3
2
1
300.0
200.0
100.0
.0
-100.0
-200.0
-300.0
PHASE ANGLE - DEG
10 -1
10 0
10 1
FREQUENCY-RAD PER SEC

D2

N85 14489

STATISTICAL TIME SERIES MODELS OF PILOT CONTROL WITH APPLICATIONS TO INSTRUMENT DISCRIMINATION

R. E. Altschul
P. M. Nagel
F. Oliver

The Boeing Company
Post Office Box 3707
Seattle, Washington 98124-2207

June 1984

INTRODUCTION

Advanced information displays have altered the way pilots interact with the airplane and the way they exercise control. Use of these displays inpacts the cognitive skills used to effect vehicle control in subtle ways. A method of modeling continuous human flight path control has been developed that has proved useful in understanding the effect of these displays on performance and in providing a more precise quantitative description of the pilot vehicle interaction. The method utilizes new technology in multivariate statistical time series for identifying and estimating multi-input/output transfer function models. It is completely data driven and does not depend on any prior knowledge of the system under consideration, but only on a definition of the loop being investigated in terms of the variables involved. Autoregressive moving average models are evaluated in the time domain using state space estimation techniques developed by H. Akaike (1). Once the models are identified, the observed process vector is regarded as the output of a linear system with a rational transfer function matrix subject to white noise input and considered in the frequency domain.

Models have been obtained for a variety of flight situations based on pilot-aircraft performance data obtained from a series of full mission flight simulations and tests in actual flight. One of the primary issues of concern during these tests was a comparison of overall pilot performance using a new flight deck MAP navigation display versus performance using the standard VOR direction indicator over several subjects. The methods used provided evidence to the effect that a pilot's continuous control was measureably different as a function of the navigation information display. They also proved useful in providing performance based quantitative measures for exploring pilot variablity and for comparing control strategies of individual pilots as they respond naturally to the varying demands of the flight path.

Although this study is far from complete, the paper includes:

(i) a general description of the methodology used in obtaining the transfer function models and verification of model fidelity,
(ii) frequency domain plots of the modeled transfer functions,
(iii) numerical results obtained from an analysis of poles and zeroes obtained from z plane to s-plane conversions of the transfer functions, and
(iv) the results of a study on the sequential introduction of other variables, both exogenous and endogenous into the loop.

EXPERIMENT

The analysis is based on a series of flight simulation experiments conducted over a period of months in 1981 in a 767 flight simulator in concert with a series of flight tests on an actual 767 airplane.

The simulations were conducted in the 767 Systems and Workload Display cab at the Renton Flight Simulation Facility of The Boeing Company. Although several flight scenarios were simulated, this analysis is based on a replica of a standard flight profile of a line operation night flight from Seattle to Moses Lake. All of the flight test measurements were obtained from flights over the same route in full daylight.

The objective of the tests was to obtain a workload data base that includes data on eye movement and fixation times, execution times for discrete, manual, verbal and auditory tasks and time traces of continuous control movement and aircraft attitude and flight condition measures. For the simulations the continuous data series were recorded on magnetic tape at a sampling rate of 6.41 per second (one every .156 seconds) and, for flight test, the sampling rate was 5.0 per second (one every 0.2 seconds).

Data was recorded for five pilot - copilot combinations for each of the simulations and for three crews in flight test. The study was designed to determine if two of the presentation formats of navigation information affect pilot control. Specifically, each crew flew two flights, one using the more conventional VOR display mode on the Electronic Horizontal Situation Indicator (EHSI) for navigation guidance throughout the flight and the other with the MAP mode displayed. Figure 1 compares the two display modes. Not all cases in the design resulted in a successful record, hence this analysis is based on a subset of comparable cases. In particular, there was only a single pilot-copilot combination that was common to both instrumentation conditions across both simulation and flight.

ANALYSIS TECHNIQUES

The analysis performed in this study is based on the general class of linear functions of sampled data systems represented by autoregressive moving average (ARMA) models of the form:

$$z(t) - A_1 z(t-1) - \ldots - A_p z(t-p) = e(t) + C_1 e(t-1) + \ldots + C_q\, e(t-q)$$

where $z(t)$ is the vector of the observed process, p and q are numbers representing the model structure, A and C are constant matrices and $e(t)$ is a vector of zero mean white noise Gaussian processes. The use of this ARMA model in the modeling of a single time series is extensively discussed by Box and Jenkins (2).When the series $z(t)$ and $e(t)$ are univariate processes, practical methods for estimating the matrices A and C and the structure identification parameters p and q are relatively recent. The extension of the application of ARMA models to

the analysis of multivariate time series where $z(t)$ is a set of possibly dependent variables is considerably more difficult particularly with regard to structure identification. In the last four to five years several computer codes have been written to perform this task, one of which is based on a method proposed by Akaike. See references (3 and 4) for more detail in addition to reference (1).

In a statistical estimation procedure an estimate is best if it fits optimally to a set of observed data relative to some criterion. Akaike extends this concept to include estimates of the statistical model identification parameters as well, namely, the parameters p and q. Therefore the performance of the model as well as the estimates of the free parameters of the model are influenced by the choice of criterion of model fit. The one proposed by Akaike minimizes an information criterion called AIC where:

$$\text{AIC} = -2(\log \text{likelihood}) + 2(\text{number of independent parameters})$$

and $$\text{MAICE} = \min(\text{AIC})$$

where the minimum is taken over all models of the candidate class. The model that attains the value of MAICE gives the final estimate.

Starting from the ARMA multivariate model in an equivalent canonical Markovian state space stochastic representation, Akaike has shown that the MAICE solution solves the problem of identifiability under very general conditions on the stochastic process.

The code used in this study is based on Akaike's methods of state space parameter identification as implemented in the Statistical Analysis System (SAS) general purpose time series analysis package procedure STATESPACE, reference (5). The state space model on which the code is based can be developed from equation (1) according to the following steps. By solving this equation iteratively for z in terms of e, the infinite series

$$z(t) = e(t) + D_1 e(t-1) + D_2 e(t-2) + \ldots , \quad D_0 = 1$$

is obtained. Denoting the conditional expectation (projection) of $z(t+i)$ on all the past history of z up to time t by $z(t+i|t)$, then:

$$z(t+i|t) = D_i\, e(t) + D_{i+1} e(t-1) + \ldots$$

and

$$z(t+i|t+1) = z(t+i|t) + D_{i-1}e(t+1)$$

Furthermore from Equation (1):

$$z(t+r|t) = A_1 z(t+r-1|t) + \ldots + A_r z(t).$$

where $r = \max(p, q+1)$

These equations can then be summarized in the following form:

$$\begin{bmatrix} z(t+1) \\ z(t+2|t+1) \\ \cdot\ \cdot\ \cdot\ \cdot\ \cdot \\ z(t+r|t+1) \end{bmatrix} = \begin{bmatrix} 0 & 1 & 0 & \ldots & 0 \\ 0 & 0 & 1 & \ldots & 0 \\ \cdot & \cdot & \cdot & \cdot\ \cdot\ \cdot\ \cdot & \\ A_p & A_{p-1} & A_{p-2} & \ldots & A_1 \end{bmatrix} \begin{bmatrix} z(t) \\ z(t+1|t) \\ \cdot\ \cdot\ \cdot\ \cdot \\ z(t+r-1|t) \end{bmatrix} + \begin{bmatrix} 1 \\ D_1 \\ \cdot \\ D_{r-1} \end{bmatrix} e(t+1)$$

or $v(t+1) = Fv(t) + Ge(t+1)$

Since the state vector $v(t)$ is comprised of conditional expectations of $z(\cdot)$ and its first components are $z(t)$, it allows for the representation

$$z(t) = H\,v(t) \text{ where } H = \begin{bmatrix} I & 0 \end{bmatrix}.$$

In summary therefore:

$$\begin{aligned} v(t+1) &= Fv(t) + Ge(t+1) \\ z(t) &= Hv(t) \end{aligned} \qquad (2)$$

which is the Markovian state space representation of the ARMA model (1).

Starting with the ARMA model in the form of (2), the objective of Akaike's method is to compute the maximum likelihood estimates of the free parameters of a given model and then select that model which gives a minimum value of AIC. Although the objective is simple to describe, most implementations are time consuming and potentially unstable. All depend on the choice of an appropriate initial value for success. The SAS implementation uses a method recommended by Akaike. The method proceeds by first fitting an AR model to the observed series by solving a sequence of Yule Walker equations. A final order, M, is then selected that minimizes the AIC information criterion. This order is then used as the number of lags into the past in a canonical correlation analysis that searches for linear

dependence among the linear predictors of the future z(t), z(t+1), ... based on a finite number of past observations z(t), z(t-1), ..., z(t-m). The algorithm proceeds sequentially, successively adding new components, z(t+i), until the canonical correlations are no longer significant. The importance of the correlation associated with the additon of a new component is judged according to another information criterion. This analysis also provides an initial estimate of the remaining free model parameters as well as an initial estimate of the innovation variance-covariance matrix. These values are input to a nonlinear optimization procedure that calculates final estimates of the model parameters based on an approximate maximum likelihood procedure.

If the process converges, the procedure supplies an estimate of the model in statespace form (2), and a covariance matrix for the innovation process e(t). Forecasts and residual plots are also obtainable. The ARMA form of the model is then retrievable by reversing the steps outlined above. Software has been developed for this procedure and is available in SAS.

Once the model is identified, z(t) can be regarded as the output of a linear system with a rational transfer function $K(\omega)$ subjected to a white noise input. See e.g. Priestly (6). The transfer function matrix has the form

$$K(\omega) = A(\omega)^{-1}C(\omega) \tag{3}$$

where

$$A(\omega) = I + A_1 e^{-i\omega} + \ldots + A_p e^{-i\omega p} \tag{4}$$

and

$$C(\omega) = I + C_1 e^{-i\omega} + \ldots + C_q e^{-i\omega q} \tag{5}$$

for the matrices A_i and C_i defined in (1).

If Σ is the variance covariance matrix of the innovation process e(t), then the spectral matrix F of the process Z is given by

$$F(\omega) = K(\omega)\Sigma^{-1}K^{*}(\omega) \tag{6}$$

where K^{*} = conjugate transpose of K .

For the two dimensional closed loop system representation of Figure 2 (a) with open loop representations (b) and (c), let z = (x, y). Then, analytically, the two, open loop, input-output representations become:

$$x(t) = \sum_{0}^{\infty} j(u)y(t-u) + V(t)$$

and

$$y(t) = \sum_{0}^{\infty} h(u)x(t-u) + N(t)$$

where

$$J(\omega) = \sum_{-\infty}^{\infty} j(u)\exp(-i\omega u)$$

is the transfer function at A and

$$H(\omega) = \Sigma h(u)\exp(-i\omega u)$$

is the transfer function at B. If, for this case, the matrices A and C of equations (4) and (5) have elements $a_{ij}(\omega)$ and $c_{ij}(\omega)$, respectively, then the transfer functions J and H are estimated from:

$$J = (a_{11}c_{22}-a_{21}c_{12})^{-1}(a_{22}c_{12}-a_{12}c_{22}) \tag{7}$$

$$H = (a_{22}c_{11}-a_{12}c_{21})^{-1}(a_{11}c_{21}-a_{21}c_{11}) \tag{8}$$

and the noise filters $S(\omega)$ and $R(\omega)$ corresponding to the outputs N(t) and V(t), respectively, from

$$S = (a_{22}c_{11}-a_{12}c_{21})^{-1}(c_{11}c_{22}-c_{12}c_{21})$$

$$R = (a_{11}c_{23}-a_{21}c_{12})^{-1}(c_{11}c_{22}-c_{12}c_{21}).$$

Note that J, H, S and R are rational functions. In general, ARMA models lead to rational functions in the frequency domain. See e.g. Priestly (6).
For two dimensional loops, procedures have been written for plotting the transfer functions J, H, S and R both amplitude and phase, modeled spectra for X, Y, V and N and the corresponding coherency spectra. Three and four dimensional models have also been considered although not all of the above software has been developed for all cases.

Although the use of the SAS code appears to be nearly automatic, there are several decision points in the process that make model fitting at this time take on some of the characteristics of a subjective process. The primary decision has to do with loop definitions: what variables should be included and what the consequences are of leaving variables out, what

interdependent structure exists and whether there are subloops with special structures; whether the subloops should be modeled as a suboptimization conducted prior to the final modeling exercise, what variables are exogenous and how they should be modeled; should the variables be detrended and how nonstationarity should be treated.

Other decisions are a consequence of the evaluation process after models are produced. The MAICE procedure is consistent with the principle of parsimony. That is, increasing the number of parameters in a model has an adverse effect on the minimum unless the increase is balanced with an equivalent increase in the likelihood. Thus this procedure has a definite tendency to converge on models with small values of the identification parameter, that is small values of p and q. It is therefore advantageous at times to force other model orders into consideration after the initial values of the innovation matrix or the residuals indicate an ill fitting model in some respect. Usually the immediate neighborhood of the fitted parameter was searched for improvement.

The STATESPACE procedure can be used in a mode that prespecifies a particular model for a given time series or particular values for the identification parameters. In this way the user of the program can exercise a significant degree of control and guidance over the nature of the subsequent convergence.

APPLICATION AND VALIDATION

The characteristics of a human operator cannot be put into a single class. Over time the human controller of an aircraft displays a wide variety of control behavior: linear, nonlinear, time varying, and adaptive, with varying degrees of randomness in the control. The controller can act as a servo in response to various information sources in the flight deck or can respond by acting upon information or internal motivation from outside the control loop. Therefore, since no single model of human control can be completely comprehensive, the hypothesis of the model building of this study is that valid models can exist for restricted classes over relatively short time periods.

Model development has proceeded on the climb portions of the simulations and flight test from a few seconds after rotation to cruise altitude. For each test condition plots of altitude, airspeed and heading were examined and comparable time periods of approximately one and one-half minutes were selected across the five pilots at various points along the flight path. These periods formed the basic data set for this part of the study.

Since this study is based entirely on a black box look at both the pilot and the vehicle, four graphs from an earlier study are included in Figure 3 that provided insight into the nature of pilot-instrument interaction, pilot to pilot variations and within pilot variation in strategy as the goals of the flight plan are executed. Figures 3 (a) and (b) superimpose the estimated raw spectral densities of aircraft pitch, the displayed aircraft pitch command on the flight director, and the corresponding pilot

column performance. Figures 4(c) and (d) are similar graphs for roll and wheel. The graphs are for two pilots and at a high level of wind turbulence. In all cases the displayed information has a band width that is broader than the corresponding aircraft response and is encouraging a response in the pilots that is broader in band width. Pilot A has matched his response fairly carefully to the indicator but pilot B has a much noisier response that seems to have been propagated by the noise in the indicator. In all cases the pilots seem to be working harder than necessary caused to a degree by the displayed information. The flight director information was not available to the pilot in any of the subsequent experiments.

Figure 4 provides graphs of wheel and column standard deviation for three pilots computed over one and one-half minute intervals at various positions during climb. The data was gathered during an experiment in a flight simulator conducted prior to the one described in the previous section. The subjects were instructed to climb to 31,000 feet in three stages: first, climb to 5,000 feet while making a heading change of 140 degrees, second, climb to 10,000 feet while making a heading change of 100, and third, climb to 31,000 feet turning 20 degrees just before level off. The series have been aligned vertically by the time of rotation. These graphs illustrate clearly the degree of similarity in pilot performance when executing similar tasks and that a pilot's performance varies widely as the task changes. Indeed, for these pilots, there is more variation in a pilot's performance due to changes along the flight path strategy than there is between pilots at any given time or comparable flight condition.

Since this paper is primarily related to display related pilot responses the data sets that are discussed are those comparing:

pilot to pilot variation in control behavior,
pilot variation and navigation display mode (MAP versus VOR),
pilot variation during climb along the flight path,
navigation display mode usage during climb, and
pilot control performance during simulation and actual flight.

Subsets of the basic data set have been selected for making these comparisons and models fitted based on the SAS/STATESPACE procedure. In most cases the modeling process was based upon the control loop structure illustrated in Figure 2 with H as the human transfer function and J that of the aircraft. Since navigation display mode was thought to influence lateral control more than vertical, the initial study was conducted on a loop defined by $x(t)$ = aircraft roll response and $y(t)$ = pilot wheel control response with $N(t)$ as the pilot residual and $V(t)$ as the aircraft residual. A later study, performed on a loop defined by column control and airplane pitch response, was extended systematically to include other variables. For the current study, however, it did not seem necessary to do so, although for a complete understanding of pilot response it is essential.

Wind turbulence is the disturbing force in the loop and would have been used in defining the loop had it been recorded in flight. Since it was not available for the flight tests, the variable was not used in the results presented here and its effect was presumed to affect the pilot only in terms of the roll variable. The lack of this variable distorted the aircraft residual and reduced precision in the loop but did not seriously effect pilot gain.

Box and Jenkins (2) discuss differencing as a method of removing trend and achieving stationarity in a sampled series. On occasion it seemed necessary to do this in one or more of the observed series. As the simulator model of the aircraft developed over time, however, it became less and less necessary, and the current models are based on the original observed data series.

Several tests, both quantitative and subjective, were applied to a model before it was considered acceptable. As a first step, the modeled innovation variance-covariance matrix was examined. For acceptance the entries had to be small relative to the observed series. Convergence itself demonstrated that there was sufficient information in the defined loop, and that the model used by the pilot in that time frame was sufficiently stable to produce a model. This was not always the case. Lack of convergence sometimes occurred and was usually of two types. During dynamic periods with large control inputs on the part of the pilot, convergence was often achieved by sliding the time unit slightly. This indicated a very dynamic change in model with time such that a badly chosen time frame might span two or more separate models. During the least dynamic part of the climb, about midclimb, convergence was also sometimes difficult to achieve. During this period, the pilot seemed to have achieved the desired stability in the flight dynamic variables and was acting more in the capacity of an instrument monitor rather than a linear processor. This was also the case after level off at cruising altitude.

STATISTICAL GOODNESS OF FIT

Statistical goodness of fit tests were performed on the model residuals. The Bartlett's Kolmogorov-Smirnov white noise test was performed on both residuals and only those series passing both tests at the 5 percent level were accepted. SAS made it also possible to plot model residuals against the observed series for visual inspection of the effects of model fitting. In general, the residuals were very small and had the characteristics of white noise. The largest deviations from the observed series occurred primarily when the first differences of the series were large such as, after a period of relative stability in control movement. In figure 5 are residual plots for roll and wheel, respectively, for a typical case of model development.

The subjective elements of model validation has to do primarily with prior expectations regarding the nature of the models themselves. One of the first things that was checked was the stability of the aircraft model across pilot and, to a degree, across flight conditions. Though not known in advance, the resultant equations did display the required model con-

stancy. The pilot models on the other hand, did not; a result which was also expected. The pilot models did, however, exhibit expected trends with flight path.

Integrating the modeled output spectral densities computed from equation (3), produced values for the variances of the modeled series which were then compared to the original sample variances computed from the raw data series. Table 1 compares these estimates in terms of standard deviation for the models discussed in this paper. Models for simulation are much closer, as expected, than those for flight with respect to this measure. In flight the roll percentage differences average 5.9 percent compared to .7 percent in simulation and for wheel the percentages are 2.4 and .7, respectively.

Figures 6 and 7 superimpose the model based spectral densities on the estimated densities calculated from the raw data series. In general, the modeled spectral density is much smoother and has a broader band width than the raw data spectrum and without noticeable peaks and valleys reflecting the overall parsimony of the fitted equations. In every case but one, the fitted spectra track the raw spectra very closely in overall features. For the one case, the low frequency aircraft response is badly modeled and should have perhaps been filtered by a difference filter to improve the modeling.

When convergence was not achieved on the innovations or the residual variances were too high for a model to be acceptable, alternatives were explored. The data series were often shifted by ten to twenty data points at either end in an attempt at locating a fixed model rather than one in transition. A high pass difference filter was also used, though somewhat sparingly, as a device to improve model fit. Other segments were set aside to be investigated in conjunction with larger loop definitions.

These results verify the fidelity of statistical time series techniques applied to the problem of modeling pilot control performance. Good quantitative models of the pilot exercising his control task can be produced that have both statistical and physical validity. The next question then, is to determine what they say about the pilot and how they can be used to provide insight into the control process.

RESULTS

There are thirty-nine modeled flight segments in all, a subset of which are represented in Table 2. The segments consist of twenty-six from the simulation results and thirteen from the results in the aircraft. Of the simulated flight segments, ten are from a flight segment common to each of five pilots flying once with the VOR navigation display and again with the MAP navigation display. The other sixteen simulated flight segments consist of nine VOR and seven MAP segments flown by a single pilot. The thirteen aircraft flight segments consist of five VOR and eight MAP segments all flown by this same pilot. The models are closed loop roll-wheel models, corresponding to Figure 1 for the original roll signal

Most of the control literature on the human transfer function is in terms of a continuous control function, and for this reason the z domain transfer function was transformed into the s domain. Since the z-domain transfer function is a rational function, it can be written as a partial sum:

$$H(z) = \sum_{i=1}^{m} A_i/(1-e^{-s_i T} z^{-1})$$

where m is the number of poles, T is the sampling interval and $z = e^{i\omega T}$. Using the correspondence:

$$H(z) = \sum_{i=1}^{M} A_i/(1-e^{-s_i T} z^{-1}) \longrightarrow \sum_{i=1}^{M} \frac{B_i}{s+s_i} = Y(s)$$

the general form of the pilot transfer function is still a rational function:

$$Y(s) = Ke^{-Ts} \Pi(s+z_i)/ \Pi(s+p_i)$$

where K is pure gain and the z_i's and p_i's are the zeroes and poles of Y, respectively. The use of this correspondence in human operator control modeling also appears in Shinners (9) and Osafo-Charles (10).

The z_i's and p_i's are not always real numbers but frequently occur as complex pairs causing second order factors in the numerator and denominator. The complex poles are more likely to be the two smallest in simulation and the two largest in flight. Complex zeroes are not nearly as frequent. Writing the complex term in the denominator as

$$[(s+(a+bi)][(s+(a-bi)] = \omega^2(s^2/\omega^2+2\zeta s/\omega+1)$$

where ζ = damping ratio

and ω = normalization frequency

The damping ratio was computed for the models developed for the one pilot flying both in the simulator and in actual flight. In the simulator, of the eleven models with second order poles, ζ ranged from .41 to .98 with approximately two thirds of the ratios above .71. For flight the situation was somewhat reversed; of the nine models with second order poles, one was above .71, one at .71, and the rest were below.

sampled at the display mode and the original wheel signal. Neither signal has been filtered.

Graphs of the modeled pilot roll to wheel transfer functions are given in Figures 8 and 9. The graphs cover small flight segments for a single pilot, flying in actual flight, covering a total time span from rotation to cruise altitude. Two flights are represented with different display modes. The graphs are plotted in the z domain using formula (8). The functions are typical of those published by other authors. See e.g., Tanaka (7) and Shirley (8).

The similarity in control exercised by the pilot over comparable time periods between the two flights is worth noting. This is obviously related to the similarity in flight goals during comparable periods of different flights. The dissimilarity of models along the time axis is a measure of the variety of strategy required of the pilot in achieving these goals.

Some thought has been given to the concept of pilot remnant relative to the pilot models developed for these series. Since the concept was originally defined in an open loop context, there is some confusion as to its meaning when the loop is closed. Several authors have defined remnant in terms such as "that part of the output not related to the forcing function" or as "that part of the output not correlated with the input." In closed loop time series modeling the only term of the ARMA time function satisfying this concept is the pilot innovation.

This can be made more explicit, by writing the ARMA model for the pilot in the form:

$$\theta(B)y(t) = \phi(B)x(t) + \beta(t) + \gamma(B)B\beta(t) + \delta(B)B\alpha(t) \qquad (9)$$

where B is the backward shift operator defined by

$$Bx(t) = x(t-1)$$

and θ, ϕ, γ and δ are polynomials in B. Since $\beta(t)$ is white noise it is independent of its own past. $\alpha(t)$ and $\beta(t)$ are contemporaneously dependent only. Therefore $\beta(t)$ is independent of the γ and δ terms of equation (9). $x(t)$ depends only on the past history of $\beta(t)$ and not on its present or future, hence $\beta(t)$ is also independent of the ϕ term.

Often the last three terms of equation 9 are combined into a single remnant term $N(t)$. Not only is this term correlated both with the input series x and both innovation series, it also has more information in it than the concept of remnant usually implies. In particular, in its final form, the transfer function associated with the pilot's innovation series $\beta(t)$ seems to represent the pilot's compensation based on his memory of past "remnants." Although, this term has not yet been studied in detail, it could provide some interesting information on the pilot's cognitive process.

Table 3 summarizes the differences in the poles and zeroes of the pilot's describing function when using the two navigation information display modes for a single flight segment across five of the six pilots who participated in the simulation test. The segment was 90 seconds in duration and a careful attempt was made to match flight conditions across all five pilots even though not all pilots encountered the same conditions at the same time in flight. Pilot control was tapped approximately seven and one-half minutes into flight when the altitude was 14,700-16,700 ft, heading 68.5^{0}-69^{0}, and airspeed approximately 300 knots. But, even though this criterion was somewhat fuzzy in definition, three of the five pilots demonstrated very similar control behavior.

If the complex zeroes and poles are replaced by their corresponding absolute values, this data suggests certain tentative hypotheses:

a) The second zero is usually very large and can be ignored as it has little effect on the frequencies of interest.

b) The time constant associated with the largest pole is measuring an aspect of the pilot's response delay. The time is nearly constant over all of the conditions and averages .126 seconds with a standard deviation of .025.

c) The control lead time constants associated with the first zer are longer using the MAP display than for VOR.

d) The control lag time constants as measured by the first pole are generally shorter when using the MAP display although this effect is not as pronounced as the lead time effect.

e) Pilot equalization as measured by the ratio of the first zero to the first pole is generally less than one for pilots using the MAP display and greater than one for the VOR display.

Thus, in effect, by introducing the MAP display the pilots are demonstrating higher lead times with less lag than their performance using the VOR display. The general positive acceptance of the MAP display obtained from pilots in debriefings implies that this result has been achieved without an adverse effect on pilot workload.

In order to determine if these results were particular to the flight conditions and control strategy in effect at the time selected for analysis, pilot control strategies at several different time segments during the climb phase were investigated. The investigation was conducted on data from both simulation and actual flight for the one pilot flying both models. Figure 10 summarizes the definition of the selected segments in terms of the flight condition measures: heading, airspeed and altitude. Pilot control strategies for these segments were analyzed in terms of the poles and zeroes of the transfer function in the canonical form for both MAP and VOR navigation display modes.

Figure 11 contains graphs of the first zero and first pole, as a function of time into flight from rotation, for the simulation experiment's MAP and VOR mode results. Each plotted point represents a time interval of approximately 90 seconds. Since the VOR zeroes dominate the MAP zeroes, the MAP lead time constants are longer than VOR which substantiates the previous results. The MAP poles are larger in general than the VOR poles though not as consistently. This too substantiates the previous results.

There is a substantial change in lead and lag time constants as a function of time into flight. As the climb progresses the pilot has less to do; flight path variation in performance decreases, lead and lag time constants decrease and the aircraft flight control stabilizes. As cruise altitude is reached, the strategy changes: performance variation increases and the lead and lag time constants increase. The pilot is adapting performance behavior to fit the control task.

Figure 12 portrays a similar scenario for the experiment involving actual flight. MAP zeroes are generally less than VOR zeroes making MAP lead time constants larger. MAP poles are generally greater than VOR poles making VOR lag time constants greater than MAP. The trend with time into flight is also evident with the lead time constants generally larger when the flight control goals are more dynamic.

By comparing the scales of Figures 11 and 12 it can be determined that the simulation zeroes are for the most part larger than those for actual flight. A similar determination is also possible for the poles. Thus, in general, the lead and lag time constants are both smaller for simulation than flight which implies that the flight simulator requires less lead input from the pilot for control compared to actual flight and lags less.

Figure 13 is a graph of the pilot equalization ratio in order to determine if the control is dominated primarily by lags or by leads over the lower end of the frequency band. All four test conditions are superimposed. In general, this graph shows that, except for the MAP condition in simulation, pilots generally lag more with VOR than with the MAP navigation display and more in flight than in simulation. In both the simulator and in actual flight the MAP display results shows a significant decrease in the equalization ratio.

In these models, as in those represented in Table 3, there is a relatively high frequency pole representing pilot response time. During simulation the average was .15 seconds or slightly larger than the average for Table 3, due to a wider variety of flight conditions. For flight the average is .25 seconds. The degree to which these results are confounded with the sampling rate is not known.

MULTI-INPUT, MULTI-OUTPUT PILOT CONTROL MODELS

A cursory investigation was conducted to explore the effect of removing the lateral component of the wind turbulence vector, v_g, from the roll

wheel simulation models of the previous section. The investigation was performed on a single time interval from a simulated flight of 70 seconds, starting approximately 5 minutes into flight. As wind is an exogenous variable, a univariate ARMA model was fit to the time series of the lateral wind component prior to formulating the problem as a multivariate statespace model. This ARMA model was then introduced into the statespace model and remained unchanged during the remainder of the model fitting process. The final model indicates, as expected, that roll has a strong dependence on v_g but that the wheel dependence on v_g is very weak. Figure 14(a) is the power spectrum of the model residuals between the one step ahead forecast and the observed data for wheel. There was no visible difference before and after v_g was introduced. The same comparison is made for roll in Figures 14(b) and (c). The change in the roll spectrum, however, clearly demonstrates that much of the lack of model fit for the lateral variable is directly attributable to this component of wind. The pilot's response to wind is almost completely through the roll variable whereas the aircraft's response is direct. Figure 14 (d) is a time history of the roll residual after v_g was introducted superimposed on the observed roll series. Comparing this plot to the residual in figure 5 for the same case before v_g was introduced, clearly demonstrates that the fit improvement is both in amplitude and over the low frequency part of the spectrum.

A second study of the effect of adding more variables in the loop was performed on a loop that initially involved just the pitch and column variables where pitch was differenced for trend removal. The variables airspeed and the vertical component of wind turbulence w_g were then added sequentially to the model. As before, a univariate ARMA model was fit to the wind component and then added to the statespace model as an exogenous variable.

Figure 15 gives the results of sequentially adding variables to the defined loop as they affect the pilot transfer of the differenced pitch signal. The lowest curve is the pilot transfer of the differenced pitch signal with no other variables in the model. The middle curve is the same transfer function but with airspeed added to the model. The increased pilot gain is frequency selective over the lower frequencies. The upper curve represents the addition of w_g to the model. Again, the added variable is frequency selective affecting only the higher frequencies.

CONCLUSION

This approach seems to have general application as a human factor design aid in display development with regard to such characteristics as the selection of format and information content, the placement and integration of displays, the selection of color/contrast and brightness levels, etc. It is based on minimal model assumptions of linearity and "optimality" of performance. The results not only have provided quantitative measures that have discriminated between display modes, but seem also to have objectively quantified some of the cognitive features of pilot workload. Indeed, its real value as an analysis tool seems to be its sensitivity to the natural control choice of the pilot at the time it is made, as opposed to having to rely on information gained from intrusive measuring devices to understand this process, or having to evaluate mission performance as a whole in terms of arbitrary success criteria or subjective debriefings.

The method does not appear to be limited to continuous performance models. An investigation has already been initiated in applying statistical time series methods to model the pilot as a supervisor or monitor of states combining visual clues with control movements.

Because the method depends on information obtained from expensive simulation, it does not replace other methods currently in use to predict and design information systems. Instead it can be used to complement this activity, e.g., as a research tool to confirm the applicability of these methods or to develop them further with a better understanding of their strengths and weaknesses. The methods of this paper can also be used after the fact, that is, after initial design decisions have been implemented, to fine tune the displays and control system parameters that involve pilot input. Finally, the methods can provide a better understanding of the job of piloting aircraft: in quantifying variation within pilots, in quantifying the interplay of the information variables and the corresponding control, and in quantifying the variation in control and the use of information as a function of the resultant maneuver.

References

1. Akaike, H. "Canonical Correlations Analysis of Time Series and the Use of an Information Criterion." In R. Mehra and D. G. Lainiotis (eds.), Advances and Case Studies in System Identification. New York Academic Press, 1976.

2. Box, G.E.P., and Jenkins, G. Time Series Analysis: Forecasting and Control. Holden Day, 1976.

3. Akaike, H. "Markovian Representation of Stochastic Processes and its Application to the Analysis of Autoregressive Moving Average Processes." Annals of The Institute of Statistical Mathematics, 26: (1974), pp. 363-387.

4. Akaike, H. "On the Identification of State Space Models and Their Use in Control." In D. R. Brillinger and G. C. Tiao (eds.), Directions in Time Series. Proceedings of the IMS Special Topics Meeting on Time Series Analysis. Iowa State University, Ames, Iowa, May 1978.

5. SAS/ETS User's Guide: Econometric and Time Series Library, 1982 Edition, SAS Institute, Cary, North Carolina.

6. Priestly, M. B., Spectral Analysis and Time Series Vol. I and II, Academic Press, 1981.

7. Tanaka, K., Gato, N. and Washizu, K. "A Comparison of Techniques for Identifying Human Operator Dynamics Utilizing Time Series Analysis" Proc. Twelfth Annual Conf. on Manual Control, NASA TM X-73170, pp. 673-693, 1976.

8. Shirley, R. S., "A Comparison of Techniques for Measuring Human Operator Frequency Responses" Proc. Sixth Annual Conference on Manual Control, AFFDL, pp. 803-869, April 1970.

9. Shinners, Stanley M. "Modeling of Human Operator Performance Utilizing Time Series Analysis," IEEE Transactions on Systems, Man and Cybernetics, Vol SMC-4, No. 5, pp. 446-458, September 1974.

10. Osafo-Charles, Frank; Agarwall, Cyan C.; O'Neill, W. D. and Gottlieb, Gerald L. Application of Time-Series Modeling to Human Operator Dynamics," IEEE Transactions on Systems, Man, and Cybernetics, Vol. SMC-10, No. 12, pp. 849-860, December 1980.

		ROLL			WHEEL		
	TIME (SEC.)	Observed	Modeled	% DIFFERENCE	Observed	Modeled	% DIFF
SIMULATION				MAP			
	360-450	4.371	4.391	0.4	3.887	3.887	0.0
	450-540	6.049	6.339	4.8	2.752	2.746	0.2
	540-630	1.561	1.561	0.0	1.538	1.538	0.0
	630-720	1.298	1.299	0.08	1.106	1.106	0.0
	730-790	0.992	0.992	0.0	0.849	0.849	0.0
	800-890	1.383	1.383	0.0	1.728	1.728	0.0
	980-1070	1.742	1.743	0.0	1.661	1.661	0.0
				VOR			
	110-200	13.871	14.527	4.7	4.729	4.707	0.5
	200-290	11.060	11.127	0.6	4.269	3.850	9.8
	300-370	1.699	1.699	0.0	2.302	2.302	0.0
	380-470	2.924	2.924	0.0	2.699	2.699	0.0
	470-560	2.579	2.579	0.0	1.938	1.938	0.0
	560-650	2.281	2.282	0.04	2.074	2.074	0.0
	650-740	3.466	3.465	0.03	2.451	2.451	0.0
	740-830	1.193	1.193	0.0	0.961	0.961	0.0
	8 0-920	3.566	3.566	0.0	2.991	2.990	0.03
FLIGHT				MAP			
	90-180	8.656	9.446	9.1	4.936	4.922	0.3
	180-250	11.491	10.806	8.4	3.396	3.079	9.3
	270-360	9.557	9.838	2.9	2.719	2.566	5.6
	340-400	2.277	2.340	2.8	1.521	1.517	0.3
	450-540	0.857	0.913	6.5	0.870	0.896	3.0
	540-630	0.739	0.738	0.1	0.656	0.655	0.2
	630-720	2.151	2.196	2.1	1.144	1.168	2.1
	720-810	1.677	1.731	3.2	1.075	1.079	0.4
				VOR			
	90-180	9.043	10.905	20.6	4.256	4.288	0.8
	180-270	8.829	9.218	4.4	2.309	2.287	1.0
	270-360	9.857	10.027	1.7	2.154	2.138	0.7
	360-450	0.927	0.958	3.3	1.008	1.012	0.4
	630-720	0.544	0.608	11.8	0.373	0.400	7.2

TABLE 1 Modeled and Observed Standard Deviation Comparison: Simulation (Top) and Flight (Bottom)

ORIGINAL PAGE IS
OF POOR QUALITY

		COEFFICIENT									
	TIME	a_1	a_2	a_3	b_1	b_2	b_3	r_1	r_2	s_1	s_2
SIMULATION					MAP						
	160-450	-1.251	0.252		-1.420	1.390		0.328		1.094	
	450-540	-1.249	0.232		-1.100	1.087		0.335		1.246	
	540-630	-1.218	0.325		-0.360	0.272		0.111		0.559	
	630-720	-1.547	0.639		-0.202	0.158		-0.389		0.537	
	730-790	-1.212	0.496		0.516	-0.652		-0.366		-0.505	
	800-390	-1.427	0.542		-0.076	-0.024		-0.075		0.157	
					ROP						
	110-200	-1.440	0.474		-0.347	0.342		0.292		0.342	
	200-290	-1.347	0.404		0.00	-0.012		0.326		-0.044	
	300-370	-1.139	0.313		-0.034	-0.138		0.284		0.221	
	380-470	-1.464	0.878	-0.359	0.00	-0.505	0.554	0.129	0.195	-0.264	0.358
	470-550	-1.078	0.179		0.217	-0.263		0.263		-0.187	
	560-650	-1.442	0 316	0.186	0.00	0.039	-0.069	-0.329	-0.324	-0.157	0.052
	6 0-740	-1.369	0 452		-0.101	0.075		0.114		0.254	
	740-830	-1.074	0.345		0.273	-0.336		0.115		-0.253	
	830-320	-1.161	0.254		-0.049	0.003		0.450		0.027	
FLIGHT					MAP						
	90-180	-1.270	0.447		0.510	-0.506		0.369		-0.644	
	180-250	-1.265	0.285		0.00	-0.305		0.413		-0.106	
	270-360	-2.049	1.522	-0.461	0.00	0.00	-0.002	-0.481	0.045	0.329	-0.310
	340-400	-1.146	0.277		0.00	-0.043		0.272		0.205	
	450-530	-1.229	0.498		1.681	-1.769		0.230		-2.007	
	540-630	-1.253	0.537		1.195	-1.263		0.200		-1.483	
	630-720	-1.159	0.303		1.330	-1.335		0.441		-1.282	
	720-810	-0.397	0.076		0.227	-0.265		0.366		-0.226	
					ROP						
	90-180	-1.548	0.785		2.479	-2.481		-0.382		-2.551	
	180-270	2.214	1.782	-0.548	0.00	0.00	-0.003	-0.799	0.032	-0.394	0.071
	270-360	-1.903	1.263	-0.337	0.00	0.00	-0.003	-0.355	-0.178	0.322	-0.309
	360-450	-1.203	0.324		0.481	-0.515		0.360		-0.331	
	630-720	-0.787	0.222		4.496	-4.497		0.443		-4.511	

Model: $y_t + a_1 y_{t-1} + a_2 y_{t-2} + a_3 y_{t-3} = b_1 x_{t-1} + b_2 x_{t-2} + b_3 x_{t-3} + \beta_t + r_1 \beta_{t-1} + s_1 \beta_{t-1} + s_2 \alpha_{t-1}$

TABLE 2 ARMA Coefficients Wheel (y) Output vs. Roll (x) Input, Wheel Innovation (β), Roll Innovation (α)

CREW-PILOT		MAP		EQUALIZATION	VOR			EQUALIZATION
1 - 1	ZERO	1.59		4.18	3.21	25.79		1.01
	TIME CONSTANT	0.63			0.311			
	POLE/MODULUS	0.38	6.17		1.89±2.55i/3.17	9.89		
	TIME CONSTANT	2.63	0.162		0.315	0.101		
3 - 5	ZERO	0.25	1.48	0.16	0.90	20.20		0.63
	TIME CONSTANT	4.00						
	POLE/MODULUS	1.13±1.11i/1.58	6.61±4.64i/8.08		1.43	7.35±0.86i/7.39		
	TIME CONSTANT	0.633	0.124		0.699	0.135		
4 - 7	ZERO	1.61	66.72	0.37	2.62	6.39		3.54
	TIME CONSTANT	0.621			0.382			
	POLE/MODULUS	2.42±3.57i/4.31	11.55		0.74	3.30	9.52	
	TIME CONSTANT	0.232	0.087		1.35		0.105	
5 - 9	ZERO	1.72	21.61	0.52	-3.02±5.40i/6.19			6.95
	TIME CONSTANT	0.581			0.162			
	POLE/MODULUS	2.79±1.79i/3.31	7.55		0.89	7.59±0.74i/7.62		
	TIME CONSTANT	0.302	0.132		1.12	0.131		
6 - 11	ZERO	0.84	∞	0.33	4.01	∞		1.50
	TIME CONSTANT	1.19			0.249			
	POLE/MODULUS	1.87±1.68i/2.51	8.53		0.96±2.50i/2.68	6.16		
	TIME CONSTANT	0.398	0.117		0.373	0.162		

TABLE 3 Wheel Model Poles and Zeroes of five pilots approximately 7½ minutes into flight, 300 KN airspeed, 68.5° - 69.5° heading, and 14,700 - 16,700 feet altitude. Roll-wheel loop.

VOR/ILS Mode – Partial Compass Rose – Heading Up

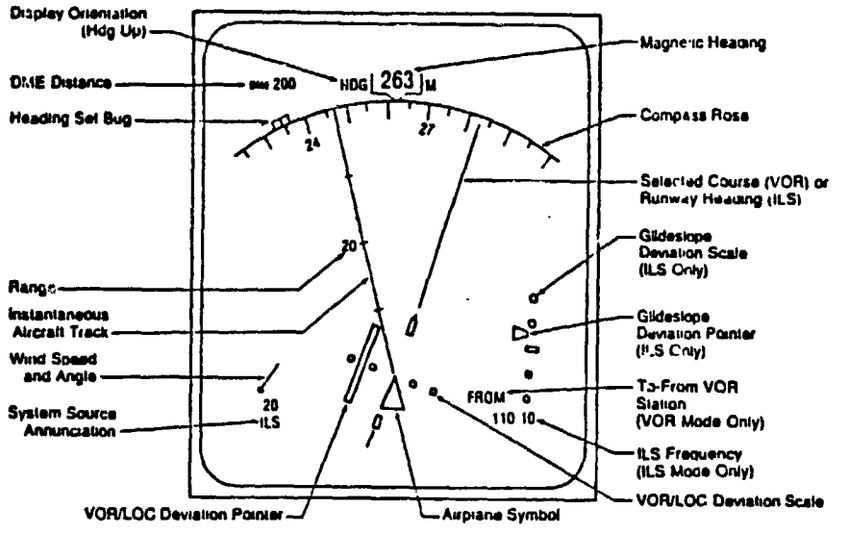

(a)

Map Mode – Track Up

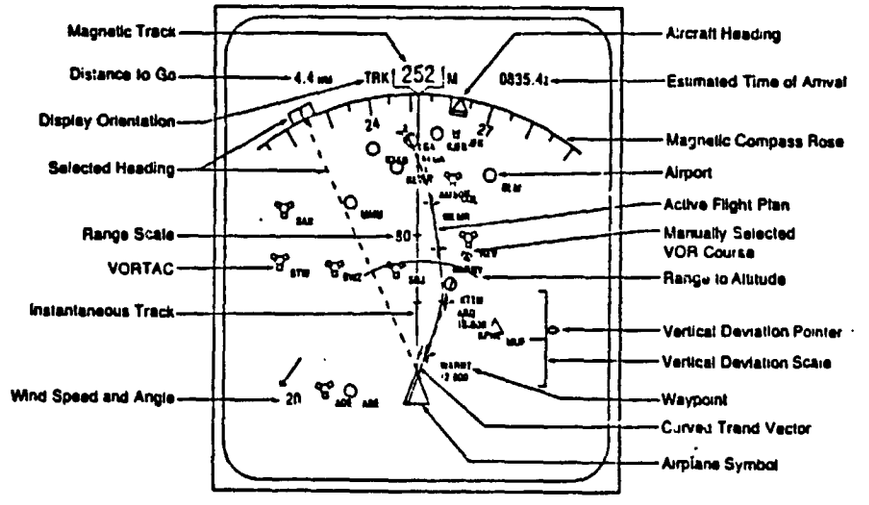

(b)

Figure 1 Horizontal Situation Indicator showing VOR/ILS Navigation Mode (a) and Map Mode (b)

ORIGINAL PAGE IS
OF POOR QUALITY

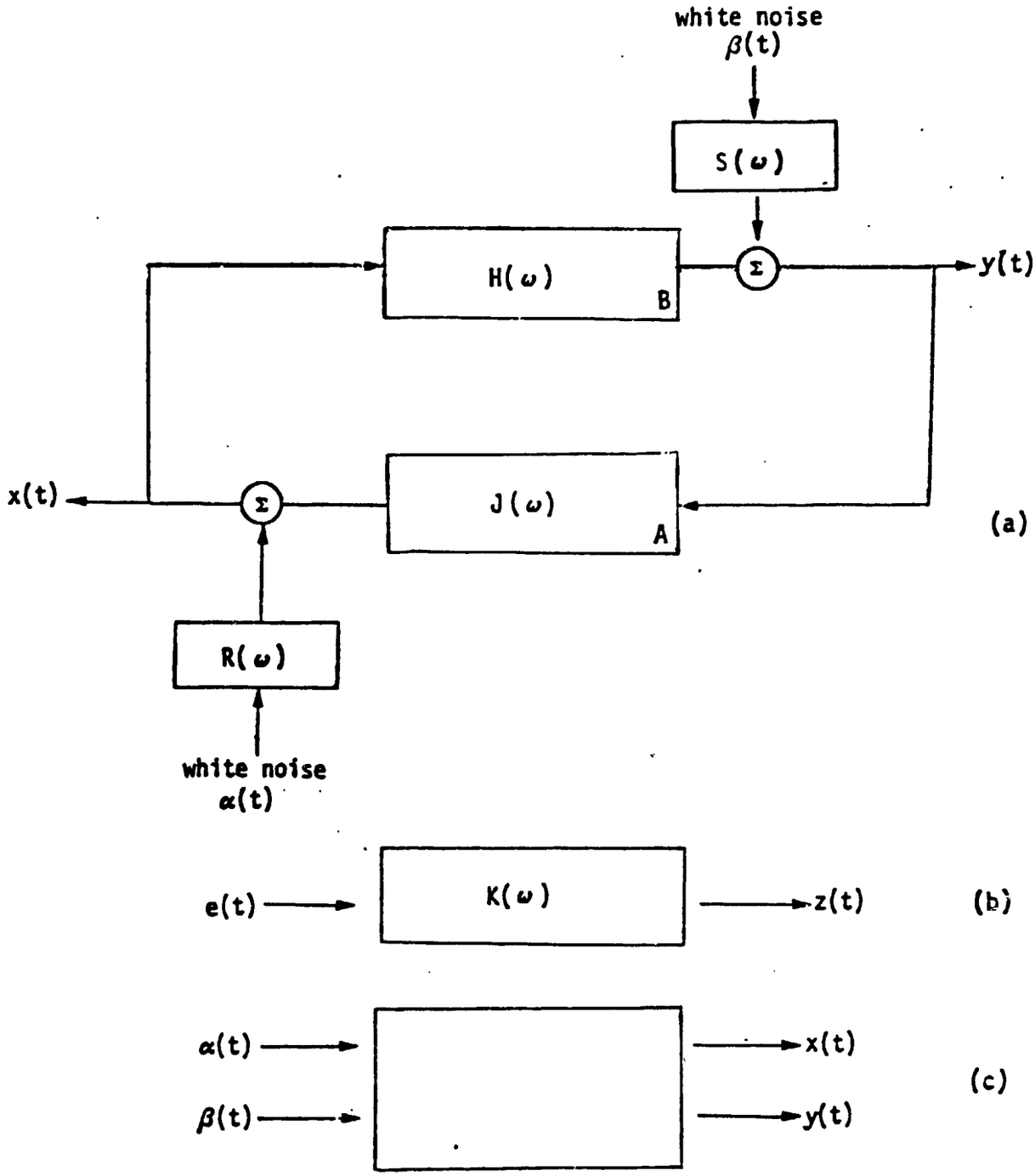

Figure 2 Two Dimensional Open and Closed Loop System Representations

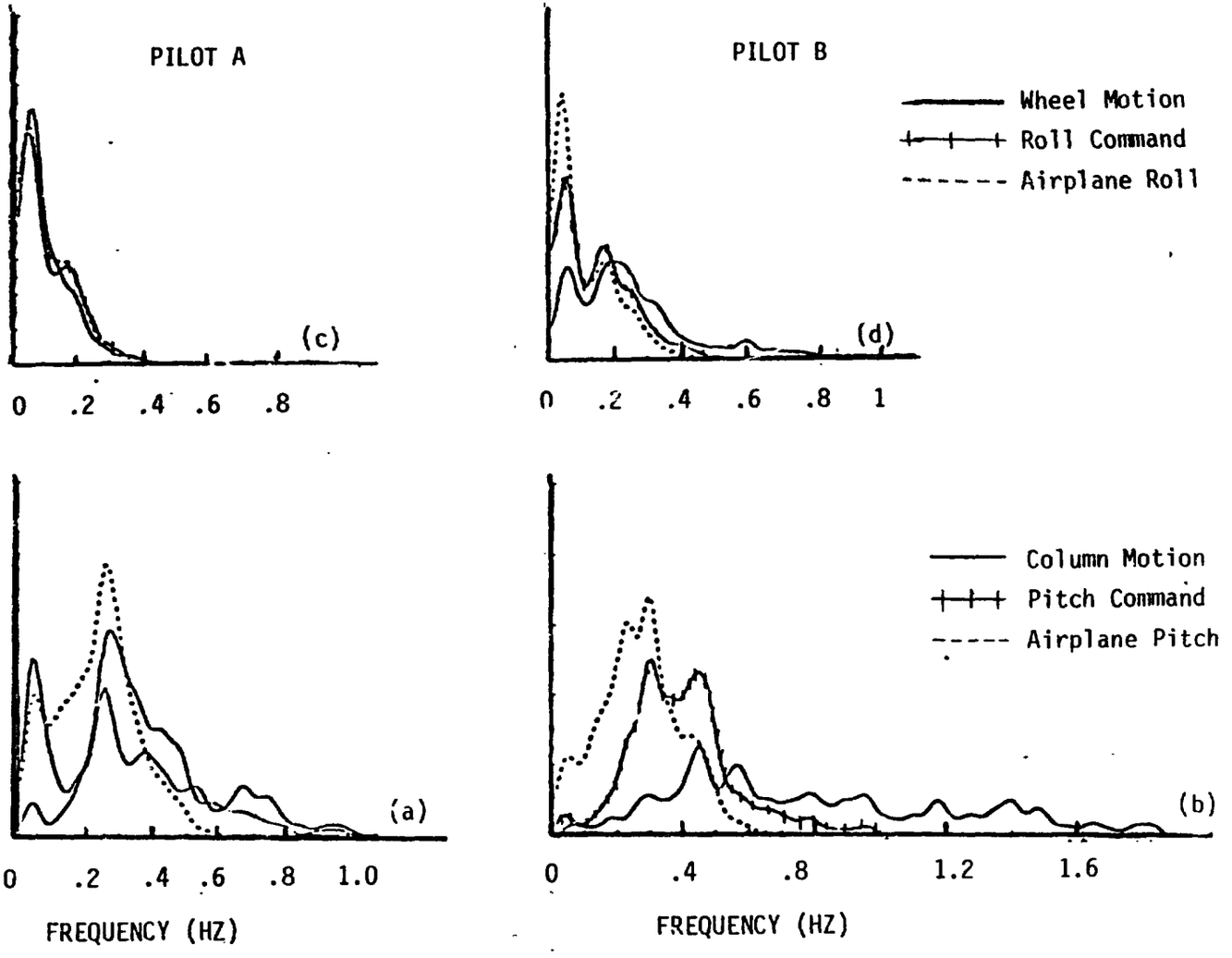

FIGURE 3 Spectral Densities: Roll-related (Top), and Pitch-related (Bottom), for Two Pilots, A (Right), and B (Left)

ORIGINAL PAGE IS
OF POOR QUALITY

ORIGINAL PAGE IS
OF POOR QUALITY

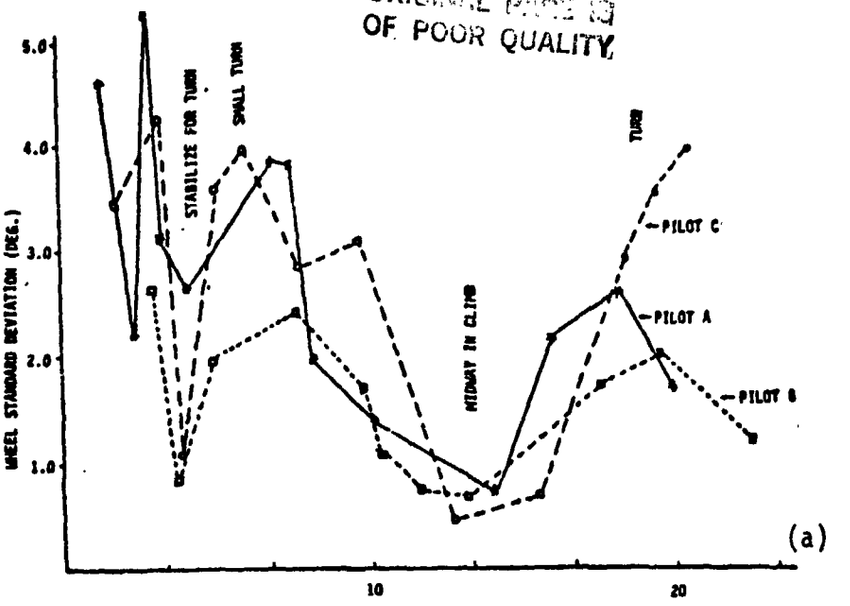

PILOT WHEEL PERFORMANCE

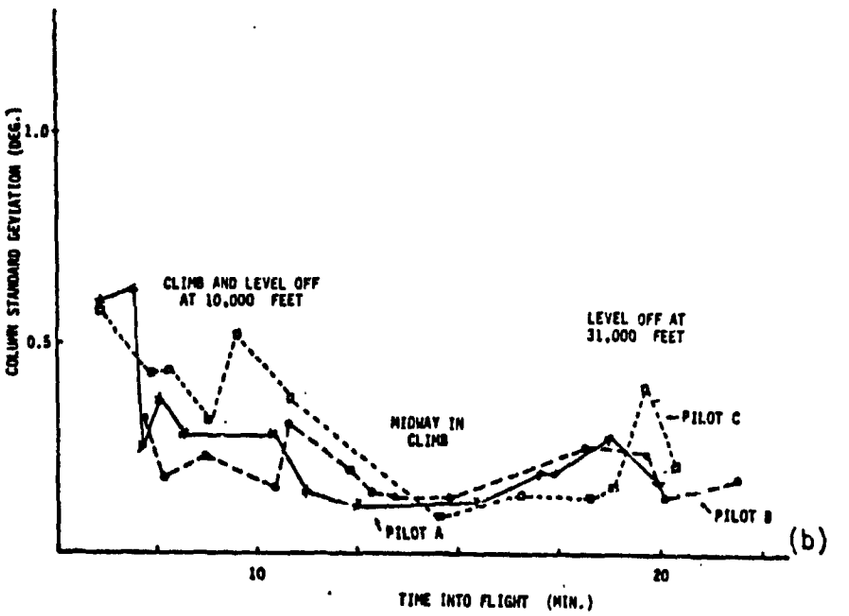

PILOT COLUMN PERFORMANCE

Figure 4 Standard Deviation of Pilot Wheel (a) and Column (b) Performance During Climb Averaged over 1½ minute Intervals -- High Turbulence

ORIGINAL PAGE IS
OF POOR QUALITY

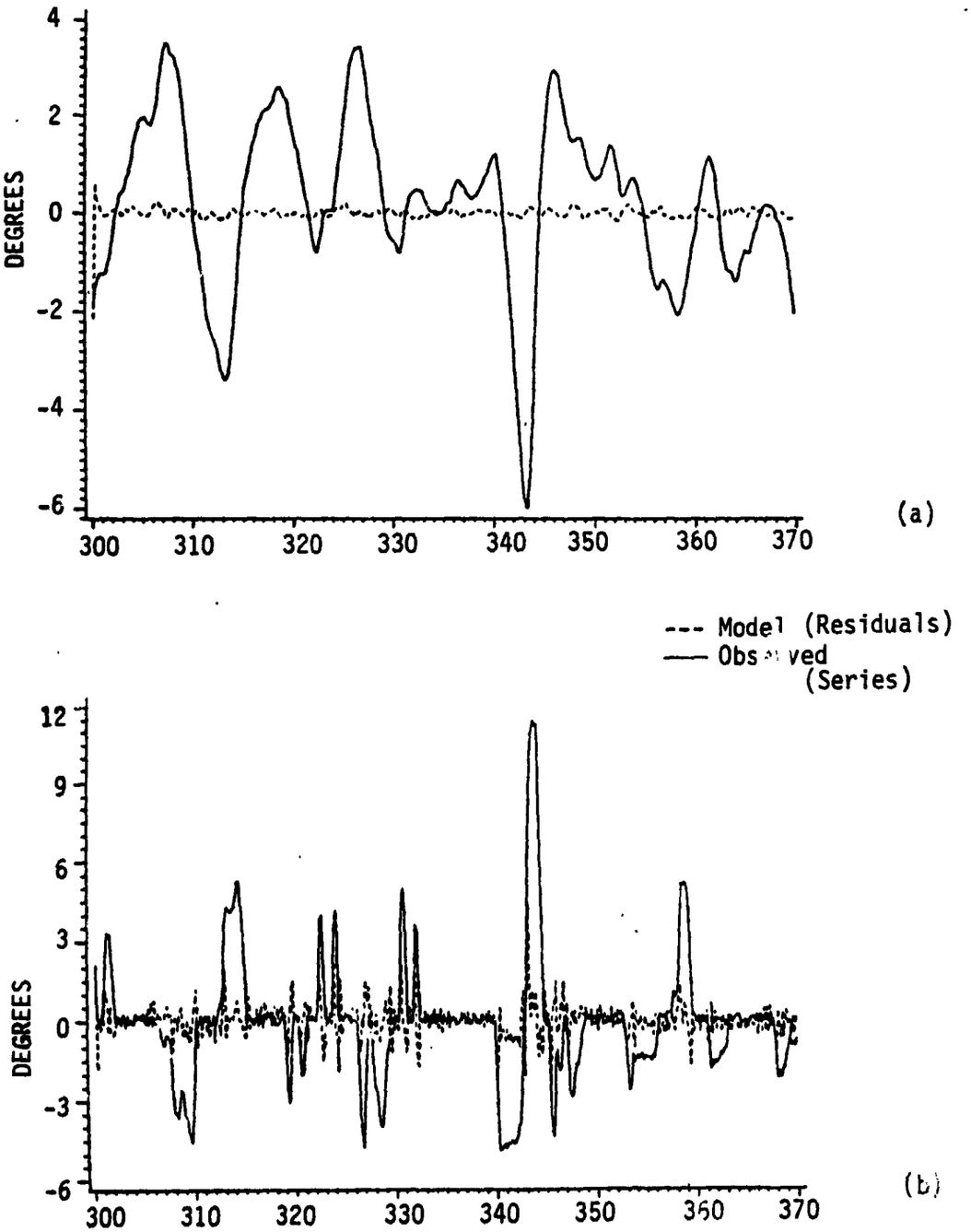

FIGURE 5 Model Residuals superimposed on Roll series (a) and Wheel series (b)

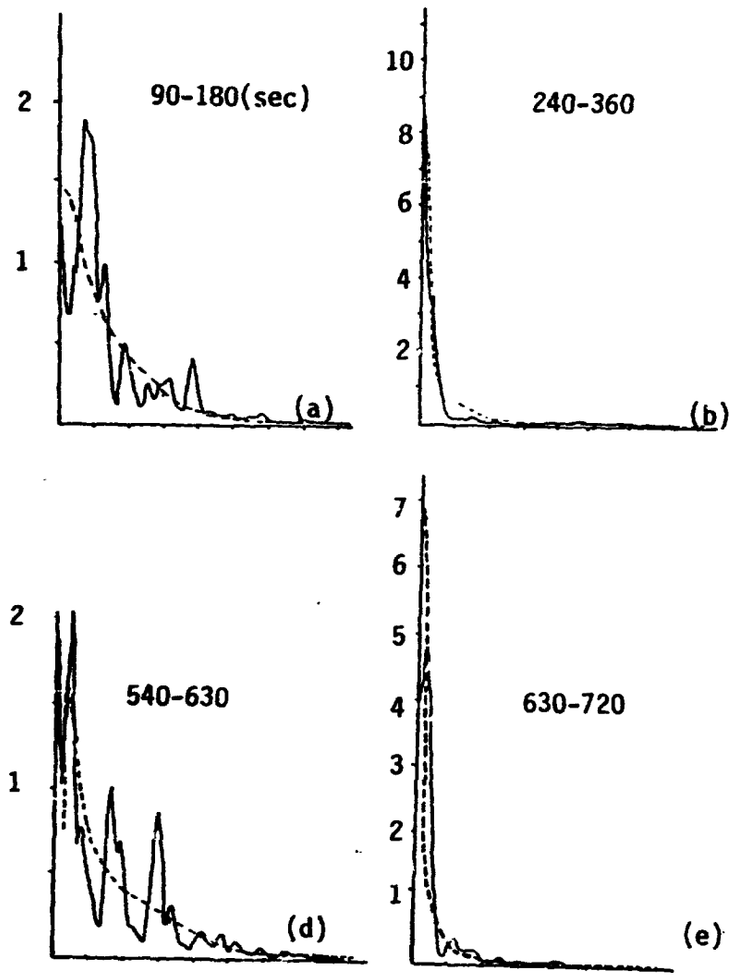

--- Model
—— Data Estimated

FIGURE 6 Modeled Wheel Spectra, MAP navigation display superimposed on Raw Data Estimated Spectra by Time Into Flight averaged over specified interval.

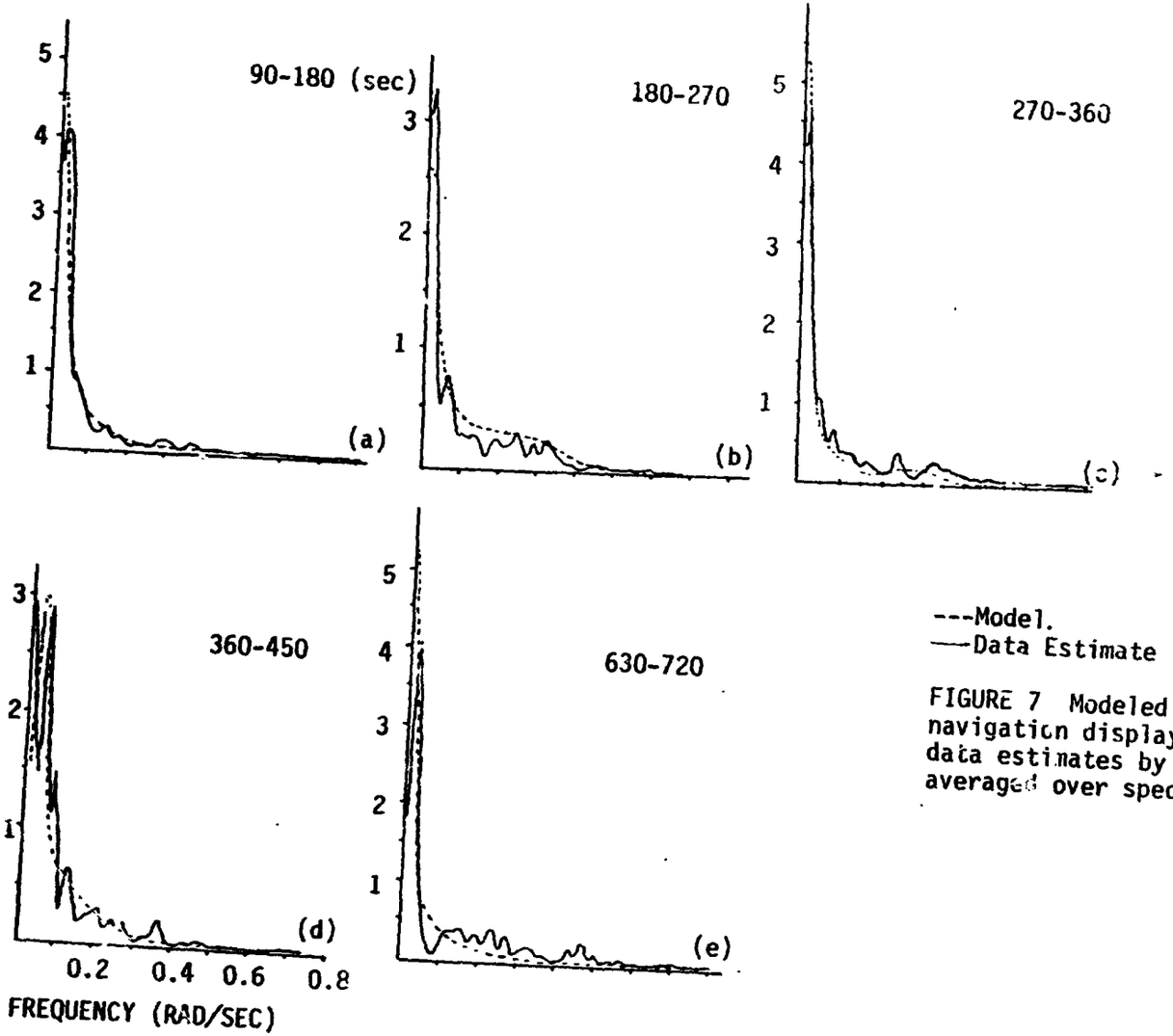

---Model.
——Data Estimate

FIGURE 7 Modeled Wheel Spectra, VOR navigation display superimposed on raw data estimates by time into flight averaged over specified interval

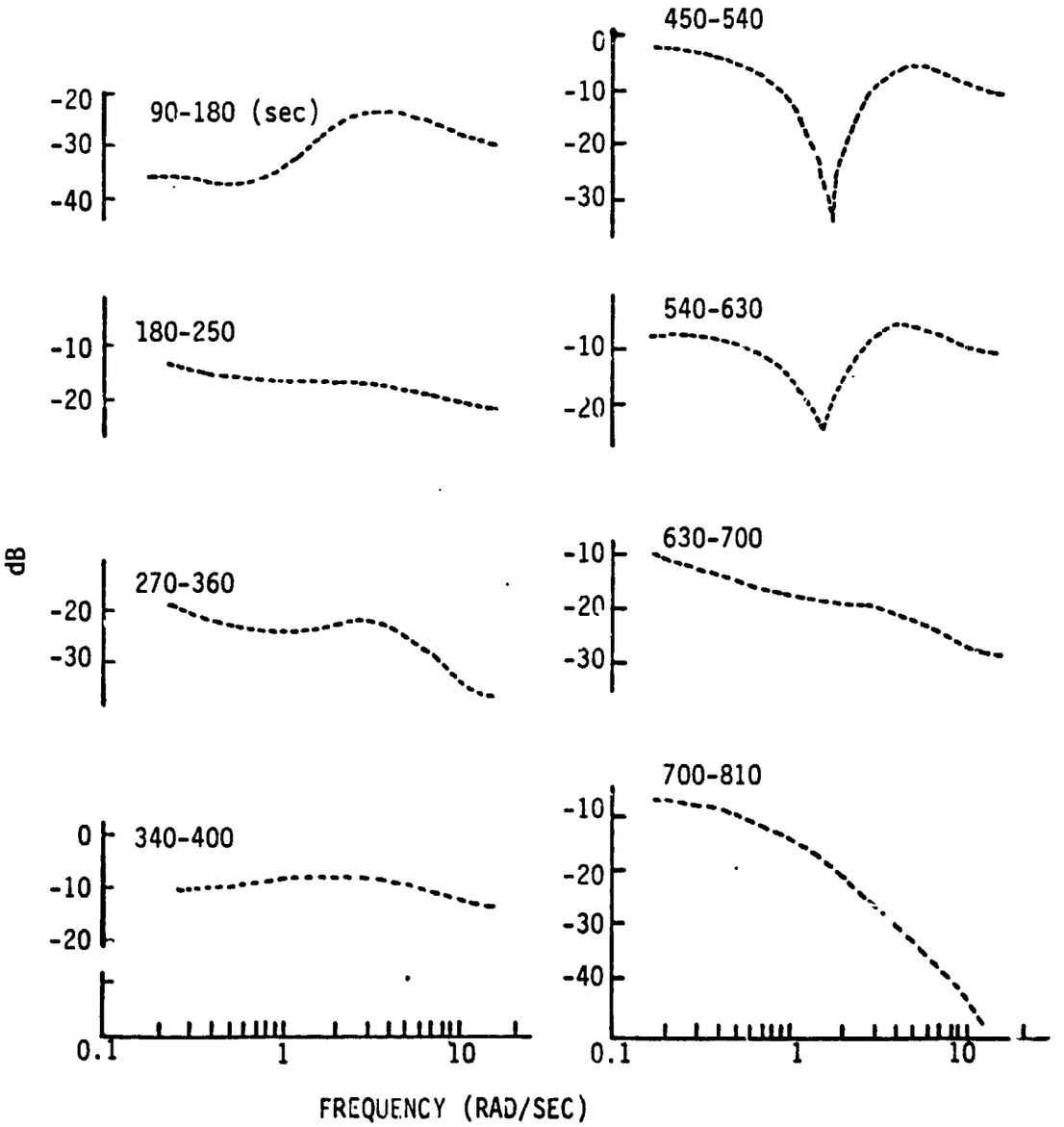

FIGURE 8 Pilot Transfer Functions by Time Into Flight, takeoff to early cruise. Wheel output, Roll input, single pilot: actual flight, MAP navigation mode.

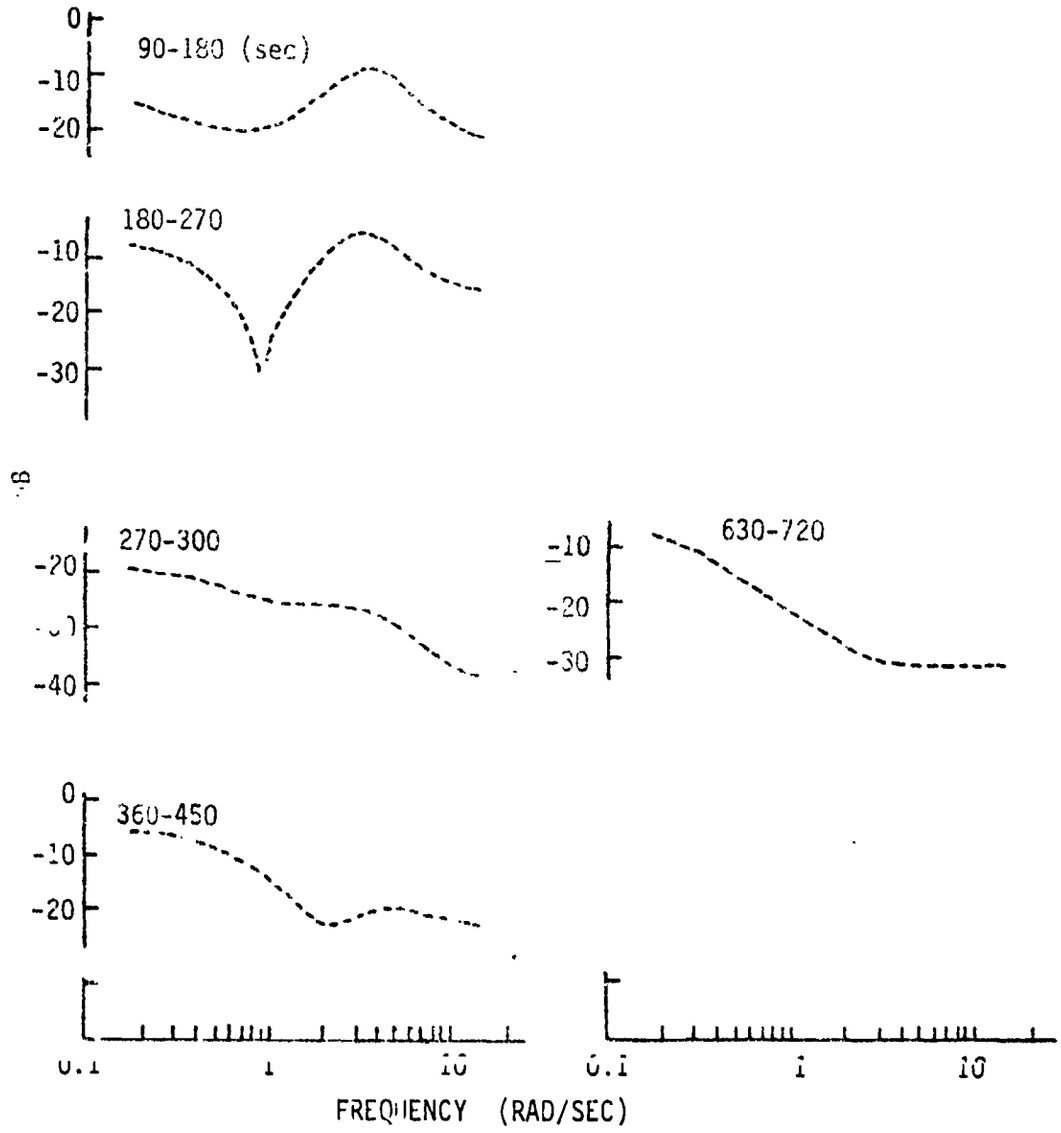

FIGURE 9 Pilot Transfer Functions by Time into Flight, takeoff to cruise, Wheel output, Roll input, Single Pilot: actual flight, VOR navigation mode

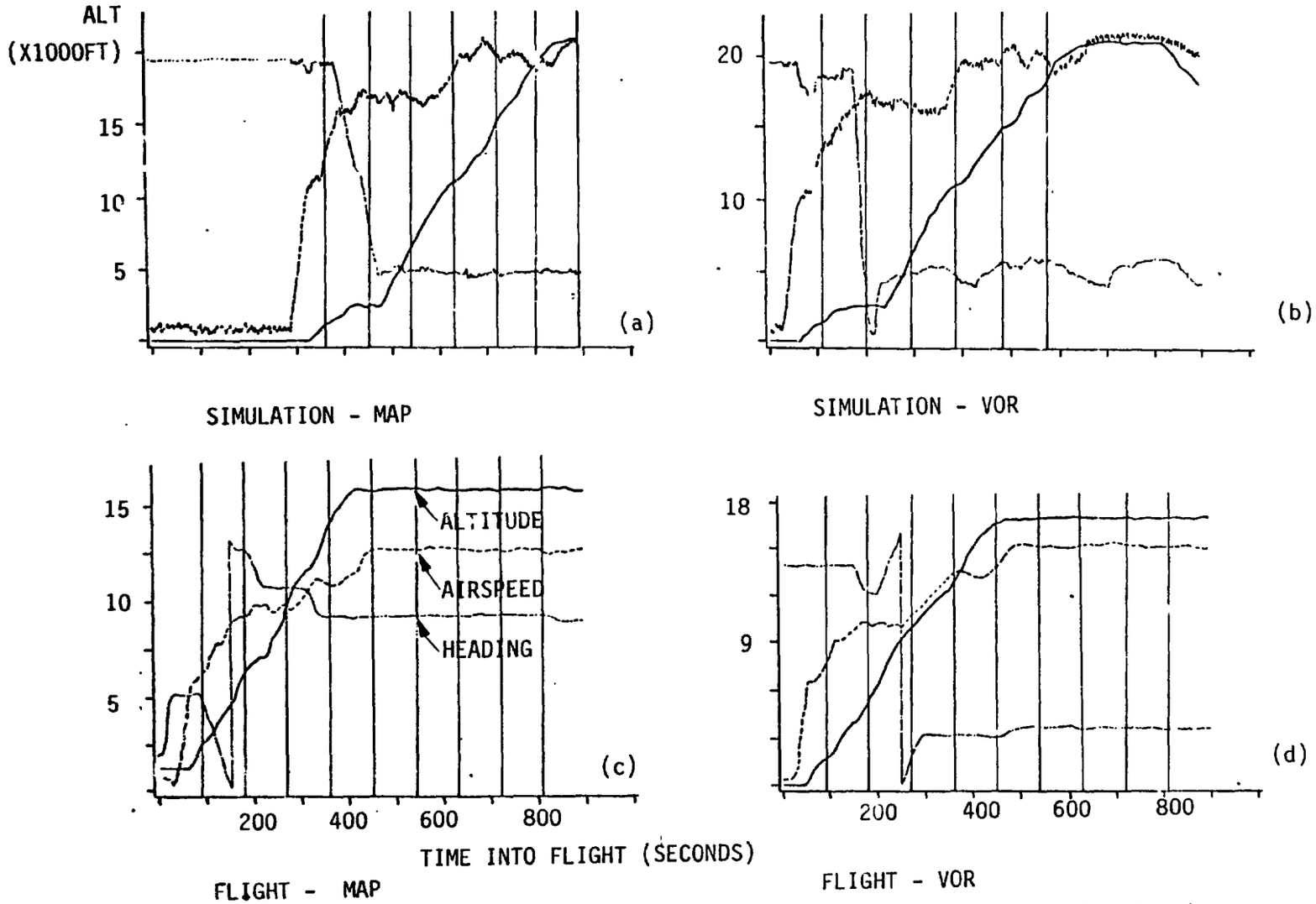

FIGURE 10 Climb Flight Condition Profiles, showing Interval selection. Single pilot, Simulation and flight test, two navigation modes, MAP and VOR.

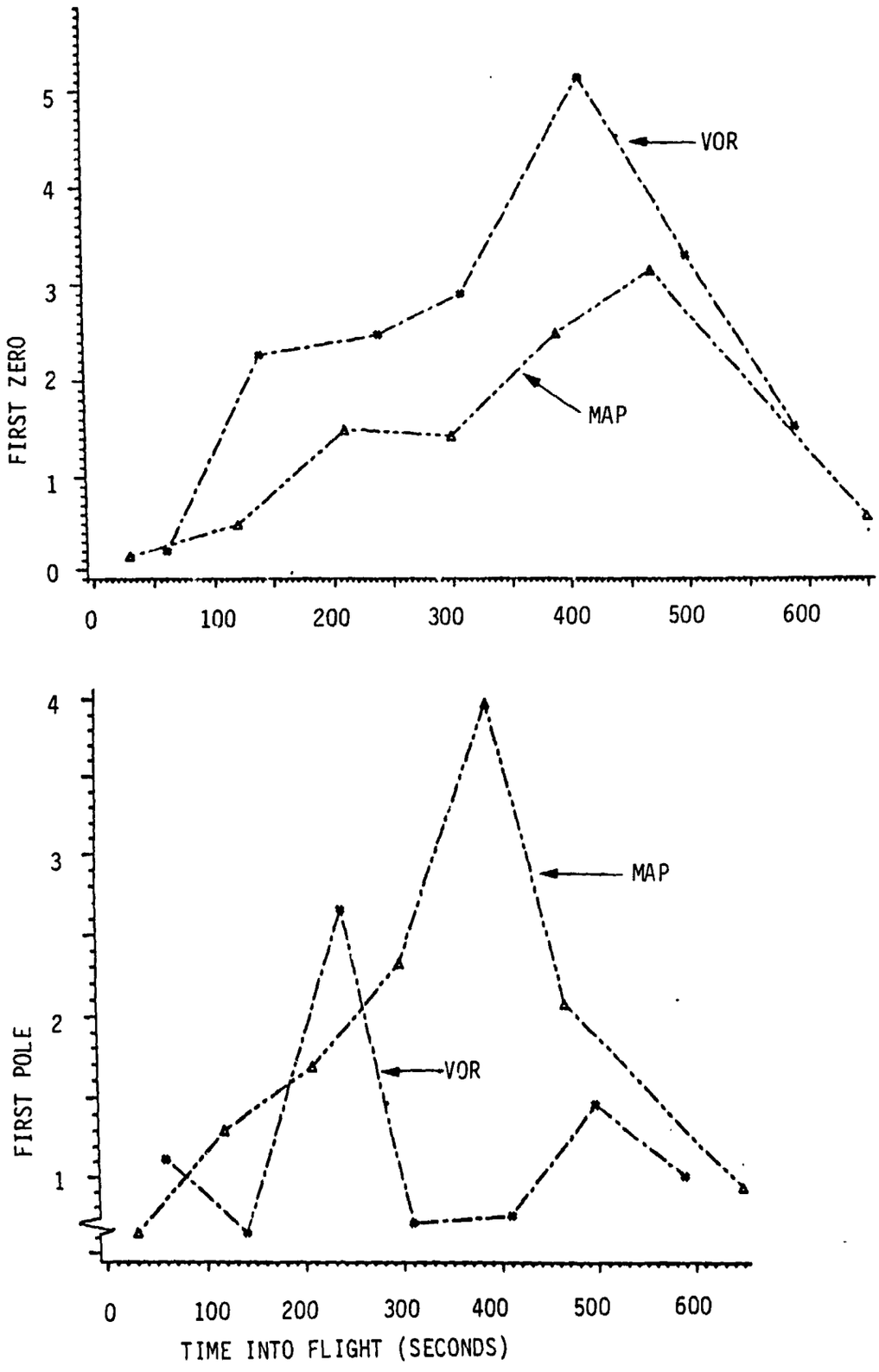

FIGURE 11 Zeroes and Poles of the Pilot Transfer Function, Single Pilot, Simulation, Two Navigation Modes: MAP and VOR

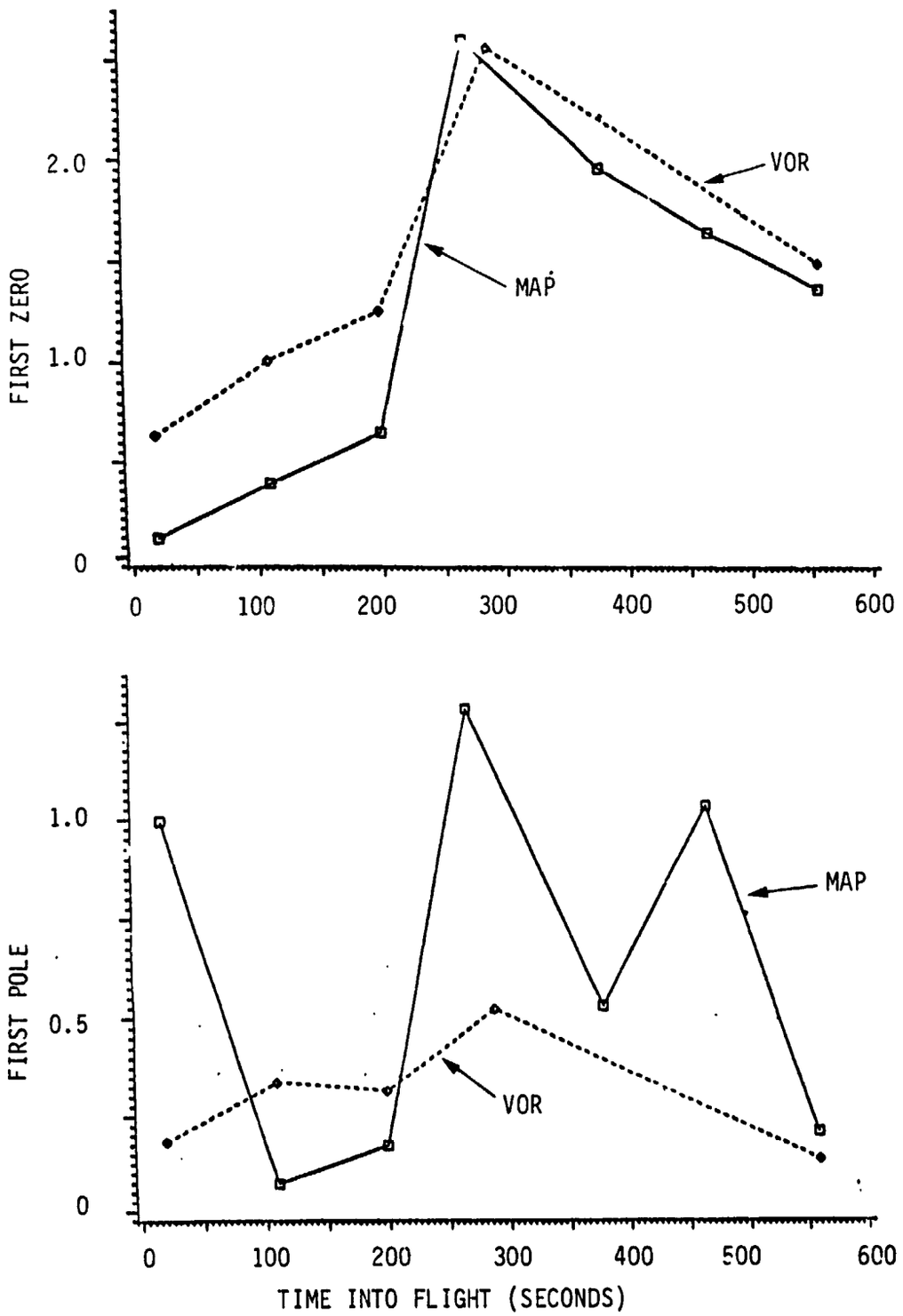

FIGURE 12 Zeroes and Poles of the Pilot Transfer Function, Single Pilot, Actual Flight, Two Navigation Modes, MAP and VOR

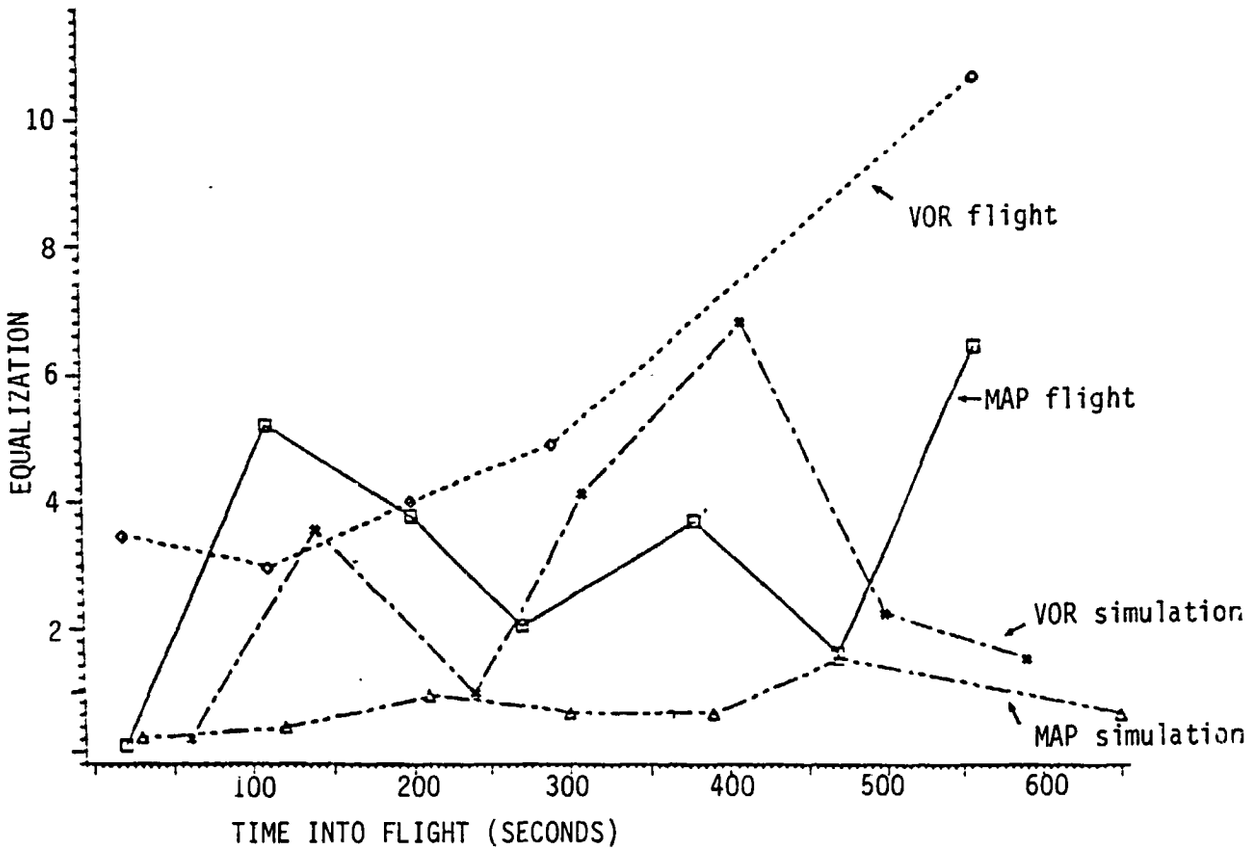

FIGURE 13 Pilot Equalization: First Zero/First Pole
Two navigation modes: MAP and VOR. Single pilot: simulation and flight tests.

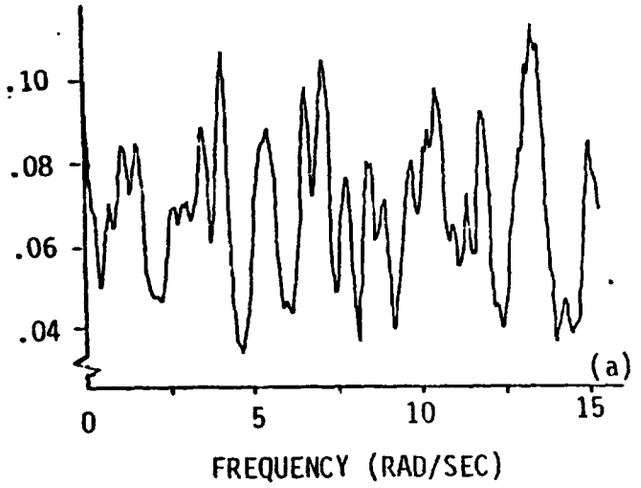

Wheel Residual Spectrum Before and After V_g

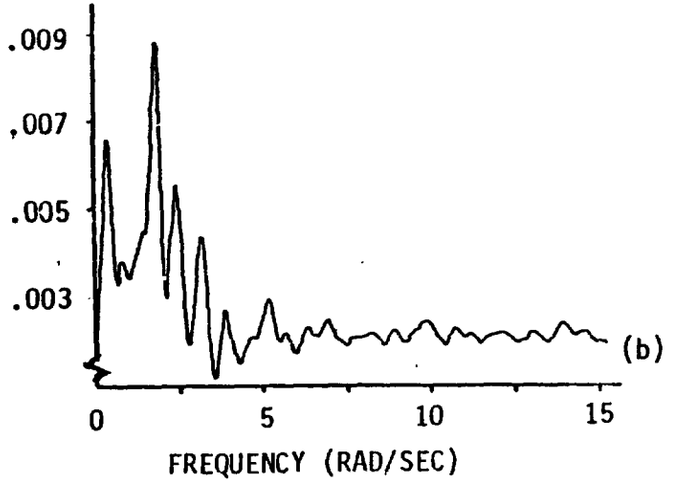

Rate Residual Spectrum Before V_g

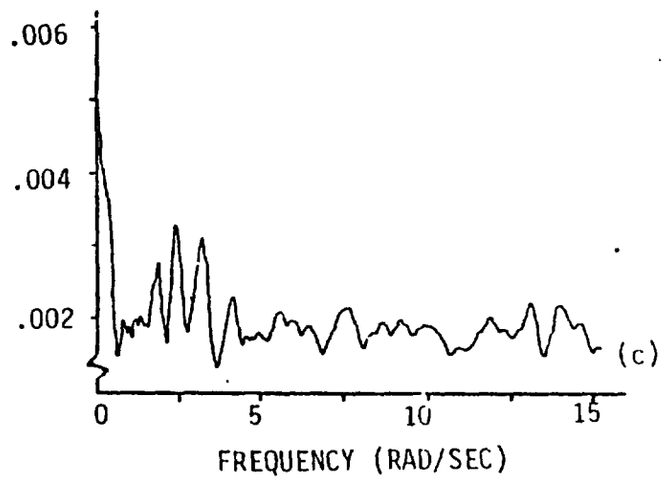

Rate Residual Spectrum After V_g

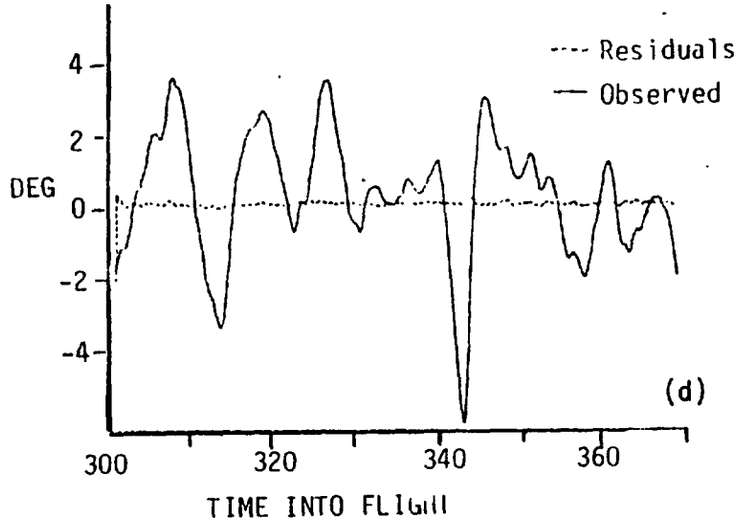

Time History: Model Residuals and Observed Roll Series

FIGURE 14 The Effect of the Lateral Wind Component V_g on the Roll Wheel Model Residuals

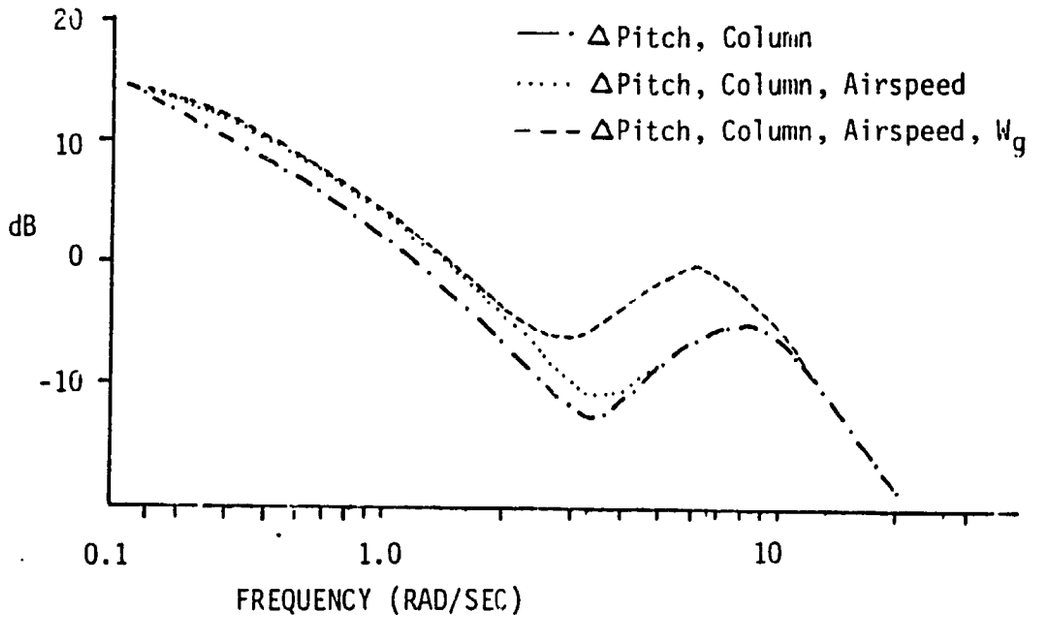

FIGURE 15 Effect of Variable Addition on Test Pilot Transfer Function: Δ Pitch to Column Initially, Airspeed and Vertical Wind, W_g, Added in Sequence

N85 14490

UTILIZATION OF HISTORIC INFORMATION IN AN OPTIMISATION TASK*

Tom Bösser
Psychologisches Institut der
Westfälischen Wilhelms-Universität
Schlaunstr.2
D-44 Münster
West-Germany

*(Complete paper not available in time for publication; it can be furnished upon request)

One of the basic components of a discrete model of motor behaviour and decision making, which describes tracking and supervisory control in unitary terms, we assume to be a filtering mechanism which is tied to the representational principles of human memory for time-series information.

Optimisation of tracking performance, tuning of a system in supervisory control, fault detection under certain conditions, all require the estimation of statistical parameters of time-series data (mean, variance, spectrum), as also assumed in the Optimal Control Model or the Crossover Model. Little empirical evidence is available about the representational principles for time-series information, although generally it is assumed that humans are capable of estimating variances (e.g. in Signal-Detection and Decision Theory).

We use a task where a window of constant length of a time-series, time-course and momentary values of two cost-variables are displayed. The subjects task is to optimize total payoff by adjusting one parameter, the optimal value of which is dependent upon the distribution of the time-series.

In a series of experiments subjects used the time-series information with certain significant limitations: There is a range-effect; asymmetric distributions seem to be recognized, but it does not seem to be possible to optimize performance based on skewed distributions. Thus there is a transformation of the displayed data between the perceptual system and representation in memory involving a loss of information. This rules out a number of representational principles for time-series information in memory and fits very well into the framework of a comprehensive discrete model for control of complex systems, modelling continuous control (tracking), discrete responses, supervisory behaviour and learning.

Manual Control

N85 14491

QUANTIFICATION OF CROSS-COUPLING AND MOTION FEEDTHROUGH FOR MULTIAXIS CONTROLLERS USED IN AN AIR COMBAT FLYING TASK

Wayne F. Jewell
Systems Technology, Inc.
2672 Bayshore-Frontage Road, Suite 505
Mountain View, California 94035

Kevin D. Citurs
McDonnell Aircraft Company
Box 516, Bldg. 32, Level 2, Post 280
St. Louis, Missouri 63166

SUMMARY

A real-time piloted simulation of an air-to-air combat flying task using a "wings-level-turn" aircraft and various novel controllers was conducted at the U. S. Air Force Flight Dynamics Laboratory (USAFFDL), Wright-Patterson Air Force Base, Ohio, on the Large Amplitude Multimode Aerospace Research Simulator (LAMARS). One objective of this on-going Air Force-sponsored research is to quantify how the pilot interacts with the controllers and control modes, including:

1. Controller versus aircraft response (i.e., pilot control strategy and describing functions).

2. Proprioceptive cross-coupling among axes of the controllers.

3. Biodynamic cross-coupling between the aircraft motions and the controllers.

In order to aid in identifying the items listed above, both the target aircraft and the LAMARS motion system were disturbed with qausi-random sums-of-sinusoids. Since the disturbances were separated in frequency, spectral analysis techniques could be used to identify the three items listed above. This paper presents the results of the spectral analysis of controller motions from the two-axis side stick, a twist grip mounted on the side stick, a thumb button mounted on the side stick, and conventional rudder pedals. Conclusions and recommendations for further research are also presented.

INTRODUCTION

The results presented in this paper are based on work performed under a U. S. Air Force contract to develop design criteria and gather appropriate substantiating data for cockpit control devices for use with six-degree-of-freedom (6-DOF) uncoupled aircraft. The purpose of this study was to insure compatibility among the pilot, the control device(s), and the aircraft response which will allow efficient utilization of the 6-DOF capability. The prime contractor was the McDonnell Aircraft Company, and

ORIGINAL PAGE
OF POOR QUALITY

Systems Technology, Inc., (STI) acted as a subcontractor for the work reported herein.

The project evaluated many different tasks, uncoupled aircraft motions, and controller configurations. A complete description of the overall project can be found in Refs. 1 and 2. This paper will be restricted to an air-to-air combat task using an aircraft with "wings-level-turn" (WLT) capability and three different cockpit controllers which can be used with the WLT mode.

DESCRIPTION OF THE CONTROL TASK

The control task is depicted in the block diagram of Fig. 1. For the experiments analyzed herein, the pilot was instructed to track the target motions (i.e., keep the target in the pipper) using the WLT controller (δ_{WLT}) and to keep the wings level using the roll controller (δ_p).

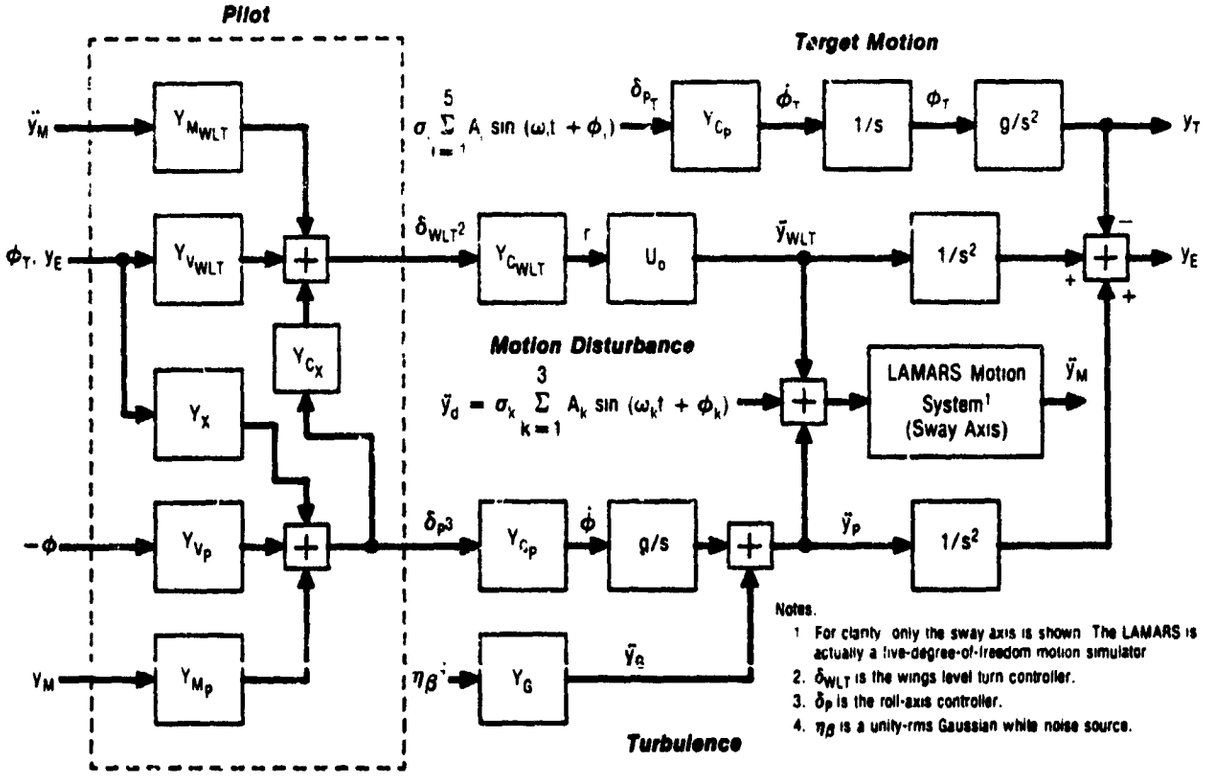

Figure 1. Functional Block Diagram of Pilot Control Task, Target Motion, and Motion Disturbance for Air-to-Air Tracking Task

Using the WLT mode (also referred to as a flat turn mode), the pilot can turn the aircraft without creating a side slip and without changing the roll attitude. The appropriate transfer functions for the WLT mode are shown below.

$$\frac{r}{\delta_{WLT}} = \frac{1.0}{0.5s + 1.0} N_{\delta_{WLT}} \equiv Y_{C_{WLT}} \tag{1}$$

$$\frac{\beta}{\delta_{WLT}} = 0 \tag{2}$$

$$\frac{\phi}{\delta_{WLT}} = 0 \tag{3}$$

$$n_y = \frac{U}{g} r \tag{4}$$

Where $N_{\delta_{WLT}}$ was used to set the maximum control power. For the experiments described herein, the control power was $n_{y_{max}} = 1.0$ g at the specified maximum control force.

The appropriate transfer functions for the roll mode are shown below:

$$\frac{p}{\delta_p} = \frac{L_{\delta_p}}{0.35s + 1} \equiv Y_{C_p} \tag{5}$$

$$\frac{\beta}{\delta_p} = 0 \tag{6}$$

Where $L_{\delta p}$ was used to set the maximum control power. For the experiments described herein, the control power was $p_{max} = 150$ deg/sec at maximum side stick deflection. The roll side stick sensitivity was 12.5 deg/sec per pound of δ_p.

The pilot's control actions shown in Fig. 1 are represented by a sum of linear feedbacks proportional to the aircraft's bank angle (ϕ), the target's bank angle (ϕ_T), the difference between the aircraft and the target aircraft, the pipper error (y_E), and the lateral acceleration (n_M). The y_E and ϕ feedbacks are represented by $Y_{V_{WLT}}$ and Y_{V_p}, respectively. The crossfeed term, Y_X, is in Fig. 1, because some pilots might "cheat" by using the roll controller, δ_p, to chase the target. The target bank angle is fed back through $Y_{V_{WLT}}$, because it is possible to use ϕ_T to

anticipate the target motion and thus generate lead. Controller cross-coupling is represented by the term Y_{C_X}. The coupling is shown with the roll controller summing with the WLT controller, but the opposite direction is also possible. "Biodynamic" feedthrough is represented by the terms $Y_{M_{WLT}}$ and Y_{M_P}, which represent how the aircraft's lateral acceleration, $\ddot{y}$, affect the pilot's controls, δ_{WLT} and δ_P, respectively.

The aircraft is being disturbed by two noise sources, as shown in Fig. 1. Dryden turbulence is injected into the equations of motion, while the motion disturbance is injected directly into the LAMARS motion system; thus, it is uncorrelated with the aircraft motion. The purpose of the Dryden turbulence is to add realism to the simulation. The transfer function for the Dryden turbulence is:

$$Y_G = \frac{\ddot{y}_G}{n_\beta} = \frac{\omega_{dr}^2 \, n_{y_\beta} (g/U) \, \sigma_{v_g} (3R_\beta)^{1/2}}{[\zeta_{dr}; \omega_{dr}] \; (s + 1.5R_\beta)} \qquad (7)$$

where $R_\beta = U/1750$ rad/sec, $\sigma_{v_g} = 3.0$ fps, $\omega_{dr} = 4.47$ rad/sec, $\zeta_{dr} = 0.68$, $n_{y\beta} = -5.73$ g/rad, and n_β is a unity amplitude Gaussian noise source.

The purpose of the motion disturbance is to quantify how aircraft accelerations will affect the use of the various controllers. Since the motion disturbance, $\ddot{y}_d$, is formed by a sum of three discrete sine waves, it is possible to "trace" the signals through to the controllers, δ_{WLT} and δ_P. Thus the terms $Y_{M_{WLT}}$ and Y_{M_P} could theoretically be identified. The amplitudes, A_k, and frequencies, ω_k, used to form $\ddot{y}_d$ are listed in Table 1. The phase angle, ϕ_k, were randomly chosen from run to run. The magnitude of the motion disturbance was subjectively set such that the motion could be felt but was not a dominant effect. The subject test pilots were not informed of the motion disturbance.

The target aircraft motions, ϕ_T and Y_T shown in Fig. 1, were formed by using a sum of five sine waves as the input to the roll controller. The target motions were recorded on magnetic tape and then played back during realtime simulation. The phasing between the sine waves, ϕ_i, was set such that a zero-mean process for ϕ_T was obtained, and the target aircraft was constrained to remain in the same vertical plane. The magnitude of the input, σ_i, was set such that the root-mean-square (rms) bank angle of the target aircraft was approximately 15 deg. The amplitudes, A_i, and frequencies, ω_i, used to form δ_{P_T} are shown in Table 2. Because the power in the target motion exists at discrete frequencies, it is theoretically possible to identify the terms $Y_{V_{WLT}}$, Y_X, Y_{C_X}, and Y_{V_P}.

OBJECTIVES

The overall objective of the analysis contained herein is to quantify how the pilot interacts with the various novel controllers and control modes described herein, including:

TABLE 1. PARAMETERS USED TO FORM THE MOTION DISTURBANCE FUNCTION, y_d

k	A_k	N_k	ω_k	ϕ_k
(-)	$(-)^3$	$(\text{cycles}/T_y)^1$	$(\text{rad/sec})^1$	$(\text{rad})^2$
1	0.9698	9 (1.8 Hz)	11.310	--
2	0.7886	13 (2.6 Hz)	16.336	--
3	0.6610	19 (3.8 Hz)	23.876	--

Notes: (1) $\omega_k = 2\pi N_k/T_y$, $T_y = 5$ seconds

(2) The ϕ_k are random numbers computed at the beginning of a run. They are constant throughout a run.

(3) Amplitude shaping is based on first-order power spectra with a break frequency at 0.5 rad/sec and unity rms.

TABLE 2. PARAMETERS USED TO FORM THE TARGET MOTION FUNCTION, δ_{P_T}

i	A_i	N_i	ω_i	ϕ_i
(-)	$(-)^3$	$(\text{cycles}/T_T)^1$	$(\text{rad/sec})^1$	$(\text{rad})^2$
1	0.9328	4 (0.04 Hz)	0.2513	--
2	0.7838	10 (0.10 Hz)	0.6283	--
3	0.5825	30 (0.30 Hz)	1.885	--
4	0.3519	70 (0.70 Hz)	4.398	--
5	0.2290	150 (1.5 Hz)	9.425	--

Notes: (1) $\omega_i = 2\pi N_i/T_T$, $T_T = 100$ seconds

(2) The ϕ_i are set such that the target bank angle, δ_T, is a zero-mean process (see Fig. 1)

(3) Amplitude shaping is based on first-order power spectra with a break frequency at 1.5 rad/sec and unity rms.

1. Controller versus aircraft response behavior (e.g., pilot control strategy and describing functions). This can be quantified by the terms $Y_{V_{WLT}}$, Y_X, and Y_{V_P} in Fig. 1.

2. Proprioceptive cross-coupling among the axes of the controllers (e.g., roll commands due to twist grip deflections). This can be quantified by the term Y_{C_X} in Fig. 1.

3. Aircraft motion-to-controller coupling ("biodynamic cross-coupling"). This can be quantified by identifying the terms $Y_{M_{WLT}}$ and Y_{M_P} in Fig. 1.

ANALYTICAL TECHNIQUES

As mentioned above, it is theoretically possible to identify the terms in Fig. 1 by using describing function and/or time domain analysis techniques. Due to time and resource constraints and the intensive level of computations required, however, we were unable to complete the analysis. Instead, the next section presents the power spectra and power fractions of the roll and WLT controllers for a selected group of runs. By examining the power spectra, we can tell if the disturbances are present in the controllers; that is, if the pilot can be modeled as a linear system as shown in Fig. 1, then all of the power in δ_{WLT} would be at the target frequencies, ω_t. Furthermore, if the pilot did not use the roll controller to track the target, then the power in δ_P would be "white" (i.e., because the Dryden turbulence is shaped white noise). If biodynamic coupling exists, then there will also be power in δ_P and/or δ_{WLT} at the motion disturbance frequencies, ω_k.

SOME EXAMPLE RESULTS

The analysis contained below compares the data from three different types of controllers used to perform an air-to-air tracking task using a wings-level-turn (WLT) mode. The three controllers were:

1. Conventional rudder pedals, δ_{RP}.

2. An isotonic twist grip, δ_{TG}. This was the twist axis of a right-handed side-stick controller.

3. The thumb button controller, δ_{TBC}, mounted on the right-handed side-stick controller.

Table 3 is a summary of the runs analyzed. Note that the maneuver gradient was held constant for each of the WLT controllers while either the dead band (DB) for the twist grip or thumb button or breakout force (BO) for the rudder pedals was varied. As shown in Table 3, the pilot-opinion rating (POR) varied from 2 to 5 as a function of either deadband or breakout force.

TABLE 3. SUMMARY OF RUNS ANALYZED

Run No.	WLT Controller	Controller Characteristics	POR	Pilot Comments	Analysis Comments
3145	Rudder Pedals*	4.0 lb BO**	2	None	Very little motion feedthrough to δ_{RP}. Lots to δ_p. Some possible crosscoupling.
3137		7.0 lb BO	3	"Not bad"	No motion feedthrough to δ_{RP}. Still lots to δ_p. Some possible crosscoupling.
3141		15.0 lb BO	3	"Feet got tired"	Same as above.
3143		25.0 lb BO	5	"Too much pedal to start and stop"	Strange looking spectra for δ_{RP}. Note jump in CH from 3 to 5.
3081	Twist Grip#	0.5 in-lb DB	2	"No problem"	Lots of motion feedthrough. Definite cross-coupling at ω = 1.8 rad/sec.
3084		2.7 in-lb DB	3	"Has a little lag"	Same as above.
3092		4.8 in-lb DB	4	None	Motion feedthrough and crosscoupling reduced.
3086		9.6 in-lb DB	5	"Too much delay"	Definite crosscoupling. No motion feedthrough.
3188	Thumb Button##	0.05 lb DB	3	"Little loose"	Lots of crosscoupling and motion feedthrough.
3190		0.50 lb DB	3	"Good"	Reduced coupling and motion feedthrough.
3194		1.0 lb DB**	3	"Had to work a little harder than normal"	Further reduction in coupling and motion feedthrough. Note that CH remains 3.
3192		1.5 lb DB	5	"Bad"	Increased use of δ_p. Note that CH jumped to 5.

*Rudder pedals had 2 inches of travel and a maneuver gradient of 40 lb/g.
**DB = deadband, BO = breakout.
#Twist grip had a maneuver gradient of 24 in-lb/g and was the rotational axis on the two-axis right-handed side stick.
##Thumb button has a maneuver gradient of 3.3 lb/g and was mounted on the two-axis right-handed side stick.

Figures 2 through 4 contain power spectra and power fraction plots of the roll controller and the appropriate WLT controller. The power fraction is a unique way to visualize the spectral distribution in a signal. It is defined as follows:

$$PF(\omega) = \frac{1}{\sigma_x^2} \int_0^{\omega} \Phi_{xx}(\omega)dx$$

Note that $\sigma_x^2 \equiv PF(\omega = \infty)$, thus $PF(\omega)$ is a fraction from 0.0 to 1.0. The unique feature of the power fraction is that it defines the bandwidth of a signal in terms of a percentage (e.g., 90 percent of the power is below 5.2 rad/sec).

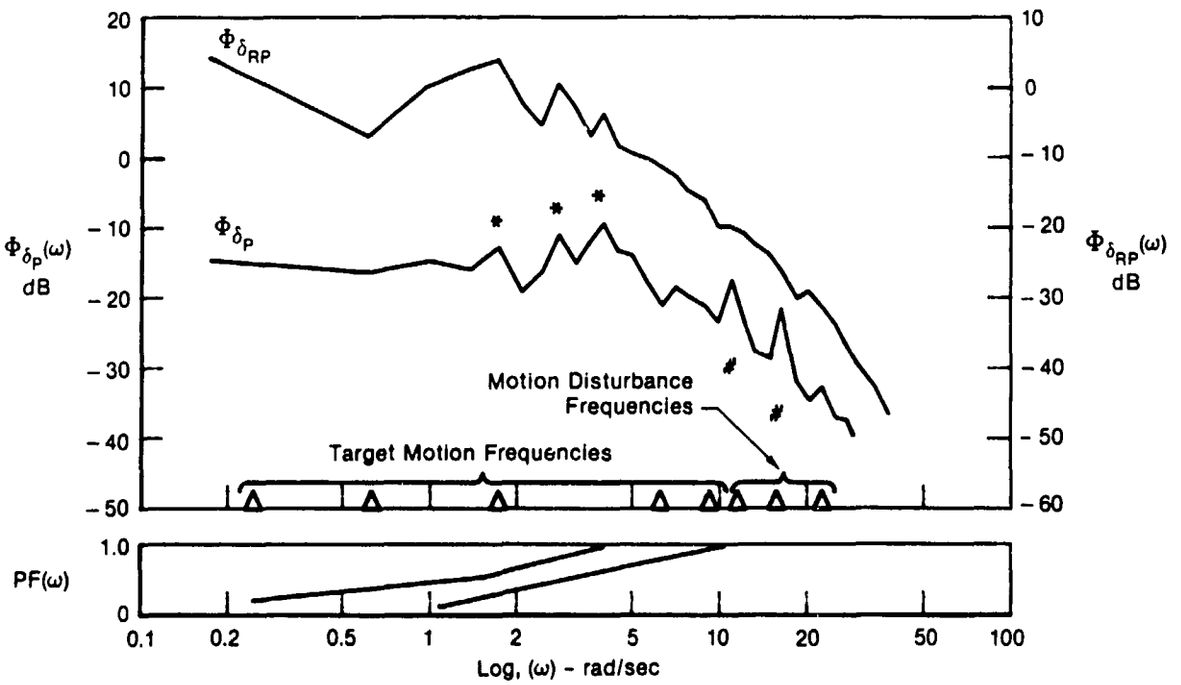

Notes:

* Crosscoupling between controllers suggested by the line spectra in Φ_{δ_P} and $\Phi_{\delta_{RP}}$ at the same frequency. However, at the target disturbance frequency, this could also be due to the pilot using δ_P to "chase" the target (even though he was instructed not to do so).

\# Motion feedthrough evidenced by line spectra at motion disturbance frequencies.

Figure 2. Power Spectra [Φ(ω)] and Power Fraction [PF(ω)] for Wings Level Turn and Roll Control Inputs Rudder Pedal, 2 in. Deflection; 7 lb Breakout; 40 lb/g Maneuver Gradient; Cooper-Harper Rating = 3

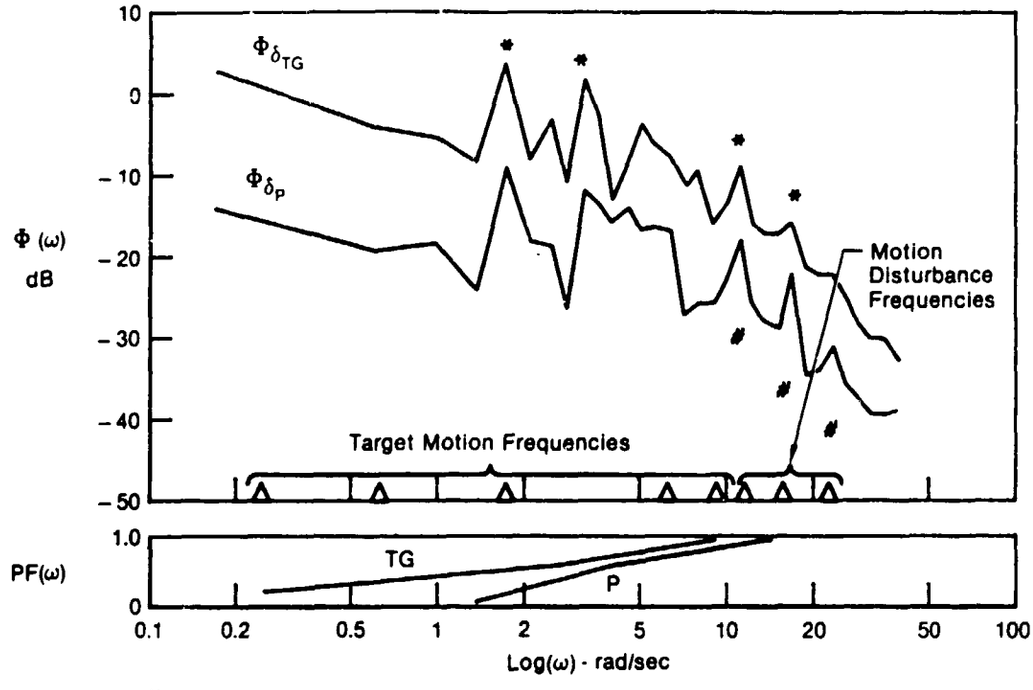

Notes:

* Crosscoupling between controllers suggested by the line spectra in Φ_{δ_P} and $\Phi_{\delta_{TG}}$ at the same frequency. However, at the target disturbance frequency, this could also be due to the pilot using δ_P to "chase" the target (even though he was instructed not to do so)

\# Motion feedthrough evidenced by line spectra at motion disturbance frequencies.

Figure 3. Power Spectra [Φ(ω)] and Power Fraction [PF(ω)] for Wings Level Turn and Roll Control Inputs Twist Grip Sidestick; 2.7 in-lb Deadband; 24 in-lb/g Maneuver Gradient; Cooper-Harper Rating = 3

The following observations were made after carefully examining these plots:

1. There are large amounts of motion feedthrough ("biodynamic coupling") to the roll controller (i.e., lateral side stick) for all runs. This is evidenced by the "line spectra" (i.e., the spikes for apparent discontinuities in the power spectra) at the motion disturbance frequencies. It is interesting to note that none of the pilots complained of motion-to-controller coupling. This is probably because the accelerations were small in amplitude and were masked by the Dryden turbulence. However, motion-to-controller coupling can have extremely detrimental effects in actual flight where the accelerations are much larger.

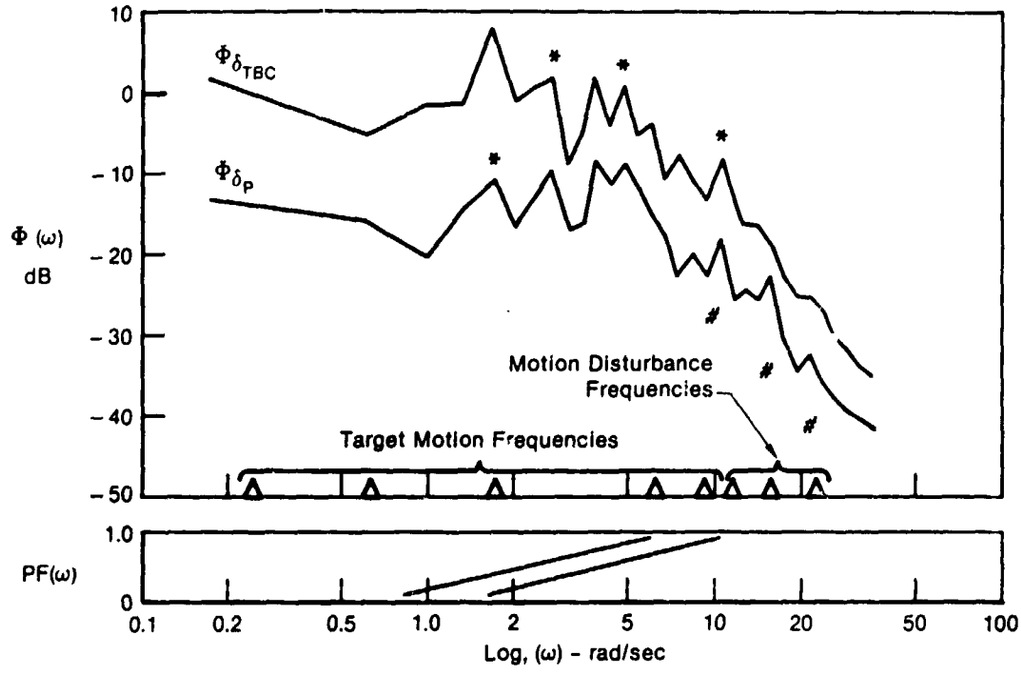

Notes:

* Crosscoupling between controllers suggested by the line spectra in Φ_{δ_P} and $\Phi_{\delta_{TBC}}$ at the same frequency. However, at the target disturbance frequency, this could also be due to the pilot using δ_P to "chase" the target (even though he was instructed not to do so).

\# Motion feedthrough evidenced by line spectra at motion disturbance frequencies

Figure 4. Power Spectra [Φ(ω)] and Power Fraction [PF(ω)] for Wings Level Turn and Roll Control Inputs Thumb Button Controller; 0.05 lb Deadband; 3.3 lb/g Maneuver Gradient; Cooper-Harper Rating = 3

2. There is evidence of motion feedthrough on all of the WLT controllers, with most on the twist grip and the least on the rudder pedals. As the deadband is increased, the evidence of motion feedthrough is decreased.

3. There appears to be controller cross-coupling between the roll and WLT controllers for the twist grip and thumb button but very little for rudder pedals. This is evidenced by the line spectra in δ_P and δ_{WLT} at the same frequencies. This is especially true (and consistent) at the motion disturbance frequencies and makes sense, because the pilot must the grab the sidestick in order to use the twist grip or the thumb button but not to use the rudder pedals.

4. Note that the rudder pedals are the only controller for which clear line spectra <u>do</u> appear at the target disturbance frequencies and <u>do not</u> appear at the motion disturbance

frequencies. All of the other controllers (roll side stick, twist grip, and thumb button) exhibit line spectra at both disturbance frequency levels. Note also that, for the rudder pedal plots, line spectra do appear for the roll controller at the target disturbance frequencies. Since physical coupling is not possible between these controllers, the plots suggest that the pilot is either consciously or unconsciously using the roll controller to assist in chasing the target. It is probably a combination of both, as the coupling seems stronger in the twist grip and thumb button plots (i.e., the magnitudes of the spikes in the roll controller are larger) where proprioceptive coupling is possible.

5. Line spectra at all of the disturbance frequencies were not clearly or consistently observed (ω = 1.8 rad/sec is the only possible exception to this observation). This is probably due to nonlinearities in the pilot's control technique such as saturation (e.g., bang-bang control) or aperiodic sampling.

CONCLUSIONS AND RECOMMENDATIONS

Using spectral analysis techniques, it was possible to identify controller cross coupling for the air-to-air combat task described herein. However, because of the nature of the task, it was not possible to discern whether the coupling was proprioceptive (e.g., twisting the side stick to effect the wings-level-turn mode without affecting the roll controller) or whether the pilot was intentionally using both controllers to improve tracking performance. We recommend performing two additional tasks which will help to isolate the coupling effects:

- Track the target without the WLT controller. This will reveal how much roll control is being used when the pilot is not using the WLT controller.

- Track the target with the roll axis of the aircraft fixed (i.e., short the connection between δ_p and the roll axis equations of motion). Reduce the dead band on δ_p to zero, and measure the spectra of δ_p.

The first task would assist in giving the analyst a feel for what to expect in $\Phi_{\delta p}(\omega)$ for a pilot actively chasing the target with only the roll controller. The second task would yield spectra for the use of the WLT controller without roll axis chasing contamination. Some caution must be applied when using this task, however. Since there would be no penalty (i.e., roll response) for making roll inputs, the pilot might modify his technique to such an extent as to invalidate the spectra of δ_p. This effect could be minimized by providing the pilot with some form of feedback, other than roll response, to indicate when roll inputs are being made.

Spectral analysis of the controller signals also revealed large amounts of biodynamic coupling; that is, the aircraft accelerations were feeding through to the controllers by way of the pilot's limbs. Because the simulated accelerations are quite small relative to the real world, none of the subject pilots complained of motion feedthrough problems. We recommend that analytic techniques be used to predict the amount of acceleration to expect in real flight and how the accelerations will affect overall performance of the pilot-aircraft system. Existing tools such as Biodyn (Ref. 3) and USAM (Ref. 4) could be used to perform this task.

We also recommend a complete pilot-vehicle analysis. Using a loop structure like the one shown in Fig. 1, the closed-loop characteristics of the pilot-vehicle system could be predicted. The effects of cross coupling and motion feedthrough could be quantified.

REFERENCES

1. Citurs, Kevin D., Controller Requirements for Uncoupled Aircraft Motion. Volumes I and II of Final Report for Period August 1981 to April 1984, McDonnell Aircraft Company Report, April 1984, forthcoming as an AFML TR.

2. Citurs, Kevin D., "Controller Requirements for Uncoupled Aircraft Motion," to be presented at the 11th Annual Atmospheric Flight Mechanics Conference, Seattle, Washington, August 1984.

3. Magdaleno, Raymond E., and Henry R. Jex, Biodynamic Models for Effects of Low-Frequency Vibration on Performance, Systems Technology, Inc., Paper No. 307, presented at the Naval Biodynamics Laboratory Workshop on Research Methods in Human Motion and Vibration Studies, New Orleans, LA, September 16, 1981.

4. Teper, Gary L., The STI Library of Control System Design Programs, Systems Technology, Inc., Working Paper No. 407-1, February 11, 1974, Revised August 1976.

N85 14492

D5

Six Degrees of Freedom Control With Each Hand?

Mike L. King

C A E Electronics Ltd.

Montreal, Quebec, Canada

SIX DEGREE OF FREEDOM CONTROL WITH EACH HAND?.

For some time man has made six degree of freedom inputs to a pair of dextrous manipulators using both hands simultaneously by the use of the master/slave concept.The advent of the micro-processor has the potential to make the master/slave concept redundant by replacing the master with a mathematical model.

Due to inevitable cabin limitations the first spaceborne remote manipulator, the CANADARM, could not utilise the master/slave concept.Resolved motion rate control of the end effector was borne, and has been proven as a satisfactory control method.However the problem of the man machine interface remained. All spacecraft to date, including the space shuttle, that have been flown in six degrees of freedom have been controlled by using both hands, the left hand controlling translation and the right rotation. Almost inevitably the same principle was applied to the CANADARM.

At the instigation of NASA we embarked on the development of a device whereby both translation and rotation could be combined allowing full control with one hand.

This paper describes the development and testing of the device, and the extension of its application into spaceflight control. Also the concept of an adaptable workstation for multi-manipulator and spacecraft flight control is discussed.

N85 14493

A NONLINEAR FILTER FOR COMPENSATING FOR TIME DELAYS IN MANUAL CONTROL SYSTEMS

Ronald A. Hess and Andrew A. Myers
Department of Mechanical Engineering
University of California
Davis, California 95616

ABSTRACT

The existence of time delays in manual control systems can have a significant and deleterious effect upon closed-loop system performance and stability. Modern flight control systems often exhibit such delays owing to digital control law implementation and higher-order control system dynamics. Modern flight simulators also share this problem owing to computational delays associated with computer-generated graphics. Thus, the need for an effective method for time delay compensation is becoming increasingly urgent. Linear methods of compensation provide needed phase lead but also introduce a significant gain distortion. To date, little research has been directed toward possible nonlinear compensation methods. This study analyzes and experimentally evaluates a nonlinear filter configured to provide phase lead without accompanying gain distortion. The nonlinear filter is superior to a linear lead/lag compensator in its ability to maintain system stability as open-loop crossover frequency is increased. Test subjects subjectively rated the filter as slightly better than a lead/lag compensator in its ability to compensate for delays in a compensatory tracking task. However, the filter does introduce unwanted harmonics. This is particularly noticeable for low-frequency pilot inputs. A revised compensation method is proposed which allows such low-frequency inputs to bypass the nonlinear filter. A brief analytical and experimental evaluation of the revised filter indicates that further evaluation in more realistic tasks is justified.

INTRODUCTION

Control systems which incorporate a human as a component in the system, such as an aircraft, are called manual control systems. Manual control systems have certain characteristics which make them highly sensitive to time delays in the system. This paper will discuss the sources and effects of time delays, some basics of manual control theory, and the results of an analysis on the effectiveness of a nonlinear filter as compared to a lead-lag filter for time delay compensation in manual control systems.

PRECEDING PAGE BLANK-NOT FILMED

TIME DELAY SOURCES AND EFFECTS

Aside from the operator's reaction time, delay in manual control systems have three basic sources. One source is computational delays in processing input signals. Examples would be modern high-performance aircraft with sophisticated digital control systems, and flight simulators with computer generated imagery[1,2]. Another source is the sampling delay caused by analog-to-digital conversion in digital control systems. This delay can be shown to be T/2 seconds where T is the sampling interval. The final source of time delays would be apparent delays introduced into the system by higher-order high-frequency system components. These delays are termed apparent because they are not actual time delays; however, the phase lags introduced into the system by these components are perceived by the operator to be time delays.

Time delays effect manual control systems in two ways: first in demanding tasks, delays cause a reduction in closed-loop stability and hence handling qualities, and second in less demanding tasks, delays induce fundamental changes in pilot characteristics[3].

In demanding tasks such as mid-air refueling in an aircraft, pilots tend to increase their open-loop gain. This important characteristic of manual control systems makes time delays a serious concern, as the reduction in gain margin caused by the time delay may cause the pilot to drive his aircraft unstable as he increases his gain[4].

The changes in pilot characteristics caused by time delays in less demanding tasks are also serious particularly when considering flight simulators. When acting as compensatory elements in single loop tasks, Hess[3] has shown that pilot's attempt to generate lead (evidenced by stick pulsing) to compensate for the time delay. Pilots are often asked to rate the handling qualities of a particular simulation configuation. When the pilot is forced to alter his flying technique to compensate for time delays caused by the simulator, he is unable to give an accurate rating of the aircraft being simulated[4].

SOME BASICS OF MANUAL CONTROL THEORY

McRuer and Krendel[5] have shown that, in single-loop man-machine control systems such as Figure 1, pilots adopt compensatory equalization so that the forward loop transfer function, Y_pY_C, resembles ω_C/s in the region of the crossover frequency ω_C. If in this configuration $Y_C = K/S$, the pilot would tailor his own dynamics so that the combined open-loop transfer function, Y_pY_C, would exhibit ω_C like behavior at crossover, i.e. $Y_p = K_p$, a pure gain. If Y_C itself were a pure gain, K, the pilot would adopt a transfer function of the form,

$$Y_p = \frac{K_p}{T_I S + 1} \qquad (1)$$

Pilots also prefer to have this crossover to take place around 2-4 rad/sec depending upon the controlled element dynamics and the input bandwidth[6].

When considering the design of a time delay compensator, this range of crossover frequency becomes one of the design parameters. This is because we are interested in providing the maximum amount of phase lead at the point where it is most important, namely at the crossover frequency. Another design parameter would be the amount of time delay for which one is attempting to compensate. For piloted aircraft flight control systems, it has been shown that handling qualities reach the unacceptable region (pilot ratings beyond 6.5) at delays of approximately 0.225 to 0.250 seconds[1].

Much attention has been devoted to finding the best method of compensating for time delays in manual control systems. The technique most commonly used to date is simple lead-lag compensation. The reminder of this paper will compare, both computationally and experimentally, the effectiveness of a nonlinear and lead-lag filter as time delay compensators in manual control systems.

LEAD-LAG FILTER DESIGN

A typical lead-lag filter can be given by the transfer function

$$G_f(s) = K_d \frac{T_n S + 1}{T_d S + 1} \tag{2}$$

Phase lead is generated when $1/T_d > 1/T_n$. A Bode plot is shown in Figure 2. As can be seen from the figure the phase lead generated is always accompanied by a gain distortion. This gain distortion has several undesirable effects[4]. Any gain increase can cause an amplification of high frequency noise and disturbance input making accurate control more difficult. In flight simulators a gain increase will corrupt the replication of aircraft dynamics, so that the simulation is not an accurate reproduction of the aircraft handling qualities.

Crane outlines a simple technique to design a lead-lag compensator for manual control systems. For the transfer function given as Equation (2), the design process goes as follows:

1) Locate the filter zero, $1/T_n$, at the estimated crossover frequency, ω_c.

2) Determine T_d using the following equation which equates the amount of phase lead generated to the phase lag produced by the time delay at ω_c.

$$\tan^{-1}\omega_c T_n - \tan^{-1}\omega_c T_d = \omega_c t_d \tag{3}$$

3) Choose K_d so that the gain of G_f is unity at ω_c.

This design process results from attempting to minimize the effects of the gain distortion while providing the amount of phase lead necessary to compensate for the time delay. The gain distortion is forced to stay within an envelope of least perceived changes in plant dynamics[2]. Such envelopes result from studies done on simulating high order systems with low order models. Changes in the system dynamics are made at various frequencies, and pilot ratings are used to determine in what frequency ranges the changes are most noticeable[7]. Choosing a conservative crossover frequency of 2 rad/sec and a time delay of 0.250 seconds, this design process leads to a lead-lag filter of

$$G_f(d) = \frac{0.737(0.50S+1)}{(0.1467S+1)} \tag{4}$$

THE SPLIT-PATH NONLINEAR FILTER

The problems encountered with the gain distortion of the lead-lag filter suggest that an ideal time delay compensator would provide phase lead with no gain change. Foster, Gieseking, and Waymeyer[8] propose a nonlinear filter which is capable of providing independent magnitude. The filter they propose is called a split-path nonlinear filter (SPAN filter), a block diagram of which is shown in Figure 3.

The filter input is processed through two branches. One branch adjusts phase; the other adjusts magnitude. The phase branch is composed of a linear filter, F_1, and a nonlinear bistable element. The parameters of F_1 are adjusted to provide the desired phase change. This signal is then input to the bistable element which destroys all amplitude effects and retains only the phase changes. The magnitude also consists of two elements: a linear filter, F_2, and an absolute value. Parameters of F_2 are adjusted to provide the desired magnitude changes. The absolute value of this signal is then multiplied by the output of the bistable element to form the SPAN filter would produce output as shown in Figure 4. The describing function for this configuration shows phase lead without gain increase but instead a slight gain attenuation. For the analysis performed in this paper the SPAN filter was configured with a lead-lag filter having zero at -1 and pole at -10 for F_1, and unity gain for F_2. The Bode plots of the SPAN filter just described and the lead-lag compensator described in the previous section are shown in Figure 5.

COMPUTER ANALYSIS

Harmonic Analysis

Because SPAN is a nonlinear filter it is capable of generating sub- and higher harmonics. To assess the nature of these harmonics a Fourier analysis was performed on the output of the SPAN filter where the input consisted of a single sinusoid of variable frequency. The results are shown in Figure 6. Notice that the harmonics contribute most at the 3-4 rad/sec frequency range which is the region where the SPAN filter produces maximum lead. A Fourier analysis was also performed to check for the existence of subharmonics. None were found.

Steady-State Stability Comparison

To compare the effectiveness of the lead-lag filter vs. the SPAN filter in maintaining system stability, a computer simulation was performed using the configuration in Figure 7. The time delay was chosen to be 0.39 seconds to include the contribution of the pilot's reaction time. The input consisted of a sum of twelve sine waves as shown in Table 1. Compensation was accomplished using the lead-lag and SPAN filters configured as described earlier. For comparison a simulation was also performed using no compensation. Mean square values of r(t), c(t), c(t), and e(t) were calculated. These are denoted R^2, C^2, and E^2 respectively. Values of R^2, C^2, and E^2 were calculated for values of crossover frequency ranging from 0.5 to a value where stability was lost. The results are shown in Figures 8 through 10.

Examining the figures shows the SPAN filter superior in maintaining system stability. The lead-lag filter actually becomes unstable before the case of a time delay with no compensation. This is a result of the gain distortion of the lead-lag filter. The design process described by Crane is "strictly applicable to constant parameter linear systems[2]." A lead-lag filter design based on constant system parameters is unsatisfactory when the design crossover frequency is exceeded.

Closed-Loop Power Ratio

The harmonic analysis described previously gave an indication of the nonlinear nature of the SPAN filter in the open-loop case. To better understand now these nonlinearities would affect closed-loop performance an additional computer analysis was performed on the system of Figure 7. The input to the system was the same as that described in Table 1. The crossover frequency was increased from one to a value where stability was lost. The total power contained in the output was calculated and divided by the power in the output at the input frequencies. Table 2 shows the values obtained. This "power ratio" is an indication of the nonlinear nature of the closed-loop output. It indicates the amount of power in the closed-loop not at input frequencies, and thus attributes to the nonlinearity. The steady increase in the values of Table 2 indicates that, as the crossover frequency is increased, SPAN itself introduces increasing power in the output.

Transient Response

As a final step in the computer analysis the closed-loop step responses were calculated for the system in Figure 7 using the same three configurations as in the steady-state stability analysis. A unit step was the input. The crossover frequency, ω_c, was increased in unit increments from one up to a value which caused the response to diverge. Figures 11 through 13 show the step responses for the case of SPAN compensation for ω_c equal to 1, 2, and 3 rad/sec. Notice the jagged discontinuities present for ω_c = 1 rad/sec. This effect dies out for larger values of ω_c. Figures 14 and 15 shown the step responses for the cases of no compensation and lead-lag compensation respectively when ω_c = 3 rad/sec. Notice that the SPAN filter's response is less oscillatory.

The existence of discontinuities in the output of the SPAN filter, in effect, introduces high frequency noise into the system. The lead-lag filter on the other hand amplifies only existing high frequency noise. Since most physical systems have large reductions in gain at high frequencies, the effects of this noise injection or amplification may be mitigated. to demonstrate this with the SPAN compensation, the ω_c/S plant of Figure 7 was replaced with

$$\frac{\omega_c}{S(0.1S + 1)^2} \tag{5}$$

and the step responses for this new system were calculated. The step response for $\omega_c = 1$ rad/sec is shown in Figures 16. The smoothing effect of additional dynamics is evident compared to Figure 11.

EXPERIMENTAL ANALYSIS

Description

Next, an experiment was performed to obtain subjective and objective measures of the effectiveness of the two compensation methods. The experiment was a single-axis compensatory tracking task involving a human operator, as shown in Figure 17. The error was displayed on a CRT as shown in Figure 18. The test subject was provided with an isometric control stick, his task being to null the error in the presence of a disturbance input.

Procedure

Four different combinations of delay and compensation method were used in the experiment: no delay, no compensation (nominal case); 0.25 second delay, lead-lag second delay, no compensation. A total of five subjects were used. Performance measures included mean square error, mean error, mean square stick output, and mean stick output. Each subject performed five data runs after adequate training.

In addition to the quantitative data obtained, a subjective comparison of each of the different configurations was also performed. Each subject was asked to rate each of the off-nominal configurations on a scale of 0 to 10, based on how closely each approximated the nominal case in terms of response characteristics, etc. The nominal case was given a value of zero.

Results

Figure 19 shows typical root-mean-square error scores for the subjects. Figure 20 shows typical data for root-mean-square stick output. Figure 21 shows data obtained in the comparison test.

Examining the graph of average RMS error scores shows that the three off-nominal cases result in RMS error scores which are approximately equal and larger than the nominal case. No significant reduction in error scores is

seen for either the lead-lag or SPAN filter. For the lead-lag filter this is probably due to the amplification of remnant injected by the pilot. For the SPAN filter the larger RMS error scores probably are a result of harmonics produced by SPAN itself.

The graphs of the RMS stick output show that in most cases the SPAN filter has the largest value followed in order by the nominal case, lead-lag compensation, and delay with no compensation. These values of RMS stick output are in a logical order when the phase and gain characteristics of each configuration are considered under the assumption of constant crossover frequency. The case of a time delay with no compensation causes a reduction in system gain margin as compared the nominal; therefore, the pilot must reduce his gain to maintain adequate stability. The lead-lag filter causes an increase in the "effective plant" gain as compared to the nominal. Thus the operator can reduce his gain with resulting lower RMS stick output scores. The SPAN filter causes a slight reduction in the "effective plant" gain thus allowing a larger pilot gain with accompanying lower RMS stick output.

Examining the graph of subject ratings shows the SPAN filter being ranked most like the nominal case. The average performance for SPAN may be due to subjects disliking the reduced gain margin for the no compensation case and the noise amplification of the lead-lag filter. This seems like the only reasonable explanation since the error scores for the SPAN filter show no significant improvement over either the lead-lag or no compensation cases.

A NEW CONFIGURATION FOR THE SPAN FILTER

The experimental results just obtained indicate that the SPAN filter increases system stability. However, SPAN does not increase tracking accuracy over the lead-lag filter. The results of the computer analysis indicate that this is caused by the harmonics produced by the SPAN filter which degrade closed-loop performance. The step responses also indicate that this detrimental influence of the harmonics on closed-loop performance is most noticeable for low frequency inputs. These results suggest a new configuration for the SPAN filter as shown in Figure 22.

The input to the filter is passed through two branches. The lower branch contains a low-pass filter which allows low frequency signals to by-pass the SPAN filter. Frequencies above a value of $1/T_1$ rad/sec are passed through the SPAN filter with parameters set as before. The output of the SPAN filter is then passed through a filter with break frequency at 20 rad/sec to reduce the amplitude of higher harmonics generated. Finally, the signals in the two paths are added together. A Bode plot of this configuration with $T_1 = 1.5$ is shown in Figure 23.

Calculating the closed-loop power ratios for the new configuration shows no improvement over the original filter. Closed-loop step responses were also calculated. Figures 24 shows the step response for $\omega_c = 1$ rad/sec. The new filter seems to significantly improve the form of the step resporse. Limited experimentation with the filter implemented in the simulation described earlier showed no improvement in tracking random command signals, but smoother responses in following step-like commands.

SUMMARY AND CONCLUSION

The results of the analysis described in this paper show that the SPAN filter's main strength lies in its ability to maintain system stability as the open-loop crossover frequency is increased. The lead-lag filter actually reduces system stability as the crossover frequency increases due to the gain distortion it introduces into the system. The SPAN filter's relative insensitivity to increase in crossover frequency is an important attribute since in manual control systems the crossover frequency is task dependent. The nonlinear nature of the SPAN filter, which enables it to perform so favorably in maintaining system stability, unfortunately also degrades its closed-loop performance. These effects are partially mitigated by replacing the K/S plant of the simulation with one more typical of those found in physical systems. Finally, a new arrangement for the SPAN filter was proposed which allows low frequency inputs.

The research described in this paper indicates that the split-path nonlinear filter shows definite promise as a compensation method for time delays in manual control systems. The next step would be actual implementation of the filter in a sophisticated system simulation and evaluation of its performance and pilot acceptability.

REFERENCES

1. Smith, R. E., Bailey, R. E., "Effect of Control System Delays on Fighter Flying Qualities," AGARD Conf. Proceedings No. 333, Criteria For Handling Qualities of Military Aircraft, pp. 18-1 to 18-16.

2. Crane, D. F., "Compensation for Time Delays in Flight Simulator Visual-Display Systems," AIAA Flight Simulation Technologies Conference, Niagara Falls, NY, 1983.

3. Hess, R. A., "The Effects of Time Delays on Systems Subject to Manual Control," AIAA Guidance and Control Conference, San Diego, CA, 1982.

4. Crane, D. F., "Flight Simulator Visual-Display Delay Compensation," Proceedings of the Winter Simulation Conference, Atlanta, Ga., 1981.

5. McRuer, D. T., and Krendel, E. S., "Mathematical Models of Human Pilot Behavior," AGARD-AG-188, Jan., 1974.

6. McRuer, D. T., Graham, D., Krendel, E., and Reisener, W., "Human Pilot Dynamics in Compensatory Systems," Air Force Flight Dynamics Laboratory, AFFDL-TR-65-15, 1965.

7. Hodgkinson, J., "Equivalent Systems Criteria for Handling Qualities of Military Aircraft," AGARD Conference Proceedings No. 333, pril 22, 1982, pp. 3-1 to 3-11.

8. Foster, W. C., Gieseking, D. L., and Waymeyer, W. K., "A Nonlinear Filter for Independant Gain and Phase (With Applications)," Journal of Basic Engineering, June, 1966, pp. 457-462.

Table 1. Sum of sinusoids input

$$r(t) = \sum_{i=1}^{12} A_i \sin(\omega_i t + \theta_i)$$

ω_i rad/sec	A_i/A_1	Number of cycles in run
0.16419	1.0	3
0.27366	1.0	5
0.76624	1.0	14
1.25883	1.0	23
1.86087	1.0	34
2.68185	0.1	49
3.66702	0.1	67
5.03531	0.1	92
7.16984	0.1	131
9.79695	0.1	179
13.73763	0.1	251
20.96219	0.1	383

Table 2. Closed-loop power ratios

Crossover Frequency ω_c	Power Ratio
1.0	1.02
2.0	1.03
3.0	1.04
4.0	1.06
5.0	1.11
6.0	2.07

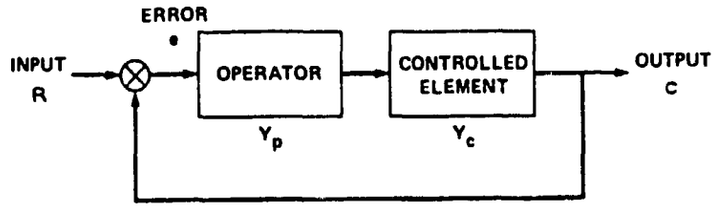

Figure 1. Single-loop compensatory task (from reference 3).

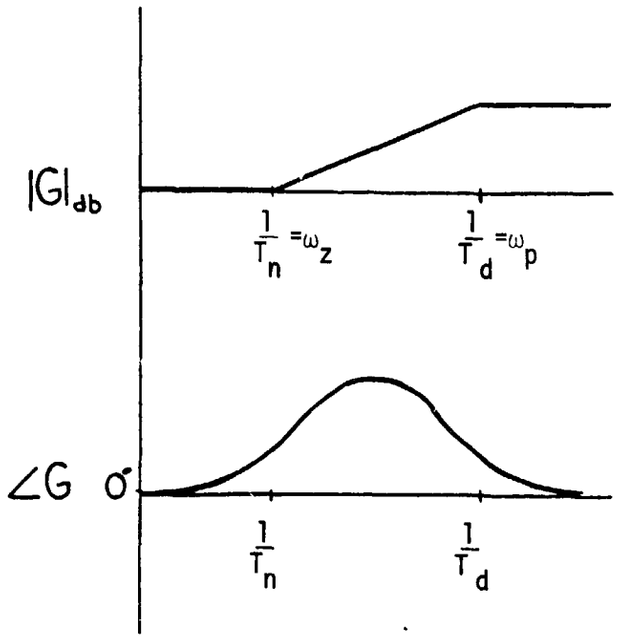

Figure 2. Bode plot of lead-lag filter (from reference 4).

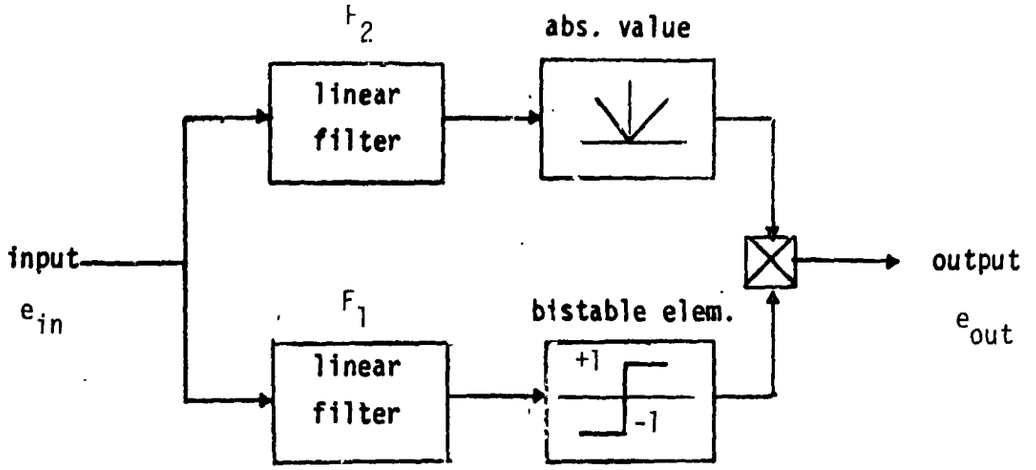

Figure 3. SPAN filter (from reference 8).

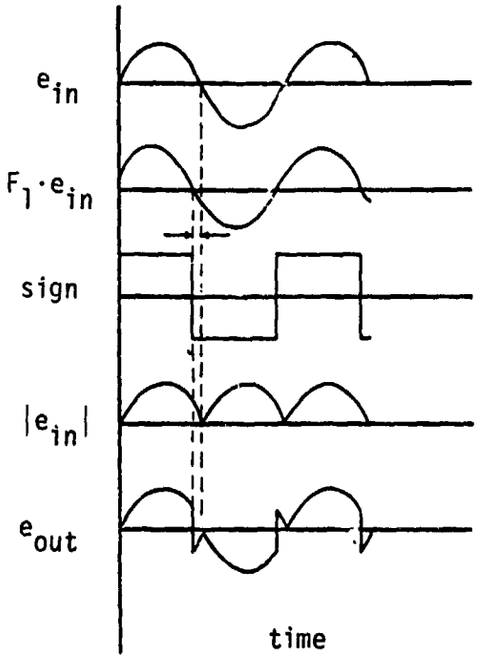

Figure 4. Filter waveform characteristics with lead-lag filter in F_1 (from reference 8).

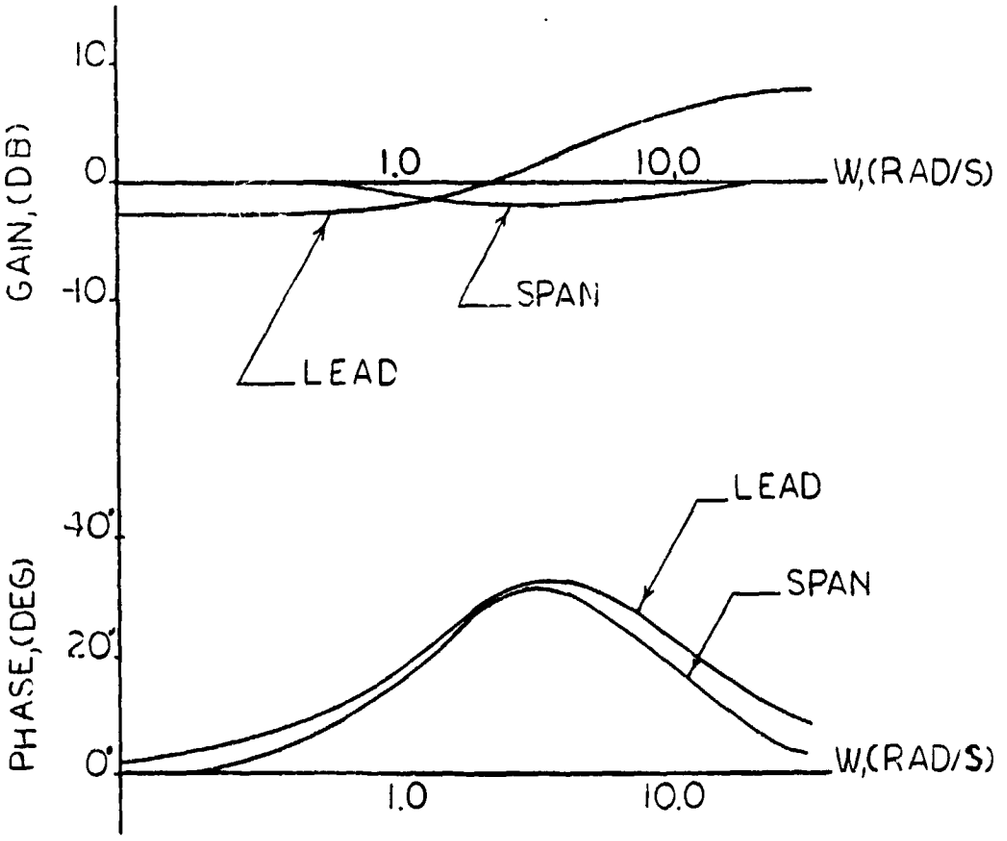

Figure 5. Bode plots for SPAN and lead-lag filters.

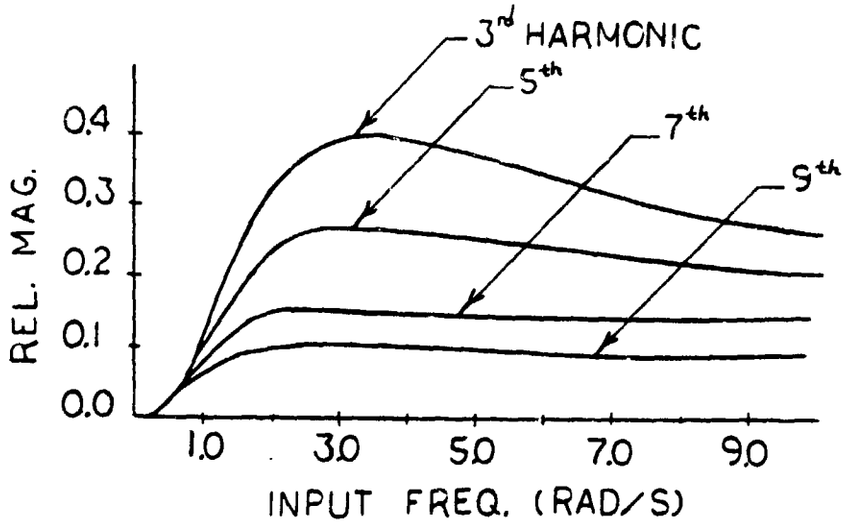

Figure 6. Relative magnitude of nth higher harmonic.

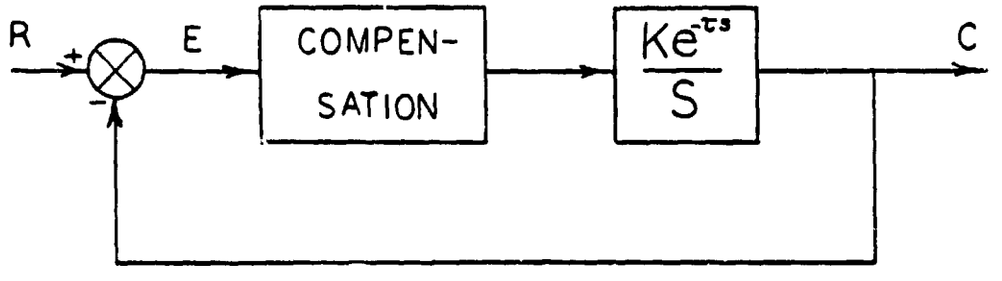

Figure 7. Single-loop system used for computer analysis.

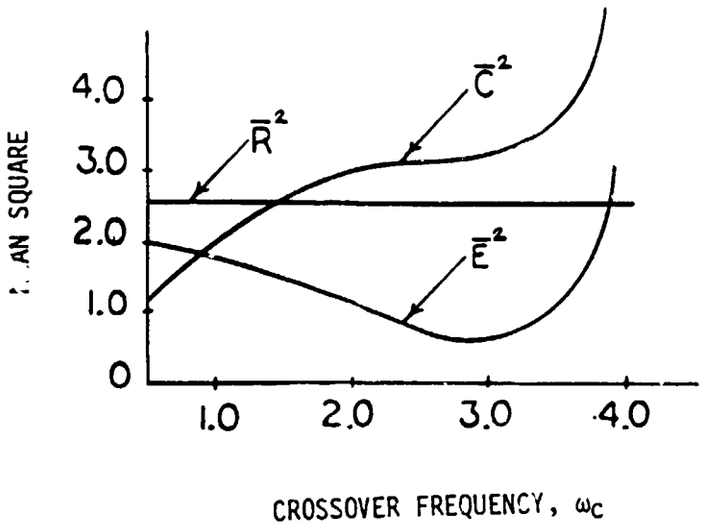

Figure 8. Mean square values for Fig. 7 with a time delay and no compensation.

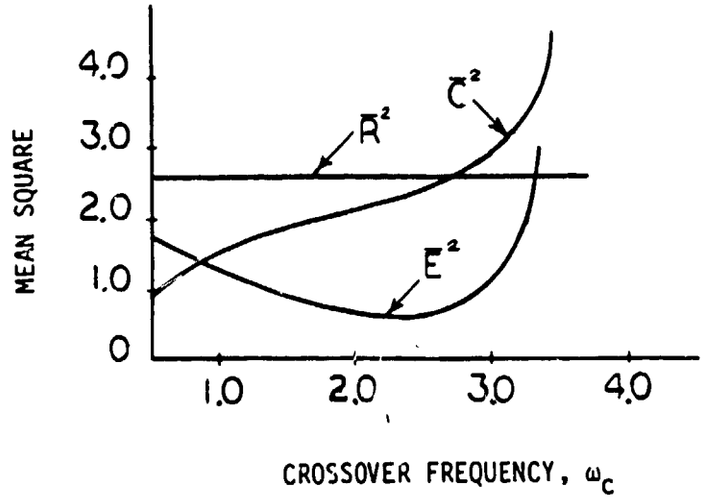

Figure 9. Mean square values for Figure 7 with a time delay and lead-lag compensatic .

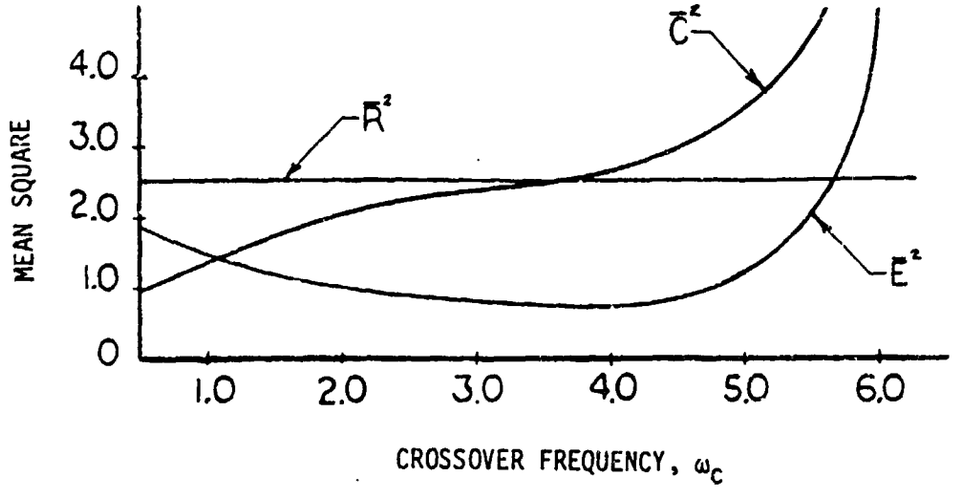

Figure 10. Mean square values for Fig. 7 with a time delay and SPAN compensation.

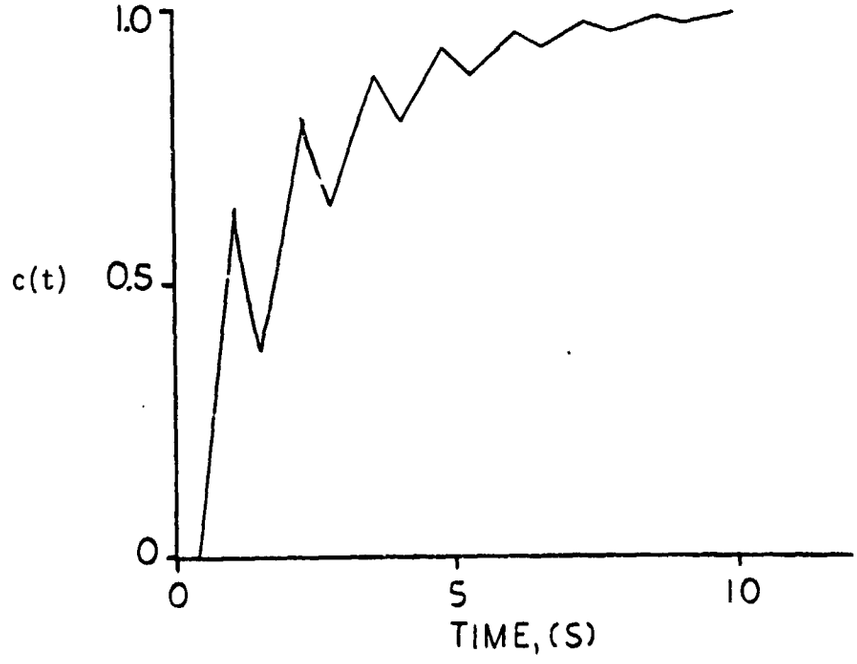

Figure 11. SPAN compensation, ω_c=1.0.

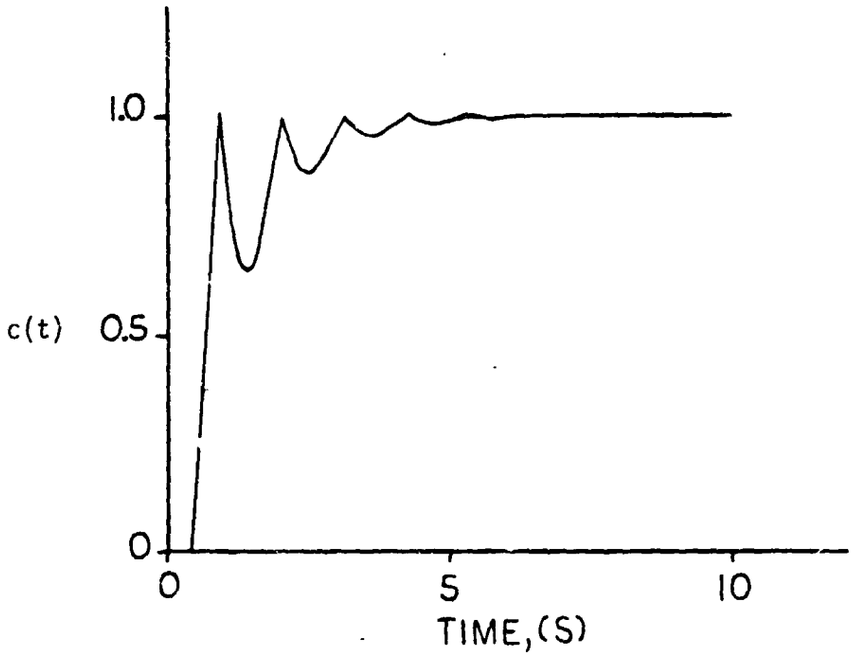

Figure 12. SPAN compensation, ω_c=2.0.

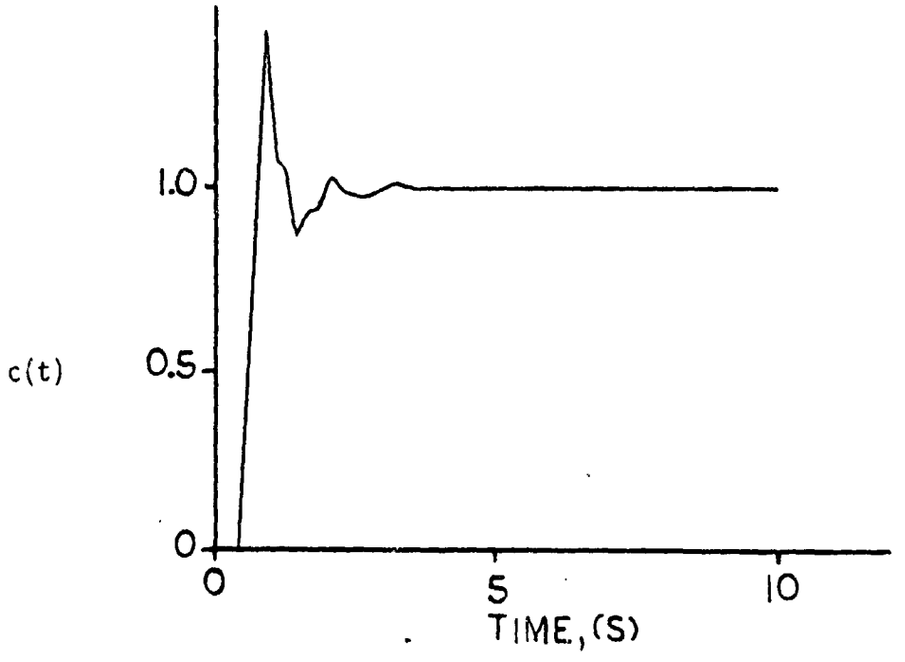

Figure 13. SPAN compensation, ω_c=3.0.

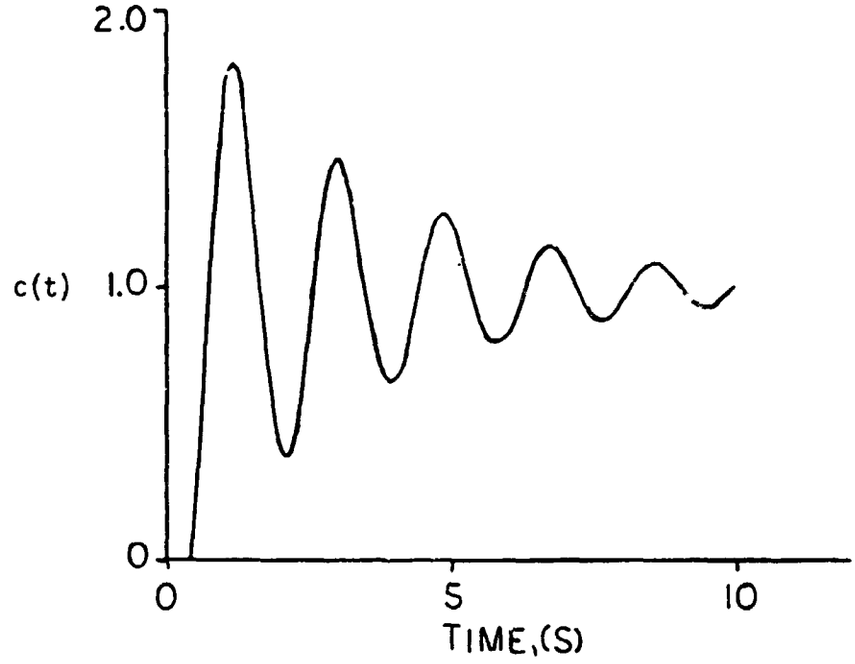

Figure 14. No compensation, ω_c=3.0.

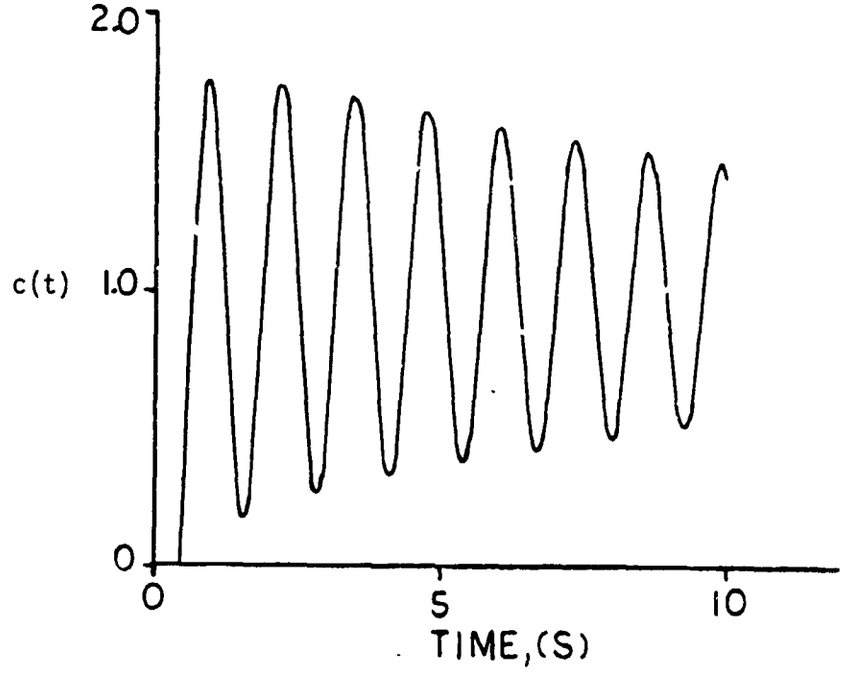

Figure 15. Lead-lag compensation, ω_c=3.0.

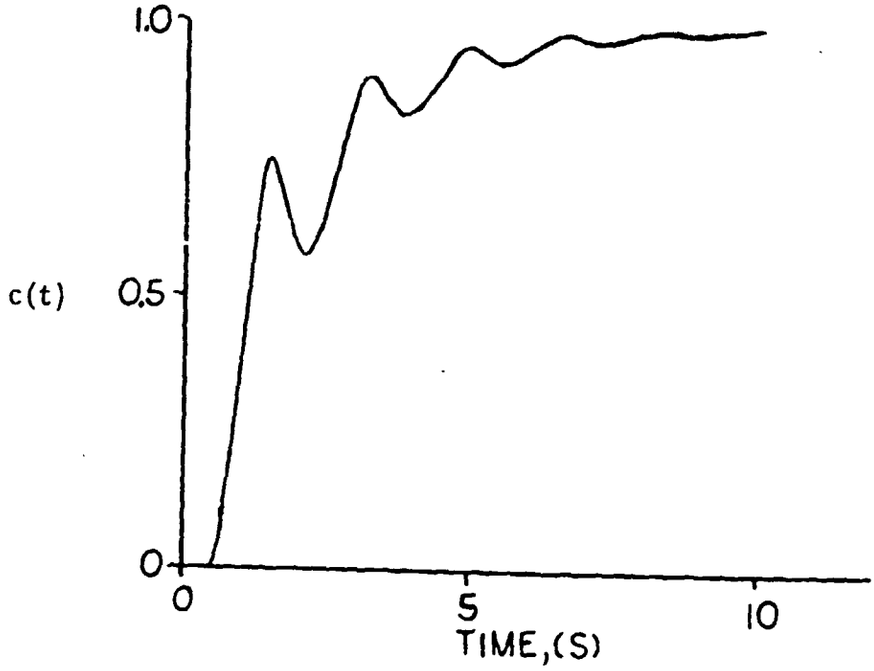

Figure 16. SPAN compensation with $\omega_c/S(0.1S+1)^2$ replacing ω_c/S, $\omega_c = 1.0$.

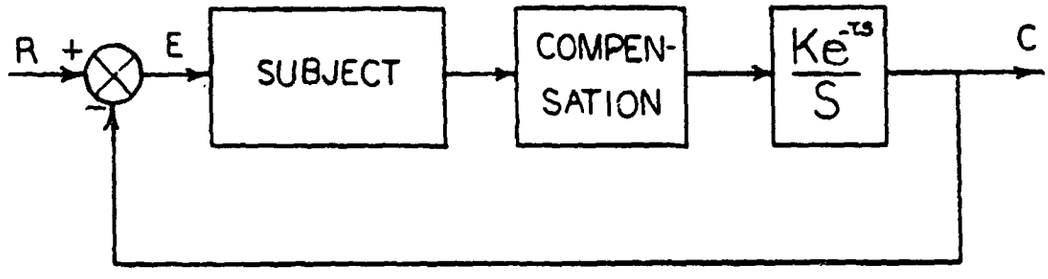

Figure 17. Diagram of single-axis, compensatory tracking task used in experimental analysis.

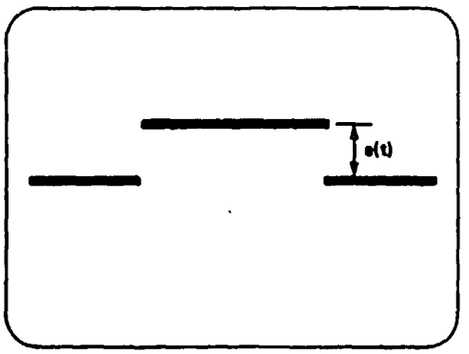

Figure 18. CRT display used in experimental analysis (Reference 3).

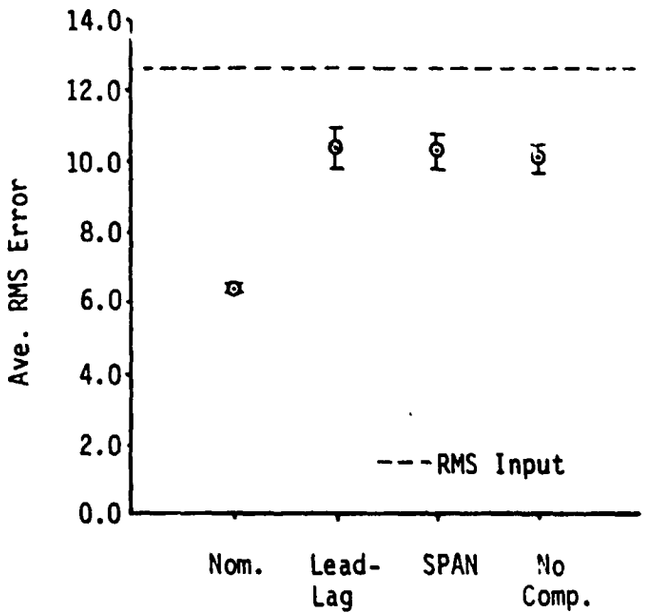

Figure 19. Plot of typical RMS error scores.

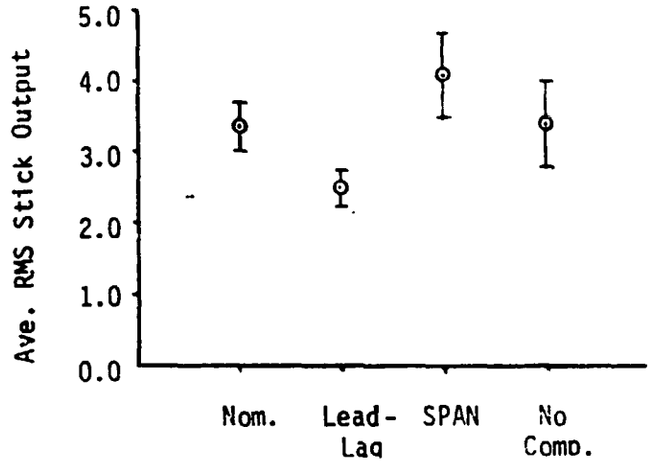

Figure 20. Plot of typical RMS stick output.

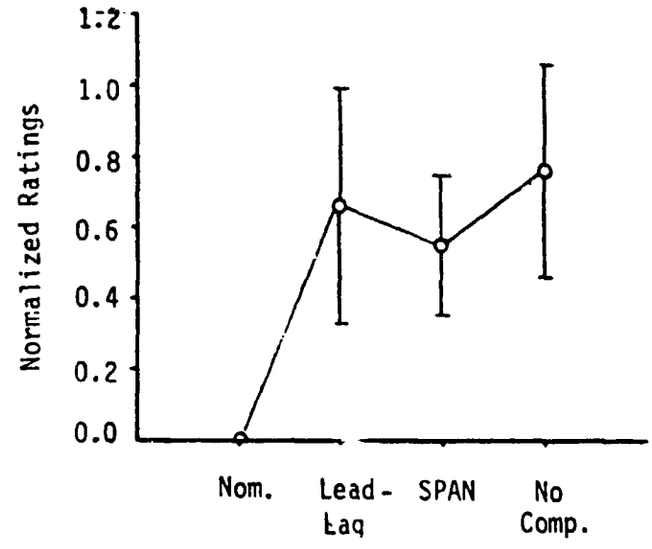

Figure 21 Plot of normalized subject ratings

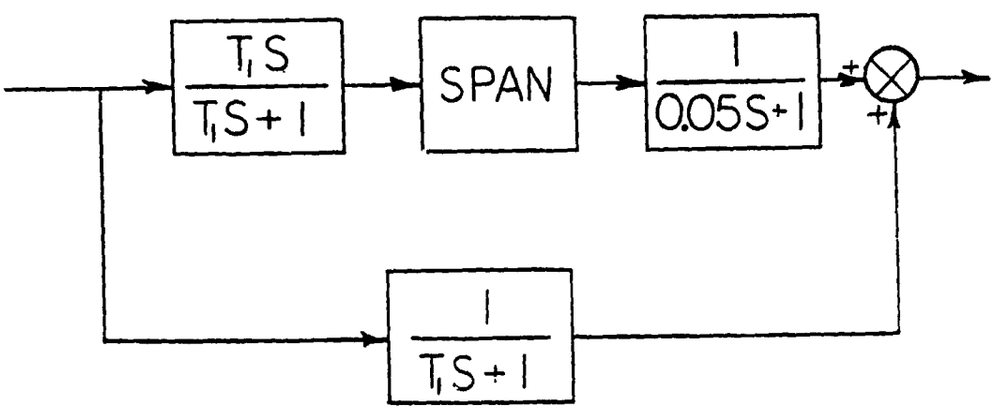

Figure 22. New configuration for SPAN filter.

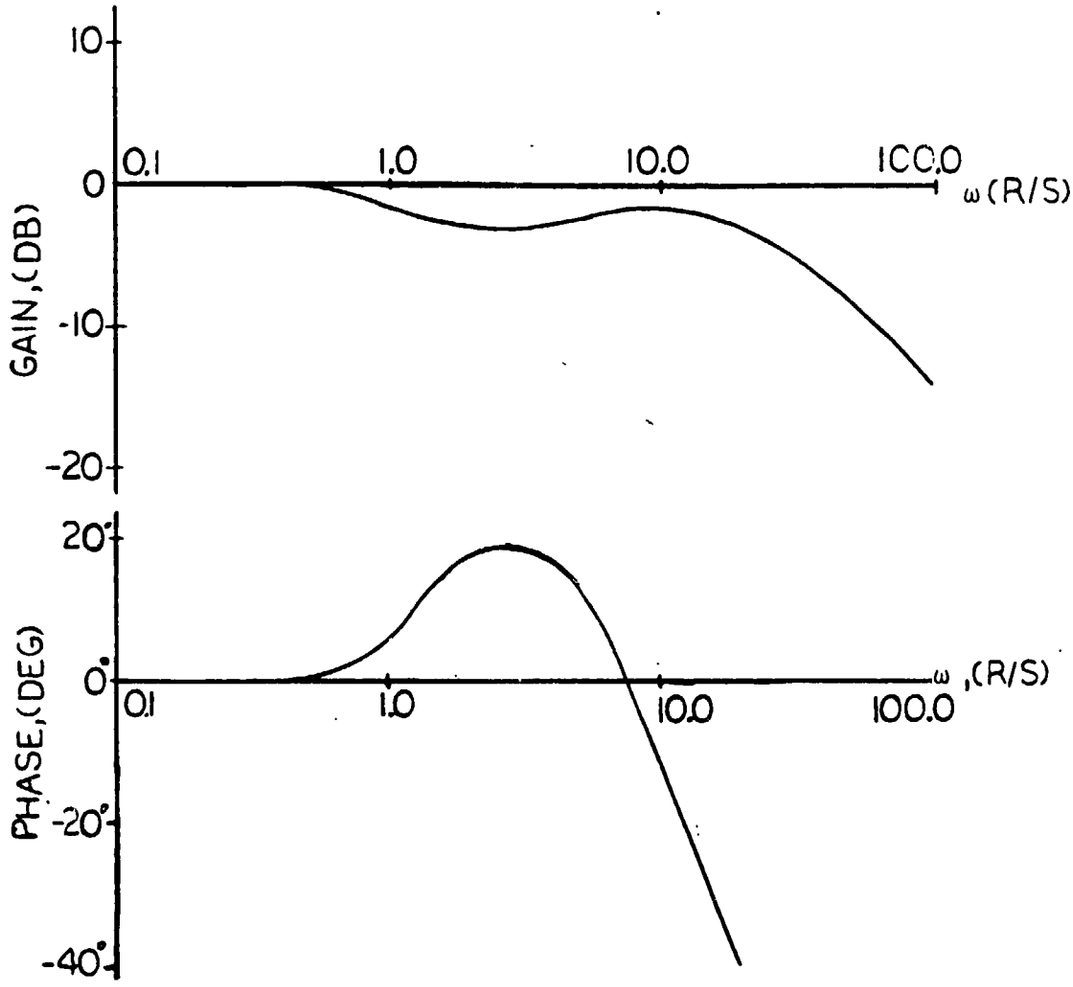

Figure 23. Bode plot of new configuration for the SPAN filter with $T_1 = 1.5$.

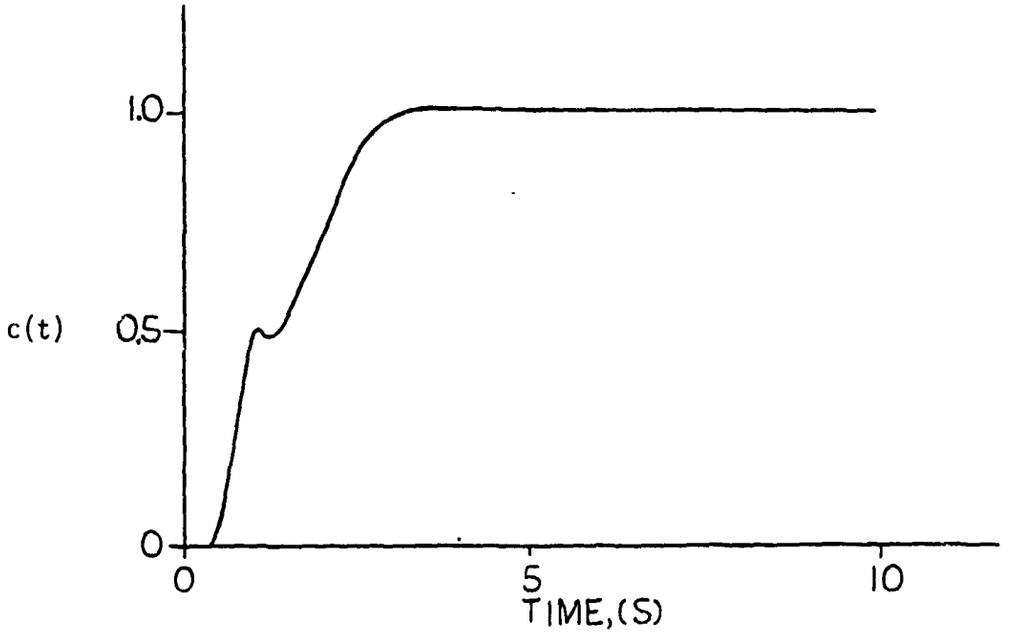

Figure 24. Closed-loop step response of new configuration with T_1=1.5, and ω_c =1.0.

N85 14494

Model Estimation and Identification of Manual Controller Objectives in Complex Tracking Tasks

by

David K. Schmidt* and Pin-Jar Yuan**

School of Aeronautics and Astronautics

Purdue University

West Lafayette, IN

A methodology is presented for estimating the parameters in an optimal-control-structured model of the manual controller from experimental data on complex, multi-input/multi-output tracking tasks. Special attention is devoted to estimating the appropriate objective function for the task, as this is considered key in understanding the objectives and "strategy" of the manual controller. The technique is applied to data from single-input/single-output as well as multi-input/multi-output experiments, and results discussed.

---

*Professor

**Doctoral Candidate

Introduction

In this paper, we will present and apply a methodology for identifying from experimental data the parameters in a multi-input/multi-output model of manual control, suitable for analysis of complex tasks. In this context, "complex tasks" refers to tasks in which multiple loop closures are expected to be present, such as multi-axis tracking or aircraft landing approach, as opposed to compensatory tracking in the laboratory, for example. The structure of the model is compatible with the well-known[1] optimal-control model (OCM) of the human operator, and among the model-related parameters we seek to obtain is an estimate of the manual controller's objective function "weightings". This is considered important because by doing so, the modeler may obtain insight into the operator's strategy and perception of the task. Furthermore, the magnitude this function takes on has been hypothesized[2,3] to correlate with the operator's subjective rating of this task. Hence, an experimentally determined metric related to the subjective assessment of the task may hopefully result.

In addition to establishing a model structure useful for identification, we will also evaluate two procedures for the determination of the desired model parameters. One uses frequency-domain measurements, and as a result is similar to previous methods.[4,5] However, a variation on this technique will be presented to facilitate multi-input/multi-output model determination. The second procedure proposed is based entirely on time-domain data. As a result, the constraints on the experimental procedure, such as special tracking signals, required in the frequency-domain approaches are avoided. Results from both methods will be presented.

Model Structure

Since the model structure to be used is to be compatible with the OCM, we will briefly note its key features. Readers unfamiliar with this modeling approach are referred to the references. The hypothesis upon which the model is based is that the well trained, well motivated human controller chooses his control inputs (e.g. stick force) to meet his (internal) objective in the task, subject to his human limitations. This objective is further assumed to be expressible in terms of a quadratic "cost" function

$$J_p = E\left\{\lim_{T\to\infty}\frac{1}{T}\int_0^T (Y_p^T Q Y_p + u_p^T F u_p + \dot{u}_p^T R \dot{u}_p)dt\right\}$$

where Y_p = vector of human's observed variables (e.g., attitude, acceleration)

u_p = vector of his control inputs

Q,F,R = Controller-Selected (internal) weightings

The human limitations modeled include information-acquisition and processing time delay, observation and control input errors, and neuromuscular dynamics. A block diagram of the resulting model structure is shown in Figure 1.

The components of this model may be grouped into two parts, one dealing with the information acquisition and state estimation, and one related to the control law or control policy operating on the estimated state. As has been shown in the references on this modeling approach, the "solution" for the human's control inputs, as predicted by the model, is expressed as

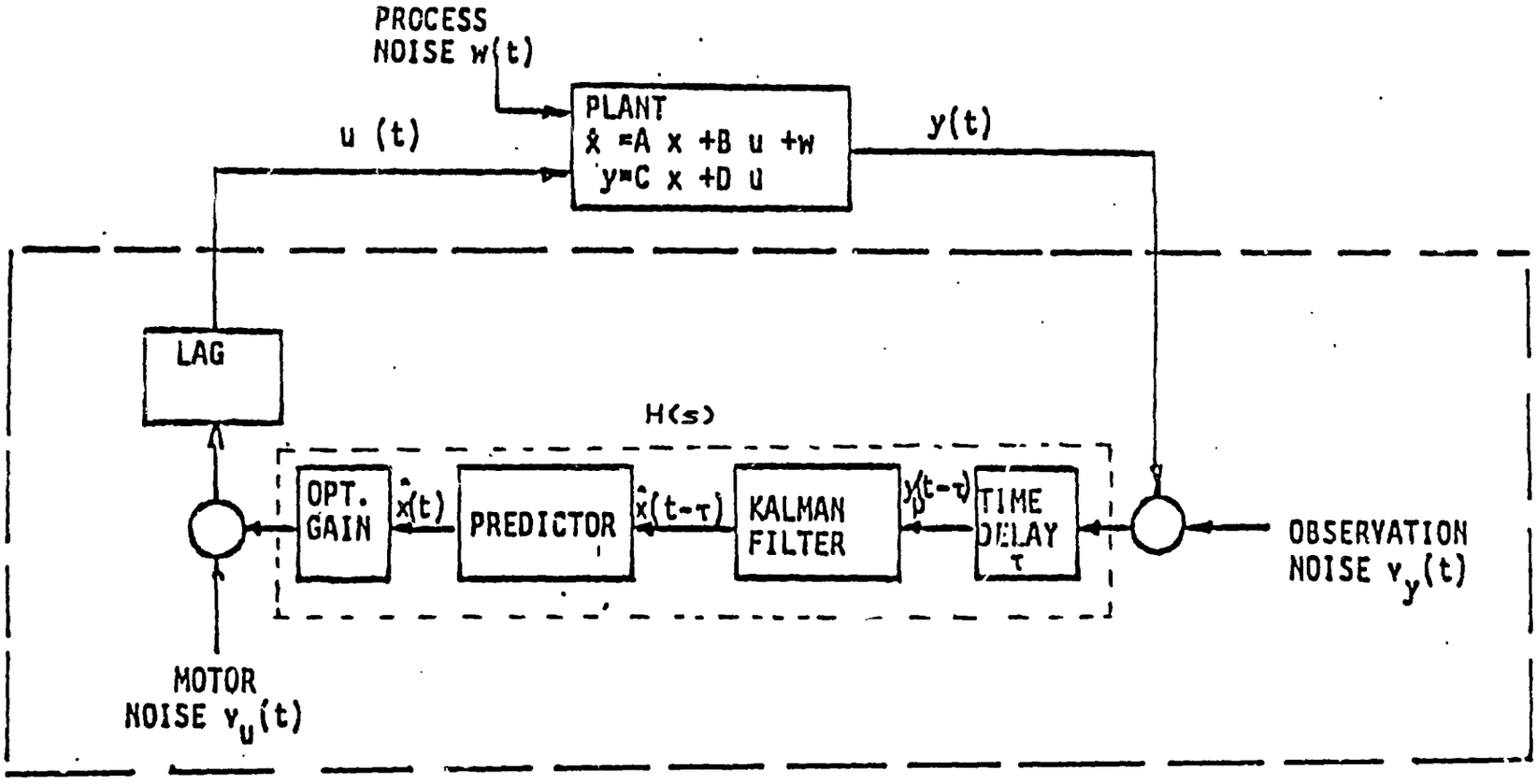

Figure 1. Optimal Control Model

$$\dot{u}_p = -G_x\hat{x} - G_u u_p + v_u \qquad (1)$$

where $\hat{x}$ = internal estimate of the system states

G_x, G_u = control gain matrices

v_u = motor noise, or control input errors

The system dynamics are taken as

$$\dot{x} = Ax + Bu_p \quad ; \quad y = Cx$$

where y = vector of system response

and if a tracking task is considered, the dynamics of the tracking signal vector y_c may be represented as

$$\dot{y}_c = A_c y_c + Dw$$

where w is a disturbance input of "white" noise. Usually, the tracking dynamics are combined with the system dynamics, resulting in an augmented state vector col$[x, y_c]$. Finally, the manual controller is considered to observe delayed system responses and commands, with some observation error, or

$$y_p = \begin{bmatrix} C_p x(t-\tau) \\ \hline y_c(t-\tau) \end{bmatrix} + v_y$$

where v_y = vector of observation errors. Usually, tracking error $\varepsilon = y_c - y$ is observed, plus the commands themselves if the task is that of pursuit. Additionally, other system responses may be observed but not actually regulated or tracked. Therefore, for our purposes we will arrange the human's observation vector as follows (dropping the $t-\tau$ here for brevity)

$$v_p^T = [\varepsilon^T, \dot{\varepsilon}^T, y_c^T, \dot{y}_c^T, y_o^T] + v_y^T$$

with $y_o = C_o x$ representing observed responses other than errors and commands. Clearly, the above expression can always be represented in the form

$$y_p = \bar{C}\bar{x}(t - \tau) + v_y$$

where $\bar{x}^T = [y_c^T, x]$ and $\bar{C}$ is partitioned accordingly to yield

$$\bar{C} = \begin{bmatrix} C_\epsilon \\ \hline C_c \\ \hline C_o \end{bmatrix} \tag{2}$$

Reference 1, for example gives closed-form expressions for the state covariance matrix $E\{xx^T\}$ for this structure, under assumptions of independence and "whiteness" on w, v_u, and v_y. A compatible frequency domain representation of the manual controller may also be obtained that effectively has the following form

$$U_p(s) = T_n^{-1}(s)H(s)[Y_p(s) + N_y] + T_n^{-1}(s)N_u \tag{3}$$

where $Y_p(s)$ = Laplace Transform of $y_p(t)$ (not delayed)

$T_n^{-1}(s)$ = Neuromotor Dynamics (= $[G_n^{-1}s + I]^{-1}$ if Eqn. 1 is considered)

$H(s)$ = Manual Controller Transfer Function Matrix (Refer to Fig. 1)

N_y, N_u = Noise Vectors - Related to v_y and v_u

Also, the command and system dynamics expressed as

$$Y_c(s) = [sI - A_c]^{-1}DW(s) = \Phi_c(s)DW(s)$$

and

$$X(s) = [sI - A]^{-1}BU_p(s) - \Phi(s)BU_p(s)$$

may be combined to form

$$x(s) = \begin{bmatrix} Y_c(s) \\ X(s) \end{bmatrix} = \begin{bmatrix} \Phi_c(s)DW(s) \\ \Phi(s)BU_p(s) \end{bmatrix}$$

Then

$$Y_p(s) = \bar{C}x(s) = \left[\begin{array}{c} C_\varepsilon \\ \hdashline C_c \\ \hdashline C_o \end{array}\right] x(s) \qquad (4)$$

where recall $\bar{C}$ is partitioned as in Equation 2. If we now partition $H(s)$ and N_y to be compatible with $Y_p(s)$, we may let

$$H(s) \overset{\Delta}{=} [H_\varepsilon(s), H_c(s), H_o(s)]$$

$$N_y^T = [N_\varepsilon^T, N_c^T, N_o^T]$$

With this structure, we may represent the system as in Fig. 2, where we have used the following definitions

$$C_c \Rightarrow [I \vdots 0] \qquad (I = \text{Identity})$$

$$C_\varepsilon \Rightarrow [I \vdots -C_r]$$

and

$$C_o \Rightarrow [0 \vdots C_o]$$

to make the matrices have compatible dimensions. Note that not only is this structure consistent with the OCM with multiple inputs and outputs, but in the scalar case with $H_c = H_o = 0$ the structure also reduces to the conventional compensatory tracking block diagram. Shown in Fig. 3 is this simpler case.

For experimentally estimating a scalar $Y_p(j\omega)$, measurements are taken of $\theta_c(t)$, $\varepsilon(t)$, and $u_p(t)$. Spectral analysis is then performed to obtain

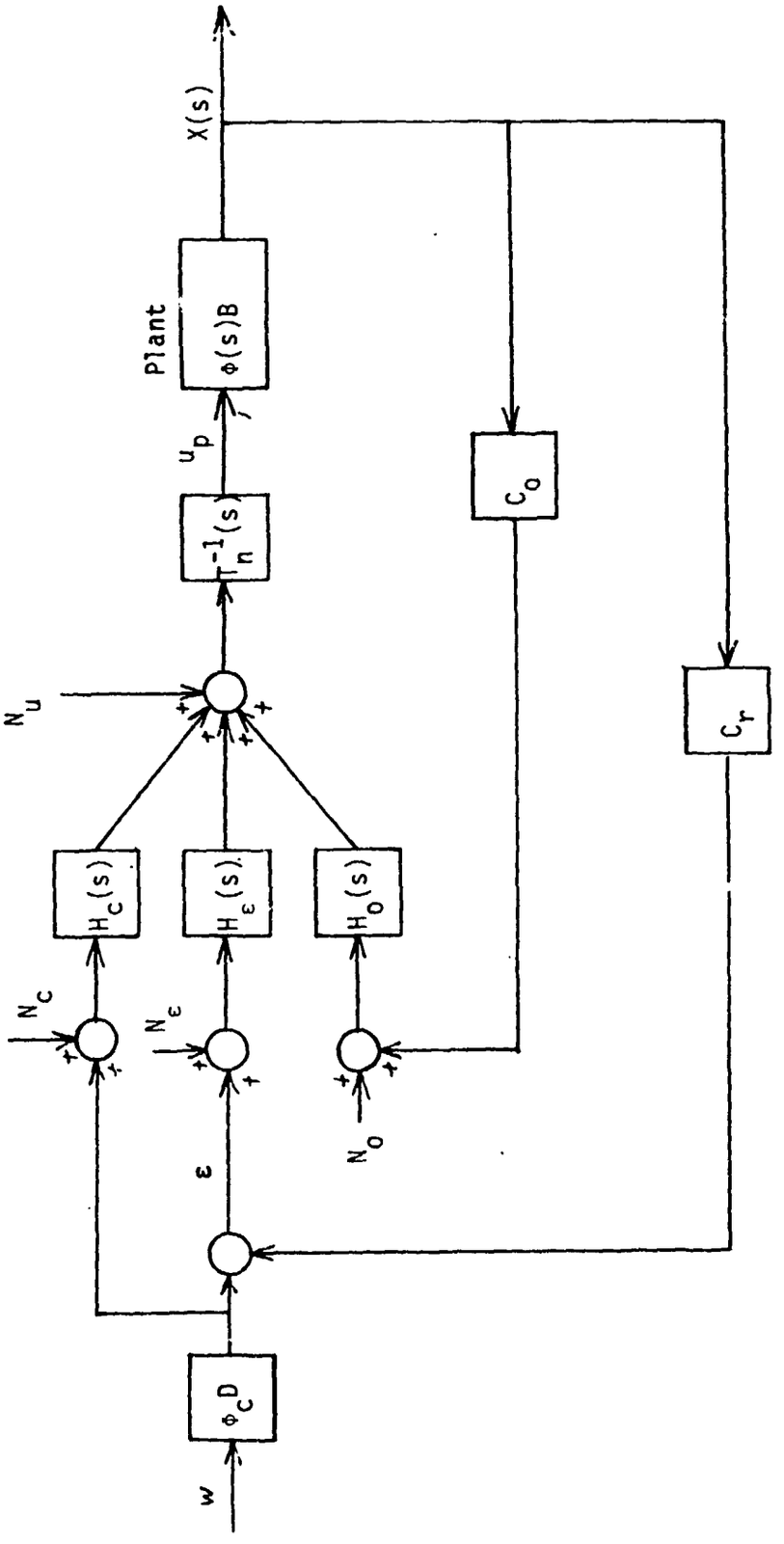

Figure 2. General Model Structure

$\Phi_{cu}(j\omega)$ = Cross spectrum between Θ_c and u_p

$\Phi_{c\varepsilon}(j\omega)$ = Cross spectrum between Θ_c and ε

and the desired relation is

$$Y_p(j\omega) = \Phi_{cu}(j\omega)/\Phi_{c\varepsilon}(j\omega)$$

which can be derived from block diagrm algebra (see for example Refs. 4 and 5).

Now, as discussed in Ref. 5, special experimental conditions must be invoked to identify multiple human operator transfer functions, as in H(s) discussed above. Specifically, independent excitation of all inputs to H(s) must be present, and this is frequently not possible in many practical situations. However, some alternate expressions will be developed which yield identifiable transfer functions directly related to the general model structure discussed here, but are not human operator transfer functions, like $Y_p(j\omega)$ in the scalar case cited above.

Referring to Eqns. 3 and 4 above, or equivalently Fig. 2, we have

$$U_p(s) = T_N^{-1}(s)[H_\varepsilon(s)(\varepsilon(s) + N_\varepsilon) + H_c(s)(Y_c(s) + N_c) + H_o(s)(Y_o(s) + N_o) + N_u]$$

$$\varepsilon(s) = Y_c(s) - C_r\Phi(s)BU_p(s)$$

$$Y_o(s) = C_o\Phi(s)BU_p(s)$$

Substituting $\varepsilon(s)$ and $Y_o(s)$ into the first expression, and solving for $U_p(s)$ yields

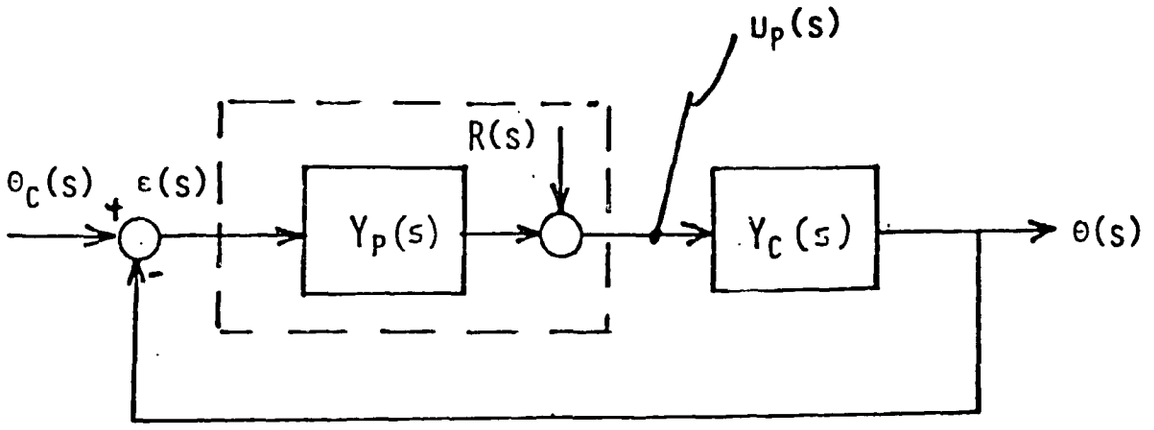

Figure 3. Scalar Model

$$U_p(s) = [T_{uc}(s)]Y_c(s) + [T_{uy}(s)]N_y + [T_{uu}(s)]N_u \tag{5}$$

where $N_y^T = [N_\varepsilon^T, N_c^T, N_o]$

$$T_{uc}(s) = [I + T_n^{-1}(s)\{H_\varepsilon(s)C_r - H_o(s)C_o\}\Phi(s)B]^{-1}[T_n^{-1}(s)\{H_\varepsilon(s)+H_c(s)\}]$$

$$T_{uy}(s) = [I + T_n^{-1}(s)\{H_\varepsilon(s)C_r - H_o(s)C_o\}\Phi(s)B]^{-1}[T_n^{-1}(s)[H_\varepsilon(s)\vdots H_c(s)\vdots H_o(s)]]$$

$$T_{uu}(s) = [I + T_n^{-1}(s)\{H_\varepsilon(s)C_r - H_o(s)C_o\}\Phi(s)B]^{-1}T_n^{-1}(s)$$

Substitution back into the relation for $\varepsilon(s)$ and $Y_o(s)$ yields

$$\begin{aligned} \varepsilon(s) &= [T_{\varepsilon c}(s)]Y_c(s) + [T_{\varepsilon y}(s)]N_y + [T_{\varepsilon u}(s)]N_u \\ Y_o(s) &= [T_{oc}(s)]Y_c(s) + [T_{oy}(s)]N_y + [T_{ou}(s)]N_u \end{aligned} \tag{6}$$

where

$$T_{\varepsilon c}(s) = [I - C_r\Phi(s)BT_{uc}(s)]$$

$$T_{\varepsilon y}(s) = -C_r\Phi(s)BT_{uy}(s)$$

$$T_{\varepsilon u}(s) = -C_r\Phi(s)BT_{uu}(s)$$

$$T_{oc}(s) = C_o\Phi(s)BT_{uc}(s)$$

$$T_{oy}(s) = C_o\Phi(s)BT_{uo}(s)$$

and

$$T_{ou}(s) = C_o\Phi(s)BT_{uu}(s)$$

Now the three transfer function matrices T_{uc}, $T_{\varepsilon c}$, and T_{oc} are related to the matrices of cross-spectra between u_p and y_c, ε and y_c, and y_o and y_c, respectively, assuming the "noises" N_y and N_u are uncorrelated with y_c. Or using matrix notation

$$\begin{aligned} T_{uc}(j\omega) &= [\Phi_{y_c u_p}(j\omega)][\Phi_{y_c y_c}(\omega)]^{-1} \\ T_{\varepsilon c}(j\omega) &= [\Phi_{y_c \varepsilon}(j\omega)][\Phi_{y_c y_c}(\omega)]^{-1} \\ T_{oc}(j\omega) &= [\Phi_{y_c y_o}(j\omega)][\Phi_{y_c y_c}(\omega)]^{-1} \end{aligned} \tag{7}$$

So, if frequency-domain data were used to estimate the above spectra, the transfer functions in Eqn. 7 may be identified, but not necessarily the elements of H(s). However, these identifiable transfer functions, due to their direct relationship to the OCM, for example, may be used for model identification and/or validation in exactly the same manner estimates for H(s) may be used, so they are just as meaningful.

Additionally, referring back to Equation 5, under the assumption that the noise vectors N_y and N_u consist of elements mutually uncorrelated, and uncorrelated with y_c, a model-related expression for the power of the remnant in each of the i'th components of u_p is expressible as

$$\begin{aligned} \Phi^i_{rr}(\omega) = &\sum_j |T_{u_i y_j}(j\omega)|^2 \Phi_{y_j y_j}(\omega) \\ &+ \sum_k |T_{u_i u_k}(j\omega)|^2 \Phi_{u_k u_k}(\omega) \end{aligned} \tag{8}$$

where $\Phi_{y_j y_j}(\omega)$ = Power spectrum of the j'th element in the noise N_y

$\Phi_{u_k u_k}(\omega)$ = Power spectrum of the K'th element in the noise N_u.

So if $\Phi^i_{rr}(\omega)$ is estimated experimentally, it is relatable to the model-based parameters on the right hand side of the above equation for further model comparison or validation. Similar expressions for all the above development are available in Ref. 6, for further reference.

Parameter Search Technique

Now that the model structure is obtained to allow direct comparisons between measured variables and their model-based counterparts, attention is now turned to obtaining the parameter set of interest. This parameter set, denoted p, consists of the "independent" variables of the model, such as objective function weights Q and R, time delay τ, and noise covariance matrices C_{n_y} and C_{n_u}, for example. We will make direct application of the quasi-Newton search approach of Refs. 5, 7 and 8, with two variations fundamental to our purpose. The first is that in the above references, a scalar objective function weight on tracking error alone was used exclusively, while we desire to estimate more complex expressions for the cost, or weighting matrices. Secondly, we will compare using two forms of experimental data, one strictly time domain and the other frequency domain, to determine if using only time domain data leads to sufficiently accurate results. This is desirable since a purely time domain approach is simpler and greatly reduces the requirement on the experimental technique for obtaining the required data.

The scheme is implemented to minimize a scalar matching cost of the form

$$M = \sum_{i=1}^{N} w_i e_i^2$$

where e_i is the difference between the i^{th} measured data point and the corresponding model prediction, w_i is a weighting coefficient. Or in matrix form:

$$M = e^T W e$$

with $e = \text{col}[e_1 e_2, \ldots]$, $W = \text{diag}[w_1]$.

For a trial set of model parameters p_1, we have its corresponding modeling cost

$$M_1 = e_1^T W e_1$$

For a new set of parameters $p_2 = p_1 + \Delta p$, we obtain a new modeling error Δe, related to Δp by

$$\Delta e = Q \Delta p$$

where $q(i, j) = \frac{\partial e_i}{\partial p_j}$ can be obtained by a numerical perturbation of the model. The change in the parameter vector Δp yielding the minimum modeling error, given the initial vector e_1 and the assumption of linearity between ΔM and Δp is

$$\Delta p = -[Q^T W Q]^{-1} Q^T W e_1$$

Thus an iteration procedure is established, which proceeds until no more improvement in matching cost M, or the required changes in the parameters in Δp are very small.

In addition to obtaining the best match to a given set of data, we also wish to determine some measure of the reliability of the identified

parameter values. A qualitative indication of parameter estimation reliability can often be obtained through sensitivity analysis relating changes in the scalar matching cost to perturbations in the model parameters. In general, estimates of parameters that have a high impact on the matching cost can be considered more reliable than estimates of parameters having a smaller impact.

As shown in Ref. 8, this sensitivity may be estimated from the relation

$$\Delta M_i = V^T Q^T W Q V (\Delta p_i)^2$$

where V is a column vector that has a value of unity for the i^{th} element and values for remaining elements V_r as determined from

$$V_r = -[Q_r^T W Q_r]^{-1} Q_r^T W q_i$$

where $q_i = \text{col}[q_{i,1}, q_{i,2}, \ldots]$ and the subscript r indicates vectors and matrices which omission of the ith row and column.

Pursuit Tracking Analysis

For comparing the time-vs. frequency-domain data for model determination, and to relate the above methodology to an established situation, a single axis pursuit tracking task is considered.[6] Subjects tracked a command signal generated by a sum of sinusoids

$$\Theta_c = \sum_{i=1}^{10} A_i \sin(\omega_i t + \phi_i)$$

for 100 seconds, with the frequencies ω_i evenly spaced between 0.25-17 rad/sec, and amplitudes A_i selected such that the spectrum of the command approximated a random signal generated by

$$\Theta_c / W = \frac{1}{s^2 + 3s + 2.25}$$

with "white" noise w intensity taken to be $\sigma_w^2 = 13.5\ \delta(t)$, - $\delta(t)$ a delta function.

In addition to Θ_c, the subjects observed the plant response $\Theta(t)$, and therefore the error $\Theta_c - \Theta$, where the two plants (Θ/δ_p) were K/s and K/s^2. A representative block diagram is shown in Figure 4. (Note the correspondence between this block diagram and that of Figure 2.) Since error, Θ_c, and Θ are not all linearly independent, only two need be included for observation. Therefore, the subjects observation vector may be taken as

$$y_p^T = [\varepsilon, \dot{\varepsilon}, \Theta_c, \dot{\Theta}_c]$$

for both K/s and K/s^2 plants. Finally, including the subjects' control input δ_p in the state vector x, we may define

For K/s , $x^T = [\Theta_c, \dot{\Theta}_c, \Theta, \delta_p]$

For K/s^2 , $x^T = [\Theta_c, \dot{\Theta}_c, \Theta, \dot{\Theta}, \delta_p]$

Referring back to Eqns. 5 and 6, one may consider $T_{uc}(s)$ and $T_{\varepsilon c}(s)$ to be scalars,

$$T_{uc}(s) = \frac{1}{\tau_n s+1}\,[H_1 + sH_2 + H_3 + sH_4][1 + F(H_1+sH_2)/(\tau_n s+1)]^{-1}$$

$$T_{\varepsilon c}(s) = [1 - F(H_3+sH_4)/(\tau_n s+1)][1 + F(H_1+sH_2)/(\tau_n s+1)]^{-1}$$

From the experimental data, the state covariance matrices $E[xx^T]$ were estimated, as well as the cross-spectra between Θ_c and δ_p, and Θ_c and ε (error), or $\Phi_{\Theta_c\delta_p}(j\omega)$ and $\Phi_{\Theta_c\varepsilon}(j\omega)$. Finally, although not possible in more complex situations, since $T_{uc}(s)$ and $T_{\varepsilon c}(s)$ are scalars in this case, an effective operator transfer function may be defined as

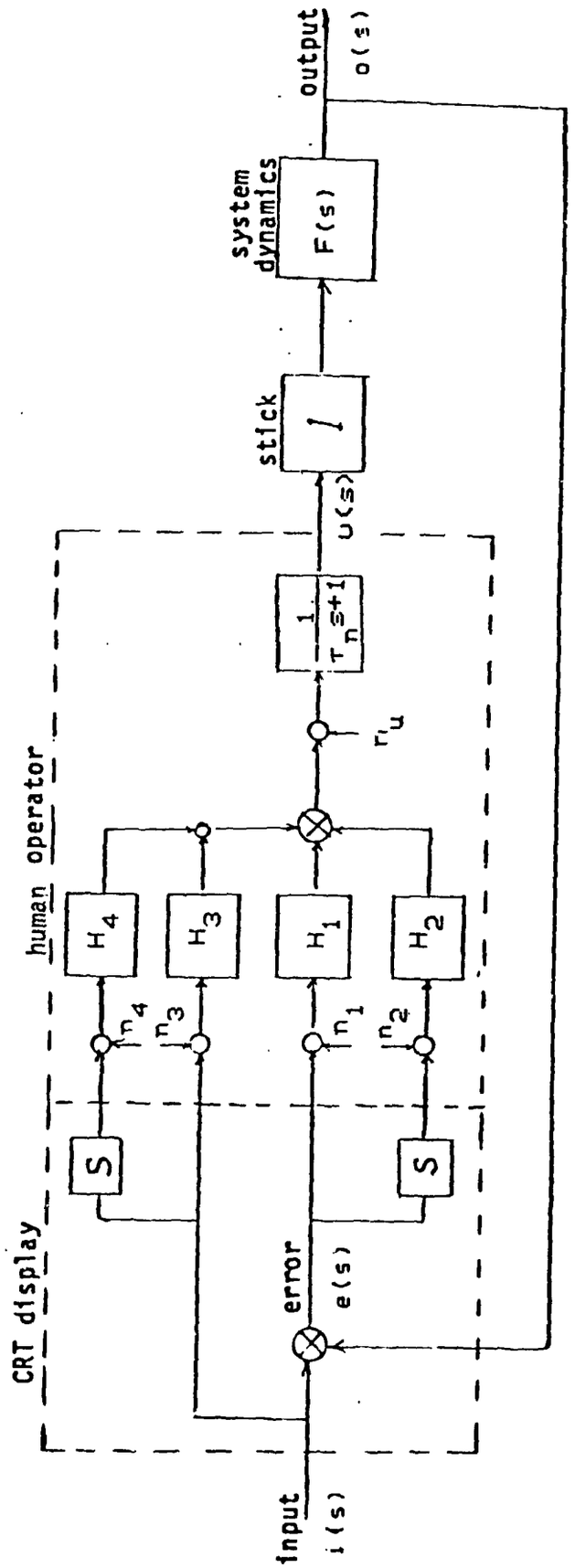

Figure 4. Pursuit Tracking Model Structure

$$y_{p_{eff}}(j\omega) \triangleq T_{uc}(j\omega)/T_{\varepsilon c}(j\omega)$$

$$= \Phi_{\Theta_c \delta_p}(j\omega)/\Phi_{\Theta_c \varepsilon}(j\omega)$$

These time and frequency-domain results were used for the quasi-Newton parameter search to estimate

$$p^T = [q_\varepsilon, q_{\dot{\varepsilon}}, \tau_n, \tau, C_{n_y}^T, C_{n_u}]$$

where q_ε, $q_{\dot{\varepsilon}}$ = objective function weights on error and error rate

τ_n = neuromotor time constant

τ = observation time delay

C_{n_y} = observation noise intensities (expressed as noise-to-signal ratios in dB relative to the variance of each observation)

C_{n_u} = motor noise intensity (expressed as noise-to-signal ratio in dB relative to control input variance)

Two separate parameter searches were performed. One used only the state covariance matrix for computing model matching cost, or

$$M_T = \frac{1}{N} \sum_{i,j}^{N} \left(\frac{X_{ij} - \hat{X}_{ij}}{\sigma_{ij}}\right)^2$$

where X_{ij} = element in experimentally-obtained state covariance matrix

$\hat{X}_{ij}$ = corresponding element from the covariance matrix from the model

σ_{ij} = standard deviation in the experimental value of X_{ij} over the repeated runs.

The second used only the frequency-domain result for $y_{p_{eff}}(j\omega_i)$,

$$M_F = \frac{1}{N}\sum_i^N \left[\left(\frac{G_i-\hat{G}_i}{\sigma_{G_i}}\right)^2 + \left(\frac{\psi_i-\hat{\psi}_i}{\sigma_{\psi_i}}\right)^2 + \left(\frac{R_i-\hat{R}_i}{\sigma_{R_i}}\right)^2\right]$$

where $G_i, \psi_i = |y_{p_{eff}}(j\omega_i)|$, and $\arg y_{p_{eff}}(j\omega_i)$, ω_i input frequencies in command signal, measured experimentally from spectra

$\hat{G}_i$ $\hat{\psi}_i$ = corresponding magnitude and phase of the model-estimated transfer function

R_i = estimated power of the remnant in the control input δ_p, from experiment. Obtained from the spectrum of δ_p at frequencies other than those in the command.

$\hat{R}_i$ = remnant power obtained from the model (or Eqn. 8)

$\sigma_{G_i}, \sigma_{\psi_i}, \sigma_{R_i}$ = standard deviation of the experimental data

The estimates for desired model parameters p obtained using both approaches are listed in Tables 1 and 2, for the K/s and K/s^2 plants, respectively. Note the estimated values of the parameters do not differ significantly between the results obtained from minimizing M_T (time domain) and those from minimizing M_F (frequency domain). In some cases, the sensitivities in these costs to small relative changes in these parameters do vary, depending on whether frequency or time domain data is used.

Another interesting result is the comparison between the state covariance matrices obtained from the frequency-data - matched model and the time-data - matched model. The results for the K/s plant are given in Table 3, while those for K/s^2 are shown in Table 4. These results show not only excellent agreement with simulation results, but the result from the frequency-domain match agrees very well with the time domain

OCM pilot-related parameters	Time Match identification results	Time Match sensitivity	Frequency Match identification results	Frequency Match sensitivity
time delay, τ	.14 sec	.47	.13 sec	10.
weighting on error, q_ε	2707.	.19	2380.	.2
weighting on error, $q_{\dot{\varepsilon}}$ rate	348.	.09	377.	4.1
motor noise, c_{u_u}	-18. db	1.39	-18. db	3.2
observation noise of command, c_{y_c}	-6. db	.21	-7. db	2.2
observation noise of command rate, $c_{\dot{y}_c}$	-10. db	.68	-10. db	2.9
observation noise of error, c_ε	-11. db	.02	-11. db	3.5
observation noise of error rate, $c_{\dot{\varepsilon}}$	-10. db	.05	-10. db	3.4
neuromotor lag, τ_n	.09 sec			

Table 1. Matching Results - K/s Plant

OCM pilot-related parameters	Time Match identification results		sensitivity	Frequency Match identification result		sensitivity
time delay, τ	.10	sec	.65	.09	sec	10.
weighting on error, q_ε	2130.		.25	2320.		.1
weighting on error rate, $q_{\dot{\varepsilon}}$	319.		.18	380.		2.8
motor noise, c_{u_u}	-19.	db	1.20	-19.	db	.3
observation noise on command, c_{y_c}	-7.1	db	.48	-5.8	db	2.1
observation noise on command rate, $c_{\dot{y}_c}$	-7.5	db	.34	-9.5	db	1.4
observation noise on error, c_ε	-15.	db	.67	-11.	db	1.
observation noise on error rate, $c_{\dot{\varepsilon}}$	-9.7	db	.55	-10.	db	1.5
neuromotor lag τ_n	.20 sec					

Table 2. Matching Results - K/s^2 Plant

Table 3. Augmented State Covariance Matrix for K/s Plant

simulation result:

1.0	0.	.80	.46	θ_c(deg)
0.	2.25	−.46	.71	$\dot{\theta}_c$ (deg/sec)
.80	−.46	.93	−.1	θ (deg)
.46	.71	−.1	3.7	δ_p (in)

frequency domain match:

1.0	0.	.77	.28
0.	2.25	−.28	.91
.77	−.28	.76	0.
.28	.91	.0	3.5

time domain match:

1.0	0.	.79	.29
0.	2.25	−.29	.91
.79	−.29	.80	0.
.29	.91	.0	4.0

Table 4. Augmented State Covariance Matrix for K/s^2 Plant

simulation result:

1.0	0.	.73	.46	-.3	θ_c (deg)
0.	2.25	-.48	.13	1.8	$\dot{\theta}_c$ (deg/sec)
.73	-.48	1.27	0.	-3.	θ (deg)
.46	.13	0.	2.8	-.32	$\dot{\theta}$ (deg/sec)
-.3	1.8	-3.	-.32	35.	δ_p (in)

frequency domain match:

1.0	0.	.67	.39	-.36
0.	2.25	-.39	.36	2.0
.67	-.39	1.18	0.	-2.7
.39	.36	0.	2.7	0.
-.36	2.0	-2.7	0.	38.

time domain match:

1.0	0.	.73	.44	-.32
0.	2.25	-.44	.32	1.9
.73	-.44	1.24	0.	-3.0
.44	.32	0.	2.9	0.
-.32	1.9	-3.0	0.	41.

model, obtained by matching these statistics.

On the other hand, the frequency-matched model, as expected, matches that experimental data well, as shown in Figures 5 and 6. Note, furthermore, that the time-matched model does not do a poor job of matching this data as well.

From the above results, the following is noted:

1. The model obtained from time-domain matching is very close to the model obtained using frequency-domain data.
2. The sensitivity of the match to model parameter variations, however, differs between the time-and frequency-domain matches.
3. From the frequency-domain matches especially, the sensitivity of the match to variation in the cost function weighting on error rate, q_ε, is quite large. This indicates that including this parameter in the cost function is significant.

Multi-Axis Tracking Analysis

As a final example, we will summarize the results of an analysis of a complex multi-axis tracking task.[9] The task involves fixed-base simulated air-to-air tracking, with the display symbology as shown in Fig. 7. The sight symbol (box) is dynamic, representing a lead-computing sight. It's position relative to the fixed screen reference is defined by the coordinates λ_{EL} and λ_{AZ}. The relative position of the target is defined by β_{EL} and β_{AZ}. And the relative bank angle ϕ_{Rel} between the target and attacker is indicated by the target's bank angle on the screen. (Note, ϕ_{rel} is zero for situation shown in the figure.) The linearized system dynamics are representative of tracking during a 4g, constant altitude turn. The input (or command) driving the closed-loop

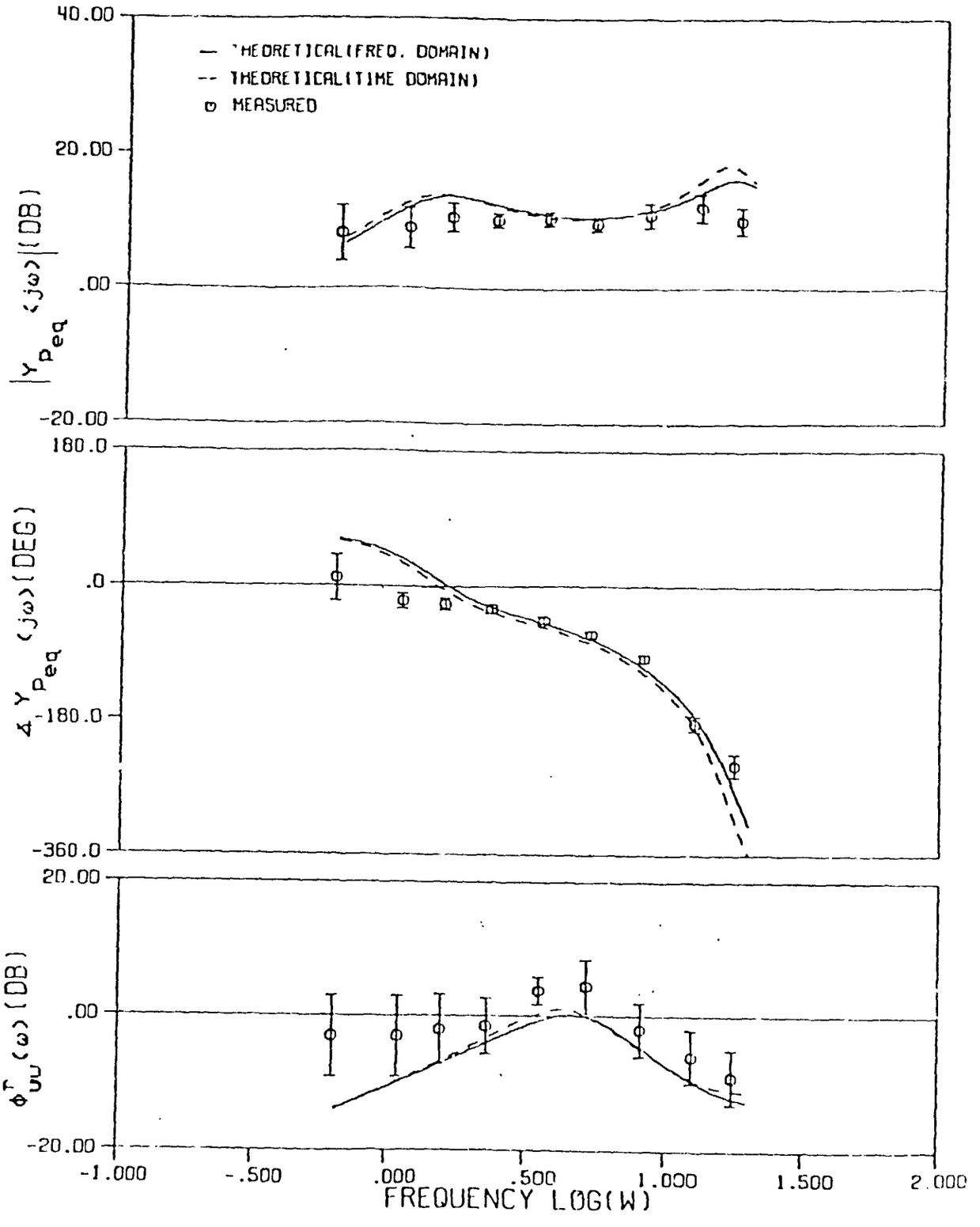

Figure 5. Human Describing Function and Controller Remnant-Correlated Spectrum of Simple Pursuit Task with k/s Plant

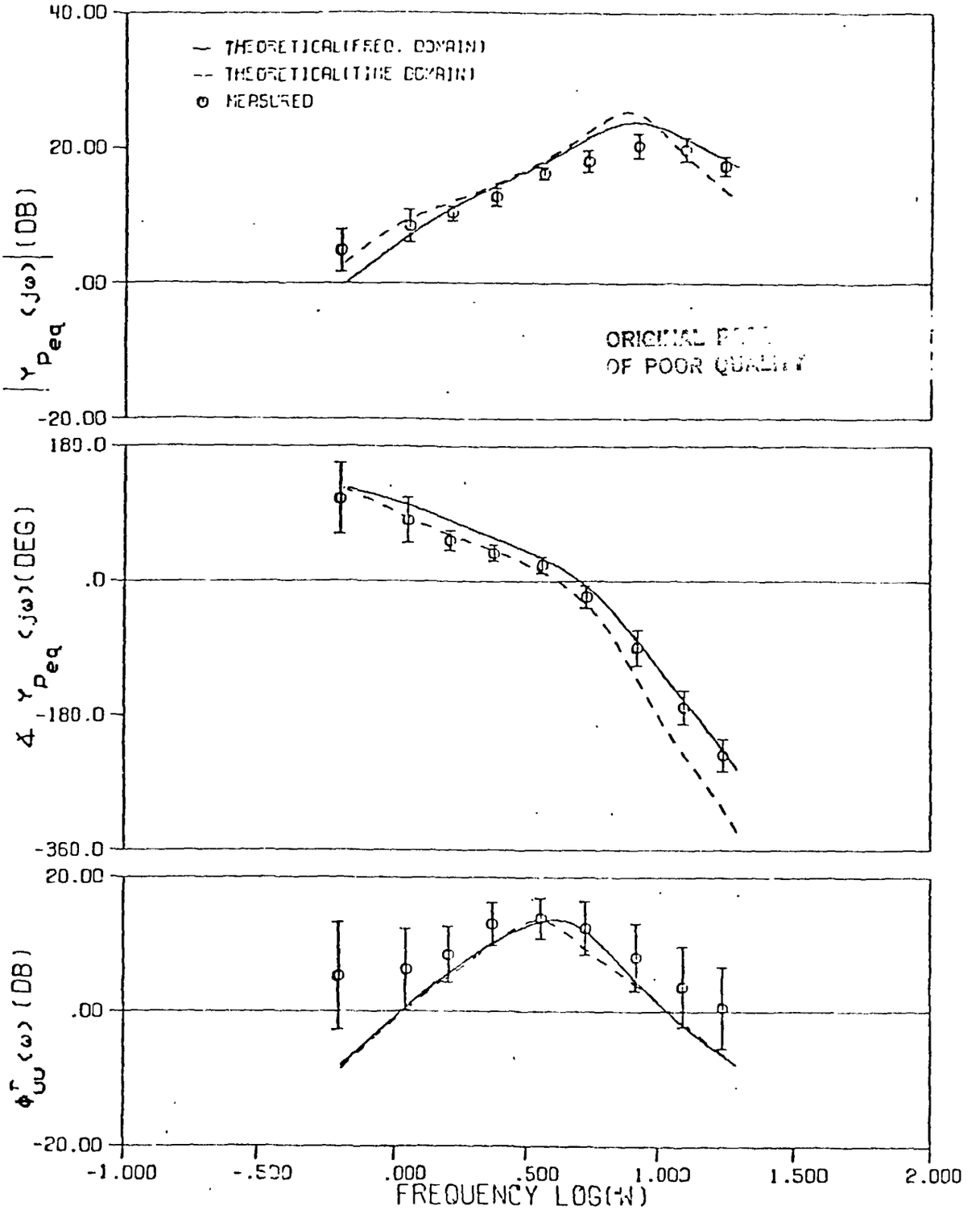

Fig. 6 Human Describing Function and Controller Remnant-Correlated Spectrum of Simple Pursuit Task with k/s^2 Plant

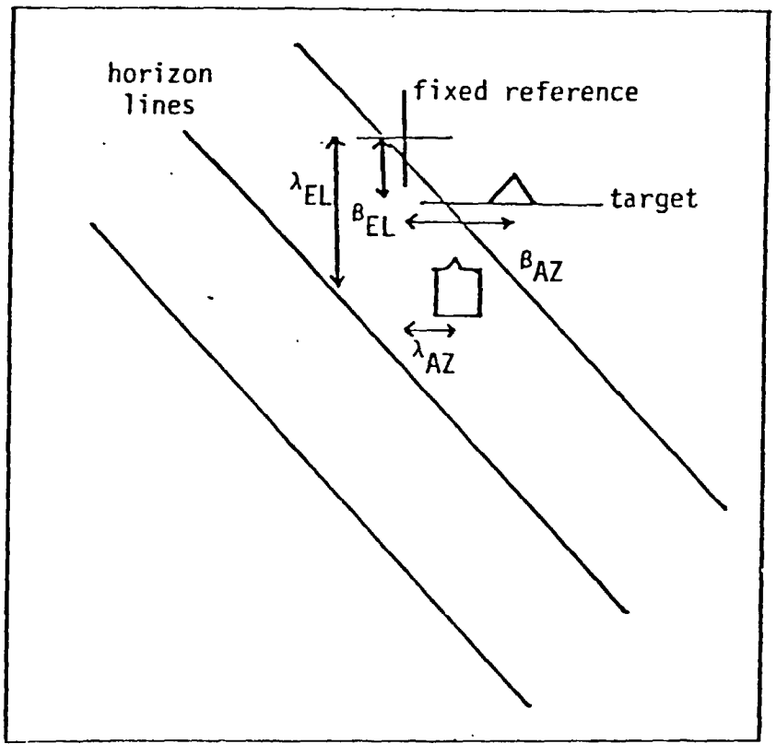

CRT Display for Multiaxis Air-to-Air Tracking Task

Fig. 7

system is the target's inertial (not relative) bank angle ϕ_T, which is generated by the relation

$$\dot{\phi}_T = -1/\tau\ \phi_T + w$$

with τ = 13 sec., and the intensity of the random w selected to yield an rms value of ϕ_T of 5.25 degrees.

One selected set of the pilot's observed variables is

$$y_p^T = [\varepsilon_{EL},\ \dot{\varepsilon}_{EL},\ \varepsilon_{AZ},\ \dot{\varepsilon}_{AZ},\ \beta_{EL},\ \dot{\beta}_{EL},\ \beta_{AZ}\ \ \dot{\beta}_{AZ},\ \phi]$$

where $\varepsilon_{(\cdot)} = \beta_{(\cdot)} - \lambda_{(\cdot)}$, tracking errors

ϕ = attacker's bank angle

Other combinations of observations could also be selected, and this set may not be optimum. Variations on this are under investigation. The pilot's control input is the stick and rudder, or δ_E, δ_A, and δ_R.

The model parameters will be estimated by a time-domain matching of the (16 x 16) state covariance matrix, including the three control inputs, obtained from several simulation runs. The parameter set to be discussed includes the (3 x 3) T_n matrix (or G_u^{-1}) associated with the three control inputs, the cost function weights

$$[q_{\varepsilon_{E1}},\ q_{\dot{\varepsilon}_{E1}},\ q_{\varepsilon_{AZ}},\ q_{\dot{\varepsilon}_{AZ}},\ q_{\beta_{E1}},\ q_{\dot{\beta}_{E1}},\ q_{\beta_{AZ}},\ q_{\dot{\beta}_{AZ}}]$$

and the noise intensities

$$(c_{\delta_E},\ c_{\delta_A},\ c_{\delta_R}) = \text{Variances on motor noises}$$

$$(c_{\varepsilon_{E1}},\ c_{\dot{\varepsilon}_{E1}},\ c_{\varepsilon_{AZ}},\ c_{\dot{\varepsilon}_{AZ}}) = \text{Variances on measurement noises}$$

The variances on the noises associated with the additional measurements

were fixed at - 13 dB after some initial studies.

As with the selected observation vector, the selection of cost function weights is based on subjective judgement, and one set may in fact be more meaningful than the other. For example, the use of a weighting on relative bank angle between target and attacker, rather than on β_{E1} and β_{AZ} could be considered. For the set selected here, however, the results are given in Table 5, and the T_n matrix is

$$T_n = \begin{bmatrix} .27 & 0 & 0 \\ 0 & .31 & -.15 \\ 0 & -.15 & .30 \end{bmatrix} \text{ (sec)}$$

for $$u_p^T = (\delta_E, \quad \delta_A, \quad \delta_R).$$

Note the relatively high sensitivity on the cost weightings on $\dot{\beta}_{EL}$ and $\dot{\beta}_{A2}$ in Table 5. This is consistent with the results of Harvey[10] in his evaluation of a similar single-axis task, in that weightings on observations in addition to tracking error and error rate were significant in obtaining a good model match. This fact is basic to the desire to be able to identify more complex cost functions, as noted in the introduction.

Finally, although this match used the simple-to-obtain state covariance matrix, comparisons or matching of frequency domain data is certainly possible if available from the experiment. If not, the frequency domain results from the model is available as a "prediction" of those human operator characteristics.

Note that slightly more general expressions for the transfer function matrices $T_{uc}(s)$, $T_{\varepsilon c}(s)$ and $T_{oc}(s)$ in Equations 5 and 6 result in the above example.[6] This arises due to the fact that the system dynamics

Table 5. Identification Result - Time Domain for Multiaxis Air-to-Air Tracking Task

OCM pilot-related parameters	identification results		sensitivity
time delay, τ	.13	sec	.2
weighting on elevation error, q_{E1}	1501.		3.4
weighting on eleva. error rate, $q_{E1}^{\cdot}$	340.		.1
weighting on azimuth error, q_A	1741.		2.4
weighting on azimu. error rate, $q_A^{\cdot}$	320.		.1
weight. on target elevation angle, $q_{\beta_{E1}}$	1575.		.2
weight. on target eleva. angle rate, $q_{\beta_{E1}}^{\cdot}$	248.		1.
weight. on target azimuth angle, q_{β_A}	1556.		.2
weight. on target azimu. angle rate, $q_{\beta_A}^{\cdot}$	226.		1.
elevator noise, c_{δ_E}	-21.3	db	2.0
aileron noise, c_{δ_A}	-20.6	db	.4
rudder noise, c_{δ_R}	-19.2	db	1.3
meas. noise on eleva. error, c_{ϵ_E}	-12.8	db	.8
meas. noise on eleva. error rate, $c_{\epsilon_E}^{\cdot}$	-13.2	db	1.4
meas. noise on azimuth error, c_{ϵ_A}	-13.3	db	1.1
meas. noise on azimu. error rate, $c_{\epsilon_A}^{\cdot}$	-13.2	db	.9

are not decoupled into command and plant dynamics, as assumed previously. As a result, the equation for $U_p(s)$ and $\varepsilon(s)$ (Eqns. 5 and 6) are developed from the relation

$$\chi(s) = [sI - \bar{A}]^{-1}[\bar{B}U_p(s) + \bar{D}W(s)]$$

where

$$\bar{A} = \begin{bmatrix} A_c & A_c' \\ 0 & A \end{bmatrix}, \quad \bar{B} = \begin{bmatrix} 0 \\ B \end{bmatrix}, \quad \bar{D} = \begin{bmatrix} D \\ 0 \end{bmatrix}$$

In the development of Eqns. 5 and 6, A_c' in $\bar{A}$ was assumed zero. With this change, the development of the desired matrices proceeds directly, along with modifying Figure 2 accordingly.

Summary and Conclusions

An approach has been presented for identifying and/or validating multi-input/multi-output models for the manual controller in complex tracking tasks. In the more general case, the conventional human describing functions may not be directly identifiable, but measurable transfer matrices directly related to the model were derived. In terms of model identification or validation, these transfer matrices are just as useful and meaningful as the conventional describing functions.

Model-parameter identification using strictly time-domain data was demonstrated to yield excellent results for the single-axis pursuit task. The use of this approach avoids the necessity of obtaining frequency domain data, sometimes a practical constraint. However, shown in Ref. 11, time-series techniques may be used effectively to obtain frequency-domain representations directly compatible with the parameter identification method presented here. Furthermore, the time-series methods

would appear to circumvent several of the practical problems in obtaining frequency-domain representations - such as the necessity to be able to define the command signal characteristics. Therefore, model parameter estimation using frequency-domain representations are certainly of interest, and will remain useful.

The results obtained from evaluation of a two-axis air-to-air tracking task with complex, high-order dynamics were briefly noted, primarily to demonstrate the type of analysis possible with this approach.

Acknowledgement

This work is being performed with the cooperation of NASA Dryden Research Facility under NASA Grant NAG4-1. Mr. Donald T. Berry is the technical monitor, and his support, and that of NASA, is appreciated.

References

1. Kleinman, D., Baron, S., and Levison, W.H., "An Optimal Control Model of Human Response, Part I: Theory and Validation," Automatica, Vol. 6, 1970, pp. 357-369.

2. Hess, R.A., "Prediction of Pilot Opinion Rating Using an Optimal Pilot Model," Human Factors, Vol. 19, Oct. 1977, pp. 459-475.

3. Schmidt, D.K., "On the Use of the OCM's Objective Function as a Pilot Rating Metric," 17th Annual Conf. on Manual Control, UCLA, June, 1981.

4. McGruer, D.T., and Krendel, E.S., Mathematical Models of Human Pilot Behavior, AGARDograph, No. 188, Jan. 1974.

5. Levison, W.H., "Methods for Identifying Pilot Dynamics," Proceedings of the USAF/NASA Workshop on Flight Testing to Identify Pilot Workload and Pilot Dynamics, AFFTC-TR-82-5, Edwards AFB, Jan. 19-21, 1982.

6. Yuan, Pin-Jar, "Identification of Pilot Dynamics and Task Objectives From Man-in-the-Loop Simulation," Ph.D. Dissertation, School of Aeronautics and Astronautics, Purdue University, May, 1984.

7. Lancraft and Kleinman, "On the Identification of Parameters in the OCM," Proc. of the Fifteenth Annual Conf. on Manual Cont., Wright State Univ., Dayton, OH, Mar. 1979.

8. Levison, "A Quasi-Newton Procedure For Identifying Pilot-Related Parameters of the OCM," Proc. of the 17th Annual Conf. on Manual Control, UCLA, Los Angeles, June, 1981.

9. Yucuis, "Computer Simulation of a Multi-Axis Air-to-Air Tracking Task and the Optimal Control Pilot Model," M.S. Thesis, School of Aeronautics and Astronautics, Purdue University, Dec., 1982.

10. Harvey, T.R. "Application of an Optimal Control Pilot Model to Air-to-Air Combat," AFIT Thesis GA/MA/74M-1, Mar., 1974.

11. Biezad, D. and Schmidt, D.K., "Time Series Modeling of Human Operator Dynamics in Manual Control Tasks," Proc. of the 20th Annual Conf. on Manual Cont., NASA Ames Research Center, CA, June, 1984.

N85 14495

STRUCTURE ERRORS IN SYSTEM IDENTIFICATION*

G. A. Bekey and F. Y. Hadaegh
Department of Electrical Engineering-Systems
University of Southern California
Los Angeles, California 90089-0781

1. INTRODUCTION

System identification is concerned with the determination of a model whose behavior approximates that of a given physical system as closely as possible, under approximately restricted experimental conditions. In practice, linear system identification is often separated into two parts: (a) determination of the order of the optimum linear model, and (b) estimation of the parameter values of the resulting linear model. Clearly, in a linear system, the model structure is determined by the choice of order. However, when the system is not linear and the nonlinearities are either omitted or incorrectly represented in the model, erroneous estimates of parameters may be obtained. This problem, i.e., the effect of erroneous assumptions of model structures on parameter values has received inadequate attention in the past. A number of books (e.g., [1]) describe variety of algorithms for system identification. The effect of erroneous assumptions of model structure generally shows up in the covariance matrix of the estimated parameters. However, this is at best an indirect indication, since an increase in the variability of the estimated parameters may also be due to a neglect of time variations and other factors. Incorrect structure assumptions may also manifest themselves in the goodness of fit criteria by which the quality of the model is judged. Thus, an incorrect structural assumption may produce a worse agreement between model outputs and system outputs. It is important to note that this is not always the case since it may be possible for the identification algorithm to select incorrect parameter values in order to compensate for erroneous assumptions of structure. This paper is concerned with an approach to system identification which explicitly takes structure errors into account and hence provides a systematic way for answering questions concerning the magnitude of estimated parameter errors resulting from structural errors.

2. FORMULATION OF THE PARAMETER IDENTIFICATION PROBLEM

Assume that there exists a physical process (the system) with inputs $u(t)$ and outputs $y_p(p)$, which are measurable. We characterize the process by the assumed mathematical model

$$\dot{x}_m(\theta,t) = f(x_m(\theta,t),u(t),x_0,\theta,t) \qquad (1)$$

*This research was supported by the National Science Foundation under Grant No. NSF 8200382.

and

$$y_m(\theta,t) = g(x_m(\theta,t),\ u(t),\ x_0,\ \theta,\ t) \tag{2}$$

where the dimensions of the vectors x, y, u and θ are n, m, r and q respectively. x_m represents the state of the model while y_m are the model outputs. The function $f(\cdot)$ represents our assumption about the structure of the process, while the function $g(\cdot)$ represents the measurement operations. Equations (1) and (2) are in fact a class of models which is parameterized by the vector θ. Hence, the process of parameter identification leads to a selection of a member of this set of models, on the basis of observations of inputs and puts of both process and model.

In the real world our assumption of model structure is never in complete agreement with that of the process itself [2]. Let us assume that we can represent the structural difference between model and process by means of an additive term. Furthermore, process measurements are always more or less corrupted by noise so that an "ideal model," which accurately and completely represents the process, will be given by

$$\dot{x}_p(\theta^*,t) = f(x_p(\theta^*,t),u(t),x_0,\theta^*,t) + e_s(\theta^*,t) \tag{3}$$

and

$$y_p(\theta^*,t) = g(x_p(\theta^*,t),u(t),x_0,\theta^*,t) + v(t) \tag{4}$$

The term $e_s(\theta^*,t)$ specifies the modeling or structural error which represents our lack of complete knowledge. It can be considered deterministic or stochastic. Measurement noise, v(t), is included in equation (4) for completeness but will be assumed to be zero for the moment. The symbol θ^* represents the true parameter values of the system. Clearly, the ideal model of equations (3) and (4) can never be known exactly in practice, but it forms a reference against which actual models, like equations (1) and (2), can be judged. In this case the ideal model corresponds to the "base model" defined by Zeigler [3]. The relation between the system true model and the class of models under consideration is illustrated in Figure 1.

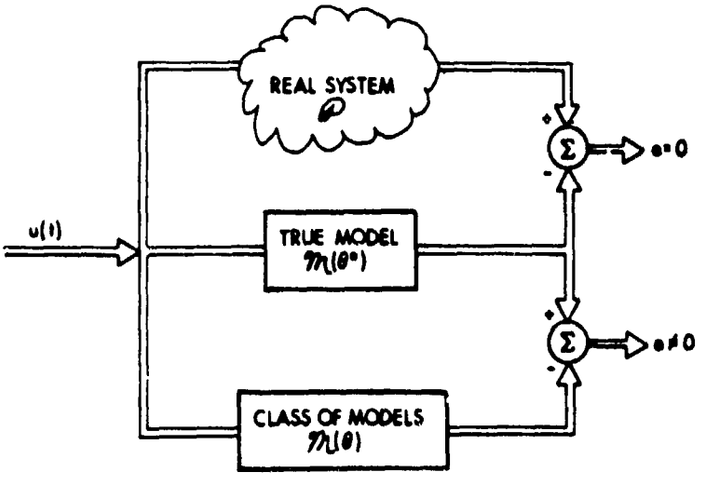

Figure 1

3. THEORETICAL IDENTIFICATION

We now define the theoretical identification problem as follows, following Zadeh [4]:

Given (a) a physical process under test, (b) a class of inputs u(t), (c) a class of models $\mathcal{M}(\theta)$.

From input/output observations of $\mathcal{P}$ determine a member of $\mathcal{M}$ which is equivalent to $\mathcal{P}$, in the sense that its responses to all $u(t) \in \mathcal{U}$ are identical to those of $\mathcal{P}$, i.e.,

$$y_p(t) \equiv y_m(t) \quad \forall\, u(t) \in \mathcal{U},\ t \in [0,T] \tag{5}$$

It is evident that the solution of this identification problem is only possible if both measurement noise and structural error are identically equal to zero. If only one parameter value θ exists for which such a solution is possible, the model is set to be globally identifiable [5].

Much controversy exists in the literature concerning the theoretical identification problem. It seems to us that such problems, while interesting, have very limited usefulness in the real world.

4. PRACTICAL IDENTIFICATION

In practice, of course, the modeling error is never identically zero, and hence the model outputs can only approximate the process outputs. Let us define a scalar criterion function, $J(\mathcal{M}(\theta), \mathcal{P})$ which is a measure of the match between y_p and y_m. We can then define the real world identification problem as follows:

Definition 1. Given

(a) a physical process under test, $\mathcal{P}$
(b) a class of inputs $\mathcal{U} = \{u\}$
(c) a class of models $\mathcal{M}(\theta)$ characterized by equations (1) and (2)
(d) a criterion function $J_p(\mathcal{M}(\theta), \mathcal{P})$
(e) an allowable modeling error ϵ_p.

The real world identification problem consists of the determination, on the basis of input and output observations of $\mathcal{P}$ and $\mathcal{M}(\theta)$, of a model parameter vector θ for which

$$J_p(\mathcal{M}(\theta), \mathcal{P}) \leq \epsilon_p$$

where ϵ_p is the allowable process identification error. If such a parameter vector can be found, we shall term the process R-W identifiable.

Note that this definition does not require exact agreement between model and process outputs. In fact, now define the notion of near equivalence by specifying a magnitude on the norm of the difference between model and process outputs. If we select a value for this norm, say δ, then we can state that:

Given that

$$\|y_p(t) - y_m(\theta,t)\| \leq \delta \tag{6}$$

the model and process are nearly equivalent. Note that criterion function appearing in Definition 1 may be the same as equation (6), or it may be an alternate criterion which measures the quality of approximation of the behavior of the process and the model. In any case, it is evident that if equation (6) is used for the criterion function in Definition 1, then we can state that models which are nearly equivalent to a given process are also R-W identifiable.

5. RELATIONS BETWEEN MODELS

In practice, we frequently approximate the model of equations (3) and (4) by a simpler and more tractable set of equations. For example, we may choose to approximate (3) by the linear model:

$$\dot{z}(\theta,t) = A(\theta)z(t) + B(\theta)u(t) + e_s'(\theta,t) \tag{7}$$

$$y_m(t) = C(\theta)z(t) + D(\theta)u(t) \tag{8}$$

where it is assumed that measurement errors are negligible. The new structural error $e_s'(\theta,t)$ in eq. (6) now includes the effects of model simplification. Similarly, a linear high-order model may be approximated by a lower-order linear model. Let us assume that such a simpler class of models can be found, without reducing the order of the parameter vector θ, (the argument which follows can be extended to the case where the simpler model has fewer parameters than the complex model).

Consider a complex model $\mathcal{M}_1$ of the process which is being approximated by a simpler model $\mathcal{M}_2$. Under these conditions, even in the absence of measurement noise, the models $\mathcal{M}_1$ and $\mathcal{M}_2$ will not be equivalent, since the outputs y_{m_1} of $\mathcal{M}_1$ will not be identical to the outputs y_{m_2} of $\mathcal{M}_2$ for all time in the interval of observation.

To make these ideas more precise, consider model $\mathcal{M}_1$ with parameter vector θ and model $\mathcal{M}_2$ with a different structure but the same parameter vector.

We now now define the relation between these two models independent of the quality of their approximation to the physical process.

Definition 2. Model-Model Near Equivalence (MMNE)

Two models $\mathcal{M}_1$ and $\mathcal{M}_2$ with different structures and with outputs y_{m_1} and y_{m_2} respectively are termed model-model nearly equivalent if there exists a criterion $J_m(\mathcal{M}_1(\theta), \mathcal{M}_2(\theta))$ and appropriate bounds ϵ_m and δ_m such that

$$|J_m(\mathcal{M}_1(\theta), \mathcal{M}_2(\theta) \leq \epsilon_m \quad \text{and} \tag{9}$$

$$\|y_{m_1}(\theta,t) - y_{m_2}(\theta,t)\| \leq \delta_m \tag{10}$$

A further discussion of the near-equivalence concept and its implications is given in [6].

6. SOME SIMPLE EXAMPLES

Consider first an electrical circuit as illustrated in Fig. 2a. This is a diagram of the process. It contains a condenser with capacitance θ_1, a coil with inductance θ_2 and a small resistor R in series. Over a given range of frequencies we assume that the current in the circuit is described by the equation (the "true" model):

$$\theta_2 I''(t) + R\, I'(t) + (1/\theta_1) I(t) = 0 \tag{11}$$

$$I(0) = I_0\,, \qquad I'(0) = I_0'$$

If we neglect the small resistance of the circuit (which may represent the resistance of the coil), we obtain a model equation

$$\theta_2 i''(t) + (1/\theta_1) i'(t) = 0 \tag{12}$$

$$i(0) = I_0\,, \qquad i'(0) = I_0'$$

If one is interested in the solution only on a short time interval, the solutions of (11) and (12) may be very close. We can select a modeling error ϵ_p such that

$$|I(t) - i(t)| \leq \epsilon_p \tag{13}$$

It is evident that (13) will be satisfied only over an interval (t_0, t_f). If, however, the final time t_f is allowed to increase, the two solutions will differ since $I(t) \to 0$ as $t \to \infty$ while $i(t)$ performs periodic oscillations with constant amplitude. The neglect of R represents the structural error and can lead to qualitatively different behavior as $t_f \to \infty$. The solution of (12) and (13) as well as the left hand side of (13) are plotted in Figure 3.

As a second example consider a linear process with time delay described by the process equation

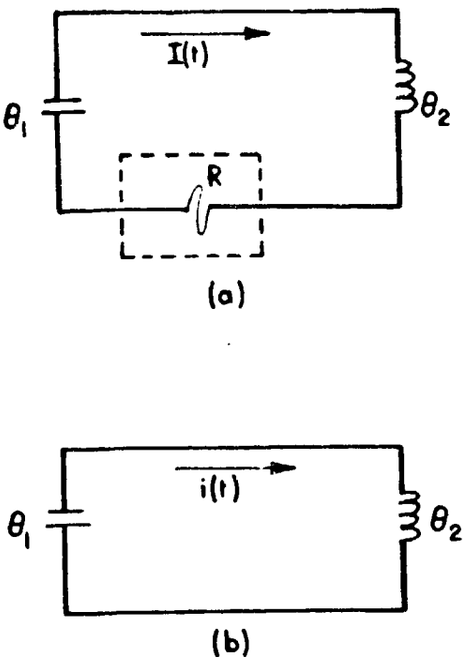

Figure 2

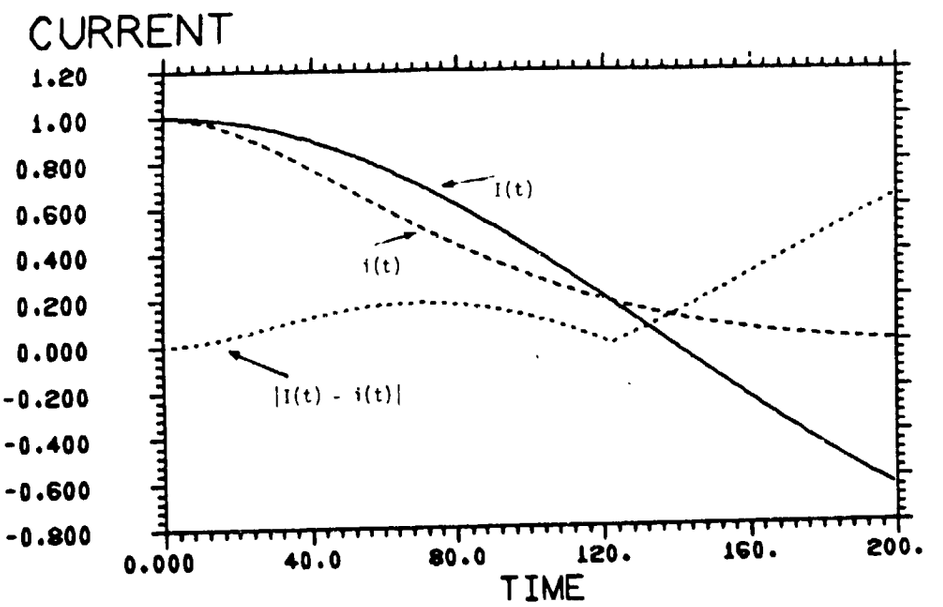

Figure 3

$$\dot{x}_p = a^* x_p + b^* u(t) + c^* x_p(t-\tau) \tag{14}$$

We assume that both c^* and τ are small and model the system as

$$\dot{x}_m = a\, x_m + b\, u(t) \tag{15}$$

where both (14) and (15) have zero initial conditions. In order to examine the effect of the structural error we compare the transfer functions of model and process. Since the time delay is small, we approximate the Laplace transform of the delay by

$$e^{-\tau s} \cong 1-\tau s \tag{16}$$

which leads to

$$G_p(s) = \frac{X_p(s)}{U(s)} = \frac{b^*/(1+\tau c^*)}{s - \left(\frac{a^* + c^*}{1 + \tau c^*}\right)} \tag{17}$$

while the model transfer function becomes

$$G_m(s) = \frac{X_m(s)}{U(s)} = \frac{b}{s - a} \tag{18}$$

Comparison of (17) and (18) reveals that identification of the model leads to incorrect values of the parameters a and b due to the structural error. Even if the identification is exact, the resulting values will differ from the "true" values a* and b* by terms which depend on the structural error parameters τ and c*.

The above examples are very simple, but they illustrate the nature of the problem.

7. THEORETICAL RESULTS

An extensive theoretical analysis of the structural error problem has been performed for both the deterministic and stochastic case [7]. The major results in [7] can be summarized as follows:

A. Solution Error Bounds

If the time dependence of the structural error $e_s(t)$ is given, it is possible to express the solution error as a function of $e_s(t)$, i.e.,

$$|\delta y(t)| = |y_p(t) - y_m(t)| = g(e_s(t))$$

under appropriate conditions.

B. Near Equivalence

Necessary and sufficient conditions under which process and model are

near-equivalent have been found, i.e., for a given ϵ,

$$|y_p(t) - y_m(t)| \leq \epsilon$$

C. For given values of maximum structural error $e_{s\ max}$ and solution error $|\delta y|_{max}$, bounds on the solution time have been obtained.

D. RW-Identifiability

Conditions under which the given class of models is real-world identifiable in the sense of Def. 2 have also been obtained.

The discussion of these results is beyond the scope of this paper. However, they will be published in the near future [8,9].

8. CONCLUSION

This short paper has presented a point of view on modeling and identification which includes (rather than evading) the structural difference between models and systems. We have indicated that, from this point of view, it is possible to define "near-equivalence" between process and model and to obtain meaningful theoretical results on solution error and system identification. It remains to apply these results to large realistic problems such as those involving models of complex man-machine systems.

REFERENCES

1. Eykhoff, P., "System Identification, Parameter and State Estimation," Wiley, London, 1974.

2. Bekey, G. A., "Models and Reality: Reflections on the Art and Science of Simulation," Simulation, 29; 161-164, January 1978.

3. Zeigler, B. P., Theory of Modeling and Simulation, Wiley, 1976.

4. Zadeh, L.A., "On the Identification Problem," Trans. AIEE, AC-8; 255-256, 1956.

5. DiStefano III, J.J. and Cobelli, C., "On Parameter and Structural Identifiability," IEEE Trans. Automatic Control, AC-25; 830-833, Aug. 1980.

6. Bekey, G.A. and Hadaegh, F.Y., "Equivalence Problems in Structural Identifiability," Math. and Comp. in Simulation, 24: 460-465, 1982.

7. Hadaegh, F.Y., "The Effects of Structural Error on Parameter Identifiability of Dynamical Systems," Ph.D. Dissertation, Department of Electrical Engineering, University of Southern California, June 1984.

8. Hadaegh, F.Y., and Bekey, G.A., "Structural Error and Identifiability," Proceedings of 7th IFAC Symposium on the System Identification and Parameter Estimation, 1985 (to appear).

9. Hadaegh, F.Y., and Bekey, G.A., "Near-Identifiability of Dynamical Systems," to appear in the Journal of Mathematical Biosciences.

N85 14496

Effects of Control Stick Parameters on Human Controller Response

D. W. Repperger*, W. H. Levison**

* Air Force Aerospace Medical Research Laboratory
Wright Patterson Air Force Base, Ohio 45433
** Bolt, Beranek, and Newman Inc., Cambridge, Massachusetts 02238

Abstract

Much interest has arisen on the comparison of the effects of force versus displacement sticks on pilot tracking ability. To investigate this effect, a fixed base laboratory tracking study was conducted to determine the effects of stick displacement and stick force characteristics on human tracking performance. Three different levels of control stick force/displacement characteristics and stick electrical gain were varied to observe their influence on RMS (Root Mean Square) tracking error and RMS control activity (stick output).

The results of this study indicated that both RMS tracking error and RMS control activity were influenced by the three different levels of control stick force/displacement characteristics and stick electrical gain. One method of investigating human controller response is to study the empirical data obtained from this experiment and to compare it to the Optimal Control Pilot Model (OCPM) which represents standard forms of human response. Fitting the Optimal Control Pilot Model to these data showed that the effect of changing electrical control gain markedly changed the motor time constant parameter of the OCPM. In model fitting these data for changes in the force/displacement characteristics of the stick, the time delay parameter of the OCPM had to be changed significantly so that the empirical data would match the model. In summary, this paper reports that the human neuromotor time constant was affected by the electrical control gain of the stick while the spring stiffness of the stick influenced the time delay characteristics of the human response behavior.

Introduction

Direct control of translational modes is being designed into certain high-performance fighter aircraft to enhance maneuverability in air-to-air combat situations. The ability of the pilot to control such a vehicle is affected by the presence of biomechanical feedback between the airframe and the control stick [1]*. For example, if the pilot commands lateral translation (i.e., side force), the aircraft will accelerate in the commanded direction, but the inertia of the arm/hand/stick system will act on the stick to partially cancel out the intended input. Laboratory studies suggest that such biomechanical coupling will tend to degrade performance in an air-to-air tracking task (Korn and Kleinman, [2]).

The Air Force has conducted studies to develop methodologies for

* A more detailed version of this paper can be found in reference [1].

the optimal design of control sticks in high-acceleration environments. While near-optimal tracking performance can usually be obtained for a wide range of stick parameters in a fixed-base tracking task, the presence of biomechanical coupling can appreciably narrow this range when the task is performed in a high-acceleration environment (Korn and Kleinman [2]). Some initial work has been done to develop a design methodology using the combination of a pilot/vehicle performance model and a model for biomechanical coupling (Levison and Houck [3], Jex and Magdaleno [4], Levison, [5]).

Levison and Houck [3] used the optimal control model (OCM) for pilot/vehicle systems as the basis for their combined model, and they suggested that control-stick characteristics be accounted for partly by the structure of the quadratic performance criterion used in obtaining a model solution, and partly by the introduction of a second-order dynamical submodel to represent the pilot/stick interface. They also recommended that further studies be undertaken to refine and validate the aspects of the OCM related to motor limitations.

The purpose of the study discussed herein was to provide a detailed look at the pilot/stick interface as suggested in Levison and Houck [3]. A fixed base laboratory study was conducted with the major experimental variables being stick force/displacement characteristics and electrical control gain. Both parameters were varied over a sufficiently wide range to exceed optimality.

Description of The Experiment

Nine test subjects ranging in age from 24 to 39 years participated in a fixed-base laboratory experiment involving tracking. Laterally-directed control forces resulted in lateral movement of a cursor displayed electronically in an inside-out format. Tracking dynamics were pure rate control (K/s) plus an effective time delay of 80 msec induced by the simulation and display apparatus. A sum-of-sines forcing function was designed to simulate a first-order noise process having a break frequency at 4 rad/sec. The forcing function was treated as a vehicle disturbance and was injected in parallel with the operator's control input. Additional experimental details may be found in Repperger, et al., [6].

The principle experimental variables were control stick mechanical characteristics (i.e. force/displacement relationship) and electrical gain. Three mechanical configurations were explored: a nearly isometric "force stick", a "strong displacement stick" having significant displacement and a modest force restraint, and "weak displacement stick" having significant displacement and a relatively small force restraint.

Three electrical gains were explored for each stick configuration. A mid-range gain was selected to lie within the optimal gain range; a gain approximately one tenth the optimal gain was selected to require

substantial control forces and/or displacements; and a gain approximately nine times the optimal gain was selected to explore effects of motor-related limitations such as tremor.

Table 1 shows the force/displacement characteristics and electromechanical gains of the nine control-stick configurations. The force/displacment ratio was essentially infinite for the force stick, .071 pounds/ degree for the strong displacement stick, and about .014 pounds/ degree for the weak displacement stick.

The fourth and fifth columns of Table 1 show the electrical control gains in terms of volts of effective control input per mechanical unit (pounds force or degrees displacement). Control requirements on the part of the pilot, however, are best seen from the last two columns, which show the amount of physical activity required to generate 1 volt of control input - approximately the average force level generated by the test subjects in the experimental study. Force requirements range from about 0.2 to 15 pounds for the force stick configurations. Required forces decrease by nearly an order of magnitude for the strong displacement stick and by another factor of 5-6 for the weak displacement sticks. Displacement requirements for both displacement sticks range from about 0.3 to about 25 degrees per volt control input.

Table 1 - Control Stick Characteristics

Configuration		Mechanical and Electrical Characteristics				
Stick	Gain	Force/Disp.	Volt/Lb.	Volt/ Deg.	Lb/Volt	Deg/Volt
Force	Low	∞	.0673	—	14.9	—
	Mid		.797		1.25	
	High		4.24		0.236	
Strong Disp.	Low	0.0714	0.572	.0403	1.75	24.8
	Mid		5.18	.375	0.193	2.67
	High		46.6	3.37	0.022	0.297
Weak Disp.	Low	0.0138	2.87	0.0403	.348	24.8
	Mid		27.3	.374	.037	2.60
	High		246.	3.37	.004	.297

Experimental Results

Performance Scores

Standard deviation (SD) scores were computed from time histories of the tracking error and of the pilot's control input. These scores were computed first from individual time histories, and then averaged across replications to obtain mean SD scores for each subject, each condition. These within-pilot average scores were then averaged across pilots to yield population means and an across-subject standard deviations of the SD scores for each experimental condition. These statistics were then subjected to paired-difference t-tests to determine the statistical significance of changes in mean performance resulting from changes in experimental conditions. A test on outliers was performed jointly on two variables (the error and control SD

scores.). A value of L=3.0 standard deviations was selected to reflect (cf. Levison and Muralidharan [7]) a 1% probability criterion of a trial being outside the normal population. Thirteen outliers were identified out of a data base of 243 experimental trials.

The effects of stick configuration on error and control SD scores are illustrated in figure (1). Response variables are shown in physiological units; error scores in degrees visual arc, and control scores in both pounds force and degrees displacement. Figure (1a) illustrates that slightly lower error scores were obtained for the force stick than for either of the displacement sticks for the mid-range (baseline) electrical gains. Low control gain degraded performance of the force stick configuration, whereas high gain degraded performance for both displacement-stick configurations.

Figure (1b) shows that control force scores varied by almost two orders of magnitude with electrical gain for a given manipulator, and by over three orders of magnitude across the entire experiment. Because of this large variation, control SD scores have been plotted on a logarithmic scale.

As anticipated, control effort (force and displacement) varied inversely with electrical gain. Control forces decreased with decreasing force/displacement ratios. Control displacements, however, were similar for both displacement sticks.

Paired-difference t-tests were performed on the SD scores to indicate the statistical significance of performance changes with changes in force/displacment characteristics and electrical gain. Table 2a shows the alpha significance levels obtained by comparing pairs of electrical gains for each control stick; Table 2b shows the results of comparing control sticks for each relative gain level. Differences yielding an alpha level of .05 or less are considered "significant" in the ensuing discussion. The following trends were observed:

1. Control scores consistently increased with electrical gain.
2. For each control stick, minimum (or near-minimum) tracking error was achieved with the mid-range mechanical gain.
3. Force/displacement characteristics had less of an influence on performance then the electrical control gain.

Frequency Response

Analysis procedures followed in previous laboratory tracking studies (Levison, [8]) were employed to compute estimates of the linear portion of the pilot's response strategy (gain and phase shift) as well as estimates of the stochastic portion ("pilot remnant"). The sum-of-sines type of input used in the experiments facilitated decomposition of the tracking error and the pilot's control response into input-correlated and remnant-related components. Comparison of input-correlated spectral estimates with estimates of remnant at neighboring frequencies provided a means for determining the reliability of the describing function measurements. A gain or phase

TABLE 2. RESULTS OF PAIRED-DIFFERENCE T-TESTS ON SD SCORES

a) Effects of Electrical Gain

Basis for Comparison

VARIABLE	Force			Strong Disp.			Weak Disp.		
	LOW, MID	HIGH, MID	HIGH, LOW	LOW, MID	HIGH, MID	HIGH, LOW	LOW, MID	HIGH, MID	HIGH, LOW
Error	.001	--	.001	--	.01	.02	--	.01	.01
Err. rate	.01	.01	.001	.02	.001	.001	.01	.05	.02
Control	.001	.01	.001	.02	.001	.001	.01	.01	.01
Ctr. rate	.01	.001	.001	.01	.001	.001	.01	.001	.001

b) Effects of Force/Displacement Characteristics

Basis for Comparison

VARIABLE	Low Gain			Mid Gain			High Gain		
	FS, SDS	FS, WDS	SDS, WDS	FS, SDS	FS, WDS	SDS, WDS	FS, SDS	FS, WDS	SDS, WDS
Error	--	--	--	.02	.01	--	.001	.01	--
Err. rate	.02	.01	--	--	.02	--	.001	.05	--
Control	.05	.01	--	--	--	--	.001	.01	--
Ctr. rate	.01	.01	--	--	.02	--	.001	.01	--

Entries show alpha levels of significance.

Dash indicates alpha greater than 0.05.

* From Reference [27]

measurement was considered valid at a given frequency only if the input-correlated power was at least 6 db greater than the corresponding average remnant power for both the error and control signals.

The effects of electrical control gain on frequency response measures are shown in figure 2 for the three mechanical stick configurations. Figure 3 shows the effects of force/displacement characteristics on frequency response, with the electrical gain at the mid (and presumable near-optimal) level for each configuration. For all figures, 0 db gain represents one control/volt/degree tracking error and 0 db remnant represents a power density of 1 volt^2 per radian/second.

Overall, increasing the control gain from the smallest to greatest values results in significant increases in pilot gain and remnant, and small decreases in phase lag. These effects differed in detail, however, across the stick configurations. Taking the mid control gain as a reference condition, Figure 2 shows that a decrease in control gain resulted in a substantial decrease in pilot gain at all frequencies, and a decrease in pilot remnant at high frequencies. An increase in control gain produced the opposite trends, but the effects were considerable smaller.

Taking the mid control gain as the reference condition, figures 4 and 5 show that, for the displacement sticks, an increase in control gain produced the greatest effects. The major effect was to increase pilot remnant at all frequencies; small increases in pilot gain were also seen. Smaller effects were obtained when the control gain was lowered with remnant reductions occurring mainly at the higher measurement frequencies.

Figure 3 shows frequency response trends consistent with the trends of the error scores; namely, that tracking response degrades as the restoring spring constant is reduced. Specifically, the largest pilot gain, least phase lag, and least remnant were observed for the force stick; and the lowest gains, greatest phase lags, and greatest remnant were found for the weak displacement stick. In general, these effects were smaller than the differences caused by varying control gain.

Model Analysis

As part of the procedure for developing a predictive model for closed-loop performance, the data presented above were further analyzed in order to identify independent (or "pilot related") parameters of the optimal control model (OCM) for pilot/vehicle systems.

Identification of Pilot Related Parameters

A quasi-Newton gradient search procedure was employed to identify the following five model parameters: (1) Observation noise variance associated with perception of error displacement, (2) Observation noise variance associated with perception of error rate,

(3) Motor noise covariance, (4) Time delay, and (5) Relative "cost" weighting on control-rate variance.

No constraints were placed on these parameters during the search, other than the requirement that they remain positive. The control-rate cost coefficient was converted to an equivalent "motor time constant". The resulting parameters of interest, and their units are defined in table 3:

TABLE 3 - OCM PARAMETERS IDENTIFIED BY THE QUASI-NEWTON PROCEDURE

Pe = Observation Noise/Signal Ratio on Tracking Error, dB
Pė= Observation Noise/Signal Ratio on Error Rate, dB
Pm= Motor Noise/Signal Ratio, dB
Td= Effective Operator Time Delay, seconds
Tm= Motor Time Constant, seconds

Exploration of Alternative Model Parameterization

Alternative model structures were also explored in an attempt to find a set of invariant "pilot related" parameters that would account for the effects of both force/displacement characteristics and electrical control gain.

The independent model parameters identified for each experimental condition are shown in figure 6. The observation noise/signal ratios associated with error and error rate were averaged to provide a composite observation noise/signal ratio. Qualitative tests for statistical significance (discussed in [8,9]) showed that, for all three mechanical stick configurations, the motor time constant was the parameter most significantly influenced by electrical control gain, observation and motor noise/signal ratios collectively were less significantly influenced, and time delay differences were not significant. On the other hand, changes in the stick force/displacement characteristics (for a given relative electrical gain) had a significant influence only on the time delay parameter.

This effort focused on explaining the apparent task-related changes in two parameters: motor time constant, and time delay. The mathematical formulation of the OCM was not modified in this exercise; rather, alternative parameterizations consistent with the existing model framework were explored. The approach adopted by Levison and Houck [3] was pursued: the performance index was modified to include true penalties on control activity, and second-order models were explored for the man/stick interface.

The following four mutually-exclusive hypotheses were tested:
1. The cost coefficient associated with control-rate variance represents a true penalty for generating physical control activity. Thus the data should be explained by a cost function of the following form:

$$J = \sigma^2_e + G\,\sigma^2_{\dot{u}} \qquad (1)$$

2. The cost coefficient associated with control-rate reflects both a response bandwidth limitation and a penalty on rate-of-change of control force.

3. The performance index includes penalties on error, control, and control rate. Thus,

$$J = \sigma^2_e + R\,\sigma^2_u + G\,\sigma^2_{\dot{u}} \qquad (2)$$

4. The performance index includes penalties on error, control, and control rate as before, except the penalty is associated with rms control, not control variance. Thus,

$$J = \sigma^2_e + r\,\sigma_u + G\,\sigma^2_{\dot{u}} \qquad (3)$$

To test the last three hypotheses, a fixed value of Tm was selected on the basis of the original identification, the coefficient relating to physical control activity (G,R, or r) was identified for each of the force stick conditions, the average value for this control-related coefficient was computed, and matching error ratios were identified. To determine matching errors, an average "G" was identified for each of the three stick conditions by the gradient search scheme. Then using a fixed value of G to re-identify the remaining model parameters, new matching errors were computed. These new matching errors were normalized with respect to the original matching errors to provide a measure of the degradation in model-matching capability resulting from the assumption of a fixed penalty on physical control activity.

The matching error ratio (MER) [8,9] provides a qualitative test for significance. That is, if any MER obtained when testing a given hypothesis is greater than some criterion level, we consider the model match to be "significantly" worse than the baseline match (i.e., no constraints on the independent model parameters), and therefore grounds for rejecting the hypothesis. A matching error ratio of 1.4 was selected as the criterion to provide a treatment consistent with similar model applications in previous studies.

Table 4 shows that the simplest hypothesis (consistent penalty on physical control rate) provided the least good match to the data (maximum MER of 3). The most consistent results were obtained with the hypothesis that the human operator is characterized by a fixed motor time constant and a fixed penalty on rms control force. In this case, the MER ranged from less than unity to 1.3 for the three conditions tested. Less consistent results were obtained with the hypothesis that the invariant parameters are motor time constant and penalty on control-force variance, where a maximum MER of 1.7 was obtained.

Table 4 - Tests of Hypotheses Concerning Invariant Control Related Model Parameters

Electrical Control Gain	Hypothesis			
	1	2	3	4
Low	3.0	1.2	1.9	<1
Mid	1.1	1.7	---	1.3
High	3.4	1.3	---	1.1

Summary and Conclusions

A fixed-base laboratory study of mechanical and electrical control-stick parameters yielded the following major results:

1. Effective control input to the plant increased with electrical control gain for the three mechanical sticks explored. This was initially modeled as a change in the time constant.
2. For each mechanical control stick, minimum or near-minimum tracking error was achieved with the mid-range gain.
3. Force/displacement characteristics had less of an influence on performance than did the control gain. These effects were modeled largely by changes in effective time delay.
4. The quadratic performance index was revised by including a penalty on RMS control activity. A greater degree of parameter invariance was obtained from the modeling.
5. Attempts to find an invariant set of model parameters to account for mechanical stick parameters were unsuccessful. A second-order mass spring/damper submodel for the pilot/stick interface was explored, but a reasonable selection of parameters yielded effects that were substantially greater than those found experimentally. The notion of a second-order stick interface submodel need not be ruled out. The parameterization of such a model, however, should take account of the pilot's active control over his effective spring constant and damping characteristics; measurement of such parameters in a strictly passive setting are likely to be inadequate.

References

[1] Levison, W.H., "Effects of Control Stick Parameters on Human Controller Response", Report No. 5510, Bolt, Beranek, and Newman, Inc., January, 1984.

[2] Korn, J. and Kleinman, D.L., "Modeling Lateral Acceleration Effects on Pilot Performance", Proc. of The Sixteenth Annual Conference on Manual Control, Cambridge, MA, pp. 340-349, May, 1980.

[3] Levison W.H., and Houck, P.D., "Guide For The Design of Control Sticks in Vibration Environments", AMRL-TR-74-127, February, 1975.

[4] Jex, H.R., and Magdaleno, R.E., "Biomechanical Models For Vibration Feedthrough To Hands and Head For a Semisupine Pilot", Aviation Space and Environmental Medicine, vol. 49, No. 1, pp. 304-317, January, 1978.

[5] Levison, W.H., "Model For Human Controller Performance in Vibration Environment", Aviation Space and Environmental Medicine, vol. 49, No. 1, pp. 321-327, January, 1978.

[6] Repperger, D. W., Levison, W.H., Skowronski V., O'Hear, B., Frazier, J.W., and Hudson, K.E., "Stick Controller Design For Lateral Acceleration Environments", Proc. of The Eighteenth Annual Conference on Manual Control, Dayton, Ohio, June, 1982, pp. 427-440.

[7] Levison, W.H. and Muralidharan, R., "Analysis of Manual Control Tasks in Support of The Chemical Defense Program", Report No. 5168, Bolt, Beranek, and Newman, Inc., Cambridge, MA, November, 1982.

[8] Levison, W.H., "The Effects of Display Gain and Signal Bandwidth on Human Controller Remnant", AMRL-TR-70-93, March, 1981.
[9] Levison, W.H., "A Quasi-Newton Procedure for Identifying Pilot-Related Parameters of the Optimal Control Model", Proc. of the Seventeenth Annual Conf. on Manual Control, Los Angeles, CA, June, 1981.

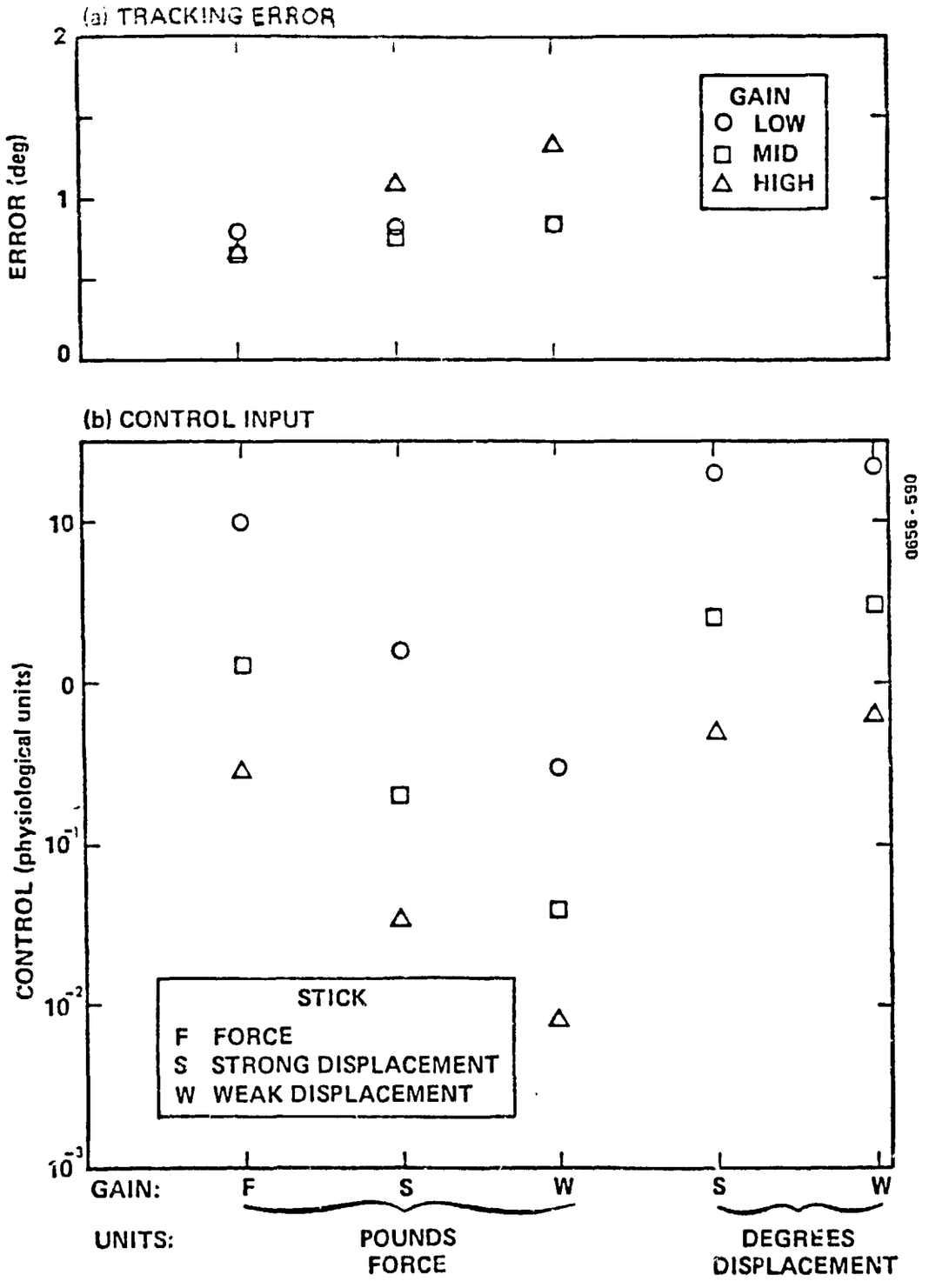

Figure 1. Effects of Stick Configuration on SD Performance Scores, Physiological Units

Average of 9 subjects, 3 trials/subject.

* From Reference 1

a) Force Stick

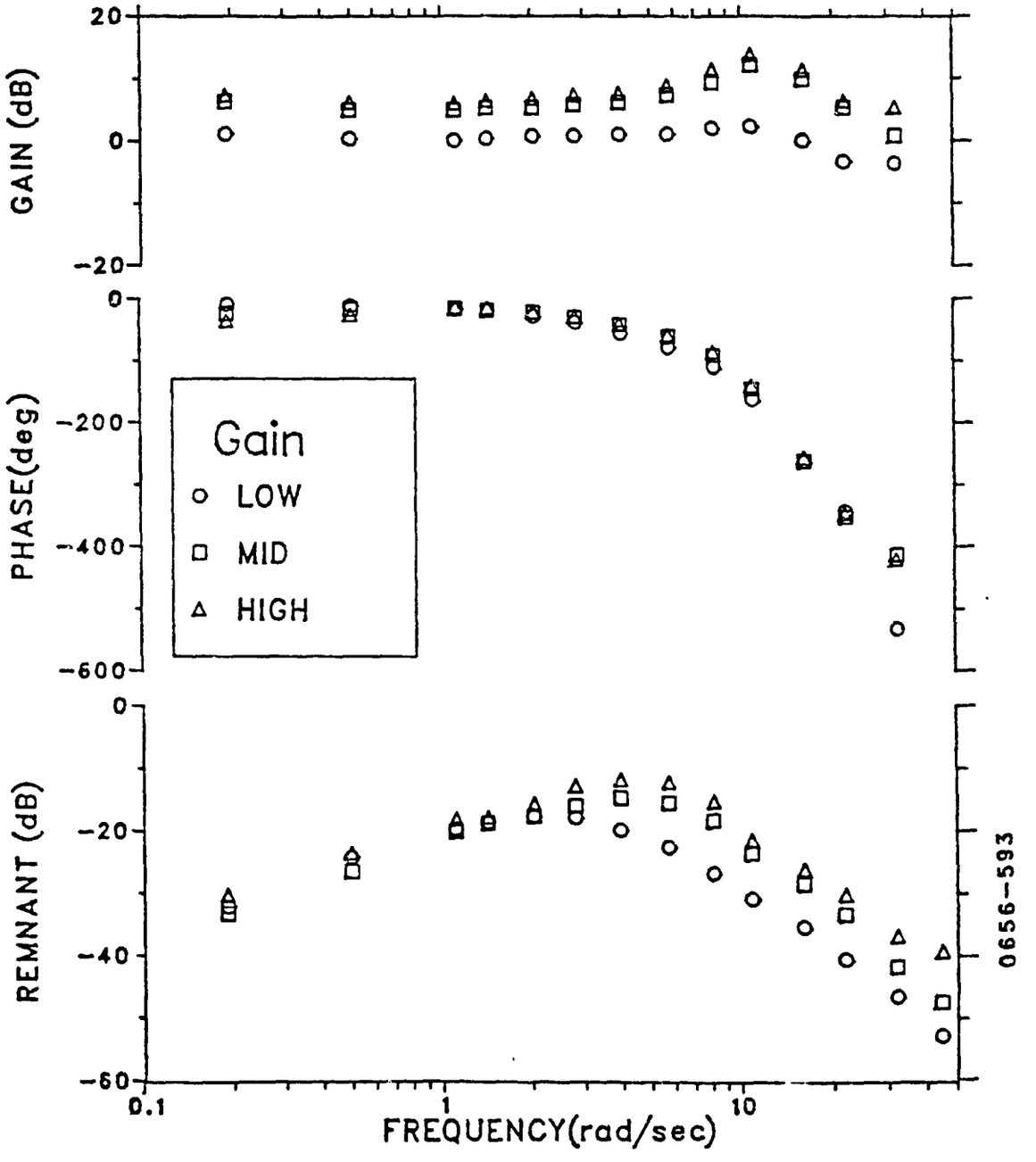

Figure 2.* Effects of Electrical Control Gain on Frequency Response

Average of 9 subjects, 3 trials/subject

* From Reference 1

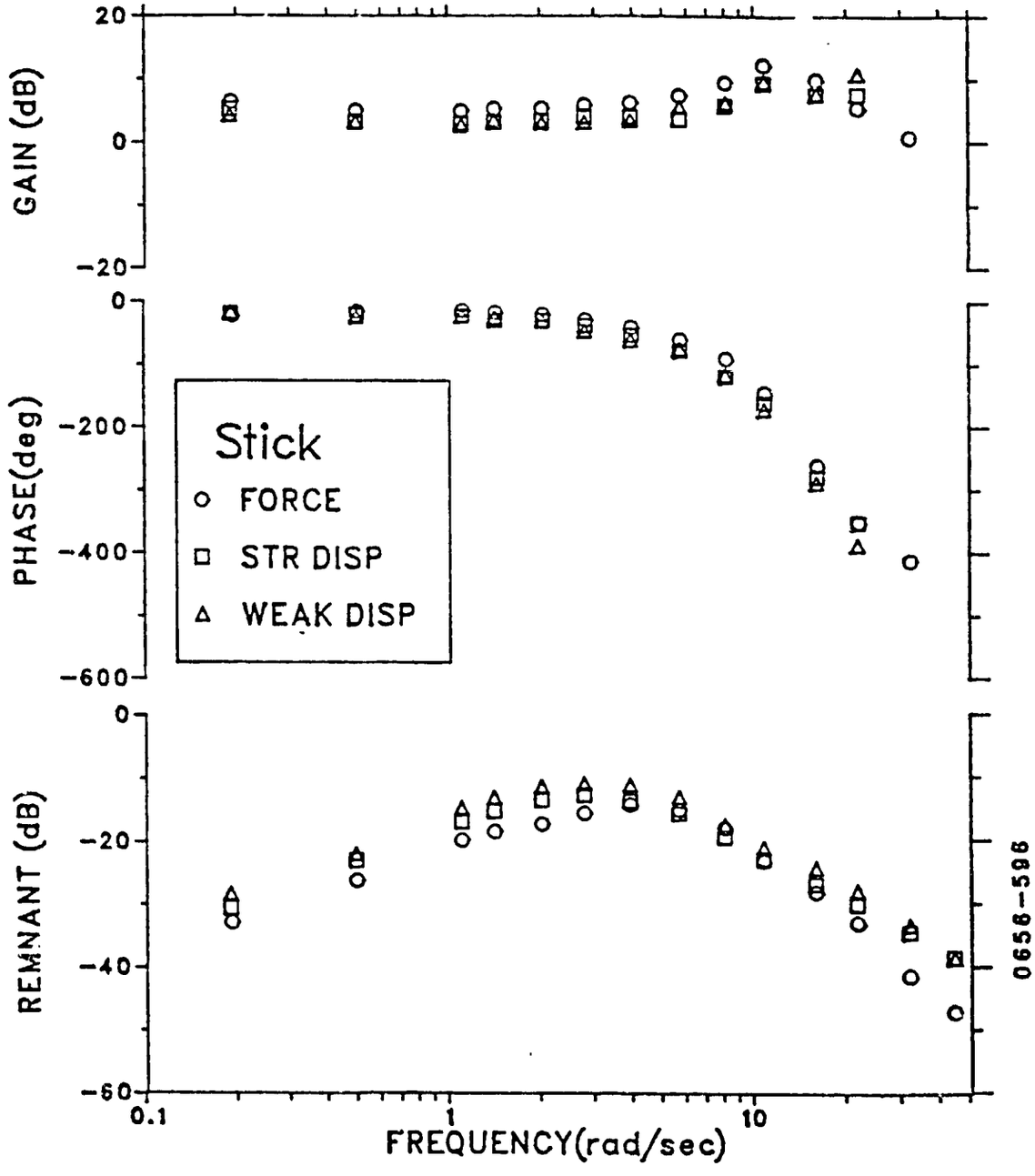

*

Figure 3. Effects of Force/Displacement Characteristics on Frequency Response

Mid Gain.
Average of 9 subjects, 3 trials/subject.

* From Reference 1

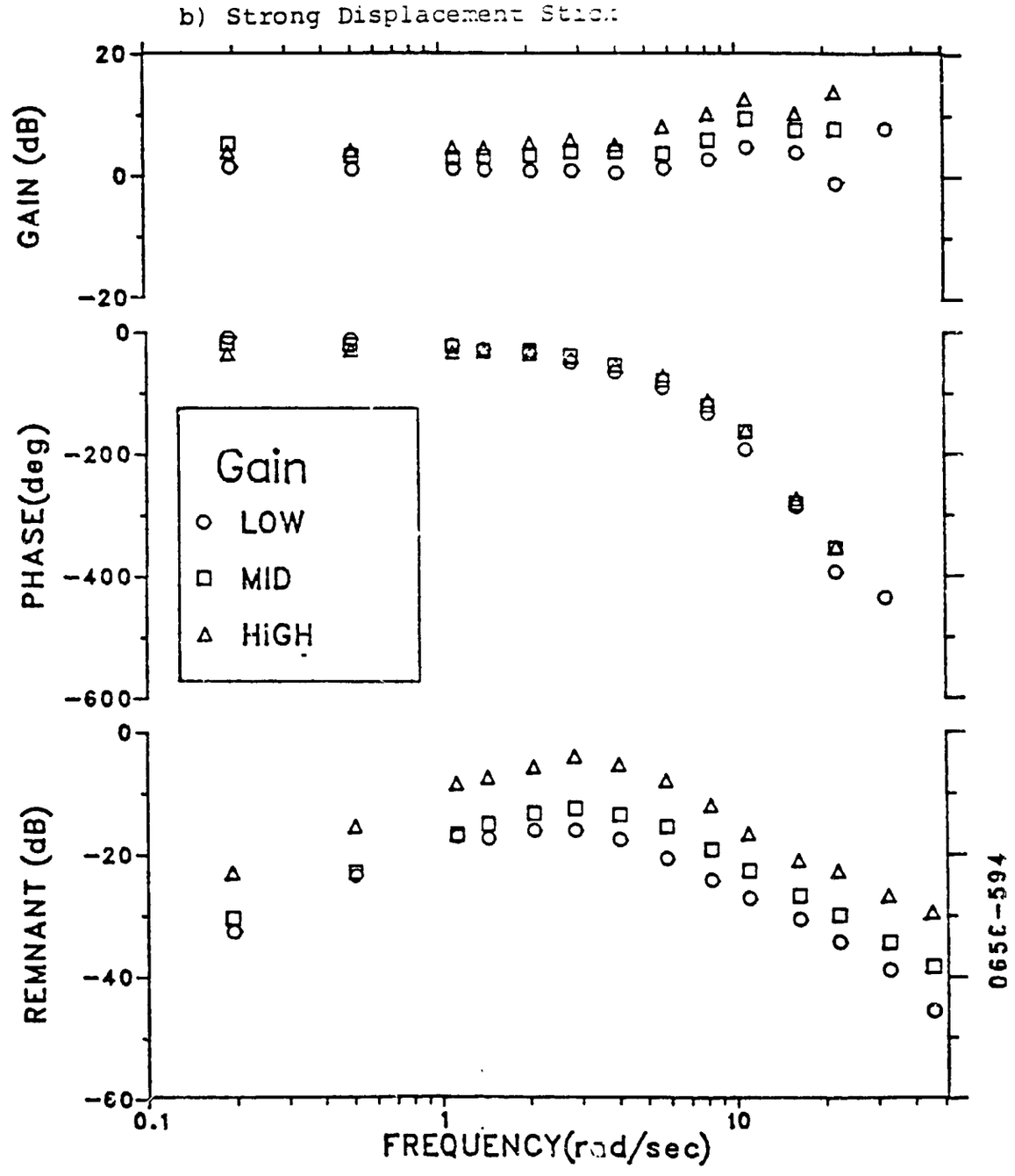

Figure 4.*

* From Reference 1

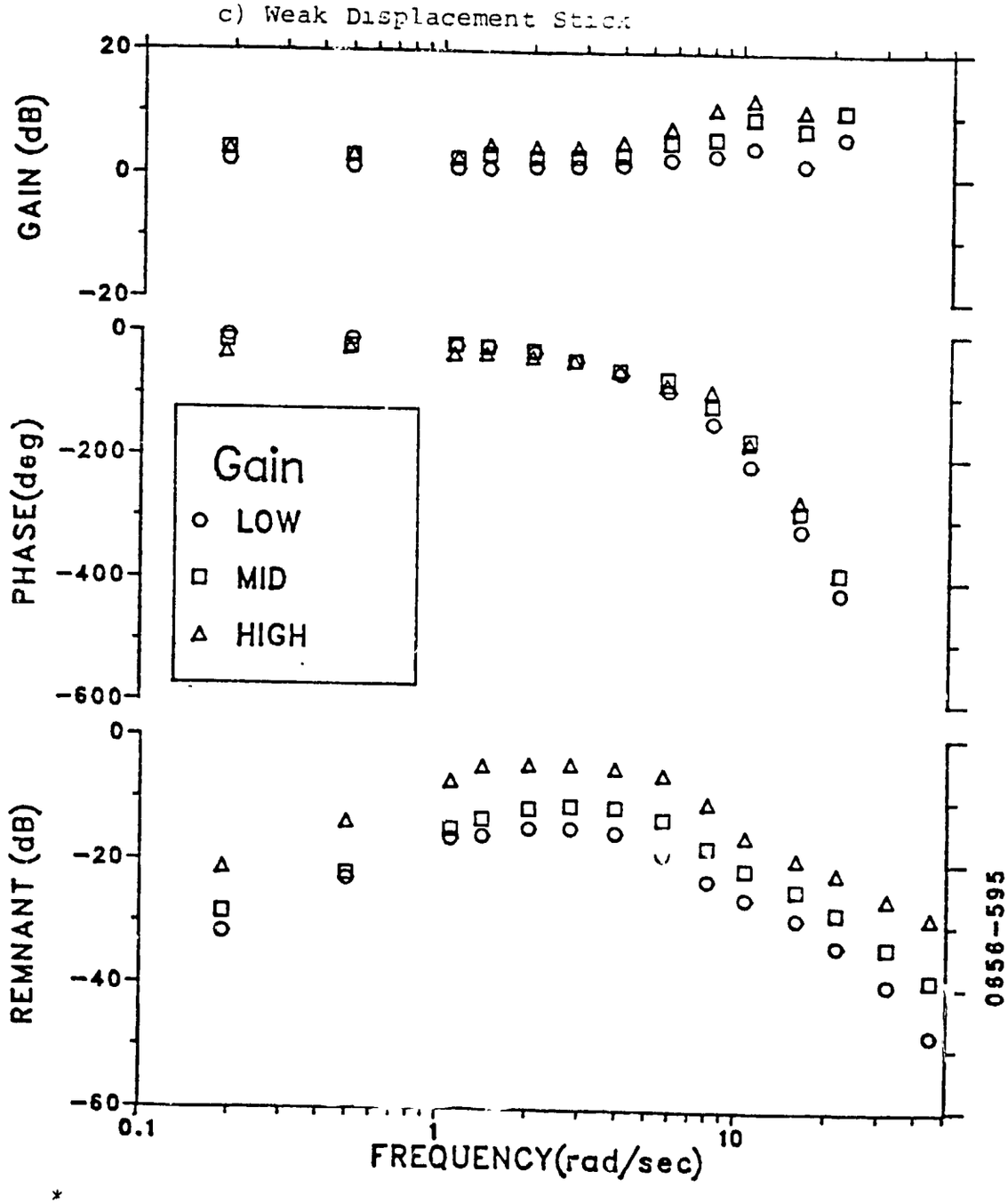

Figure 5.

* from Reference 1

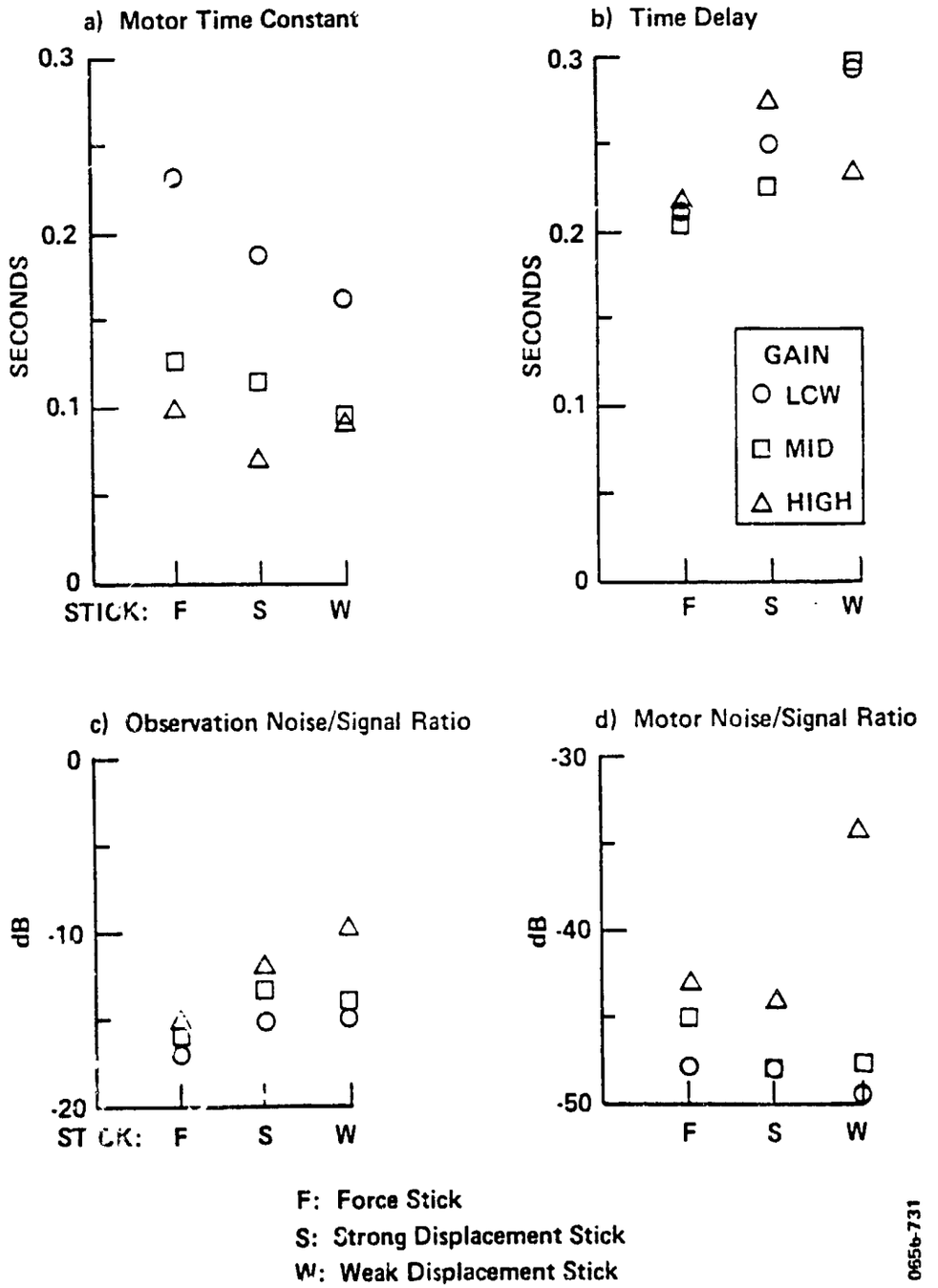

FIG. 6.* EFFECTS OF STICK CONFIGURATION ON MODEL PARAMETERS

* From Reference 1

Effects of Transport Delays in Simulator Performance

N85 14497

D10

A METHOD FOR MEASURING THE EFFECTIVE THROUGHPUT TIME DELAY IN SIMULATED DISPLAYS INVOLVING MANUAL CONTROL

Wayne F. Jewell, Senior Research Engineer
Warren F. Clement, Principal Research Engineer
Systems Technology, Inc.
2672 Bayshore-Frontage Road, Suite 505
Mountain View, California 94043

SUMMARY

The advent and widespread use of the computer-generated image (CGI) device to simulate visual cues has had a mixed impact on the realism and fidelity of flight simulators. On the plus side, CGIs can provide greater flexibility in scene content than terrain boards and closed-circuit television-based visual systems can, and they have the potential for a greater field of view. However, on the minus side, CGIs introduce into the visual simulation relatively long time delays. In many state-of-the-art CGIs, this delay is as much as 200 ms, which is comparable to the inherent delay time of the pilot. Because most GCIs use multiloop processing and smoothing algorithms and are linked to a multiloop host computer, it is seldom possible to identify a unique throughput time delay, and it is therefore difficult to quantify the performance of the closed-loop pilot-simulator system relative to the "real world" task. This paper describes a method to address these issues using the STI-developed Critical Task Tester (CTT). Some empirical results from applying the method are presented, and a novel technique for improving the performance of CGIs is discussed.

BACKGROUND AND INTRODUCTION

Modern flight simulators usually employ a "host" digital computer in order to represent the mathematical model of the aircraft dynamics, the flight control system, the equations of motion, and the environmental disturbances. A "satellite" digital computer generates the dynamic external visual field which is output to one or more cathode-ray tube (CRT) displays. The combined process of generating and displaying the external visual field is usually referred to as a computer-generated image (CGI). The pilot "flies" the aircraft by monitoring the CGI, and his control outputs, ϕ, are inputs to the host computer. This closed-loop process is depicted in the block diagram shown in Fig. 1.

In order to conserve computer resources and minimize digital delays, both the host and the CGI computers usually employ multiloop architectures. In addition, the CGI computer uses smoothing algorithms in order to prevent the visual scene from "jumping" on the display. The data transfer between the host and CGI computers is almost always asynchronous.

C-3

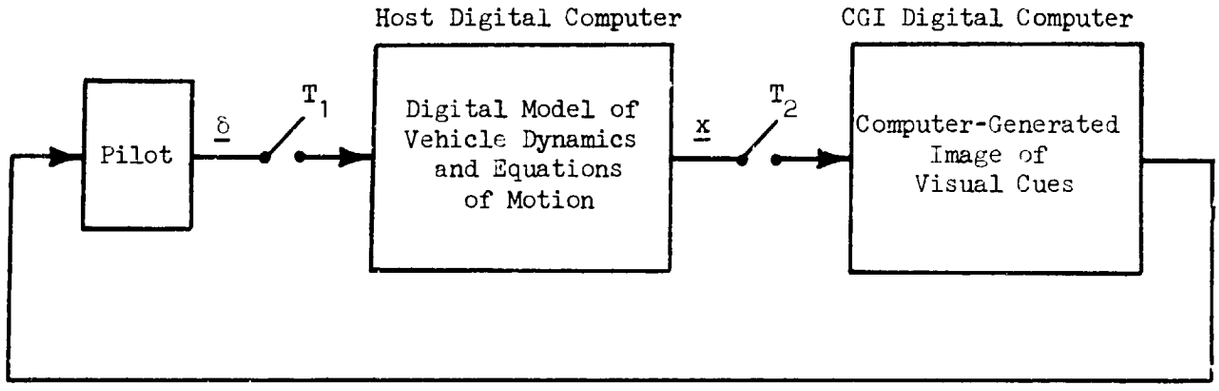

Figure 1. Functional Block Diagram of Architecture for Host and CGI Computers Used in Modern Flight Simulators

Because of the complex architecture used in the computers of modern flight simulators, it is very difficult to identify the effective time delay of the overall system, or, more importantly, to identify how the performance of the simulator compares to that of the real world. In many state-of-the-art CGIs, this delay is as much as 200 ms (Ref. 1), which is comparable to the inherent delay time of the pilot. For some flight tasks (e.g., up-and-away flight), this much delay is tolerable. For others (e.g., precision hover or landing), it is intolerable and completely unrealistic. When a pilot is unable to perform a task in a simulator, he often does not know exactly what is wrong; he knows only that he can perform the same task in the real world (Ref. 2). On the other hand, if the pilot can perform the task, he often complains that the workload is much higher than that in the real world. One explanation for both of these problems is that the pilot must generate lead in order to compensate for the lag in the CGI.

The primary purpose of this paper is to describe a method which can both measure the effective time delay of a modern flight simulator and quantify the performance of the closed-loop pilot-simulator system relative to the "real world." Since this method is independent of the hardware and software of the computers used in the simulator, it offers a rational means for evaluating hardware and/or software changes to any part of the flight simulator.

The remainder of this paper describes the proposed method and presents some empirical results of applying the method. A novel technique for improving the performance of visual simulators is also presented and discussed.

DESCRIPTION OF THE METHOD

The proposed method is based on human operator (HO) performance degradation in performing a manual control task. The particular manual control task is to stabilize an unstable controlled element using the critical tracking task (CTT, Refs. 3 and 4), as depicted in Fig. 2. The HO uses a manipulator, δ, to null the error, e, which is displayed on a CRT. The task is automatically paced in the sense that the unstable pole, λ, increases slowly with time, thus making the task progressively more difficult. At some point, the HO can no longer control the error, e, and the value of e exceeds a preset value. At this point, the task ends, and the corresponding final value of λ is defined to be the critical task score, λ_c.

The CTT has been used in numerous experiments involving the human operator. Most of these experiments have examined the performance degradation of the HO due to exogenous effects such as alcohol, drugs, and prolonged bed rest (Refs. 5 through 8). It is also possible, however, to use the CTT in order to examine the performance degradation of the HO due to divided attention (Refs. 9 and 10) and other causes within the display (Refs. 11 and 12), the manipulator (Ref. 13), or the order of the unstable controlled element itself (Refs. 13 and 14). It is the causes of HO performance degradation between the operator's manipulator and a CGI display that forms the basis for the proposed method.

Consider now the modified CTT block diagram shown in Fig. 3. A CGI with sample update period, T_e, is now used to display the error signal, e. The control output of the HO, δ, is sampled at period T_δ. (T_e and T_δ were equal but not synchronized for the results described herein.) Figure 3 represents the essential features of a modern flight simulator that uses one or more digital computers to sample and process the pilot's output and a CGI to display the state of the vehicle to the pilot in terms of a simulated appearance of the external field of view. Figure 2 can be thought of as the "real-world" counterpart of Fig. 3, where the display is continuous, and there is no delay due to sampled data effects.

Because the variability in λ_c for a well-trained subject is sufficiently low (Refs. 3 and 15), the continuous (i.e., Fig. 2) and discrete (i.e., Fig. 3) versions of the CTT offer a unique means for comparing the effects of sampled data systems and CGI displays on the performance of the human operator.

SOME EMPIRICAL RESULTS

The results of an initial investigation of the effects of T_e and T_δ from the sampled, first-order CTT described in Fig. 3 are shown in Fig. 4. Note that the mean score, λ_c, is a linear function of the sample periods, T_e and T_δ. Also note that there is low variability in the data, as evidenced by the low values of the standard deviations. Using the zero time delay score as a reference point (i.e., $\lambda_c \approx 6.5$ rad/sec), the

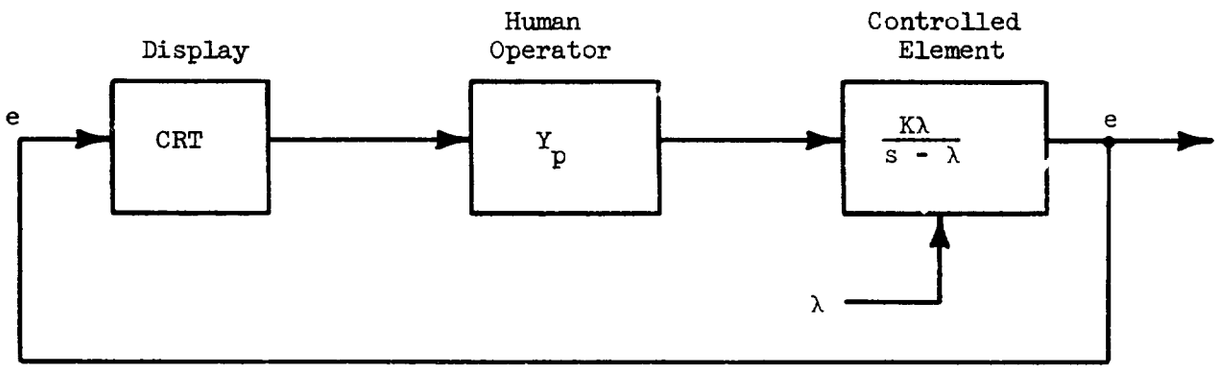

$$\lambda = \lambda_o + \int \dot{\lambda}\, dt$$

$$\dot{\lambda} = \begin{cases} 0.20 \text{ rad/sec/sec} & \text{for } |e| < e_c \\ 0.05 \text{ rad/sec/sec} & \text{for } |e| > e_c \end{cases}$$ one-way switch

Note: Task is automatically stopped when $|e| > e_s$

Figure 2. Functional Block Diagram of Critical Task Tester (CTT)

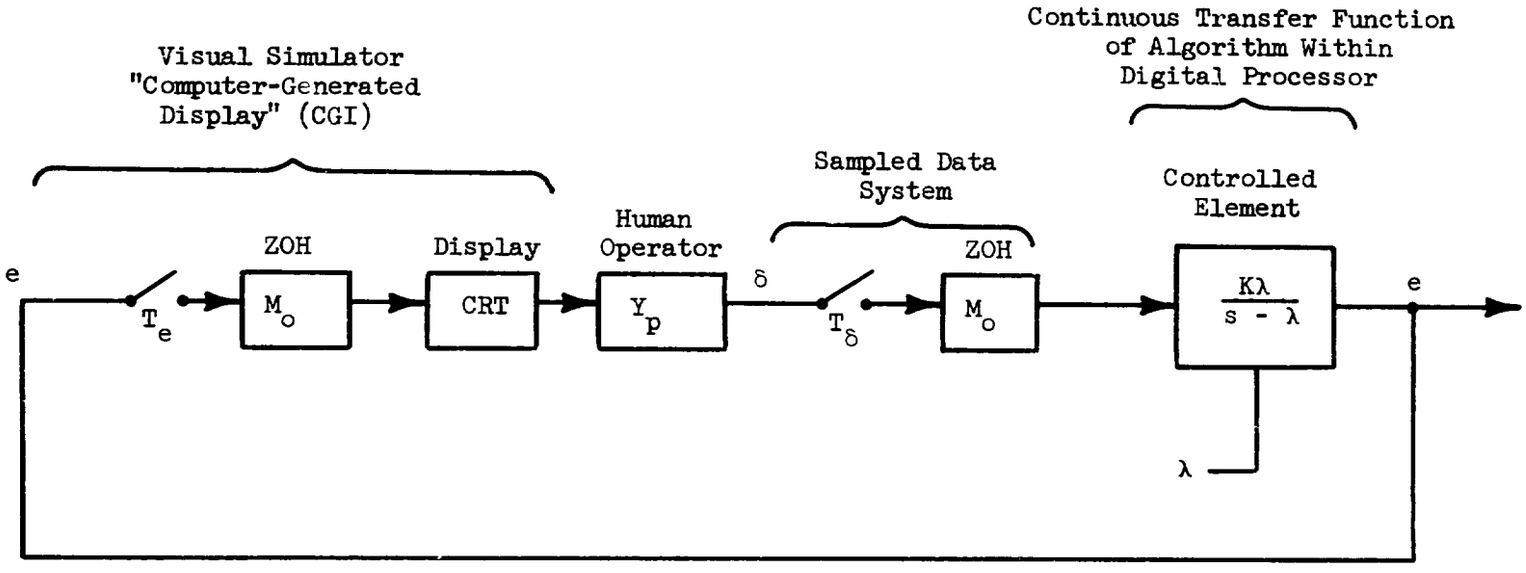

Note: The process of updating and holding a sample for one frame time, T, is modeled with a zero-order hold (ZOH):

$$M_o = (1 - e^{-Ts})/s$$

where T is the time delay associated with either T_e or T_δ

Figure 3. CTT with Computer-Generated Display and Sampled Data System

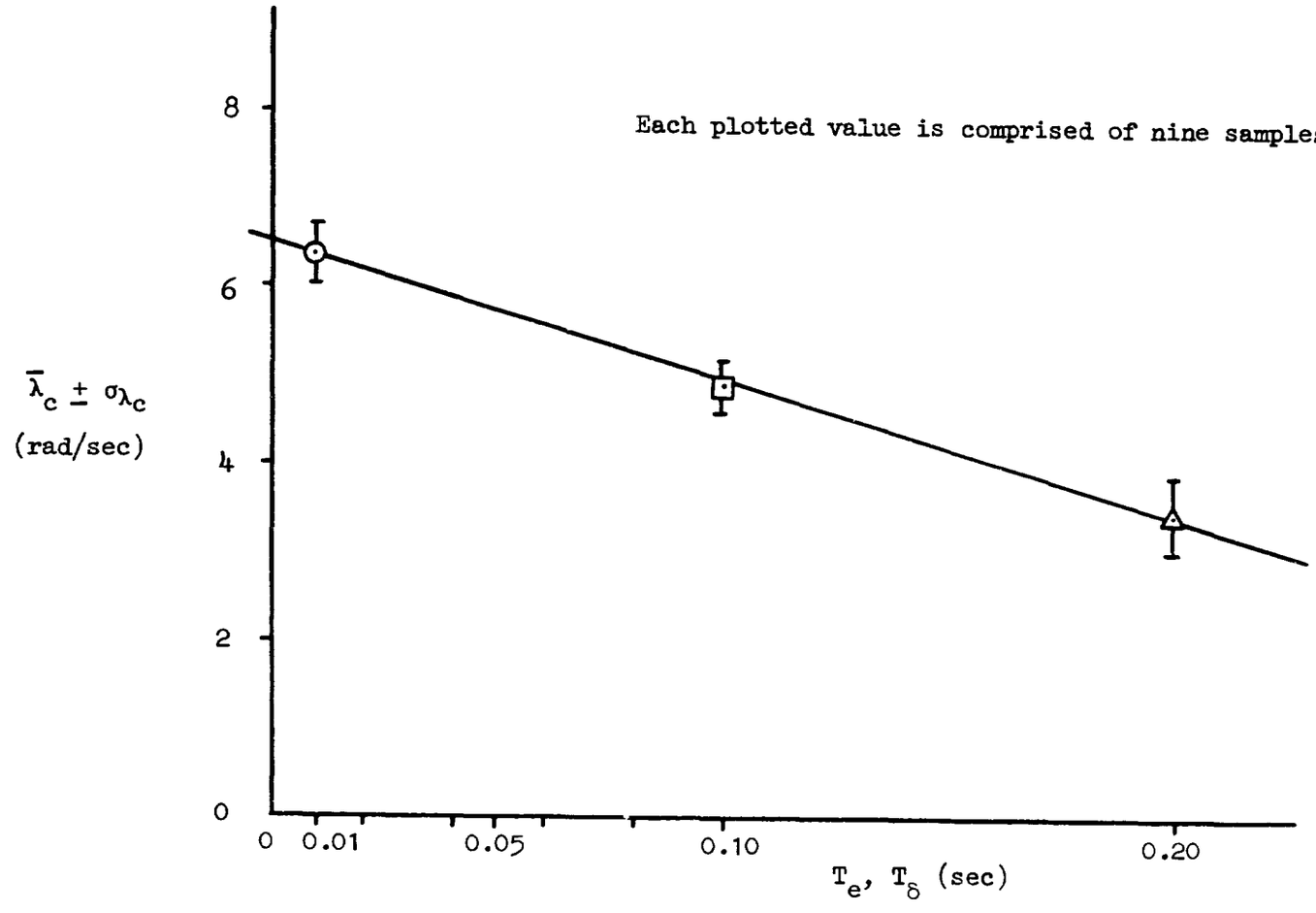

Figure 4. Effects of T_e, T_δ on λ_c

performance at 100 ms throughput delay is degraded by about 26 percent and, at 200 ms, by 49 percent! If we can extrapolate these results to other flight tasks, it is no wonder that pilots complain that they cannot perform real-world tasks in a flight simulator.

The discrete version of the first-order CTT in Fig. 3 thus offers a simple, convenient, and portable means for comparing the degradation in HO performance which accompanies throughput time delay and update rate between the pilot's manipulator and the CGI. It also meets the objectives stated at the beginning of this paper, i.e., to measure the effective time delay of a modern flight simulator and to quantify the performance of the closed-loop pilot-simulator system relative to the real world. The procedure for doing this in any given flight simulator is as follows:

1. Program the CTT algorithm in the host computer. Options for driving any one of the six axes of the CGI should be provided.

2. Establish a reference curve for λ_c versus the cycle time of the host computer. A separate curve must be established for each controller-display-operator combination.

3. Since the host computer will not be able to run at zero cycle time, each controller-display-operator combination must be extrapolated to the zero cycle time point. This point, λ_{co}, will be used as the "real world" reference point.

4. The effective throughput time delay of the total simulator, i.e., host computer and CGI, is calculated as follows:

$$T_{eff} = \frac{1}{\lambda_{ct}} - \frac{1}{\lambda_{co}}$$

where λ_{ct} is the value of λ_c at the normal operating point of the host computer. The above equation is based on the total throughput delay of the HO and digital computers being proportional to the inverse CTT score (Ref. 4). In general, the value of T_{eff} will not be the same as the "exact" throughput time delay. Hence the name "effective throughput time delay" is given.

Note that the procedure outlined above offers a rational means of evaluating the performance of a flight simulator. It also provides a method for evaluating changes to any component of the simulator. For example, the technique for improving the performance of a CGI that is discussed in the next section could be evaluated by this procedure.

A NOVEL TECHNIQUE FOR IMPROVING THE PERFORMANCE OF COMPUTER-GENERATED IMAGES

One way to compensate for the lag due to time delay in the combined host computer and CGI is to use lead in the signals being sent to the CGI. There are limitations in doing this, because the host computer cannot generate lead beyond the Nyquist frequency, and linear lead filters distort the amplitude response at the expense of obtaining the correct phase response. To overcome the first of these restrictions, the hybrid approach shown in Fig. 5 could be used.

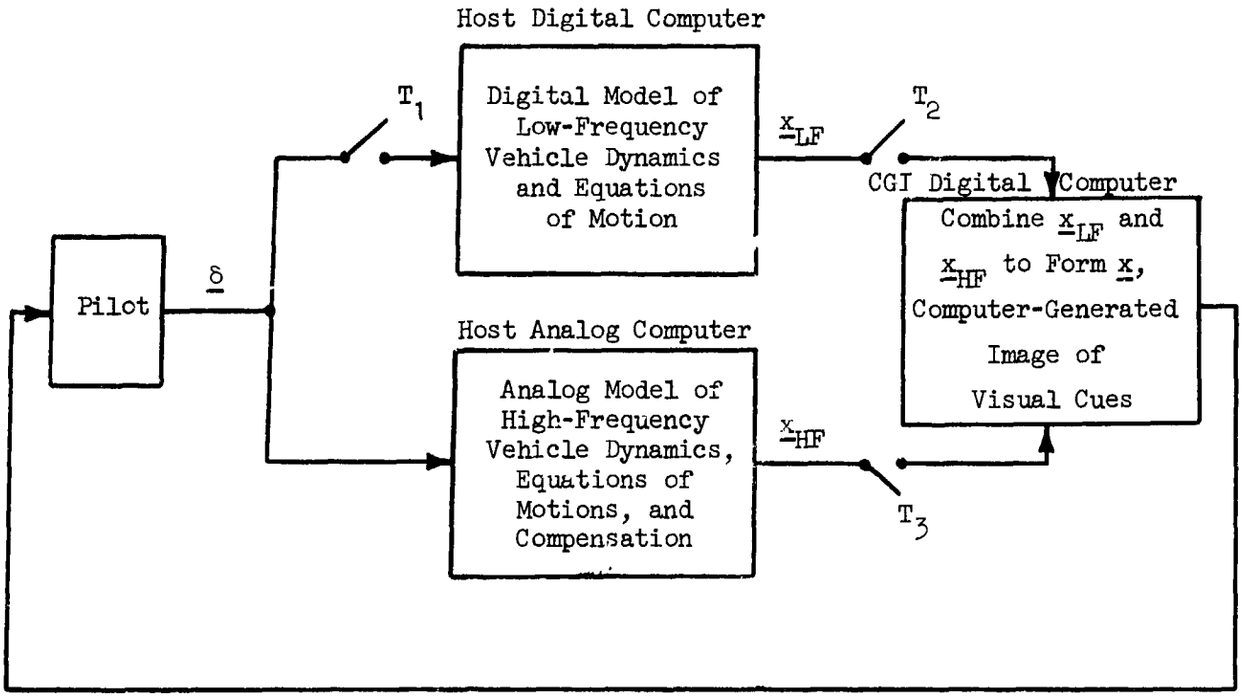

Figure 5. Functional Block Diagram of Advanced Hybrid Architecture Proposed for Host and CGI Computers

Note that there are two "host" computers, one digital and one analog (hence the name "hybrid"). The host digital computer simulates the low-frequency vehicle dynamics ($\underline{x}_{LF}$), where "low frequency" means up to the Nyquist frequency, π/T_1; the host analog computer simulates the high-frequency vehicle dynamics ($\underline{x}_{HF}$), where "high frequency" means above π/T_1; and it compensates $\underline{x}_{HF}$ to account for lags in the CGI digital computer. The CGI digital computer then combines $\underline{x}_{LF}$ and $\underline{x}_{HF}$ via "complimentary filtering" in order to form the final vehicle states, $\underline{x}$, which are displayed to the HO. A simple first-order complimentary filter is shown below,

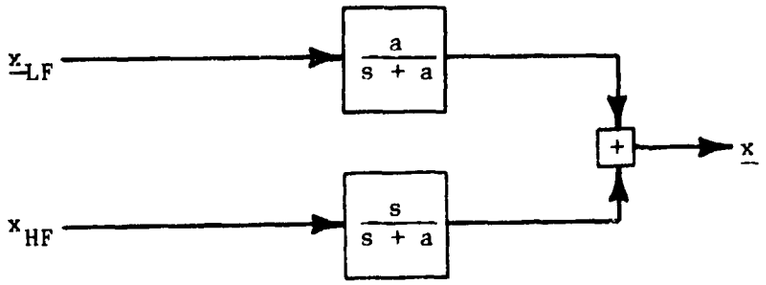

where the break frequency, a, is chosen to be just below the Nyquist frequency, π/T_1.

The compensation technique we propose to implement in the host analog computer was first reported in Ref. 16 and then later in Ref. 17. The technique, called the Split Path Nonlinear Filter or SPAN is shown in Fig. 6. The advantages of SPAN are that (1) it provides conditionally independent magnitude and phase angle specification (e.g., it can generate phase lead without amplitude distortion!) and (2) it is not dependent on input signal amplitude. On the other hand, the possible disadvantages of SPAN are that (1) the output will contain harmonic distortion which may need to be attenuated and (2) if the linear filter in the magnitude control path (F_m) contributes phase shift, it will be reflected in the output, hence the magnitude control path is conditionally independent.

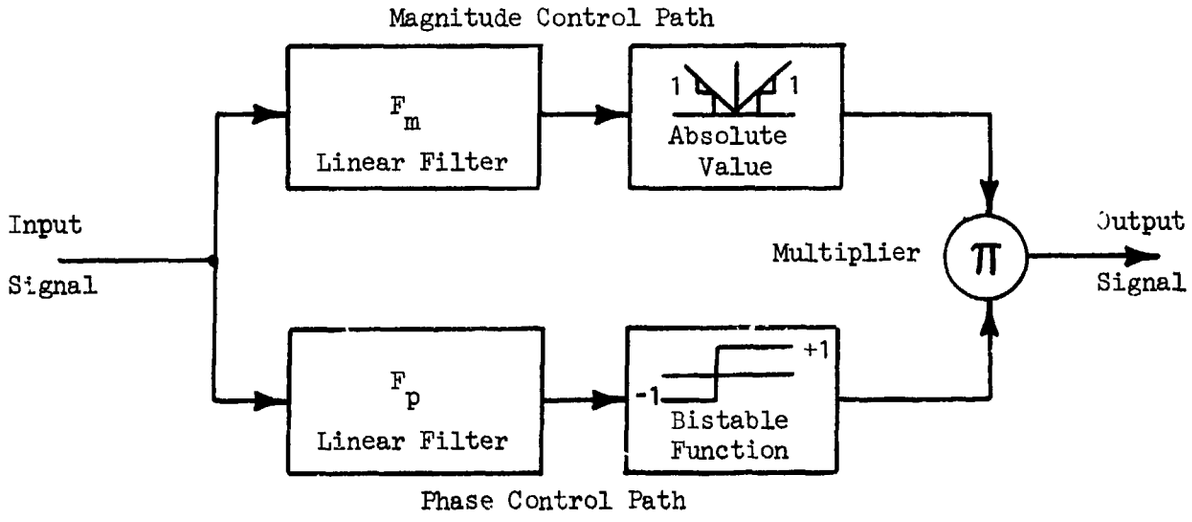

Figure 6. Flight Simulator Delay Compensation by Means of Split-Path Nonlinear Independent Magnitude and Phase Filters

The procedure outlined above needs to be tested under carefully controlled conditions. The CTT method described in this paper offers a unique way of quantitatively evaluating this novel technique for improving the performance of visual simulators.

REFERENCES

1. Paulk, Clyde H., Jr., David L. Astill, and Shawn T. Donley, Simulation and Evaluation of the SH-2F Helicopter in a Shipboard Environment Using the Interchangeable Cab System, NASA TM-84387, August 1983.

2. Woomer, Lt. C. (USN), and D. Carico, A Program for Increased Flight Fidelity in Helicopter Simulation, NATC TM 77-1 RW, April 27, 1977.

3. Jex, H. R., J. D. McDonnell, and A. V. Phatak, "A 'Critical' Tracking Task for Manual Control Research," IEEE Transactions on Human Factors in Electronics, Vol. HFE-7, No. 4, December 1966, pp. 138-145.

4. Jex, H. R., J. D. McDonnell, and A. V. Phatak, A "Critical" Tracking Task for Man-Machine Research Related to the Operator's Effective Delay Time. Part I: Theory and Experiments with a First-Order Divergent Controlled Element, NASA CR-616, November 1966.

5. Allen, R. Wade, Henry R. Jex, Duane T. McRuer, and Richard H. Klein, "Control Characteristics of Alcohol-Impaired Operators," AIAA Paper No. 74-1300, November 1974.

6. Allen, R. Wade, Stephen H. Schwartz, Anthony C. Stein, Raymond E. Magdaleno, and Jeffrey R. Hogue, Effects of Alcohol and Marihuana on Driver Control Behavior. Volume I: Laboratory Simulation Experiment, Systems Technology, Inc., Interim Technical Report No. 1066-1-I, April 1978.

7. Allen, R. W., and Henry R. Jex, "Visual-Motor Response in Crewmen During a Simulated 90-Day Space Mission as Measured by the Critical Task Battery," Seventh Annual NASA-University Conference on Manual Control, NASA SP-281, 1972.

8. Allen, R. Wade, and Henry R. Jex, Visual-Motor Response of Crewmen During a Simulated 90-Day Space Mission as Measured by the Critical Task Battery, NASA CR-2240, May 1973.

9. Jex, H. R., "Two Applications of the Critical Instability Task to Secondary Workload Research," IEEE Transactions on Man, Machines, and Systems, Vol. MMS-10, No. 4, December 1969, pp. 137-140.

10. Allen, R. W., W. F. Clement, and H. R. Jex, Research on Display Scanning, Sampling, and Reconstruction Using Separate Main and Secondary Tracking Tasks, NASA CR-1569, July 1970.

11. Jex, Henry R., R. Wade Allen, and Raymond E. Magdaleno, Display Format Effects on Precision Tracking Performance, Describing Functions, and Remnant, AMRL-TR-71-63, August 1971.

12. Jex, H. R., R. W. Allen, and R. E. Magdaleno, "Vibration Effect Manual Control Performance," Eighth Annual NASA-Univer Conference on Manual Control--University of Michigan, AF.. TR-72-92, May 1972.

13. McDonnell, J. D., and H. R. Jex, A "Critical" Tracki g T ek for Man-Machine Research Related to the Operator's Effective Delay Time. Part II. Experimental Effects of System Input Spectra, Control Stick Stiffness, and Controlled Element Order, NASA CR-674, January 1967.

14. Jex, H. R., and R. W. Allen, "Research on a New Human Dynamic Response Test Battery. Part I: Test Development and Validation. Part II: Psychophysiological Correlates," Sixth Annual Conference on Manual Control, AFIT/AFFDL Report, Conference Paper G-5, April 1970.

15. Jex, H. R., W. F. Jewell, and R. W. Allen, "Development of the Dual-Axis and Cross-Coupled Critical Tasks," Eighth Annual NASA-University Conference on Manual Control--University of Michigan, AFFDL-TR-72-92, May 1972, pp. 529-552.

16. Levinson, Emanuel, "Gain-Phase Relations of Nonlinear Circuits," IRE National Convention Record, Part 4, 1958, pp. 141-152.

17. Foster, W. C., D. L. Gieseking, and W. K. Waymeyer, "A Nonlinear Filter for Independent Gain and Phase (With Applications)," Transactions of the ASME, Journal of Basic Engineering, June 1966, pp. 457-462.

N85 14498

EFFECTS OF TRANSPORT DELAYS ON MANUAL CONTROL SYSTEM PERFORMANCE

R. Wade Allen
Richard J. DiMarco

Systems Technology, Inc.
13766 S. Hawthorne Blvd.
Hawthorne, CA 90250

Telephone No. 213/679-2281

ABSTRACT

Throughput or transport delays in manual control systems can cause degraded performance and lead to potentially unstable operation. With the expanding use of digital processors, throughput delays can occur in manual control systems in a variety of ways such as in digital flight control systems in real aircraft, and in equation-of-motion computers and CGI's in simulators. Previous research has shown the degrading effect of throughput delays on subjective opinion and system performance and dynamic response. A generic manual control system model is used in this paper to provide a relatively simple analysis of and explanation for the effects of various types of delays. The consequences of throughput delays of some simple system architectures is also discussed.

A. OVERVIEW AND BACKGROUND

Past literature surveys associated with flight simulation fidelity have found that system response lags and computational delays cause performance and pilot subjective rating problems (Refs. 1 and 2). Pilot/vehicle model analysis has shown that delays on the order of 50 to 100 msec can have an appreciabl influence on performance and workload (Ref. 3). Recent experiments have shown performance effects of time delays which are consistent with model analysis (Refs. 4 and 5).

The above literature indicates that simulator computational delays can have a serious effect on aircraft simulation fidelity. Ground vehicles typically have faster response dynamics than aircraft in terms of path control, and it is suspected that the problem may be even more serious for driving simulators. To further understand the effect of various potential sources of transport delays a computer model analysis was undertaken using a generic vehicle control model as described below. The analysis was carried out to study the effect of several sources of computational delay including host computer system, display system, and motion system. (This analysis does not address another important simulation artifact, that of the mismatch between visual and motion cues, which can lead to vertigo and/or sickness.)

PRECEDING PAGE BLANK NOT FILMED

B. ANALYSIS MODEL

The basic control example for the analysis model concerns generic vehicle tracking (e.g., dogfighting) where the operator must point his vehicle at a target or aim point at some fixed distance in front of the vehicle. An example for a typical aircraft is shown in Fig. 1 (Ref. 6). A similar arrangement holds for ground vehicle steering control as illustrated in Fig. 2 (Ref. 7). The only dynamic difference between the car and aircraft examples is the T_{θ_2} path lag which is ignored for the car. (It actually exists in the car, but as a very high frequency lag corresponding to an aircraft with steep lift or side-force curve slopes.)

A generic operator/vehicle pointing control model was prepared for analysis based on an expansion of the Figs. 1 and 2 models. A block diagram of the analysis model is shown in Fig. 3 which has additional dynamic complexity over the simplified models of Figs. 1 and 2 as follows:

- Pilot lead generation to compensate for effective vehicle lag, T_{eq}, is provided by angular rate feedback which is assumed to represent a composite of motion perception (i.e., acceleration, angular rotation and proprioceptive sensations).
- Lightly damped, second-order limb/manipulator dynamics.
- Human operator transport delay associated with visual (τ_v) and motion (τ_r) perception.
- System transport delays associated with dynamic computations (τ_c), display generation (τ_d), and motion feedback (τ_m).
- A low frequency trimming operation to minimize low frequency "hang off" errors.

In the Fig. 3 analysis model, a disturbance (δ_d) is added at the input to the equivalent vehicle dynamics to represent the effects of wind gusts, and roadway inputs in the case of ground vehicles. The equivalent vehicle dynamics are represented by s simple first-order time constant, T_{eq}, to approximate lags in vehicle rotational rate in response to control inputs. Path lag, T_{θ_2}, is assumed to be zero for this analysis. Transport delay representations are defined below.

C. TRANSPORT DELAY SOURCES

The model analysis was arranged to assess the effects of three sources of computational delay. The first is a transport delay associated with the vehicle dynamics equations of motion (τ_c). This delay could represent the equivalent delay used in specifying vehicle handling qualities (Ref. 8) which can result from the composite effect of stick filters, digital flight control system delays, and control system and other high frequency vehicle dynamics effects. It could also represent the composite effect of A/D and D/A sampling holds, integration routines and computational cycle time. The analysis considered either no delay, which might correspond to an analog vehicle or an

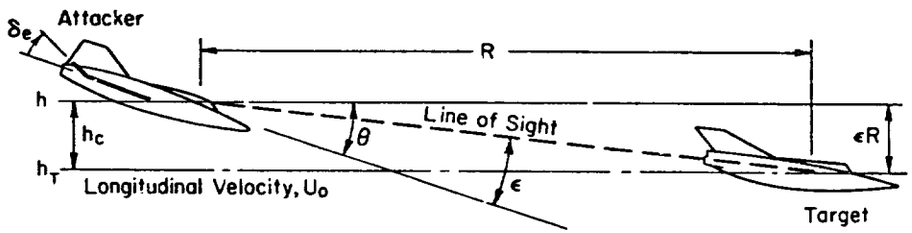

a) Model Scenario

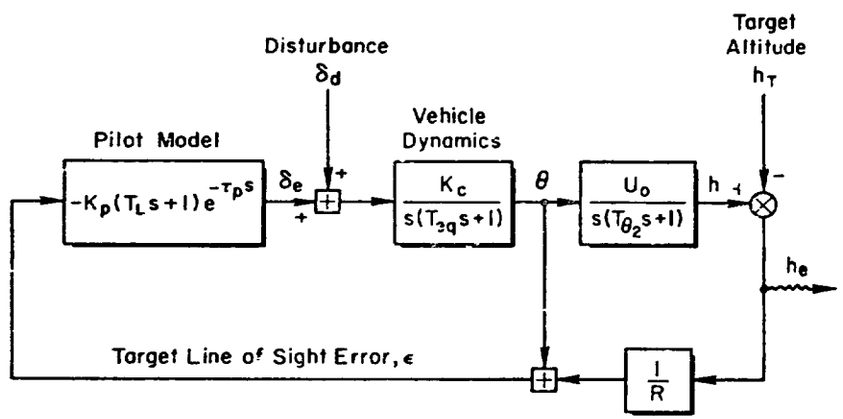

b) Pilot-Aircraft System Dynamics

Figure 1. System Model for Air-to-Air Target Tracking

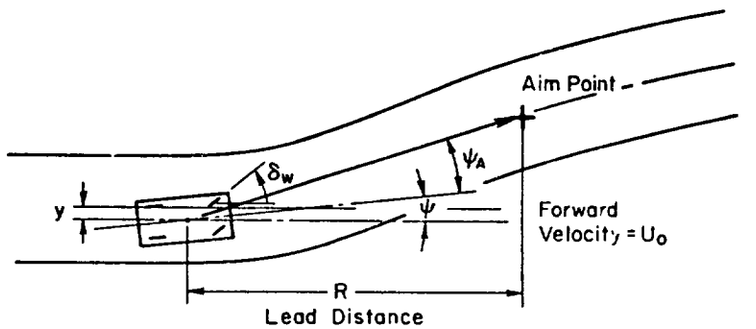

a) Model Scenario

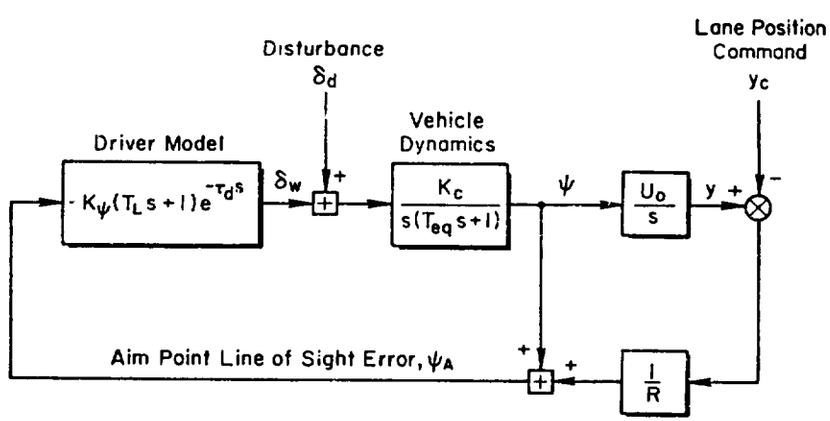

b) Driver-Automobile System Dynamics

Figure 2. System Model for Car/Driver Path Following a Commanded Path

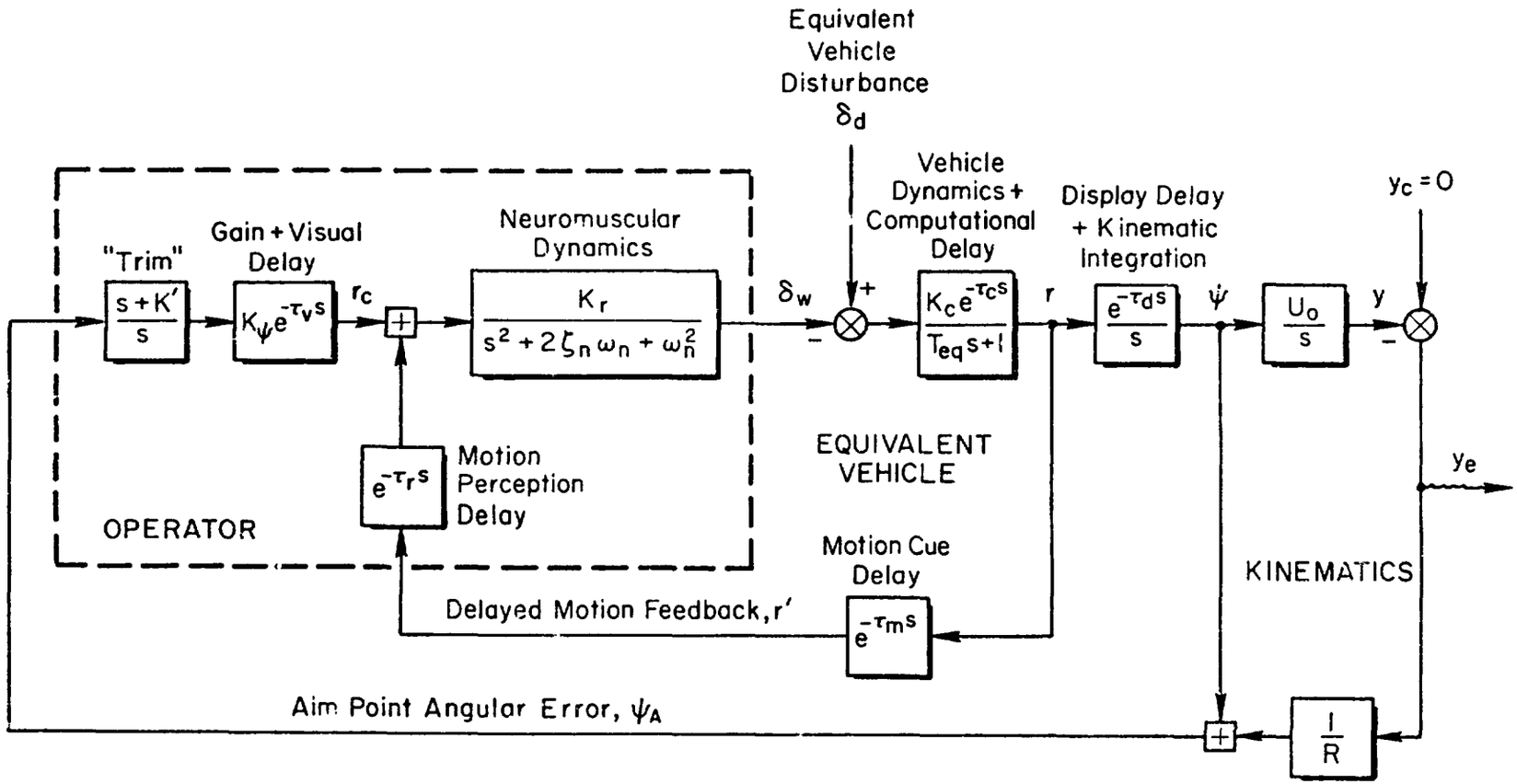

Figure 3. Generic Operator/Vehicle Tracking Dynamic Model for Analyzing Transport Delay Effects

analog simulation computer, or a delay of 0.075 sec, which is a common equivalent delay time associated with complicated digital simulation computations or modern high performance aircraft with digital flight control systems.

The second delay source considered was that due to display system characteristics. Analysis conditions included either no delay, which might be associated with an analog processor, or 100 msec delay which is common to many of the current generation simulation CGI raster scan devices. The delay time condition might also be associated with the camera servos on a terrain board system, or digital processing in HUD or EADI instruments.

The final delay factor was concerned with motion feedback to the human operator. Analysis conditions included no delay, or a rather long delay of 250 msec. The long-delay condition might be associated with a fixed-based simulator environment where there were no motion cues available, and the human operator has to generate heading rate cues visually. This could also result from motion lags in a simulator motion system combined with computational delay in generating the motion base drive commands. The additional 250 msec was calculated to give model behavior that was consistent with past measurements made under both fixed-based and moving base conditions (Ref. 9), and is also consistent with delays identified in flight simulators (Ref. 10).

D. MODEL PARAMETER SELECTION

The Fig. 3 model has a variety of parameters that must be set to represent either vehicle characteristics or human operator behavior. A nominal vehicle heading time constant (T_{eq}) of about 0.2 sec was selected. This might represent a light weight, high performance aircraft, or a compact to intermediate size automobile. The vehicle gain is somewhat arbitrary, depending both on control gain and vehicle stability derivatives.

The human operator model parameters can be divided into two groups; those which are relatively fixed and were assumed to be constant for this analysis, and other parameters which the human operator typically adapts in order to achieve stable and desirable closed-loop performance. The trim constant (K') was assumed to be constant at 0.5 rad/sec which is consistent with driver measurements discussed in Ref. 7. The visual time delay (τ_v) was assumed to be constant at 0.05 sec. The time delay associated with motion feedback perception (τ_r) was also set at 0.05 sec. The second-order limb/manipulator system dynamics were set at a break frequency of 20 rad/sec and a damping ratio of 0.5. The pure delay and lag characteristic were set to give a composite effective time delay, with the motion feedback loop closed, of 0.17 seconds which is consistent with past car-driver measurements (Ref. 7).

The human operator can arbitrarily adapt his inner and outer loop gains (K_r and K_ψ respectively) and has some control over aim point range, R, to optimize system performance and control stability. For the model structure assumed here, K_r was adjusted to obtain as wide a frequency response as possible in the motion feedback loop while maintaining a reasonable closed-loop damping ratio (i.e., $\zeta_{CL} \cong 0.5$). For a real vehicle without any computer delay or extra motion feedback delays the variable K_r would be adjusted to

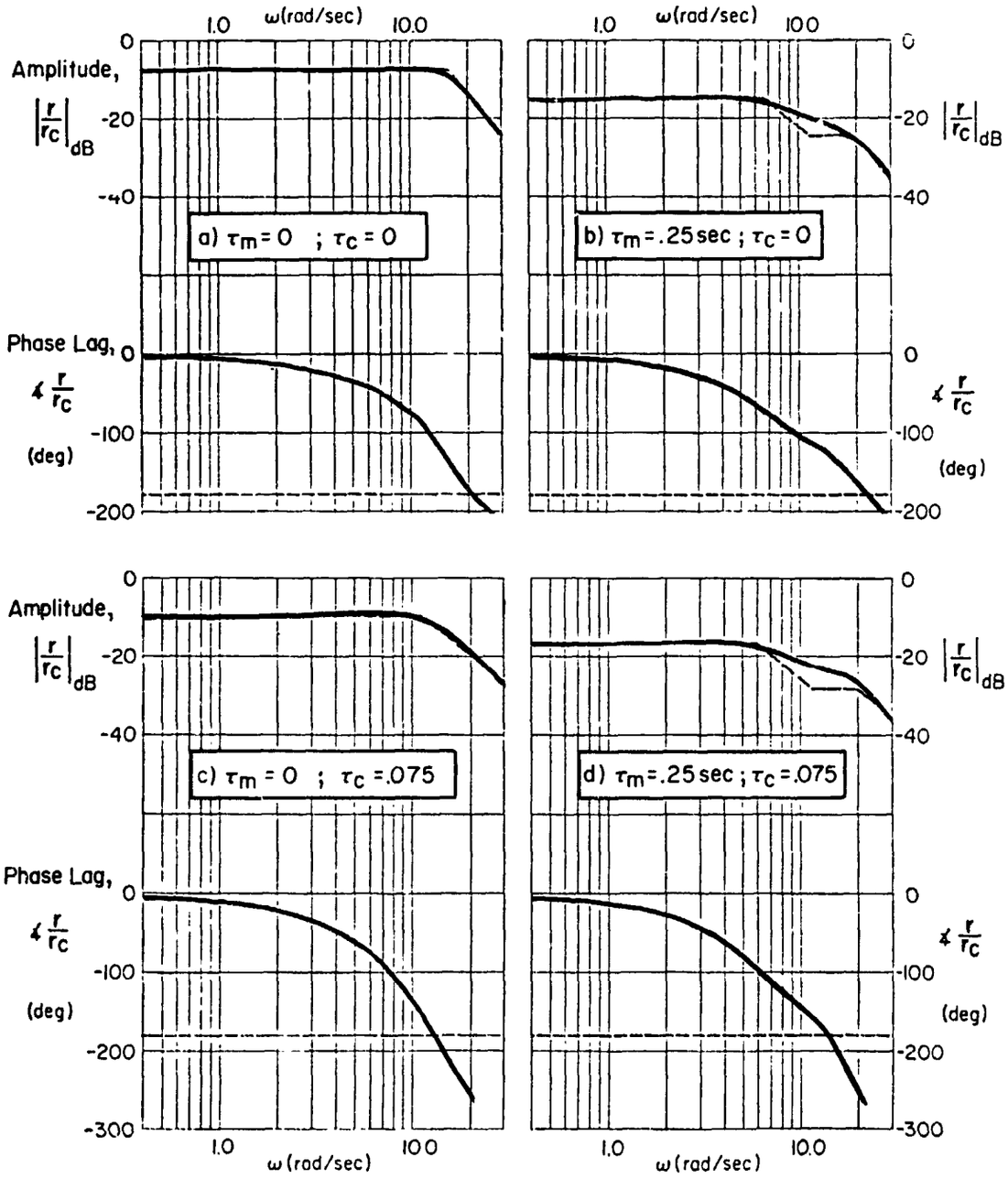

Figure 4. Motion Feedback Closed-Loop Response Functions
(Equivalent Closed-Loop Parameters Given in Table 1)

TABLE 1. MOTION FEEDBACK LOOP PARAMETERS FOR VARIOUS LEVELS OF MOTION FEEDBACK (τ_m) AND COMPUTATIONAL (τ_c) DELAY

OPEN LOOP			EQUIVALENT CLOSED	
τ_m (sec)	τ_c (sec)	$K_{\tau-1}$ (sec^{-1})	K_{eq} (sec)	τ_o (sec)
0	0	500	0.414	0.12
	0.075	350	0.331	0.20
0.25	0	150	0.175	0.16
	0.075	125	0.150	0.235

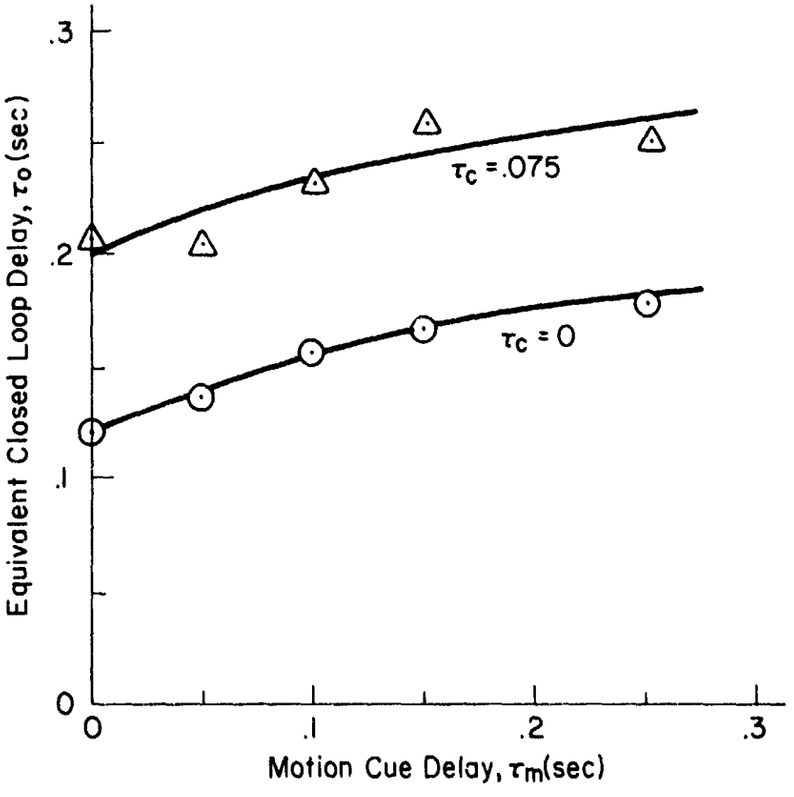

Figure 5. Equivalent Motion Feedback Delay for Various Levels of τ_m and τ_c

cancel out the effects of the vehicle equivalent heading lag, T_{eq}. As computational delay is added or the heading rate feedback delay is changed, K_r would then be adjusted to still achieve as wide a bandwidth as possible with this inner loop.

When K_r is properly adjusted a fairly flat closed-loop amplitude ratio can be achieved for the motion feedback loop as illustrated in Fig. 4. When the conditions in Fig. 4 are achieved the closed-loop response of the motion feedback loop can then be approximated by a gain and an equivalent time delay up to the point where the amplitude ratio begins to roll off:

$$\text{Motion Feedback Closed-Loop Response} \cong K_{eq} e^{-\tau_o}$$

Closed-loop equivalent parameters are given in Table 1 for the Fig. 4 response functions.

Note that when there are no extra computational delays and a low feedback delay, as in the upper lefthand corner of Fig. 4, the closed-loop bandwidth of the heading rate loop can be adjusted to be quite high. Theoretically, in this case the bandwidth is on the order of 15 rad/sec, and the equivalent time delay is quite small (about 120 msec). If τ_o is added to the visual time delay (τ_v), the result is an overall equivalent time delay for the driver of about 0.17 sec, which is consistent with measurements discussed in Ref. 7. On the other hand, when a significant amount of delay is put into the motion feedback loop, as in the lower righthand corner of Fig. 4, the closed-loop bandwidth of the heading rate loop is reduced considerably. In this case it is reduced to the vicinity of the vehicle's heading rate time constant (i.e., delayed feedback effectively opens the loop). In the second case the equivalent time delay for the heading rate loop is increased to about 235 msec.

E. EQUIVALENT OPERATOR/VEHICLE TIME DELAY EFFECTS

The equivalent closed-loop time delays that are achieved over a wide range of motion feedback delays (τ_m) and two levels of computational delay are illustrated in Fig. 5. Here, note that the computer computation delay (τ_c) has a much greater influence on the equivalent closed-loop delay than does the motion feedback time delay which is actually in the feedback of this loop. These induced delays will have two effects on human operator/vehicle performance. First, the increased equivalent closed-loop time delay will affect the operator's ability to achieve an overall bandwidth in controlling outer loop errors. Second, the effect of disturbances that act on the vehicle will be delayed in their feedback to the operator. Thus, there will be an overall delay in the human operator responding to a disturbance, and, once the operator responds, he will be limited in the bandwidth of his response.

The parameters that remain to be selected in the Fig. 3 model are K_ψ and U_o/R. Procedures for optimizing human operator performance by the selection of these two variables has been discussed for car driving in Ref. 7. The procedure involves breaking the Fig. 3 model loop at the r_c point and then considering the composite driver/vehicle open-loop transfer function proceeding around the loop.

Given that the inner loop closed-loop dynamics can be interpreted as an equivalent time delay over the outer loop bandwidth, then an Extended Crossover Model describing function for the Fig. 3 model can be written as:

$$Y_p{}^*Y_c = \underbrace{\frac{s + K'}{s}}_{\text{Low Frequency Trimming}} \cdot \underbrace{\frac{s + U_o/R}{s}}_{\substack{\text{Low Frequency Kinematic Lead} \\ + \text{ Integration}}} \cdot \underbrace{\frac{\omega_c e^{-\tau_e s}}{s}}_{\substack{\text{Crossover} \\ \text{Model}}} \qquad (1)$$

The kinematic zero at U_o/R is at low enough frequency that the dynamics become K/s-like in the region of magnitude crossover (the classical crossover model law). Now the optimum K_ψ and U_o/R values can be interpreted in terms of crossover frequency and phase margin.

The $Y_p{}^*Y_c$ transfer function is illustrated in Fig. 6 for each combination of induced time delays under consideration. As noted in Fig. 6, the low frequency effects of aim point kinematics $(s + (U_o/R))/s$ plus trimming $(s + K')/s$ have resulted in a conditionally stable system. The variable U_o/R which corresponds to lead distance or look-ahead range for the human operator's aim point was adjusted to give the stable phase region indicated in Fig. 6. As can be noted, U_o/R was varied for each combination of the various time delays in Fig. 6 in order to get a similar stable phase region for all conditions. Once this form had been achieved, then the remaining variable K_ψ was selected in order to give a specified phase margin. The low frequency kinematic and trim effects cause a significant reduction in phase margin in the crossover frequency region and cannot be neglected for tasks requiring control to aim points with speed-to-range ratios in the region of 0.1-1.0 rad/sec. It should be noted that situations which constrain the look ahead distance R to small values (e.g., driving in the fog, pointing at short range ground or air targets) could decrease the region over which the phase is stable.

Phase margin has been used previously as a metric for quantifying the stability of car/driver closed-loop steering performance (Ref. 11). K_ψ is set to achieve a desired phase margin at the crossover frequency which can be considered the bandwidth of the closed-loop operator/vehicle control system. The phase margin quantifies the stability or oscillatory nature of the operator's steering control behavior. The bandwidth or crossover frequency defines how rapidly the control can be carried out. For this analysis an attempt was made to maintain a constant phase margin of 30 deg for all cases. This level has been typically found in past car driving studies (Ref. 7). The achievable crossover frequency depends on the total system time delay which includes the inner loop equivalent time delay, visual perceptual delay, and display system transport delay:

$$\tau_e = \tau_o + \tau_v + \tau_d$$

Gain and crossover model parameters are summarized in Table 2.

ORIGINAL PAGE IS
OF POOR QUALITY

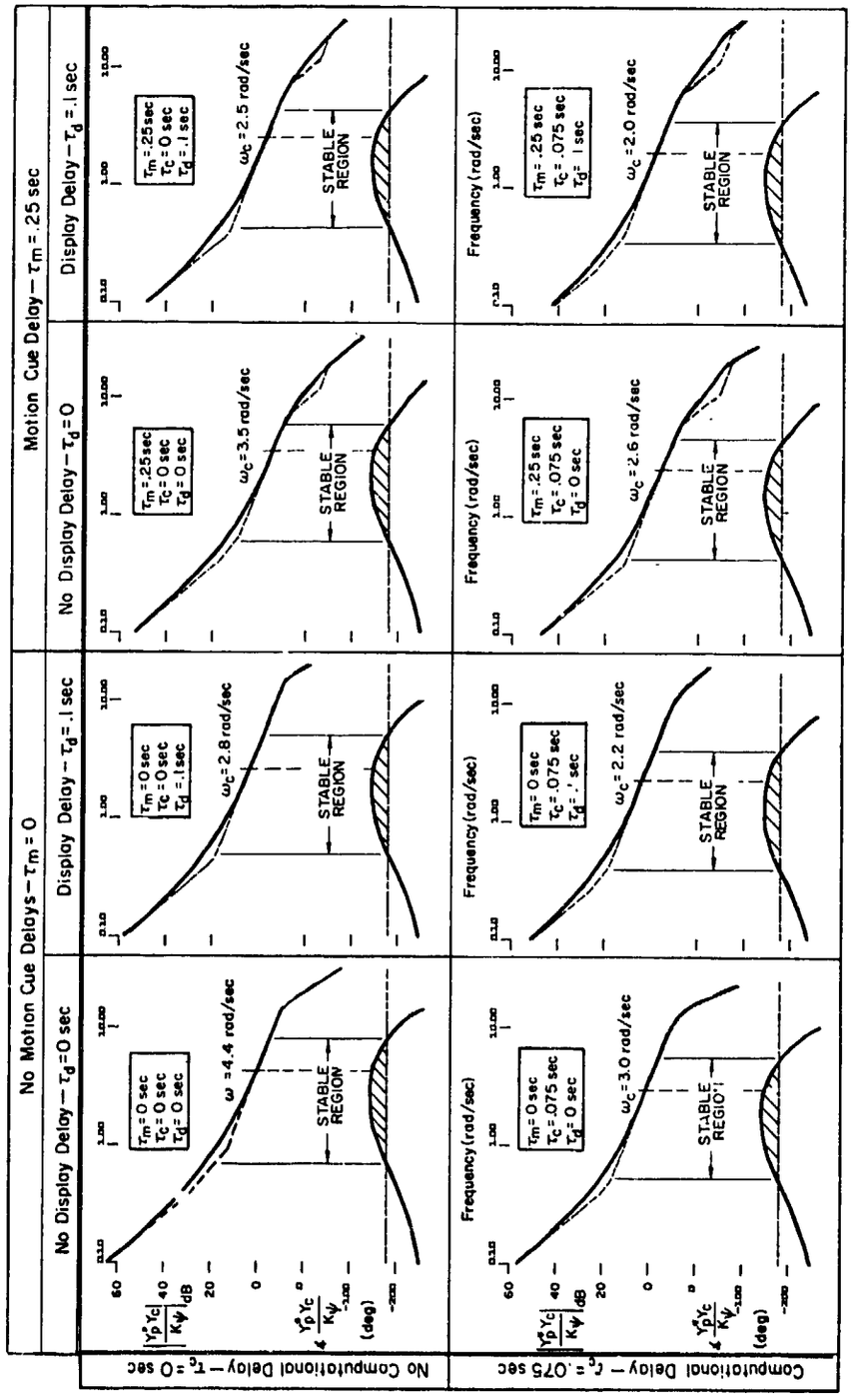

Figure 6. Equivalent Open-Loop Human Operator/Vehicle Describing Functions For Various Levels of Simulation Time Delays

TABLE 2. HUMAN OPERATOR/VEHICLE GAIN AND CROSSOVER MODEL PARAMETERS FOR VARIOUS COMBINATIONS OF INDUCED VEHICLE/SIMULATOR DELAYS

VEHICLE/SIMULATOR INDUCED DELAYS			GAINS		CROSSOVER MODEL PARAMETERS	
τ_m (sec)	τ_c (sec)	τ_d (sec)	U_o/R (rad/sec)	K_ψ (sec^{-1})	ω_c (rad/sec)	τ_e (sec)
0	0	0	0.92	10.26	4.4	0.17
		0.1 sec	0.44	6.59	2.8	0.27
	0.075 sec	0	0.50	8.60	3.0	0.25
		0.1 sec	0.26	6.39	2.2	0.345
0.25 sec	0	0	0.65	18.51	3.5	0.215
		0.1 sec	0.35	13.47	2.5	0.305
	0.075 sec	0	0.38	16.13	2.6	0.29
		0.1 sec	0.20	12.58	2.0	0.38

F. BANDWIDTH EFFECTS

The consequences of the above adjustment procedures can be seen in Fig. 7. Here observe that the control bandwidth of the operator/vehicle system drops dramatically as various delays are added into the simulation loop. Adding the 0.1 sec display delay has the largest single impact on equivalent time delay and system bandwidth. Motion cue delays had the least impact. Computational delays had an effect somewhere in between motion cue delays and display delays. Perhaps if the computational delay had been 100 msec it would have had a similar effect to the display delay. The concatenation of these various delay sources deteriorates the system bandwidth to an even greater degree. When all the delay sources were combined, the system bandwidth was cut by more than 50 percent.

The relationship shown in Fig. 7 is a consequence of maintaining a constant phase margin. If we had changed the desired phase margin, or chosen a different aim point range (thus changing the low frequency kinematic root U_o/R) then a different constant would have resulted. In any case, we can use the hyperbolic relationship between ω_c and τ_e to determine how changes in effective system time delay affect achieveable bandwidth. Assume that a 25 percent decrease in system bandwidth is permissable. Then

$$\frac{\omega_c'}{\omega_c} = 0.75 = \frac{K/\tau_e'}{K/\tau_e} \rightarrow \tau_e' = \frac{\tau_e}{0.75}$$

or

$$\tau_e' - \tau_e = \Delta\tau_e = \frac{1}{3}\tau_e$$

Thus, an increase of one third in the total effective system time delay (τ_e) would be acceptable. For exceptionally responsive real world systems, such as cars which can result in effective time delays on the order of 0.17 seconds (Ref. 7), such an incremental increase in time delay due to simulator characteristics, would be on the order of 50 msec. (Maximum time delays on the order of 40 msec have previously been recommended for driving simulators, Ref. 12.) For sluggish real world systems where effective system time delays might be 0.3-0.4 seconds, then incremental time delays on the order of 100 msec might be acceptable.

Regardless of the value of the constant in the Fig. 7 relationship, the tradeoff between system bandwidth and effective system time delay is fundamental, and gives some insight into the consequences of added computational delays, whatever their origin.

G. PERFORMANCE EFFECTS

A v_d impulse disturbance was applied to the Fig. 3 model as indicated in order to investigate the performance consequences of various time delay sources. The impulse input might be attributable to a wind gust or road input

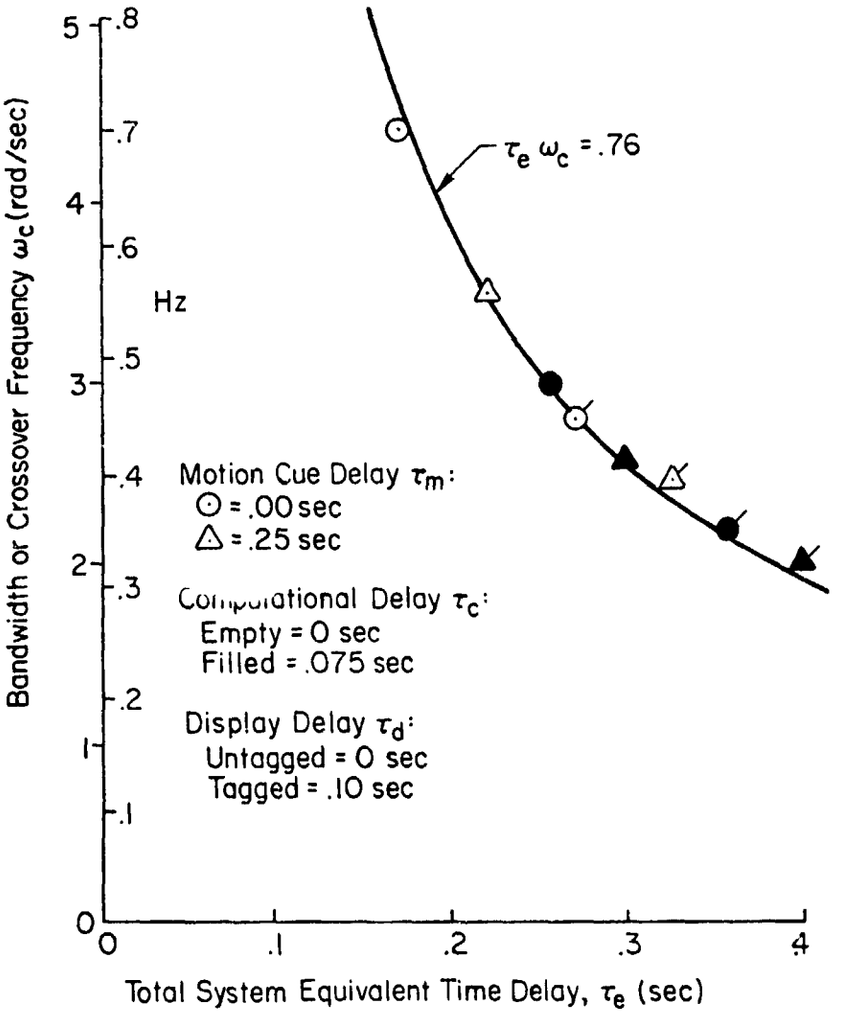

Figure 7. System Bandwidth as a Function of System Time Delay

in the case of ground vehicles. Time histories of the model transient response to an impulse disturbance input are illustrated in Fig. 8 for an automobile traveling at U_o = 80 ft/sec (55 mph). For the low frequency kinematic characteristics given in Table 2 (U_o/R = 0.2-0.92) the Fig. 8 transients could also be scaled to represent airplane motions in the Fig. 1 model (e.g., at 800 ft/sec this would represent target ranges of roughly 900-4000 ft).

The effects of the various transport delays on system performance are quite evident in Fig. 8. Note that the model's ability to maintain lane position deteriorates radically as the amount of simulator delay is increased. The effect of the various delay sources are directly observable in the steering wheel response of the model driver. As the delay sources are concatenated, the model driver takes longer and longer to initially respond to the input disturbance. This is consistent with the data given in Table 2 which shows the total effective system time delay increasing from a no delay level of 0.17 seconds to 0.38 seconds in the worst delay case.

The cycle time of the system transient response also obviously increases with increasing delay sources in Fig. 8. This effect is consistent with the decreasing bandwidth as a function of time delay shown in Fig. 7. Because of the driver/vehicle system's increasingly delayed regulatory response to the transient input, the maximum vehicle heading deviation nearly doubles in the worst delay case compared to the no delay condition, and the lane deviation increases by more than a factor of three with the increasing delay. Note also that each of the delay components considered separately in Fig. 8 have a similar effect on system performance, as does the concatenation of any two delay sources.

H. SYSTEM ARCHITECTURE AND DELAY COMPENSATION

The effective system delays analyzed herein can arise from a variety of sources. Effective computational delays are due to a composite of A/D and D/A operations, computational algorithms (e.g., integration routines) and general software architecture. Cycle time may not be a true measure of effective delay if some routines are updated more often than others (e.g., high frequency modes might be updated more rapidly than kinematic integrations). Motion drive computations can have analogous considerations, and the frequency response of the drive servos must also be accounted for. CGI systems must maintain high refresh and update rates to portray smooth motion (i.e., typically 50 Hz or above), but multiple frame times may be required for angular and translational commands work their way through typical pipeline architectures.

Delay compensation can be considered at various stages in the system architecture. Minimum delay integration routines should be considered for dynamic computations (Ref. 13). The update of motion and angular orientation cues are more critical to closed-loop operator/vehicle system response than outer loop translational information that is already delayed by kinematic integration. Thus in computing equations of motion, angular rates and orientation, and accelerations could be updated more rapidly than inertial velocity and position. In CGI display systems, angular transformations could be updated more rapidly than perspective transformations.

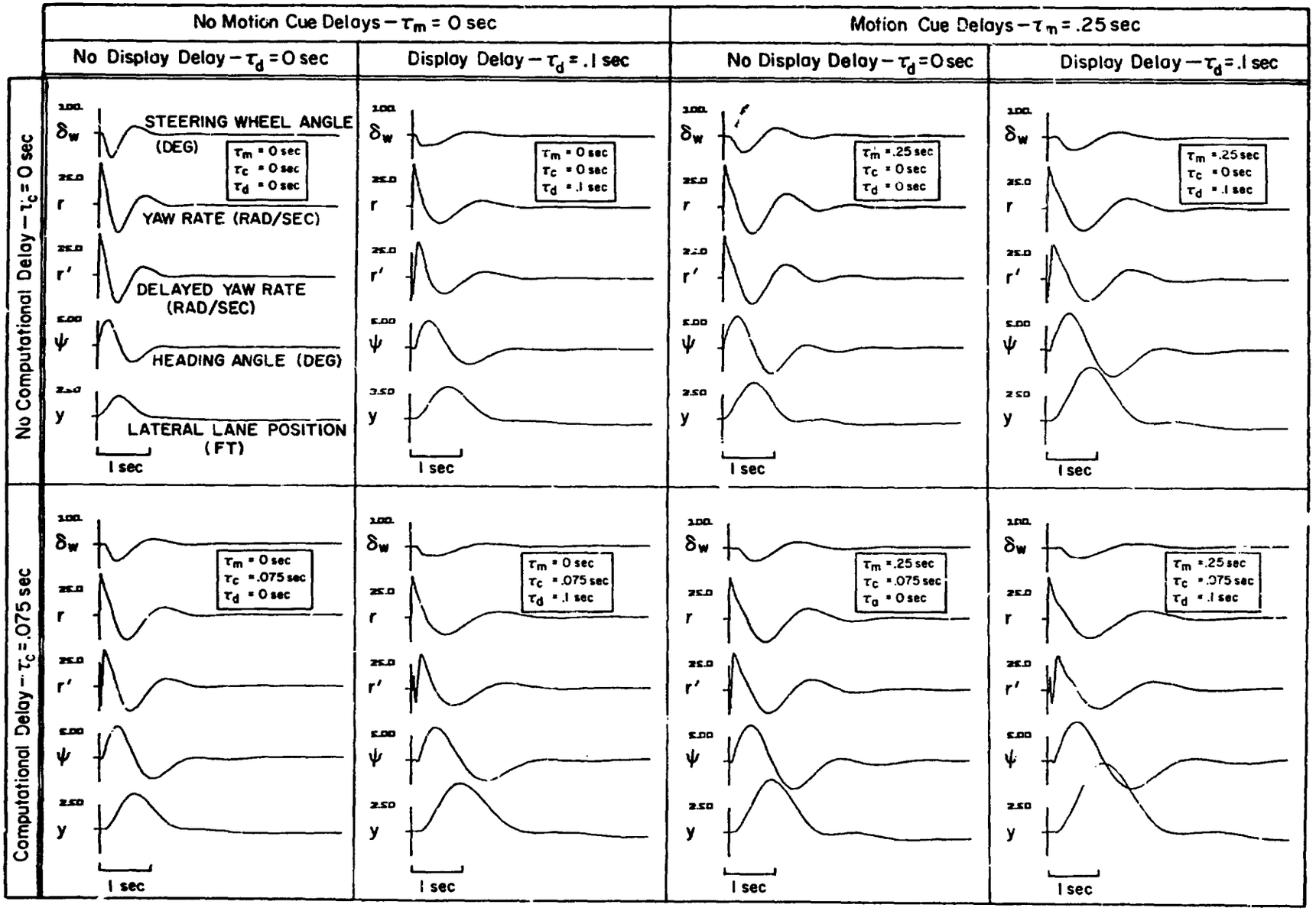

Figure 8. Driver/Vehicle System Closed-Loop Response to an Impulse Disturbance

ORIGINAL P
OF POOR QUALI

Lead or rate compensation might be considered for both host computer and CGI computations. Overall system dynamics should be considered here, however. The transfer functions in Figs. 4 and 6 suggest that for systems with adequate motion cues, lead frequencies in the region of the human operators limb/manipulator bandwidth (> 10 rad/sec) might be acceptable, while in the case of delayed or no motion cues, lead compensation could be increased to cover the bandwidth above the basic vehicle dynamics bandwidth. In general lead frequency must be above system crossover frequency (ω_c) in orcer to avoid compromising system gain margin.

I. CONCLUDING REMARKS

The model analysis herein shows that the effects of several computational delay sources in manual vehicle control systems can be evaluated to a first approximation by their effect on a composite effective system time delay. This effective time delay constrains the closed-loop bandwidth that can be achieved by the human operators. Tolerable computational delays can be determined by specifying a permissable system bandwidth reduction. The model analysis also shows that degradation in performance, such as regulation against transient disturbance, is consistent with system bandwidth reduction.

In general, compensation for effective system delays must be considered in an overall system context. System delays and compensation effects should be measured with input/output identification procedures using appropriate system inputs and sensors to measure outputs (e.g., gyros and accelerometers to measure platform motions and photo detectors to measure display system response). Response functions should be compensated to approach the less delayed response of the ideal target system. Finally, the fidelity of the system response should be considered from the human operator's point of view. In moving base systems, visual and motion cues should be consistent, and in general perceived vehicle response should be consistent with the operator's expectations. The analytic consequences of these fidelity considerations are not well understood, and typically would require final empirical tuneup.

REFERENCES

1. Puig, Joseph A., William T. Harris, and Gilbert L. Ricard, Motion in Flight Simulation: An Annotated Bibliography, NAVTRAEQUIPCEN IH-298, July 1978.

2. Semple, Clarence A., Robert T. Hennessy, Mark S. Sanders, et al., Aircrew Training Device Fidelity Features, AFHRL-TR-80-36, Feb. 1980.

3. Baron, Sheldon, Ramal Muralidharan, and David Kleinman, "Closed Loop Models for Analyzing the Effects of Simulator Characteristics," AIAA Paper 78-1592, presented at the AIAA Flight Simulation Technologies Conference, Arlington, TX, 18-20 Sept. 1978, pp. 138-148.

4. Parrish, Russell V., Burnell T. McKissick, and Billy R. Ashworth, "Comparison of Simulator Fidelity Model Predictions with In-Simulator Evaluation Data," NASA TP-2106, Feb. 1983.

5. Hess, Ronald A., "The Effects of Time Delays on Systems Subject to Manual Control," AIAA Paper 82-1523, presented at the AIAA Guidance and Control Conference Proceedings, San Diego, CA, 9-11 Aug. 1982, pp. 165-172.

6. Hoh, Roger H., Thomas T. Myers, Irving L. Ashkenas, et al., Development of Handling Quality Criteria for Aircraft with Independent Control of Six Degrees of Freedom, AFWAL-TR-81-3027, Apr. 1981.

7. Allen, R. Wade, "Stability and Performance Analysis of Automobile Driver Steering Control," SAE Paper 820303, presented at the 1982 SAE International Annual Congress and Exposition, Detroit, MI, 22-26 Feb. 1982.

8. Hodgkinson, J., W. J. LaManna, and J. L. Heyde, "Handling Qualities of Aircraft with Stability and Control Augmentation Systems -- a Fundamental Approach," Aeronautical Journal, Vol. 80, No. 782, Feb. 1976, pp. 75-81.

9. McRuer, Duane T., and Richard H. Klein, "Comparison of Human Driver Dynamics in an Automobile on the Road with Those in Simulators Having Complex and Simple Visual Displays," Systems Technology, Inc., P-173A, presented at the 55th Annual Meeting of the Transportation Research Board, Washington, D.C., 19-23 Jan. 1976.

10. Gum, D. R., and W. B. Albery, "Time-Delay Problems Encountered in Integrating the Advanced Simulator for Undergraduate Pilot Training," J. Aircraft, Vol. 14, No. 4, Apr. 1977, pp. 327-332.

11. Allen, R. Wade, "Modeling Driver Steering Control Behavior," Systems Technology, Inc., P-322, presented at the 1982 IEEE International Conference on Cybernetics and Society, Seattle, WA, 28-30 Oct. 1982.

12. Allen, R. Wade, and Henry R. Jex, "Driving Simulation -- Requirements, Mechanization and Application," SAE Paper 800448, presented at the SAE Congress and Exposition, Detroit, MI, Feb. 1980; also SAE Trans., Vol. 89, 1981, pp. 1769-1780.

13. Howe, R. M., "Special Considerations in Real-Time Digital Simulation," The Proceedings of the 1983 Summer Computer Simulation Conference, Volume 1, 11-13 July 1983, Vancouver, B.C., Canada.

D/V

N85 14499

STOL SIMULATION REQUIREMENTS FOR DEVELOPMENT OF INTEGRATED FLIGHT/PROPULSION CONTROL SYSTEMS

by

K. E. Sanders, Senior Engineer
Dr. D. C. Anderson, Senior Engineering Specialist
J. H. Watson, Engineering Chief
Flight Control Systems Section
General Dynamics Fort Worth Division

ABSTRACT

The role and use of simulation as a design tool in developing integrated systems where design criteria is largely unavailable is well known. This paper addresses additional simulation needs for the development of Integrated Flight/Propulsion Control Systems (IFPCS) which will improve the probability of properly interpreting simulation results. These needs are based on recent experience with power approach flying qualities evaluations of an advanced fighter configuration which incorporated Short Takeoff and Landing (STOL) technologies and earlier experiences with power approach flying qualities evaluations on the AFTI/F-16 program. Specific topics addressed in this paper are:

(1) The use of motion base platforms with axial and normal degrees of freedom will help in evaluating pilot coupling and workload in the presence of high frequency low amplitude axial accelerations produced by high bandwidth airspeed controllers in a gusty environment. This would also help quantify the airspeed controller bandwidth necessary for adequate STOL performance.

(2) The use of high resolution visual scenes or helmet mounted displays capable of providing better depth perception, HUD symbology, and simulated FLIR imagery will help in evaluating precision (no flare) all weather landing techniques.

(3) The use of higher computational capability to adequately model and execute more complete visual display, landing gear, and engine models will help in evaluation of high speed roll out dynamics.

These needs can be met with unique government simulation facilities such as the NASA Ames Research Development Center (NARDC) which have special capabilities.

Copyright © 1984 by General Dynamics Corporation
All rights reserved

INTRODUCTION

Development of a STOL integrated flight control system will require extensive manned simulation because design criteria and guidelines are incompletely developed for the STOL task (References 1 and 5). Therefore, the requirements on ground-based simulation equipment to aid in the development of a STOL control system become very important to developers of STOL aircraft. Specifically, simulations must be capable of supporting evaluations in the following areas:

1. Evaluations of normal axis and axial axis gust sensitivity effects on pilot workload and control effectiveness
2. Cockpit constraint system evaluations
3. Control gradient evaluations
4. PIO susceptability and cross control axis coupling
5. Crew station human factors evaluations
6. Safety evaluations
7. High speed roll-out and ground handling evaluations
8. Hydraulic flow demand evaluations
9. Evaluation of more complex landing gear and engine/nozzle/reverser operations
10. Low altitude ground effects and flying qualities evaluations with good visual peripheral cues and depth perception.

Realistically, pilot workload and effectiveness in precision STOL control tasks cannot be fully measured without these evaluations.

MOTION CUES

Recent STOL studies (Reference 1) and IRAD results (Reference 2) indicate that landing precision may be obtained to the required level by providing high-bandwidth pitch rate control for flight path adjustments in combination with tight, high bandwidth regulation of aircraft airspeed. This combination of control features is readily implemented on a STOL configuration which utilizes the thrust reversing feature of a 2-dimensional thrust vectoring/thrust reversing (2-D TV/TR) nozzle to achieve more then 0.2 g acceleration capability axially (fore and aft) and 0.5 rps^2 pitch acceleration. The high bandwidths achievable with this nozzle permit pinpoint control precision in piloted simulations of STOL landings in fixed base simulations, but aircraft gust sensitivity is high in the normal and axial axes due to the high system control loop gain associated with the powerful control forces available from the nozzle. For instance, from Reference 2, a generic STOL longitudinal axis control law was designed to provide decoupled pitch rate/airspeed control. The desired bandwidth of the pitch rate controller was well defined from the simulation results, but the desired bandwidth of the airspeed controller was not as clearly indicated. The airspeed controller was designed to provide the maximum decoupling purity between pitch rate and airspeed while maintaining a critically damped airspeed response to an incremental step command. The resulting design demonstrated the capability of providing very precise airspeed control, as shown in the left column of

Figure 1, even in the presence of 1.2 FPS RMS (1-Sigma, Dryden Spectrum) random atmospheric gusts. However, it is not apparent what effect the small amplitude, high-frequency gust-generated axial accelerations will have on pilot performance. It is also clear that the desired engine actuator requirements will have a direct impact on the bandwidth of the airspeed controller. A first-order-lag filter was placed in the airspeed feedback path in the studies of Reference 2 to evaluate the capability to reduce axial gust responses. As shown in the right column of Figure 1, a .02 filter time constant significantly reduced the axial acceleration activity. With the control system gain levels used in this study, a filter with time constants as large as .2 seconds could be used without adversely affecting system performance or stability. Therefore, there is a large range of airspeed control bandwidths which appear to be acceptable to pilots on a fixed base simulator. Figure 2 illustrates nozzle control activity during a typical approach in a gusty environment with the 0.2 second time constant airspeed feedback filter. While the illustrated control activity is not unreasonable, the actuators were occasionally operating near their assumed maximum rate. Figure 3 shows the relationship between nozzle control activity and axial acceleration. Since the degree of airspeed augmentation provided by the controller can have an impact on other aircraft systems such as the hydraulics, pilot vehicle interface, and engine control, it is important to determine the pilot acceptance of high frequency axial accelerations and how these accelerations are coupled through the pilot into axial control and into other axes. One example of pilot coupling experienced in flight but not experienced during simulation evaluations is the pilot coupled oscillations encountered during the AFTI/F-16 flight tests (Reference 3). Gust sensitivity in the normal axis can be evaluated, to some degree, based on common pilot experience, however, notable failures in evaluation of normal axis gust sensitivity have been experienced (e.g., Reference 4) on fixed base simulation equipment in the AFTI/F-16 program. Gust sensitivity effects on pilot workload in the axial axis will be difficult to evaluate with fixed base simulation equipment since pilots have not previously experienced the combination of high axial acceleration levels and bandwidths which are possible on a STOL aircraft. A study of this type can be accomplished on a moving base simulator with axial and normal degrees of freedom similar to capabilities on NASA-Ames moving base simulator facilities.

VISUAL CUES

Important primary visual cues used during a landing approach are associated with depth and peripheral vision. In the simulation of a STOL approach, the use of a limited area projection type of visual system does not provide the best result such as a wide field of view and good depth perception would provide. Also, because the scene is projected out in front of the pilot, landing biases can occur causing the pilot to land short of the intended touchdown point. Our recent experience (Reference 2) points to the need for a wrap-around virtual image type visual system which is mounted closer to the pilot. The use of a vertically collimated raster display utilizing simple solid color pastels to form a cartoon-like picture could significantly increase resolution near the ground. The wrap around feature would improve peripheral vision. Peripheral vision provides the pilot with sink rate information he cannot obtain very well over the nose at STOL approach angles of attack. This reinforces the pilot's perception of descent through the visual-motion system and thus increases his stress level. Since pilot gain is strongly influenced by stress level, real pilot workload could be more accurately determined with improvements in the visual system. The pilot must subconsciously feel that he is in real danger if the landing maneuver is not successfully executed for best evaluation results.

Helmet mounted displays have a significant application to a STOL approach and landing. They enhance peripheral and depth perception in simulation applications but also provide HUD information and simulated FLIR imagery in actual aircraft applications to perform

precision all weather and night landings. Operational use of Helmet Mounted Sight/Displays (HMSD) allow the pilot to view the landing scene under poor visual conditions and safely land the aircraft with a minimum of additional workload. This technology can give the pilot night vision, allowing the pilot to look anywhere in the forward quadrant through the aircraft to locate the landing field by merely directing his line-of-sight (LOS) to the desired area. The pilot's line of sight (LOS) commands the FLIR to follow his helmet (head) movements thus providing a large field of view (FOV) for landing the aircraft at large crab angles and high angles of attack. Symbology to aid the pilot in landing with minimum dispersion is superimposed on the FLIR video and projected onto the pilot's visor by a miniature CRT mounted on the helmet. The aircraft becomes "transparent" and he experiences a true kinetic sense of where the landing field is, relative to the aircraft, thus enabling him to land the aircraft using the scene on his visor. Proof of application and operational readiness will first have to be shown in a realistic simulation environment before deployment in the field.

COMPUTATIONAL CAPABILITY

Computer power may be the most easily attainable, yet least definable, quantity in a development simulator. Computers are constantly being improved from the standpoint of speed and memory capabilities. What is difficult to define is how the computing power is to be assembled to provide engineering flexibility, growth, and eventual hot-bench support. A STOL development simulator must provide capabilities in several key areas. First, adequate input/output (I/O) capability is important to support visual scene and motion base drives, advanced cockpit development, output data recording (both analog and digital), and eventual flight control and avionics hardware-in-the-loop simulation. Secondly, several simulation models which have traditionally been kept simple in their implementation such as engine, actuator, and landing gear models must be made more complete in order to lower program risk by providing timely hydraulic demand, engine operation, and critical high speed ground roll-out information. And thirdly, the addition of an all new Nozzle Drive Unit (NDU) complex will further tax existing computer modeling computational power. In order to achieve adequate computational fidelity several computers, operating at different rates, must be employed in parallel. Most importantly the computer simulation complex architecture must be such as to not compromise the fidelity of the presentation of the flight characteristics to the pilot.

SUMMARY AND CONCLUSIONS

Based on recent experience with power approach flying qualities evaluations of an advanced fighter configuration which incorporated STOL technologies, general requirements for adequate STOL flight simulation have been developed. Specific topics addressed in this paper were:

(1) The use of motion base platforms to and in evaluating pilot coupling and workload in the presence of high frequency low amplitude axial accelerations produced by high bandwidth airspeed controllers in a gusty environment. (This would also help quantify the airspeed controller bandwidth necessary for adequate STOL performance.)

(2) The need for high resolution visual scenes or helmet mounted displays capable of providing better depth perception, HUD symbology, and simulated FLIR imagery in evaluating precision (no flare) all weather landing techniques.

(3) The need for higher computation capability to adequately model and execute

more complete visual display, landing gear, and engine models.

The importance of a high fidelity presentation of the flight characteristics to the pilot cannot be overstressed.

REFERENCE

1. STOL Demonstrator Design Study, R. W. Woodrey, et. al., AFWAL-TR-83-3022, Vol II, General Dynamics Corp., March 1983.

2. Man-in-the-Loop General STOL Simuation, D. C. Anderson, K. E. Sanders, J. W. Roberts, ERR-FW-2345, General Dynamics Corp., Report in Progress.

3. AFTI/F-16 Pilot Coupled Roll Oscillation, Merle G. Allen, AIAA Paper No. 83-2282-CP, August 1983.

4. The Role of Simulation in Development of the AFTI/F-16 Digital Flight Controls, D. C. Anderson, K. E. Sanders, AIAA Paper No. 83-2283-CP, August 1963.

5. Design Criteria for Flightpath and Airspeed Control for the Approach and Landing of STOL Aircraft, J. A. Franklin, et. al., NASA TP-1911, March 1982.

6. An Operational Evaluation of Head-Up Displays for Civil Transport Operations, J. K. Lauber, et. al., NASA TP-1815, August 1982.

7. AIAA Paper No. 84-1901CP, Piloted Simulation Evaluation of Advanced Fighter Integrated Flight/Propulsion STOL Controls, D. C. Anderson, K. E. Sanders, AIAA G&C Conference, Seattle, Washington, 20-22 Aug 1984.

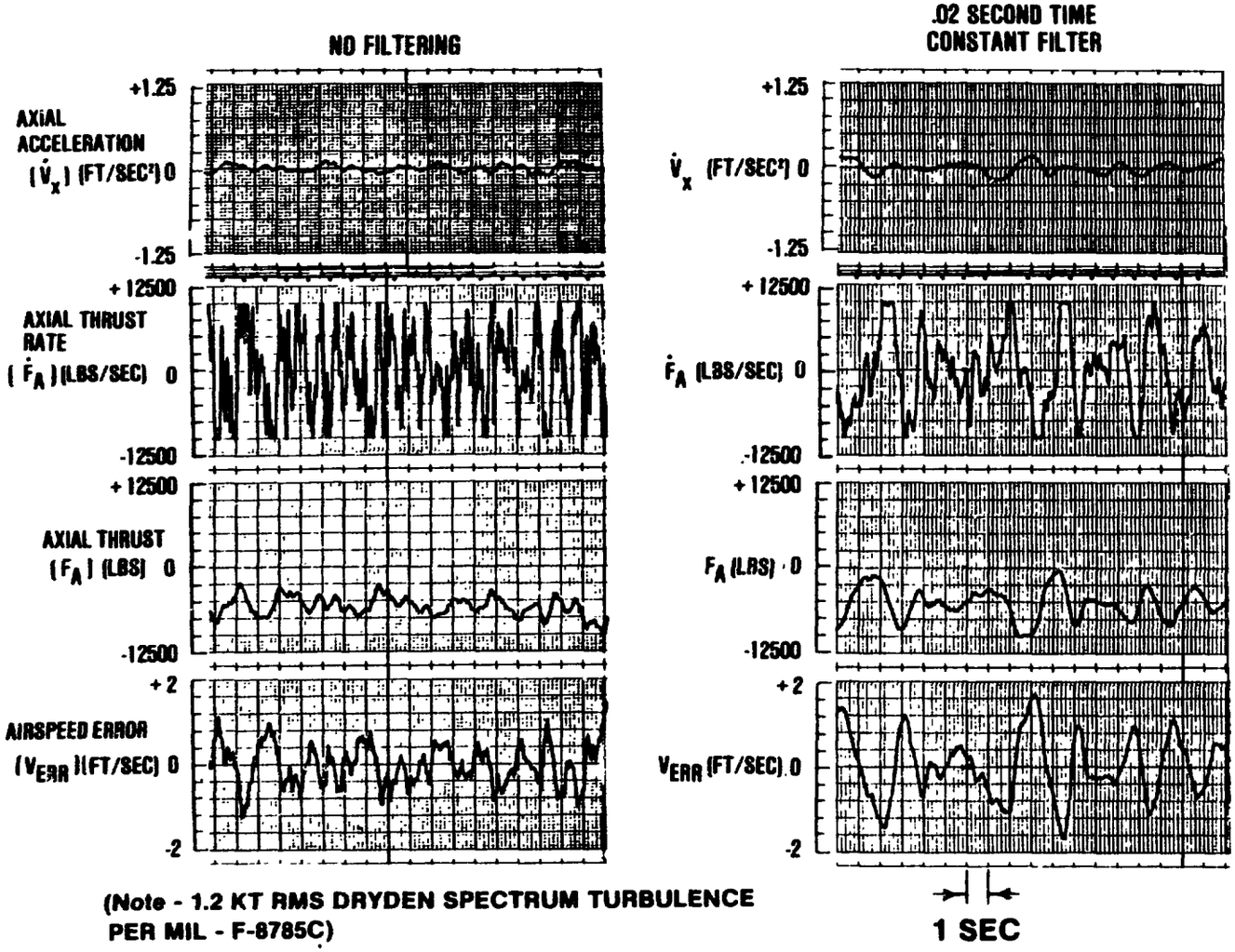

Figure 1 High Bandwidth Airspeed Controller Introduces High Frequency Axial Accelerations During STOL Approach

ORIGINAL PAGE IS OF POOR QUALITY

ORIGINAL PAGE IS
OF POOR QUALITY

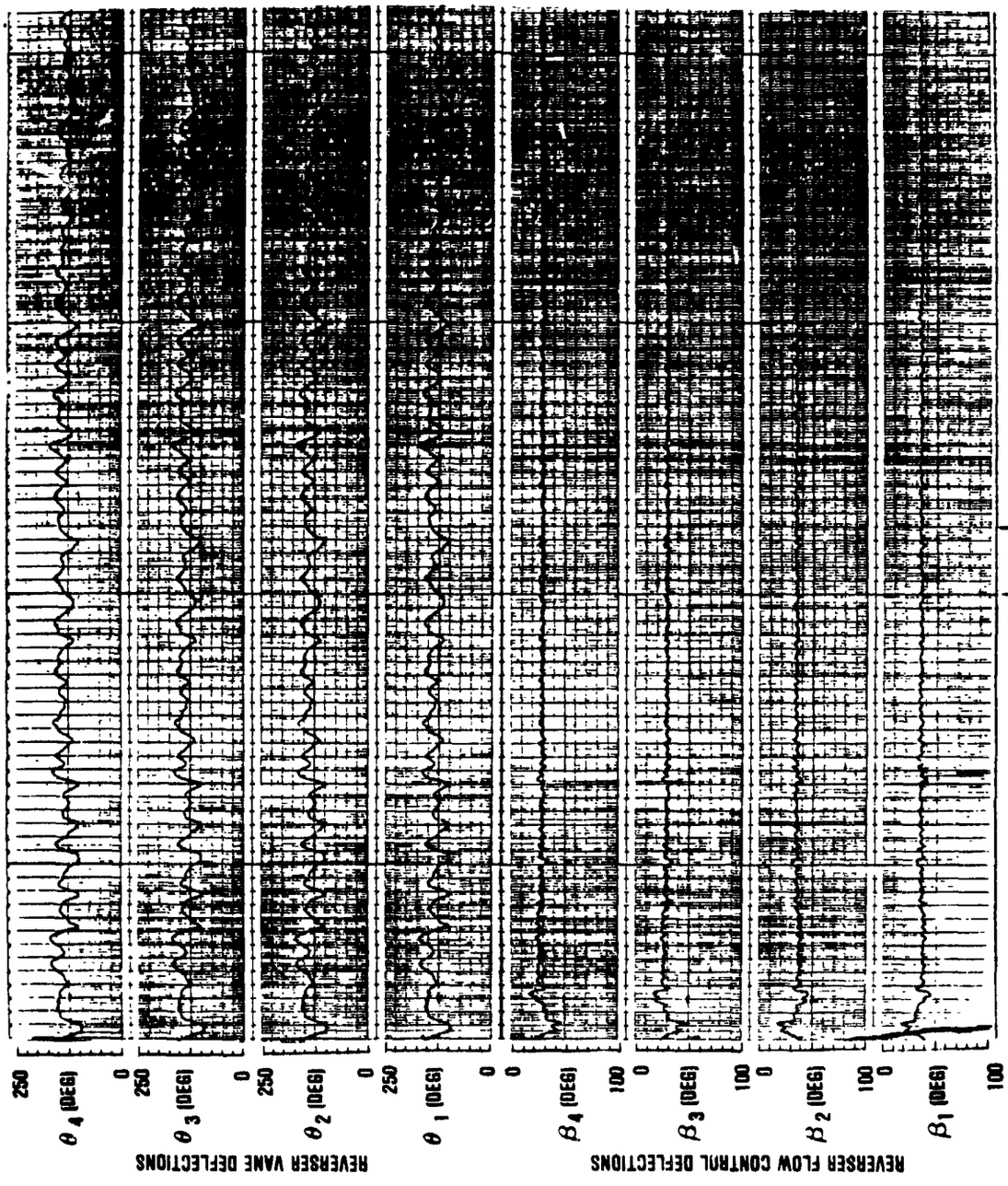

Figure 2 Nozzle Control Activity During a Typical STOL Approach

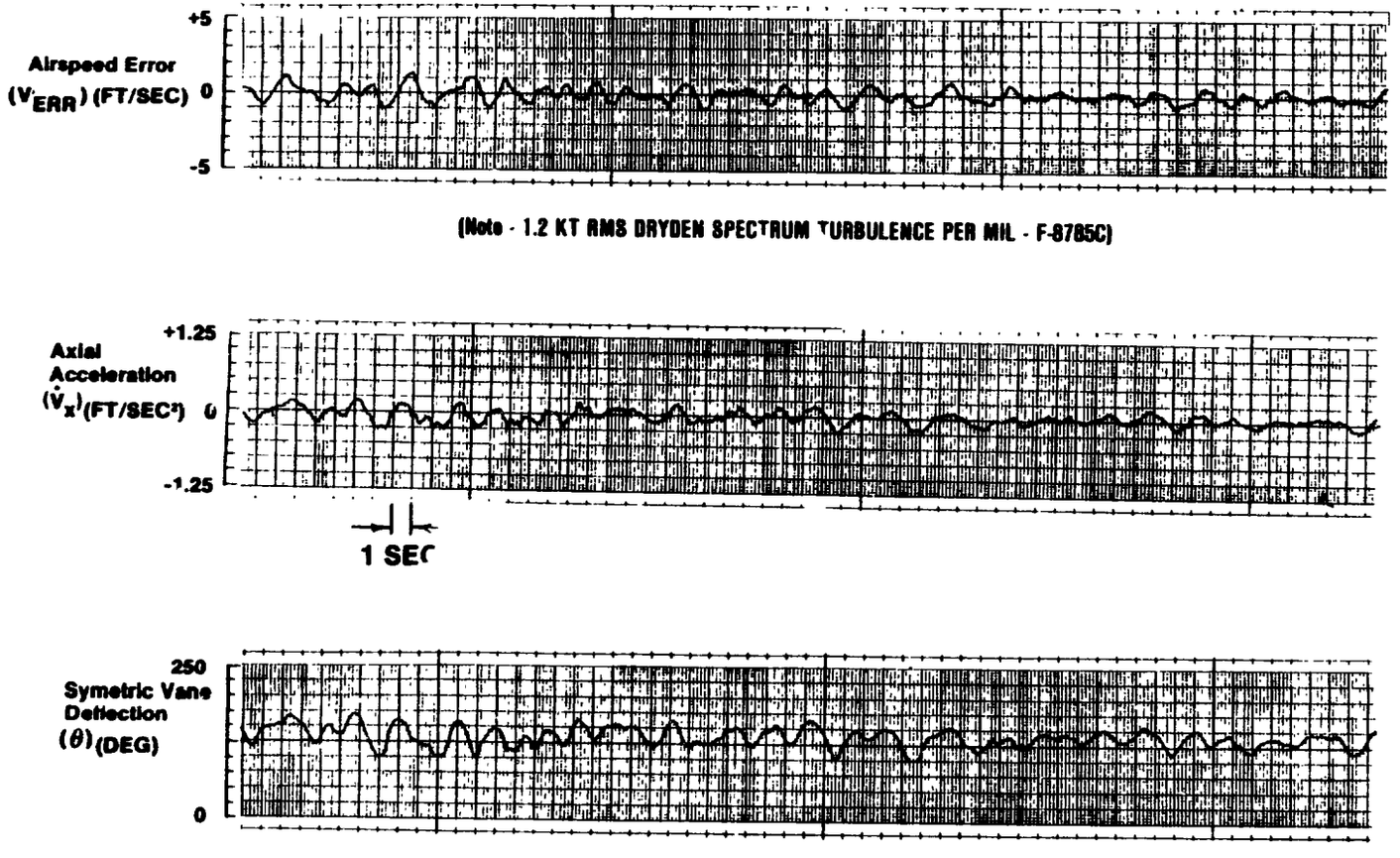

Figure 3 Nozzle Control Activity and Axial Accelerations as a Function of Airspeed Error

ORIGINAL PAGE IS
OF POOR QUALITY

D13

N85 14500

MEASUREMENTS OF PILOT TIME DELAY AS INFLUENCED BY CONTROLLER CHARACTERISTICS AND VEHICLE TIME DELAYS

Cynthia M. Privoznik, Donald T. Berry, and Adrian G. Bartoli
NASA Ames Research Center
Dryden Flight Research Facility
P.O. Box 273
Edwards, California 93523

ABSTRACT

A study to measure and compare pilot time delay when using a space shuttle rotational hand controller and a more conventional control stick was conducted at NASA Ames Research Center's Dryden Flight Research Facility. The space shuttle controller has a palm pivot in the pitch axis. The more conventional controller used was a general-purpose engineering simulator stick that has a pivot length between that of a typical aircraft center stick and a sidestick. Measurements of the pilot's effective time delay were obtained through a first-order, closed-loop, compensatory tracking task in pitch. The tasks were implemented through a space shuttle cockpit simulator and a critical task tester device. The study consisted of 450 data runs with four test pilots and one nonpilot, and used three control stick configurations and two system delays. Results showed that the heavier conventional stick had the lowest pilot effective time delays associated with it, whereas the shuttle and light conventional sticks each had similar higher pilot time delay characteristics. It was also determined that each control stick showed an increase in pilot time delay when the total system delay was increased.

NOMENCLATURE

CTT	critical task tester
e	base of natural system of logarithms (2.718)
K_c	controlled element constant
j	imaginary number
K_p	operator describing function constant
s	LaPlace operator
SHARP	Summer High School Apprentice Research Program
Y_c	controlled element
Y_p	operator describing function

λ	inverse time constant, rad/sec
λ_c	inverse time constant at critical time
τ_d	total system delay, sec
τ_p	pilot effective time delay, sec
ω	frequency

INTRODUCTION

The space shuttle control stick is different than a conventional aircraft stick in that it has a palm pivot in the pitch axis and is essentially a wrist rotation controller. A conventional controller has a longer pivot length and a more translational movement. Because of this difference there is an interest in how this may affect pilot time delay. Past studies conducted by Systems Technology Incorporated (refs. 1 and 2) have shown a difference in pilot effective time delay due to manipulator characteristics and the order of the controlled element. Total system time delays, which consist of pilot and vehicle system delays, are critical parameters in aircraft handling qualities. For example, pilot-induced oscillations can be encountered in critical tasks such as landing and inflight refueling when excessive time delays exist. The pilot's effective time delay can be an important component of the total system time delay when the pilot is in the loop. In some circumstances small changes in vehicle system time delays result in large changes in flying qualities (ref. 3).

In a study performed at NASA Ames Research Center's Dryden Flight Research Facility, a critical task tester (CTT) was used to obtain pilot effective time delay (τ_p) values for the shuttle stick and a more conventional stick. The experiment used two system time delays. Variations in the values of τ_p are used to show how the shuttle stick compares to a more conventional control stick and what effect the total system delay has on the pilot's effective time delay.

At the completion of this experiment, the equipment was available for the NASA Summer High School Apprentice Research Program (SHARP). A high school student in a science and engineering program measured operator time delay for a diverse group of subjects, mostly SHARP students. Results as a function of background and flying experience are briefly summarized in this paper.

DESCRIPTION OF EQUIPMENT

Three control stick configurations were used in this study with the shuttle cockpit simulator in the Ames Dryden simulation laboratory. One configuration was a space shuttle stick, which is a three-degree-of-freedom rotational manipulator with nonlinear gearing. The other two configurations used a more conventional general-purpose engineering simulation stick with two different spring constants. All sticks were center mounted. The

general-purpose stick was used in a variety of engineering simulators and represented a compromise among a broad range of stick characteristics. It had two degrees of freedom and linear gearing; however it had a pivot point between that of a typical aircraft center stick and a sidestick. This general-purpose stick was tested first with a stiff set of springs and was designated the heavy conventional stick. Later, a softer set of springs was installed to obtain the light conventional stick. The designations light, heavy, and conventional are only relative, however, since the force gradients are lighter and pivot arms are shorter for this stick than that used in most aircraft center sticks. For stick characteristics see table 1 and figures 1, 2, and 3.

The control stick signal that is processed through the cockpit simulator is operated with a 40-msec frame time and is sent through the CTT. The total inherent time delay between the pilot input and the CTT was 46 msec; 20 msec was due to the average sampling delay of the 40 msec frame time, and 26 msec was due to the computation time.

The CTT uses a first-order compensatory tracking task with an unstable controlled element:

$$Y_c = K_c\lambda/(s - \lambda)$$

where λ is the inverse time constant. Under these conditions it can be assumed that the operator can be described by:

$$Y_p = K_p e^{-\tau_p s}$$

where τ_p is the pilot's effective time delay. Figure 4 shows the block diagram and root locus of these elements using a first-order Pade' approximation for the $e^{-\tau_p s}$ term. λ is increased as a function of time and error magnitude, making the system more unstable until control is lost. The value of λ at that critical point approximates the reciprocal of the operator's effective time delay, $\lambda_c = 1/\tau_p$. This simplified summary is based on more detailed explanations of the critical tracking task theory which includes systems with additional system delays. These explanations can be found in references 1 and 2.

The pitch indicator is displayed on an oscilloscope as a horizontal bar that moves vertically in pitch. The λ_c values are read directly from a voltmeter. Figures 5 and 6 show the setup of the equipment.

TEST PROCEDURE

The test subjects for this study included four test pilots and one nonpilot engineer. All of the subjects were orientated to the experimental setup through a series of trial runs.

A series of 15 runs for each of the three stick configurations was conducted. Adding runs with a system delay of 250 msec brought the total number

of runs for each of the five test subjects to 90. The λ_c values were recorded for each run, and the average for the 15 runs was computed for each case. The λ_c values, which were read directly off the voltmeter, contained the 46 msec inherent time delay but did not contain the added system delay of 250 msec when it was applied. A time delay of 250 msec was chosen to simulate the total system delay nearer to the value of the space shuttle. The total average λ_c value from each set of 15 runs was converted to time delay and the 46 msec computational delay was subtracted from it to obtain the pilot's total effective time delay.

RESULTS AND DISCUSSION

Figure 7 shows the averaged τ_p values for each subject and the total average for all the subjects; these averages are denoted by solid bars. The data obtained from the runs with no added time delay (46 msec τ_d) is on the left and the data for the 250 msec added system delay run (296 msec τ_d) is on the right for each stick. Based on the total average for all the test subjects, the heavy conventional control stick had the lowest τ_p values with and without added system delay. The shuttle and the light conventional manipulator had similar τ_p values. The shuttle and light conventional sticks both had the same τ_p (200 msec) value for runs with no added system delay. On runs with added system delay, the shuttle stick τ_p was slightly higher than with the light conventional stick. Scatter can be seen in the data in figure 7 but the trends with any given pilot look very consistent.

The changes in τ_p values for each control stick because of added system delay are evident in figure 7. In every case the subject's effective time delay increased with an added system delay of 250 msec. On the average, the shuttle controller showed the most change: 70 msec. For the heavy conventional stick the average increase in subject delay was 50 msec. The average increase for the light conventional stick was 60 msec.

These data show that the changes in pilot time delay due to differences in manipulator characteristics are much less than the changes in pilot time delay due to differences in total system time delay. This is consistent with previous results (fig. 8). These data are unpublished results obtained under NASA Contract NAS2-4405 with Systems Technology, Incorporated. The data show very small changes in τ_p for a first-order controlled element as the gradient for a pencil controller changes from a rigid (force) stick to a free (unconstrained) stick. However, for a second-order controlled element, the τ_p is much larger and more sensitive to stick force gradient. Figure 9 presents the results of the Ames Dryden experiment in a format similar to that in figure 8. Figures 8 and 9 cannot be directly compared because of the differences in controller geometry, gradient, and controlled element time delay. However, some observations on gross trends are valid. The increase in τ_p for the second-order controlled element (Y_c, fig. 8) can be attributed to the additional mental processing the pilot must perform to compensate for the

integrator lag. The time delay in the controlled elements of figure 9 would also require pilot compensation (or lead); an increase, therefore, in τ_p would be expected. The change in pilot time delay for this experiment is not as large as that seen in figure 8. However, the variation in stick gradient for this experiment is not nearly as extreme as that used in figure 8. Perhaps even more significant is the difference in compensation required for the time delay compared to the integrator.

The secondary experiment conducted by a SHARP student was done in a similar manner to that of the primary experiment except that only one control stick configuration was used (the light Ames Dryden stick); the subjects included SHARP students and some adults. None of the subjects were professional pilots, although some were amateur pilots. The results of this experiment are summarized in figures 10 and 11. Figure 10 compares results of the secondary and primary experiments, and indicates that previous piloting experience did not affect the pilot's time delay; nonpilots, amateur pilots, and professional pilots scored alike. The student investigator, a video game enthusiast, correlated the results with video game playing experience. These results are shown in figure 11, and improvements in the raw score are shown as the number of video games played per week increased.

Although these data are insufficient to be statistically conclusive, they do suggest some interesting speculation. For example, the indication that pilot time delay is affected by video game experience, but not real-world piloting experience, suggests that laboratory setups that are too "game-like" may not give the same results as an operational environment. This, however, does not impair the usefulness of laboratory results in establishing trends and measuring differences.

CONCLUDING REMARKS

The space shuttle manipulator controller and a more conventional controller with two different force gradients were evaluated in the pitch axis using a first-order, closed-loop, compensatory tracking task implemented through a critical task tester device. Five test subjects performed a total of 450 data runs using the three control stick configurations with a total system delay of 46 and 296 msec. The data indicate that the heavy conventional controller had the lowest effective pilot time delay values associated with it, with and without the added system delay. The shuttle and light conventional controllers had similar pilot time delay characteristics. Each control stick experiment showed an increase in pilot time delay when there was an increase in total delay.

Changes in pilot time delay because of increases in system time delay were much more significant than changes because of manipulator characteristics.

A secondary experiment using the critical task tester indicated that the pilot time delay is unaffected by previous piloting experience but is influenced by video game experience.

REFERENCES

1. Jex, H. R.; McDonnell, J. D.; and Phatak, A. V.: A "Critical" Tracking Task for Man-Machine Research Related to the Operator's Effective Delay Time, Part I: Theory and Experiments with a First-Order Divergent Controlled Element. NASA CR-616, 1966.

2. McDonnell, J. D.; and Jex, H. R.: A "Critical" Tracking Task for Man-Machine Research Related to the Operator's Effective Delay Time, Part II: Experimental Effects of System Input Spectra, Control Stick Stiffness, and Controlled Element Order. NASA CR-674, 1967.

3. Berry, Donald T.; Powers, Bruce G.; Szalai, Kenneth J.; and Wilson, R. J.: In-Flight Evaluation of Control System Pure Time Delays. J. Aircraft, vol. 19, no. 4, Apr. 1982, pp. 318-323.

Table 1 Control stick characteristics

Characteristics	Pitch
Shuttle stick	
Breakout, in-lb	1.2
Travel, deg	±19.5
Gradient, in-lb/deg	1.2
Pivot point, in*	0
Heavy conventional stick	
Breakout, in-lb	0.5
At stop, lb	11.0
Travel, in	±2.0
Gradient, lb/in	5.3
Pivot point, in*	7.0
Light conventional stick	
Breakout, lb	0.5
At stop, lb	6.5
Travel, in	±2.0
Gradient, lb/in	3.0
Pivot point, in*	7.0

*Measured from middle of palm point on control stick.

ORIGINAL PAGE IS
OF POOR QUALITY

ORIGINAL PAGE IS
OF POOR QUALITY

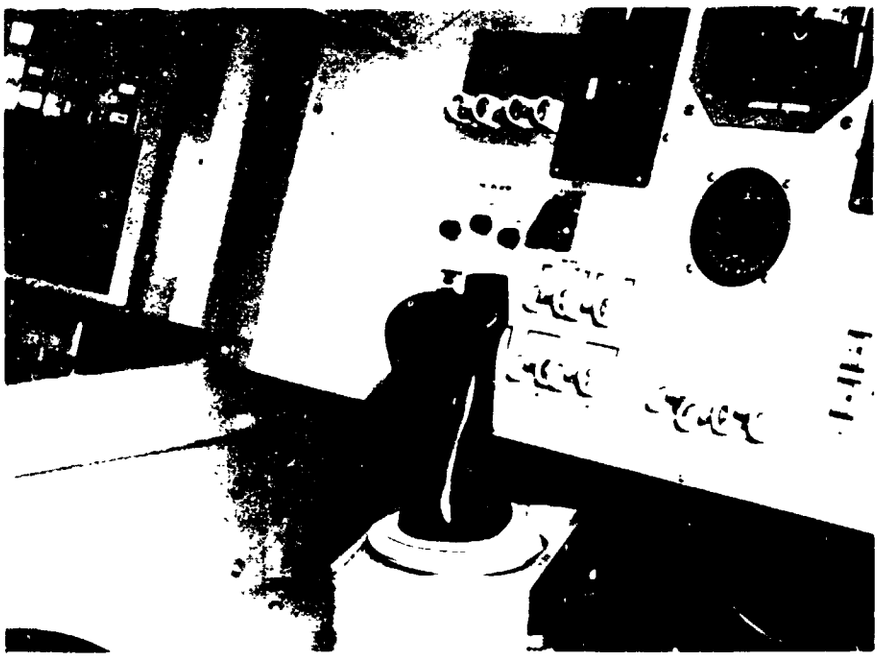

ECN 24922A

Figure 1. Space shuttle rotational hand controller.

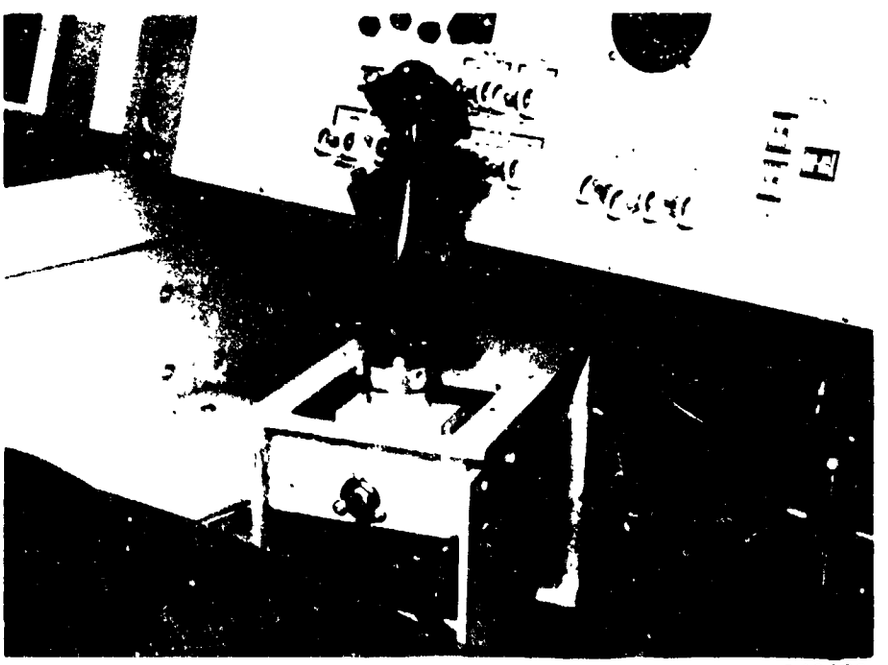

ECN 24919A

Figure 2. Conventional control stick.

OF POOR QUALITY

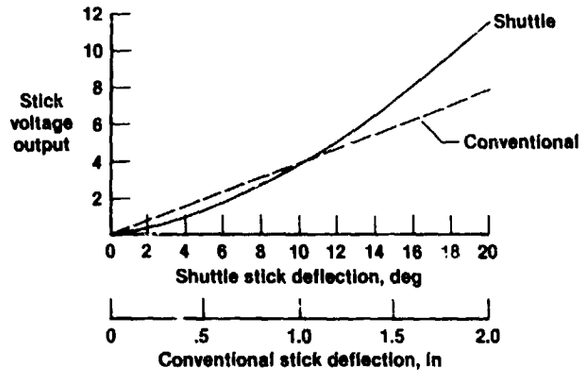

Figure 3. Pitch axis stick shaping.

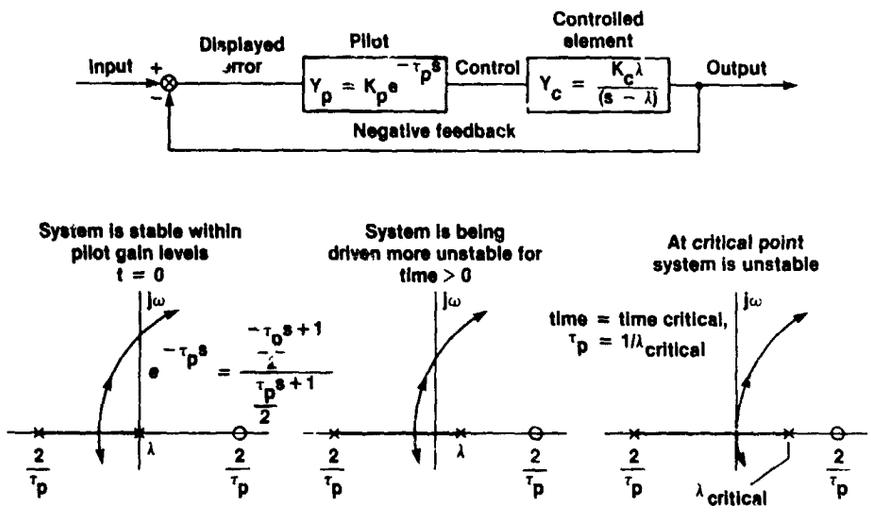

Figure 4. Critical task tester block diagram and root locus.

ORIGINAL PAGE IS
OF POOR QUALITY

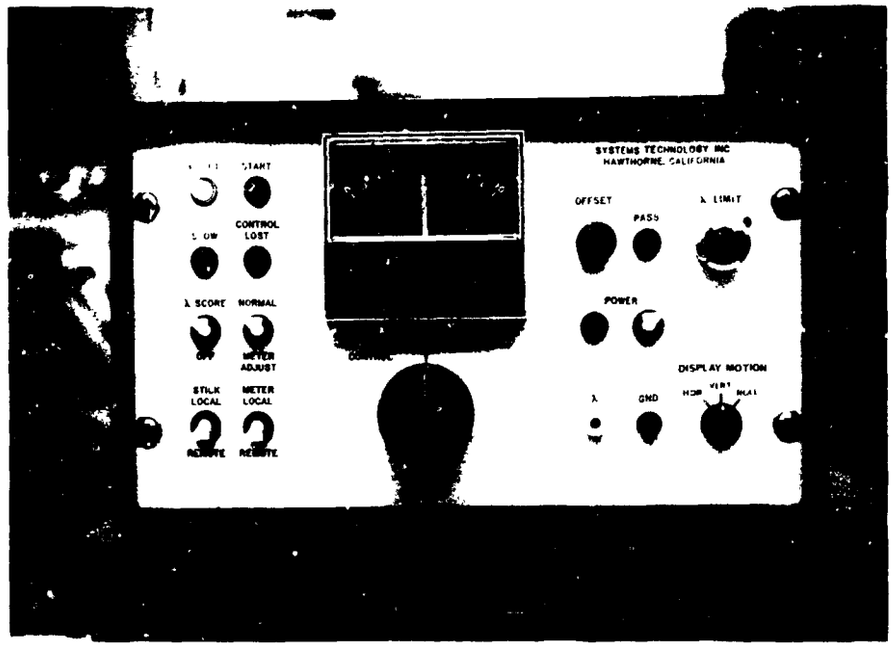

ECN 24923A

Figure 5. Critical task tester.

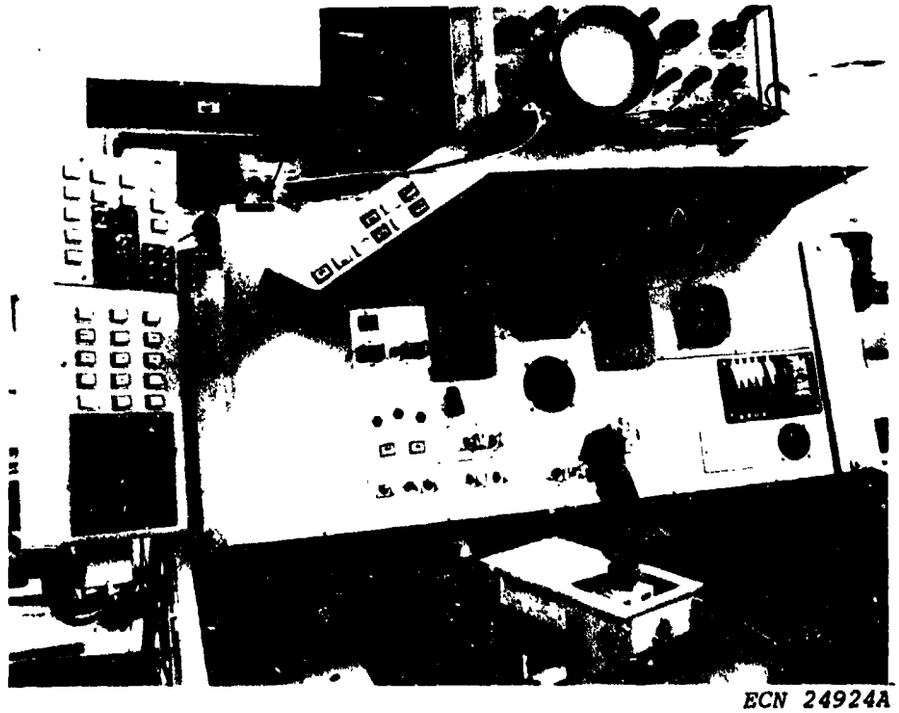

ECN 24924A

Figure 6. Simulator cockpit.

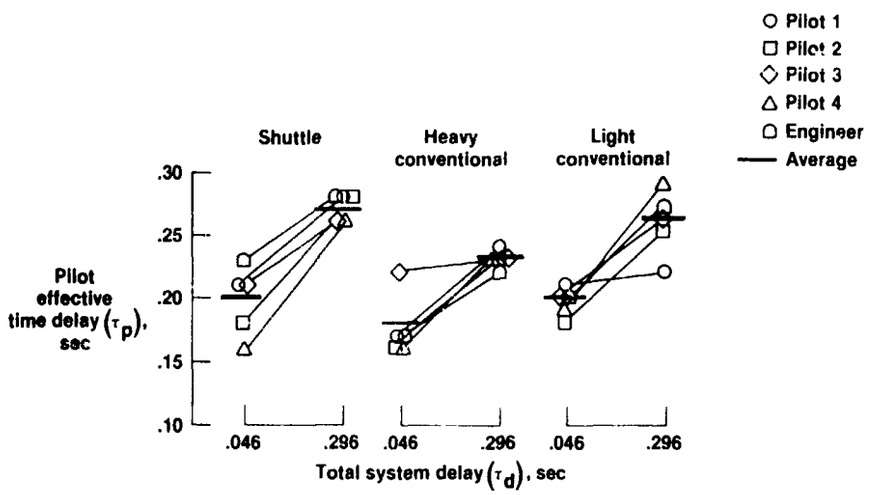

Figure 7. Summary of pilot time delay results.

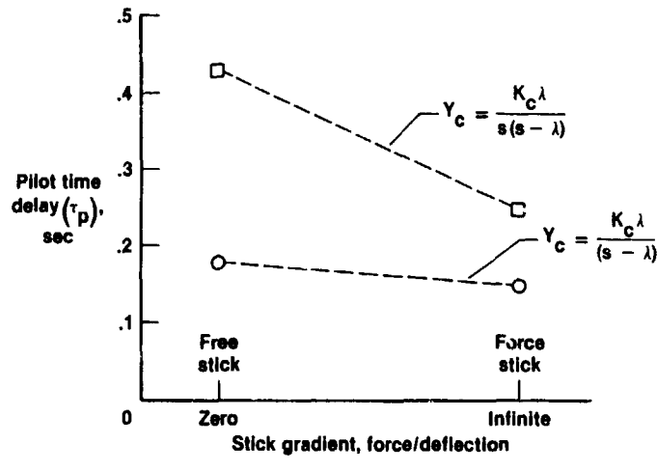

Figure 8. Pilot time delays for pencil controller.

ORIGINAL PAGE IS
OF POOR QUALITY

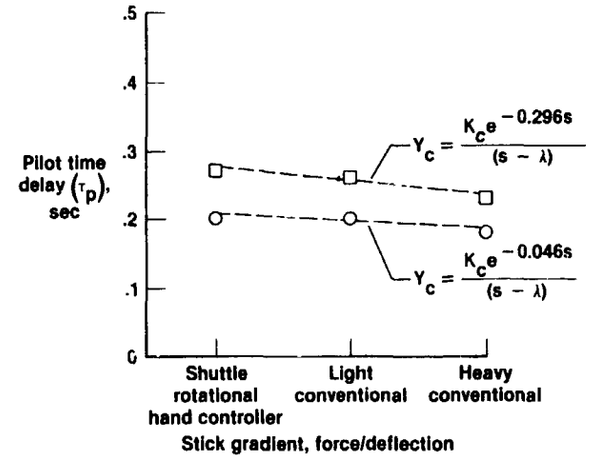

Figure 9. Pilot time delays for shuttle and conventional control sticks.

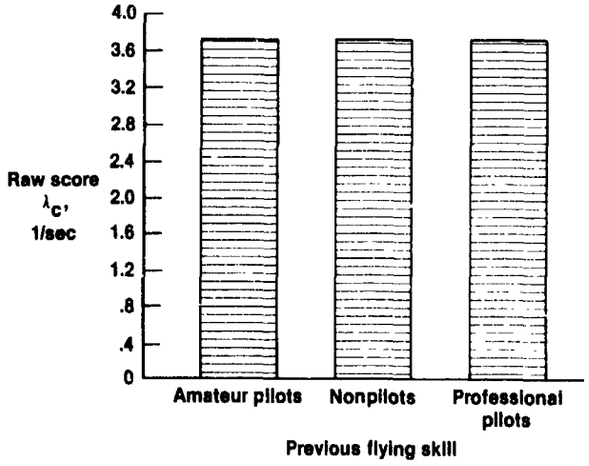

Figure 10. Raw scores as a function of flying skill.

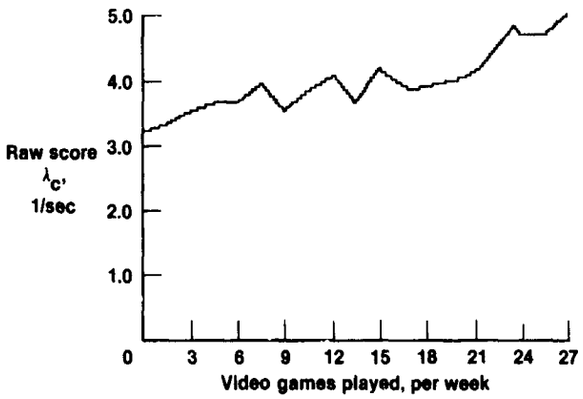

Figure 11. Raw scores as a function of video games played.

D14

N85 14501

Psychophysical Research in Development of a Fibre-Optic Helmet Mounted Display

R. V. Kruk[1] and T. M. Longridge[2]

The Fibre Optic Helmet Mounted Display (FOHMD) was conceived as an innovative solution to existing flight simulator display deficiencies. An initial (breadboard) version of the system was fabricated to permit experimentation which would help define design requirements for a more refined engineering prototype.

A series of visual/human factors studies is being conducted at the USAF Human Resources Laboratory (AFHRL) Operations Training Division, Williams AFB, Arizona to determine the optimum fit of human observer operating characteristics and fibre optic helmet mounted display technology.

Pilot performance within a variety of high resolution insert/binocular overlap combinations is being assessed in two classes of environment. The first two of four studies planned incorporate an air-to-air combat environment, whereas the second two studies will use a low level environment with air to ground weapons delivery.

This paper presents the research results to date from the air to air portion of the program.

1. CAE Electronics Ltd., 8585 Cote de Liesse, Montreal, Quebec, Canada.
2. USAF Human Resources Laboratory, Williams AFB, Arizona.

Flying Qualities

N85 14502

HELICOPTER PILOT PERFORMANCE FOR DISCRETE-MANEUVER FLIGHT TASKS

Robert K. Heffley and Simon M. Bourne
Manudyne Systems, Inc.
Los Altos, California

William S. Hindson*
Consultant
Stanford, California

Introduction

In order to address effectively the topics of aircraft handling qualities, pilot workload assessment, or aircrew training, it is sometimes necessary to describe and quantify adequately the associated flight tasks. Traditionally only labels have been used to do this (e. g., "landing", "climb", "turn", ...), but labels are insufficient to portray the level of aggressiveness, the amplitude of maneuvering, the degree of closed-loop damping, and other features of task execution crucial to success.

This paper describes a current study of several basic helicopter flight maneuvers. This is part of an effort sponsored by the U. S. Army Aeromechanics Laboratory under the Reference 1 contract. The data base consists of in-flight measurements from instrumented helicopters using experienced pilots. The analysis technique is simple enough to apply without automatic data processing, and the results can be used to build quantitative math models of the flight task and some aspects of the pilot control strategy. In addition to describing the performance measurement technique, some results are presented which define the aggressiveness and amplitude of maneuvering for several lateral maneuvers including turns and sidesteps.

Analysis Approach

The main purpose of this paper is to outline a general procedure for interpreting and analyzing pilot performance of certain discrete-maneuver flight tasks. The scope is limited to a few basic roll-axis helicopter maneuvers with emphasis on the inner-loop control of bank angle. Nevertheless, this permits useful connections to be made with the topics of pilot workload, handling qualities, pilot skill development, and vehicle performance.

One important concept is the recognition of the task as being an integral part of the man-machine system. As the piloting task varies, so must the control strategy and the closed-loop interactions between pilot and aircraft. In fact, the dynamics of task execution should be and usually are the dominant response modes of the pilot-vehicle combination. In addition, it is important to note how quickly a task is executed with respect to the time or space available. In short, there are several dimensions to task performance which are involved in the formula for success besides the more traditional precision metrics (such as tracking or trajectory errors, for example).

---

*Senior Research Associate, Department of Aeronautics and Astronautics, Stanford University.

Discrete maneuvers represent an important class of piloting tasks. Most tasks, in fact, are composed of a series of several discrete commands of attitude and power. These commands may not be either very periodic or numerous. Thus classical spectral analysis techniques requiring long record lengths and normally applied to long-term continuous tracking tasks may be of only limited use.

The analysis of discrete maneuvor tasks is not necessarily more difficult than continuous tasks. Discrete tasks can be portrayed using conventional feedback control block diagrams and Laplace transforms as shown in Figure 1. This formulation is more thoroughly described in Reference 2.

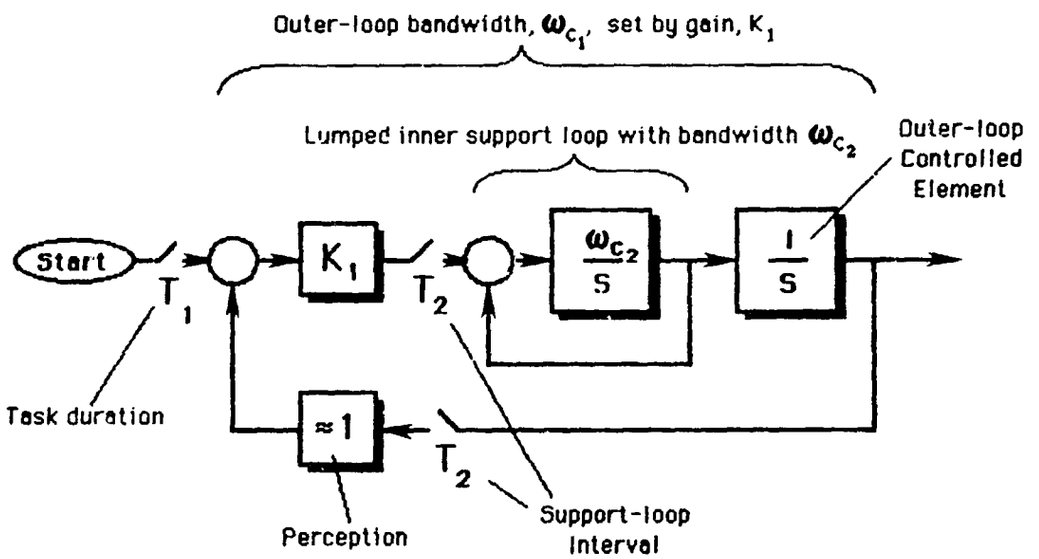

Figure 1. Block Diagram Structure for a Discrete Manuever Task and Support Loop

One factor which can complicate effective task performance measurement is the sometimes short, transitory nature of task execution. For example, a simple sideward translation of a helicopter might span only a dozen seconds and involve one quick bank to start, a second one to stop, and perhaps a third for fine adjustment of the final position. Each command might typically occur every three or four seconds, and the closed-loop response to a command need be only about one half cycle of the dominant mode of the bank angle task. Finally, bank angle commands may not be very periodic. Some of these features are illustrated in a timing diagram of an actual sidestep maneuver as shown in Figure 2. The term "timing diagram" is used because of the resemblence of the sequence of commands to a digital computer software timing sequence. The outer-loop lateral position commands correspond to a

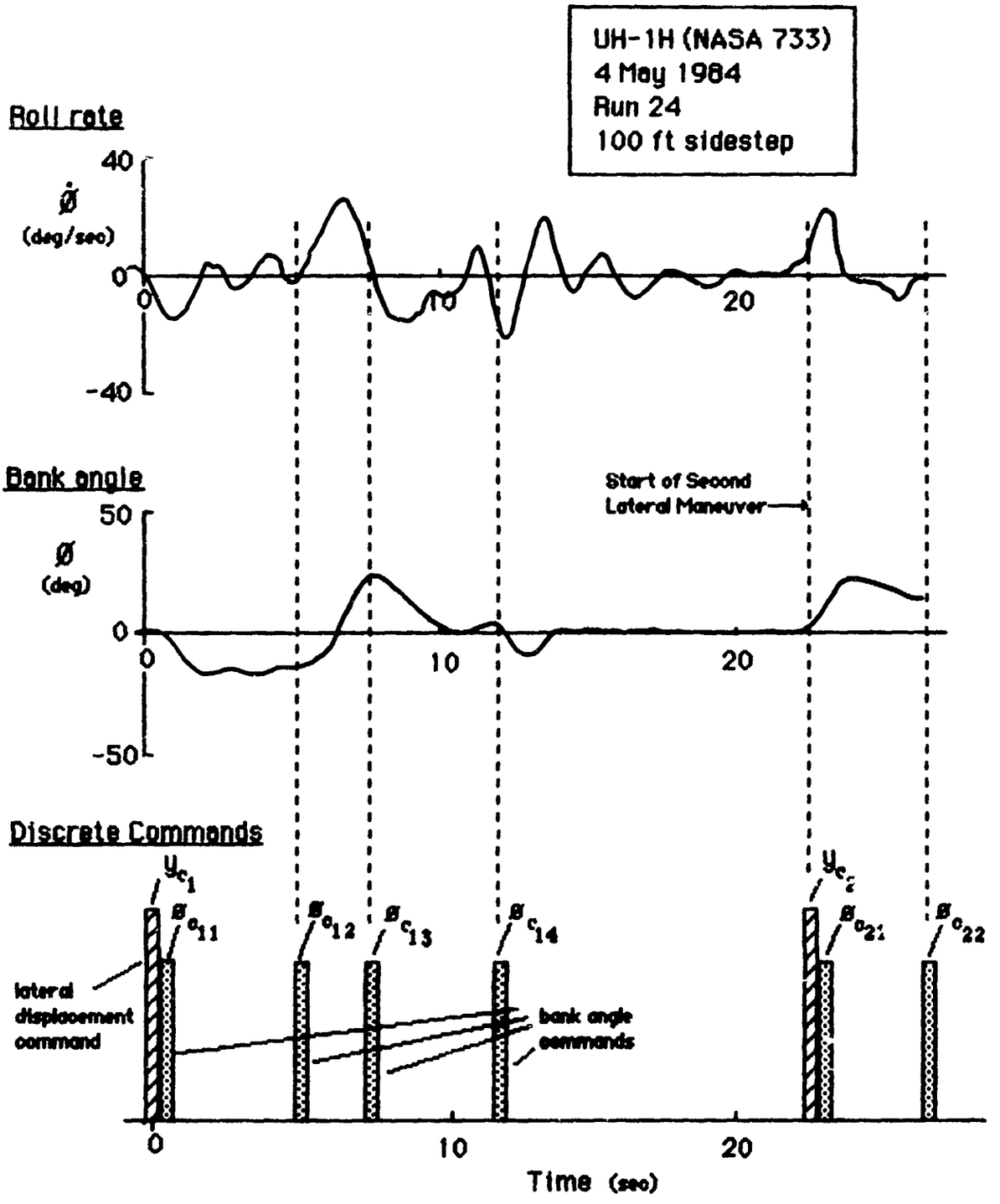

Figure 2. A Timing Diagram for a Typical Helicopter Sidestep Maneuver

kind of slow duty cycle while the inner-loop bank angle commands occur much more frequently. However, a typical flight task may involve only a few cycles of commands, and it is therefore necessary to use response identification techniques which will work over a fairly short sample.

One method for handling individual short-term discrete maneuvers is illustrated in Figure 3. If the features of a roll maneuver are to be studied, the first step is simply to obtain time history information which indicates the magnitudes of roll rate and corresponding bank angle change. Alternatively, this can be expressed on a phase-plane portrait in which case two important features can be clearly seen: (1) The net bank angle change and (2) the peak roll rate during that change. Finally these two features can be cross-plotted.

Roll rate versus net bank angle change can be interpreted in at least two ways. First, as explained in Reference 3, the proportion of peak rate to the net change in displacement is proportional to closed-loop natural frequency or bandwidth:

$$\omega_C \approx \frac{\text{peak rate} \times 2.4}{\text{net change in displacement}}$$

A detailed explanation of this relationship is given in Reference 4 using general second-order system phase plane plots. The valid range of damping ratios is about 0.4 to 1. A more exact determination of closed-loop frequency could be made using standard system identification techniques.

The second important facet of the roll rate versus incremental bank angle change is the magnitude of the maneuver in terms of either roll rate or bank angle. It was found that the former is perhaps a more significant parameter to use in connection with handling qualities since it can be directly compared with the vehicle roll rate capability. This will be discussed further at a later point.

It should be noted that the main purpose in applying the above analysis technique is to permit rapid assessment of flight or simulator data quickly and with minimal dependence on complicated data analysis techniques and complex data processing equipment. It is possible to examine on-line strip chart records of roll rate, bank angle, and lateral control and extract data points within a few moments of the actual generation of data. This permits better correlation of data with the conditions surrounding the data collection and factors affecting the pilot and aircraft.

Examination of Flight Data

Several flight maneuvers have been examined in the above manner. As part of the previously mentioned Army program, two experienced test pilots flew a NASA UH-1H through a series of aggressive turns, slalom courses, lateral sidesteps, and lateral jinking maneuvers. The objective was to observe the magnitude and aggressiveness and possible variations in piloting technique among these various maneuvers. Figure 4 is representative of how the discrete maneuver data appeared for one important class of lateral maneuver, the sidestep from hover. In this case the individual maneuvers combined to form a nearly straight line, i. e., the peak roll rate tended to be proportional to each roll attitude change. By multiplying the slope of the trend line by 2.4, the resultant closed-loop bandwidth appeared to be slightly in excess of 3 rad/sec—a fairly high value for a multiloop/multiaxis flight task. A typical value for routine approach and landing bank angle regulation would be about one half as much.

ORIGINAL
OF POOR QUALITY

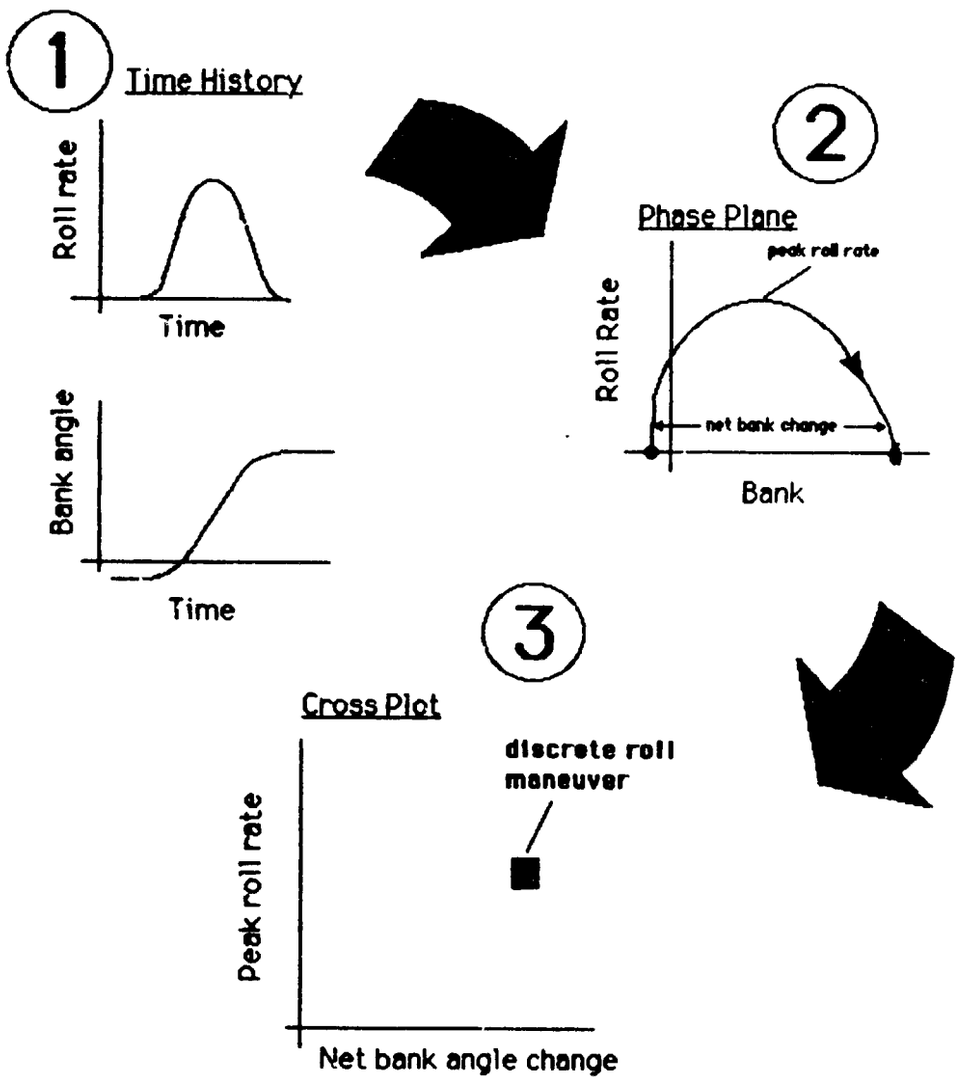

Figure 3. Analysis of Roll Maneuver Data

ORIGINAL PAGE IS
OF POOR QUALITY

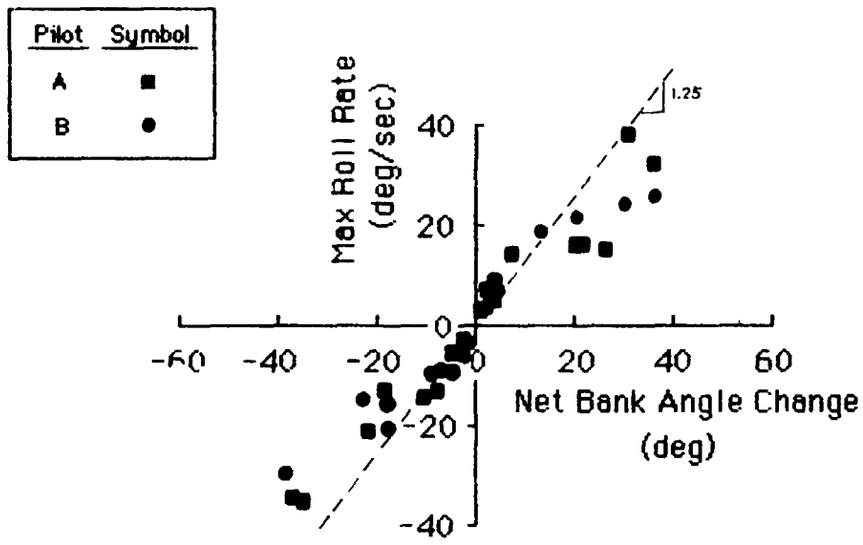

Figure 4. Aggressive Sidesteps from Hover with a UH-1H

Other maneuvers performed in forward flight generally were somewhat less aggressive, involved larger bank angle changes but were limited in the values of peak rollrate to about 40 deg/sec. One aspect being actively studied is why rollrates in excess of this value do not appear to be used by the pilots even though the helicopter may be capable of substantially greater rollrates.

In addition to the flight data that have been obtained in the course of this study, a number of other data bases have also been examined. One set of data involving an interesting comparison of two helicopters was furnished by the DFVLR* in Reference 5. The aircraft were a UH-1D (teetering rotor) and a Bo-105 (rigid rotor). The UH-1D is characterized by a modest level of rolldamping with some quickening provided by a mechical stabilizer bar. The Bo-105 has considerably faster short-term roll response as a result of the directly applied flapping moment on the rotor hub. A preliminary assessment of the discrete maneuver performance, however, indicates that the two helicopters were operated at comparable levels of aggressiveness in the slalom-type test that were conducted.

The maneuvers from this study along with the flight results from the DFVLR tests are listed in Table 1.

*Deutsche Forschungs- und Versuchsanstalt für Luft- und Raumfahrt e. V.

Table 1. Summary of Lateral Maneuver Flight Data

Source	Aircraft	Maneuver	Airspeed (kt)	ω_c (rad/sec)	$\dot{\phi}_{Pk}$ (deg/sec)
Hindson/ Wilson	UH-1H	Straight-line slalom	60	1.5	40
		" " "	80	2.4	40
		50° intersection turn	60	2.4	46
		130° " "	60	2.4	30
		30 ft Lateral jink	30	2.4	40
		Sidestep	Hover	3.1	37
DFVLR	UH-1D	Straight-line slalom	60	2.4	25
	Bo-105	" " "		1.7	23
	UH-1D	'German slalom'		1.6	47
	Bo-105	" "		1.8	32
	UH-1D/ Bo-105	High-g turn		-	33

The above performance data are valuable in gauging the demands of a given maneuver against the cabability of the aircraft—a fundamental handling qualities aspect. Figure 5 shows how maneuver requirements and aircraft capabilities can be expressed on a common scale. One aircraft characteristic is the maximum rollrate available. For a helicopter this is dependent upon basic rotor design parameters including rotor rpm, Lock number, and swashplate deflection angle. A second essential characteristic is the effective bandwidth or short-term rollresponse. For an augmented helicopter this is directly related to the rolldamping stability derivative.

Conclusions

The analysis of discrete-maneuver task performance from flight data has been found to be feasible using simple, easy-to-apply techniques.

From the time history data recorded on strip charts, the inner-loop task performance features readily obtained included measures of pilot aggressiveness, amplitude of maneuvering, and inner- or support-loop command intervals. This was adequate for portrayal of the task demands versus aircraft capabilities.

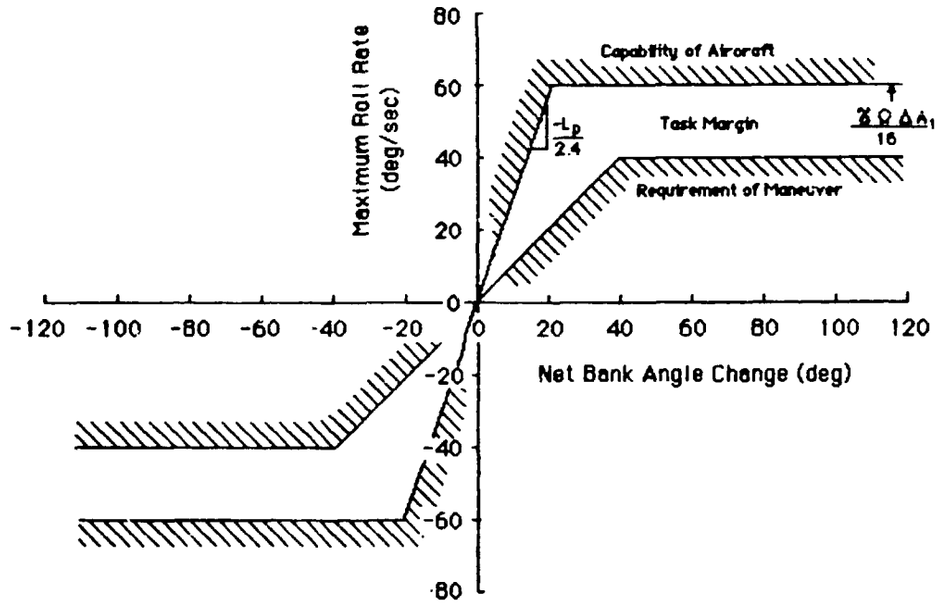

Figure 5. Interpretation of Discrete Maneuver Performance

In general, performance of several helicopter flight tasks varied between quick, small-amplitude discrete maneuvers and slower (lower bandwidth), large-amplitude maneuvers. In both cases, the peak rollrates observed were comparable.

Two modes of pilot operating conditions seemed to be involved over the range of discrete maneuvers. For small-amplitude maneuvers the magnitude of peak rollrate was about proportional to the magnitude of the bank angle command. Hence a linear, fixed-gain pilot model generally applies. For large-amplitude maneuvers, the peak rollrate was fairly independent of the bank angle command, thus a contactor-type control model is a better representation (i. e., a "saturated" or "limited" control). Both these operating modes—linear or contactor—can simultaneously be expressed by a simple linear gain in series with a limiter.

Sidestep maneuvers involved the highest level of pilot aggressiveness observed. Closed-loop bandwidths in excess of 3 rad/sec were typical. Peak roll rates as high as 40 deg/sec were employed by the pilots. These values tended to represent the most critical demands placed on this helicopter of any of the tasks explored.

Forward flight maneuvers such as turns or slalom maneuvers involved large amplitude bank angle commands with maximum peak rollrates of about 40 deg/sec. However for the inner loop, the maximum closed-loopbandwidths were typicallyabout 2.5 rad/sec.

Further analyses of outer-loop task performance are yet to be done. Typicallythis is more difficult only because of the data processing needed to handle translationalposition and velocity states. The same simple bandwidth and timing measurement techniques used for the inner loops are applicable, however.

The ultimate objective of this work is to catalog pilot performance parameters on a task-by-task basis and relate them to specific handling qualities features required.

References

1. Anon., "Study to Develop Helicopter Roll Control Effectiveness Criteria", Contract NAS2-11665, July 1983.

2. Heffley, Robert K., Pilot Workload Modeling for Aircraft Flying Qualities Analysis, NADC Report No. NADC-82094-60, May 1984.

3. Heffley, Robert K., Pilot Models for Discrete Maneuvers, AIAA 82-1519-CP, August 1982.

4. Heffley, Robert K., Ted M. Schulman, and Warren F. Clement, An Analysis of Airline Landing Flare Data Based on Flight and Training Simulator Measurements, NASA CR 166404, August 1982.

5. Pausder, H-J., Informal transmittal of flight data from UH-1D and Bo-105 aircraft, December 1983.

N85 14503

MAXIMUM NORMALIZED RATE AS A FLYING QUALITIES PARAMETER

E.D. Onstott

J.S. Warner

J. Hodgkinson

Northrop Corporation
Aircraft Division
Hawthorne, California

ABSTRACT

Discrete attitude commands have become a standard task for flying qualities evaluation and control system testing. Much pilot opinion data is now available for ground-based and in-flight simulations, but adequate performance measures and prediction methods have not been established. The Step Target Tracking Prediction method, introduced in 1978, correlated time-on-target and rms tracking data with NT-33 in-flight longitudinal simulations, but did not employ parameters easily measured in manned flight and simulation. Recent application of the Step Target Tracking Prediction method to lateral flying qualities analysis has led to a new measure of performance. This quantity, called Maximum Normalized Rate (MNR), reflects the greatest attitude rate a pilot can employ during a discrete maneuver without excessive overshoot and oscillation. MNR correlates NT-33 lateral pilot opinion ratings well, and is easily measured during flight test or simulation. Furthermore, the Step Target MNR method can be used to analyze large amplitude problems concerning rate limiting and nonlinear aerodynamics.

INTRODUCTION

Although the lateral roll mode of a conventional aircraft is perhaps the most easily understood aspect of aircraft dynamics, there exists at the present time a number of unresolved aspects relating to roll performance. On the one hand, theoretical and fixed-base flight simulation data dictate that the shortest roll mode time constants should characterize an ideal configuration. On the other hand, in-flight simulations and experience with real-world aircraft development programs show clear disadvantages in such highly damped aircraft. This in-flight experience is exemplified in the fundamental data

PRECEDING PAGE BLANK NOT FILMED

base obtained using the NT-33 aircraft. This is published in two volumes as AFWAL-TR-81-3171, "Lateral Flying Qualities of Highly Augmented Fighter Aircraft" by Monagan, Smith, and Bailey, Reference 1. Part of this difficulty lies in a confusion of real-world aircraft considerations such as ride qualities and control system actuator response, with pure isolated flying qualities of closed-loop pilot control dynamics as seen in analysis and flight simulators.

Beyond this, the plaguing occurrence of roll ratcheting has caused the appearance of numerous articles on lateral flying qualities in recent years, References 2, 3. If these publications are examined, it becomes clear that an insufficient flight data base is at the root of this failure to understand these aspects of lateral flying qualities. The associated lack of comprehensive criteria is now a major concern in the development of highly augmented tactical aircraft. The resolution of the above dichotomy between ideal aircraft response, and real-world aircraft constraints constitutes the main problem of designing roll command augmentation systems (roll CAS) for state-of-the-art, highly augmented tactical aircraft. The aircraft control system designer's primary objective can be stated:

DESIGN OBJECTIVE:	Alleviate the aircraft constraints as much as possible so that the best control dynamics can be realized.

The main categories of "Ideal Dynamics," and "Real Aircraft Constraints" are shown in Figure 1 in relation to the above DESIGN OBJECTIVE.

As indicated in Figure 1, the design process is a contest between the ideal and the real. Northrop is currently pursuing this tradeoff roll CAS technology through four basic approaches:

- Review and analysis of current literature and flight test data.
- Development of more discriminating analysis methods.
- Ground-based flight simulation.
- Contractual participation with NASA Dryden Flight Research Facility in a "Cooperative Program for Investigation of Superaugmented Aircraft Lateral Flying Qualities," involving in-flight simulation using the DFBW F-8 aircraft.

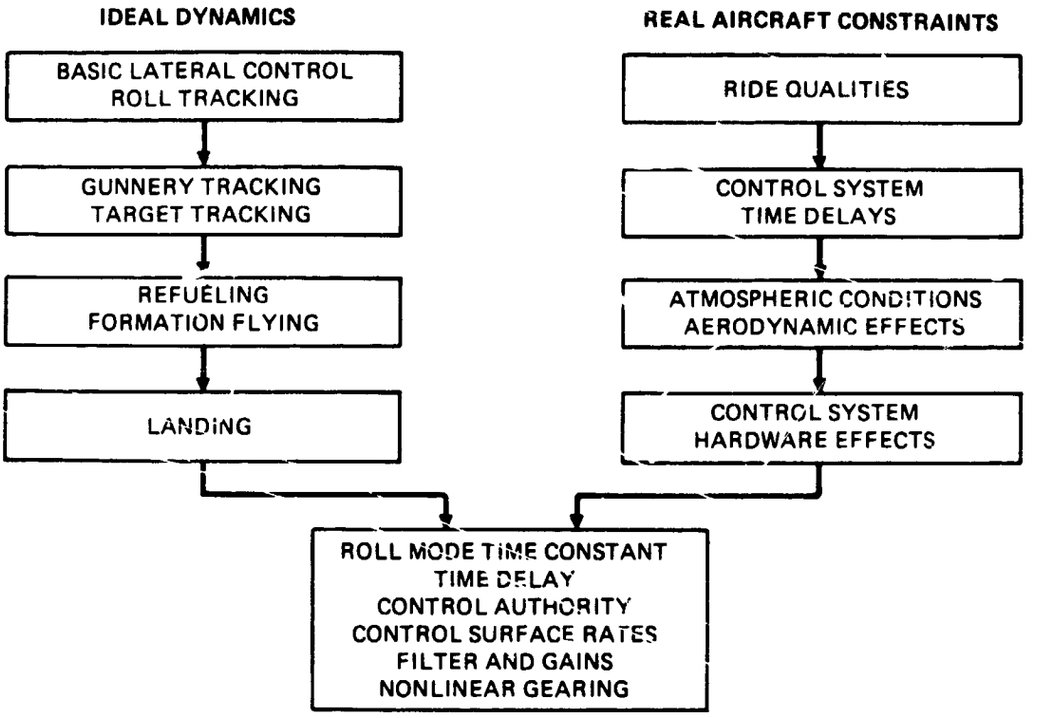

FIGURE 1. ROLL COMMAND AUGMENTATION DESIGN SELECTION

The following presentation will summarize an analysis of existing data using a new flying qualities concept, and show how this method is being used to evolve test matrices for ground-based and in-flight simulations.

ANALYSIS OBJECTIVES AND SELECTION OF METHOD

Although historically the design of lateral flight control systems has been a somewhat routine activity, the advent of highly augmented and unconventional aircraft configurations requires a much more careful selection of dynamic characteristics for acceptable flying qualities. In fact, the in-flight experiment of Reference 1, which will be referred to as LATHOS – for LATeral High Order System, has partially supplied a much needed data base including roll mode time constant, control system time delay, a limited variation of prefilters, nonlinear stick gearing, and Dutch roll damping. In addition to the difficulties in interpreting lateral flying qualities in the presence of high lateral acceleration at the pilot station, attempts to verify the resulting LATHOS criteria for acceptable roll mode time constant by ground-based flight simulation has not been successful. For example, a fixed-base study was performed at McDonnell Aircraft Company in 1984, Reference 4. The relation of the LATHOS and McAir data is shown qualitatively in Figure 2.

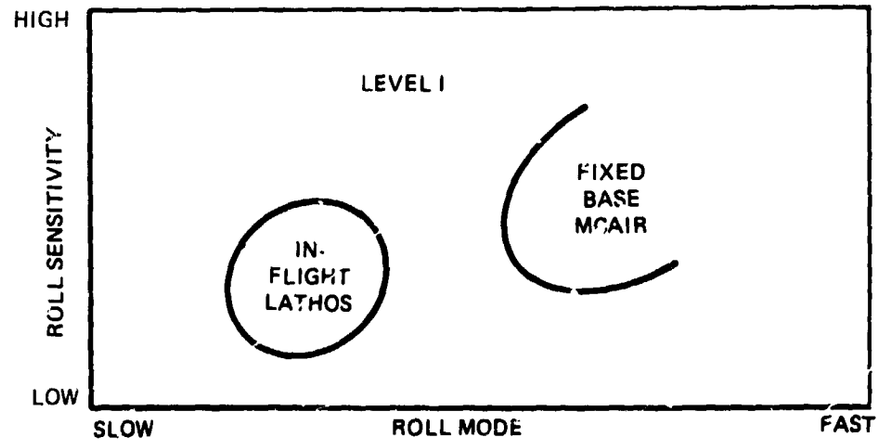

FIGURE 2. DIFFERING CRITERIA FROM IN-FLIGHT AND FIXED-BASE SIMULATION

This discrepancy in placement of roll mode time constant for Level I flying qualities presents a fundamental problem in aircraft control design. For this reason, study of the LATHOS data base using closed-loop pilot-vehicle methods was undertaken at Northrop in 1983.

There were four basic objectives in this undertaking.

1) Develop a methodology that will be applicable to nonlinear lateral flight control systems including prefilters and actuator limiting.

2) Identify a minimal dimensional metric that can be correlated with the LATHOS pilot rating data so that interpolations of the LATHOS test matrix can be made.

3) Employ the metric of 2) to analyze discrepancies in the LATHOS data, identify sensitivities, and recommend improved test procedures.

4) Interpolate the LATHOS survey to develop test matrices that will augment the existing data base in a manner resolving deficiencies and inconsistencies.

The first objective requires that the methods used can incorporate nonlinearities. For this reason, time domain methods were selected.

The LATHOS program included a HUD tracking task consisting of discrete bank angle commands as shown in Figure 3, redrawn from Reference 1.

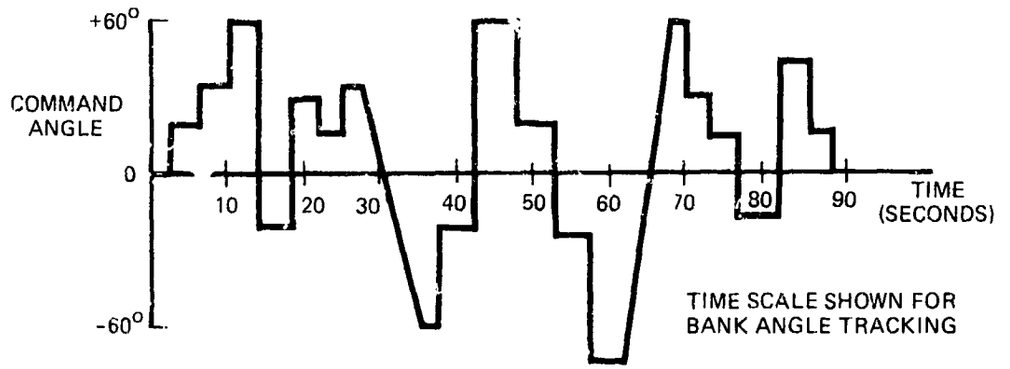

FIGURE 3. LATHOS HUD TRACKING COMMAND TIME HISTORY

This task was selected for analysis of the bank angle tracking task. In the LATHOS program, the HUD task was also flown in a heading task, and the other evaluations consisted of air refueling, formation flying, and gun tracking. These are multiloop lateral-directional tasks; thus they do not qualify for a lateral analysis. Even so, correlations between pilot data for these tasks and the lateral analysis results are possible and will be presented.

For these reasons, it is natural to employ a method developed to solve a similar discrete tracking problem in longitudinal flying qualities, the Northrop Step Target Tracking Method. For the sake of completeness, this method is briefly described next for a pitch step attitude tracking task.

INTRODUCTION TO THE STEP TARGET METHOD

Current flight test and flight simulation practice make extensive use of piloted attitude capture tasks as diagnostics for flight control performance. This procedure consists of having the pilot close on a target attitude as rapidly as he can without exciting excessive residual oscillations. Although this is a simple and effective flight simulation method, there are the following advantages in approximating such results by purely analytical means:

- Simulation time can be reduced
- Uniformity in pilot techniques can be maintained
- An assessment of task severity can be made
- An exact comparison of control system variants can be made.

An analytical method for accomplishing this has been developed and reported in References 5 and 6. These reports should be consulted for further details of the method. Briefly, the calculations consist of the following: For a typical analysis, a step attitude command of 0.1 radian is presented to a mathematical model of the pilot and aircraft. For a total tracking time of 5 seconds, the performance is scored by two statistics, Time-on-Target (TOT), and the normalized root mean square tracking error (RMS). TOT is scaled up with respect to an error tolerance of 0.0025 radian and represents a measure of how much time during the 5 second tracking period that the aircraft is within tolerance of the commanded value. The other statistic, RMS, is primarily a measure of rise time and, in some cases, overshoot. In this way, the TOT and RMS pair give a description of how quickly the aircraft can respond to the step pitch command, and how well it will settle to the commanded value.

There are two elements in the step target method – the airframe and the pilot. The aircraft is modeled by aerodynamic and control descriptions

that represent the aircraft along with appropriate position and rate limits on the control surfaces. The equations of motion are either fixed point or fully general large angle body axes equations and the time histories are generated using a suitable integration and frame time. These can be chosen so that the difference equations represent the control system filters exactly corresponding to the on-board flight control computer algorithms.

The pilot model reflects the following capabilities and limitations of the human controller:

- Ability to generate control compensation consisting of a proportional blend of error, error rate, and integral control.
- Ability to use, if required, separate control compensation for the initial response and final precision tracking phases of the tracking task.
- The limitation of a total cerebral and neuromuscular human equivalent transport delay of 0.3 seconds.

The definition of the model and the full pitch task is shown in Figure 4.

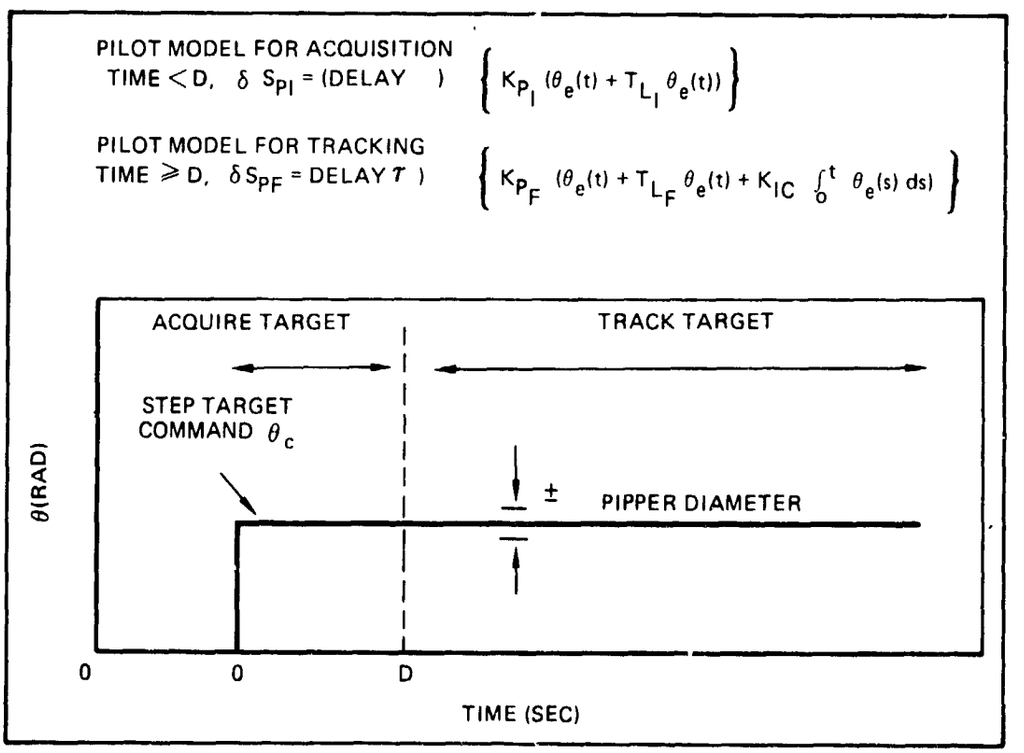

FIGURE 4. DEFINITION OF PITCH STEP TARGET TRACKING TASK

The adjustment rule for the pilot model is simple: maximize TOT. This is done by adjusting the gains K, and lead coefficients T_L. The time at which the tracking phase is initiated, D, is also a parameter along with K_{IC}.

Validation of this approach is provided in Reference 6 and further demonstrations of the utility of this approach have been made in applications to both pitch and yaw CAS systems during aircraft development. The method is also described in the USAF specification MIL-F-8785C, Reference 7.

An analysis of NT-33 in-flight simulation of longitudinal flying qualities performed by Neal and Smith shows an essential two-dimensional relationship between the time-on-target, TOT, and the RMS statistics as shown in Figure 5, which is reproduced from Reference 7.

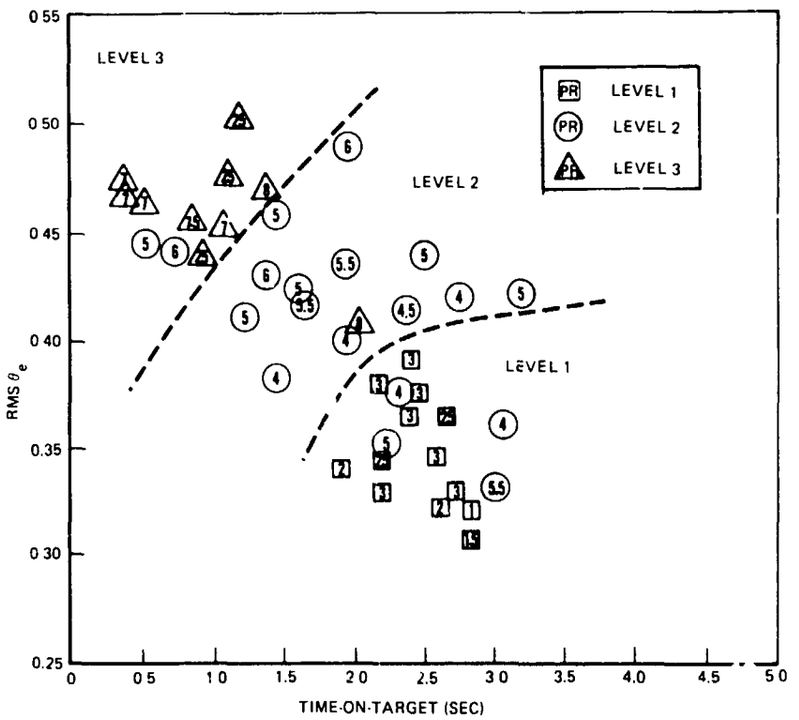

FIGURE 5. PILOT RATINGS AS FUNCTIONS OF RMS AND TIME ON TARGET FOR FIVE SECOND TRACKING TASK

APPROPRIATENESS OF THE STEP TARGET METHOD

The appropriateness of the step target method as a means of analyzing the LATHOS data base and suggesting further test requirements can be summarized as follows:

- The LATHOS experiment used a succession of step target commands exclusively for all HUD evaluations of lateral control. Thus the method models and studies this exact LATHOS flight test maneuver.
- The method gives good resolution in the Level I region where information is usually difficult to obtain.
- The method with its two stage acquisition – track model generates realistic time-varying pilot control strategies. In these cases, steady-state concepts such as gain or phase margins, and bandwidth are not even definable.
- All system nonlinearities can be incorporated along with full control and aerodynamic models where necessary. Thus exact time delays and amplitude-related nonlinear characteristics can be analyzed.

The following analysis will develop a promising new parameter easily obtained from in-flight or ground-based simulations as well as from flight tests:

- The time-on-target and RMS statistics are highly correlated with the amount of roll rate that the pilot can generate without overshoot and oscillation. This quantity normalized by commanded step size is an invariant that is easy to measure in piloted flight or simulation and is related to closed-loop bandwidth.

STEP TARGET ANALYSIS OF THE LATHOS DATA

An attempt to analyze the LATHOS data using the approach outlined above was documented by the authors in 1983, Reference 8. Since then, improvements in the methods used to optimize time on target, TOT, along with greater care in applying the LATHOS pilot opinion rating data, have led to considerable refinement of this earlier preliminary analysis. Fortunately, the basic conclusions of Reference 8 remain valid, and the improved resolution of the method allows greater insight into the discrete lateral step bank angle maneuver. A full analysis of this problem is not yet completed, however, a summary of current findings will be presented next.

Objectives of LATHOS Step Target Analysis

There are a number of questions to be addressed in the analysis:

1) Will analysis using the optimized single-stage step target suffice, or is the two-stage model necessary?

2) Do HUD POR data correlate with the step target parameters RMS and TOT?

3) Is there a one-dimensional metric obtainable from the step target analysis that correlates with HUD POR data?

4) Are correlations independent of the source of lateral flying qualities characteristics i.e., time delay, roll mode time constant, or prefilter coefficients?

A further question regarding the multiloop control flight tasks:

5) Do the metrics used in the analysis of the HUD tasks correlate with the gun tracking and formation flying tasks?

Selection of Baseline LATHOS Pilot Rating Data

The first task in the analysis is to identify the LATHOS evaluation flights which are applicable to the study of the HUD discrete maneuver problem. A validation data base is required for calibration of the metrics used in the analysis in terms of pilot opinion ratings, POR. The analysis presented here will be confined to one pilot supported by the corresponding safety pilot POR data. The pilot selected, "B" of Reference 1, demonstrated the best self-consistency, the broadest participation in the experiment, the widest range of ratings, and the best agreement with the safety pilot ratings. Since this analysis will assume ideal pilot-controller interface characteristics, evaluation flights suitable for the validation baseline data set must meet the following criteria:

1) The principal evaluation task must be the HUD task.

2) There must be no significant pilot comments expressing dissatisfaction with control forces, stick sensitivity, or control harmony.

3) Of various stick sensitivities tested, the configuration with best POR must be used.

With these restrictions a set of LATHOS flight evaluations was selected which will be referred to as the HUD validation data set. A second set of

evaluations was also selected for the tasks of gun tracking, TR, and formation flying, F, performed together. Gun tracking performed alone was also considered.

The complete list of the selected NT-33 evaluation flights is contained in Table I.

Single-Stage Analysis of the LATHOS Data

In accordance with the above description of the single-stage step target model, the validation data configurations were optimized for maximum TOT using a computerized exhaustive search algorithm. The results for the combined data sets are presented in Table I. The significance of these data is more clearly understood when viewed graphically. In analogy to Figure 5, Figure 6 presents the HUD validation data in the form of pilot ratings placed at their coordinates of TOT and RMS.

Figure 6 shows two characteristics of importance:

- The rating data lie on a well defined line in the RMS versus TOT plane.
- The POR data are monotonic increasing along this line.

These two observations indicate the possible existence of a single dimensional metric. In addition to TOT and RMS, another measure of this performance was identified, the Maximum Normalized Rate, MNR. This quantity is the maximum rate that the pilot can use and yet avoid overshoot and oscillation, normalized by the commanded step size. MNR can be interpreted in terms of flying qualities as expressed in Section 6.2 of Reference 9 in which Neal and Smith comment:

> "The first step in the analysis is to identify the performance which the pilot is trying to achieve when he "adapts" to an airplane configuration. The pilot comments indicate quite clearly that he wants to acquire the target quickly and predictably, with a minimum of overshoot and oscillation. The question that remains is how to translate this observation into mathematical terms."

TABLE 1. SINGLE-STAGE STEP TARGET ANALYSIS DATA FOR VALIDATION LATHOS CONFIGURATIONS

CONFIGURATION	EVAL NO.	TASK	POR	SPOR	TOT	RMS	MNR
2-3T2	95	F, TR	5	5	2.925	0.4784	0.909
2-4	17	HUD	2	3	3.200	0.4430	1.021
2-4F1	18	HUD	4	4	3.000	0.4672	0.922
2-4F2	179	TR	3	3	2.825	0.4851	0.847
3-3	44	F, TR	5	4	3.375	0.4233	1.153
3-3F3	135	HUD	7	7	2.825	0.4848	0.853
3-4F4	213	HUD	8	7	2.575	0.5090	0.751
1-3T2	112	TR	8	9	2.725	0.4989	0.809
2-2T1	45	F, TR	2	2	3.000	0.4698	0.935
2-2T4	15	HUD	9	8	2.600	0.5186	0.799
2-4F3	94	F, TR	7	7	2.525	0.5137	0.734
2-3T1F1	113	TR	6	7	2.800	0.4924	0.853
3-4F5	97	F, TR	8	8	2.150	0.5431	0.629
3-3T1F1	125	TR	7	7	3.025	0.4700	0.966
5-2	12	F, TR	7	7	3.500	0.4072	1.276
5-2F2	127	TR	5	5	3.225	0.4436	1.062
5-3F3	188	TR	4	4	3.025	0.4647	0.945

DEFINITIONS:
POR – PILOT OPINION RATING FOR PILOT "B"
SPOR – SAFETY PILOT RATING
CONFIGURATION – SEE REFERENCE 1 FOR CODE
TOT – TIME-ON-TARGET
RMS – NORMALIZED ROOT MEAN SQUARE TRACKING ERRCR
MNR – MAXIMUM NORMALIZED RATE – MAXIMUM ROLL RATE DEVELOPED IN OPTIMIZED MANEUVER NORMALIZED BY THE COMMAND STEP SIZE
TASK – F: FORMATION FLIGHT, TR: GUN TRACKING, HUD: HEAD UP DISPLAY STEP ATTITUDE TRACKING

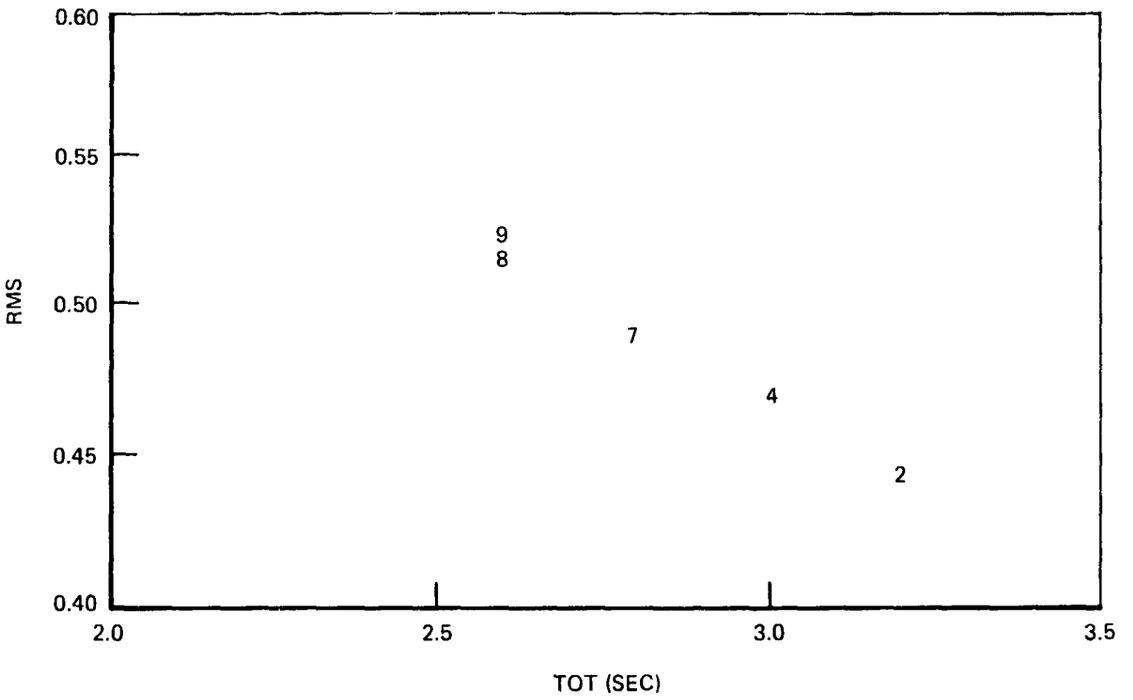

FIGURE 6. HUD PILOT RATINGS AS FUNCTIONS OF TOT AND RMS

Viewed in this way, the step target method with MNR as a metric suffices for two reasons:

- The optimized TOT corresponds to the condition of "acquiring the target quickly and predictably with a minimum of overshoot and oscillation."
- The MNR is a measure of just how quickly the pilot can undertake the maneuver in response to the requirement "to translate this observation into mathematical terms."

If POR data are plotted versus MNR for the HUD cases, the result is a strong linear correlation as shown in Figure 7.

With this successful correlation for the HUD tasks, it is natural to look for agreement of the multiloop lateral-directional pilot ratings with the inner loop MNR data. Interpretation in this case becomes more difficult and uncertain owing to the intrusion of ride qualities effects, and possible insufficiency of the tests used to evaluate the configurations. Figure 8 presents both the HUD and the multiloop evaluations consisting of gun tracking and formation flight perfcrmed together in each evaluation.

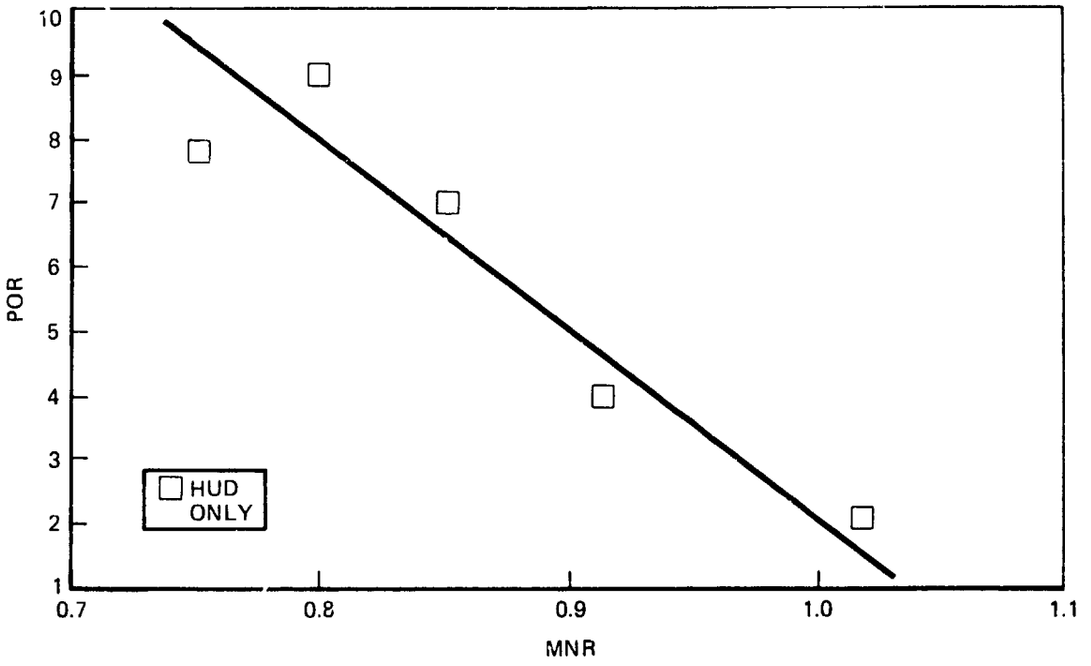

FIGURE 7. POR vs. MNR FOR HUD VALIDATION CASES

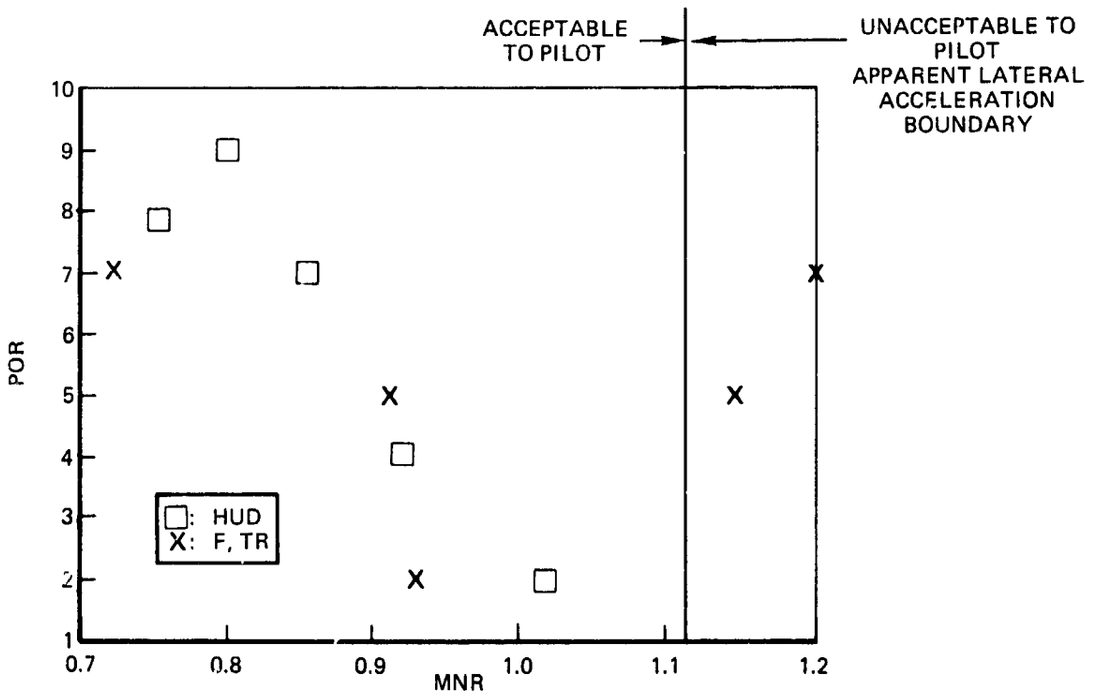

FIGURE 8. POR vs. MNR FOR HUD AND F, TR TRACKING TASKS

Examination of Figure 8 shows a general agreement between the F, TR tasks and the HUD cases for sufficiently low MNR. For MNR greater than 1.1, there are very sharp pilot rating degradations. In both of these cases, the roll mode time constant is 0.15 sec, and in the worst case the pilot comments indicate "quick, sharp ratcheting."

On the other hand, if the gun tracking cases are plotted against MNR, the result is as shown in Figure 9.

The wide scatter of Figure 9 in contrast to the linear correlations of Figures 7 and 8 indicate that the gun tracking task alone may not lead to consistent evaluations with the HUD and formation flying tasks. This difficulty is possibly exhibited in the data reported in Reference 1 where the LATHOS POR data is presented in the form of inter and intra pilot rating correlations which are poor in some cases. Furthermore, the correlation of the HUD and other tasks shows a strong trend, but includes points that are as far as 4 units of POR from the line of agreement, and with a spread of 5 units of POR in several cases. Figure 9 might explain some of this disagreement, however, it seems inescapable that there are dynamic considerations beyond the closed loop piloted control of inner loop roll angle required to fully understand the outer loop maneuvers.

Two-Stage Analysis of the LATHOS Data

From the above data presentations, it is clear that MNR derived from the single-stage step target model leads to sharp and discriminating analysis of control configurations with variations in time constant, time delay, and prefilters. Even so, it is natural to inquire into the possible use of the two-stage model illustrated in Figure 4. Automatic computer optimization algorithms were developed for this problem, and the results obtained were of little use, not because the method broke down in this instance, but because the problem was not sufficiently well defined.

The difficulty lies with the distinction between open loop maneuvers and closed loop tracking. With the single-stage model, the model coefficients are maintained constant throughout the 5-second tracking interval so that the compensation must be stable. This places a considerable compromise on the initial transient response and the final tracking compensation compared to the

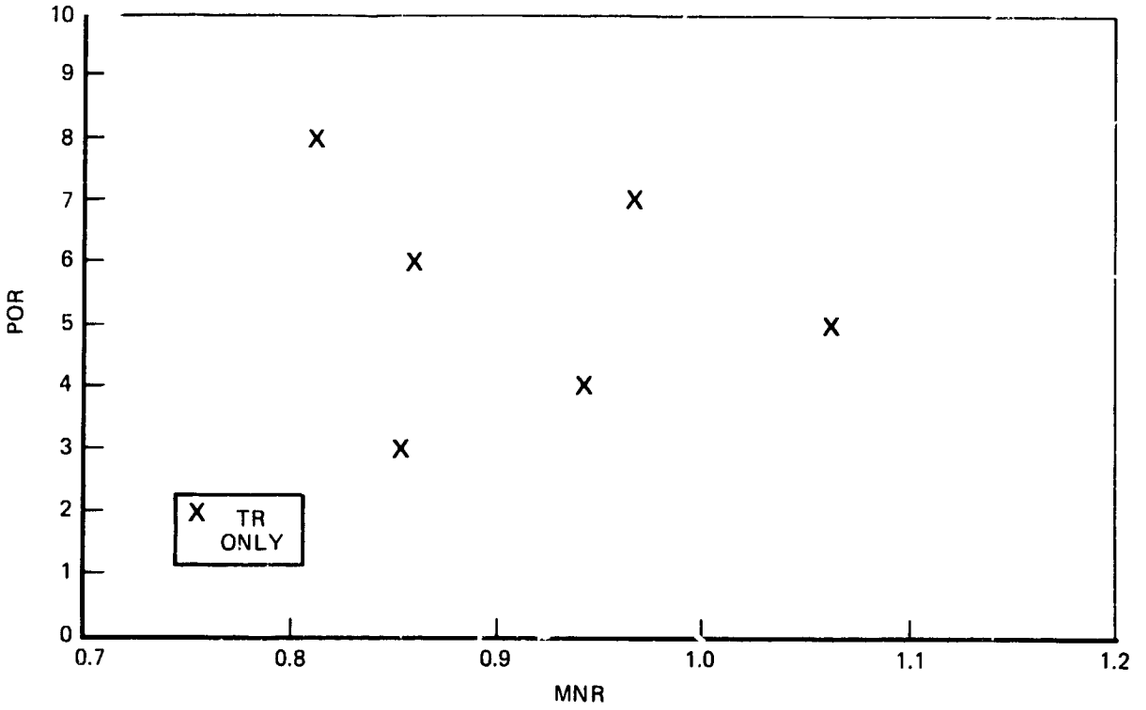

FIGURE 9. POR vs. MNR SHOWING POOR CORRELATION FOR TR ONLY TRACKING TASKS

two-stage model. In the two-stage case, the initial coefficients can be maintained for a short period at values that in a steady-state sense would be unstable. This can then be followed by a set of coefficients that correctly terminate the initial transient and provide a sufficient amount of error correction during the final tracking stage to prevent drift, or to correct small offset at the end of the acquisition phase of the problem.

This advantage of the two-stage model leads to unrealistic TOT and associated MNR for most of the LATHOS cases. The situation is this: For the idealized model consisting of just the transfer functions of the prefilter, the roll mode, and the Dutch roll dynamics plus the time delay, there is no restriction of "real world" characteristics encountered in the actual flight tests.

These considerations are of two basic kinds:

> The NT-33 has finite surface rate limits. The two-stage model in many cases generates extremely high roll accelerations depending on instantaneous surface rates.

2) The human pilot has resolution limitations in 1) judging the exact command magnitude, 2) adopting exact compensation ratios of error to error rate, and 3) initiating of any discontinuities he may use to perform the maneuver.

If the pilot is allowed to fly the exact same step over and over, his performance can be dramatically improved, but in this case he is developing an open loop control history, and is abandoning closed loop tracking. Each of the above two limitations can be built into the two-stage model, and work in this direction is in progress.

This difficulty in maintaining a suitable distinction between open loop maneuvers and closed loop tracking is a feature of discrete flying qualities where both kinds of maneuvers need to be studied. The MNR metric for the two-stage model has difficulty, not because of model deficiencies, but because it is sensitive to all aspects of aircraft model, task definition, and human pilot characteristics. For these reasons, it is anticipated that the step target method with the MNR metric will lead to sensitive and discriminating methods for assessing the influence of control and aerodynamic nonlinearities as well as pilot/aircraft interface problems of controllers and displays.

Summary of Step Target LATHOS Analysis

At this point the five questions listed at the front of this subsection can be answered. In brief:

1) For the LATHOS analysis, the single-stage step target model suffices.

2) HUD POR data correlate well, linearly in fact, with RMS and TOT, Figure 6.

3) MNR is a suitable one-dimensional metric for lateral flying qualities evaluation, Figure 7.

4) The correlations include configurations with variations in roll mode time constant, control system time delay, and prefilters. Thus the method can account for all these influences on pilot ratings, Figure 7.

5) POR data for gun tracking and formation flying performed during the same evaluation correlate acceptably with the HUD data, Figure 8. Gun tracking alone is not correlated with the HUD data in terms of MNR, Figure 9.

This completes the analysis of the LATHOS data of Reference 1. However, there are a number of further comments and applications of the MNR metric of the step target method that will be presented next.

OTHER APPLICATIONS OF THE MNR METRIC

There are several practical considerations of MNR as a flying qualities parameter that project a wide range of applications. Although little data has been obtained for these applications, they appear promising and are presented in the hope that some of the ideas may help clarify several troublesome problem areas.

Effects of Actuator Rate Limiting on Lateral Flying Qualities

In the last section, limiting of surface deflection rates was identified as a "real world" aspect of flying qualities to which the two-stage model MNR was sensitive. In fact, the single stage model is also sensitive to actuator rate limiting. Consider the aircraft model shown in Figure 10.

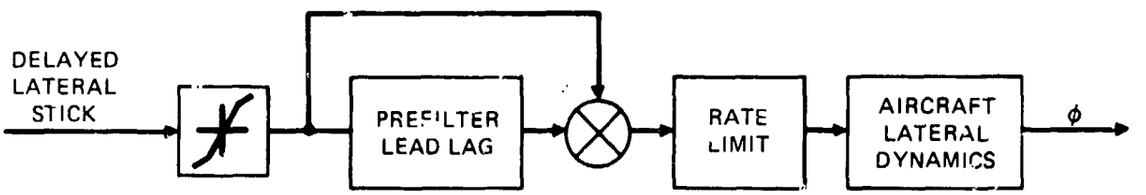

FIGURE 10. RATE LIMITING AIRCRAFT MODEL

For a given rate limit, the command step size will determine the extent to which the limiting is encountered. To apply the step target MNR metric, the model is optimized for each command size of interest. As the command step size increases, the limiting retards the maneuver onset acceleration resulting in reduced MNR, even for the model fully optimized for the particular step size. This is illustrated in Figure 11 for a roll mode time constant of 1.0 sec. The maximum slope, thus normalized, is MNR for each curve.

Equivalently, the rate limit for the actuator can be varied for a fixed commanded step size. Figure 12 presents data in this form for a configuration with a roll mode time constant of 0.5 sec and a control system time delay of 100 ms. Dutch roll and prefilter dynamics are also present.

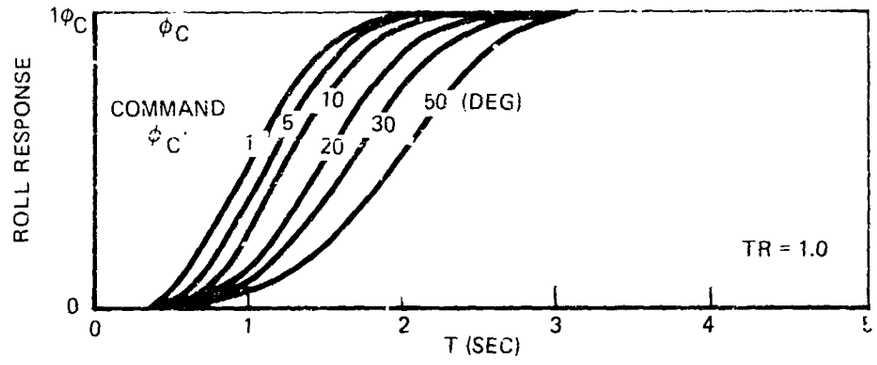

FIGURE 11. EFFECT OF RATE LIMITING ON OPTIMIZED STEP TRACKING RESPONSE

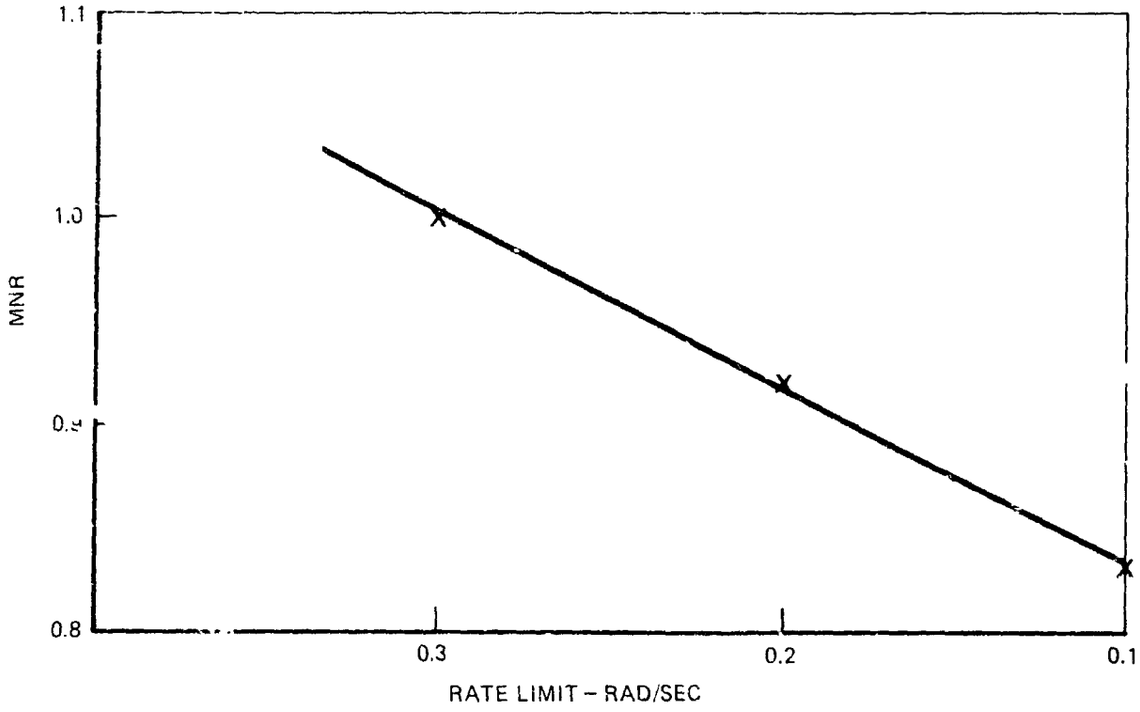

FIGURE 12. DEGRADATION OF MNR WITH DECREASING ACTUATOR RATE LIMIT

The importance of this example illustrates two useful attributes of the MNR metric:

- The MNR metric using the single- or two-stage model can incorporate all system nonlinearities.
- The MNR metric can be used to assess amplitude dependent flying qualities aspects.

In this way, MNR can be used to assess the characteristics of roll control not only for small perturbation maneuvers, but large amplitudes as well. By examining the profile of MNR versus command amplitude, many aspects of the large maneuver problem can be approached by analysis or in simulation. The use of MNR as a flight test and simulation performance measure will be discussed next.

MNR as a Flight Test and Simulation Performance Measure

When the step target method was first developed, the idea was put forward to use TOT and RMS as experimental measures of step attitude acquisition tasks. Such tasks are now standard in control system development and flying qualities assessment, and with the success of the analytical measures it seemed natural to obtain RMS and TOT in experimental testing. However, attempts to obtain these data were frustrated for two reasons:

1) The distinction between open- and closed-loop maneuvers was clouded in the tests.

2) The TOT metric is extremely sensitive to small variations in piloted compensation. Consequently, the data for TOT was badly scattered.

The first problem will always remain, and must be addressed in the design of the test, the task descriptions and performance criteria given to the test pilot, and the order of presentation of the steps in training and data flights and simulations. Thus it can be controlled, or at least made consistent in a known manner. The second problem is much less critical for MNR. For variations in pilot model parameters in the step target model that produce great variations in TOT, the variations in MNR remain small. Flight simulations are now being developed at Northrop to investigate MNR as an experimental performance parameter.

Quantification of Control Harmony in Terms of MNR

If MNR is regarded as a piloted flight or simulation performance parameter or as an analytically derived quantity, the ability of MNR to analyze amplitude dependent flying qualities may provide a way to quantify control harmony.

Control harmony has always been one of the most elusive aspects of flying qualities. It is neither quantified by performance in the sense of tracking data, nor by workload as such, yet has strong influence on the Cooper Harper ratings of test pilots. This influence is mostly in the form of annoyance, as expressed in pilot comments. There is one aspect of harmony, at least, that MNR should be able to identify, predict, and analyze.

Consider an aircraft which has a certain falloff of roll MNR with increasing step command size. Now suppose that the pitch MNR falls off at the same rate. In such a case, if the relative control gearings and forces are well-chosen for small amplitudes, the pilot has only to restrain his aggressiveness for the larger maneuvers. However, if the MNR of one axis decreases more sharply than the other, or if one should in fact increase, then the pilot is faced with restraining one axis while staying or becoming more aggressive on the other. This would seem to be a circumstance that could be quite annoying, and might be an area where MNR can identify some aspects of harmony in a quantitative way. This approach to control harmony will also be tested at Northrop by ground-based flight simulation.

Use of MNR Step Target Analysis to Develop Test Matrices

The correlations of MNR with the LATHOS data, and the understanding of inconsistencies in that data base that the MNR metric provides allows the method to be used to predict where further testing should be performed. By using the MNR metric for interpolation of the LATHOS data, areas of high expected pilot rating gradients can be identified for more thorough testing, while in areas of low sensitivity, testing can be reduced. In this way, time on simulators or test aircraft can be used to better advantage. Also, by testing along the gradients and the lines of apparent equal rating, better definitions of the boundaries of the flying qualities Levels can be obtained. By calibrating the MNR metric to any set of test data, this process can be employed to generate a well selected test matrix for further study. If a data base is unavailable, the method will still show where dense testing should be recommended, and where sparse testing should suffice.

NASA/Northrop Cooperative Program

Northrop is currently under contract to NASA Dryden Flight Research Facility to perform "A Cooperative Program for Investigation of Super-augmented Aircraft Lateral Flying Qualities." Ten flights using the Digital Fly-By-Wire F-8 aircraft will be performed at DFRF, and Northrop will provide engineering support to develop specific test plans, analyze flight test data and document the entire activity. The technology presented above is currently being used to generate the required test plans, and the resulting flight tests will extend the existing data base represented by the LATHOS program.

The basic dynamical interplay among the lateral flying qualities parameters is between control system transport time delay and the roll mode time constant T_R. Therefore the test plan will establish a baseline test matrix and an extended matrix. The baseline test objectives are:

1) Confirm LATHOS.

2) Adequately extend LATHOS.

3) Test small amplitude motions to avoid lateral acceleration N_{yP} effects.

4) Avoid prefilters.

5) Be restricted to linear gearing.

Once this basic matrix has been established and tested, then the matrix will be extended as follows by by examining:

1) N_{yP} lateral acceleration ride qualities.

2) Prefilter and nonlinear gearing alleviation of acceleration detriments.

3) Roll ratcheting identification and boundary study.

4) Establish criteria and verify by air-to-air target tracking.

The relationship between these test objectives is shown graphically in Figure 13.

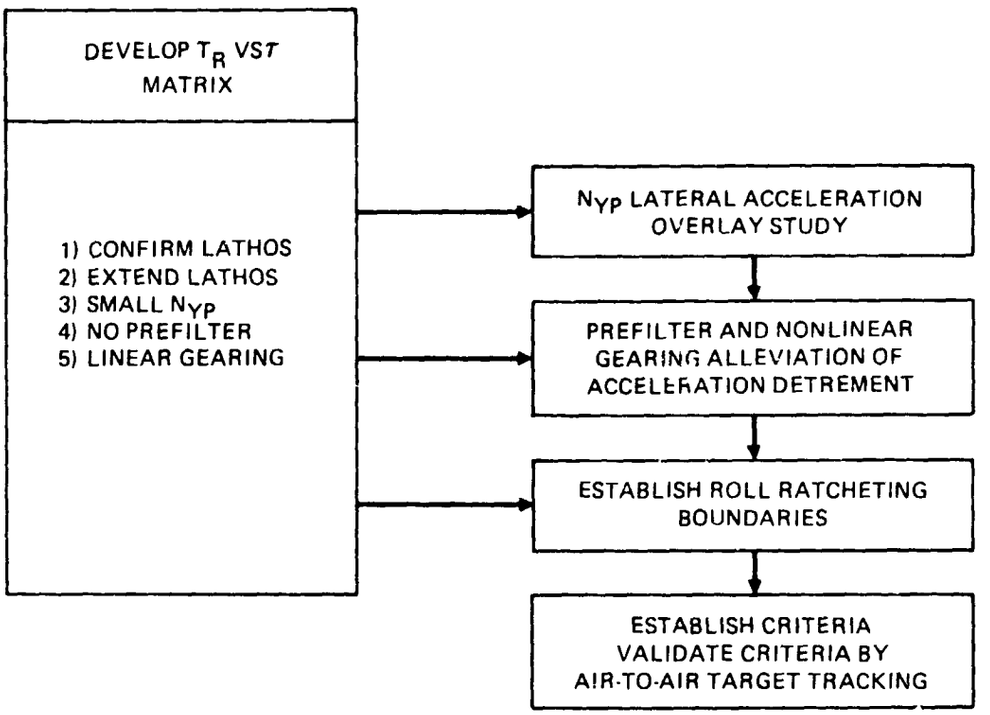

FIGURE 13. NASA/NORTHROP STUDY OBJECTIVES

VISTAS AND PROSPECTS

The data and analysis presented above in no way is offered as validation of any sort of pilot rating prediction method. What has been attempted, is to illustrate the utility of developing time domain models and metrics that can provide insight into some of the difficult aspects of control system development and flying qualities assessment. From this point of view, many more questions have been raised than answered. However, this general approach to the problem has demonstrated the following useful features:

- Ability to incorporate nonlinear system dynamics.
- Ability to incorporate discontinuous control dynamics and transient pilot control strategies.
- Ability to correlate with discrete task flight test data.
- Ability to analyze amplitude dependent flying qualities effects.

These together with the suggested areas of application in the study of rate limiting effects and control harmony demonstrate a need for continued

investigation of the basic step target methodology. Simulations and further analysis are in progress at Northrop, and the utility of this MNR metric is being demonstrated in developing suitable test matrices by interpolation of the LATHOS data base. These matrices are being evaluated by fixed-base flight simulation at the present time. Moving-base and in-flight simulation tests for the NASA/Northrop cooperative program will commence in mid 1984.

REFERENCES

1. Monagan, Stephen J., Smith, Rogers E., and Bailey, Randall E., Lateral Flying Qualities of Highly Augmented Fighter Aircraft, AFWAL-TR-81-3171, June 1982.

2. Chalk, C.R., Excessive Roll Damping Can Cause Roll Rachet, Paper 82-1606 AIAA Guidance and Control Conference, San Diego, California, August 9-11, 1982.

3. Mitchel, David G., and Hoh, Roger, Flying Qualities Requirements for Roll CAS Systems AIAA, 1982.

4. Wood, J.R., Comparison of Fixed-Base and In-Flight Simulation Results for Lateral High Order Systems.

5. Onstott, E.D. and Faulkner, W.H., Prediction, Evaluation, and Specification of Closed Loop and Multiaxis Flying Qualities, AFFDL-TR-78-3, February 1978.

6. Onstott, E.D. and Faulkner, W.H., Discrete Maneuver Pilot Models for Flying Qualities Evaluation, J. of Guidance and Control Vol. 1, Number 2, March-April 1978.

7. Moorhouse, David J. and Woodcock, Robert J., Background Information and User Guide for MIL-F-8785C, Military Specification - Flying Qualities of Piloted Airplanes, AFWAL-TR-81-3109, July 1982.

8. Onstott, E.D., A Definitive Lateral Flying Qualities Test Plan for Ground-Based and In-Flight Simulation, Northrop Technical Report NOR 83-120, June 1983.

9. Neal, T.P., and Smith, R.E., An In-Flight Investigation to Develop Control System Design Criteria for Fighter Airplanes, AFFDL-TR-70-74, Air Force Flight Dynamics Laboratory, Wright-Patterson Air Force Base, Ohio, February 1971.

N85 14504

PREDICTIONS OF COCKPIT SIMULATOR EXPERIMENTAL OUTCOME USING SYSTEM MODELS*

John A. Sorensen and Tsuyoshi Goka

Analytical Mechanics Assoc., Inc.
2483 Old Middlefield Way
Mountain View, CA 94043

ABSTRACT

This study involved predicting the outcome of a cockpit simulator experiment where pilots used cockpit displays of traffic information (CDTI) to establish and maintain in-trail spacing behind a lead aircraft during approach. The experiments were run on the NASA Ames Research Center multi-cab cockpit simulator facility. Prior to the experiments, a mathematical model of the pilot/aircraft/CDTI flight system was developed which included relative in-trail and vertical dynamics between aircraft in the approach string. This model was used to construct a digital simulation of the string dynamics including response to initial position errors. The model was then used to predict the outcome of the in-trail following cockpit simulator experiments. Outcome included pilot performance and sensitivity to different separation criteria. The experimental results were then used to evaluate the model and its prediction accuracy. Lessons learned in this modeling and prediction study are noted.

INTRODUCTION

This study was concerned with pilot manual control in a multiple cockpit simulator experiment at NASA Ames Research Center. Each pilot used a device called the Cockpit Display of Traffic Information (CDTI) to follow some assigned lead aircraft on approach to landing. In this way, several successive pilots formed a string of decelerating aircraft in the terminal area using some preassigned separation criterion. The CDTI application has three potential benefits - (1) reduced controller workload, (2) increased terminal airspace efficiency, and (3) increased flight safety.

To begin to answer many questions regarding the pilot interface and equipment requirements for the CDTI application, many previous cockpit simulator experiments had been run [1-3]. These experiments simulated the pilot following one or more lead aircraft while on approach to landing. One set of shakedown tests to evaluate in-trail following using the CDTI was made in April 1982 on the multi-cab simulator. Much was learned from these tests, and based on this information, the experimental scenario and simulator equipment were revised. With these modifications, a new in-trail following experiment using the multi-cab facility was run in February-March 1983.

* This work was supported by NASA Ames and Langley Research Centers under Contract No. NAS1-16135. Dr. Renwick E. Curry was technical monitor, and Dr. Roland L. Bowles was technical administrator.

PRECEDING PAGE BLANK NOT FILMED

Previous to and during the simulator experiment, this study was organized into the following three phases:

1. Before the experiment was conducted, data and models from previous experiments and tests were combined to formulate a new flight system model. This model represented (a) the relative in-trail dynamics of the CDTI-equipped (Own) aircraft as it achieves and maintains designated in-trail spacing, and (b) the vertical aircraft dynamics, as the pilot attempts to remain on the glideslope. This model was used to predict the outcome of the simulator experiment.
2. The experiment was conducted, and data were collected and processed. The performance results were then plotted and compared to that predicted before the experiment.
3. Because differences existed between the predicted experimental outcome and the actual results, these differences were analyzed in terms of modeling error. The model was tuned to match the experimental results on a statistical basis. This required revision of the model structure as well as tuning of model parameters.

In going through this three-phase process to predict and analyze the outcome of the CDTI-based in-trail following experiment, we learned something. The following sections outline the results of the above three phases of study and the lessons that we learned.

FLIGHT SYSTEM MODEL

In the previous study [4], a mathematical model of the pilot/aircraft/CDTI flight system was developed to match the one-dimensional in-trail dynamics of "daisy chain" experiments conducted at NASA Langley Research Center (LaRC) [2]. A first-level block diagram of this heuristic model is divided into three subsystems - aircraft, cockpit displays, and pilot. The model is driven by the recorded groundspeed V_T of the lead aircraft. The model state variables are initialized to values recorded in the experimental runs; thereafter, the model runs itself. Model parameters are chosen for each run so that the root-mean-square differences between the model groundspeed V_M and actual simulator groundspeed are minimized. This previous model was used as a starting point to postulate an upgraded model to predict the outcome of the in-trail following experiments from the NASA Ames Research Center (ARC) multi-cab simulator facility.

The upgraded model was expanded to include vertical dynamics, as each pilot had the additional manual control task of keeping the aircraft on the 3° glideslope after capture. Previous to capture, the aircraft were to pass through two altitude windows at 12000 ft and 8800 ft when waypoints of 36 and 26 nmi-to-touchdown were passed on approach to San Jose airport. The new model was divided into the three subsystems as before - aircraft, display, and pilot; each is now discussed.

ORIGINAL PAGE IS
OF POOR QUALITY

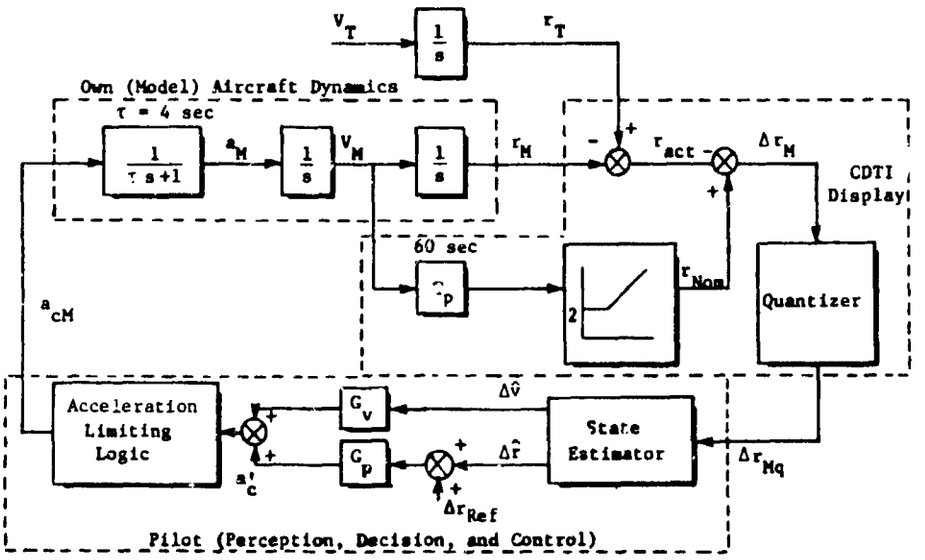

Fig. 1. First Level Block Diagram of In-Trail Following Flight System Model with CTP Criterion

Aircraft Dynamics

To simplify the aircraft longitudinal dynamics over a sample period of 4 sec, it was assumed that the short period motion of the aircraft dampens out from sample-to-sample. This implied that the pitch acceleration, pitch rate, and vertical acceleration terms could be set to zero. The control inputs were considered to be flight path angle γ, throttle setting δ_T, spoiler setting δ_S, flap setting δ_F, and gear position δ_G Flaps and gear were set on an open-loop basis, dependent upon approach speed and altitude. The resulting equation governing angle-of-attack was

$$-3060\delta_F - 3040\delta_S - (9400 + 47\delta_S)\alpha + (160 - 1950\delta_F)\alpha^2 + \frac{2W}{\rho V_M^2} = 0 , \quad (1)$$

where the numerical terms are generic for a B-727 [5]. Equation (1) is solved for each pass through the integration cycle to get the nominal angle-of-attack α.

The relationship for pitch angle is

$$\Theta = \gamma + \alpha . \quad (2)$$

The in-trail acceleration equation was

$$\dot{V}_M = -g\Theta + \frac{g\rho}{2W} V_M^2 [- 47\delta_S - 700\delta_F^2 - 28 - 20\delta_G + (110\delta_F - 304\delta_S)\alpha + 6400\alpha^2] + \frac{g\rho}{2W} \frac{T_{max}}{\rho_o} (1 - 0.72\ U/U_o)\delta_T \quad . \quad (3)$$

In Eq. (3), the throttle input δ_T is at idle when the spoiler δ_S is on, and vice versa. Details of this dynamic model can be found in Ref. 6. The other equations governing the aircraft model are for altitude h_M and in-trail distance r_M, or

$$\dot{h}_M = V_M \gamma \quad , \quad (4)$$

$$\dot{r}_M = V_M \quad . \quad (5)$$

Equations (3)-(5) are integrated to derive the aircraft motion each sample time. The cross-coupling between the longitudinal and vertical axes is from the - $g\Theta$ term in Eq. (3). Thus, the pilot can control longitudinal acceleration by using the throttle/spoiler combination (δ_T/δ_S) or by changing his pitch attitude Θ.

Displays

The model of the glideslope indicator is shown in Fig. 2, where r_{TD} is the initial range to touchdown. The modeled glideslope deviation measurements $\Delta\lambda_M$ seen on the cockpit displays are the actual deviation plus a noise contribution η_λ.

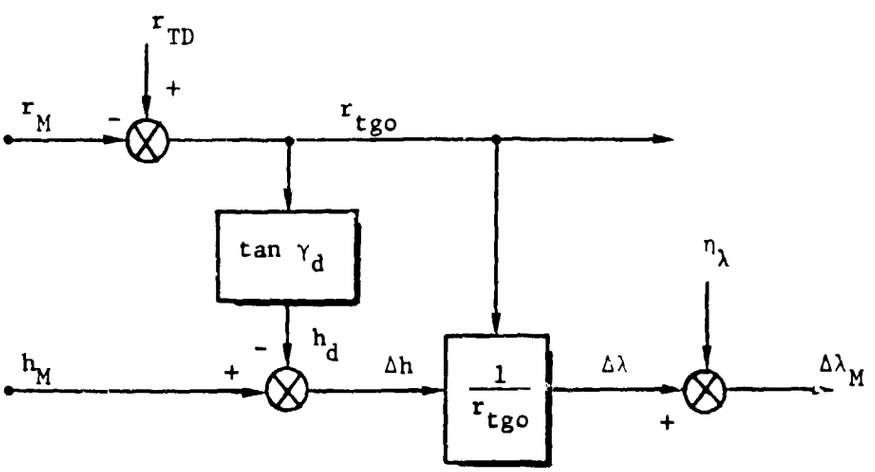

Fig. 2. Glideslope Indicator Model

For the experiments, the standa l approaches began outside of localizer/ glideslope coverage. Here, the pilots were assumed to maintain the 3 nmi-range-to-1000 ft-altitude sink rate (3-to-1 rule), based on displayed DME distance to runway. They also controlled .ltitude to pass through the two altitude windows mentioned earlier.

The primary quantities obtained from the CDTI display are the relative in-trail position r_{act} of own aircraft with respect to the immediate lead, the nominal separation r_{Nom}, and the separation error Δr_M. The nominal separation is dependent upon the separation criterion. For the Constant Time Predictor (CTP) criterion, this is a time constant T_p multiplied by own aircraft's groundspeed V_M. This is usually indicated by a vector protruing from own aircraft's symbol such as seen in the sketch in Fig. 3. For the actual separation to equal the nominal value, the tip of the follower's predictor vector should coincide with the lead aircraft (or target) position. Figure 1 contains the model of the CDTI display with CTP separation error Δr_M and its computation.

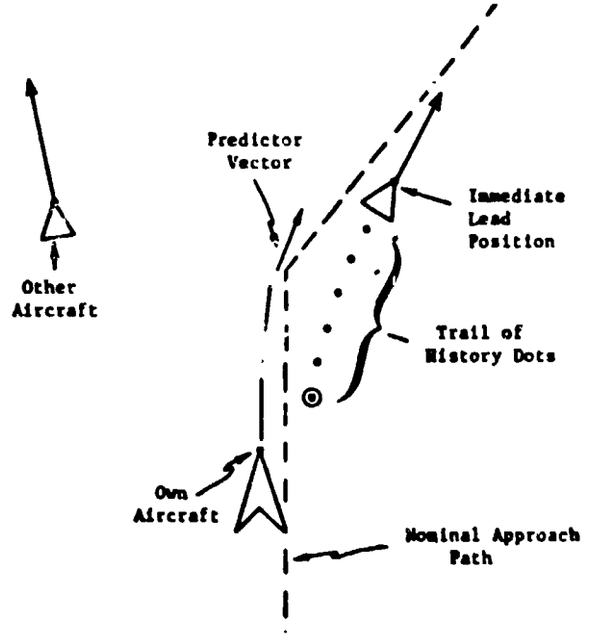

Fig. 3. Simplified Sketch of CDTI Display

For the Constant Time Delay (CTD) criterion, own aircraft is to be where the lead aircraft was a time constant T_D sec earlier. This is indicated by a trail of history dots dropped by the lead aircraft. For the actual separation to equal the nominal value, own aircraft's symbol should coincide with the history dot dropped T_D sec earlier. Figure 4 depicts the model of the CDTI display with CTD separation error and its computation.

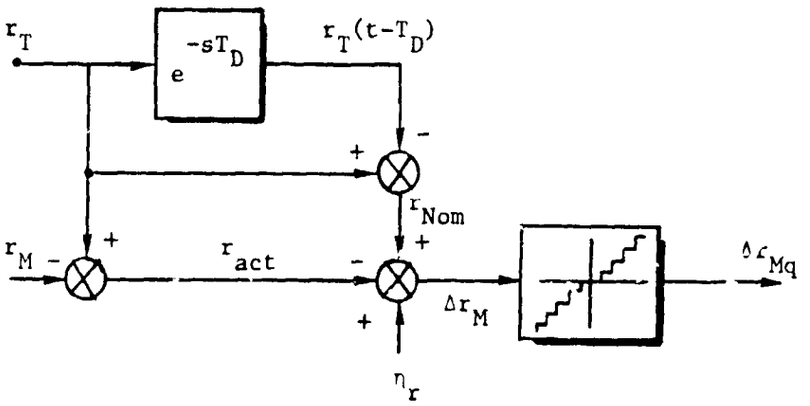

Fig. 4. Model of CDTI Display of Separation Error with CTD Criterion

For the third criterion of the experiment, the CDTI display was modified to indicate the effect of current acceleration on future longitudinal position. This was referred to as the acceleration cue (AC) criterion. Its display was a variation on both the CTD and CTP criteria. For the AC display, history dots are dropped at T_D, $T_D - \tau_d$, $T_D - 2\tau_d$, and $T_D - 3\tau_d$ sec earlier. These were 90, 70, 50, and 30 sec, respectively, in the experiment. The time predictor is modified to include the effect of currently measured acceleration a_M. The displayed predictor vector is cut into segments and used to predict where the own aircraft will be τ, 2τ and 3τ sec into the future. In the experiment, τ was 20 sec. For perfect separation, speed, and acceleration, the predictor vector segment tips will line up with the history dots. When there is separation error, the pilot can use the AC display to determine if current acceleration will yield the desired future position.

Pilot Modeling

In these experiments, the displayed quantities had low noise levels, so estimation inaccuracy was not considered to be a significant source of piloting error. The quantized signals taken from the CDTI display models were used to drive an estimation model which was assumed to be an α-β filter. The same estimation process was assumed to obtain vertical glideslope error and its rate.

There are four stages of decision making that a pilot goes through during an in-trail following task with the CDTI. These are (a) his choice of role to be in (controller, monitor, or inattention), (b) which displays to observe, (c) whether to be an active controller or to continue to monitor, and (d) which active control mode to use. The relevance of each stage is dependent upon the decision made in the previous stage.

The inattention choice was modeled to be of cyclic periods, initially of longer duration, but as the aircraft approached landing, the cycles

became shorter but occurred more frequently. This model is based on the fact that as landing approaches, the pilot focuses more often on steering, his control tolerances tighten, and he changes roles more rapidly. The cyclic pattern of the attention/inattention decision and the corresponding model discrete D_1 are depicted in Fig. 5.

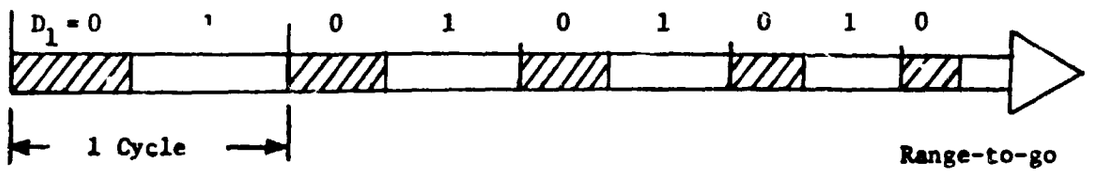

Fig. 5. Cyclic Pattern of Decision to Monitor/Control Aircraft (D_1 = 1) or Other Activity (D_1 = 0)

It was assumed prior to the experiments that the pilots would use their flight path angle control only to regulate vertical position and null out glideslope errors. It was also assumed that they would use throttle and spoiler control primarily to regulate in-trail spacing. Inherent in these assumptions is that vertical and in-trail control are independent.

The pilot model used the discrete D_2 to represent the in-trail control decision and D_3 to represent the vertical control decision. These discretes could be enabled or changed when the monitor/control discrete of Fig. 5 was set to 1. They remained fixed at their set positions until the state variable being controlled crossed a threshold indicating that a new control strategy was needed.

In the experiments, the initial separations between consecutive aircraft were set so that the followers were either too close (positive Δr_M), too far back (negative error), or within some acceptable threshold. Thus, it was assumed that the in-trail control would consist of initial capture followed by regulator control. The in-trail error term $\hat{r}_{fac}$ was defined as

$$\hat{r}_{fac} = C_1 \Delta\hat{r} + C_2 \Delta\hat{v} \; ; \qquad (6)$$

this is a combination of estimated separation error $\Delta\hat{r}$ and its rate $\Delta\hat{v}$. This term was used to govern which in-trail control was appropriate.

The model discrete logic governing the in-trail control decisions is shown in Fig. 6. For being initially too far back ($\hat{r}_{fac} < \varepsilon_1$), the decision/control logic of the following pilot model is

C-4

ORIGINAL PAGE IS
OF POOR QUALITY

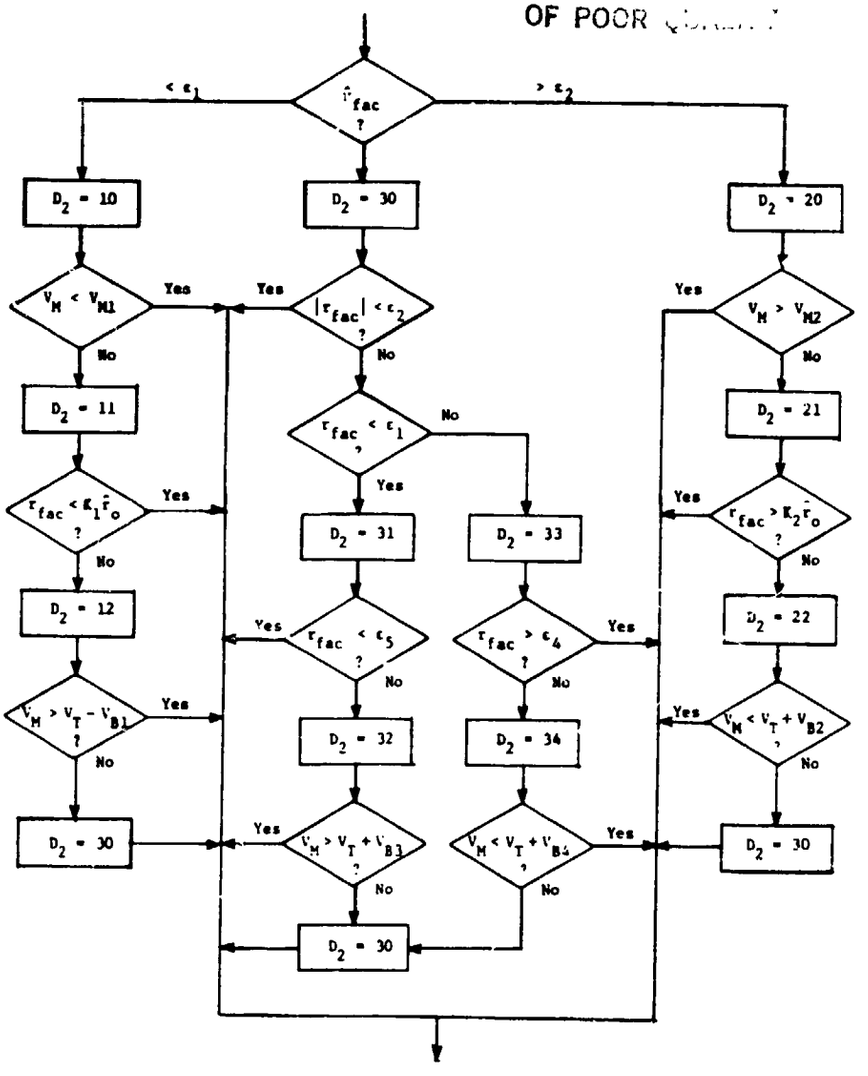

Fig. 6. Decision Logic to Predict Experimental Outcome

D_2 = 10 : Accelerate with throttle until $V_M \geq V_{M1}$;

= 11 : Hold speed constant until $\hat{r}_{fac} \geq K_1 \hat{r}_0$;
$(\hat{r}_0 = \hat{r}_{fac}(t=0))$

= 12 : Decelerate with spoilers until speed V_M is within V_{B1} of target.

This is using the throttle/spoiler to first accelerate, then coast, and then decelerate to null the error and return to an appropriate following speed.

The same model procedure was used in reverse to remove an initial "too close" error by using discrete D_2 set at 20, 21, and 22. Here, parameters, V_{M2}, K_2, and V_{B2} govern logic switching, as shown in Fig. 6.

After initial capture has taken place, the discrete D_2 is set to 30 to indicate $\hat{r}_{fac}$ is within ϵ_2 of null. D_2 is set to 31 and then 32 for catchup control if the follower falls behind ϵ_1 of the target. This indicates that throttle followed by spoiler control is required. If the follower becomes closer than ϵ_2, D_2 is set to 33 and then 34 to activate spoiler and then throttle control to cause the follower to drop back. The discrete D_2 was used subsequently to govern position of throttle δ_T and spoiler δ_S as inputs to the aircraft dynamic model (Eq. 3).

Each follower began at 15000 ft altitude, 340 kt speed, and 52-55 nmi from touchdown. The initial vertical objective was to pass through the two windows at 12000 ft and 8800 ft. The model governing vertical control was open loop in nature with the discrete D_3 set to five consecutive values:

$D_3 = 0$: Descend at $\gamma_{CM} = G_{M1}$ until altitude h_{C1} (= 12000 ft);

$= 1$: Hold $\gamma_{CM} = G_{M2}$ (~ 0) until range r_{t1} (= 36 nmi);

$= 2$: Descend at $\gamma_{CM} = G_{M3}$ until h_{C2} (= 8800 ft);

$= 3$: Hold $\delta_{CM} = G_{M4}$ (~ 0) until r_{t2} (= 26 nmi);

$= 4$: Glideslope capture and hold.

PREDICTED EXPERIMENTAL OUTCOME

The flight system model just described was used to simulate strings of six following aircraft. The string model was driven by recorded lead profiles, where the data were taken from the cockpit simulator. These data represented the profile followed by the lead aircraft in the experiments. Each run of six followers represented a prediction of the performance of the in-trail following experiments. The parameters in the decision and control logic of the model were modified until "reasonable" performances were achieved in terms of string following dynamics.

Three cases (or strings) of six followers were run - one for each of the three separation criteria. For each case, the initial separation errors were set to alternate between being too close, too far back, and nominal.

An example of the predicted performance of a follower using the CTD criterion and being initially too far back is shown in Fig. 7. This compares own and lead groundspeed, separation error (where nominal is 90 sec), altitude, and throttle/spoiler inputs as functions of range-to-go. As seen, the initial separation error of 3 nmi is driven to less than 0.5 nmi by 30 nmi-to-go. In-trail control alternates between throttle and spoiler input.

ORIGINAL PAGE IS
OF POOR QUALITY

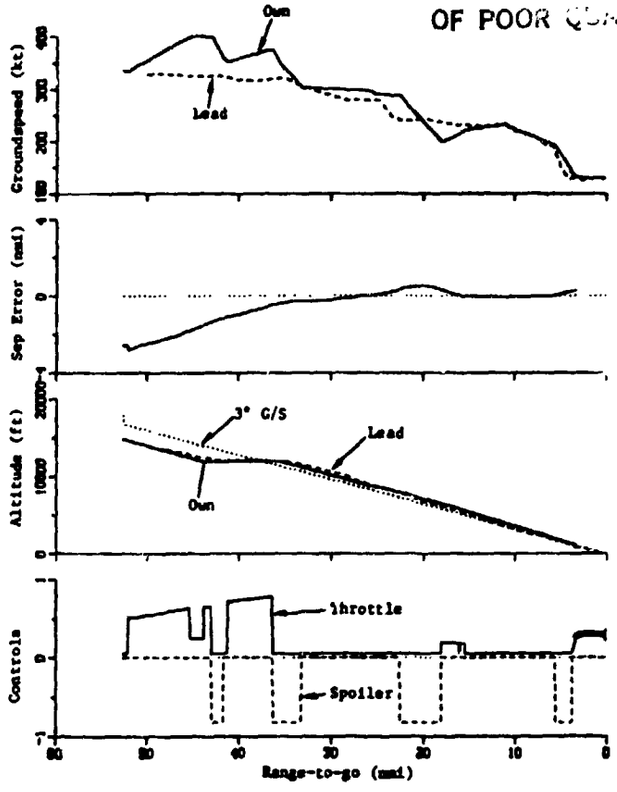

Fig. 7. Predicted Performance for the CTD Criterion. No. 1 Follower

The speed vs range-to-go prediction summary for every other follower using the CTD criterion is shown in Fig. 8. It is seen that there is about a 100 kt band of speeds about the lead profile after capture. This was consistent with previous shakedown results from the multi-cab simulator [3].

In terms of estimated performance, there are various statistical measure which could be used to categorize the overall following performance of the six aircraft. For the CTD criterion, these included, for six followers:

Own - Target Groundspeed	Mean: 0.2 kt; 1σ : 33.2 kt;
Longitudinal Error	Mean: -0.19 nmi; 1σ : 0.37 nmi;
Average Throttle	0.16;
Vertical Error	Mean: 0.32°; 1 : 0.06°;
Time to Land Six Aircraft	4515 sec;

where 1σ is the standard deviation. Vertical error is measured after glide-slope capture.

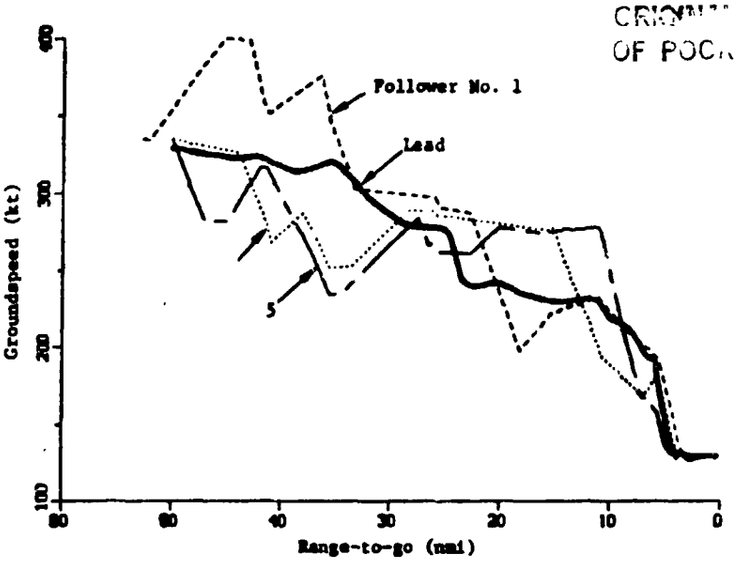

Fig. 8. Predicted Groundspeed vs Range-to-go in String with CTD Criterion

To design good performance into the model, the objectives would have been to keep the landing times for all six aircraft reasonably close, to use minimum throttle to remove the separation errors, and to minimize separation error after capture. In examining the data used to generate Figs. 7 and 8, it was seen that flight times (time to land) varied from 735 to 764 sec, or under 4% variation. The mean longitudinal error varied from +0.091 nmi to -0.454 nmi. These values depended upon whether the particular modeled follower was initially too close, too far back, or at a nominal separation.

Similar results to those shown in Figs. 7 and 8 were generated for strings of six followers using both the CTP and AC criteria. The estimated speed vs range-to-go summarizes for the AC criterion is shown in Fig. 9.

ACTUAL EXPERIMENTAL OUTCOME

The NASA Ames Research Center multi-cab simulator facility was used to conduct the CDTI in-trail following studies in February-March 1983. Six weeks of experiment were conducted, where six different sets of three airline pilots were used as test subjects each week. The first two weeks were devoted to using the CTD criterion; the CTP criterion was used the second two weeks. Eight sets of nine-aircraft strings were generated for each criterion. Thus, a total of twenty-four sets of nine-aircraft strings (192 followers in all) were generated.

The approach paths used for the experiments are shown in Fig. 10. Both the Shark and Big Sur paths were used which caused dog-leg lateral maneuvers to be required for the approach. The pilots were instructed to cross the first waypoints t 12000 ft (down from 15000 ft.) and the second waypoints at 8800 ft. The indicated airspeed was to be kept below 250 kt when flying below 10000 ft.

ORIGINAL PAGE IS
OF POOR QUALITY

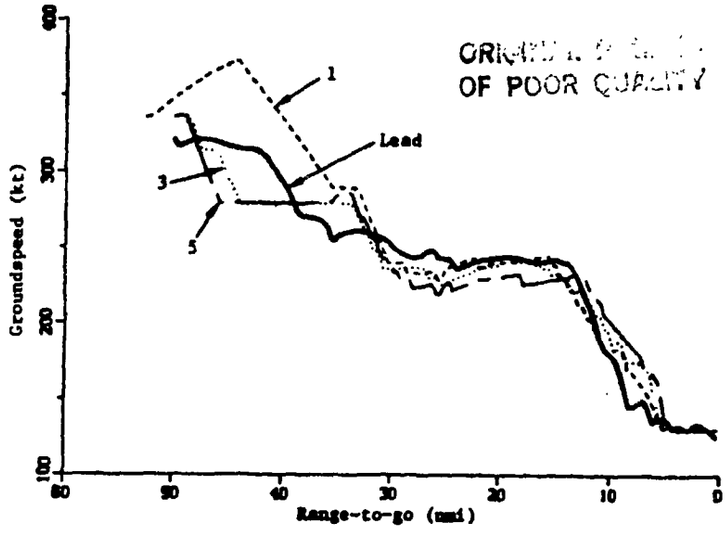

Fig. 9. Predicted Groundspeed vs Range-to-go in String with AC Criterion

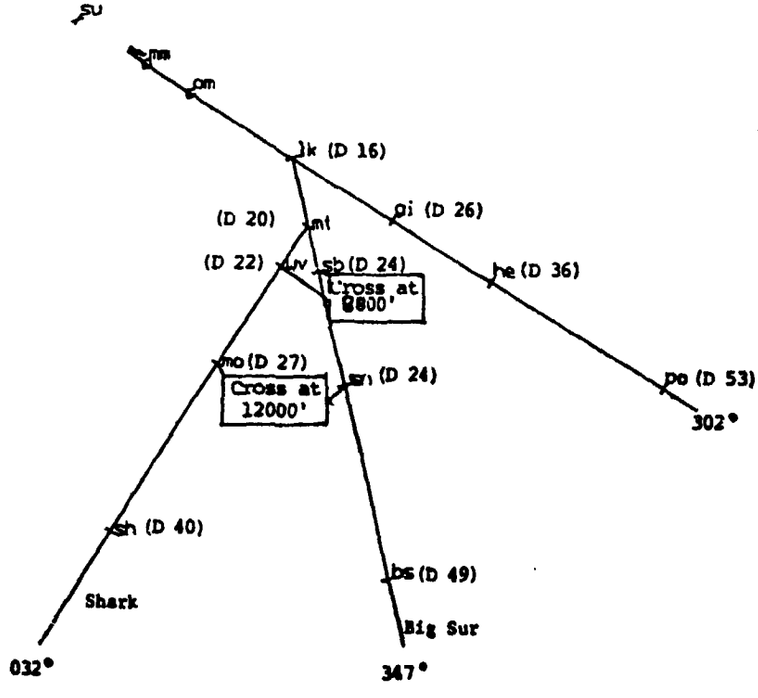

Fig. 10. Shark and Big Sur Approach Paths to San Jose Airport

ORIGINAL PAGE IS
OF POOR QUALITY

The display for the Acceleration Cue criterion is shown in Fig. 11. Note that the predictor vector has three 20-sec segments, and three history dots are shown at 30, 50, and 70 sec behind the lead's location. In addition, the 90-sec history dot is replaced by a "box" consisting of two parallel lines at ± 15 sec about the 90-sec point. The predictor vector length is adjusted to account for own aircraft's measured longitudinal acceleration.

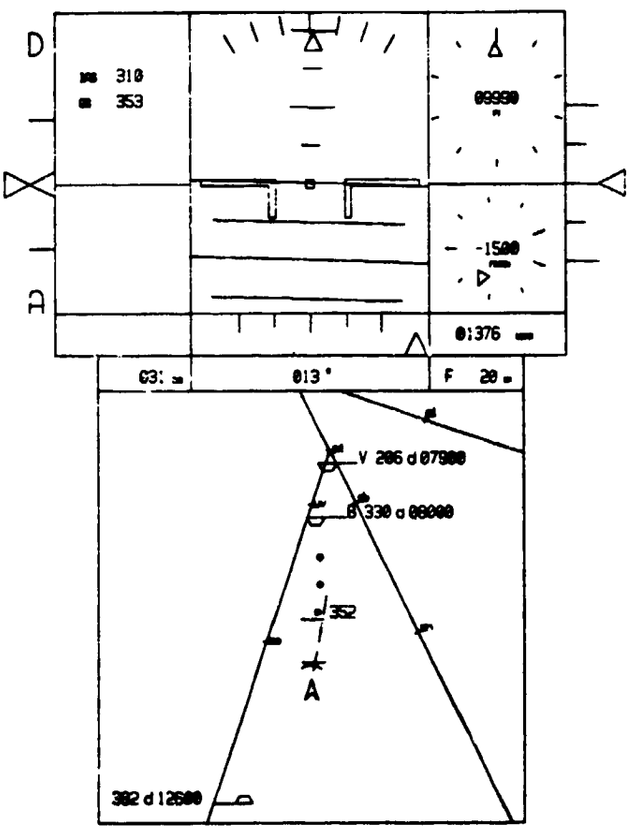

Fig. 11. Multi-cab Display for Acceleration Cue Logic

Three strings, each using a different separation criterion, were chosen to evaluate our specific prediction results in terms of the qualitative dynamic characteristics of the string. The CTD and AC strings chosen can be qualitatively summarized by the groundspeed vs range profiles as shown in Figs. 12a-b. These should be compared to the predicted results of Figs. 8 and 9, for a quick assessment.

Figure 12a is compared to the CTD predicted profiles of Fig. 8, As can be seen, the actual speed profiles lie in a close band after 30 nmi-to-go. Followers 1 and 5 have 40 kt changes between 20 and 10 nmi, but this is closer than predicted in Fig. 8. Also, there is less variation in speed than is shown in the prediction plot after the first maneuver to capture,

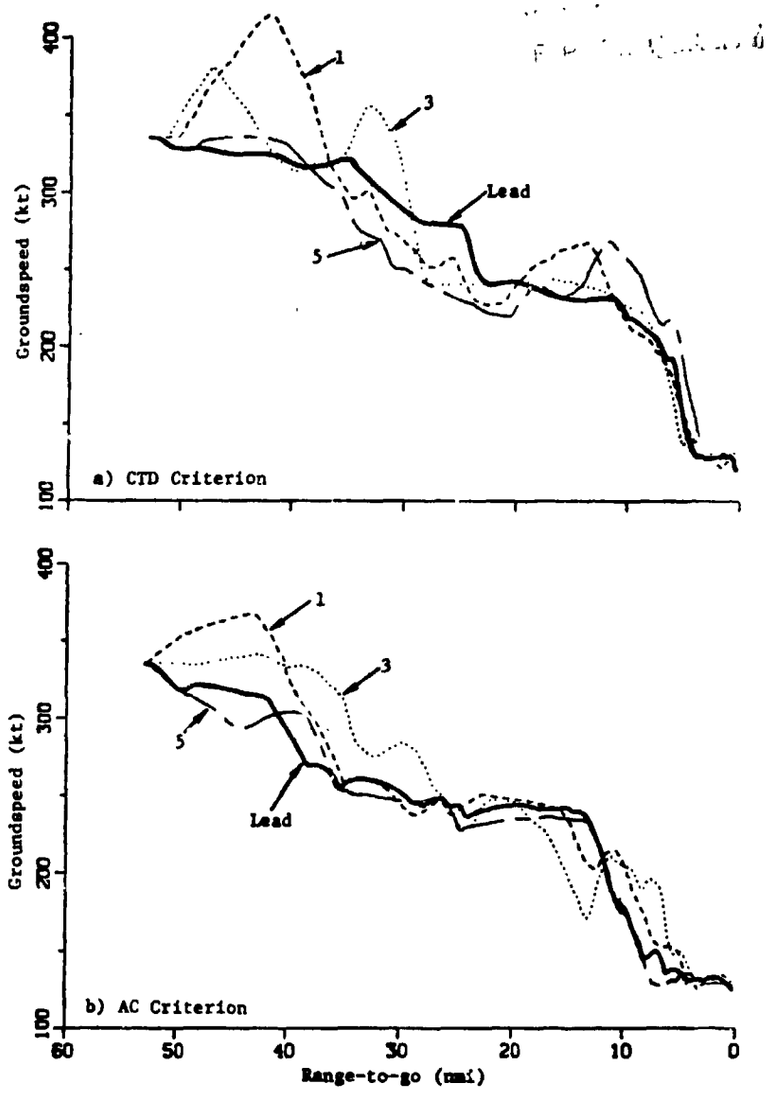

Fig. 12. Groundspeed vs Range-to-go for Every Other Aircraft

For the CTD criterion, the performance statistics for eight followers of the chosen string were:

Own - Target Groundspeed	Mean: -1.2 kt; 1σ : 24.9 kt;
Longitudinal Error	Mean: -0.12 nmi; 1σ : -.37 nmi;
Average Throttle	0.17
Vertical Error	Mean: 0.05°; 1σ : 0.35°;

Time to land varied between 745 and 807 sec which is a ± 4.2% variation. In comparing these values with our predictions, we see actual own - target speed difference deviation was 8 kt less; longitudinal error was very close; and actual average throttle was 6% higher. Actual glideslope error was considerably more than we modeled (0.35° vs 0.06°), indicating that either the pilots continued to use glideslope for partial control or just did not control this dimension as accurately as we had supposed.

Figure 12b is compared to the AC predicted profiles of Fig. 9. Here, our predicted profiles look good. The actual speed profiles have some uneven variations (No. 3 has a 40 kt variation at 15 nmi). The other differences seem to be due to the order of initial separation errors modeled.

In our predicted results, there was a great deal of on-off spoiler control activity. For the actual performances, the spoilers were used only sparingly. The throttle was used mostly for catchup speed control before 40 nmi. Thereafter, it was mostly set at idle. Thus, the chief control from about 35 nmi-to-go to 15 nmi was flight path angle. This was contrary to our assumption that the vertical control was independent. During this period, the speed was held close to 250 kt. Gear and flaps were used for the final deceleration.

Another observation was that aircraft initially too close (No. 2 and No. 4 in the AC string) did not decrease speed rapidly to reduce this error. Rather, they let the aircraft that were initially too far back (No. 1 and No. 3 in the AC string) first accelerate to remove their separation errors; this also took care of the "too close" problem. This indicated that the pilots look ahead to assess what their immediate leads' strategy will probably be. This feature was not included in our predictive model.

It was seen, for all three separation criteria, that there frequently was large (more than 15 sec) separation errors that built up after 10 nmi-to-go was passed. This is illustrated in Fig. 13 for Follower Nos. 2-4 from the AC criterion string. Apparently after 10 nmi, the pilots tend to neglect separation error and concentrate on landing. Thus, our prediction of tight separation control at the end was not correct.

Finally, it is useful to compare the statistics of the errors in the displayed longitudinal separations and glideslope deviations of all the experimental runs to those predicted by our models. In this way, we get an overall average of experimental performance that takes into account differences in pilots, pilot order of flight, and approach paths. These comparisons are made in Table 1 for the three separation criteria.

We note two points from this table. First of all, there was little difference in the overall experimental results between the three criteria. Separation error was about -0.1 ±0.6 nmi, and glideslope error was about ±0.5°, for the three criteria. The second point is that our model predictions are consistently optimistic for both the vertical and in-trail standard deviations. The model predicts a mean of about 0.25° with small variation (±.06°) for the vertical. This indicates that more randomness is required in the model's pilot behavior to get the same in-trail and vertical

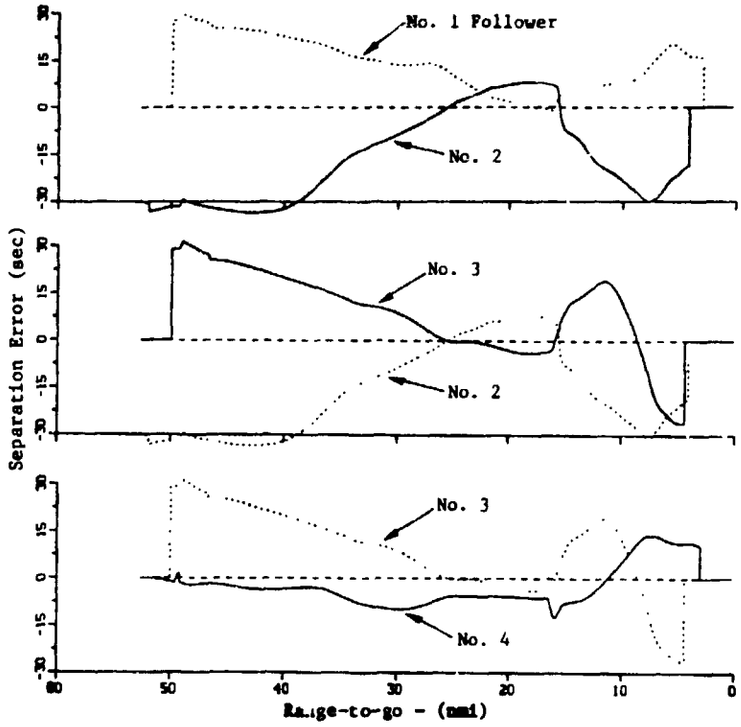

Fig. 13. Separation Errors in Time for Actual AC Data

Table 1. Comparison of Predicted and Actual Separation and Glideslope Tracking Performance After Capture Using All Experimental Data

Criterian	Longitudinal Error (nmi)				Vertical Error (deg)			
	Actual		Predicted		Actual		Predicted	
	m	σ	m	σ	m	σ	m	σ
Constant Time Delay	-.134	.606	-.190	.370	.08	.52	.32	.06
Constant Time Predictor	-.131	.586	-.048	.261	-.01	.48	.22	.05
Acceleration Cue	-.069	.585	-.077	.154	.03	.52	.22	.06

variations. This means that we have to increase drag in the model so that the average glideslope error can be lowered 0.25°

MODEL ADJUSTMENTS TO MATCH EXPERIMENTAL RESULTS

To match experimental results, we began by adjusting the model which uses the CTD criterion. Model parameters and structure were changed to achieve a closer match in the groundspeed vs range-to-go record and the in-trail statistical measures.

First, the sequence of initial separation errors of the mod. changed to be the same as that of the chosen CTD experimental st. second change was to put minimum and maximum speed limits into eff. 10000 ft (after nominal in-trail capture) for each follower. These l. represent the fact that each pilot has a nominal app. ach speed profile that he tends to follow. He deviates from this prof.le o null separation error but only up to some acceptable amount that is consistent with his training. The speed limits and point of gear deployment were then tuned to adjust model profiles.

The result of this CTD model adjustment of speed vs range is shown in Fig. 14; a qualitative agreement exists with the experimental results shown in Fig. 12a. The revised statistical parameters of the modified CTD model are presented in Table 2, along with the experimental results. Good agreement exists in all but the glideslope error statistics. By using the model sensitivity results, it is possible to tune the model to get as close as we wish for in-trail statistics comparison. Thus, the tuned mathematical model is a good representation of the piloted multi-cab simulator using the CDTI for in-trail spacing. However, we next had to address the descrepancies in the control and glideslope error time histories.

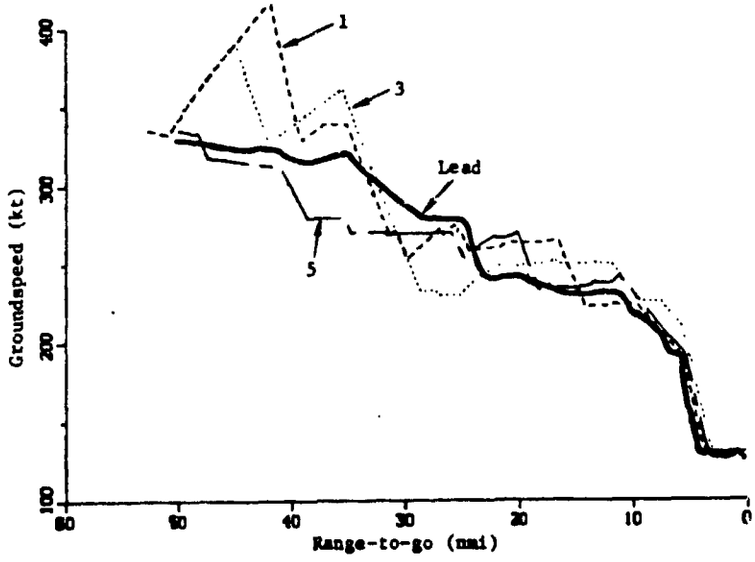

Fig. 14. Modified CTD Model Results

Table 2. Statistical Comparison of Revised CTD Model and Experimental Results

Quantity	Model	Actual
Longitudinal Separation Error (nmi) (After Capture)	-0.11 ±0.34	-0.12 ±0.37
Vertical (Glideslope) Error (deg) (After Capture of Localizer)	0.22 ±0.06	-0.05 ±0.35
Ground Speed Difference (kt)	1.8 ±27.6	-1.2 ±24.9
Average Throttle	0.172	0.170

Figure 15 is a comparison of the vertical profile (altitude vs range) and control sequence used by the first follower in the Experimental and modeled AC criterion string. Note that the actual flight path angle has considerable more fluctuation than does the model. The model has more throttle/spoiler activity than the experiment. This same results was true for the other followers. This indicates that the pilots tend to use flight path angle to a greater extent for in-trail control than we assumed in the model. (i.e., the pilots use flight path angle for both in-trail and vertical control.)

To show that flight path angle could be used for both in-trail and vertical control by the model, the acceleration cue (AC) based model was modified to use primarily γ control by inhibiting the use of spoilers. The resulting model was tuned so the resulting speed vs range curves approximated those results shown in Fig. 12b. The match of separation error for the No. 1 follower in the model and the experiment is shown in Fig. 16. Similar results for all followers proved that the aircraft is fully controllable with flight path angle and throttle variations.

The statistical results before and after the AC model was modified based on the actual experimental outcome are shown in Table 3. We see that using γ for primary control shifts the mean separation error forward 0.15 nmi, increases both the mean and standard deviation of vertical error, and decreases the average throttle position. If throttle activity was increased to 0.17, as in the experiment, it would be required to have an even larger mean flight path angle error.

Changing the model did succeed in raising the glideslope error standard deviation from 0.06 to 0.19. Larger variations in this control are possible with an accompaning increase in standard deviation in separation error.

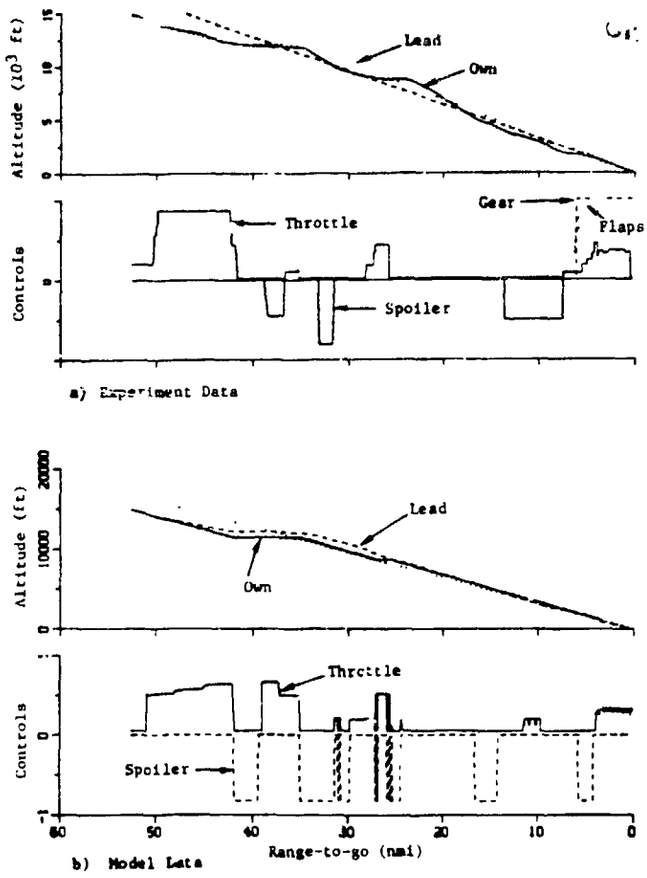

Fig. 15. Comparison of Flight Path Angle and Spoiler/Throttle Control for No. 1 Follower (AC)

That is, if the glideslope variation was tuned to increase from $\pm 0.19°$ to $\pm .35°$, the separation error deviation would move from ± 0.15 nmi closer to the ± 0.37 nmi of the actual results.

The vertical mean error of $+0.38°$ indicates that the model has to have a mean positive (pitch up) error to slow the aircraft successfully for landing. This indicates that the actual similator dynamics has a drag (or decay) term affecting speed that is not in the model. The idle thrust level could be tuned in the model to improve the match between actual and modeled results.

CONCLUSIONS

This study demonstrated that a system model can be devised which duplicates the statistical performance, qualitative character, and control strategies of pilot and aircraft in a multi-cab experiment. This model can be used for future fast time simulation of in-trail following tasks. The process of

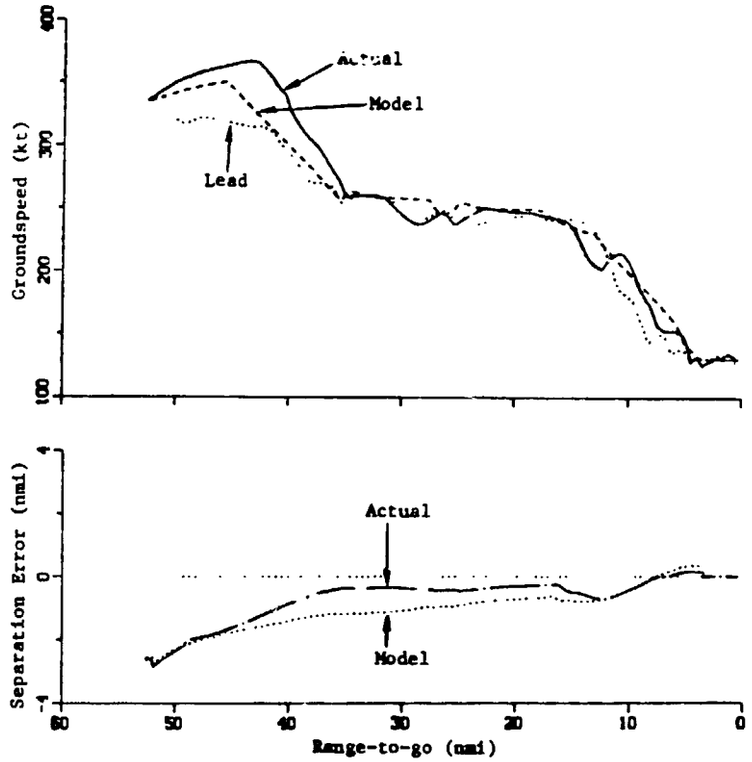

Fig. 16. Modified AC Model Match of No. 1 Follower Separation Error

Table 3. Statistical Comparison of AC Models and Experimental Results

Quantity	Original Model	Modified Model	Actual Experiment
Longitudinal Separation Error (nmi) (After Capture)	-0.08 ±0.15	0.07 ±0.15	0.02 ±0.37
Vertical (Glideslope) Error (deg) (After Localizer Capture)	0.22 ±0.06	0.38 ±0.19	-0.07 ±0.35
Groundspeed Difference (kt)	0.1 ±20.6	1.2 ±13.5	-0.2 ±17.8
Average Throttle	0.13	0.08	0.17

duplicating the actions of the pilot using the CDTI to regulate his aircraft position was facilitated by breaking those actions into estimation, decision, and control components.

The more significant lessons we learned were those resulting from our incorrect assumptions in predicting the outcome of the experiment. Some of the more important lessons were as follows:

1. In our design logic for decision and control to model the actual experiments, we assumed that because spoilers were present, the pilot would use primarily throttle and spoilers for in-trail spacing control. We assumed he would use flight path angle control strictly for meeting altitude windows and then later capturing and maintaining the glideslope. (i.e., we assumed that the two axes would be split by the control mechanisms used.) This was not the case. The pilots used the spoilers as little as possible. They used flight path angle for both speed control and vertical control, which is consistent with their training. The lesson: Build control logic based as closely as possible to the way pilots normally fly, even though a new requirement (regulating in-trail spacing) is added to their control requirements.

2. We assumed that the in-trail following task would be the primary objective that would govern the pilots' control of the speed of the aircraft during most of the approach. This was not true. After the initial capture phase where pilots would remove most of the initial separation error, they would stay close to a nominal approach speed as a function of range-to-go. Thus, this nominal speed had to be included in the longitudinal control laws and decision process of the model. The lesson: Again, the way the pilot flys a nominal approach must be factored into the model for prediction.

3. We assumed that tight in-trail spacing control would continue to the outer marker. The data incidated that the pilots would switch to a strategy of just concentrating on landing sooner than this, and the in-trail spacing errors would grow near the end. Again, this is inherent in the way they have been trained and what they have experienced over years of flying.

These lessons are all logical, and they would enable us to design a more accurate model and make better predictions of the experimental outcome sooner the next time.

References

1. Palmer, E.A., et al., "Perception of Horizontal Aircraft Separation on a Cockpit Display of Traffic Information," Human Factors, Vol. 22, No. 5, Oct. 1980, pp. 605-620.

2. Kelly, J.R. and Williams, D.H., "Factors Affecting In-Trail Following Using the CDTI," Proceedings of the 18th Annual Conference on Manual Control, Dayton, Ohio, June 1982.

3. Sorensen, J.A., "Analysis of In-Trail Following Dynamics of CDTI-Equipped Aircraft - Phase II," Report No. 82-31, Analytical Mechanics Assoc., Inc., Mtn. View, CA., August 1982.

4. Sorensen, J.A., and Goka, T., "Analysis of In-Trail Following Dynamics of CDTI-Equipped Aircraft," J. of Guidance, Control, and Dynamics, Vol. 6, No. 3, May-June 1983, pp. 163-169.

5. Heffley, R.K., and Schulman, T.M., "Mathematical Model Descriptions for a Medium Jet Transport and a Light Twin," System Technology, Inc. Report No. 1164-2R, Mtn. View, CA, June 1981.

6. Sorensen, J.A., and Goka, T., "System Modeling to Predict Pilot Performance During an In-Trail Following Experiment," Report No. 83-16, Analytical Mechanics Assoc., Inc., Mtn. View, CA, July 1983.

N85 14505

MULTILOOP MANUAL CONTROL OF DYNAMIC SYSTEMS

Ronald A. Hess and B. David McNally
Department of Mechanical Engineering
University of California
Davis, California 95616

ABSTRACT

Modern, high performance aircraft increasingly rely upon high-authority stability and command augmentation systems to achieve satisfactory performance and handling qualities. In addition, certain tasks which have traditionally been allocated to the human pilot are candidates for automation in the near future. This situation has accentuated a long-standing need for a thorough understanding of the human's capabilities, limitations and preferences when interacting with complex dynamic systems, particularly when the question of task allocation between man and machine arises. In this work, an analytical and experimental study was undertaken to investigate human interaction with a simple, multiloop dynamic system in which the human's activity was systematically varied by changing the levels of automation. The control loop structure resulting from the task definition parallels that for any multiloop manual control system, and hence, can be considered as a stereotype. The analytical work concentrated upon developing simple models of the human in the task, and upon extending a technique for describing the manner in which the human subjectively quantifies his opinion of task difficulty. The experimental work consisted of a man-in-the-loop simulation providing data to support and direct the analytical effort.

INTRODUCTION

Automation has become a central issue in the design of man-machine systems in the past decade, particularly as regards manned aircraft. The pilot's role as a systems manager or supervisor is being emphasized as the capabilities of modern avionics systems, in particular, digital computers, evolve. Indeed man-machine interaction has become nearly synonomous with man-computer interaction in describing the activity of the pilot in the cockpit of the future.

It is worth emphasizing that the fundamental role of the human in the aircraft cockpit is still that of a "controller" in that nearly all his activity has, as its ultimate aim, the control of the vehicle's velocity vector.

A convenient means of explaining the nature of tasks involving the manual or automatic control of dynamic systems such as aircraft is shown in Fig. 1. Here, Ω_i represents a generalized "bandwidth" indicating the relative time scales involved in each of the loop shown. The nesting of feedback loops with $\Omega_1 > \Omega_2 > \Omega_3 \ldots > \Omega_n$ is a characteristic of nearly all dynamic control systems, no matter how complex. As an example of an aircraft flight control

problem, the loops of Fig. 1 could be interpreted as follows: The block denoted Ω_1 represents attitude control with a relatively high bandwidth. Block Ω_2 represents altitude control with a lower bandwidth while block Ω_3 represents navigation activity with a still lower bandwidth.

The ways in which a man and a computer can interact in the system of Fig. 1 can be quite subtle and have been outlined, classified and discussed by Rouse [1]. They are obviously dependent upon which function are under manual and which are under computer (automatic) control. Figure 1 invites a simple and practical allocation of tasks between man and computer (manual and automatic control). One can start at the inner-most loop and begin automating the feedback activity loop-by-loop. This means that the human is responsible for fewer loop closures as the automation proceeds and these with lower and lower bandwidths. Conversely, one can start at the outer-most loop and begin the automation process. Again, as the automation proceeds, the human is responsible for fewer loop closures, but the bandwidth of the manual control task is, in this case, dominated by the inner-most loop. Both of these schemes are consistent with current practice in aircraft flight control automation. For example, the first is exemplified by an automatic landing system while the second is exemplified by the same landing task, except using a cockpit flight director. Both schemes can result in increased man-machine performance and decreased "workload".

It is of some interest to analyze these two automation approaches, particularly when outer-loop preview information is available to the human. To this end, an analytical and experimental study was undertaken to investigate human interaction with a simple, multiloop dynamic system in which the human's activity was systematically varied by changing the level of control augmentation (automation level). The control loop structure resulting from the task definition is consistent with that of Fig. 1 and, as such, can be considered as a simple steroetype. The analytical work concentrated upon developing simple models of the human in the task, including preview effects, and for extending a technique for describing the manner in which the human subjectively quantifies his opinion of task difficulty [2] . The experimental work consisted of a man-in-the-loop simulation providing data to support and direct the analytical effort.

EXPERIMENT

A simple man-in-the-loop simulation was conducted on a fixed-base laboratory type simulator at NASA Ames Research Center. The actual task considered was that of the longitudinal control of a hovering helicopter or VTOL vehicle. The multiloop system is shown in Fig. 2. This figure indicates completely manual operation in its present form and the basic vehicle possesses so-called rate-command, attitude-hold pitch attitude dynamics. Vehicle attitude determines vehicle velocity, which, in turn, determines vehicle displacement from some command position. Figure 2 also outlines the automation levels which were examined in this study. If the inner-most loop of Fig. 2 is automated, the human is left with an attitude-command, attitude-hold "inner" loop, with velocity and position loops unchanged. If the next inner-loop of Fig. 2 is also automated, the human is left with a velocity-command, position-hold system. Finally, by automating all the loops of Fig 2 but leaving the pilot

the option of providing a position-command signal to the automated system, a position-command, position-hold system results. Conversely, of the outer-most loops are closed and an inner-loop command signal displayed to the pilot, a flight director system results (not indicated in Fig. 2).

The unagumented vehicle dynamics were very simple and can be given as:

$$\dot{x} = u$$

$$\dot{u} = -g\theta + X_u u$$

$$\dot{\theta} = K\delta$$

where x represents vehicle position, u vehicle velocity, θ vehicle attitude and δ control deflection.

A color, raster-type display was used in the experiment to provide the subjects with the pertinent information needed to close the loops in Fig. 2. The display format is shown in Fig. 3. An isometric manipulator was used in all but the position command configuration where an unrestrained finger manipulator was employed. Each of the automated closures were implemented in a manner similar to that which would be employed by the human were he asked to close the loops in question.

The human pilot dynamics were estimated by using the simplifed crossover model of the human [3] for each loop closure:

$$Y_{p_i} Y_{c_i} = (\omega_{c_i}/s)e^{-\tau_e s} \qquad (1)$$

where Y_{p_i} represents the human pilot dynamics in the closure in question, Y_{c_i} represents the pertinent vehicle dynamics in that closure, and ω_{c_i} represents the open-loop crossover frequency (or closed-loop bandwidth). For example, the attitude-command system was implemented by allowing Y_{p_θ} in Fig. 2 to take the form

$$Y_{p_\theta} = \omega_{c_\theta}/K$$

where ω_{c_θ} is the appropriate crossover frequency and K is the gain appearing in θ/δ. Of course, the human's effective time delay τ_e was deleted in implementing the automated loop closures.

The command signal x_c was chosen as a square wave with a fundamental frequency of 0.2 rad/sec. This command signal was displayed to the subject in preview fashion as the horizontal translation of the square waveform on the display of Fig. 3. The amplitude of the command signal was 50 ft. The loop crossover frequencies were chosen by equating the position-loop crossover frequency, ω_{c_x}, to that of the fundamental component of the command signal and then separating the remaining crossover frequencies by a factor of three. This factor was suggested by other multiloop manual control experiments [4].

The position command signal was chosen as periodic to encourage higher levels of skill development on the part of the subjects.

Four naive subjects participated in the experiment. Each simulation run lasted approximately 95 seconds. Each subject saw the 5 different configurations presented in the following order: (1) velocity command, (2) rate command, (3) flight director, (4) attitude command, and (5) position command. Root-mean-square (RMS) performance scores were recorded as were pilot opinion ratings of task difficulty quantified on a non-adjectival rating scale [5]. The subjects were instructed to minimize position errors while maintaining realistic vehicle pitch rate. The quantify the latter, an audio alarm sounded whenever $\dot{\theta}$ exceeded 10 deg/sec. Data was taken only after RMS performance scores stabilized.

RESULTS

Figure 4 summarizes the outer-loop position performance for the subject with the best performance (subject 3) for each configuration. The unfilled symbols in Fig. 5 show the subjective task difficulty ratings for each configuration averaged across all the subjects. A technique for obtaining objective measures of task difficulty from analysis of control movements was investigated [6]. Specifically, the number of individual "control movements" during any run were measured and recorded. As implemented in this study, a "control movement" was said to occur when the subject's control input exceeded a criterion value defined as a percentage of the RMS value of the output for that run. A criterion value of 75% was found to produce trends in the control movement data which compared well with those of the subjective opinion data with the exception of the flight director. This discrepancy will be discussed in the next section. The control movement results are shown in Fig. 6 for each configuration, averaged across all subjects.

Figure 7 shows typical time responses in x, u, and θ for subject 3 for each of the automation configurations. This figure also demonstrates one of the most important results of the experimental study. Namely, with the exception of the flight director, all configurations allowed the subjects to synchronize the vehicle position $x(t)$ with the command input $x_c(t)$. Since the flight director was the only configuration which forced compensatory behavior on the part of the subjects, the remaining configurations apparently allowed higher levels of skill development associated with preview tracking.

PILOT MODELING

A simple pilot modeling effort was undertaken to identify, at least approximately, the pertinent model parameters in the completely manual system of Fig. 2. An off-line computer simulation of that system was implemented. Nominal pilot models of the following form were examined:

$$Y_{p_\theta} = \omega_{c_\theta} e^{-\tau_e s} = 1.8e^{-0.3s}$$

$$Y_{p_u} = \omega_{c_u} = 0.6 \qquad (2)$$

$$Y_{p_x} = \omega_{c_x} = 0.2$$

It was found that no choice of the parameters in Eq. (2) would yield model time responses that provided adequate matches to the data, even when the command input x_c was advanced in time to model preview. However, when the actual square wave time history for x_c was replaced with the position command which the subject generated in using the position command system, a dramatic improvement was seen in the modeling results. Fig. 8 comapres the subject-generated position command for subject 3 with tha actual square wave position command. It should be noted that all the subjects generated commands which were similar in nature to that of Fig. 8 when using the most automated, position command system. An accurate approximation to the subject-generated position command was implemented in the off-line computer simulation using the pilot model of Eqn, (2) with the nominal parameter values shown. The resulting time histories are shown in Fig. 9. They are seen to compare quite favorably with the experimental traces shown in Fig. 7a.

Finally, an analytical means for determing task difficulty using a structural model of the human pilot [7] was investigated. The approach was introduced in Ref. 2, but dealt soley with single-loop tracking tasks in that study. Figure 10 shows a simplified version of the structural model of the human pilot [2] . Following the lead of Smith [8] , it was shown in Ref. 2 that the RMS value of the signal u_m in the model of Fig. 10 correlated quite well with pilot opinion ratings of vehicle handling qualities when model parameters were selected which produced human operator transfer functions which matched those measured in experiment. It was hypothesized here that the method of Ref. 2 could be extended to multiloop tasks by considering the activity only in the inner-most loop of any multiloop task. For example, consider Y_{p_θ} for the completely manual configuration of Fig. 2. One can see from Fig. 10 that the RMS value of u_m is determined by the characteristics of the inner-loop command θ_c once the structural model parameters have been selected to provide a realistic Y_{p_θ}. Now the simplified structural model of Fig. 10 is parameterized by K_e and K_m. However, for K/s controlled element dynamics, Fig. 10 indicates

$$u_m = (sK_m/(s/\omega_c + 1))\theta_c$$

Thus, the effect of manual outer-loop closures in determining u_m is contained in the characteristics of θ_c.

Thus, using the nominal bandwidths of Eqn. (2), the RMS value of u_m can be determined in terms of the model parameter K_m for each automation level using the off-line computer simulation. The fact that the inner-most manual closure for any automation level always (except the position command) involves K/s dynamics and the control sensitivities have been optimized for each closure, leads to the final assumption that, in terms of the model, K_m can be considered invariant across all configurations.

The filled symbols shows the RMS u_m values obtained from the off-line

simulation for each automation level, except the position command, in which K/s open-loop dynamics were not in evidence. In generating the RMS values of u_m (σ_{u_m}), the subject-generated position command was used in place of the actual task position command as discussed previously. To model the effects of noisy observations, broadband noise with an RMS value of 10 ft was injected in parallel with the position command. The noise was removed in modeling the human using the flight director since the single, compensatory closure would involve minimal observation noise as compared to the other closures.

DISCUSSION

Control strategy and automation level

The control strategy adopted by the subjects for each automation level can best be interpreted in terms of the resulting vehicle velocity time histories in Fig. 7. As the figure indicates, in configurations where preview information was available (all but the flight director) the velocity responses appear as a series of relatively uniform alternating pulses. With the outer position loop open in Fig. 2, the effective open-loop dynamics are approximately 1/s in the frequency region around ω_{c_u}. McRuer, et al, [9] have shown that a constrained time-optimal step-response control input to a K/s system under manual control is a rectangular pulse. The duration of the pulse was shown in 11 to be a physical constraint in manual control problems. In the simple single-loop experiments of [9] , the pulse duration was related to the duration of a "force program", i.e., the minimum time possible for the human neuromuscular system to generate an accurate pulsive control motion with an ideal manipulator. This concept can be adopted here and the duration of the velocity pulse is seen to be approximately 3 to 4 times the reciprocal of the pertinent loop crossover frequency, ω_{c_u}.

It must be emphasized again that the time histories evident in Figs. 7a - 7d cannot be adequately explained via Fig. 2 using the step position command x_c, only Fig. 7e, the flight director, can. This means that the available preview information has led to the generation of time optimal behavior on the part of the human, regardless of the automation level. As Fig. 4 indicates, position performance was also nearly independent of automation level when preview information was available.

Control movement analysis

The failure of the control movement analysis in following the subjective rating trends for the flight director can be traced to the fact that, in using the director, all the subjects adopted a very aggressive control strategy. This was attributed to the fact that the subjects were aware of the rather sluggish response of the flight director configuration relative to the other configurations where preview was available. The subjects tried to null director errors almost instantly by using pulsive control inputs. Although this strategy did not seem to detract from their subjective estimates of control difficulty, it certainly would effect the control movement analysis and can explain the flight director results of Fig. 6 as compared to Fig. 5.

Analytical task difficulty measure

The extension of the single-loop theory for interpreting the manner in which the human quantifies his subjective opinion of task difficulty to multiloop tasks appears feasible. The extension implies that task difficulty is determined by the activity in the inner-most loop being closed by the human regardless of automation level. Outer-loop effects, of course, influence the subjective estimates through the characteristics of the command signal to the inner-most loop.

ACKNOWLEDGEMENTS

This work was supported by a grant from the Aircraft Guidance and Navigation Branch of the Flight Systems and Simulation Research Division, NASA Ames Research Center, Moffett Field, CA.

REFERENCES

[1] Rouse, W. B., "Human-Computer Interaction in the Control of Dynamic Systems," Computing Surveys, Vol. 13, No. 1, March 1981, pp. 71-99.

[2] Hess, R. A., and Sunyoto, I., "Toward a Unifying Theory for Aircraft Handling Qualities," AIAA Paper No. 84-0236, 22nd Aerospace Sciences Meeting, Jan. 1984.

[3] McRuer, D. T., and Krendel, E., "Mathematical Models of Human Pilot Behavior," AGARDograph No. 188, 1974.

[4] Heffley, R. K., "A Pilot-in-the-Loop Analysis of Several Kinds of Helicopter Acceleration/Deceleration Maneuvers," Proceedings of a Specialists Meeting on Helicopter Handling Qualities, NASA Ames Research Center, April, 1982 NASA Conf. Pub. 2219, pp. 221-231

[5] Hess, R. A., "Nonadjectival Rating Scales in Human Response Experiments," Human Factors, Vol. 15, No. 3, 1973, pp. 275-280.

[6] Weirwille, W. W., and Connor, S. A., "The Sensitivity of Twenty Measures of Pilot Mental Workload in a Simulated ILS Task," Proceedings of the Eighteenth Annual Conference on Manual Control, June, 1982, pp. 150-162.

[7] Hess, R. A., "A Structural Model of the Adaptive Human Pilot," Journal of Guidance and Control, Vol. 3, No. 5, Sept.-Oct. 1980, pp. 416-423.

[8] Smith, R. H., "A Theory for Handling Qualities With Application to MIL-F-8785B," AFFDL-TR-75-119, 1976.

[9] McRuer, D. T., et al, "New Approaches to Human Pilot/Vehicle Dynamic Analysis," AFFDL-TR-67-150, 1968.

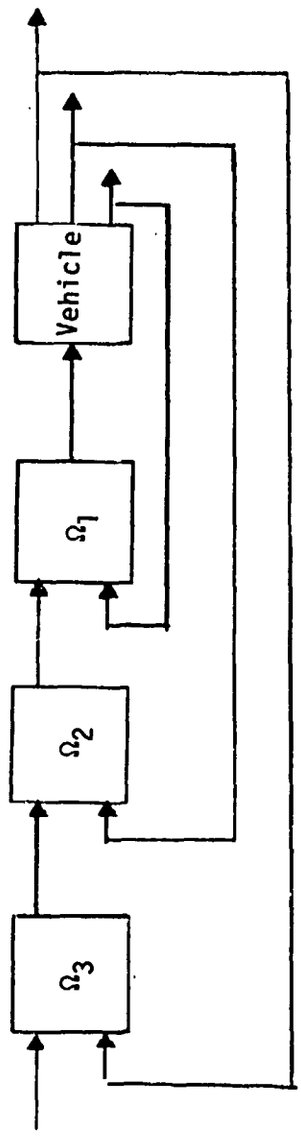

Figure 1. The general structure of dynamic systems

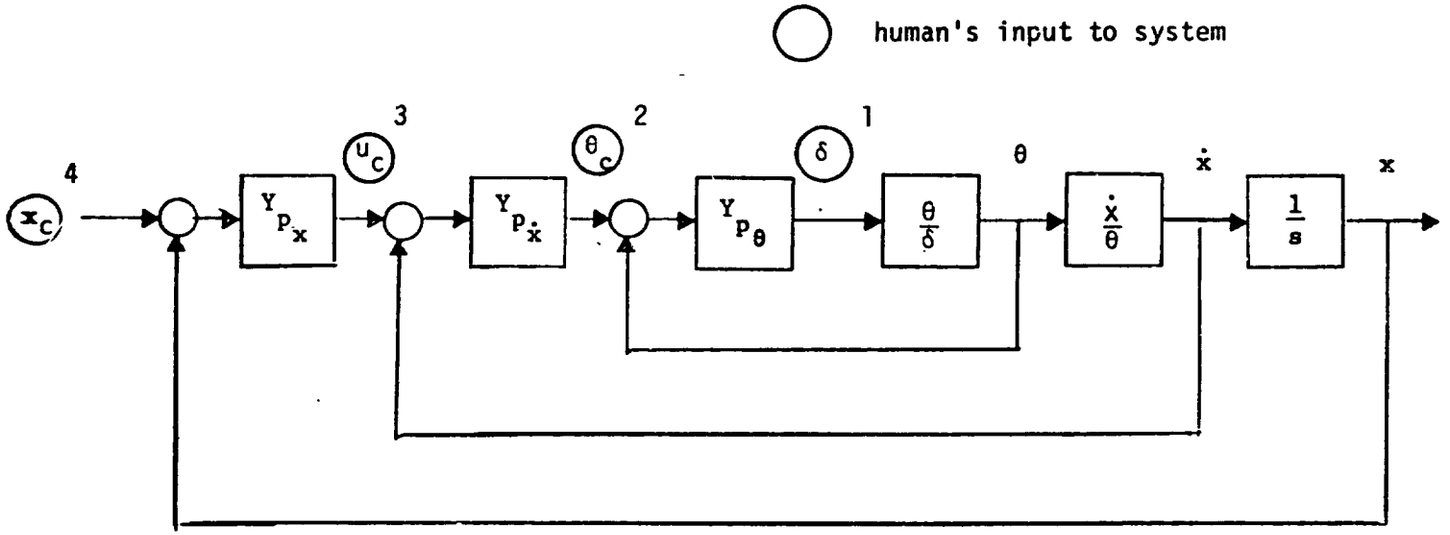

1 = human control input for rate-command system

2 = " " " " attitude-command system

3 = " " " " velocity-command system

4 = " " " " position-command system

Figure 2. The stereotype multiloop system - hypothesized pilot loop closures for a longitudinal VTOL hover task

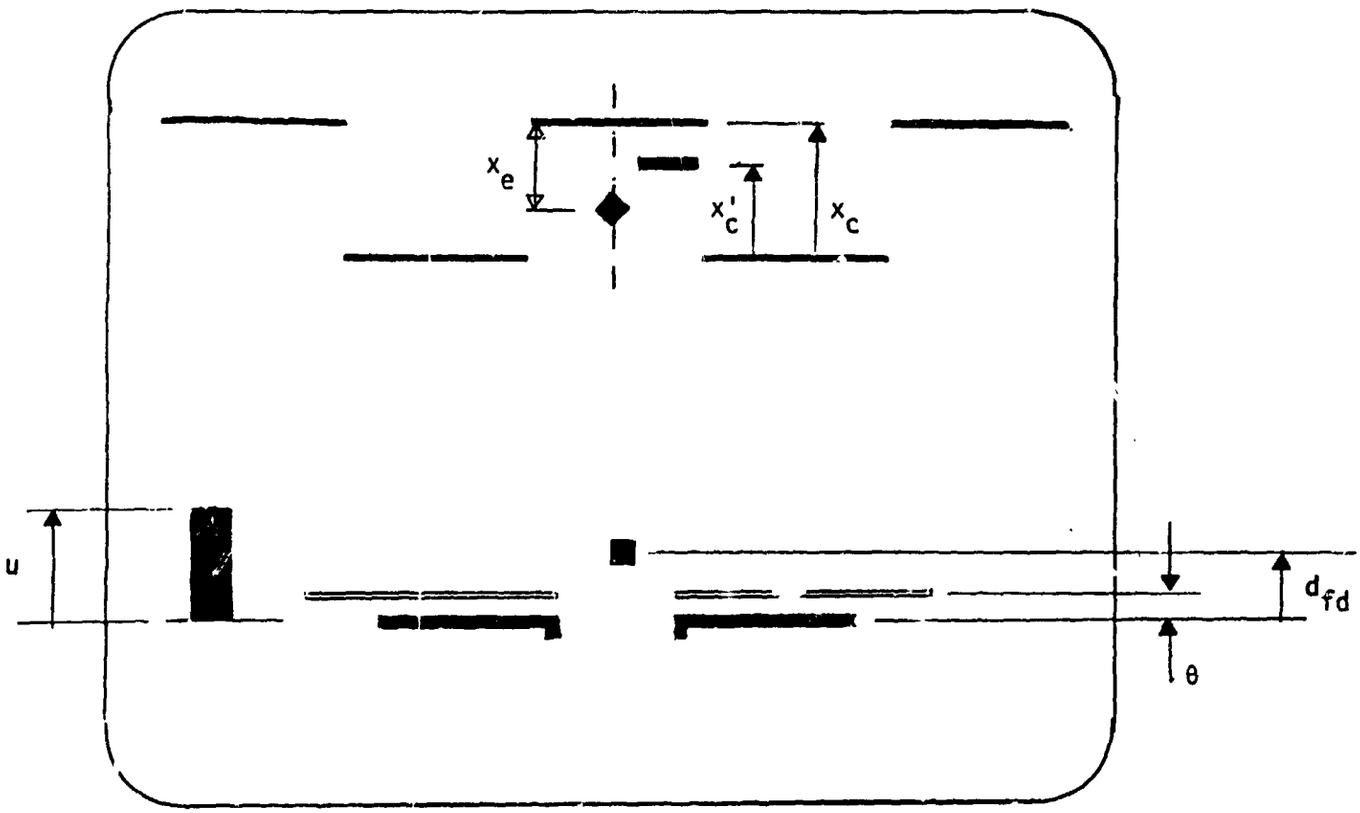

u = vehicle velocity

θ = pitch attitude

d_{fd} = flight director command

x_c = actual task position command

x'_c = subject-generated position command

x_e = position error

Figure 3. Display format for longitudinal hover experiment

ORIGINAL PAGE IS
OF POOR QUALITY

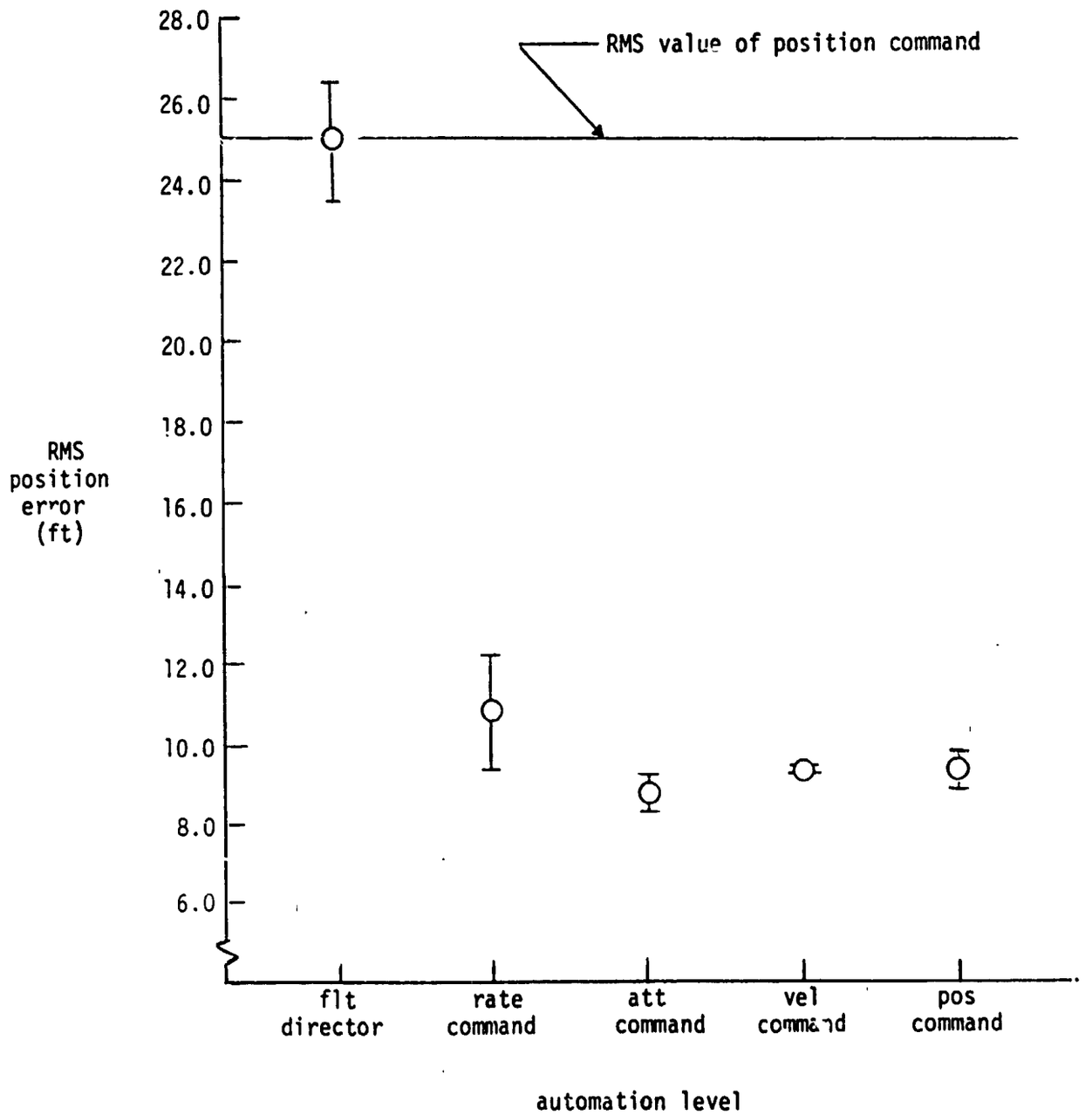

Figure 4. RMS position performance for one subject for various automation levels. Average of 5 runs.

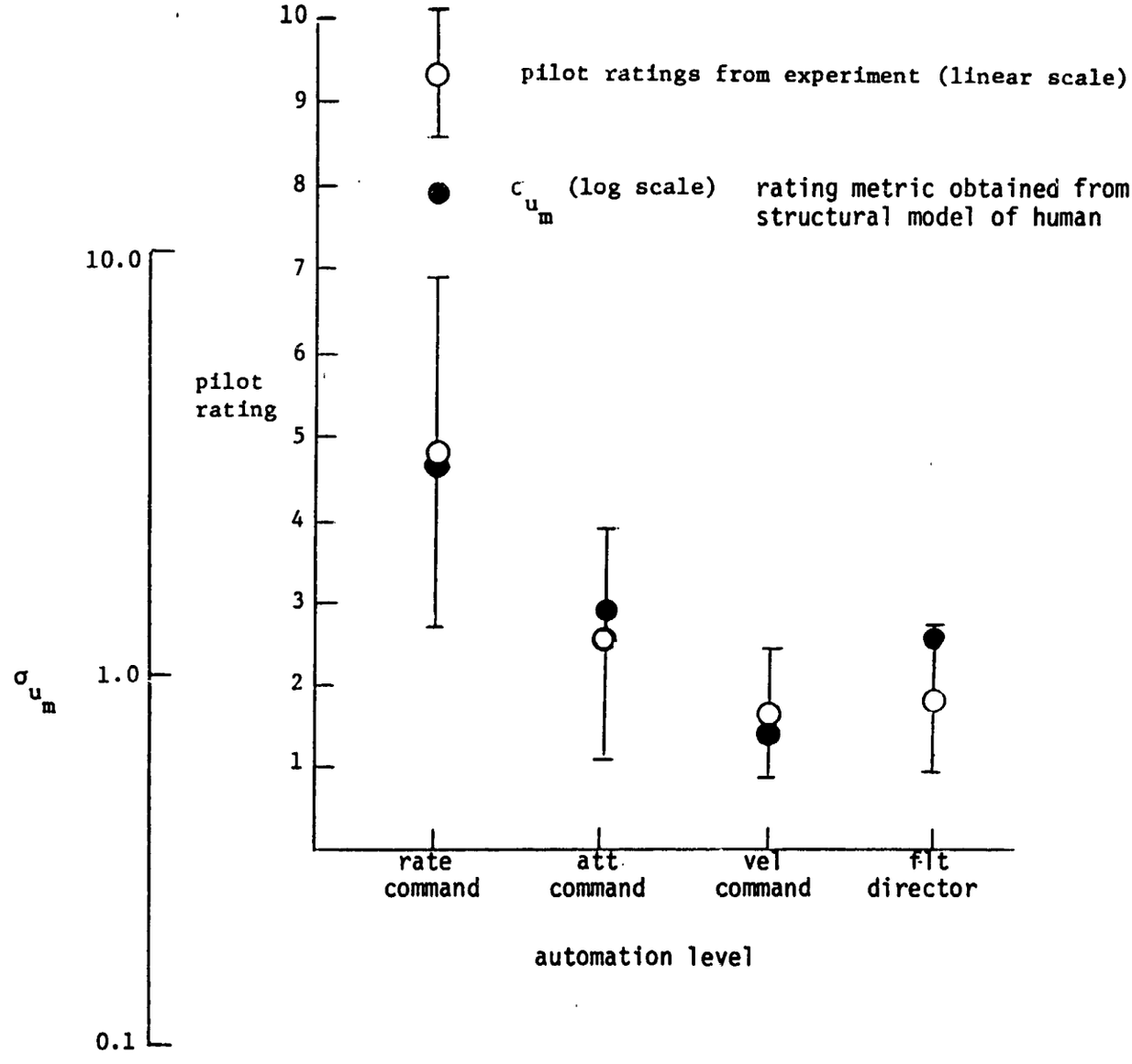

Figure 5. Comparison of subjective task-difficulty ratings with model-based metric

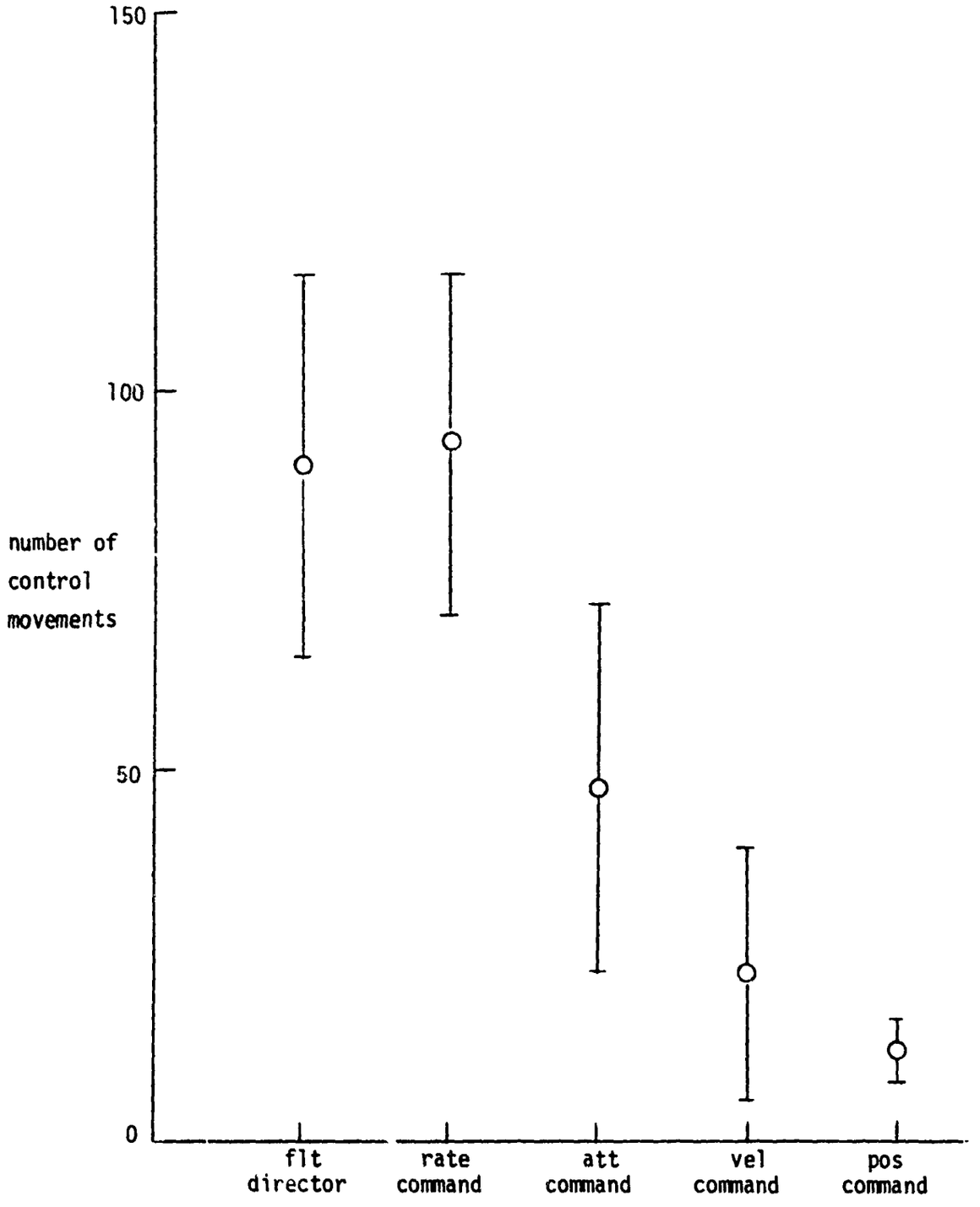

Figure 6. Control movements analysis

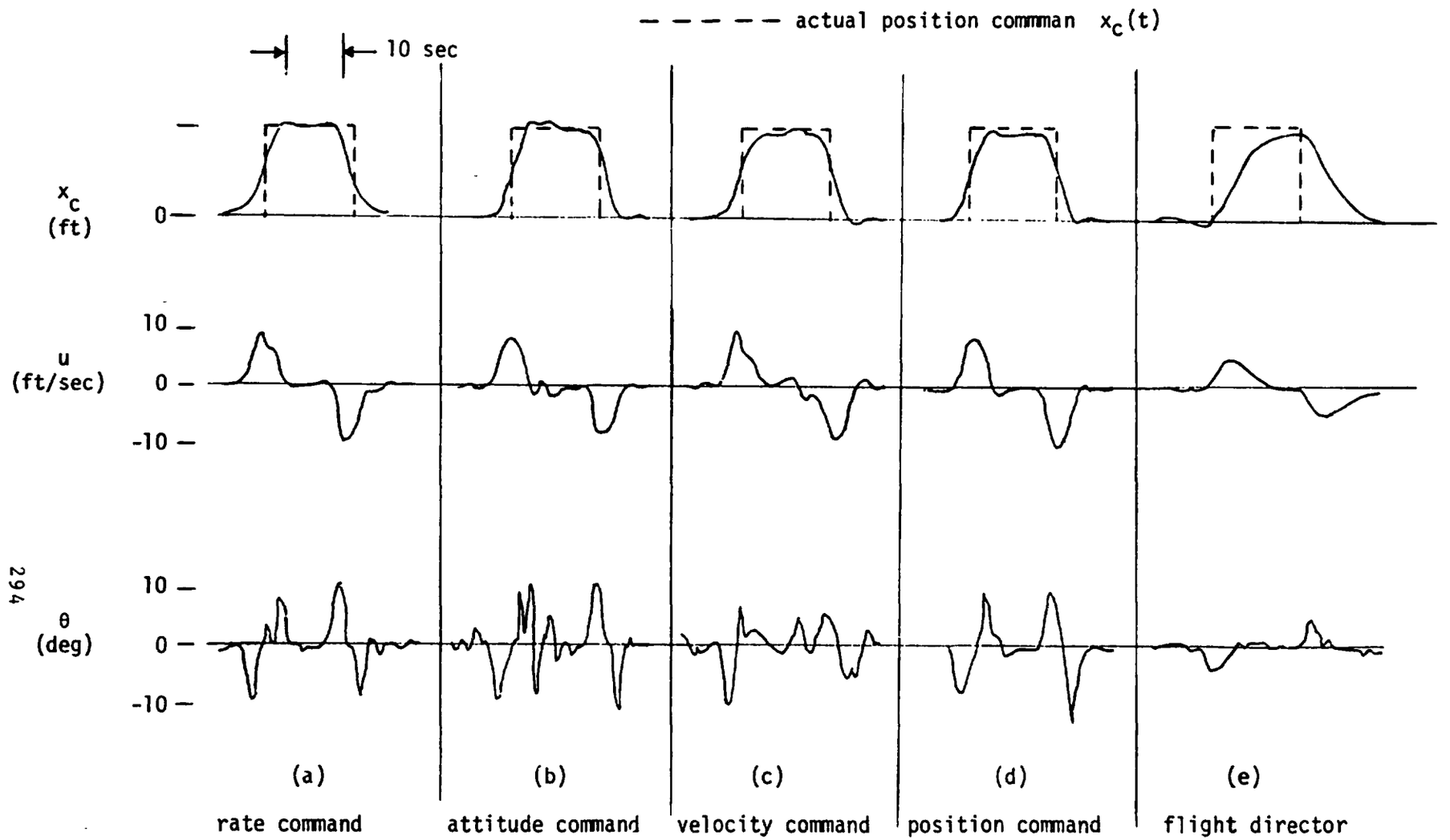

Figure 7. Typical time responses for one subject

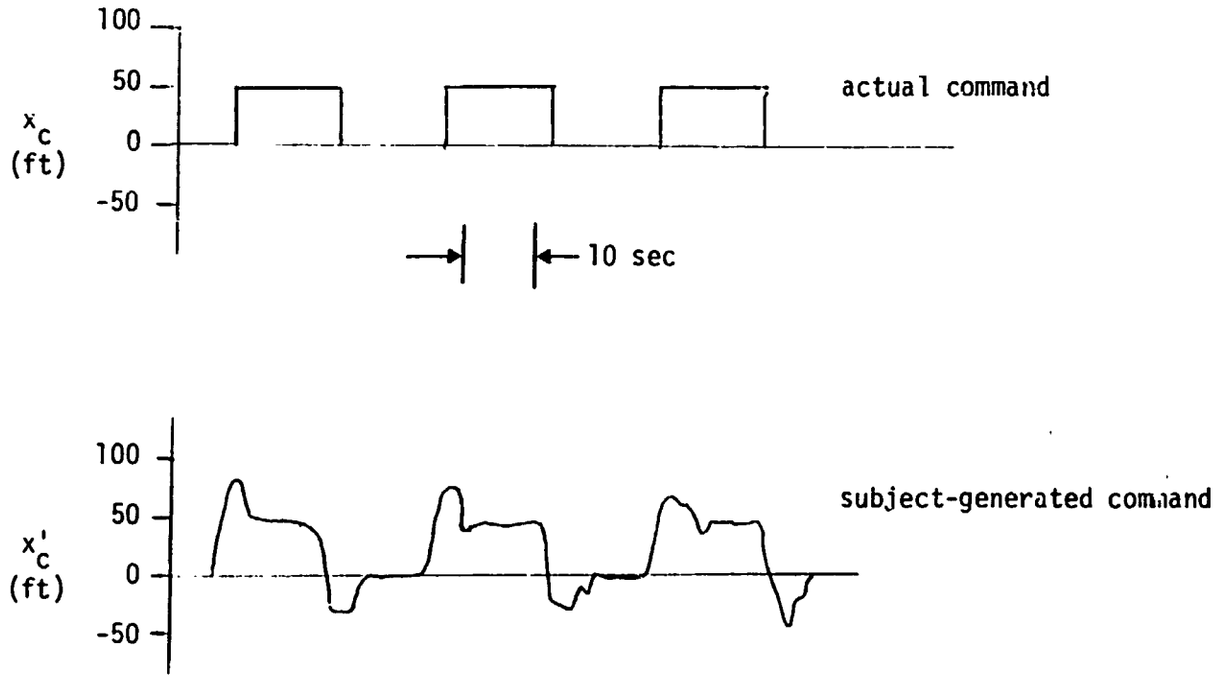

Figure 8. Comparison of actual position command with subject-generated command

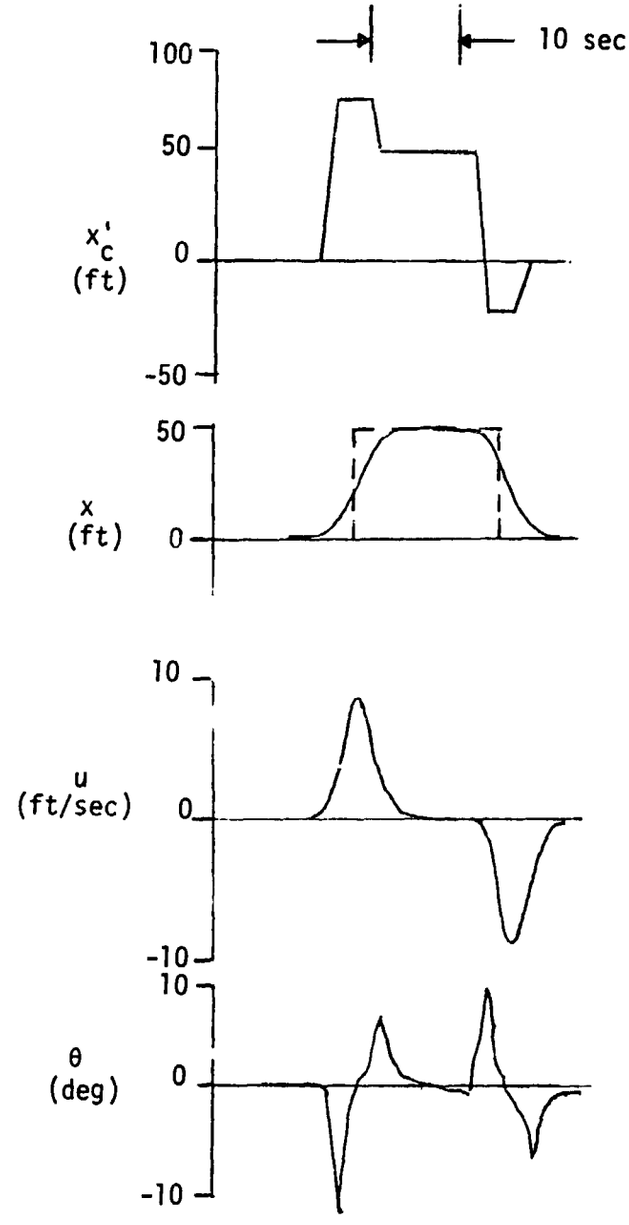

Figure 9. Model generated time responses

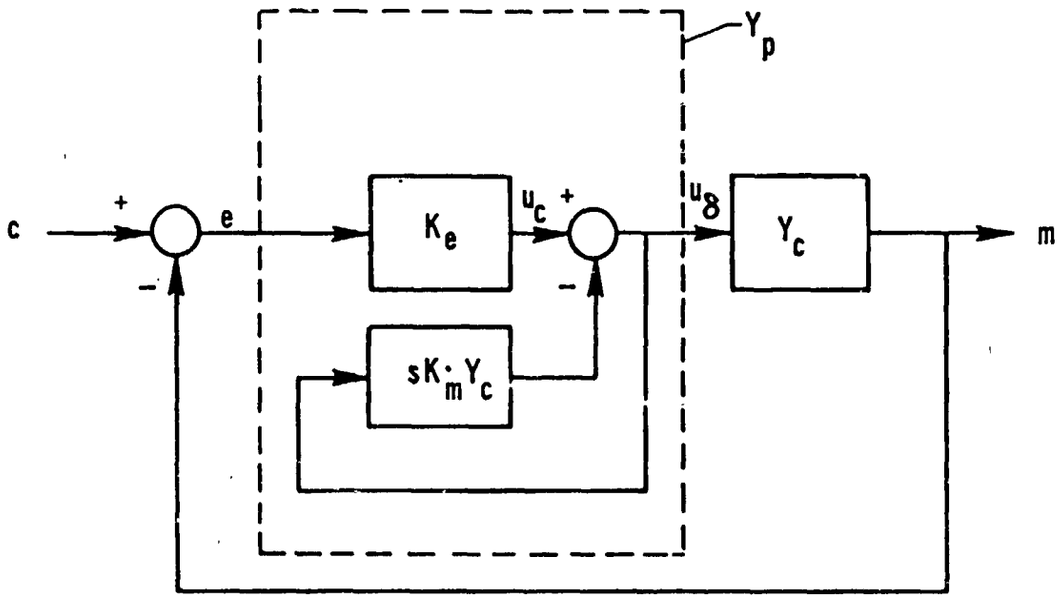

Figure 10. A simplified structural model of the human controller for single-loop tasks.

Fault Diagnosis/Modeling

D19

N85 14506

Submitted to the 20th Annual Conference on Manual Control

A MODEL FOR THE EFFECTIVENESS OF AIRCRAFT ALERTING AND WARNING SYSTEMS

Renwick E. Curry
NASA Ames Research Center

James E. Neu
Major, USAF

ABSTRACT

There are many behaviors that have been observed with Cockpit Alerting and Warning Systems (CAWS). We know that pilots ignore alerts from a CAWS with high false alarm rate; pilots come to rely on the CAWS as a primary system instead of a backup system; pilots miss alerts during periods of high workload; pilots adopt "unusual" criteria when evaluating alerts; pilots confuse one alert with another; and pilots turn off or otherwise defeat CAWS systems.

This paper presents an analysis of the effectiveness of an alerting system with a single alert. The pilot's decision behavior is modeled by the Theory of Signal Detection and therefore accounts for different "strengths" of cross-check information and different pilot criteria. The model includes the effects of the CAWS error rate; the pilot's past experience with the CAWS accuracy; his reliance on the CAWS rather than independent monitoring; missed alerts (due to high workload or other reasons); and adoption of a minimum error or Neyman-Pearson objective rather than minimum cost objective. (The model does not account for a pilot turning off the CAWS or confusing one alert with another.)

Exercising the model in a sensitivity analysis shows, among other things, that for rare events (a) the expected cost is greatly increased if the pilot ignores the a posteriori information in the existence of an alert; (b) the expected cost is insensitive to CAWS Type I (missed event) errors; and (c) the expected cost is sensitive to CAWS Type II (false alarm) errors only when the cross-check information is ambiguous.

N85 14507

D20

DEVELOPMENT AND CERTIFICATION OF A NEW STALL WARNING AND AVOIDANCE SYSTEM

W.M. Gertsen
Group Engineer
Gates Learjet Corporation

and

J.D. Hawkins
Engineering Specialist
Gates Learjet Corporation

PRECEDING PAGE BLANK NOT FILMED

TABLE OF CONTENTS

		PAGE
I.	ABSTRACT	1
II.	SUMMARY	1
III.	INTRODUCTION AND BACKGROUND	3
IV.	ORIGINAL MODEL 55 STALL WARNING AND AVOIDANCE SYSTEM	5
	A. System Description	
	B. Functional Block Diagram	
	C. System Performance	
V.	ANALOG COMPUTER REPRESENTATION OF THE AIRPLANE & STALL WARNING AND AVOIDANCE SYSTEM	7
VI.	MODIFICATIONS INVESTIGATED AND FLIGHT TESTED	7
	A. First Modification	
	B. Second Modification	
	C. Third Modification	
	D. Fourth Modification	
	E. Fifth and Final Modification	
VII.	STALL WARNING AND AVOIDANCE SYSTEM PERFORMANCE & TOLERANCE EFFECTS	17
VIII.	STALL WARNING AND AVOIDANCE SYSTEM TURBULENCE SENSITIVITY AND TOLERANCE EFFECTS	20
IX.	CONCLUSIONS	24

I. ABSTRACT

In order to improve natural stall characteristics, several methods may be employed. The method employed on all Learjets to obtain improved stall characteristics (either to prevent roll-off or pitch-up at the stall) has been a stall warning and avoidance system that employs angle-of-attack vanes, an electronic computer, a control column shaker motor, and a torquer which drives the control column in a pusher mode to avoid unwanted further build-up of angle-of-attack. The early systems were designed in such a way that the shaker and pusher actuation occurred only as a function of angle-of-attack. Later, time rate of change of vane angle ($\dot{\alpha}$) was added to permit higher angle-of-attack for pusher actuation. This permitted lower stall speeds with retention of satisfactory stall characteristics.

The new system, recently developed and FAA certified was developed with certain changes that improved system response with no performance penalty or increase in turbulence sensitivity. Changes that were made included modified system time constants and $\dot{\alpha}$ dead zone and the addition of an $\dot{\alpha}$ signal limiter and an $\dot{\alpha}$ cut-out below a specified angle-of-attack.

II. SUMMARY

Aircraft of the T-Tail configuration have, in general, a propensity toward steady state deep stall for aft center-of-gravity locations. Some aircraft avoid this flight regime by means of restrictions against loading behind the critical center-of-gravity. This approach is unsatisfactory for some configurations that require a wide range of center-of-gravity for operational efficacy. Some configurations with deep stall tendencies have been certified on the basis of placarding against stalls for loadings in the region where pitch-up can occur. However, today's regulatory environment discourages such a basis. Thus to improve stall characteristics, several methods have been employed. The method employed on all Learjets to obtain improved stall characteristics (either to avoid roll-off or pitch-up at the stall) has been a stall warning and avoidance system that employs angle-of-attack vanes, an electronic computer, a control column shaker, a nudger circuit, and a torquer which drives the control column in a pusher mode to avoid unwanted further build-up of angle-of-attack. (NOTE: The nudger circuit is a current (torque) limited push at a 3 Hz rate. The nudger function is utilized to indicate to the pilot that the pitch torquer is operating normally.) The early systems were designed in such a way that the shaker and pusher actuation occurred only as a function of angle-of-attack. With the advent of the Learjet Century III configurations in 1976, the desire to enhance safety by reducing takeoff and landing speeds led to adding time rate of change of vane angle ($\dot{\alpha}$) to the vane angle signal for shaker and pusher actuation. Because of this change the angle-of-attack for pusher actuation was raised to a point higher on the lift curve, while retaining satisfactory stall characteristics for the high entry rate stalls (4 kt/sec deceleration). The system as originally designed

had some inherent lag due to gust filtering to prevent nuisance actuation in turbulence, but no problems had been observed in many years of operational experience. It has been determined, however, that an unsteady approach to the stall with a pause in angle-of-attack increase (close to the stall) followed by a rapid increase in angle-of-attack could result in late firing of the pusher and pitch-up. The pusher must fire at or before a given angle-of-attack (depending on rate of increase in angle) in order to retain enough control authority to counteract the unstable moments that occur at extremely high angles. The pause that was mentioned above has the effect of resetting the stall warning system and its $\Delta\alpha$ lead to zero. The new system that has recently been certified was developed by making certain changes that improved system response with no performance penalty or increase in turbulence sensitivity. Changes that were made included modified system time constants and $\dot{\alpha}$ dead zone and the addition of an $\dot{\alpha}$ signal limiter and an $\dot{\alpha}$ cut-out below a specified angle-of-attack.

Figure 1 illustrates a normal steady approach to the stall, whereas Figure 2 is representative of the unsteady ('pause and pull') maneuvers referred to above.

FIGURE 1

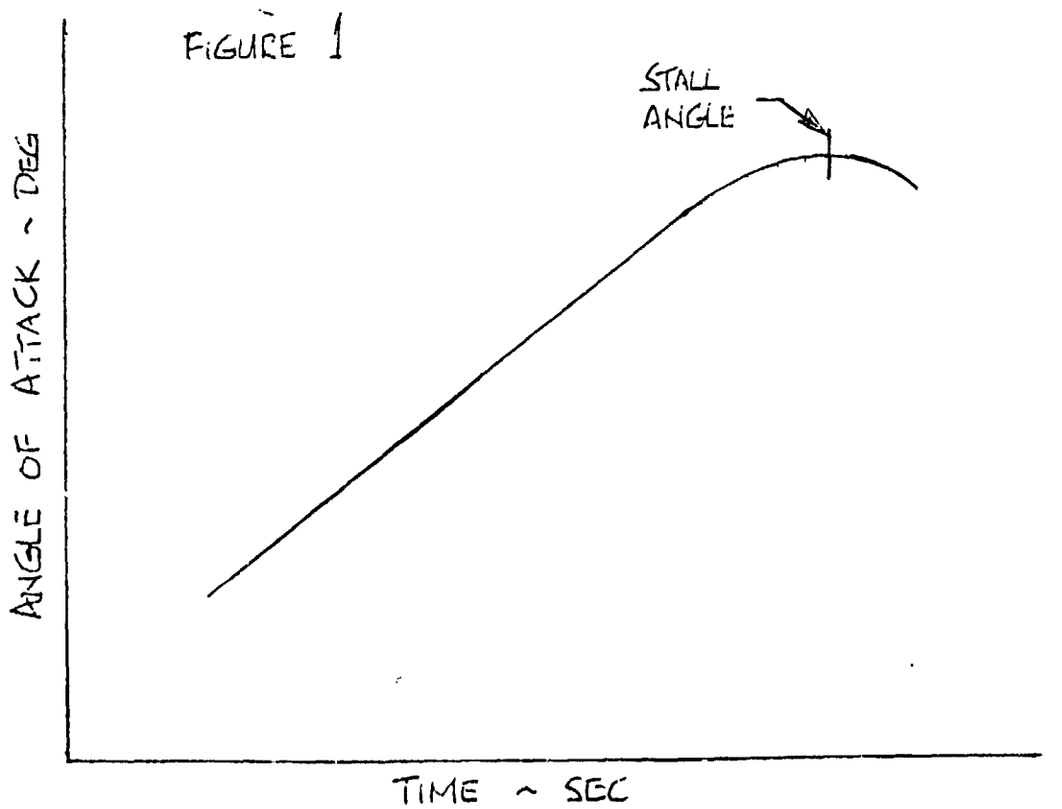

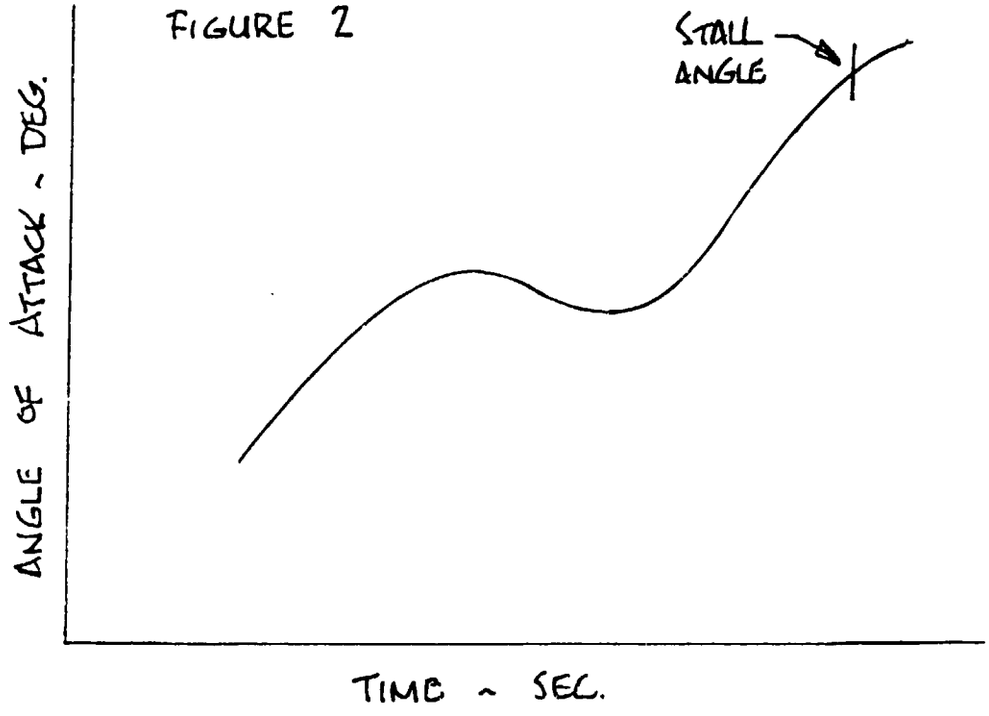

III. INTRODUCTION AND BACKGROUND

During developmental flight testing of the Learjet Model 23 it became apparent that the airplane would not meet the appropriate FAR's in the area of stall characteristics due to a wing drop tendency at the stall. Consequently, the original stall warning and avoidance system was developed to provide warning of the approach to the stall through a stick shaker that oscillates the control column at between two and three cycles per second through a small amplitude. The shaker actuation occurs at a speed approximately 7% above stall speed. In order to avoid inadvertent aerodynamic stall, a strong push force (equivalent to no less than 60 lb. of pilot force) is imparted to the pilot's control column. The push force remains constant until the angle of attack is reduced below the designated pusher angle. The pusher angle of attack is established to provide protection in the case of accelerated or high entry rate stalls (4 kt/sec deceleration). As can be seen in Figure 3, the requirement for pusher actuation to be at a lower angle of attack than the angle for aerodynamic stall results in higher effective stall speeds than would be the case if aerodynamic stall could be used. The consequence of this is higher takeoff and landing speeds and longer takeoff and landing distances.

In conjunction with the development of the Learjet Century III models in 1976, the desire to reduce stall speeds as much as possible led to a new stall warning and avoidance system that utilized an additional signal, that being time rate of change of vane angle ($\dot{\alpha}$). Because this signal added lead to the system response, the angle for pusher actuation could be raised to a point closer to the angle for $C_{L_{MAX}}$ as in Figure 4 below.

FIGURE 3

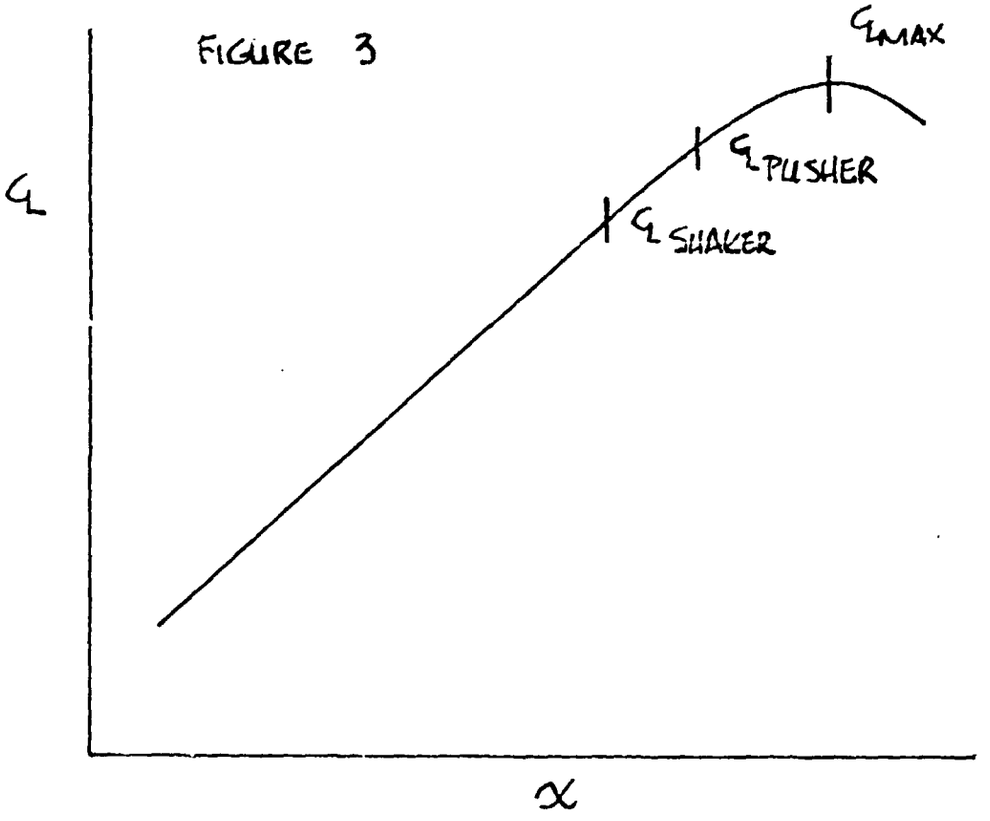

FIGURE 4

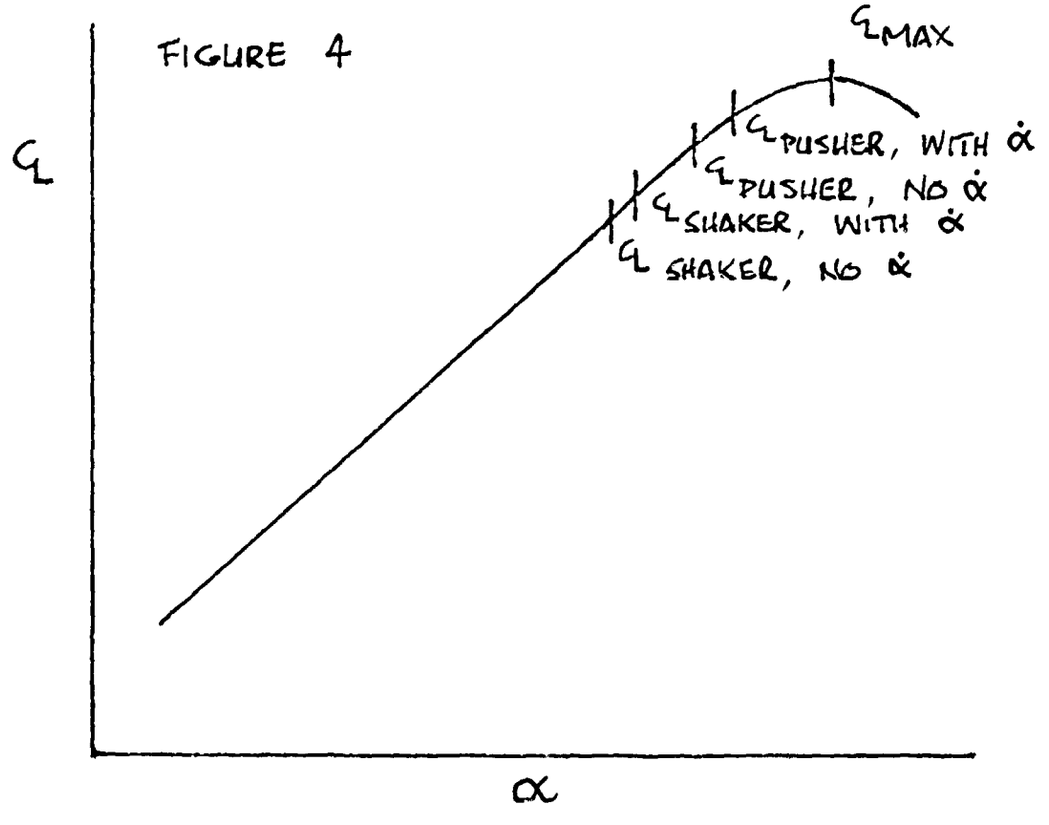

The result of adding the $\dot{\alpha}$ signal was reduced stall speeds, reduced takeoff and landing speeds, shorter field lengths, enhanced operational safety and retention of satisfactory stall characteristics for high entry rates.

IV. ORIGINAL MODEL 55 STALL WARNING AND AVOIDANCE SYSTEM

A. System Description

The original Model 55 stall warning and avoidance system was designed to be functionally similar to that in the earlier Model 35A. Only minor differences existed, such as small differences in time constants. The systems consist of dual vanes for sensing local angle of attack on each side of the fuselage somewhat ahead of the pilots station (see Figure 5), potentiometers, a dual angle of attach indicator, a dual computer, a dual accelerometers that deactivate the pusher when the airplane normal acceleration decreases to 0.5 g, and a servomotor that applies the appropriate pusher forces to the control column.

B. Functional Block Diagram

The stall warning and avoidance system functional block diagram is shown on Figure 6, next page. The forward loop converts vane angle to a voltage, amplifies and filters the signal to reduce the effects of turbulence to minimize nuisance firing of the shaker and pusher. The rate taker lead-lag circuit generates an effective signal and takes the signal through a dead zone or threshold. The signal is then summed with the signal and a flap bias signal. The summed signal is amplified and measured by a voltmeter. When the system output reaches 1.95 volts the shaker is actuated, and when the value goes to 0 volts, the pusher is actuated.

FIGURE 5

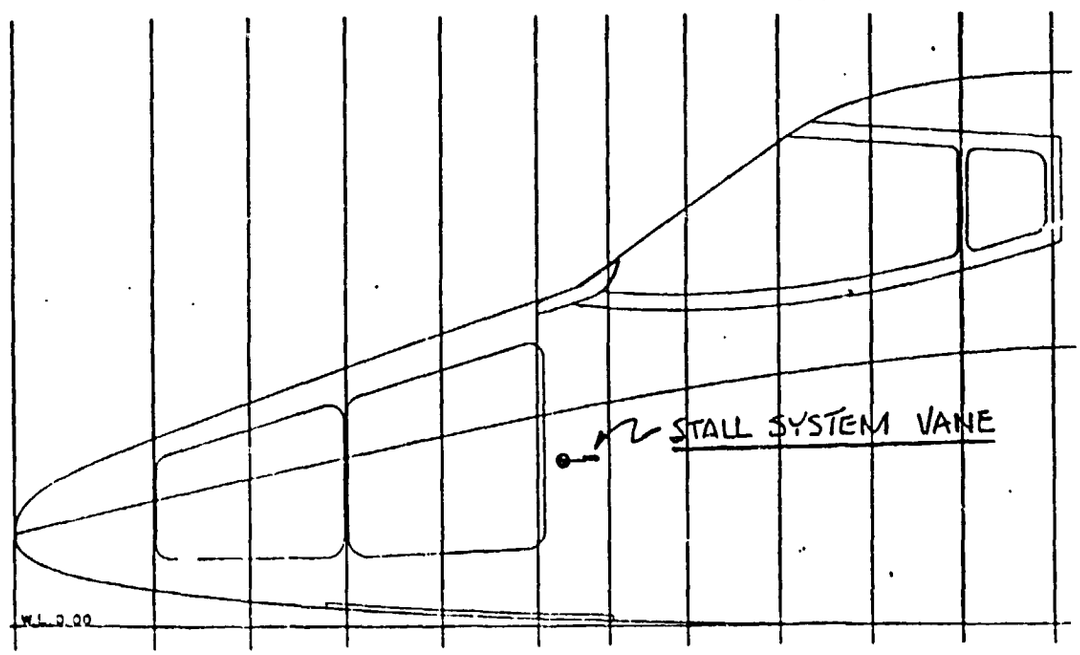

ORIGINAL PAGE IS OF POOR QUALITY

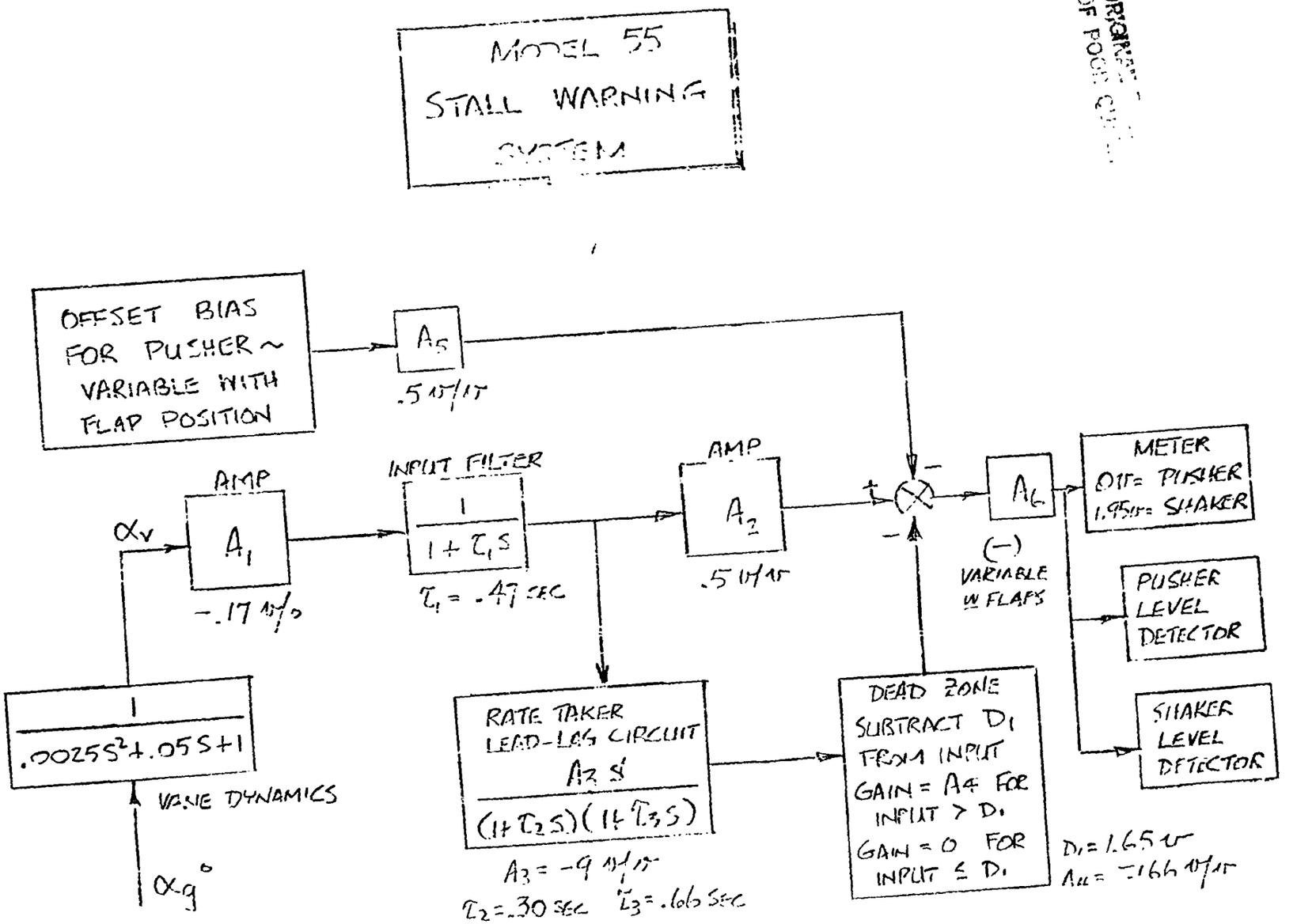

Figure 6

C. System Performance

If the system block diagram is converted into the equivalent differential equations, the system response to a ramp input of vane rate can be calculated for various values of vane rate and for various initial values of vane angles below the pursher ground set angle. The results of a series of such calculations have been plotted and are presented in Figures 7 and 8. The solid lines represent the baseline or original Model 55 system performance, while the new (modified) system performance is given by the dashed lines. For example, for an initial vane angle at 10° below pusher angle and for a vane rate of 10. deg/sec, the system would actuate the pusher at 1.3° before the static setting of 27°. Thus the pusher would fire at 25.7° vane angle.

By comparison, the new system would actuate the pusher at a point 5.4° prior to 27°, or at 21.6°, thus affording 4.1° more lead than the original (baseline) system. Figure 9 is similar to the previous two charts but only 5° away from pusher is shown for the several configurations tested during the flight test program.

V. ANALOG COMPUTER REPRESENTATION OF THE AIRPLANE & STALL WARNING AND AVOIDANCE SYSTEM

The mathematical model of the airplane degrees of freedom and the stall warning and avoidance system are shown on Figures 10 through 14 in analog computer diagram form The digital computer program that was used for the analytical studies accepts as input data the problem formulation in analog format. Figure 10 contains the forcing functions available, which are a ramp, a continuous sine wave, of variable frequency and magnitude, a one-cycle (1-cosine) discrete disturbance of variable wave length and amplitude, and a random disturbance of variable intensity. Next, Figure 12 represents the stall warning system shown functionally in Figure 10. The airplane longitudinal degrees of freedom are shown in Figures 13 and 14.

VI. MODIFICATIONS INVESTIGATED AND FLIGHT TESTED

A large number of modifications were investigated analytically by means of the computer program described in Section V above. The purpose of the analytical work was to evaluate before flight testing all proposed modifications and thus minimize the number of flight hours required to achieve the program objectives. Of all the configurations analyzed only five were actually flown and tested. These five modifications will be discussed in the following paragraphs. The ground rules for the project were that the stall warning and avoidance system modifications had to be relatively simple, such as substitution of one value of component for another, and with no loss in airplane performance capability, and retention of acceptable turbulence sensitivity. Analytical investigations included system response for the nominal system and for the system with the maximum adverse component tolerances. Also analyzed was the system response in turbulence for the nominal system and for the system with the maximum adverse system tolerances.

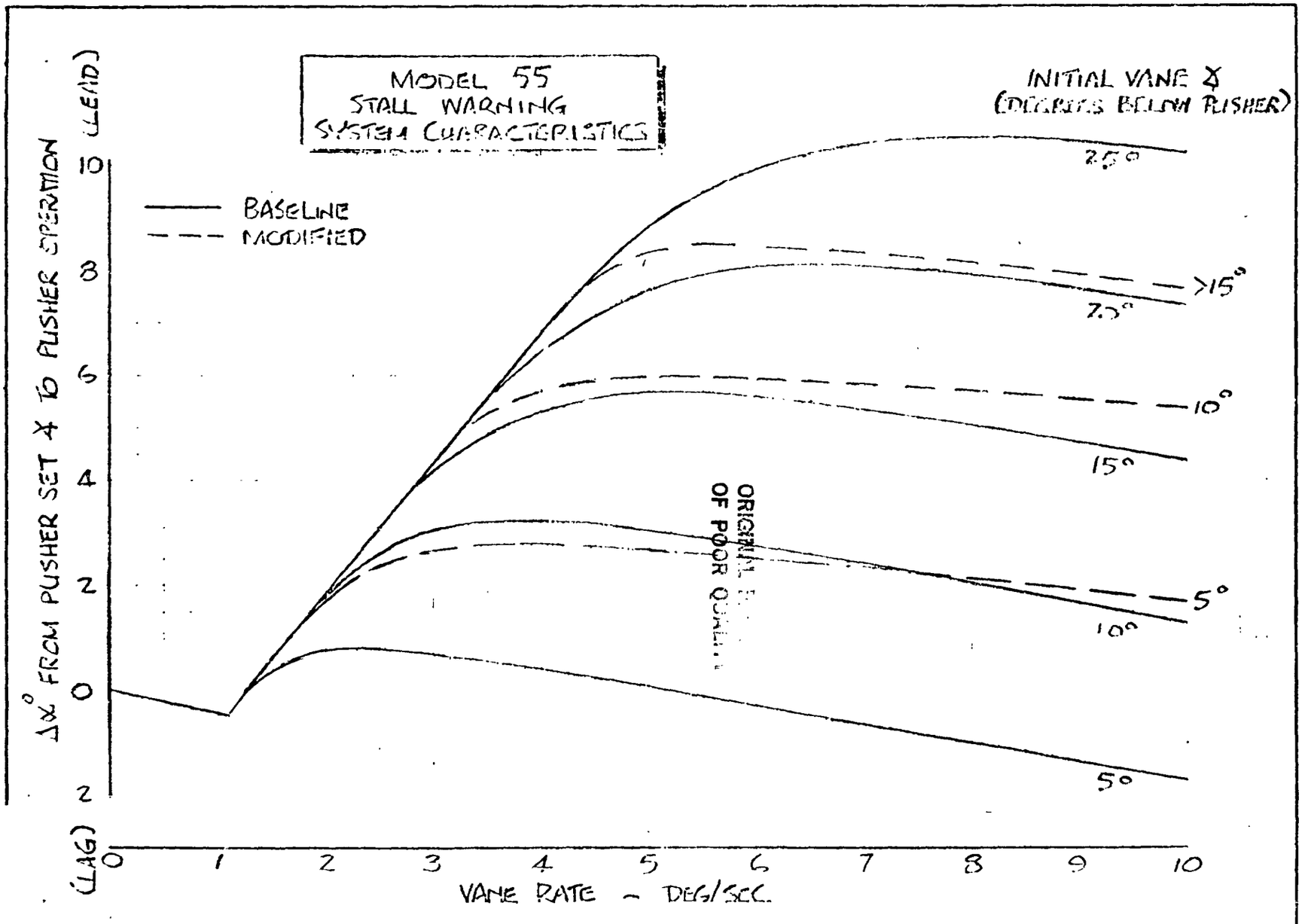
MODEL 55
STALL WARNING
SYSTEM CHARACTERISTICS
INITIAL VANE α
(DEGREES BELOW PUSHER)
BASELINE
MODIFIED
25°
>15°
7.5°
10°
15°
5°
10°
5°
ORIGINAL [illegible]
OF POOR QUALITY
Δα° FROM PUSHER SET α TO PUSHER OPERATION
10 (LEAD)
8
6
4
2
0
2 (LAG)
0 1 2 3 4 5 6 7 8 9 10
VANE RATE - DEG/SEC.

Figure 7

MODEL 55
STALL WARNING
SYSTEM CHARACTERISTICS
BASELINE
MODIFIED
INITIAL VANE ∠
(DEGREES BELOW
PUSHER)
25°
20°
15°
10°
5°
ORIGINAL
OF POOR QUALITY
VANE RATE - DEG/SEC
5
6
7
8
9
10
11
12
13
14
15
Δα° FROM PUSHER SET ∠ TO PUSHER OPERATION
2
0
2
4
6
8
10
(LAG)
(LEAD)

FIGURE 8

ORIGINAL PAGE IS
OF POOR QUALITY

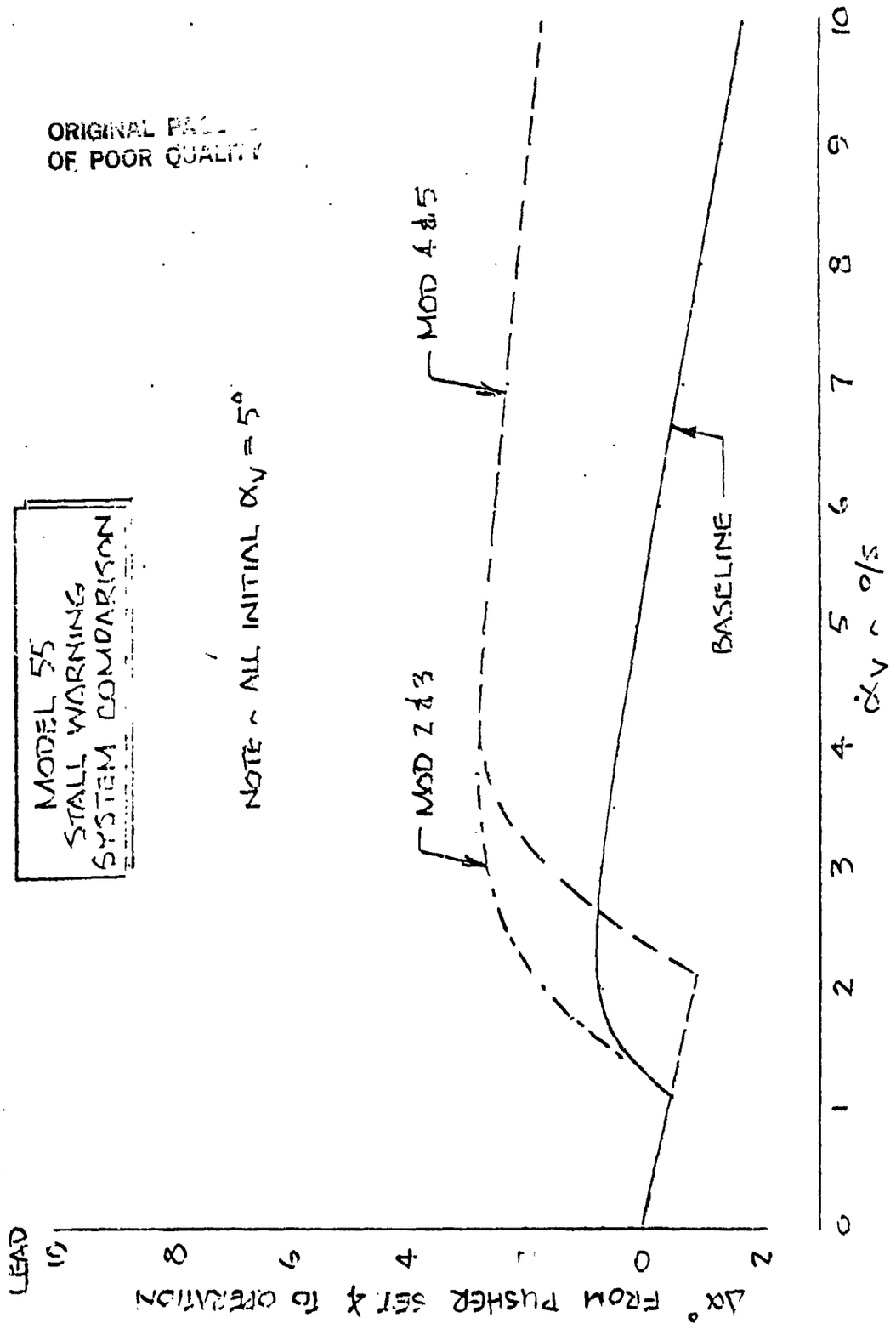

figure 9

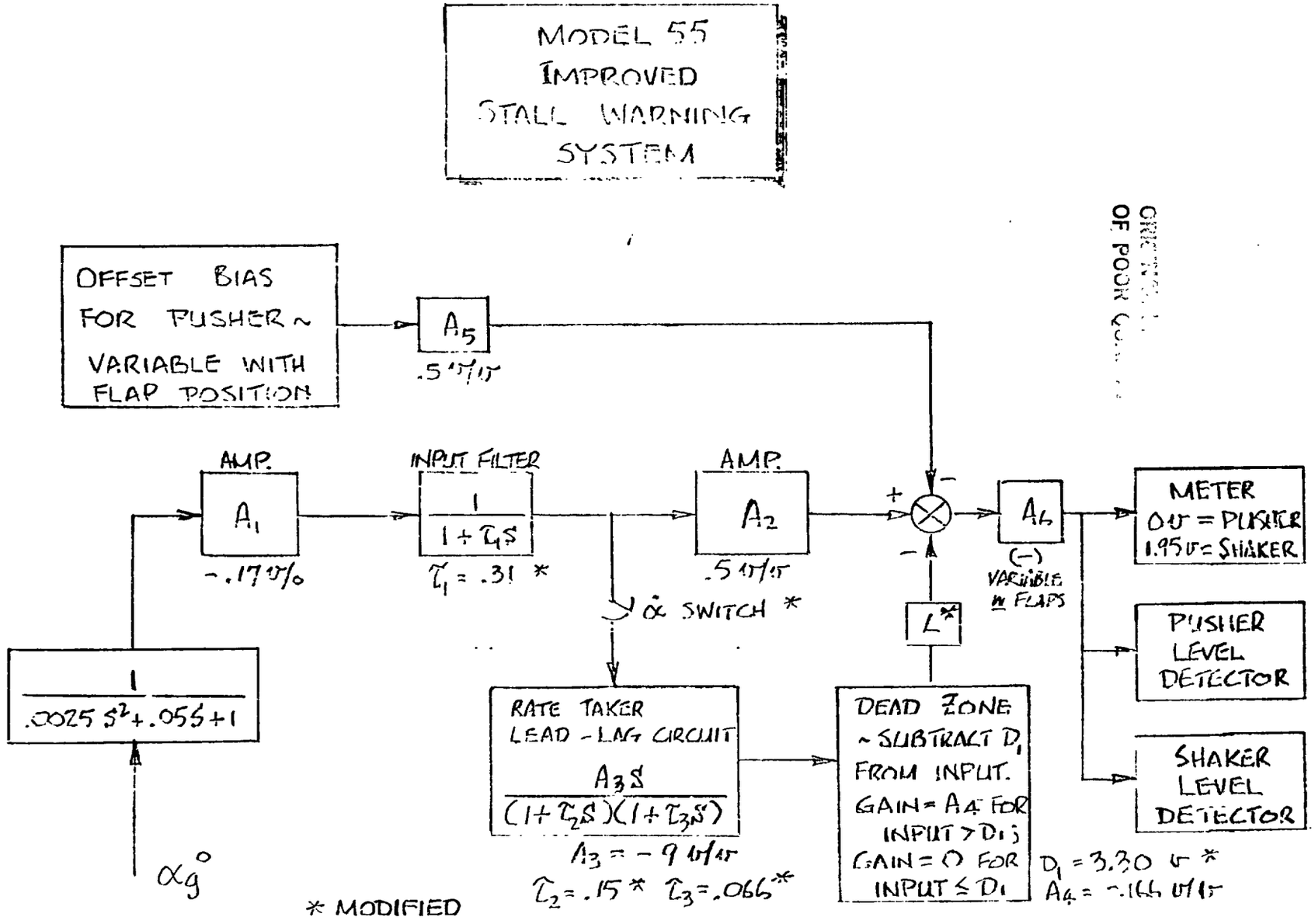
MODEL 55
IMPROVED
STALL WARNING
SYSTEM
OFFSET BIAS
FOR PUSHER ~
VARIABLE WITH
FLAP POSITION
A_5
.5 U/U
AMP.
A_1
-.17 U/U
INPUT FILTER
$\frac{1}{1+\tau_1 S}$
τ_1 = .31 *
AMP.
A_2
.5 U/U
$\dot{\alpha}$ SWITCH *
A_6
(-)
VARIABLE W/ FLAPS
METER
0 U = PUSHER
1.95 U = SHAKER
PUSHER
LEVEL
DETECTOR
SHAKER
LEVEL
DETECTOR
L^*
$\frac{1}{.0025 S^2 + .05 S + 1}$
α_g °
RATE TAKER
LEAD - LAG CIRCUIT
$\frac{A_3 S}{(1+\tau_2 S)(1+\tau_3 S)}$
A_3 = -9 U/U
τ_2 = .15 * τ_3 = .066 *
DEAD ZONE
~ SUBTRACT D_1
FROM INPUT.
GAIN = A_4 FOR
INPUT > D_1;
GAIN = 0 FOR
INPUT ≤ D_1
D_1 = 3.30 U *
A_4 = -.166 U/U
* MODIFIED

FIGURE 10

FORCING FUNCTIONS

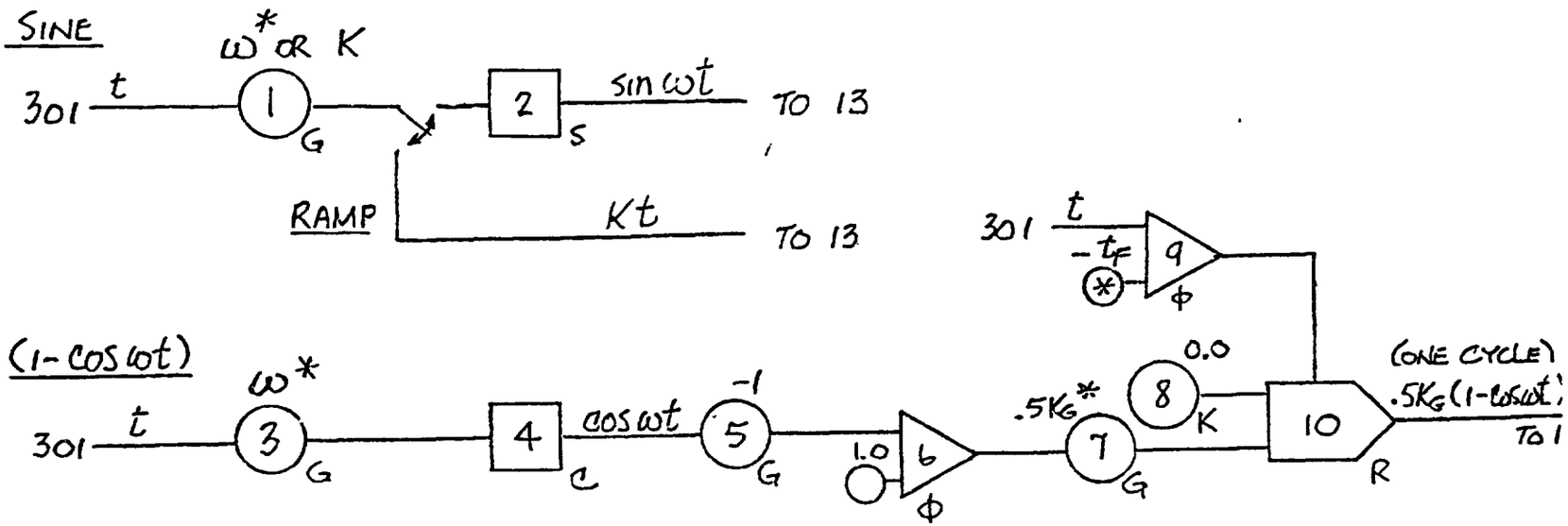

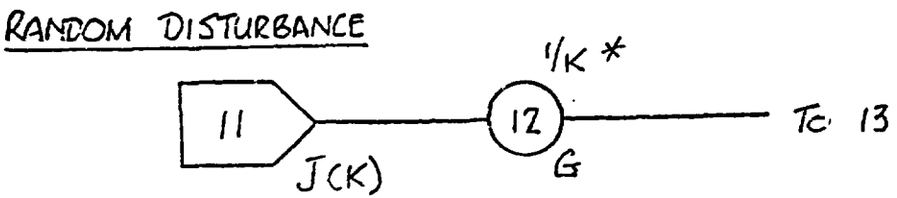

* VARIABLE

figure 11

STALL WARNING SYSTEM

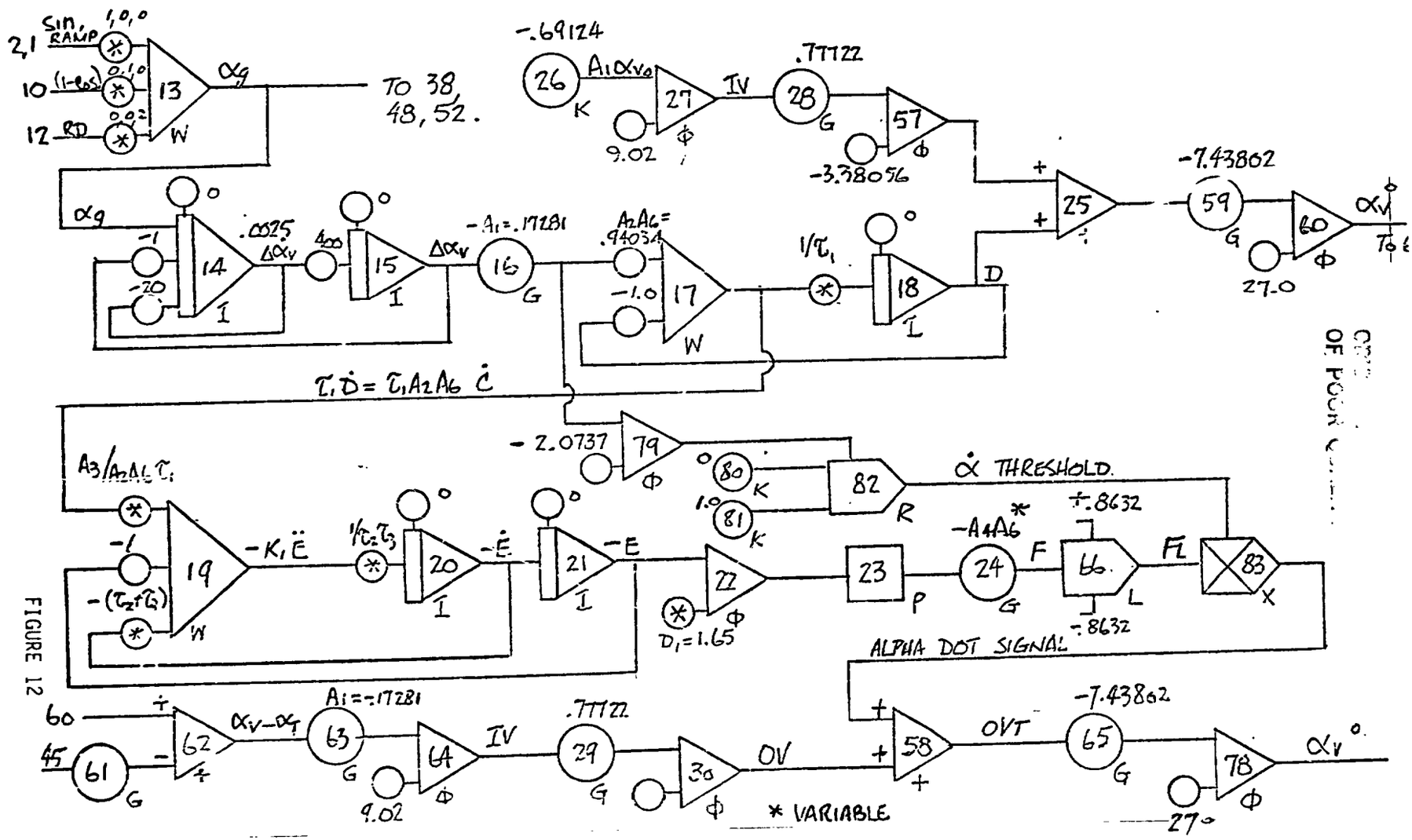

FIGURE 12

THREE DOF LONGITUDINAL SIMULATION

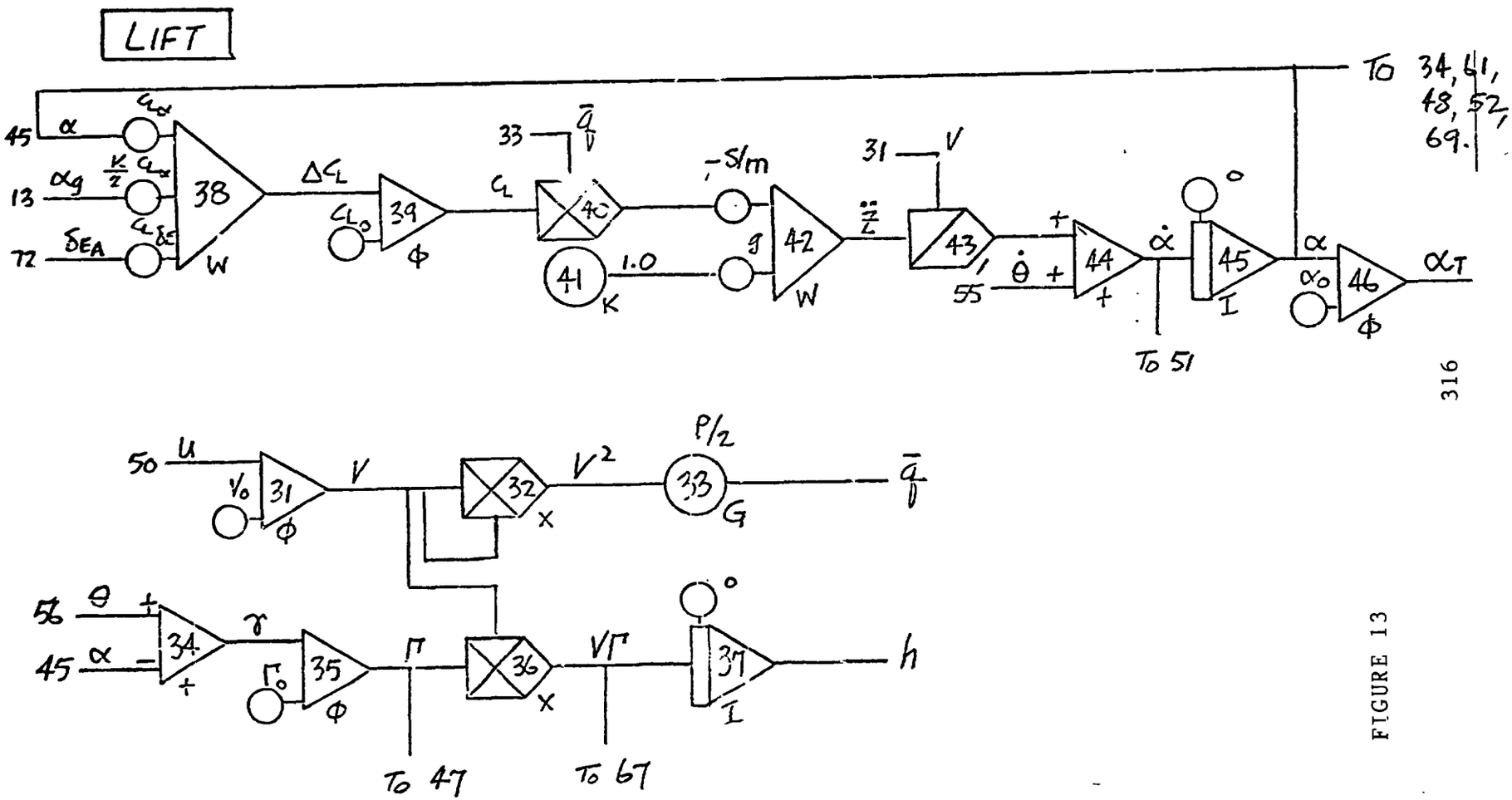

FIGURE 13

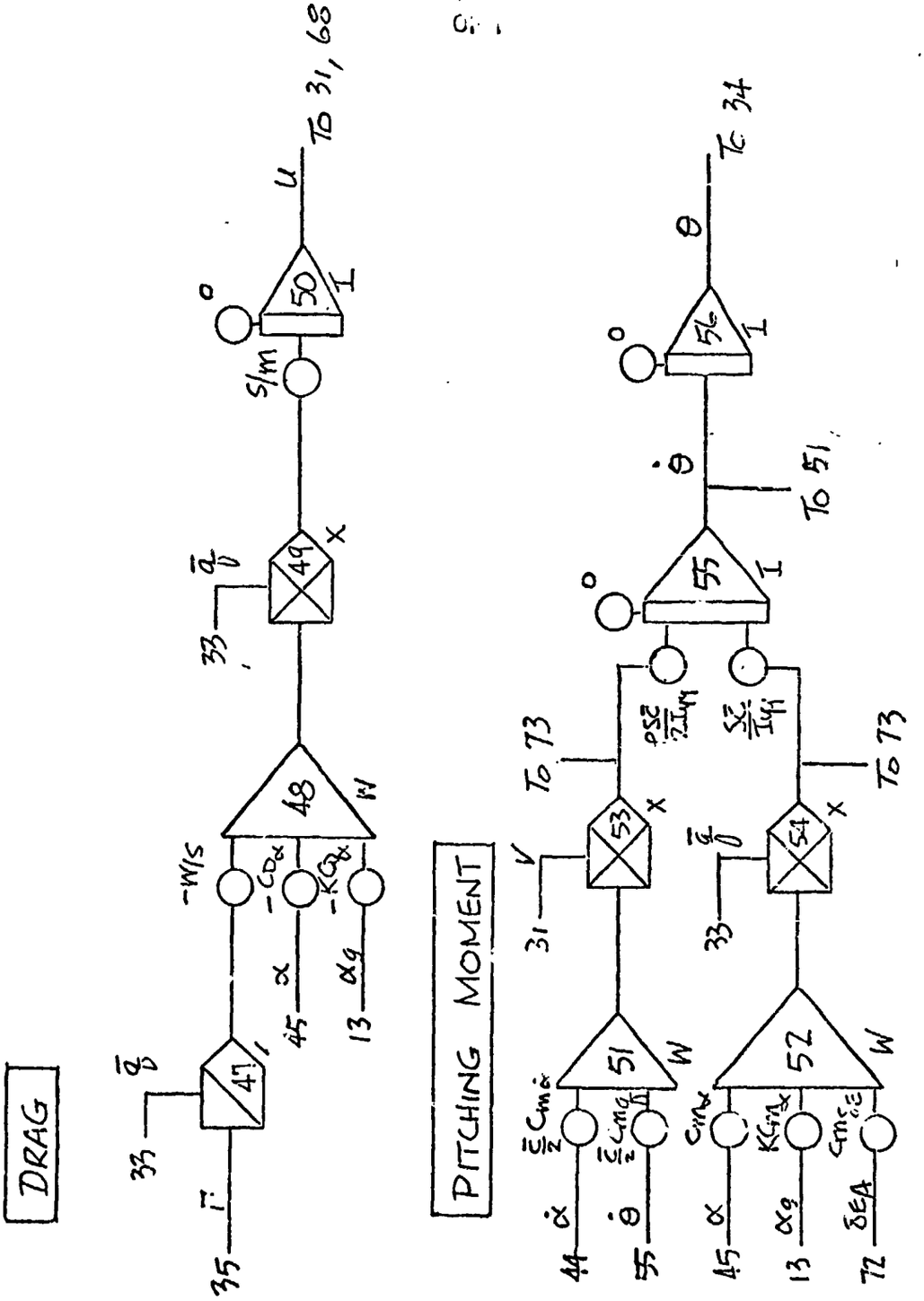

FIGURE 14

A. First Modification

In an effort to overcome some of the system lag, the first modification that was analyzed and tested both in the laboratory and in flight had two time constants reduced. τ_1 was reduced from 0.47 sec. to 0.31 sec., and τ_3 was reduced from 0.66 sec. to 0.066 sec. This configuration gave sufficient responsiveness but was too sensitive in turbulence. The system was noticeably more sensitive than the original Model 55 configuration.

B. Second Modification

The second configuration that was analyzed and tested retained the τ_1 and τ_3 changes but also added a voltage limiter in the $\dot{\alpha}$ circuit to reduce the turbulence sensitivity. This system provided an improvement but was still too sensitive.

C. Third Modification

The third modification that was analyzed and tested replaced the limiter with a lower valued limiter. This configuration met all the original criteria except that a little more lead was desired at high vane rates, and a little less lead was required at low vane rates corresponding to normal 1 kt/sec deceleration rate that is used for stall speed determination.

D. Fourth Modification

In order to increase the system lead at the higher vane rates, τ_2 was decreased from 0.30 sec. to 0.15 sec. At the same time the $\dot{\alpha}$ dead zone was increased from 1.65 volts to 3.3 volts to desensitize the system at low vane rates. This modification proved to be satisfactory in nearly every respect.

E. Fifth and Final Modification

The final modification that was analyzed and tested was the same as the fourth modification, with the addition of an $\dot{\alpha}$ cut-out switch that is open at vane angles up to just above the snaker angle, and closed above that point. Thus the $\dot{\alpha}$ function is only in effect in the higher angle of attack range. The effect of this addition was to desensitize the system still further in turbulence without affecting the basic system function at or near the stall. The block diagram for the final configuration tested and FAA certified is shown in Figure 10. Comparison of Figure 10 with Figure 6 which represents the original unmodified system illustrates the similarity of the two systems. In summary, three time constants, τ_1, τ_2, τ_3 were decreased, the $\dot{\alpha}$ dead zone was increased, an $\dot{\alpha}$ switch and an $\dot{\alpha}$ limiter were added.

VII. STALL WARNING AND AVOIDANCE SYSTEM PERFORMANCE AND TOLERANCE EFFECTS

The system performance curves shown previously on Figures 7 and 8 were generated analytically by using a ramp input in vane angle at various vane rates. The system performance was also checked by tying the actual system computer to a fast Fourier analyzer and obtaining performance data. Then during actual flight testing, the system performance was closely monitored by means of a telemetry system that is routinely used at GLC for certain exploratory testing. All three sources of data correlated very well throughout the flight test program. The good correlation increased the confidence level in new configurations before flight, and also helped to identify problems with hardware as they occurred during the program. Figure 15 is a typical working plot that was used during the course of the telemetered flights. The deep stall region had previously been estimated from wind tunnel data and revised as flight test data was accumulated. By plotting points on such a plot as the testing progressed the test pilot could be immediately informed concerning the validity of the previous test condition and could be cleared to perform the next test point, or advised to discontinue the test series. He was also advised concerning the magnitude of his control inputs and rates, and angles obtained compared with expected values. The learning curve was thereby accelerated and safety enhanced. Figure 16 is a plot of pitch acceleration available through elevator input as a function of vane angle at the time of maximum recovery nose down elevator input. As zero pitch acceleration is approached, recovery with elevator alone is not possible. This plot was useful in establishing the estimated deep stall boundary shown on Figure 15.

For tolerance effects, a maximum build-up of component tolerances was assumed in the direction of minimum system responsiveness. Tolerance values used are as follows:

A_1: ±5%
A_2: ±2%
A_3: ±10%
A_4: ±2%
A_5: ±2%
τ_1: ±15%
τ_2: ±15%
D_1: ±20%
L: ±20%

System performance was calculated for the maximum tolerance case for several values of vane angular rate and initial vane angle. For the critical range of rates (10-15^0/sec) and initial vane angle (5-10^0 below pusher angle) the loss in

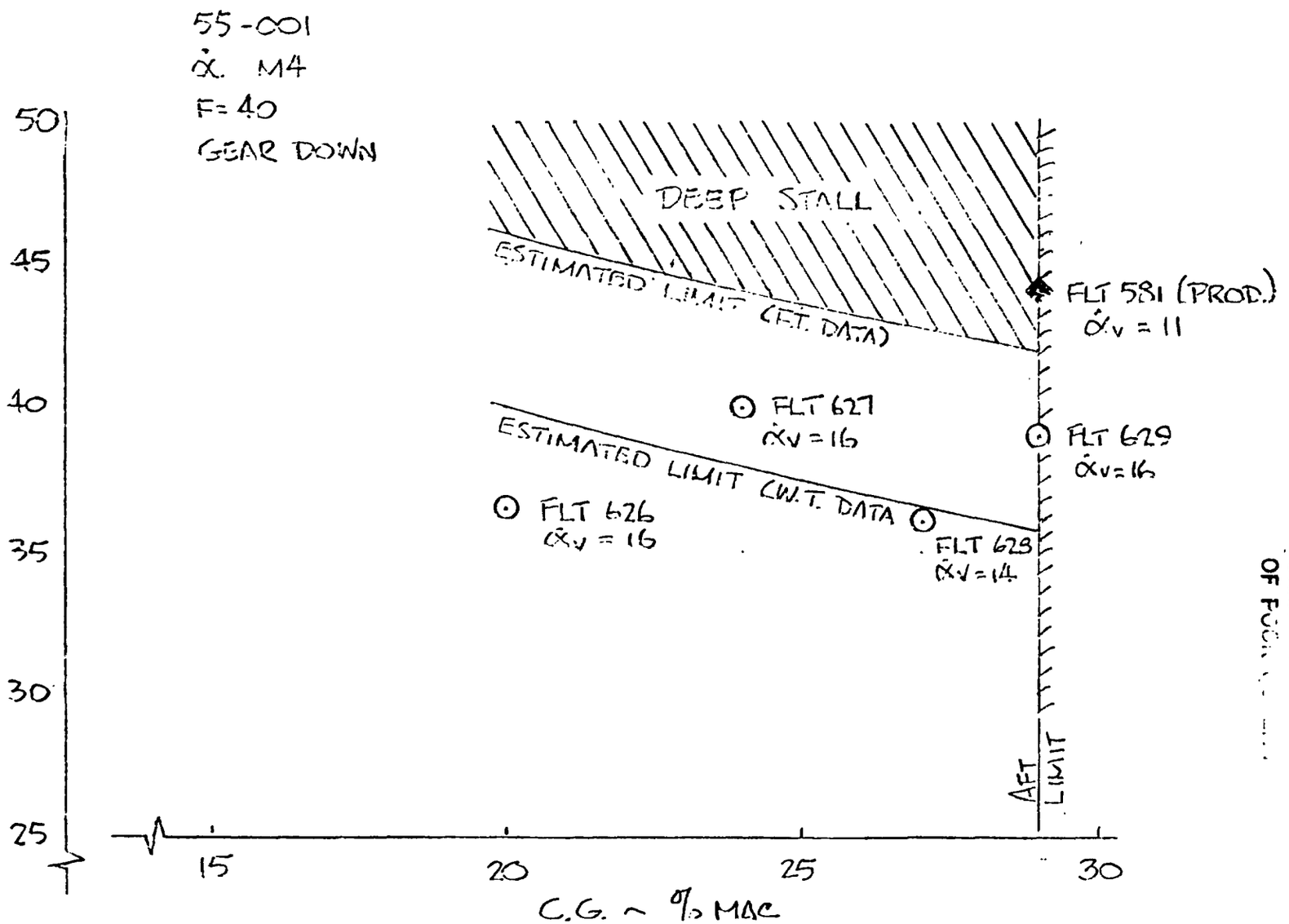
55-001
$\dot{\alpha}$. M4
F=40
GEAR DOWN
DEEP STALL
ESTIMATED LIMIT (FLT. DATA)
FLT 581 (PROD.)
$\dot{\alpha}_V$ = 11
FLT 627
$\dot{\alpha}_V$ = 16
FLT 629
$\dot{\alpha}_V$ = 16
ESTIMATED LIMIT CW.T. DATA
FLT 626
$\dot{\alpha}_V$ = 16
FLT 628
$\dot{\alpha}_V$ = 14
AFT LIMIT
MAX. VANE ANGLE - DEG.
50
45
40
35
30
25
15
20
25
30
C.G. ~ % MAC

figure 15

ORIGINAL IS
OF POOR QUALITY

55-001 SWS DEVELOPMENT, M4

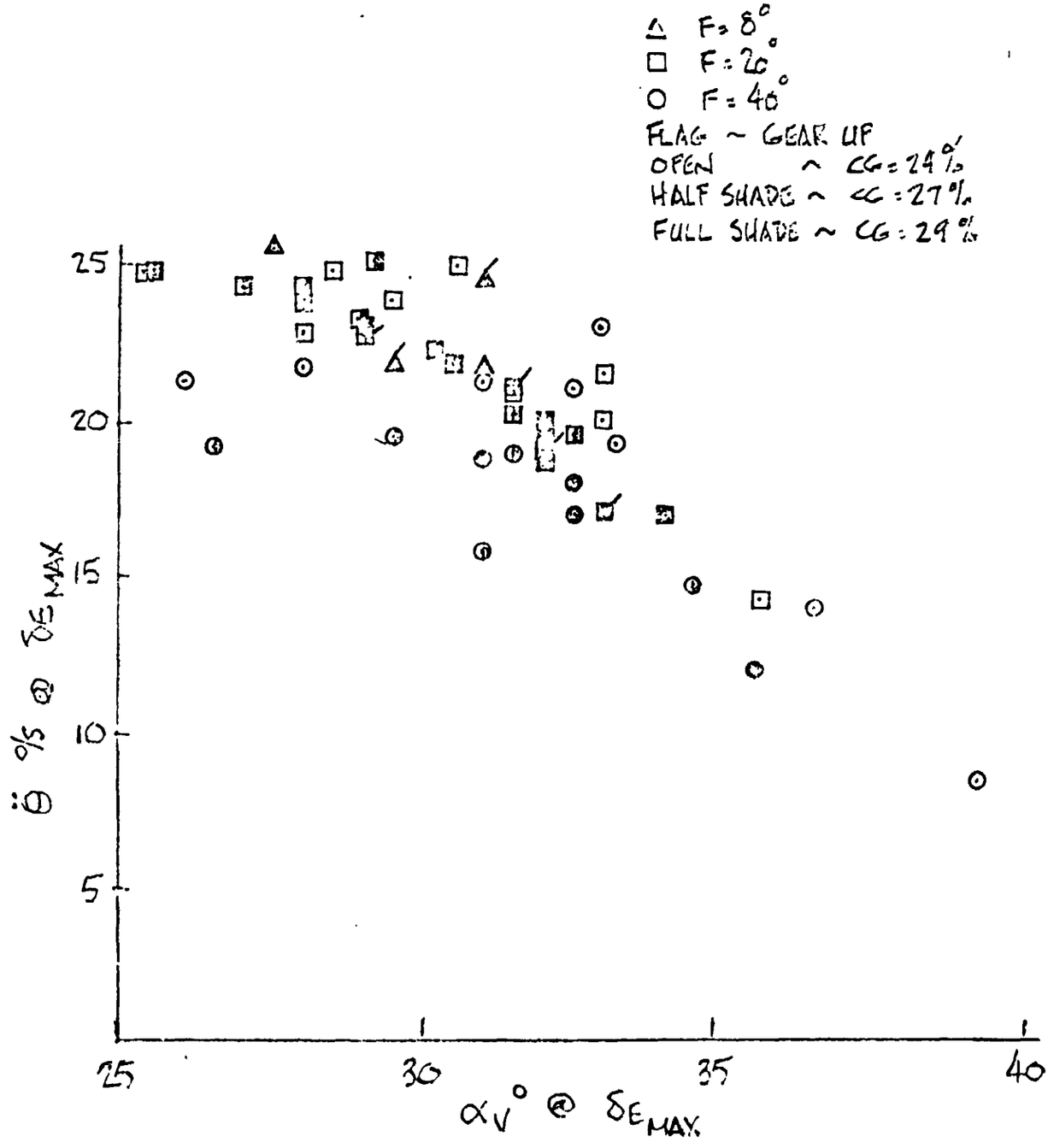

FIGURE 16

lead was found to be approximately 1.5^{o}. Additional system tolerances were found to add 2.0^{o} for a total of 3.5^{o}. Accordingly for purposes of flight testing the system the pusher was set to fire 3.5^{o} higher than the production setting. All the test conditions were accomplished satisfactorily. Thus it was concluded that the expected component and system tolerances will be satisfactory for production and for use in the field.

VIII. STALL WARNING AND AVOIDANCE SYSTEM

TURBULENCE SENSITIVITY AND TOLERANCE EFFECTS

In addition to the primary concern of system function for stall warning and avoidance, another important consideration is the sensitivity of the system in atmospheric turbulence and the resulting frequency of nuisance shaker and pusher occurrences. The criterion that was used in the development of the new system was that the new system should have approximately the same or less turbulence sensitivity as the original system. In order to investigate this prior to flight each candidate system was analyzed with the computer program described in Section V of this paper. The baseline (original) system was also investigated. All the systems were analyzed for effects of maximum tolerance build-up of the various system components. In the case of turbulence effects, tolerances in the direction toward greatest responsiveness were investigated, whereas for the primary function of the system, maximum tolerances in the direction of least responsiveness were analyzed.

Two types of turbulence environments were used. The first was a 15 ft/sec (1-cosine) discreet gust across a spectrum of wavelengths that was sufficient to define a maximum system response point. Figure 17 presents the results of this part of the study for the baseline system and for the final configuration (Mod. 5) in the form of maximum output voltage vs frequency. The modified system exhibits less sensitivity to the discrete gusts and much less sensitivity to the effects of system component tolerances. The magnitude of the gust input was based upon the assumption that if the root mean square (RMS) turbulence level exceeds 5 ft/sec., a landing would not be attempted. Therefore, 15 ft/sec. (3σ) was selected as the largest probable gust that would be encountered in a landing situation.

The second type of turbulence environment that was used was simulated random turbulence of varying intensity up to an extremely heavy 20 ft/sec. RMS. System response in the form of maximum voltage range vs turbulence intensity is shown in Figure 18. Similarly Figure 19 shows number of shaker occurrences as a function of turbulence intensity. For reasonable levels of turbulence the new system response was comparable to the old. Based upon the analytical studies, laboratory hardware tests and flight tests of the prototype system in turbulent air, it was concluded that the modified stall warning system was better than the original and less likely to cause nuisance pusher occurrences.

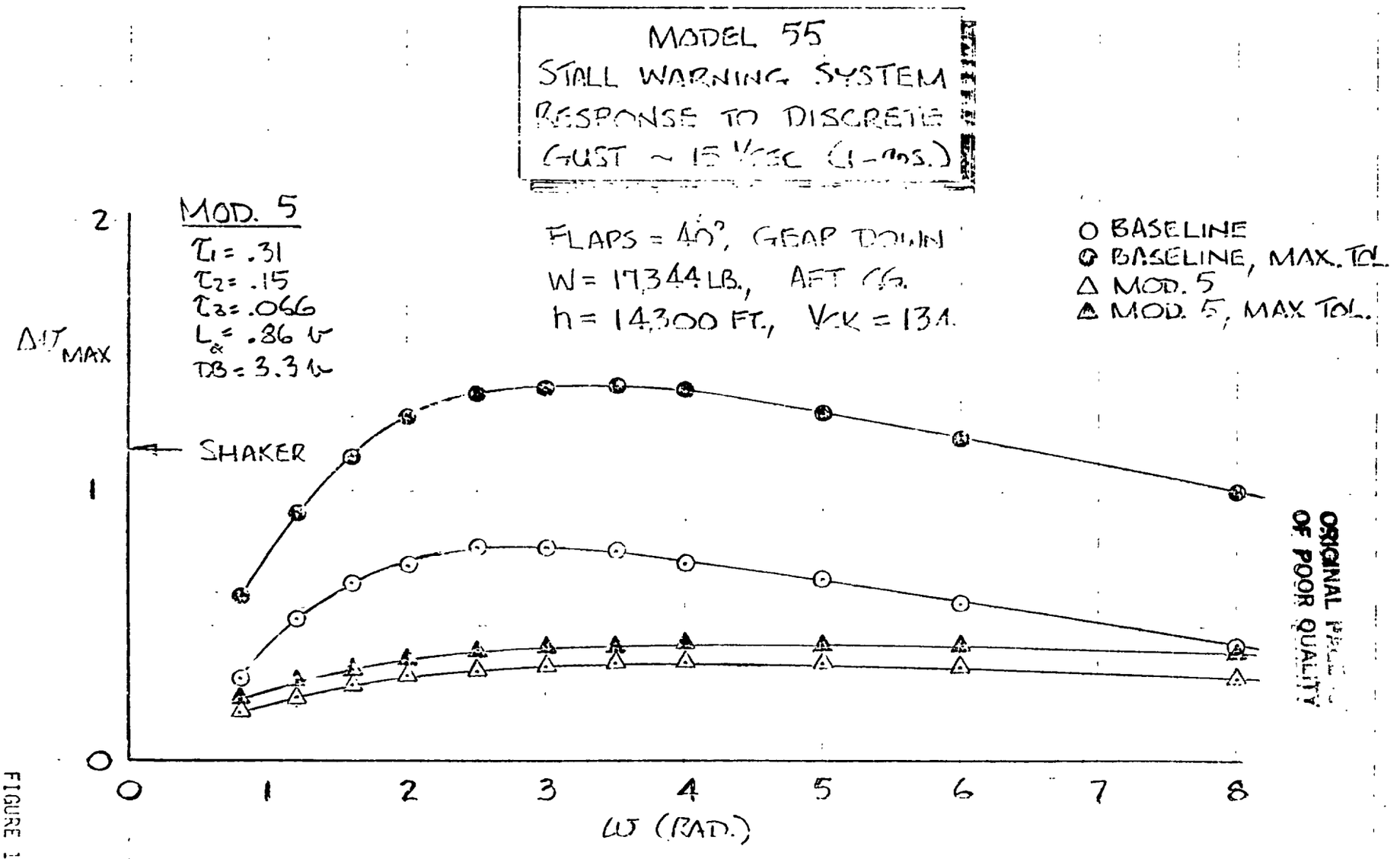
MODEL 55
STALL WARNING SYSTEM
RESPONSE TO DISCRETE
GUST ~ 15 V/SEC (1-COS.)
MOD. 5
τ_1 = .31
τ_2 = .15
τ_3 = .066
L_α = .86 U
TB = 3.3 U
FLAPS = 40°, GEAR DOWN
W = 17,344 LB., AFT CG.
h = 14,300 FT., VEK = 134
O BASELINE
⊙ BASELINE, MAX. TOL.
Δ MOD. 5
▲ MOD. 5, MAX TOL.
Δn_{MAX}
SHAKER
2
1
0
0
1
2
3
4
5
6
7
8
ω (RAD.)
ORIGINAL PAGE IS OF POOR QUALITY

FIGURE 17

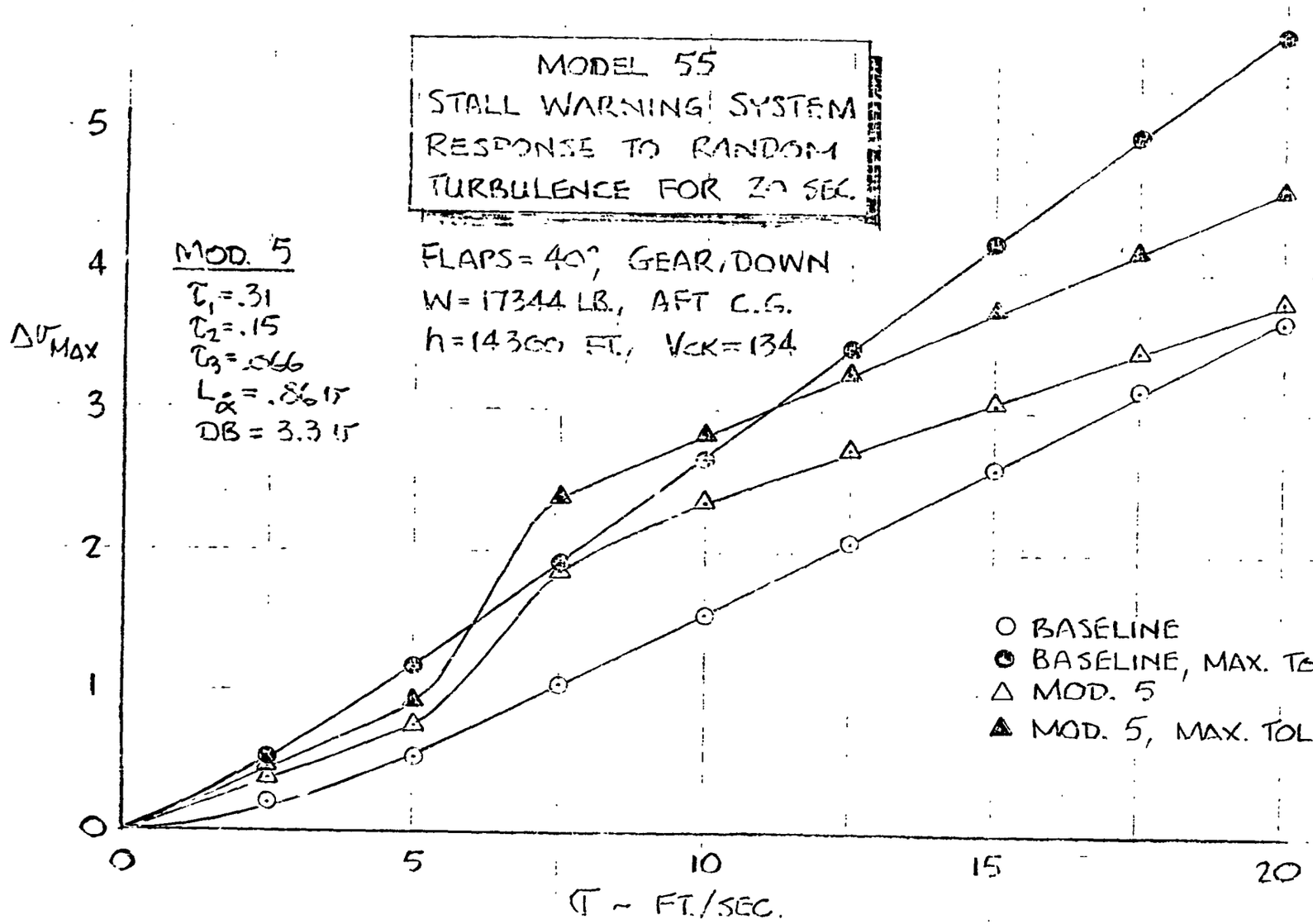

FIGURE 18

ORIGINAL PAGE IS OF POOR QUALITY

ORIGINAL PAGE IS
OF POOR QUALITY
MODEL 55
STALL WARNING SYSTEM
RESPONSE TO RANDOM
TURBULENCE FOR 20 SEC.
FLAPS = 40°, GEAR DOWN
W = 17344 LB., AFT C.G.
h = 14300 FT., VCK = 134
MOD. 5
ζ1 = .31
ζ2 = .15
ζ3 = .056
Lα = .85 U
τB = 3.3 U
O BASELINE
● BASELINE, MAX. TOL.
△ MOD. 5
▲ MOD. 5, MAX. TOL.
P=5
P=2
NUMBER OF SHAKER OCCURRENCES
40
30
20
10
0
0
5
10
15
20
σT ~ FT./SEC.

FIGURE 19

IX. CONCLUSIONS

The following conclusions can be drawn from the results of this program:

1) Computer analyses and hardware bench tests proved to be valuable in speeding the development of a new stall warning and avoidance system.

2) Good correlation was observed between analytical results and flight test results. Analysis of system modifications prior to flight enhanced flight safety during flight tests in high angle of attack regimes.

3) A superior system was developed at no penalty in performance or in turbulence sensitivity, and with minimal design changes.

N85 14508

EVALUATION OF FUZZY RULEMAKING FOR EXPERT SYSTEMS FOR FAILURE DETECTION

Frank Laritz and Thomas B. Sheridan
Man-Machine Systems Laboratory
Massachusetts Institute of Technology

INTRODUCTION

Computer aids in the form of so called "expert systems" have been proposed repeatedly for making diagnoses of failures in complex systems.

The fuzzy set theory of Zadeh[1] has been shown to offer an interesting new perspective for modeling the way humans think and use language. In particular, we assume that real expert human operators of aircraft, power plants and other systems do not think of their control tasks or failure diagnosis tasks in terms of control laws in differential equation form, but rather keep in mind a set of rules of thumb in fuzzy form. For the reader ignorant of fuzzy sets the experiment described below communicates by example the gist of the idea.

FIRST EXPERIMENT

Five subjects repeatedly adjusted two "inputs" A and B to a "black box" to any value between 10 and 100, set a "failure mode" to any one of four available settings including "no failure", and observe two "outputs" C and D. The contents of the black box were not revealed. The subjects' task was to correlate inputs and outputs with failure modes and from this infer rules by which to assert whether and in what mode the black box had "failed" as a function of the two inputs and two outputs.

Actually the black box was a simple resistor network as shown in Figure 1 in which one of the resistors 1,2,3,4 was selectively opened (or none was).

After each subject had completed a number of trials (they were all really learning trials) he was asked to formulate rules in terms of easy-to-remember descriptors for the four variables like "low", "medium" and "high" using these descriptors he was to generate rules such as:

"when A is low and B is medium or high and C is high and D is medium or high, the failure is mode 2".

There could be any number of such (fuzzy) descriptors and any number of such rules, and the subjects were free to format them in tables or however they wished. They could also combine variables in forms such as C/D and C-D.

The subjects were also asked to produce functions of each descriptor (fuzzy set) defining what they "meant". Each function specified "membership" or "truth" as a function of the values of the corresponding variable (in the range 10-100). Two of the five subjects observed the black box behavior first, then devised the rules, and lastly devised membership functions.

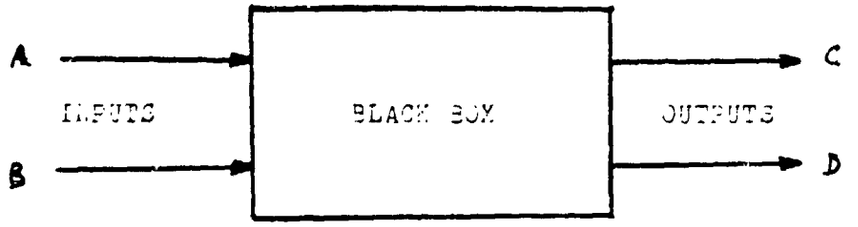

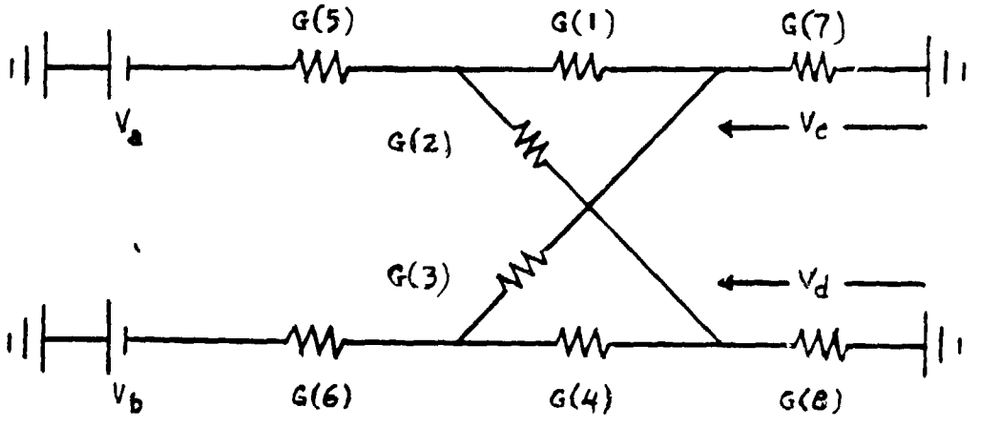

Resistors Allowed to Fail: G(1) = 61 mhos
G(2) = 87
G(3) = 59
G(4) = 76

Other Resistors: G(5) = 95
G(6) = 55
G(7) = 74
G(8) = 85

Figure 1. Simple resistor network comprising the "black box"

The others chose to invent terms and define the membership functions first.

As an example Figure 2 lists the rules given by one subject (JR) and Figure 3 presents his membership functions. Note that certain regions of A,B and D-C were (apparantly intentionally) not covered by his membership functions (and rules). For contrast the membership functions of a second subject are also shown (Figure 4).

For each subject independently the experimenter derived the state-action matrix (failure mode as a function of input and output numerical values) using the conventioanl "max m" for "or" and min m" for "AND". He then proceeded to evaluate each resulting expert system not only against single complete failures (the basis in which the subjects made up their rules) but also on multiple complete failures and single partial failures (5% changes rather than 100% changes in resistance). For a given set of inputs and outputs each subject's expert system yielded a "truth value" for each failure mode for each combination of A,B,C,D. A simple procedure is to assert failure for that mode having the greatest truth value greater than some threshold and no failure for truth less than that threshold. Laritz used this as one decision criterion (which he called the "most true" criterion) but also counted the number of times u for each mode exceeded 0.5 (the "times true" criterion), and the sum of truth values for each mode ("truth summation" criterion). Figure 5 summarizes the rather impressive success of subject JR's expert system, and for comparison Figure 6 summarizes that of subject DM. The performances of the other fuzzy expert systems lay somewhere in between.

CONCLUSIONS FROM FIRST EXPERIMENT

From this first experiment we concluded:

1. The method of observing trends, then formulating rules, and then defining fuzzy values captures more of the human's ingenuity and pattern recognition ability and provides a better expert failue detection system than the method or creating fuzzy values, then gathering data, and then deducing rules.

2. If the second method is used, it is best to put the membeship functions for the fuzzy values on paper at the outset so that there will be no loss of information later.

3. Expert systems using non-fuzzy values require perfect failure rules. When the rules are not perfect, the expert system does not perform well.

4. Although not explicitly defined for this purpose in the investigation, the fuzzy expert systems did remarkably well in detecting and locating multiple and partial failures. This means that fuzzy methods have some robustness.

(1,1) If A is high and B is low and D is significantly greater than C, then the system is in failure mode 1.

(2,1) If A is high and B is low and C is significantly greater than D, then the system is in failure mode 2.

(3,1) If A is low and B is high and D is significantly greater than C, then the system is in failure mode 3.

(4,1) If A is low and B is high and C is significantly greater than D, then the system is in failure mode 4.

(5,1) If A is high and B is high and D is slightly greater than C, then the system is in failure mode 0.

Figure 2. Fuzzy decision rules inferred by subject JR

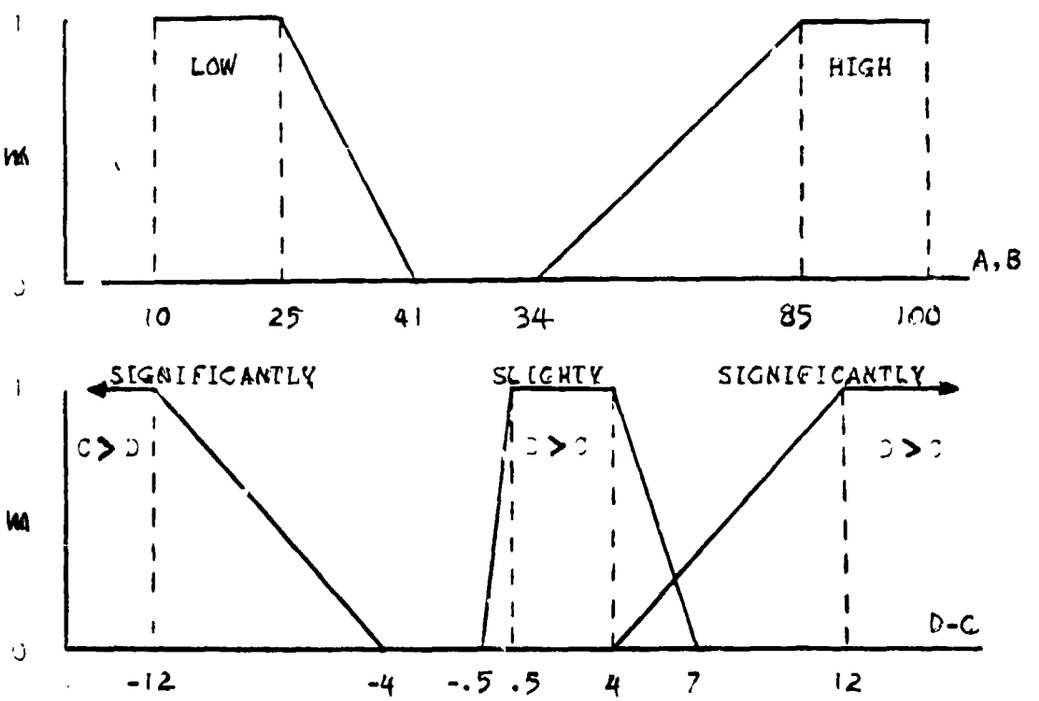

Figure 3. Membership functions devised by subject JR

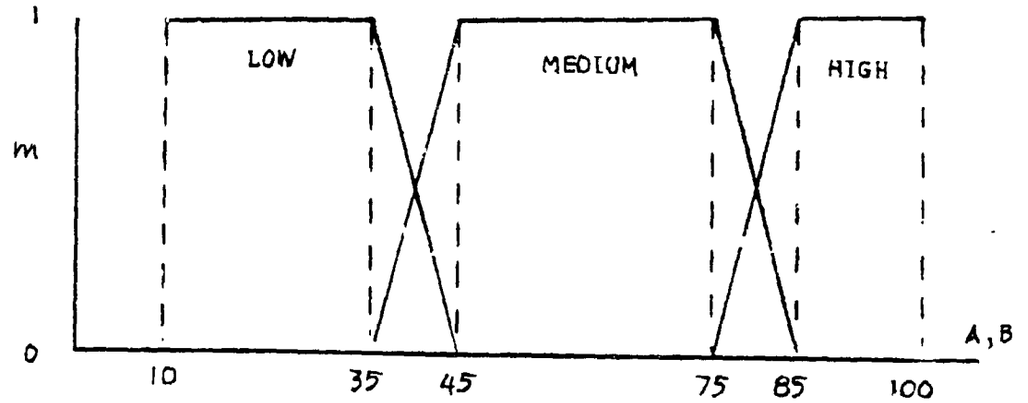

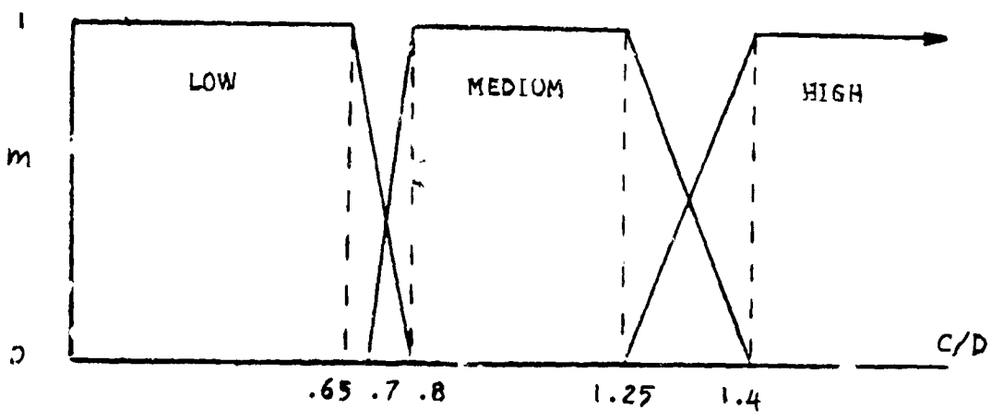

Figure 4. Membership functions devised by subject DM

TEST 1: SINGLE COMPLETE FAILURE

ACTUAL FAILURE	IDENTIFIED FAILURE		
	MOST-TRUE	TIMES-TRUE	TRUTH-SUMMATION
1	1	1	1
2	2	2	2
3	3	3	3
4	4	4	4
0	0	0	0
SCORE:	5/5	5/5	5/5

TEST 2: MULTIPLE COMPLETE FAILURES

ACTUAL FAILURES	IDENTIFIED FAILURE		
	MOST-TRUE	TIMES-TRUE	TRUTH-SUMMATION
1,3	3	3	1
1,4	1,4	1	1
2,3	2,3	3	3
2,4	2,4	2	2
SCORE:	4/4	4/4	4/4

TEST 3: SINGLE PARTIAL FAILURE

ACTUAL FAILURE	IDENTIFIED FAILURE		
	MOST-TRUE	TIMES-TRUE	TRUTH-SUMMATION
1	1 (55%)	1 (50%)	1 (55%)
2	2 (75%)	2 (70%)	2 (55%)
3	3 (70%)	3 (70%)	3 (65%)
4	4 (80%)	4 (75%)	4 (65%)
SCORE:	4/4	4/4	4/4
TOTAL SCORE:	13/13	13/13	13/13

* = INCORRECT DECISION

Figure 5. Results of applying JR's expert system

TEST 1: SINGLE COMPLETE FAILURE

ACTUAL FAILURE	IDENTIFIED FAILURE		
	MOST-TRUE	TIMES-TRUE	TRUTH-SUMMATION
1	1	1	1
2	* 1,2	2	2
3	* 1,3	* 1	* 1
4	* 1,4	4	4
0	0	0	0
SCORE:	2/5	4/5	4/5

TEST 2: MULTIPLE COMPLETE FAILURES

ACTUAL FAILURES	IDENTIFIED FAILURE		
	MOST-TRUE	TIMES-TRUE	TRUTH-SUMMATION
1,3	1,3	1	1
1,4	* 1,4,0	1	1
2,3	* 2,3,4,0	2	2
2,4	2	2	2
SCORE:	2/4	4/4	4/4

TEST 3: SINGLE PARTIAL FAILURE

ACTUAL FAILURE	IDENTIFIED FAILURE		
	MOST-TRUE	TIMES-TRUE	TRUTH-SUMMATION
1	1 (80%)	1 (55%)	1 (50%)
2	* 4	* 4	* 4
3	3 (70%)	3 (65%)	3 (60%)
4	* 1,4	4 (30%)	* 1
SCORE:	2/4	3/4	2/4
TOTAL SCORE:	6/13	11/13	10/13

* = INCORRECT DECISION

Figure 6. Results of applying DM's expert system

5. The decision method can be chosen to suit the strength and tightness of the rules. Stronger rules require less margin for error.

6. Expert systems which have approximately the same number of rules for each failure mode perform better than those with an uneven distribution

SECOND EXPERIMENT

As a second experiment the first author used himself as a subject on a black box resistor network that was much more complex (sufficiently so that he had no advantage over a subject who did not know what was inside). Again there were two adjustable inputs and two resulting outputs but this time eight failure modes. The first author experimented and observed, then derived his rules, (Figure 7) then defined his membership functions, and finally derived an expert system on the same basis as before. Results showed that the expert system worked perfectly on complete failures but faltered on multiple complete failures and partial failures (Figure 8). Further attempts to refine his decision rules showed little gain in discriminabililty.

CONCLUSIONS FROM SECOND EXPERIMENT

One can conclude from these results that a computer, given relatively little knowledge in fuzzy form from persons who are "expert" in the behavior of a sufficiently simple system under complete failures, can perform very well in identification of such failures. But when the system is complex and failures are multiple or partial and the expert's knowledge is not derived on the basis of experiencing such failures, an expert system cannot be expected to perform very well.

REFERENCES

1. Zadeh, L.A., Fuzzy Sets, Information and Control, 8, 338-353.

2. Laritz, F.J., The Use of Fuzzy Sets in Failure tection, MIT SM Thesis, December 1983.

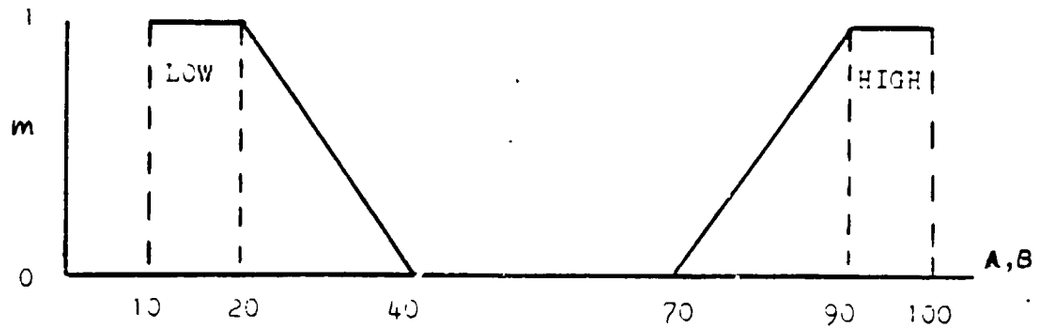

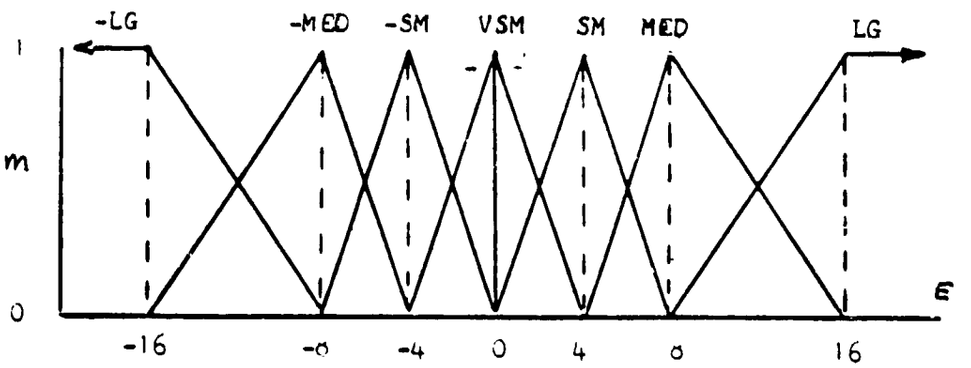

Figure 7. Membership functions devised by Laritz for variables of complex resistor network

ORIGINAL PAGE IS
OF POOR QUALITY

TEST 1: SINGLE COMPLETE FAILURE

ACTUAL FAILURE	IDENTIFIED FAILURE		
	MOST-TRUE	TIMES-TRUE	TRUTH-SUMMATION
1	1	1	1
2	2	2	2
3	3	3	3
4	4	4	4
5	5	5	5
6	6	6	6
7	7	7	7
8	8	8	8
0	0	0	0
SCORE:	9/9	9/9	9/9

TEST 2: MULTIPLE COMPLETE FAILURES

ACTUAL FAILURES	IDENTIFIED FAILURE		
	MOST-TRUE	TIMES-TRUE	TRUTH-SUMMATION
1,2	2	2	2
1,3	1	1	1
1,4	1	1	1
1,5	1	* 1,7	1
1,6	1	1	1
1,7	* 5	* 5	* 5
1,8	8	8	8
2,3	2	2	2
2,4	4	4	4
2,5	* 4	* 4	5
2,6	6	6	6
2,7	7	7	2
2,8	2	* 1,2	* 1
3,4	4	4	4
3,5	5	5	5
3,6	6	6	3
3,7	7	7	7
3,8	8	8	8
4,5	* 7	* 7	* 7
4,6	6	6	6
4,7	* 5	* 5	* 5
4,8	* 6	* 6	* 6
5,6	* 1	* 1	* 1
5,7	* 0	* 0	* 0
5,8	* 2	* 0	* 2
6,7	* 4	* 8	* 8
6,8	6	6	6
7,8	* 4	* 4	* 1
SCORE:	18/28	16/28	18/28

TEST 3: SINGLE PARTIAL FAILURE

ACTUAL FAILURE	IDENTIFIED FAILURE		
	MOST-TRUE	TIMES-TRUE	TRUTH-SUMMATION
1	1 (55%)	1 (55%)	* 2
2	2 (65%)	2 (65%)	2 (25%)
3	3 (60%)	3 (60%)	* 2
4	* 3	* 3	* 2
5	* 2	* 2	* 2
6	* 8	* 8	* 8
7	* 4	* 4	* 2
8	8 (55%)	8 (55%)	* 2
SCORE:	4/8	4/8	1/8
TOTAL SCORE:	31/45	29/45	28/45

* = INCORRECT DECISION

Figure 8. Results of applying Laritz' expert system to failures of complex resistor network

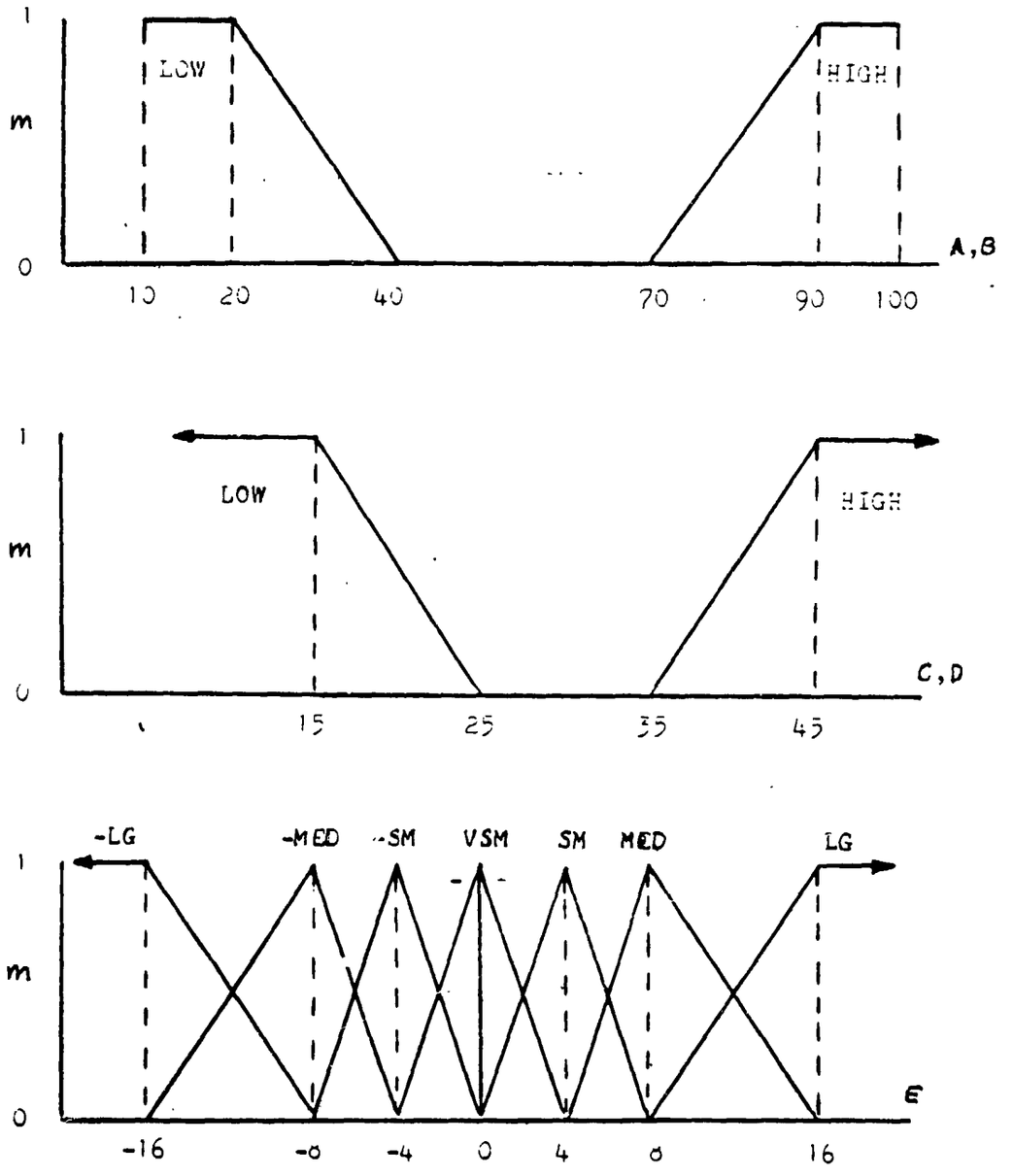

Figure 7. Membership functions devised by Laritz for variables of complex resistor network

TEST 1: SINGLE COMPLETE FAILURE

ACTUAL FAILURE	IDENTIFIED FAILURE		
	MOST-TRUE	TIMES-TRUE	TRUTH-SUMMATION
1	1	1	1
2	2	2	2
3	3	3	3
4	4	4	4
5	5	5	5
6	6	6	6
7	7	7	7
8	8	8	8
0	0	0	0
SCORE:	9/9	9/9	9/9

TEST 2: MULTIPLE COMPLETE FAILURES

ACTUAL FAILURES	IDENTIFIED FAILURE		
	MOST-TRUE	TIMES-TRUE	TRUTH-SUMMATION
1,2	2	2	2
1,3	1	1	1
1,4	1	1	1
1,5	1	* 1,7	1
1,6	1	1	1
1,7	* 5	* 5	* 5
1,8	8	8	8
2,3	2	2	2
2,4	4	4	4
2,5	* 4	* 4	5
2,6	6	6	6
2,7	7	7	2
2,8	2	* 1,2	* 1
3,4	4	4	4
3,5	5	5	5
3,6	6	6	3
3,7	7	7	7
3,8	8	8	8
4,5	* 7	* 7	* 7
4,6	6	6	6
4,7	* 5	* 5	* 5
4,8	* 6	* 6	* 6
5,6	* 1	* 1	* 1
5,7	* 0	* 0	* 0
5,8	* 2	* 0	* 2
6,7	* 4	* 8	* 8
6,8	6	6	6
7,8	* 4	* 4	* 1
SCORE:	18/28	16/28	18/28

TEST 3: SINGLE PARTIAL FAILURE

ACTUAL FAILURE	IDENTIFIED FAILURE		
	MOST-TRUE	TIMES-TRUE	TRUTH-SUMMATION
1	1 (55%)	1 (55%)	* 2
2	2 (65%)	2 (65%)	2 (25%)
3	3 (60%)	3 (60%)	* 2
4	* 3	* 3	* 2
5	* 2	* 2	* 4
6	* 8	* 8	* 8
7	* 4	* 4	* 2
0	8 (55%)	8 (55%)	* 2
SCORE:	4/8	4/8	1/8
TOTAL SCORE:	31/45	29/45	28/45

* = INCORRECT DECISION

Figure 8. Results of applying Laritz' expert system to failures of complex resistor network

N85 14509 D22

THE ROLE OF KNOWLEDGE STRUCTURES IN FAULT DIAGNOSIS

Philip J. Smith
Walter C. Giffin
Thomas H. Rockwell
Mark E. Thomas

Department of Industrial and Systems Engineering

The Ohio State University

210 Baker Systems Engineering Building

1971 Neil Avenue

Columbus, Ohio 43210

An experiment was conducted to study how a person whose memory contains well-developed knowledge structures relevant to a particular problem uses these knowledge structures to direct fault diagnosis performance. In particular, the performances of twenty pilots with instrument flight ratings were studied in a fault diagnosis task (detection of a vacuum system failure). The pilots were initially read a scenario describing the conditions of flight under which symptoms indicative of a problem were detected. They were asked to then think out loud as they requested and interpreted various pieces of information (instrument readings, visible condition of the aircraft, etc.) in an effort to diagnose the cause of the problem. Only eleven of the twenty pilots successfully diagnosed the problem.

Pilot performance on this fault diagnosis task has been modeled in terms of the use of domain-specific knowledge organized in a frame system. Eighteen frames, all having a common structure, were necessary to account for the data from all twenty subjects. (Each pilot utilized some subset of these eighteen frames while diagnosing the fault.)

These frames represent prototypical states of nature (e.g., NOSE-DOWN DESCENT, STRUCTURAL ICING). Each frame has associated with it a set of enabling events and two slots. One slot represents alternative causes of the state of nature represented by the frame (e.g., POWER LOSS can cause DESCENT). The second slot indicates expected instrument readings and other observable conditions if that state of nature actually exists.

The eighteen frames are organized in a set of hierarchies, with one frame linked to another as a slot-filler in the "Possible Causes" slot of that frame.

When listening to the scenario, the pilot is hypothesized to activate one of the top-level frames in the frame system. This activation process may not utilize all of the information available in the scenario. Instead, certain cues are given selective attention. Three possible determinants of attention will be discussed.

Upon activation of a frame, the contents of its two slots ("Possible Causes" and "Expectations" are used to achieve certain objectives (find cause, check for instrument malfunction, etc.). The selection of objectives appears to be of critical importance in determining ultimate success or failure in diagnosing the fault.

Other factors contributing to the failures to correctly diagnose the fault include:

1. memory distortions;

2. activation of incorrect default values;

3. inheritance based on incorrect assumptions;

4. missing slot-fillers.

Teleoperators

N85 14510

The Effect of Part-Simulation of Weightlessness on Human Control of Bilateral Teleoperation: Neuromotor Considerations

Kevin Corker and Antal Bejczy
Jet Propulsion Laboratory, California Institute of Technology
Pasadena, California 91109

Experimental investigations have been undertaken at JPL to study the effect of weightlessness on the human operator's performance in force-reflecting position control of remote manipulators. A gravity compensation system has been developed to simulate the effect of weightlessness on the operator's arm. In the experiments, a universal force-reflecting hand controller (FRHC) and task simulation software were employed. The controller device is a backdrivable six-dimensional isotonic joystick which conforms to the range of motion of the operator in position control. The simulation software provides experimenter manipulable task parameters which interact with the hand controller in real time operation. In light of anticipated disturbances in neuromotor control specification on the human operator in an orbital control environment, two experiments were performed in this study: (i) investigation of the effect of controller stiffness on the attainment of a learned terminal position in the three dimensional controller space, and (ii) investigation of the effect of controller stiffness and damping on force tracking (subject to unit pulse disturbance) of the contour of a simulated three dimensional cube using the part-simulation of weightless conditions: . The results of the experiments: (i) support the extension of neuromotor control models, which postulate a stiffness balance encoding of terminal position, to three dimensional motion of a multi-link system, (ii) confirm the existence of a disturbance in human manual control performance under gravity compensated conditions, and (iii) suggest techniques for compensation of weightlessness induced performance decrement through appropriate specification of hand-controller response characteristics. These techniques are based on the human control model, and instituted through FRHC control parameter adjustment.

INTRODUCTION

Remote manipulators (teleoperators) are devices that extend human manipulative abilities to operational environments that are either hostile to or remote from the human operator. Teleoperation is distinguished by the explicit and active inclusion of the human operator (HO) in the ongoing control of

the teleoperated device. The operator brings to the control task impressive intellectual and analytic capabilities, as well as, a rich and subtle control language in the movement and proprioceptive functions of the human arm and hand. This study addresses bilateral control in space teleoperation in which the transmission of control signals and the reception of feedback information occurs simultaneously at the operator's hand. The critical elements in this control are (i) the neuromotor characterisitcs of the human's arm and hand, including motion control functions, their stability, and their sensitivity to environmental perturbations (in particular micro-gravity effects in control of space teleoperators) and (ii) the hand controller that serves as a control and feedback transmission device in consonance with the human neuromotor parameters in motion control.

In the investigation of human/teleoperator control interactions in the orbital operational environment, we have employed a model describing human neuromotor control as a linear damped harmonic oscillator, i.e.,

$$I\ddot{\Theta} + B\dot{\Theta} + K\Theta = N \qquad (1)$$

where: $\Theta, \dot{\Theta}, \ddot{\Theta}$ represent joint position, angular velocity, and acceleration, respectively, for the links of the kinematic chain effecting end point position, I represents system inertia, B represents system viscosity, and K represents system stiffness. N, the torque input to the system, is assumed to account for the various nonlinearities and nonstationary physiological characterisitics of actual muscle movement. The control methods inferred from this model, eg., impedance control (Hogan, 1982), or stiffness control for end point positioning (Polit and Bizzi, 1978), have been the focus of recent neuromotor research. (See Corker (1984) for a review of this research base). We explore the application of this model for the specification of the end point position in teleoperator control. It is of value to man/machine interface design that neuromotor control models be formulated in the same terms as control system descriptions for

the hand controller. Human neuromotor parameters and hand controller characteristics interact as coupled systems to produce the total system response. If human and teleoperator control in position and the first and second time derivatives (velocity and acceleration), are expressed with a similar nomenclature and found to obey similar control laws, interactions can be described, and compensations for machine or human limitations in control can be more easily accommodated in the design for optimal system function.

The first experiment was undertaken to verify and extend to teleoperator control current theories in human achievement of final limb position, as a function of balanced stiffness among muscle groups contributing to movement. The second experiment examined the effects of micro-gravity on force tracking performance using computer generated resistance planes in the control volume of the FRHC, and tested compensation techniques to counteract environment induced performance disruption.

EQUIPMENT

Hand Controller.

The JPL universal FRHC provides a generalized bilateral force-reflecting control of teleoperated manipulators. In a departure from the standard practice of master/slave control systems requiring kinematic and dynamic replication between the master and the slave, the FRHC control function is implemented through a hand controller that can be dissimilar to a particular slave both dynamically and kinematically. The hand controller is a six degree of freedom (DOF) isotonic joystick which can be backdriven by commands from the control computer (Figure 1). The control algorithms of the FRHC (i) transform the operator's six-dimensional hand motion into an equivalent six-dimensional motion of the particular slave hand and (providing appropriate instrumentation of the manipulator) (ii) transmit ("reflect") the acting forces from the slave arm back to the operator's hand. Thus the FRHC as a man-machine interface device

performs feedforward and feedback motion, and force transformation and transmission between the operator's hand and the remote manipulator's hand.

The FRHC provides feedback to the operator identifying position and velocity mismatch between the commanded endpoint and the actual (or simulated) manipulator end point. This feedback is instituted as a stiffening and damping of the FRHC motion through active backdrive of torque motors affecting the FRHC handgrip motion. The controller feedback gains K_p,K_v, and K_f (for sensor based force reflection) are software manipulable and were varied in the course of the experimentation reported. These gains can be varied independently for each of the six DOFs of the hand controller (Bejczy and Salisbury, 1980).

Simulation Software.

In this investigation the FRHC was decoupled from control a physical manipulator so that task parameters and disturbance inputs could be closely controlled by the experimenters.

A task simulation system was developed based on the following concept: the computer, the FRHC and the operator form a closed loop, the computer simulates a slave arm to be driven by the FRHC (Figure 2). In the feedforward path, positioning commands received from the controller are interpreted and processed in the computer. In feedback, the force and torque resulted from the simulated task environment are computed and sent by the computer to the FRHC to back drive the joint motors (Fong and Corker, 1984).

The simulation system was used in both experiments to manipulate the characterisitics of the response of the FRHC to operator task performance.

EXPERIMENTS

The purpose of the first experiment was to verify and extend the linear harmonic oscillator model of human neuromotor control to control of a teleoperator device in three dimensional space. This verification of the model was undertaken to provide a basis

for analyzing performance in the zero gravity performance scenerio, described in Experiment Two.

Experiment One.

A terminal position for the hand controller was learned in the three dimensional control space of the FRHC by blindfolded subjects. The reattainment of that position was subject to stiffness constraints imposed through the simulation system. The stiffness imposed, by software specification of stiffness gain on the three translational axes of motion, either resisted or augmented the operator's movement to the learned target position. The conditions of stiffness and the magnitude of the gain were an operator dependent function based on prior calibration of system response stability for each partcipant in the study. The simulation system provided the capability to (i) specify augmentative and resistive stiffness vectors for an arbitrary position in three dimensional operator referenced Cartesian coordinates, (ii) record the achieved position (AP) to .01 inch accuracy in the free space of operator movement. Figure Three illustrates the task workspace in relation to the FRHC.

A repeated measures analysis of variance (ANOVA) was performed to determine if the target, resisted AP, and augmented AP differed significantly from each other across subjects, and to determine if that difference was orthogonal among the axial coordinates (X,Y,Z) defining those positions.

The analysis indicates a significant effect of stiffness gain (K_p) on position. The null hypothesis that stiffness would not affect achieved position in relation to the target is rejected with a $p < .001$, ($F_{(2,14)} = 18.21$). The analysis also indicates no significant difference among axes of motion, and no significant interaction between stiffness and axis, thereby supporting the hypothesis that the effect of stiffness gain is orthogonal among axes.

The results of this experiment indicate that achievment of final position in three dimensional space, effected through coordinated multi-joint motion of a multi-articulated limb

system, is affected by an imposed stiffness on the moving limb. This effect differs between an augmentative and resitive stiffness in relation to a target position (learned in the absence of imposed stiffness conditions). The resultant APs are reliably short of the target in the case of resistive stiffness and beyond the target in the case of augmentative stiffness. This directional deviation is orthogonal among the major translation axes defining the AP in relation to the target. The model of multi-articulated limb control that can be inferred from these data is currently under development.

The results support the concept of stiffness balance as a position specification in human neuromotor control, and provide an extension of that model to three dimensional positioning with a control manipulanda. The results indicate a lack of precision in blind limb placement, even for a trained position, as a function of an imposed change in the relative stiffness of the muscles driving the limb movement. This effect is observed despite the availabilty of kinesthetic feedback as to the limb's actual position. The inference drawn from these results is that changes in relative muscle stiffness as a function of a zero g operating environment could potentially affect blind limb positioning in control.

Experiment Two.

The second experiment examines the effect of a zero gravity operating environment on human performance in manual control of a teleoperator in a bilateral position control mode. In order to provide an experimental platform for this research, a mechanical gravity compensation system for the upper limb has been designed and fabricated. The system is based in part on work performed at Case Western University, as reported in NASA CR-1234 (1968). The system supports the operator's upper arm an hand throughout the range of motion for control of the force reflecting hand controller (FRHC).

The system was designed to meet the following suspension

requirements:

1) The compensation system should provide a constant force at the center of mass of each limb segment that is equal and opposite the gravity force acting on that limb. Determination of that force requirement is as follows:

For a limb in an arbitrary position in a 1g environment, Figure 4 illustrates the parameters of interest.

Where:

F_o = Force of support of shoulder girdle

M_1, M_2, M_3 = Mass of Limb segments

T_1, T_2, T_3 = Torque about shoulder, elbow, and wrist

L_1, L_2, L_3 = Length of limb segments

l_1, l_2, l_3 = Length to center of mass for each segment

$\theta_1, \theta_2, \theta_3$ = Segment angle to gravity perpendicular

Force balance requires that:

$$F_o = g\,(M_1 + M_2 + M_3)$$

In this design each limb segment will be supported at the center of mass of each segment. Consequently, the compensation forces (f_1, f_2, f_3) can be calculated independent of the joint torques, assuming frictionless coupling at the joints.

The arm and hand of each subject were analysed to determine the approximate weight and center of mass of each limb segment using anthropometic measurement and regression techniques developed by Clauser et al. (1969). The approximate weight determined the particular spring system to be used. Each spring system was adjustable within a range of +/- .25 lbs.; as is described below. The exact segment balance was determined by examining the response of a suspended and relaxed subject to a unit pulse disturbance, and adjusting spring tension to result in a balanced positive and negative amplitude for the response trajectory.

System Design:

The suspension system consists of two parts:

a) Negator springs to provide a constant gain spring tension

for vertical compensation. The torque from the spring can be adjusted to balance the individual limb segment weight by selecting the width and breadth of the spring, and adjusting the selected spring by varying the interior diameter of the spring coil through adjustment of the radius of the take up spool. The exact spring characteristic to torque relationship has been developed for several classes of spring coils. Figure 5 shows several details. The limb segment is secured using velcro pads and the placement of the spring support is adjustable.

b) For translational motion and as a support for the negator springs an x-y roller bearing system was designed and fabricated (see Figure 5). The system will be adjustable for a standing and seated operator and mounted in front of the FRHC control/display panel.

Figure 6 illustrates an operator using the compensation system and the FRHC in control simulation experiments.

The second experiment made extensive use of the simulation system capability to configure a software defined interactive workspace for the FRHC, and to present that workspace to the operator proprioceptively, through FRHC backdrive.

In this experiment the task was defined as moving the FRHC along the surface inside or outside a simulated box , a typical task which can generate force feedback in all possible directions. The hand controller is free moving inside/outside the 'virtual' box and encounters backdriving force when exceeding the workspace limits. This backdriving force is determined by one unique parameter called 'position error' defined as

$$\underline{E} = \underline{X} - \underline{X}_o \qquad (2)$$

where

$\underline{E}$ is the position error,

$\underline{X}$ is the hand controller's position,

$\underline{X}_o$ is the workspace limit.

Subjects learned to follow the outline of the three dimensional cube defined by force resistance within the working space of the hand controller. This three dimensional tracking trajectory was approximately 27 inches around the perimeter of the force cube and was completed in 20 seconds. A unit pulse disturbance of approximately 70 msec. duration and 65 in-lbs. in amplitude, defined through the simulation system, was delivered randomly in a 4 second window as the subjects performed the trajectory. The disturbance was delivered randomly in the positive or negative direction along each axis of motion.

Subjects performed the force tracking task under conditions of micro-gravity, through suspension, and in one gravity. The velocity feedback gain (damping) of the hand controller was varied between maximum stable value for each subject, and one quarter that value

A test sequence consisted of ten trials in each of two damping gain conditions in both a suspended and unsuspended operating state. FRHC position data were collected for each of the three translational axes of motion at a rate of 70 $msec^{-1}$.

Results:

The velocity profile of each trial for each subject was subjected to a spectral analysis through the application of a Fast Fourier Transform (FFT) technique. The data were so treated to enable statistical analysis of the effects of the imposed conditions on the amplitude of response for a specified frequency range. The FFT resulted in amplitude data for frequencies from 0 to 15 Hz. digitized in .10 Hz. steps. The data were further reduced by averging amplitudes for the first five Hertz.

The averaged performance in simulated zero g shows a higher amplitude response to disturbance in each axis of motion illustrated in Figure 7. Statistical analysis indicates a significant difference in amplitude of response to disturbance as a function of the axis observed with an $F_{(2,4)}= 9.23$. The differential response among axes of motion is in keeping with the

results of an analysis of damping effects on control reported in Corker (1984).

The level of damping applied did not result in significant effects in the averaged data. An analysis of the individual response to damping was undertaken to investigate this lack of effect. Figure 8 illustrates the result of this analysis. Averaged across axes, damping in one g performance has the expected effect. However, in the suspended condition the response pattern of the subjects diverged. Group 1 response amplitudes indicate that the effect of damping is enhanced in the suspended condition resulting in response amplitudes further reduced than those of one g performance. Group 2 showed the opposite effect in response to damping in the suspended condition.

The factors contributing to the differential response to damping under zero g performance are currently being investigated. It is hypothesised that some individual's response to control in the zero g condition result in an impedance mismatch between control damping and stiffness and the neuromotor activation state that results in the instability observed.

CONCLUSION

The results indicate the potential utility of relatively simple models of neuromotor control processes in investigating the interaction of the human operator and controller in teleoperation. Stiffness manipulation in the control system significantly affected the accuracy of final position attainment in three dimensional space. Gravity compensation for the human operator through part-simulation resulted in increased instability in the operator's response to disturbance in a force tracking task. Additionally, preliminary data indicate that this increased instability can be successfully compensated, in some subjects, by selection of hand controller damping and stiffness parameters to match reduced natural damping which obtains as a function of the micro-gravity conditions.

Acknowledgment

This work has been carried out at the Jet Propulsion Laboratory, California Institute of Technology, under NASA Contract No. NAS7-918.

REFERENCES

Bejczy, A. K., and Salisbury, J. K., Jr., Kinesthetic Coupling Between Operator and Remote Manipulator, Proceedings of ASME Computer Technology Conference, Volume 1, San Francisco, CA., August 12-15, 1980; and, Controlling Remote Manipulators Through Kinesthetic Coupling, Computers in Mechanical Engineering, Vol. 1 No. 1, July 1983, pp. 48-60.

Clauser, C. E., J. T. McConville, and J. W. Young, (1969) Weight, Volume, and Center of Mass of the Segments of the Human Body. (AMRL-1R-69-70), Aerospace Medical Research Laboratory, Wright Patterson Airforce Base, Ohio, NASA CR 11262.

Corker, K. M., Investigation of Neuromotor Control and Sensory Sampling in Bilateral Teleoperation, Ph.D Thesis, UCLA, Department of Psychology, 1984.

Fong, C. P. and Corker, K. (1984). Force/Torque feedback task simulation for advanced remote manipulators. Society for Computer Simulation SCS Conference, July 23-25, (In Press).

Hogan, N. (1982). Mechanical impedance control in assistive devices and manipulators. in Robot Motion. M. Brady, J. M. Hollerbach, T. L. Johnson, T. Lozano-Perez, and M. T. Mason (eds.), pp. 631-372, MIT Press, Cambridge, Ma.

Morgen, R. J. (1969). A lunar Cravity Simulator, Volume II. Case Western Reserve University, Cleveland, Ohio, NASA CR-1234.

Polit, A., & Bizzi, E. (1978) Processes controlling arm movements in monkeys. Science, 201 (4362), 1235-1237.

ORIGINAL PAGE IS
OF POOR QUALITY

Figure 1. FRHC Mechanical Design Schematic

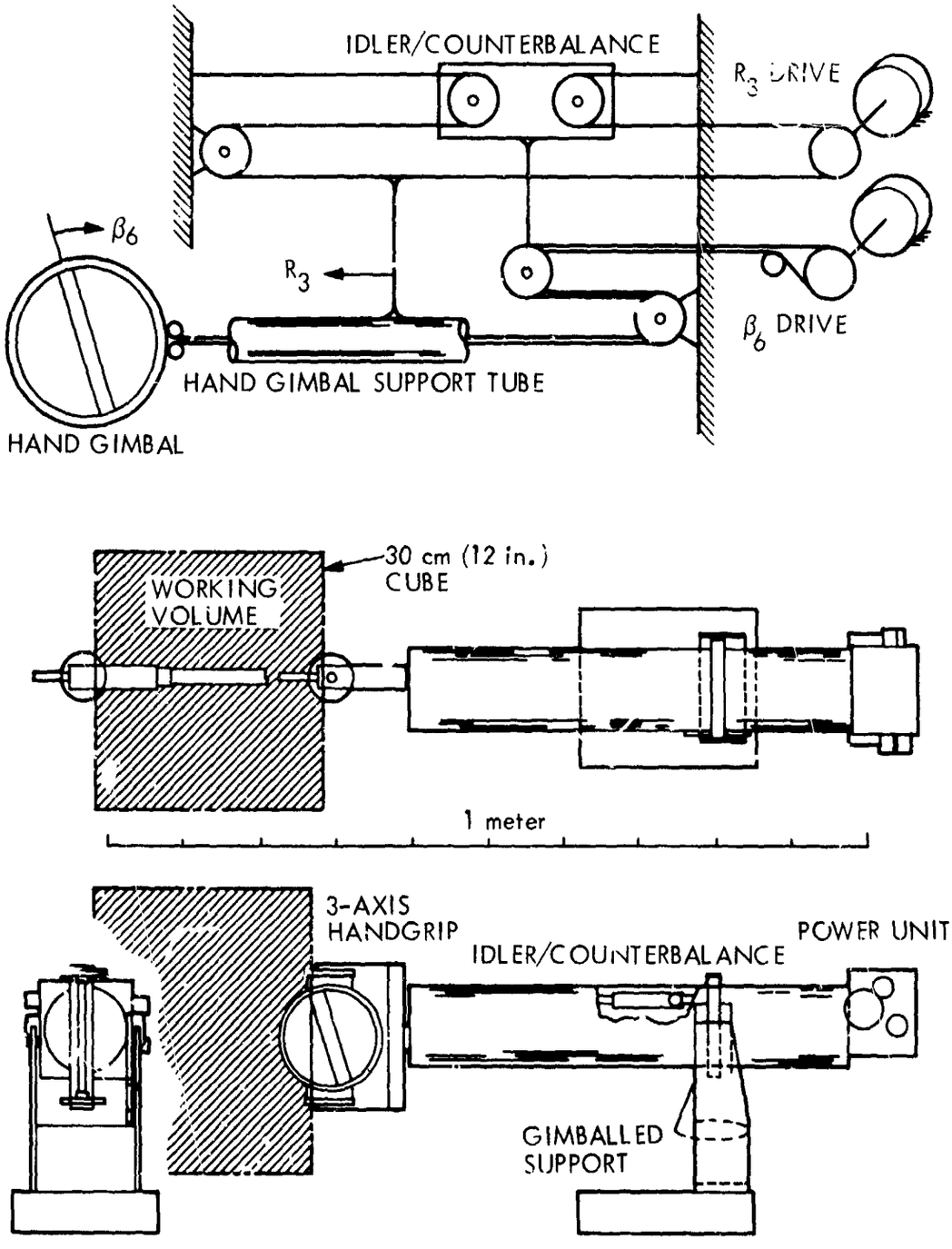

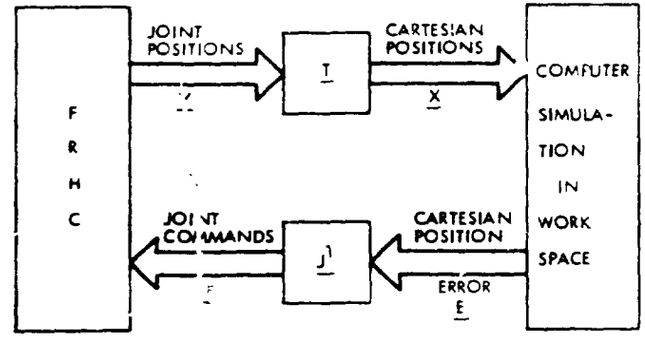

Figure 2.

FRHC Backdrive simulation system configuration.

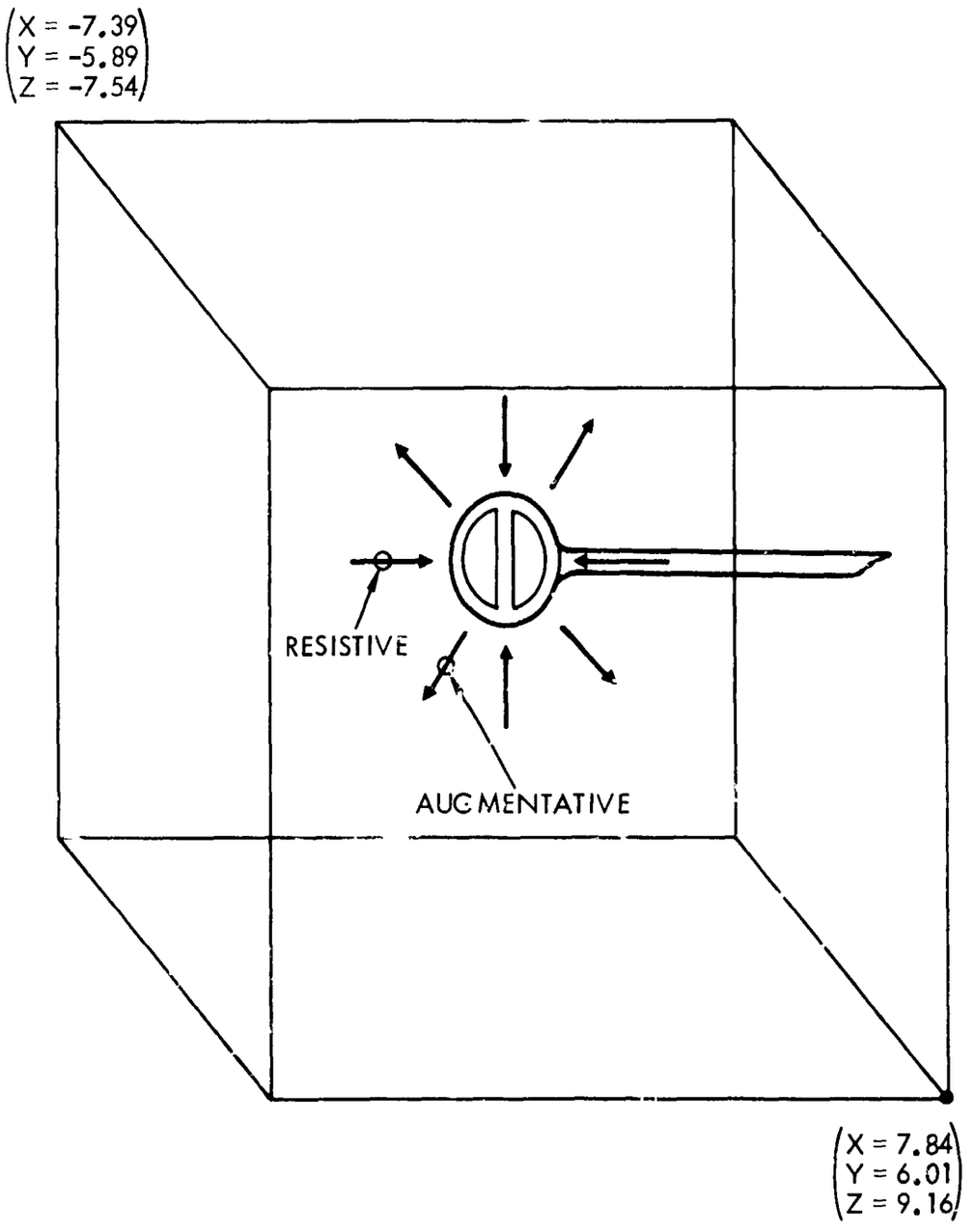

Figure 3.
Working Volume of FRHC

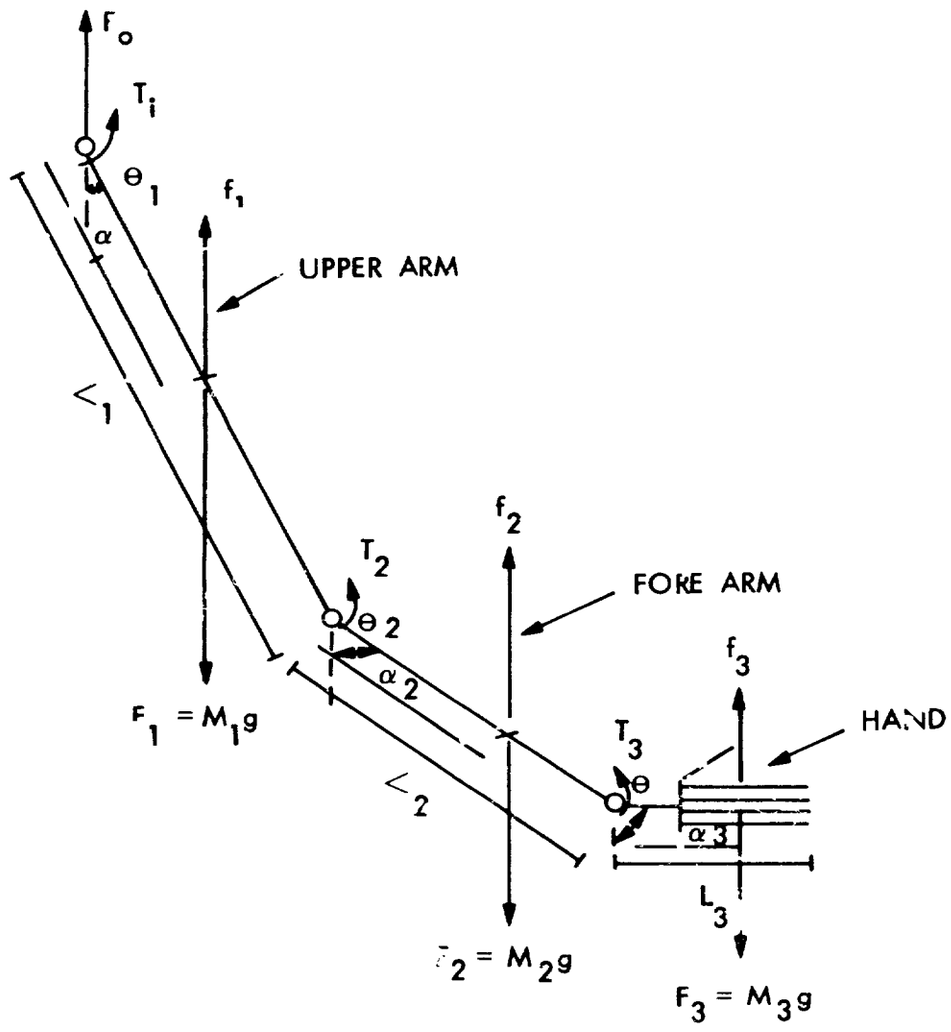

Figure 4.
ARM COMPENSATION FOR 1 GRAVITY:
MASS AND FORCE FACTORS

Figure 5.
Variable Radius Take-up Spool

ORIGINAL PAGE IS
OF POOR QUALITY

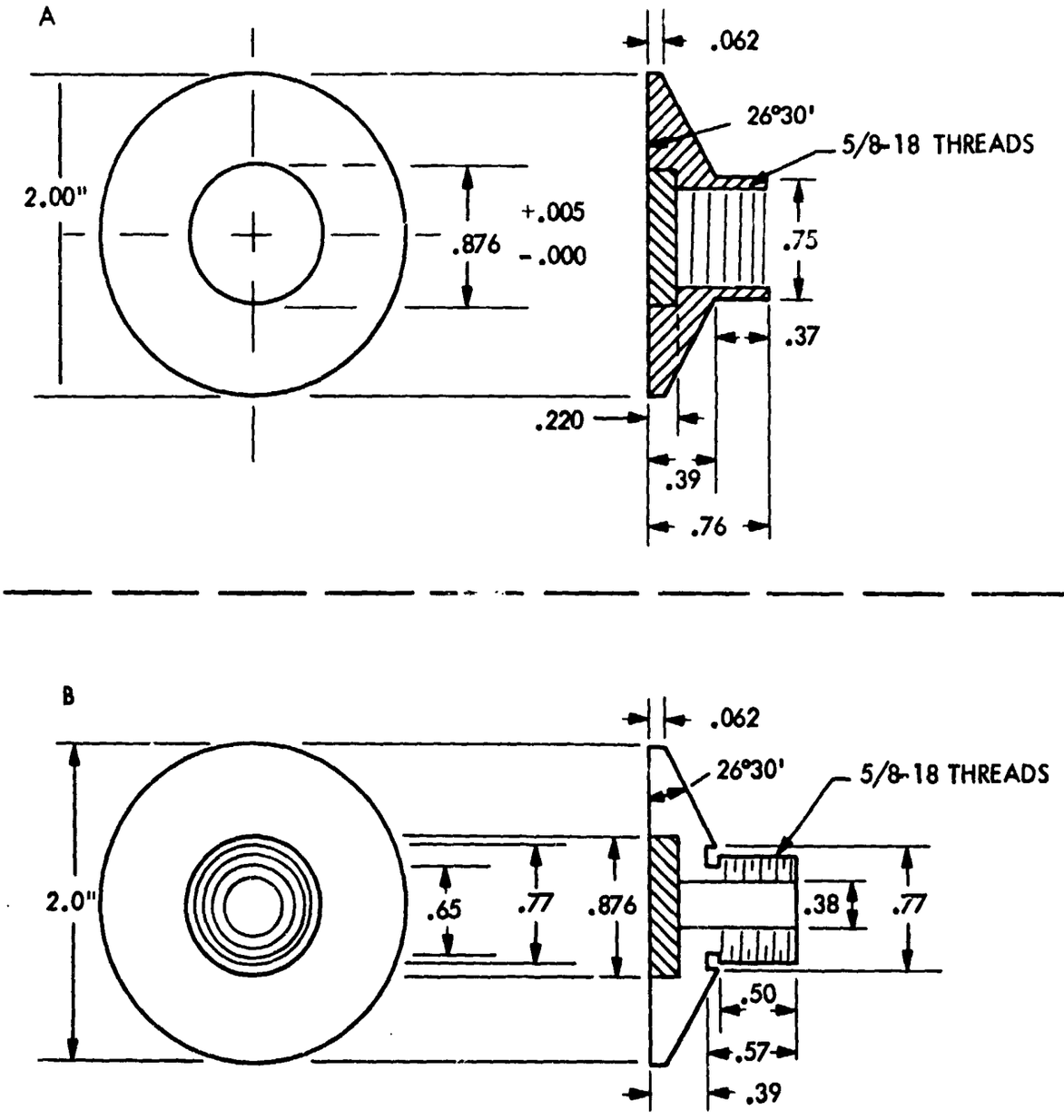

MAKE FROM 7075 T7 ALUM OR QUIV.
CONICAL SPOOL NEGATOR SPRING
SK 2-24-83 REV. B

C-5

Figure 5.

X-Y Translation Support System

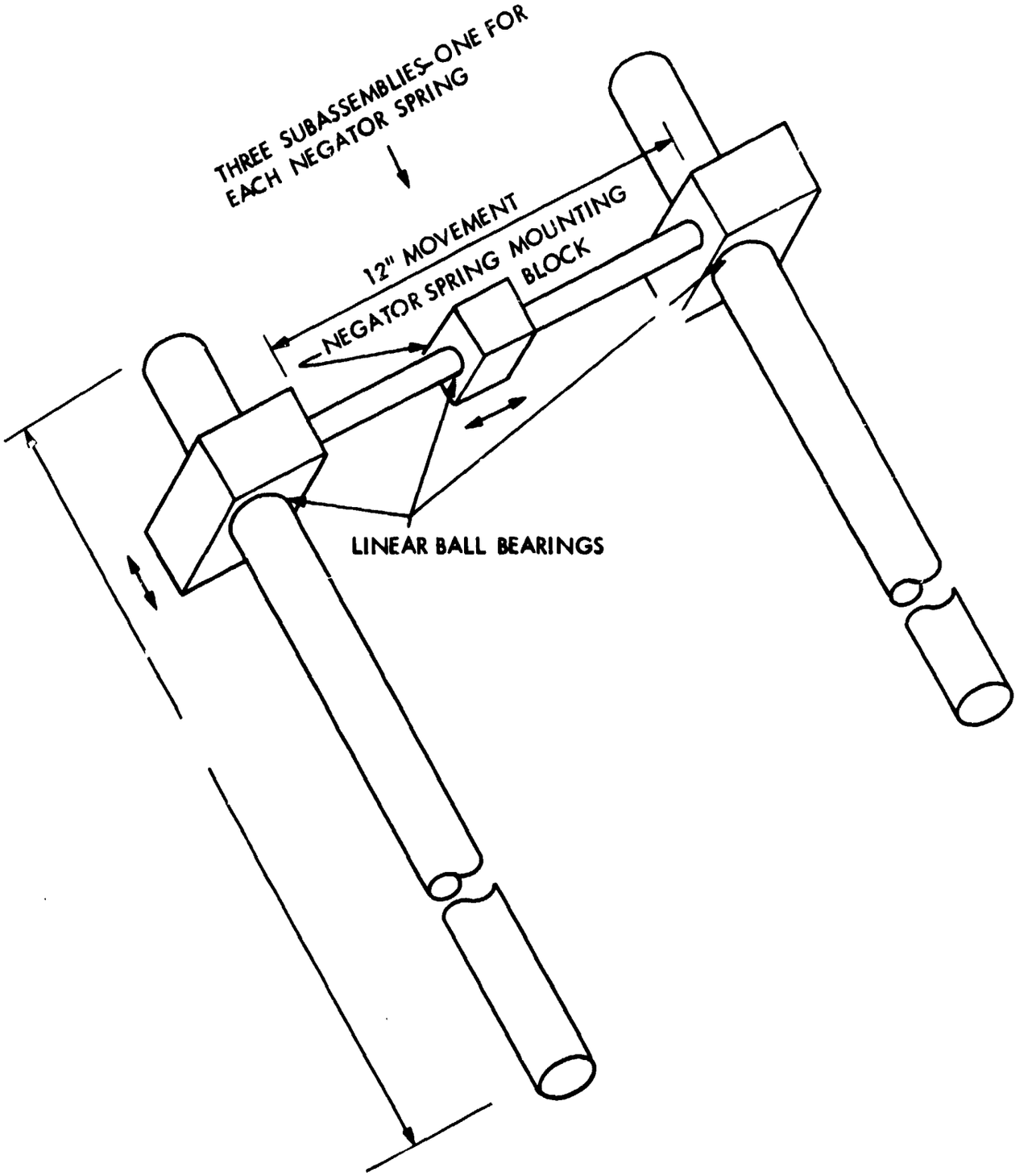

TRANSLATION MOTION UNIT
SK 2-25-83

ORIGINAL PAGE IS
OF POOR QUALITY

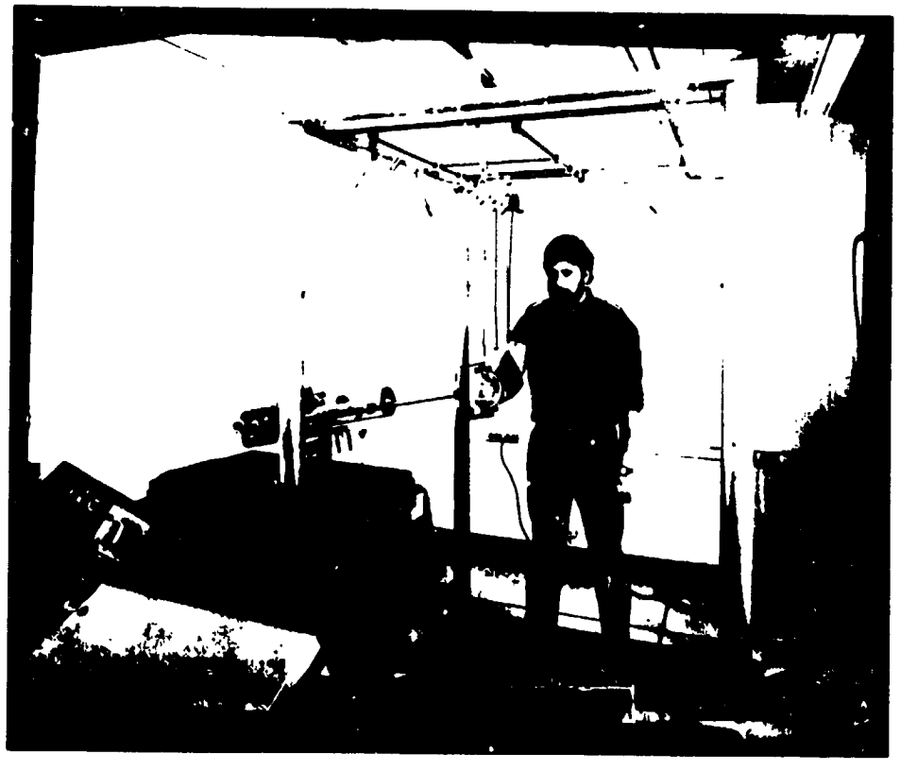

Figure 6.

Operator Using Suspension System in Simulation Task.

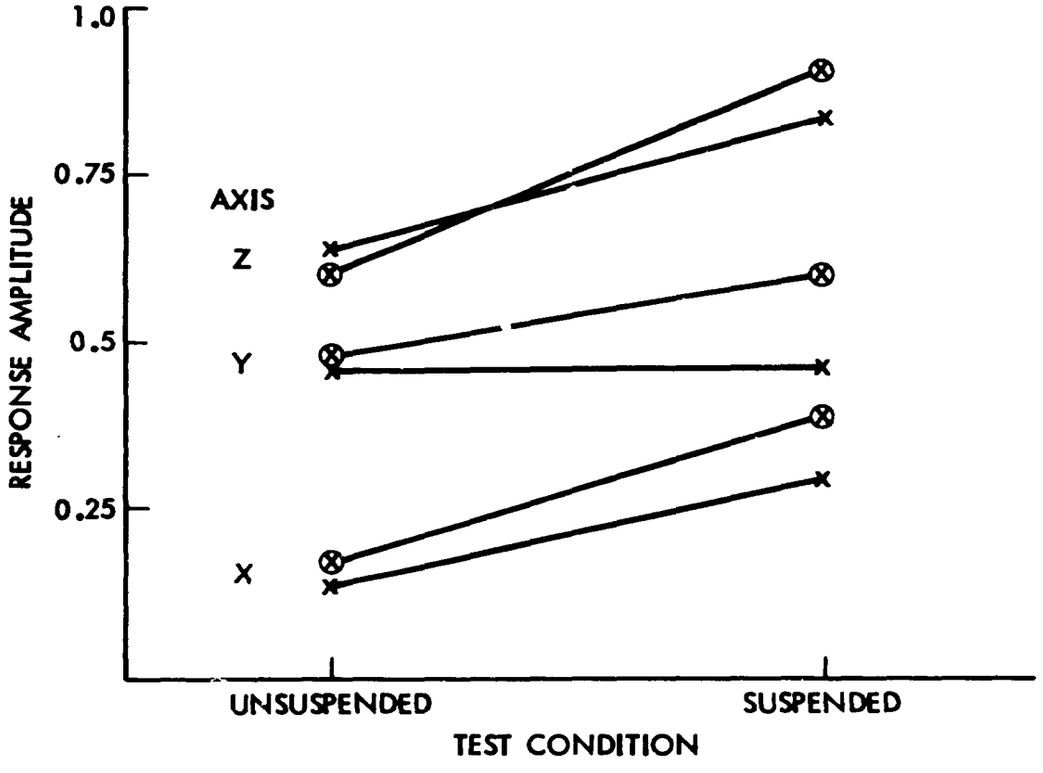

x = MODERATE DAMPING
⊗ = HIGH DAMPING

Figure 7.

RESPONSE TO DISTURBANCE INPUT
AS A FUNCTION OF DAMPING AND OPERATING CONDITION

PRECEDING PAGE BLANK NOT FILMED

INTENTIONALLY BLANK

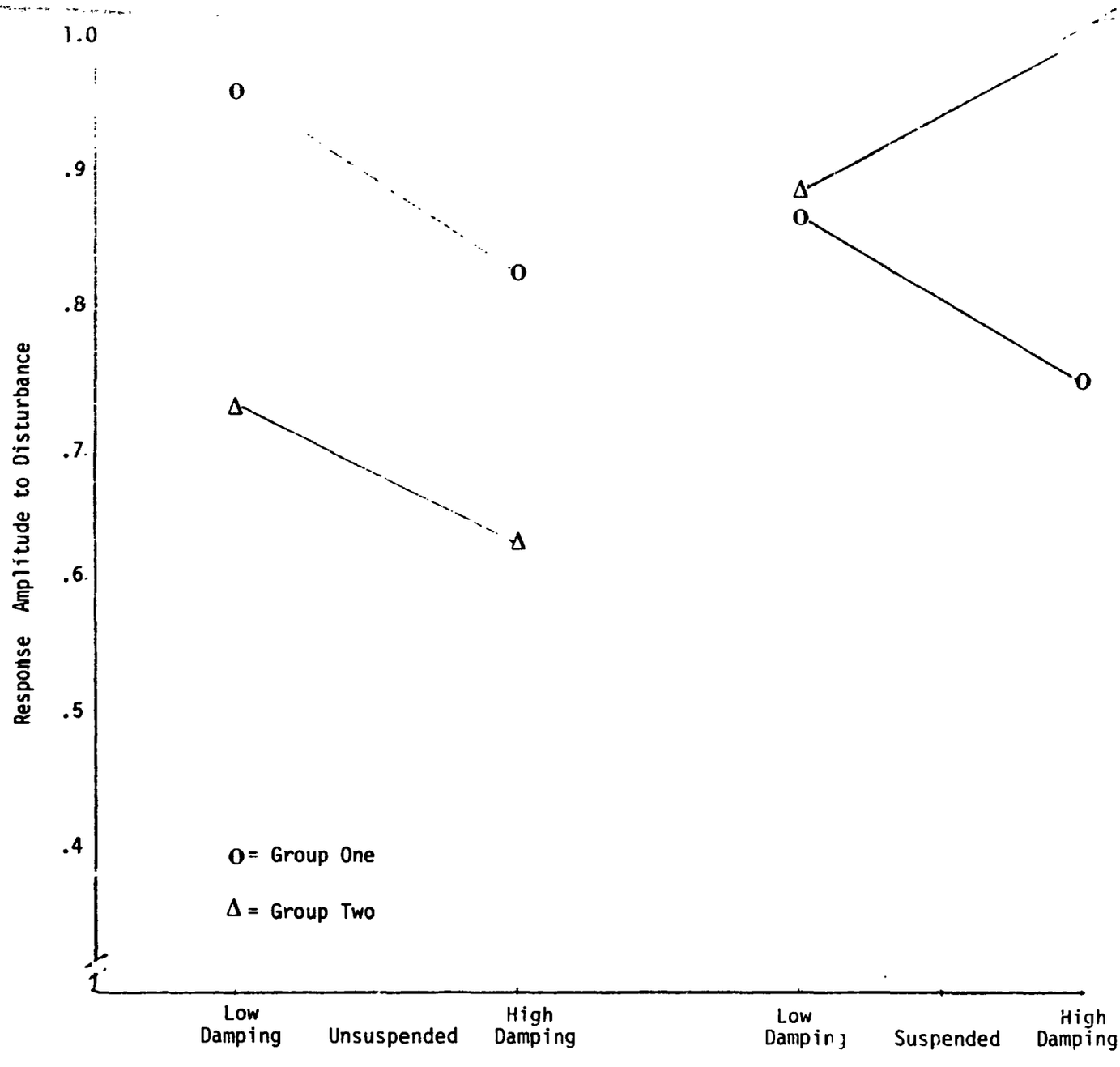

Figure 8.

Kruk, R. V. & Longridge, T. M. Psychophysiological research in development of a fibre-optic helmet mounted display. 221

FLYING QUALITIES
Chairman: Professor Ronald Hess

Heffley, R. K. , Bourne, S.M. & Hindson, W. S. Helicopter pilot performance for discrete-maneuver flight tasks. 223

Onstott, E. D., Warner, J. S. & Hodgkinson, J. Maximum normalized rate as a flying qualities parameter. 233

Sorenson, J. A. & Goka, T. Predictions of cockpit simulator experimental outcome using system models. 259

Hess, R. A. & McNally, B. D. Multi loop manual control of dynamic systems. 281

FAULT DIAGNOSIS/MODELING
Chairman: Dr. William Rouse

Curry, R. & Neu, J. E. A model for the effectiveness of aircraft alerting and warning systems. 299

Gersten, W. M. & Hawkins, J. D. Development and certification of a new stall warning and avoidance system. 301

Laritz, F. & Sheridan, T. Evaluation of fuzzy rulemaking for expert systems for failure detection. 327

Smith, P.J., Giffin, W. C. & Rockwell, T. H. The role of knowledge structure in fault diagnosis. 337

TELEOPERATORS
Chairman: Professor Thomas B. Sheridan

Corker, K. & Bejczy, A. The effect of part-simulation of weightlessness on human control of bilateral teleoperation: Neuromotor considerations. 339

Sheridan, T. B. Review of teleoperator research. 361

Rezek, T. Visual systems for remotely controlled vehicles. 367

SUPERVISORY CONTROL MODELS/TASKS
Chairman: Dr. Azad Madni

Berg, S. & Sheridan, T. B. Measuring workload differences between short-term memory and long-term memory scenarios in a simulated flight environment. 397

N85 14511

REVIEW OF TELEOPERATOR RESEARCH

Thomas B. Sheridan
Man-Machine System Laboratory
Massachusetts Institute of Technology

This is a progress report of four current projects, all dealing with teleoperator control.

1. A NOVEL PREDICTOR DISPLAY FOR TELEMANIPULATION THROUGH A TIME DELAY

Remote operation of manipulators, vehicles or other devices in earth orbit or deep space by human operators on the earth's surface is seriously impeded by signal transmission delays imposed by limits on the speed of light (radio transmission) and computer processing at sending and receiving stations and satellite relay stations. For vehicles in low earth orbit round-trip delays (the time from sending a discrete signal until any receipt of any feedback pertaining to the signal) are typically 0.4 seconds and for vehicles on or near the moon this is typically three seconds. It has been shown that the time to accomplish even simple manipulation tasks can increase by many fold, depending upon the time delay and the complexity of the task. This is because the human operator, in order to avoid instability (which is quite predictable from simple control theory) must adapt what has come to be called a "move and wait strategy", wherein he commits to a small incremental motion of the remote hand or vehicle, stops while waiting (the round trip delay time) for feedback, then commits to another small motion, and so on. To control continuously is literally not possible.

Because of this problem, requirements for control by human operators has required astronauts to do such controlling from nearby locations in orbit themselves, i.e., where signal transmission delays are very small. However, as more and more devices are put in space the requirement will increase for humans to perform remote manipulation and control, and if this can be done entirely from earth there will be great savings in not having to send humans into space. Thus the problem is how to make such remote control more efficient.

A similar problem is encountered with remote operation of manipulators and vehicles in the deep ocean from the surface if acoustic telemetry is employed, where sound transmission is limited to around 5000 ft/second in water. Except for the time delays and energy dissipation such acoustic telemetry is an attractive alternative to dragging many miles of wire cable through the water.

"Predictor displays" have been implemented where cursors or other indications are driven by a computer which extrapolates forward in time, based upon current state and time derivatives (Taylor series extrapolation). These have been employed in gun sights and "head-up" optical landing aids for aircraft pilots. Such techniques are adequate for continuous control of vehicles, but not for "move-and-wait" control

PRECEDING PAGE BLANK NOT FILMED

through finite time delays. Further, in the case of telemanipulation, it may be necessary to predict the position of a number of parts, i.e., a whole configuration of a device, relative to the environment, beyond a simple cursor.

The system we have conceived, constructed and tested is designed explicitly for control of a manipulator or other multi-degree-of-freedom device through finite time delay. The technique is made possible by new commercially available computer technology for video display which we have used for superposing artificially generated graphics on to a regular video picture (Figure 1).

The video picture is a (necessarily) time-delayed picture from the remote location, generated as a coherent frame (snapshot) so that all picture elements in a single scan are delayed the same. (Otherwise the lower part of the screen would be delayed more than the upper part). The computer-generated graphics is a line drawing of the present configuration of the manipulator arm, vehicle or other device. The latter is generated by using the same control signals which are sent to the remote manipulator (device) to drive a computer model of it. The computer model is drawn on the video display in exactly the same location as where it will actually be after a one-way time delay and where it will be seen to be on the video after one round-trip time delay. Since the graphics are generated in perspective and scaled relative to the video picture, if one waits at least one round-trip delay without moving, both the graphics model and the video picture of the manipulator (device) are seen to coincide. Using such a display operators can "lead" the actual feedback and take larger steps with confidence.

Experiments were performed with trained human subjects performing various telemanipulation tasks using both continuously updated video and buffered video (to intermittently generate and hold each video frame). The predictor technique proved to work well and has been shown for time delays in the 1-3 second range to reduce completion times for a variety of manipulation tasks by 50-150 percent reliably. It is still to be evaluated for longer time delays.

2. IMPEDANCE CONTROL

The common servomechanism provides position control: an actuator is forced in proportion to and to reduce a position error. When measured position corresponds to desired or reference position, the position error goes to zero and forcing stops.

Servomechanisms can also provide force control. Applied force is adjusted until the measured force matches the reference force.

Impedance control generalizes the relation between measured and actual to make the force-position relation (position being referenced to any fixed point in the environment) conform to whatever relation is desired. It may be desired that the relation between teleoperator hand and a fixed point environment be like a soft spring. It may be desired that it be like a

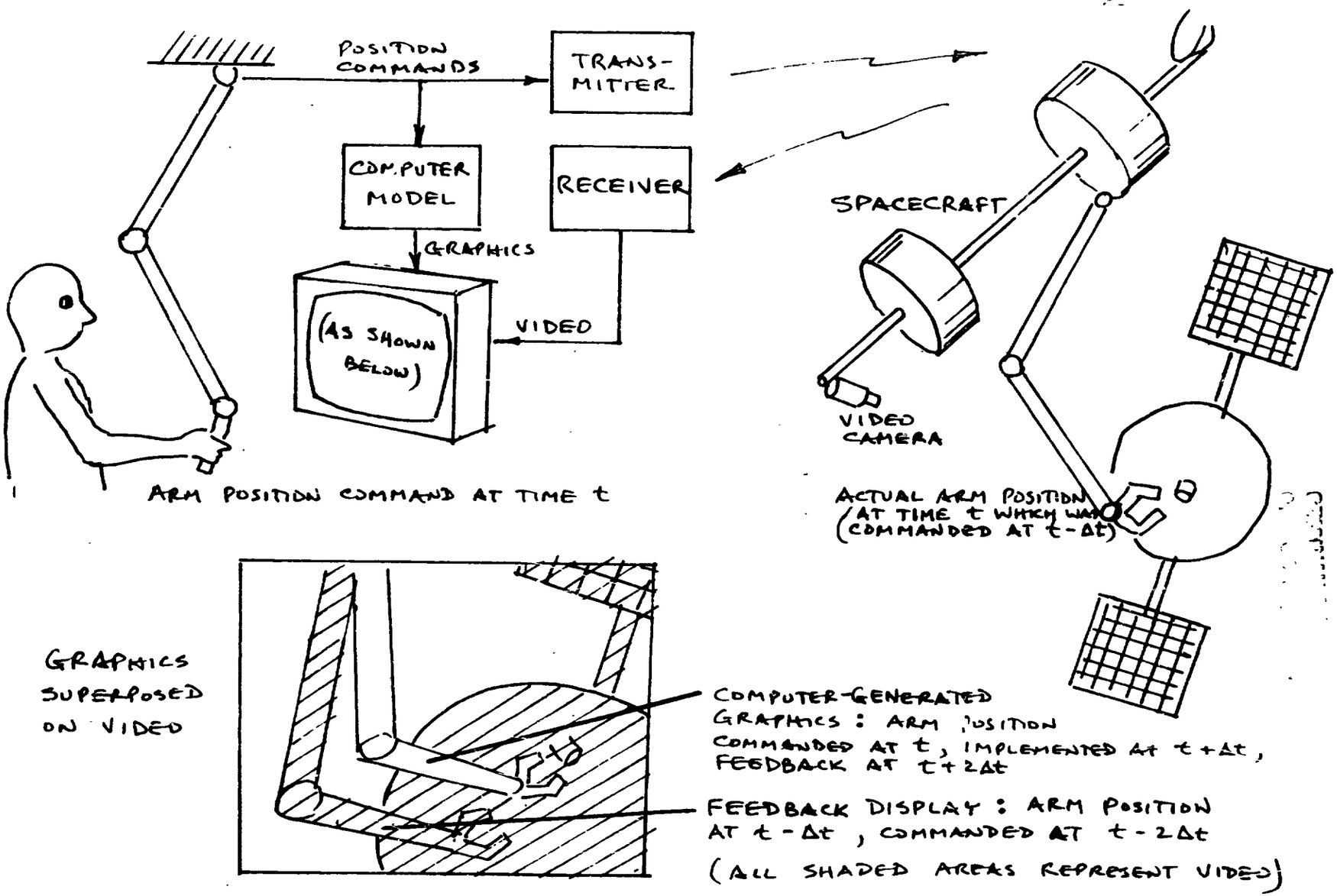

FIGURE 1. SYSTEM FOR REMOTE CONTROL THROUGH TIME DELAY

stiff spring. It may be desired that it be like a spring preloaded to a given level. It may be that it be like a dashpot (damper) with a given constant or some combination of spring and dashpot. Since in general we are talking about six degrees of freedom it may be that each degree of freedom has a different impedance.

An example of impedance control is afforded by the act of opening a door at a fixed angular rate. This requires a high gain or "rigid" position control in the trajectory described by the doorknob. However any inaccuracy in position normal to the arc could rip the doorknob off the door. Thus the impedance in all but one direction wants to be that of a very soft spring with enough damping to prevent oscillation.

In the deep ocean or space environment, as in technical climbing on a rock face, one wants to tether oneself (or the teleoperator) to constrain some motions, but still control one's force-position in other directions. This also poses an impedance control problem.

An analytical technique has been devised to permit the design of an impedance control system.[2] Stability and robustness conditions have been satisfied.

3. OPERATOR ADJUSTABLE BILATERAL TELEOPERATOR

The golfer selects a club from his bag to achieve the desired "feel" when he swings the club and/or when the club head hits the ball. This he does in order to adjust the impedance between his own neuromuscular system and the club as it interacts with its environment. Similarly the baseball hitter selects a bat, the tennis player a racket, the carpenter a hammer, the musician a bow, and so on. The handled "tool" or "implement" is subject, of course, to the impedance between itself and its environment (ball, nail, violin string, etc).

One can imagine that it would be nice to have a teleoperator which "feels" appropriate to the handling task to be done. That is, one would like to adjust the "feel" (to the operator) of the control handle. (Primarily we are thinking of a master-slave manipulator).

We have devised a computer simulation which includes the human arm-hand, the master, the slave, the mechanical environment of the slave, and all the couplings between these including both directions of feedback control between master and slave (e.g., position control from master to slave plus force feedback). This is a complex interaction which has not been well studied or understood in the past, even for only one degree of freedom for each element. With this we are studying questions of performance stability and limits of adjustment.

We are in the process of devising a one-degree-of-freedom force-reflecting mechanical master-slave system (based on DC brushless motor) which has a great deal of flexibility for parameter changes and impedance. This will be used experimentally with actual human operators.

4. SUPERVISORY CONTROLLED SUBMARINE-MANIPULATOR

An unmanned submarine is being constructed and is expected to undergo initial supervisory control trials this summer, first in a tank and then in the Atlantic Ocean.

The vehicle, which we call Sea Grant I, is actually a reconstructed the Perry Oceanographic RECON 5. It is approximately 2 1/2 meters length, weighs approximately 300 Kg, has five individually controlled hydraulic motor thrusters to allow control effectively in all degrees of freedom excepting pitch and roll, has on-board compass, inclinometer, sonar altimeter and a microcomputer.

A video camera can be controlled in pan and tilt. A novel parallel link six-degree-of-freedom manipulator is being designed for its front end. Both are controlled with hydraulic motors.

The onboard computer is connected through 1000 feet of tether to a second microcomputer on the surface, through which the human operator will give supervisory commands. The language structure will be based in large measure on the recently compiled supervisory control structure of Yoerger.[5]

REFERENCES

1. Noyes, Mark V., Superposition of Graphics on Low Bit-Rate Video as an Aid in Teleoperation, SM Thesis, Dept of MEchanical Engineering, MIT, June, 1984.

2. Kazerooni, Homayoon, Ph.D. Thesis, Dept of Mechanical Engineering, MIT, in progress.

3. Raju, Jagganath, Ph.D. Thesis, Dept. of MEchanical Engineering, MIT, in progress.

4. Gallardo, Kleber, SM Thesis, Dept. of Mechanical Engineering, MIT, in progress.

5. Yoerger, Dana, Supervisory Control of Underwater Telemanipulators: Design and Experiment, Ph.D. Thesis, MIT, 1982.

Time Series Modeling

N85 14512 D25

VISUAL SYSTEMS FOR REMOTELY CONTROLLED VEHICLES

Terrence Rezek
Ames Research Center
Dryden Flight Research Facility
Edwards, CA

The Dryden Flight Research Facility of the National Aeronautics and Space Administration's Ames Research Center has been working with unmanned vehicles for 15 years. These Remotely Controlled Vehicles (RCVs) provide valuable research tools for testing aircraft performance in situations too hazardous to risk human operators. Even though the costs for thorough testing of high-performance aircraft continue to rise, this testing could not be reduced without jeopardizing operational pilots who might fly such aircraft after they went into production. RCVs provide an excellent way to test the high risk periods of an aircraft's lifespan than by removing the pilots from physical danger while leaving them in complete control of the vehicle.

Visual systems were simple and direct in the first RCVs. Since the early techniques derived from radio-controlled model work, the beginning visual information system was direct observation. When it was time to test full-scale vehicles, they were dropped from helicopters and flown under the control of a pilot on the lakebed below (Fig. 1). An experienced test pilot sat in an open cockpit copied from those used for simulators and flew the vehicle to within 200 meters of the ground, at which point an experienced RC model pilot took over and landed the vehicle.

Even in these early experiments, the effects of differences in visual information inputs were apparent. Both pilots had direct view of the vehicle, but the test pilot in the cockpit had supplemental information (Fig. 2). The cockpit had airspeed, altitude, angle of attack, control surface positions, and an attitude indicator showing roll, pitch, heading, and sideslip; all telemetered from the flight vehicle. With this information, the test pilot was able to detect and damp out oscillations as the vehicle was being towed by the helicopter. When the RC pilot took over, he was forced to command large excursions in the vehicle so that he could see the results of his command inputs.

Through the years of development which followed, a powerful flight test technique evolved (Fig. 3). The most important feature of this methodology has been the inclusion of the pilot in the control loop. Unlike military drones, an RCV is intended to explore unknown engineering territory, the nature of which precludes the use of autopilots or preprogrammed control systems, unless they are what is being tested. The uniqueness of each flight may require that control systems be changed during a flight to compensate for unexpected responses. Just as in flight testing with human operators, flight profiles and attempted data points may be changed to respond to dynamic conditions.

RCV SYSTEMS

The current configuration of our RCV systems was developed with active input from the test pilots. The cockpits used for RCV flights are based on a common framework (Fig. 4). The layout for instrumentation is largely a matter of pilot preference unless the particular study involves scan patterns, displays, or the effects of innovative instrumentation. In this respect, the

PRECEDING PAGE BLANK NOT FILMED

RCV cockpit is treated as an extension of simulation techniques and is designed to be easily modified. The instrument panels are plug-ins and can be interchanged in a few minutes. The panel formats are not representative of a specific aircraft but are tailored to the immediate task. These cockpit stations also have a graphics display system, an X-Y plotting system, and various input/output (IO) devices.

Despite the variety of potential information systems in these cockpits, the pilots consistently reported difficulty in perceiving position relative to the ground during the last 100 meters to touchdown. Operationally, this is handled by having the flight test engineer, who is always at the RCV pilot's side during a test, call out the closing altitude from a radar altimeter. This was necessary because the pilot's entire attention was focused on the forward field of view, and the only deviation he allowed himself was the briefest of glances at the airspeed. The pilots felt that the workload was unecessarily high and could be reduced with better video. The problem of height perception was critical and felt to be related to the degradation of depth cues.

The visual systems used for the RCVs were developed using a single vehicle (Fig. 5). The Piper Comanche, or PA-30, is our flying workbench, laboratory, simulator, and trainer. Originally used for experimental control systems work, the left seat controls can be operated electrically while the right seat controls are not modified. In addition to its usefulness in developing video systems for RCV forward field of view, the PA-30 was especially valuable for training pilots in the unique environment of remote flight (Fig. 6). The dual controls in the vehicle allow the rapid installation and testing of untried concepts since the vehicle can be instantly returned to normal operation and is always flown with an onboard safety pilot.

When the transition from outside to inside visual systems began, the press of time and the limitations of available equipment dictated a configuration which was functional, if limited. In the PA-30, this took the simple form of a nose mounted camera with a single fixed focal length lens and a single 22 cm (9 inch) diagonal monochromatic monitor. In the training setup, the monitor was mounted in the left side cockpit panel and hardwired to the nose camera. The pilot learned to fly the PA-30 while "under the hood" using only the monitor for forward visual information. In the RCV arrangement, the monitor was atop the cockpit panel inside the RCV facility and the video signal was telemetered down from the vehicle along with aircraft instrumentation information.

A great variety of vehicles were flown with this configuration (Fig. 7). In addition to the PA-30, which is still in use, there was the 3/8 scale F-15 which later became the Spin Recovery Vehicle. High-performance and exotic aircraft were well represented by the HIMAT and DAST vehicles. A vehicle with an oblique wing was tested in a cooperative program with Ames-North. Presently the world's largest RCV, a Boeing 720, is being prepared for the Controlled Impact Demonstration program (Fig. 8).

VISUAL SYSTEMS

There are definite perceptual limitations inherent in a narrow field of view system. Depending on the orientation of the the Line of Sight (LOS) of the video system relative to the vehicle's longitudinal axis, a steep approach may cause the horizon to be lost from view. If the vehicle is pitched up, the runway may not be seen. When close to touchdown with a very narrow field of view, this situation may result in both the horizon and the runway

disappearing. Use of a motorized zoom lens is not acceptable because it would give the pilot another variable and another control at a critical point in the flight. Even a programmed zoom would introduce a variable at a time when the pilot needs a consistent visual field for reference.

All RCV pilots commented on the difficulty of perceiving height during the approach and landing. A possible solution was a three-dimensional video system (Fig. 9). This was tested using an adaptation of a system originally suggested for use with the Space Shuttle Remote Manipulator Arm. Two separate video systems were paralleled and the views presented to the pilot with a fresnel imaging system which did not require the use of special glasses (Fig. 10).

This concept has numerous advantages over other possible stereo displays. Since the fresnel lens collects light over a large field and concentrates it at the exit pupils, image illumination is optimized. The lack of operator worn optical aids is important for RCV work. Cockpit instrumentation and peripheral displays may be scanned without re-accommodating. This mechanization has one major disadvantage; a restriction of available head movement. Visual information is perceived in a realistic manner as long as the eyes are within a 3.3 cm horizontal by 7.6 cm vertical by 15.2 cm longitudinal volume.

This system was evaluated in flight using the PA-30 and met with limited success. In general, the system worked and provided the pilot with binocular vision far beyond the normal 6 meter limit of unaided human vision. However, spacing the viewing lenses at interocular distances necessary to achieve such spatial resolution, produced another perceptual problem. The eye-brain system apparently rescaled the perceived images to match normal interocular distances and caused size discrimination difficulties. In addition, the unavailability of an independent dual video transmission system neccessitated the multiplexing of the incoming signals. Equipment design flaws prevented adequate separation of the received signals and the resultant images were always contaminated with ghosted images. The system was judged to be impractical without extensive development.

PRESENT APPROACH

Flying current RCVs produces a loading effect on the pilots which is due in large part to the restrictive nature of the forward field of view. The normal aspect ratio, broadcast quality, monochromatic video system does not provide the normal visual cues present in live flight. Pilots have been more dissatisfied with this aspect of the system than with any other. Of course, the early work was intended to produce a workable method in the shortest possible time. In that regard, it was successful. However, as the flight tests gained in complexity and the RCV vehicles gained capabilities, the need for augmented video systems became great.

As mentioned, the stereo system was not viable given the current state of development. The spatial perception problem remained. The human (eye-brain) vision system uses many more cues than just binocular disparity to establish spatial position. Among these are relative sizes and perspective in both static and dynamic conditions, and also closure rates and streaming in dynamic conditions. Considering the motion sensitivity of the peripheral vision and the effect of the large human visual field in establishing orientation, a very wide angle video system would seem to answer many of the forward view questions. However, cramming a wide field of view into a limited bandwidth system results in very small images across the entire field and poor resolution. This combination of factors led to the use of a non-linear lens system.

VARVS

The Variable Acuity Remote Viewing System (VARVS) was conceived as a technique for resolving the FOV/resolution/ bandwidth tradeoffs that exist in remote viewing systems (Fig. 11). This system is based on the fact that integration of the human eye acuity function shows only about 130,000 pixels are required to fully support the human vision. This quantity is well within the capabilities of conventional video systems.

The technique utilizes a non-linear optical system in both the sensing and display equipment. The non-linearity is achieved by a special lens which translates a uniform pixel array on its image plane into the object field as a variable angular array. This can be contrasted with the "Fish Eye" wide angle lens which projects into the object field with equal angular increments. In another sense, this lens will record the same angular detail the eye would see when viewing the same scene and compress this detail into a uniform matrix of equal sized picture elements on its image plane. This image can be scanned with a broadcast quality tv having a 525 line raster scan. Conventional transmission equipment can then also be used to send the image information to a remote location. When received, the image is projected by a light valve projector onto a hemispherical screen by an identical non-linear lens (Fig. 12).

This projected image is viewed in apparent high acuity and correct geometric perspective when the observer's eye is aligned with the projector's optical axis. In the original design, an eye position sensor was postulated as a means to eliminate image to eye misalignment by repositioning the sensor through a narrow band control link. This motion subsystem has not been used in RCV work since the vehicles are generally too small to accomodate a slewing camera mount. The camera-lens system alone achieves an effective 140 degree FOV, which is more than usually seen from a normal cockpit. High resolution occurs in a 20 degree cone centered on the head position axis. The head tracking capability will be used in simulator studies.

The key to this idea is the non-linear lens (Fig. 11). This lens was originally designed by McDonnell Aircraft and fabricated from glass using numerically controlled grinding machines, a difficult and expensive process. Modern optical fabrication techniques including laser polishing, plastic casting, and graded density optical materials can be expected to reduce the cost, size and weight.

The difference between the non-linear lens and a fish-eye lens is best seen in comparison. Apparent positive magnification exists near the center of the image, decreasing towards the perimeter. A 525 line raster can extract the same angular detail from this image that would take a 10,000 line raster for the fish-eye image. The very unique properties of this optical system form the basis for a series of psychophysiological studies on the interaction of human operators and Remotely Controlled Vehicles.

LANDING CUE ASSESSMENT STUDY (LCAS)

In LCAS, the peripheral motion thresholds of pilot observers will be quantified in roll, pitch, vertical rate and forward velocity. The Peripheral Visual Cue Assessment Laboratory at Ames North is presently determining these parameters using very sparse computer generated imagery. To successfully apply the results of this study to the real world of flight, it is necessary to verify and amplify those results in a more realistic visual environment.

The motions created by the computer in the laboratory phase of LCAS will be duplicated as closely as possible by video taping live scenes from a precisely controlled camera platform atop a moving truck. These scenes will simulate the subtle maneuvers made during the last moments before touchdown in a normal landing. The responses by observers will be compared to the results of the Ames North Laboratory experiments.

This experiment will be repeated using the PA-30 as an RPV to assess the effect of this visual system on the landing qualities of RCVs.

DOD INTERESTS

The USAF Human Resources Laboratory is using the VARVS as a development tool in the design and evaluation of a full field of view simulator for combat aircraft training. Ultimately, this would envision the use of highly realistic computer generated imagery. Since current equipment of sufficient power to do this in real time is huge, rare, and extremely expensive; interim designs will use the video method to present realistic, interactive scenes to simulator operators.

The United States Naval Ocean Systems Command has expressed an interest in using this methodology to provide better visual input from a free-roaming ground vehicle operating in a forward observer mode.

Both of these applications fit well within the capabilities of the VARVS. Additional development is required for special purposes, such as light weight, probably plastic lenses, for the USAF and ruggedized equipment for the USN.

ORIGINAL PAGE IS
OF POOR QUALITY

Figure 1. The Hyper III reentry vehicle an early full scale RCV

ORIGINAL PAGE IS
OF POOR QUALITY

Figure 2. Early RCV ground cockpit

PRECEDING PAGE BLANK NOT FILMED

NASA
DFRC 79-190

REMOTELY PILOTED VEHICLE (RPV)/REMOTELY AUGMENTED VEHICLE (RAV) FACILITY

PURPOSE: Low Cost Flight Test of Advanced High Risk Concepts on Control Systems Development

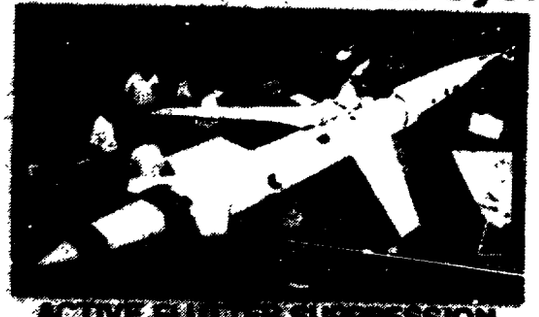

ACTIVE FLUTTER SUPPRESSION TESTING

HIGHLY MANEUVERABLE AIRCRAFT TECHNOLOGY

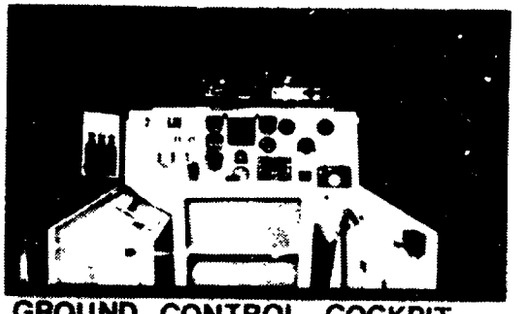

GROUND CONTROL COCKPIT

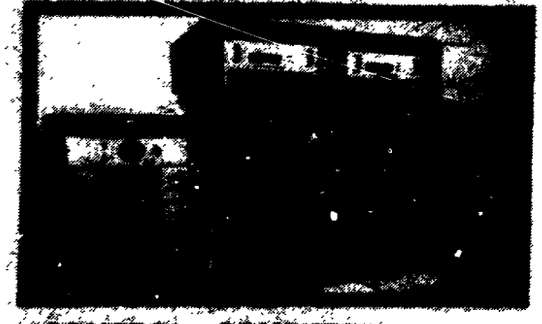

CONTROL COMPUTER

SPIN RESEARCH TESTING

ADVANCED CONTROL LAW VERIFICATION (RAV)

Figure 3. Some aspects of Remotely Controlled/Remotely Augmented Vehicle operations at Dryden

ORIGINAL PAGE IS OF POOR QUALITY

ORIGINAL PAGE IS
OF POOR QUALITY

Figure 4. A typical RCV cockpit at Dryden

PRECEDING PAGE BLANK NOT FILMED

ORIGINAL PAGE IS
OF POOR QUALITY

Figure 5. PA-30 aircraft. Primary camera locations are in the nose and atop the cabin

PRECEDING PAGE BLANK NOT FILMED

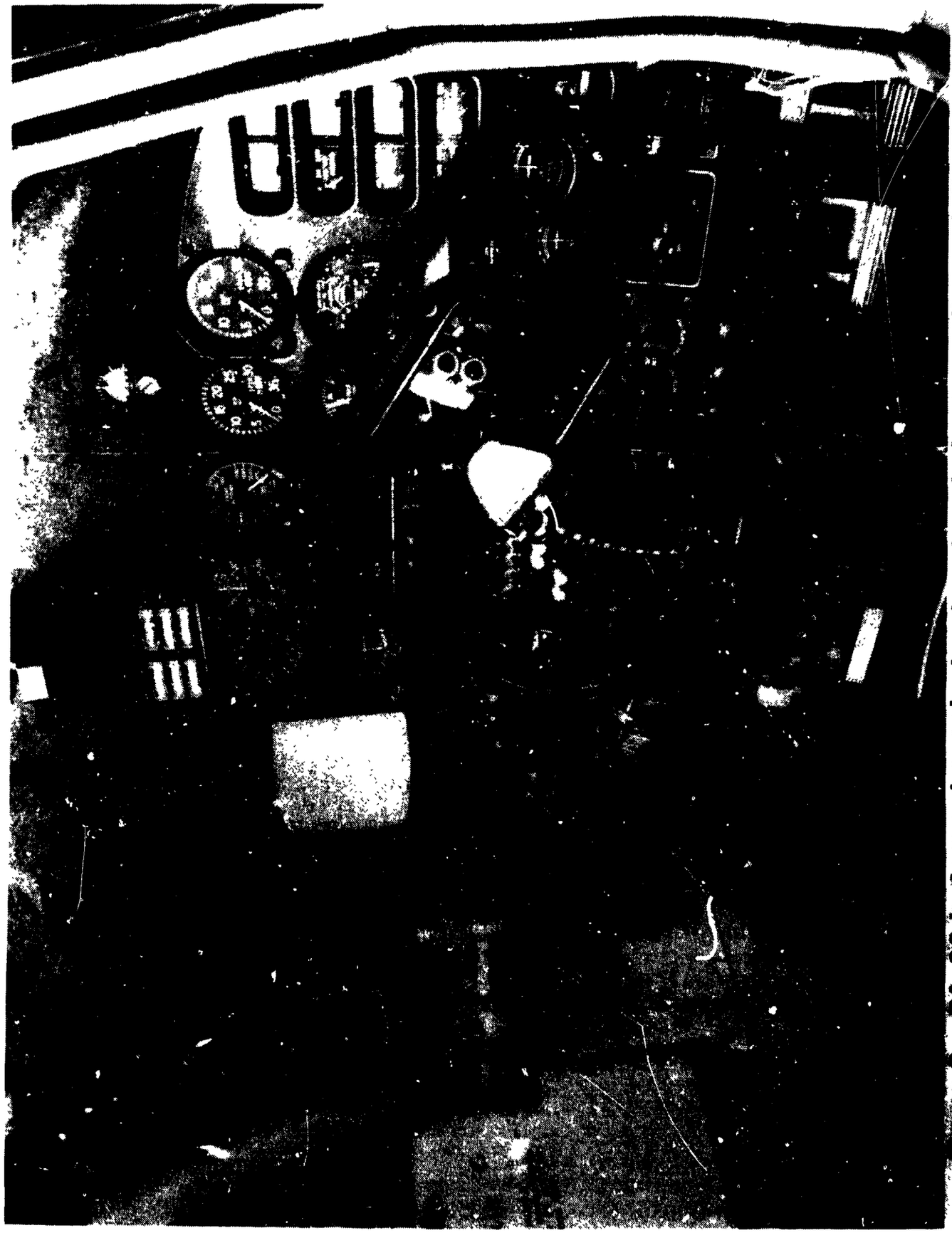

PRECEDING PAGE BLANK NOT FILMED

ORIGINAL PAGE IS
OF POOR QUALITY

ORIGINAL PAGE IS
OF POOR QUALITY

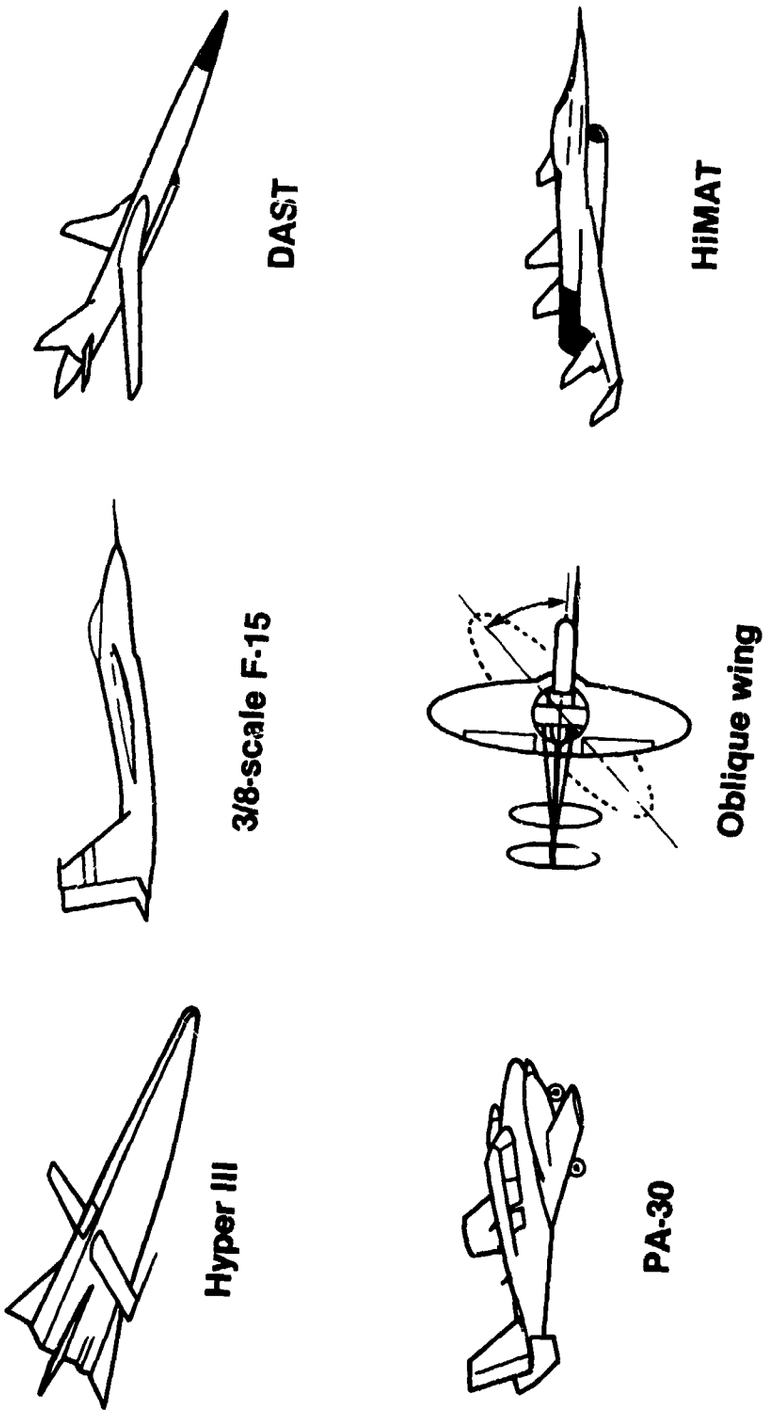

Figure 7. Some RCVs flown at Dryden

PRECEDING PAGE BLANK NOT FILMED

ORIGINAL PAGE IS
OF POOR QUALITY

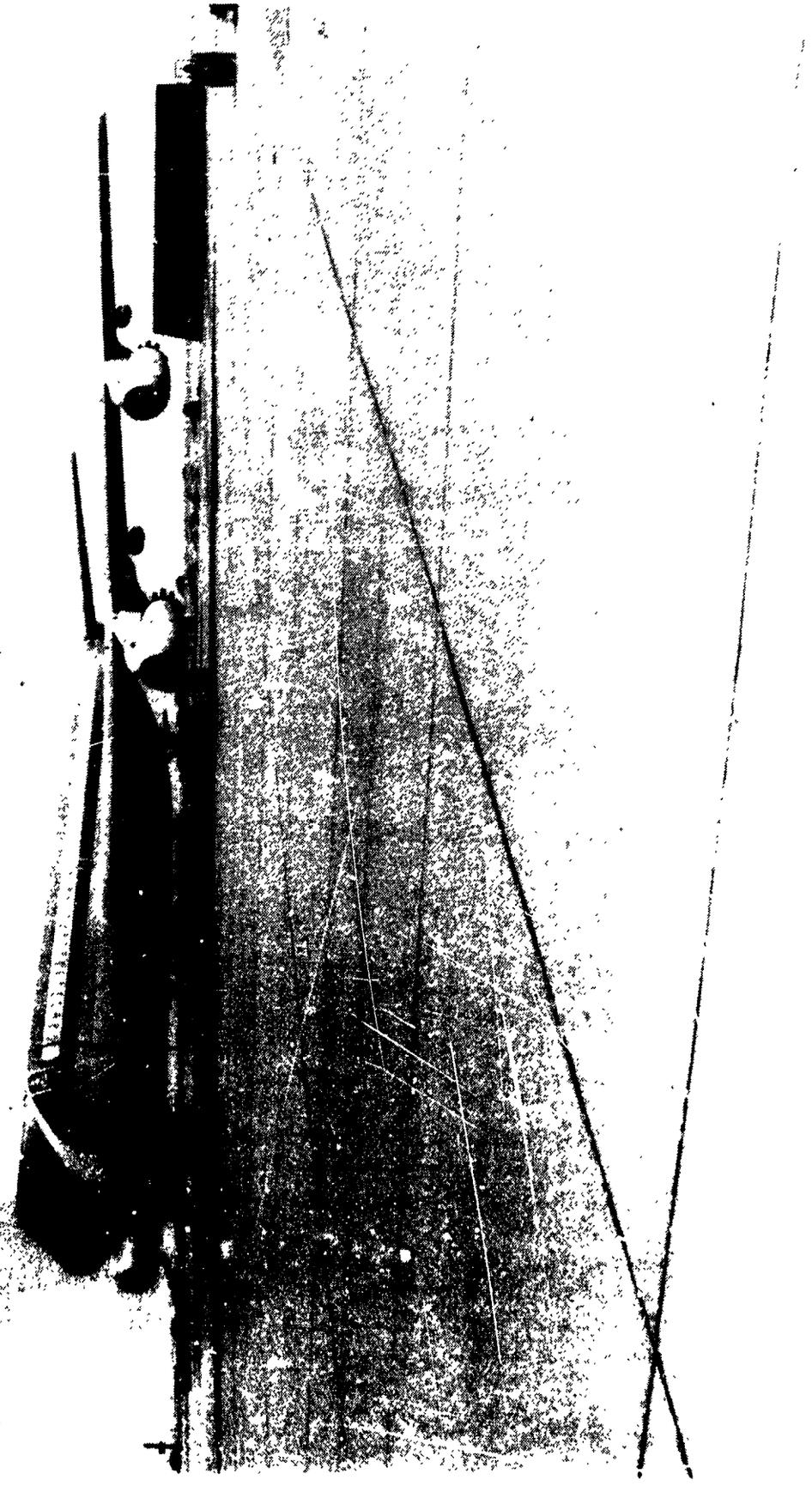

Figure 8. Controlled Impact Demonstration

PRECEDING PAGE BLANK NOT FILMED

ORIGINAL PAGE IS
OF POOR QUALITY

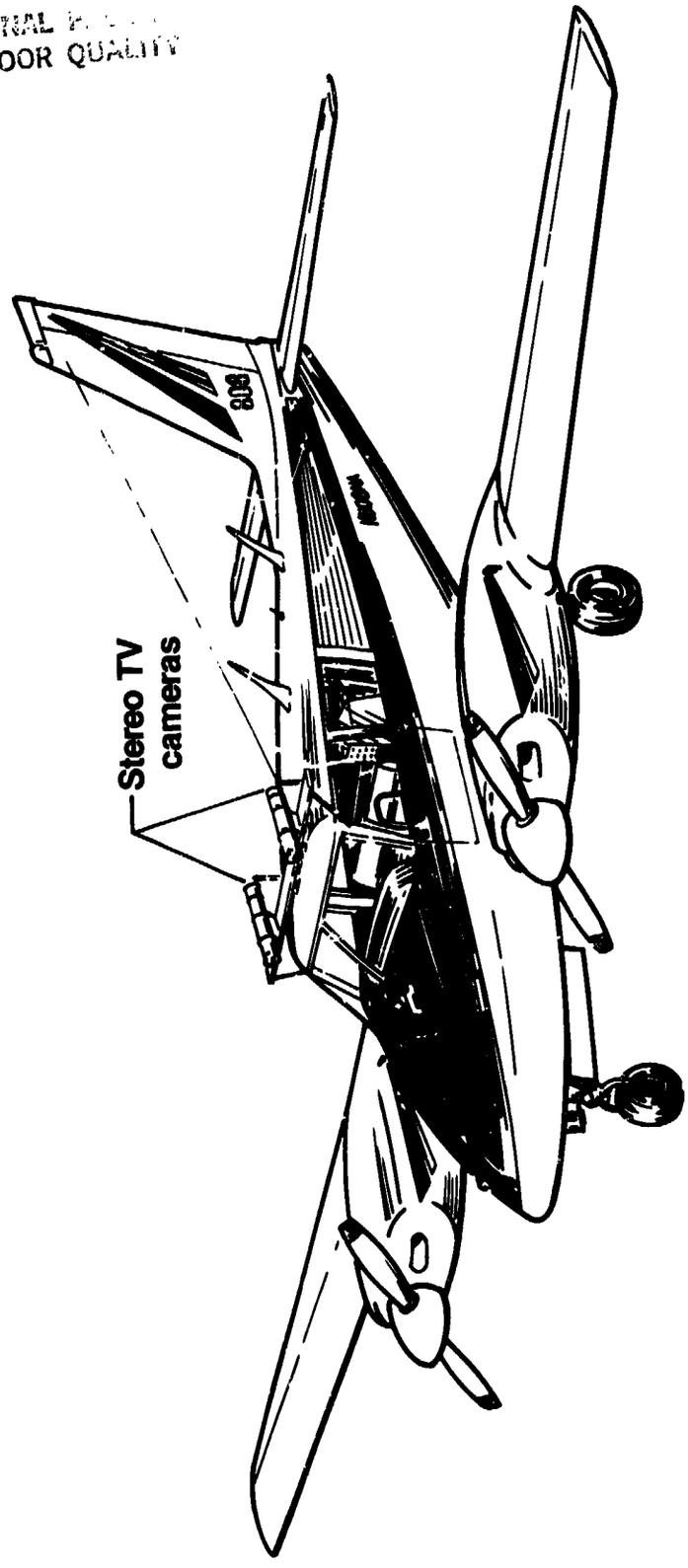

Figure 9. PA-30, showing the location of the Stereo-TV cameras

PRECEDING PAGE BLANK NOT FILMED

ORIGINAL
OF POOR

Figure 10

PRECEDING PAGE BLANK NOT FILMED

NON-LINEAR LENS

LENS RESOLUTION CHARACTERISTICS

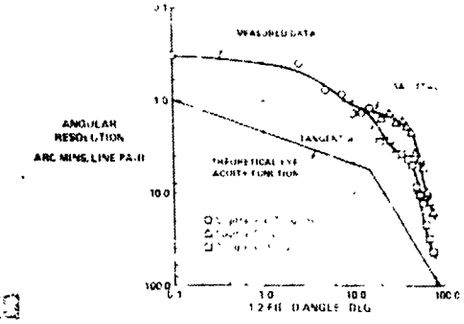

ORIGINAL PAGE IS
OF POOR QUALITY

NON-LINEAR LENS IMAGE

LENS DRAWING

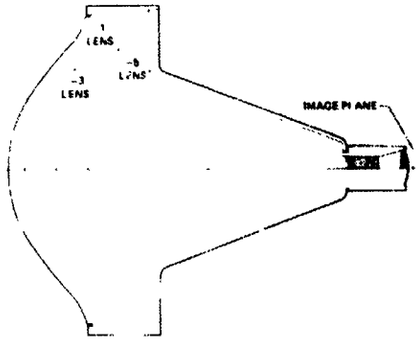

LENS IMAGE/OBJECT TRANSFER CHARACTERISTICS

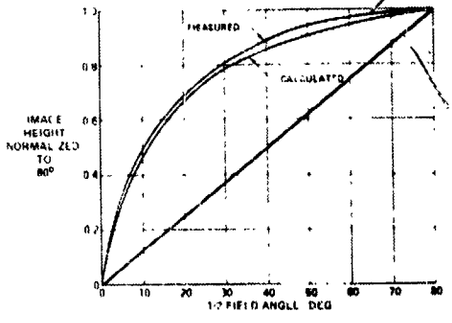

CONVENTIONAL FISH EYE LENS IMAGE

NON-LINEAR LENS USED WITH CONVENTIONAL TV RASTER GIVES

- 160° FOV
- EYE ACUITY RESOLUTION

SIGNIFICANT REDUCTION OF DATA TRANSMISSION BANDWIDTH EVEN IN NARROW FOV APPLICATION

Figure 11. Variable Acuity Remote Viewing System (VARVS)

ORIGINAL
OF POOR QUALITY

Figure 12. VARVS projection dome with RCV cockpit in place

PRECEDING PAGE BLANK NOT FILMED

Table 3, increases both with pilot rating and with the added workload of the three-channel task (as measured by the spectral density).

For the three-channel case studies, the total power in the pilot's aileron deflection signal for each configuration is shown in Figure 9. As in the two-channel ease study, the power spectral density peak magnitude increases for configurations with the higher (worse) rating, suggesting a proportional increase in pilot workload.

It is noted that the peak power tends to occur at the dutch roll frequency for each configuration, indicating that this mode is clearly present if not dominant in the pilot's output. If this is the case this mode may be a contributing cause to the lateral PIO occurring for Configuration 3 (refer to Table 1 for comments).

The plots depicting noise contributions into the aileron and rudder deflection signals are shown in Figures 10 and 11. In addition to the large increase in peak spectral density of Configuration 3 over the other configurations, note that command disturbance noise is not dominant in the frequency range of maximum power as in the two-channel case (Figure 8). In the aileron deflection channel, pilot injected noise contribution exceeds the command disturbance noise contribution. This same trend is even more noticeable in the noise contribution plots for the rudder channel in Figure 11, where the primary noise source is clearly pilot injected noise into the rudder channel.

To summarize the data analysis of the identified models, there is evidence that the cause of the PIO and resultant poor pilot rating is self-induced coupling caused by rudder excitation of a dutch roll mode with level 3 flying qualities. Recall in the two-channel case study for Configuration 3 that no lateral PIO occurred when the rudder input was denied the pilot. The command disturbance in each case was identically provided using Equation (69).

The frequency response of the pilot model, obtained from the approximation of Equation (24), is shown for each configuration for the three-channel cases in Figures 12 and 13. Note that for for poorly rated Configuration 3 that pilot aileron deflection is out of phase at low frequencies with displayed bank angle error.

As seen from the JIR analysis, the amount of information from the identification, validation, and analysis of models obtained from actual

N85 14513 D26

MEASURING WORKLOAD DIFFERENCES BETWEEN SHORT-TERM MEMORY AND LONG-TERM MEMORY SCENARIOS IN A SIMULATED FLIGHT ENVIRONMENT

Scott L. Berg and Thomas B. Sheridan
Man-Machine Systems Laboratory
Massachusetts Institute of Technology
Cambridge, Massachusetts 02139

Abstract

Four highly experienced Air Force pilots each flew four simulated flight scenarios. Two scenarios required a great deal of aircraft manuevering. The other two scenarios involved less manuevering, but required remembering a number of items. All scenarios were designed to be equally challenging. Pilot's Subjective Ratings for Activity-level, Complexity, Difficulty, Stress, and Workload were higher for the manuevering scenarios than the memory scenarios. At a moderate workload level, keeping the pilots active resulted in better aircraft control. When required to monitor and remember items, aircraft control tended to decrease. Pilots tended to weigh information about the spatial positioning and performance of their aircraft more heavily than other items.

Research Supported by NASA Ames Research Center

PRECEDING PAGE BLANK NOT FILMED 395 - 396

I. Introduction

Deregulation is having a profound impact on the airline industry. It has brought increased competition, cut-throat "fare wars", and demands by management for greater employee productivity. This new economic environment has intensified the pressure to cut cockpit crews from three to two persons.

In addition, the nation's airways are becoming more crowded every day, absorbing an ever greater mix of aircraft types, sizes, and performance characteristics. Thus, the need for pilots to spend more time looking outside the cockpit is of major concern.

These conflicting demands for less "in cockpit" workload while simultaneously cutting the cockpit workforce by 33%, have accelerated the push to automate and computerize today's aircraft. New display technologies and microprocessors have led to the widespread use of programmable calculators and a growing number of computer-monitored, computer-flown, and computer-display-dominated flight decks.

This technology has relieved a great deal of the pilot's physical labor in aircraft configured with the latest equipment. However, this equipment has generated its own set of concerns and problems:

(1) At what point and to what extent does boredom or the lack of "something to do" impact performance?
(2) Given that pilots must plan, program, and monitor "automatic" equipment, when do these mental tasks begin to overwhelm a crewmember?
(3) How can this mental workload be measured?
(4) Can one determine how close a given crew member is operating to his or her "breaking point"?

This research examines these questions using a fixed-base simulator. This intermim report looks at the problem of measuring mental workload by subdividing it into short-term mental operations and long-term mental functions such as information "storage" and "retrieval".

II. Objective

This research examines whether certain objective and subjective measures can distinguish between two types of simulated flight scenarios: (1) a scenario emphasizing short-term memory tasks; (2) a scenario with a large number of long-term memory tasks.

III. Simulator Configuration

The flow of information to and from various elements of this experiment is represented schematically on Figure A-1. The PDP-11 Computer acts upon an aircraft dynamics simulation program (four engine Lockheed Jetstar) and presents information on the present flight condition to a Megatek CRT display. (For an in-depth description of the simulation program and aircraft dynamics, see Mental Workload in Supervisory Control of Automated Aircraft, by Tanaka, Buharali, and Sheridan, 1983).

The Megatek display (Figure A-2) simulates an aircraft cockpit display. The upper part of this CRT display gives a simplified "out the window" perspective of an airport and three runways. Below this is a set of instruments in the familiar "T" pattern. An Airspeed Indicator, Attitude Deviation Indicator (ADI) with Glide Slope Deviation Indicator (GSI), and Altimeter comprise the top row. A Horizontal Situation Indicator (HSI) with the selected course (CRS) and distance (DME) to a selected navigation aid, is directly beneath the ADI. A Vertical Velocity Indicator (VVI) is to the right of the HSI. Landing Gear Position (Up, Down), Flap Position (Up, Down), Thrust Setting, Stability Augmentation Selection (On, Off), Navigation Radio Selection (Off, VOR, ILS, channel number), Lateral Autopilot Selection (Off, Manual Heading, VOR Course, Localizer Course), and the Longitudinal Autopilot Selection (Off, Altitude Hold, Speed Hold, Altitude/Speed Hold, Glide Slope/Speed Hold) are also presented.

The subject interprets the displayed flight information and manipulates the controls on the Control Box (Figure A-3) to make the "aircraft" respond in a desired fashion. The Control Box contains an aircraft-type control-stick or joy-stick, a throttle, and a number of other controls. On the top-rear of the box are eight Radio Toggles. To the left of the Throttle are the Course Set Knob and the Flaps and Landing Gear Selector. To the right of the joy-stick is a longitudinal Trim Control. The front panel has six controls: Heading Set Knob, VOR/ILS Selector; Lateral Autopilot Selector; Longitudinal Autopilot Selector; Radio-Navigation Channel Selector; and Stability Augmentation Selector.

Electrical signals convey information on control positions from the Control Box to the Computer. The Computer then uses these inputs to update the flight condition, aircraft dynamics, and display.

The Experimenter (XPRMNTR) interacts with the Computer via a separate Video Display Terminal (VDT). After experimental runs are completed, the experimenter can get an output of data stored by the Computer, on a Line Printer.

IV. Data

Every ten seconds, the computer stores aircraft x, y, and z positions. In addition, it stores every control box manipulation along with the magnitude and time of the event. This data yielded Ground Track information. By correlating the aircraft's x, y position with time and the chosen scenario, altitude error was derived.

Since part of each flight consisted of maintaining certain magnetic courses, altitude deviations were much more useful than heading deviations could have been. Furthermore, since the aircraft responds to altitude change commands more quickly than airspeed change commands, and since the range of altitudes and potential altitude deviations are much greater, altitude information was better than airspeed data for monitoring flying precision. This altitude error data was converted into Absolute Altitude Error (Feet) and Root-Mean-Square (RMS) Altitude Error (Feet).

Subjects were simply instructed to follow instructions as precisely as possible; thus, they had no indication of what types of deviations would be used as the scored parameter.

In addition, each subject scored a set of five Subjective Workload Ratings at three points during each run. These Subjective Ratings were Activity-Level, Complexity, Difficulty, Stress, and Workload. Ratings were taken at three points rather than taking one overall rating to see if any "point" loading of workload might be occuring and biasing the ratings.

V. Subjects

Four subjects participated in this experiment. All four were highly experienced Air Force pilots and had flown this simulator several times. An experience summary follows:

B:	Fighter-Type:	1250 Hours
	Jet:	1250
	Total:	1250
H:	Fighter-Type:	3200
	Jet:	2750
	Total:	3200
L:	Light Aircraft:	550
	Fighter-Type:	1000
	Heavy Aircraft:	600
	Jet:	1000
	Total:	2150
W:	Light Aircraft:	100
	Fighter-Type:	700
	Heavy Aircraft	1300
	Jet:	2000
	Total:	2100

VI. Instructions

Figure A-4 is a reproduction of the typewritten instructions given to each subject before each session. A few points require emphasis or explanation. Subjects were instructed to fly as "precisely" as possible. Further, all simulated ARTCC instructions were handled verbally between the subjects and experimenter. The CWS switch is the Stability Augmentation Switch mentioned in Section III.

Along with these instructions, two other items were given each subject. A Subjective Rating Sheet (Figure A-5) was provided, and the subjects were asked to examine it and ask questions pertaining to it. They were instructed to consider each scale as continuous rather than discrete. That is, the subdivisions were provided simply as references for the subjects and

experimenter. Each score sheet was used for one day's activities: two runs. Subjects were also instructed that they would give each of the ratings three times during each run, and were to place a 1 at their first rating, a 2 at their second rating, and a 3 at their final rating, as well as give an overall rating (T).

Figure A-6 was also provided, and served as a reference for rating Workload. This "Modified Cooper-Harper" system was adopted from earlier work by Sheridan and Simpson. (See Ref. 18)

VII. Experimental Design

As mentioned in the instructions of Figure A-4, there were two different ground tracks used. Each subject flew both ground tracks during each session. Two different ground tracks were employed in order to minimize the effects of transfering prior knowledge from one run to the next, "learning" the scenario, and consciously or subconsciously anticipating tasks.

Each ground track was flown in two versions. One version was highly loaded with a number of tasks to perform. Most of these tasks were similar to following the instruction, "Climb and Maintain 4000". Such tasks exercise short-term memory because, in executing them, the pilot must constantly remind himself to follow the new parameter. The second version exercised long-term memory by instructing subjects to take some action at some time in the future.

Ground tracks and versions were counterbalanced between and within subjects. Each day's data runs included one run of each ground track and one run of each version (long-term memory and short-term memory).

"Navigational Charts" and Note Pads were provided to enable pilots to record instructions (as in real flight). The Navigational Charts contained Navigational Aid positions, courses, bearings, point identifiers, and distances to and from various points.

Figure A-7 shows such a "Navigational Chart" for the alpha ground track. Subjects began heading 360 degrees at 5000 feet, five nautical miles (nm) due south of VOR #1. They then proceeded to Point A (VOR #1: 021/15.0), VOR #2, Point B (#2: 228/10.0), Point C (#1: 144/5.0), and then headed 045 degrees until intercepting the Localizer for an ILS to Runway 36 (ILS 4).

Figure A-8 shows the nominal alpha ground track flown in its skill - or task-loaded version. Please note how ARTCC directed headings result in significant ground track deviations from the direct course. Figure A-9 pictures the nominal alpha ground track in its memory (long-term memory) version.

Figures A-10, -11, -12 are the corresponding examples for the beta ground track. Referring to Figure A-11, subjects began on a heading of 045 degrees at 5000 feet, Southwest of VOR#2. Then, they proceeded to VOR #2, Point D (#2: 312/22.8), VOR #1, Point E (#1: 156/6.7), and then headed 045 degrees until intercepting the localizer for Runway 36 (ILS 4). Figure A-12 clearly shows the 360 degree turn which is directed at VOR #1 for this version.

The differences between the skill- or task-loaded scenarios (short-term memory) and mentally- or memory-loaded scenarios (long-term memory) is best illustrated by picturing the time history of altitude, heading, and airspeed for each.

Figures A-13 and A-14 illustrate the airspeeds which subjects were commanded to maintain for each version of the alpha groundtrack. Compare task-loaded Figure A-13 with memory-loaded A-14.

Similarly, Figure A-15 can compared to Figure A-16 for Magnetic Headings. Finally, Figure A-17 can be compared with Figure A-18 for commanded Altitudes.

Every effort was made to make the alpha and beta ground tracks as similar as possible while mal ing the task and memory versions as different as possible. Thus. total Mental Workload Units and Total Physical Workload Units were calculated and plotted for each ground-track/memory-version combination.

The technique used to calculate these "Workload Units" can best be explained with two examples. For a task such as, "Climb 1000 feet", it was assumed that the pilot would climb at approximately 1000 feet per minute. The pilot must respond to the instruction, initiate the climb, monitor his progress in the climb, and execute a level off. For a 1000 foot climb, this entire proces was estimated to last 90 seconds. Workload Units were calculated for 30 second intervals, so this task required 1 Workload Unit (WU) for three 30 second intervals, or three Physical WU's. However, in the process of performing this task, the pilot had to constantly update his short-term memory with this immediate goal: climb 1000 feet. Thus, the task <u>also</u> was credited with three memory or mental WU's, and labeled a short-term memory task.

For an example of a long term memory task, assume that ARTCC directs, "Report at Point D". The pilot must respond, usually make some note of the request, keep it in mind until he gets to Point D, and then report arriving at Point D. This also requires both task and memory work. It was assumed that the initial response and copying of the request would be handled in one, 30 second task unit. The same applied to the call to ARTCC at Point D. So this task generated one 30 second task unit at the time of the request, and one unit at the time of fulfilling the request. When receiving the request, the pilot stores it in his memory and hopefully retains it until arriving at Point D. Thus, it required one 30 second mental WU for each 30 second period from the time of the request until arriving at Point D. It also counts as one long-term memory task.

A Time/Workload history was done for each task the pilots were expected to perform for each ground-track. These workloads were then combined for each ground-track/version and plotted against an approximate time-line. Figure 19 is an example of one of these workload plots. Standing alone, these charts are not very enlightening, but they were useful for plotting workload data.

For instance, Figure A-20 shows the Accumulative Number of Physical WU's as a function of time for each type of run. This graph suggests that the physical workload is higher for the skill- or short-term memory versions than the long-term memory versions. Furthermore, it looks like the rate of

physical workload for the alpha and beta ground-tracks are similar within each version.

Figure A-21 is a plot of the Accumulative Mental (Memory) WU's versus time. Again, it appears that within each version, alpha and beta scenarios are similar, and that the overall workload for the skill version is different from that for the memory versions.

Figure A-22 shows the Accumulated number of memory tasks as a function of time. Here, the short-term memory tasks of the skill-or task scenarios balance out the additional long-term memory tasks of the memory versions. Thus, although the physical and mental workloads vary in some details across versions, the total number of mental tasks are roughly equivalent for each.

Figure A-23 breaks out the long-term memory tasks and shows that the long-term memory versions have roughly twice the number of long-term tasks as the short-term memory versions. Notice, also, the good balance between the alpha and beta ground tracks for each version. Comparing Figures A-22 and A-23, one can see that the skill versions must have a higher number of short-term memory tasks than the long-term memory versions.

VIII. Training and Experimental Procedure

After the subjects read the instructions (described in Section VI) and had all their questions answered, they then spent 20 to 30 minutes flying the simulator. This practice consisted of changing headings, altitudes, airspeeds, intercepting courses, and several ILS approaches.

When they felt ready, the subjects were given the Navigational Charts to study (Section VII) and the Charts were explained to them. The data runs then began with the Computer storing x, y, z positions every 10 seconds, and Control Box inputs as they occured. The runs were frozen at roughly 8 to 10 minutes and 18 to 20 minutes of elapsed time. These two freezes and run termination were used to take the subject's Subjective Ratings.

IX. Results and Comments

The Subjects' Subjective Rating data is summarized in Figure A-24. Each rated category's mean rating and rating standard deviation are given for both alpha and beta ground-tracks, and for the arithmetic combination of alpha and beta.

Student t-tests and F-tests were performed on the data with the following results. For both long- and short-term memory versions, there were no significant difference between alpha or beta ground tracks at the 95 percent confidence level for any of the five categories. This implied that the effort to make the workload levels similar for the two ground tracks was successful from the standpoint of pilot perceptions. For each type of run

(for example, alpha/long-term memory), there was no significant difference between segments 1, 2, or 3 at the 90 percent confidence level. This implied a low likelihood of "point loading" occuring. That is, workload was fairly constant over time.

Student t-tests were performed on the mean subjective ratings to determine if there was a significant difference between the skill and mental versions for each category. There was a statistically significant difference at the 90 percent confidence level for Complexity and Stress. The difference was significant at the 95 percent level for Activity-level, Difficulty, and Workload.

The weaker confidence levels for the Complexity and Stress ratings can possibly be explained. All runs were performed manually, that is, with the autopilot off. Thus, the "complexity" changed little. The relative weakness in the Stress rating may be due to the relatively low workload level. Future experiments, run at greater workload levels, may show greater sensitivity for this rating category.

The Skill or Short-term Memory version was consistently rated higher (harder, more difficult) than the Mental or Long-term Memory version. This was a bit surprising since the average total (physical and mental) workload for the long-term memory version was greater than that for the task version. (218.5 WU vs. 187 WU: 116.8 percent)

Since other tests gave good confidence in the validity of this "workload unit" technique, several possible explanations come to mind. The 17 percent difference in workload units may not be significant at these workload levels. (One should keep in mind that the mean workload ratings were only in the three to five range on a ten-point scale.) Second, because subjects were "busier", doing a greater number of relatively simple tasks, this may have translated into a perception of greater workload.

Figure A-25 shows the Root-Mean-Squared (RMS) Altitude Deviations and the Mean and Standard Deviation of the Absolute Altitude Deviations. (Altitude Deviations were not measured during climbs and descents.) This information is given for each subject and across all subjects. It is also broken down, giving values for alpha and beta scenarios, and combined alpha-beta scores for the short-term memory and long-term memory versions.

Student t-test analyses of these errors for short-term memory versus long-term memory indicates a significant difference between these versions. Mean Absolute Altitude Errors are significant at an 80 percent confidence level and RMS Altitude Errors are significant at a 70 percent confidence level.

The relative weakness in differentiating the two versions may be due to the fact that there was no "baseline" version. Both versions were designed to be difficult, but difficult in different ways. The data only produced small differences between two fairly well-matched versions. Furthermore, both versions were rated only moderately difficult. If subjects are worked harder in future tests, more meaningful distinctions may appear.

Referring to Figure A-25, both the Mean Absolute Altitude Error and the RMS Altitude Error were greater for the long-term memory case than the short-term memory case. This is somewhat surprising since reference to Figures A-17 and A-18 clearly show that the short-term memory case had a much more difficult Altitude profile.

One possible explanation is that subjects became bored during the long-term memory scenario. I reject this hypothesis for three reasons. (1) No individual run lasted more than 30 minutes, and runs were broken by several "freezes" for subjective ratings. (2) Subjects knew that their performance was being measured, increasing interest. (3) The long-term memory version had few "quiet" periods longer than several minutes. Therefore, boredom was unlikely.

Two other, more promising, explanations relate to interest or attention. In the short-term memory or skill version, subjects were repeatedly asked to change airspeed, altitude, and heading. Thus, they probably channelled more effort and attention to these tasks, resulting in smaller deviations. This would also help explain the slightly higher subjective ratings for this version.

Alternatively, another type of prioritizing may have occurred. Given a lower task workload, the subjects may have shifted the task of aircraft control to a lower priority. This would produce a certain level of complacency about altitude, while subjects paid additional attention to memory items.

Mean Absolute Altitude Errors and RMS Altitude Errors were compared with the Subjective Ratings for each of the five Subjective Categories. For all cases, the magnitude of Altitude Error was inversely proportional to the Subjective Rating. That is, task loading resulted in lower Altitude Errors than mental loading, but higher Subjective Ratings.

Figure A-26 gives data on Long-term Memory Errors. (An example of a long-term memory task was given in Section VII). However, this chart further differentiates among long-term memory tasks. Here, these events were divided into "Positional" and "Non-Positional" Memory Tasks. A "Positional" task pertains to some performance required of the aircraft. For example, "Descend to 3000 at Point D." A "Non-Positional" task refers to something required of the pilot. For example, "Report at Point D".

Although it's difficult to generalize because of the small total number of tasks, the percentage of forgotten "Positional" tasks was similar for all versions/ground tracks, and the percentage of forgotten "Non-Positional" tasks was also similar for all versions/ground tracks. The interesting part of this data, however, lies in the fact that, on average, only 12.5 percent of "Positional" tasks were missed, while 40.6 percent of "Non-Positional tasks were missed.

Professional Pilots are constantly reminded that no matter what happens, maintaining aircraft control should be their top priority. Therefore, this "Positional" information is given first priority. ARTCC requirements for informaton, etc., may be given second, or even third priority. This lower

priority for "Non-Positional" tasks may explain the poorer performance for these types of memory tasks.

X. Findings and Conclusions

1. Alpha and beta ground-cracks were roughly equivalent in perceived workload.

2. During each run, the perceived workload did not vary significantly with time.

3. At a moderate workload level, subjects consistently ranked the task-loaded version more diffiuclt than a memory-loaded version, even though both were designed to be equally demanding.

4. At a moderate workload level, higher subjective workload ratings correlated with lower altitude deviations, possibly due to greater subject interest or attention.

5. Higher Long-term memory workload appears to interfere with, or lower the priority of short-term memory items.

6. Objective measurements (Altitude Error) differentiated between long-term and short-term memory scenarios at a 70 to 80 percent Confidence Level.

7. Pilots systematically weighted information about the physical positioning of their aircraft in space more heavily than other items.

8. Subjects can be worked much harder in future tests.

XI. Follow-up Studies

The next phase of this investigation will build upon these results to further differentiate between task or short-term memory workload, and long-term memory workload.

In an attempt to widen the differences between task workload and memory workload, the following scenarios will be tested:

Workload Type	Aircraft Control
Baseline Scenario	Manual
Task (Short-term Memory)	Manual
Memory (Long-term Memory)	Autopilot
Overload	Manual

The Baseline scenario will be a low workload scenario.

The Task scenario will be similar to the Baseline scenario, but involve many additional tasks: Heading changes, Altitude changes, Airspeed changes. The simulator will be manually flown and long-term memory items will be kept to a minimum.

The Memory scenario will allow the subjects to use the autopilot, freeing them to remember, monitor, and plan. Tasks will be kept to a minimum, but subjects will be repeatedly told to remember certain things for various lengths of time and then perform the directed tasks.

Finally, an "Overload" scenario will attempt to saturate the subjects. Subjects will be forced to fly manually while performing a large number of tasks and told to remember and do a variety of things.

Civilian pilots with less flight experience than the present subject group will be added.

Altitude Deviations, Subjective Ratings, and the percentage of memory items which are missed or not executed properly will be noted.

We postulate the following results:

1. Workload ratings will directly relate to prior flight experience.

2. Subjects of all experience levels will do equally well and give similar ratings for the Memory Scenario.

3. There will be a direct relationship between performance, ratings, and experience for the Task and Overload Scenarios.

4. If given enough memory items, workload ratings will be as high in the Memory/Autopilot Scenarios as the Task/Manual Scenarios.

5. As workload ratings approach the high end of the scale, memory errors, or altitude deviations, or both will increase.

6. Subjects will tend to allow the number of memory errors to increase rather than aircraft control to decrease.

XII. References

1. Heffley, R. K. and Jewell, W. F.; Aircraft Handling Qualities Data, NASA CR-2144, Dec. (1972).

2. McRuer, D., Ashkenas, I. and Graham, D.; Aircraft Dynamics and Automatic Control, Princeton (1973).

3. Sheridan, T. B.; Simpson, R. W.: Toward the Definition and Measurement of the Mental Workload of Transport Pilots, DOT-OS-70055, Jan. (1979).

4. Anon.; Air Traffic Control, U.S. Air Traffic Service, Federal Highway Administration, 7110.65c, Jan. (1982).

5. Anon.; A300FF Minimum Flight Crew Determination, Airbus Industries, AI/VF-AI/TE4-023/82, Jan. (1982).

6. Soulsby, E.P.; Human Operator Workload; A Survey of Concepts and Assessment Techniques, Technical Report of EECS TR-82-4, School of Engineering, University of Connecticut (1982).

7. Johannsen, G. and Rouse, B.; Studies of Planning Behavior of Aircraft Pilots in Normal, Abnormal, and Emergency Situations.

8. Sheridan, T. B.; Supervisory Control: Problems, Theory and Experiment for Application to Human-Computer Interaction in Undersea Remote Systems, Man-Machine Systems Laboratory, Technical Report, MIT, March (1982).

9. Sheridan, T. B.; Mental Workload in Decision and Control, Proc. of IEEE (1979) pp. 997-982.

10. Bird, K. L.; Subjective Rating Scale as a Workload Assessment Technique, Proc. of 17th Annual Conf. on Manual Control (1981).

11. Hart, S. G.; Childress, M.E. and Bortolussi, M. R.; Defining the Subjective Experience of Workload, Proc. of the Human Factor Society 25th Annual Meeting (1981) pp. 527-531.

12. Hart, S. G.; Effect of VFR Aircraft on Approach Traffic with and without Cockpit Displays of Traffic Information, Proc. of 18th Annual Conf. on Manual Control (1982).

13. Hauser, J. R., Childress, M. E. and Hart, S. G.; Rating Consistency and Component Salience in Subjective Workload Estimation, Proc. of 18th Annual Conf. on Manual Control (1982).

14. Hart. S. G., Childress, M. E. and Hauser, J. R.; Individual Definitions of the term 'Workload', Proc. of 1982 Psychology in the DOD Symposium (1982).

15. Childress, M. E., Hart, S. G. and Bortolussi, M. R.; The Reliability and Validity of Flight Task Workload Ratings, Proc. of the Human Factor Society 26th Annual Meeting (1982) pp. 319-323.

16. Rasmussen, J.; Outlines of a Hybrid Model of the Process Plant Operator, in Sheridan, T. and Johannsen, G. Eds., Monitoring Behavior and Supervisory Control, Plenum, N.Y. (1976).

17. Sheridan, T. B.; Proposal to Study the Relationship between Aircraft Control Automation, Mental Workload and Pilot Error in a Laboratory Simulator.

18. Tanaka, K.; Buharali, A.; and Sheridan, T. B.: Mental Workload in Supervisory Control of Automated Aircraft, Proc. of 19th Annual Conf. on Manual Control (1983).

A-1

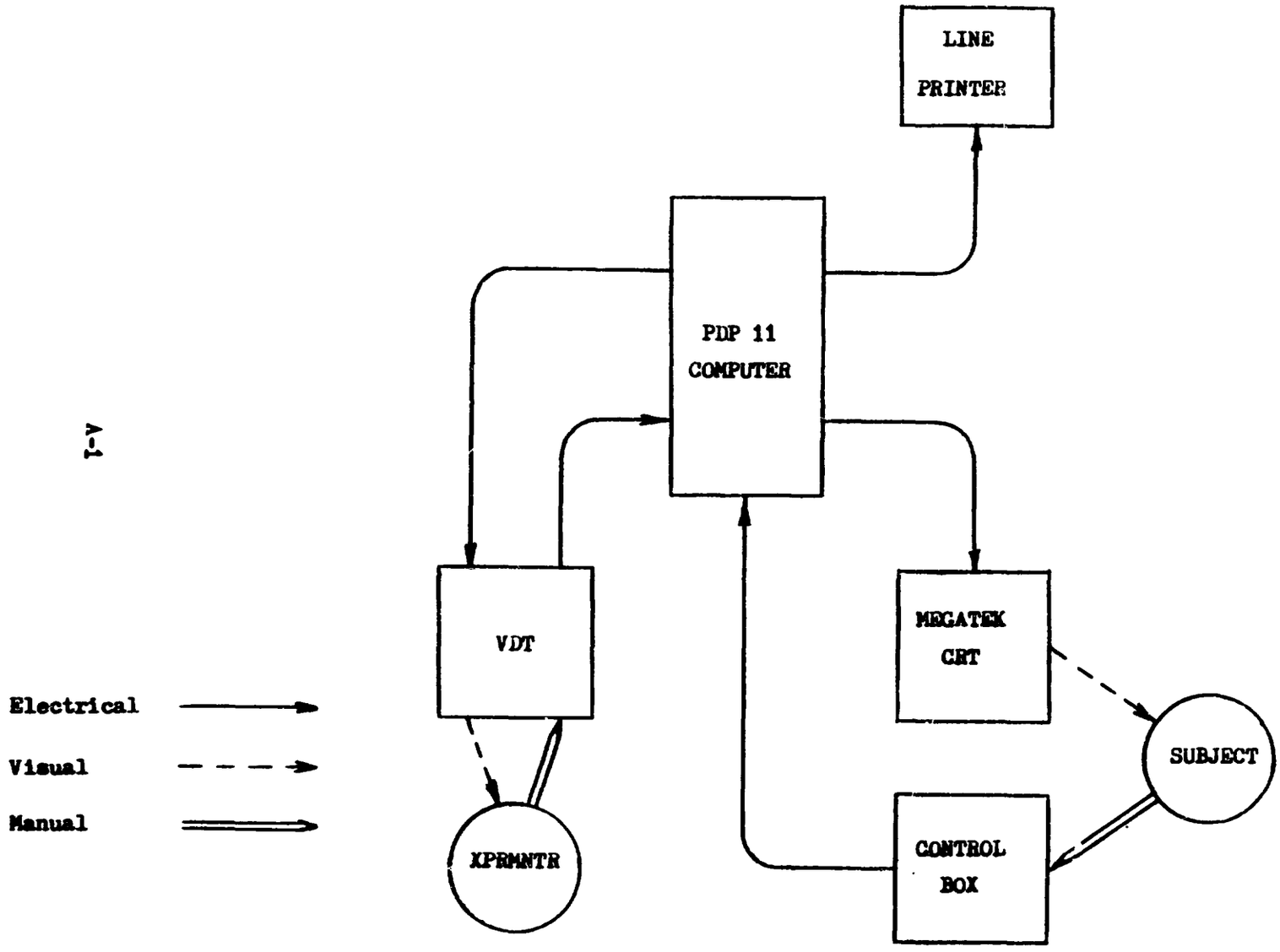

EXPERIMENTAL SET-UP

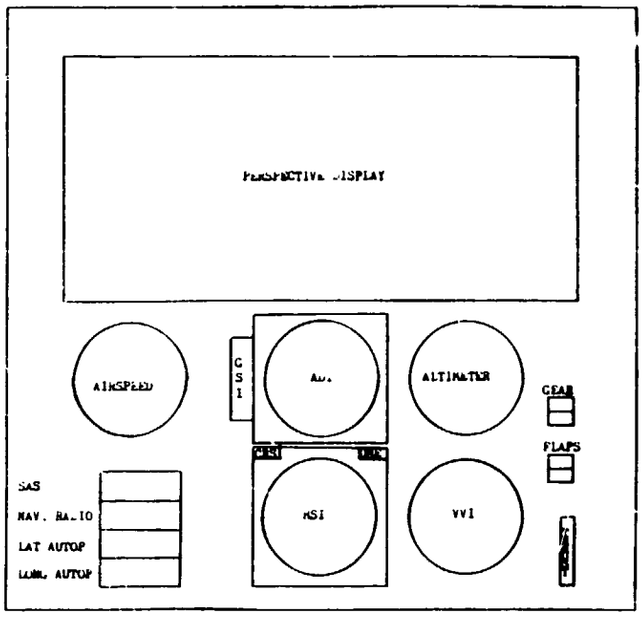

RELATED CRT DISPLAY

A-2

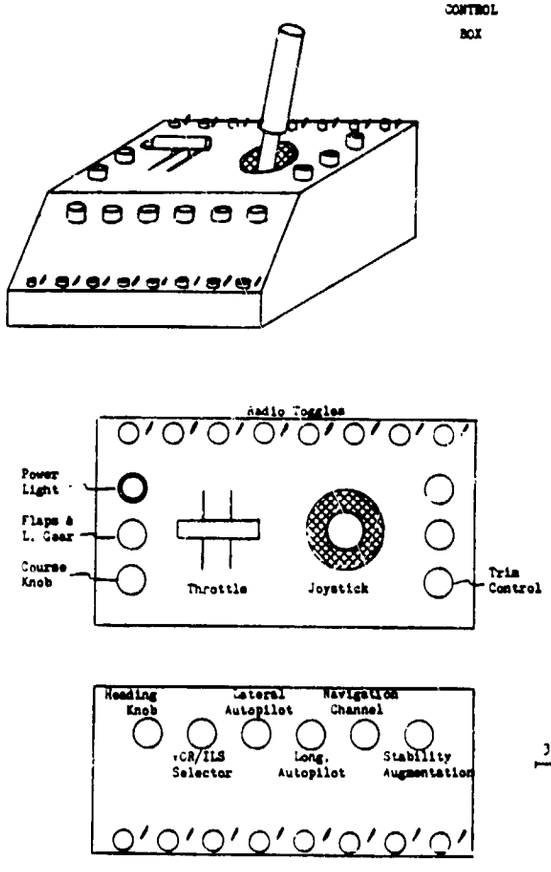

A-3

INSTRUCTIONS

The experiment you are participating in will provide information on pilot workload. The experiment consists of four "flights": two now and two another day. On each day you will fly two different ground tracks, terminating in an ILS approach. For each flight, the number of manual and control tasks will be varied.

Your task is to fly as precisely as possible while following instructions to the best of your ability.

Ignore any ATC statements or instructions which appear on the display. All instructions and ATC statements will be handled verbally. However, when contacting a new "Controller", toggle off (away) the old radio and toggle on (toward) the new channel. Since all flights will be performed manually, you can ignore the two autopilot controls. In addition, the Trim and CWS switches are best left as set.

You will use 3 Navigation aids: VOR 1, VOR 2, and ILS 4. ILS 4 provides an ILS for Runway 36. Please note that the signal is only received within 10 miles of the runway. So, when on a degleg to the ILS, hold heading until the Course Deviation Bar comes off the stops or the Glide Slope Indicator shows movement.

The "nominal" airspeed for these runs is 200 kts. Final approach will be flown at 150 kts. with Gear and Flaps down. Usually, a throttle position near center will maintain a stable airspeed.

You can expect the following level flight attitudes:

200 kts:	Clean	-2 deg
	Flaps	-5 deg
	Gear & Flaps	-2 deg
150 kts:	Clean	0 deg
	Flaps	+2 deg
	Gear & Flaps	+6 deg

During and after each run, you will be asked to make several subjective ratings. Thank you for your time and effort.

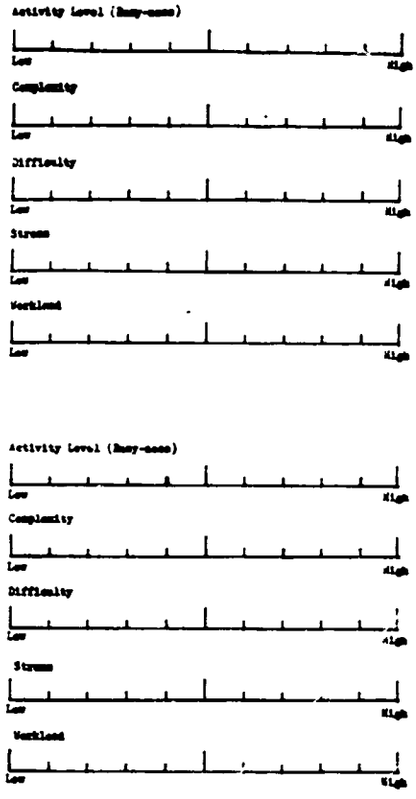

Subjective Rating Sheet

ORIGINAL PAGE IS
OF POOR QUALITY

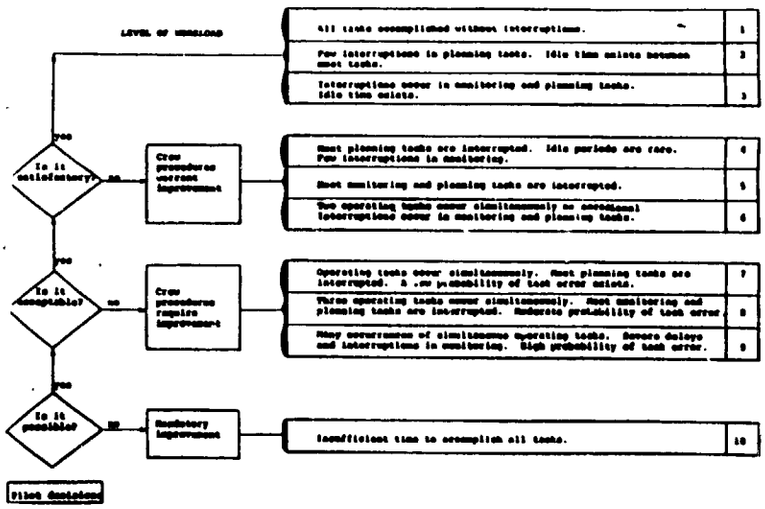

WORKLOAD RATING SYSTEM

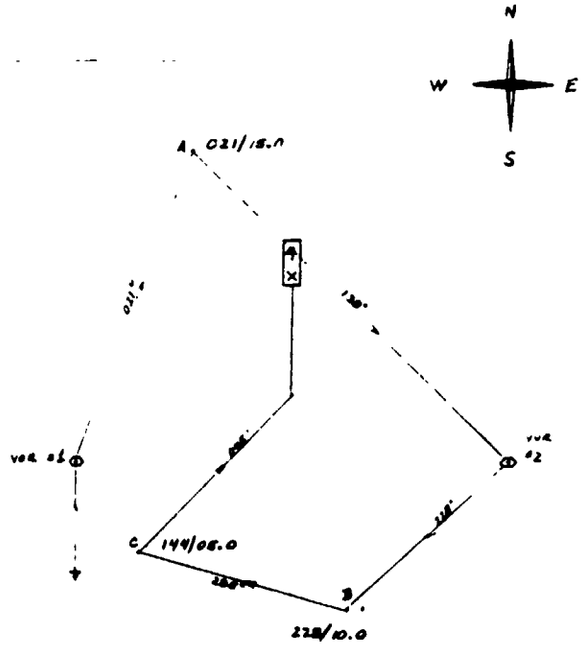

NAVIGATIONAL CHART: ALPHA SCENARIO

NOMINAL GROUND TRACK: ALPHA SCENARIO
SHORT-TERM MEMORY

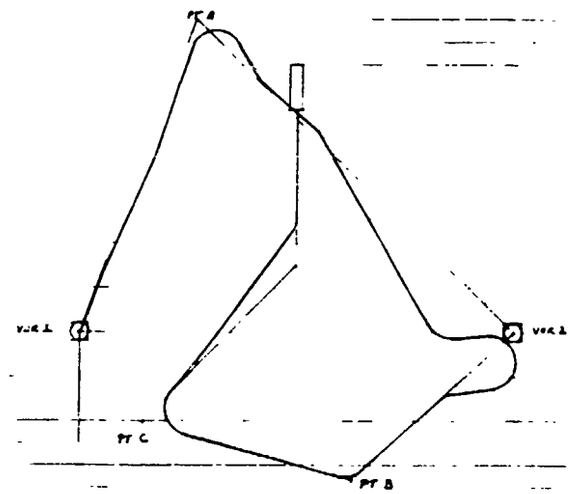

A-8

NOMINAL GROUND TRACK: ALPHA SCENARIO
LONG-TERM MEMORY

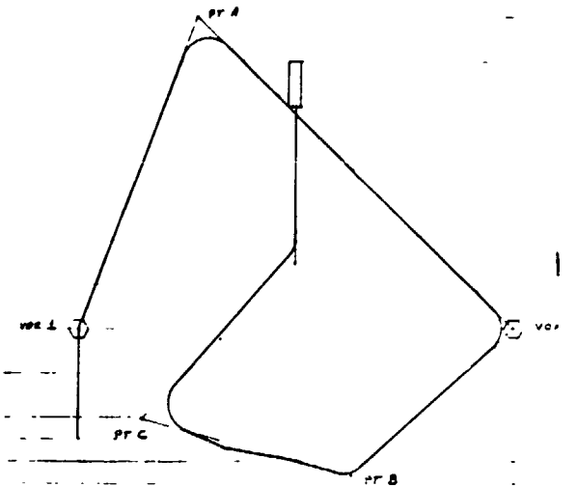

A-9

NAVIGATIONAL CHART: BETA SCENARIO

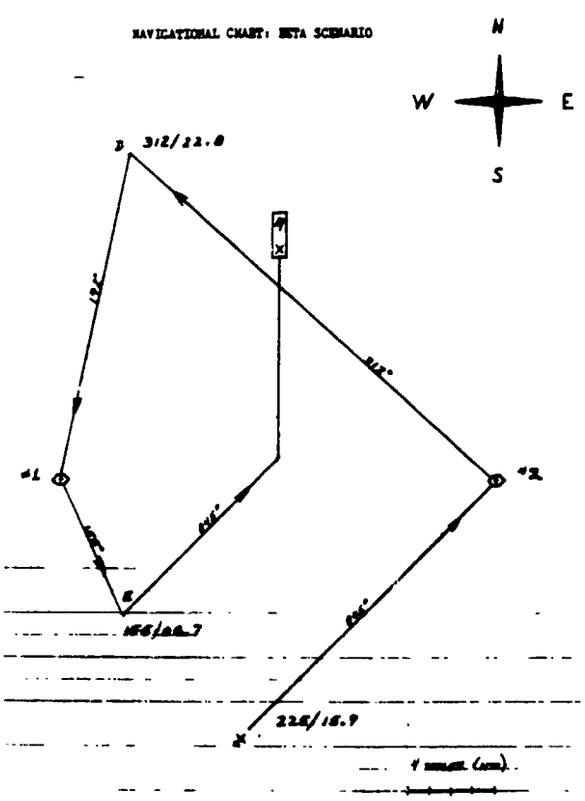

A-10

NOMINAL GROUND TRACK: BETA SCENARIO
SHORT-TERM MEMORY

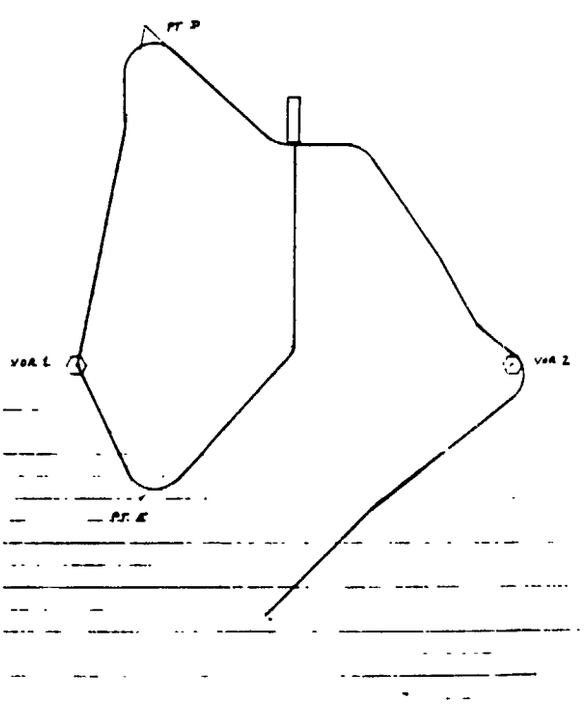

A-11

ORIGINAL PAGE IS
OF POOR QUALITY

NOMINAL GROUND TRACK: BETA SCENARIO
LONG-TERM MEMORY

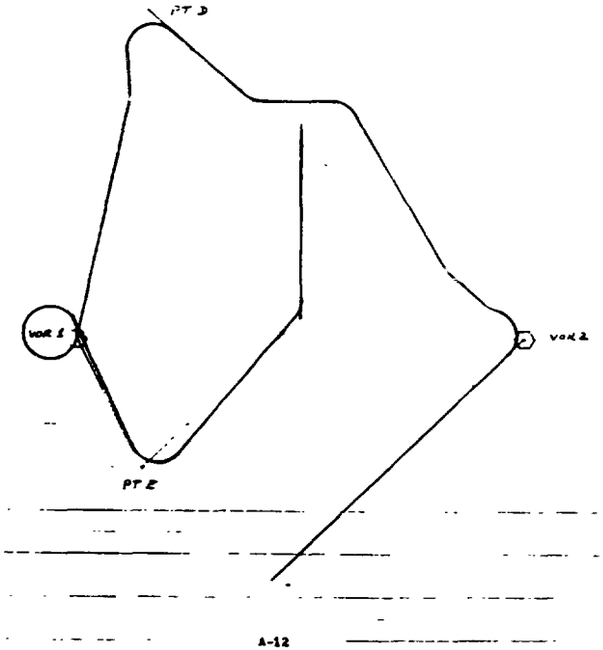

A-12

ALPHA SCENARIO: SHORT-TERM MEMORY

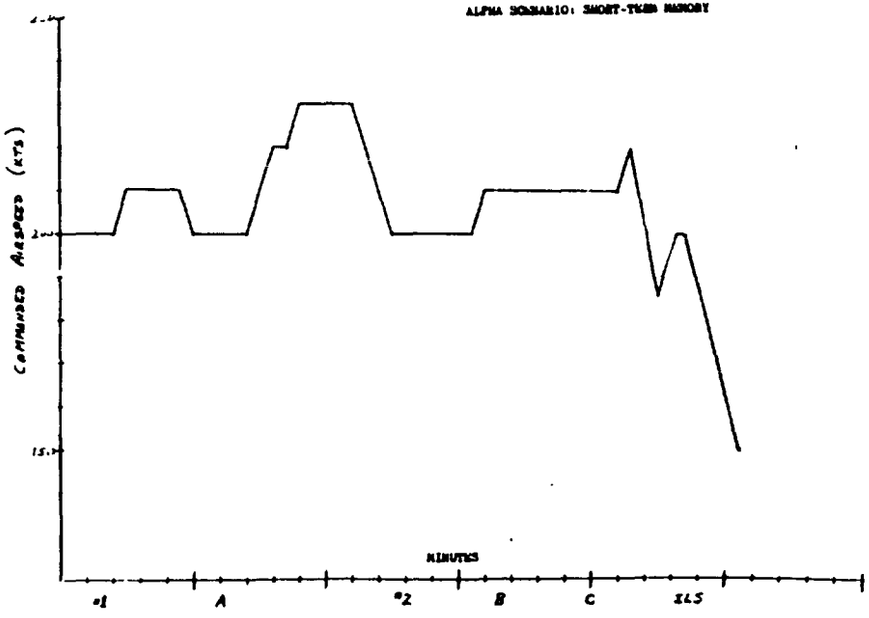

A-13

ALPHA SCENARIO: LONG-TERM MEMORY

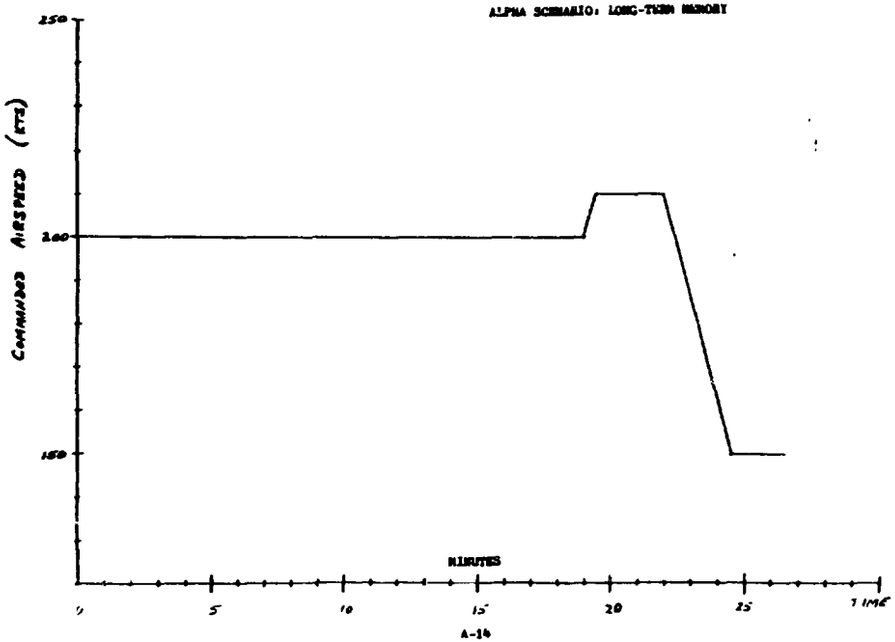

A-14

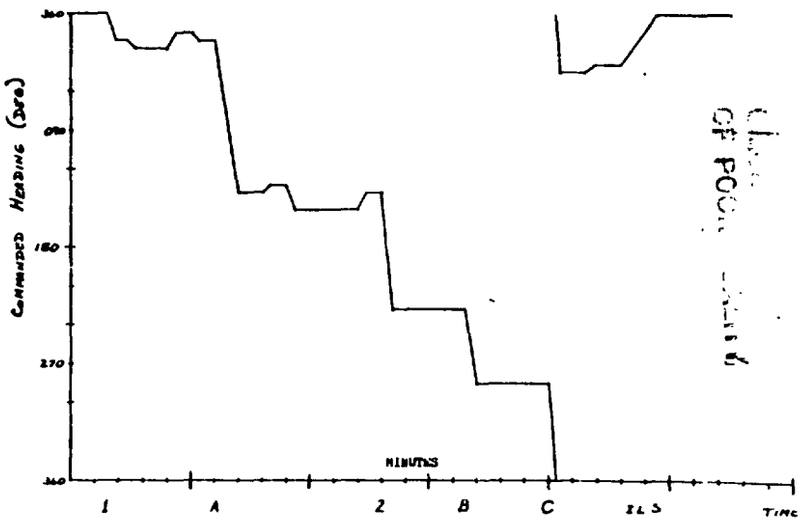

ALPHA SCENARIO: SHORT-TERM MEMORY

A-15

ORIGINAL PAGE IS
OF POOR QUALITY

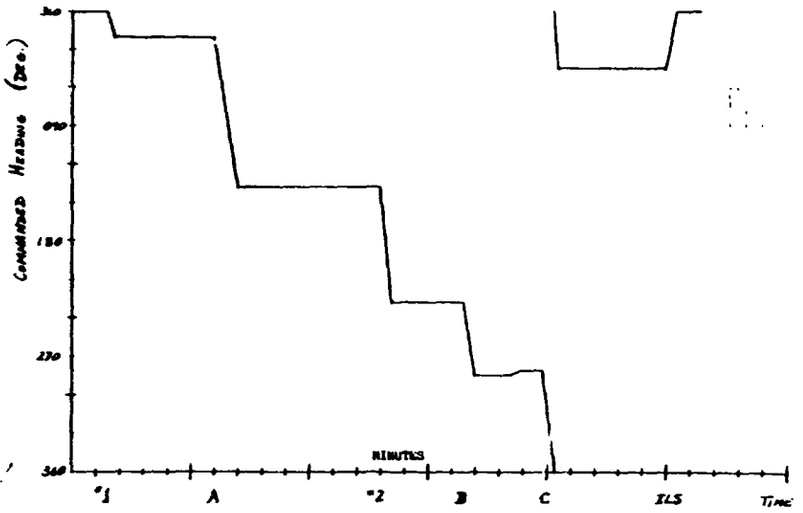

ALPHA SCENARIO: LONG-TERM MEMORY

A-16

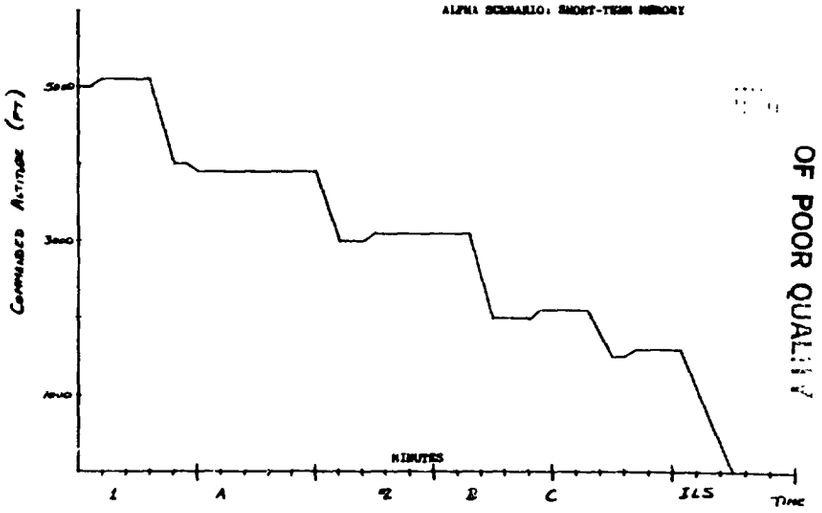

A-17

ORIGINAL PAGE IS
OF POOR QUALITY

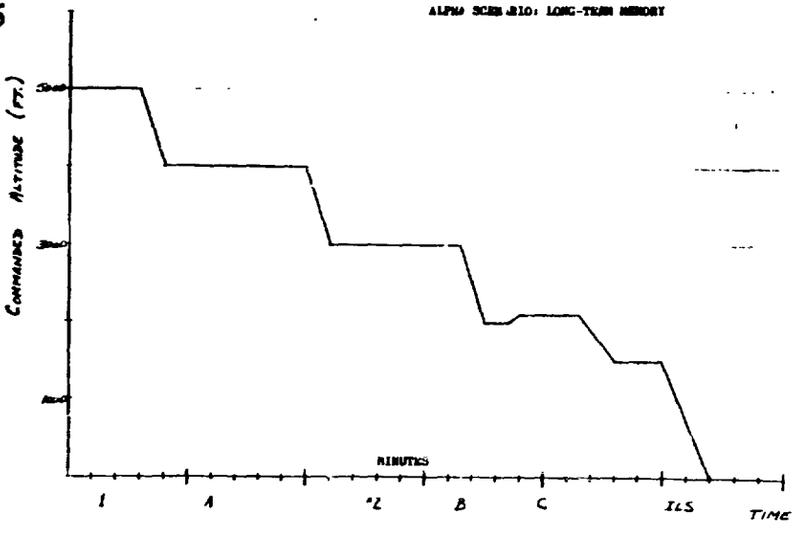

A-18

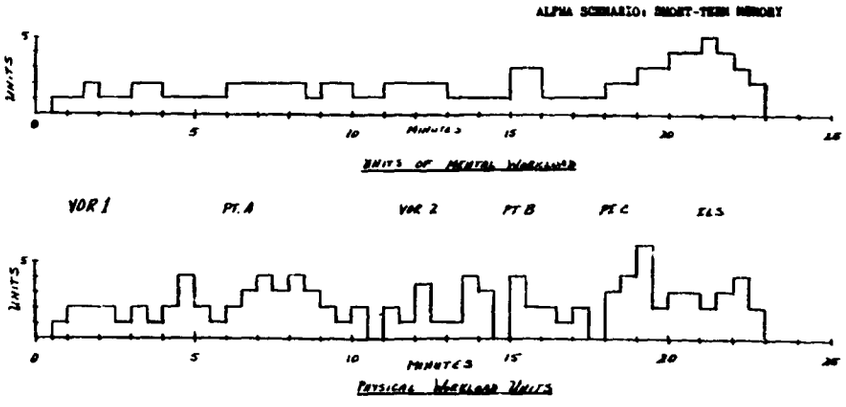

A-19

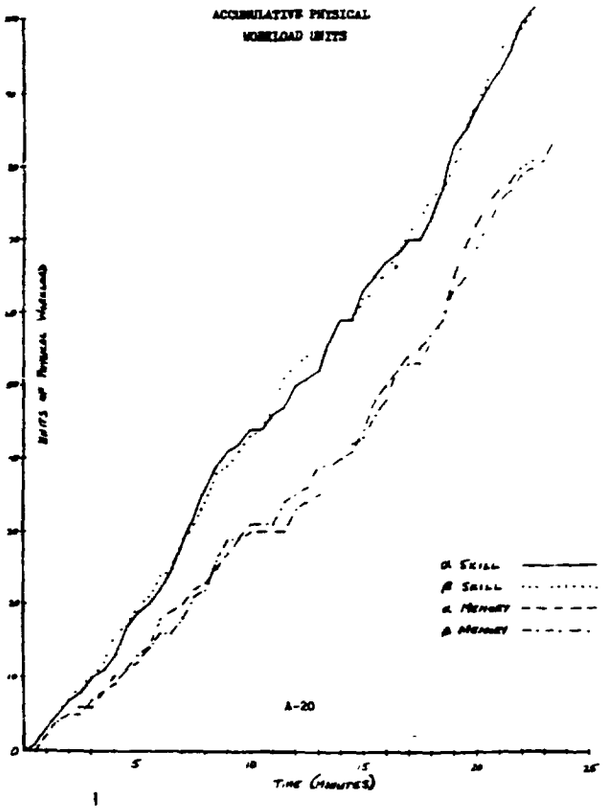

A-20

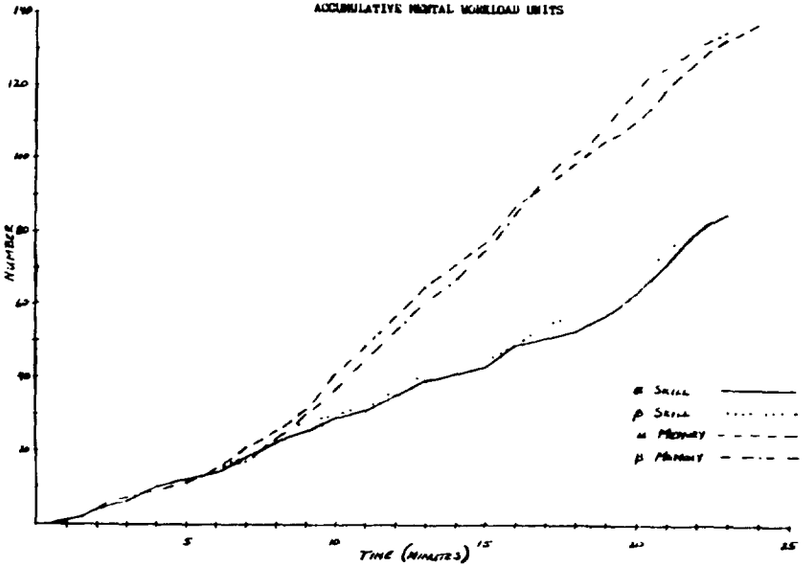

A-21

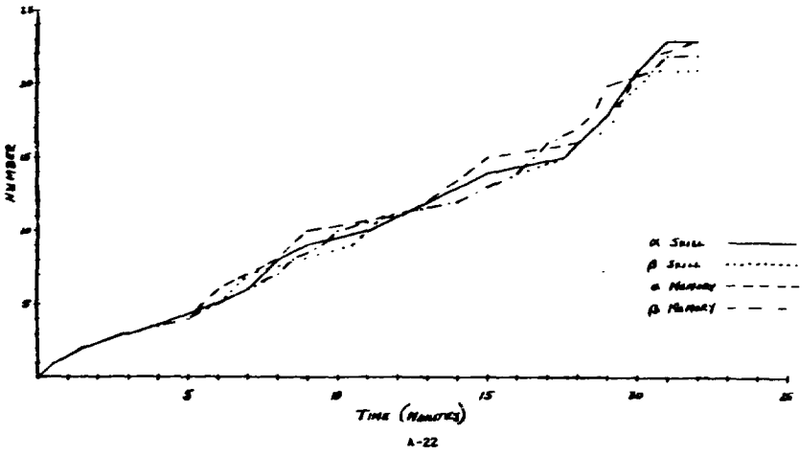

A-22

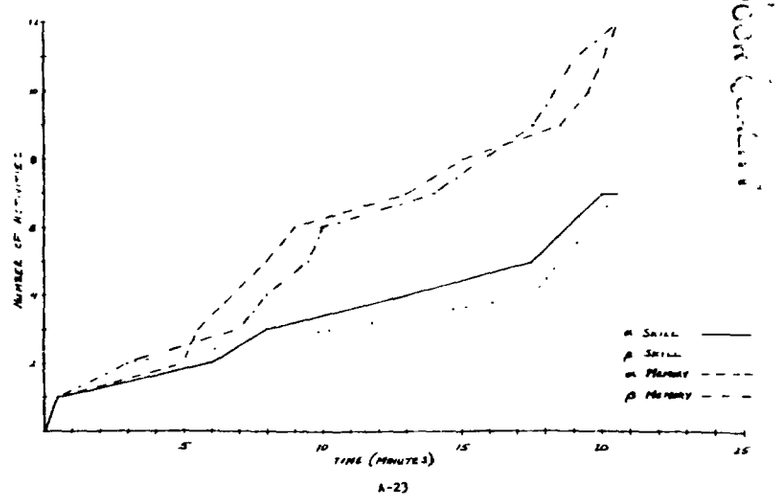

A-23

ORIGINAL IS
OF POOR QUALITY

OVER-ALL SUBJECTIVE RATINGS

	mean			std. dev.			
	A	B	adj	A	B	adj	
Activity-Level	4.93	4.35	4.64	1.42	1.60	1.54	SHORT-TERM MEMORY
Complexity	4.17	4.18	4.18	1.70	2.15	1.93	
Difficulty	5.08	4.33	4.69	1.54	2.15	1.90	
Stress	4.54	4.13	4.33	1.82	2.12	1.98	
Workload	5.00	4.47	4.73	1.68	2.37	2.07	

A-24

	mean			std. dev.			
	A	B	adj	A	B	adj	
Activity-Level	3.85	3.18	3.52	1.68	1.20	1.50	LONG-TERM MEMORY
Complexity	3.49	2.78	3.13	2.03	1.39	1.78	
Difficulty	3.98	3.14	3.56	1.79	1.54	1.72	
Stress	3.53	3.11	3.32	1.80	1.82	1.82	
Workload	3.79	3.18	3.49	2.19	1.66	1.97	

ALTITUDE ERRORS

		B	H	L	W	AVER.		
SHORT-TERM MEMORY A	mean	59.0	77.3	95.71	69.4	74.36		
	σ	36.11	71.4	134.78	59.32	79.97		
	rms	69.17	105.19	157.26	91.30	109.20	74.46	mean
SHORT-TERM MEMORY B	mean	60.69	95.0	59.13	99.06	74.59	76.19	σ
	σ	53.33	57.6	60.68	105.80	71.05	106.53	rms
	rms	80.79	111.08	84.72	144.94	103.01		

A-25

LONG-TERM MEMORY A	mean	81.77	163.06	72.41	121.60	103.06		
	σ	49.70	134.80	57.48	94.39	90.38		
	rms	95.69	211.55	92.45	153.93	137.08	93.58	mean
LONG-TERM MEMORY B	mean	93.2	122.3	74.38	53.41	84.14	81.08	σ
	σ	70.86	80.60	61.63	45.69	69.48	123.82	rms
	rms	117.08	146.48	96.59	70.28	109.12		

LONG-TERM MEMORY ERRORS

Scenario/ Version	Positional Memory Events	Number of Errors	Percent of Errors	Non-Positional Memory Events	Number of Errors	Percent of Errors
Short-term A	0	0	0	4	2	50
Short-term B	0	0	0	4	2	50
Long-term A	8	1	12.5	12	5	41.7
Long-term B	8	1	12.5	12	4	33.3

A-26

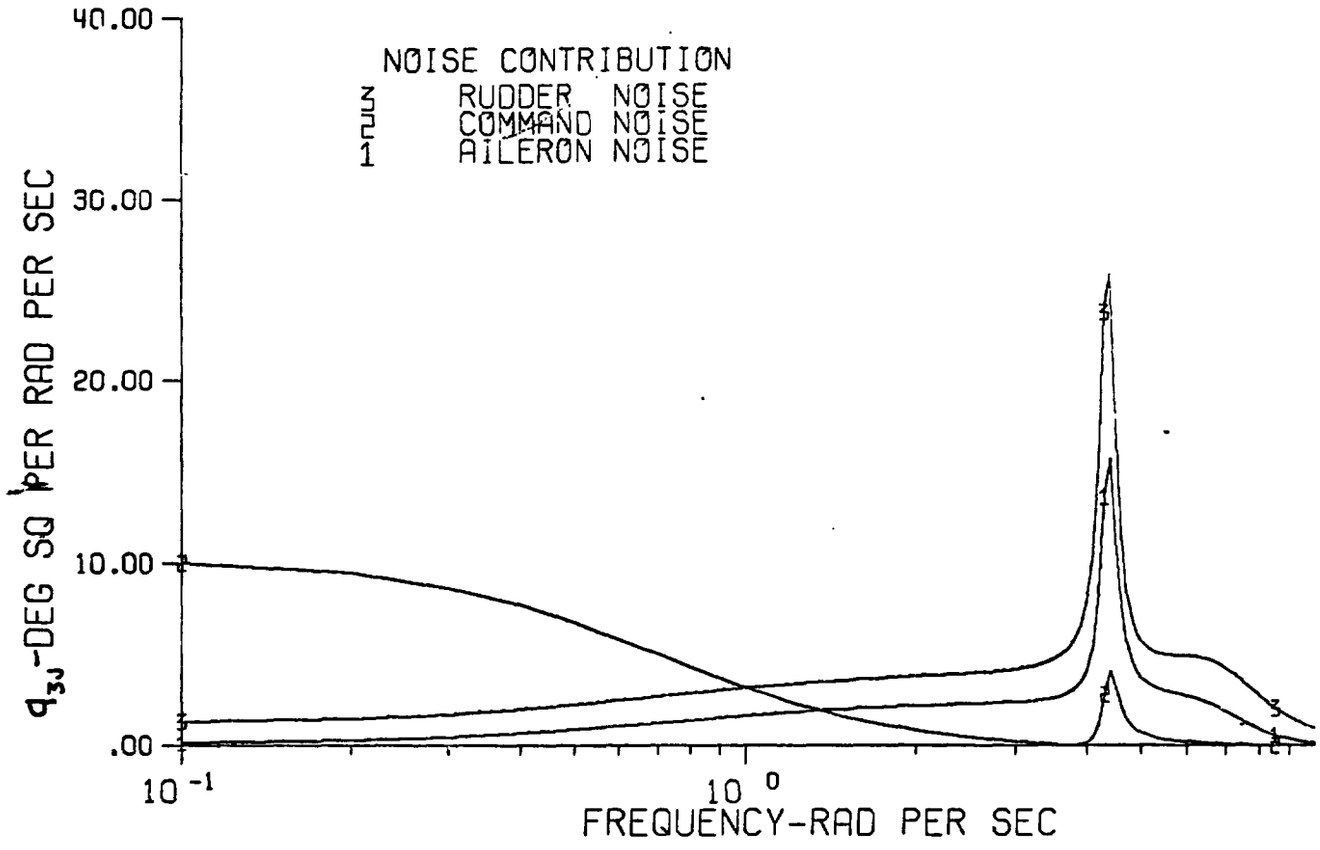
NOISE CONTRIBUTION
RUDDER NOISE
COMMAND NOISE
AILERON NOISE
40.00
30.00
20.00
10.00
.00
q_{3J}-DEG SQ PER RAD PER SEC
10^{-1}
10^{0}
FREQUENCY-RAD PER SEC

N85 14514 D27

Visual Attention to Radar Displays

Neville Moray, Dept. of Industrial Engineering, University of Toronto
Mark Richards & Corinne Brophy, Department of Psychology, University of Stirling

Abstract

A model is described which predicts the allocation of attention to the features of a PPI radar display. It uses the growth of uncertainty and the probability of near collision to call the eye to a feature of the display. The main source of uncertainty is forgetting following a fixation, which is modelled as a two dimensional diffusion process. The model was used to predict information overload in intercept controllers, and preliminary validation obtained by recording eye movements of intercept controllers in simulated and live (practice) interception.

Introduction

The task of an intercept controller is to use the information displayed on a PPI radar to direct one or more fighters to the vicinity of one or more hostile aircraft. Because of the very low rates of change of the positions of ehcos at long radar range the kind of model for visual sampling which was proposed by Senders, et al. (1966) is inappropriate. The rate of generation of information (uncertainty) by the signal is slight compared with rate of generation of uncertainty by endgenous forgetting of the information acquired by fixations. The basic assumption of the model is therefore that the observer has an uncertainty threshold for his estimate of the position of the echos of aircraft, and when his uncertainty exceeds that threshold, he will again look at the echo (or other source of information) to reduce his uncertainty.

In order to model this process, we require an estimate of the rate of forgetting for radar-like information, and a model for its interaction with the operator's uncertainty threshold. A problem arises in how to validate such a model, since for a given interception there are many acceptable flight paths which will result in a successful interception. The model was therefore used not to predict the degree of success in completing an interception, but merely to predict the proportion of time spent in looking at different parts of the display, and statistics such as the mean first passage time for fixations.

Method

Two series of experiments were conducted. The first was to establish the form of the forgetting function. Intercept controllers were shown pictures of "radar-like" patterns for 10 seconds, (which was approximately the scan rate of the radar). The pictures consisted of one, two, or three small marks in a 8" diameter circle. The picture was removed, and the controller then was required to wait for a period from 3 seconds to thirty seconds. He was then shown a second, but blank, circle, and asked to mark the position(s) of the "echos". An estimate of the basic accuracy

without forgetting was obtained by allowing the controller to mark the positions of echos on a blank circle while the stimulus was still visible, so that the only limitation on his accuracy was perceptual. Each operator performed the task for several different patterns, and several times for each pattern, at 5 recall delays, and with and without a map grid superimposed on the radar. Performance was measured in terms of the standard deviation of the estimate of the target position.

The second series of experiments consisted of recording the eye movements of interceptors while they conducted interceptions either in a simulator or with real aircraft. In the latter case, both aircraft were friendly but one played the role of intruder. The intruders did not take evasive action and no ECM were used. Data were collected from trainees and from experienced controllers, and on a variety of sorties. The data to be reported here are restricted to a series of simulated sorties in which a flight of 10 intruders approached, and were intercepted by 1-6 fighters. We were asked to predict which scenario would first lead to overload and a failure to complete interceptions.

The model was programmed in FORTRAN and run on a VAX computer.

Experiments on Forgetting

A summary of the results is shown in Figure 1. The latter shows forgetting curves for 1, 2, and 3 "echos", and for 3 "echos" with a superimposed reference grid. The results are pooled over all participants. The data from the several experiments are all described by the same equation,

$$sd(t) = a + b(t)^{3/2} \qquad \text{EQN (1)}$$

where sd(t) is the standard deviation of the estimated position in millimetres after a recall delay of t seconds. All the data are well fitted by a value for b of 0.02. The constant a depends on the difficulty of the task, ranging from 8.25 for 1 echo to 11.0 for 3 echos, and falling 4.2 for 2 echos when a reference grid was provided.

It appears that forgetting proceeds at a constant rate independent of the complexity of the display, but that the uncertainty of the initial perceptual judgement is affected by complexity. The standard deviation when no memory was involved was 4.2 mm., so that approximately 86% of all estimates would fall within a circle 2 cm. in diameter, and 40% within a circle 1 cm. in diameter.

A Model for Visual Attention

Because new information appears only every ten seconds, and because the positions of the aircraft change only slightly each sweep on long range radar, we assume that most of the uncertainty is generated by forgetting. The effective bandwidth is too low for attention to be driven by the uncertainty in the display.

Assume that the observer makes an estimate of the position, course, and velocity of an echo, $\underline{x}$, at time t_0, and that thereafter he looks elsewhere. His uncertainty is represented by the s.d. of his estimate, and this increases with time,

$$U_x(t) = f(t)$$

where $\underline{t}$ is the time which has elapsed since x was fixated.

We make five assumptions.

1. For each source of information, $\underline{i}$, there is a threshold of uncertainty PTH_i. If this is exceeded due to forgetting (increasing $U_i(t)$) the observer will look back at $\underline{i}$ to reduce $U_i(t)$ to $U_i(t_0)$.

2. There is a PTH for all features of the display, each fighter, each intruder, and "console features" such as weather information, compass bearings, etc.

3. The value of PTH_i depends on the perceived value of the source of information as subjectively estimated by the controller.

4. Although the task of the controller is to bring aircraft into close proximity, (the "inverse Air Traffic Control" problem), it is not desirable to allow aircraft to approach too close for fear of collision. (This also applies to the relation of the fighter to any "strangers", that is aircraft not involved in the interception, which may be general aviation or commercial aircraft). We assume that the controller has a second threshold, CTH, which is related to the probability that two aircraft occupy the same position in air space. If CTH is exceeded, then he will look at both aircraft.

5. Following a pair of looks induced by CTH, PTH will be adjusted for each in such a way that PTH = a' + b'/exp(-d) where d is the separation of the aircraft. As the aircraft approach, the uncertainty threshold falls rapidly so that more attention will be paid to aircraft close to another.

The rate of forgetting was taken from the experiment described above.

The program provided a printout of the positions, courses, and speeds of each aircraft, the values of PTH and CTH, and the time since each source of information was last examined. If PTH or CTH called for a source of information to be examined, the source was flagged in the printout at the time it was examined. Importance values were tuned to some extent to improve the behaviour of the model.

Model outputs are shown in Tables 1 and 2. F1 - F4 are fighters, T1 - T4 are intruders. Other variables are "console variables". In Scenario 1, one fighter intercepted on intruder. In Scenario 2, two fighters intercepted two intruders, one fighter being launched thirty seconds after the other. In Scenario 3, three fighters (launched at 30 second intervals) intercepted three intruders. The tables give data for the early part of the sortie when the fighters were distant from the intruders, and also for the final minute as the interceptions were completed. "Console variables" model all sources of information other than aircraft which were fixated. "PTHs" for them were given typical values based on early empirical data.

From these data it is apparent that Scenario 3 is the first in which the mean first passage time rises substantially. The Scenario 3 MFPT, and the standard deviation are such that for a substantial proportion of the time more than 10 seconds will elapse between fixations. Looking back at Figure 1, it is after about 6 seconds that significant forgetting sets in, and we therefore predicted that overload would first occur at Scenario 3.

Note that in Scenario 2, a switch of attention is predicted. Early in the sortie, most attention is paid to two fighters, as they leave their base and begin the interception. Late in the sortie, Fighter 1 and Intruder 4 receive most attention as the interception is completed.

Experimental Data on Eye Movements

The same scenarios were programmed on the simulator at RAF Boulmer, and three controllers carried out the interceptions. They were given complete freedom to choose their own tactics. Their eye movements were recorded using a NAC eye mark recorder, modified to make its calibration more reliable. Summary data for these sorties are given in Tables 3,4 and 5. In these tables, the s.d. of the MFPT are the square root of the mean. As predicted, Scenario 3 is that in which MFPTs become unacceptably long. In fact, several interceptions failed, and one controller lost a fighter completely by flying it off the edge of the radar.

Switches of attention can be seen in Table 4. For example, in Scenario 2, two controllers showed strong bias early in the sortie but more equally distributed attention late in the sortie. In Scenario 3 Controller #1 shows a dramatic example of "cognitive tunnel vision".

Early in the sortie, there is a fairly uniform distribution of attention across the fighters, and a lower fairly uniform distribution over the intruders. Late in the sortie, 60% of attention is devoted to F2 and T2. The MFPT for these aircraft falls markedly and the fixation duration rises. We have seen even more dramatic examples of such "cognitive lockup" in real interceptions. In some cases, almost no attention is paid to anything except the two aircraft to the extent that they are allowed, for example, to wander into a civilian air traffic lane without the controller noticing. An example of such data is shown in Table 6 and 7. These are experienced controllers. Note the case of RHE who gives less than 10% of his attention to aircraft in the vicinity other than the interception. The model also shows this behaviour under certain conditions, particularly if the importance weighting function is inappropriately high.

General Comments

The model is a very rough first approximation, and no time was available for tuning it or for sensitivity analysis. It appears able to capture the general features of intercept controller attention, including switching attention, cognitive lockup, etc. The forgetting function seems to generate eye movement statistics of the right order of magnitude with little parameter twiddling.

The empirical data are of great interest, and show some very interesting features. They confirm the model's prediction that cognitive lock up can occur, and may reach levels which while sensible from the point of view of interception, may be hazardous to other aircraft. (It would be interesting to collect similar data on air traffic controllers). It is also interesting that fixation times are remarkably short. Taken with the MFPT, this means that within the 10-second period during which the antenna completes a rotation, each echo is examined as many times as possible, although no new information arrives. This suggest that controllers are very sensitive to forgetting and try to minimise forgetting by a repeated rapid superficial scan, rather than using an intense examination to minimise initial uncertainty which would result in a rise and fall of uncertainty over a large range.

More data are available through the author, and the eye movement recordings are lodged at RAF Farnborough, U.K. See also Moray, Richards and Low (1980) and Moray, Neil and Brophy (1983).

ACKNOWLEDGEMENTS

This work was supported by the U.K. Ministry of Defense.

REFERENCES

Moray, N., Richards, M., and Low, J. 1980. The Behavior of Fighter Controllers. U.K. Ministry of Defense.

Moray, N., Neil, G., and Brophy, C. 1983. Final Report into the Selection of Fighter Controller Trainees and the Modelling of Fighter Controller Behaviour. U.K. Ministry of Defence.

Senders, J.W., Elkind, J.I., Grignetti, M.C., and Smallwood, R. 1966. An Investigation of the Visual Sampling Behavior of Human Observers. NASA-CR-434.

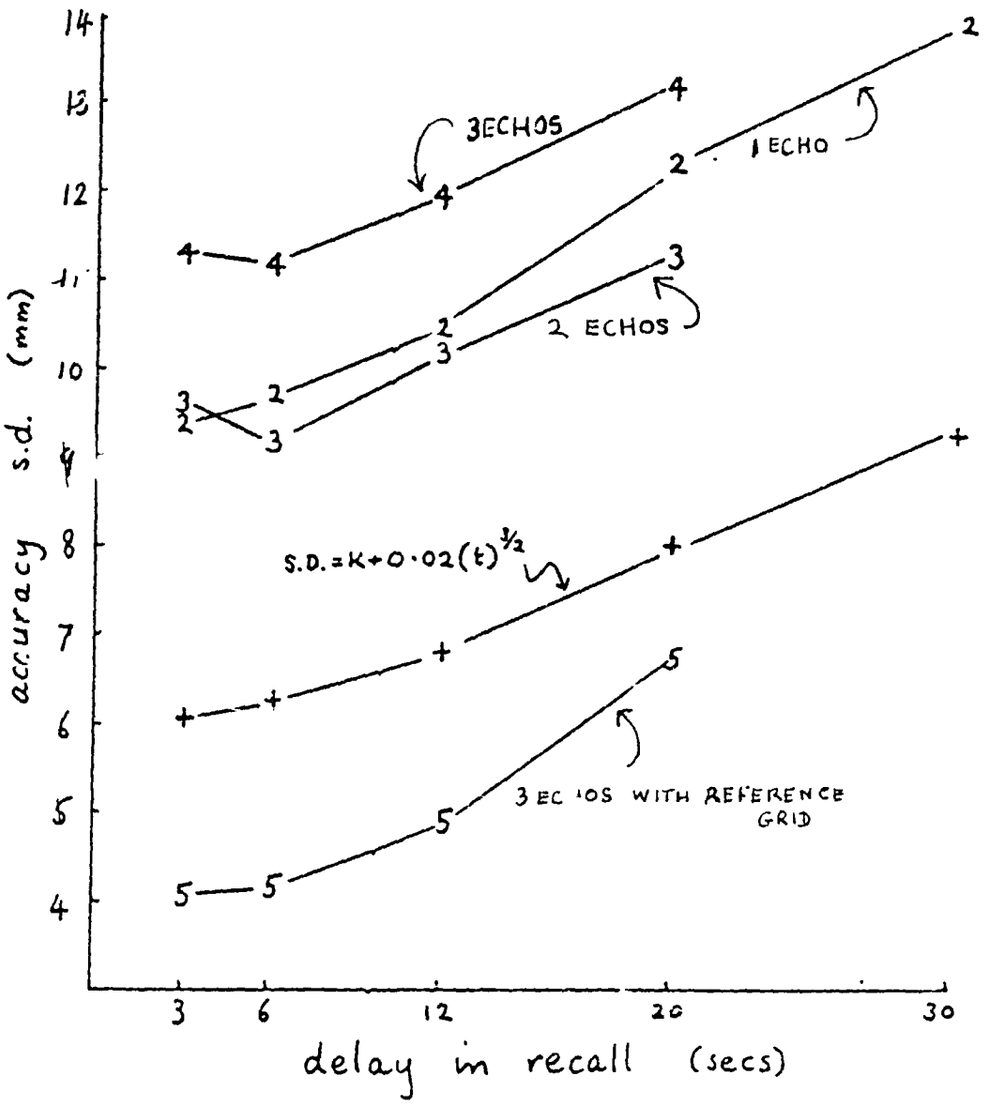

FIGURE 1

data pooled over all subjects

SCENARIO #1

MEANS OF MEAN FIRST PASSAGE TIMES (SECONDS)

	F1	T1	Console Variables			
EARLY	1.81	2.65	67.43	25.22	36.89	62.78
LATE	2.07	2.03	81.61	26.36	36.56	81.29

SCENARIO #2

MEANS OF MEAN FIRST PASSAGE TIMES (SECONDS)

	F1	F2	T1	T2	Console Variables			
EARLY	3.00	3.26	6.02	5.38	82.25	31.70	47.09	83.77
LATE	3.20	6.42	5.43	3.39	18.03	43.14	105.32	16.83

SCENARIO #3

MEANS OF MEAN FIRST PASSAGE TIMES (SECONDS)

	F1	F2	F3	F4	T1	T2	T3	T4	Console Variables			
EARLY	6.40	7.02	7.77	7.71	12.98	13.87	7.27	5.56	101.28	49.97	110.61	115.68

Table 1

Summary of Mean First Passage Times in Seconds for Eye Movements as Predicted by the Model.

SCENARIO #1

PROPORTION OF TIME SPENT ON SOURCES OF INFORMATION

	F1	T1	Console Variables			
EARLY	0.43	0.43	0.01	0.06	0.04	0.01
LATE	0.44	0.44	0.01	0.05	0.05	0.01

SCENARIO #2

PROPORTION OF TIME SPENT ON SOURCES OF INFORMATION

	F1	F2	T1	T2	Console Variables			
EARLY	0.30	0.30	0.15	0.15	0.01	0.04	0.04	0.01
LATE	0.24	0.16	0.18	0.26	0.06	0.03	0.02	0.06

SCENARIO #3

PROPORTION OF TIME SPENT ON SOURCES OF INFORMATION

	F1	F2	F3	F4	T1	T2	T3	T4	Console Variables			
EARLY	0.15	0.15	0.13	0.13	0.07	0.07	0.13	0.12	0.01	0.02	0.02	0.01

Table 2

Summary of Distribution of Attention as Predicted by Model

SCENARIO #1

MEANS OF MEAN FIRST PASSAGE TIMES (SECONDS)

		F	T	OL	CON	S	INFO	U
CONTROLLER #1	EARLY	2.37	1.09	3.50	24.08	7.50	---	---
	LATE	1.12	1.12	19.18	---	73.00	12.63	---
CONTROLLER #2	EARLY	1.64	2.00	1.31	---	---	---	79.39
	LATE	1.14	1.14	5.38	---	37.45	---	---
CONTROLLER #3	EARLY	1.77	0.85	5.65	61.02	60.69	---	---
	LATE	1.18	1.18	5.12	34.41	---	---	---
CONTROLLER #4	EARLY	1.14	1.15	---	---	42.08	---	22.81
	LATE	1.05	1.05	---	---	12.35	---	---

SCENARIO #2

MEANS OF MEAN FIRST PASSAGE TIMES (SECONDS)

		F1	F2	T1	T2	OL	S	U	INFO
CONTROLLER #1	EARLY	2.93	5.52	2.45	3.75	2.82	14.92	---	---
	LATE	1.92	2.63	1.93	2.64	13.06	---	---	101.53
CONTROLLER #2	EARLY	1.49	6.39	3.33	10.62	3.45	1[illegible].72	72.52	---
	LATE	2.93	2.54	2.62	2.52	3.09	40.72	---	---
CONTROLLER #3	EARLY	3.37	2.36	3.68	7.16	1.51	---	---	---
	LATE	2.82	1.87	2.82	1.82	---	---	---	---

SCENARIO #3

MEANS OF MEAN FIRST PASSAGE TIMES (SECONDS)

		F1	F2	F3	F4	T1	T2	T3	T4	OL	S
CONTROLLER #1	EARLY	5.48	4.73	4.25	4.17	39.61	9.56	8.74	19.81	2.66	72.09
	LATE	6.73	1.96	5.85	9.55	6.73	1.91	5.85	9.55	---	----
CONTROLLER #2	EARLY	6.58	4.70	4.43	6.72	6.55	4.70	4.43	6.22	3.74	---
	LATE	7.50	5.52	8.92	9.83	7.39	5.60	11.52	28.18	2.10	104.83
CONTROLLER #3	EARLY	4.48	5.64	3.02	6.79	4.54	70.38	4.22	18.16	3.90	---
	LATE	4.42	5.11	8.82	2.73	4.42	5.11	8.82	2.23	44.58	---

TABLE 3

SCENARIO #1

PROPORTION OF TIME SPENT ON FEATURES OF DISPLAY

		FIGHTER	TARGET	OL	CON	SEARCH	INFO	UNKNOWN
CONTROLLER #1	EARLY	0.19	0.49	0.22	0.02	0.07	--	--
	LATE	0.56	0.46	0.03	--	0.05	0.01	--
CONTROLLER #2	EARLY	0.30	0.27	0.42	--	--	--	0.01
	LATE	0.44	0.44	0.10	--	0.01	--	--
CONTROLLER #3	EARLY	0.34	0.52	0.13	0.01	0.01	--	--
	LATE	0.43	0.43	0.12	--	0.02	--	--
CONTROLLER #4	EARLY	0.55	0.40	0.02	--	--	--	0.03
	LATE	0.48	0.48	0.04	--	--	--	--

SCENARIO #2

PROPORTION OF TIME SPENT ON FEATURES OF DISPLAY

		F1	F2	T1	T2	OL	S	U	INFO
CONTROLLER #1	EARLY	0.18	0.13	0.22	0.13	0.29	0.05	--	--
	LATE	0.28	0.19	0.28	0.19	0.05	--	--	<0.01
CONTROLLER #2	EARLY	0.20	0.08	0.23	0.05	0.19	0.04	0.01	--
	LATE	0.18	0.20	0.21	0.21	0.18	0.01	--	--
CONTROLLER #3	EARLY	0.16	0.22	0.15	0.08	0.39	--	--	--
	LATE	0.20	0.30	0.20	0.30	--	--	--	--

SCENARIO #3

PROPORTION OF TIME SPENT ON FEATURES OF DISPLAY

		F1	F2	F3	F4	T1	T2	T3	T4	OL	S
CONTROLLER #1	EARLY	0.12	0.12	0.13	0.12	0.01	0.06	0.09	0.04	0.31	0.01
	LATE	0.07	0.30	0.08	0.05	0.07	0.30	0.08	0.05	--	--
CONTROLLER #2	EARLY	0.07	0.11	0.08	0.09	0.10	0.12	0.06	0.02	0.35	0.01
	LATE	0.09	0.12	0.12	0.09	0.09	0.12	0.12	0.19	0.15	--
CONTROLLER #3	EARLY	0.11	0.10	0.17	0.09	0.12	0.01	0.16	0.[illegible]	0.21	--
	LATE	0.14	0.10	0.06	0.20	0.14	0.10	0.06	0.20	0.01	--

TABLE 4

OF POOR QUALITY

SCENARIO #1

FIXATION DURATIONS (SECONDS)

		F	T	OL	CON	S	INFO	U
CONTROLLER #1	EARLY	0.76	1.19	1.03	0.50	0.55	--	--
	LATE	0.93	0.93	0.62	--	0.66	0.50	--
CONTROLLER #2	EARLY	0.76	0.71	1.01	--	--	--	0.50
	LATE	0.91	0.91	0.62	--	0.50	--	--
CONTROLLER #3	EARLY	0.78	1.06	0.89	0.50	0.50	--	--
	LATE	0.90	0.90	0.68	--	0.53	--	--
CONTROLLER #4	EARLY	0.96	0.69	--	--	1.00	--	0.75
	LATE	0.96	0.96	--	--	0.54	--	--

SCENARIO #2

FIXATION DURATIONS (SECONDS)

		F1	F2	T1	T2	OL	S	U	INFO
CONTROLLER #1	EARLY	0.66	0.78	0.65	0.59	1.16	1.75	--	--
	LATE	0.72	0.66	0.72	0.66	0.64	--	--	0.50
CONTROLLER #2	EARLY	1.02	0.61	0.90	0.62	0.82	0.50	0.50	--
	LATE	0.64	0.62	0.71	0.68	0.68	0.50	--	--
CONTROLLER #3	EARLY	0.68	0.70	0.63	0.59	0.03	--	--	--
	LATE	0.76	0.79	0.71	0.79	--	--	--	--

SCENARIO #3

FIXATION DURATIONS (SECONDS)

		F1	F2	F3	F4	T1	T2	T3	T4	OL	S
CONTROLLER #1	EARLY	0.68	0.56	0.62	0.58	0.50	0.56	0.75	0.70	1.08	0.50
	LATE	0.50	0.78	0.52	0.50	0.50	0.78	0.52	0.50	--	--
CONTROLLER #2	EARLY	0.61	0.65	0.63	0.63	0.61	0.65	0.63	0.63	0.65	--
	LATE	0.54	0.64	0.71	0.85	0.68	0.64	0.80	0.50	0.95	0.50
CONTROLLER #3	EARLY	0.50	0.62	0.54	0.54	0.61	1.00	0.64	0.50	0.91	--
	LATE	0.67	0.60	0.52	0.67	0.67	0.60	0.52	0.67	0.62	--

TABLE 5

Controller	Early in Sortie			Late in Sortie		
	F	T	S	F	T	S
SBU(L)	3.12	2.71	6.04	1.79	1.41	19.03
SBU(L)	1.78	1.55	3.75	1.12	0.91	10.95
SBS(S)	1.45	1.75	1.81	1.12	1.18	2.45
RH(L)	1.45	2.25	4.55	1.29	1.60	4.32
RHE(S)	2.04	1.51	7.43	1.52	1.59	38.19
PH(S)	1.93	1.13	11.16	1.28	1.07	8.14
PH(L)	3.18	1.63	-	1.37	1.31	9.52
PH(L)	1.62	0.97	51.05	0.96	0.93	6.33
STH(S)	1.35	1.02	1.52	0.93	0.89	3.13

Table 6. MFPT for Fighter, Target and Stranger in Live and Simulator Sorties. Time in seconds.

	Experienced Controllers					
Controller	Early in Sortie			Late in Sortie		
	F	T	S	F	T	S
SBU(L)	21	25	11	39	43	3
SBU(L)	25	27	12	39	41	4
SBS(S)	31	25	25	34	33	18
RH(L)	33	26	12	35	28	12
RHE(S)	30	41	9	45	46	1
PH(S)	29	45	5	35	47	6
PH(L)	21	42	0	38	40	6
PH(L)	28	37	1	37	38	8
STH(S)	32	37	24	41	40	15

Table 7. Proportion of time spent on Fighter, Target, and Stranger, in Live (L) and Simulator (S) sorties.

ORIGINAL PAGE IS
OF POOR QUALITY

Controller	Early in Sortie			Late in Sortie		
	F	T	S	F	T	S
SBU(L)	3.12	2.71	6.04	1.79	1.41	19.03
SBU(L)	1.78	1.55	3.75	1.12	0.91	10.95
SBS(S)	1.45	1.75	1.81	1.12	1.18	2.45
RH(L)	1.45	2.25	4.55	1.29	1.60	4.32
RHE(S)	2.04	1.51	7.43	1.52	1.59	38.19
PH(S)	1.93	1.13	11.16	1.28	1.07	8.14
PH(L)	3.18	1.63	-	1.37	1.31	9.52
PH(L)	1.62	0.97	51.05	0.96	0.93	6.33
STH(S)	1.35	1.02	1.52	0.93	0.89	3.13

Table 6. MFPT for Fighter, Target and Stranger in Live and Simulator Sorties. Time in seconds.

Experienced Controllers

Controller	Early in Sortie			Late in Sortie		
	F	T	S	F	T	S
SBU(L)	21	25	11	39	43	3
SBU(L)	25	27	12	39	41	4
SBS(S)	31	25	25	34	33	18
RH(L)	33	26	12	35	28	12
RHE(S)	30	41	9	45	46	1
PH(S)	29	45	5	35	47	6
PH(L)	21	42	0	38	40	6
PH(L)	28	37	1	37	38	8
STH(S)	32	37	24	41	40	15

Table 7. Proportion of time spent on Fighter, Target, and Stranger, in Live (L) and Simulator (S) sorties.

Most of the control literature on the human transfer function is in terms of a continuous control function, and for this reason the z domain transfer function was transformed into the s domain. Since the z-domain transfer function is a rational function, it can be written as a partial sum:

$$H(z) = \sum_{i=1}^{m} A_i/(1-e^{-s_i T} z^{-1})$$

where m is the number of poles, T is the sampling interval and $z = e^{i\omega T}$. Using the correspondence:

$$H(z) = \sum_{i=1}^{M} A_i/(1-e^{-s_i T} z^{-1}) \longrightarrow \sum_{i=1}^{M} \frac{B_i}{s+s_i} = Y(s)$$

the general form of the pilot transfer function is still a rational function:

$$Y(s) = Ke^{-Ts} \Pi(s+z_i)/ \Pi(s+p_i)$$

where K is pure gain and the z_i's and p_i's are the zeroes and poles of Y, respectively. The use of this correspondence in human operator control modeling also appears in Shinners (9) and Osafo-Charles (10).

The z_i's and p_i's are not always real numbers but frequently occur as complex pairs causing second order factors in the numerator and denominator. The complex poles are more likely to be the two smallest in simulation and the two largest in flight. Complex zeroes are not nearly as frequent. Writing the complex term in the denominator as

$$[(s+(a+bi)][(s+(a-bi)] = \omega^2(s^2/\omega^2+2\zeta s/\omega+1)$$

where ζ = damping ratio

and ω = normalization frequency

The damping ratio was computed for the models developed for the one pilot flying both in the simulator and in actual flight. In the simulator, of the eleven models with second order poles, ζ ranged from .41 to .98 with approximately two thirds of the ratios above .71. For flight the situation was somewhat reversed; of the nine models with second order poles, one was above .71, one at .71, and the rest were below.

N85 14515

POPCORN: A Supervisory Control Simulation for Workload and Performance Research

Sandra G. Hart
NASA-Ames Research Center
Moffett Field, CA

Vernol Battiste and Patrick T. Lester
San Jose State University
San Jose, CA

ABSTRACT

A multi-task simulation of a semi-automatic supervisory control system was developed to provide an environment in which training, operator strategy development, failure detection and resolution, levels of automation, and operator workload can be investigated. The goal was to develop a well-defined, but realistically complex, task that would lend itself to model-based analysis. The name of the task ("POPCORN") reflects the visual display that depicts different task elements milling around waiting to be released and "pop" out to be performed. The operator's task was to complete each of 100 task elements that were represented by different symbols. by selecting a target task and entering the desired a command. The simulated automatic system then completed the selected function automatically. Task difficulty, operator behavior, and experienced workload were varied by manipulating: (1) the number of elements per task; (2) the number of discrete tasks; (3) the penalties for lagging behind the system; (4) task schedule; and (5) payoff structure for performing or failing to perform task elements. Highly significant differences in performance, strategy, and rated workload were found as a function of all experimental manipulations (except reward/penalty). In addition, a proposed technique for reducing the between-subject variability of workload ratings was described and applied successfully. The first simulation conducted with this task defined a range of scenarios that imposed distinctly different levels of workload on operators and resulted in different levels of performance and operator strategies.

INTRODUCTION

The introduction of computer aiding, artificial intelligence, and automation into advanced systems has changed the roles of human operators. Their primary functions have become scheduling, monitoring, decision making, and planning rather than direct mechanical control. Furthermore, the interfaces between the operators and the systems that they control have become indirect, periodic, and discrete rather than direct and continuous as computers are placed between the human operator and the mechanical system.

Automation is a generic term for replacing human actions by human decisions executed by machines and for accomplishing clusters of related tasks by simple executive commands (refs. 1, 2). Often, the decision to automate some or many system functions stems from a desire to enhance system capabilities without overloading operators. Alternatively, it is introduced to allow existing crewmembers (or a reduced number of them) to perform additional tasks or operate in environments in which they could not function without aiding. In the past, automation has been provided to reduce the physical workload of

activities, a goal that has been accomplished with great success. However, a potential consequence of adding automation could be a substantial increase in mental workload to replace the reduced physical workload, due, in part, to the added burden of supervising or monitoring the automation itself. Such a tradeoff between physical and mental workload has been inferred rather than proven, however, because mental processes are difficult to observe or quantify directly. Thus, there is an increasing need to monitor, measure, define, and control whatever "mental workload" is in order to keep it within the capabilities of human operators.

In order to develop valid and sensitive measures of mental workload and performance, standardized primary tasks are needed to test candidate measures. These tasks must impose controlled levels of load with the dynamic decision-making and task-selection activities typical of current and future man-machine systems. Procedures for performing combinations of subtasks under normal and failure conditions should simulate the complexities and alternative solutions typical of advanced systems and computer aiding might be provided to assist operators with specific functions. Manual control issues may receive less emphasis, as the focus of the research will be on activities that are more typical of automated systems. The interface between man and machine will continue to be an important issue, however. With such tasks, theoretically and practically interesting topics, such as training, development of performance strategies, and the subjective experience of workload, could be investigated and models of human performance appropriate for multi-task, supervisory control systems developed.

Laboratory tasks that impose controlled levels of load across a range of functions typical of advanced systems (refs. 3, 4) have been used in many research efforts. These tasks may be manipulated and controlled with precision and predictions about performance may be made from a sound theoretical point of view. One disadvantage, however, is that the workload imposed by a realistically complex combination of such tasks may be substantially different than the sum of the workloads imposed by the components individually. For example, depending on the strategies selected and the degree to which groups of related subtasks are performed automatically, subjective experiences and objective performance might be significantly different than would be predicted from single-task performance.

A multi-task dynamic simulation was developed to represent the environment in which decision makers responsible for semi-automatic systems work (ref. 5). It involved a computer display of tasks (represented by boxes) which appeared according to different random schedules and moved toward a deadline. Operators could perform only one task at a time and were required to develop different performance strategies to accomplish specific experimental scenarios. Interarrival rates, the time until tasks reached the deadline and the time required to perform them, the number of tasks, and the "values" assigned to them were manipulated. The goals of the research were to develop an objective index of task load and to model subject's behavior. In a later study, (ref. 6) three task variables (interarrival rate, task duration, and number of tasks) were manipulated to determine their relative contributions to the subjective experiences of workload. It was found that the number of tasks to be processed per unit of time was the dominant factor.

A similar simulation was developed to extend the optimal control model methodology to characterize human monitoring, information processing, and task

selection in a dynamic multi-task environment (ref. 7). Five stylized tasks that varied in value, processing time, and velocity competed for the operator's attention. The decision process was dynamic, as new tasks with different characteristics continued to arrive, the opportunity window to perform available tasks shrank, and unperformed tasks reached the deadline.

The design of the current simulation was derived, philosophically, from the earlier simulations (refs. 5, 6, 7), however it expanded on them by increasing task complexity, incorporating dependencies among task elements, varying task attributes as a function of human decisions, and providing an extensive procedural structure. Its name, "POPCORN", reflects the appearance of the task elements waiting to be performed (they mill around and then "pop" out of the computer-displayed containers). The operator's job is to decide which tasks to do and which procedures to follow based on an assessment of the current and projected situation, the urgency and difficulty of the tasks, and the reward or penalty for performing or failing to perform them. The system is controlled by operators who select functions to be performed by automatic subsystems (barring preprogrammed "hardware" failures or operator error).

The first study conducted with this simulation was designed to examine the effects of a variety of phenomena typical of supervisory control tasks on operator strategies, performance, and the workload they experience. The goal was to establish task scenarios that would present operators with predictable variations in imposed workload (by varying scheduling, the number of elements per task, time pressure, and availability of tasks for performance) and to provide opportunities for operators to adopt different strategies (depending on whether they were leading, lagging, or level with system demands). A variety of control functions were simulated to provide alternative solutions to different combinations of circumstances. Different penalties for procrastination were invoked whenever an operator failed to meet task schedules and deadlines: (1) Imposition of additional operations to perform on delayed tasks, (2) Loss of points for performing deferred tasks, and (3) Transfer of delayed task elements to a penalty box where immediate performance was required. In addition, the longer a task element remained unperformed, the faster it moved in half of the scenarios, so that less and less time was available for its performance when the operator did attend to it. Interarrival rates were varied so that each task could be completed by a trained operator before another was scheduled. Because the acceleration function made tasks available for performance more quickly, the scheduled arrival times between accelerated tasks was less than it was between fixed-rate tasks to maintain a steady flow of activities. The interval of time during which a task element could be performed (its "opportunity window") was, therefore, influenced by the presence or absence of acceleration and the number of elements per task. The minimum time to perform a task was fixed by the speed at which elements exited from the boxes and the number of elements per task. The maximum time to perform a task was defined by the scheduled interval between successive tasks per box.

Performance on the primary task was evaluated by examining the scores obtained under each experimental condition, to complete it, and the number of errors. Strategies were evaluated by analyzing the functions that were selected. The effect of experimental manipulations, operator strategy, and performance on the subjective experiences of the operators was assessed by responses to rating scales presented immediately after each scenario.

The workload imposed by the tasks was determined by a weighted combination of operators' evaluations of 10 relevant factors. These evaluations were related not only to the experimental manipulations, but to the operators' strategies, performance and pre-existing biases about what aspects of a situation contribute to variations in experienced workload, as well. Ratings on many different scales were obtained because workload is thought to be a multi-dimensional construct (refs. 1, 8, 9). Factors such as the difficulty of the task imposed on the operator, the physical or emotional stress experienced, time pressure, and the amount of effort exerted have been suggested as potential components. In addition, there may be individual differences in which aspects of a task are considered to be relevant to the level of workload experienced (refs. 10, 11). For some individuals, the difficulty of a task may completely define the workload experienced. For others, the physical or mental effort exerted may create the conscious experience of workload. For yet others, feelings of stress, frustration, or fatigue that accompany task performance may affect the conscious experience of workload. Tasks that are performed successfully may be experienced as having low workload whereas those that are performed poorly may be equated with high workload (regardless of the level of effort applied in either case).

A technique for combining ratings on different workload-related dimensions (each weighted to reflect its subjective importance to individual operators) was developed and tested in this and other recent studies (refs. 12, 13). Nine factors that have been found to provide the most complete description of operators' experiences were the basis for the weighting procedure. Unlike other methods of extracting subjective biases from workload ratings, such as the Subjective Workload Assessment Technique (SWAT) (refs. 11, 14), this technique allows a weight of zero to be given to a dimension that is considered to be irrelevant and incorporates a sufficiently broad range of dimensions to characterize the biases of most individuals. In addition, it does not require an abstract prediction of the possible effects of complex combinations of different levels of different dimensions as does the SWAT technique.

METHOD

Subjects

Eight male general aviation pilots served as paid participants in the experiment. They ranged in age from 22 to 35 years. Two additional male subjects participated in a pilot study.

Equipment

The simulation was programmed on a Digital Equipment Corporation PDP-11/40 computer and an Evans and Sutherland Picture System I. The display was presented in a 25.60 cm square area on a Xytron black and white monitor. Operators interacted with the system by positioning a stylus on a magnetic response pad and entering selections by depressing the tip of the stylus. The 25.6 cm display area was projected onto a 5.1 cm area on the response pad (an area approximately equivalent to the dimensions of the display depicted in Figure 1). The operators rested their right arms on the response pad and were able to reach every function with minimal hand movements. The response area was delimited by cut-out area of a 0.6 cm thick plexiglass overlay on the pad.

The experiment was conducted in a secluded area of a computer room with dim lighting levels and no distractions. The operators were seated at a small table that contained the stylus and response pad and the operations manual. The display was located immediately in front of the subjects at a distance of approximately 1.0 m.

Experimental Task

Basic Functions

The information, control functions, and displays for the simulated system were presented on a computer display. (Figure 1) The five task types were each represented by a unique symbol (*, +, -, #, =), consistently mapped so that only one symbol appeared in each box. Five types of tasks that occurred several times each were included so that operators had to shift their attention from one to another, as they do in operational environments. Each task served as an abstract representation of a different type of function (e.g., communications, navigation, monitoring, checklists, and autopilot control) that might be performed in a complex system, such as a modern aircraft. In the current experiment, the values assigned to elements from each box, the functions and time required for performance, and element rates were identical for all tasks within each scenario, however these variable are under experimental control and different levels and combinations of levels could be selected for subsequent simulations.

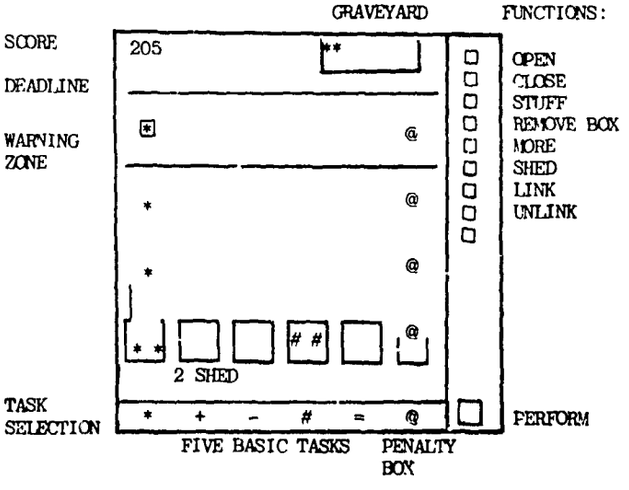

Figure 1. The POPCORN simulation display.

If a new task was scheduled to enter an occupied box, elements from the existing task were transferred to a "penalty box". This marked the end of the window of opportunity to perform the remaining task elements for score points. The operator's goal was to perform as many tasks as possible, maximizing the score and minimizing the time per scenario.

The initial decision to ready a task for performance was made by touching the symbol located immediately below the selected box with the stylus (the SELECT function). Task selections remained in force until a different task was selected; only one task could be operated upon at a time in the basic system. The functions that could be performed on any task were displayed on the right side of the display. Functions were generally momentary; each actuation caused the selected function to be applied one time to the current task. The operator's job was to decide which functions to apply to which tasks. Their actions prompted automatic subsystems to effect the selected functions, much as when a pilot selects a new altitude or navigational point, enters it into a navigation computer, and an autopilot achieves the desired change.

Task elements arrived at scheduled times and milled around in their boxes until they were SELECTed. Once the lid of a box was removed (by the OPEN function), task elements streamed out in a vertical line at a rate determined by their initial velocity (12.5 cm/sec) and the acceleration function for that scenario (either 0 or 1.52 cm/sec/sec). One box could opened at a time or several could be left open. Elements of the currently selected task were performed by touching the PERFORM key area. Each actuation caused the topmost element in the stream of task elements to disappear and the score to be incremented by five points. The maximum possible score for any scenario was 500 (5 points each for 100 task elements).

Boxes could be closed after each task was completed (in anticipation of the arrival of the next task) or with elements remaining to be performed. If any elements were actively exiting from a box, the operator had to place them back in the box (by actuating the STUFF command) before selecting the CLOSE command. By selectively opening and closing one or more boxes, operators could control the number of task elements available for performance and by rapidly selecting and performing one task then another, several tasks could be completed in parallel. An alternate strategy was complete each task, one at a time, before going on to the next. The optimal strategy differed as a function of the schedule and circumstances for each scenario.

Penalties and Procedures for Lagging Behind

If operators waited too long to perform a task element after it had left its box, the symbol moved into a "warning zone" where each element was surrounded by a square symbol. The task could still be performed with no loss of score, but at the cost of an extra procedure. This represents the additional problems encountered in operational settings when operators wait too long to finish a task once it has been started. In order to perform task elements in this zone, the task must be SELECTed, the warning box removed from the symbol (REMOVE BOX), and the topmost task PERFORMed. This two-stage process had to be repeated for each successive task that entered the warning zone. The most efficient strategy was one that allowed tasks to be completed before they entered this area. If tasks did enter this area, however, the operator could either elect to perform the two-stage REMOVE BOX/PERFORM procedure or STUFF the elements back in their original boxes, in effect resetting that task. If a task element was not performed by the time it reached the "deadline", its symbol was placed in the "graveyard" and no points were scored.

Since more than one task of each type was scheduled per box, operators had to complete each task before the next one arrived or the unperformed elements

from the previous task would be transferred to the penalty box. Once in the penalty box, task elements lost their identity (they were represented by "@"), they had to be performed immediately (the box had no lid), and no score points could be gained by performing them (although a five-point penalty was levied if they were not performed). Thus, once operators had begun to lag behind the system to the point that tasks were being transferred to the penalty box, they had to shift to a reactive strategy in which they could accomplish no more than preventing additional loss of points.

If operators decided that things were out of control, two strategies were available: closing some or all of the boxes or shedding the elements in one or more boxes. If the SHED function was selected, the elements remaining in the selected box could no longer be performed (thereby losing the potential for gaining those points), however the five-piont penalty for unperformed tasks could be avoided. This function was provided to allow the operators to elect a strategy available in operational settings (e.g. the decision to ignore certain tasks when loading levels are perceived as excessive).

Functions that Allow Operators to Lead the System

If operators wished to complete tasks ahead of schedule, they could request MORE tasks. For half of the scenarios, only two tasks of each type (with 10 elements each) were scheduled, limiting the opportunity to use this command. For the remaining scenarios, however, five tasks of each type (with four elements each) were scheduled, providing many opportunities to select it.

One form of automation is the performance of multiple related tasks by a single command. This type of activity was simulated with the LINK and UNLINK functions. If LINK was selected, elements from two of the five basic tasks could be acted upon with a single command; every function applied to one task was applied to the other so that tasks could be completed twice as fast. There were limits to the utility of this function, however. If one task was completed before the other, or if elements from one task entered the warning zone, the tasks had to be UNLINKed to be completed.

Experimental Variables

Two levels of each of four experimental variables were combined to create sixteen scenarios. The variables were: (1) reward and penalty for performing (or failing to perform) subtasks, (2) task schedule, (3) number of elements per task, and (4) the consequences of delaying task performance. The experimental design may be seen in Figure 2. The payoff structure was manipulated to determine the impact of penalties (decrements in score) for failing to perform subtasks on operators' strategies and experienced workload. Five points were given for each task element performed within the appropriate amount of time. In half of the scenarios, there was no additional penalty (other than loss of score) for failing to perform tasks (+5/0). In the other scenarios, an additional five-point penalty was levied for each unperformed task element (+5/-5).

Two task schedules were imposed: (1) **MASSED** (tasks appeared simultaneously in the five boxes whenever new tasks were scheduled to appear); and (2) **STAGGERED** (tasks appeared at different, predetermined times in each box). This manipulation was included to assess the effect of organizational complexity.

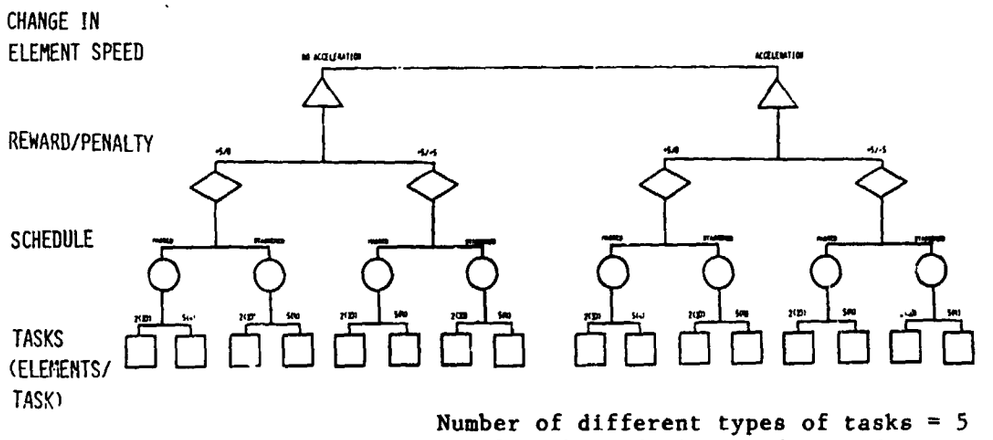

Number of different types of tasks = 5
Total number of elements/type of task = 20
Maximum score possible/scenario = 500

Figure 2: Design of the 16 experimental scenarios.

The scenarios were designed to provide operators with a predictable and reasonable set of requirements; the intervals between successive tasks were sufficiently long for trained operators to complete one task before the next arrived. The number of elements/task (analogous to the time-to-perform tasks in the earlier studies) and the presence or absence of acceleration (accelerated tasks exited more quickly, thus the opportunity for performing them occurred more often, even though the opportunity window for their performance was reduced by speed of their movement toward the deadline) were considered in computing the task schedules. The 16 schedules are depicted in Appendix A.

The number of task elements per scenario was constant (20 elements for each of 5 task types), however, the way they were grouped was varied: (1) Two tasks with 10 elements each [2(10)] per box, or (2) Five tasks with five elements each [5(4)] per box. Each element took the same amount of time to perform, thus, tasks with many elements took longer to complete than those with few elements, however there was less time lost switching among tasks and the schedule was less complicated with the larger tasks. This variable was included so that strategies and performance differences resulting from the tradeoff between task complexity (e.g. elements/task) and number of discrete tasks (10 or 25) could be evaluated.

The longer operators waited to perform tasks, the more urgent they became. In eight of the scenarios (**ACCELERATION**), urgency was simulated by accelerating the movement of task elements in the boxes as long as they remained unperformed. In the other eight scenarios (**no ACCELERATION**), task elements moved at a constant rate that was so leisurely that it inhibited well-trained operators from performing tasks as quickly as they could. The accelerations were 0 and 1.53 cm/sec/sec for the **no ACCELERATION** and **ACCELERATION** conditions, respectively. Although acceleration substantially increased the time pressure under which operators worked, accelerated tasks could be completed more rapidly once a box was opened (a potentially positive factor).

Rating Scales

Operators rated their experiences along 10 workload-related dimensions: task difficulty, time pressure, performance, mental effort, physical effort, frustration, stress, fatigue, type of activity, and overall workload. The scales were presented on the display immediately after each scenario. A stylus was used to position a cursor at the desired scale value. Each scale was a 11.0-cm vertical line labeled with a title (e.g. "MENTAL EFFORT ") and bipolar descriptors (e.g. "EXTREMELY HIGH/EXTREMELY LOW"). Numerical values were assigned to the selected scale positions with a range from 0 to 100 during data analysis.

Two estimates of workload were obtained: a direct rating provided by the operators (with the "OVERALL WORKLOAD" bipolar scale), and a combination of the remaining nine scales weighted to reflect the importance placed on each factor by each subject. The relative importance of the nine factors (e.g. the weights) was determined by a pretest in which the 36 possible pairs of the nine factors were presented one at a time. The member of each pair that was considered to be most relevant to workload by that subject was recorded. The number of times each factor was selected was computed; the possible values each factor might have ranged from 0 (the dimension was not at all relevant) to 8 (it was more important than every other factor), with a total possible sum of 36.

Procedure

A brief introduction that described the purpose of the simulation and the research to be performed with it was read to the participants. An operations manual was given to them to read while the experimental manipulations were described and demonstrated. A one-hour training session was provided to familiarize them with the tasks, equipment, and procedures.

At the end of the training period, the 16 experimental scenarios were presented in a different random order to each subject. A description of the upcoming scenario and a schedule of task arrival times was provided before each scenario and the 10 rating scales were presented following each scenario. At the conclusion of the experiment, the operators rank ordered the four experimental variables with respect to the impact that they felt each had had in influencing the level of workload. The experiment lasted approximately 5 hr, with a long break in the middle and shorter breaks between scenarios.

RESULTS AND DISCUSSION

A three-way analysis of variance for repeated measures was the primary statistical procedure applied to the dependent measures. Analyses were performed on 12 measures of performance (e. g. score, task duration, and inappropriate function selections), 10 measures of operator behavior (e. g. function selections), and 11 subjective ratings (e. g. 10 bipolar scales and the combined weighted workload scale). In addition, the correlations among scores, task durations, selected measures of behavior, and the weighted workload rating were computed. Differences in performance, operator behavior, and subjective experience were examined on a subject-by-subject basis to determine the association between operator strategies and behavior, and the resulting performance and subjective experiences.

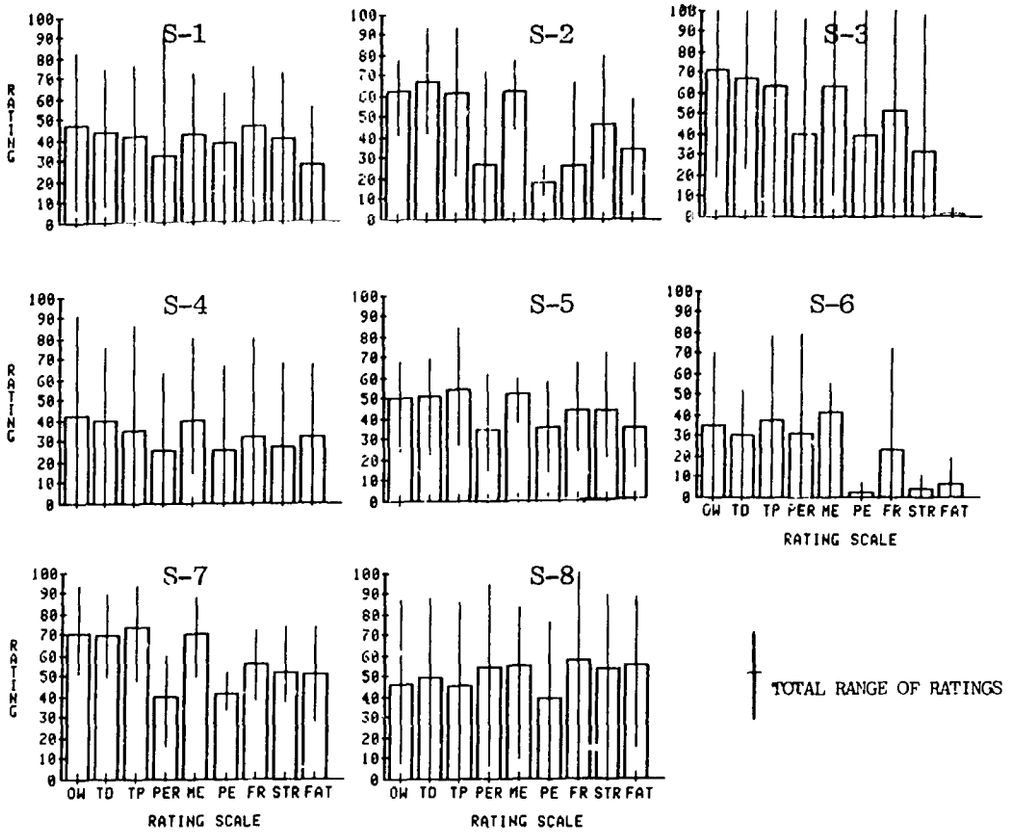

Figure 3. Average and range of bipolar ratings obtained from each of 8 experimental subjects across 16 experimental conditions.

Overview of Dependent Measures

Bipolar Ratings

The average and range of ratings given by each subject across experimental conditions may be seen in Figure 3. It is clear from an examination of the data that individual subjects differed in the magnitudes of ratings given from one scale to the next and also in the range of the rating scales used within and between scales. For example, the between-subject standard deviation (SD) of overall workload ratings across conditions and subjects was 25.5, more than half of the mean value of the rating (52.7).

Workload Weights

The relative importance each subject placed on the nine workload-related factors may be seen in Figure 4. As expected, the subjects disagreed about how much influence the different factors were predicted to have on their experience of workload. It is precisely because of this expected difference of opinion that the preliminary test was conducted, however, to facilitate the statistical removal of this source of between-subject variability from the combined bipolar ratings. In general, Time Pressure, Own Performance, Frustration, and Stress were each selected as more relevant than the other

items more than half of the time. Physical Effort was rarely selected as a relevant variable, and Task Difficulty and Mental Effort (which are usually considered to be important) were just moderately important for this group. For each of the 16 experimental conditions, the nine original bipolar scales, multipled by the appropriate weight, were combined and averaged for each subject. The resulting weighted workload estimate could be conceptualized as the combined area of a bar graph with nine variables; the width of each bar determined by the importance of that factor to the individual (the weight) and the height of each bar determined by the subjective magnitude of the factor in a given experimental condition (the bipolar ratings). (see Appendix B for examples by subject and experimental condition)

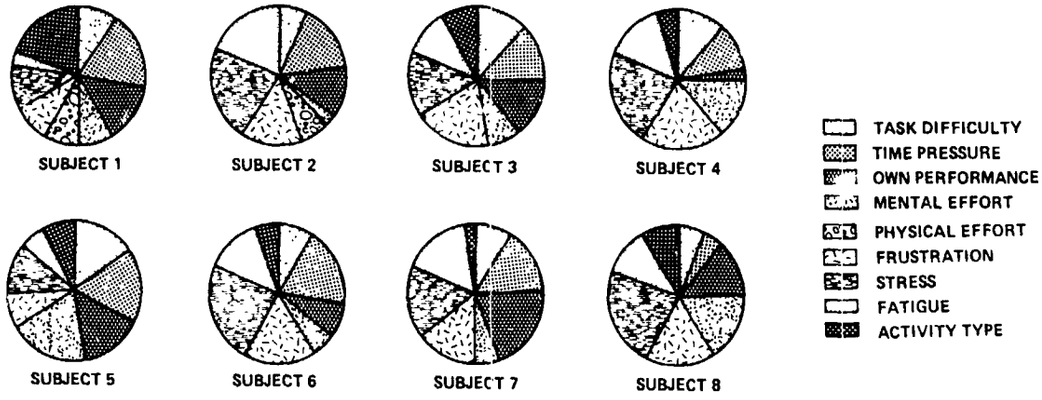

Figure 4: Relative importance to the subjective experience of workload assigned to each of 9 factors by each subject (n = 8)

The magnitude of the weighted workload estimates was less, on the average, (43.4 versus 52.7) than was the overall bipolar rating of workload, however the relationships among the experimental conditions was the same for the two estimates of workload, as illustrated in Figure 5. This reduction in magnitude is expected, as a single rating of overall workload represents the subjective total of whatever factors the individual considered were relevant to an exrerience of workload, whereas the weighted combination of ratings is statistical average of all of the factors. The benefit of performing the weighting procedure was that the between-subject SD was reduced for every experimental condition taken one at a time. Overall, the reduction 17% (from 25.5 to 21.3). Using a simple linear combination of the nine unweighted ratings also resulted in reduced between-subject variability (with the relationships among experimental conditions maintained), but the reduction was considerably less.

The reduction in between-subject variability achieved with the weighting procedure was less than has been found in other recent applications (see, for example, refs. 12, 13). In other applications, between-subject variablity was reduced by as much as 50% overall. Since the participants in the current study were in greater accord about the relative importance of the different factors than has been found for other groups of subjects, the influence of individual differences in the definition of workload wcs not as great in the current study as in the others. This weighted workload rating will be used as the primary measure of subjective workload for the remainder of the study.

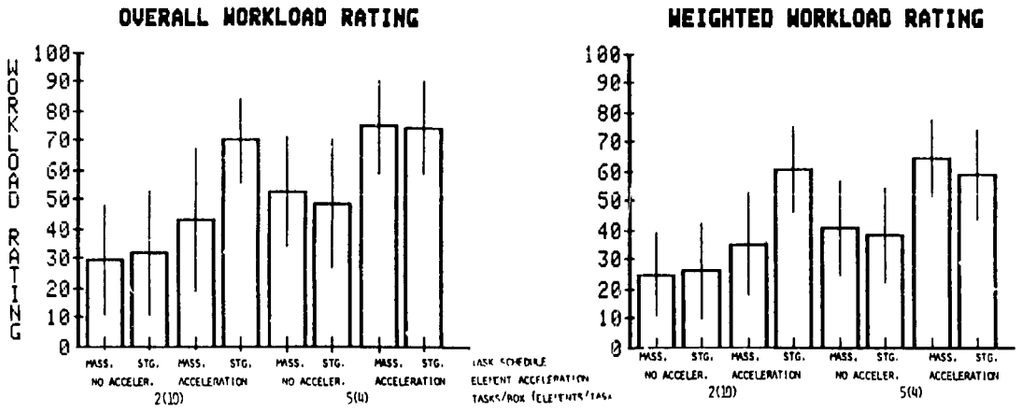

Figure 5: Unweighted and weighted ratings of overall workload by experimental condition (n=8; I depicts +/-1 SD)

Score

The scores ranged from a maximum of 500 to a low of 55. The grand mean was 375 (SD = 125). Thus, the 16 combinations of experimental variables did produce the desired range in performance levels across subjects and scenarios. (Figure 6) On an individual basis, the average scores obtained by individual subjects across experimental conditions ranged from 409 to 321. High scoring subjects performed more consistently than low scoring subjects, and there was a highly significant correlation between score and rated workload (rxy = -0.71), high scores being associated with low workload ratings.

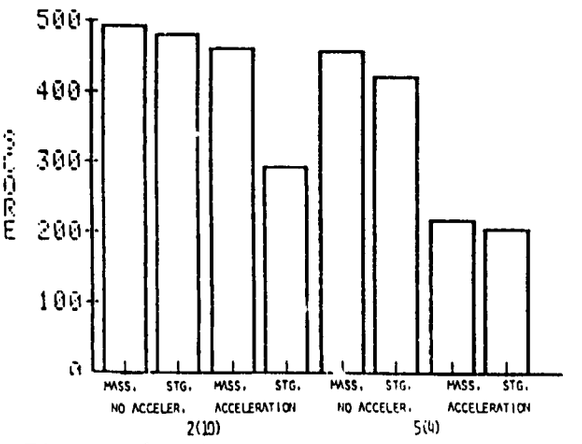

Figure 6: Average scores by experimental condition. (n = 8)

Scores were examined in the order that the scenarios were presented to determine whether or not there was a continuing improvement in performance from the beginning to the end of the experiment across the counterbalanced experimental conditions. No such improvement was found, indicating that the training given was sufficient to achieve stable levels of performance.

Task Duration

The scenario durations ranged from 615 to 216 sec. The average length of time was 383 sec (SD = 117 sec). On an individual basis, the average time taken to perform a scenario ranged from 410 to 369 sec. The subjects with the best scores also had the fastest times, suggesting there that was no speed/accuracy tradeoff, however the overall correlation between score and duration was only +0.49. The correlation between scenario duration and workload was -0.41, shorter sessions being associated with greater workload. The presence of ACCELERATION resulted in a sharp decrease in session length, as can be seen in Figure 7, because task elements moved more quickly and were, therefore

available for performance with less delay. In all cases, the obtained session durations were less than the baseline durations used to create the schedules. When the schedules were designed, it was assumed that tasks would be performed one at a time, that LINK, MORE, SHED, etc. would not be used to decrease time-to-completion, and that all tasks would be performed so as to impose schedules that would allow time for an average operator to complete most of the tasks.

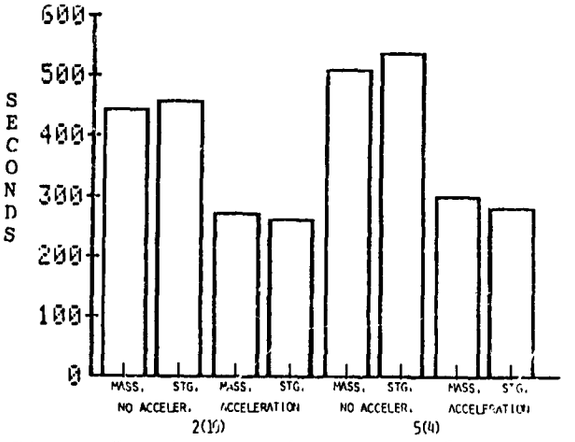

Figure 7: Average durations of the experimental conditions. (n = 8)

Operator Strategies

The relative proportion of function key actuations made be each subject may be seen in Figure 8. There was relatively little difference among subjects in PERFORM key actuations, although high-scoring subjects, obviously, used it more often than low-scoring subjects because they operated on several tasks at the same time, rapidly switching from one open task to another. Thus, the two high-scoring subjects (mean = 409) averaged 80 different task selections per scenario (S-5 and S-7), while the low-scoring subject (mean = 321) averaged 25 selections per scenario (S-8). High-scoring subjects used the OPEN, CLOSE, STUFF, and MORE commands nearly twice as often as low-scoring subjects, thereby controlling the flow of active tasks. Although there was considerable variation in the use of the LINK and SHED commands, their use was not significantly correlated with score, rated workload or task duration.

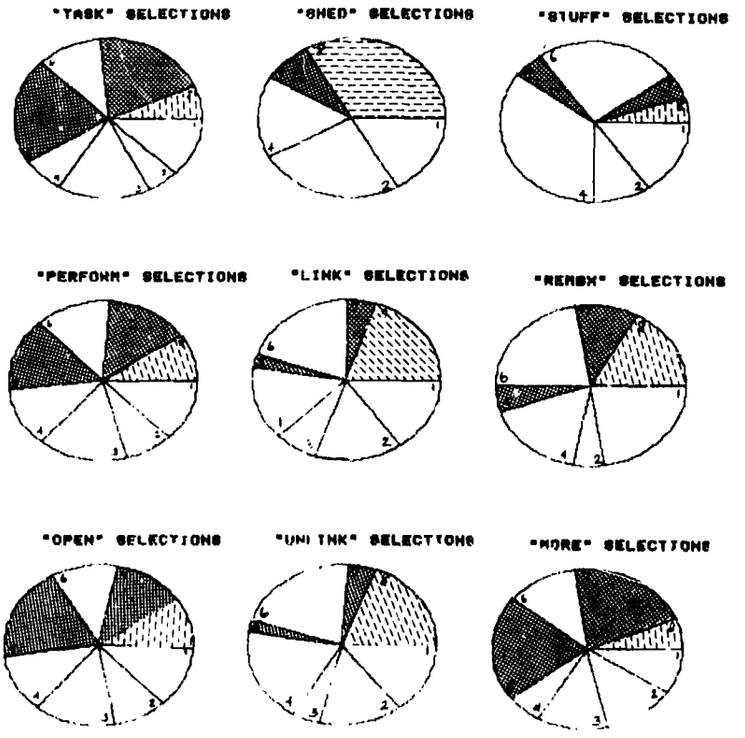

Figure 8: Relative proportion of times each function was selected by subjects whose score was low ( ), high ( ), or average ( ).

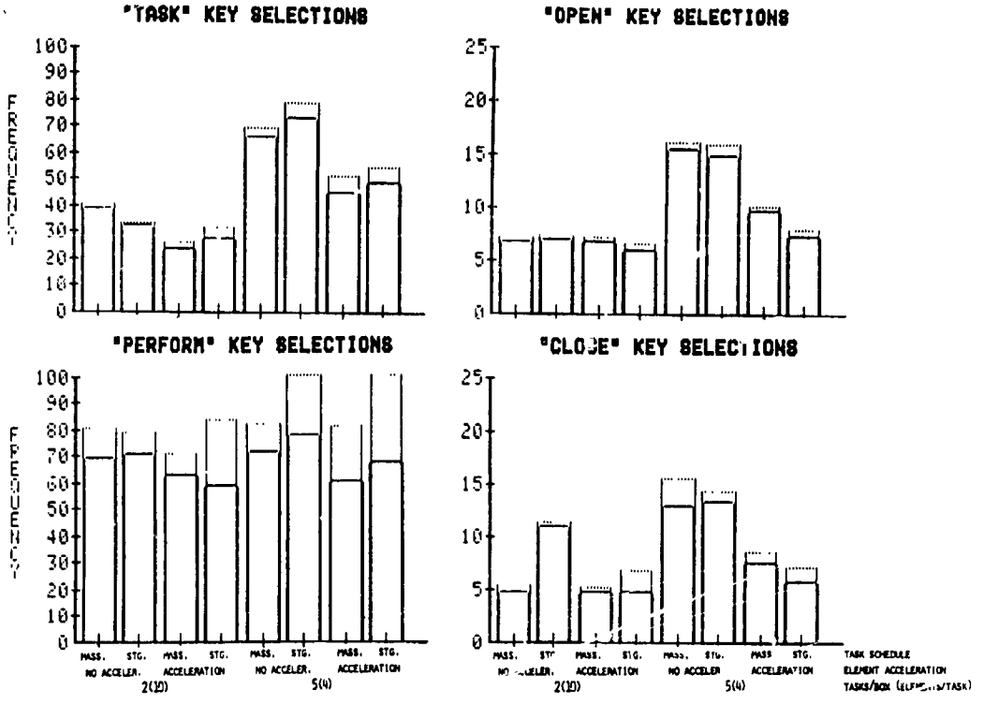

Figure 9: Frequency of appropriate (┌─┐) and inappropriate (┌┄┐) selections of the basic functions by experimental condition (n = 5).

Basic Functions

The scenarios were designed so that each task had the same payoff, rate, number of elements/tasks, and schedule, thus, similar performance was anticipated across the five tasks. Individual analyses of variance for repeated measures were performed for each function to determine whether each was selected equally often for the five tasks task across experimental conditions. Since no significant differences were found for any function, subsequent analyses were performed collapsed across task type.

On the average, the four basic functions were selected 152 times per scenario. Of these selections, 85%, were made correctly. The remaining selections were slips (the operator intended to select one function but actuated another instead) or errors (the opearato# selected an inappropriate function). An inappropriate TASK or PERFORM selection occurred when no task elements were available. An inappropriate OPEN or CLOSE selection was one that was made when the selected box was already open or closed. Different TASKS were selected 48 times (96% correctly), PERFORM was selected 85 times (83% correctly), and OPEN and CLOSE were selected 10 and 9 times, respectively (99% correctly), across experimental conditions. (Figure 9)

Problem-solving functions

The four functions that were provided as solutions to [illegible] behind the system were selected two times each, on the average. Use of the [illegible] and the performance of tasks from the penalty box characteristic [illegible]. (Figure 8) The REMOVE BOX command was used only once per scenario by high-

Comparison of Experimental Conditions

Measures of performance, behavior, and subjective experience were analyzed to determine the relative impact of the four experimental variables. Significant variations in measures of performance may be seen in Figures 6 and 7. Significant variations in the selections of functions may be seen in Figures 9, 10, and 11. Workload ratings may be seen in Figure 5.

REWARD/PENALTY Conditions

Performance There were no significant variations in scores or duration

Workload Rating There was no significant variation in rated workload

Use of Basic Functions There were no significant variations in the frequency with which any of the basic functions were selected as a function of the **REWARD/PENALTY** condition.

Use of Problem-Solving Functions There was a significant increase in the use of the SHED command (from 0.6 to 2.25 selections/scenario) when a penalty was levied for failing to perform task elements. If it was clear to the operator that he could not perform one or more elements before they reached the graveyard or were transferred to the penalty box, this was the correct strategy (on +5/-5 trials) to avoid an additional five-point penalty. Since as many as 10 elements could have been shed with a single command (all those remaining in the box), this measure may underestimate the impact of this function on the subsequent structure of the task. None of the other commands were used significantly differently due to the **REWARD/PENALTY** condition.

Use of Lead-Generating Functions There was no significant change in the of use of these commands as a function of the **REWARD/PENALTY** condition.

Schedule

Performance There was a significant ($F(1,7) = 19.16$, $p<.01$) decrease in score (from 404 to 347) between the **MASSED** and **STAGGERED** schedules. Overall, the length of time taken to complete scenarios was not affected by the schedule, even though the scheduled durations were offset by 5 sec in the **STAGGERED** condition, potentially increasing the time required to complete a task.

Workload Rating Rated workload increased significantly ($F(1,7) = 19.11$, $p< .01$) from 41 (**MASSED**) to 46 (**STAGGERED**) as schedule complexity was increased, reflecting the additional mental processing load imposed by more complex schedules.

Use of Basic Functions There were no significant differences in the use of any of the basic functions due to schedule alone. The same number of boxes were OPENed, CLOSEed, and SELECTed. The PERFORM key was actuated more often with the **STAGGERED** schedule than with the **MASSED** schedule, but 25% of the selections were made in error. This resulted in a significant difference in the number of erroneous PERFORM key selections ($F(1,7) = 14.5$, $p<.01$).

Use of Problem-Solving Functions All of the problem-solving functions were used more often with the **STAGGERED** condition, indicating that the operators were lagging the system. STUFF ($F(1,7) = 13.72$, $p<.01$) and REMOVE BOX

($F(1,7) = 13.75$, $p<.01$) commands increased significantly, and more tasks ended up in the penalty box ($F(1,7) = 9.17$, $p<.05$).

Use of Lead-Generating Functions The LINK and UNLINK commands were selected significantly ($F(1,7) = 9.01$, $p<.05$) less often with the **STAGGERED** condition, as expected, because it was rare that two tasks were at the same stage of performance and were, therefore likely candidates for LINKing. MORE tasks were selected half as often with the **STAGGERED** schedule ($F(1,7) = 11.46$, $p < .05$), another indication that subjects were not able to get ahead of the system in this condition.

Acceleration of elements

Performance There was a highly significant difference in scores due to the presence (460) or absence (291) of **ACCELERATION** ($F(1,7) = 773.2$, $p<.001$), particularly when **ACCELERATION** was combined with a **STAGGERED** schedule and when there were a greater number of different tasks. These synergistic effects were reflected in a significant **SCHEDULE** by **ACCELERATION** interaction ($F(1,7) = 8.43$, $p<.05$) and in a significant **ELEMENTS/TASK** by **ACCELERATION** interaction ($F(1,7) = 20.77$ $p<.01$).

Scenarios with **ACCELERATION** were completed significantly more quickly ($F(1,7) = 168.7$, $p<.001$) than those without (488 versus 277 sec, respectively). With **ACCELERATION**, task elements arrived more quickly and were available for performance at a faster rate once in a box, thus, operators were not constrained by system delays in completing tasks.

With **ACCELERATION**, the number of times that functions were selected inappropriately was increased, possibly because operators were under greater time pressure. Significantly more tasks ended up in the graveyard ($F(1,7) = 83.41$ $p<.001$) and penalty box ($F(1,7) = 31.29$, $p<.001$) with **ACCELERATION**.

Workload Rating There was a significant ($F(1,7) = 30.56$, $p<.001$) increase in workload ratings with **ACCELERATION** (from 32 to 55). The influence of **ACCELERATION** on experienced workload was particularly great when it was combined with a **STAGGERED** schedule with many elements to be performed per task. This was reflected in a significant three-way interaction among **SCHEDULE**, **ACCELERATION**, and **ELEMENTS/TASK** ($F(1,7) = 14.44$, $p<.01$). Rated workload may have been highest in the 2(10), **ACCELERATED** scenarios because tasks with many elements took longer to complete and were thus subject to the effects of acceleration for a longer time.

Use of Basic Functions There was no significant change in the use of the TASK select or the PERFORM functions due to **ACCELERATION**. There was, however, a significant decrease in the number of times that the OPEN ($F(1,7) = 15.29$, $p<.01$) and CLOSE ($F(1,7) = 9.07$, $p<.01$) functions were used, particularly when there were many different tasks per box. There was a significant three-way interaction among **ACCELERATION**, **SCHEDULE**, and **ELEMENTS/TASK** for the OPEN function ($F(1,7) = 119.62$, $p<.001$). Boxes were OPENed 6.5 times per scenario, on the average, in the 2(10) condition regardless of **SCHEDULE** or **ACCELERATION**, whereas they were OPENed as often as 16 times per scenario without **ACCELERATION** in the 5(4) condition and 10 times with **ACCELERATION**. In the easier conditions, and when only two tasks with 10 elements each were scheduled, subjects OPENed each box one time and left it that way. They did not OPEN and CLOSE boxes as a management strategy. When five tasks were scheduled per box,

however, they did close the boxes occasionally between different tasks, but considerably less often than once for every one of the 25, four-element tasks.

Use of Problem-Solving Functions All of these functions were used more often with **ACCELERATION** than without. Significantly more tasks had to be SHED ($F(1,7) = 9.36$, $p<.01$), STUFFed $F(1,7) = 5.67$, $p<.05$) and performed with the additional REMOVE BOX procedure ($F(1,7) = 6.12$, $p<.05$). These differences indicate that subjects were more likely to lag behind the system with **ACCELERATION** than without.

Use of Lead-Generating Functions A related finding was that there were fewer requests for MORE tasks ahead of schedule with **ACCELERATION** than without ($F(1,7) = 19.24$, $p<.01$). The difference was particularly great when more tasks were actually available (in the 5(4) condition). There was a significant interaction between **SCHEDULE** and **ELEMENTS/TASK** ($F(1,7) = 12.13$, $p<.01$). **ACCELERATION** did not affect the use of LINK and unLINK.

Number of ELEMENTS/TASK

Performance There was a significant ($F(1,7) = 114.1$, $p<.001$) decrease in score (from 430 to 322) when there were more different tasks with fewer elements each. This decrease was accentuated by **ACCELERATION** ($F(1,7) = 20.77$, $p<.01$) and by a **STAGGERED** schedule ($F(1,7) = 15.13$, $p<.01$).

The time taken to complete a scenario was significantly longer when there were more discrete tasks to be performed ($F(1,7) = 43.3$, $p<.001$) than when the same number of elements were grouped into fewer (albeit more complex) tasks. To some extent, this increase in time occured because four-element tasks did not remain in the boxes as long as ten-element tasks and thus never developed the same rates of speed due to **ACCELERATION** .

More functions were selected inappropriately as the number of discrete tasks increased (18 versus 23%). The decrease in score, increase in time-to-complete a scenario, and increase in errors in the 5(4) condition may reflect the cost of shifting attention among 25 smaller tasks, even though each was individually less complex.

Workload ratings The greatest increase in rated workload was found between the 5(4) and 2(10) conditions. This significant increase ($F(1,7) = 51.2$, $p<.001$) reflected the operators' perceptions that an increase in the number of different tasks that they were required to do (even if the total number of subtask elements remained the same) imposed a substantial increase in their workload.

Use of Basic Functions Not surprisingly, there were significantly ($F(1,7) = 50.8$, $p<.001$) more TASK selections with the 5(4) condition than with the 2(10) condition, because subjects had to shift their attention among many discrete tasks. The difference (33 versus 64) was not as great, however, as the 250% increase in the actual number of different tasks scheduled for each box. Although the OPEN function was selected significantly ($F(1,7) = 42.6$, $p<.001$) more often in the 5(4) conditions than in the 2(10) conditions, the increase (from 7 to 13 times per scenario) was proportionally less than would be expected from the actual increase in number of different tasks per scenario (from 10 to 25). Relatively speaking, subjects shifted their attention from one task to the next less often as the number of discrete tasks was increased.

Use of Problem-Solving Functions There was no significant change in the use of the REMOVE BOX and STUFF commands as a consequence of the number of tasks per box. There was, however, a significant ($F(1,7) = 9.23$, $p<.05$) increase in the use of the SHED command when there were fewer elements, but more tasks. This might have occurred because the SHED command had a less dramatic effect on reducing the number of tasks remaining to be performed for score points when there were only 4 elements per task rather than 10. There were significantly more tasks transferred to the penalty box ($F(1,7) = 29.6$, $p<.001$) in the 5(4) scenarios than in the 10(2) scenarios. Seven times as many elements were performed from the penalty box (but with no increase in score) in the 5(4) scenarios than in the 2(10) scenarios. This occurred because there were five separate arrivals of tasks in each box, thereby increasing the chance (by 250%) that a new task would enter an box still occupied by an existing task. Since there was no significant difference in the number of times the PERFORM function was selected, the lower scores obtained with the 5(4) conditions occurred because more tasks were SHED and more ended up in the penalty box (thus no points were gained for them even if they were performed), not because they selected the PERFORM function less often.

Use of Lead-Generating Functions Although more tasks were requested ahead of schedule in the 5(4) condition than in the 2(10) condition (5.3 times per scenario versus 3.1), the difference was not significant. In addition, the increase was considerably less than would be expected by the increased opportunities to request tasks ahead of schedule provided by the 5(4) scenario (4 times per box) than the 2(10) scenario (once per box). The LINK and UNLINK commands were used considerably less often than they could have been in 5(4) scenarios. The difference in usage between the two conditions was not significant.

Relative Importance of Experimental Conditions

The relative impact of the different experimental manipulations was analyzed by examining the amount of variance accounted for by each of them in the statistical analyses performed on the scores, workload ratings, and function selections. In addition, each subject was asked to rank order the four factors with respect to the impact that they felt each had had on workload. The **REWARD/PENALTY** conditions contributed little to variations in performance, behavior or opinion. The **ELEMENTS/TASK** had the greatest impact on the frequency of basic function selections. Presence or absence of **ACCELERATION** and **MASSED** versus **STAGGERED** schedules, particularly when they covaried, had the greatest impact on problem-solving behavior, lead-generating responses, and score. Although the number of **ELEMENTS/TASK** contributed most to the variance of workload ratings, the factor selected as most influential by the subjects at the end of the experiment was the **SCHEDULE** (a relatively less important influence on measures obtained during and immediatly after the scenarios).

CONCLUSIONS

All of the experimental manipulations, alone and in combination, generated highly significant differences in operator behavior, performance, and experienced workload with the exception of the **REWARD/PENALTY** condition. Each variable had slightly different influences on individual measures, however,

scorers. Instead of performing the additional REMOVE BOX step for tasks in the warning zone, they selected the STUFF option, using this strategy six times more often per scenario than did the low-scoring subjects. The STUFF and REMOVE BOX commands were selected in error at least once per cenario, although the SHED command was never selected erroneously. (Figure 10)

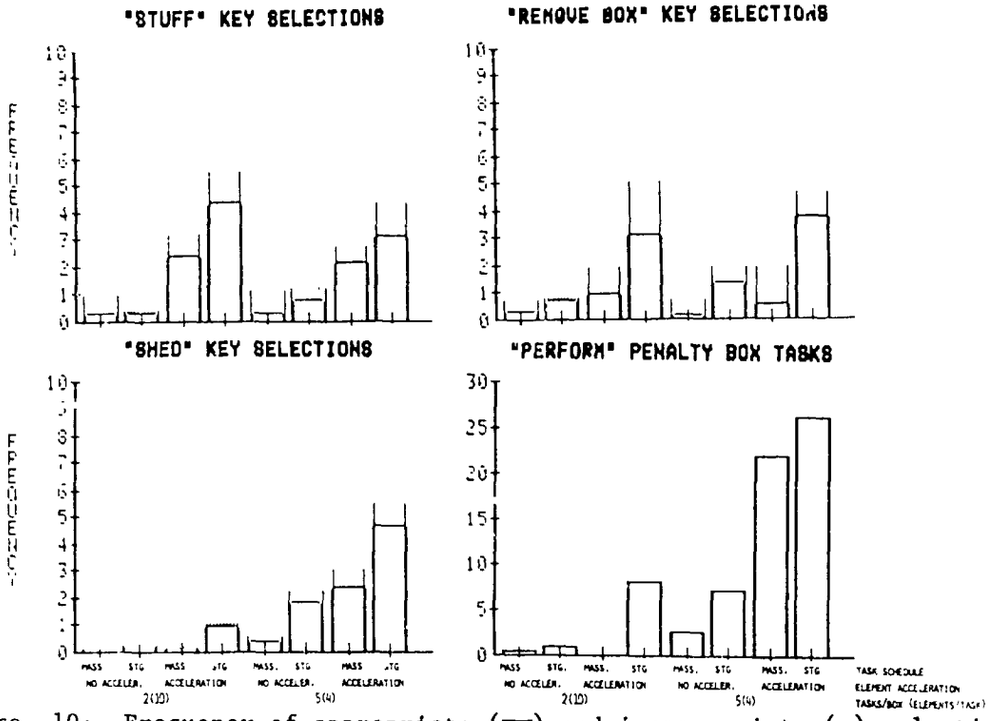

Figure 10: Frequency of appropriate (⌐¬) and inappropriate (¬¬) selections of problem-solving functions by experimental condition (n = 8)

Lead-generating Functions

The LINK command was used rarely by high-scoring subjects (once or twice per scenario), but relatively often by the other (seven times per scenario). It was usually selected appropriately. (Figure 11) On the average, the MORE command was selected four or five times per scenario, however more than half of the time more tasks were requested none were available for the selected box. High-scorers used the MORE command three times more often than low-scorers because they were able to complete tasks ahead of schedule.

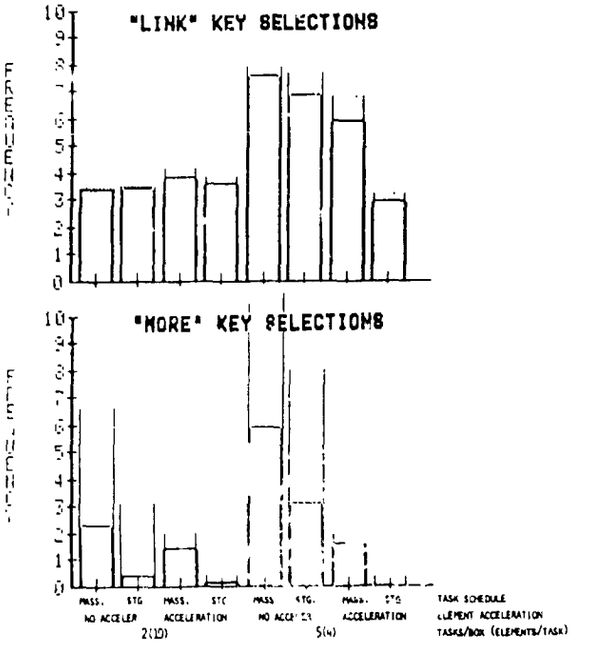

Figure 11: Frequency of appropriate (⌐¬) and inappropriate (¬¬) lead-generating function selections (n=8)

allowing a detailed and informative analysis of the effect of experimental manipulations of imposed workload on different aspects of operators' behavior and performance. The initial objective of developing a set of scenarios that imposed a range of variations in performance and workload and investigating the impact of different penalties for procrastination was satisfied. In addition, the efficacy of the proposed weighted combination of workload components in reducing between-subject variability was demonstrated.

In future experiments, the effects of training must be determined to establish optimal procedures and asymptotic levels. In addition, the influence of task rate and value should be manipulated so as to replicate the critical variables in the earlier studies (refs. 5, 6, 7) using the current paradigm. In future research, particular attention should be given to the impact of machine-aiding, automation, and system failures on performance, behavior, and workload. Given the success of this simulation in generating significant variations in performance and workload, this paradigm should continue to provide a useful environment in which measures of workload and performance can be developed, tested and calibrated once standardized levels of imposed task load have been established. This experiment was designed to evaluate utility of the POPCORN simulation as an experimental task. It remains to future researchers to apply the different theoretical and mathematical models (depending on their experimental goals) to use this simulation as a prototype of multi-task, automated and semi-automated supervisory control systems.

REFERENCES

1. Hart, S. G. and Sheridan, T. S. Pilot workload, performance, and aircraft control automation. Proceedings of the AGARD Symposium on Human Factors Considerations in High Performance Aircraft.. Williamsburg, VA, April 1984. (in Press)

2. National Research Council. Automation in Combat Aircraft. Committee on Automation in Combat Aircraft. Washington, D. C.: National Academy Press, 1982.

3. Shingledecker, C. A., Crabtree, M. S. and Acton, W. H. Standardized tests for the evaluation and classification of workload metrics. Proceedings of the Human Factors Society - 26th Annual Meeting. Seattle, WA, 1982, 648-651.

4. Derrick, W. L. and Wickens, C. D. A Multiple Processing Resource Explanation of the Subjective Dimensions of Operator Workload. Urbana-Champaign, IL. Engineering Psychology Research Laboratory Technical Report EPL-84-2/ONR-84-1, February 1984.

5. Tulga, K. M. and Sheridan, T. S. Dynamic decisions and workload in multitask supervisory control. IEEE Transactions on Systems, Man and Cybernetics, 1980, SMC-10, 217-231.

6. Daryanian, B. Subjective scaling of mental workload in a multi-task environment. Proceedings of the 16th Annual Conference on Manual Control. Massachusetts Institute of Technology, 1980, 172-188.

7. Pattipati, K. R., Kleinman, D. L., and Ephrath, A. R. A dynamic decision model of human task selection performance. IEEE Transactions on Systems, Man,

and Cybernetics, 1983, SMC-13(3), 145-156.

8. Sheridan, T. S. & Stassen, H. Definitions, models, and measures of human workload. In N. Moray (Ed.) Mental Workload: Its Theory and Measurement. New York: Plenum Press, 1979, 219-234.

9. Moray, N. Subjective mental workload. Human Factors, 1982, 24(1), 25-40.

10. Hart, S. G., Childress, M. E. & Hauser, J. R. Individual definitions of the term "workload". In the Proceedings of the 1982 Psychology in the DOD Symposium. U. S. Air Force Academy, 1982.

11. Reid, G. B., Eggemeier, F. T. and Nygren, T. E. An individual differences approach to SWAT scale development. Proceedings of the Human Factors Society - 26th Annual Meeting. Seattle, WA, 1982, 639-62.

12. Kantowitz, B. H., Hart, S. G., Bortolussi, M. R., Shively, R. J., and Kantowitz, S. C. Measuring pilot workload in a moving-base simulator: II. Building levels of workload. Proceedings of the 20th Annual Conference on Manual Control., 1984 (in press)

13. Miller, R. C. and Hart, S. G. Assessing the subjective workload of directional orientation tasks. Proceedings of the 20th Annual Conference on Manual Control., 1984 (in press)

APPENDIX A: Scheduled arrival times of tasks

SCHEDULED ARRIVAL TIME OF TASKS (BY SCENARIO)

SUMMARY OF RESULTS (BY SCENARIO)

10 ELEMENTS/TASK; NO ACCELERATION; MASSED SCHEDULE

DIFFICULTY RANK: 1 (least)
SCORE: 454
DURATION: 512
WORKLOAD RATING: 40
BASIC FUNCTION SELECTIONS: 70/82/16/16=186
PROBLEM SOLVING FUNCTION SELECTIONS: 1/1/1/3=6
LEAD-GENERATION FUNCTION SELECTIONS: 11/8=19

4 ELEMENTS/TASK; NO ACCELERATION; MASSED SCHEDULE

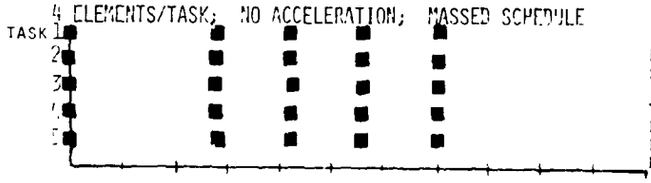

DIFFICULTY RANK: 2
SCORE: 491
DURATION: 444
WORKLOAD RATING: 25
BASIC FUNCTION SELECTIONS: 40/81/7/5=133
PROBLEM SOLVING FUNCTION SELECTIONS: 1/0/1/0=2
LEAD-GENERATION FUNCTION SELECTIONS: 7/3=10

10 ELEMENTS/TASK; NO ACCELERATION; STAGGERED SCHEDULE

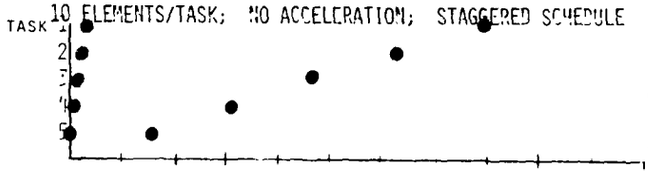

DIFFICULTY RANK: 3
SCORE: 417
DURATION: 539
WORKLOAD RATING: 38
BASIC FUNCTION SELECTIONS: 79/101/16/14=210
PROBLEM SOLVING FUNCTION SELECTIONS: 1/2/2/7=12
LEAD-GENERATION FUNCTION SELECTIONS: 8/8=16

4 ELEMENTS/TASK; NO ACCELERATION; STAGGERED SCHEDULE

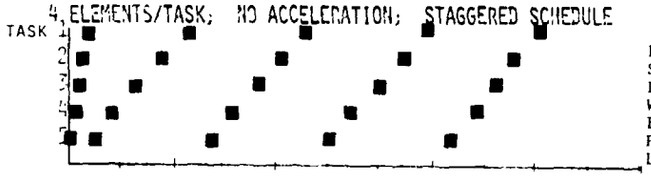

DIFFICULTY RANK: 4
SCORE: 477
DURATION: 456
WORKLOAD RATING: 26
BASIC FUNCTION SELECTIONS: 33/79/7/11=130
PROBLEM SOLVING FUNCTION SELECTIONS: 0/0/1/1=2
LEAD-GENERATION FUNCTION SELECTIONS: 3/3=6

10 ELEMENTS/TASK; ACCELERATION; MASSED SCHEDULE

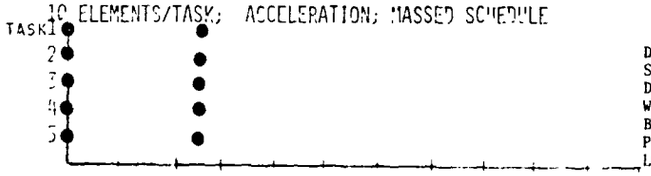

DIFFICULTY RANK: 5
SCORE: 460
DURATION: 272
WORKLOAD RATING: 35
BASIC FUNCTION SELECTIONS: 26/71/7/5=109
PROBLEM SOLVING FUNCTION SELECTIONS: 3/0/2/0=5
LEAD-GENERATION FUNCTION SELECTIONS: 2/4=6

4 ELEMENTS/TASK; ACCELERATION; MASSED SCHEDULE

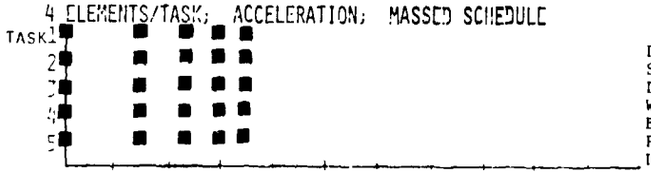

DIFFICULTY RANK: 6
SCORE: 213
DURATION: 300
WORKLOAD RATING: 64
BASIC FUNCTION SELECTIONS: 52/81/10/9=152
PROBLEM SOLVING FUNCTION SELECTIONS: 3/3/2/22=30
LEAD-GENERATION FUNCTION SELECTIONS: 2/7=9

10 ELEMENTS/TASK; ACCELERATION; STAGGERED SCHEDULE

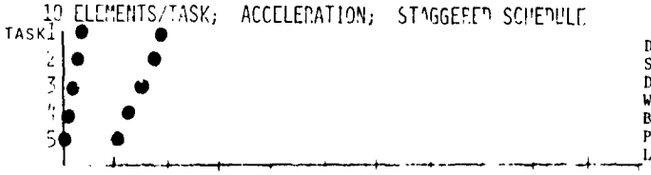

DIFFICULTY RANK: 7
SCORE: 203
DURATION: 278
WORKLOAD RATING: 59
BASIC FUNCTION SELECTIONS: 55/100/8/7=170
PROBLEM SOLVING FUNCTION SELECTIONS: 4/5/5/27=41
LEAD-GENERATION FUNCTION SELECTIONS: 0/3=3

4 ELEMENTS/TASK; ACCELERATION; STAGGERED SCHEDULE

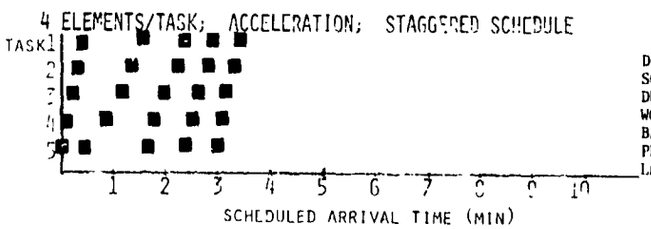

DIFFICULTY RANK: 8 (most)
SCORE: 290
DURATION: 260
WORKLOAD RATING: 60
BASIC FUNCTION SELECTIONS: 31/84/7/7=129
PROBLEM SOLVING FUNCTION SELECTIONS: 6/1/5/8=20
LEAD-GENERATION FUNCTION SELECTIONS: 0/4=4

● TASKS WITH 10 ELEMENTS EACH
■ TASKS WITH 4 ELEMENTS EACH

OF POOR

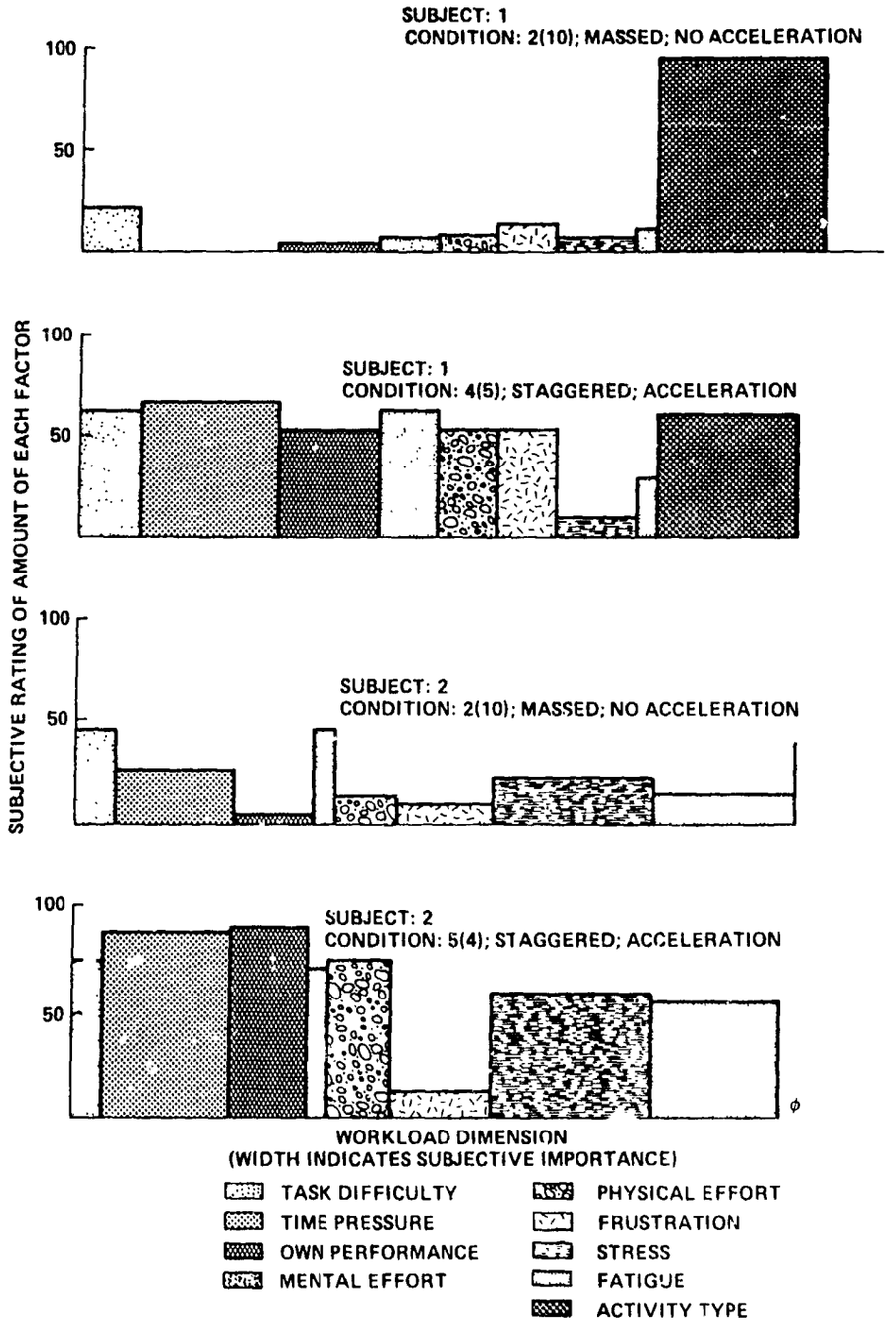

Appendix B: Eaxmpie of weighting procedure applied to the bipolar ratings obtained from each of two different operators after performing a relatively easy scenario and a relatively difficult scenario. (See Figure 4 for the importance placed on each of the factors by these two subjects).

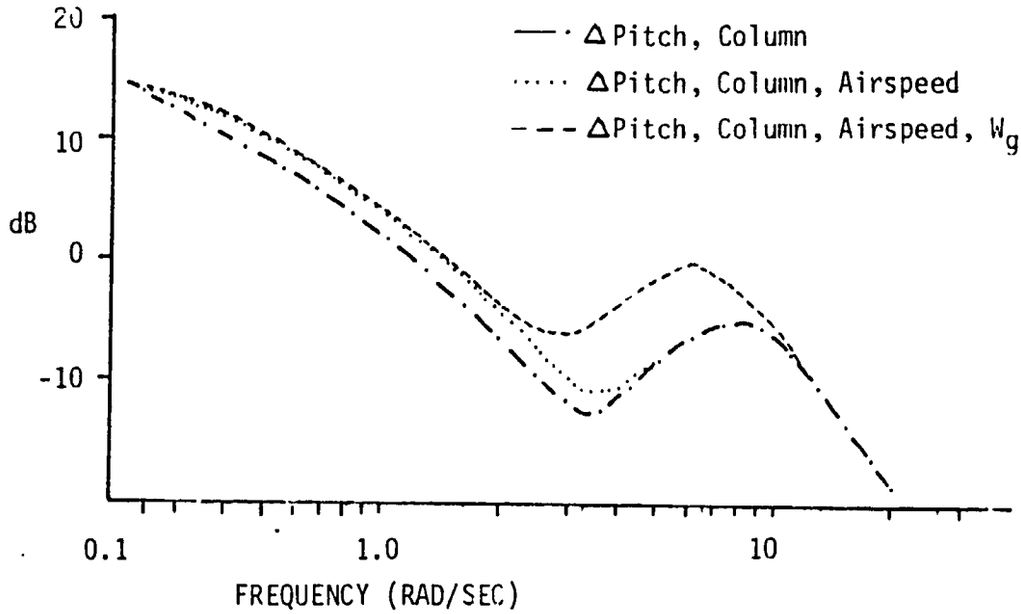

FIGURE 15 Effect of Variable Addition on Test Pilot Transfer Function: Δ Pitch to Column Initially, Airspeed and Vertical Wind, W_g, Added in Sequence

N85 14516

PSYCHOLOGICAL ISSUES IN ONLINE ADAPTIVE TASK ALLOCATION

Nancy M. Morris*, William B. Rouse*,
Sharon L. Ward**, and Paul R. Frey*

*Search Technology, Inc.
Norcross, Georgia 30092

**Air Force Aerospace Medical Research Laboratory
Wright-Patterson Air Force Base, Ohio 45433

ABSTRACT

Adaptive aiding is an idea that offers potential for improvement over many current approaches to aiding in human-computer systems. The expected return of tailoring the system to fit the user could be in the form of improved system performance and/or increased user satisfaction. Although the utility of the concept has been demonstrated in limited ways in a variety of contexts, there has been no substantial research effort devoted to addressing the many issues relevant to adaptive aiding. These include such issues as the manner in which information is shared between human and computer, the appropriate division of labor between them, and the level of autonomy of the aid.

In order to investigate these and other issues relevant to human-computer interaction, a simulated visual search task has been developed. Subjects are required to identify targets in a moving display while performing a compensatory sub-critical tracking task. It is also possible for the computer to identify targets. By manipulating characteristics of the situation such as imposed task-related workload and effort required to communicate with the computer, it is possible to create conditions in which interaction with the computer would be more or less desirable. The results of preliminary research using this experimental scenario are presented, and future directions for this research effort are discussed.

INTRODUCTION

The idea of providing the human operator with some form of computer assistance is not new. Computers have been used for years in a variety of applications. Often the complexity of modern systems and the potentially high costs of system failure have been invoked as justification for computerizing portions of the operator's job.

The decision as to which tasks will be performed by computer has all too often been based upon which tasks could be automated. In situations where total automation was not feasible, the task

PRECEDING PAGE BLANK NOT FILMED

allocation decision has been based upon relative abilities of human and computer. For example, humans would be given tasks requiring "flexibility" and computers would perform tasks requiring "consistency". A number of lists of human vs. computer abilities are available for this purpose (e.g., Licklider, 1960).

For several reasons, this "traditional" approach to computer aiding may be less than satisfactory. For example, thanks to progress in artificial intelligence, the distinction between human and computer abilities is much less clear. Thus, the human and computer may be viewed as partners, with abilities which partially overlap. As a result, it may be inappropriate to allocate tasks based solely on computer abilities.

Another factor which should be considered is individual differences. Aptitudes and abilities, cognitive styles, and attitudes have been cited as affecting human behavior in a number of situations. Lists of human abilities are characteristic of a prototypical human and do not reflect these differences.

Human performance varies not only across individuals but also within individuals over time. People become fatigued. They have a limited capacity to perform. The "mix" of required tasks may impose an inordinate amount of workload, and performance may degrade as a result.

Finally, the quality of the computer's performance may depend upon conditions. For example, suppose the computer must have certain state information in order to make decisions. If the quality of that information is degraded, performance of the computer will be affected.

In light of these shortcomings, it seems desirable to make computer aids adaptive. An adaptive aid could step in when needed and provide assistance in a form appropriate to the situation. In situations where no assistance was needed, the aid could remain inactive. In principle, it seems that such an approach to aiding could improve overall system performance substantially.

RELEVANT ISSUES

The concept of adaptive aiding is also not new (Chu & Rouse, 1979; Rouse, 1975, 1981). However, it has not been implemented in any real-world applications, probably because the manner in which this should be done is not at all straightforward. A number of issues must be considered before progress can be made (Rouse & Rouse, 1983). For example, what should the <u>focus</u> of adaptation be? Should the aid be adapted to group characteristics, or to individuals? Should adaptation be done once, or dynamically over time?

Another issue is the method of adaptation. At least three approaches are imaginable. Tasks may be allocated, with either the human or computer in control of task performance. Alternatively, tasks may be partitioned between the two partners, with each performing task components. Finally, one partner may assist the other by performing a transformation of a task (e.g., the computer could filter noise from a visual display).

If human and computer are to be partners, then there must be some means for the two to communicate. But what should be the nature of communication? If communication is explicit, there is less uncertainty as to what is being communicated, but the human must invest resources in receiving and transmitting information. This resource demand may be less if communication is implicit, but there may be less certainty as to what is communicated. There may also be a need for the human to invest resources into determining what the computer is doing.

When system control is shared by human and computer, which partner should be in charge? Suppose tasks are to be allocated dynamically. Which partner--human or computer--should make the decision as to task allocation? As with the nature of communication, the resources required to make decisions and inform the partner must be considered.

Finally, if it appears that it would be advantageous to have the computer make decisions such as task allocation, what is the basis for decision making? It will be necessary to imbed models in the computer's knowledge base if such decisions are to be possible. These models must incorporate characteristics of the task situation, the human's task performance, and the computer's performance in order to be effective. Although the results of research in human problem solving and information processing provide a partial data base to support such models, many parameters must be obtained via specific research in human-computer interaction. The goal of the work reported here is to investigate these and other relevant issues.

EXPERIMENTAL APPROACH

In explaining the approach adopted in this research effort, it helps to consider a hypothetical situation. Suppose a variety of tasks must be performed for overall system operation to be successful. Human performance of these tasks on an individual basis is acceptable, but the degree to which tasks may be time-shared successfully depends upon the level of difficulty and combination of concurrent tasks. Further, suppose a computer is available which may perform a subset of these tasks. The computer's task performance may or may not be as good as the human's best performance, but may be preferable if the human's performance degrades.

An attempt was made to create this situation experimentally.

In designing the experimental scenario, one goal was to maintain a semblance of realism, rather than create an "artificial" laboratory task. However, the characteristics of the task environment were determined analytically, and little attempt was made to provide a high-fidelity simulation of an actual task.

A target recognition task was created as one of the tasks in the scenario because of differences in human and computer abilities in this area. Humans readily impart meaning into what is seen, and are excellent at "perceptual organization". Computers, on the other hand, have a great deal of difficulty analyzing scenes, but excel at figure rotation and template matching. Thus, humans should be better at identifying features in a meaningful scene, whereas computers should be better if the scene is a relatively homogenous field of objects.

Description of Experimental Tasks

The target recognition task employs a color graphic terrain display, as illustrated in Figure 1. The terrain display depicts an intracoastal waterway with varying proportions of water. Water areas are colored blue. Also included in the terrain are green trees, tan ground, black buildings, white roads and parking lots, and cars and boats of assorted colors. To simulate flight over the terrain the display pans down the CRT. Subjects are given the goal of identifying or spotting boats of a certain type which are in use in the waterway.

Targets may be identified only when they are in the region defined by the heavy black horizontal lines. When the subject is identifying targets, identification is accomplished by using a mouse to position the cross-hair cursor on top of the target and then pressing a button on the mouse. When the button is pressed a "+" appears on the screen to acknowledge the action. Hits and false alarms are tallied in the upper left corner of the screen. (See Figure 1.)

It is also possible for the computer to perform the spotting task. If the human is in control of the allocation decision, the aid may be activated by positioning the cursor on top of the word "AID" (to the left of the terrain display in Figure 1), and pressing the button on the mouse. The cursor then disappears, and the aid identifies targets until the human resumes control by again pressing the button on the mouse.

The relative performance of human and computer may be expected to vary over time. In light of the human's perceptual abilities, this task should be easier for the human when the proportion of water in the picture is low (such as when flying over a narrow channel). This is because the human is able to organize the scene and automatically exclude a large portion (i.e., the land areas) from consideration.

The computer, on the other hand, is deficient in these organizational abilities, and scans the whole scene, identifying boats with a "template matching" approach.* As a result, the computer does not always differentiate land from water, and its false alarm rate increases with the proportion of land in the display. Thus, the human may be expected to excel when the proportion of water is low, and there is greater potential for the aid to excel when the proportion of water is high.

Target identification is not the only task which must be performed. In addition to looking for boats, the human must also perform a subcritical tracking task. The tracking display is shown in the upper left corner of Figure 1.

The tracking display contains a green region flanked by yellow and red regions. The horizontal black line to the right of these regions moves up and down, and the arrow within the green region indicates the direction of the control input. The degree of instability of the controlled element is determined by a difficulty parameter which is entered by the experimenter at the beginning of a run and remains constant throughout the run. The human's goal is to keep the black line within the green region by using bang-bang control via the space bar on the terminal keyboard. When performing both tasks, the subject identifies targets with the right hand and tracks with the left.

The primary reason for incorporating the tracking task into the scenario is to create conditions in which assistance from the computer is required in order to maintain satisfactory performance. If target identification were the only task required, it is conceivable that a subject could maintain acceptable performance over a wide range of difficulty. However, performance should be more sensitive to difficulty manipulations (i.e., changes in terrain composition) if tracking is also required. The difficulty parameter of the tracking task may be varied to insure that such is the case, and the option of "shedding" the tracking task in favor of the target identification task is eliminated by disabling mouse inputs whenever the tracking indicator is in a red region.

With respect to the adaptive aiding concept, it is possible to specify qualitatively when the computer should be used in this environment. First, the aid should be used if its potential target identification performance exceeds that of the human. It is expected that this occurrence is most likely when tracking is non-trivial and the terrain is mostly water. Second, the aid should be used to look for boats if the human's tracking

---

*In reality the computer "knows" the identity and location of every object in the display and makes responses on a probabilistic basis. The template matching explanation is provided to subjects.

performance degrades to an unacceptable level. Excluding the case in which acceptable tracking is impossible due to the level of tracking difficulty, it is anticipated that this occurrence would also be related to the amount of water in the display.

AN EXPERIMENT

A pilot study was conducted to evaluate the accuracy of some of these ideas by assessing the effects of task parameters on subject's performance. Since one of the purposes of this experiment was to identify conditions in which the need for computer assistance would be likely, no aid was available to subjects.

Two subjects served in three sessions each. The first session served as training and consisted of one 5-minute run at each of four levels of tracking difficulty. In the second and third sessions, the easiest tracking condition was excluded and only three levels of tracking difficulty were used. Thus, there were two independent variables in the pilot study: tracking difficulty and terrain composition. Dependent measures included rms tracking error, spotting accuracy (i.e., percent identified) and spotting latency (i.e., average time to identify a target once it entered the spotting window).

The results of this study are presented graphically in Figures 2-4. Time is represented on the abscissa of each graph, as the values shown represent the sequence of terrain types encountered by subjects over the course of a run. One interval on the abscissa corresponds to approximately 20 seconds of real time. To facilitate interpretation of these figures, terrain is also identified as either predominantly land or predominantly water. The break or dashed line in the middle of each graph reflects missing data. Due to hardware constraints, targets in these areas are not accessible to subjects, and there is a 1-2 second interval of "dead time" in the middle of each run.

Figure 2 depicts rms tracking error for three levels of tracking difficulty, averaged across both subjects. Two characteristics of Figure 2 are noteworthy. First, rms tracking error increased with increases in the difficulty parameter of the tracking task. Second, rms tracking error increased with the amount of water in the display. This effect seems to have been stronger when tracking was relatively easy, but is noticeable at each of the levels of tracking difficulty employed in this study.

From Figures 3 and 4, it may be ascertained that performance on the target identification task was also affected by changes in the terrain composition. Increases in the proportion of water in the display were accompanied by decreases in spotting accuracy (although small) and increases in spotting latency. Unlike rms tracking error, there was no noticeable effect of tracking difficulty manipulations upon target identification; as a

result, the plots in Figures 3 and 4 represent performance averaged across three levels of tracking difficulty.

If the three dependent measures are compared to each other, some clear relationships emerge. First, there is an obvious negative relationship between spotting accuracy and spotting latency. Product-moment correlations at different levels of tracking difficulty ranged from -.61 to -.70. Of course, these results were obtained with only two subjects, so generalizations should be made with caution; however, if further experiments continue to reveal this relationship, this may have implications for online adaptation.

Although spotting accuracy is the stated performance criterion, its utility as an online measure is limited due to two factors. First, observed decrements in spotting accuracy were quite small, usually no more than 2-3 missed targets. Second, it seems desirable to be able to offer assistance before a target is missed, rather than stepping in too late to do any good. Spotting latency is easily assessed online; if the relationship of latency to accuracy proves to be sufficiently strong, the latency measure may be useful as a basis for online computer adaptation.

It may also be noted that rms tracking error is related to both spotting accuracy and spotting latency. Since it is an easily calculated, continuous measure, rms tracking error may also be useful as a basis for decision making. However, the results from this pilot study indicate that rms tracking error may not be as useful for this purpose as spotting latency, because its response to task changes considerably lags the response of spotting latency to these changes. (A comparison of Figures 2 and 4 reveals a difference of almost 20 seconds in the most difficult tracking condition.)

PLANS FOR FUTURE RESEARCH

Current plans are to conduct a full-scale experiment this summer. Independent variables will be the same as those reported here: terrain composition and tracking difficulty. Additionally, an initial attempt will be made to have the computer make the decision as to allocation of the target identification task. Undoubtedly the decision algorithm will be rather simplistic; however, this should provide insights necessary for more effective decision aiding in the future.

At present, it is possible to imagine several alternative approaches to allocation which might be appropriate. For example, in addition to unilateral decision making by human or computer, a "hybrid" approach could prove to be useful. In this case, the computer could monitor the human's performance and assume control of the target identification task when his performance on either task began to degrade. The human could

then resume control of target identification when he felt able to do so.

If online adaptation is to be effective, it will be necessary to identify appropriate measures to serve as the bases for decision aiding, and to develop adequate models of how important variables interact. Effort will be devoted to achieving both of these goals. Identification of measures will be approached in a manner similar to that described here, by obtaining multiple performance measures and noting relationships between intermediate behavior and ultimate performance. A preliminary conceptual model of human-computer interaction has been developed (Morris, Rouse, & Ward, 1984, in preparation), and will be evaluated as research results become available. An "armchair" analysis of the problem indicates that such a model should include not only aspects of the task situation but also should take into account such factors as the human's perception of his own and the computer's performance, and human information processing resource limitations.

Also of interest are a number of issues relevant to problems which may arise when the computer aid degrades in some way. For example, under what conditions will the human realize that the aid has degraded, and will it be possible for the human to cope with the loss of the aid? Investigation of these and other questions may entail consideration of knowledge requirements and the human's "mental models" of the aid and situation.

REFERENCES

Chu, Y.Y., & Rouse, W.B. Adaptive allocation of decisionmaking responsibility between human and computer in multitask situations. IEEE Transactions on Systems, Man, and Cybernetics, 1979, SMC-9, 769-778.

Licklider, J.C.R. Man-computer symbiosis. IRE Transactions on Human Factors in Electronics, 1960, HFE-1, 4-11.

Morris, N.M., Rouse, W.B., & Ward, S.L. Human-computer interaction: A conceptual model. Proceedings of the International Conference on Cybernetics and Society, 1984, in preparation.

Rouse, W.B. Human interaction with an intelligent computer in multi-task situations. Proceedings of the Eleventh Annual Conference on Manual Control, 1975, 130-143.

Rouse, W.B. Human-computer interaction in the control of dynamic systems. Computing Surveys, 1981, 13, 71-99.

Rouse, W.B., & Rouse, S.H. A framework for research on adaptive decision aids (Tech. Rept. AFAMRL-TR-83-082). Norcross, GA: Search Technology, October 1983.

ORIGINAL PAGE
OF POOR QUALITY

Figure 1. Task display.

ORIGINAL PAGE IS
OF POOR QUALITY

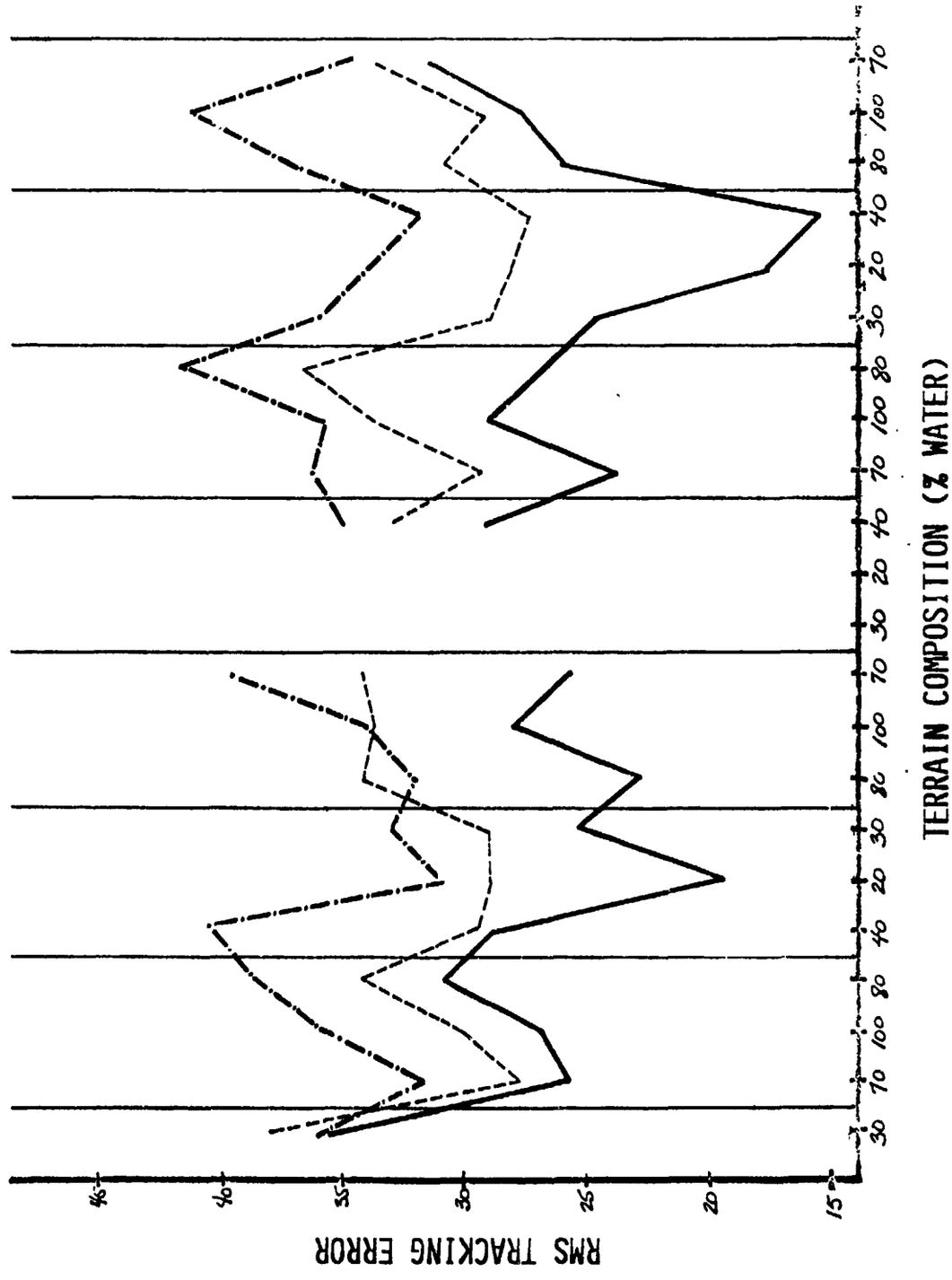

Figure 2. RMS tracking error.

ORIGINAL
OF POOR QUALITY

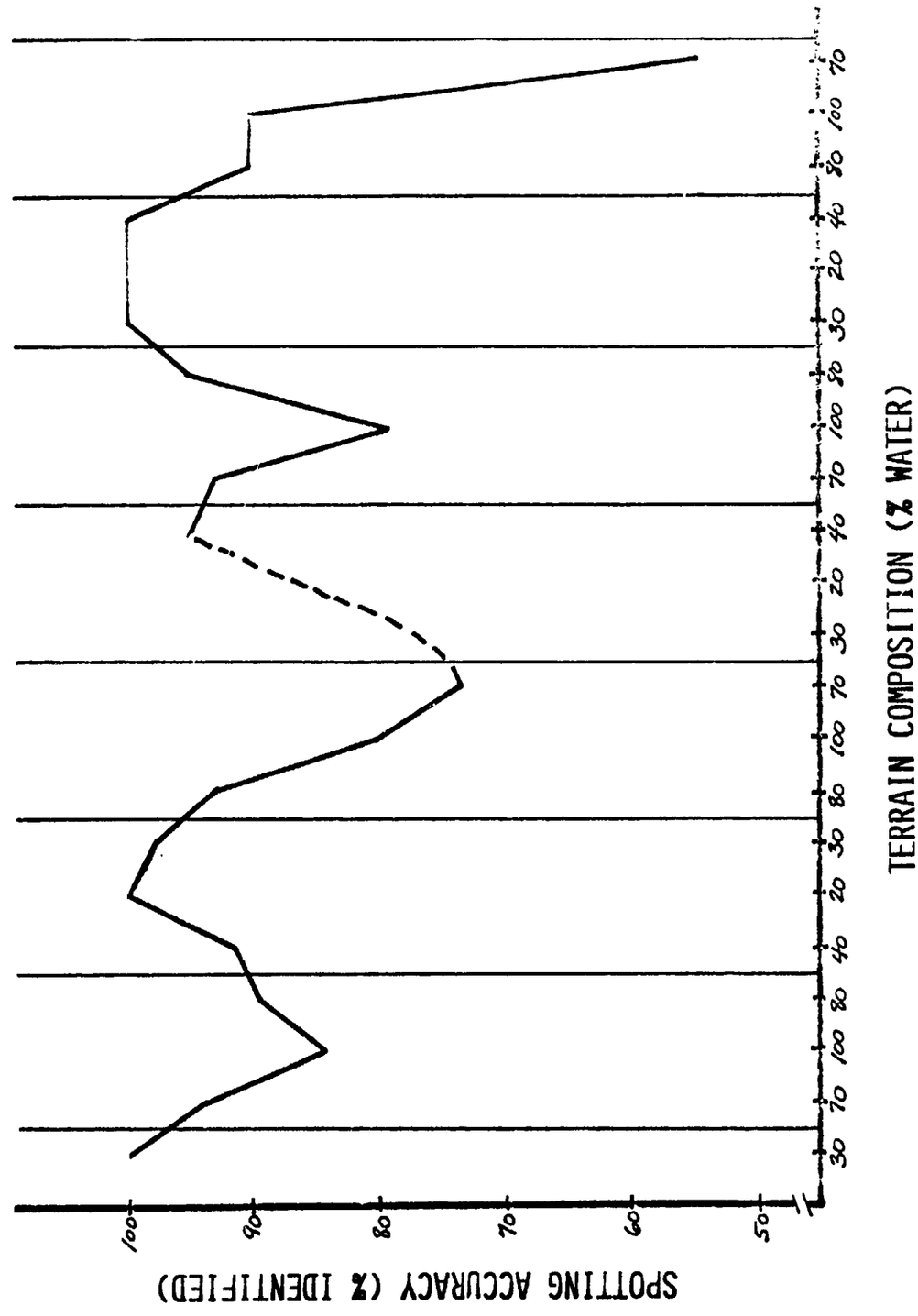

Figure 3. Spotting accuracy.

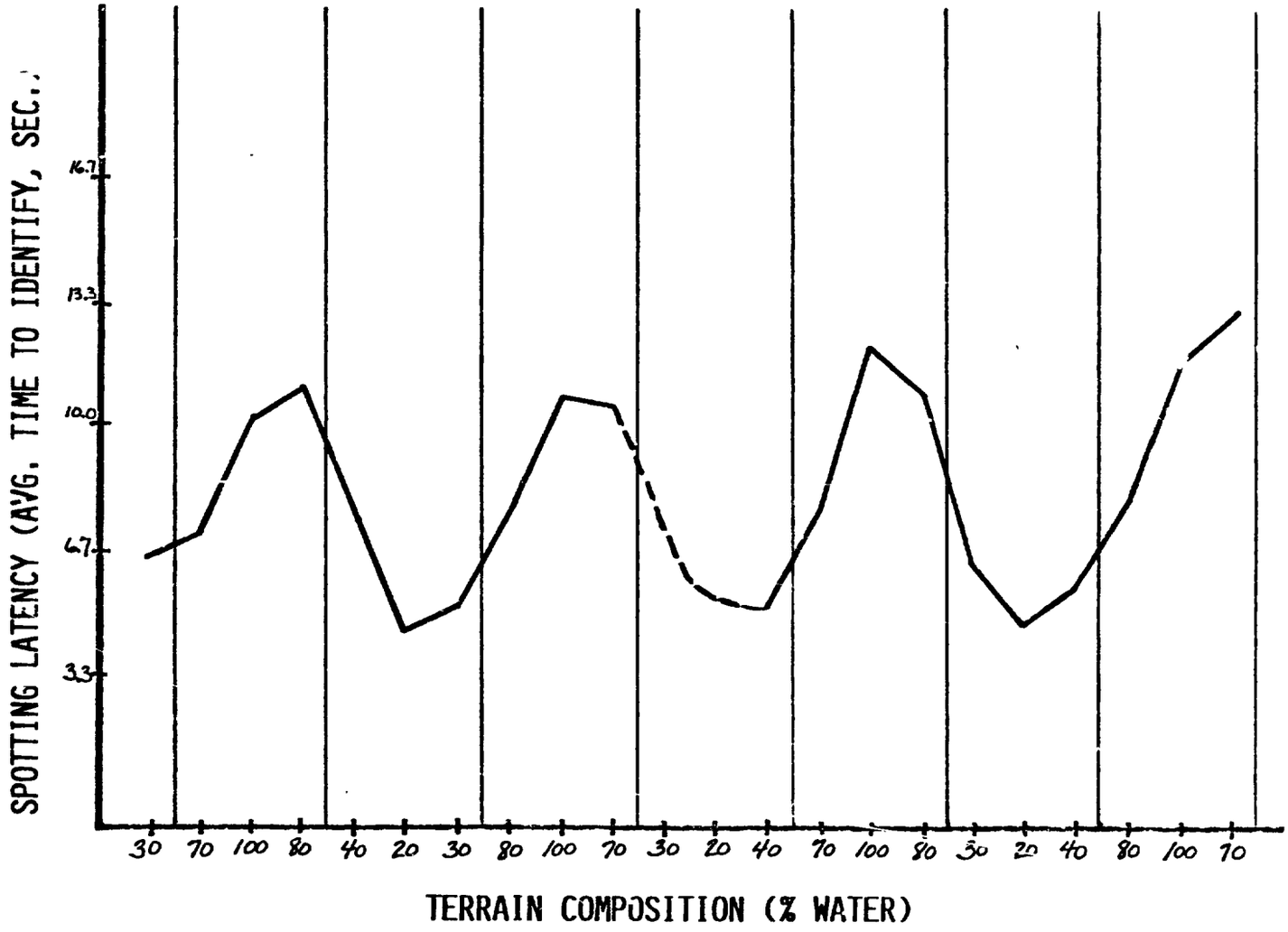

Figure 4. Spotting latency.

Perception and Action in Simulator Displays

N85 14517 D30

USE OF LINEAR PERSPECTIVE SCENE CUES IN A SIMULATED HEIGHT REGULATION TASK

William H. Levison
Bolt Beranek and Newman Inc.
10 Moulton St.
Cambridge, MA 02238

Rik Warren
AFAMRL/HEF
Wright-Patterson Air Force Base
Ohio 45433

Submitted to the
20th Annual Conference on Manual Control
June 12-14, 1984, NASA-ARC, California

ABSTRACT

As part of a long-term effort to quantify the effects of visual scene cuing and non-visual motion cuing in flight simulators, the Air Force Aerospace Medical Research Laboratory (AFAMRL) has completed an experimental study of the pilot's use of linear perspective cues in a simulated height-regulation task. Six test subjects performed a fixed-base tracking task with a visual display consisting of a simulated horizon and a perspective view of a straight, infinitely-long roadway of constant width. Experimental parameters were (1) the central angle formed by the roadway perspective (30 or 60 degrees) and (2) the display gain (-0.3 or -0.6 degrees change in central angle per foot change in altitude). The subject controlled only the pitch/height axis; airspeed, bank angle, and lateral track were fixed in the simulation.

The average RMS height error score for the least effective display configuration (60 degree central angle, lower display gain) was about 25% greater than the score for the most effective configuration (30 degree angle, larger gain). Overall, larger and more highly significant effects were observed for the pitch and control scores. Model analysis was performed with the optimal control pilot model to characterize the pilot's use of visual scene cues, with the goal of obtaining a consistent set of independent model parameters to account for display effects.

INTRODUCTION

The Air Force Aerospace Medical Research Laboratory (AFAMRL) is studying visual scene cuing and non-visual motion cuing in operational and simulated aircraft missions. A set of experiments has been designed to provide a data base which will

support development of a cuing model centered on the optimal control model (OCM) of the human operator. This model is intended to permit prediction of cuing effects in experimental situations not tested, and ultimately to aid in the specification of simulation hardware.

The task of low-level flight is the operational mission simulated in the experimental program. (In the military context, low-level flight may involve high-speed flight relatively close to the terrain to avoid detection while over enemy territory.) This task was chosen because of its relevance to Air Force operations, and because it provides a realistic framework for exploring the pilot's use of various visual and non-visual cues.

Research into visual scene cuing is being concentrated on cues provided by lines and texture elements in the visual scene. This paper summarizes the results of an initial experiment involving the use of linear perspective cuing -- specifically, the cues provided by a perspective display of a straight, indefinitely- long roadway. The reader is referred to recent articles documenting modeling efforts related to the pilot's use of texture-related cues [1,2], and to another paper presented at this Conference summarizing a study of g-seat cuing [3], also conducted as part of the AFAMRL research program.

METHOD

Displays

The displays were computer generated scenes consisting of line drawings of a perspective view of a road and a horizon. The central perspective angle of the road changed as a function of altitude, and the vertical position of the horizon line and simulated roadway changed as a function of the pitch state of a simulated aircraft. The left two frames of Figure 1 indicate level flight at low and high altitudes. The right two frames indicate pitch down and pitch up states. When the aircraft was level, the horizon was at eye level. The screen was 38 cm wide and viewed from 38 cm resulting in a horizontal optical size of 53.1 deg. The image of the road was always symmetrical but the horizontal location of the vanishing point was continuously perturbed using a sum-of-three-sines forcing function. This resulted in a quasi-random simulated "crabbing" motion of the aircraft beyond the control of the observer and uncorrelated with the vehicle states. The purpose was to eliminate any spurious cues arising from unintended static reference marks.

The experimental design called for four scene classes formed by crossing two levels of the central angle of the road (30 and 60 deg) and two levels of the display sensitivity or gain (-.3 and -.6 deg/ft). Display gain refers to the change in road angle per unit change in altitude. The relationships between central angle and roadway parameters are:

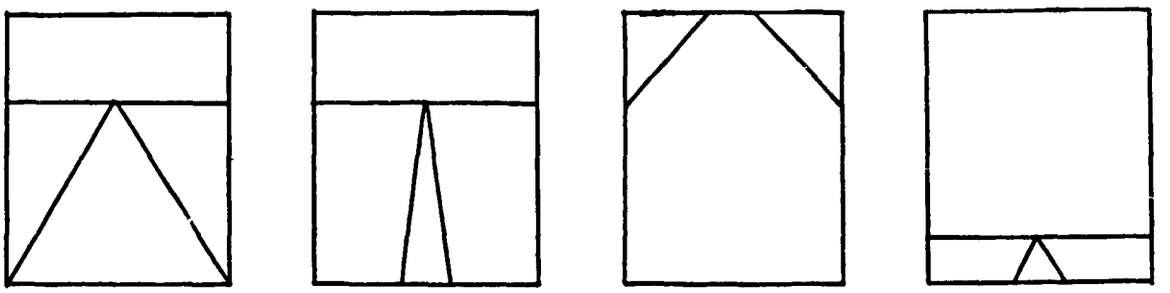

FIG. 1. EXAMPLES OF DISPLAY STATES

$$\beta = 2 \tan^{-1} \frac{W}{2H} \tag{1}$$

$$\frac{\partial \beta}{\partial H} = -\frac{W}{H^2 + \frac{W^2}{4}} \tag{2}$$

where β is perspective central angle in radians, H is height above roadway in feet, and W is the width of the road in feet. Because the central angle decreases with increasing altitude, the display gains are negative as indicated by Equation 2.

The gain and angle requirements uniquely determine the physical roadway width and initial altitude values which in turn are used for computer scene generation. Table 1 presents the values.

NOMINAL CONDITIONS

Height ft	Width ft	Road Angle deg	Display Gain deg/ft
95.5	51.2	30	-.3
47.7	25.0	30	-.6
165.0	191.0	60	-.3
83.0	95.0	60	-.6

Because it is more consistent to model perceptual limitations in terms of perceptual units, rather than simulation units, visual variables (central angle and display gain) were selected as the primary experimental variables, and values for the corresponding physical scene variables (road width and

height) were selected to yield the desired combination of visual values. Treatment of perceptual limitations within the OCM is discussed later in this paper in the presentation of model results.

Control.

The displays changed from their initial condi . . a function of observer pitch control and simulated ver . The actual relationship between these inputs and disp . . . cs was determined by a simulation of the flight dynamics o . . 16 aircraft flying at 400 knots at a 100 ft a . . de. For d . ails see Levison, Zacharias, and Sinacori [4].

The observer controlled the simulated aircraft by means of a force stick mounted to the side of an aircraft seat. Only pitch commands were registered.

Forcing Functions

The forcing function was formed by summing 13 sinusoids with amplitudes and frequencies to approximate a first-order gust spectrum having a break frequency of 12 rad/sec and an RMS amplitude of 7.7 ft/sec. This gust spectrum is, in turn, an approximation to the Dryden gust spectrum appropriate to a nominal flight condition of 400 kts at 100 feet above sea level -- a gust model that is recommended for aircraft flying qualities studies [5].

Procedure

Six people (three men, three women) participated as test subjects. None were pilots. The observer's task was to keep altitude constant during the course of each simulated flight. An alternate conception of the task is that it involved compensatory tracking of the central roadway angle. This task is interesting in that, once a trial began, no reference angle was presented: An observer tracked his or her concept of what 30 or 60 deg looked like.

Each flight or trial began with 15 sec of viewing the static display corresponding to the initial scene of one of the four conditions. A ready signal was then given and both the gust and force stick were activated. The dynamic phase lasted 120 sec of which only the last 102.4 sec were used as data. At the end of each trial, the observer's mean, standard deviation, and RMS height error were displayed. Four trials, one for each condition, constituted a session and observers ran for two session a day.

Conditions were uniquely randomized within each training session, and were further constrained to form a Latin Square over the last four session (16 data trials). These sessions, which

began when an observer reached an asymptote based on RMS height error, provided the data for formal analysis. On the average, the subjects received 43 training sessions.

DATA ANALYSIS

Performance Scores

Standard deviation (SD) height error scores were averaged across replications to provide mean performance scores for each subject, each condition. Subject means were then averaged to provide group mean performance and subject-to-subject variability. T-tests were performed on subject-paired SD scores to determine potentially significant differences between all pairs of experimental conditions.

Average SD scores for height error, pitch error, "stick" (operator's control input), and stick rate are plotted in Figure 2. Solid symbols indicate group means, vertical bars indicate the standard deviation of the subject means. Figure 2a shows that superior tracking performance (lower height error scores) was achieved with the larger display gain and the smaller reference angle. Display gain had the greater effect: doubling the gain decreased tracking error by about 17% on the average, whereas reference angle influenced the score by about 7%.

Display parameters had numerically greater effects on the remaining SD scores, with gain again having the greater influence. Pitch error SD score showed the greatest fractional change, being about 45% greater for the larger display gain. Stick and stick rate also showed substantial increases for the larger display gain.

If we consider the perspective angle seen by the operator -- rather than height error -- as the major "outer-loop" variable, then the effects of display gain are consistent in that all display and control variables of interest increase with increasing display gain. The RMS central angle increased by less than a factor of 2 with a doubling of the display gain, however, as indicated by the improved tracking error. Perceptual-motor mechanisms responsible for this improvement are suggested later in the section on model results.

Results of subject-paired t-tests of differences in SD scores are shown in Table 2. Entries indicate alpha levels of significance; differences having alpha levels greater than 0.05 are considered "not significant" and are indicated by dashes. Two major trends are indicated by this table: (1) differences due to changes in display gain (Table 2a) were overall more significant than differences due to reference central angle (Table 2b), and (2) display-related differences in pitch and control variables were more significant than differences in height error. Because

a) Height Error

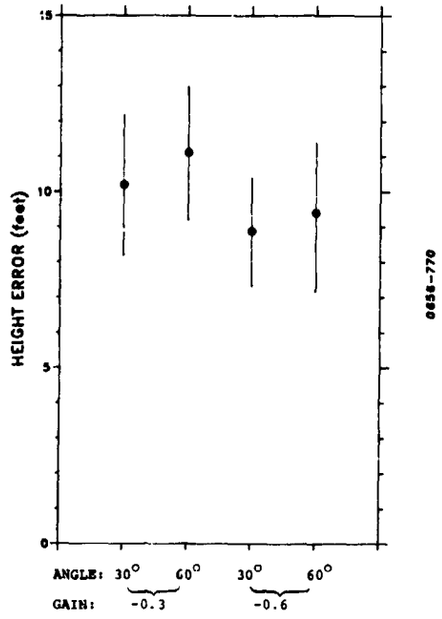

b) Pitch Error

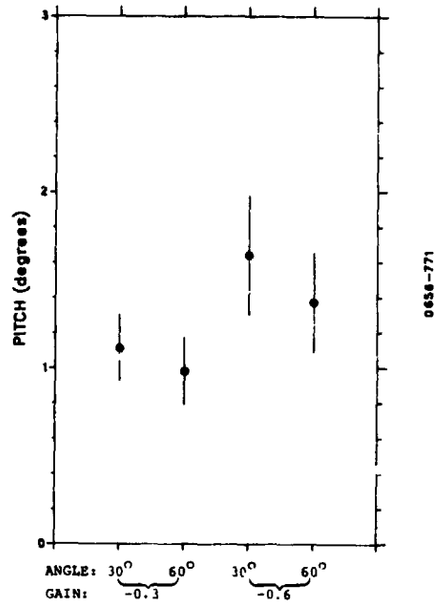

c) Stick

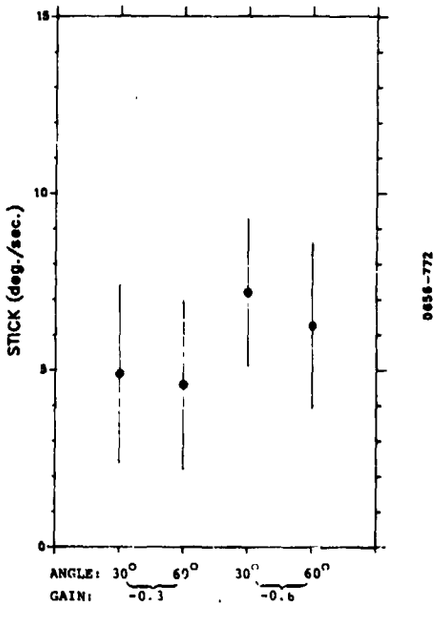

d) Stick Rate

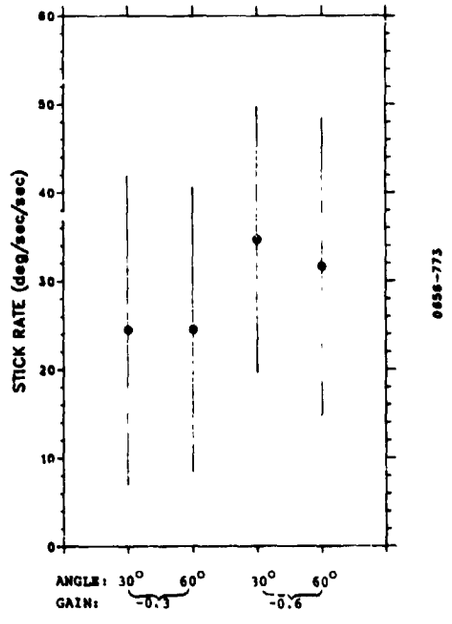

Figure 2. Effect of Display Conditions on SD Score
Average of 6 subjects, 4 trials/subject

ORIGINAL PAGE
OF POOR QUALITY

Table 2. Results of Paired-Difference T-Tests on SD Scores

Condition	Height	Pitch	Control	Ctrl Rate
a) Effects of Display Gain				
30 degrees	--	.01	.02	--
60 degrees	.05	.001	.01	.02
b) Effects of Nominal Central Angle				
-0.3 deg/ft	--	.05	.05	--
-0.6 deg/ft	--	.05	--	--

Entries indicate alpha significance levels. Alpha levels greater than 0.05 indicated by dashes.

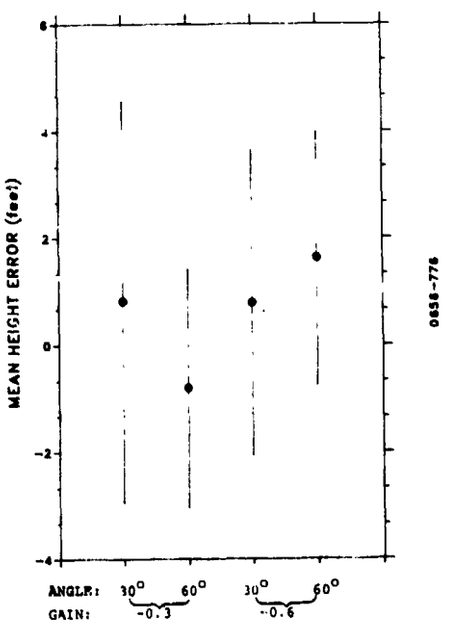

Figure 3. Effects of Display on Mean Height Error
Average of 6 subjects, 4 trials/subject

central angle effects were only weakly significant (alpha = Ø.5), we consider angle effects on the whole as not significant.

Mean height error, averaged over the subject population, is plotted in Figure 3. There were no significant differences in mean error across conditions and, overall, the mean error was relatively small. The absence of a substantial error bias, which is somewhat surprising given the lack of an explicit zero reference during data collection, suggests that the subjects were able to develop a relatively accurate impression of the desired roadway perspective during training.

Frequency Response

The effects of display gain on average operator frequency response are shown in Figure 4a. Results have been averaged across the two central-angle conditions; thus, each curve reflects the average of six subjects, eight replications per subject.

a) Effects of Display Gain

b) Effects of Reference Central Angle

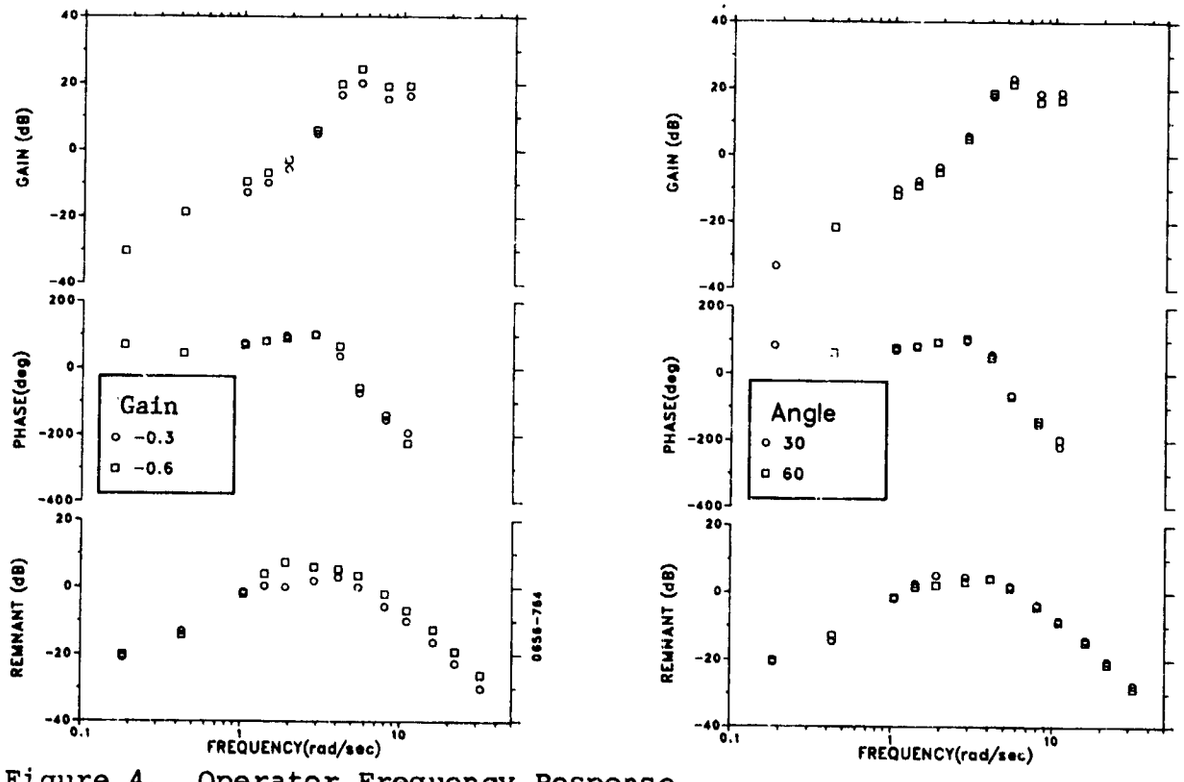

Figure 4. Operator Frequency Response
Average of 6 subjects, 8 trials/subject

Note that the term "gain" has two meanings: the sensitivity of the display in terms of degrees change of central per foot change of altitude, or the amplitude-ratio component of the

ORIGINAL PAGE IS
OF POOR QUALITY

operator describing function. The particular meaning intended should be clear from the context of the discussion.

Each pair of gain and phase curves represents the effective describing function relating operator response to height error (i.e., the Fourier transform of the control response divided by the Fourier transform of the height error). Zero dB gain corresponds to one unit of control input per foot of height error; zero dB remnant indicates one unit of control power (at a given frequency) not linearly correlated with the tracking input.* These curves have not been corrected for measurement bias due to simulation delays of around 50 msec. Thus, the true operator phase shift is somewhat more positive (i.e., less phase lag) than shown here and in subsequent plots.

Each describing function shown in Figure 4 reflects the subjects' use of all available cues (e.g., height error, height error rate, pitch, and pitch rate). The frequency dependencies of these curves, therefore, should not be expected to resemble those observed in previous studies of single-variable tracking tasks.

Figure 4a shows that, on balance, the subjects tracked with a higher gain when provided with the more sensitive display, whereas differences in phase shift were negligible. This result is consistent with the trend in the error SD scores, which indicated more effective tracking with the higher display sensitivity.

The larger display gain also yielded larger stick remnant at mid and high frequencies. This result should not necessarily be interpreted to mean that the operator's response was relatively more noisy under these conditions; it may simply reflect the wider man/machine bandwidth achieved with the larger display gain. T-tests of paired differences showed that the larger gain and remnant differences were generally statistically significant.

The SD scores of Figure 2 and the frequency response measures of Figure 4a indicate that the subjects did not fully compensate for the change in display gain. Had they done so, both the scores and the frequency response measures would have been invariant with regard to display gain. Perceptual mechanisms to account for this lack of complete compensation are suggested in the discussion of model analysis.

---

*The F-16 control augmentation designed for this laboratory study was configured to provide the operator with a pitch-rate command. The operator's control input, therefore, has units of degrees/second.

As we would expect from the foregoing analysis of error scores, Figure 4b shows relatively small changes in frequency response due to a change in the nominal central angle. In general, angle-related differences were not statistically significant.

MODEL ANALYSIS

As mentioned earlier, the optimal control model (OCM) for the human operator is expected to provide a theoretical framework for coalescing and extending the data on visual scene cuing obtained in the AFAMRL experimental program. This model has yielded reasonable results in previous applications involving both symbolic and pictorial displays, and we believe it allows the appropriate parameterization to handle relatively simple visual scene cues such as linear perspective. Additional theoretical developments have been undertaken to develop a separate submodel for visual flow-field cuing [1,2] which, it is hoped, will eventually be integrated into the OCM.

Problem Formulation

The reader is assumed familiar with the general structure and parameterization of the OCM. For convenience, however, we review here the treatment of display-related issues.

The OCM, as currently implemented, allows a treatment of a display along the following three dimensions: (1) the state-related information provided by the display, (2) the quality of this information, and (3) dynamical aspects of the display (e.g., bandwidth limitations) that may be important. Each perceptual input provided by the display is assumed to be a linear combination of one or more of the problem state variables; if no such relationship can be found, the display is deemed irrelevant to the task. The quality of the information is represented by an observation noise, and possibly by a delay.* Dynamics associated with the physical display create new state variables which are simply lumped with the original problem state variables as part of the total "system dynamics". Because the display used in this study was free of significant bandwidth limitations, we shall discuss only the informational aspects of the display.

---

*The OCM, as currently configured, allows for a single pure time delay, which is often selected to reflect the time delay associated with the human operator (typically, 0.2 seconds). Display-related delays may be lumped into this operator delay (if all such delays are equal), or they may be included by means of Pade approximatic s.

The linear relationships between state (problem) variables and perceptual (display) variables were as follows:

$$\begin{bmatrix} \beta \\ \dot{\beta} \\ \theta \\ q \end{bmatrix} = \begin{bmatrix} K & 0 & 0 & 0 \\ 0 & K & 0 & 0 \\ 0 & 0 & 1 & 0 \\ 0 & 0 & 0 & 1 \end{bmatrix} \cdot \begin{bmatrix} h \\ \dot{h} \\ \theta \\ q \end{bmatrix} \tag{3}$$

where the vector on the left includes visual variables in degrees, and the vector on the right includes state variables in problem units. The parameters of this expression were defined as follows:

β = perspective central angle, degrees
$\dot{\beta}$ = central angle rate, deg/sec
θ = pitch, degrees
q = pitch rate, deg/sec

The display gain K was computed as

$$K = -\frac{57.3\ W}{H^2+\frac{W^2}{4}} = 57.3 \cdot \partial\beta/\partial H \tag{4}$$

where H and W are roadway height and width in feet.

This formulation reflects a small-signal linear analysis about the nominal (reference) condition. The display and state vectors shown above, therefore, include only the variational components and do not include reference values or mean errors. On the other hand, all coefficients of the transformation matrix (including the reference height H) were fixed at reference values, and variations in central angle were therefore proportional to variations in height. This approximation was not made in the experimental study, where the full trigonometric relation between perspective angle and roadway parameters was implemented continuously during each experimental trial.

In keeping with previous analysis, each perceptual variable was assumed to be corrupted by an additive white noise process with autocovariance determined by:

$$V_y = \frac{\pi P}{f} \quad (\sigma_y^2 + \sigma_{yo}^2) \tag{5}$$

where V_y is the autocovariance, P a noise/signal ratio to account for the scaling aspects of this "observation noise" process, "f"

the fraction of attention allocated to the perceptual variable, σ_y^2 the variance of the signal as presented on the display, and σ_{yo}^2 a "residual noise" variance to provide a statistical representation of perceptual resolution limitations (i.e., perceptual "threshold"). The reader is referred to Baron and Levison [6] for further details on the display submodel, and to Levison [7] for a discussion of the treatment of attention-sharing.

Note that one of the experimental variables -- display gain -- was reflected directly in the linear relationship between state and perceptual variables (Equation 3). The other experimental variable -- nominal central angle -- influenced the model analysis in the selection of residual noise levels associated with perception of central angle and angle rate. That is, the fidelity with which the operator could extract height-related information from the display was assumed to be potentially dependent on the nominal central angle.

Pre-Experiment Model Analysis

Pre-experiment model analysis was performed to aid in the selection of values for the major experimental variables (central angle and display gain). Using the results of a recent modeling effort as a basis [8], the following values were assigned to independent "pilot-related" model parameters:

Observation noise/signal ratio = -20 dB

Motor noise/signal ratio = -60 dB

Time delay = 0.2 seconds

Motor time constant = 0.13 seconds*

Additional parameters related to the perceptual process were adjusted to reflect various assumptions concerning attention-sharing and perceptual resolution limitations, as described below.

A baseline observation noise/signal ratio of -20 dB was

---

*Readers familiar with applications of the OCM will recall that motor time constants of around 0.1 seconds have typically been specified when using the model as a predictive tool. We felt that this larger value, which was based on a recent study involving roll-axis tracking in the presence of important simulation-related lags, would be more appropriate than the lower value based on idealized tracking dynamics (e.g., no simulation lags).

associated with nominal "full attention" to the tracking task. Noise ratios associated with particular display quantities were scaled inversely with attention (see Equation 3) to reflect attention-sharing penalties between attitude and path variables. Preliminary model analysis revealed that a simulated attention split of 50% to path and attitude variables yielded predicted performance scores very close to those predicted for optimal allocation of attention. Therefore, the bulk of the model analysis was performed for equal attentional allocation (i.e., a noise/signal ratio of -17 dB for all perceptual inputs).

Pre-experiment predictions of the (zero-mean) RMS height error are shown in Figure 5 for a variety of assumptions concerning perceptual resolution limitations. Condition A reflects an idealized perceptual environment without perceptual resolution limitations and serves as a baseline for exploring the effects of such limitations. Conditions B through D reflect increasingly pessimistic assumptions concerning effective perceptual thresholds associated with the pitch and roadway (angle) display variables. (See Levison et al for additional details [4]).

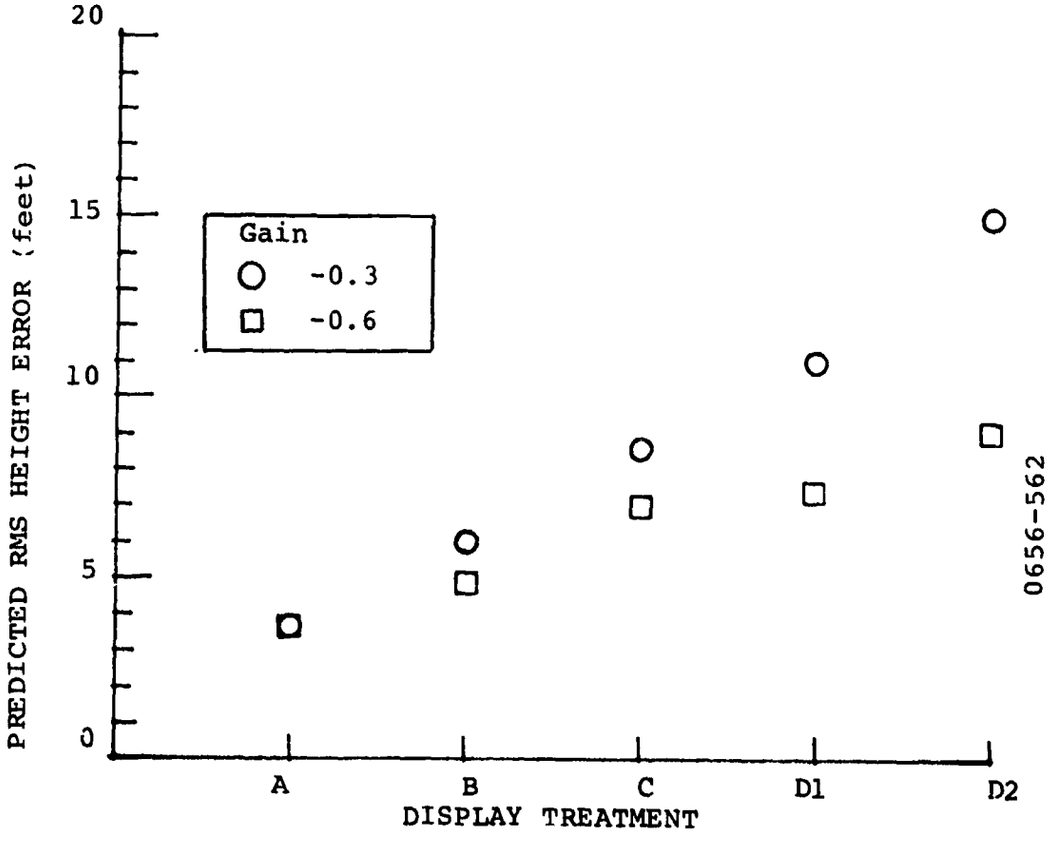

Figure 5. Effects of Display-Related Limitations on Predicted RMS Height Error

Conditions B and C assume constant (but different) thresholds associated with perception of the perspective central angle and angle rate. For these cases, the OCM predicts performance effects due to display gain, but not due to differences in nominal central angle. (As the display gain increases, the RMS variation in central angle increases with respect to the assumed perceptual "threshold", allowing the subject to obtain better estimates of his altitude and therefore track more effectively.)

To account for performance effects related to central angle, condition D assumes that the residual noise variance (Equation 5) associated with perception of central angle varies with the mean-squared value of the central angle. In this case, a larger residual noise is associated with the 60 degree central angle (condition D2) than with the 30 degree angle (D1), and, as Figure 5 shows, performance effects of both central angle and display gain are predicted.

As noted above, the primary objective of this pre-experiment analysis was to aid in the experiment design; specifically, to allow us to select parameters having a reasonable likelihood of showing a performance effect. On the basis of Figure 5 we predicted that, for the display gains and angle selected, there would very likely be a measurable performance effect due to display gain, and possibly one due to central angle. A comparison of the predictions of Figure 5 with the experimental height error scores of Figure 2 shows that the data fell within the range of pre-experiment predictions and corresponded most closely to the set of (relatively pessimistic) assumptions reflected in condition D1.

Post-Experiment Model Analysis

The condition yielding best performance (30 degree reference angle, -0.6 deg/foot display sensitivity) was selected as the baseline condition for initial model analysis. Group-mean performance scores and frequency response measures were matched via the OCM with all independent parameters allowed to vary. The parameter set consisted of four observation noise quantities: one each for the presumed observations of height error, height error rate, pitch "error", and pitch rate; a motor noise; a time delay; and a motor time constant.

The resulting model response (smooth curve) is compared with experimental results (discrete symbols) in Figure 6. At all but the lowest and highest measurement frequencies, model and data exhibited very close correspondence. The composite scalar matching error (which includes SD performance scores as well as frequency response) indicated that experimental measures were matched to within about 1 standard deviation on the average.

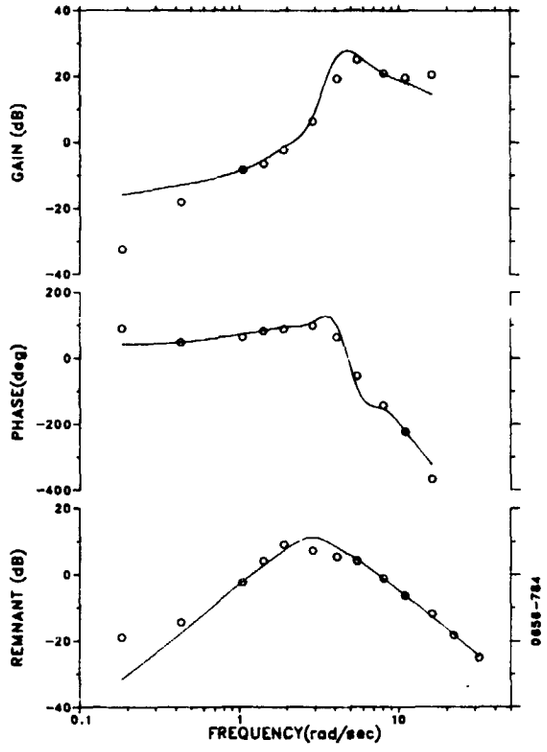

Figure 6. Model Match to Average Operator Frequency Response. 30 degree reference angle, -0.6 deg/foot. Average of 6 subjects, 4 trials/subject.

With seven model parameters adjusted in the search procedure, there existed substantial potential for "tradeoff" among parameters in obtaining a near-optimal match to the data; thus, the resulting parameter set cannot be expected to provide a reliable estimate of intrinsic human information processing limitations.* Rather, the goal of this initial post-experiment model analysis was to provide a baseline against which to compare model analysis employing reasonable constraints among the independent parameters.

Further model analysis was pursued with the goal of developing a tool having useful predictive capabilities. The approach adopted was to fix as many operator-related parameters as possible at values based on previous results, and to "search"

---

*Some of the parameter values yielded by this unconstrained search were outside the range of expectations. For example, the observation noise associated with perception of central angle was unusually low, whereas unusually large values were found for the time delay and motor time constant parameters.

the parameter space as little as possible. Accordingly, the observation noise/signal ratio was fixed at -20 dB; baseline equal attention to height- and pitch-related display variables was assumed; motor noise was set to -50 dB; the time delay parameter was set to 0.25 seconds (0.2 for the human operator plus 0.05 for simulation delays); and the motor time constant was set to 0.133 to provide an apparent best match for this particular parameter.

RMS residual noise levels* associated with pitch and pitch rate were fixed respectively at 3.0 degrees and 0.84 deg/sec, respectively, and a residual noise of 3.0 deg/sec was specified for perception of central angle rate. (These values correspond to those selected for condition D during pre-experiment analysis.) The remaining free parameter -- residual noise for perception of central angle -- was then adjusted to a value of 30 degrees (RMS) to provide the best match to data from the baseline experimental condition (30 degrees, -0.6 deg/foot). The resulting scalar matching error was within 20% of that obtained previously with no constraints on the seven independent parameters.

Having matched the baseline condition, our next modeling objective was to determine whether or not a consistent treatment of visual scene cues (along with other operator limitations) would allow the OCM to mimic the experimental trends. Accordingly, the model was tested against a low-display-gain condition (30 degree central angle, -0.3 deg/foot display gain) with the parameters fixed at values determined from matching the baseline condition.

There was some ambiguity, however, as to what constituted a "fixed" parameter set. Recall* that the motor time constant parameter derives from a performance penalty associated with rate-of-change of control (i.e., a "cost" on control rate variance). For a given set of system dynamics, there is a unique relationship between these two parameters (provided other

---

*Other applications of the OCM have tended to use an alternative treatment of effective perceptual threshold in which the observation noise is a more severe function of "threshold" than indicated by Equation 5 above. For equivalent influence on estimation and control performance, the "residual noise" of the current treatment is about 3 times as great as the "threshold" parameter of the alternative model described in Baron and Levison [6].

*Readers unfamiliar with the mathematical structure of the OCM are directed to References [9,10].

components of the quadratic performance index are invariant.* When the system matrices are changed, however, this relationship changes. Thus, we had the choice of fixing either the motor time constant (which would require a corresponding change in the control-rate cost coefficient), or of fixing the cost coefficient and accepting a different motor time constant. The first option would imply a consistent human operator bandwidth limitation, the second, a consistent subjective penalty on control activity.

Because the motor time constant has tended to be less variable across conditions than the control-rate penalty [8], this parameter was held fixed in the first test of the low-display-gain data. While an increased height error score was predicted, the model did not mimic the trends of the pitch and control-related scores, nor did it replicate the experimental trends in operator frequency response.

Considerably better results were achieved by maintaining a constant performance penalty. Table 3 shows that experimental trends were replicated; specifically, a reduction in display gain resulted in a larger predicted height tracking error and in lower pitch and control-related scores. While not demonstrating the type of precision match usually obtained in a laboratory setting, the predicted frequency response shown in Figure 7 also mimics certain important trends; specifically, the generally lower operator gain and lower high-frequency bandwidth observed for tracking with the low display gain. The overall scalar matching error for the low-gain experimental condition was on the order of 1 standard deviation, which compares favorably with the initial model-matching exercise in which all parameters were adjusted for optimum match.

DISCUSSION

Experimental results and model analysis support the following hypotheses concerning the effects of display gain on operator performance:

1. As the display gain increases, the variations in perspective angle are increased relative to the operator's limitations in resolving angle differences, and the resulting signal/noise enhancement provides better height-related information with resulting improvement in height tracking performance.

2. Because the operator maintains with a fixed subjective

---

*The control-rate weighting term was actually identified by the gradient search procedure, then converted to a motor time constant for presentation.

Table 3. Comparison of Experimental and Model SD Scores

	High Display Gain			Low Display Gain		
Variable	Model Mean	Experimental Mean	Experimental Std Dev	Model Mean	Experimental Mean	Experimental Std Dev
Height	7.83	8.87	1.57	11.0	10.2	2.03
Pitch	1.41	1.64	0.34	1.23	1.11	0.19
Stick	8.27	7.20	2.10	4.46	4.88	2.53
Stick Rate	40.6	34.7	15.1	22.6	24.5	17.5

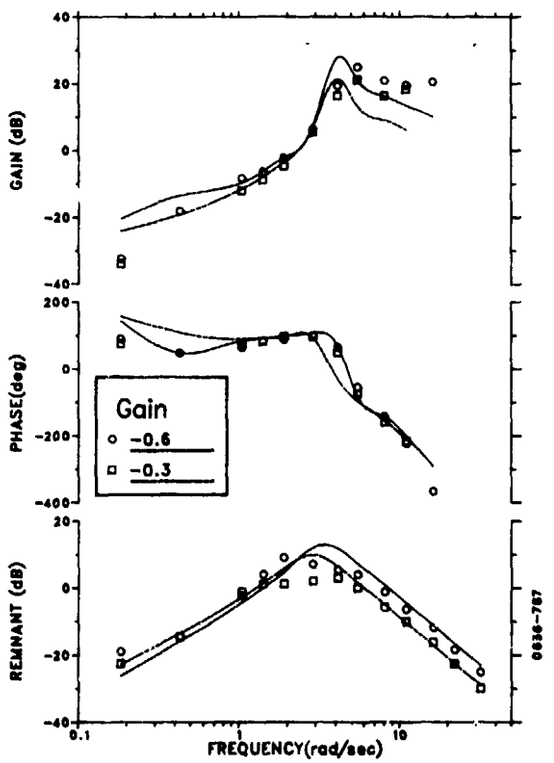

Figure 7. Comparison of Experimental and Model Frequency Response. Experimental results shown by discrete points, model results indicated by smooth curves.

penalty on mean-squared control-rate, relative to mean-squared display error, the larger display excursions accompanying the larger display gain motivate the operator to respond more aggressively, thereby increasing closed-loop system bandwidth and reducing height error.

The first-cited of these display-gain effects was anticipated prior to initiation of the experimental study and was revealed in the pre-experiment model analysis. The second hypothesis is based on post-experiment analysis and was not specifically anticipated. Other interpretations of the experimental results are discussed shortly.

Effects of central angle were not so obvious prior to the experiment. One could argue for certain angle configurations (say, very small or close to 180 degrees) for which small variations could be readily detected by the human observer, but it was not clear how performance should differ between a 30-degree and a 60-degree central angle. The hypothesis that a perceptual noise variable would scale with mean-squared central angle proved overly pessimistic. The experiment revealed a small and not statistically significant effect of central angle on height error. Additional experimentation would be necessary to determine whether this result extends to other values for central angle and other tracking tasks.

The residual noise value of 30 degrees associated with perception of central angle was much larger than expected. Based on previous experience with the OCM, we would relate this noise level to a "threshold" of around 10 degrees as might be measured in a standard psychophysical experiment. Previous studies [11], however, have shown that operators can discriminate angle differences much more precisely. It is worth noting that the composite scalar model-matching error was relatively insensitive to this residual noise parameter (provided the noise was relatively large), and that adjusting this noise influenced mainly the match to height tracking error (which, of course, is the major variable of concern when performing low-level flight).

Because height error, for this task, was a relatively low-bandwidth "outer-loop" variable, we suspect that the residual noise parameter may have accounted for more than simply perceptual resolution limitations. Two possibilities are suggested. First, despite the extensive training given the test subjects (an average of 43 trials prior to data collection), it is possible that there was some tendency for the subjects to average their response strategies across tasks. Such a tendency would cause the subjects to track with a higher response gain when presented with the higher display gain. One way to model this behavior would be to modify the "internal model" element of the OCM to contain an average representation of display gain.

Another internal-model deficiency to consider is the potential interaction between the pilot's internal model and the difficulties posed by the task environment (perceptual limitations, system lags and delays). Previous analysis [8] provides some qualitative support for the notion that significant system lags and delays, for example, impede the operator's ability to construct an accurate internal model. It is possible that there may have been a double effect associated with the central angle display: namely, the relatively large perceptual resolution limitations associated with the angle display may have interfered with development of an adequate model for low-frequency system response; an inadequate model, in turn, would cause still larger height errors.

We noted above two methods of treating the control-rate cost coefficient: either hold this parameter fixed across tasks, or let it vary in a way that maintains an invariant motor time constant. A recent study of control-stick parameters suggests a more general treatment; namely, that this coefficient be adjusted to reflect both an operator response bandwidth limitation as well as a true subjective penalty on control response [12].

Although certain modeling issues remain to be resolved, we feel that the OCM provides a suitable model framework for integrating the effects of various cuing environments and various task environments to yield useful predictions of the operator's estimation and control strategies. To include the effects of a perceptual cue that has not been previously explored, some "calibration" is required to quantify appropriate model parameters to reflect the information content, information quality, and dynamical characteristics of the display providing the cue.

There are a number of ways to perform such a calibration. The procedure followed in the pre-experiment design phase of this study was to look to the tracking and psychophysical literature for guidelines concerning perceptual limitations. In our case, this process yielded an experiment design for which operator performance was significantly influenced by at least one of the experimental variables.

Another calibration method is to develop a separate submodel for the perceptual cue(s) of interest, and use this model to determine relevant OCM parameters. This approach was followed in the design of an experiment to explore flow-field cues [4]. A third procedure is to perform an experiment in a tracking or psychophysical setting to explore directly the operator's ability to utilize the cues of interest.

One of the lessons learned from this study is that a complex task simulation is not well-suited to display calibration because of the complex cuing environment. Because the operator will typically utilize all relevant cues available, his response to a

particular cue of interest is confounded by his response to the remaining cues. Simulations of this sort are most useful for testing hypotheses in operationally-relevant settings, but not in performing detailed diagnosis.

Display calibration is best executed in simple experiments in which the cuing environment is tightly constrained; ideally, only the cue of direct interest should be available. Constructing an experiment of this sort is not always a trivial task, particularly when attempting to isolate one of many cues that may be present in a rich visual scene; nor is it clear how to extrapolate measures obtained in a passive psychophysical setting to a manual control task in which the displayed variables are influenced by operator actions. Further methodological development remains to be done in this area.

SUMMARY AND CONCLUSIONS

Six test subjects performed a fixed-base tracking task with a visual display consisting of a simulated horizon and a perspective view of a straight, infinitely-long roadway of constant width. Experimental parameters were (1) the central angle formed by the roadway perspective (30 or 60 degrees) and (2) the display gain (-0.3 or -0.6 degrees change in central angle per foot change in altitude). The subject controlled only the pitch/height axis. The subject's primary task was to maintain a fixed height above ground in the presence of simulated random gusts.

Experimental results showed the following trends:

- Display gain had a greater influence on the average height error standard deviation (SD) score than did central angle. Doubling the display gain resulted in an average reduction in tracking score of about 17%, whereas doubling the central angle increased the height error score by only 7%.
- Display parameters had greater influence on pitch and control-related scores, with a doubling of the display gain resulting in a 45% increase in the pitch SD score.
- The larger display gain resulted in a larger operator response gain (i.e., amplitude ratio), little change in phase shift, and greater high-frequency remnant. The increased remnant is attributed to increased man-machine system bandwidth, not to increased "noisiness" in the operator's information processing.
- Gain-related effects tended to be statistically more significant than angle-related effects.

- The relatively small mean height errors suggests that the subjects were able to construct good internal models of the reference central angle.

A fixed set of model parameters was found to replicate the trends of the display-gain variations. Model analysis supports the notion that two factors accounted for the improvement in height regulation with increasing display gain: (1) excursions of the perspective central angle are increased relative to the effective perceptual threshold, and (2) the larger apparent tracking error indicated by the display motivates the operator to track more vigorously and thereby increase closed-loop system bandwidth.

In order to match experimental results with an otherwise reasonable set of independent model parameters, a relatively large value was required for the "residual noise" model parameter associated with perception of central angle deviations. We therefore speculate that this parameter reflected other, non-perceptual, limitations on operator performance, including (1) a tendency to adopt an average response strategy for the four experimental conditions, and (2) some imperfections in the operator's ability to construct an accurate internal model of system response at low frequencies.

On the basis of this study we conclude that the OCM, as currently configured, provides a suitable framework for modeling the effects of visual scene cues of the type explored here, and that it can be used very effectively in the design of simulation experiments. We also conclude that simulations of complex realistic flight tasks should not be employed for quantifying the operator's use of specific perceptual cues, but rather for testing hypotheses in task-relevant settings. Instead, we recommend that studies of cue utilization employ relatively simple tasks in which the cuing environment is constrained as much as possible to include only the cues of specific interest.

To enhance the accuracy of the model as a tool for predicting visual cuing effects, we suggest the following two areas for further attention:

Improved methodology for "calibrating" the operator's utilization of various perceptual cues, and for extrapolating measures obtained in a standard psychophysical setting to model parameters relevant to estimation and control.

Refine the OCM to account for the possible interaction between certain task parameters and the operator's internal model of the task environment.

ACKNOWLEDGEMENT

This research was supported by the Air Force Aerospace Medical Research Laboratory under contract F33615-81-C-0515 with John B. Sinacori Associates, Inc.

REFERENCES

1. Zacharias, G.L., Caglayan, A.C., and Sinacori, J.B., "A Model for Visual Flow-Field Cueing and Self-Motion Estimation", Proc. of the AIAA Flight Technologies Simulation Conf., Niagara Falls, NY, June 1983.

2. Zacharias, G.L., Caglayan, A.K., and Sinacori, J.G., "A Visual Cueing Model for Terrain-Following Applications", Proc. of ther AIAA Flight Technologies Simulation Conf., Niagara Falls, NY, June 1983.

3. Levison, W.H., McMillan, G.R., and Martin, E.A., "Models for the Effects of G-Seat Cueing on Roll-Axis Tracking Performance", Proc. of the 20th Annual Conference on Manual Control, NASA-ARC, CA, June 12-14, 1984.

4. Levison, W.H., Zacharias, G.L., and Sinacori, J.B., "Design of an Experiment to Study the Pilot's Use of Visual and Motion Cues in a Height-Regulation Task", BBN Report No. 5028, Bolt Beranek and Newman, Inc., Cambridge, MA, December 1982.

5. MIL-F-8785B(ASG), "Flying Qualities of Piloted Airplanes", August 1969.

6. Baron, S., and Levison, W.H., "Display Analysis with the Optimal Control Model of the Human Operator", Human Factors, 1977, 19(5), pp. 437-457.

7. Levison, W.H., "A Model for Mental Workload in Tasks Requiring Continuous Information Processing", in Mental Workload Its Theory and Measurement, Neville Moray (Ed.), Plenum Press, NY, 1979.

8. Levison, W.H., "Development of a Model for Human Operator Learning in Continuous Estimation and Control Tasks", BBN Report No. 5331, Bolt Beranek and Newman, Inc., Cambridge, MA, September 1983.

9. Kleinman, D.L., Baron, S., and Levison, W.H., "An Optimal-Control Model of Human Response, Part I: Theory and Validation", Automatica, Vol. 6, pp. 357-369, 1970.

10. Kleinman, D.L., Baron, S., and Levison, W.H., "A Control Theoretic Approach to Manned-Vehicle Systems Analysis", IEEE Trans. on Auto. Control, Vol. AC-16, pp. 824-833, No. 6, December 1971.

11. Smit, J., "Thresholds for the Visual Perception of Position Deviations and Motion", NLR TR 79025, National Aerospace Laboratory NLR, November 1978.

12. Levison, W.H., "Effects of Control Stick Parameters on Human Controller Response", BBN Report 5510, Bolt Beranek and Newman, Inc., Cambridge, MA, January 1984.

COCKPIT WINDOW EDGE PROXIMITY EFFECTS ON JUDGEMENTS OF HORIZON VERTICAL DISPLACEMENT

Richard F. Haines

Aerospace Human Factors Research Division
N-239-3
Ames Research Center - NASA
Moffett Field, Calif. 94035

January 30, 1984

ABSTRACT

To quantify the influence of a spatially fixed edge on vertical displacement threshold, twenty-four males (12 pilots, 12 non-pilots) were presented a series of forced choice, paired comparison trials in which a 32° arc wide, thin, luminous horizontal stimulus line moved smoothly downward through five angles from a common starting position within a three second-long period. The five angles were 1.4, 1.7, 2, 2.3, and 2.6°. Each angle was presented paired with itself and the other four angles in all combinations in random order. For each pair of trials the observer had to choose which trial possessed the largest displacement. A confidence response also was made. The independent variable was the angular separation between the lower edge of a stable "window" aperture through which the stimulus was seen to move and the lowest position attained by the stimulus. Three lower edge positions were studied making a total of 15 angular separation values between 0.4° and 5.6° upon which a threshold curve could be derived. It was found that vertical displacement accuracy is inversely related to the angle separating the stimulus and the fixed window edge ($p = .05$). In addition, there is a strong tendency for pilot confidence to be lower than that of non-pilots for each of the three angular separations. These results are discussed in terms of selected cockpit features and as they relate to how pilots judge changes in aircraft pitch attitude.

ACKNOWLEDGEMENTS

The following persons have provided valuable assistance during this study for which I am grateful. Dan Gundo (Northrup Services), assisted in the construction and set-up of the optical displays designed by Bob Miller (Systems Integration Branch) while Patricia Musser and Rieka McCain (Evans & Sutherland) assisted with hardware and software calibration of the picture system. Paul Bilibin (Informatics) provided invaluable help in developing stimulus input control software and output data formating for later statistical testing. Finally, Tony Murabito (Bellarmine High School, San Jose) helped in collecting and plotting portions of the data.

COPY FURNISHED

INTRODUCTION

This investigation was conducted to gain a better understanding of how the visual system uses a nearby stable frame of reference to assist in judging vertical displacement of a horizontal line. Research by Bonnet (1975), Brown (1927, 1931), Cartwright (1938), Duncker (1929), Johnson and Scobey (1982), Koffka (1935), Legge and Campbell (1981), and Tyler and Torres (1972) showed that motion is discriminated more accurately in the presence of a fixed visual reference. This work suggested that the nearer this reference was to the moving stimulus the more sensitive is the visual system to motion. This will be referred to as the "proximity effect." Portions of this literature will be reviewed in the following section labelled "background research on motion judgments." Of more practical relevance is the possibility that pilots may be influenced in their ability to judge aircraft pitch attitude and pitch attitude changes by how angularly near the (distant) horizon appears to some part of their cockpit window frame. This topic is discussed later in a section labelled "practical applications for these data."

Background Research on Motion Judgments.

The subject of how humans perceive motion has been of interest to a great many investigators over the years. The interested reader may want to consult reviews by Brown (1931), Gibson (1950), Graham (1962), LeGrand (1965), and Spigal (1965). Of particular interest here are those studies dealing with the influence of a spatially fixed frame(s) of reference or visual field detail, including inhomogeneous backgrounds immediately behind a moving stimulus. Work on the former topic has been carried out by Breitmeyer (1974), Brown (1931), Brown (1965), Cartwright (1938), Duncker (1929), Graham (1968), Johnson and Scobey (1982), Leibowitz (1955), Mates and Graham (1970), and Mattson (1976) and on the latter by Brandt et al. (1973), Brown (1931), Harvey and Michon (1974), Owen et al. (1981), and Tynan and Sekuler (1982).

Perhaps the earliest work on the proximity effect was that of Brown (1927) who reported that when a horizontally moving row of equally spaced black circles (pasted on a white background) are viewed moving behind a small rectangular aperture of a given size and another identical pattern is placed along side the first there is almost no difference in their phenomenal speed as long as their angular velocities are equal. However, when one of the two apertures and moving stimuli are spatially separated so that the comparison must be made in succession, Brown reported a striking difference of speed. The larger circles seen in the larger aperture now appeared much slower than did the smaller circles moving behind the smaller aperture. Also, the darker the surrounding room was the more conspicuous was the effect. Differential subjective motion as great as 1:7 was reported. It should be noted that Brown's method was a

temporally and spatially separated, paired- comparison, forced choice requiring a judgment of which of the two stimulus fields appeared faster. An experimenter adjusted the variable stimulus' velocity until a match was achieved. Earlier research on motion sensitivity by Aubert (1886, 1887) and Bourdon (1902) had considered such field factors as extraneous.

In a subsequent paper (1931), Brown found that in an opening four times the area as another (both with identical stimuli), the physical velocity had to be 3.8 times as great in the smaller aperture if a just perceptible movement was to be perceived correctly. Unfortunately, this early work did not attempt precise quantification of this type of effect.

Koffka (1935) suggested that visual sensitivity to such differential motion may depend on the magnitude of the angle between the moving stimulus and the nearest edge of a surrounding frame. Cartwright (1938) then offered that "...objective velocities will...appear inversely proportional to the linear dimensions of these frames; and objective velocities will have to be changed in proportion to these dimensions, if equal phenomenal speeds are to be obtained." (Ibid., pg. 324)

Considered from a Gestalt viewpoint, for situations in which an observer judges stimulus motion relative to a fixed aperture, the edge (of the aperture) that is being approached should exert an increasingly strong proximity effect to prod .ce a perception of motion while the opposite edge should exert a diminishing effect over time. If, on the other hand, such judgments are mediated by non Gestalt and/or more localized retinal capabilities one might expect no such effect.

In all of the early work the immediate background for a stimulus (within an aperture) was homogeneous. The influence of spatial detail or texture immediately behind the moving stimulus did not receive much interest until 1955 when Leibowitz considered an aspect of it by including a series of parallel, vertical grid lines behind which the equally spaced black stimuli moved horizontally. Bonnet (1975; 1977), Johnson and Scobey (1982), Legge and Campbell (1981), and Tyler and Torres (1972), also have studied the effect reference lines have on the proximity effect. More closely related to the present study is work by Johnson and Scobey (1982) who studied the influence of a vertical, fixed, luminous reference line (3.2' arc thick by 30' arc long) upon the displacement threshold for a vertically oriented moving stimulus which moved at constant velocity and which was 1' arc thick, 50' arc long, and only 11' arc away at the start of each trial. The stimulus always moved horizontally away from the reference line; both lines were viewed on the screen of a cathode ray tube measuring 10° arc high by 30° arc wide. Each of the two Os had to respond whether or not the stimulus had moved. The results showed that for all stimulus durations studied (from 10 msec to 2.5 sec), the reference line reduced displacement threshold by about five times (e.g., from about 6.5' arc to about 1.6' arc for one O and from about 5' arc to about 0.8' arc for the other for the 2.5 second stimulus duration condition. The question can be raised whether this proximity effect of a stable reference line exists for larger separation angles. While one might consider this as a reasonable possibility for foveally imaged stimuli (e.g., viewing with a separation angle of only 11' ar mechanisms might need to be invoked if a proximity effect is found to

separation angles of (say) more than one degree. The present study was conducted to investigate this possibility.

Concerning the matter of proximity effects produced by the edge of the stimulus' display area, Brown (1931) tried to make the edges of his aperture more conspicuous by including a high contrast "wall paper pattern" of squares so that a relatively thin rim of black cardboard remained around each aperture. He reported that this type of pattern lead to higher phenomenal velocities of the horizontally moving stimulus than when the entire apparatus up to the edge of the aperture was covered with the patterned wall paper. He stated, "It may be concluded that the physical velocity of the stimulus alone conditions the phenomenal velocity only when all of the properties of the visual field are kept constant." (pg. 228-9) Or put another way, there is no single perceptual criterion which can be applied to predict the magnitude of a particular phenomenal velocity or whether one velocity is more correct than another in a given matching task.

Brown (1931) suggested that phenomenal velocities were determined in a *"...dynamical field, the essential nature of which can not be described as a sum of independent local events. They correspond to dependent events in the functional whole. Therefore the whole functional structure of the excited field, not the excitation present at any given point within the field, must be considered in order that one understand the physiology of the visual perception of velocity." (Ibid., pp. 229-30; italics mine).* Of course, one implication of such a view is that the concept of an absolute threshold for movement is virtually meaningless, particularly when all of the relevant independent variables are not known, not controllable, and/or not even reported as is the case in actual airplane flight and its simulation.

Thus, for useful insights to be gained from laboratory motion perception studies it is necessary to hold virtually everything constant except the variable of interest. This was attempted here. Because of the confounding influences produced by the many visual variables that are present during actual and simulated flight (see Owen et al., 1981; Warren and Owen, 1982), the present study was designed to vary only one of the six degrees of freedom of motion (pitch) while holding the other five constant.

In this study the major objective was to obtain vertical displacement threshold measurements when the angular separation between the stimulus line and a nearby stable reference (window edge) was varied systematically over a relatively large range of angles. As will be noted, the basic temporal and spatial parameters approximated the apparent movement of the horizon as viewed from a turbojet type commercial airplane cockpit during a nose up pitch (flare) maneuver just prior to touchdown.

METHOD

Procedure.

The test procedure can best be described in the following sections: instructions, eye tests, practice, and data collection.

Instructions. The test instructions were read by each observer (O) and a brief black board demonstration was given to emphasize the required visual fixation location, displacement judgement, which response toggles to use, and the importance of maintaining a stable eye position (hereafter called the *Reference Eye Position; REP).*

A *Bausch & Lomb* Orthorater (far series) battery of vision tests was given to insure that all Os possessed at least 20:20 distance acuity, normal horizontal and vertical phoria balance. This required about 20 minutes.

Practice. The practice session consisted of 16 paired comparison trials having vertical displacements different from but similar to those used during data collection. All stimulus movement was downward starting from the center of the optical display. Presentation order of all trials was randomized. O had an opportunity to ask questions and try different response toggles. A typical response interval lasted about eight seconds.

O was carefully positioned in an adjustable seat through the use of a low light level TV system; his eyes were positioned at the REP of the display unit. An experimenter (E) visually monitored eye location continuously during data collection to insure that no deviations greater than +/- 0.1 inch occurred in any direction.

Data Collection. O remained in the semi-darkness of the laboratory for at least 20 minutes. Temporal intervals were identical for each of the two trials in a pair, viz., the horizontal stimulus was stationary for two seconds in its initial position at the center of the display which was at the same level as O's eyes; it descended through one of the five displacement angles over a three second period (ramp displacement); it remained stationary in its final position for two more seconds; it disappeared for 0.2 seconds between the two trials. It disappeared after the second trial indicating the start of the response period. The instructions were to choose whether the first or second stimulus trial had moved (down) the farthest.

Because each trial was initiated by O it was not possible to control total test time or total trial time. An average trial lasted about 20 seconds; 25 trials

required about nine minutes.

Prior to data collection and unknown to O, an E positioned the diffuse black lower window surface (hereafter called the *edge*) into one of the three positions of interest. The following steps were followed to insure that O would not be influenced in his displacement judgments because of prior knowledge of a positional change in the window's lower edge. First, the moveable edge was carefully located so that it was -3°, -4°, or -7° below and parallel to the stimulus' starting position (as measured from a level line of sight). O was never permitted to watch this operation but was led to believe that another variable was being tested. Second, O was told that his head and eyes had to be checked for position and that (subsequently) he would be shown the horizon (stimulus) and that he should adjust his seat up or down appropriately so that it appeared to lie exactly on top of the window's edge. Third, the stimulus was then located in such a position that it's displacement equalled the pre-set vertical edge position. Since O did not have to adjust his seat (but only sit a little taller or shorter), he was led to believe that nothing had changed from earlier testing conditions. When asked after testing was completed whether anything had been varied during testing no O was consciously aware of the deliberate repositioning of the edge. Finally, the stimulus was turned off and the data collection period began.

Since the stimulus moved downward through five angles and the lower window edge was located in each of three positions, there were a total of fifteen angular separations presented to each O upon which a mean threshold curve could be based. These angles are shown on the abscissa of Figure 5; they ranged from 0.4° to 5.6° arc from the stimulus' final (displaced) position.

Apparatus.

The apparatus consisted of three basic elements: digital computer to calculate stimulus equations of motion, stimulus derivation/display computer, and display collimating optics. A DEC PDP 11/60 digital computer was used to solve rate and amplitude equations for the stimulus which was displayed at apparent optical infinity as will be described. The stimulus line was programmed to lie 50,000 feet away with a vertical "eye height" of 50 feet to the imaginary ground plane which is a nominal airplane altitude at initiation of the flare maneuver.

An Evans and Sutherland Picture System II was used to generate the mathematical coordinates and display the stimulus on a calligraphic (stroke) CRT display. This 21 inch Zytron (model A21R-7C) monitor was collimated (-0.01 diopter) by means of a mirror/beam splitter imaging system of 25 inch (63.5 cm) focal length.

The stimulus subtended 0.033° (0.58 mrad) in width and 34.5° (0.602 rad) in length. Its intensity was adjusted by E prior to testing while being viewed by O through a 2.0 log ND Wratten filter (after prolonged adaptation to ambient illuminance) to be just visible over its full length. Of course, all stimulus viewing during data collection was without this filter. The stimulus appeared white against a very evenly dark background.

As is shown in Figure 1, a large, flat, rigid plastic aperture surface was located between the eyes and the collimating optics. O's side of this aperture surface was flat black with a reflectance of approximately six percent. This surface was illuminated by two 25 watt frosted, tungsten incandescent filament lamps operated at 40 volts and aimed so as to produce even illumination of approximately 0.54 lx (0.05 ft-c). The contrast (C) between the dimly illuminated aperture surface and the darker background of the moving stimulus was 6 where:

$$C = Lt - Lb/Lb$$

and Lt = aperture surface illuminance and Lb = background illuminance.

The plumb bob indicates the REP, a curved, padded head rest is seen to its left, and a response panel with white top and a row of spring-loaded toggle switches also is visible. The bottom edge of the aperture was adjustable as described above. Except for its lower edge, this aperture possessed the same frontal area and occupied the same position relative to O's eyes as the forward window in a B-727 type airplane on the captain's side. It subtended approximately 63° arc width across its upper edge with 18° vertically above the center of the stimulus (at its initial position) to the upper edge. There was no glass within the aperture, however. Figure 2 illustrates the shape and angular dimensions of this aperture as viewed from the REP.

Figure 1.

Photograph of Observer's Seat, Window Aperture, and Other Apparatus.

ORIGINAL PAGE IS
OF POOR QUALITY

Figure 2.

Diagram of Aperture with Dimensions

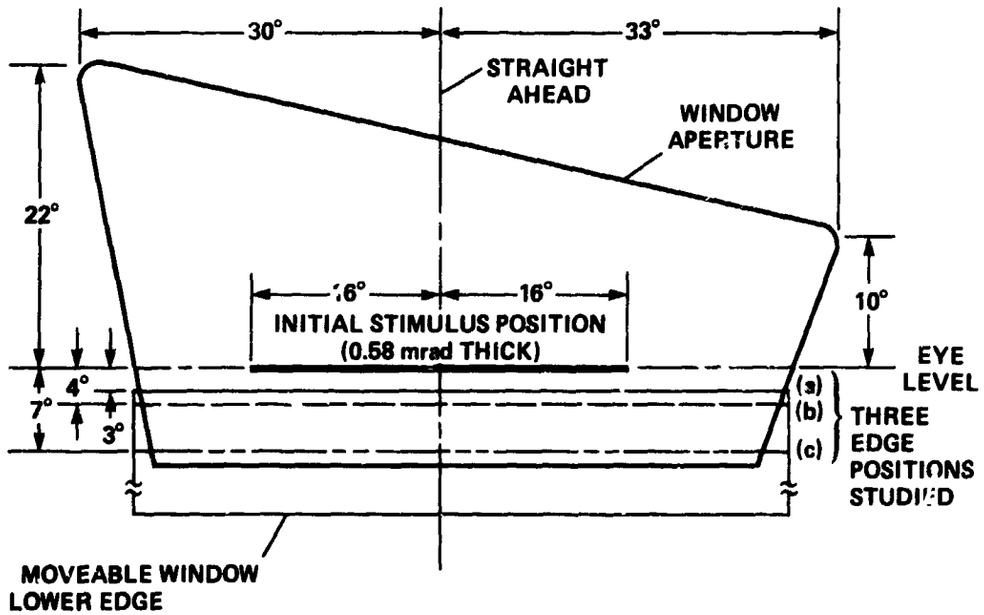

Experimental Design.

The experimental design may be characterized as an observer by treatment design with the five stimulus displacement angles nested within each treatment. The three edge positions and five stimulus displacement angles were presented in random order.

Observers.

Twenty four males took part as paid Os. They were obtained through a NASA contractor. Twelve were non pilots (mean age = 27.9; SD = 8.8 yrs) and twelve were pilots (mean age = 26; SD = 10.7 yrs). Except for one non pilot all Os possessed 20:20 or better uncorrected distance acuity. The single O wore glasses which corrected his acuity to 20:20. The total flight time of the pilot group ranged from 70 to 14,000 hours (mean = 1,727). Table 1 presents selected O information.

Table 1.

Observer Information

	Age	Acuity	Pilot Flight Hours (heaviest airplane flown)
Pilots			
A	19	20:20	650 Hrs. Multi-engine rating
B	23	20:17	110 Hrs. (2,300 lbs.)
C	34	20:17	135 Hrs. Cessna 182
D	21	20:17	120 Hrs. Cessna 172
E	27	20:20	70 Hrs. Archer 2
F	33	20:20	1,200 Hrs. Cessna 420
G	35	20:17	534 Hrs. Cessna 206
H	45	20:18	14,000 Hrs. B-747
I	31	20:17	4,100 Hrs. B-727
J	25	20:20	500 Hrs. Piper-Turbo Lance
K	23	20:18	275 Hrs. Piper-Apache
L	22	20:20	100 Hrs. Cessna 206
Non Pilots			
M	29	20:20	
N	39	20:17	
O	30	20:20	
P	33	20:17	
Q	18	20:20	
R	29	20:18	
S	31	20:17	
T	45	20:20 (corrected)	
U	20	20:20	
V	25	20:17	
W	18	20:18	
X	31	20:17	

RESULTS

Two separate responses were required on each pair of trials (I. vetical displacement comparison; II. confidence). Each type of response is presented and discussed separately.

I. Vertical Displacement Comparison Results:

Analysis of Variance Results. An analysis of variance was performed on the mean proportion data (Univ. of Calif., 197 ; BMD-08V). The Os were considered as a random factor and the three edge positions as a fixed factor. The five displacement angles were nested within each edge position. The only significant factor found was the edge position main effect ($F = 3.04$; $df = 2/44$; $p = 0.05$). It is of value to consider this significant edge position effect more closely.

Proportion Data. The data were analyzed following procedures set forth in detail elsewhere (Guilford, 1954). The proportion of total responses on which these Os responded that the first trial in a pair possessed the larger displacement is referred to as P. The bivariate normal transform of P also was determined and is referred to as Z. Tables of P and Z values for all 25 cell conditions, averaged across the 24 Os, are given in Appendix 1 through 3.

The mean data from Appendix 1 - 3 were plotted with the percent of responses correct on the ordinate and the angular magnitude of the difference between the two trials of a given pair on the abscissa. For instance, a difference of 0.6° is obtained from three pairs of angles presented (-1.4° vs. -2°; -1.7° vs. -2.3°; and -2° vs. -2.6°). Figures 3 through 5 present these threshold curves for the -3°, -4°, and -7° edge position conditions, respectively. Dots represent trials in which the larger angle was presented second in a pair while crosses represent the opposite. Each curve is fit by eye.

Figure 3.

Mean Displacement Threshold Curve for the -3° Edge Position Condition.

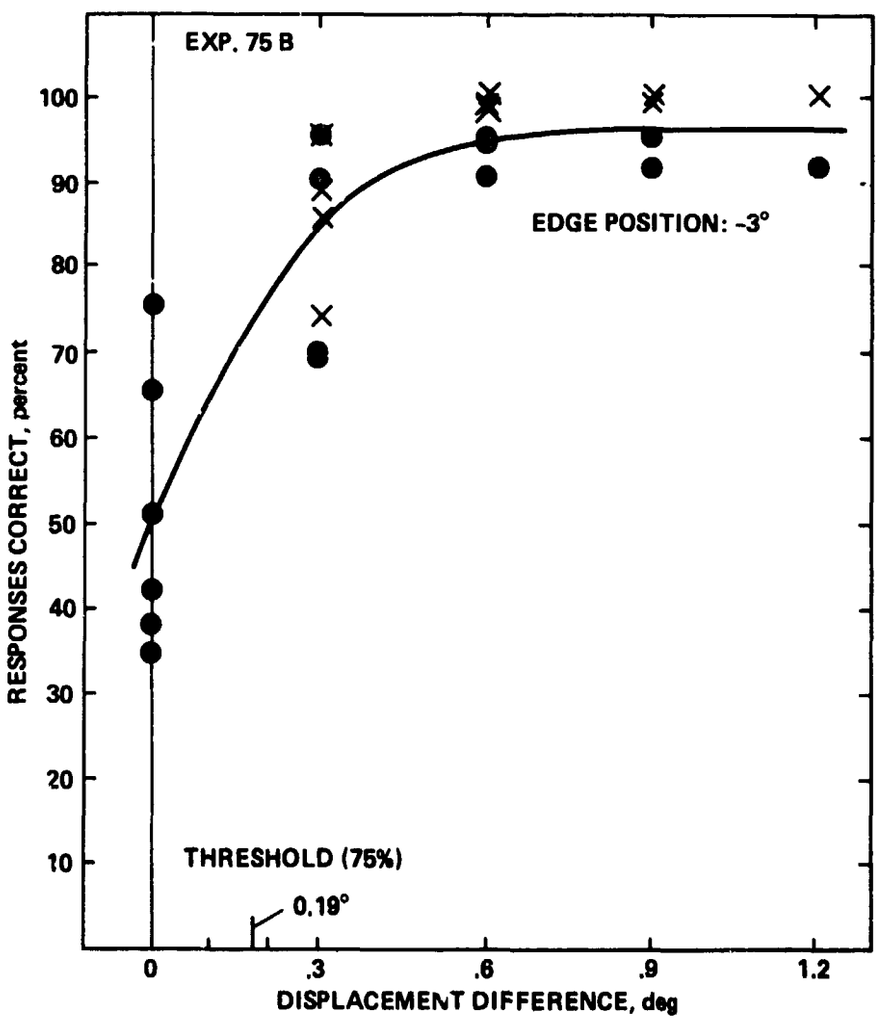

Figure 4.

Mean Displacement Threshold Curve for the -4° Edge Position Condition.

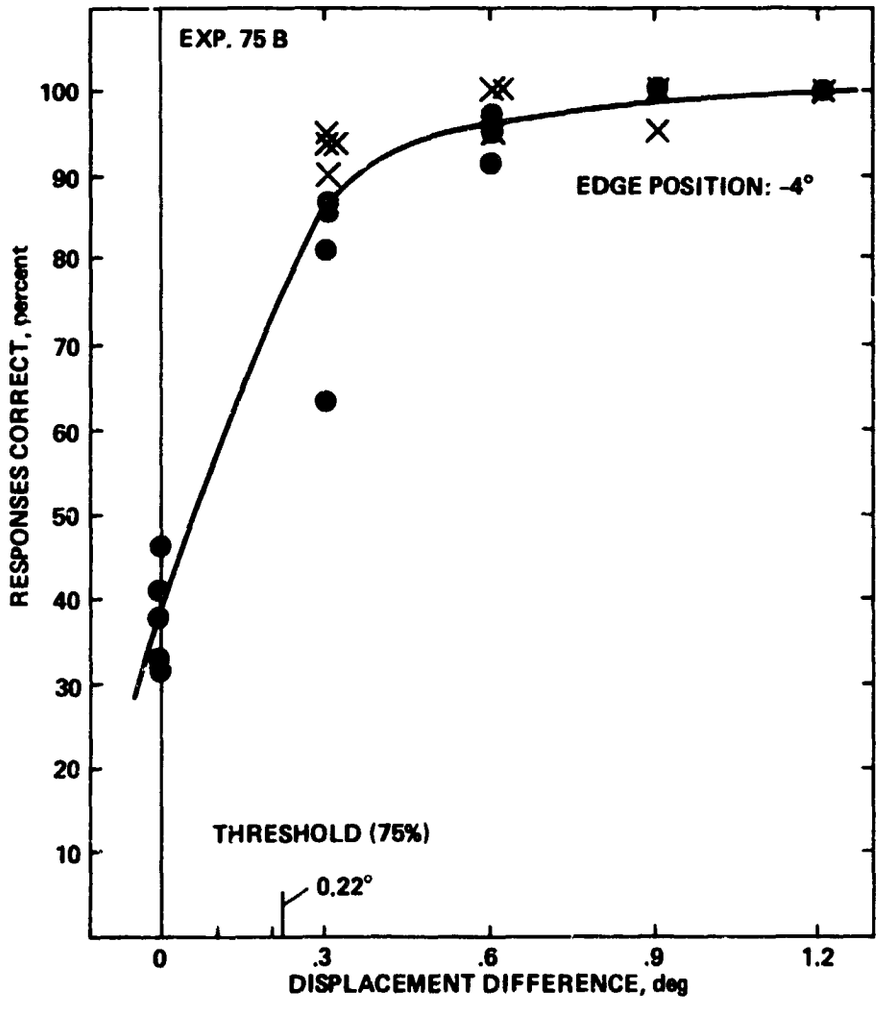

Figure 5.

Mean Displacement Threshold Curve for the -7° Edge Position Condition.

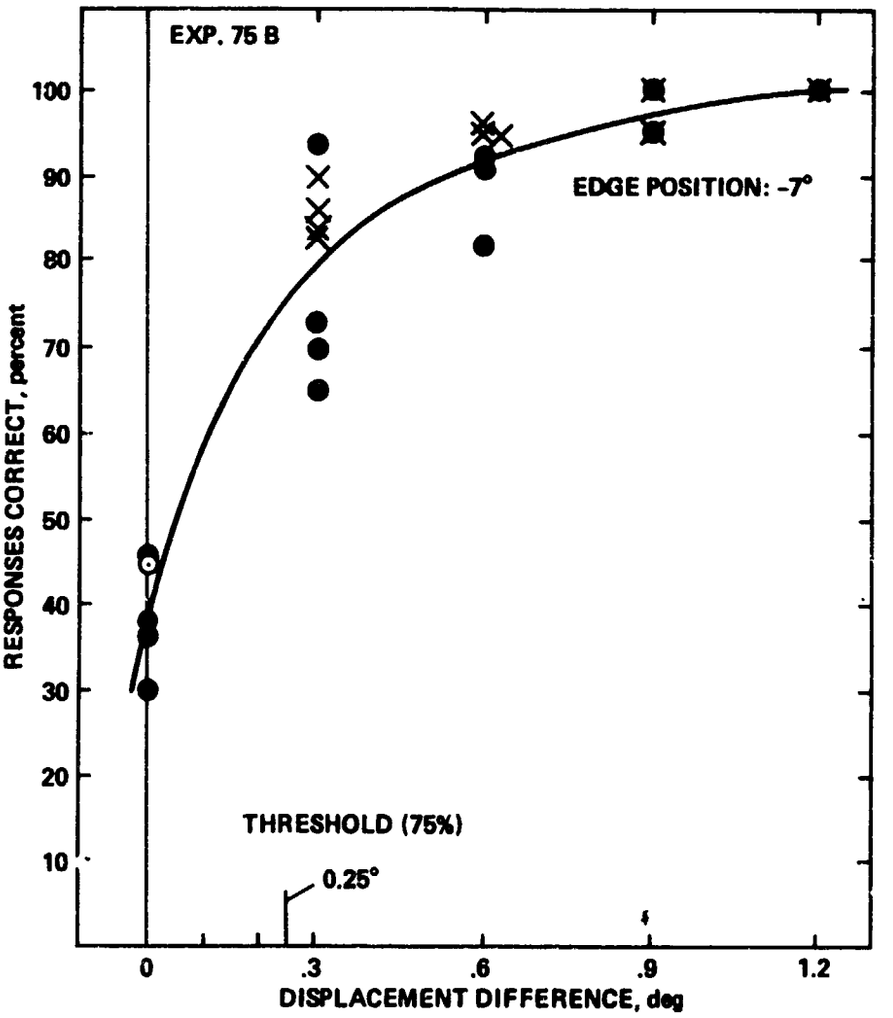

Using a threshold criterion of 75 percent correct yields mean displacement thresholds of 0.19°, 0.22°, and 0.25° for the above three edge positions, respectively (see vertical tick on abscissa).

All of the mean data from Figures 3 through 5 were combined in Figure 6 to show percent correct as a function of the angular separation between the stimulus' final position and the edge regardless of which of the three edge positions was presented. Each data point is the mean of 24 responses. Two linear, least square fit curves are shown intersecting at an angular separation of 1.7° which is the angle which divides the data used for each curve. The data points have been coded to permit identification of which displacement angle each represents.

Figure 6.

Percent Correct as a Function of Stimulus - Edge Angular Separation.

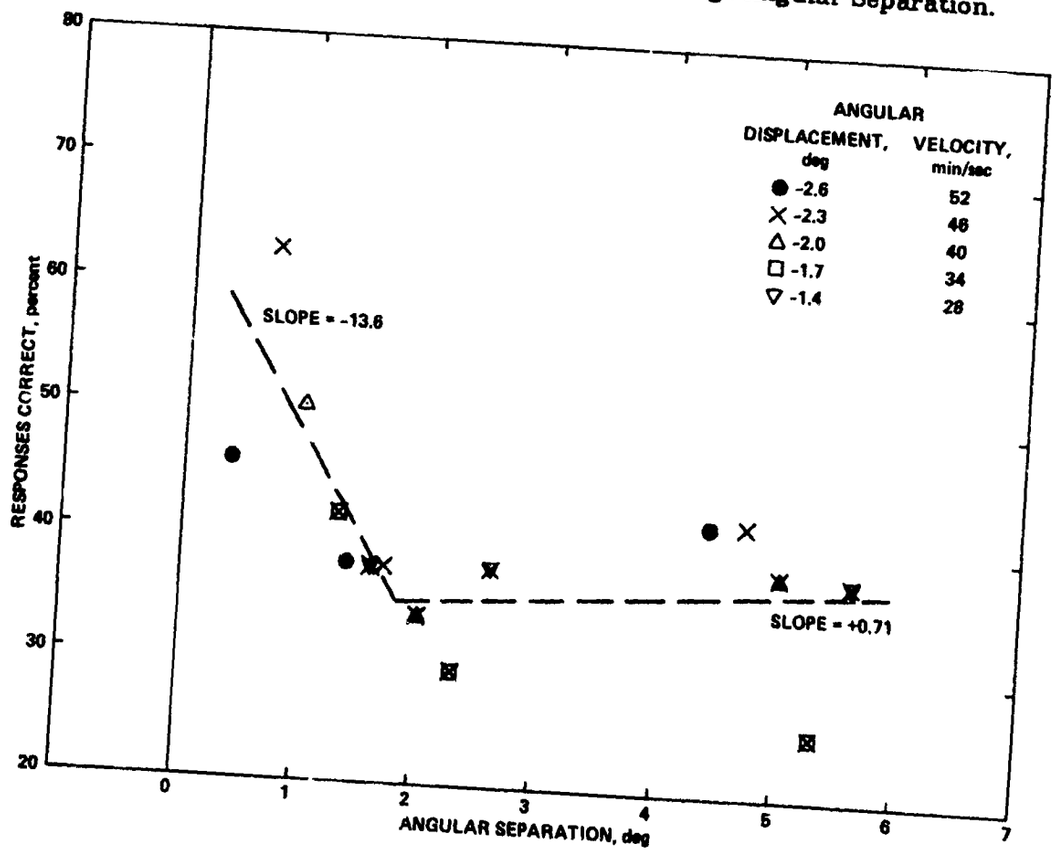

Referring to Figure 6 it can be seen that it is only within about 1.7° arc of the window's edge that the percent of responses that are correct is influenced to any marked degree.

Normal Bivariate (Z) Transform Results. Guilford (Ibid.) provides both the mathematical derivation for and suggested approaches to interpretation of paired comparison, forced choice data. He points out that for data which meets certain requirements, Z transformed data provide useful insights about the underlying data upon which they are based. For example, (a) the slope of a least squares linear fit curve of Z data is inversely proportional to the standard deviation of that data, (b) the degree of linearity of a Z curve is positively related to the normalicy of the distribution of data underlying the data, (c) given sufficient data, each curve should cross the level Z = 0 at a value corresponding to the standard or mid-stimulus value for that data set, and (d) the degree to which all curves are non- overlapping and ordered in the same order as the original stimulus dimension gives useful insights as to whether the perceptual mechanism(s) involved in the discrimination also is mediating regular, ordered discriminations.

The mean proportion data of Figures 3 through 5 are replotted as Z in Figures 7 through 9. Referring to Figure 7 for the -3° edge position condition it is seen that the five curves are not only spaced relatively evenly but possess decreasing slope (increasing standard deviation) with an increase in the magnitude of the stimulus displacement. Thus, the farther the stimulus is from the window's lower edge the greater is response variability. The (presumed) "edge effect" seems to have diminished by the time the stimulus is 7° from the edge, i.e., while the five curves are still ordered correctly their slopes do not change regularly. A similar effect has been found in earlier unpublished research from this laboratory in which the same five stimulus displacement angles were presented but in the center of a much larger field of view where, presumably, the display edges would not be expected to exert any effect on the judgment.

Figure 7.

Mean Z Deviate as a Function of Stimulus Displacement for the -3° Edge Position Condition.

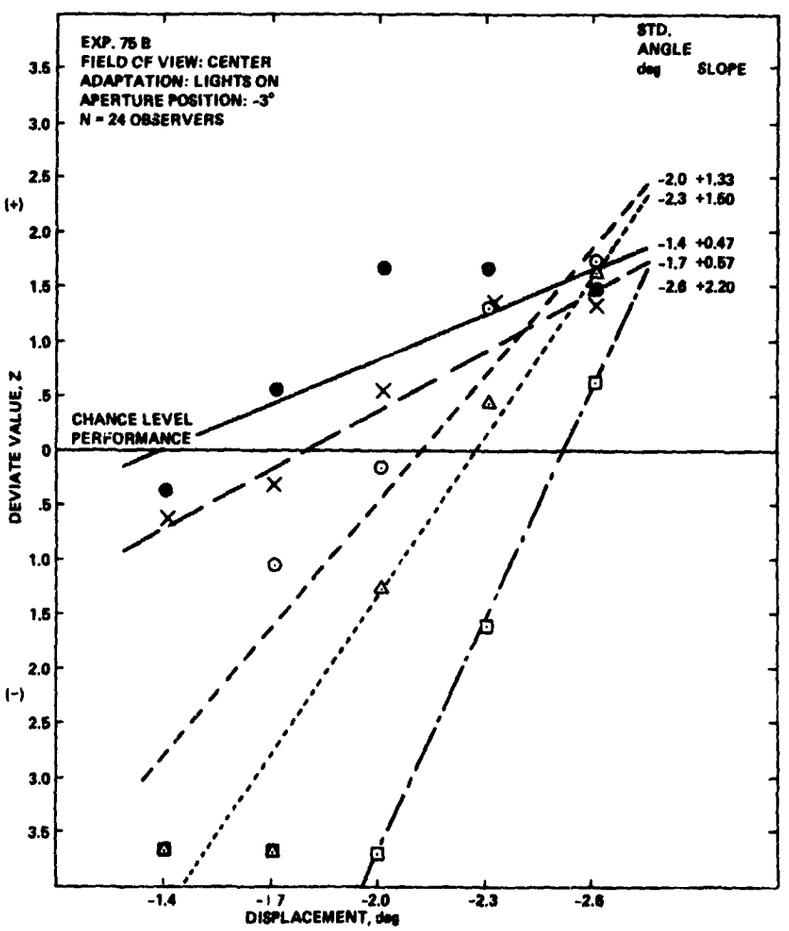

Figure 8.

Mean Z Deviate as a Function of Stimulus Displacement for the -4° Edge Position Condition.

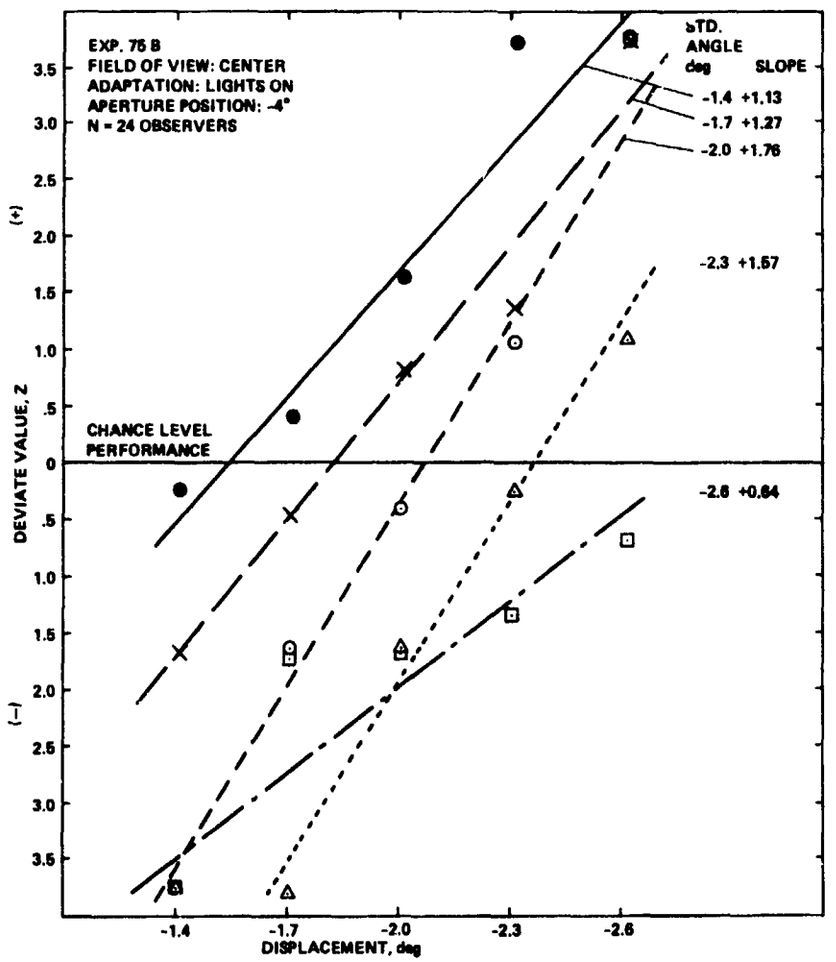

Figure 9.

Mean Z Deviate as a Function of Stimulus Displacement for the -7° Edge Position Condition.

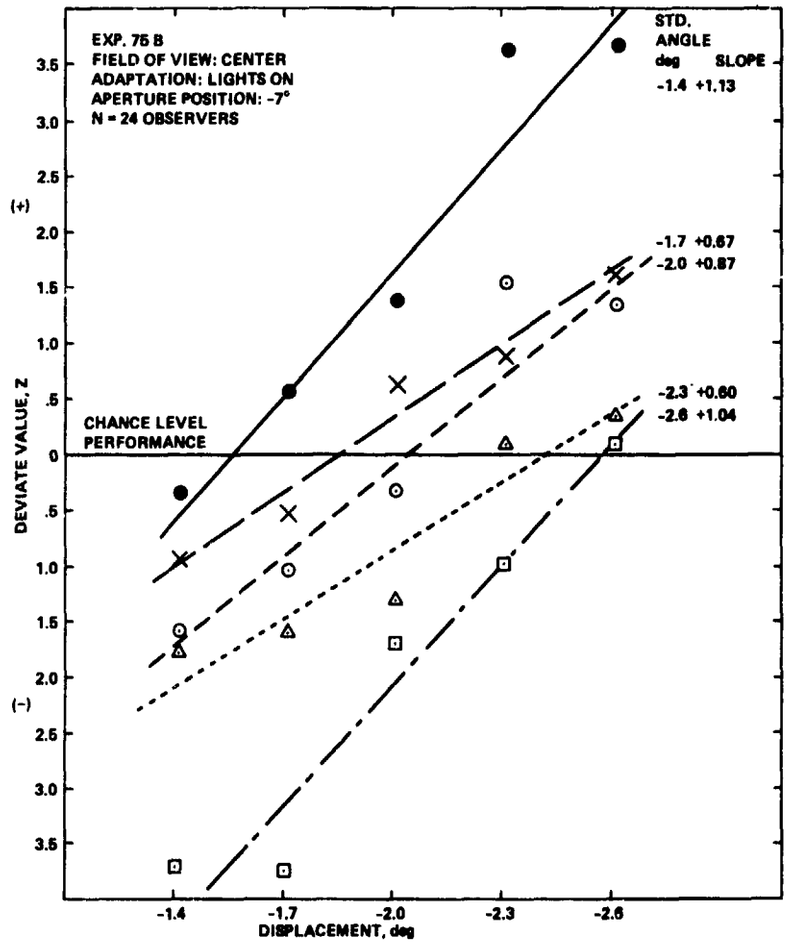

ORIGINAL PAGE IS
OF POOR QUALITY

II. Confidence Response Results:

An analysis of variance was conducted on the mean confidence data (cf. Appendix 4 - 6) using the same program as was used earlier. No significant main effects or interactions were found. A prominant trend was noted, however, in that the twelve pilots tended to give lower confidence responses than the twelve non pilots at each of the three edge positions ($F = 3.73$; $df = 1/22$; $p = .06$). Within the confidence scale from 2 to 9, the pilots' mean confidence ranged from 3.4 to 3.6 while the non pilot's mean confidence ranged from 4.3 to 4.9 across the five stimulus displacement angles studied. While it is interesting to speculate on the possible reason for this finding, it is probably just the result of the usual conservative attitudes that pilots tend to bring into a laboratory situation.

DISCUSSION

This study has shown that vertical displacement accuracy is inversely related to the angular separation between a horizontal stimulus line and a nearby fixed window edge. The effect appears to exist (for the present test conditions) within only one or two degrees arc of the edge. An "edge proximity effect" on phenomenal velocity was suggested earlier by Koffka (1935) and Cartwright (1938); both suggested that the edge that is being approached will exert an increasingly strong influence on the perception of phenomenal movement. The edge from which the stimulus is receding will exert a progressively decreasing influence. Unfortunately, the nature of this proposed "influence" has yet to be discovered.

Correlated and Uncorrelated Motion-inducing Parameters.

CMIPs in the present study include those visual cues that do not influence the stimulus displacement judgment, i.e., they are highly correlated with the perception of displacement and do not offer a source of "differential" information. It is suggested that the primary CMIPs include:

1) field of view
2) stimulus collimation angle and magnification
3) stimulus intensity and contrast with the background
4) stimulus temporal characteristics
5) retinal image position of stimulus
6) head position

It is suggested that the primary UMIPs include:

1) line of sight
2) stimulus angular velocity

According to the above view, these two UMIPs act not only to make the stimulus' displacement perceptible but also to isolate stimulus displacement and/or angular velocity as the sole contributor(s) to the judgment. Let us consider the line of sight parameter. As O visually fixates the stimulus during its downward displacement its retinal image remains approximately cen-

tered on the fovea (+/- approx. 0.1°; Yarbus, 1967). To the extent that the edges of the window are visible, however, the retinal image of the top and bottom edges will be displaced downward over the peripheral retina. It is possible that the displacement is perceived because of this image translation.

The second possible displacement cue is that of the differential angular velocity possessed by each of the five displacement angles studied Each displacement occurred over a three second-long period. Consequently, each displacement is associated with a different angular rate; the possibility exists that the discrimination is based (partially or entirely) on a rate discrimination rather than displacement despite the fact that the criterion that was supposed to be used was, by instruction, a displacement criterion. The angular rates corresponding to each displacement angle are:

-1.4° = 28'/sec
-1.7° = 34'/sec
-2.0° = 40'/sec
-2.3° = 46'/sec
-2.6° = 52'/sec

The shape-coded data points in Figure 6 permit an assessment of this possibility. It is noted that within and across the three edge position conditions, there is no particular spatial ordering of the mean proportion data on the basis of angular velocity. A follow-on study is underway to investigate this issue further.

Practical Application of These Data.

Consider a pilot who is about to land a modern, swept-wing, turbo-jet airplane of the B-727 type in weather and illumination conditions which permit a good view of the horizon. Let us assume that he has stabilized his approach, i.e., that he is on the ILS localizer and glideslope, is at the correct approach and vertical speed, and is not deviating from the correct flight path. Until the moment of flare initiation, he will try to maintain a constant pitch attitude along with the other parameters just mentioned. This pitch attitude will cause the distant horizon to be seen imaged within the front window at some fixed angular separation above his glare shield top surface or window lower edge (whichever cuts off his LOS over the airplane's nose). The present data provides an idea about how small an amount he can pitch his airplane up and still detect it correctly. This angle is about 0.2° for a 75 per cent criterion. As Figures 3 - 5 show, this value increases at higher criterion values with an asymptote at about 0.6° threshold for a criterion of 98 per cent (for the -3° edge position condition). Slightly different values are found for the other two edge position conditions. This study also found that the larger the angular separation between the horizon and the lower edge of the window (during displacement comparison judgments), the larger must the displacement be in order to be perceived correctly.

Returning to the (above) cockpit illustration, the typical pilot alternates his line of sight (LOS) many times during an approach between cockpit display

information and outside scene information (Haines, Fischer & Price, 1980). During these intra-cockpit information scans he will check his attitude direction indicator (ADI) for his basic pitch attitude, his air speed indicator (ASI), and his instantaneous vertical rate indicator (IVSI). It is important to point out that most ADIs provide pitch attitude in reduced visual angle such that one degree of actual airplane pitch is displayed as about a 0.2° index line displacement. Interestingly, this is very nearly the same vertical displacement amplitude that can be discriminated by the present observers. Once the pilot looks up through his window at the runway he typically fixates the touchdown zone and tries to notice changes in his airplane's pitch attitude by displacement of the horizon (and other ground detail).

It is suggested that the major reason why pilots cross-check flight instruments other than their ADI for pitch attitude is that they simply cannot obtain sufficient pitch attitude resolution from it. While they are able to correctly discriminate a vertical displacement of a *simulated* horizon as small as about 0.2', they cannot discriminate pitch attitude changes equivalent to one degree of airplane pitch from this flight instrument.

CONCLUSIONS

In this investigation the horizontal (line) stimulus was located 18° arc below the top of the window's edge and either 3°, 4°, or 7° arc above its lower edge at the start of each displacement trial. After its displacement downward it was from 0.4° to 5.6° above the window's lower edge due to the fact that five different displacement angles were presented. Evidence was found to support the view that displacement sensitivity improves when the horizontal stimulus is within from one to two degrees arc of the lower edge but not more than this. It also appears that angular velocity was not a prominant cue to account for this displacement sensitivity among the five conditions tested which ranged from 28 to 52 minutes of arc per second.

REFERENCES

Aubert, H., Die Bewegungsempfindung. Arch. ges. Physiol. (Pfluger's), vol. 39, Pp. 347-370, 1886.

Bonnet, C., A tentative model for visual motion detection. Psychologica, vol. 18, Pp. 35-50, 1975.

Bonnet, C., Visual motion detection models: features and frequency filters. Perception, vol. 6, Pp. 491-500, 1977.

Bourdon, B., La perception Visuelle de l'Espace. Paris, Librarie C. Reinwald, 1902.

Brandt, Th., J. Dichgans, & E. Koenig., Differential effects of central versus peripheral vision on egocentric and exocentric motion perception. Exp. Brain Res., vol. 16, Pp. 476-491, 1973.

Breitmeyer, B. G., Velocity sensitivity and discriminability in centeral and peripheral vision. (Paper presented at the 1974 Optical Society Meeting, Houston, Texas).

Brown, J.F., Uber gesehene Geschwindigkeit. Psychol. Forschg., vol. 10, Pp. 84-101, 1927.

Brown, J.F., Thresholds for visual movement. Psychol. Forsch., vol. 14, Pp.249-268, 1931.

Brown, J. F., The visual perception of velocity. In (I. M. Spigel (ed.), Visually Perceived Movement. New York, Harper & Row, 1965, Pp. 64-107.

Cartwright, D., On visual speed. Psychol. Forsch., vol. 22, Pp. 320-342, 1938.

Dixon, W. J., (ed.), BMD: Biomedical Computer Programs. School of Medicine, Univ. of California, Los Angeles, 1975.

Duncker, K., Uber induzierte Bewegung. Ein Beitrag zur Theorie optisch Wahrgenommener Bewegung. Psychol. Forsch., vol. 12, Pp. 180-259, 1929.

Gibson, J. J., The Perception of the Visual World. New York, Houghton Mifflin, 1950.

Graham, C. H., Visual Perception. In S. S. Stevens (ed.), Handbook of Experimental Psychology. New York, John Wiley & Sons, Inc., 1962.

Guilford, J. P., The method of pair comparisons. Chpt. 7 in J. P. Guilford, Psychometric Methods, New York, McGraw-Hill Book Co., Inc., 1954.

Haines, R. F., E. Fischer, & T. A. Price, Head up transition Behavior of pilots with and without a head-up display in simulated low-visibility approaches. NASA Technical Paper No. 1720, 1980.

Johnson, C. A., and R. P. Scobey, Effects of reference lines on displacement thresholds at various durations of movement. Vision Research, vol. 22, Pp. 819-821, 1982.

Koffka, K., Principles of Gestalt Psychology. London, Routledge & Kegan Publ., 1935

Legge, G. E., and F. W. Campbell, Displacement detection in human vision. Vision Research, vol. 21, Pp. 205-213, 1981..

Le Grand, Y., Vision of movements. Chpt. 11 in Y. Le Grand, Form and Space Vision, Bloomington, Indiana University Press, 1965.

Leibowitz, H. W., Effect of reference lines on the discrimination of movement. J. optical Soc. Amer., vol. 45, Pp. 829-830, 1955.

Mates, B., and C. H. Graham, Effect of rectangle length on velocity thresholds for real movement. Proc. of the National Academy of Sciences, vol. 65, Pp. 516-520, 1970

Mattson, D. L., Stimulus length and orientation variables interact in peripheral motion perception. Perceptual & Motor Skills, vol. 43, Pp. 95-98, 1976.

Owen, D. H., R. Warren, R. S. Jensen, S. J. Mangold, & L. J. Hetlinger, Optical information for detecting loss in one's own forward speed. Acta Psychologica, vol. 48, Pp. 203-213, 1981.

Owen, D.H., R. Warren, and S.J. Mangold, Sensitivity to optical information specifying loss in one's own altitude. Perception and Psychophysics, (in press).

Spigel, I. M., (ed.), Readings in the Study of Visually Perceived Movement. New York, Harper & Row, Publ., 1965.

Tyler, C. W., and J. Torres, Frequency response characteristics for sinusoidal movement in the fovea and periphery. Perception and Psychophysics, vol. 12, Pp. 232-236.

Tynan, P. D., & R. Sekuler, Motion processing in peripheral vision: Reaction time and perceived velocity. Vision Research, vol. 22, Pp. 61-68, 1982.

Warren, R., and D.H. Owen, Functional optical invariants: A new methodology for aviation research. Aviation, Space, and Environmental Medicine, vol. 53, no. 10, Pp. 977-983, 1982.

Yarbus, A. L., Eye Movements and Vision. New York, Plenum Press, 1967.

N85 14519

MEAN AND RANDOM ERRORS OF VISUAL ROLL RATE PERCEPTION FROM CENTRAL AND PERIPHERAL VISUAL DISPLAYS

by

J.C. van der Vaart and R.J.A.W. Hosman

DEPARTMENT OF AEROSPACE ENGINEERING
Delft University of Technology
Kluyverweg 1 - 2629 HS Delft
The Netherlands

ABSTRACT

A large number of roll rate stimuli, covering rates from zero to plus or minus 25 deg/sec, were presented to subjects in random order at 2 sec intervals. Subjects were to make estimates of magnitude of perceived roll rate stimuli presented on either a central display, on displays in the peripheral field of vision, or on all displays simultaneously. Response was by way of a digital keyboard device, stimulus exposition times were varied.
The present experiment differs from earlier perception tasks by the same authors in that mean rate perception error (and standard deviation) was obtained as a function of rate stimulus magnitude, whereas the earlier experiments only yielded mean absolute error magnitude. Moreover, in the present experiment, all stimulus rates had an equal probability of occurrence, whereas the earlier tests featured a gaussian stimulus probability density function.
Results yield a good illustration of the non-linear functions relating rate presented to rate perceived by human observers or operators.

INTRODUCTION

Earlier and related experiments

The perception accuracy experiment reported here is a part of a large series of experiments on motion perception in piloting tasks that was started off with a moving base simulator experiment by the same authors (Ref. 1). A better performance and notable changes in pilot control behaviour were found in roll tracking tasks whenever peripheral visual field motion and/or cockpit motion was added to the basic display configuration of a central, artificial (CRT) horizon display. Peripheral field motion could be displayed by moving checkerboard patterns on TV-monitors mounted on either side of the cockpit, in the peripheral field of vision of the subjects.
These results and the subsequent questions raised about the rôle of motion perception and that of mental processing of perceived motion by pilots in the control of an aeroplane, resulted in a long-term research program, at the Department of Aerospace Engineering of Delft University, into visual and whole-body motion perception by pilots in a typical flight-deck situation.
By lack of data on the accuracy of motion perception, a rather extensive series of experiments was carried out on accuracy and speed of visual roll

PRECEDING PAGE BLANK NOT FILMED

attitude and roll motion perception, on target-time estimation accuracy and, more recently, on accuracy of visual and vestibular motion perception in a moving base flight simulator. In order to assure a sound basis of comparison, the experimental apparatus remained basically unchanged throughout the entire series.

Experiments on visual motion perception

Accuracy and speed of visual perception of roll attitude and roll rate, from the same visual displays as used in the tracking experiment of Ref. 1, were assessed in tests where subjects were required to make accurate and quick estimates of the magnitude of discrete stimuli of roll angle or roll angular velocity (Refs 2 and 3). Subjects responded by pressing the appropriate button of a digital keyboard device, followed by immediate feedback of errors by displaying error angle or rate after each response. The temporal aspect of motion perception appeared to be twofold.

Firstly, there is the exposure duration necessary for a subject to attain a reasonably accurate estimate of the stimulus magnitude. By varying exposure times, it was shown that attitude (roll angle) perception could very accurately be done down to exposure times as short as 0.05 sec, whereas roll rate perception appe red to deteriorate badly at exposure times shorter than 0.4 sec.

Secondly, there is the time taken by subjects to decide on the magnitude of their estimate and to press the appropriate key. It was shown that response times for attitude stimuli were around 0.1 sec shorter than those to roll stimuli, but response times to roll stimuli were slightly, but significantly quicker if peripheral field motion was present.

As to the accuracy of responses, it was shown that peripheral field motion decreased overall standard deviation of the response error for short exposure duration.

Target-time experiments

The perception tests were succeeded by a series of target-time estimation tests (Refs 4 and 5) where subjects were to combine roll attitude and roll rate, as perceived from a rotating horizon line, to obtain an estimate of the time of zero-crossing (target-time).

The accuracy of subject's responses in this sort of interception or motion extrapolation tasks could be shown to be partly related to the known accuracy of rate perception, but some other questions could not be answered due to lack of certain data on rate perception.

Present experiment

Unfortunately, in the rate perception experiments of Refs 2 and 3 only the mean error and standard deviation over a completed run, and absolute errors as a function of rate were determined. Moreover, the discrete stimuli in these experiments were generated by quantization of a random, zero mean, gaussian white noise process. This resulted in rather few data points at the extremes of the range of stimuli and considerable scatter in results for large rates was found.

Therefore, the present tests on rate perception accuracy were carried out, featuring a straight distribution of stimuli and a set-up yielding mean errors, standard deviation of the mean and standard deviation of total error as a function of stimulus rate magnitude.

TEST FACILITY AND DATA REDUCTION

Tests were done in a low-noise room where, in front of the subject's seat, a central (foveal) CRT display (Tektronix 604 monitor), was mounted in a dull gray panel. Peripheral visual field motion was provided by two TV-monitors (Bosch Fernseh Monitor) placed on either side of the subject's seat, see Fig. 1. Subjects gave their responses via a digital keyboard device, see Fig. 2.
The relative positions of central and peripheral displays and the subject's eye reference point are shown in Fig. 4. No head restraint was used. Subjects were free to sit relaxed and at ease, just as in an actual airline cockpit. Also shown in Fig. 4 is the image of the central display, simulating an artificial horizon. The repetition rate was 250 Hz and the position of the horizon line was updated at 50 Hz.
The peripheral displays showed a black and white checkerboard pattern with squares of 5x5 cm, generated by a moving pattern generator (developed at Delft University), at a rate of 30 frames per second. The patterns on the displays moved in conjunction with the rotating horizon line.
All experimental runs were controlled by a hybrid computer (EAI Pacer 100).

A single run consisted of 105 discrete stimuli, presented in random order at fixed intervals of 2 seconds, the sequence during one interval being as follows, see Fig. 3.
At the beginning of the n-th presentation within a run, a random discrete value $\dot{\varphi}_{st}(n)$ of roll rate was presented and this event was marked by a short audiotone in the subject's headphone. After observing the stimulus, the subject was required to respond by pressing the appropriate key of the keyboard. The response magnitude is designated here by $\dot{\varphi}_p(n)$ (perceived rate magnitude). Immediately after the response, the rate error value

$$\Delta\dot{\varphi}_e(n) = \dot{\varphi}_p(n) - \dot{\varphi}_{st}(n) \tag{1}$$

was shown on the display, thereby giving the subject immediate knowledge of the result after a single presentation and response.
According to eq. (1) a positive value of $\Delta\varphi_e$ would indicate an overestimation of rate for positive stimulus rates. In order to facilitate the combination of results of clockwise and counter-clockwise stimuli, the error $\Delta\dot{\varphi}_e$ was computed as

$$\Delta\dot{\varphi}_e(n) = \{\dot{\varphi}_p(n) - \dot{\varphi}_{st}(n)\}.\mathrm{sign}(\dot{\varphi}_{st}(n)) \tag{2}$$

so that positive $\Delta\dot{\varphi}_e$ indicates overestimation of absolute rate magnitude throughout.
For reasons to be explained below, a next (n+1) rate stimulus magnitude was set by

$$\dot{\varphi}_{st}(n+1) = \Delta\dot{\varphi}_e(n) + \Delta\varphi_1(n+1) \tag{3}$$

where $\Delta\varphi_1(n+1)$ is a discrete, random value of rate magnitude, set by a random number sequence in the program software.
The stimulus exposure time Δt_{exp} could be varied and was set at a constant value by the experimentor prior to each run.

In one particular experimental condition, exposure was retained until the subject's keyboard response. In all other conditions, the stimulus was made to disappear at the end of the preset exposure time by entirely blanking the displays. In that case, subjects were required to give responses only after exposure termination, responses during exposure time being neglected by the program software. Provisions were also made to neglect responses later than 2.0 sec after exposition onset. Very few missed responses (only one or two in thousand) occurred during actual tests.
During a run, the values of $\dot{\varphi}_{st}(n)$, $\Delta\dot{\varphi}_e(n)$ and the response e RT were recorded and stored on disk for subsequent analysis. Immediatel after a run, a printout of overall means and standard eviations of $\Delta\dot{\varphi}_e$ and RT was available.

From replicated runs, overal means and standard deviations of $\Delta\dot{\varphi}_e$ and RT were computed, together with an error score parameter, defined by

$$S_c = \frac{\sigma^2_{\Delta\dot{\varphi}_t}}{\sigma^2_{\dot{\varphi}_{st}}}$$

where $\sigma^2_{\Delta\dot{\varphi}_t}$ is the total error variance defined below.

In addition, means and standard deviations of $\Delta\dot{\varphi}_e$ and RT were computed, together with the standard deviation of total error (relative to zero mean), per stimulus rate level. Total error variance $\sigma^2_{\Delta\dot{\varphi}_t}$ was computed according to

$$\sigma^2_{\Delta\dot{\varphi}_t} = \frac{\Sigma(\Delta\dot{\varphi}_e)^2}{n-1}$$

whereas variance of mean rate error was obtained by

$$\sigma^2_{\Delta\dot{\varphi}_e} = \frac{\Sigma(\Delta\dot{\varphi}_e - \overline{\Delta\dot{\varphi}_e})^2}{n-1}$$

EXPERIMENT

The experimental design was similar to that described in Refs 2 and 3, except for the frequency distribution of the rate stimulus magnitude. The former experiment featured a quantized gaussian white noise stimulus, the present one was run with a range of 0±10 levels of discrete stimuli having an equal probability of occurrence.
The range of stimuli was, just as in the former experiments chosen to be representative of routine airline flight (φ_{max} = ±25 deg/sec). The range of keys to be used nominally was set again at ±10, corresponding with ±25 deg/sec on the displays. Including zero rate, a number of 21 rate levels was obtained. The discrete values of $\Delta\dot{\varphi}_i$ were set by a random number sequence in the program

software in such a way that each rate level was replicated 5 times during a run, bringing the number of presentations at 105 per run.
During pre-experimental evaluation, the rate stimulus magnitude was first set by

$$\dot{\varphi}_{st}(n) = \Delta\varphi_i(n)$$

giving a completely 'fresh' stimulus for each presentation. In this way, the complete range of stimuli was covered and was replicated five times when the random sequence was completed. As a consequence, only zero errors or underestimation of absolute rate can occur at the extreme rate magnitudes, since subjects are very soon aware of the fact that no rates larger than those corresponding with ±10 keys on the keyboard, will occur. This peculiarity was suspected to be the cause of a measured tendency for negative mean errors towards the extremes of the range of rates.
In order to remove this phenomenon from the range of rates of interest, it was decided to present a next stimulus according tot eq. (3). Given the fact that errors will be made, this arrangement will cause stimuli greater than ±25 deg/sec to occur frequently. In this way, the possible artifact could be excluded, without having to increase the nominal range of rates and the number of presentations within a run.

Based on the results of Refs 2 and 3, the exposition times in the present experiments were set at 0.1 sec, 0.3 sec and equal to the response time (Δt_{exp} = RT). Just as in the former experiments, three display configurations were used i.e. central display only (configuration C), peripheral displays only (configuration P) and all displays (configuration CP). With the three exposition times this yielded 9 types of experimental runs, each subject replicating 5 times the 9 types of runs.
After checking that no systematic differences occurred due to clockwise and counter-clockwise rotations of the horizon line, results for positive and negative rates were taken together. Since each stimulus rate level was (nominally) replicated 5 times within a run, a total number of approximately 5x5x2 = 50 replications per non-zero rate level per subject was obtained.

SUBJECTS AND TEST PROCEDURE

Two subjects, who also participated in the other experiments mentioned above, volunteered in the experiment. They are University staff members and both qualified jet transport pilots.
They were instructed to respond primarily as accurate, and secondly as quickly as possible to the presented stimuli. They were not required to continua y fixate their eyes on the central display, but were free to look at the keyboard device when giving responses. When only peripheral displays were used, subjects were instructed to fixate their eyes, after responding, on the blank central display, until the next response. Apart from the immediate feedback of the error after each keyboard response, subjects were informed of the total rate error standard deviation after a run.
The experiment was run during a number of morning sessions in which subjects completed series of the 9 types of different runs, presented in random order. After a series of 9 runs, which took around 45 minutes to complete, subjects

were always allowed a break of at least 15 minutes. A total of 9x5x2 = 40 runs were completed. Different random number sequences setting the order of 105 presentations within a run, were used for successive runs and the random number sequences themselves were frequently refreshed in order to prevent subjects becoming familiar with particular random sequences. Because of the equal probability of occurrence, more stimuli at larger rates occurred than with the gaussian probability density function in the earlier rate experiments. This made the present task a more difficult one. However, a sufficiently large number of runs was made during preliminary evaluation to assure a steady level of performance.

RESULTS

The overall results for the 9 combinations of exposition time and display configurations have been summarized in Table 1. Figure 5 shows the standard deviation of the total error (relative to zero mean). For $\Delta t_{exp} = 0.3$ the decrease in total error standard deviation due to addition of peripheral displays (configuration CP compared to configuration C) is just significant ($\alpha < 0.10$). The changes due to peripheral displays for $\Delta t_{exp} = 0.1$ sec are highly significant ($\alpha < 0.01$).

Also shown for comparison (solid symbols in Fig. 5) are the corresponding values obtained in the experiments of Ref. 3. Figure 6 shows the error scores. It can be seen that although standard deviations are larger throughout for the present experiment, the error scores are lower than for the earlier tests. The effects due to exposition time and display configuration are quite similar. For example, addition of peripheral displays to the central display at 0.1 sec exposition time, decreases the total error standard deviation by around 65% in both experiments.

Mean reacton times and standard deviations have also been summarized in Table 1. For all exposition times, mean reaction times for peripheral displays only and for central and peripheral displays are significantly ($\alpha < 0.01$) smaller than those for the central display alone, confirming the earlier findings of Ref. 3. In Figs 7 and 8 mean perception errors, standard deviation and standard deviation of total error have been plotted as a function of stimulus rate magnitude for $\Delta t_{exp} = 0.3$ and 0.1 sec respectively.

With decreasing exposure time, a tendency for overestimating low rates and underestimating higher rates can be observed and addition of peripheral displays to the central display is seen to suppress this range effect. Also, an apparent tendency to more underestimating the larger rates than to overestimating the smaller rates, can be observed.

An interesting feature is the increase of standard deviation of the mean error as a function of rate. It follows from Figs 7 and 8 that the increase of total error standard deviation, for rates up to around 20 deg/sec, is largely caused by the increase in random error, except for the case of $\Delta t_{exp} = 0.1$ sec in the configuration C. Although the overall effect of peripheral displays for $\Delta t_{exp} = 0.3$ sec is small, it is remarkable to see that for zero rate, a highly significant ($\alpha < 0.01$) decrease in error standard deviation occurs.

In order to put the present results into the proper perspective, mean perceived rates and standard deviations have been plotted as a function of stimulus rate magnitude in Figs 9 and 10.

DISCUSSION AND CONCLUDING REMARKS

A comparison of overall results for the 9 combinations of exposure times and display configurations shows that the results as obtained are dependent on the probability density function of the rate stimulus magnitude. Since results are apparently task-dependent, some care should be taken when extrapolating them to other tasks, for instance tracking tasks. On the other hand, relative changes due to display configurations or exposition times seem to have rather constant magnitudes.

As concerned individual differences, it should be remarked that, as far as total rate error standard deviation is concerned, subjects showed only significant differences in the case of all displays (configuration CP) for exposition times of 0.1 and 0.3 seconds.

Subjects showed consistent and highly significant ($\alpha < 0.01$) differences in mean reaction times (around 0.11 sec) but both showed a decrease in mean RT and standard deviation at $\Delta t_{exp} = 0.1$ sec between the C and the P configuration.

The 'slower' subject seemed to profit more from the peripheral displays, both in terms of lower mean RT, lower RT standard deviation and decrease in total rate error standard deviation. An illustration of individual differences is given in Fig. 11 where total error standard deviation is plotted as a function of mean RT for both subjects, for $\Delta t_{exp} = 0.1$ sec.

It would appear from the data of subject 2 that a decrease in mean RT is consistent with a decrease in rate error standard deviation. A larger number of subjects would be necessary to see whether this is a general trend.

Apart for the case of zero rate magnitude, where RT mean and standard deviations are slightly smaller, mean reaction time and standard deviation are fairly constant over stimulus rates.

A range effect is evident in the present results and more so if task difficulty increases (shorter Δt_{exp}). This probably reflects a strategy, adapted by subjects in difficult perception tasks, to guess for the mean absolute stimulus rate to be expected.

The gross underestimation of large rates in the present experiment might be due to the fact that pilots, experienced in closed loop control, are reluctant to overcontrol in the case of large deviations.

When the present data are to be applied to closed-loop control, however, it appears that this phenomenon would be of relatively little importance when very few excursions greater than 5 to 10 degr/sec would occur, for instance in the case of the roll control of a jet transport in mild turbulence.

TABLE 1: Results for 2 subjects, 5 replications each.

Conf.*)	Δt_{exp} (sec)	Reaction Time (sec)	Perceived rate error (deg/sec)	Stand deviation total error (degr/sec)	Score**)
C	= RT	0.832±0.103	-0.24±3.59	3.60	0.0532
P	= RT	0.816±0.123	-0.54±3.55	3.59	0.0539
CP	= RT	0.805±0.098	-0.11±3.49	3.49	0.0501
C	0.3	0.824±0.095	-0.62±3.51	3.57	0.0525
P	0.3	0.794±0.105	-1.28±3.39	3.58	0.0540
CP	0.3	0.800±0.091	-0.22±3.20	3.21	0.0449
C	0.1	0.898±0.198	-3.60±7.48	8.30	0.2564
P	0.1	0.792±0.126	-1.11±5.61	5.72	0.1269
CP	0.1	0.812±0.116	-1.57±5.59	5.80	0.1300

*) C central display only
P peripheral displays only
CP central and peripheral displays

**) Error score parameter, defined by:

$$S_c = \frac{\sigma^2_{\Delta\varphi_t}}{\sigma^2_{\varphi_{st}}}$$

REFERENCES

1. Hosman, R.J.A.W. and Van der Vaart, J.C.
Effects of vestibular and visual motion perception on task performance. Acta Psychologica 48 (1981) 271-287, North-Holland Publishing Company.

2. Hosman, R.J.A.W. and Van der Vaart, J.C.
Accuracy of visually perceived roll angle and roll rate using an artificial horizon and peripheral displays. Proceedings of the second european annual conference on human decisionmaking and manual control. Bonn, Forschungsinstitut für Anthropotechnik, 1982.

3. Hosman, R.J.A.W. and Van der Vaart, J.C.
Perception of roll rate from an artificial horizon and peripheral displays. Proceedings of the 19th annual conference on manual control, Cambridge MA, 23-25 May, 1983.

4. Van der Vaart, J.C. and Hosman, R.J.A.W.
Roll rate, roll attitude on target-time estimation by subjects using an artificial horizon display and peripheral displays. Proceedings of the third european annual conference on human decisionmaking and manual control, Roskilde, Denmark, 1983.

5. Van der Vaart, J.C. and Hosman, R.J.A.W.
Influence of uninterrupted display of peripheral visual field motion on target-time estimation from a rotating artificial horizon display with blanking. Paper presented at the fourth european annual conference on human decisionmaking and manual control. Institute for Perception TNO, Soesterberg, The Netherlands, May 28-30, 1984.

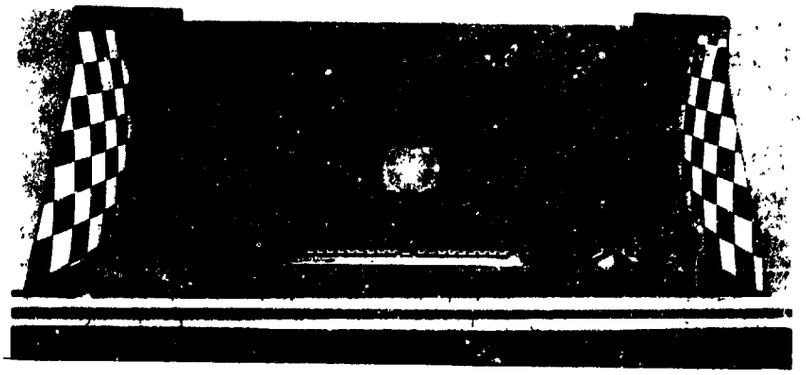

Fig. 1. Overview of test facility showing central display, the perihperal displays and the digital keyboard.

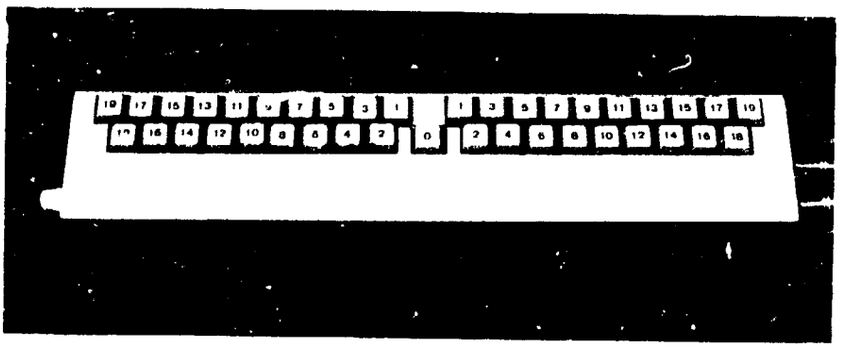

Fig. 2. Digital keyboard device.

ORIGINAL PAGE IS
OF POOR QUALITY

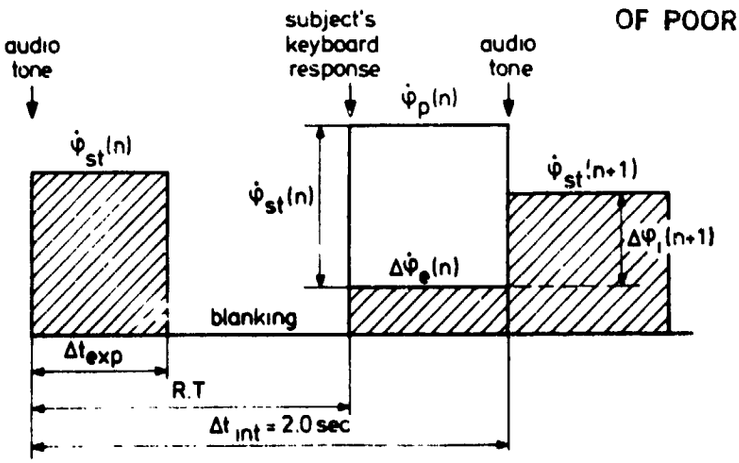

Fig. 3, Sequence during one interval of a test run. Shaded areas represent rate magnitude as displayed.

ORIGINAL
OF POOR QUALITY

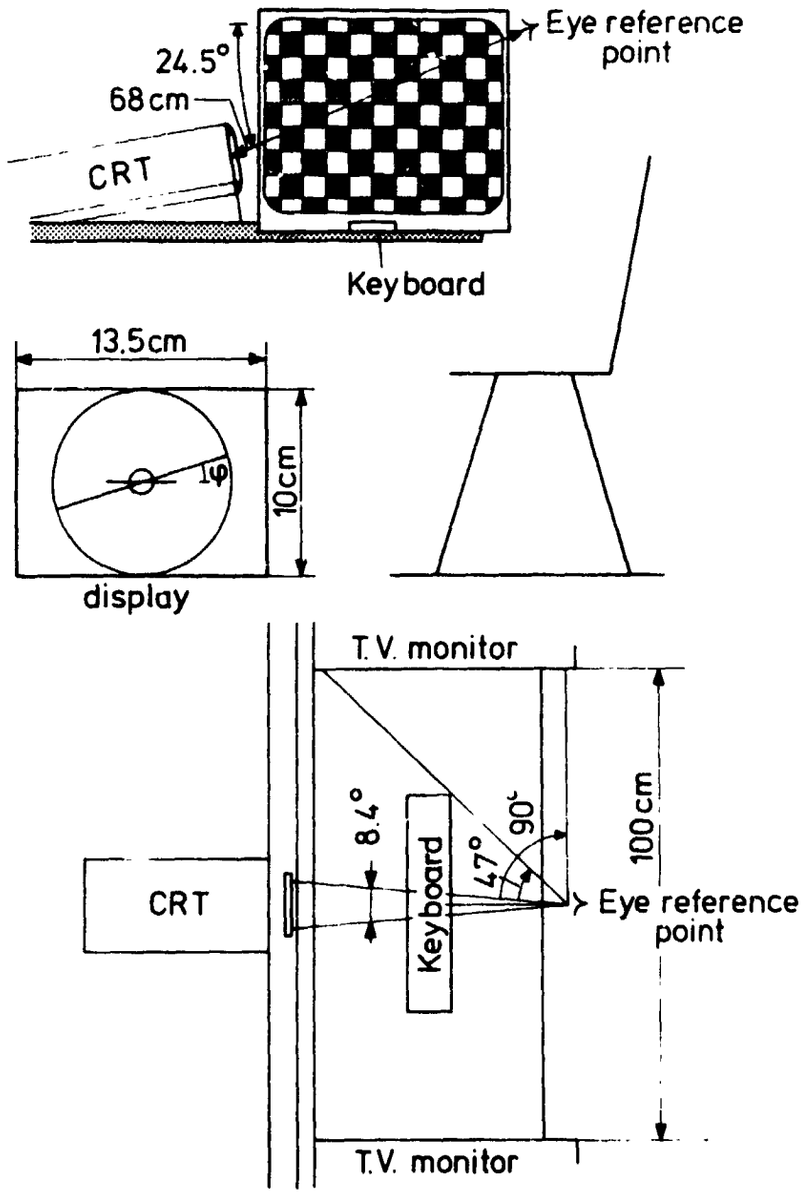

Fig. 4. Positions of displays relative to the subject's eye reference point. Central display image and dimensions.

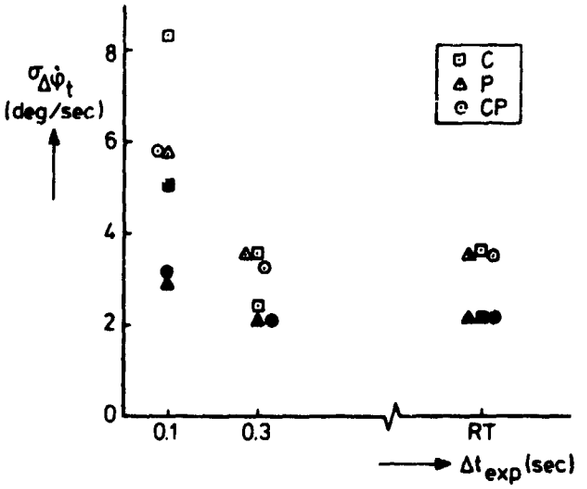

Fig. 5. Standard deviation of total rate perception error as a function of exposure time Δt_{exp}. Solid symbols: data from Ref. 3.

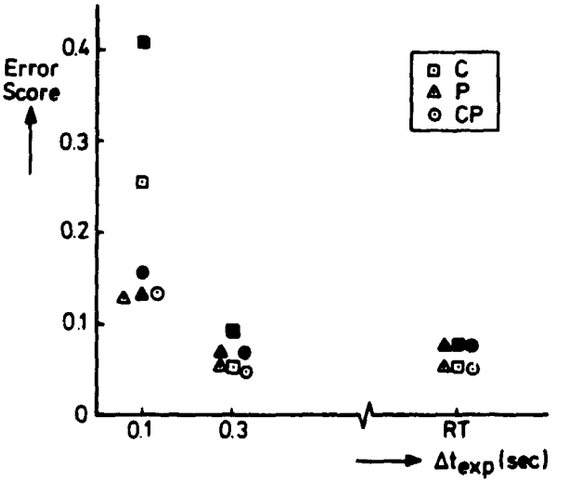

Fig. 6. Error score as a function of exposure time Δt_{exp}. Solid symbols: data from Ref. 3.

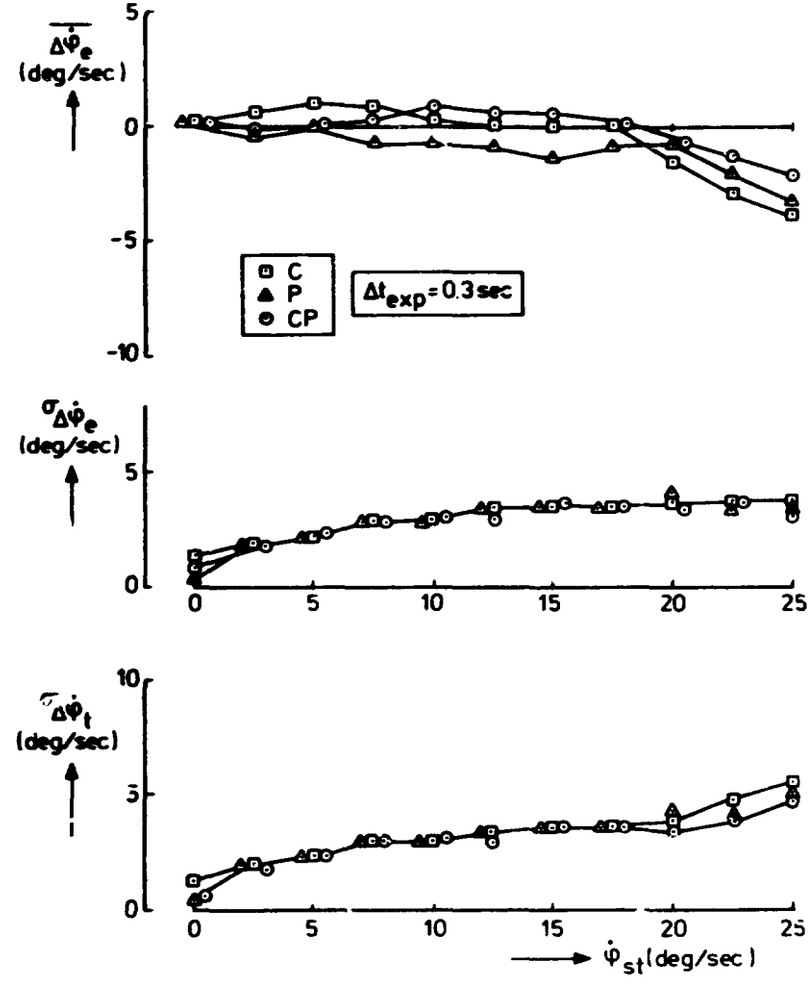

Fig. 7. Mean rate perception error, standard deviations of mean error and total error as a function of stimulus rate magnitude, Δt_{exp} = 0.3 sec.

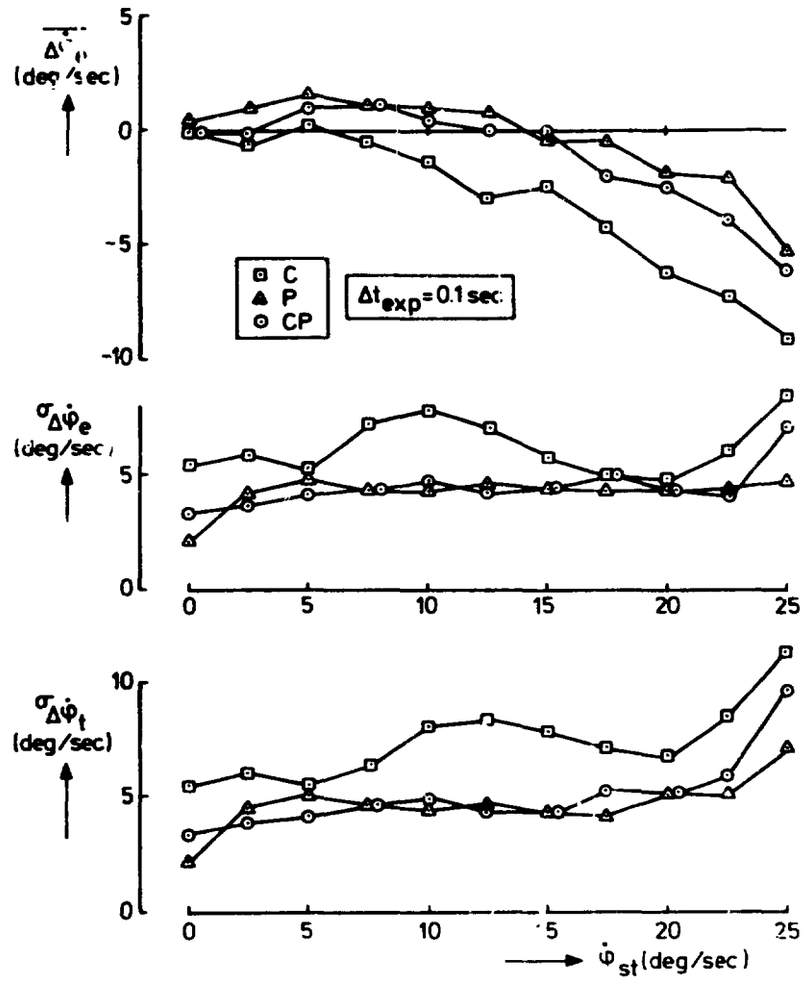

Fig. 8. Mean rate perception error, standard deviations of mean error and total error as a function of stimulus rate magnitude, Δt_{exp} = 0.1 sec.

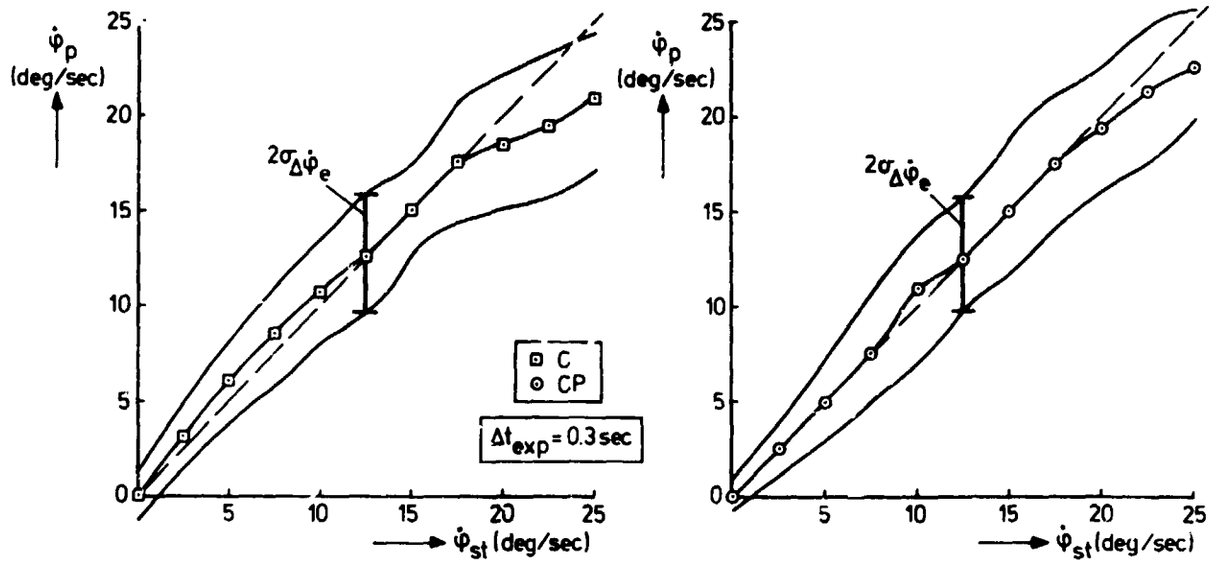

Fig. 9. Mean perceived rate and standard deviation as a function of stimulus rate magnitude, Δt_{exp} = 0.3 sec.

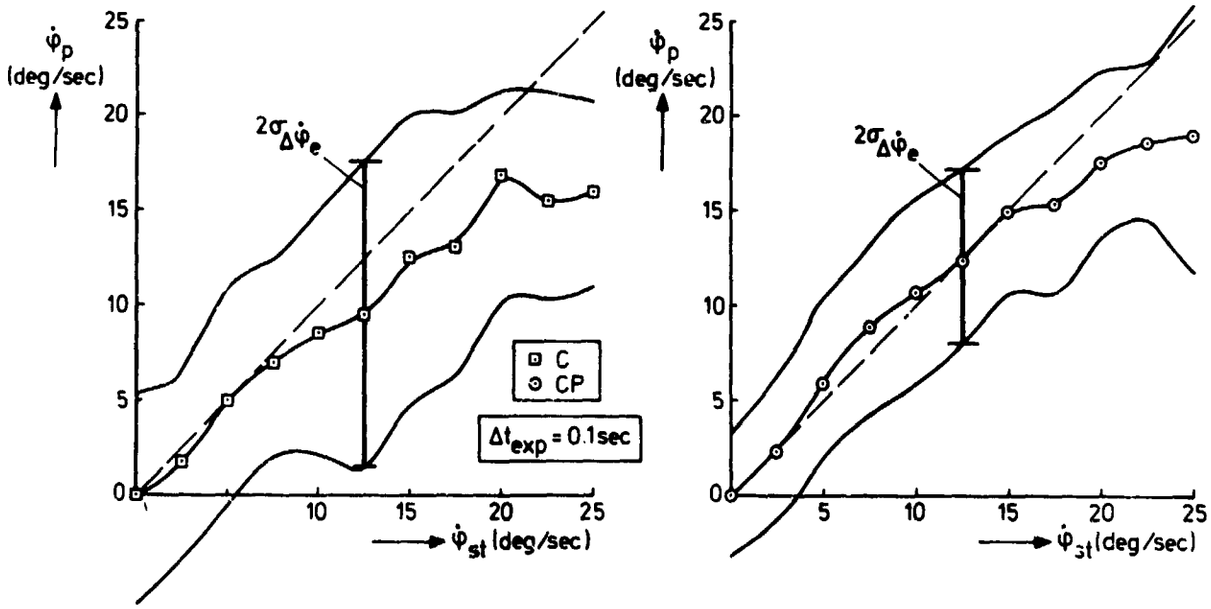

Fig. 10. Mean perceived rate and standard deviation as a function of stimulus rate magnitude, Δt_{exp} = 0.1 sec.

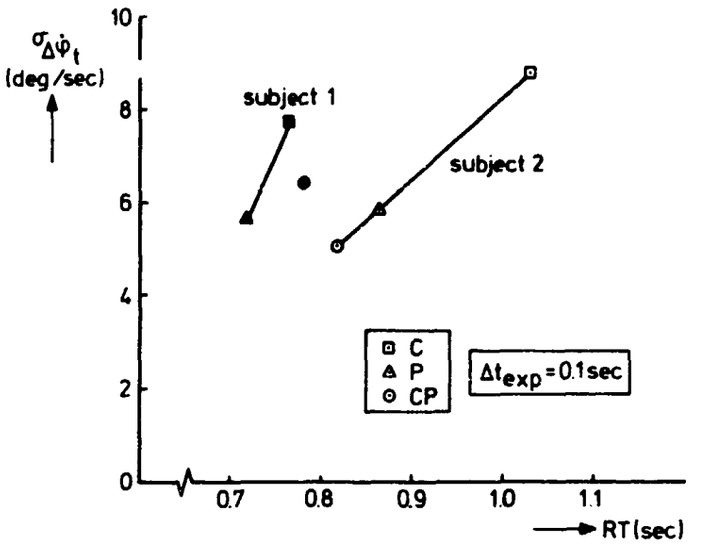

Fig. 11. Total error standard deviation as a function of reaction time RT for the two subjects, Δt_{exp} = 0.1 sec.

N85 14520

Direction Judgement Errors in Perspective Displays

Michael Wallace McGreevy
Stephen R. Ellis

NASA Ames Research Center
Moffett Field, CA 94035

ABSTRACT

In a study of spatial information transfer characteristics of perspective situation displays, eight subjects judged the directions of displayed targets relative to a fixed position in the center of computer generated perspective scenes. Their errors in judging azimuth angles varied sinusoidally with the azimuth of the targets. Errors alternated between clockwise and counterclockwise from one direction quadrant to the next. As the perspective geometry was varied between 'telephoto lens' and 'wide angle lens' views, the direction of error gradually reversed in all quadrants. The results can be explained by systematic differences between the three-dimensional stimulus angles and the perspective projections of those angles onto the display screen.

Introduction

Use of pictures as spatial information instruments has been of particular interest in aerospace [Getty, 1992], [Jauer and Quinn, 1982], [Jones et. al., 1950], [Roscoe et. al., 1981], [Warner, 1979]. Primary tasks involve maneuvering through a three dimensional space, amid other moving or fixed objects, both physical (aircraft, missiles, mountains, weather systems) and virtual (traffic control regions, threat zones). Assistance in monitoring the spatial relationships among objects of interest can best be provided by instruments matching the spatial dimensions of the tasks for which they are used. A typical approach has been to map two dimensions of information to the two dimensions of a display and to encode the collapsed dimension. Recent designs have used perspective projections to capitalize upon our natural spatial abilities. There is

PRECEDING PAGE BLANK NOT FILMED

some evidence that perspective displays can have advantages over planview displays [Ellis et. al., 1984].

Although it is fairly simple to make a display that looks spatial, the quality of the spatial information transfer between the system and the user must be examined. When three dimensional information is projected onto a two-dimensional screen, the original information must be mentally reconstructed by the user. No matter how accurate the data base, the user may introduce distortions in the act of interpretation of the projection.

Complicating the design of perspective displays is the fact that the 2D projection varies dramatically in appearance depending upon the values of the perspective parameters (fig. 1). An example of a perspective parameter is the geometric field of view angle (fig 1). It is often referred to in this paper simply as the field of view. It is defined as the the visual angle of the display screen as seen from the station point, which is sometimes called the center of projection or geometric eyepoint. An example of the effect of field of view can be seen in figure 2. A narrow field of view, such as 30 degrees, produces an image that is similar to that obtained with a telephoto lens. A wide field of view, such as 120 degrees, produces an image that is similar to that obtained with a "wide angle" lens. Another perspective parameter is the distance between the station point and an object of interest located at the reference point. These two parameters are the major factors defining the geometry of the projection of the 3D information onto to 2D display screen. The purpose of the following experiment was to determine whether the differences in appearance that are due to these perspective parameters result in differences of interpretation.

Experiment

The perspective scene used in this experiment (fig. 3) was abstracted from a perspective display of air traffic for the cockpit [McGreevy, 1982] which

compared to a plan-view display in a previous experiment [Ellis, et. al., 1984](fig. 4). In the scenes used in this experiment the aircraft symbols representing ownship and an intruder were replaced by cubes. The cube replacing ownship was always at the center of the display screen and served as a reference for judgement of the relative position of the target cube. For this reason, the ownship cube is also referred to as the reference cube and the intruder is called the target. A grid represented a "ground" plane below the reference cube. A line connected each cube with a point directly below it on the grid. A horizontal cross marked the point on the target cube's line where the reference cube's altitude plane intersected it.

In the experiment, subjects viewed a series of perspective scenes and judged the azimuth and elevation angles of the target relative to the reference (fig. 3). The azimuth angle of the target is the angle between the reference cube's heading and the horizontal direction to the target. The elevation angle is the angle from reference cube's altitude and the vertical direction to the target. In these scenes the viewing vector is rotated 22 degrees relative to a heading of 0 degrees azimuth and elevated 22 degrees above the altitude plane of the reference cube. Subjects responded by using a stylus and digitizer pad [1] to control two angle indicator dials that were drawn on the display screen, next to the perspective scene.

The experiment was a fully crossed, repeated measures design, with eight subjects. Five were airline pilots and 3 were non-pilots. Each subject was shown 640 perspective stimuli. The target cube appeared in 40 different orientation regions on a sphere centered on the reference cube.

[1] The center of the pad was the origin, where the (horizontal) azimuth axis crossed the (vertical) elevation axis. The range of azimuth was from minus 180 degrees to the far left, to plus 180 degrees to the far right. Elevation ranged from minus 90 degrees at the bottom of the pad, to plus 90 degrees at the top of the pad.

Four geometric fields of view, 30, 60, 90, 120 deg., were crossed with four distances between the reference cube and the station point [2], for a total of 16 perspectives. In this paper analysis will be limited to the subjects' judgments of the azimuth angles of the targets.

The subject's eye position was 61 cm. (24 in.) from a 19 cm. (7.5 in.) square image on a 25 cm. (10 in.) square screen of an Evans and Sutherland Picture System II monitor. The image subtended a visual angle of 8.9 degrees. Since the geometric fields of view were greater than this, the corresponding station points were closer to the screen: 14.0 in. (30 deg. fov), 6.5 in. (60 deg. fov), 3.8 in. (90 deg. fov), 2.2 in. (120 deg. fov).

Geometry of the Stimulus Angles

Since the task in this experiment required that the subjects interpret a three-dimensional stimulus angle from its two-dimensional projection, it seemed reasonable that the difference between the true 3D stimulus angle and its 2D projection would influence the subjects' judgements. Accordingly, this difference was plotted as a function of 3D azimuth to suggest the amount and direction of error that might be expected if the subject's 3D judgement is biased by the 2D projection of the stimulus angle. This function is the "2D difference effect" function (fig. 5). At narrow fields of view which produce perspectives similar to telephoto lenses, the magnitude of this function is large. As field of view increases, the magnitude decreases. This function is independent of the actual eye position of the viewer.

A second possible source of influence on subjects' judgements involves the position of the station point relative to the viewer's actual eye position. When

[2] The distances can be described in terms of the distance, d, of the reference cube above the grid. The four distances were 0.66d, 4.61d, 8.97d, 13.12d, approximately in a ratio of 1:5:9:13.

the eye is not at the geometrically correct station point the projectors are effectively bent at the point where they pierce the viewing screen (fig. 6). We call this the "virtual space effect." [1] If the subject assumes that all projectors are straight, just as they are when looking through a window, then the apparent 3D scene will differ from the true 3D scene. We call the subject's assumption the "window assumption."

The virtual azimuth and elevation angles that result from the window assumption can be computed. Our computation assumes shape alteration without translation. The difference between the actual 3D stimulus and the virtual 3D stimulus can be plotted as a function of the 3D stimulus angle to define the virtual space difference function (fig. 7). This describes the expected influence upon direction judgements if the concept of a window assumption is valid. The magnitude of this function varies directly with the distance between the station point and the actual eyepoint of the viewer.

Results

Direction judgement error was measured in terms of azimuth and elevation. The median of each subject's responses at each azimuth position was taken as his typical estimate.

Sixteen plots were made, one for each of the sixteen perspective conditions. While there were apparently only minor differences among the plots with respect to the distance parameter, there were obvious differences as field of view varied. The data were then grouped into four sets, one for each field of view. As a first approximation of these theoretically sinusoidal curves [1], a sixth order polynomial was fitted by least squares to each set of points to

[1] Farber and Rosinski (1978) studied a similar effect but assumed a translation along the viewing axis of the 3D stimulus to its virtual position. This would result in a significantly different virtual space.

obtain a summary curve for each field of view (eg. fig. 8). The standard error of estimate overall for each curve was approximately 7 degrees. When plotted together, the four data summary curves can be seen to vary systematically as field of view changes (fig. 9). These curves summarize the statistically significant interaction between field of view and the azimuth of the intruder cube shown by the analysis of variance of azimuth error. ($F = 10.3$; $df = 21, 147$; $p < .001$).

Since the two model components, the 2D and the virtual space difference functions, may be combined and fitted to the direction judgement data in a variety of ways, several different combinations were tried. The combination resulting in a fit most like the data summary polynomials is obtained when the component curves are separately weighted and added. The weights and an additive constant are determined by regression of each set of data points (four sets, one for each fov) against the expected errors based on the two model components. A visually good fit (see fig. 10) is achieved when the component curves are shifted 22 degrees counter-clockwise, prior to being fitted to the data. This could correspond to a process in which subjects make judgements relative to a line directly into the displayed space (22 deg. azimuth) and then rotate 22 degrees to account for the fact that the heading (zero deg. azimuth) is 22 degrees counter-clockwise of their actual reference direction.

A particularly interesting aspect of the best model curves is that they reproduce a trend seen in the original data which was not explicitly incorporated into the model itself. This trend shows a gradual general change in the direction of the azimuth error from counterclockwise to clockwise as the

[1] The fitted curve should be a projected sinusoid since the set of azimuth stimulus angles step around a circle of bearings in regular intervals. Projecting the positions of these stimulus angles onto a line in the plane of the circle, and translating this line in a direction perpendicular to the line, will trace out a sine-cosine function. Since the circle is viewed from an oblique angle, and in perspective, the sine-cosine function will be modified by the projection.

azimuth region changes from the left quadrants to the right quadrants. The trend corresponds to a significant main effect of azimuth ($F = 3.146$; $df = 7, 49$; $p < .008$).

CONCLUSIONS

The spatial interpretation of the data summary polynomials (fig. 9) is that for narrow fields of view, some azimuths are interpreted as being as much as 10 degrees farther to port or starboard than they are in fact. This bias gradually changes until it reverses at wide fields of view. For these, the azimuths are interpreted as being closer to the line of flight. The bias reverses by as much as 15 degrees in all four azimuth quadrants.

The set of four data summary polynomials and the four composite model curves are very similar (fig. 10). As field of view steps through 30, 60, 90, 120 degrees, the model follows the data through its reversal of the sign of the sinusoid, in regular steps. This suggests that the suspected influences represented by the 2D and virtual space difference functions could account for the systematic errors in direction judgements. Whether these influences actually cause the subject to err systematically remains to be confirmed by subsequent experiments.

It appears that the difference between the true 3D stimulus angle and its 2D projection has the greatest biasing effect when the magnitude of the difference is greatest, that is, at narrow fields of view (regardless of actual eye position of the observer). Similarly, it seems that the difference between the true 3D stimulus angle and the virtual 3D angle, the angle that would be required for the projectors to be straight, has the greatest biasing effect when the magnitude of this difference is greatest, that is, when the geometric station point and the actual eye position are at widely separate locations. Consistently, at intermediate fields of view, as one influence increases and the other

decreases, the judgement bias is correspondingly intermediate.

The next experiment will involve keeping the virtual space difference function fixed as the 2D difference function varies and vice versa. This will help clarify the relative biasing effects of these two influences on direction judgements. It is possible that the use of 2D dials on the screen for elevation and azimuth responses was partly responsible for the subjects' tendency to be biased by the two dimensional projection of the three dimensional stimulus angles. Later experiments will use alternative responses, such as egocentric visual direction, and should resolve this question. In these experiments the subjects will be allowed to use a hand-held pointing device to indicate the visual direction of the target. These experiments will thus further test the quality of spatial information transfer that is accomplished when perspective displays are used as spatial information instruments.

REFERENCES

Ellis, Stephen R., McGreevy, Michael W., Hitchcock, Robert J. Influence of a perspective cockpit traffic display format on pilot avoidance maneuvers. Proceedings of the AGARD Aerospace Medical Panel Symposium on Human Factors Considerations in High Performance Aircraft. Williamsburg, Virginia, April 30 - May 4, 1984.

Farber, James, Rosinsky, Richard R. Geometric transformations of pictured space. *Perception, vol. 7*, pp. 269-282, 1978.

Getty, David J. 3-D Displays: Perceptual research and applications to military systems, National Academy of Sciences, Washington, D.C., January 29, 1982.

Jauer, R.A., Quinn, T.J., Pictorial formats, vol 1: Format development, AFWAL-TR-81-3156, Flight Dynamics Laboratory, Air Force Wright Aeronautical Laboratory, Air Force Systems Command, Wright-Patterson AFB, Ohio, February 1982.

Jones, Loren F., Schrader, H.J., Marshall, J.N. Pictorial display in aircraft navigation and landing. Proceedings of the I.R.E., pp 391-400, April 1950.

McGreevy, Michael W. A perspective display of air traffic for the cockpit. Proceedings of the 18th annual conference on manual control.

Dayton, Ohio, June 10, 1982.

Roscoe, Stanley N., Corl, L., Jensen, R. S. Flight display dynamics revisited. Human Factors, vol. 23, no. 3, pp. 341-353, June 1981.

Warner, Debra A. Flight path displays. Air Force Flight Dynamics Laboratory Technical Report AFFDL-TR-79-3075, Wright-Patterson Air Force Base, Ohio, June, 1979.

fig. 1
Example of projection

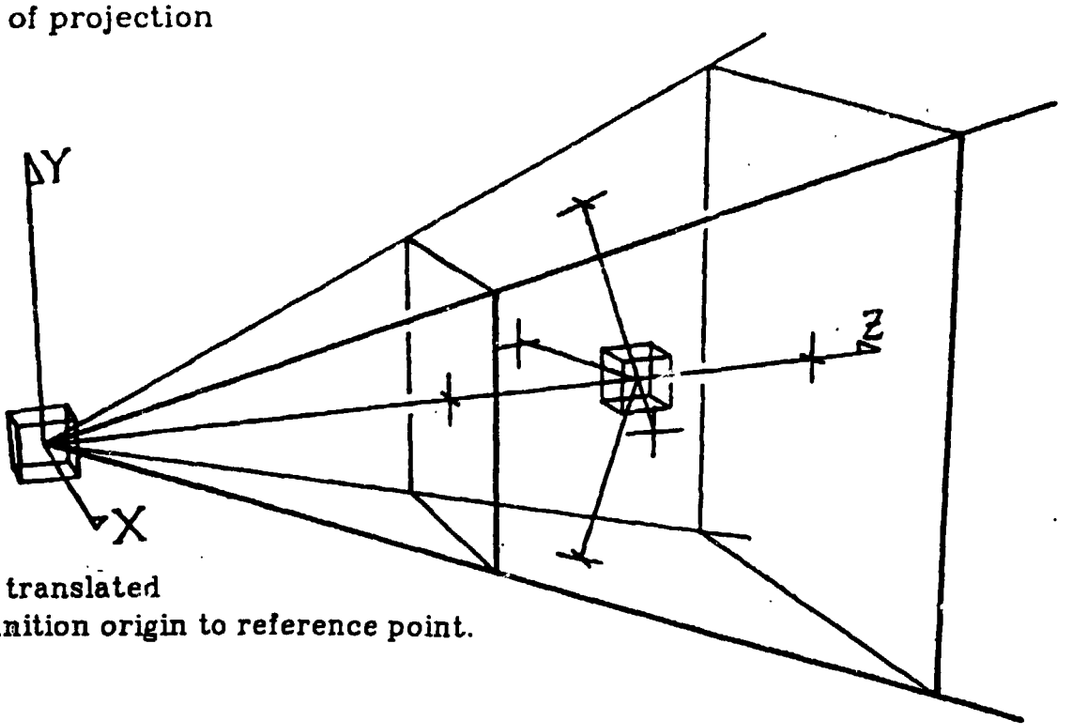

Object is translated
from definition origin to reference point.

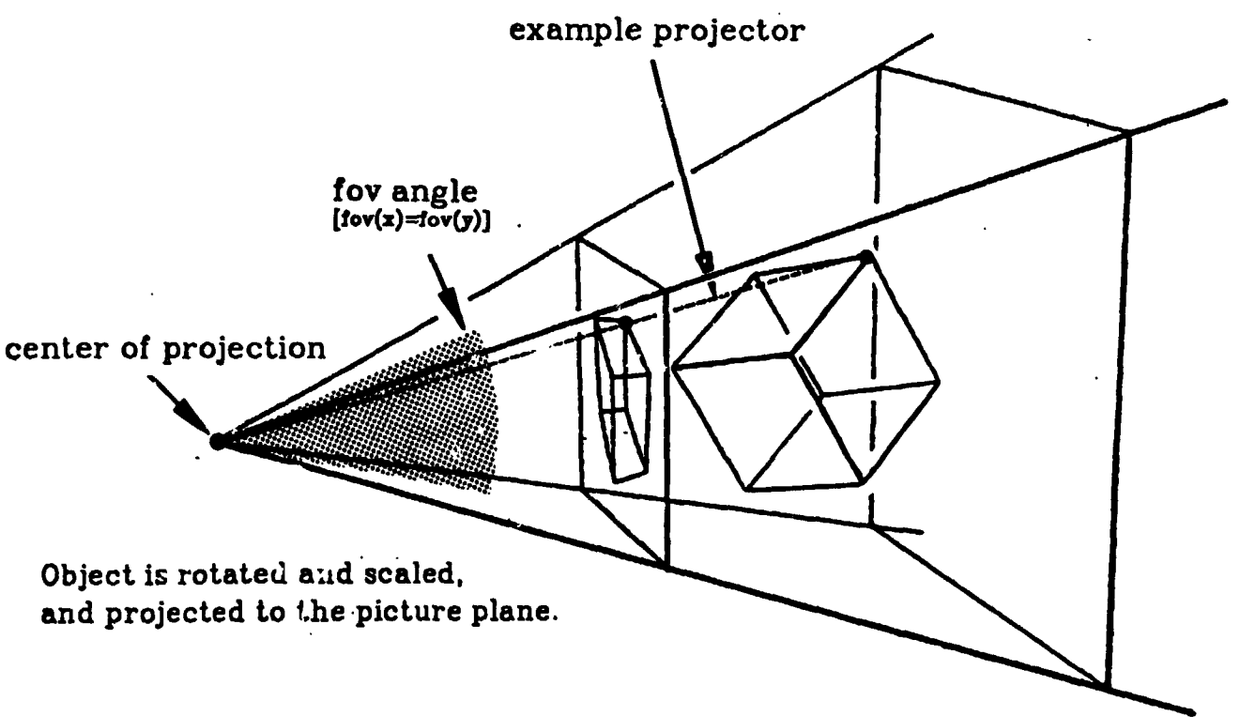

Object is rotated and scaled,
and projected to the picture plane.

fov = visual angle of display screen as seen from center of projection

ORIGINAL IS
OF POOR QUALITY

fig. 2
Field of View Effect
(constant viewing distance and direction)

fov = 30°("telephoto lens")

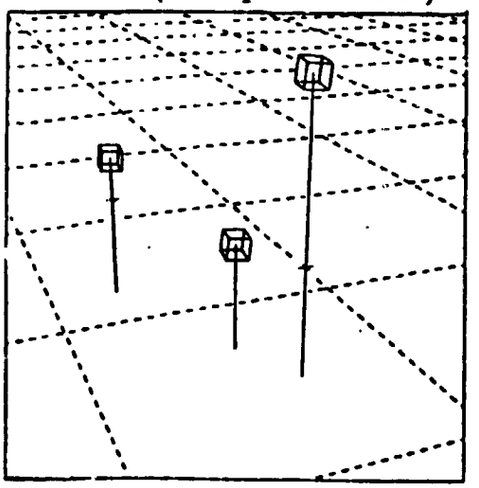

fov = 60°

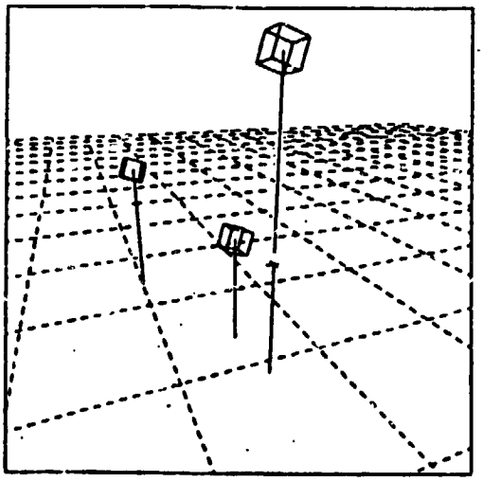

fov = 90°

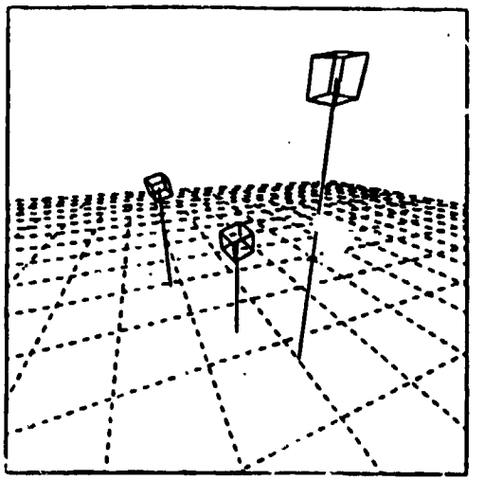

fov = 120°("wide angle lens")

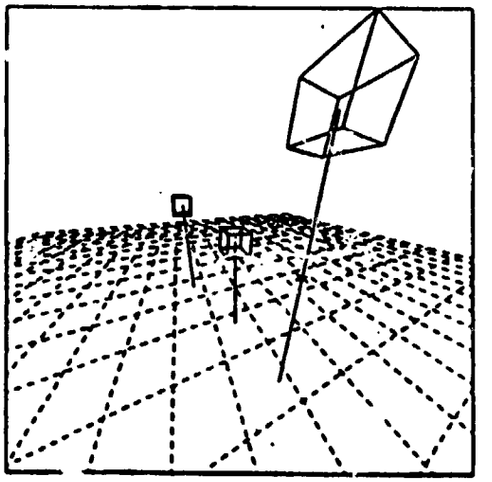

ORIGINAL PAGE IS
OF POOR QUALITY

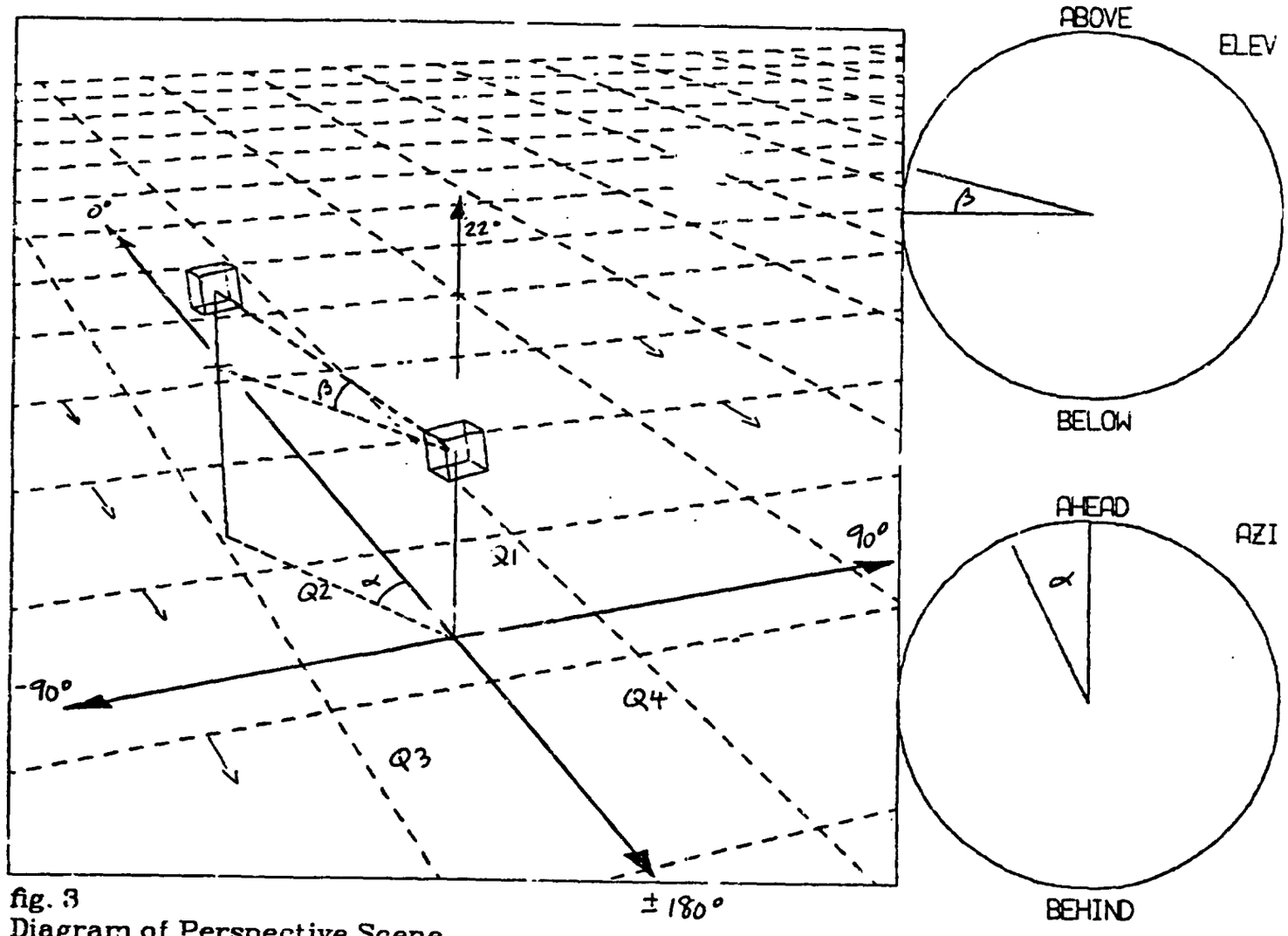

fig. 3
Diagram of Perspective Scene
Used in Experiment

fov = 38	elev= 22	azi = 22	hro= 3537	vro= 3537	seq 3	tID 81
ue=-13667	uh= -3537	uv= -3537	ul= -2714	ur= 2714	ub= -2714	ut= 2714

fig. 4
Examples of Spatial Displays

PLAN-VIEW DISPLAY

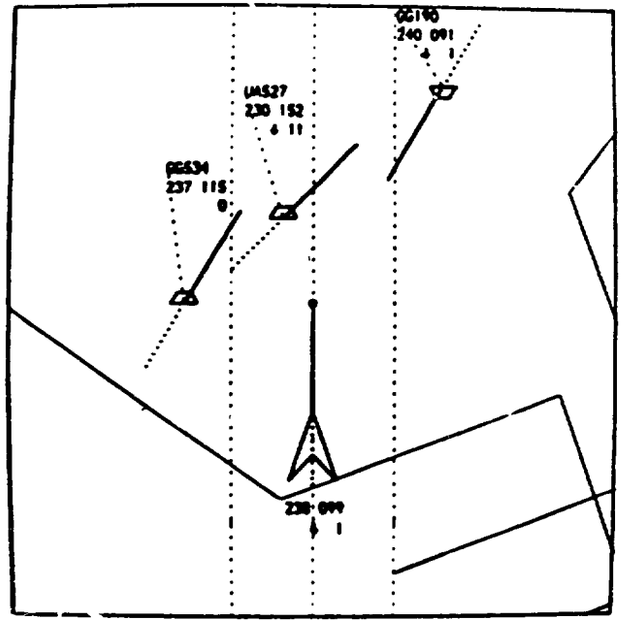

PERSPECTIVE DISPLAY

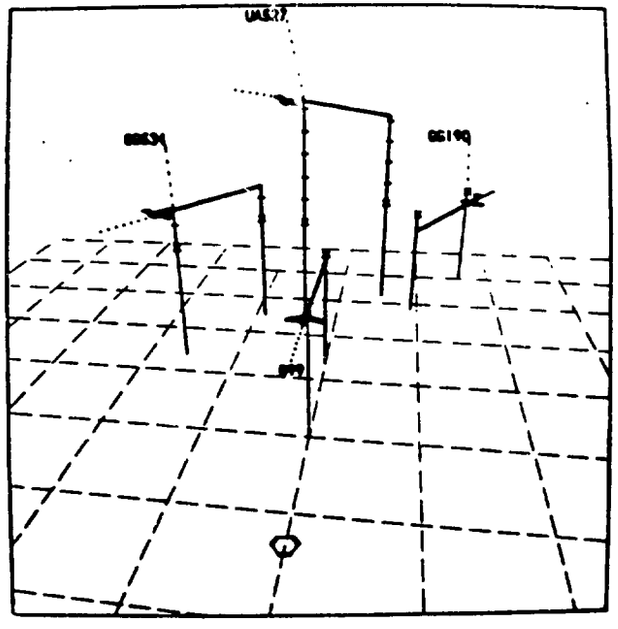

ORIGINAL PAGE IS
OF POOR QUALITY

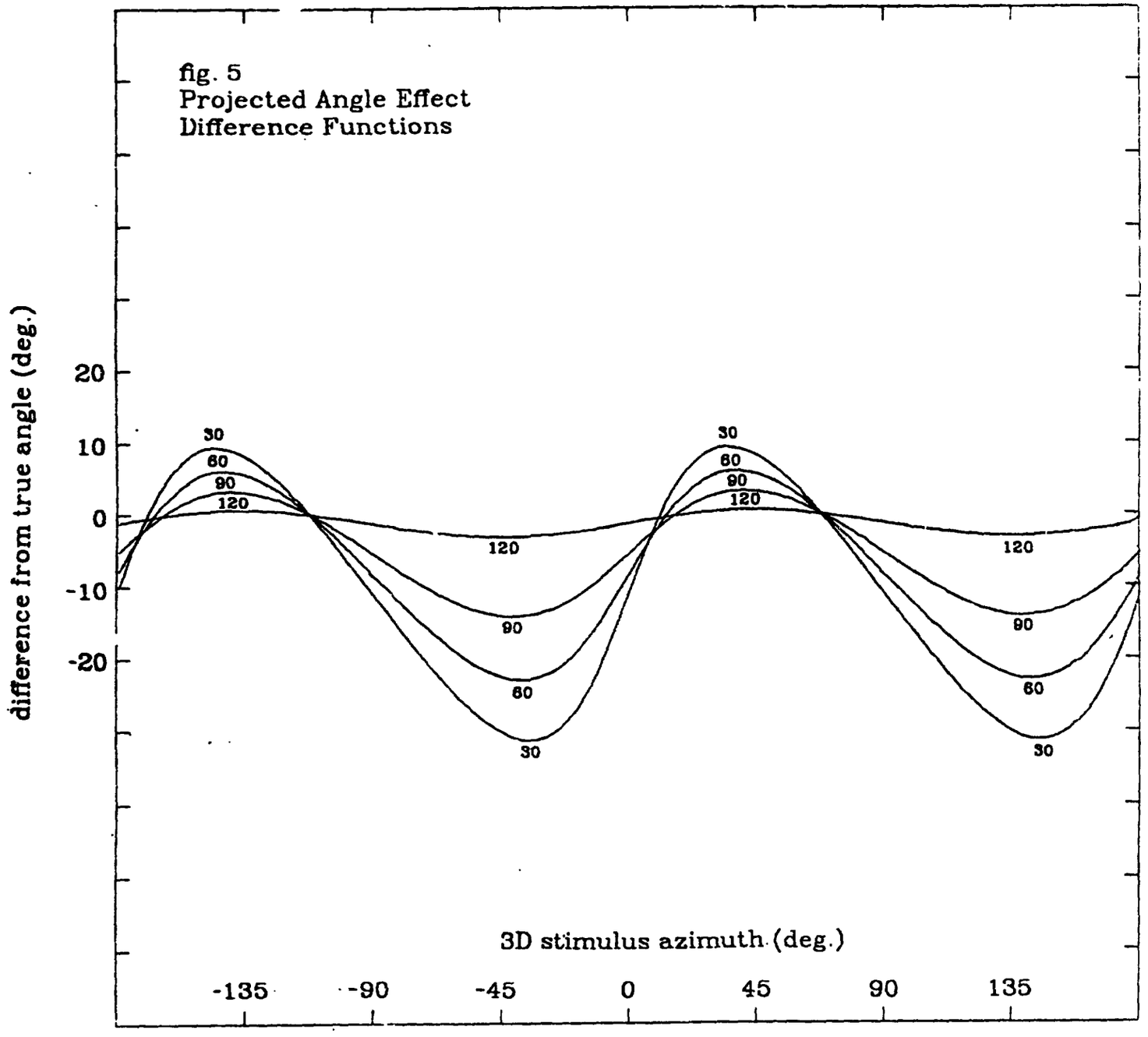
fig. 5
Projected Angle Effect
Difference Functions
difference from true angle (deg.)
20
10
0
-10
-20
30
60
90
120
3D stimulus azimuth (deg.)
-135
-90
-45
0
45
90
135

fig. 6
Virtual Space Effect

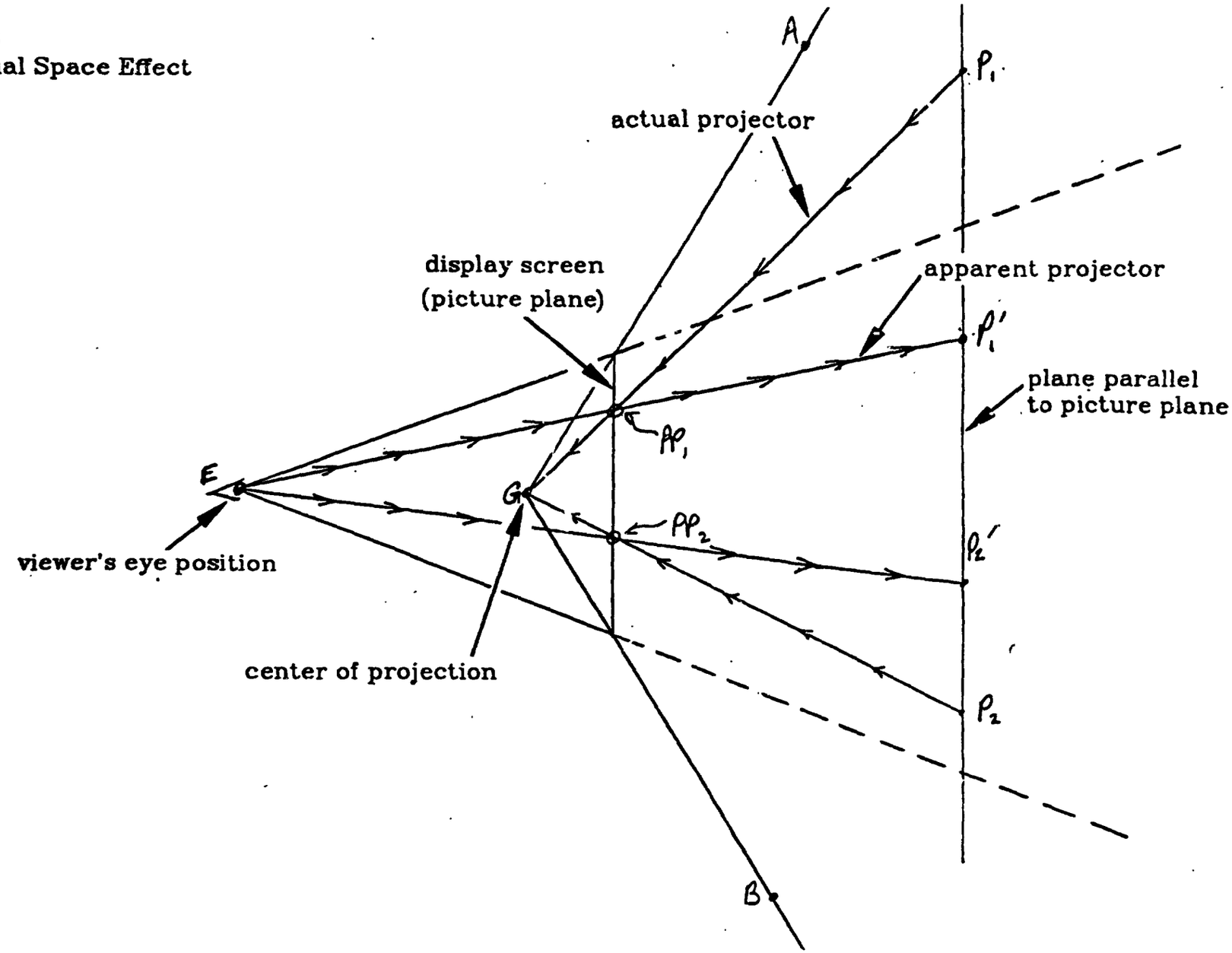

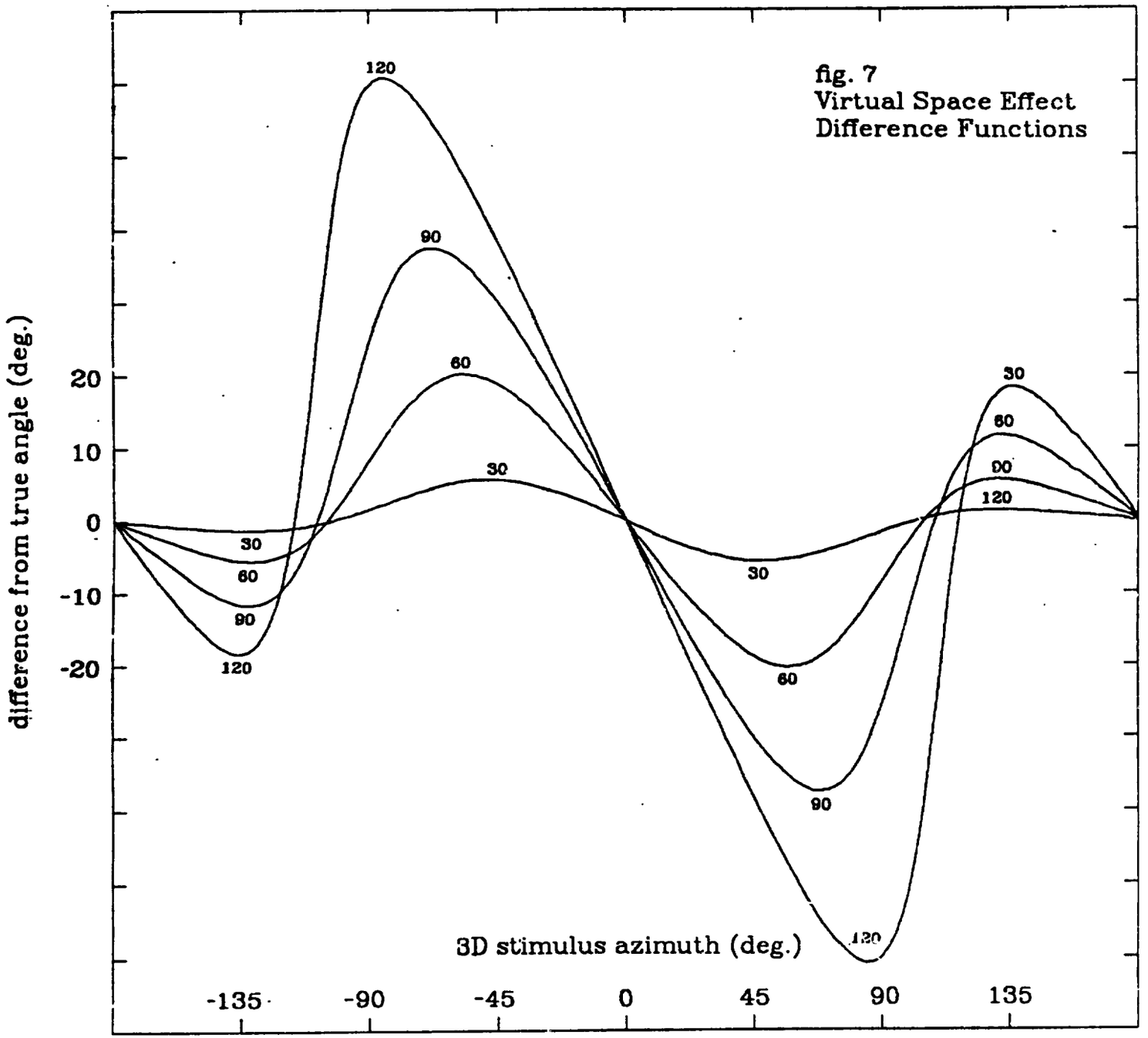
fig. 7
Virtual Space Effect
Difference Functions
difference from true angle (deg.)
20
10
0
-10
-20
120
90
60
30
30
60
90
120
30
60
90
120
30
60
90
120
3D stimulus azimuth (deg.)
-135
-90
-45
0
45
90
135

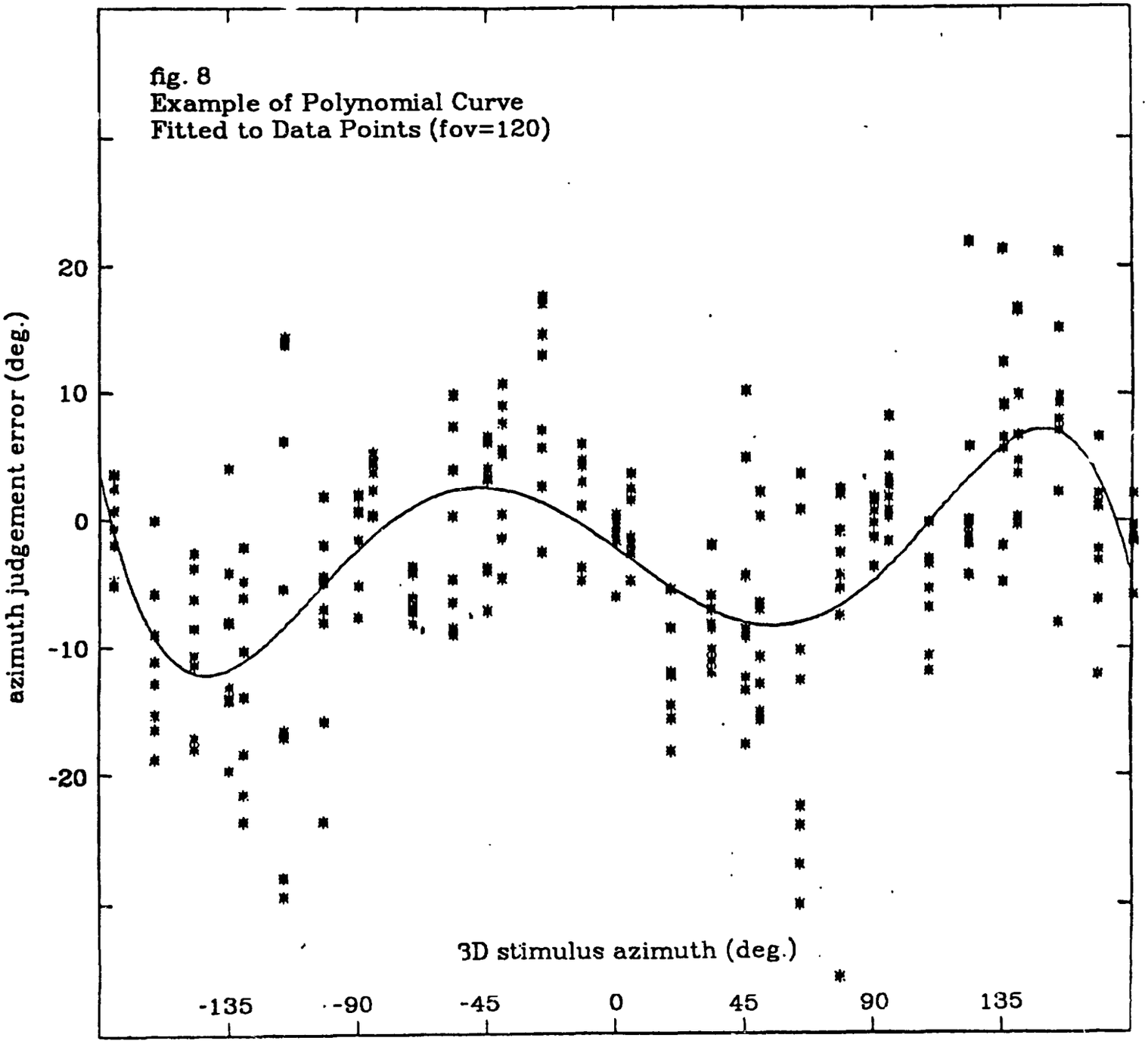
fig. 8
Example of Polynomial Curve
Fitted to Data Points (fov=120)
azimuth judgement error (deg.)
20
10
0
-10
-20
3D stimulus azimuth (deg.)
-135
-90
-45
0
45
90
135

fig. 9
Data Summary Polynomials
and their Spatial Interpretation

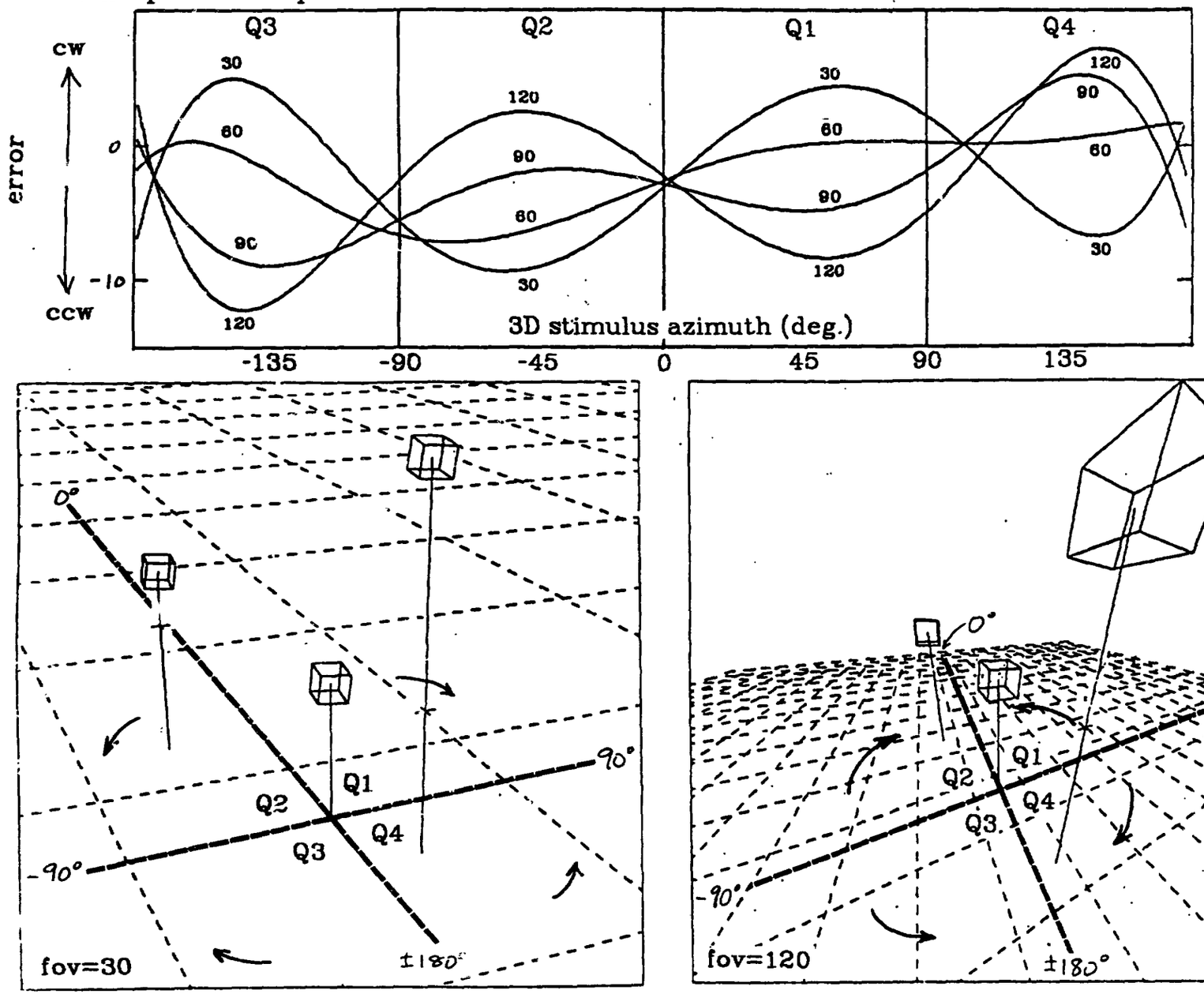

fig. 10
Comparison of Data Polynomials
and Composite Model Curves

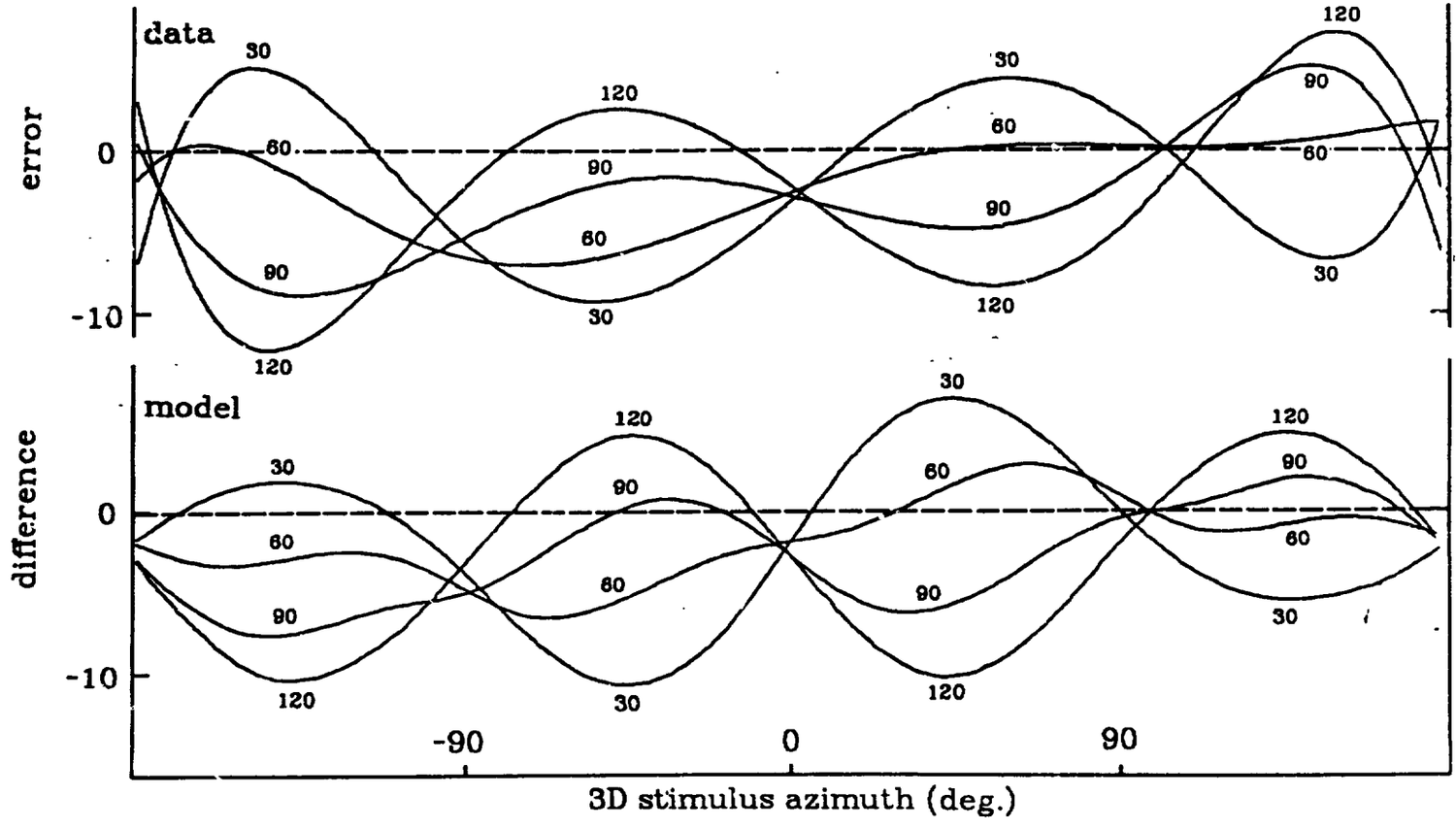

N85 14521

THE INTERACTION OF FOCUSED ATTENTION WITH FLOW-FIELD SENSITIVITY

Tom Stoffregen
Department of Psychology
Cornell University
Ithaca, New York 14853

ABSTRACT

Two studies were performed to determine whether a subject's response to naturalistic optical flow specifying egomotion would be affected by a concurrent attention task. In the first study subjects stood in a 'moving room' in which various areas of the optical flow generated by room movement were visible. Subjects responded to room motion with strong compensatory sway when the entire room was visible. When the side walls of the room were completely obscured by stationary screens, leaving only the front wall visible, sway was significantly reduced, though it remained greater than in an eyes-closed control. In Exp. 2 subjects were presented with either the full room (large sway response) or the room with only the front wall visible (moderate response), each in combination with either a hard or easy verbal addition task. Preliminary results show that swaying in the fully visible room and in the room with only the front wall visible increased when combined with either the hard or easy tasks. These preliminary results suggest that at the least the pick-up of optical flow specifying egomotion is not affected by concurrent attentional activity, supporting the notion of dual visual systems, and of the direct, non-attentional nature of the pick-up of optical flow.

INTRODUCTION

In recent years a growing amount of work has investigated the role of optical information in the control of both postural stability and guidance of actions, such as standing, running, and flying. Generally these studies have dealt with automatic pick-up of flow information, and have tacitly assumed that active attentional processes are unimportant in these areas. In fact the role of active, exploratory attentional pick-up during egomotion has hardly been addressed at all. One of the few studies related to this issue was carried out by Fischer, Haines and Price (1981) who investigated pilots performance in simulators with Head-Up Display (HUD) instrumentation. The tasks involved in this study were quite complex, and while subjects typically showed no decrement in simulator performance while reading HUD, there were some cases in which flight-critical information went completely undetected. The present paper reports the results of the first two experiments in a series

PRECEDING PAGE BLANK NOT FILMED

devoted to the basic question "What is the role of attention during locomotion?" To what extent, if any, must we actively attend to the optical information accompanying motion in order to successfully get around? Can we pick up information for our own motion through the environment while at the same time attending to some task?

For an initial look at this issue it was decided to use a situation for which something is already known about the usefulness of optical flow. In a series of experiments with the well-known 'swinging room' Lee (Lee & Lishman 1975, Lee & Aronson, 1974) has shown that large scale optical flow is naturally used in the control of standing posture. Subjects in the swinging room sway in response to exclusively optical room motion; the effect is robust, and the sensation of egomotion very compelling. Such a paradigm could easily be augmented by a variety of attention tasks.

If attention does have an effect on concurrent pick-up of flow field information, we would expect that such effects would be to some extent a function of the difficulty of the attention task. Similarly, a given level of attention task difficulty could have differential effects on the use of flow information depending on the ease with which the latter could be picked up; pick-up of restricted or otherwise impoverished flow could be less efficient while active attention was being used than otherwise. Experiment 1 sought to determine conditions under which optical flow specifying egomotion might be rendered less effective in controling posture.

EXPERIMENT 1

Method A moving room was constructed for use in these experiments. The 'room' is a large cubical box, 2.5m on a side, mounted on four wheels such that it can be rolled along the floor. The walls have reinforced wooden frames, faced on the inside with rigid cardboard, which is itself covered with a semi-random visual texture. The room has no floor, such that a subject inside it stands on the floor of the laboratory as the room moves around them. One wall of the room is left open; subjects stand with their backs to this open wall, facing into the room.

Postural adjustments in response to room motion were registered by a potentiometer. A grooved wheel was fixed to the axle of the potentiometer, and a string passed over the wheel and around the subject's neck, such that anterior/posterior movements caused the wheel to turn, generating a position-specific voltage which could be recorded. A second potentiometer registered motion of the room; data from the two could be correlated as

ORIGINAL PAGE IS
OF POOR QUALITY

time series to determine the effect of room motion on stance.

Stationary cardboard screens could be placed in the room in order to restrict the optical motion available to subjects. The screens could be placed so as to occlude the three vertical walls of the room. Subjects wore a hat with a wide bill which prevented their seeing the ceiling.

The room was moved sinusoidally along an axis parallel with the subject's line of sight. The total magnitude of the movements was 2.5cm, with a period of 12 seconds per cycle. Each one minute trial consisted of a continuous series of five of these cycles. Subjects were instructed to look straight ahead, keeping their gaze within a small square outlined on the front wall. They were not given any task to do, and were not imformed about room movements in advance, but were simply told to stand still and look at the wall.

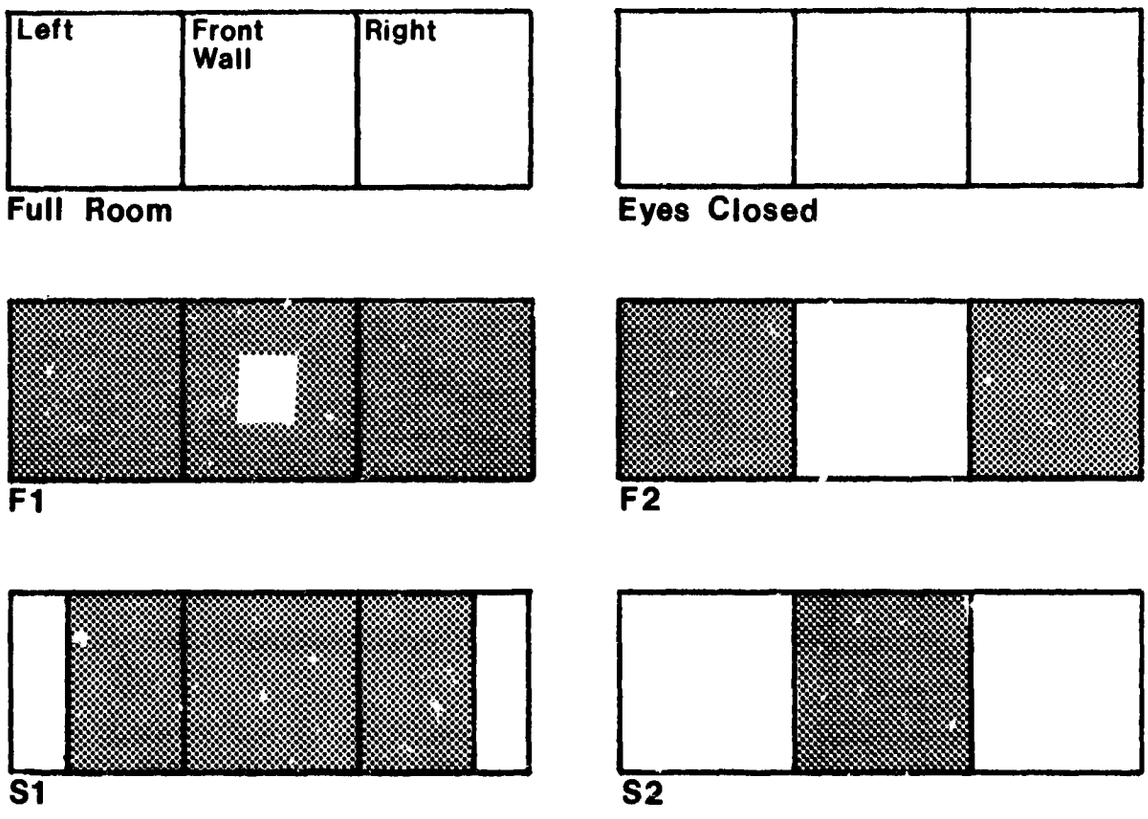

Figure 1. Experimental conditions. Dotted areas were blocked by stationary screens. The ceiling was always blocked. The floor was visible but did not move.

Conditions Conditions are illustrated schematically in figure 1. The Full Room condition served as a baseline to establish the magnitude of the basic sway response. In the control condition subjects stood as normal in the room, but kept their eyes closed throughout the trial. In the four experimental conditions the side and front walls of the room were blocked off by the stationary cardboard screens, leaving flow available to either the retinal center or periphery. Each of 27 subjects participated in the five experimental conditions, and 12 of these also were in the eyes closed control.

Results The data shown in figure 2 are the mean correlations (across subjects) between room motion and subject motion for each condition.

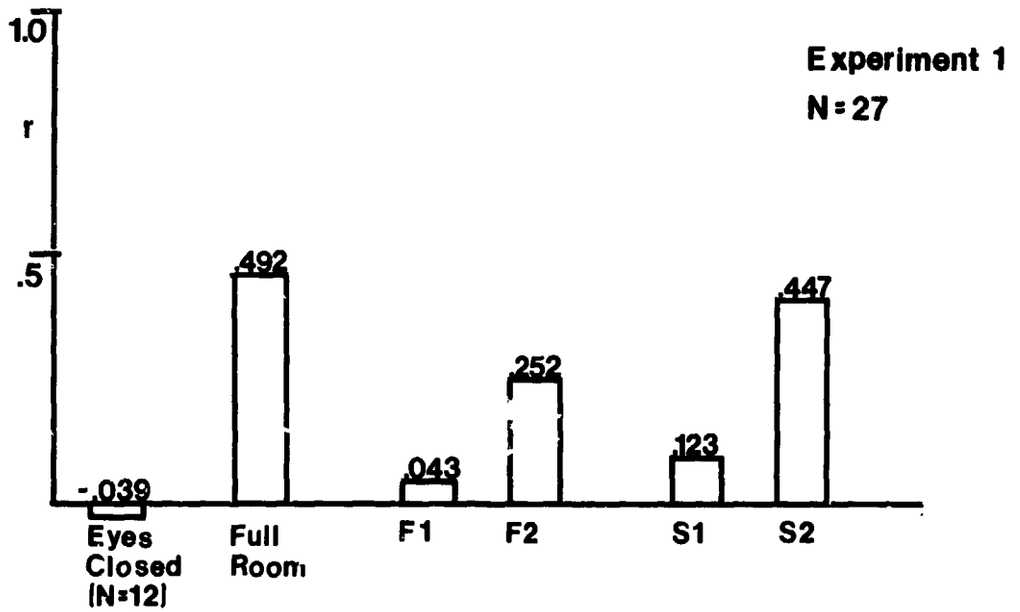

Figure 2. Mean correlations between room movement and subject sway.

With their eyes closed subjects movements were unrelated to those of the room. With eyes open and the entire room visible there was a strong and consistent sway response. In the four experimental conditions the greatest overall sway came in response to the larger peripheral exposure, such that for this condition subjects swayed nearly as much as when the whole room was visible. By contrast, the larger front wall exposure produced only half as much sway as its peripheral counterpart, and

significantly less than the full room. Neither of the smaller exposures produced any more sway than in the eyes closed control.

Discussion Experiment 1 showed that by limiting optical flow to the front wall of the experimental room (and thereby blocking off flow from the far retinal periphery), compensatory sway could be significantly reduced, though the larger front wall exposure still produced significantly more sway than the eyes closed control. These results suggest a peripheral dominance for the pick-up of flow information for postural stability, and are consistent with the findings of Brandt, Dichgans and Koening (1973), who found a similar peripheral dominance for sensations of egomotion induced by rotatory optical stimulation. With respect to the goals of this project, the major result is the finding that exposing the entire front wall of the room results in a significant but reduced sway response; the difference between Full Room and Front Wall conditions could be used in the next experiment.

EXPERIMENT 2

The second experiment combined the two levels of sway response established in experiment 1 with two levels of difficulty in a verbal addition task as a preliminary test of the interaction between attention and flow pick-up. Subjects were presented with both the full room and with the room with the side walls completely occluded by the stationary screens. Each of these exposures was paired with both the hard and easy verbal tasks. In the easy task the subject was presented with a three digit number at the beginning of a trial, which they would increment by 2 continuously over the course of the trial, announcing the sums in time with the beating of a metronome (50 beats/minute). The hard task was identical, except that subjects added 3 instead of two. Nine subjects were run.

Results Since this was a preliminary study only sway data were analyzed; task performance as a function of flow exposures will be evaluated in future studies. Results are presented in figure 3. As can be seen from the figure, the addition of either the hard or the easy task produced no decrement in sway in either full room or front wall conditions. On the contrary, the presence of either of the verbal tasks produced an increase in induced sway. Multiple comparisons done with the Tukey test showed no significant differences between the full room by itself and in combination with either of the tasks, or between the partially blocked room by itself and in combination with either of the tasks.

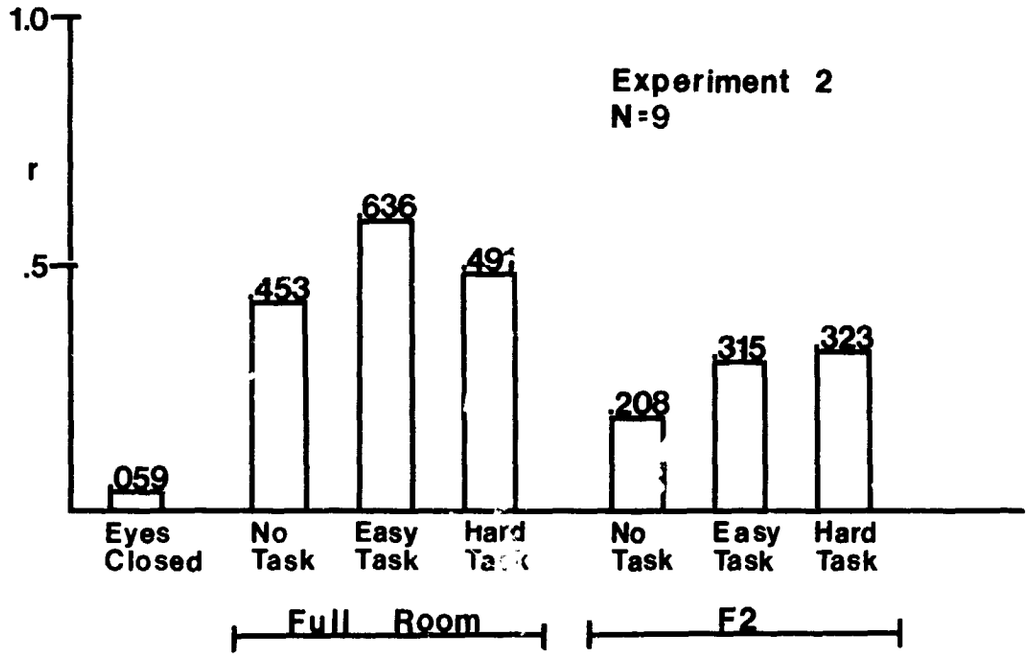

Figure 3. Mean correlations between room movement and subject sway.

Discussion These results, though preliminary, indicate that in the present experiment the presence of an ongoing attention task did not diminish adaptive responding to large scale optical flow specifying egomotion. This is consistent with the notion that optical information used for maintaining postural stability is picked up 'automatically'. The suggestion in these data that a concurrent verbal task may increase sway would be more difficult to interpret.

Future studies in this series will again investigate the effects of attention tasks on response to visual motion, but also the reverse; the effects, if any, of flow pick-up on performance of an attention task. They will also examine the interaction of flow pick-up with visual attention tasks (such as might be found in flight situations), and will extend the requirements on flow pick-up by having subjects execute an active movement task which is dependent on the pick-up of flow information.

REFERENCES

Brandt, T., Dichgans, J. and Koenig, E., "Differential Effects of Central Versus Peripheral Vision on Egocentric and Exocentric Motion Perception", 1973, Experimental Brain Research, 16, 476-491.

Fischer, E., Haines, R. and Price, T., "Cognitive Issues in Head-Up Displays", 1980, NASA Technical Paper 1711.

Lee, D. and Aronson, E., "Visual Proprioceptive Control of Standing in Human Infants", 1974, Perception and Psychophysics, 15(3), 529-532.

Lee, D. and Lishman, R., "Visual Proprioceptive Control of Stance", 1975, Journal of Human Movement Studies, 1, 87-95.

D35

ACCURACY OF SYSTEM STEP RESPONSE ROLL MAGNITUDE ESTIMATION FROM CENTRAL AND PERIPHERAL VISUAL DISPLAYS AND SIMULATOR COCKPIT MOTION

by

N85 14522

R.J.A.W. Hosman and J.C. van der Vaart

DEPARTMENT OF AEROSPACE ENGINEERING
Delft University of Technology
Kluyverweg 1 - 2629 HS Delft
The Netherlands

ABSTRACT

The present experiment is an extension of work done in previous years, at Delft University, on the accuracy and temporal properties of visual roll attitude and roll rate perception.
In earlier perception tasks, discrete stimuli of roll attitude were presented on a central artificial horizon type display. Roll rate tests were done with the same display and with peripheral visual field displays showing moving checkerboard patterns.
From tracking tasks in a flight simulator it was found that cockpit motion improved tracking accuracy and the present experiment was designed to assess the improvements of perception due to cockpit motion.
As it is not possible to present and to manipulate discrete motion stimuli in a moving cockpit just as in the case of visual stimuli alone, a different set-up had to be chosen in which dynamic system step responses of roll angle were the stimuli to be presented.
After the onset of the motion, subjects were to make accuracte and quick estimates of the final magnitude of the roll angle step response by pressing the appropriate button of a keyboard device. The differing time-histories of roll angle, roll rate and roll acceleration caused by a step response will stimulate the different perception processes related the central visual field, peripheral visual field and vestibular organs in different, yet exactly known ways.
Experiments with either of the visual displays or cockpit motion and some combinations of these were run to asses the roles of the different perception processes.
Results show that the differences in response time are much more pronounced than the differences in perception accuracy.

1. INTRODUCTION

A few years ago a research program on pilot's motion perception was started at the Department of Aerospace Engineering of the Delft University of Technology. The aim is to investigate how the pilot perceives the state of the aircraft from the central visual field (artificial horizon), the peripheral visual field (outside world) and motion cues (aircraft motions).
The motive for this program was the wellknown fact that peripheral field

PRECEDING PAGE BLANK NOT FILMED

displays and simulator motion improve pilot's tracking performance and dynamic behaviour. See Refs 1, 2, 3 and 4.
It was assumed that, due to the fact that these improvements in tracking performance can be achieved only by changing the display configuration, these improvements resulted from changes in the perception proces.
It was hypothesised that only two reasons could exist for changes in the perception process. The first was that by adding peripheral visual cues and/or motion cues redundant information becomes available and the subject is able to use this information to improve the perception of the motion variables.
The second reason could be that due to the different (dynamic) characteristics of the neural processing of stimuli received by the central visual field, the peripheral visual field and the vestibular system the duration of the perception and the information handling process is changed. The aim of the research program was to test these hypotheses.

In Refs 5 and 6 experiments are described on the perception of roll attitude and roll rate from central - and peripheral displays.
It was shown that roll attitude can be perceived faster and more accurate than roll rate from the central display. In addition it turned out that roll rate could be perceived faster from the peripheral field display. After these facts had been established an experiment including motion cues was prepared.
An important difference between visual displays on one hand and motion systems on the other is, that motion systems have to move the simulator mass and have dynamic characteristics. Thus the choice of input stimuli is limited by the characteristics of the simulator motion system. It is not possible for instance to present or to manipulate pure attitude, rate or acceleration stimuli separately, since a motion stimulus is now to be considered as a mixture of these three variables.
After some evaluation, the step response of a dynamic system with rather low natural frequency was shown as the input stimulus to the subject. All combinations of the central and peripheral displays and motion were used in the experiment. After stimulus onset the subject was asked to predict the final magnitude of the step response and to answer by pressing the corresponding key on a keyboard. This subject's response corrected the input to the dynamic system and the resulting system output was displayed thus presenting a direct feedback to the subject.
The main output variables of the experiment were perception accuracy and response time. In the final experiment two dynamic systems (second order and third order) were used.

2. TEST FACILITY

All measurements were performed in the research simulator of the Department of Aerospace Engineering. In front of the right hand seat a central (foveal) CRT display (Tektronix 604 monitor), was mounted in the instrument panel. Peripheral visual cues were provided by two TV monitors (Bosch Fernseh Monitor) placed on either side of the simulator cockpit. See Fig. 1. Subjects gave their responses via a digital keyboard, see Fig. 2. The relative positions of the central and peripheral displays and the subject's eye reference point are shown in Fig. 3. In Fig. 3 the image on the central display, simulating the artificial horizon, is als shown. The repetition rate was 250 Hz. The peripheral displays showed a movable checkerboard pattern with squares

of 5x5 cm generated by a moving pattern generator (developed at Delft University) at a repetition rate of 30 frames per sec.
The three degrees of freedom motion system of the flight simulator has high fidelity motion characteristics, making the simulator a very suitable tool for the present experiment. The application, in this motion system of so called 'hydrostatic' bearings in the electrohydraulic servo actuators, assures a very smooth and almost rumble free simulator motion, see Ref. 7. The control of the motion system was compensated for its second order characteristics (ω_o = 43 rad/sec, ζ = 1.5) leading to a gain of unity and phase shift of around zero up to 15 rad/sec. All experimental runs were controlled by a hybrid computer (EAI Pacer 100).
The step response stimulus was generated by either a second or third order system simulated in the analog part of the computer installation. The maximum step magnitude of 12 degrees was well within the limitations of the motion system, see Table 1. The sequence of one stimulus interval is presented in Fig. 4. At the beginning of the n-th interval a new step input φ_{i_n} was given to the system. This event was marked by an audiotone.
The system outputs φ, $\dot{\varphi}$ and φ were used to control the central and peripheral field displays and the motion system, thus presenting the system response to the subject in a number of different ways. After observing the response onset, the subject was asked to respond by pressing the appropriate key of the keyboard in order to return the system output to zero.
The response magnitude is designated by φ_p. The keyboard response changed the input step magnitude of φ_i of the system to the error value $\Delta\varphi$

$$\Delta\varphi_n = \varphi_{i_n} - \varphi_{p_n}$$

In order to inform the subject about the error value and next to bring the simulator back to the zero roll angle, the system response to $\Delta\varphi_n$ is displayed first. Next the system input is reset to zero and the displays blanked as the simulator is being rolled back to the zero roll angle. The total interval length was approximately 7 sec.
During each run the variables φ_{i_n}, $\Delta\varphi_n$, φ_{p_n} and the subjects response time RT_n were recorded and stored on disk for subsequent analysis.

3. EXPERIMENT

As already mentioned the aim of the experiment was to investigate the accuracy with which subjects can perceive simulator motion by observing the central and peripheral displays and cockpit motion.
In Refs 5 and 6 experiments are described where in the perception of roll attitude and roll rate was investigated by using discrete stimuli presented on a central and peripheral displays. In the present experiment, however, the motion system of the simulator was involved. Discrete stimuli were not longer possible due to the limitations of the simulator (see Table 1) and for safety of the subjects.
Therefore a motion stimulus had to be chosen which would be comparable to normal aircraft motions and had characteristics from which the magnitude can be perceived and quantified by subjects. It was decided to use the step response of a second order system (ω_o = 2 rad/sec, ζ = 0.7) as the roll stimulus

for the experiment.
In Fig. 5a the roll angle φ, the roll rate $\dot{\varphi}$ and the angular acceleration $\ddot{\varphi}$ are shown for such a step response.
The advantage of the step response as a stimulus is that after some time a steady state roll attitude is reached. The task of the subject was to estimate the final steady state value of the roll angle. As shown in Fig. 5a the initial roll acceleration is rather sharp ($4°/sec^2$ for a 1 degree step input). This roll acceleration causes an initial lateral acceleration of the subjects head of $0.056\ m/sec^2$ for a step input of 1 degree. The roll and lateral acceleration, due to the maximum step input of 12 degrees caused rather strong proprioceptive cues. To prevent that these proprioceptive cues should have an undesirable effect on the results of the experiment a more gradual input stimulus was used for a limited number of display configurations. This stimulus was the step response of a third order system ($\omega_0 = 2$ rad/sec, $\zeta = 0.7$, $\tau = 0.5$ sec). In Fig. 5b the roll angle φ, roll rate $\dot{\varphi}$ and acceleration $\ddot{\varphi}$ are shown. The maximum roll acceleration for a 1 degree step input decreased to $1°/sec^2$.
The motion perception was investigated with all seven combinations of the central display C, the peripheral displays P and the cockpit motion M using the second order step response stimulus. The third order stimulus was used only for three display configurations (C, M and CM).
The step magnitudes used in the experiment were 0, ±2, ±4, ±6, ±8, ±10 and ±12 degrees. During one run 5 replications of these 13 magnitudes were presented in random order. Each subject replicated all 10 different runs 5 times.

4. SUBJECTS AND TEST PROCEDURE

Two subjects, University staff members and both qualified jet transport pilots, volunteered in the experiment. They were instructed to respond primarily as accurate as possible and secondly as quickly as possible to the presented stimuli. They were not required to fixate their eyes continually on the central display but were free to look at the keyboard when responding. If the central display was not used, subjects were asked to fixate on the central display just before the next stimulus was presented. Apart from the feedback of the error after each keyboard response, subjects were informed of the error standard deviation and the mean response time after each run.
For preliminary evaluation and training a total of 150 runs were made. After a steady level of performance was obtained the two parts of the experiment were carried out during morning sessions. The number of runs for the first part was 7x5x2 = 70 runs. For the second part 3x5x2 = 30 runs were carried out.

5. RESULTS

In Table 2 the means and standard deviations of the step response perception error and the response time are presented as a function of display configuration and system step response stimulus.
The means and standard deviations of the error as a function of step magnitude are shown in Fig. 6. There is a tendency to overestimate the step input for steps of 4, 6 and 8 degrees, while the step of 12 degrees is underestimated. This partly results from the limited range of stimuli of the experiment. The

subjects were aware of the fact that the maximum step input was 12 degrees. This made an overestimation of the maximum step vertually impossible, whereas underestimations still occured. However, overestimating small stimuli and underestimating large stimuli is also present in a pure rate perception task, see Ref. 8.
The error standard deviation is increasing as a function of step magnitude up to a step of 8 degrees. For steps of 10 and 12 degrees, the error standard deviation remains approximately constant. This is also found in the rate perception experiment of Ref. 8, but it is assumed that this phenomenon depends among others on the stimulus range of the experiment.
In Fig. 6c the error mean and standard deviation of the third order step response stimulus is shown. It is clear that the standard deviation for the step inputs of 0, 2 and 4 degrees increased relative to the case of the second order response stimulus, see Fig. 6a. This increase is significant only for the configuration including motion (M, CM) and is not surprising in view of the low value of the maximum roll acceleration during the third order step response, although this roll acceleration is well above threshold, see Ref. 9.
The differences in mean value and standard deviation of the error for each configuration are in some cases significant ($\alpha < 0.01$). The error standard deviation of display configurations including motion are in general smaller than of those not including motion.

The differences between the response times are significant ($\alpha < 0.01$). Notable is the difference in interference between the central display on one hand and the peripheral displays and motion on the other. The response time with the central display C only is the longest. Peripheral displays P and motion M both cause shorter response times. The response times for the combinations CP, CM and CPM are in between those for C and P, C and M and C and PM respectively. For the combination PM however the effect is enhanced and the response time is shorter than for P and M separately.
For the third order system longer response times are found, just as could be expected, but the trend is the same as for the second order system. In Fig. 7 the response time is plotted as a function of stimulus magnitude. The change due to the step magnitude is significant and is found for all display configurations.

6. DISCUSSION AND CONCLUSIONS

As shown in the preceeding chapter the perception accuracy as expressed in error standard deviation is not essentially influenced by the display configuration or sort of input stimulus (second or third order system response). This is in agreement with an earlier experiment on rate perception where except for short exposure times no essential difference in perception accuracy was found between the display configurations central display, peripheral displays and central and peripheral displays. See Ref. 6.
Although the present experiment features notable differences in the time course of the roll angle, roll rate and roll acceleration - the primary input variables for the central visual field, the peripheral visual field and the vestibular system - it turns out that the step magnitude can be perceived equally well from the central display and the peripheral displays and slightly better with motion. Extension of the display configuration to CP, CM etc. did not influence the perception accuracy.

As explained in Chapter 4 the task of the subject was to respond primarily as accurate as possible and secondly as quickly as possible. For each display configuration and stimulus there should be an optimal response time, based on the fact that especially the peripheral and motion cues will vanish with time (see Figs 5a and b). Based on this notion it is next assumed that a change in subject's instruction (obtain maximum accuracy regardless of the response time) should hardly influence the perception accuracy.
It has been suggested that man, as an observer, should be able to combine in some optimal way, independent sources of information on attitude and motion. If in the present task perceptions from central and peripheral displays and from cockpit motion were independent and if indeed some kind of optimal or suboptimal combination were present, then greater accuracy of subjects estimates would appear in, for instance the CPM configuration when compared to the C, P and M configurations separately. Table 2 shows that this is not the case.

Comparison of the estimation error of the present experiment with the attitude perception experiment of Ref. 5 shows a same order of magnitude ($\sigma_{\Delta\varphi}$ present experiment configuration C = 1.393 degrees, $\sigma_{\Delta\varphi}$ attitude perception = 1.543 degrees).

As already mentioned in Chapter 5 the differences in response time due to the seven display configurations are significant. Part of these differences correspond remarkably well with the corresponding differences from the rate perception experiment in Ref. 6, see Table 3.
From the response times resulting from the second order and third order step-response stimuli it should be concluded that the trend of changes in response time due to different display configurations is independent of the stimulus but the actual values are dependent on the sort of stimulus, see Table 4.
From the data presented so far it may be concluded that addition of peripheral visual cues and motion cues to central visual cues does not essentially improve the perception accuracy but makes the perception process faster.
Going back to earlier experiments performed in Delft and by others (see Refs 1 to 4) it is well known that tracking performance can be improved by the addition of peripheral visual cues and motion cues. The question arose whether a connection can be established between the results of the present experiment and these tracking tasks experiments.
In Ref. 10 Levison and Junker describe an experiment investigating the influence of simulator motion system time delays on a roll tracking task. From this experiment data are plotted in Fig. 8 which clearly demonstrate the relation between time delay and tracking performance. This figure shows that in the particular experimental configuration motion cues had to be delayed by 0.26 sec to make tracking performance equal to that in the no motion configuration.
It is shown in the present experiment that motion cues speed up the response times. If these motion cues are delayed, the advantages of the motion cues are nullified. If the differences in response times of the present experiment can be ascribed to the perception proces alone, then these differences can be interpreted as differences in duration of the perception proces.
As described in the introduction this research program was started with a tracking task experiment, see Refs 3 and 4, wherein the same display configurations have been used as in the present experiment. With the tracking

performance of that experiment and the response times of the present experiment a comparable figure as Figure 8 can be drawn, see Fig. 9.
The results of three configurations (P, M, PM) however have to be excluded from this analysis due to the lack of accurate roll attitude information in the tracking task which has influenced the tracking performance.
The evident relation between tracking performance and response time, demonstrates that the improvements in tracking performance due to motion and peripheral visual cues results only from the shorter duration of the perception proces.

7. REFERENCES

1. Moriarity, T.E., Junker, A.M. and Price, D.R.
   Roll axis tracking improvements resulting from peripheral vision motion cues. Proceedings of the Twelfth Annual Conference on Manual Control, NASA TM-X-73, 1976.

2. Stapleford, R.L., Peters, R.A. and Alex, F.R.
   Experiments and a model for pilot dynamics with visual and motion inputs. NASA CR-1325, 1969.

3. Hosman, R.J.A.W. and Van der Vaart, J.C.
   Effects of visual and vestibular motion perception on control task performance. Proceedings of the First European Annual Conference on Human Decision Making and Manual Control, Delft, 1981.

4. Hosman, R.J.A.W. and Van der Vaart, J.C.
   Effects of vestibular and visual motion perception on task performance. Acta Psychologica 48 (1981) 271-287.

5. Hosman, R.J.A.W. and Van der Vaart, J.C.
   Accuracy of visually perceived roll angle and roll rate using an artificial horizon and peripheral display. Proceedings of the Second European Annual Conference on Human Decision Making and Manual Control, Bonn, 1982.

6. Hosman, R.J.A.W. and Van der Vaart, J.C.
   Perception of roll rate from an artificial horizon and peripheral displays. Proceedings of the 19th Annual Conference of Manual Control.

7. Den Hollander, J.G. and Baarspul, M.
   Measurement of motion quality of a moving base flight simulator. Delft University of Technology, Department of Aerospace Engineering. Memorandum M-264, 1977.

8. Van der Vaart, J.C. and Hosman, R.J.A.W.
   Mean and random errors of visual roll rate perception from central and peripheral displays. 20th Annual Conference on Manual Control, NASA Ames Research Center, 12-14 June, 1984.

9. Hosman, R.J.A.W. and Van der Vaart, J.C.
Vestibular models and thresholds of motion perception. Results of test in a flight simulator. Delft University of Technology, Department of Aerospace Engineering, Report LR-265, 1978.

10. Levison, W.H., Lancroft, R.E. and Junker, A.M.
Effects of simulator delays on performance and learning in a roll-axis tracking task. Proceedings of the fifteenth Annual Conference on Manual Control, AFFDL-7R-79-3135, 1979.

TABLE 1: Limits of the flight simulator motion system.

mode	maximum displacement	maximum rate	maximum acceleration
heave	0.3 m	0.65 mh	10 m/sec^2
pitch	16 degrees	44 deg/sec*	650 deg/sec^2*
roll	15 degrees	32 deg/sec*	340 deg/sec^2*

* computed values.

TABLE 2: Mean response time and perception error as a function if display configuration and input stimulus.

display configuration	2nd order step response				3rd order step response			
	$\overline{RT}$ sec	σ_{RT} sec	$\Delta\overline{\varphi}$ degrees	$\sigma_{\Delta\varphi}$ degrees	$\overline{RT}$ sec	σ_{RT} sec	$\Delta\overline{\varphi}$ degrees	$\sigma_{\Delta\varphi}$ degrees
C	1.163	0.162	0.148	1.343	1.563	0.251	0.332	1.439
P	1.098	0.174	0.317	1.388				
M	0.948	0.191	-0.062	1.194	1.260	0.248	-0.071	1.414
CP	1.127	0.178	0.028	1.339				
CM	0.992	0.231	0.018	1.216	1.353	0.282	0.148	1.267
PM	0.905	0.173	0.157	1.259				
CPM	0.940	0.212	0.092	1.253				

TABLE 3: Comparison of response times from the rate perception experiment (Ref. 6) and the present experiment.

	Rate perception experiment Ref. 6	Present step response experiment
RT_C	0.83 sec	1.16 sec
RT_P	0.77 sec	1.10 sec
RT_{CP}	0.80 sec	1.13 sec
RT_C-RT_P	0.06 sec	0.06 sec
RT_C-RT_{CP}	0.03 sec	0.03 sec
RT_{CP}-RT_P	0.03 sec	0.03 sec

TABLE 4: Comparison of response times resulting from the second order and third order step respons stimuli.

	2nd order stimulus	3rd order stimulus
RT_C	1.15 sec	1.56 sec
RT_M	0.95 sec	1.26 sec
AT_{CM}	0.99 sec	1.35 sec
RT_C-RT_M	0.21 sec	0.30 sec
RT_C-RT_{CM}	0.17 sec	0.21 sec
RT_{CM}-RT_M	0.04 sec	0.09 sec

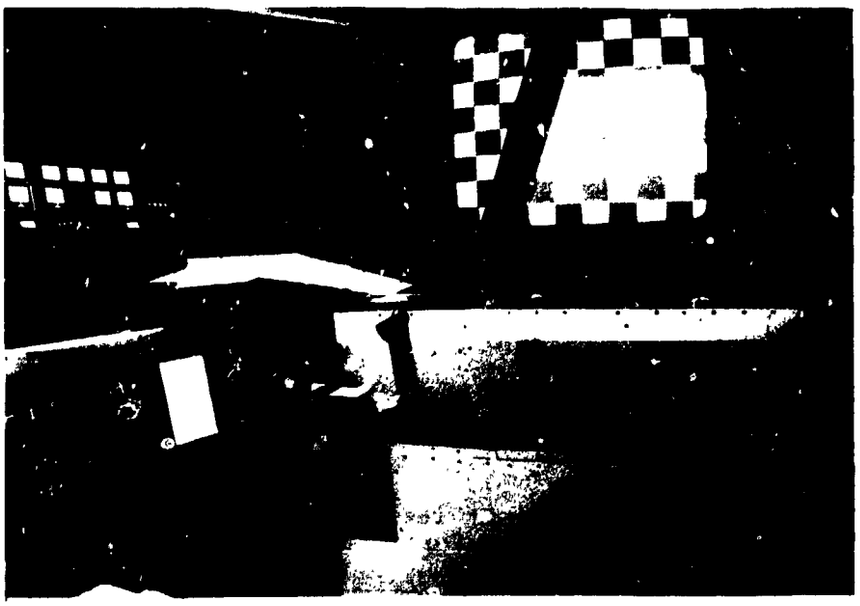

Fig. 1. Overview of the simulator cockpit with central display and the right hand peripheral display.

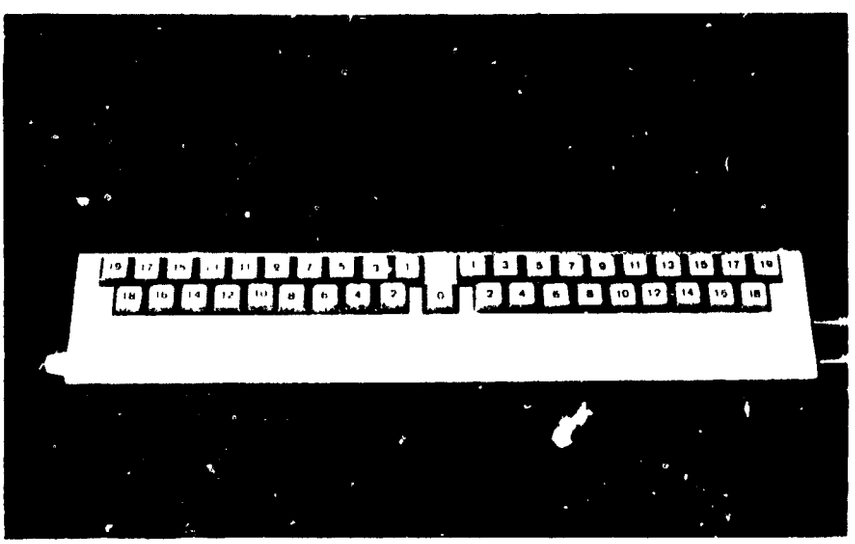

Fig. 2. Digital keyboard.

ORIGINAL PAGE IS
OF POOR QUALITY

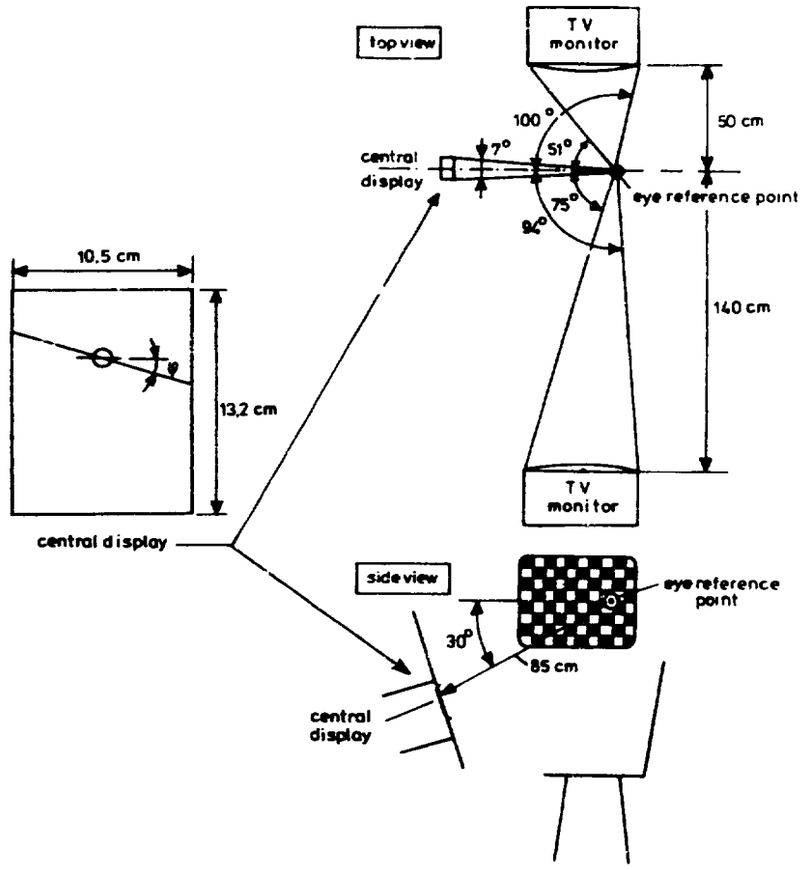

Fig. 3. Positions of displays relative to the subject's eye reference point. Central display image and dimensions.

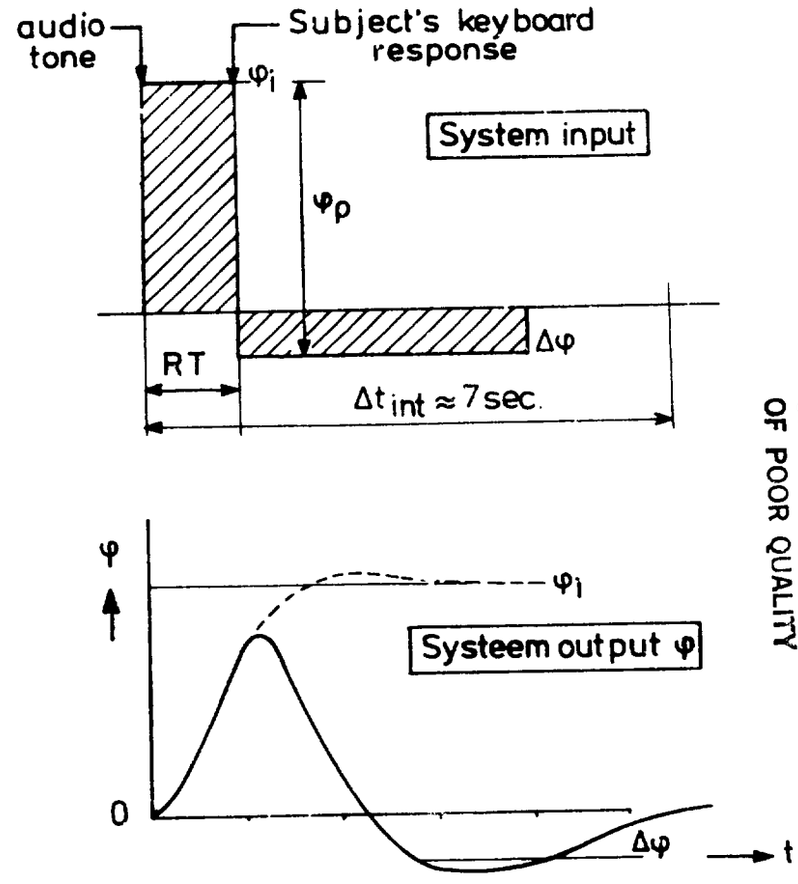

Fig. 4. Sequence of one interval of a test run.

ORIGINAL PAGE IS OF POOR QUALITY

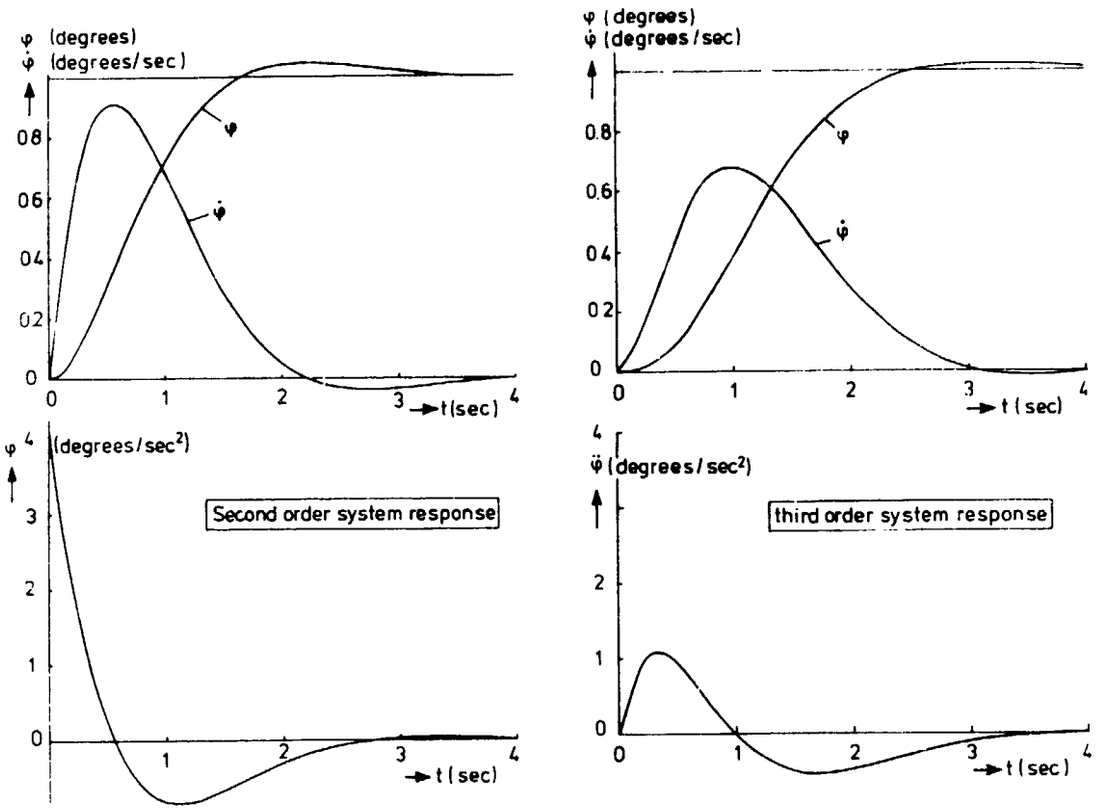

Fig. 5. The roll angle, roll rate and roll acceleration of the second and third order system step responses.

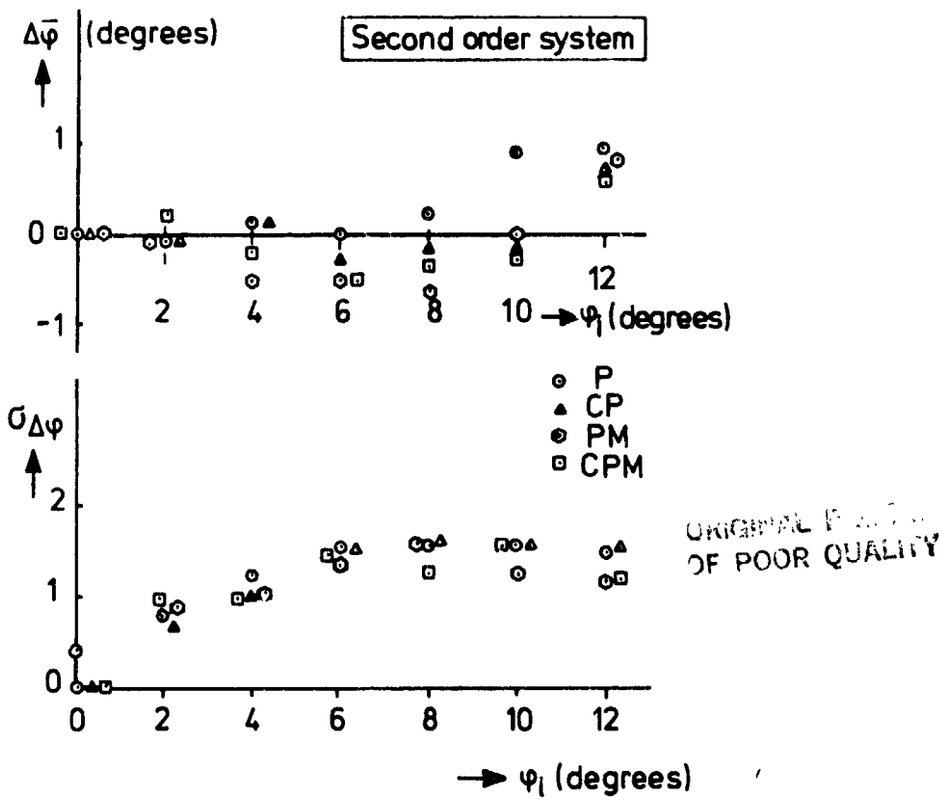

ORIGINAL PAGE IS
OF POOR QUALITY

Fig. 6a. Mean roll angle perception error Δφ and its standard deviation as a function of stimulus magnitude.

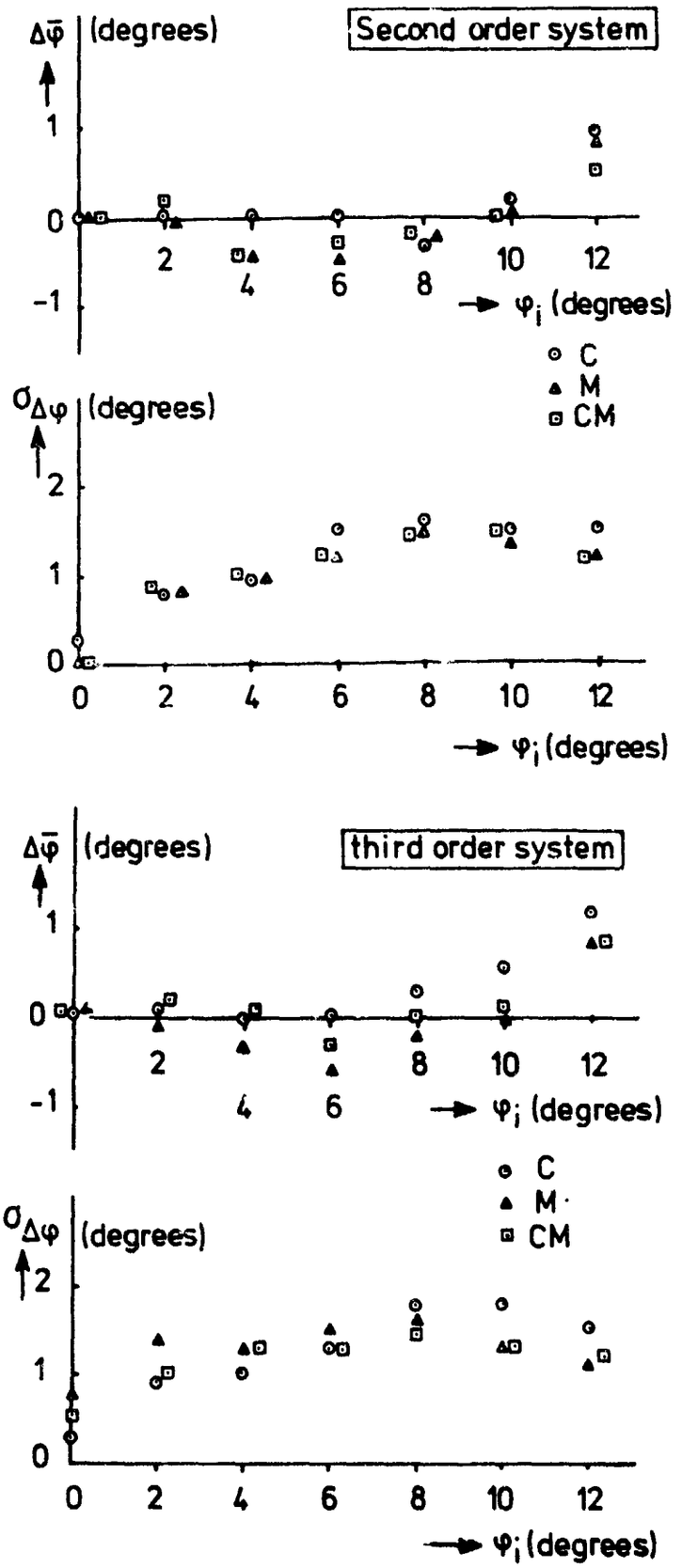

Fig. 6b. Mean roll angle perception error $\Delta\varphi$ and its standard deviation as a function of stimulus magnitude.

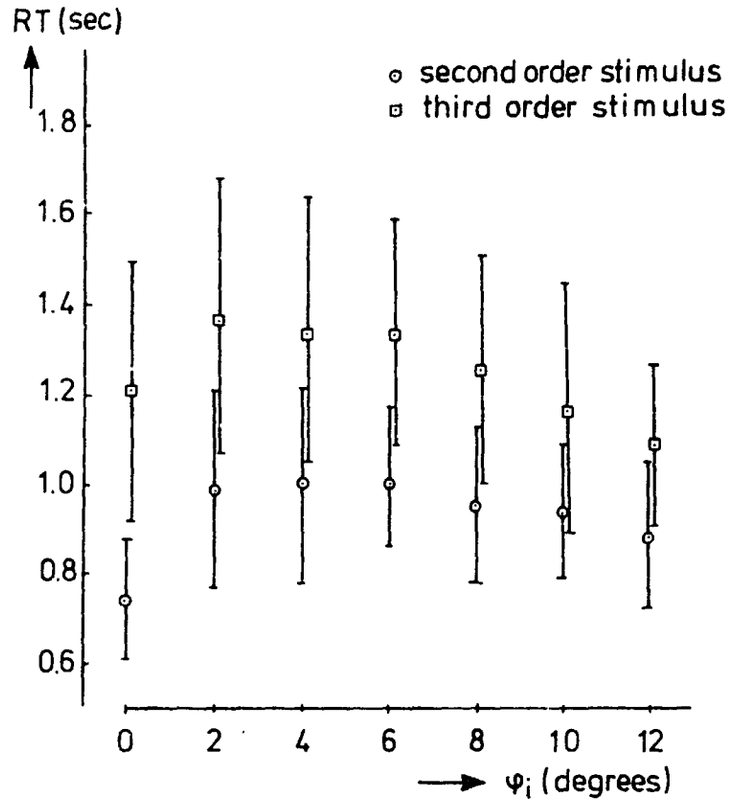

Fig. 7. Response time as a function of stimulus magnitude for the motion configuration M.

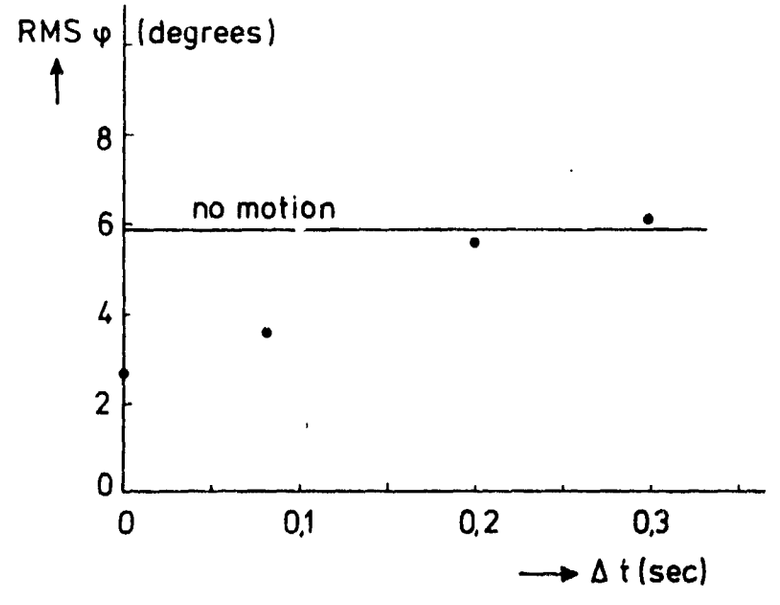

Fig. 8. Root mean square of the roll angle φ in a roll tracking task as a function of simulator motion time delay Δt compared with the no motion performance, from Ref. 10.

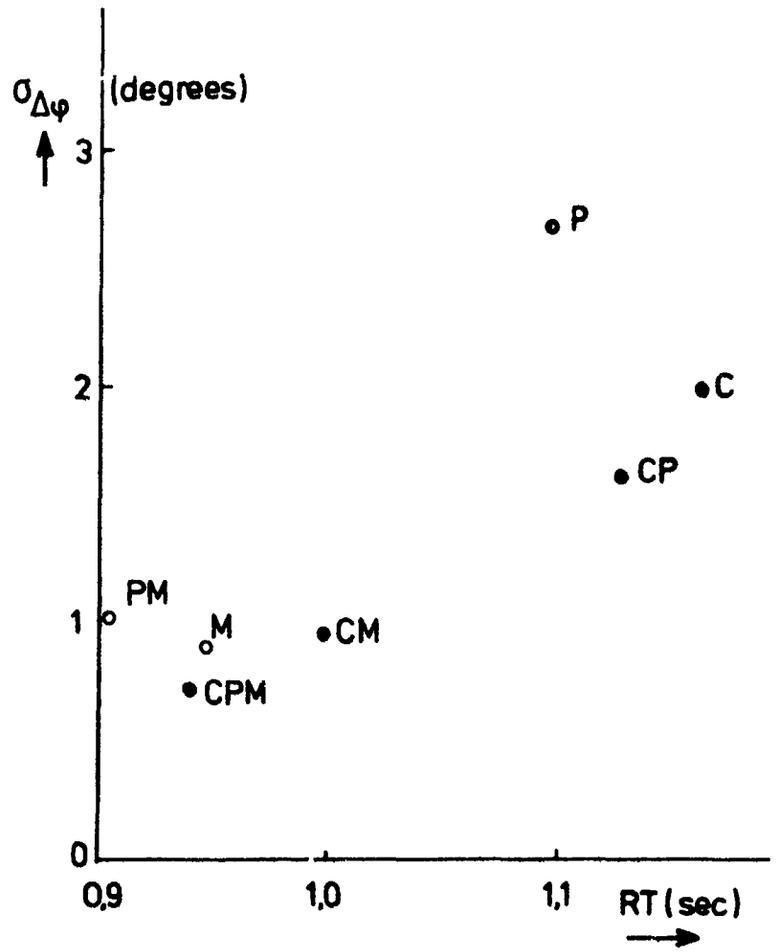

Fig. 9. Tracking performance σφ of the roll tracking task from Ref. 4 as a function of the response time RT of the present experiment for similar display configurations.

Models of Target Acquisition

N85 14523

D36

HITTS' LAW? A TEST OF THE RELATIONSHIP BETWEEN INFORMATION LOAD AND MOVEMENT PRECISION

Mathew Zaleski
Department of Industrial Engineering
University of Toronto

Penny Sanderson
Department of Psychology
University of Toronto

Abstract

An experiment was run to test the independence of information load (Hick's Law) and movement precision (Fitts' Law) using additive factors methodology.

There were two elements to the subjects' task. Firstly, subjects were required to classify stimuli according to a decision rule with a variable entropy. The stimuli were presented in the centre of the CRT screen. In response, subjects had to move a cursor from a starting point near the stimulus to the appropriate target. The targets were arranged in an annular pattern around the central point. The precision of the response movement was varied by manipulating the ratio of the radius of the annulus to the width of the target area.

The dependent measure was elapsed time between onset of the stimulus and completion of the response movement. Independence of the Hick's Law and Fitts' Law components of the reaction time was tested with an analysis of variance. Presence of an interaction would suggest that a decision stage and a response stage are dependent, and cannot be considered discrete steps in a serial process.

- Zaleski, Mathew; Sanderson, Penny.
- Annual Mental
- Informal paper
- Perceptual-motor performance

ORIGINAL PAGE IS
OF POOR QUALITY

With the increasing popularity of icon driven software systems there has been a trend towards "pointing" input devices such as the mouse, touch screen and joystick. These devices help reduce the cognitive and motor complexity required to recode an intention as an action. Operators are required to make a decision about a situation or an item of information and act upon the decision by moving a cursor to a designated area on CRT screen. What factors influence the efficiency and accuracy of such a task?

The operator's task can be divided into two parts, a decision part and a movement part, and there exist information theoretic measures predicting reaction time for each of these parts. Hick [1952] and Hyman [1953] proposed that reaction time increased with the number of bits per decision:

$$RT = a + bH \tag{1}$$

where

$$H = -\sum p_i \log_2(p_i)$$

Fitts [1954] proposed that movement time increased with the $\log_2$ of the ratio of movement amplitude to target width:

$$MT = c + d \log_2(2A/W) \tag{2}$$

Following Jagacinski, the combined RT and MT will be called capture time (CT). Reaction time (RT) will refer to the time between stimulus onset and the start of the joystick movement, while movement time will refer to the time between the start of the joystick movement and target capture. Operational definitions of the above events will be given below.

It is generally found that movement precision has very little effect on RT. This supports the notion that perceptual or cognitive processing is independent of the processing of motor movements. Fitts and Peterson [1964] found that as movement amplitude (A) was increased or target width (W) decreased, RT increased consistently, but only very slightly. However, manipulations of stimulus probablity did have an effect on RT. RT was longer the more uncertainty there was as to which of two targets would be signalled (Fitts and Peterson Practice Session, Experiments I and II). They also found that by making one of the two targets more probable, thus increasing redundancy, RT decreased to the more probable target (Experiment III). More recently, Jagacinski, Hartzel, Ward and Bishop [1978] tested the applicability of Fitts' Law as system dynamics and target uncertainty were varied. They found that movement precision and RT were independent. Finally, Gopher, Hartzell,Hart S. G., Lee E., and Dunbar S. [1983] have attempted a combination of Sternberg's memory scanning task with Fitts' Law and have on the whole found independence of the two subtasks.

Given these results, it could be hypothesized that overall capture time in an X-Y sorting task should be an

ORIGINAL PAGE IS
OF POOR QUALITY

additive combination of RT and MT. Combining Hick's and Fitts' Laws:

$$CT=\alpha + \beta H + \gamma \log_2(2A/W). \quad (3)$$

There appear to have been few explicit attempts to combine Hick's and Fitts' Laws in this fashion, even though it must follow from the findings outlined above. One attempt was made by Beggs, Graham, Monk, Shaw and Howarth [1972]. They proposed the combination in equation 3 and varied the accuracy of each movement and the number of possible movements in a continuous task. Subjects held a pencil and moved their hand between a home position and any of several targets, paced by a metronome. However, the combination of the two laws was not possible as a negative minimum movement time for the Fitts' law component made that Law invalid. Beggs et al. [1972] suggested that their rather unusual methodology may have been responsible for this.

The present experiment tests equation 3 in discrete trials and when movements are made with a joystick. The joystick is used to control the position of a cursor on a CRT screen. The dynamics are of order zero, with constant gain. Response uncertainty was manipulated by making the number of equiprobable responses either 2,4 or 8, resulting in 1,2 or 3 bit decisions. Subjects viewed the stimulus in the centre of the CRT screen, and made their response by moving the cursor to the target indicated by the stimulus. The mapping from stimulus to target was one to one, targets were labeled A,B, .. ,H and the stimuli were identical to the labels. Targets were arrayed in an annular fashion around the stimulus position, in a radially symmetrical arrangement. Movement precision was manipulated by varying the inner and outer radii of the targets. In this geometry the ratio of 2A/W used in (3) corresponds to the ratio of:

$$(radius_{outer}+radius_{inner})/(radius_{outer}-radius_{inner}) \quad (4)$$

In the present experiment, movement precision was either 3,4 or 5 bits. Jagacinski and Monk [in Press] and Card, English and Burr [1978] have found that with a joystick, diagonal movements, like those required to reach half the targets in this experiment, take slightly longer than vertical or horizontal movements. However, Jagacinski and Monk [in Press] show that Fitts' law still holds.

Response uncertainty and movement precision were crossed in a factorial design. If (3) is correct then there should be independent effects of response uncertainty and movement precision, but no interaction. Analysis of variance should show only response uncertainty to have a significant effect on Reaction Time (RT) and only movement precision to have a significant effect on Movement Time (MT). Capture Time (CT) should show significant effects of both response uncertainty and movement precision, but no interaction. Regression analysis ought to be able to fit a model akin to equation 3 to the data obtained.

ORIGINAL PAGE IS
OF POOR QUALITY

METHOD

Design

There were three levels of response uncertainty (1,2,3 bits) and three levels of movement precision (3,4,5 bits). These were crossed in a factorial design and each subject served under all 9 conditions. The trials were chosen such that the subject made movements in each of the possible orientations an equal number of times at each level of response uncertainty.

The subjects' task was to view a letter which appeared in the centre of the CRT screen and move the cursor to the target which matched the letter. In the 1,2,3 bit decisions, subsets of the letters A,B, ..,H were used. Specifically, in the 1 bit decision, the subject had to choose between A and E, B and F, C and G, and D and H. In the two bit decisions the subject had to choose from A,C,E and G or from B,D,F and H. In the three bit decisions, the stimulus could be any one of the eight letters. In all cases, only targets corresponding to possible stimuli were displayed. Movement precision was manipulated within each response uncertainty block according to a latin square.

Apparatus

The experiment was run on an Apple IIe micro computer. Responses were made with a Measurement Systems joystick without spring return to centre. The maximum deflection of the joystick was about 30°. The gain was approximately 0.25° of visual angle for each 1° of joystick deflection. After presentation of the stimulus the position of the joystick was sampled every 10 mSec by installing an interrupt handler which trapped interrupts from a Mountain Equipment Inc. Clock card and read a Mountain Equipment Inc. analog to digital converter (ADC). Reaction and capture times were not calculated on line, and so were not fed back to the subject after each trial. ADC samples were spooled onto floppy disk, and analyzed off line by another program. All software, including the clock and ADC handler, was developed under the Apple version of the UCSD Pascal operating system.

Procedure

Subjects were run in eight 20 minute blocks, each of which comprised either the first or second half of the experimental design. They took between 3 and 7 days to run through the experimental design four times.

The instructions to the subjects asked them to be as time-efficient as possible while maintaining good accuracy. If their results showed any systematic inaccuracy, such as moving away from the cross hairs less than 200 mSec after stimulus onset, they were asked to avoid such errors when they next performed the task. Reaction time was operationally defined to be the time between the onset of the stimulus and when the joystick was deflected 0.3°. Capture time was the time between the onset of the stimulus and the

beginning of a 350 mSec capture of the target.

Subjects

Seven undergraduate and graduate students at the University of Toronto served as subjects.

RESULTS

Three analyses of variance and three multivariate regressions will be discussed. The analysis of variance [1] took the within subjects experimental design into account. Much of the variation was found to stem from differences between subjects. The regression analysis employed six dummy variables in addition to response entropy and the index of difficulty in order to take between subject differences into account. In this way the regression analysis was made more consistent with the ANOVAs.

Reaction time was found to vary significantly with response entropy ($F(2,12)= 41$, $MSE=71$, $p<0.001$). There was a significant interaction between response entropy (H) and index of difficulty (ID) ($F(4,24)=3$, $MSE=3$, $p=0.037$) detected, but the amount of variance actually involved was neglible. The regression analysis showed an r^2 of 0.95.

Movement time varied significantly with both H and ID, but the ANOVA showed that by far the greatest part of the variation can be attributed to the ID ($F(2,12)= 87$, $MSE= 71$, $p<0.001$) as opposed to the H ($F(2,12)= 5.6$, $MSE= 17$, $p = 0.019$). There was no significant interaction found between H and ID. The regression showed an r^2 of 0.90, but with a negative intercept (about -100 mSec).

Capture time showed a significant effect of H ($F(2,12)= 89$, $MSE= 44$, $p<0.001$) and, ID ($F(2,12)= 91$, $MSE= 67$, $p<0.001$) but no interaction at all. In fact, the F score of the interaction term was almost precisely 1.

The best fit of equation 3 (Hitts' Law) for this data is thus:

$$CT=344 + 137H + 170\log_2(ID)$$

with an r^2 of 0.96.

DISCUSSION

It appears that the data supports a relation of the form of equation 3. Both the ANOVA and regression analysis

[1]The joystick was sampled every 10 mSec, and so all the ANOVAs are in terms of this unit of time.

indicate that most of the variance in subject performance can be accounted for by such an expression. As hypothesized, response entropy and movement precision have independent effects on capture time over a fairly broad range of uncertainties.

The analysis of variance showed a great amount of the variation was due to differences between subjects. Thus, adding dummy variables to the regression analysis increased the r^2 for CT from about .45 to about 0.96. This would indicate that the difference between subjects was in large part due to different intercepts, and can probably be attributed to the relative lack of practice of the subjects, as well as the lack of on line performance feedback.

Movement time was found to vary not only with ID, but also with H. Examination of Figure 3 will indicate that this effect seems to occur in those trials with H=3. One possible explanation starts with the observation that only in the H=3 trials does the subject have to deal with targets separated by 45°. This could be tested by adding such configurations into H=2 and H=1 cells.

A few subjects showed little difference in movement time between ID=4 and ID=5. This is possibly due to the fact that the difference between these two movement precisions was manipulated using width of the target rather than amplitude of the motion.

Within the conditions tested in this experiment Hitts' law appears to hold. The next step might be to generalize the manipulation of H, since response entropy was varied here by controlling the number of equiprobable targets, and not by presenting targets with different probabilities. This would have the aditional benefit that a wider range of H could be tested.

Finally, in the procedure described here the task of the subject was a highly discrete one. The subject had several seconds to contemplate the targets before the onset of the stimulus. It is possible that the subject was able to prepare himself for the upcoming movement in a way which contributed to the high degree of independence between H and ID. In contrast, in a setting in which each trial led into the next with no gaps inbetween, and in which there may be more incentive for the subject to overlap reaction and movement times, the independence of H and ID might disappear.

References

Beggs W.D.A, Graham J.C., Monk T.H., Shaw M.R.W., and Howarth C.I., Can Hick's Law and Fitts' law be combined?, *Acta Pschologica* 1972, 36 348-357

Card S.K., English W.K., Burr B.J., Evaluation of mouse, rate controlled joystick, step keys and text keys for text selection on a CRT, *Ergonomics* 1978, 21 601-613.

Fitts P.M., The information capacity of the human motor system in controlling the amplitude of movement, *Journal Experimental Psychology* 1954, **47**, 381-391.

Fitts P.M., Peterson J.R., Information capacity of discrete motor responses, *J of Experimental Psychology* 1964, **67**, 103-112.

Hartzell E.J., Gopher D., Hart S.G., Lee E., Dunbar S., The Fittsberg Law: The joint impact of memory load and movement difficulty, *Proceedings of the Human Factors Society* 1983.

Hick, W.E., On the rate of gain of information, *Quarterly Journal Experimental Psychology* 1952, **4**, 11-26.

Hyman R., Stimulus Information as a determinant of reaction time, *Journal Exp. Psychology* 1953, **45** 188-199.

Jagacinski R.J., Hartzell, J., Fitts' law as a function of system dynamics and target uncertainty, *Journal of Motor Behaviour* 1978, **10** ,123-131.

Jagacinski R.J., Monk D. L., Fitts Law in two dimensions with head and hand movements *In Press*.

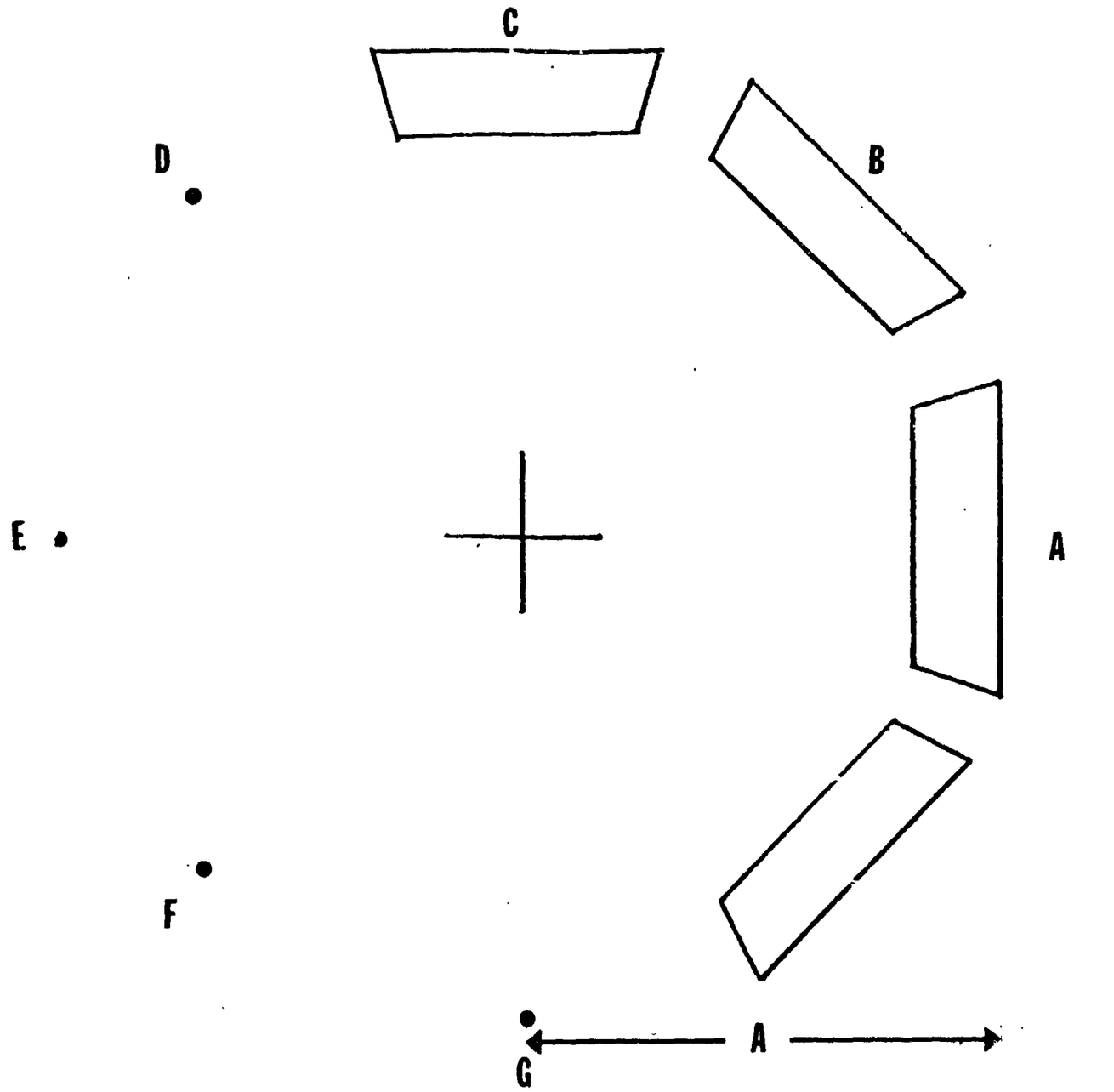

$$ID = \log_2\left(\frac{2A}{W}\right)$$

FIG. 1

reaction time (mSec) vs response entropy

Fig 2

ORIGINAL PAGE IS
OF POOR QUALITY

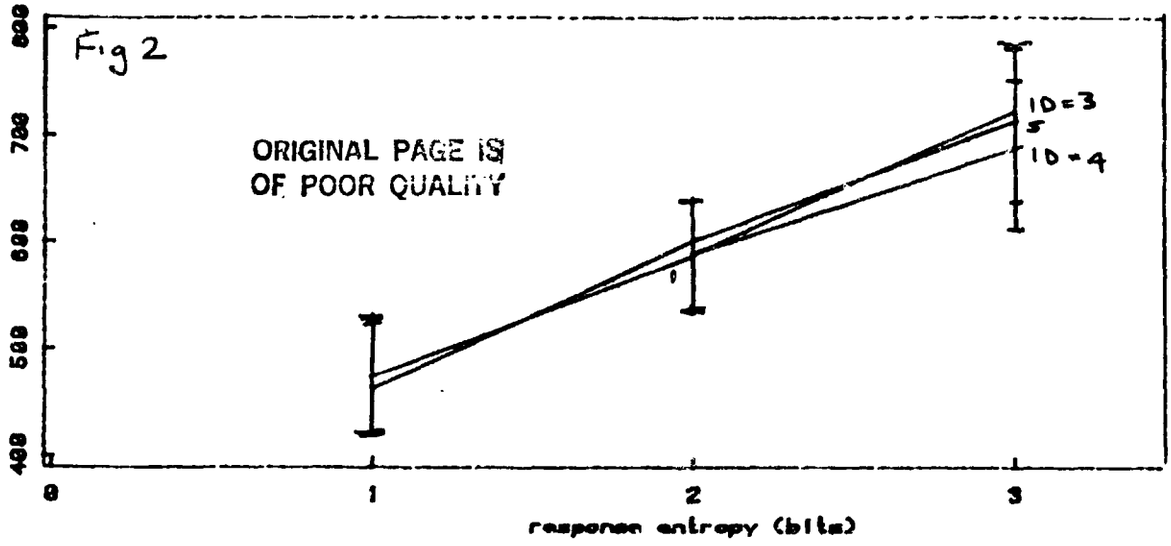

movement time (mSec) vs response entropy

Fig 3

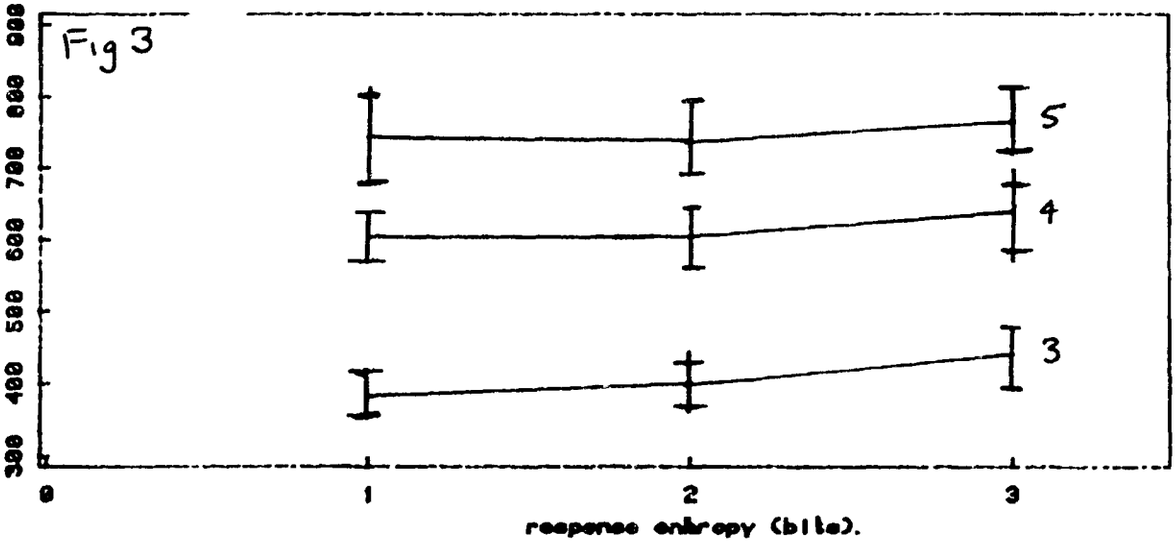

capture time vs response entropy

Fig 4

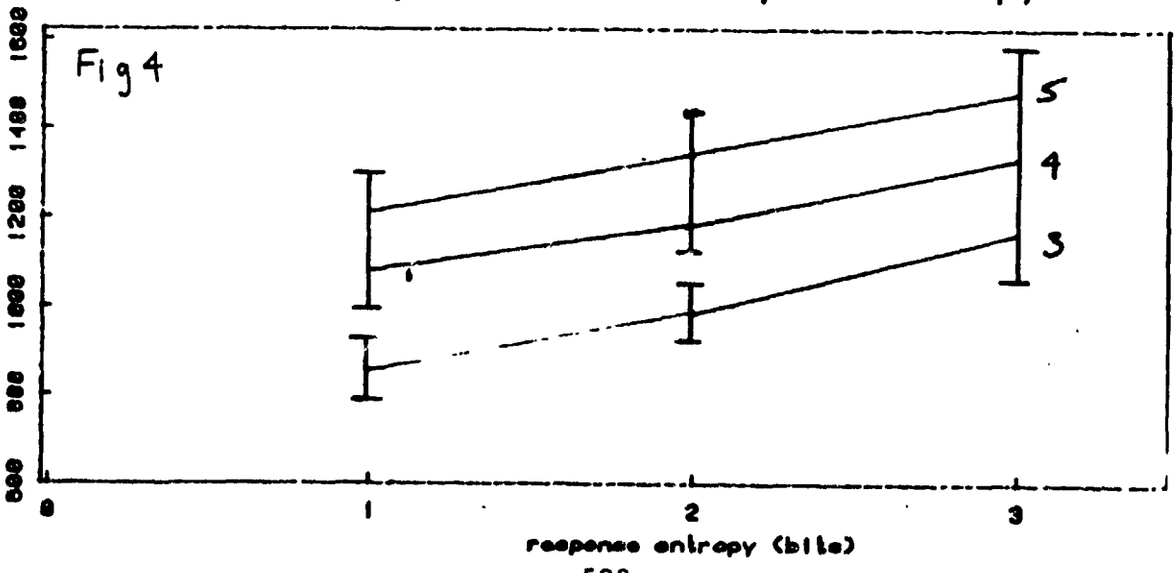

N85 14524 D37

A PRODUCTION SYSTEM MODEL OF CAPTURING REACTIVE MOVING TARGETS

Richard J. Jagacinski, Brian D. Plamondon, and Richard A. Miller

The Ohio State University
Columbus, Ohio 43210

ABSTRACT

Subjects manipulated a control stick to position a cursor over a moving target that reacted with a computer-generated escape strategy. The cursor movements were described at two levels of abstraction. At the upper level, a production system described transitions among four modes of activity: rapid acquisition, close following, a predictive mode, and herding. Within each mode, differential equations described trajectory generating mechanisms. A simulation of this two-level model captures the targets in a manner resembling the episodic time histories of human subjects.

INTRODUCTION

There seems to be a growing consensus that complex motor behavior must be described at multiple levels of abstraction. This notion is at least as old as Bryan and Harter's (1899) work on telegraph operators. More recently Rasmussen (1983) has discussed skill-based, rule-based and knowledge-based behaviors. The present experiment used two levels of abstraction to describe the way people capture a moving target. The more abstract level of description consisted of a production system which exhibited discrete transitions among modes of capture behavior. The more detailed level of description consisted of the trajectory generating mechanisms that were active within each mode. The simulated time-histories of this two level model contained sequences of episodes corresponding to the activation of different tracking modes. The time histories of human subjects were similarly episodic.

The episodic nature of manual tracking was emphasized by Craik (1947) in his characterization of the human operator as an intermittent correction servo. A number of subsequent sampled-data models exemplified this approach (e.g., Lemay and Westcott, 1962; Bekey, 1962; see Pew, 1970 for additional discussion of this issue). In contrast, smooth continuous descriptions of tracking such as the McRuer Crossover Model (McRuer and Jex, 1968) and continuous optimal control models (e.g., Kleinman, Baron, and Levison, 1971) have not emphasized episodic aspects of performance.

PRECEDING PAGE BLANK NOT FILMED

A somewhat intermediate class of models has described episodic aspects of manual tracking as switching among a set of control modes, some or all of which were smoothly continuous. For example, Costello (1968), Phatak and Bekey (1969), and Burnham and Bekey (1976) partitioned the error phase plane into several regions, and associated a different tracking mode with each region. The episodes in these latter models were thus event-driven, rather than time-driven as in the sampled-data models. The simulation used in the present study was a generalization of this event-driven approach, in which the events that triggered the beginnings of episodes included aspects of the target and cursor movement in addition to error and error rate.

METHOD

Four undergraduate students served as subjects for ten 45-minute sessions. Subjects sat approximately 50 cm away from a 10-cm wide oscilloscope display on which they saw a target and a cursor. The target consisted of two vertical lines separated by 2 mm, and the cursor was a single dot. Both target and cursor moved only in the horizontal dimension. At the beginning of a trial the cursor was centered, and the target randomly appeared 2 cm to the right or left of center. The subjects' task was to manipulate an isometric control stick (gain = .35 kg per 1° of visual angle) so as to hold the cursor dot between the two target lines for an uninterrupted period of 400 ms. When this criterion was achieved, the target was considered "captured," and it disappeared from the display. If the target was not captured within 15 seconds, or if the target exceeded the display boundaries of 5 cm to the right and left of center, the target was considered to have "escaped," and it also disappeared from the display. The subjects' task was to capture the target as quickly as possible.

The target reacted to the movement of the cursor with an escape strategy represented in Figure 1. A nonlinearity plus an integrator made the target move away from the cursor with a velocity that increased as the cursor came closer (a "panic" function). The resulting velocity was then filtered through a second-order underdamped system that made the target movement oscillatory. There was a 15 cm/sec saturation on velocity and a $15\omega_n$ cm/sec^2 saturation on accelaration in this filter that is not represented in Figure 1. ω_n is the undamped natural frequency of the filter. The purpose of the filter was to have the target make evasive side-to-side movements analogous to the juking maneuvers performed by footbal players attempting to elude a tackler.

ω_n was set at either 3 or 5 rad/s, and the per unit critical damping, ζ, was set at either 0 or .25 . A factorial crossing of these values produced four targets of varying degrees of evasiveness.

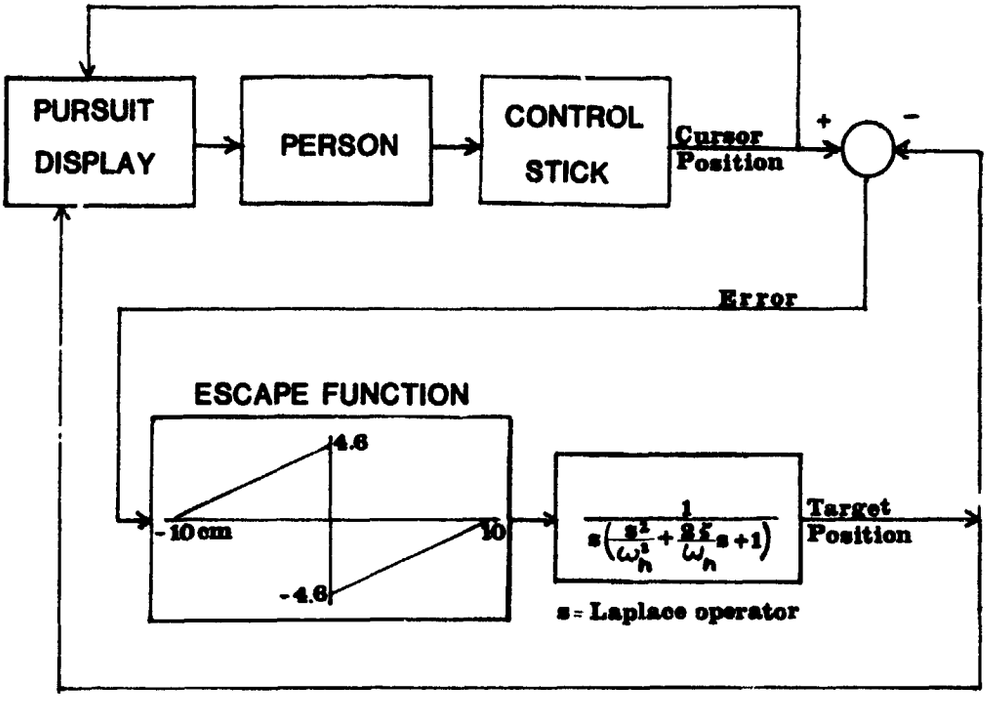

Figure 1 - Escape strategy for reactive targets.

For each of the four targets, subjects received two practice trials followed by two 20-trial blocks. Each session thus consisted of 160 data trials, 40 trials for each target. The order of presentation of targets was randomized within a session; however, subjects were informed as to which target they would receive at the beginning of each block. Subjects were instructed to capture the targets as quickly as possible, and were given feedback after each block as to the sum of their capture times over the twenty trials. Whenever the target escaped, a capture time of 15 s was recorded for that trial. There was thus a strong penalty for an escape. Subjects were also given daily feedback on their total capture time across all 160 trials, and a bonus of $5.00 was offered to the subject with the lowest total capture times for Sessions 9 and 10.

RESULTS

State Definitions

Mean capture times on Sessions 9 and 10 ranged from 3.2 s for Subject 1 to 6.1 s for Subject 4. For all four subjects, mean capture times increased

monotonically across targets in the following order: (ω_n = 3 rad/s, ζ= .25), shortest capture time; (ω_n = 3 rad/s, ζ = 0); (ω_n = 5 rad/s, ζ = .25); (ω_n = 5 rad/s, ζ = 0), longest capture time. A single trial for Subject 1 capturing the most difficult target is shown in Figure 2. Qualitatively, this time history appears to contain a sequence of short episodes of very different types of pursuit behavior. After a reaction time interval of approximately 300 ms (RT segment, Figure 2), the cursor moves very rapidly toward the target to reduce the initial large distance from the target (first A segment, Figure 2). Once the cursor nears the target, the cursor begins to follow the target closely and mimic the target trajectory (first F segment, Figure 2). After several changes of direction, the discrepancy between the target and cursor builds up, and the cursor no longer mimics the target trajectory (segment P, Figure 2). Rather, the cursor moves much more slowly than the target, coming close to the target only at its upper turnaround points. The cursor then begins to follow the target closely again (second F segment, Figure 2) until the target approaches the 5-cm escape boundary. The cursor then exhibits a quick pulse that has the effect of reversing the target movement (second A segment, Figure 2). Finally, the cursor again begins to follow the target closely, and the target is captured (third F segment, Figure 2).

The boundaries of the episodes indicated in Figure 2 were determined by a computer program that was basically looking for three patterns:

1. A - "fast acquisition" Cursor velocity is much greater than target velocity.
2. F - "close following" Cursor velocity is approximately equal to target velocity.
3. P - "predictive mode" Cursor velocity is much less than target velocity.

The distinction between a fast acquisition as in the first A segment in Figure 2 and close following is similar to the two modes in Costello's (1968) surge model. Large errors are corrected proportionately more rapidly than small errors. The second A segment in Figure 2 keeps the target in bounds rather than reducing a large discrepancy. This type of response might better be labelled "herding". More will be made of this distinction later in this paper. The predictive mode is also quite different from close following. The subject seems to know that the target is eventually going to turn around and oscillate back toward the cursor. This behavior seems to involve more long-range prediction of target behavior.

The three patterns, A, F, and P were more quantitatively defined as a trichotomy on the ratio of target velocity to cursor velocity. However, such a definition is based on very local movement characteristics rather than more global pattern recognition, and it ran into problems when the target paused or reversed direction, or when cursor and target had approximately equal velocities of opposite sign. The computerized pattern recognition scheme was therefore supplemented with additional

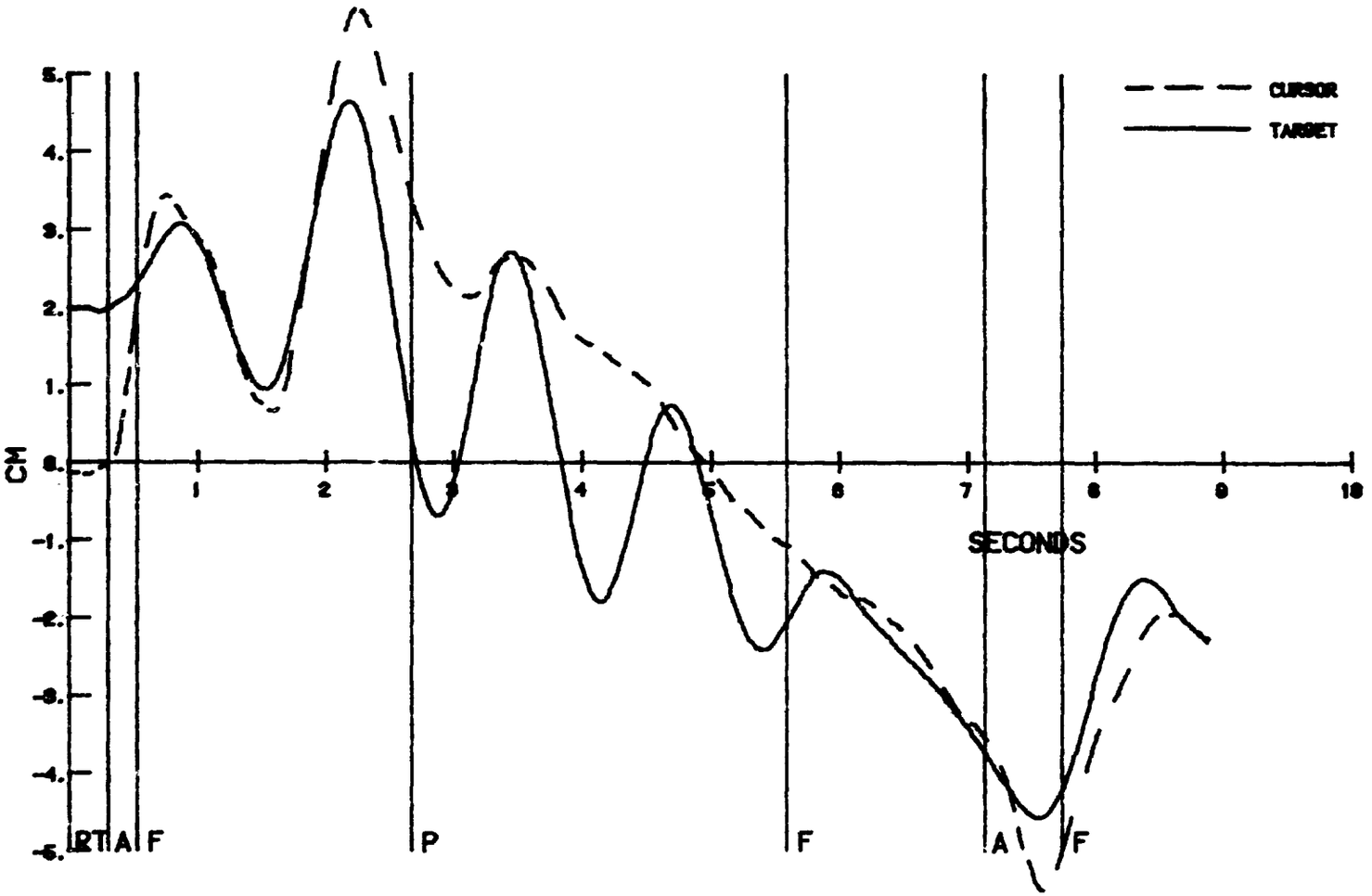

Figure 2. Time history of Subject 1 capturing the most difficult target.

local tests of error magnitude and cursor velocity, as well as more global tests of tracking mode continuity. The details of these pattern recognition procedures are beyond the scope of the present summary (see Plamondon, 1982).

Markov Descriptions

Using the three state definitions A, F, and P, a computer program segmented the continuous time history of each of the trials into a sequence of discrete states. For each target, the pattern of state transitions across trials was represented as a first order Markov process. Figure 3 shows the Markov representations for Subjects 1 and 4 capt ıg the most difficult of the four targets (ω_n = 5 rad/s, ζ = 0). For e... subject, the represe.ıtation is based on a total of 80 trials from Sessions 9 and 10. The number in each circle is the mean duration of that state in seconds. The number on each arrow between states represents the probability of going to a particular new state given that a transition occurred from the old state. Transitions which occurred on less than five percent of the trials are not shown in the figure.

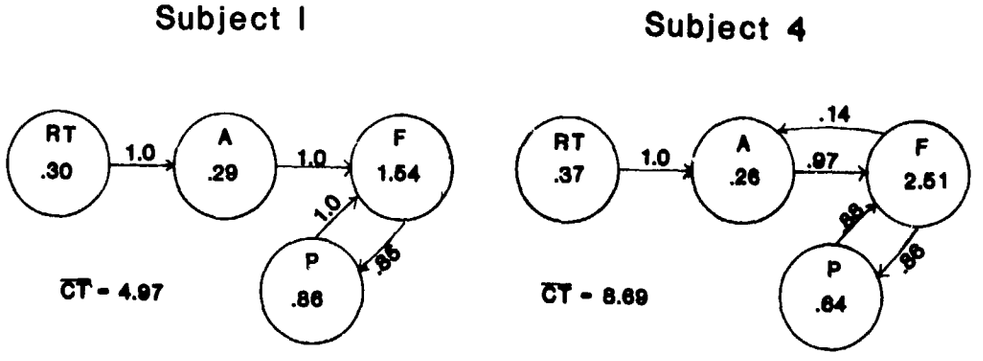

Figure 3 - Markov representations of subjects' strategies in capturing the most difficult target.

At this very abstract level of representation, the subjects' strategies for capture look quite similar. After an initial acquisition mode, close following occurred. Transitions to the predictive mode and

a return to close following might occur subsequently. Subject 4 occasionally transitioned from close following to the acquisition mode, and the mean duration of Subject 4's following mode was about 1 second longer than for Subject 1. On the other hand, mean capture time for Subject 4 (8.69 s) was almost four seconds longer than the mean capture time for Subject 1 (4.97 s). Subject 4 captured only 47 of 80 targets, while Subject 1 captured 76 out of 80. Given these large differences in overall performance, it is somewhat surprising that the Markov diagrams are so similar.

One aspect of performance missing from these diagrams is the states of the cursor and target when the mode transitions occurred. Phase plane diagrams of cursor, target, and error revealed striking individual differences between Subjects 1 and 4 when transitioning into the P mode. Subject 1 transitioned into the P mode primarily when the error was increasing (a well defined linear locus in the first and third quadrants of the error phase plane), and target velocity was greater than 5 cm/s. Subject 4 had a more diffuse spread of points in the first and third quadrants of the error phase plane, and no well defined pattern in the target phase plane. Cursor velocity was less than 1 cm/s for 28% of Subject 4's entries into the P mode, indicating that some of the activity classified as "predictive" may have simply been pausing. In contrast, Subject 1 tended to generate ramp-like cursor movements during the P mode, and cursor velocity was never less than 1 cm/s at entry to the P mode.

Production System Model

Based on the previous analysis, a two-level model of capture performance was constructed. The upper level was a production system model that generated transitions among four different modes of activity (Table 1). The fourth mode arose from treating herding and the reduction of the initial large tracking error at the beginning of a trial as two separate A modes. Each mode has an associated goal, and the productions are ordered to reflect the urgency of these goals. Preventing an escape (herding) has the highest priority, and reducing large oscillations via the predictive mode has second priority. Staying close to the target to achieve capture (close following) cannot be successful if the target is about to escape or if it is wildly oscillating. This goal was therefore given third priority. The fourth goal, reducing the large initial error, applies only at the beginning of trials.

The trigger conditions for entering the P and F modes were based on the phase plane patterns for Subject 1. Very few herding responses were detected by the computer pattern recognition scheme previously described, so the entry conditions for the herding maneuver are not derived from subjects' data.

Once begun, a mode of tracking continues until it produces states of target and cursor that match the entry condition for a different mode to begin. If more than one entry condition is satisfied simultaneously,

Table 1 - Annotated Production System

Goal	Triggering Condition	Movement Trajectory
1. Keep target away from boundary	$\lvert T \rvert > 3.5$ cm and $\lvert T + .25\,\dot{T} \rvert > 5.0$ cm and $\lvert E \rvert < .65$ cm	Herding response (A_2) Rapid, preprogrammed pulse
2. Reduce large oscillations	$\lvert \dot{T} \rvert > 5$ cm/sec and $\lvert \dot{T} \rvert > \lvert \dot{C} \rvert$ and $\lvert E \rvert$ increasing and $\lvert E \rvert > .3$ cm	Predictive response (P) Ramp response to closest predicted turn-around point by damped sinusoidal schema $\hat{T} = T_o + e^{-bt}\, r \sin(\omega t + \theta)$ and closed-loop error nulling (low gain) and strong velocity limiting
3. Stay very close to target to achieve capture ($\lvert E \rvert < .10$ cm for .4 sec)	$\lvert E \rvert < .65$ cm	Close following response (F) Position cursor at short-range damped sinusoidal extrapolation of target position and closed-loop error nulling (high gain) and slight velocity limiting

Table 1 - continued

Goal	Triggering Condition	Movement Trajectory
4. Reduce initial large error	Initial conditions	Fast acquisition response (A_1) Rapid, preprogrammed step

T = target C = cursor E = error = T - C

the highest priority condition takes precedence. This system is thus deterministic. The probabilistic nature of mode transitions in the Markov description is resolved by the explicit entry conditions in the production system.

The second level of the overall model is the trajectory generating mechanism within each tracking mode. The initial acquisition response, A_1, was generated from the step response of a second-order underdamped system. Low damping and a high undamped natural frequency generated a fast rise time. The damping was then increased and the undamped natural frequency was decreased to shape the overshoot aspect of the response. This preprogrammed response was protected from interruption by other tracking modes for 450 ms. The herding maneuver, A_2, was similarly generated from the pulse response of a second-order system with high undamped natural frequency and low damping. This preprogrammed response was protected from interruption for 400 ms.

The trajectories for the predictive or P mode were generated from a combination of three mechanimsm: a predictive element, a closed-loop error nulling element, and a velocity limiter. The predictive element used a damped sinusoidal model of target motion. Target position and target velocity 150 ms and 300 ms into the past were used to estimate continuously the target model parameters for amplitude, frequency, phase, and offset. The damping constant was fixed as apriori knowledge of the target. In the predictive mode the cursor does not keep up with the target. The subject anticipates that the fleeing target is going to turn around and start coming back, and then turn around again in an oscillatory manner. The predictive element therefore continuously predicted the position and time of the nearer turnaround, and generated a cursor velocity sufficient to intercept the target at turnaround (see the P segment in Figure 2). This predictive behavior was combined with a closed-loop error nulling element in the form of a simplified McRuer Crossover Model with low gain and 150 ms time delay. A velocity limiter approximated neuromuscular smoothing.

The close following or F mode used the same three elements as the predictive mode, but modified their interaction. The predictive element used the damped sinusoidal model to predict present target position based on target position and target velocity 150 ms and 300 ms into the past. The change in cursor position necessary to match this predicted target position was weighted by a factor reflecting how accurately the damped sinusoidal model had recently predicted past target position. This predictive element was combined with a high gain McRuer Crossover Model and a less severe velocity limiter than was used in P mode.

The production system is a deterministic model. Given the constant initial condition at the beginnings of trials, only a single time history would be generated for each of the four targets. Subject data, however, exhibited considerable trial to trial variability even after ten days of practice. To introduce trial to trial variability into the production system, the initial acquisition response was stochastically varied as

well as a 200 ms exponential blending function that was implemented to avoid transients when mode switching occurred. Any of the other tracking modes could also have been varied. However, the present stochastic variations were sufficient to generate an interesting variety of time histories. Three sample time histories of the model capturing the most difficult target (ω_n = 5 rad/s, ζ = 0) are shown in Figure 4.

The performance of this multi-level model has to be judged at multiple levels of detail. At the grossest level, one can simply count how often it captures targets. The model captured the most difficult target about sixty percent of the time. This level is comparable to Subject 4 (59%), but not as good as Subject 1 (95%) on Sessions 9 and 10. A slightly more detailed measure of model performance is the mode transitions it exhibits. Like Subjects 1 and 4, the model captured the most difficult target by primarily transitioning between the P and F modes. At still a lower level of detail one can compare the trajectory shapes in the different tracking modes with those exhibited by the subjects. At least qualitatively, there is strong similarity. Much work remains to be done in more formally evaluating this production system model. However, even this cursory evaluation does lend additional credence to the multi-level description of target capture behavior.

DISCUSSION

The present study has demonstrated the usefulness of combining production systems and trajectory generating mechanisms to describe the episodic nature of target capture behavior. The present authors believe these different levels of describing behavior are examples of what Rasmussen (1983) has referred to as rule-based and skill-based behaviors. In more complex environmental situations a third level of organization corresponding to problem-solving aspects of knowledge-based manipulations might be added to the present model.

The decomposition of behavior provided by the definitions of different tracking modes proved useful in developing a simulation to match human performance. An alternative would have been to work at only one level of abstraction, and attempt to represent all of the varied aspects of the target capture behavior in a single linear or non-linear differential equation. This approach probably would have been considerably more difficult given the nature of the time histories exemplified by Figure 2.

The present simulation has also demonstrated the usefulness of a simplified predictive element for successfully capturing a higher order non-linear target. Although the form of the simplified target model (a damped sinusoid) was not uniquely identified from the subjects' time histories, earlier versions of the simulation suggested that some kind of predictive mechanism was essential for achieving the tracking

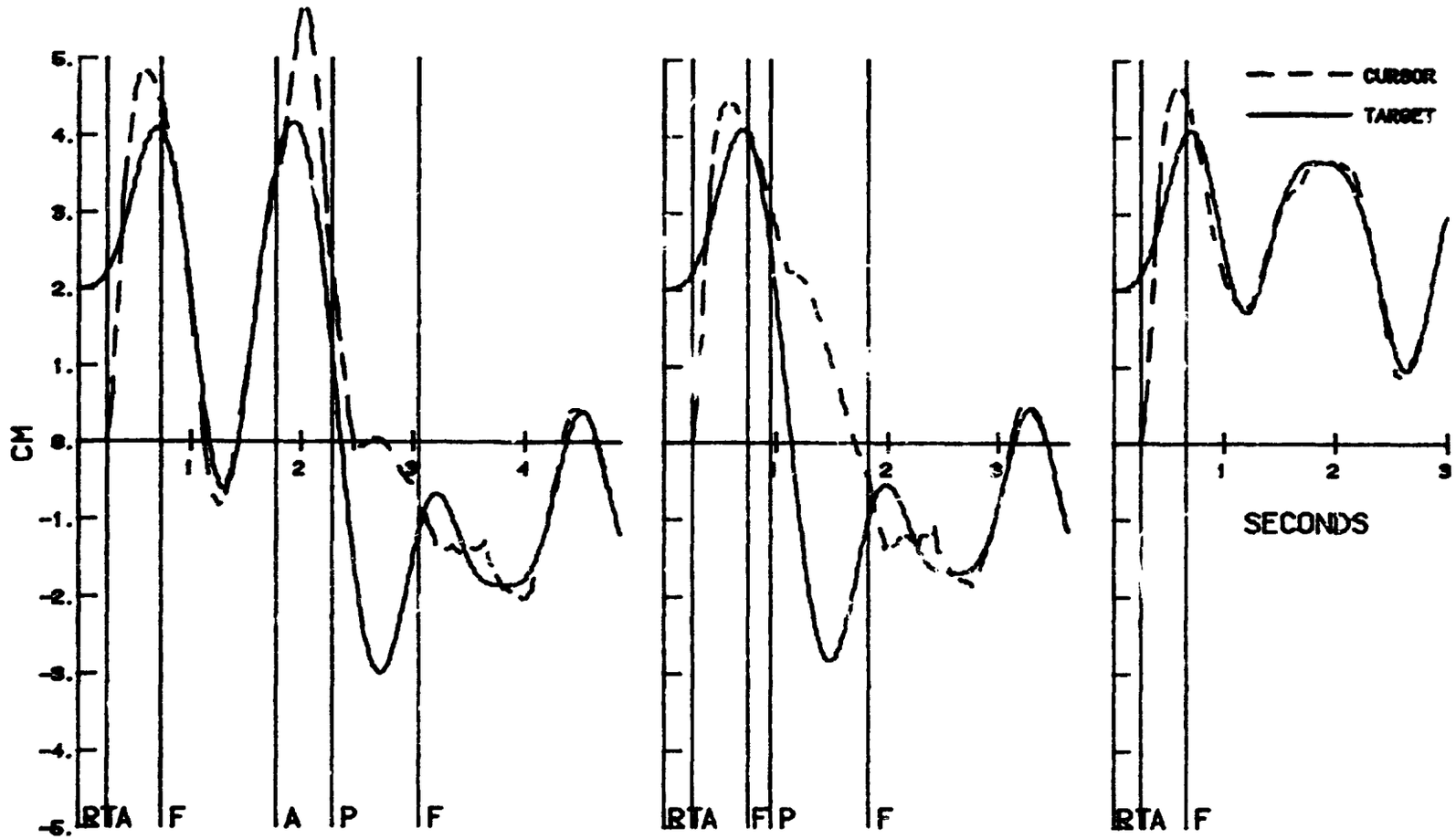

Figure 4 - Time histories of the production system model capturing the most difficult target.

accuracy required in this very demanding task. Closed-loop error nulling did not appear to be sufficient. On the other hand, complete veridical knowledge of the target dynamics was not necessary for capture. The damped sinusoidal predictive element in the P and F modes did not explicitly represent the nonlinear velocity generating escape mechanism that preceded the oscillatory filter, nor was the time history of past tracking error modeled as an input to the damped sinusoidal approximation. The usefulness of approximate prediction has also been noted by other investigators including Kelley (1962), Murril (1967), and Herzog (1968). Additional work on incorporating more global pattern recognition capability might improve the present model without resorting to full veridical knowledge of the target.

The close following (F) and predictive (P) tracking modes utilized the same basic elements of damped-sinusoidal prediction, closed-loop error nulling, and velocity limiting, but the two modes differed in the way these elements interacted (Table 1). This recombination of the same basic elements captures the spirit of what Greene (1972), Turvey (1977), Gallistel (1980) and others have termed coordination. Although the present production system model has this property, there may be other ways of representing the trajectory generating mechanisms for these two modes. The present authors do not claim that the present representation is unique.

The tracking modes used in the present production system model appear to be closely related to distinct styles of tracking noted by previous investigators. For example, Costello (1968) postulated a two-mode model for nulling large and small errors that is similar to the distinction between the fast acquisition (A_1) and close following (F) modes in the present study. The subjects' behavior in the predictive (P) mode is somewhat analogous to crossover regression (McRuer and Jex, 1968) in which subjects do not attempt to follow high frequency characteristics of the input signal. Subjects' ability to predict sinusoidal patterns in manual control tasks is also well documented (Magdaleno, Jex, and Johnson, 1970; Pew, 1974). Parallels such as these increase the credibility of the present mode definitions. Nevertheless, considerably more work is necessary to establish their behavioral independence as distinct modes of tracking. What is necessary is to find independent variables that can alter each mode individually without altering the other modes. For example, Subject 1 only used the P mode to any appreciable degree for the most difficult target. If the other modes were not altered in structurally significant ways by this manipulation of ω_n and ζ, one would have greater confidence that the P mode was behaviorally independent from the other tracking modes. Similarly, the addition of high frequency noise to the target might affect the close following (F) mode without significantly altering the fast acquisition and predictive modes. Much more work needs to be done on this important issue.

In summary, the present work has argued for the usefulness of combining production systems and differential equation descriptions of episodic target capture behavior. In more complex tasks involving both supervisory and active control, production systems may in turn be controlled by still more abstract levels of behavioral organization. By explicitly representing multiple levels of organization of tracking behavior as in the present study, it may be easier to incorporate tracking into more general behavioral models involving problem solving and decision making. The authors hope that the present effort will contribute toward the development of behavioral models at multiple levels of abstraction.

ACKNOWLEDGEMENT

This work was supported by Air Force Office of Scientific Research Grant AFOSR-78-3697 and by NASA Grant NAG 2-195. The project monitor for the latter grant was E. James Hartzell. Portions of this report are based on the Masters' Thesis of the second author.

REFERENCES

Bekey, G. A. The human operator as a sampled-data system. IRE Transactions on Human Factors in Electronics, 1962, HFE-3, 43-51.

Bryan, W. L., & Harter, N. Studies on the telegraphic language. The acquisition of a hierarchy of habits. Psychological Review, 1899, 6, 345-375.

Burnham, G. O., & Bekey, G. A. A heuristic finite-state model of the human driver in a car-following situation. IEEE Transactions on Systems, Man and Cybernetics, 1976, SMC-6, 554-562.

Costello, R. G. The surge model of the well-trained human operator in simple manual control. IEEE Transactions in Man-Machine Systems, 1968, MMS-9, 2-9.

Craik, K. J. W. Theory of the human operator in control systems. 1. The operator as an engineering system. British Journal of Psychology, 1947, 38, 56-61.

Gallistel, C. R. The Organization of Action: A New Synthesis. Hillsdale, New Jersey: Wiley, 1980.

Greene, P.H. Problems of organization of motor systems. In R. Rosen & F. M. Snell, (Eds.). Progress in Theoretical Biology, 1972, 2, 303-338.

Herzog, J. H. Manual control using the matched manipulator control technique. IEEE Transactions on Man- Machine Systems, 1968, 9, 56-60.

Kelley, C. R. A predictor instrument for manual control. In The predictor instrument - Final report and summary of project activities during 1961. Stanford, Connecticut: Dunlap & Associates, Inc., 1962, 15-16. Cited in T. B. Sheridan & W. R. Ferrell. Man-Machine Systems. Cambridge, Massachusetts: MIT Press, 1974, 273.

Kleinman, D. L., Baron, S., & Levison, W. H. A control theoretic approach to manned-vehicle systems analysis. IEEE Transactions on Automatic Control, 1971, AC-16, 824-832.

Lemay, L. P. & Westcott, J. H. The simulation of human operator tracking using an intermittent model. International Congress on Human Factors in Electronics, Long Beach, California, May 1962. Cited in Pew, 1970.

Magdaleno, R. E., Jex, H. R., & Johnson, W. A. Tracking quasi-predictable displays. Proceedings of the Fifth Annual NASA-University Conference on Manual Control, NASA SP-215, 1970, 391-428.

McRuer, D. T., & Jex, H. R. A review of quasi-linear pilot models. IEEE Transactions on Human Factors in Electronics, 1967, HFE-8, 231-249.

Murril, P. J. Automatic Control of Processes. Scranton, Pennsylvania: International Textbook Company, 1967, 405-425.

Pew, R. W. Toward a process-oriented theory of human skilled performance. Journal of Motor Behavior, 1970, 2, 8-24.

Pew, R. W. Human perceptual-motor performance. In B. H. Kantowitz, (Ed.). Human Information Processing: Tutorials in Performance and Cognition. Hillsdale, New Jersey: Erlbaum, 1974.

Phatak, A. V., & Bekey, G. A. Model of the adaptive behavior of the human operator in response to a sudden change in the control situation. IEEE Transactions on Man-Machine Systems, 1969, MMS-10, 72-80.

Plamondon, B. D. A finite state analysis of reactive target tracking. Unpublished Masters' Thesis, Ohio State University, Columbus, Ohio, 1982.

Rasmussen, J. Skills, rules, and knowledge; Signals, signs, and symbols, and other distinctions in human performance models. IEEE Transactions on Systems, Man, and Cybernetics, 1983, SMC-13, 257-266.

Turvey, M. T. Preliminaries to a theory of action with reference to vision. In R. Shaw & J. Bransford, (Eds.). Perceiving, Acting, and Knowing. Hillsdale, New Jersey: Erlbaum, 1977.

N85 14525

D38

INVERSE MODELLING TO OBTAIN HEAD MOVEMENT CONTROLLER SIGNAL

Won Soo Kim, Sang Hyo Lee*, Blake Hannaford & Lawrence Stark

Neurology Unit, 481 Minor Hall,
University of California, Berkeley, CA, 94720

20th Annual Conference on Manual Control
June 1984

ABSTRACT

Experimentally obtained dynamics of time-optimal, horizontal head rotations have previously been simulated by a sixth order, non-linear model driven by rectangular control signals. EMG recordings have aspects which differ in detail from the theoretical rectangular pulsed control signal. We have obtained control signals for time-optimal as well as sub-optimal horizontal head rotations by means of a newly developed inverse modelling proceedure. With experimentally measured dynamical data serving as the input, this procedure inverts the model to produce the neurological control signals driving muscles and plant. The relationships between these controller signals, and EMG records should contribute to our understanding of the neurological control of movements.

Acknowledgements: NIH Training grant in Systems and Integrative Biology (BH); Nasa-Ames cooperative agreement NCC-2-86. S.H.L. is partially supported by a grant from the Ministry of Education, Korea.

INTRODUCTION

Head movements are similar to arm movements about the elbow in dynamics and time scales (Lehman 1983) and are of interest because of their interactions with eye movements, posture, and perception. Zangemeister, et. al., 1981a-e, have studied head movements and their involvement in shifts of gaze, the eye's position in space. They have also quantified the dynamics of time-optimal horizontal head rotations in terms of the peaks of the dynamical variables position, velocity, and acceleration and plotted them in the Main Sequence diagram to show the relationship between dynamics and movement magnitude

Interest in the control mechanisms involved in head movements has lead to the study of the electromyographic activity of neck muscles involved in these movements (Zangemeister, Stark, Meienberg, & Waite & Stark, Hannaford et al. 1983) and to efforts to model the system.

* On Leave: Department of Electronics Engineering, Kwang Woon University, Seoul, Korea

PRECEDING PAGE BLANK NOT FILMED

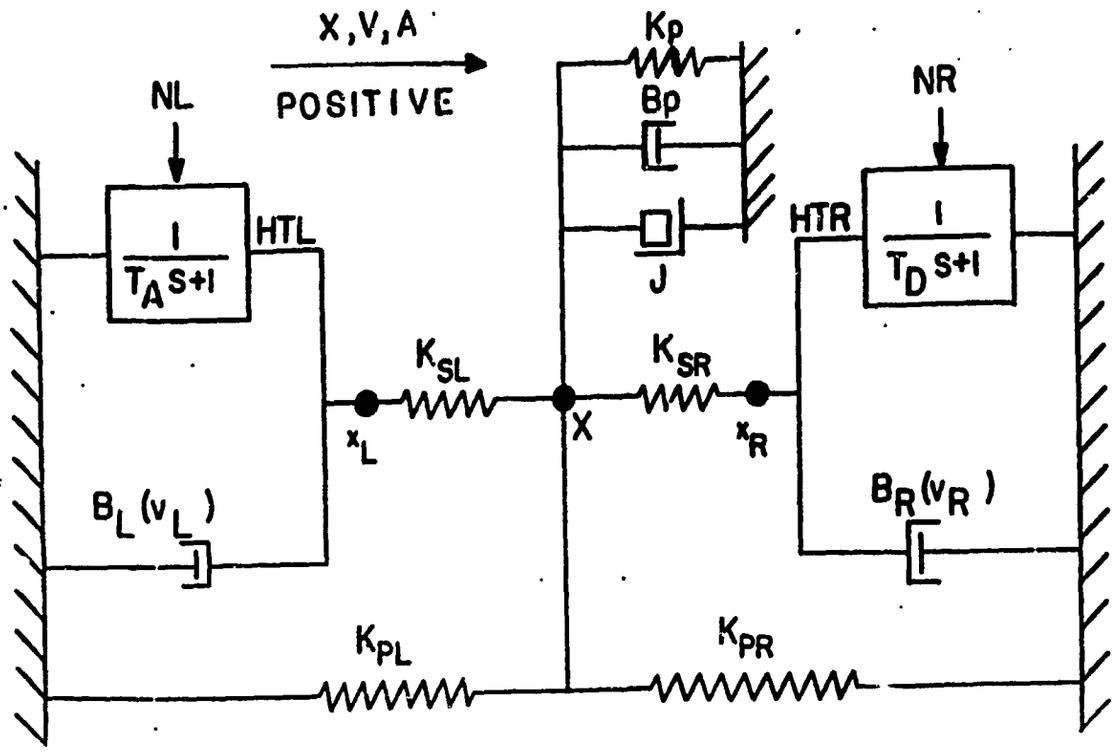

Figure 1

6th Order Non-Linear Model of the head rotation system.

Zangemeister Lehman and Stark (81ab) simulated the muscles and plant of the head movement system with a 6th order non-linear model incorporating Hill's force-velocity relationship, two antagonist muscles, and an overdamped second order plant (Figure 1). Their model matched experimentally measured Main Sequence dynamic peaks when driven by heuristically derived control signals. Versions of this model have had a fruitful history of application to many different physiological systems. Stark (1961) proposed and Atwood et. al. (1961) simulated a two-muscle model for understanding neurological control mechanisms. Cook & Stark (1968), and Clark & Stark (1975) used more detailed versions with appropriate parameter values to model saccadic and other eye movements, and it has been applied to the eyelid in modeling the dynamics of the blink (Kim, et. al. 1984b).

In some cases, it is possible to invert a numerical model and obtain controller signals as a function of dynamics. Cook (1965) linearized the model and obtained a closed form solution to the inverse problem. Recently, Kim, et. al.(84a) has developed an iterative method which has been applied to the non-linear model of the eye-movement system. An adaptation of this technique was used in the present work.

METHODS

Experimental

Horizontal head position was measured by a precision potentiometer attached to a bicycle helmet frame worn by the subject. To allow for vertical head movement and subjects of differing heights, the potentiometer was coupled to the head through a compliant fitting which unfortunately resulted in a delay of about 50 ms. between actual and recorded head position.

Electromyographic activity was measured differentially with two S&W number 737 self-adhesive Ag-AgCl disposable electrodes placed approximately 5cm apart on the skin along the major axes of the left and right splenius capitus muscles. EMG and position data was digitized at 1000 Hz by an LSI 11-23 computer with 12 bit analog to digital converters (Hannaford et.al. 1983).

The subject's head movements were made in response to light emitting diode (LED) targets alternately flashing at points on a curved screen 1 meter from the subject's head. The subject was aware of the exact position of his head by a small spot of light projected from his helmet onto the screen. When the target illumination alternated between the two positions, (at intervals of 4 seconds) the subject performed 20, 40, and 60 degree horizontal head movements.

The subjects were instructed to move their heads "as fast as possible" to produce an intent to respond to the target in a time-optimal manner. This experiment resulted in stereotyped movements which could be ensemble averaged along with their

rectified EMGs.

In a separate experiment, the targets were set 40 degrees apart and the subject was given different instructions for movements in the two different directions. For movements to the right, the subject was asked to make time-optimal movements as in the first experiments. For the leftward movements, he was instructed to move "however you want." Of the many and varied leftward movements that resulted from this paradigm, two leftward movements occurring directly after each other (with one time-optimal rightward movement between them) were selected for analysis.

Modeling

For simulation of the horizontal head rotation system, we used the sixth-order non-linear model developed by Zangemeister, Lehman, and Stark (1981ab). This model consists of two identical, antagonistic muscle elements driving a second order plant (Figure 1). The muscle elements have a force generator driven through a first order low pass filter representing the calcium activation process. The control signals, nl and nr, range from zero to one to represent the possible range of excitation from none to full excitation. To help the reader's intuition, we have plotted this signal in equivalent kilograms to suggest the steady state force that would result from constant excitation at a given level. In parallel with the force generator is a non-linear viscous element representing the Hill's force-velocity relationship (Hill, 1938). Force is transmitted to the load through a series elastic element representing the properties of muscle tendon and attached cross-bridges.

This system is modeled and simulated by a set of 6 state equations and two ancillary equations (Table 1). The values used for the parameters (Table 2) are based on previous work (Zangemeister, Lehman & Stark, 1981a) and recent, improved estimates (J.M. Winters, private communication).

State Equations

$$\dot{x} = v$$
$$vl = (htl - ks(xl-x)) / bl$$
$$vr = (-htr- ks(xr-x)) / br$$
$$a = (-kp\ x - bp\ v + ks\ (xl - x) + ks(xr - x)\ ) / j$$
$$dhtl = (nl-htl)/ta$$
$$dhtr = (nr-htr)/ta$$

Ancillary Equations

$$bl = \begin{cases} (1.25\ htl) / (bh + vl) & vl > 0 \\ 1.25\ htl / 900. & vl < 0 \end{cases}$$

$$br = \begin{cases} (1.25\ htr) / (bh + vr) & vr < 0 \\ 1.25\ htr / 900. & vl > 0 \end{cases}$$

TABLE 1
Equations for the sixth order non-linear model of horizontal head rotation.

- - -

Name	Symbol	Value	Units
Parallel Viscosity	bp	2.0	gr-f $deg^{-1}sec$
Activation Time Const.	ta	50.0	milli seconds
Hill's Constant; b	bh	350.0	deg sec^{-1}
Rotational Inertia	j	0.18	gr-f $deg^{-1}sec^2$
Series Elasticity	ks	350.0	gr-f deg^{-1}
Parallel Elasticity	kp	2.0	gr-f deg^{-1}

TABLE 2
Model Parameter Values.

Inversion by Iteration of Forward Model

The simulations typically undertaken with such a model involve applying various control signals at the model's inputs (the neurological force commands to the muscles, nl and nr, are presumably a product of firing rate and recruitment) and observing the model's output; position, velocity, and acceleration time functions. In this study, we reversed the process, obtaining the control signal as a function of experimentally recorded movement dynamics.

To do this, we used an iterative method which, at each time sample, involves finding the control signal values which result in model output that exactly matches the experimentally recorded

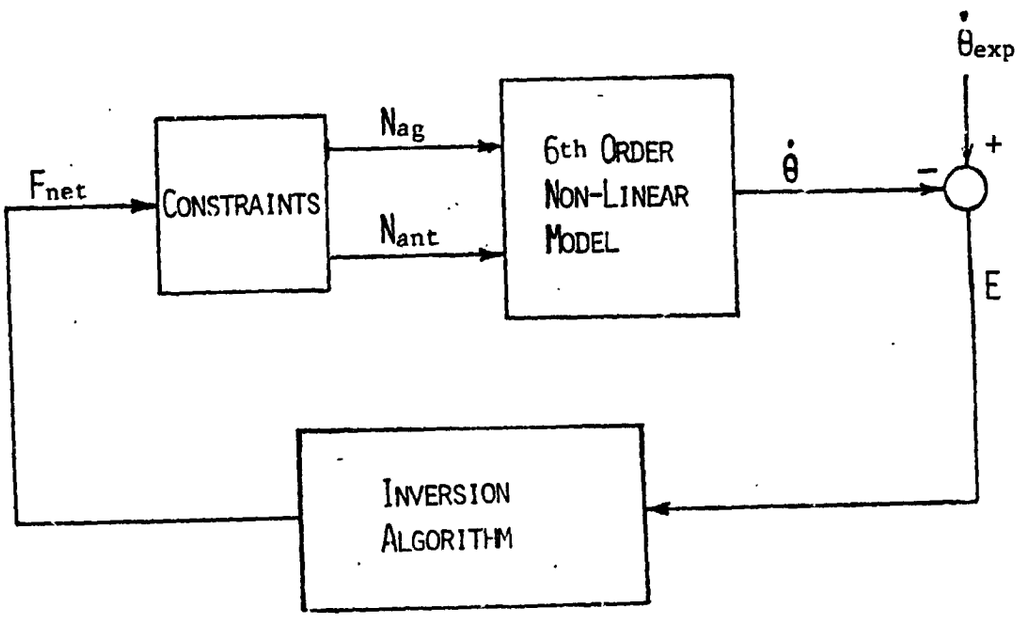

Figure 2

Block diagram of iterative model inversion process.

dynamics at that time (Figure 2). When these control signal values are obtained, the state variables are updated and the process is repeated for the next time sample. Several issues arise which must be resolved before this computation can be performed.

Because the system has only one measurable output, head position only one independent variable can be obtained by inversion of the model. In order to use an iterative method to minimize the difference between model output and experimental data, the two model inputs, agonist and antagonist control signals must be constrained to be a function of this single variable. In these simulations, the independent variable was net force (fnet) and the constraint used was:

$$\begin{aligned} f_{agonist} &= fmin + fnet \qquad fnet > 0 \\ f_{antagonist} &= fmin \end{aligned}$$

$$\begin{aligned} f_{agonist} &= fmin \qquad fnet \leq 0 \\ f_{antagonist} &= fmin + fnet \end{aligned}$$

where fnet = 80 grams-force (the small, minimal force level, fmin in each muscle is necessary for stability of the simulation). Although this constraint does not allow co-contraction, that is simultaneous activation of both muscles, other constraints are possible which do. This constraint was suggested by the absence of co-contraction shown in the EMG recordings we analyzed.

Iteration Methods

With net force driving the model through the constraints and generating agonist and antagonist force commands, the problem becomes to find the value of net force for which

$$E = 0$$

where

$$E = V_h(t) - V_m(t,fnet)$$

and $V_h(t)$ is head velocity as a function of time over ($0 < t < tmax$), and $V_m(t,fnet)$ is the model output as a a function of fnet and its previous values. Solving this equation for each value of t from 0 to tmax yields net force as a function of time. By applying the constraint, we then have agonist and antagonist force control signal as a function of time.

The method initially used to solve this equation at each time sample was an adaptation of the Newton-Raphson method in which fnet was iterated until the value of E was less than a small epsilon. After E was calculated for two values of fnet, the new estimate for fnet is

$$fnet_{j+1} = \frac{E_{j-1}f_j - E_j f_{j-1}}{E_{j-1} - E_j}$$

where j is the iteration number.

Although this method was effective, it occasionally failed to converge when $V_m(t,fnet)$ was sufficiently non-linear as a function of fnet. It was subsequently found that a binary search method would guarantee convergence of the algorithm.

In this second method, an initial range of values is selected between which it is assumed must lie the correct value of fnet. This range can easily be determined by taking the maximum expected force value and allowing fnet to vary between that value both above and below zero. The first estimate in this procedure is zero. Then each subsequent estimate is improved by an increment equal to the maximum value divided by a larger and larger power of two. If the value of E resulting from this new estimate of fnet is negative, the next increment is subtracted from fnet. If it is positive, it is added. Convergence relies on the assumption that E crosses zero at least once at some value of fnet between the initial guesses, an assumption which can always be made true by widening the initial range at a slight expense in convergence time.

Numerical precision

Compared to the eye movement system (Kim et al, 1984a), the head movement system has very long time constants; a step change in controller signal results in a very small instantaneous change in head velocity. Also, small amounts of noise, including quantization noise, in the velocity signal will require large changes in the control signal in order for the model output to match this noise. Thus attention must be paid to numerical precision and filtering if this calculation is to be successful. In our computations, we used double precision arithmetic for all calculations of state variables, ancillary equations, and system error, E. Furthermore, we filtered the input data to produce a double precision result with a sufficiently small amount of noise and quantization error. Filtering did not result in appreciable changes in movement dynamics.

Filtering and Effects of Bandwidth

Filtering of head movement trajectories was necessary to reduce undesired measurement and quantization noise. For this smoothing operation, a Hamming window, zero-phase-delay, low pass filter was used (Rabiner & Gold, 1975). The frequency response of the ideal low pass filter is

$$H(jw) = \begin{cases} 1 & \text{for } -wc < w < wc \\ 0 & \text{elsewhere} \end{cases}$$

where wc is the desired cutoff frequency. The filter we used is

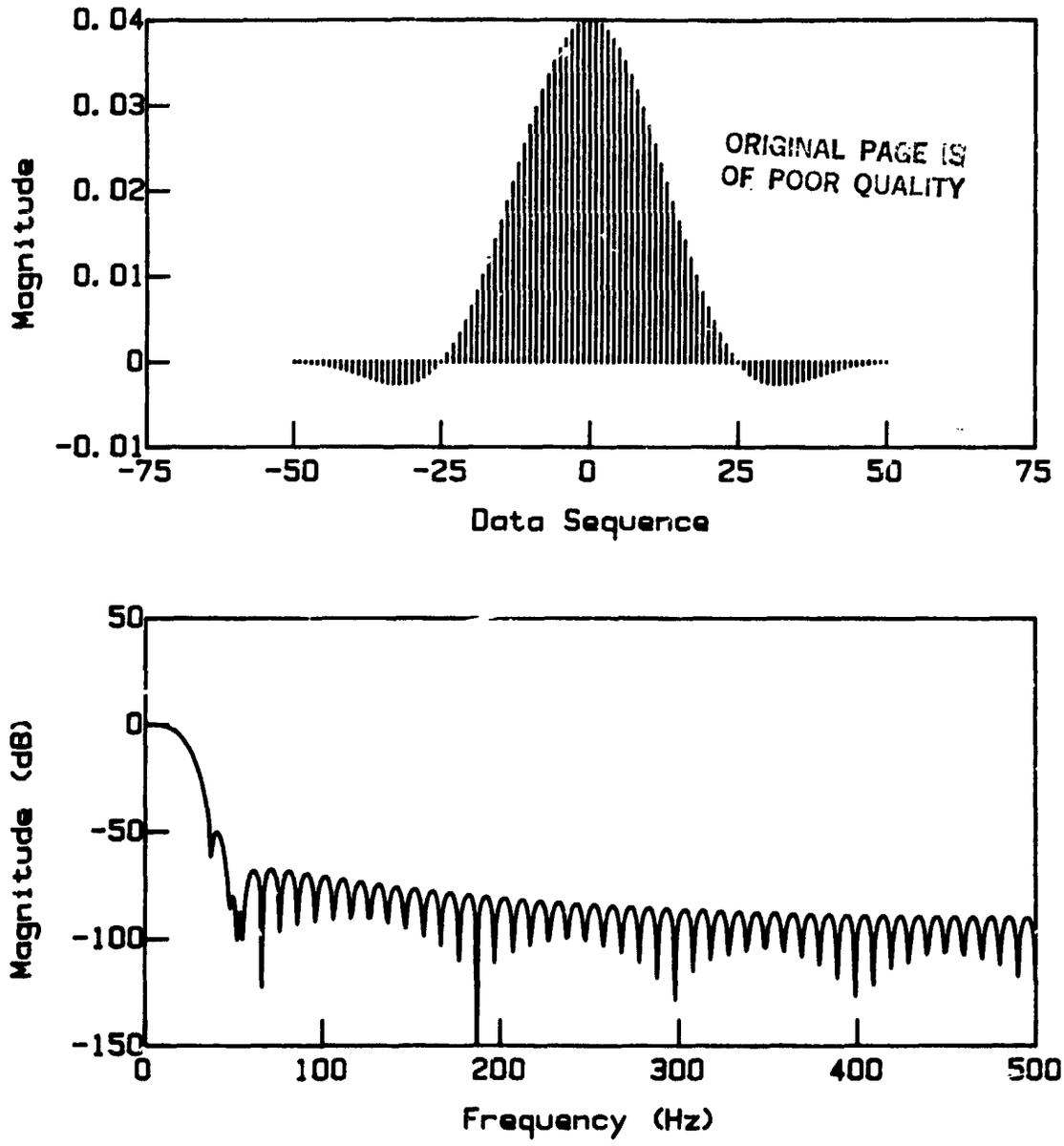

Figure 3

Smoothing of movement dynamics necessary for model inversion was performed with a [illegible] point Hamming window low pass filter. Impulse response of this filter (top) is symmetrical about zero to eliminate phase delay. Frequency response (bottom) shows sharp cutoff at 20 Hz.

one which comes close to this ideal response. The impulse response of the ideal low pass filter is

$$h(n) = \frac{\sin \frac{n\ wc}{ws}}{pi\ n}$$

where ws is the sampling frequency. The ideal impulse response extends to infinite values of n. The Hamming window is employed as a finite weighting sequence on the infinite ideal impulse response to produce smooth truncation. The weighting function of the Hamming window is

$$w(n) = 0.54 + 0.46 \cos(2pi\ n/\ N), \qquad -N <= n <= N$$

where N is the number of data points for the truncation window. The modified impulse response weighted by the Hamming window is

$$hw(n) = h(n)\ w(n).$$

The output sequence y(n) of the Hamming window low pass filter is given by the convolution of the input sequence with the modified impulse response hw(n). Note that hw(n) is symmetrical with respect to hw(0). The filtered output sequence y(n) can thus be described by a finite difference equation as;

$$y(n) = hw(0)\ x(n) + hw(1)\ (x(n-1)+x(n+1)) + hw(2)\ (x(n-2)+x(n+2)) + \ldots .$$

For smoothing the position and velocity trajectories, we used a Hamming window low pass filter of 100 data point with a cutoff frequency of 20 Hz at a sampling rate of 1000 Hz (Figure 3).

RESULTS

Time Optimal Movements

We prepared 3 ensemble averages of fast movements at amplitudes of 20, 40 and 60 degrees (n = 5). Velocity and acceleration traces show amplitude-dependent peak values characteristic of time-optimal movements (Figure 4). Full-wave-rectified EMG activity from agonist and antagonist muscles was also averaged (Figure 5). The EMGs exhibit the tri-phasic burst pattern found in fast movements about several different joints (Wachtolder, Angel, Ghez & Martin, Litvintsev & Seropyan, Wadman, van der Gon, & Derksen, Hannaford et. al., 83, Cheron & Godaux). It is difficult to quantify signals of this type in terms of height and width. However, as a function of movement magnitude, they seem to vary more in width than in amplitude although PA, the first

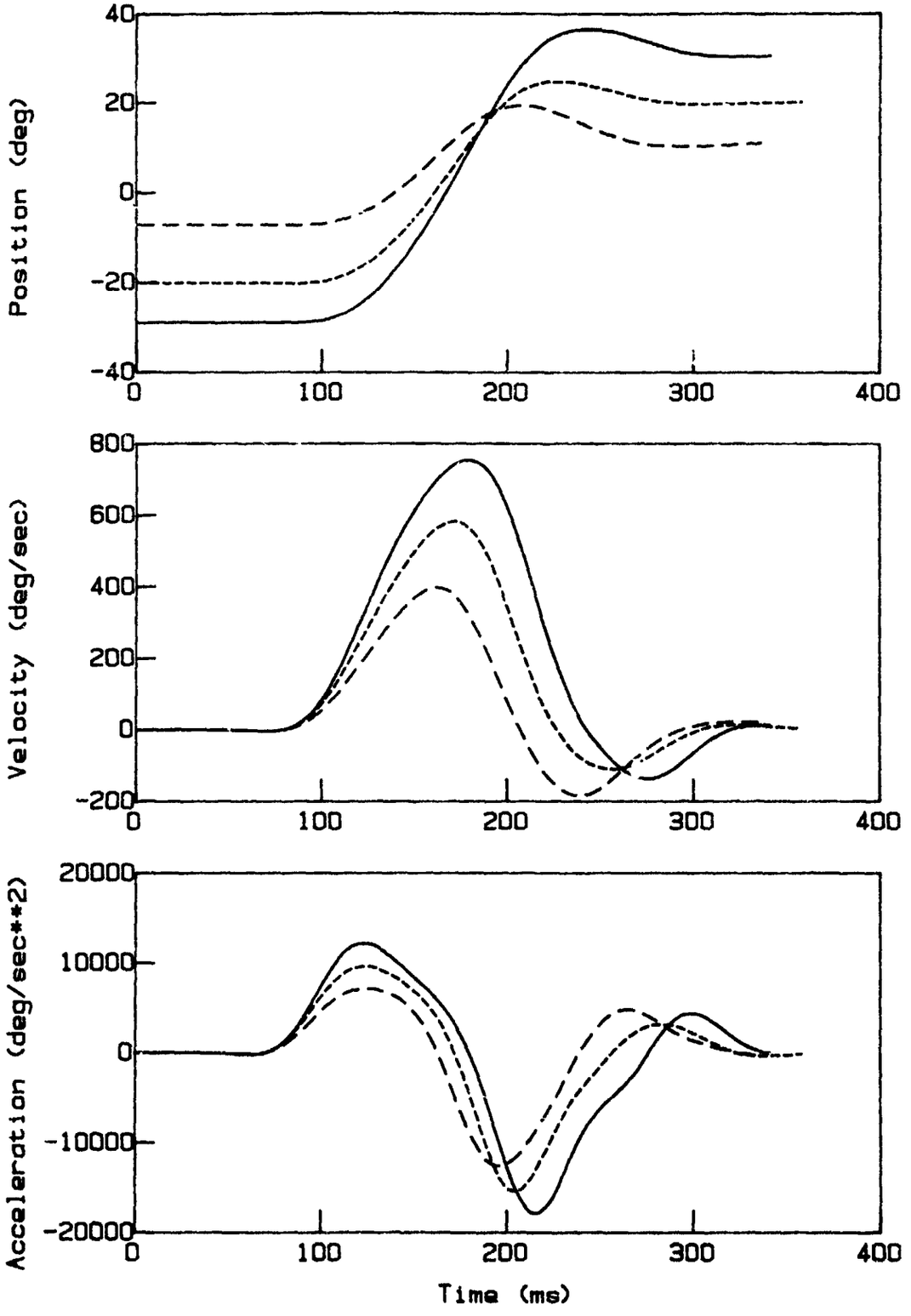

Figure 4

Three ensemble averages of time-optimal horizontal head movements of 20, 40, and 60 deg. (n=5). Also shown are velocity (middle) and acceleration (bottom) computed from the filtered data.

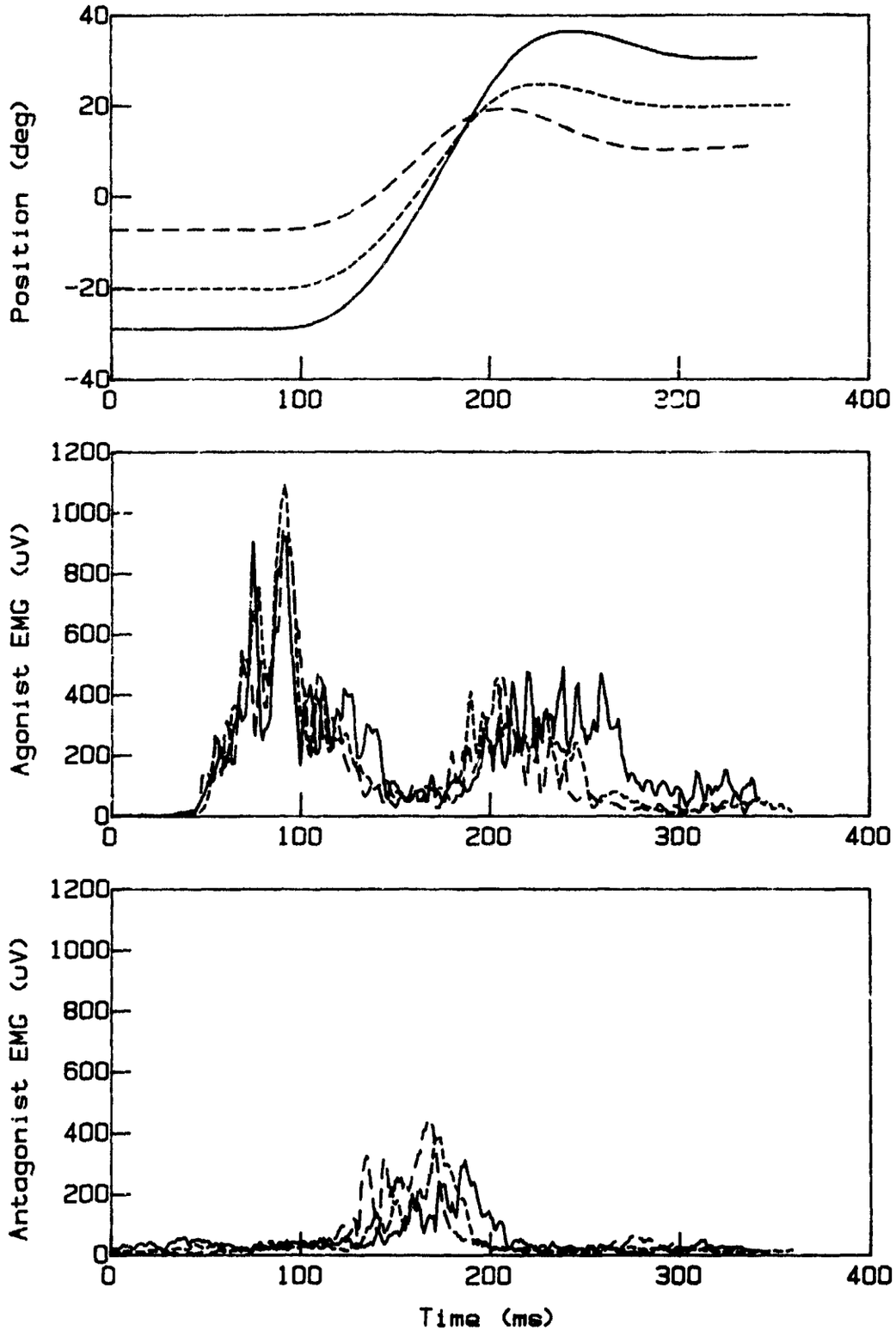

Figure 5

Rectified and averaged EMG's, taken from left and right splenius capitus muscles, during same time-optimal movements as in figure 4.

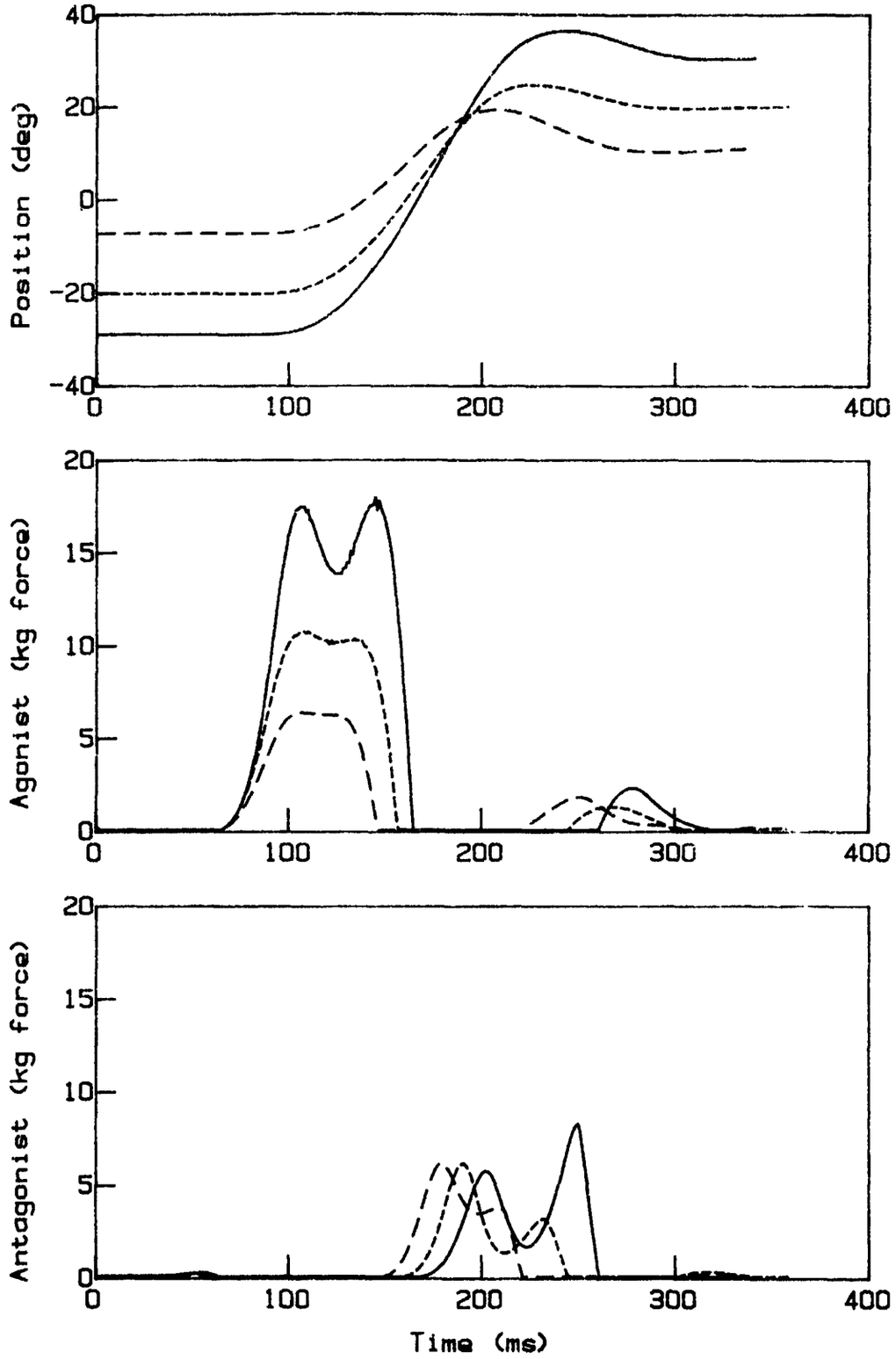

Figure 6

Controller signals obtained by inverse modelling of the three time optimal movements of figures 4 and 5. Three pulses of excitation are seen which correspond to the three EMG pulses

agonist EMG burst reaches a peak value about twice that of PB and PC.

The result of the inverse modelling process is a pair of control signals describing the excitation levels of the antagonistic muscle pair for each of the three movement magnitudes. This signal (Figure 6) also shows the tri-phasic pattern, having an initial agonist burst followed by a burst of antagonist activity and finally a second antagonist burst. PA, the first agonist pulse, increases from 75 to 100 ms in width and from 6 to 17 equivalent kilograms (kge) in amplitude as movement magnitude increases from 20 to 60 degrees. PB ranges from 70 to 100 ms in width and has a relatively constant amplitude of about 6kge except for a second peak of about 8 kge in the 60 degree case. PC appears to be fairly constant at about 40 ms in width and about 2 kge in amplitude. The skew evident in PB and PC is due to the concatenation of the three pulses; as longer pulses are concatenated, later pulses are delayed appropriately.

Comparison of the EMG records with controller signals resulting from the inversion shows a delay of about 30 ms. between EMG and control signal resulting from delay in the head position measurement apparatus not accounted for in the model. The width of PA, the first agonist EMG burst matches well with the first agonist control signal pulse for all three magnitudes. The antagonist excitation pulse shows the same increase in onset times (of roughly 10 ms./20deg) with movement magnitude as does PB, the antagonist EMG burst. But each antagonist control signal pulse is longer than the corresponding EMG pulse. While the EMG pulse, PA is of roughly constant amplitude, the first control signal pulse amplitude varies over a three to one range with movement magnitude.

PC, the second agonist EMG burst, is of roughly constant amplitude but its width varies strongly with movement magnitude from about 60 to 75 ms. Width of the third control signal pulse is difficult to ascertain because of its approximately exponential decay, but unlike the PC of the EMG, its amplitude is quite small relative to the first pulse at all three magnitudes. A hypothetical linear relationship between EMG magnitude and control signal magnitude would suggest that the third control signal pulse have an amplitude roughly half of that of PA but in fact, it is much less. This may suggest that the model is too viscous during the later phase of the movement, requiring less active damping than does the real system.

A Pair of Slow Movements

Figure seven depicts two double movements. These single records (not averages) were taken of the subject on successive leftward rotations under instructions to move "however you want to". Both records begin with a movement of approximately 15 degrees to the left which is of insufficient amplitude to reach the target. The peak velocity of this movement was 210 deg/sec for the solid and 220 deg/sec for the dashed record. A second deflection of the

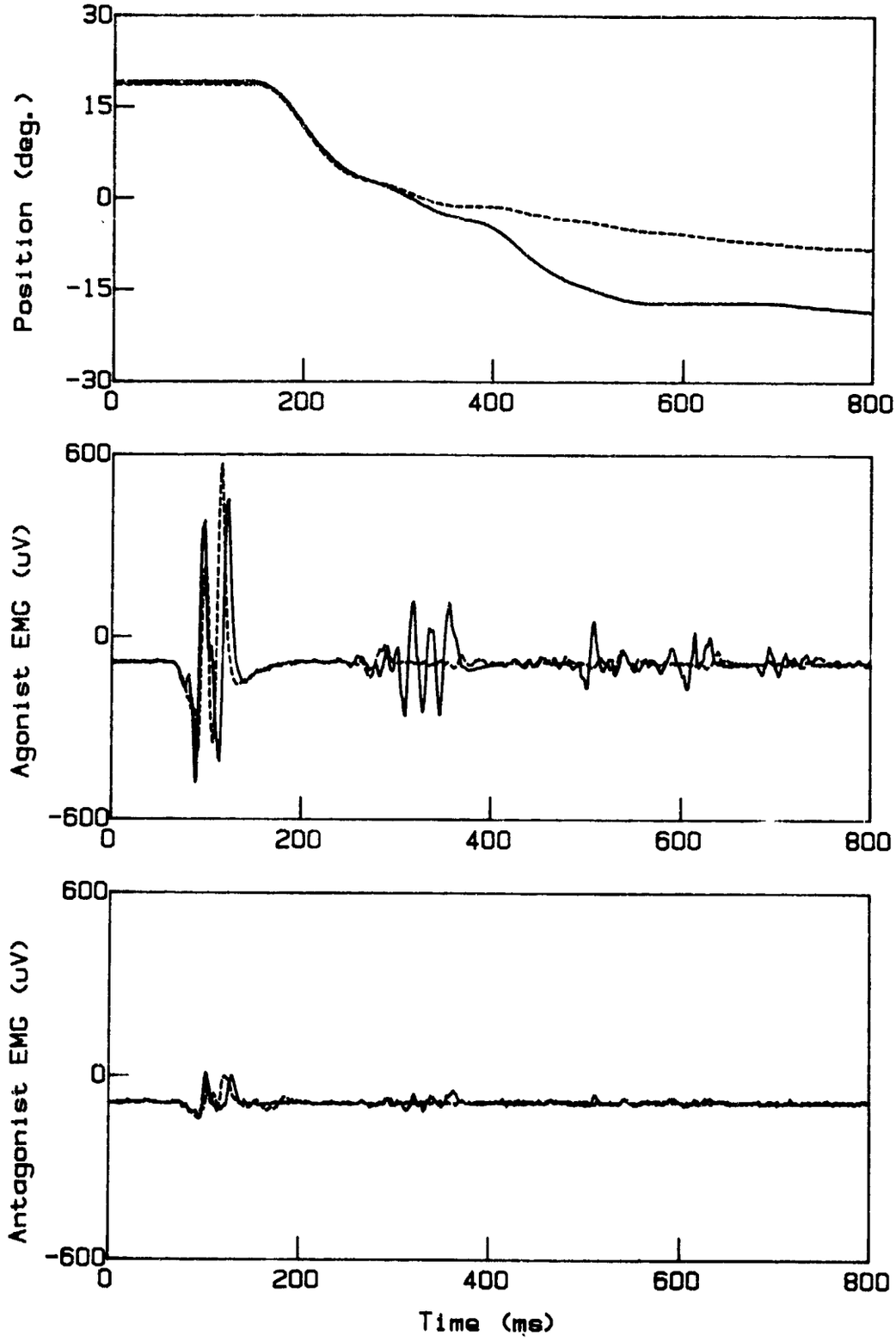

Figure 7

Records of two double movements and their EMG's. First movement is nearly identical in both records while a second, corrective, movement appears in the later record (solid trace) about 240 ms. after the first. Note similarity in duration, amplitude and number of pulses of EMG bursts causing first movement, and divergence of EMG's as dynamics diverge.

position trace appears about 100 ms. later. About 220 ms after the first movement, the subject made a second, corrective movement to cover the remaining distance. The solid record makes a discrete corrective movement of about 15 deg. with a velocity peak of 135 deg/sec. In the dashed trace, there is instead a drift at an approximately constant velocity of about 20 deg/sec. The first movement is nearly the same in both records while the second movement is of larger amplitude and velocity in the second of the two records (solid trace).

An initial burst of agonist EMG is seen in both records. These bursts are similar in amplitude, duration, and number of spikes. The antagonist channel shows a small amount of EMG activity due to either cross-talk or a small amount of co-contraction. No antagonist EMG activity appears after the initial agonist burst (PA). The second EMG burst is much more prominent in the second record (solid) and the corresponding second movement is greater.

Control signals were calculated using the inverse model on the velocity trajectories of the two records (Figure 8). The calculated control signals consist of a series of rounded, roughly triangular pulses, the first and largest ones resulting from the initial movement in both records. These pulses have a peak force value of about 5 kge. with the dashed pulse slightly greater coresponding to the slightly greater peak velocity. Both pulses are about 60 ms in duration. The slight difference in peak force corresponds to the slightly faster time course of the first movement in the first record (dashed lines). The control signal obtained by the inversion contains 6 subsequent, smaller, pulses of activity in the agonist and 6 in the antagonist.

The second agonist pulse (about 1 kge peak force, and about 50 ms duration) corresponds to the slight increase in velocity seen about 100 ms. before the start the second movement. 220 ms after the initial agonist burst, the second movement is initiated by another burst of agonist activity. Here, as the dynamics diverge between the two records, a larger agonist burst (3 kge vs less than 1 kge peak force and 60 ms vs 50 ms pulse width) appears in the later (solid) record corresponding to the larger movement.

Small pulses of antagonist force follow immediately after each agonist pulse and immediately precede the next agonist pulse. These pulses are not present in the EMG records and their presence may be due to the fact that the filtering of the dynamics results in slight dynamical changes requiring a smoothly changing or "ringing" control signal. Another possibility is that since no co-contraction is possible because of the control signal constraint, active damping may be required of the control signal to make up for lack of an active viscosity due to co-contraction but no co-contraction is evident in the EMG. Finally, it may be that other neck muscles such as the left and right sterno cleido mastoid may be activated at these times. Recording of additional EMG channels may clarify this possiblity.

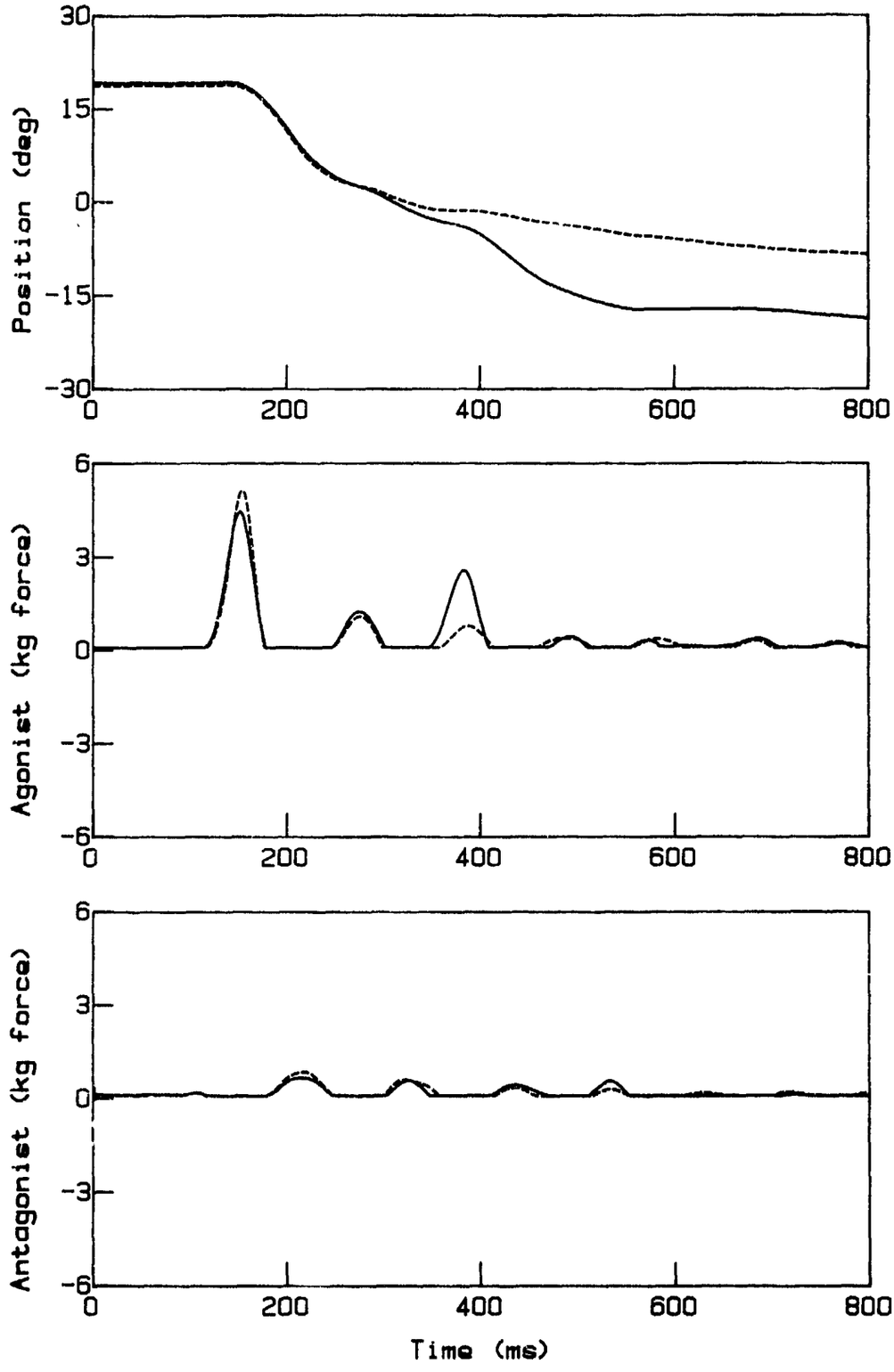

Figure 8

Control signals obtained by inverse modelling of two slow movements shown in figure 7. Timing shift between EMG's (fig. 7) and control signal pulses (this fig.) is due to time delay in experimental apparatus. Extra pulses of controller signal activity may be due to lack of co-contraction imposed by controller signal constraint, or activity of other neck muscles, not recorded in fig. 7.

DISCUSSION

Inversion of the head model is an interesting problem in numerical analysis. Because of the long time lags involved, the problem is near to being ill conditioned (Rice, 1984). Use of FORTRAN's double precision arithmetic was required both for the computation of state variables and for the results of the data filtering against which model output was matched.

Algorithms for solving for a zero of the output error function E must be sufficiently able to deal with the non-linear behavior of the model to guarantee convergence in a reasonable amount of time. A binary search algorithm was found to always converge but to take more time, in many cases, than a successive approximation method based on the Newton-Raphson algorithm. A suitable improvement would be a successive approximation method generating a rough estimated range, followed by a binary search to guarantee convergence and full double precision accuracy.

Another area for further study is that of the controller signal constraints by which net force is converted to agonist and antagonist control signals. The constraint used in this study was suggested by the fact that appreciable co-contraction was not evident in the EMG records from time-optimal movements. Cook (1965) and Kim, et.al. (1984a) in inverting the eye movement system have used another possible constraint, which specifies a given amount of co-contraction in terms of a ratio of antagonist to agonist excitation. For example, if the co-activation level is set to 20%, and the excitation level required is 1, then the agonist would be set to 1 and the antagonist to 0.2. It will be interesting to recompute the above results with this type of constraint and assess the effect of co-contraction level on antagonist activity in the slow movements.

The inverse modeling process is an aid to understanding the control of skeletal muscle in movements and helps create a conceptual link between EMG and movement dynamics. Completion of this link will yield the ability to predict movement dynamics from a knowledge of the plant and of the EMG signal. The three unresolved steps in this link are the calibration of EMG to excitation; the improvement of experimental apparatus to reduce delays, non-linearities, and frequency dependent effects; and the further elaboration of the subtle non-linearities in the model.

The above process of "Dynamic Calibration" would be a step toward an ideal EMG signal processor in the sense that the response of the Hamming window low pass filter approaches that of the ideal low pass filter. So far, the only signal processor to adequately interpret the EMG is still the living muscle.

REFERENCES

1. Angel, R.W., "Myoelectric patterns associated with ballisitic movement: effect of unexpected changes in load.", J. Human Movement Studies Vol. 1, p.96-103, 1975

2. Atwood, J., Elkind, J., Houk, J., King, M., & Stark, L. "Digital Computer Simulation of a Neurological System.", Quarterly Progress Report; Research Laboratory of Electronics, MIT, Oct. 15, 1961.

3. Cheron, G., & Godaux, E., "Ballistic Movements in Man: Pre-Programmed Activities and Reflex Influences", Pre-print 5/84

4. Clark, M. & Stark, L. "Time Optimal Behavior of Human Saccadic Eye Movements", IEEE Trans. Automatic Control, Vol AC 20, 1975 p. 345-348

5. Cook, G., "Control Systems Study of the Saccadic Eye Movement Mechanism," PhD Thesis, Department of Electrical Engineering, Mass. Inst. of Technology, 1965.

6. Cook, G., and Stark, L., "The Human Eye Movement Mechanism: Experiments, Modeling, and Model Testing," Archives of Opthalmology, vol. 79, p428-436, 1968.

7. Ghez, C., & Martin, J.H., "Control of Rapid Limb Movement in the Cat. III. Agonist-Antagonist Coupling." Exp. Brain Research. Vol. 45 pp 115-125, 1982.

8. Hannaford, B., Maduel, R., Nam, M.H., Lakshminarayanan, V., and Stark, L.,"Effects of Loads on Time-Optimal Head Movements: EMG, Oblique, and Main Sequence Relationships," Proceedings of the 19th Annual Conference on Manual Control, MIT, June 1983.

9. Hannaford, B., Nam, M.H., Lakshminarayanan, V. & Stark, L., "EMG as Controller Signal with Viscous Load," Journal of Motor Behavior, submitted 5/83 revised 10/83 accepted 11/83.

10. Hill, A.V., "The Heat of Shortening and Dynamic Constraints of Muscle," Proceedings of the Royal Society, London, Vol. 126, pp.136-195, 1938.

11. Kim, W.S., & Stark, L., "Inverse Modeling to Obtain Neurological Control Signals of the Non-Linear Eye Movement Model.", In Progress., 1984a.

12. Kim, W.S., & Stark, L., "Inverse Modeling to Obtain Neurological Control Signal in the Blinking Eye.", In progress. 1984b.

13. Lehman, S.L., & Stark, L., "Perturbation Analysis Applied to Eye, Head, and Arm Movement Models," IEEE Transactions on Systems, Man, and Cybernetics, Sept. 1983.

14. Lehman, S. & Stark, L., "Simulation of Linear and Nonlinear Eye Movement Models: Sensitivity Analysis and Enumeration Studies of Time Optimal Control", J. Cyber. & Inf. Sci. vol. 4

15. Litvintsev,A.I., & Seropyan, N. S., "Muscular Control of Movements with One Degree of Freedom: I Single Movements" Avtomatika i Telemekhanika, no. 5, pp. 88-102, May, 1977

16. Rabiner, L.R., & Gold, B., "Theory and Application of Digital Signal Processing.", Prentice-Hall, Inc. 1975. pp. 75-105

17. Rice, J.R., "Numerical Methods, Software, and Analysis", McGraw Hill, 1983

18. Stark, L., "Neurological Organization of the Control System for Movement.", Quarterly Progress Report #61, Research Laboratory of Electronics. MIT, April 15, 1961. pp. 215-217

19. Wachholder, K., Altenburger, H.,"Beitrage zur Physiologie der willkurlichen Bewegung.", 10 Einzelbewegungen Pflugers Arch Ges Physiol Vol. 214, pp 642-661, 1926

20. Wadman, W.J., van der Gon, J.J.D. & Derksen, R.J.A., "Muscle activation patterns for fast goal directed arm movements," J. Hum. Move. Stu., Vol. 6, 1980, p. 19-37.

21. Zangemeister, W. H., & Stark, L., "Dynamics of head movement trajectories: Main Sequence Relationship," Exp. Neuro., Vol. 71, 1981a, p. 76-91.

22. Zangemeister, W. H., Lehman, S., & Stark, L., "Sensitivity analysis and optimization for a head movement model," Biol. Cybern., Vol. 41, 1981b, p. 33-45.

23. Zangemeister, W. H., Lehman, S., & Stark, L., "Simulation of head movement trajectories: model and fit to main sequence," Biol. Cybern., Vol. 41, 1981c, p. 19-32.

24. Zangemeister, W.H. & Stark, L., "Active head rotations and eye head coordination," Annals N.Y. Acad. of Sci., 1981d, p. 540-559.

25. Zangemeister, W. H., Stark, L., Meienberg, O., & Waite, T., "Neurological control of head rotations: electromyographic evidence," J. Neurological Sci., Vol. 55, 1982, p. 1-14.

N85 14526 D39

A CONTROL MODEL: INTERPRETATION OF FITTS' LAW

Edward M. Connelly

Performance Measurement Associates, Inc.
1909 Hull Road
Vienna, Virginia 22180

ABSTRACT

Fitts' law has been universally cited as an index of difficulty or predictor of movement time (MT) for rapid aiming tasks since it was first published in 1954 (Fitts 1954). Many researchers report a remarkable correlation of Fitts' law and the observed movement times in aiming tasks. Other researchers report discrepancies, however, between observed movement time and the law, especially at low and high movement times, which correspond, respectively, to short movements to a large target, and long movements to a small target.

These discrepancies suggest that while the law predicts MT well for some human motions, the true basis for the law may not be known, and, as a consequence, that there may exist conditions where its application is appropriate and yet others where different laws should be used.

Fitts suggested the law as a model of the rate-limit of human information processing and movements. According to that view, the movement-problem is characterized by one half the target width (i.e., the target center-point is the aiming-point and 1/2 the target width is the error tolerance) and the movement amplitude. According to Fitts, the total movement amplitude (A) can be regarded as N units, where each unit consists of 1/2 the target width, which are "processed" by the human at a maximum rate. Hence, as the target width (W) is decreased or A is increased, the "difficulty" and MT of the task both increase. Further, if A is increased and the target width is also increased, making their ratio constant, the task difficulty and MT are constant. The remarkable ability of the law to predict these results suggests that its functional form is appropriate for at least some movement problems.

But this rate-limit model is not the only interpretation possible. Rapid movement of the hand to a target can be modeled from a different view-point: namely, as a control system. This paper gives the analytical results for several models: a first order model where it is assumed that the hand velocity can be directly controlled, and a second order model where it is assumed that the hand acceleration can be directly controlled. Two different types of control-laws are investigated. One is a linear function of the hand error and error rate; the other is the time-optimal control law.

The results show that the first and second order models with the linear control-law produce a MT function with the exact form of the Fitts' law. These models assume that the control-law aims for the center of the target, but that the motion is actually stopped when the edge of the target is reached. This corresponds to the situation in which the lateral hand movement is directed toward the center of the target and in which, if it were not for the vertical movement which causes the hand to hit the target at the target edge, the lateral movement would asymptotically approach the target center as time approaches infinity.

This control-law interpretation produces a formula for index of difficulty identical to Fitts' law, and yet it has nothing to do with information theory. It says, for instance, that the lateral hand motion is not (necesarily) a function of target width, but is instead a constant linear control function independent of target width. The control-law interpretation thus implies that the effect of target width on MT must be a result of the vertical motion which elevates the hand from the starting point and drops it on the target at the target edge. The control law interpretation further suggests that many movement time experiments may be inadequate because the end point conditions, such as the vertical and horizontal velocities, are not controlled but are allowed to vary.

The time optimal control law did not produce a movement-time formula similar to Fitts' law. However, the formula may be found to apply in yet other situations.

INTRODUCTION

Fitts' law has been cited as a predictor of movement time or an index of difficulty for rapid aiming tasks as well as other selected tasks. In 1954, Fitts published a theory of task-difficulty in which the movement time (MT) for a hand-position task was given as:

$$MT = K \log \left(\frac{A}{W/2} \right) \qquad A \geq W/2 \qquad (1)$$

where the log is log base 2, A is the movement amplitude, and W is the target width.

The rationale Fitts presented for this formula developed an analogy between the rapid positioning task and Shannon's information theory. According to that rationale, one half the target width is the target error tolerance. The movement amplitude divided by this error tolerance gives the number of "tolerance units" that must be considered for the motion. The base 2 logarithm of the number of tolerance units is the number of bits i.e., the amount of information to be processed. Fitts reported that the correlation between the actual, measured MT and the formula was .99. While these early results were obtained for serial, self-paced tasks, Fitts later, in 1964 (Fitts and Peterson 1964), showed that the formula also applied to discrete tasks.

Welford (1968) found that Fitts' law fits experimental data well except for near-zero movement times and except for the tendency of the data at the high end of the scale (i.e., for large movement times), where Fitts' law predicts a straight line function (i.e., a straight line on a log plot), to "curve gently upwards". Welford presents a number of alternative constructions of Fitts' law, including

$$MT = K \log \left(\frac{A}{W} + \frac{1}{2} \right), \qquad A \geq \frac{W}{2} \qquad (2)$$

in order to better fit the data.

Drury (1975), in studying foot pedal designs, found that both Fitts' law and the Welford formula provided a good fit to the data, with the correlation coefficient for either being of the order

of .98. Drury found that Welford's formula provided a somewhat better fit to his data, but also found a deviation for the higher movement times, where a "gentle upward curve" again appeared.

More recently, Buck (1983) proposed a modification of Fitts' law to include the effect of target location in addition to movement amplitude.

Wallace and Newell (1983) report results supporting the notion, corollary to the division of the movement amplitude into "tolerance units," that Fitts' law represents a discrete corrections model. This model assumes that the movement to the target consists of a series of discrete submovements each involving a visual error correction.

Jagacinski, Repperger, Ward, and Moran (1980) attempted to apply Fitts' law to the capture of moving targets. They found that target velocity interacts with the movement amplitude A and, consequently, that the law should be modified to include target velocity.

Sheridan and Ferrell (1974) discuss the development of Fitts' law and its information-theoretic basis. They recognize the empirical support for the law, but also state that the information-theoretic argument is "not entirely satisfying."

The researchers cited above are but a few of those who have systematically used Fitts' law in their work. Their conclusions are cited to illustrate a point: Although some researchers find Fitts' law to be highly correlated with a prescribed task MT, others find that the formula must be revised or that additional factors must be introduced.

These inconsistencies suggest that the true basis for the law may not be known, and, further, that there may exist conditions under which the law is valid and other conditions under which the law is simply not appropriate. Specification of the application-rules for the law would facilitate its correct use. Further, an investigation of the appropriate applications of the law may guide us to new laws or to a more general task-difficulty measure, representing difficulty or MT in cases where Fitts' law does not apply.

The Control-Law Derivation of Fitts' Law

The remarkably high correlation with observed data in some movement problems serves as a first clue. The log function suggests that the movement is described by an exponential solution i.e., by a function of time that exponentially approaches the steady state solution as time approaches infinity. Exponential solutions typically result from control policies where the hand velocity or acceleration is controlled as a smooth function of hand error (distance from the center of the target) and error rate. In contrast, however, to rapid aiming tasks, in which finite movement times are observed, exponential solutions require an infinite time to reach steady state.

In actual situations there is always a finite target tolerance: the motion does not need to proceed to the target center. It may stop at the target edge or anywhere in between the target edge and the target center. Such a situation, translated into mathematical terms, provides a log-solution time-function combined with a finite MT.

As an aid in presenting the mathematical development given below, consider the following aiming task. The task is to move the hand rapidly from a starting position on a table to a target, which is also on the table (see Fig. 1). The control strategy for the LATERAL portion of the hand movement can take several forms, which are described subsequently, but is assumed, in all forms, to be a linear function of error alone, or of error and error rate. Error is the instantaneous distance from the hand to the center of the target. The target center is the "aiming" point of the lateral motion i.e., the lateral hand motion is such that, if not disturbed by the vertical hand motion hitting the target, the lateral hand motion would come to rest at the target center. The vertical motion directs the hand upwards and then downwards so that the hand or a hand-held pen actually hits the edge of the target, causing the hand to stop.

In order to illustrate the mathematical development for a simple control law, assume that the lateral-movement control-law is such that the error rate ($\dot{X}$) is a linear function of the error (X):

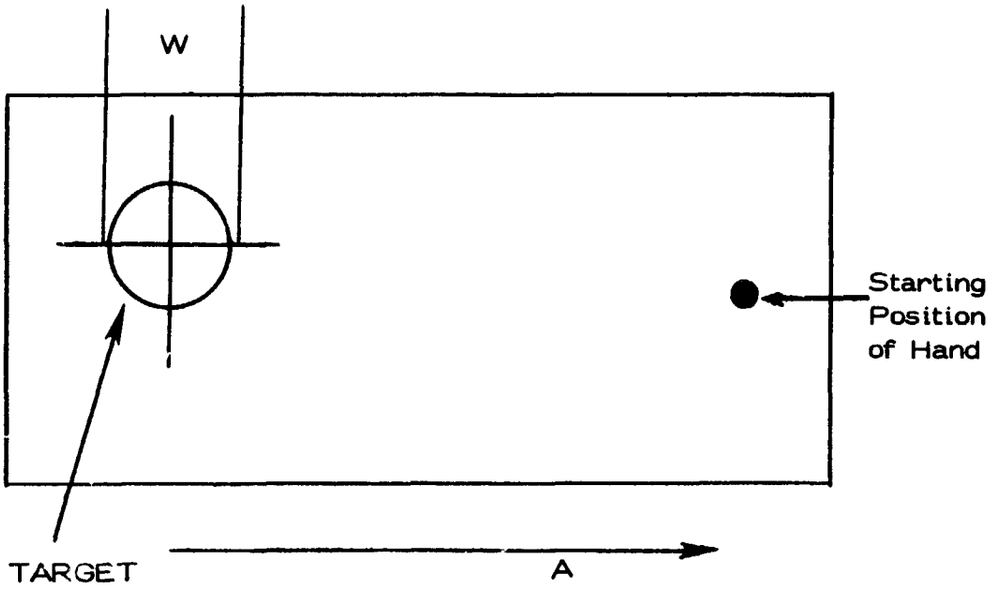

Figure 1. Hand-to-Hand Motion in Perspect.ve

$$\dot{X} = -KX, \qquad K > 0 \tag{3}$$

The solution to this equation is:

$$X(t) = X(0)e^{-Kt} \tag{4}$$

Taking the log (base 2) of both sides yields

$$\log (X(t)/X(0)) = -Kt \log(e) \tag{5}$$

Solving for t gives

$$t = c \log (X(0)/X(t)), \text{ where } c = 1/K \log(e) \tag{6}$$

Now, we recognize that X(0) is really the movement amplitude A and X(MT) is really the "error" at movement time MT, when the hand is stopped at the edge of the target.

That is,

$$X(0) = A$$

$$X(MT) = W/2 \tag{7}$$

Thus,

$$MT = c \log (2A/W), \tag{8}$$

which is the same equation as Fitts law.

As shown in the Appendix B, the same equation is obtained, except for an additive constant, when a second-order model is used with a linear control law.

Appendix C gives the MT for a "time-optimal" control-law where maximum force is applied laterally until the hand is stopped at the edge of the target. The MT equation then has the form:

$$MT = \sqrt{\frac{2\,|A-W/2|}{F}} \tag{9}$$

where F is the maximum force that can be applied to the hand and | | indicates absolute value.

Thus, even though the task is described as a "rapid" movement task, the control strategy actually used is apparently not a time optimal (i.e., a minimum time) strategy.

Theoretical Consequences

Now considering that the first and second order models using linear control laws produce MT functions that are similar or identical to Fitts' law, there exists a control-law interpretation of MT for rapid motions. There are, of course, numerous models and control laws, both linear and non-linear, that can be formulated. The key model and control-law feature may be that the lateral hand movement is governed by a smooth function of error and error rate i.e., by a control law that will tend to bring the hand error and error rate to zero simultaneously at the target center. This provides the log function for MT.

Evaluation of the control-law interpretation can be accomplished by examining data revealing the lateral and vertical position of the hand as a function of time and by computing the control-law employed. If the control-law has constant coefficients (see equation 3), a simple control-law interpretation of MT will then exist. If the computed control-law has varying coefficients along the trajectory, then another model -- perhaps a non-linear model accounting for a non-linear muscle function, or a higher order model -- must be investigated.

The control-law model says that MT is determined by the LATERAL hand motion, since it is the lateral motion that determines where the hand will be as a function of time -- for instance, when the hand will be at the target edge. The accuracy of the hand's final resting position is governed by the VERTICAL motion, which might be a ballistic response for short MT, where ballistic parameters are fixed early in the movement, or a scheduled response for longer MT, in which vertical hand movement is coordinated with lateral hand-position error via feedback.

The control-law model also says that the LATERAL hand response path as a function of time (see equation 4) is actually independent of the target width. Yet, for a fixed movement amplitude A (i.e., a fixed distance from the initial hand position to the center of the target), a smaller target width requires a longer MT (see equation 8) because the hand has a greater actual

traveling distance. This suggests that the term "index of difficulty" is misapplied since the same response path as a function of time is used for a constant amplitude A but varying target width W. Since the hand is moving with an ever decreasing velocity as the target center is approached, the time per unit distance is increasing. Consequently, small changes in target width result in large changes in MT.

Further, the control-law model says that one system differential equation explains the lateral hand movement for all amplitudes A. Different initial positions, corresponding to various amplitudes, result in different paths as a function of time; but, once a differential equation is accepted as a model for the task, it represents the hand movement for values of A and W.

The observations presented above lead naturally to the concept that the LATERAL-movement differential equation may be that suggested by spring-mass theory. As explained by spring-mass theory, muscle parameters determining final hand position are preset prior to actual movement. According to this theory, the "springs" are set so that the target center is the "final position" for lateral movement (i.e., the final position of the hand, if it were not stopped at the target edge by the vertical hand motion). Thus, there is a direct correspondence between spring-mass theory and the control-law interpretation of MT for lateral hand motion.

A further observation resulting from the control-law is that different constants are expected as multipliers of the log term as different parts (systems) of the body are used to move the hand or hand-held pointer. Thus, for short A, when only the fingers are used, one constant value is appropriate. When the wrist, and/or arm, and/or shoulder, and/or torso are used, other constants are appropriate. When a consistent set of these systems is used an appropriate set of representative constants can be determined.

But how is the constant adjusted as various systems or system combinations are used to perform a task? This problem may be the reason that Fitts' law often fails for short and long MT. For it would seem appropriate that the scaling of the amplitude factor A would be a function of all the systems used to perform the task, but that the scaling of the target width $\left(\frac{W}{2}\right)$ would be a function of only the system (or systems) used during the terminal portion of the task.

In conclusion, an alternative interpretation of Fitts' law has been identified in the control-law model. Its advantage over the information theoretic approach to Fitts' law is that its application-rules can be easily established, and, further, that the formula arising from it can be easily modified as different types of motions or combinations of types of motion are considered.

APPENDIX A

1st Order Model: Linear Control Law

Assumption: Operator can control the lateral velocity of the hand directly* and moves laterally toward the center of the target, but stops when the edge of the target is reached. The hand is stopped instantaneously because the hand or hand-held pen hits the target edge.

*Direct control of the hand's lateral velocity assumes that any acceleration required (even an infinite acceleration) can be provided to establish the desired velocity.

Equation of Motion:

$$\dot{X}_1 = -KX_1, \qquad (1)$$

where X_1 is the lateral error, i.e., the distance of the hand from the target, and

K is a constant.

Solution as a function of time:

$$X_1(t) = X_1(0)e^{-Kt} \qquad (2)$$

Taking log (base 2) yields:

$$\log\left(\frac{X_1(t)}{X_1(0)}\right) = -Kt \log (e) \qquad (3)$$

Solving for t results in:

$$t = \frac{1}{K \log(e)} \log\left(\frac{X_1(0)}{X_1(t)}\right) \qquad (4)$$

Since

$$X_1(0) = A$$

and

$$X_1(MT) = W/2, \tag{5}$$

substitution yields

$$MT = \left(\frac{1}{K \log(e)}\right) \log\left(\frac{2A}{W}\right) \tag{6}$$

or

$$MT = C \log (2A/W), \tag{7}$$

where

$$C = 1/K \log(e).$$

APPENDIX B

2nd Order Model: Linear Control Rule

Assumptions:

1. Operator can control the acceleration of the hand directly (i.e., can apply any force required to establish the desired acceleration.)

2. Operator uses a control rule which is a linear function of error and error rate.

3. Hand is stopped instantaneously at edge of target because hand or hand held pen hits the target edge.

Second order equation

$$\ddot{X}_1 = -2ZN\dot{X}_1 - N^2X_1 \qquad (1)$$

or

$$\dot{X}_1 = X_2 \qquad (2)$$

$$\dot{X}_2 = -2ZNX_2 - N^2X_1 \qquad (3)$$

where X_1 is the error (displacement from center of target)

$\dot{X}_1 = X_2$ is the error rate

Z is damping ratio

N is natural frequency

There are two types of solutions to these equations: One solution, represented by Z less than 1, corresponds to the case where, if the vertical hand motion did not hit the target edge thus stopping the hand, the lateral hand motion would overshoot the target center line before returning to oscillate about the target center line with an asymptotically decreasing oscillation. This response is shown in Figure B1. Assuming that the hand is initially at rest i.e.,

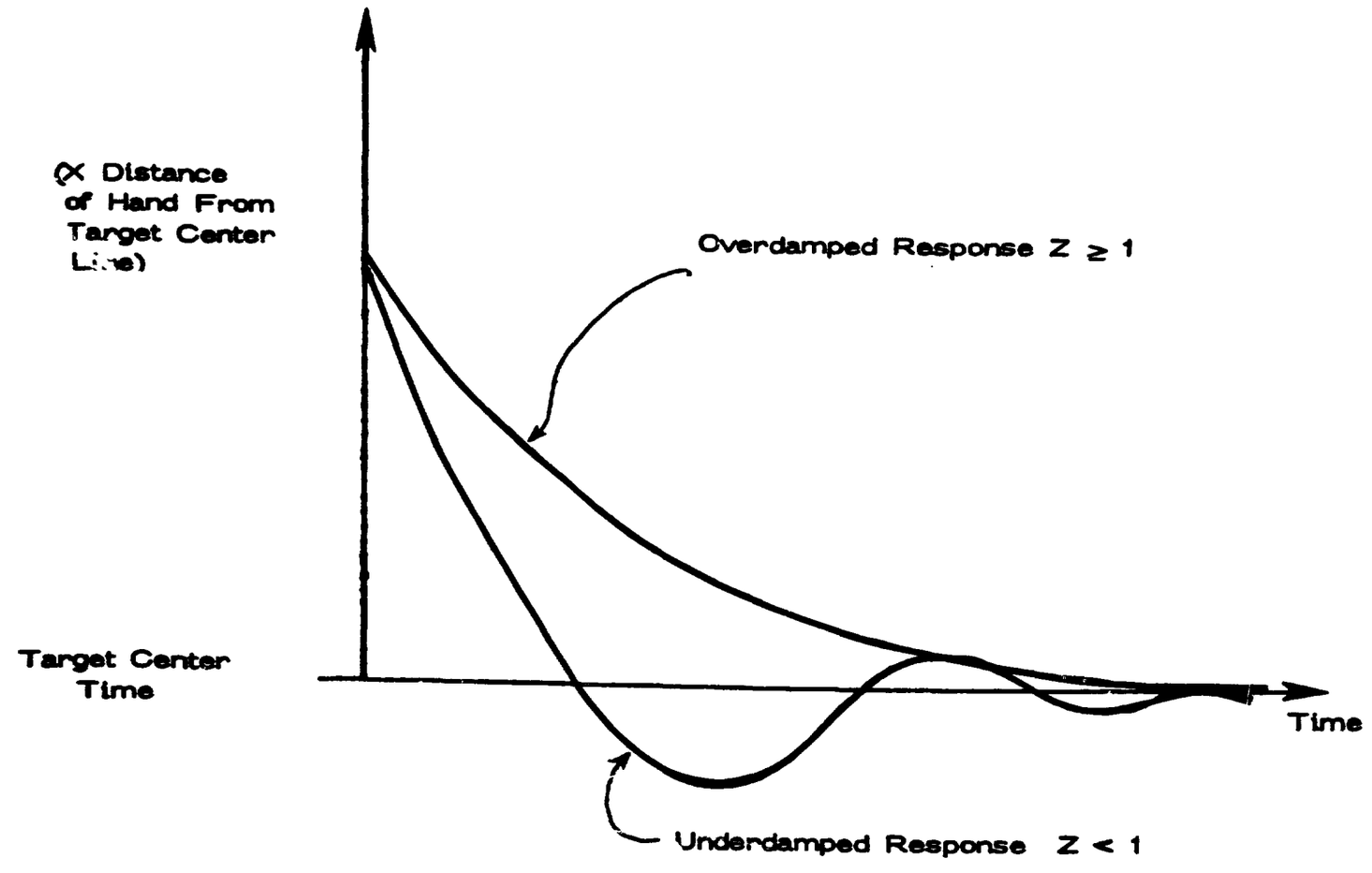

Figure B1. Two Types of Hand Movement

$$\dot{X}_1(0) = 0, \tag{4}$$

the solution to equation 1 or 2 & 3 is

$$X_1(t) = X(0)e^{-ZNt} \sin (N t \sqrt{1-Z^2}\, t + \psi) \tag{5}$$

where ψ is a constant.

Since our interest is computing the time when X_1 is less than the 1/2 the target width and remains within the target inspite of overshoots, we can replace the sin function by its largest value namely: a "1" which yields

$$X_1(t) = X_1(0)e^{-ZNt} \tag{6}$$

then taking the log of both sides

$$\log\left(\frac{X_1(t)}{X_1(0)}\right) = -ZNt \log(e) \tag{7}$$

Since the initial position of the hand is A units from the target center line and at t = MT, the hand is stopped at the edge of the target,

$$X_1(0) = A$$

$$X_1(MT) = W/2$$

thus with the substitutions:

$$MT = C \log\left(\frac{A}{W/2}\right) \tag{8}$$

where

$$C = \frac{1}{ZN\log(e)}$$

The second type of solution referred to above, represented by Z equal to or greater than 1, corresponds to the case where, if the vertical hand motion did not hit the target edge thus stopping the hand, the lateral hand motion would asymptotically approach the target center line without overshoots. This response is also shown in Figure B1.

When $Z \geq 1$, it is convenient to transform the equations with the following.

$$T_1 = 1/T_2N^2 \tag{9}$$

$$T_2 = \left(Z \pm \sqrt{Z^2-1}\right)/N \tag{10}$$

providing:

$$\ddot{X}_1 = -(T_1+T_2)\,\dot{X}_1 / T_1T_2 - X_1/T_1T_2 \tag{11}$$

or

$$\dot{X}_1 = X_2$$

$$\dot{X}_2 = -(T_1+T_2)\,X_2/T_1T_2 - X_1/T_1T_2 \tag{12}$$

Assuming that the hand is initially at rest i.e.,

$$\dot{X}_1(0) = 0 \tag{13}$$

Solving for $X_1(t)$ yields:

$$X_1(t) = X_1(0)\left\{\frac{(T_1-a)}{T_1(T_1-T_2)}\,e^{-t/T_1} - \frac{T_2-a)}{T_2(T_1-T_2)}\right.$$

$$\left.e^{-t/T_2}\right\}\quad (T_1+T_2) \tag{14}$$

$$\text{where } a = \frac{T_1T_2}{T_1+T_2}$$

The second order system has two functions of time as indicated by the two exponential terms. Normally all terms in the equation would be used to calculate the value of X as a function of time. It is possible, however, to calculate an upper and a lower bound of X as follows:

$$\frac{X_1(t)}{X_1(0)} = \frac{T_1+T_2}{T_1-T_2} \left\{ \frac{T_1-a}{T_1} - \frac{T_2-a}{T_2} e^{-C_3 t} \right\} e^{-C_1 t} \quad (15)$$

where

$$C_1 = 1/T_1$$

$$C_2 = 1/T_2$$

$$C_3 \geq 0, \; C_2 > C_1 \quad (16)$$

Now $e^{-C_3 t}$ has a maximum value of 1 and a minimum value of 0.

Thus an upper bound for X is

$$\frac{X_1(t)}{X_1(0)} = \frac{T_1+T_2}{T_1-T_2} \left\{ \frac{T_1-a}{T_1} - \frac{T_2-a}{T_2} \right\} e^{-C_1 t} \quad (17)$$

$$= K_1 e^{-C_1 t}$$

and a lower bound is

$$\frac{X_1(t)}{X_1(0)} = \frac{T_1+T_2}{T_1-T_2} \left\{ \frac{T_1-a}{T_1} \right\} e^{-C_1 t} \quad (18)$$

$$\frac{X_1(t)}{X_1(0)} = K_2 e^{-C_1 t} \quad (19)$$

Thus taking the log (base 2) yields:

$$t = K_3 \log \left(\frac{X_1(0)}{X_1(t)} \right) + K_3 \log K \quad (20)$$

where $K_3 = \dfrac{1}{C_1 \log(e)}$

$K = K_1$ or K_2 for upper, lower bound respectively.

Substituting as before:

$$X_1(0) = A$$

$$X_1(MT) = W/2$$

Yields:

$$MT = K_3 \log \left(\frac{2A}{W}\right) + K_3 \log K \qquad (21)$$

APPENDIX C

Second Order: Time Optimal Control

Assumptions:

1. Operator applies and maintains a constant maximum lateral force to accelerate the hand toward the target.

2. When the edge of the target is reached the hand is instantaneously stopped because the hand or hand held pen hits the edge of the target.

Note: A description of this response is plotted in a phase plane shown in the Figure C1. Also shown in the figure is an alternative trajectory resulting from an alternative strategy. These trajectories show that considerable variation in the control strategy and, consequently, in response time is possible within the task specification because both the lateral and vertical terminal velocities are not limited by the experiment design.

Equation of Motion:

$$\ddot{X} = \pm u \qquad (1)$$

where

$\ddot{X}$ is the second derivative of X

and

u is the applied force

According to assumption 1, u is limited such that $|u| = F$, where $|\ |$ indicates the absolute value and F is the maximum force available.

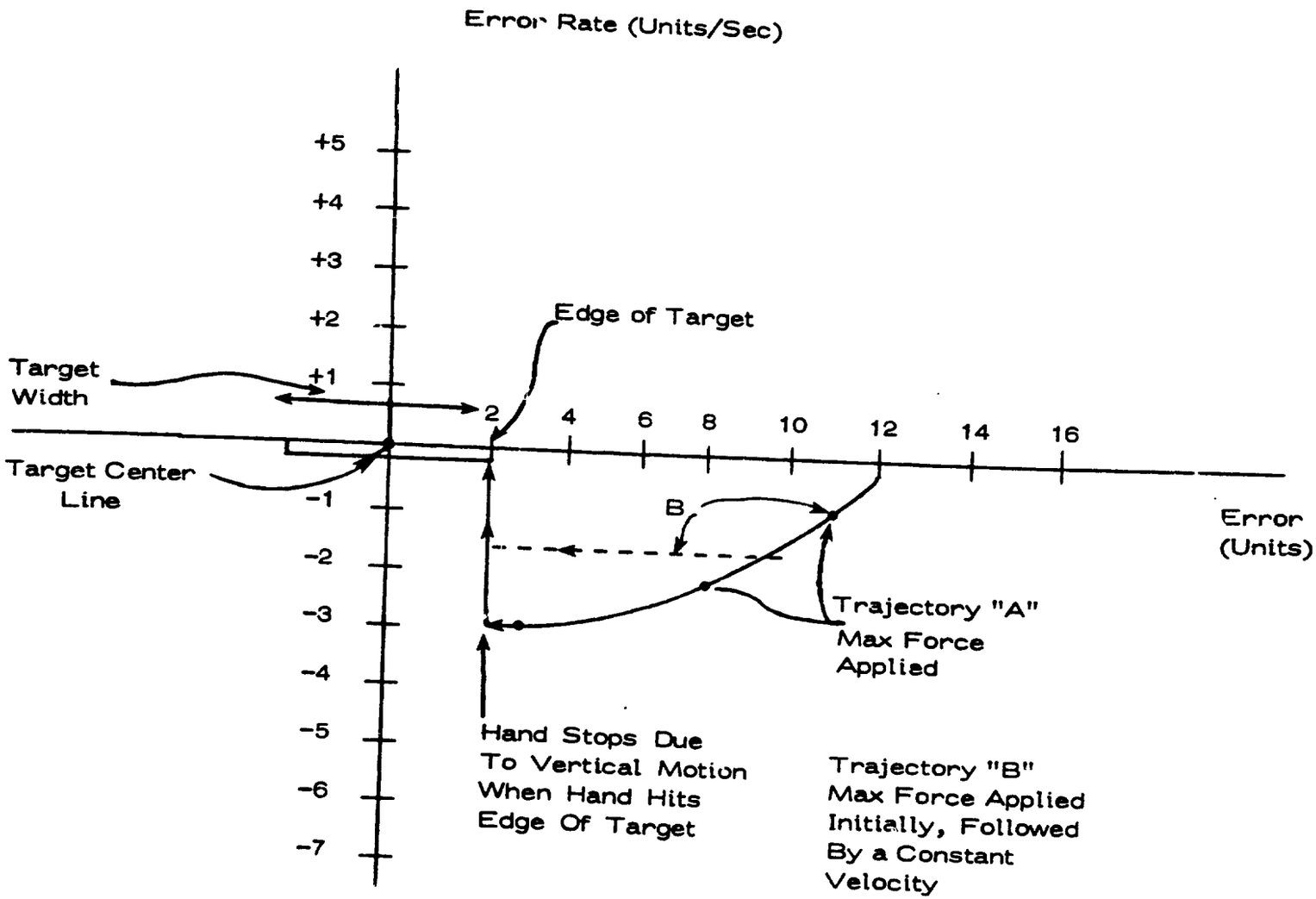

Figure C_1. Phase Plane Trajectories

According to optimal control theory (Elgerd 1967) most rapid motion for the motion system given above, occurs when

$$u = \pm F \tag{2}$$

The solution for any trajectory when F is constant is,

$$X(t) = \frac{u}{2}t^2 + X(0) + \dot{X}(0)t \tag{3}$$

Solving for t yields:

$$t = \frac{-\dot{X}(0) \pm \sqrt{\dot{X}(0)^2 - 2u\,(X(0)-X(t))}}{u}$$

If the hand is initially at rest then:

$$\dot{X}(0) = 0$$

and

$$t = \pm \sqrt{\frac{-2u(X_1(0) - X_1(t))}{u}} \quad ,$$

where

$$u = -F \text{ sgn } (X(0) - X(t))$$

But, as in the analyses given in Appendices A, B:

$$X(0) = A$$
$$X(MT) = W/2$$

Thus,

$$MT = \sqrt{\frac{2|A-W/2|}{F}}$$

REFERENCES

Buck, L. Target location in reciprocal tapping tasks. Psychology of Motor Behavior and Sport 1983, 20, (Abstract).

Drury, C. G. Application of Fitts' law to foot-pedal design. Human Factors, 1975, 17(4), 368-373.

Elgerd, O. I. Control systems theory. New York: McGraw-Hill, 1967.

Fitts, P. M. The information capacity of the human motor system in controlling the amplitude of movement. Journal of Experimental Psychology, 1954, 47, 381-391.

Fitts, P. M. and Peterson, J. R. Information capacity of discrete motor responses. Journal of Experimental Psychology, 1964, 67, 103-112.

Jagacinski, R. J., Repperger, D. W., Ward, S. L., and Moran, M. S. A test of Fitts' law with moving targets. Human Factors, 1980, 22(2), 225-233.

Sheridan, T. B. and Ferrell, W. R. Man-machine systems information, control, and decision models of human performance. MIT Press Cambridge, Mass. 1974.

Wallace, S. A. and Newell, K. M. The use of vision in controlling limb movements which vary in difficulty. Psychology of Motor Behavior and Sport 1983, 63, (Abstract).

Welford, A. T. Fundamentals of skill. London: Methuen, 1968.

N85 14527 D40

THE IMPACT OF PICTORIAL DISPLAY ON OPERATOR LEARNING AND PERFORMANCE

Richard A. Miller, Lisa J. Messing, Richard J. Jagacinski

The Ohio State University
Columbus, Ohio 43210

ABSTRACT

The objective of this study was to investigate the effects of pictorially displayed information on human learning and performance of a simple control task. The controlled system was a harmonic oscillator and the system response was displayed to subjects as either an animated pendulum or a horizontally moving dot. Results indicated that the pendulum display did not effect performance scores but did significantly effect the learning processes of individual operators. The subjects with the pendulum display demonstrated more veridical internal models early in the experiment and the manner in which their internal models were tuned with practice showed increased variability between subjects.

INTRODUCTION

The power of the computer has opened up a wide range of possibilities for displaying information to the human operator and there has been a considerable amount of research on the ergonomics of computer based displays. Intensity, color, and relative size are some of the variables which have been studied. Very little attention, however, has been paid to the effects of the representational form used to present information to the operator.

With the increased capabilities of computer graphics, the options available for pictorial representations are numerous. The state of a chemical process, for example, could be displayed by listing the information in alphanumeric form, drawing pictures of gauges, using coded schematics of the process, or using other pictorial animation.

The purpose of this research was to investigate the effects of the display form on operator performance and learning. A control task involving a simple undamped harmonic oscillator was used to compare two computer generated displays. The system was presented to different subject groups using either an abstract context-free display of a horizontally

moving dot, or a pictorial representation of an oscillating pendulum, presumably a physical system with which most people are familar. The optimal control strategy was identical in each case. The fundamental question of interest was whether the pictorial representation of a system already familiar to the operator would effect his/her performance or behavior.

It is commonly accepted that humans form internal, cognitive representations or models of the "real world" around them. There is no evidence to indicate that these internal models are structurally equivalent to the usual representations of physical systems. Behavioral (input/output) equivalence does not neccessarily indicate structural equivalence. Rasmussen (1983), for example, explains the structures of these internal models on three distinct levels of complexity relating to skill, rule and knowledge based levels of performance. Most theories not only support structural differences but also contend that the human's internal model is often behaviorally non-veridical when compared to the physical system. Larkin (1982) argues that the structure of this internal representation can vary drastically between individuals. In her analysis of expert and naive subject behavior in solving physics problems she describes the internal representations of these two types of subjects as structually different. The expert's "physical representation" is composed of combinations of context-free entities such as forces and momenta. The "naive representation" uses such physical structures as springs, pulleys and blocks as the basic entities from which cognitive representations are formed. In this type of representation the attributes of the entities are influenced by the context in which they appear.

The human operator is assumed to use an internal representation of the system to choose the control actions exerted on a dynamic system. The operator is assumed to have a collection of cognitive representations for existing physical systems which have been built up by experience (i.e., models of pulleys, springs, pendulums, etc.). Therefore, one might expect that if the operator can use one of these existing models, adjustments to a new system can be made quickly by simply adjusting the parameters of this existing model. Pictorial display is one methodology that can be used to "lead" the operator to an existing internal model.

The task used in this study was the same for all subjects but the system was represented as a pendulum to some subjects while for other subjects it was simply a horizontally moving dot. The objective was to determine if performance or learning speed were improved for those subjects given a representational context for which an existing cognitive model of the system dynamics might already exist.

METHOD

Two independent representation variables: (1) pictorial description variations (dot, pendulum), and (2) repeated motion cue variations (repeat, no repeat) were used in this experiment. These independent representational variables were combined in a 2 X 2 combinatorial design, resulting in four pictorial displays: (1) dot display with no repeated motion (DN), (2) dot display with repeated motion (DR), (3) pendulum display with no repeated motion (PN), and (4) pendulum display with repeated motion (PR). Eleven subjects were run under the DN and PR conditions. These were the conditions which provided the operator with the most (PR) and least (DN) amount of information. Five subjects were run under conditions DR and PN.

Experiments were conducted in groups of five or six subjects. For each group, eight right-handed persons (four male, four female, all college students) were screened via a critical tracking task (Jex, McDonnell, and Phatak, 1966) and the five best performers (six best in the two final groups) were selected for the experiment. All subjects were paid $3.00 per day, and an incentive prize of $10.00 was awarded to the subject in each group with the best average score at the end of the ten sessions.

A total of 32 subjects participated in the experiment; two conditions with five subjects each and two conditions with eleven subjects each.

The controlled system was an undamped harmonic oscillator. The equation of motion for this system was as follows:

$$d^2x(t)/dt^2 = -0.16x(t) \pm 0.7112$$

The variable t denotes time in seconds and x(t) the position of the system measured in centimeters. The natural frequency of oscillation of this system is 0.4 radians per second. The term ± 0.7112 defines the two control forces which the operator could use. By pushing a button the operator could switch from the +0.7112 force to the negative one.

The undamped harmonic oscillator system was simulated on a DEC PDP 11/34 digital computer and displayed with a Raster Technology Model One 512 x 512 resolution raster graphics controller. Pixel images were displayed on a Mitsubishi Model C3419 color graphics monitor. The display was viewed on a 29.3 cm x 29.3 cm area with a display grain of approximately 17.5 pixels (or points) per centimeter and was updated at a 30 hertz refresh rate. Subjects were seated 80 cm from the screen and wore headphones over which background white

noise was transmitted. The white noise was briefly interrupted prior to each trial with a 80 db tone for 200 milliseconds to signal the beginning of the next trial.

The system was displayed as a yellow dot 0.69 cm in diameter and the target was displayed as a 1.14 cm red vertical line at the center of the screen. The pendulum display differed from the dot display by drawing a yellow line connecting the center of the dot to an off-screen point 85 cm above the target which represented the center of oscillation. Motion was displayed on the arc formed from this 85 cm radius, causing a slight vertical displacement of the pendulum which reached a maximum of 0.5cm at the extremes of the dot path.

Each trial was initiated with a rightward force applied to the yellow dot (pendulum), with the dot (pendulum) moving to the left. The subject's task was to reverse the rightward force to a leftward force at the point which caused the dot (pendulum) to reach zero velocity at the target. The task was therefore equivalent to a time optimal control problem. The subjects could reverse the applied force by pressing a button with their right index finger. The button was located on an inclined board attached to the right arm of the subjects' chair. A red arrow was displayed on the screen to indicate the direction of the applied force. The magnitude of the force was constant and uneffected by how hard or how long the button was pressed.

After the force was switched the dot (pendulum) continued its rightward motion until it reached zero velocity. At this point the absolute value of the distance from the dot to the target was displayed to the subject as a score for that trial. In cases where no repeated motion was displayed the dot (pendulum) then disappeared from the screen. When repeated motion was displayed the dot (pendulum) continued its motion on the switched trajectory for another full cycle (15.7 seconds) and disappeared when it reached the rightmost position for the second time. If a subject used the well known (Athans and Falb, 1966) time optimal control strategy for this system, the score would be zero.

The subjects participated in one session per day for 10 days. Each session consisted of 84 trials, preceded by 2 additional practice trials. Subjects were given instructions prior to the first session. The 84 trials corresponded to 84 distinct system initial conditions, 7 each on 12 distinct orbits in the phase plane. The initial conditions are shown in Figure 1. The 84 initial conditions for the trials were randomly ordered each day for each subject. Each trial commenced with the word "ready" displayed for 1.5 seconds. The screen was then blanked, and 0.5 seconds later a tone was transmitted over the headphones. At this instant the 0.69 cm

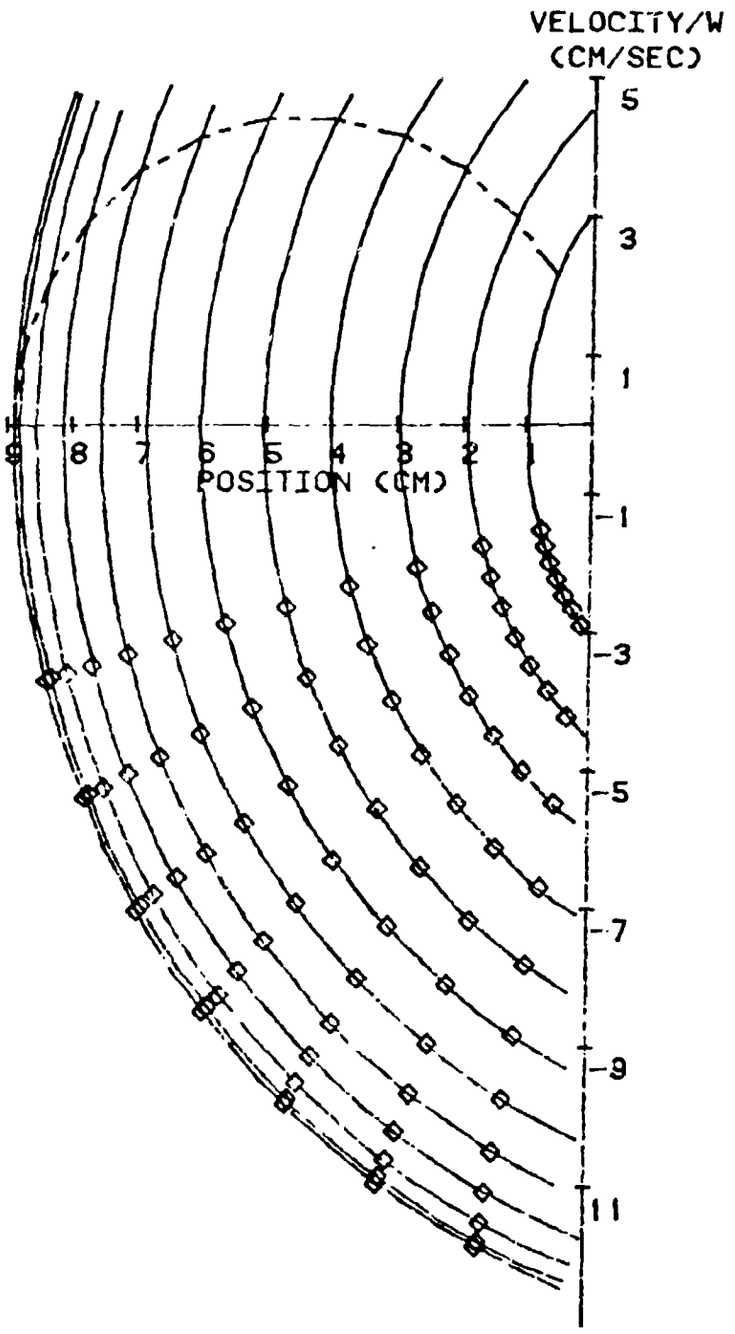

Figure 1

Initial Conditions Used in the Experiment

ORIGINAL PAGE IS
OF POOR QUALITY

diameter dot also appeared on the screen, and the trial began. There was a 5.0 second pause between trials and a two minute rest break after the first 42 trials. Subjects were given 10 seconds to make the force switch. If a subject did not respond within that time limit he/she was alerted by the appearance of the word "timeout" on the screen. The trial was then terminated and a maximum score of 1400 (i.e., 14 cm) was recorded for that subject during that trial.

In addition to feedback scores on each trial, subjects were shown their average score for that session at the end of each session. A graph of these average scores over previous sessions was displayed at the beginning and end of each session. The data recorded for each trial included the initial position and velocity, the position and velocity of the system at the time of the switch, and the switch time measured from the start of the trial.

RESULTS

An initial analysis of performance based on five subjects per group showed that the largest differences occurred between subjects given the most information (pendulum, repeat), and subjects given the least amount of information (dot, no repeat). The sample size for these two conditions was increased to eleven and the analysis was focused on these two conditions. For the purpose the following discussion the group exposed to the pendulum, repeat (PR) condition is refered to as the "pendulum" group and the group exposed to the dot, no repeat (DN) condition is refered to as the "dot" group.

One subject dropped out after three days and was excluded from the analysis. Three subjects, one under the DN condition and two under the PR condition, had an initial basic misunderstanding of the task. This misunderstanding was common to all three subjects. In these three cases, subjects switched the force very early in the trial, while the system was still moving in the leftward direction. These subjects therefore did not have the opportunity to observe the basic oscillatory characteristics of the system, and did not learn for many trials that the direction of motion would reverse at some point even if the leftward force was not applied. All subjects eventually learned this and changed their strategy to allow the system to continue its leftward motion to the turnaround point prior to switching the force. This change in strategy usually occurred several sessions into the experiment, making the comparison of groups on a session by session basis difficult since the impact on learning during these early sessions is not known. Therefore, the data from these subjects were not included in the analysis.

The criterion used to reject a subject data set required

the median locus of switch points to reside entirely in the third quadrant of the phase plane for at least one session. If a subject's performance met this criterion for one session all the data for that subject was omitted from the analysis. Figure 2 contains a phase plane example which met the rejection criterian.

The most obvious evaluation of the effect of the pictorial display on performance is through comparison of the operator feedback scores. Each subject was given a session score which corresponded to the mean of the 84 trial scores for that session.

An analysis of variance was performed for each session comparing the subject session scores of the different groups. While no significant differences were found between the pendulum and dot groups on any day of the 10 days, the mean group score of the dot group was below that of the pendulum group for all 10 days. The lack of statistical significance can be primarily attributed to the high degree of variability from subject to subject. A plot of the mean scores of the groups for successive sessions is presented in Figure 3.

Although the above comparison of operator feedback scores serves as an indication of overall performance in achieving the goal of the task, it gives no insight into the behavioral patterns of performance and how they are effected by the pictorial display. To further investigate the behaviorial differences between groups a more in depth phase plane analysis of switching behavior was conducted.

Phase Plane Analysis of Performance

The 84 initial conditions used during each session were composed of seven points on each of 12 system trajectories or orbits. Since the seven initial conditions lying on a given orbit have the same optimal switch point, the median switching point was calculated from the seven actual operator switching points on each system orbit to obtain a total of 12 median switching points for each day's performance for each subject. This median switching behavior was compared with the optimal behavior on an orbit by orbit basis. This is illustrated in Figure 4 where the locus of median switching points are depicted as data points on each orbit, and the optimal switch curve is displayed as a dashed line.

Any non-optimal switch places the system on a trajectory that reaches zero velocity at some point other than the origin, i.e., the system either undershoots or overshoots the target. In the phase plane, any such trajectory is represented by a circle with center (-4.445,0.0) and a radius either larger (overshoot) or smaller (undershoot) than the optimal 4.445. The difference between the radii of the switch-

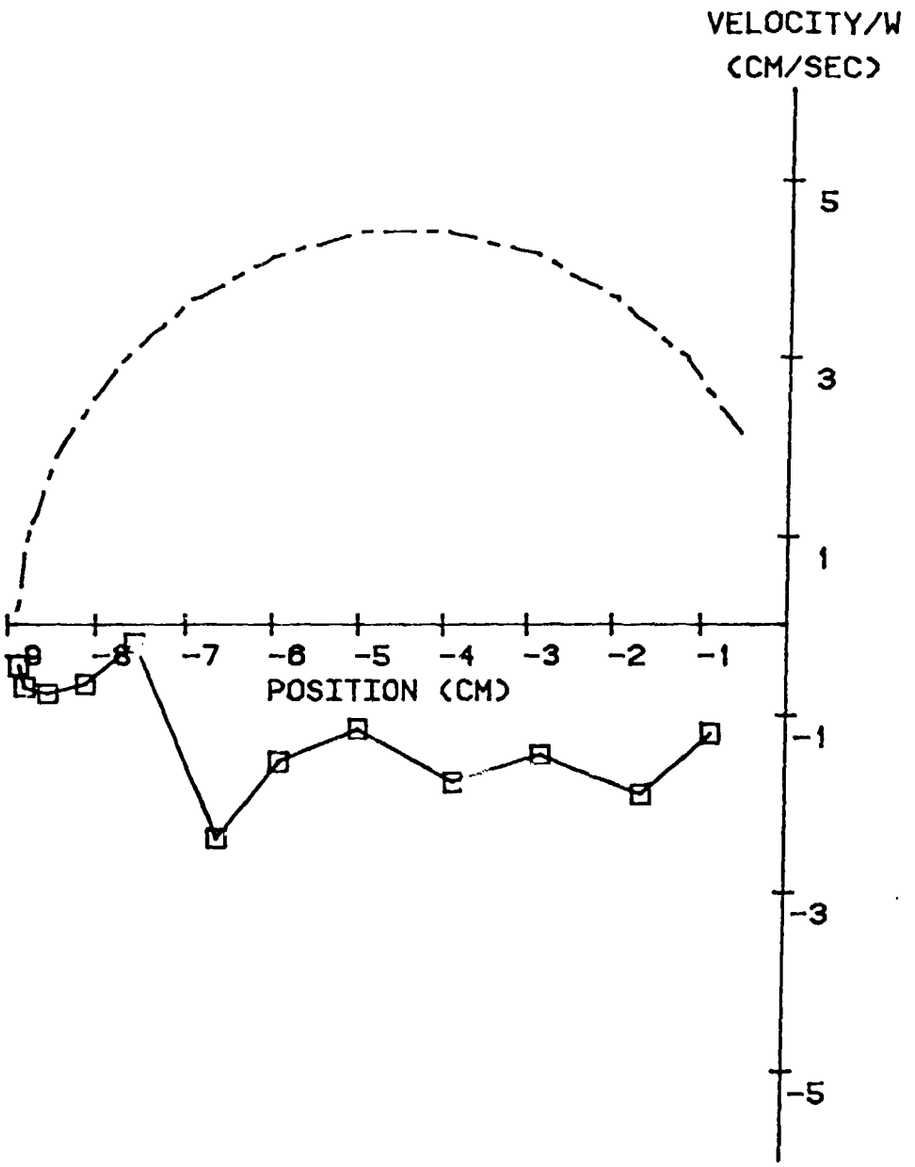

Figure 2

Subject Response Meeting the Rejection Criterion

C-8

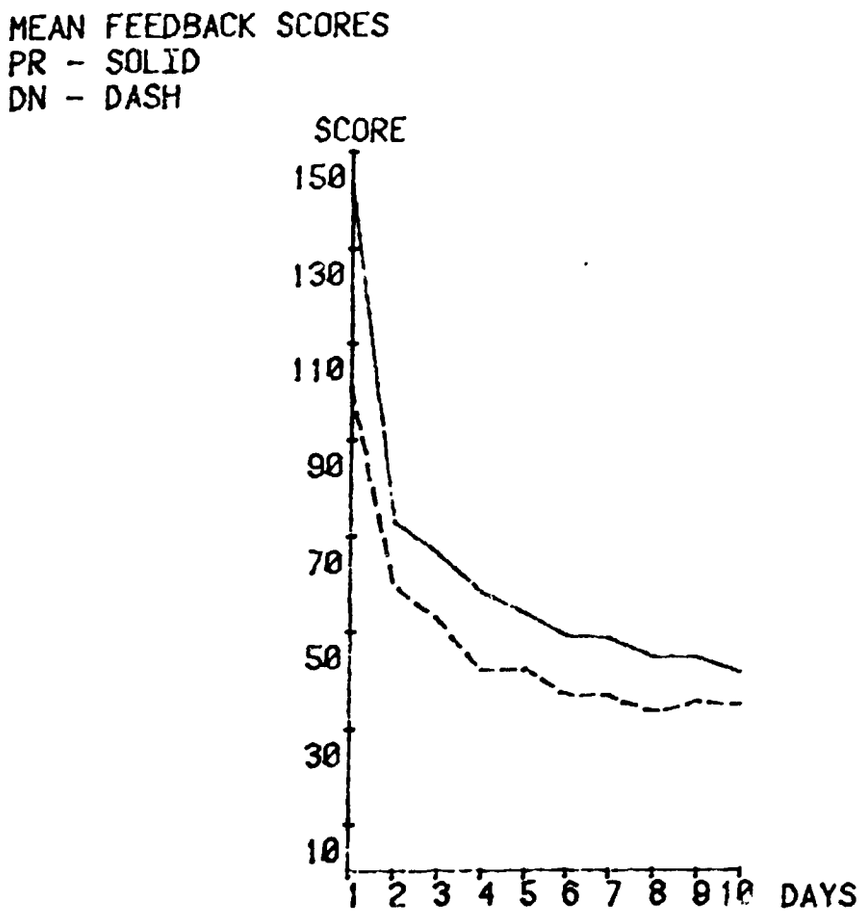

Figure 3

Average Scores by Group and Day

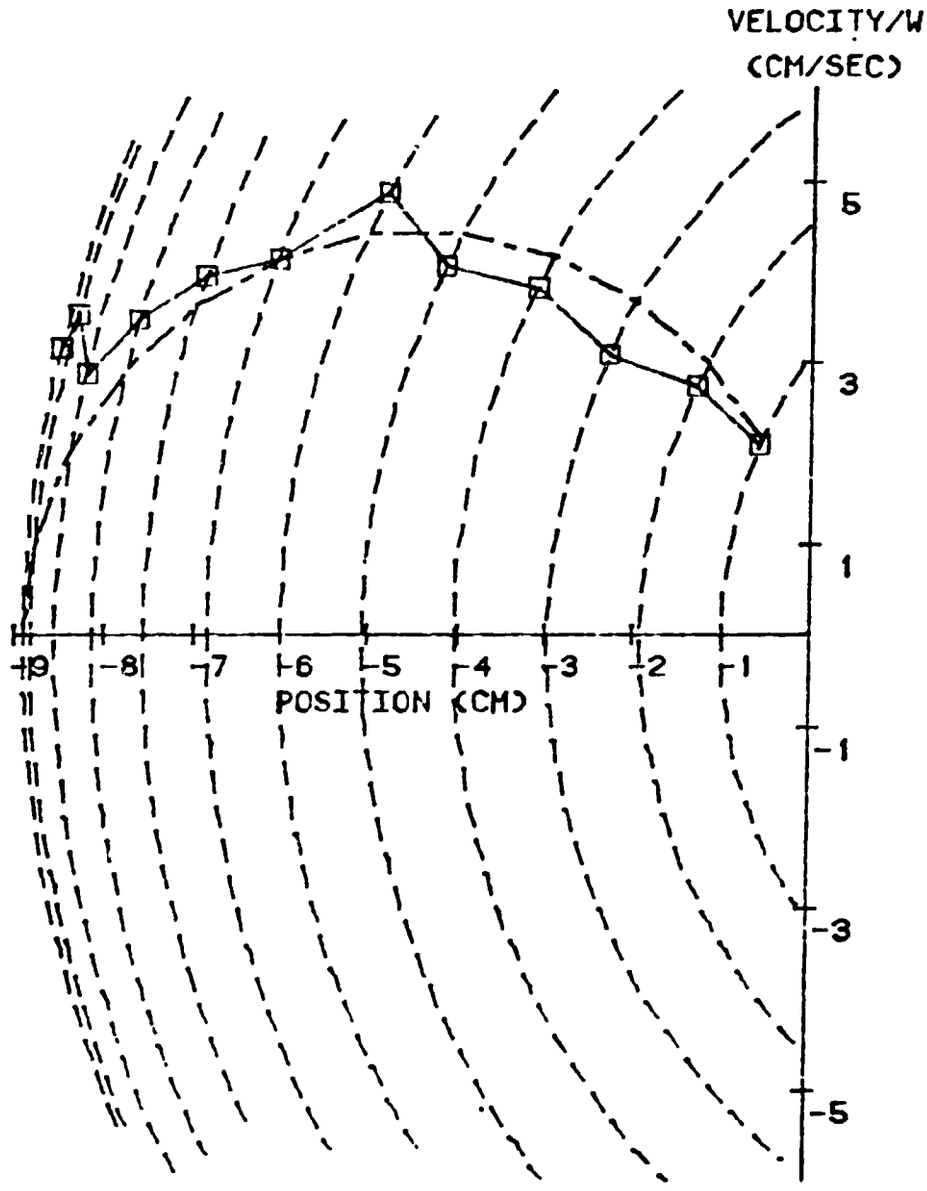

Figure 4

A Typical Subject Switch Locus
Compared With the Optimal Switch Curve

ing trajectory and the optimal trajectory was used as a measure of switching error for each orbit. Negative radial error thus indicated an early switch and target undershoot, while positive radial error indicated a late switch and target overshoot. The feedback score displayed after each trial was the absolute value of this measure multiplied by one hundred.

Typical operator behavior was characterized by early switching on the inner orbits and late switching on the outer orbits. An analysis of variance was performed on the inner orbits (1-5) and outer orbits (6-12), separately. Using radial error as the dependent variable and orbits as a within subject variable, analyses of variance were performed comparing the two groups on each day. These analyses showed no significant difference between groups for the inner orbits on any day. A marginally significant difference ($p < 0.10$) was found on the tenth day only for the outer orbits.

As a measure of intraorbit variation the time spread among the seven switches for each orbit was measured after the extreme high and low point were removed. The measure used was the angle in the phase plane between the second and sixth ordered switching point on each orbit, which is proportional to the time between these switching points. This temporal range was used as the dependent variable in comparing the two groups for the inner and outer orbits. Although the mean range for the pendulum group was consistently higher, no significant difference was found between the two groups.

Operator Internal Model Development

In order to investigate the more subtle effects of pictorial display on operator behavior, the phase phase switching locus was used to infer an operator's internal model of the system for each session. The change in these models was used to analyze the effect of the pictorial display on the orderly change of that model over time. The concept and development of the internal model used here is discussed in detail by Jagacinski and Miller (1978). A brief summary will be provided below.

Optimal performance requires switching the force when the system state lies on the trajectory which passes through the origin. If one assumes that the subject switches when he/she judges that the system state is on this trajectory, then the locus of operator switch points can be used to estimate the subject's cognitive characterization of the dynamics of the system. Assuming that the operator is behaving in accordance with some internal model he has developed of the system, the switching point locus could be described as a sampling from the trajectory of that model. The form of this cognitive model is certainly not clear and so an assumed form must be used. The form chosen by Jagacinski and Miller

(1978) and used in the present analysis is a second order differential equation of the form

$$a(t) = B0 + B1x(t) + B2v(t)$$

where a(t), v(t), and x(t) are respectively acceleration, velocity and position as functions of time, t. B0, B1, and B2 are constants.

Estimates of B0, B1, and B2 were obtained using an algorithm which fit a curve of the above form to the locus of the subject's 12 switch points for that session. The result was a parametrically determined description of the subject's internal model of the system for that day.

This alogorithm searched through the eigenvalue space of the system. The eigenvalues searches were conducted separately for zero (constant acceleration), real, and complex eigenvalues. The measurement used for determining the best fit was the sum of squared error between model and data. Error was defined as the Euclidean distance in the position, velocity plane with position expressed in centimeters and velocity expressed in centimeters per second. With the exception of Day 1, the sum of squared error estimates were consistently under 1.0, and normally under 0.5. These low error measures indicated that the estimates obtained for the three parameters B0, B1, and B2 reflected a reasonably accurate modeling of the 12 point switching loci.

The estimates of B0, B1 and B2 parameters can be used to interpret an operator's behavior. For example, early in practice the subjects exhibited low negative values of the B0 parameter. This trend indicates that the operator behaved as if the external force was stronger than it actually was. Similarly the positive B2 values which were found throughout practice indicate that the operator behaved as if there were a positive force proportional to velocity which caused a high decceleration rate for high positive velocities with this force decreasing as the velocities decreased. In other words, the subjects behaved as if there were a force related to velocity which caused the system to "slow down" faster at higher velocities than was actually the case.

To determine the change of the internal model for each group with practice, a regression analysis was performed on each parameter, fitting the parameter estimates to a quadratic function of days. The dot group showed a significant effect of days ($p < 0.001$) for all three parameter estimates, while the pendulum group did not show a significant day effect for any of the three parameters.

While the group means of the three parameters were never veridical, the progression of the parameters in both groups

moved toward their veridical values over time. Figure 5 is a graph of group parameter means by day. For example, the dot group had a group mean value for B0 of -1.68 on Day 2 and -1.28 on Day 10, thus changing with practice toward the veridical value of -0.7112. Similarly, the pendulum group went from -1.51 on Day 2 to -1.25 on Day 10 for this same parameter. For all three parameters the pendulum group began the sessions with mean parameter values which were closer to veridical than were the corresponding values for the dot group. This trend continued until Day 4 (Day 5 for the B1 parameter), when the difference between the two groups became negligible. By Day 10 the mean position and velocity parameter values for the dot group (B1 = - 0.150, B2 = 0.42) were slightly closer to veridical values than those for the pendulum group (B1 = - 0.146, B2 = 0.43). These differences are small however and not statistically significant.

In an attempt to characterize this significant effect of days on the DN group scatter plots of the parameter estimates were generated. Examination of these plots suggested a possible dichotomy in the data. There appeared to be a bipolar grouping of the data which was particularly evident in the B1 parameter fits. For this parameter most of the data points fell in the range from -0.1 to -0.3. However, there was a second significant clustering of data points about zero or slightly positive (< 0.1). Nearly all the data points fell into one of these two distinct groups. In an attempt to classify this distinction the eigenvalues of the model fits were compared. The B1 parameter fits which clustered around zero were characterized by model fits having two real eigenvalues with one of the eigenvalues either zero or very small (less than 0.1). This type of model fit is characterized in the phase plane as a trajectory which tends to "flatten out" as distance from the target increases and will be refered to as the Type I model.

The second clustering of points was characterized by model fits with either 1) complex eigenvalues or 2) positive real eigenvalues with values nearly equal (within 0.1). This type of model, which shall be refered to as the Type II model, demonstrates a degree of curvature in the phase plane. Since the eignenvalues for the system dynamics are complex (+0.4i, -0.4i) a Type II model fit is necessary to describe a veridical internal model of the system. Using this eigenvalue classification, all the models derived fell into one of these two model catagories.

The "flat" characteristics of the Type I model, as mentioned before, is an indication of the small B1 parameter. It is this parametric weight on position (often referred to as the spring constant) which provides the oscillatory or pendulumlike characteristics of the dynamics. An operator switch curve modeled with a Type I model can be interpreted

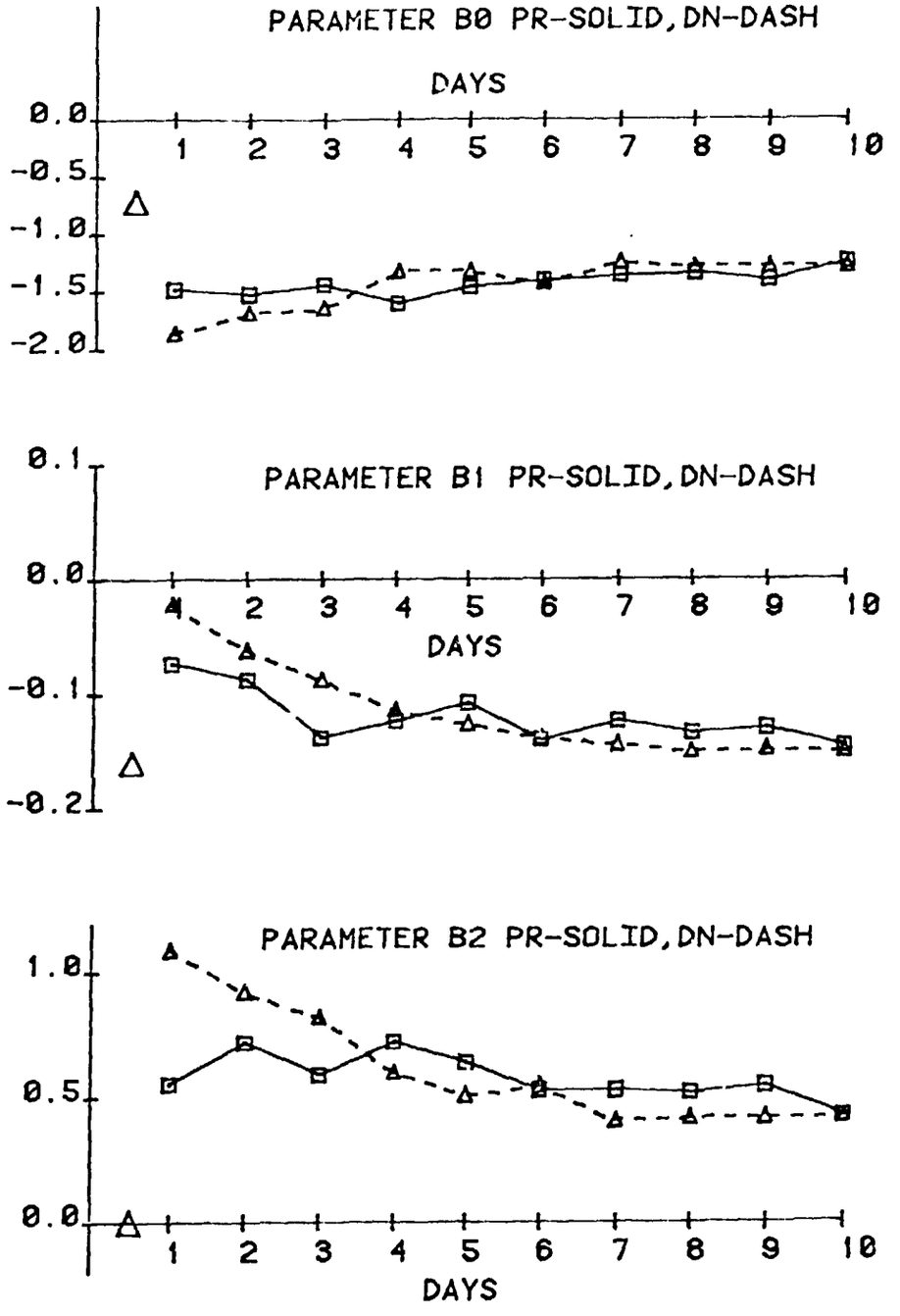

Figure 5

Average Parameter Values By Group and Day

to indicate a failure on the part of the operator to recognize and interpret the oscillatory or pendulumlike characteristics of the system correctly. Conversely, a Type II model contains a much larger weighting on position and demonstrates more curvature in the phase plane. This type of model implies a more accurate interpretation of the system's oscillatory characteristics. Typically, operator switch curves were modeled with the Type I models early in practice and Type II models later. With only two exceptions, once the Type II model was fit to a subject's switch curve on a particular day all remaining days were also modeled with a Type II model. The exceptions were two subjects in the pendulum group which were modeled by Type II models one day early in practice (Day 1 for one subject and Day 2 for the other) and then not again until several days later in practice.

Transition from Type I model fits to Type II model fits occured at various stages in practice for different subjects. For each day, the subjects of each group were catagorized by the model type used to describe their internal representation of the system. Figure 6 shows the proportion of subjects in each group which were modeled by the Type II model. As this graph shows, a much higher percentage of subjects in the pendulum group were modeled with the Type II model initially. The portion of subjects from the dot group with this model while initially lower, increased over practice and was higher than the pendulum group by the fourth day of practice. By Day 10 all subjects were modeled with the Type II model. The largest dichotomy between the groups was on Day 1 where 5 of the 9 subjects from the pendulum group and only 2 of the 10 of the subjects from the dot group were modeled with the Type II model. The probability of at least this degree of spread between groups, assuming that the distribution of subjects in the two model types was independent of the group, was calculated directly from the binomial marginal probabilities. Since the number of pendulum subjects with Type II model is expected to be higher initially this can be considered a one tailed test. This probability was found to be significantly low ($p < 0.05$) indicating that the display type significantly effected the type of model generated on the first day of practice. There continued to be more subjects from the pendulum group in this model catagory until Day 4, however, the proportional differences between the groups were not significant after Day 1. These results suggest that the pendulum display aided the subjects in initially interpreting the oscillatory chacteristics of the system. It appeared to take the subjects given the dot display longer to recognize and interpret these characteristics and demonstrate behavior captured by Type II models.

The next step was to then compare the progession of the subject's internal model once it was modeled with a type II model. Given that the subject's performance indicated that

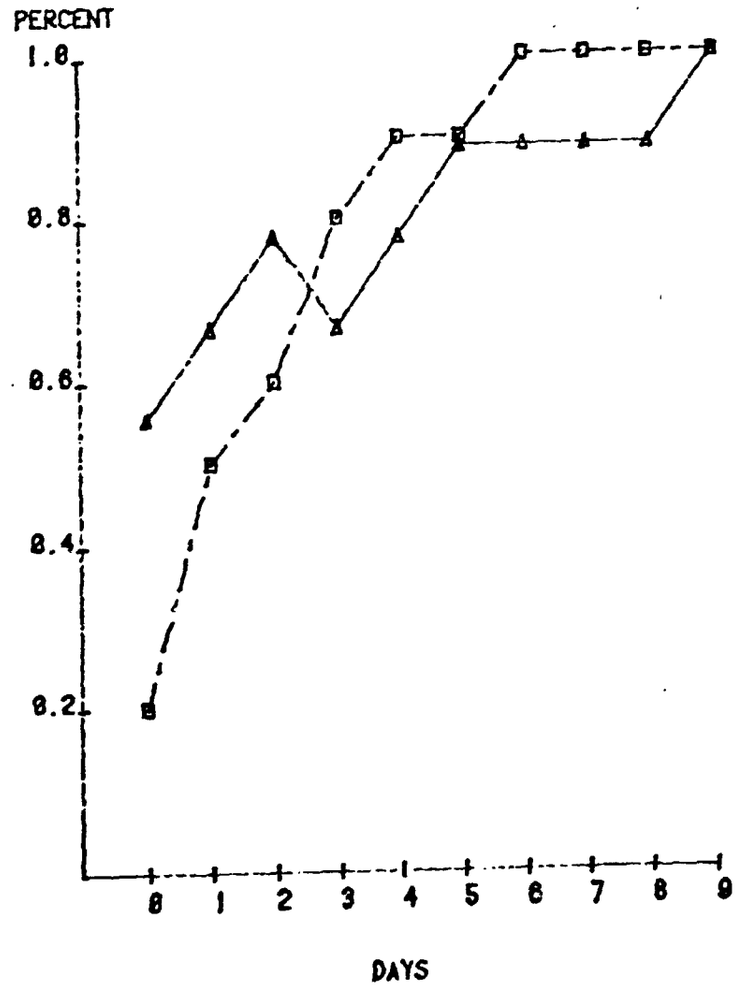

Figure 6

Proportion of Subjects
Represented by Each Model Type by Day

he/she was able to somewhat interpret the oscillatory characteristics of the system, how did the subject "tune" his/her model over practice and did the type of display effect this tuning process? A regression analysis was performed on the three Type II model parameters for each group. The results of this analysis showed significant subject differences in both groups in parameters B0 and B1 ($p < 0.001$). A significant subject effect was not found for the B2 parameter of the dot group. The subjects by day interaction effect was significant ($p < 0.05$) in all three parameters for the pendulum group. No significant subject by day interaction was found in the dot group. This indicates that for the pendulum group the parameters of the different subjects did not change in a uniform manner. This suggests that the manner in which subjects in this group tuned their model varied greatly and suggests that the use of the pendulum display resulted in greater individual differences in the way the subjects tuned their internal representations of the system with practice.

The dot group, however, showed a significant effect of day ($p < 0.001$) in the B1 parameter and no significant effect of subject by day interaction. This indicates that for the subjects in this group this parameter changed in a similiar manner with practice. Hence, one can conclude that once the subjects in the dot group begin to interpret the oscillatory chacteristics of the system (i.e., form a Type II model) it is primarily the B1 parameter, or spring constant, that characterizes the change in their model and that parameter changes in a similar manner for different subjects.

DISCUSSION

Certain assumptions are made when using the approach described in the previous section to describe the human operator's internal model of the system. The first assumption is that the operator's prediction of the motion of the system after the force is reversed can be described as a unique trajectory which passes through the origin of the phase plane. The concept of describing this trajectory with a differential equation is not new and has been used by Jagacinski and Miller (1978) with a similar control task as was used in the present case, and by Jagacinski, Johnson, and Miller (1982) in describing extrapolation performance. Through parameteric adjustment these internal models exhibited orderly changes with practice.

A second assumption of this approach is that the system is assumed to be slow enough so that the subject's ability to predict the motion after the force switch overshadows any inability to extrapolate the present movement over his reaction time. While this assumption seems appropriate for the speed of this system it may not be a reasonable assumption for faster systems. A third assumption is that any error in

the subject's estimate of the state of the system is small enough to be neglected. There may be some indication that under certain circumstances these errors should not be ignored. For example, in the present study the optimal switch point for the outer most orbit considered was the state of zero velocity and extreme positon (-4.445 cm). In interviews following the experiment subjects often indicated that their strategy for the "long oscillations", i.e. the outermost orbit, was to switch the force "right when it turned". However, the average switch points for that orbit were not for both groups. This finding suggests that there was some difficulty in perceiving a zero instantaneous velocity state that is preceeded by a high deceleration rate. In any case, such effects would be expected to effect both groups and therfore should not bias the comparison between groups.

There are two primary findings of the analysis described in the previous section. First, the pictorial display of the pendulum did not significantly aid the operator in achieving a a low session score. Secondly, it was found that the pictorial display did effect the behavioral chatacteristics and learning process of the operator. Those subjects given the pendulum display appeared to recognize the oscillatory characteristics of the system earlier. However, the manner in which their internal representations of the system changed with practice was significantly different between individual subjects. This suggests the pendulum display not only aided the subject in forming his/her initial internal model of the system, but that it also caused significant differences in the way different subjects learned the task. This second finding may mean that the pendulum display permitted the operator to use a pre-existing internal model of the pendulum dynamics improving the operator's understanding of the system dynamics initially. Although these subjects demonstated more veridical initial interpretations of the dynamics their task scores did not show an improvement over the dot subjects. Those subjects given the abstract display of the system began with highly non-veridical internal models of the dynamics but with practice these models improved substantially.

The analysis performed on the type of model used to describe the operator's internal representation has several possible implications. The probability that a subject would be modelled by the more veridical type of model (Type II model) was significantly higher for the pendulum group on the first day of practice. This suggests that the pictorial display did aid the subjects initially in interpreting this oscillatory characteristic of the system. The majority of subjects with the abstract display did not exhibit this type of behavior until later in practice. However, once the subjects entered this category of performance the abstract display subjects showed significant improvement in the B1 parameter indicating that their improvement in performance from this

point was directly related to the springlike or oscillatory system characteristics.

This analysis demonstrates the importance of the role of the non-verdical internal human model in evaluating the human operator in dynamic systems. Overall performance behavior does not give information concerning the internal structure of the human's interpretation of the system he is controlling. While improvement in performance can be detected, the characteristics of that improvement are not at all evident from gross overall performance measures. In this case, while the subjects from both groups were generating similar performance measures the type of behavior generating these performance measures was characteristically different. The internal model concept allows the analysis of some of these changes that occur in the human operator's internal representation of the system over practice. In the present experiment this concept is used to characterize the differences in learning behavior for subjects seeing different displays.

Kieras and Bovair (1983) demonstated in their study that a mental model, or so called "device" model, can aid performance if the model explains the mechanisms that are involved in fulfilling the operator's goals. They contend that if the model does not provide information explaining how or why the operator is to achieve a goal then it is not useful.

In their experiments they attempted to empirically assure that the all the subjects had approximately the same internal or "device" model prior to beginning the experiments. This was done by instructing the subjects on the model and testing them on their knowledge of the information povided to them. In the present experiments subjects were given no special training relevant to the dynamics of a pendulum. The subject was allowed to use the existing model he/she had for the physical entity of a pendulum. There is no evidence that this representation is the same for each subject. In fact the results of this study, among others (Larkin, 1983), indicate that these internal representations vary significantly from operator to operator. This suggests the extent to which the pendulum display aided the operator may have been dependent upon the nature of his/her existing model of a pendulum and whether that representation could provide the operator with information relevant to the goal of the task.

The significant differences between the two groups early in practice suggest that the pendulum subjects were using their internal representations of a pendulum. However, there is no indication that this pendulum "device" model provided the subjects with sufficiently relevant goal-seeking information to substantially improve their performance of the task. This suggests that while the pendulum display did provide the

operator with relevant information concerning the oscillatory characteristics of the system, the subjects, in general, were not able to extract the information neccessary to achieve a low score.

ACKNOWLEDGEMENT

This work was supported in part by NASA Grant NAG 2-195. The project monitor was E. James Hartzell. This paper is based on the Masters' Thesis of the second author.

REFERENCES

Athans, M. and Falb, P.L., Optimal Control, New York: McGraw-Hill, 1966.

Jagacinski, R.J., Burke, M.W., and Miller, D.P., "Use of schemata and acceleration in stopping a pendulum-like system," Journal of Experimental Psychology: Human Perception and Performance, 1977, 3, 212-223.

Jagacinski, R.J., Johnson, W.W., and Miller, R.A., "Quantify the cognitive trajectories of extrapolated movements", Journal of Experimental Psychology: Human Perception and Performance, 1983, 9, 43-57.

Jagacinski, R.J.and Miller, R.A. "Describing the human operator's internal model of a dynamic system", Human Factors, 1978, 20, 425-433.

Jex, H.R., McDonnell, J.D., and Phatak, A.V., "A 'critical' tracking task for manual control research", IEEE Transactions on Human Factors in Electronics, 1966, 7, 138-145.

Kieras, D.E. and Bovair, S., "The role of a mental mode in learning to operate a device" Technical Report No. 13 (UARZ/DP/TR-83/ONR-83), University of Arizona, March 1983.

Larkin, J.H., "The role of problem representation in physics", in D. Gentner and A.L. Stevens (Eds.), Mental Models, Hillsdale, New Jersey: Lawrence Erlbaum, 1983.

Rasmussen, J., "Skills, rules and knowledge: signals, signs, and symbols and other distinctions in human performance models", IEEE Transactions on Systems, Man, and Cybernetics, 1983, 13, 257-266.

Biodynamic Factors

N85 14528 D41

1984 ANNUAL MANUAL ABSTRACT

DOES McRUER'S LAW HOLD FOR HEART RATE CONTROL VIA BIOFEEDBACK DISPLAY?

Barbara Jex Courter
Human Engineering/Biomedical
Rockwell International, NAAO
Los Angeles, CA 90245

Henry R. Jex
Systems Technology, Inc.
Hawthorne, CA 90250

Some persons can control their pulse rate; rapidly increasing or decreasing it with the aid of a biofeedback display. If the biofeedback display is modified to show the error between a command pulse-rate and the measured rate, a compensatory (error correcting) heart rate tracking control loop can be created. An exploratory experiment is described to measure the dynamic response characteristics of this control loop when subjected to step and quasi-random disturbances.

The control loop includes a beat-to-beat cardiotachmeter differenced with a forcing function from a quasi-random input generator; the resulting "error" pulse-rate is displayed as feedback. The subject acts to null the displayed pulse-rate error, thereby closing a compensatory control loop. McRuer's Law should hold for this case, as it has for most other compensatory manual control situations.*

In this preliminary experiment, a few subjects already skilled in voluntary pulse-rate control are being tested for heart-rate control response, using the STI Describing Function Analyzer. The DFA measures the response/input fourier coefficients at five input frequencies from which various closed-loop and opened-loop transfer functions can be computed. In a method similar to past human-operator tracking research, control-law properties are derived, such as: crossover frequency, stability margins, and closed-loop bandwidth. These are evaluated for a range of forcing functions and for step as well as random disturbances.

Heart rate variation has been proposed as one measure of task-induced mental workload. In that context, this research has application to:

- Developing the applied technology needed to properly evaluate heart-rate workload measures.
- Training subjects (drivers, pilots, N-plant operators) to cope with task-induced workload via psychophysiological feedback (e.g., anticipatory heart rate rise; incipient overload).
- Screening subjects as to sensitivity to heart rate variations and heart rate control ability, as they affect the above applications.

This presentation constitutes an early status report on the results to date.

---

*McRuer's Law (sometimes called the Crossover Model for Operator Adaptation) states that the opened-loop frequency-response of a random-forcing-function compensatory man-machine control loop will be adjusted by the operator to resemble that of an integrator with time-delay in the "gain crossover" frequency range near unity magnitude-ratio.

INTRODUCTION

- SOME PERSONS CAN CONTROL THEIR PULSE RATE AT WILL VIA BIOFEEDBACK.
- DISPLAY THE "ERROR" BETWEEN PULSE RATE AND A DISTURBANCE (FORCING FUNCTION) COMPENSATORY TRACKING.
- FOR COMPENSATORY TRACKING WITH AN UNPREDICTABLE FORCING FUNCTION, McRUER'S (CROSSOVER MODEL) LAW HOLDS.
- Q: DOES McRUER'S LAW HOLD TRUE FOR HEART RATE CONTROL VIA BIOFEEDBACK DISPLAY?

HEART RATE REGULATION USING BIOFEEDBACK -

SYSTEM DIAGRAM

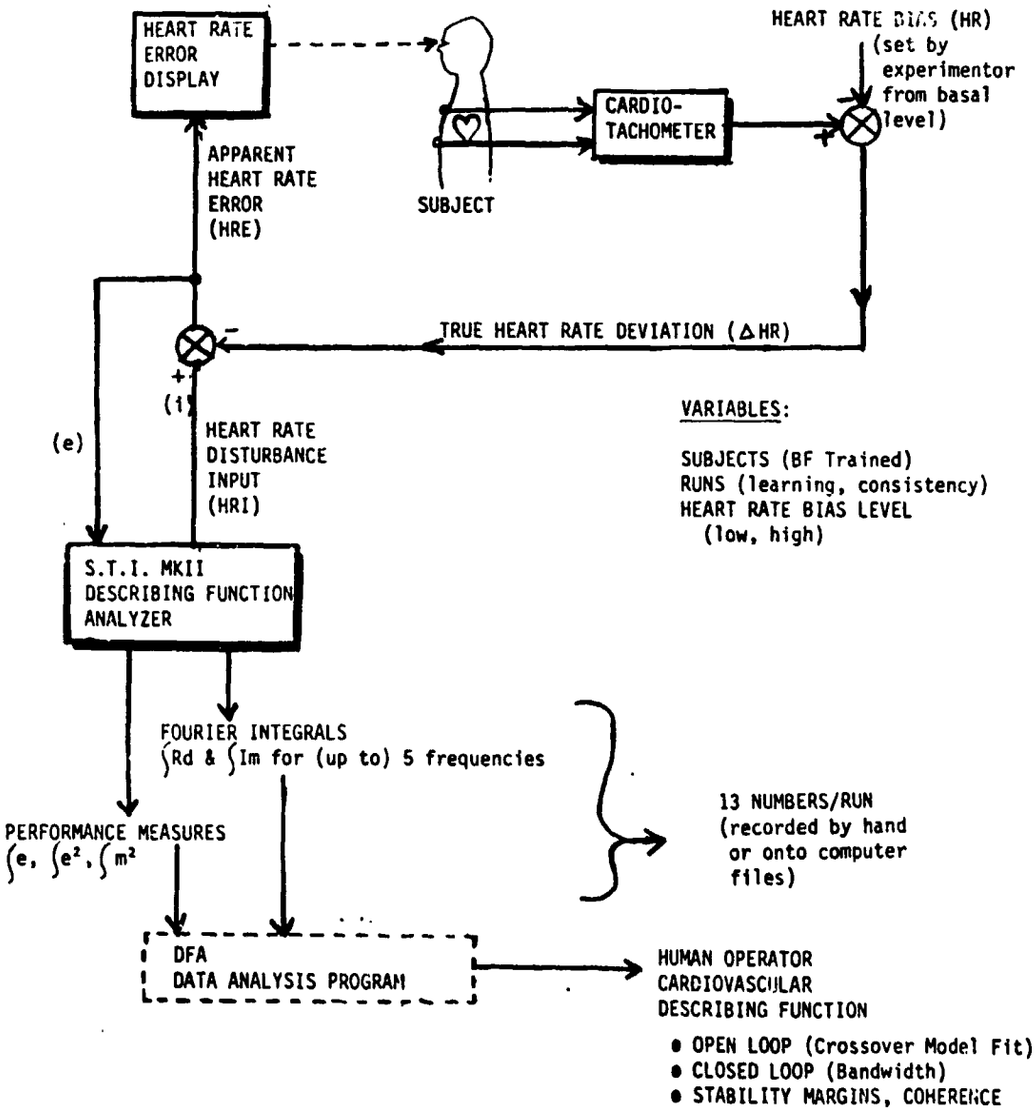

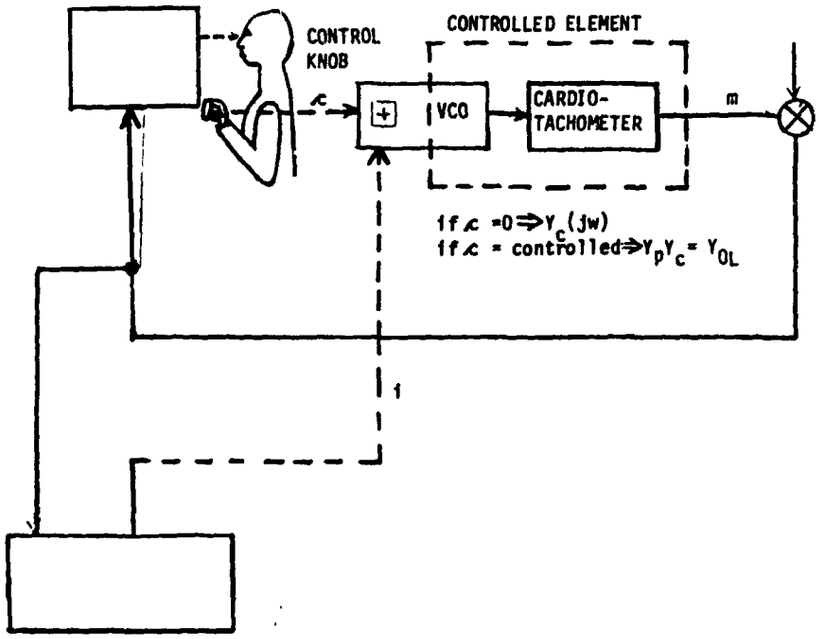
CONTROL KNOB
CONTROLLED ELEMENT
VCO
CARDIO-TACHOMETER
m
1
1 f ∠c =0 ⇒ Y_c(jw)
1 f ∠c = controlled ⇒ Y_p Y_c = Y_OL

ORIGINAL PAGE IS
OF POOR QUALITY

FREQUENCY RESPONSE OF CARDIOTACHOMETER CONTROLLED ELEMENT

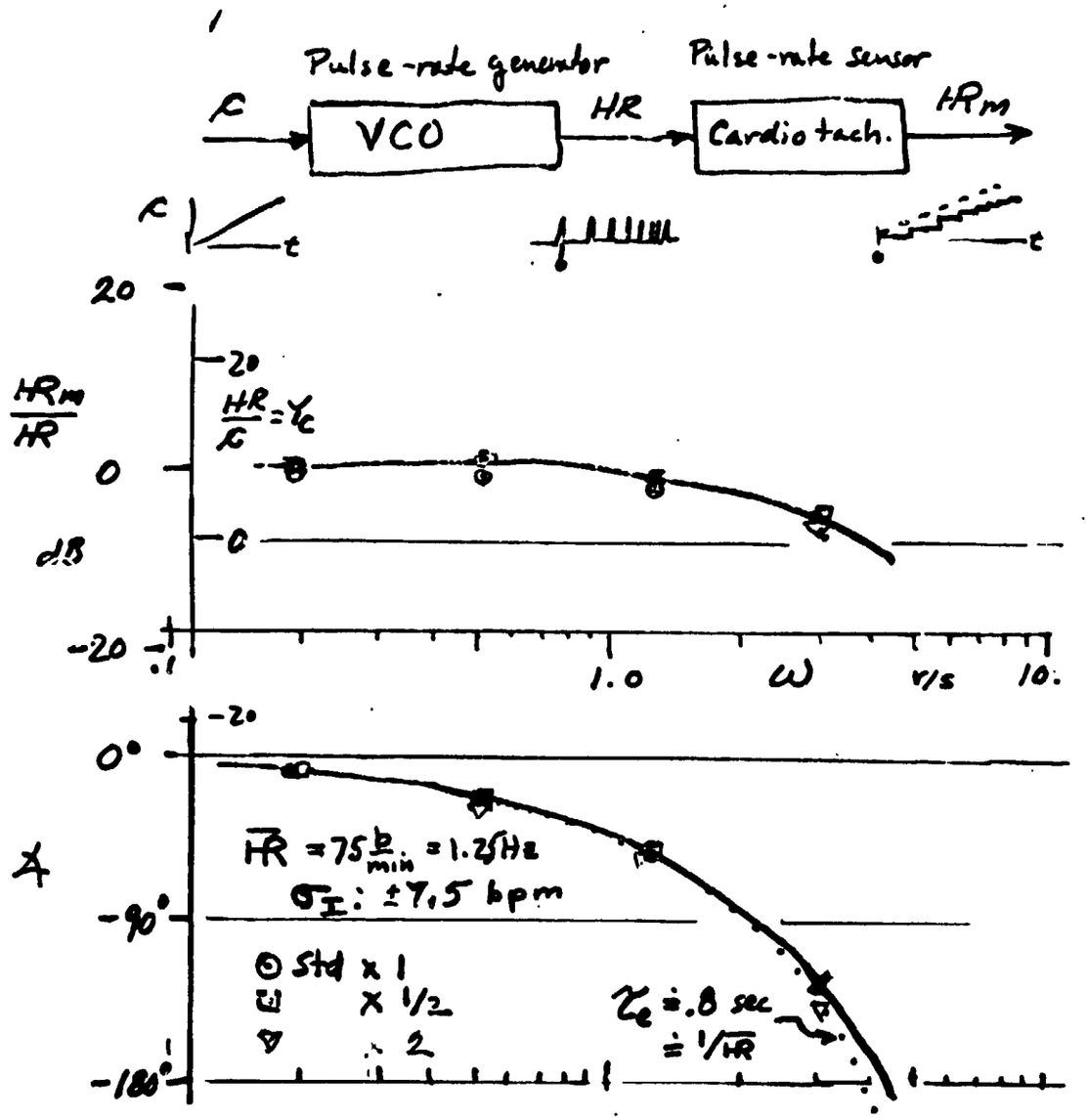

ORIGINAL PAGE IS
OF POOR QUALITY

OPEN LOOP DESCRIBING FUNCTIONS FOR COMPENSATORY TRACKING WITH A CARDIOTACHOMETER USING MANUAL CONTROL VIA A V.C.O.

Avg Pulse Rate : 75 beats/min
RMS Disturbance : ± 7.5 beats/min

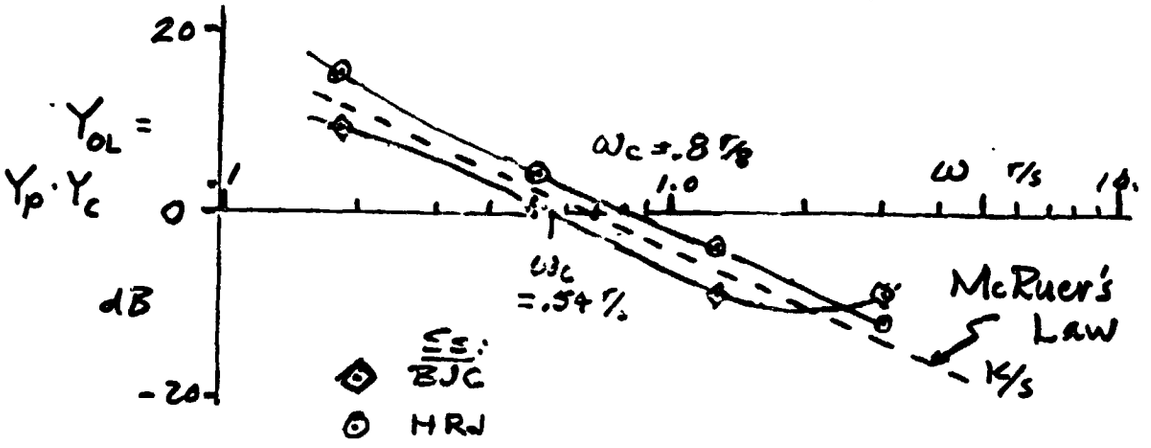

STATUS:

- McRUER'S LAW DOES HOLD FOR MANUAL TRACKING WITH A CARDIOTACHOMETER.
- NEED SKILLED HEART RATE CONTROL SUBJECTS.

APPLICATIONS

- DEVELOPING THE APPLIED TECHNOLOGY NEEDED TO PROPERLY EVALUATE HEART RATE WORKLOAD MEASURES.
- TRAINING SUBJECTS (DRIVERS, PILOTS, N-PLANT OPERATORS) TO COPE WITH TASK-INDUCED WORKLOAD VIA PSYCHOPHYSIOLOGICAL FEEDBACK.
- SCREENING SUBJECTS AS TO SENSITIVITY TO HEART RATE VARIATIONS AND HEART RATE CONTROL ABILITY, AS THEY AFFECT THE ABOVE APPLICATIONS.

N85 14529

D42

New Uses for Sensitivity Analysis: How Different Movement Tasks Effect Limb Model Parameter Sensitivity

by
Jack M. Winters and Lawrence Stark
Dept. of Engineering Science, Bioengineering Group
University of California, Berkeley

In general, sensitivity analysis is a heuristic technique for systematically evaluating how output "behaviors" are influenced by varying system "parameters". The basic method can play a major role not only directly by helping tune existing model parameters but also indirectly through the design of experiments that may allow certain parameters to be isolated and defined by certain behaviors.

The present work extends past eye and head model sensitivity efforts in a number of significant ways. First, original results for the newly developed eighth-order nonlinear limb antagonistic muscle model of elbow flexion and extension are presented. Second, a wider variety of sensitivity analysis techniques are used and a systematic protocol is established that shows how the different methods can be used efficiently to compliment one another for maximum insight into model sensitivity. Third, it is explicitly shown how the sensitivity of output behaviors to model parameters is a function of the controller input sequence, i.e. of the movement task. When the task is changed (for instance, from an input sequence that results in the usual "fast movement" task to a slower movement that may also involve external loading, etc.) the set of parameters with high sensitivity will in general also change. Such task-specific use of sensitivity analysis techniques identifies the set of parameters most important for a given task, and even suggests task-specific model reduction possibilities.

NEW USES FOR SENSITIVITY ANALYSIS: HOW DIFFERENT MOVEMENT TASKS EFFECT LIMB MODEL PARAMETER SENSITIVITY

INTRODUCTION

Sensitivity analysis techniques have traditionally been used by the systems engineer to help understand the behavior of complex systems. Although the details of the techniques seen in practise differ, the basic approach is the same: A system parameter is varied in a controlled, systematic manner, and the subsequent variations in output are measured and described quantitatively (Frank (1978), Tomovic and Vukobratovic (1972), Lehman and Stark (1982)). When the system is nonlinear, as is the usual case, numerical techniques involving computer simulation typically need to be employed. Insights gained from such techniques are of value both for systems analysis and design.

The methods presented here represent extensions of previous work (Clark and Stark (1976), Hsu et al (1976), Lehman and Stark (1979), Bahill (1980) and Zangemeister et al (1981)), only with a wider range of sensitivity tools employed. Furthermore, the model considered here is for limb flexion-extension movements, rather than for head or eye rotation. The model **structure** has also been expanded and the constitutive equations representing basic muscle properties improved so as to more accurately characterize basic neuromuscular system dynamics. Consequently, there are a larger number of internal model **parameters**. A greater number of output behaviors are also considered.

In addition to presenting this expansion of previous sensitivity analysis tools and extending these methods to a larger number of model parameters, a major role of this presentation is to show how sensitivity analysis results are a function of the model **task**. When the task under consideration is changed (i.e. the model input controller signal sequence is fundamentally different, resulting in a different type of output), the relative role of each parameter in affecting performance also changes. This fact, surprisingly neglected in the literature, is developed quantitatively here.

The result is one model that can adequately simulate any basic physiologically realizable flexion-extension task and a set of sensitivity tools that help explain the relative role of any specific parameter for any particular task - tools that can help make the goal these modeling efforts, gaining **insight** into the role of biomechanical systems in neuromotor control, a reality.

METHODS:

A. Model Structure: Before presenting the sensitivity analysis protocol employed here, it will first be advantagous to develope a basic understanding of the biomechanical system being modelled. The first step to any modeling effort is to assume a basic structure. Once chosen, this structure will be the major constraint on the success of the model - too simple a structure can result in a poor approximation of actual behavior, while too complex a structure reduces insight (or results in a model with poorly defined parameters). The basic structure for the model, based on the classical muscle work of Hill (1938) and elbow flexion-extension work of Wilkie (1950) and supported by numerous more recent experimental work on muscle mechanics, is presented in Figure 1. The sixth-order strucuture has been found to be the lowest order structure that is capable of approximating all fundamental muscle properties needed for an antagonistic pair of lumped "equivalent" muscle actuators rotating a joint.

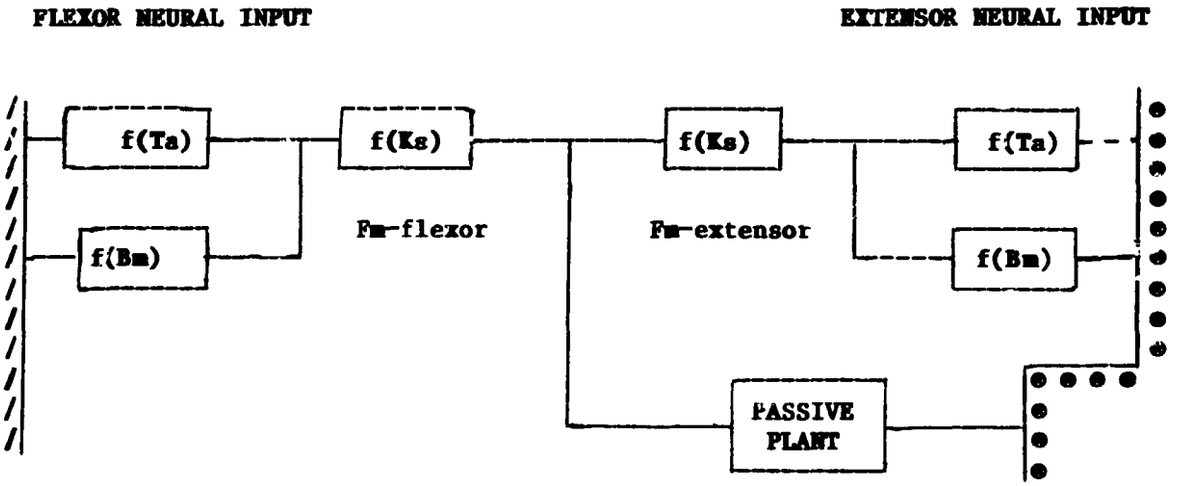

FIGURE 1: Model of System Showing the Nonlinear Blocks. Lumped Flexor Muscle is on the left, Extensor on right.

Experimental work is often able to approximately isolate each of these elements in the model. Fundamental to such an approach is this idea of an "equivalent muscle". This concept of an "equivalent" muscle for the lumping of a number of synergistic muscles has been previously developed, based on experimental work, for both the flexor group (Bouisset et al (1973, 1976) and the extensor group (Cnockaert and Pertouzon (1974)) and confirmed by Cnockaert (1978) and Le Bozec (1980). This idea is supported and expanded on here in the following sense: not only is it a good representation for the ideal case of elbow flexion-extension but it also should be expected to hold for more complex one degree of freedom movements such as wrist or head rotation because two lumped antagonistic muscles with the blocks described above should be structurally capable of approximating all basic muscle properties for such movements whenever muscles contract approximately synergistically. In these more involved movement systems, however, parameter identification is more difficult.

A good summary of much of the work on the material properties of muscle is found in the review by Close (1972). Once fiber type and fiber

orientation are determined, basic skeletal muscle material properties for a given muscle can be well estimated. Geometric data for the muscles around the elbow joint also exists (An et al (1981), Amis et al (1979)). By creating algorithms that combine material and geometrical information, first generation parameter values for the torque-velocity and series elastic elements can be established. These results are then combined with the wealth of experimental work on controlled intact limb movements, the best of which include Dern et al (1947), Wilkie (1950), Pertuzon and Bouisset (1973), Jorgensen et al (1971, 1976), Hatze (1981a,b) and Komi (1973) for torque-velocity information, Wilkie (1950), Goubel and Pertuzon (1973) and Cnockaert et al (1978) for the series elastic relation, and Boon (1973) and Hayes and Hatze (1977) for passive viscoelastic data. Limb inertial data exists in abundance. Insights from preliminary sensitivity analysis work (not presented here) are also used for fine-tuning parameters. The actual protocol followed for parameter development is beyond the scope of the present presentation and will not be described here. The resulting model parameter values for the elbow flexion / extension model, one of the five models currently under pursuit, are displayed in Table 1.

PARAMETER:	VALUE:		CONSTITUTIVE EQUATION:
Passive Plant:			
Jp:	0.06	Kg-m**2/rad	(or N-m-sec**2/rad)
Bp:	0.15	N-m-sec/rad	
Kp:	1.4	N-m/rad	$Fkp = Kp*x + Kp_1*(\exp(Kp_2*x)-1)$
Kp1:	0.0001	...	
Kp2:	10.0		
Series Elasticity:			
Ks1-f:	4.8	N-m/rad	$Fks = Ks_1*(\exp(Ks_2*(xh-x))-1)$
Ks2-f:	7.0		
Ks1-e:	4.5	N-m/rad	
Ks2-e:	7.2		
Torque-Veocity:			
Af-f:	0.34		
Bh-f:	8.0	rad/sec	$Bm = \begin{cases} \frac{(1 + Af) * Fh}{(Vh + Bh)} & Vh < 0 \\ \frac{(1 + Af*Affv) * Fh * _fv}{(Vh + Bh*bhfv)} & Vh > 0 \end{cases}$
Af-e:	0.30		
Bh-e:	7.0	rad/sec	
Fm-fv:	0.3		
Af-fv:	0.6		
Bh-fv:	0.25		
			(where Fm = Fn - Bm*Vh)
Activation Dynamics:			
Ta1:	40	ms	
Ta2:	10	ms	
Fmax-f:	60	N-m	
Fmax-e:	50	N-m	

TABLE 1: Current Parameter Values for the Elbow Flexion-Extension Model. Constitutive Equations are for: Parallel Elasticity (Fkp), Series Elasticity (Fks (=Fm)) and Torque-Velocity (Bm). (Parameter values are for 70 Kg male of average strength.)

The passive plant values represent the inertia and viscoelastic properties of the lumped joint/muscle system, with all three elements in parallel as is usual. The exponential fit for the parallel and series elasticities has become a standard representation for load-bearing collagen-elastin based soft tissue (Fung (1968), Glantz (1974) and Hatze (1981)). The "Hill's" parameters (Af and Bh) for shortening muscle are the standard representation for the classic force-velocity relation of muscle, used constantly in the literature to document experimental results (see, for instance, Close (1972)). The scaling of the instantaneous torque-velocity relation by the activation level was suggested as early as 1956 by Wilkie, and has been supported by the work of Pertuzon and Bouisset (1973). The relation used for lengthening muscle (an inverted, skewed Hill's-type equation) is a new method that appears to adequately approximate past data (Joyce et al (1969a,b), Komi (1971) and Hatze (1981)), plus numerous observations that the peak eccentric torque is about 30% above the peak isometric force. Activation dynamics is simulated by two time constants, compatible with the basic neuromuscular literature (see Close (1972) or Bahler (1967) for reviews). This second-order form represents simplifications suggested by the more detailed work of Lehman (1983) and Hatze (1981). There is also numerous isometric peak torque data available in the physical education literature - the values presented here are for a "typical" human male. For reasons of clarity, the static torque-angle parameters (based on an abundance of literature) were not presented above.

As seen above, all indications are that all of these elemental building blocks are nonlinear. The function of these nonlinear properties is still poorly understood, and one of the main problems faced is to explore the sensitivity of the system to these nonlinearities. There is ample evidence, supported here, that the relative importance of various parameters is a function of the task in question. Consequently, it can be a major mistake to over-simplify this basic system if one is interested in a variety of movement tasks. Furthermore, since sensitivity methods provide just the information needed for task-specific model simplification, it is suggested that the more complex model be considered first - any model simplification is then based on a solid foundation.

B. Computer Simulation Algorithm: The simulation algorithm is contained within a more general set of modules that are linked to a main routine, called "JAMM" (Juiced-up Antagonistic Muscle Model). This user-friendly program will simulate second, sixth and eighth order models with degrees of nonlinearity ranging from linear to highly nonlinear. Once the biomechanical model of interest is chosen, a data base, complete with all the current numerical values of parameters for any user-desired combination of linear/nonlinear parameter defaults, is read. The user is prompted for parameter modification, for various external loading options, for the type of run (interactive, sensitivity analysis, optimization), and for the controller signal input sequence for each equivalent muscle.

The options under sensitivity analysis include: determining the parameters that are to be varied, one by one, for a given run and determining the range of the parameter variation and the number of times varied. Parameter variation is by a reciprocal format (for example, 4/5 and 5/4 of nominal). Typically results for five reciprocal pairs are obtained. Raw behavior data, behavior and parameter ratios, and linear and logarithmic sensitivity coefficients are stored for later plotting and/or printing.

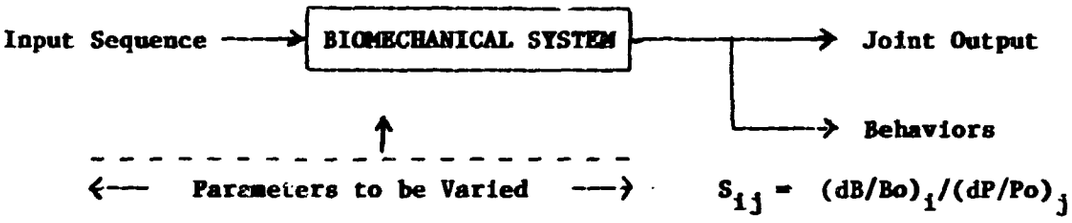

Figure 2 Schematic of Sensitivity Analysis Method. Note that varied parameters can include system, input or disturbance values, and that input sequence depends on task.

C. Sensitivty Analysis Protocol: Past sensitivity analysis work on eye and head systems concentrated on the development of a "sensitivity matrix" (Hsu et al (1976), Lehman and Stark (1979), and Zangemeister et al (1981)). A schematic of this basic method is presented in Figure 2. An input sequence that will define a certain type of task is chozen, and output trajecties are measured. In general, the input and output can be scalar or vector quantities. Here, for the generalized equivalent flexor and extensor muscles, there are two inputs, one to each of the lumped equivalent muscles. The outputs of interest are the position, velocity and acceleration of the limb, plus the muscle torques. The "behaviors" of interest are a function of these output trajectories. The parameter varied is typically an internal model parameter value, but may also be an input signal parameter value, such as a pulse height or width, or an external disturbance. Traditionally, each column would indicate the sensitivity of all the different behaviors (each on a different row) to that column's parameter.

The actual value of each matrix element is called the "sensitivity coefficient", S_{ij}, of the i-th behavior to the j-th parameter. This coefficient represents the relative change in behavior divided by the relative change in parameter $(dB/B_o)_i/(dP/P_o)_j$, where Po and Bo are the nominal parameter value and the resulting nominal behavior value, respectively. The range of the change in parameter for the determination of the matrix coefficients is up to the discretion of the user. Typically, the range chosen for the sensitivity matrix coefficient computation was from one half to twice the nominal parameter value. Another design consideration is the equation used to determine the coefficent. Two equations are used here:

"linear": $((B_2-B_1)/B_o)/((P_2-P_1)/P_o)$

"logarithmic": $(\log(B_2/B_o)/\log(P_2/P_o))-(\log(B_1/B_o)/\log(P_1/P_0))$

where P_2 is the parameter value greater than nominal and B_2 the resulting behavior value; P_1 the reciprocal fraction of P_2 and B_1 the resulting behavior due to P_1. Because the first method gives a value proportional to the relative difference in behavior without regard to one direction maybe having a greater shift, it tends to weigh behavior changes greater than B_o disproportionally more than those below. The second method weighs ratios both below and above nominal equally. For this reason, the second method is usually prefered. Notice that, if the behavior where to change in a manner proportional to the parameter change, the sensitivity coefficient for

ORIGINAL PAGE IS
OF POOR QUALITY

either method would be "1.0".

Once this "sensitivity matrix" is completed, it gives a global view of model behavior for the task under question. Table 2 presents the results for a simple "generic" run. Here, an input signal, about 30% of maximum, is applied to the flexor group for 200 ms. The extensor group is about 3% of maximum. The model is run for each of the parameters chosen for variation at values one half and twice nominal. The behaviors of interest are measured, and the sensitivity coefficients determined, here by both methods.

Each of the resulting column gives one a feel for how a given parameter effects the various behaviors, while a given row indicates what parameter(s) most influence the particular behavior. For convenience in matrix inspection, the following conventions are used: the highest value in each column is printed in italics; the highest in each row is in boldface; and the three three most influencial parameters are also printed in boldfaced italics. For this example coefficients for both the "linear" and "logarithmic" decriptions are provided. Note the similarity in coefficient values. All later work uses only the logarithmic method of determination.

TABLE 2:

SENSITIVITY MATRIX FOR TASK: "Generic, Medium-Speed Movement":

	NOMINAL	Jp	Bp	Kp	Kp1	Kp2	Ka1-f	Ka2-f	Af-f	Bb-f	Fvmax	Ta1
Magn:	114 deg	-0.012	-0.108	-0.026	-0.012	**-0.289**	-0.002	-0.004	-0.200	0.037	-0.101	-0.046
		-0.013	-0.120	-0.029	-0.013	**-0.398**	-0.002	-0.004	-0.223	0.055	-0.112	-0.050
Vmax:	565 d/s	-0.141	-0.125	0.005	-0.000	**-0.367**	-0.007	-0.019	-0.290	**0.542**	-0.059	-0.115
		-0.162	-0.138	0.006	-0.000	**-0.575**	-0.070	-0.020	-0.333	**0.593**	-0.064	-0.131
Amax:	5492 d/s/s	-0.510	-0.057	0.077	-0.002	**1.732**	-0.021	-0.039	-0.096	0.274	-0.057	**-0.415**
		-0.556	-0.062	0.082	-0.002	**0.924**	-0.023	-0.043	-0.105	0.300	-0.063	**-0.468**
Amin:	-4858 d/s/s	**-0.671**	**-0.231**	**0.150**	-0.028	**1.960**	-0.020	-0.041	**-1.128**	**5.573**	-0.002	-0.390
		-0.757	**-0.227**	**0.156**	-0.030	1.000	-0.021	-0.044	**-0.800**	**1.749**	-0.002	-0.454
Fm-f:	9.1 N-m	0.154	0.005	-0.015	-0.001	**0.295**	0.005	0.022	-0.063	0.185	0.033	-0.123
		0.166	0.006	-0.017	-0.001	**0.264**	0.006	0.040	-0.069	0.202	0.050	-0.134
Fb-f:	14.4 N-m	-0.100	-0.056	0.011	-0.000	**-0.364**	-0.001	-0.004	0.106	-0.170	-0.029	-0.138
		-0.110	-0.061	0.012	-0.000	**-0.569**	-0.020	-0.005	0.114	-0.191	-0.032	-0.160
Tmagn:	363 ms	**0.298**	0.097	-0.064	**-0.041**	0.000	-0.009	0.017	0.000	0.233	0.017	0.252
		0.302	0.104	-0.071	**-0.044**	0.000	-0.010	0.080	0.001	0.241	0.018	0.252
Tvmax:	209 ms	**0.131**	-0.013	-0.035	0.000	0.077	0.000	0.003	-0.061	0.042	-0.003	0.057
		0.147	-0.014	-0.038	0.001	0.078	0.001	0.003	-0.068	0.045	-0.003	0.061
Tamax:	59 ms	0.260	-0.023	-0.011	-0.011	-0.158	-0.068	-0.192	-0.034	0.068	0.045	**0.294**
		0.278	-0.024	-0.012	-0.012	-0.192	-0.073	0.207	-0.036	0.071	0.048	**0.320**
Tamin:	278 ms	0.103	-0.132	-0.007	-0.031	**-0.528**	-0.005	-0.017	-0.120	0.029	**-0.134**	0.089
		0.111	-0.135	-0.080	-0.033	**-1.182**	-0.005	-0.018	-0.125	0.032	**-0.136**	0.096
Tfm-f:	54 ms	0.284	0.025	-0.037	0.000	**0.877**	**-0.086**	**-0.247**	-0.037	0.099	0.037	0.247
		0.390	0.027	-0.040	0.010	**0.605**	**-0.095**	**-0.260**	-0.040	0.105	0.040	0.265
Tfb-f:	273 ms	0.023	0.000	-0.011	0.000	0.010	0.000	0.000	0.000	0.000	0.000	**0.036**
		0.050	0.000	-0.012	0.010	0.011	0.010	0.001	0.000	0.000	0.001	**0.040**

Use of a coefficient determined by two values only gives the linear slope over the operating range of the two parameters. For a nonlinear system, this may give misleading information (discussed later). For this reason, the parameter ratio range for a given sensitivity matrix is an important design variable. Thus, if one is interested in a deeper understanding of the role of a certain parameter, a simple column of coefficients is not enough.

The tools desribed here for a more in-depth examination of the role of a specific parameter will be called "sensitivity graphs" and "sensitivity trajectories". They are best used as the next step after a preliminary sensitivity matrix has been developed for the task in question. The "sensitivity trajectory" is simply the set of output versus time plots that result from a range of parameter variation, in superimposed plots (Figure 3, left panel). Inspection of these output plots can be a surprisingly effective way of coming to an understanding of the role of the parameter, making use of human talents for visualizing information, and putting the column of sensitivity coefficients in proper perspective (these coefficients can be occasionally misleading (discussed later). This simple step should be used on all parameters with significant sensitivity columns.

"Sensitivity graphs" further expand ones insight into model sensitivity to a certain parameter of interest, and also bring together sensitivity columns and trajectory information. This method consists of graphing behavior ratios versus parameter ratios for a wide range, as in Figure 3 (right panel). Notice that each "graph" is basically a graphical extension of each coefficient, basically showing the five possible coefficients (slopes) that could be placed in the particular location. Typically logarithmic scales are employed. Visual inspection of this graph provides information on how linearly the behavior changes with parameter variation. It also suggests the useful operating range of the parameter of interest. This is possibly the most important sensitivity tool from a design perspective.

ORIGINAL PAGE IS
OF POOR QUALITY

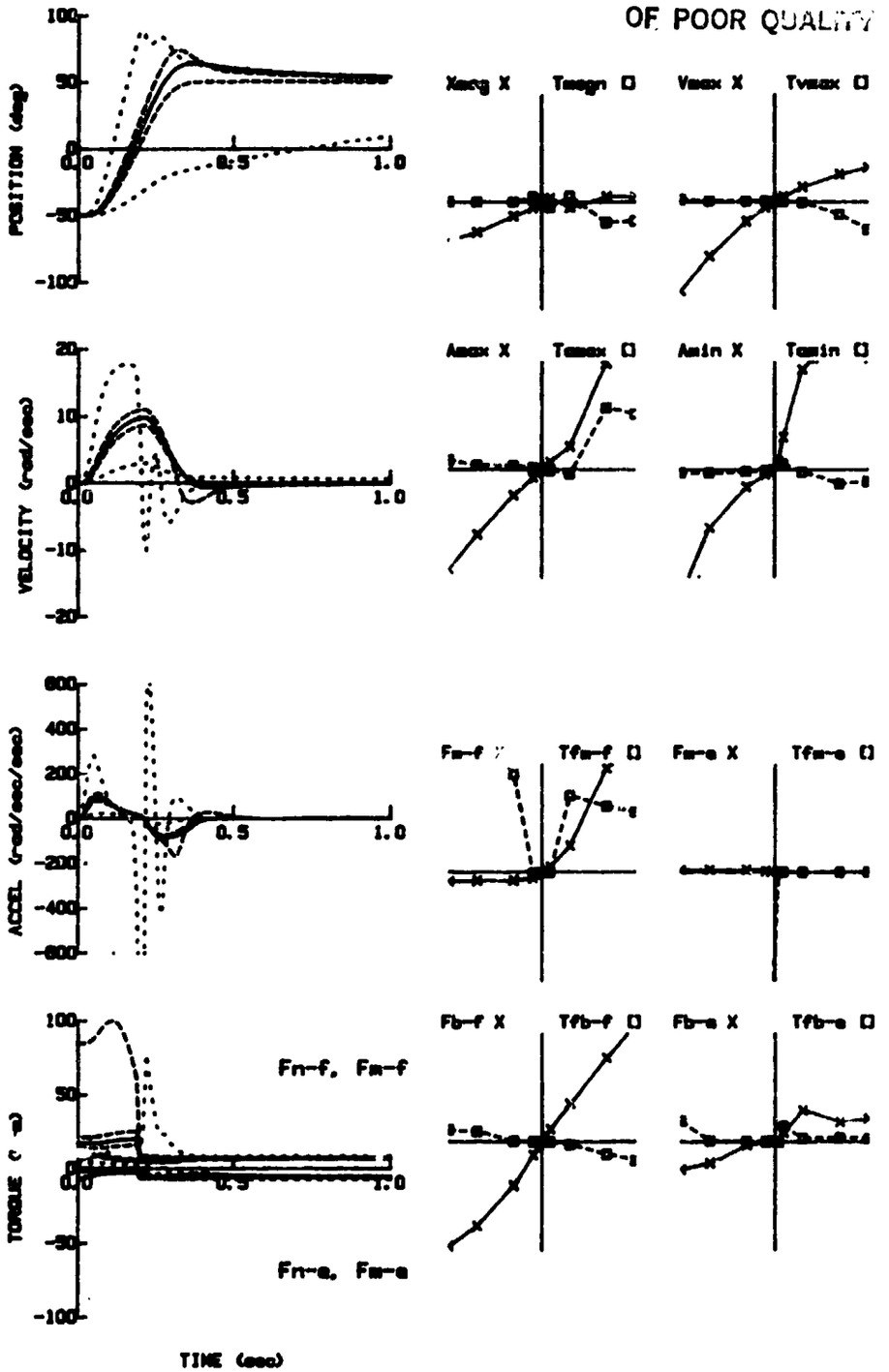

Figure 3: Sensitivity Trajectories (left panel) and Sensitivity Graphs (right panel) for the controller parameter PH-f, the pulse height for the agonist pulse, Task #1. Large dash is for 4/5 and 5/4 times nominal. For Sensitivity Graphs, range is 1/10 to 10, on logarithmic scales, for both the parameter (abscissa) and the behavior (ordinate).

RESULTS:

Task #1: "Generic" Run: Some simple results, for a "typical", moderate-speed run, were displayed in Table 2 (sensitivity matrix) and Figure 3 (sensitivity trajectories and sensitivity graphs). From the sensitivity matrix, it is seen that the most important system parameters are the plant inertia (Jp), especially for peak accelerations and for the timing of all peak values; Hill's parameter Bh-f, especially for peak magnitudes; the time constant of activation (Ta_1), and the parallel elastic fit parameter Kp_2. From the nature of the equation for the parallel elasticity (Table 1) we see that the location of the parallel elastic concavity will automatically define the position operating range. The model output is also particularily sensitive to controller signal pulse parameters such as PH1 and PH2 - not an unexpected finding since a well-designed tracking system is usually sensitive to its own input for tracking tasks.

Based on these sensitivity matrix results, the parameters mentioned above appear to be of particular interest for this task. In Figure 3, variation in the agonist pulse height parameter (PH1) is displayed using sensitivity trajectories and sensitivity graphs. These results show more explicitly the effect of varying the agonist pulse height. For reference, an average adult male can contract the flexor group to about 60 N-m. Similar plots, not presented here, are then produced for the other highly sensitive parameters.

ORIGINAL PAGE IS
OF POOR QUALITY

Task #2: Unloaded Fast Voluntary Elbow Flexion: The effects of a 60 N-m, 100 ms agonist pulse are displayed in Figure 4. The corresponding antagonist pulse during this time is only 1 N-m. Notice that the peak angular velocity is about 14 rad/sec. (For a longer pulse width, one finds a peak velocity of about 19 rad/sec both for the model and for the average intact adult human (Dern (1947), Wilkie (1950), Pertuzon and Bouisset (1973)). Zero degrees is defined here as the rest elbow position (where the lumped parallel elasticity is zero), of 100 degrees between the humerous and the ulna. Notice that movements of about 80 deg are possible in each direction, with the nonlinear parallel elastic element automatically keeping the joint position within this physiological operating range.

In Table 3 a more complete sensitivity matrix for internal system parameters, including flexor and extensor parameters for both series elastic and torque-velocity (shortening and lengthening) properties, is presented. Notice that, while the general trends in this table are similar to those in the previous table, the details are quite different. Also notice the general insensitivity of the "extensor" muscle parameters. This shows that it is the flexor parameters that are of primary importance for this particular task and furthermore shows the relative significance of the various flexor parameters to each other for each behavior.

In Figure 5 sensitivity trajectories and sensitivity graphs are obtained for a few of the more important internal system parameters such as Bh, Jp and Tal. Notice that, by combining all three techniques, a remarkably clear picture of the role of each of these parameters emerges. We see, by all three methods, that the inertial term affects mainly acceleration information and the timing of peak values. The latter two methods both show that the system is more sensitive to increases in inertia - something common in everyday life and sporting events. All three methods also show that the torque-velocity parameter Bh (Figure 5b) mainly influences magnitude information, with less effect on timing. The acrtivation time constant parameter Ta_1, which basically filters the neuromuscular signal before "passing" it, effects system behavior as might be expected. Notice that the sensitivity increases proportionally more when the parameter increases in value than when it decreases (best seen by the sensitivity graph).

TABLE 3:

SENSITIVITY MATRIX FOR TASK: "Simple, Fast, Unloaded Movement":

	NOMINAL	Jp	Bp	Kp	Kp1	Kp2	Ka1-f	Ka2-f	Ka1-e	Ka2-e	Af-f	Af-e	Bh-f	Bh-e	Bh-fv	Af-fv	Bh-fv	Ta1	Ta2
Magn:	122.6 deg	0.050	-0.065	-0.036	-0.015	-0.200	-0.002	-0.004	0.001	0.002	-0.173	-0.047	0.333	0.023	-0.073	-0.017	0.022	-0.001	-0.003
Vmax:	805 d/s	-0.347	-0.090	0.024	-0.004	-0.130	-0.017	-0.053	-0.000	-0.003	-0.323	-0.085	0.345	0.005	-0.031	-0.005	0.005	-0.226	-0.038
Amax:	16407 d/s/s	-0.527	-0.031	0.037	-0.004	-0.170	-0.013	-0.011	-0.005	-0.002	-0.166	-0.004	0.367	-0.006	-0.026	-0.004	-0.008	-0.447	-0.112
Amin:	6081 d/s/s	-0.766	-0.005	0.000	-0.002	-0.046	-0.037	-0.005	0.000	0.000	-0.005	0.022	1.932	-0.026	0.137	0.022	-0.026	-0.588	-0.051
Tmagn:	330 ms	0.131	0.750	-0.101	-0.000	-0.755	0.022	0.057	0.000	0.000	0.000	0.000	0.087	0.000	-0.017	0.000	0.000	0.333	0.049
Tvmax:	125 ms	0.160	-0.029	-0.015	0.000	0.036	-0.012	-0.029	0.002	0.000	-0.004	0.022	-0.176	0.002	0.770	0.022	0.023	0.137	-0.038
Tamax:	51 ms	0.281	-0.028	0.000	0.000	0.170	-0.015	-0.287	0.000	0.000	0.000	0.000	-0.014	0.000	0.062	0.000	0.000	0.252	-0.112
Tamin:	189 ms	0.234	-0.061	0.000	0.0058	0.078	-0.004	-0.011	0.000	0.000	-0.004	-0.000	0.134	0.000	0.038	-0.008	0.000	0.190	-0.011
Fm-f:	15.6 N-m	0.283	0.009	-0.013	-0.004	-0.069	0.003	0.040	-0.004	-0.010	-0.143	0.006	0.343	-0.017	0.036	0.006	-0.017	-0.213	-0.060
Fm-e:	8.4 N-m	0.000	0.009	0.078	0.019	1.300	0.000	-0.002	-0.000	-0.010	0.026	0.070	-0.032	-0.043	0.183	0.037	-0.043	-0.070	0.002
Fb-f:	37.6 N-m	-0.219	-0.028	0.000	-0.001	-0.063	0.016	0.039	0.001	0.001	0.181	-0.003	-0.136	0.004	-0.019	-0.030	0.004	-0.434	-0.108
Fb-e:	1.9 N-m	0.101	-0.027	-0.008	0.001	0.741	-0.004	-0.011	0.000	0.010	-0.330	0.136	0.717	-0.167	0.971	0.136	-0.167	-0.118	-0.010
Fm-fe:	11.4 N-m	0.300	0.018	-0.006	-0.034	-0.110	-0.029	-0.057	-0.008	-0.011	-0.202	-0.040	0.068	-0.007	-0.027	-0.004	-0.008	-0.488	-0.112
Tfm-f:	30 ms	0.287	0.015	-0.015	0.000	0.000	-0.188	-0.318	0.000	0.000	0.000	0.000	0.014	0.000	0.029	0.000	0.000	0.240	0.171
Tfm-e:	207 ms	-	0.000	-	-	-	0.003	0.003	0.000	-0.003	0.006	0.000	-	-0.021	-	0.000	-0.021	0.279	0.082
Tfb-f:	104 ms	0.007	-0.007	0.000	0.000	-0.021	-0.007	-0.007	0.000	0.000	0.007	0.000	0.000	0.000	0.000	0.000	0.000	0.041	0.041
Tfb-e:	193 ms	0.131	-0.000	-0.019	0.000	-4.498	0.000	-0.004	0.000	-0.004	-0.328	-0.004	0.139	-0.049	-0.484	-0.004	-0.049	0.113	0.077
Tf-fe:	55 ms	0.349	0.026	0.000	0.013	-	-0.000	-0.292	0.001	0.000	-0.026	0.000	0.013	-0.013	0.039	0.000	-0.013	0.287	0.193

ORIGINAL PAGE IS
OF POOR QUALITY

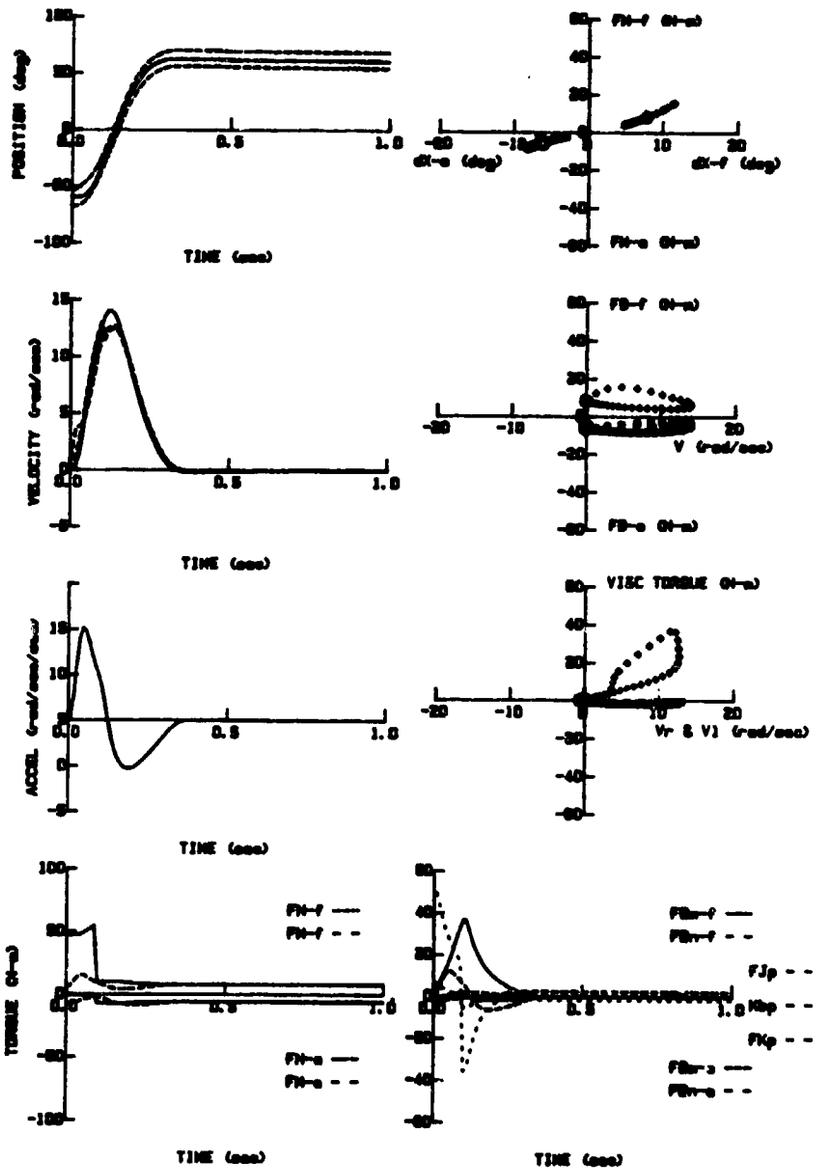

Figure 4: Plots of input, output, and internal variables for the "normal" run of Task #2. Lower left contains the model input variables (FN-f & FN-e) and the resulting muscle output torques (FM-f & FM-e). Upper and middle left contain kinematic output information as well as the positions and velocities of flexor and extensor internal nodes (dashed). On the right, from top to bottom, are internal variable plots for the series elastic element, the instantanous externally seen torque-velocity behavior, the viscous muscle torque versus node velocity, and the torque propogation for varous model elements. For the 3 top right plots, time is an implicit parameter, with a point being produces every 10 ms.

ORIGINAL PAGE IS
OF POOR QUALITY

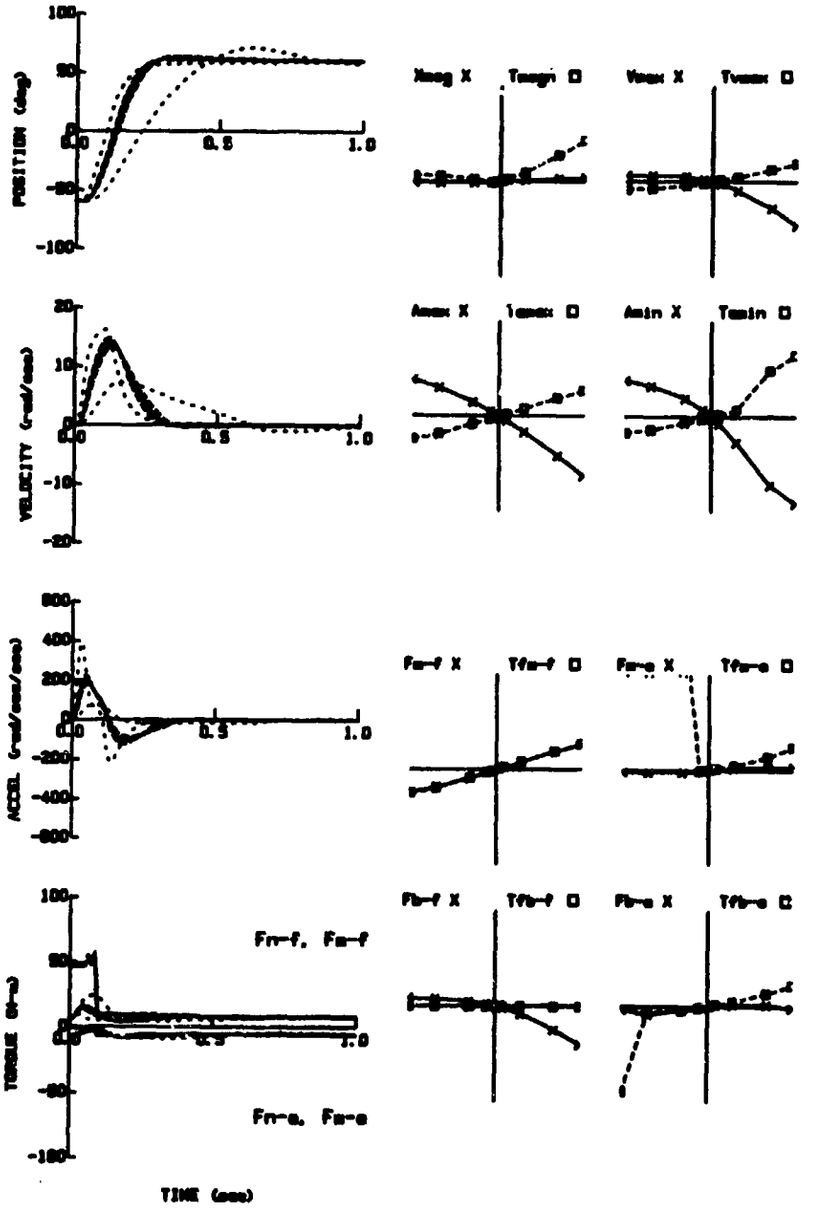

Figure 5a: Sensitivity Trajectories (left panel) and Sensitivity Graphs (right panel) for parameter Jp (plant inertia), Task #2. Large dash is for 4/5 and 5/4 times nominal, smaller dash is for 1/5 and 5 times nominal. For Sensitivity Graphs, range is 1/10 to 10, on logarithmic scales, for both the parameter (abscissa) and behavior (ordinate).

ORIGINAL PAGE IS
OF POOR QUALITY

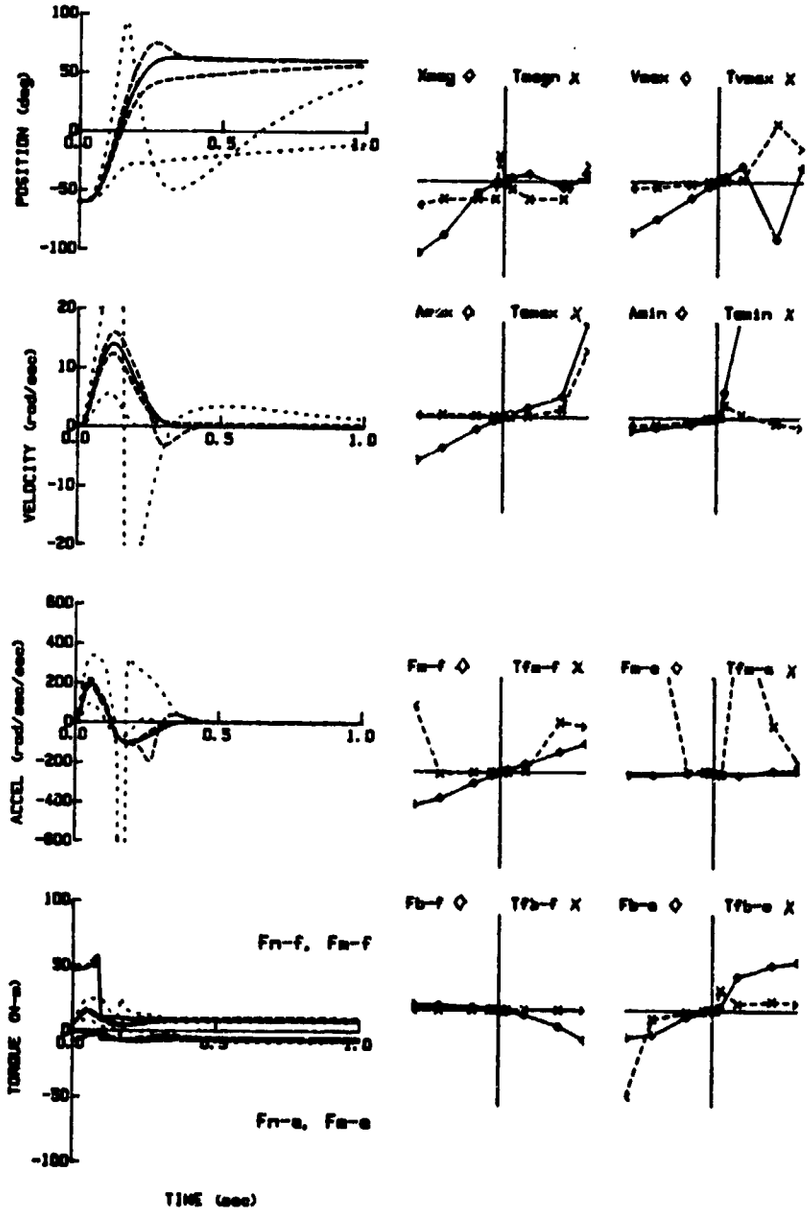

Figure 5b: Sensitivity Trajectories (left panel) and Sensitivity Graphs (right panel) for parameter Bh (one of the "Hill's" constants for shortening muscle). Large trajectory dashes: 4/5 and 5/4 of nominal, smaller dashes: 1/5 to 5 times nominal. Sensitivity Graph range: 1/10 to 10, logarithmic units, for both parameter (abscissa) and behavior (ordinate).

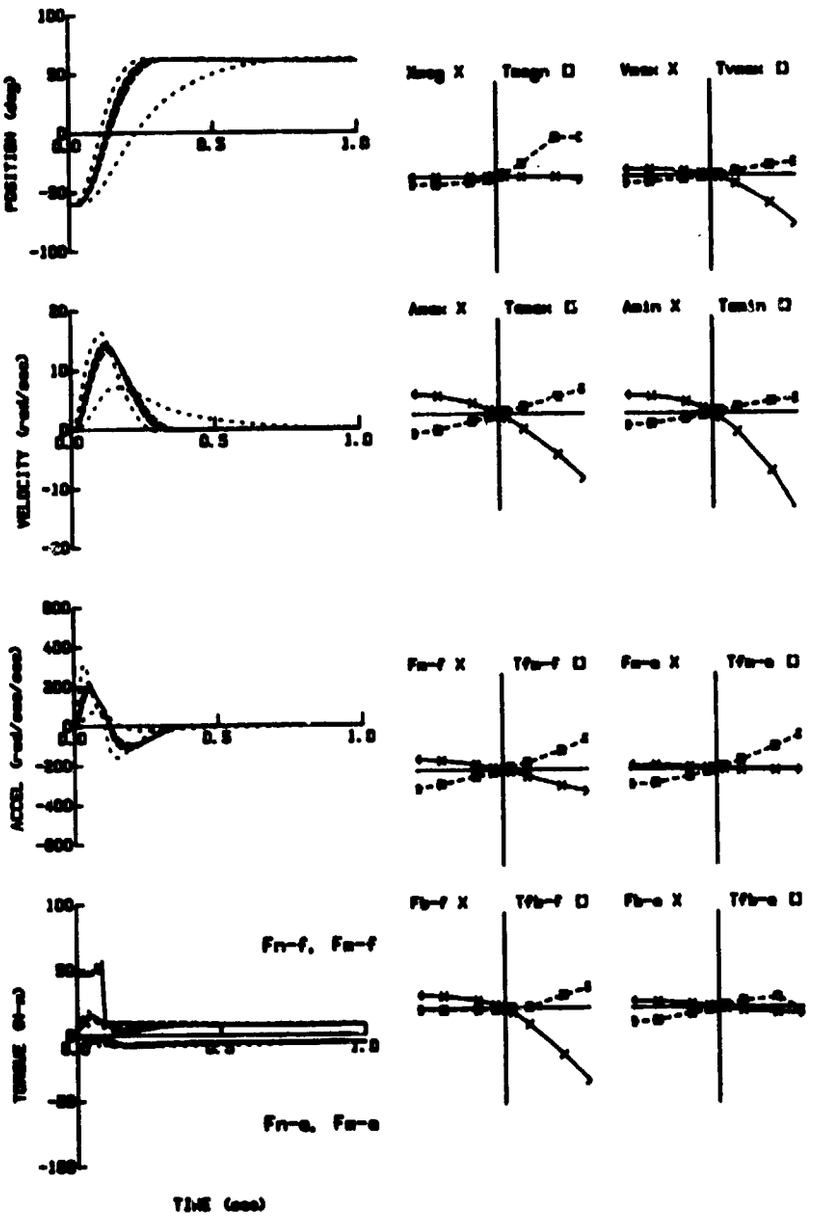

Figure 5c: Sensitivity Trajectories (left panel) and Sensitivity Graphs (right panel) for parameter Tal (one of the two time constants representing muscle activation). Large trajectory dashes: 4/5 and 5/4 times nominal, smaller dashes: 1/5 and 5 times nominal. Sensitivity Graph range: 1/10 to 10, logarithmic units, for both parameter (abscissa) and behavior (ordinate).

Task #3: Maximum Voluntary Flexion with an External Load: This task represents an extension of the previous task, only with the addition of an external "isotonic" load of 12 N-m and a 0.1 kg-m**2 added inertia (a light bar being grasped). The task is based on some of the classical experimental data of Dern et al (1947), and the results are consistent with this work. The time of contraction is now 250 msec. Run dynamics are displayed in Figure 6a. An inspection of Table 4 shows that, once again, while many of the parameters are very similar, others differ sharply. Such observations guide further analysis of this task (not presented here).

In Figure 6b we see the sensitivity to a new type of parameter - a disturbance (i.e. the external load). Here the "base" external load of 12 N-m is varied as any other parameter would be. The sensitivity of the system to such an external load becomes well understood via inspection when all three methods are used. Notice that the factor of ten parameter change (to 120 N-m) is not attempted since it would injure a normal limb.

In Figure 6c and 6d we see the sensitivity to another new type of parameter: an initial condition. In this instance it is an initial against-movement velocity of 2 and 2- rad/sec. Notice that, in the absence of any initial inertial dynamics, the lengthening torque-velocity properties are able to easily compensate for the initial condition of Figure 6d, with the effect being negligible by the time of peak velocity, position or negative acceleration - only the peak positive acceleration is significantly affected, and then only for initial velocities of greater than 4 rad/sec. The sensitivity for the "with" initial velocity is also compensated for fairly well. These findings are in contrast to previous results for the fast, low inertia eye movement system (Winters et al (1983).

TABLE 4:

SENSITIVITY MATRIX FOR: Maximal Contraction Against External Load

	NOMINAL	Jp	Bp	Kp	Kpl	Kal-f	Ka2-f	Af-f	Bb-f	Pafv	Ta1	Ta2	PB-f	PB-e	EXT LOAD	Vo-	Vo+
Magn:	114 deg	0.011	-0.032	-0.013	-0.398	-0.001	-0.006	0.095	-0.268	-0.031	-0.018	-0.003	0.135	-0.175	-0.365	-0.021	0.021
Vmax:	565 d/s	-0.131	-0.059	-0.000	-0.575	-0.003	-0.017	-0.433	0.788	-0.015	-0.096	-0.016	0.536	-0.259	-0.401	-0.007	0.004
Amax:	5492 d/s/s	-0.574	-0.024	0.002	0.924	-0.006	-0.009	-0.129	0.368	-0.101	-0.419	-0.081	0.750	-0.184	-0.475	0.386	-0.210
Amin:	-4858 d/s/s	0.228	-0.183	0.028	1.000	-0.299	-1.281	-0.512	1.839	-0.987	1.480	0.159	1.814	-0.539	-1.387	-0.068	0.384
Tmagn:	363 ms	0.268	0.056	-0.840	0.000	-0.005	0.019	0.000	-0.065	0.024	0.184	0.025	0.088	0.748	-0.196	0.038	-0.057
Tvmax:	209 ms	0.086	-0.003	0.000	0.078	0.000	0.028	-0.031	0.017	-0.003	0.052	0.039	-0.021	-0.010	-0.006	0.003	-0.006
Tamax:	59 ms	0.293	-0.010	-0.011	-0.192	-0.057	-0.274	-0.011	0.022	0.023	0.269	0.154	-0.123	-0.012	-0.069	-0.180	0.157
Tamin:	278 ms	0.385	-0.111	0.033	-	-0.020	-0.007	-0.061	-0.051	-0.113	0.141	0.031	-0.014	-0.108	-0.037	-0.097	-0.040
Fm-f:	9.1 N-m	0.137	0.002	-0.001	0.264	0.003	0.023	-0.064	0.224	0.017	-0.123	-0.028	0.536	0.036	0.170	0.133	-0.086
Fm-e:	7.1 N-m	0.029	0.000	0.019	3.388	0.001	0.000	0.006	0.060	0.079	0.000	0.000	-0.043	0.058	0.000	0.000	0.112
Fv-f:	14.4 N-m	-0.082	-0.026	-0.000	-0.569	-0.000	-0.004	0.066	-0.120	-0.007	-0.120	-0.020	1.250	-0.122	-0.317	0.009	0.000
Fv-e:	1.5 N-m	0.231	-0.04e	-0.001	3.268	-0.002	-0.018	-0.051	0.838	0.382	-0.098	0.070	0.542	-0.003	-0.406	0.020	0.314
Fm-fo:	3.0 N-m	0.229	0.004	-0.012	3.614	-0.003	-0.018	-0.075	0.377	-0.006	-0.224	-0.041	1.220	-0.237	0.144	0.147	-0.078
Tfm-f:	34 ms	0.387	0.000	0.000	0.603	-0.000	-0.311	-0.012	1.196	0.024	0.235	0.151	-0.338	0.079	-1.388	-0.145	0.165
Tfm-e:	-	-	-	0.000	0.000	-	-	-	-	-	-	-	-	-	-	0.000	-0.085
Tfb-f:	201 ms	0.041	0.000	0.000	0.011	0.000	0.000	0.000	-0.041	0.000	0.056	0.003	-0.035	0.000	0.017	0.000	-0.017
Tfb-e:	173 ms	0.006	-0.275	0.000	-1.784	-0.275	-0.271	-0.193	0.150	-0.308	0.134	0.043	0.048	-0.284	0.698	-	-
Tfm-fo:	65 ms	0.279	0.010	0.000	-	0.010	-0.284	0.022	1.120	0.022	0.288	0.188	0.026	-0.011	-1.867	-0.236	0.151

ORIGINAL PAGE IS
OF POOR QUALITY

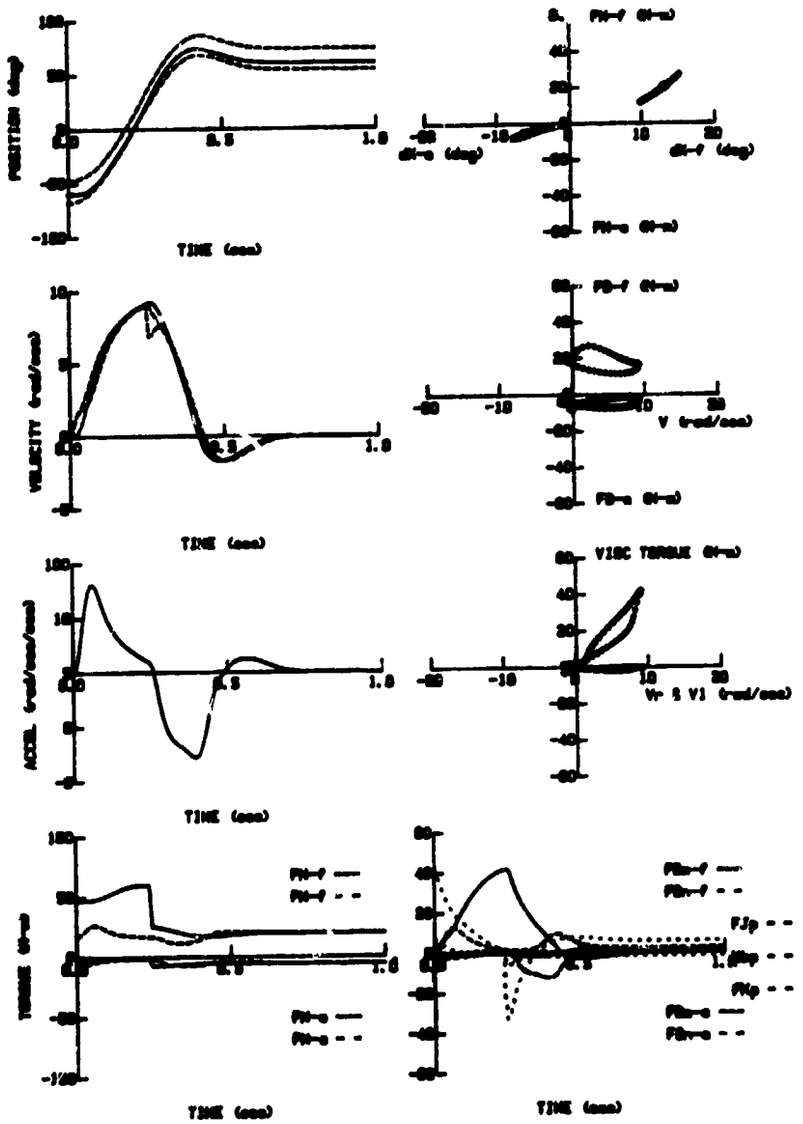

Figure 6a: Plots of input, output, and internal variables for the "normal" run of Task #3. Variables plotted are the same as for Figure 4. The input signal is a 250 ms pulse of magnitude 60 N-m for the flexor. An external load of 12 N-m (not graphed) exists throughout the movement. The steady-state input signals take this fact, plus the static torque-angle relations, into account. Notice the large torque lost to muscle viscosity.

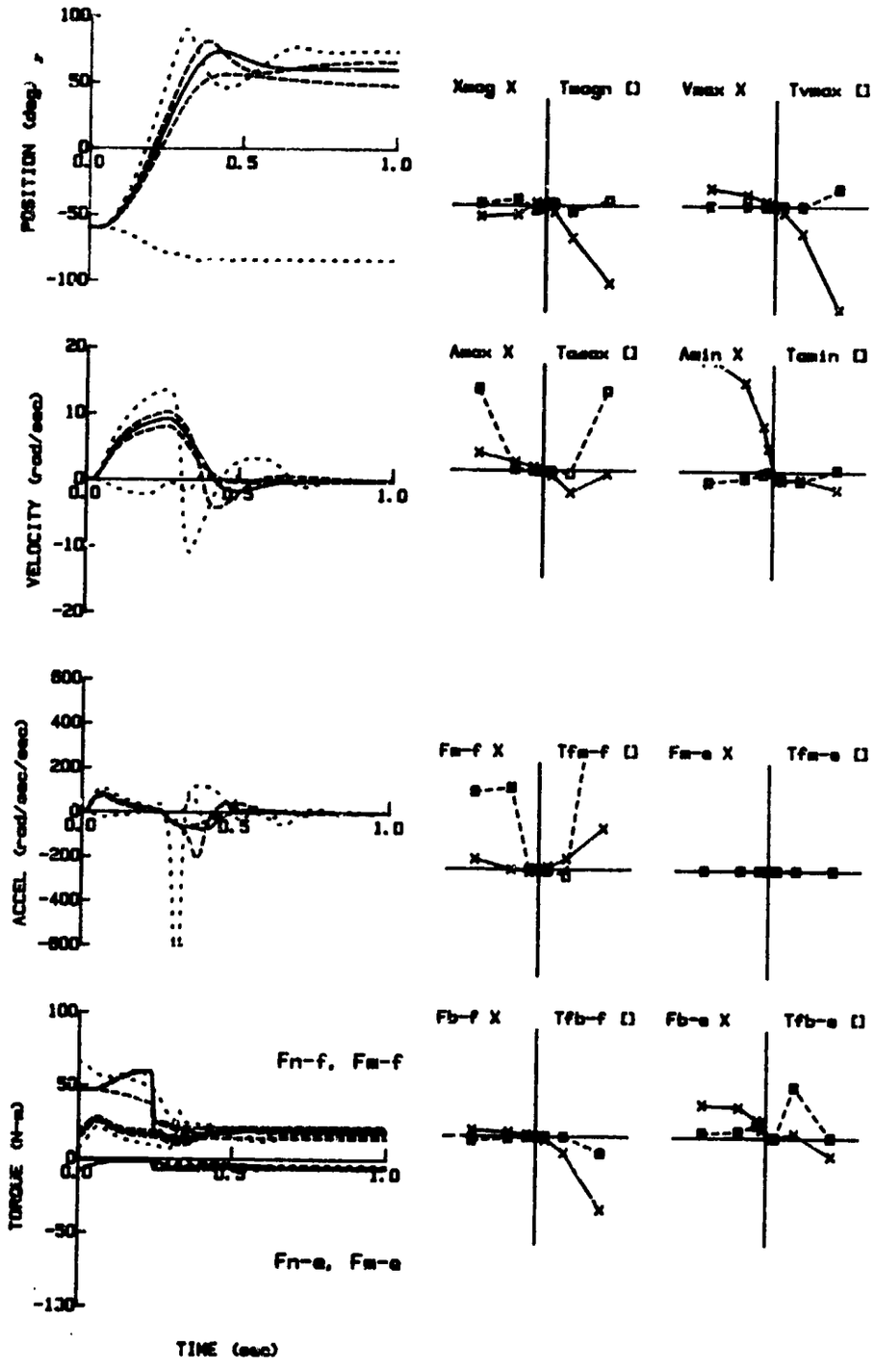

Figure 6b: Sensitivity Trajectories (left panel) and Sensitivity Graphs (right panel) for parameter "EXT LOA ", an external torque with a nominal value of . ` N-m. Variables plotted are the same as in Figure 5.

ORIGINAL PAGE IS
OF POOR QUALITY

ORIGINAL PAGE IS
OF POOR QUALITY

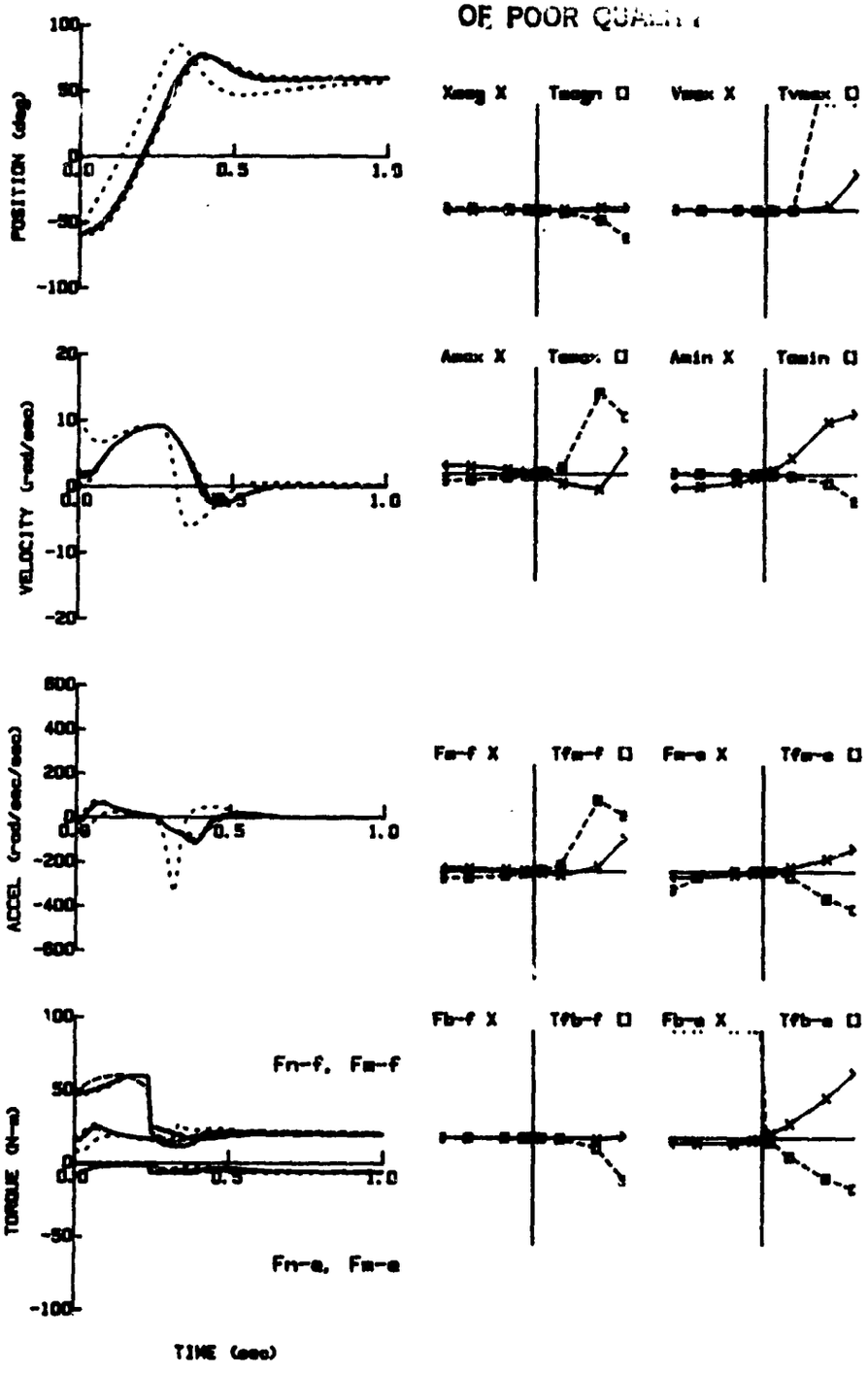

Figure 6c. Sensitivity Trajectories (left panel) and Sensitivity Graphs (right panel) for an initial velocity of 2 rad/sec (nominal). Axes ranges and behaviors plotted are the same as in Figure 5.

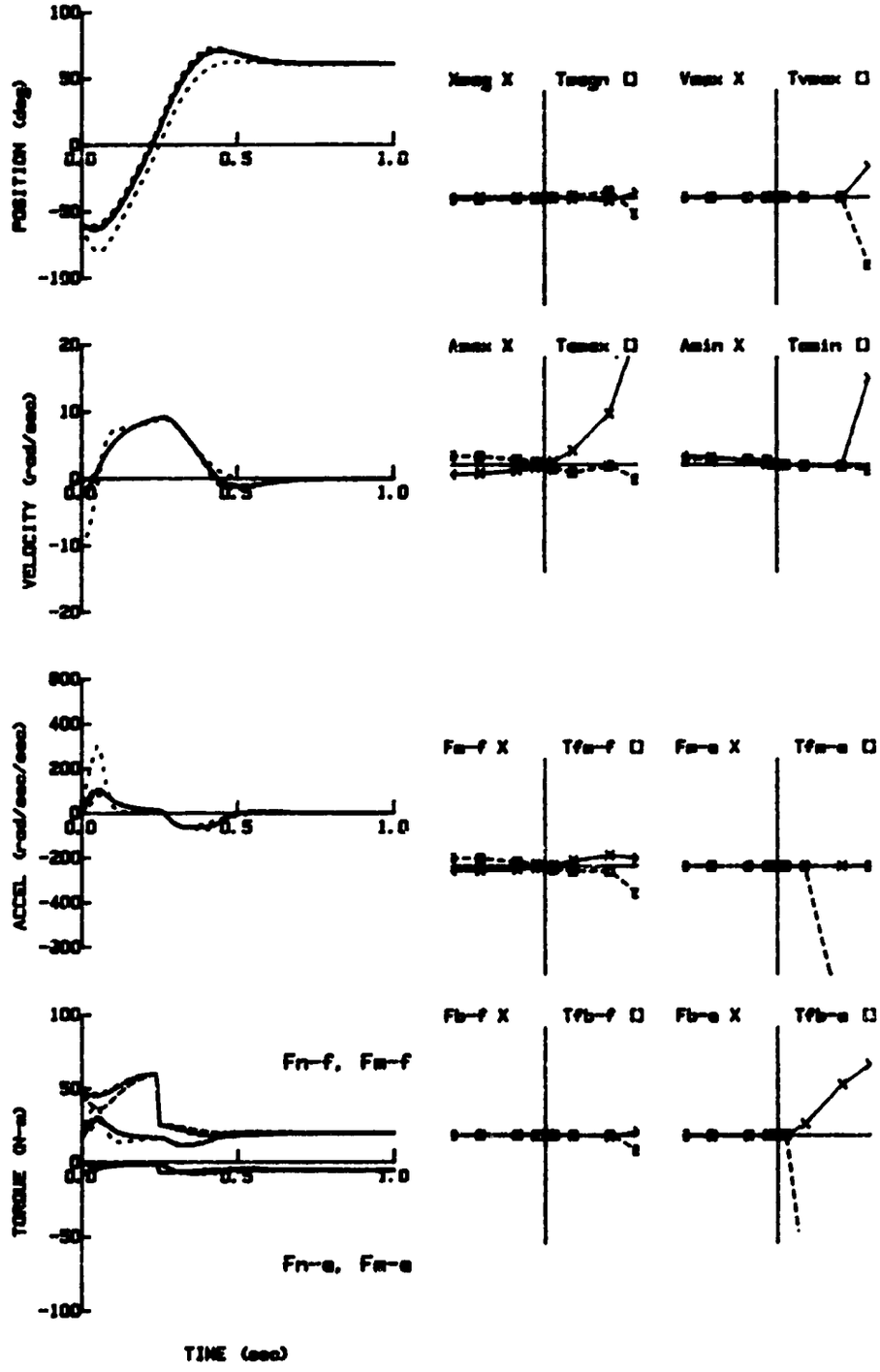

Figure 6d. Sensitivity Trajectories (left panel) and Sensitivity Graphs (right panel) for an initial velocity of -2 rad/sec (nominal). Axes ranges and behaviors plotted are the same as in Figure 5.

ORIGINAL PAGE IS
OF POOR QUALITY

Task #4: Maximal Isometric Contraction: This is a fundamentally different type of contraction than those considered above. A maximal contraction is resisted by an equal and opposite external force. An interesting question is whether or not a different set of parameters become most important. The sensitivity matrix of Table 5 shows some sharp differences both in what parameters and in what behaviors are most important. First of all, since there is no movement, there is no change in overall position, velocity or acceleration, leaving only force propogation. As expected, the passive plant parameters Jp, Bp and Kp have no effect. We now see that the series elasticity, as well as Hill's constants and the time constant of activation/deactivation, play a role. Also, because, for this task of contraction, the hypothetical internal muscle node is shortening, the lengthening muscle parameters like Fm-fv also do not play a role until after 500 msec.

Inspection of the sensitivity matrix indicates that only the viscous torque behavior seems to be effected. This result is misleading, as can be seen from the sensitivity trajectory for Ks2-f (Figure 7). This example shows one of the major limitations of sensitivity coefficients and graphs: in the process of extracting **useful** information, **other** information is invariably lost, and, furthermore, the information extracted can sometimes be misleading. It turns out that these observations are particularily true for the series elastic parameters, which tend to primarily effect movement with high frequency components, such as movement initiation or voluntary or involuntary limb oscillation. Thus, subtle information on trajectory shapes can be lost when sensitivity coefficients and graphs are restricted to behaviors such as peak output values and the corresponding time of peak values. Although such phenomena are difficult to define by the "behaviors" presented here, they are possibly discribable by other types of behavior definitions, such as oscillation frequency. In any case, sensitivity trajectories must be plotted.

TABLE 5:

SENSITIVITY MATRIX FOR TASK: "Maximal Voluntary Isometric Contraction":

		Jp	Bp	Kp	Ks1-f	Ks2-f	Af-f	Bh-f	Fmfv	Ta1	Ta2
Pm-f:	60.0 N-m	0	0	0	0.000	0.000	0.000	0.000	0	-0.002	0.000
Pb-f:	13.2 N-m	0	0	0	-0.184	-0.727	0.278	-0.727	0	-0.610	-0.135
Tfm-f:	500 ms	0	0	0	0.000	-0.001	0.000	-0.001	0	0.289	0.000
Tfb-f:	43 ms	0	0	0	-0.017	-0.360	0.132	-0.360	0	0.334	0.292

Task #5: A Simple External Load, With No Neural Control: Here we have a steady neural input signal of 6 N-m for both the flexor and extensor groups. An external load of 12 N-m is applied for 200 msec, and no effort is made to resist this disturbance via neural feedback. Inspection of the resulting sensitivity matrix (Table 6) shows again that the relative sensitivity of the various parameters and behaviors is a function of the task.

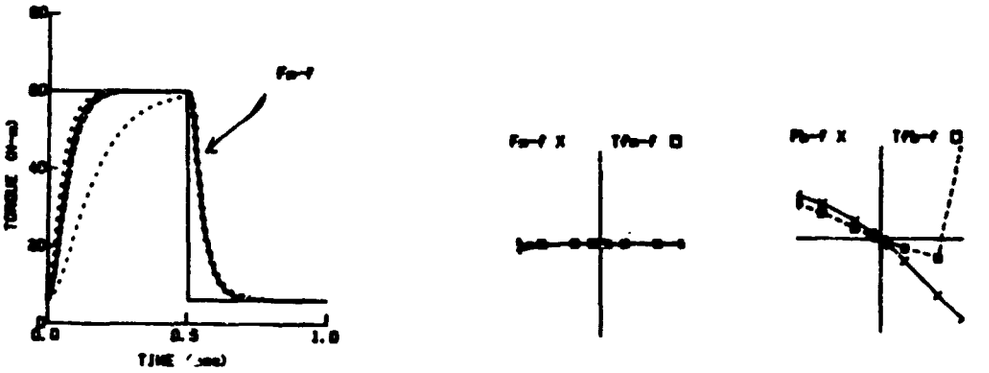

Figure 7: Sensitivity Trajectory for parameter Ks_2, a series elastic fit parameter (left panel). Small dashed is for 1/5 and 5 times nominal - note lack of symmetry. Sensitivity Graphs (right panel) are for the same parameter. Ranges are from 1/10 to 10, in logarithmic units, for both the parameter (abscissa) and the behaviors (ordinate). Note the lack of information for Fm-f.

TABLE 6:

SENSITIVITY ANALYSIS FOR: External Load with no Active Resistance

	NOMINAL	Jp	Bp	Kp	Kp2	Ksl-f	Ks2-f	Af-f	Bm-f	Fmfv	Tal
Magn:	49.4 deg	-0.172	-0.154	-0.142	-0.093	-0.015	-0.032	-0.164	**0.394**	-0.375	-0.010
Vmax:	267.5 d/s	-0.181	**-0.176**	-0.147	-0.024	-0.008	-0.018	**-0.188**	**0.437**	-0.405	-0.013
Amax:	5730 d/s/s	**-1.000**	0.000	0.000	0.000	0.000	0.000	0.001	0.000	0.001	0.000
Amin:	-5742 d/s/s	**-1.108**	0.018	0.078	0.816	-0.004	-0.010	0.018	-0.032	0.019	0.012
Tmagn:	266 ms	**0.277**	-0.030	-0.101	0.000	0.014	0.022	-0.049	0.100	-0.095	-0.008
Tvmax:	196 ms	**0.468**	-0.131	**-0.275**	**-0.223**	**0.033**	0.076	-0.158	0.335	-0.264	-0.057
Tamax:	1 ms	0.000	0.000	0.000	0.000	0.000	0.000	0.000	0.000	**0.001**	0.000
Tamin:	200 ms	**0.004**	0.000	0.000	0.003	0.001	0.000	0.000	0.000	0.000	0.000
Fm-f:	6.00 N-m	0.001	0.000	0.030	**0.115**	0.000	0.000	0.005	-0.033	0.041	0.000
Fm-e:	7.47 N-m	-0.018	-0.006	-0.030	-0.000	-0.001	-0.003	-0.006	0.017	**0.183**	0.003
Fb-f:	2.87 N-m	-0.135	-0.094	-0.062	-0.004	-0.003	-0.008	0.165	**-0.402**	-0.234	0.011
Fb-e:	1.51 N-m	-0.064	-0.039	-0.023	0.385	-0.004	-0.009	-0.041	0.101	**0.711**	0.006
Fm-fe:	4.38 N-m	-0.110	-0.074	-0.048	-0.002	-0.003	-0.008	0.096	**-0.227**	0.173	0.009
Tfm-f:	2 ms	-	0.000	-	-	0.000	0.000	-	-	-	0.000
Tfm-e:	101 ms	**0.516**	-0.014	-0.051	-0.007	0.029	0.065	-0.051	0.115	0.098	**0.107**
Tfb-f:	154 ms	**0.518**	-0.071	-0.182	-0.048	0.019	0.038	-0.087	0.226	-0.136	0.047
Tfb-e:	135 ms	**0.591**	-0.043	-0.133	**0.418**	0.032	**0.077**	-0.072	0.165	**-0.858**	0.069
Tfm-fe:	150 ms	**0.530**	-0.064	-0.169	-0.045	0.019	0.044	-0.074	0.196	-0.139	0.048

In Figure 8 the sensitivity trajectories and graphs are obtained for an interesting parameter that is not well understood. This is "Fm-fv", a torque-velocity parameter, discussed earlier, that influences only lengthening muscle (by giving the lenthening muscle torque eccentric torque saturation value, nominally 30% above isometric for any given activation level). The fact that this parameter is significant shows that, for this task, the constitutive relation used for the lengthening extensor muscle group is important.

ORIGINAL PAGE
OF POOR QUALITY

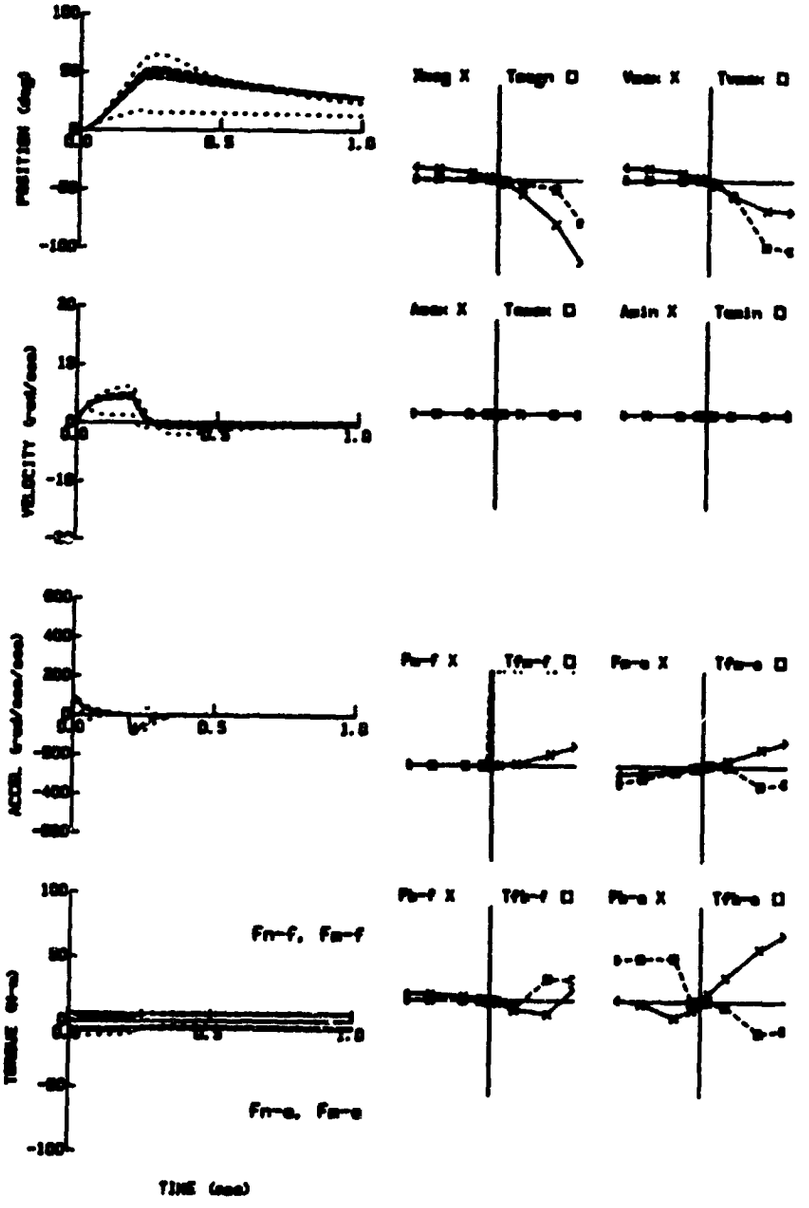

Figure 8: Sensitivity Trajectories (left panel) and Sensitivity Graphs (right panel) for parameter Fm-fv, a torque-velocity parameter for lengthening muscle. This parameter gives the percentage above isometric that a muscle can contract when lengthening at medium-to-high velocity, i.e. the saturating torque for lengthening muscle. Trajectory ranges, axes labeling, and axes ranges are as in Figure 5.

DISCUSSION:

The five simple tasks considered above barely scratch the surface of all the potential movements of the elbow joint. These movements seemed representative of the range of possibilities. Furthermore, the neural inputs were purposely kept simple for the sake of clarity of presentation.

In reality, however, neural inputs - as well as system output, are more complex. Over the last few decades a large amount of research has been done on upper limb movement, including elbow movements performed both in isolation and in conjunction with movements of other joints. Much of this data is for atheletic performance. Components of such data can be simulated using JAMM. This is possible because the model contains all of the parameters that are needed to describe all basic nonlinear muscle properities - the model is purposely constructed to be able to simulate a the full range of types of tasks seen in the literature.

By using sensitivity analysis the parameters of primary importance can be determined for any particular task. This provides insight into the movement task under analysis. It also suggests ways for task-specific model reduction, if desired.

Another area of interest is the sensitivity analysis protocol. Once a task for analysis is chosen, the following steps were found to be represent an optimal protocol: First, a **sensitivity matrix** is constructed, the size of which depends on the parameters and behaviors of interest. The coefficients in the matrix are usually best found using the "logarithmic" method. This gives one a global view of model performance and furthermore guides one to the areas of interest for more detailed work. Second, **sensitivity trajectories** are used to help visualize the effect of a given parameter. Sensitivity Trajectories are also a good way to scan for problems in coefficient values. Finally, sensitivity graphs are of considerable use in getting a feel for the model behavior as the parameter is varied over a wider operating range. Such information often descibed the potential tolerable range of the parameter and also the linearity of the change in behavior with change in parameter. As such it also can show the extent of the sensitivity matrix°s sensitivity to range used for coefficient determination.

There are a couple of observations worth noting: First, all three methods have weaknesses. Second, one of the main advantages of using such a variety of methods is that the weaknesses of any particular method are exposed by the other methods. Consequently, each method gains strength when combined with the others. Third, the work presented here was only for elbow flexion-extension. These methods are currently being found equally valuable for knee flexion-extension, wrist flexion-extension, and eye, head and wrist rotation.

CONCLUSION:

A number of sensitivity analysis tools have been used on a highly developed model of elbow flexion-extension. It has been found that maximum insight into both model performance and parameter sensitivity appears to require a systematic protocol that employs a variety of sensitivity tools. Each of the methods is strengthened when used in conjunction with the other sensitivity tools. Furthermore, it has been found that the relative sensitivity of the model parameters is a function of the task being studied. Finally, it is suggested that sensitivity analysis should be the cornerstone for task-specific model reduction.

REFERENCES:

An, K. N., Hui, F.C., Morrey, B.F., Linscheid, R.L. and Chao, E. Y., "Muscles Across the Elbow Joint: A Biomechanical Analysis", J. Biomechanics., 14: 659-669 (1981).

Amis, A. A., Dowson, D. and Wright, V., "Muscle Strengths and Musculoskeletal Geometry of the Upper Limb", Engng. Med. 8: 41-48 (1979)).

Bahill, A. T., "Development, Validation and Sensitivity Analysis of Human Eye Movement Models", Crit. Rev. Bio-Engineering, 4: 311 (1980).

Bahler, A. S., Fales, J. T. and Zierler, K. L., "The Active State of Mammalian Muscle", J. Gen. Physiol. 50: 2239, (1967).

Boon, K. L., Hof, A. L. and Wallinga-De Jonge, W., "The Mechanical Behaviour of the Passive Limb", pp 243-248, Medicine and Sport, Biomechanics III, Karger, Basel (1973).

Bouisset, S., "EMG and Muscle Force in Normal Motor Activities", pp 547-583, in: New Developements in Electromyography and Clinical Neurophysiology", J. E. Desmedt (ed) Vol. I, S. Karger, Basel (1973).

Bouisset, S., Lestienne, F. and Maton, B., "Relative Work of Main Agonists in Elbow Flexion", pp 273-279, in Biomechanics V-A, P. V. Komi (ed), Baltimore, Univ. Park Press (1976).

Clark, M. R. and Stark, L., "Senistivity of Control Parameters in a Model of Saccadic Eye Tracking and Estimation of Resultant Nervous Activity", Bull. Math. Biol. 38: 39-57 (1976).

Close, R. I., "Dynamic Properties of Mannalian Skeletal Muscle", Physiological Reviews 52: 129-197 (1972).

Cnockaert, J. C., "Comparison of the Potential El stic Energy Stored and Used by Two Antagonistic Muscular Groups", European J. of Appl. Physiol. and Occ. Phys., 39: 181-190 (1978).

Cnockaert, J. C., Pertuzon, E., Goubel, F. and Lestienne, F., "Series-Elastic Component in Normal Human Muscle", pp 73-78, in Biomechanics VI-A, E. Asmussen and K. Jorgenson (ed), Baltimore, University Park Press (1978).

Dern, R. J., Levene, J. M. and Blair, H. A., "Forces exerted at Different Velocities in Human Arm Movements", Amer. J. Physiol., 151: 415-437 (1947).

Frank, P. M., "Introduction to System Sensitivity Theory", Academic, N. Y. (1978).

Fung, Y. C., "Elasticity of Soft Tissues in Sim e Elongation", Am. J. Physiol. 213: 1532-1544 (1967).

Glantz, S. A., "A Constitutive Equation for the Passive Properties of Muscle", J. Biomech. 7: 139-146 (1974).

Goubel F. and Pertuzon, E., "Evaluation de l'elastic du muscle in situ par une methode de quick-release", Arch. Int. Physiol. 81: 697-701 (1974).

Hatze, H. "Estimation of Myodynamic Parameter Values from Observations on sometrically Contracting Muscle Groups, Europ. J. Appl. Phys. and Occ. Phys., 1981.

Hatze, H. "Myocybernetic Control Models of Skeletal Muscle, Characteristics and Applications", Univ. of S. Africa (1981).

Hayes, K. C. and Hatze, H., "Passive Visco-elastic Properties of the Structures Spanning the Human Elbow Joint", European J. of Appl. Phys, and Occ. Phys. 37: 265-274 (1977).

Hill, A. V., "The Heat of Shortening and the Dynamic Constants of Muscle", Proc. Roy., Soc. B., 126: 126-195 (1938).

Hsu, F. K., Bahill, A. T. and Stark, L., "Parametric Sensitivity Analysis of a Homeomorphic Model for Saccadic and Vergence Eye Movements", Computer Programs in Biomedicine, 6: 108-116 (1976).

Jorgensen, K., "Force-Velocity Relationship in Human Elbow Flexors and Extensors", pp 145-151, in: Biomechanics V-A, P. V. Komi (ed), Baltimore, Univ. Park Press (1976).

Jorgensen, K. and Bankov, S., "Maximum Strength of Elbow Flexors with Pronated and Supinated Forearm, pp 174-180, in: Medicine and Sport, Vol. 6: Biomechanics II, Karger, Basel (1971).

Joyce, G. C. and Rack, P. M. H., "Isotonic Lengthening and Shortening Movements of C Solfeu Muscle", J. Physiol. 204: 475-491 (1969a).

Joyce, G. C., Rack, P. M. H. and Westbury, D. R., "The Mechanical Properties of Cat Soleus Muscle During Controlled Lengthening and Shortening Movements", J. Physiol. 204: 461-474 (1969b).

Komi, P. V., "Measurement of the Force-Velocity Relationship in Human Muscle under Concentric and Eccentrtic Contractions", pp 224-229, in: Medicine and Sport, Vol. 8: Biomechanics III, Karger, Basel (1973).

Le Bozec, S., Maton, B. and Cnockaert, J. C., "The Synergy of Elbow Extensor Muscles During Dynamic Work in Man, I. Elbow Extension", Europ. J. of Appl. Phys. and Occ. Phys.43: 57-68 (1980).

Lehman, S. "A Detailed Biophysical Model of Human Extraocular Muscle, PhD Thesis, U. C. Berkeley (1982).

Lehman, S. and Stark, L., "Simulation of Linear and Nonlinear Eye Movement Models: Sensitivity Analyses and Enumeration Studing of Time Optimal Control", J. Cybern. and Inform. Sci. 2: 21-43 (1979).

Pertuzon, E. and Bouisset, S., "Instantaneous Force-Velocity Relationship in Human Muscle", pp 230-234, in: Medicine and Sport, Biomechanics III, S. Karger, Basel (1973).

Tomovic, R. and Vukobratovic, M., "General Sensitivity Theory", American Elsevier, N. Y. (1972).

Wilkie, D. R., "The Relation Between Force and Velocity in Human Muscle", J. Phys., London, 110: 249-280 (1950).

Wilkie, D. R., "The Mechanical Properties of Muscle", Brit. Med. Bull. 12: 177-182 (1958).

Winters, J. M., Nam, M. H. and Stark. L., "Modeling Dynamical Interactions Between Fast and Slow Movements: Fast Saccadic Eye Movement Behavior in the Presence of the Slower VOR", Math. Biosci. 68: 159-187 (1984).

Zangemeister, W. H., Lehman, S. and Stark, L., "Sensitivity Analysis and Optimization for a Head Movement Model", Biol. Cybern. 41: 33-45 (1981).

D43

N85 14530

SUPPRESSION OF BIODYNAMIC INTERFERENCE BY ADAPTIVE FILTERING

by

M. Velger, S.J. Merhav and A.J. Grunwald

Department of Aeronautical Engineering
Technion - Israel Institute of Technology
Haifa 32000, Israel

ABSTRACT

A novel approach for suppressing biodynamic interference by means of adaptive filtering, is described. Preliminary experimental results obtained in moving base simulator tests are presented. Both for pursuit and compensatory tracking tasks, a strong deterioration in tracking performance due to biodynamic interference is found. The use of adaptive filtering is shown to substantially alleviate these effects, resulting in a markedly improved tracking performance and reduction in task difficulty. The effect of simulator motion and of adaptive filtering on Human Operator describing functions is investigated. Adaptive filtering is found to substantially increase pilot gain and cross-over frequency, implying a more "tight" tracking behaviour. The adaptive filter is found to be effective in particular for high-gain proportional dynamics, low display forcing function power and for pursuit tracking task configurations.

I. INTRODUCTION

Biodynamic interference is a bothersome problem in the man-machine systems area. It occurs when a manual control task is performed on a platform, subjected to translatory or angular external accelerations. Typical examples are: the manual control of large flexible aircraft flying through strong convective turbulence, the manoeuvering fighters under transonic buffeting conditions, tracking tasks performed on hovering rotorcraft, high-speed vehicles travelling over rough terrain or waves, etc. [1-3]. In such tasks the manual control performance may be severely impaired by the resulting involuntary pilot control commands. These originate in the biomechanical coupling between the vibrating vehicle and the control manipulator ("stick feedthrough"), which may be either manual or head mounted, such as in helmet sights. This coupling is due to the dynamic response of various human body elements to external accelerations. In addition to the direct additive stick feedthrough, the vibration of limbs and head increases the pilot remnant noise level, either by interfering with neuromuscular feedbacks needed for precise manual control, or by degrading the visual acuity due to the relative motion between the eye point-of-regard and the display, causing image blurring, [4]

Although the severe effects of biodynamic interference on the pilot vehicle system have been recognized [1-3], successful efforts to eliminate these interferences have so far not been reported. The approach attempted has been to mechanically isolate the pilot from the aircraft by passive means, such as shock-absorbing seats, armrests, etc., [5,6] or by active isolation systems e.g.

Active Vibration Isolation Systems (AVIS), [7,8]. However, since these methods reduce the pilot's inertial accelerations, they actually increase his motion relative to the display or manipulator. Consequently no significant performance improvement was obtained [8]. Moreover, vibration isolation may be undesirable since it may impair the pilot's "seat of the pants" motion cues.

In this paper an adaptive disturbance cancellation technique to eliminate the involuntary pilot commands is described. A Least Mean Square (LMS) adaptive filter [9] has been employed. Its main advantage is its inherent ability to automatically adjust its parameters so that its design requires little or no a priori knowledge of input or human response characteristics. The adaptive filter utilizes the measurements of a platform mounted accelerometer to generate a signal which is a close estimate of the involuntary pilot command. This signal is subtracted from the stick output, thus largely cancelling the biodynamic interference. Since the adaptive algorithm requires little computational effort and memory, it can be easily implemented by a low cost microprocessor.

II. PRINCIPLE OF OPERATION

The following two major cases are considered:

1. The "biodynamic open loop" case, in which the platform motions are independent of the manipulator forcing function. Examples are: pointing of sights or weapons on a moving ship deck or helicopter.

2. The "biodynamic closed loop case" in which the platform motions partly result from the control stick command itself, such as the piloting of an aircraft. The resulting biodynamic stick feedthrough again causes a platform motion, thus constituting a circulating signal.

A block diagram of the biodynamic "open loop" case is shown in Fig. 1. The control error ε between the desired reference signal c and the actual response r is presented to the Human Operator (HO) on a display monitor as the displayed error ε_d. This signal is utilized by the HO to generate the voluntary control command u_c. On the other hand, the biodynamic interference due to the platform motions, generates an involuntary control command u_b which is added to u_c resulting in a total control command u_t. This command being either the control stick force or displacement is translated into an analog or digital signal u. The platform motions are measured by a platform mounted accelerometer. Its output a is passed through a high-pass filter in order to block low-frequency motion components which should not be subtracted. The filtered signal is applied to the adaptive filter and causes it to generate the signal u_a, which is a least squares estimate of the additive interference u_b. By subtracting u_a from u, the filtered control command u_f is obtained.

The diagram of the biodynamic "closed-loop" case is shown in Fig. 2. Unlike the biodynamic open loop case, the aircraft response constitutes the motion disturbance. Therefore, the input to the adaptive filter is now dependent on the voluntary command u_c, which causes a bias in the estimation of u_b. This difficulty can largely be overcome by the use of the high-pass filter, which separates the aircraft response to desired control, which is basically of low frequency, from the aircraft response to involuntary biodynamic disturbance, which is basically of high frequency. The feasibility of this approach has been

demonstrated by digital simulations in Ref. [10]. An example is given of a YF-12 aircraft, in which the stick feedthrough in the longitudinal axis of control results in diverging pilot induced oscillations. The adaptive filter is able to suppress these oscillations effectively without affecting the dynamic response of the aircraft.

In this paper only the biodynamic "open loop" case is evaluated experimentally. The biodynamic "closed loop" case is a subject for further study.

III. EXPERIMENTAL PROGRAM

A. Objectives of the Experiments

The objectives of the experiments were: 1) To investigate the effect of motion on tracking performance in various tasks and 2) to evaluate the effectiveness of the adaptive filter in reducing the effects of biodynamic interference. For this purpose the variances of tracking error and control command were computed and separated into three components: 1) A component correlated with the tracking task forcing function, 2) a component correlated with the simulator motions and 3) a residual uncorrelated component due to pilot remnant. Futhermore, in order to achieve better insights of cause and effect in the error and control signals components, the visual motor dynamic response properties of the human operator were analyzed and computed. In these computations the auto and cross power spectral density functions were computed first and used to determine pilot control and biodynamic transfer functions as well as tracking error and control variance components.

B. Experimental Set-Up

The experimental set-up is shown in Fig. 3. The dynamical tests were carried out with a three-degree-of-freedom moving-base simulator, designed and built at the Flight Control Laboratory at the Technion, Haifa, Israel. The simulator cabin is suspended from three rods, each of which can be moved up and down independently by separate DC torque motors. By moving the rods either collectively or differentially, heave, pitch and roll, or combinations thereof, can be generated. The total weight of the cabin and the subject is balanced by a pneumatic system consisting of an air bellow connected to a large pressure tank. The platform motions are generated digitally in real-time by a DGC Nova 3 minicomputer. The computed motions are converted into analog signals which are fed into the controllers and power amplifiers which drive the torque motors to obtain the required motion. The cabin includes (1) an aircraft ejection seat with automobile type cushions and seat belt; (2) a two-axis isomorphic side stick of an F-16 aircraft; (3) a 9 inch TV monitor on which the tracking task is displayed, and (4) a package of accelerometers and rate gyros, measuring the platform motions. The measured analog signals of the pilot's total control output consisting of voluntary and involuntary control commands as well as platform accelerations, are converted into digital signals and fed into the Nova computer. The computer implements the adaptive filter in real-time and simulates the motions of the controlled element as well as its forcing function. These computed motions are converted into analog signals, fed into a display generator and visualized on the TV monitor in the simulator cabin. During the test run

control commands, controlled element motions as well as platform motions, are recorded and stored on a 10 megabyte disk for further off-line processing.

C. Description of the Experiments

Two tracking tasks were performed in the experiments: 1) A compensatory task, representing e.g. a missile, remotely guided by a vehicle mounted TV camera and 2) a pursuit task representing a teleoperated electro-optical device. For each experimental configuration three cases were investigated. In the first case the tracking task was performed in the absence of motion (static case S), in the second case motion was present but the adaptive filter was not activated (case M) and in the third case motion was present and the adaptive filter was activated (case A). The duration of each test run was 245 seconds during which time histories of the various signals were recorded. For each experimental configuration, each of the cases S,M and A were repeated at least three times in a random sequence, unknown to the subject.

In the experimental program both the display forcing function power and the dynamics of the controlled element were parameters. Their effect on performance and effectiveness of the adaptive filter was investigated.

D. Description of the Tracking Tasks

Both in the compensatory and in the pursuit tracking task the controlled element dynamics included a pure integration combined with a proportional part. This choice was made in order to investigate the biodynamic effects and effectiveness of the adaptive filter in the basic rate and position control tasks. The transfer function of the controlled element is given by:

$$\frac{r(s)}{u_f(s)} = K \cdot \{\frac{1}{s} + K_p \cdot \frac{\omega_o^2}{(s^2 + 2\xi\omega_o s + \omega_o^2)}\} \qquad (1)$$

The second order filtering of the proportional part was included to avoid the appearance of rapid, high frequency display motions. The filter natural frequency ω_o was set to 15 rad/sec and the damping ratio ξ was set to 0.707. The tracking tasks were performed in two axes of control, where for each axis the dynamics of Eq. (1) was employed. However, the adaptive filter was implemented in the lateral axis of control only. On the display monitor a cross and a square were shown. In the compensatory task the cross was kept fixed in the center of the screen and symbolized the controlled element vehicle axis. The square symbolized the target as seen through a vehicle mounted TV camera, and the target motions c were generated for each axis of control independently by passing bandlimited zero-mean Gaussian white noise processes through second order filters with ω_o = 0.7 rad/sec and ξ = 0.3. Thus the deviations of the square from the cross at the center of the screen represented the displayed tracking error ε_d between target motion c and controlled element response r. The objective of the task was to minimize ε_d by bringing the square to the cross center. In the pursuit task the cross symbolized the controlled element and the square the target, as seen both through a platform mounted optical device. In contrast to the compensatory task, the cross deviated from the screen center, where the deviations corresponded to the controlled element response r. The motions of the square symbolized the target motions c, which were generated by the same forcing functions

as for the compensatory task. Also in the pursuit task the objective was to reduce the error ε_d in the attempt to maintain coincidence of cross center and square.

The stick gearing was the same for both axis. For the compensatory task it was set at 1.24 N/cm and for the pursuit task at 0.79 N/cm.

E. Description of the Simulator Motions

The lateral accelerations were obtained by a roll-motion of the simulator cabin. The simulator motions were generated by passing bandlimited zero-mean Gaussian white noise through a second-order filter with ω_o = 15 rad/sec and ξ = 0.707. This signal constituted the roll-angle command imparted to the controllers of the simulator. The power spectrum of the actual measured lateral accelerations is shown in Fig. 4. The notch at about 3 rad/sec is inherent to the pendulum type suspension of the simulator. The RMS value of the lateral accelerations was measured to be 0.24g.

F. Subject Background and Training

Four subjects participated in the experimental programs. Subject B was female. Only subject D had actual flight experience as a military helicopter pilot. Subjects B and D were Aeronautical Engineering students and A and C Aeronautical Engineers. Subjects A and B had extensive prior fixed base simulator training.

Each simulation session lasted one hour. An average of 5 training hours was required for the subjects to reach a stable level of performance. Only the results of subject A are presented in this paper. However, very similar trends in the results of the other subjects were noticed.

G. Experimental Results

The values of the display forcing function power σ_{in} and of the controlled element proportional gain K_p, for the various configurations, are listed in Table 1. The experimental results for subject A are summarized in Figs. 5-11.

Configuration	Tracking Task C-compensatory P-pursuit	Display Forcing Function Power σ_{in} [mm]	Proportional Gain K_p
I	C	7.8	0.022
II	C	15.5	0.022
III	C	31	0.022
IV	C	15.5	0.2
V	P	15.5	0.022
VI	P	15.5	0.2

Table 1: Tracking Task Parameters.

1. Tracking Performance in the Presence of Motion

The variance components of the error and of the stick output are shown in Figs. 5-7. Fig. 5 shows that for all compensatory tracking configurations the total variance in the presence of motion (M) is markedly larger than the variance for the static case (S). For all configurations the vibration correlated component constitutes a considerable part of the total error variance. Fig. 6 shows components of the total stick output u, i.e. voluntary command u_c plus stick feedthrough u_b. Also the total stick output in the presence of motion (M) is markedly larger than in the static case (S). For all cases the vibration correlated component of the stick output variance caused by stick feedthrough, is dominant. The input correlated component is the second largest and the remnant component is the smallest. Fig. 7 shows that for pursuit tracking, the effect of the stick feedthrough on error and on stick output is even larger than for compensatory control. Both for compensatory and for pursuit tracking a marked increase in remnant between the static case (S) and the motion case (M) is noticed. The subjects commented that tracking in the presence of motion was considerably more straining and difficult to perform.

2. Tracking Performance with the Adaptive Filter

Fig. 5 shows for all configurations a substantial reduction in the total error variance as a result of the incorporation of the adaptive filter, case A. This improvement with respect to case M is mainly due to a marked reduction in the vibration correlated component of the error variance and, to a lesser extent, to a reduction in the input correlated components. This indicates that the suppression of stick feedthrough also improves the ability to track the forcing function. On the other hand the remnant component generally increases slightly. Fig. 6 shows that also for the adaptive filter the vibration correlated component of the total unfiltered stick output u is considerably large (case A) though smaller than without the adaptive filter (case M). However, for the filtered output u_f (case A) the vibration correlated component is very small. Fig. 7 shows similar trends of the effect of the adaptive filter for pursuit tracking.

The effectiveness of the adaptive filter is demonstrated by time-histories shown in Figs. 8 and 9. Fig. 8 shows the stick output and adaptive filter output in the presence of motion while the display forcing function was set to zero, i.e. $\sigma_{in}=0$. In this case the control output is almost entirely due to stick feedthrough. Fig. 8 shows that the adaptive filter output signal closely "copies" the stick feedthrough signal and that the difference between them, being u_f, is small.

Time histories for a second example with σ_{in} = 15.5 mm are shown in Fig. 9. The tracking error in the dynamic case (M) is considerably larger than in the static case (S). The tracking error in the presence of the adaptive filter (A) is much smaller than in the dynamic case (M) and only slightly larger than in the static case (S).

The subjects commented that tracking in the presence of the adaptive filter was considerably easier than without the filter, and that the filter enabled them to improve their tracking accuracy.

3. The Effect of Display Forcing Function Power

Fig. 5 shows, as can be expected, that for a small forcing function power σ_{in}, the vibration correlated component of the error is more dominant than for

high power. Hence, for low forcing function power, the adaptive noise cancellation is more pronounced and therefore relatively more effective.

4. Effect of the Controlled Element Proportional Gain

Fig. 5 shows that an increase in proportional gain has no significant effect on the error score in the static case, (see (S) of configurations II and IV). However, in the presence of motion the total error for high-proportional gain is markedly larger than for low-proportional gain (see case M of configurations II and IV). This is mainly due to the larger effect of stick feedthrough. The incorporation of the adaptive filter strongly reduced the stick feedthrough as well as the input correlated component of the error and thus strongly improved tracking accuracy, (see case A of configurations II and IV). Therefore, for tasks with high proportional gain, it is indicated that the adaptive filter is particularly effective. A similar, but even more pronounced trend was found for pursuit tracking, see configurations V and VI in Fig. 7.

5. Effect of Motion and Adaptive Filtering on Human Operator Response

Figs. 10 and 11 show the visual motor dynamic response properties, characterized by open loop transfer function cross-over frequency and phase margin, and low-frequency pilot and biodynamic gains. For all configurations it is shown that motion (M) strongly reduces the cross-over frequency and pilot gain and increases the phase margin as compared to the static case (S). This indicates that in the presence of biodynamic interference the tracking response is more inhibitive, a fact which is confirmed by the subjects. The adaptive filter causes an increase in cross-over frequency and pilot gain and a reduction in phase margin, see (A) in Figs. 10 and 11. It should be noted that the cross-over frequency and phase margin with the adaptive filter are close in value to those of the static case. In most cases the cross-over frequency even exceeds the one of the static case and the phase margin is correspondingly smaller. This indicates that with the adaptive filter the tracking behaviour is more "tight". Consequently the low-frequency gain of the biodynamic feedthrough is considerably larger for the adaptive filter than without it, as can be seen from Figs. 10 and 11). This implies that with the adaptive filter the subject allows himself a firmer grip on the control stick, as compared to case M without the filter, in which he tends to release his grip in order to alleviate the stick feedthrough effects. This fact was also confirmed by the subjects.

6. Motion Cross-Talk

Finally it should be noted that the adaptive filter was employed in the lateral axis of control only. However, due to cross-talk effects in the simulator motion and biodynamic response, part of the interference appeared in the vertical axis of control as well. Since these disturbances were not filtered the vertical error was considerably larger than the lateral one. It is anticipated that a reduction in the vertical error by employing an adaptive filter in both axes of control, will improve the lateral tracking performance even more.

IV. CONCLUSIONS

1. For the configurations considered, lateral accelerations seriously impair tracking performance as a result of biodynamic interference.

2. Apart from the error component caused by stick feedthrough, the biodynamic interference increases the input correlated and remnant components of the error and strongly increases the task difficulty.

3. The biodynamic interference reduces the cross-over frequency and low-frequency pilot gain, implying a more inhibited tracking strategy.

4. Performance deterioration due to stick feedthrough is the strongest for high proportional gain dynamics and low tracking forcing function power.

5. The adaptive filter markedly reduces the total tracking error by reducing the vibration and input correlated components of the error and thus substantially reduces task difficulty.

6. The adaptive filter is effective in particular for high proportional gain dynamics, low display forcing function power and in the pursuit tracking configurations.

7. The adaptive filter causes a substantial increase in cross-over frequency and pilot gain and reduces the phase margin implying a more "tight" tracking behaviour.

8. The adaptive filter yields an increased biodynamic low-frequency gain and slightly increased remnant which indicates that the subject's grip of the control stick is firmer.

9. It is anticipated that even for single-axis motion excitation it is desirable to employ an adaptive filter in both axes of control.

V. ACKNOWLEDGEMENTS

This reseach is sponsored by the Department of the Air Force under Contract No. F33615-82-C-0520. Dr. Daniel W. Repperberger of the Air Force Aerospace Medical Research Laboratory, Wright-Patterson AFB, Ohio, the contract technical director.

VI. REFERENCES

1. Jex, H.R., Evaluating Biodynamic Interference with Operation Crews, Vibration and Combined Stresses in Advanced Systems, AGARD CP-145, pp. B24-1-B24-18.

2. Jex, H.R., Problems in Modeling Man Machine Control Behavior in Biodynamic Environments, Proc. 7th Annual Conf. on Manual Control, NASA SP-281, 1971.

3. Jex, H.R. and Magdaleno, R.E., Progress in Measurement and Modeling the Effects of Low Frequency Vibration on Performance, AGARD CP-253, March 1980.

4. Levison, W.H., Model for Human Controller Performance in Vibration Environments, Aviat. Space and Environ. Med. 49:321-327, Jan. 1978.

5. Jex, H.R. and Magdaleno, R.E., Biomechanical Models for Vibration Feedthrough to Hands and Head for a Semisupine Pilot, Aviat. Space and Environ. Med. 49: 304-316, Jan. 1978.

6. Levison, W.H. and Houck, P.D., Guide for the Design of Control Sticks in Vibration Environments, AMRL-TR-74-127, Aerospace Medical Research Laboratory, Wright Patterson AFB, Oh. 1975.

7. Schubert, D.W., Pepi, J.S. and Roman, F.E., Investigation of the Vibration Isolation of Commercial Jet Transport Pilots During Turbulent Air Penetration, NASA CR-1560, July 1970.

8. DiMasi, F.P., Allen, R.F. and Calcaterra, P.C., Effect of Vertical Active Vibration Isolation on Tracking Performance and on Ride Qualities, NASA CR-2146.

9. Widrow, B. et al., Adaptive Noise Cancelling: Principles and Applications, Proc. IEEE, Vol. 63, No. 12, December 1975, pp. 1692-1716.

10. Velger, M., Grunwald, A. and Merhav, S., Suppression of Biodynamic Disturbances and Pilot Induced Oscillations by Adaptive Filtering, 25th Israel Annual Conference on Aviation and Astronautics, Feb. 23-25, 1983, pp. 45-54.

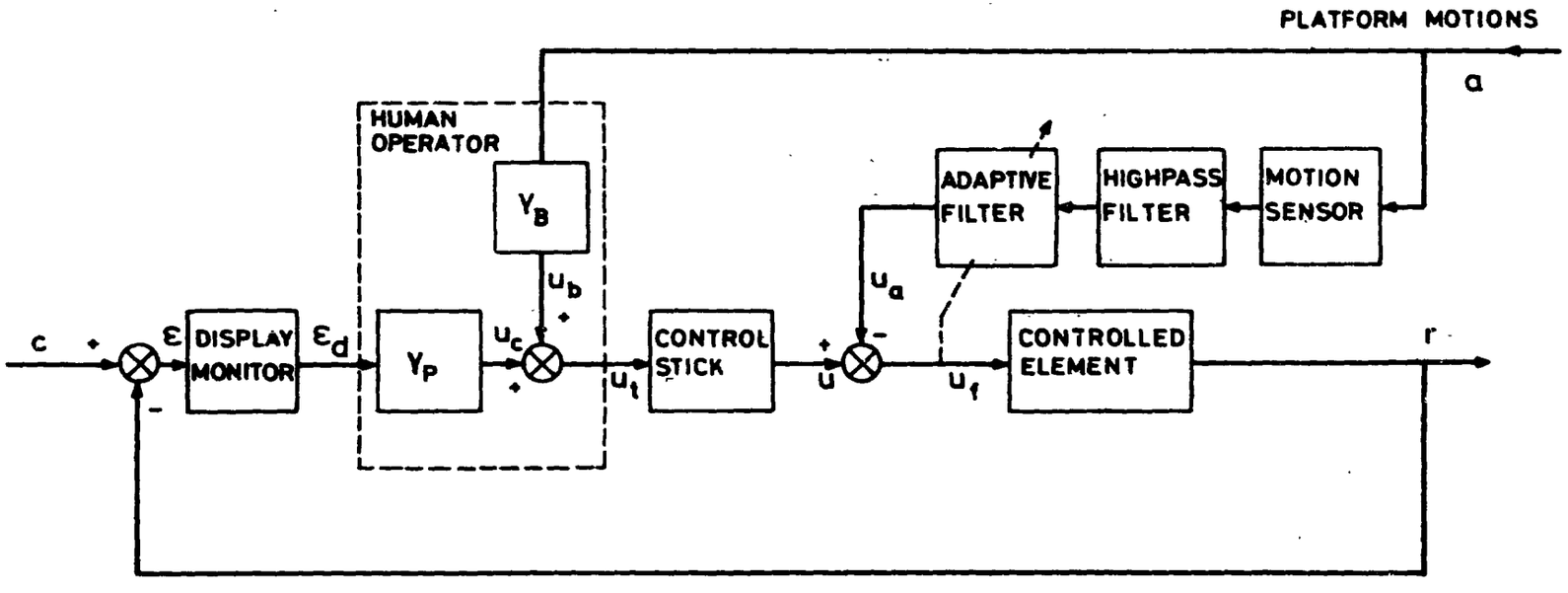

Figure 1. Adaptive Filtering scheme of Biodynamic Interference in Manipulation Tasks (Biodynamic "Open Loop" Case).

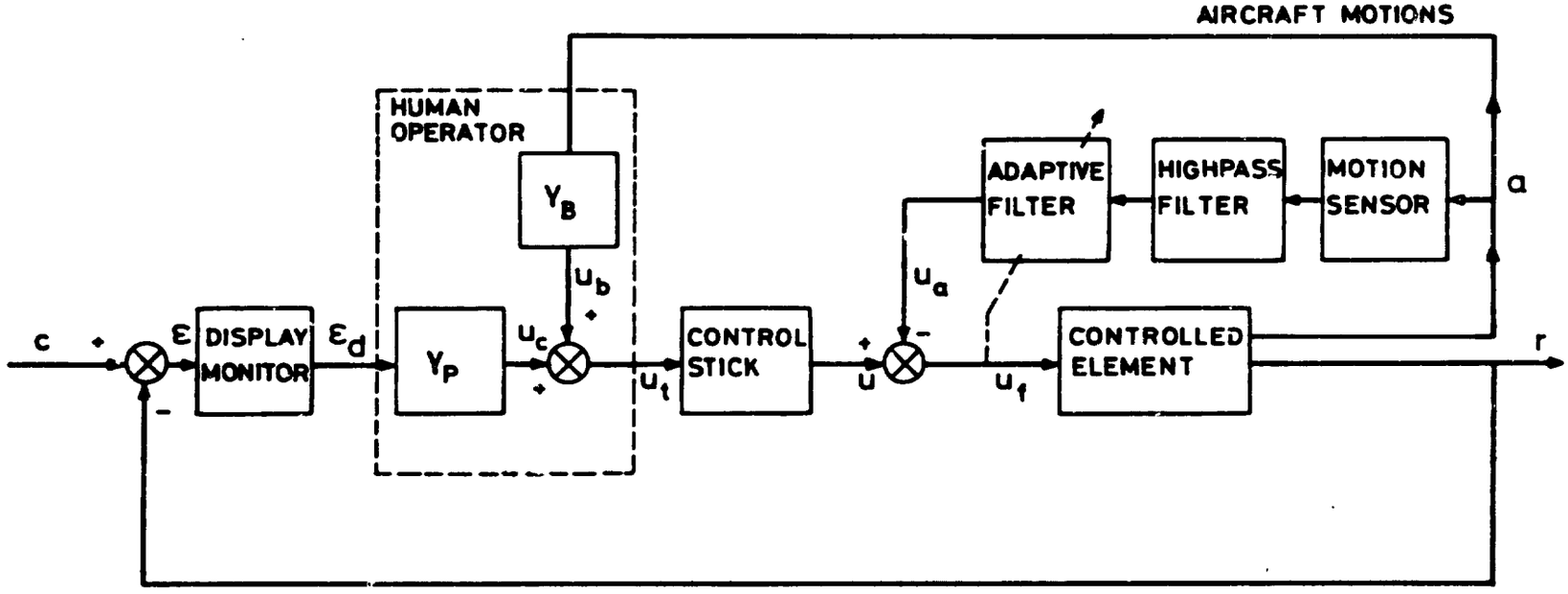

Figure 2. Adaptive Filtering Scheme of Biodynamic Interference in Vehicular Control (Biodynamic "Closed Loop" Case).

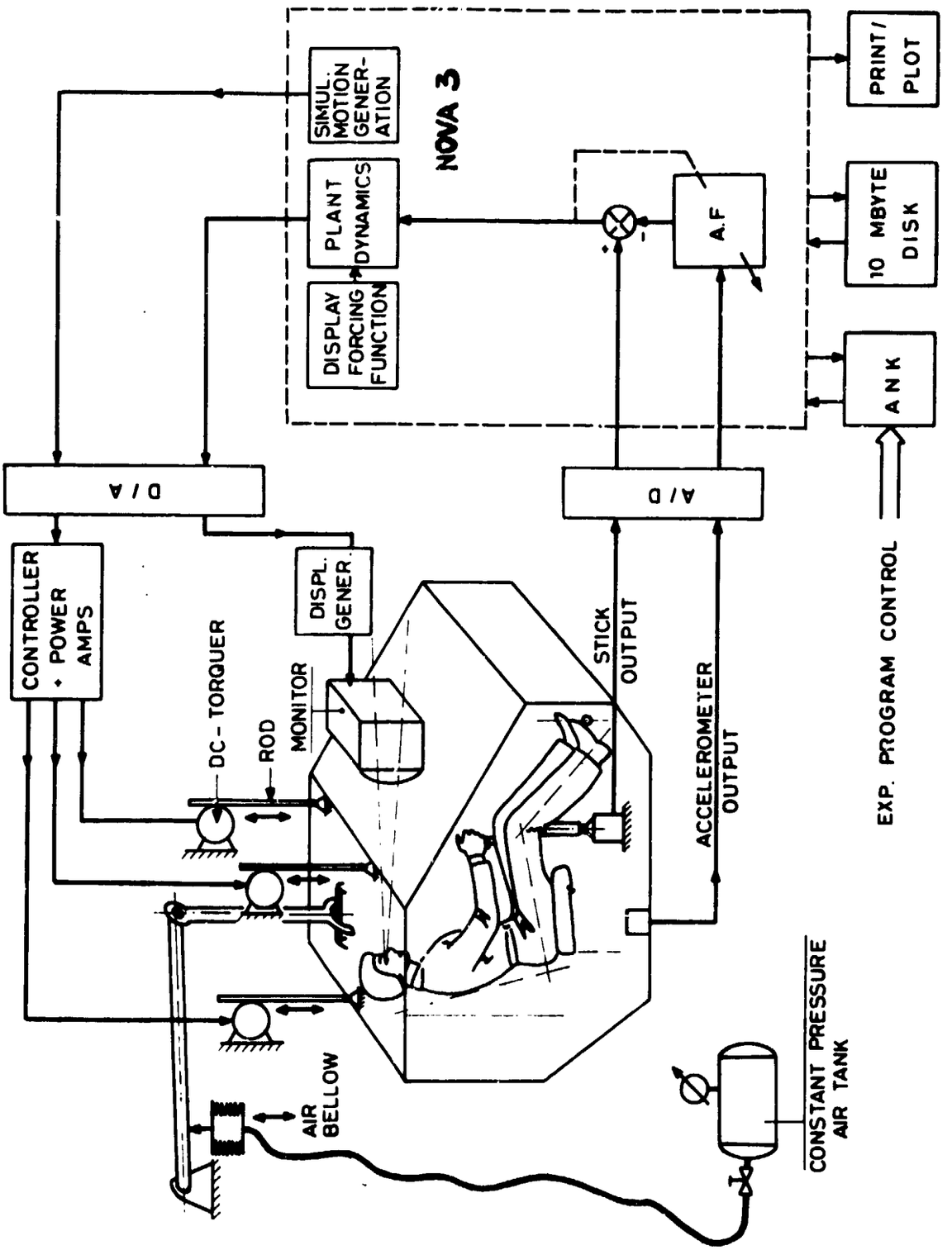

Figure 3. Experimental Setup.

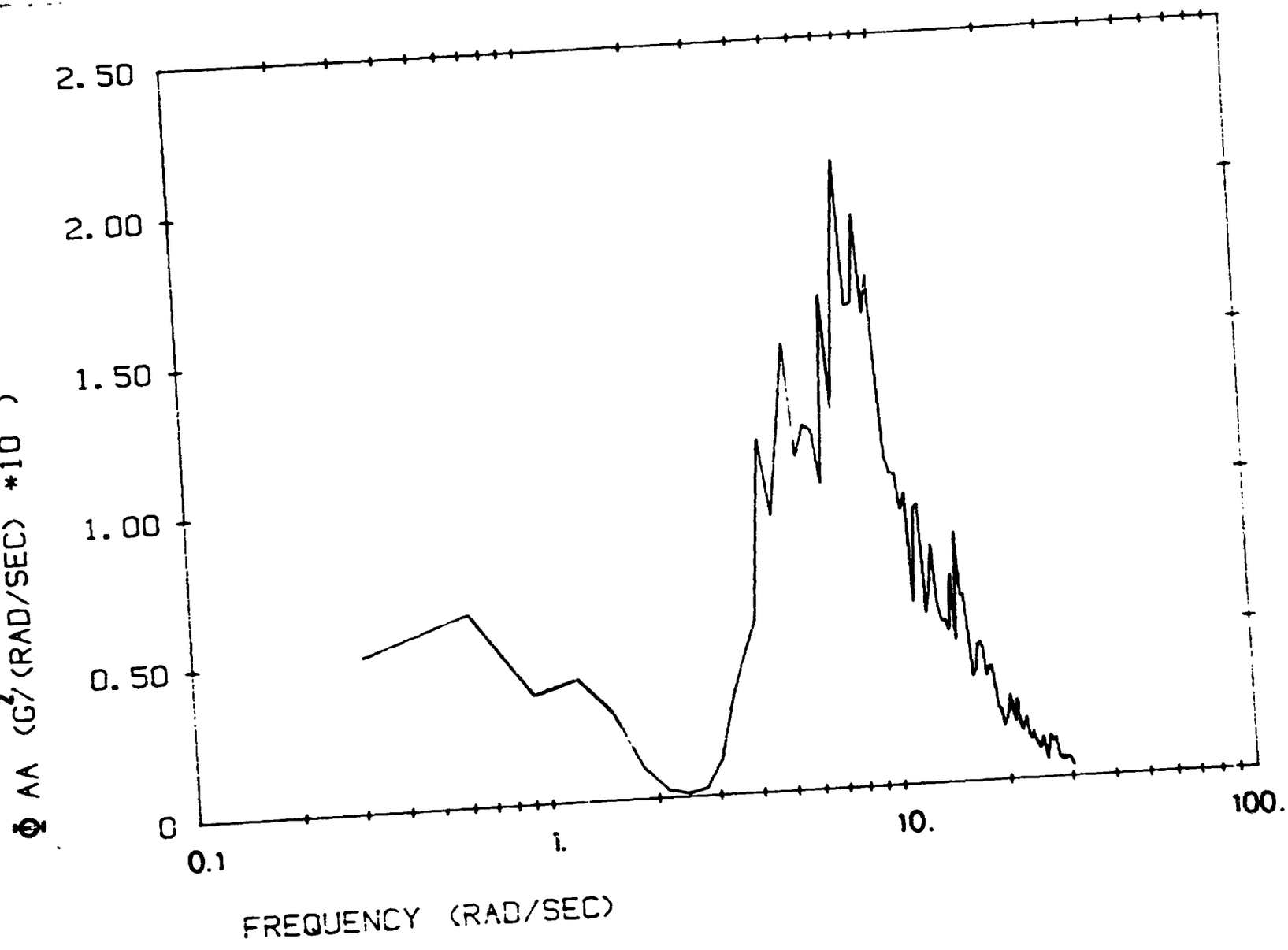

Figure 4. Power Spectrum of Lateral Simulator Accelerations.

ORIGINAL PAGE IS
OF POOR QUALITY

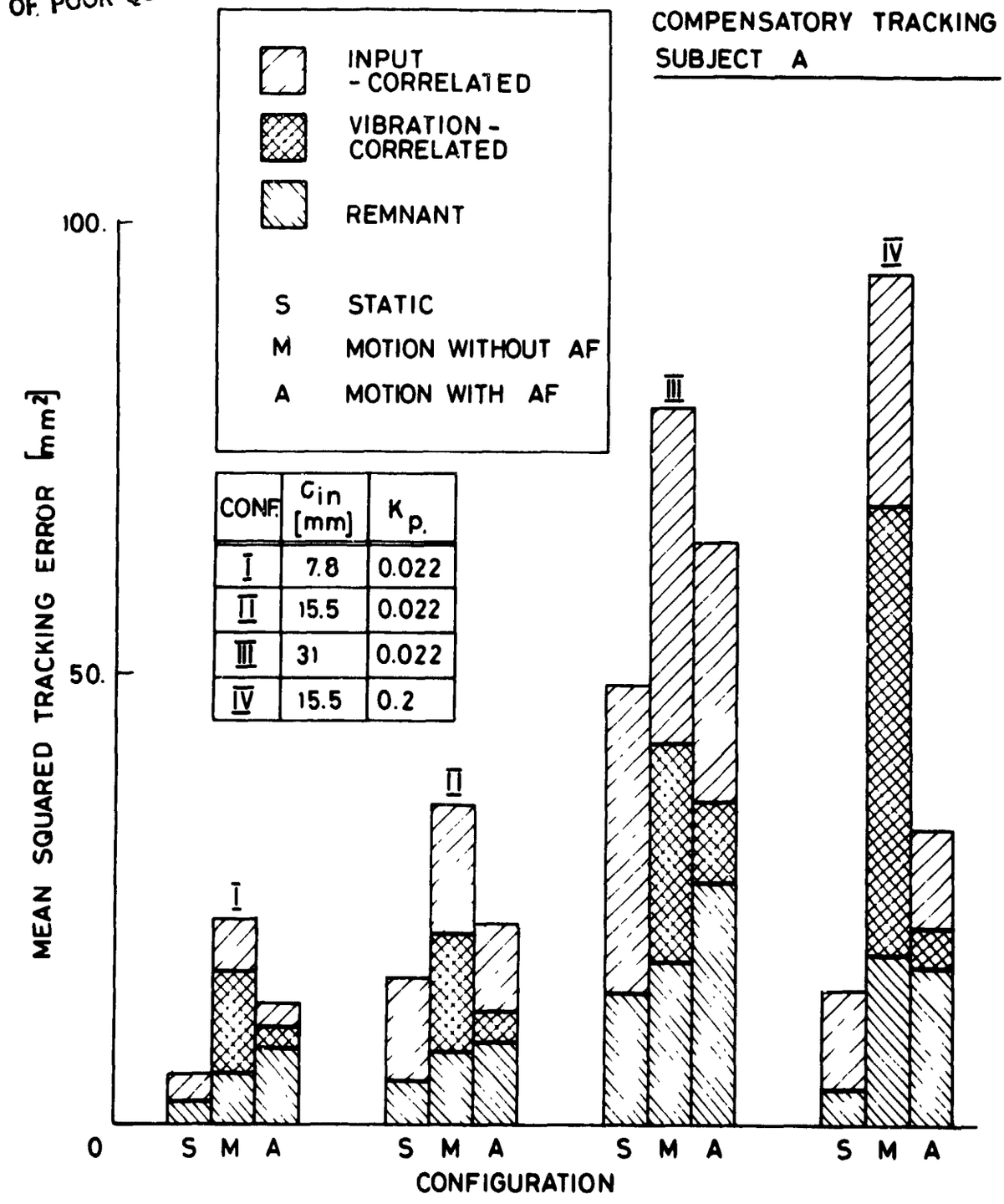

Figure 5. Variance Components of the Tracking Error for the Compensatory Task; Subject A.

ORIGINAL PAGE IS
OF POOR QUALITY

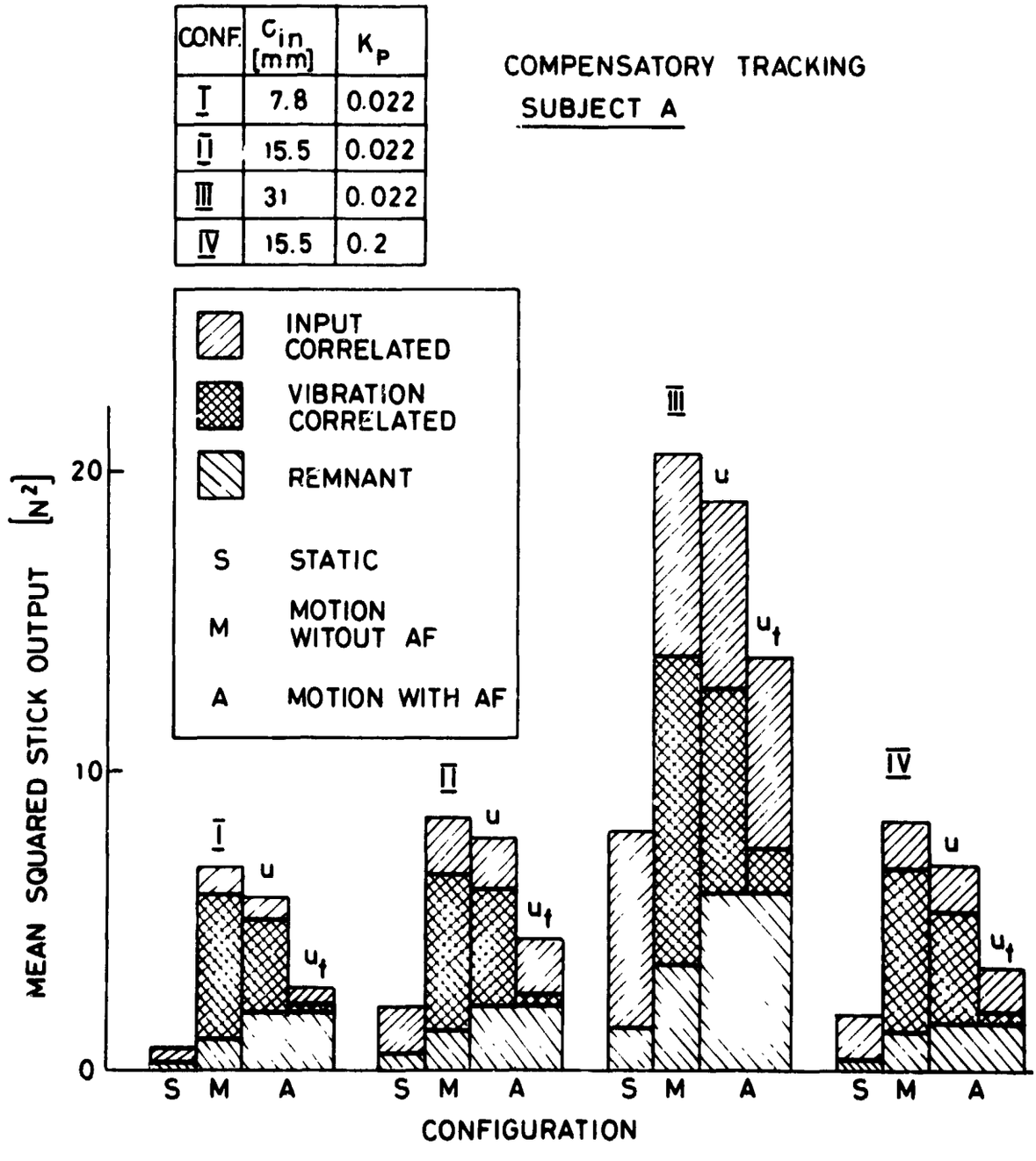

Figure 6. Variance Components of the Stick Output for the Compensatory Task; Subject A.

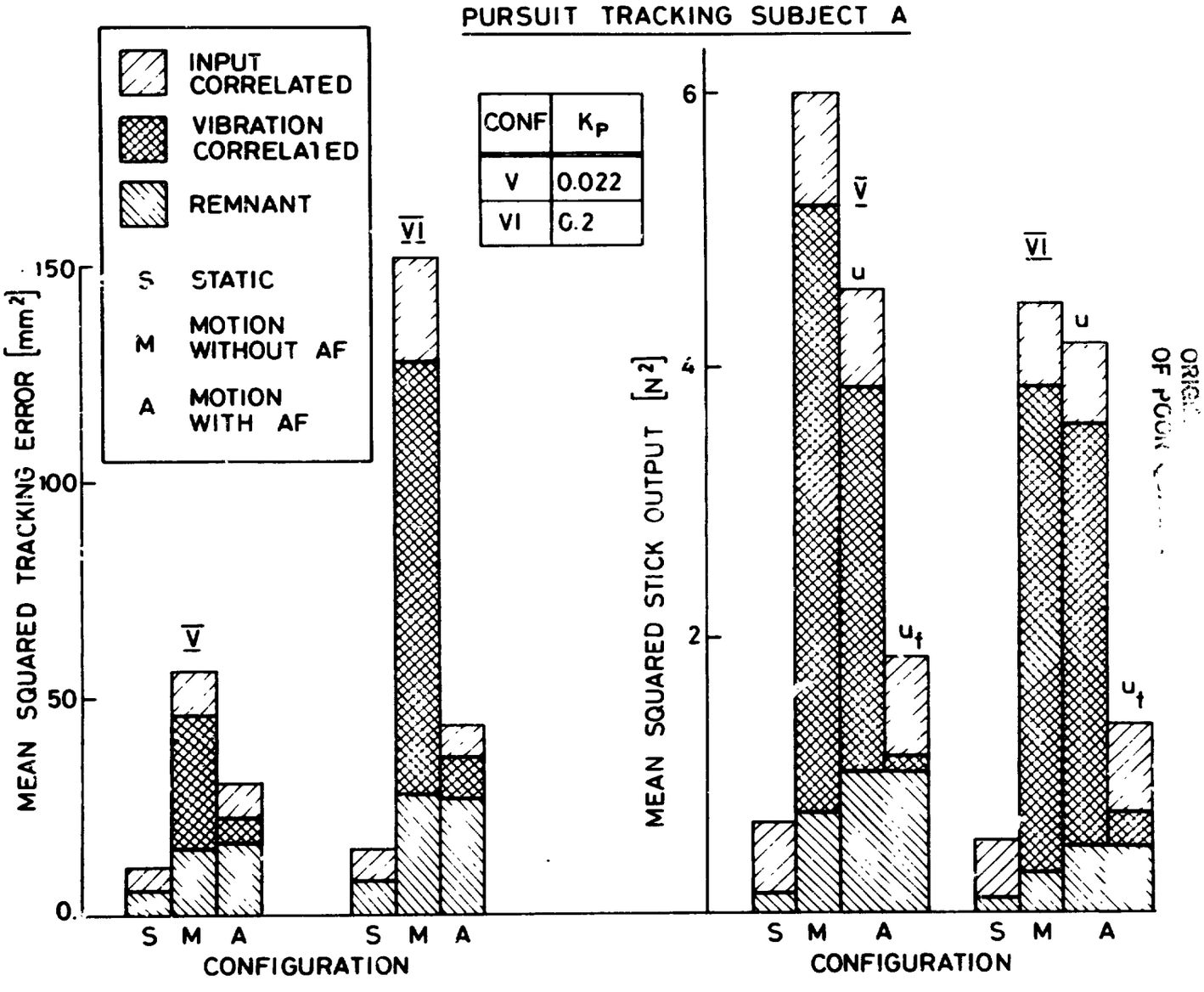

Figure 7. Variance Components of the Tracking Error and Stick Output for the Pursuit Task, Subject A.

ORIGINAL PAGE IS
OF POOR QUALITY

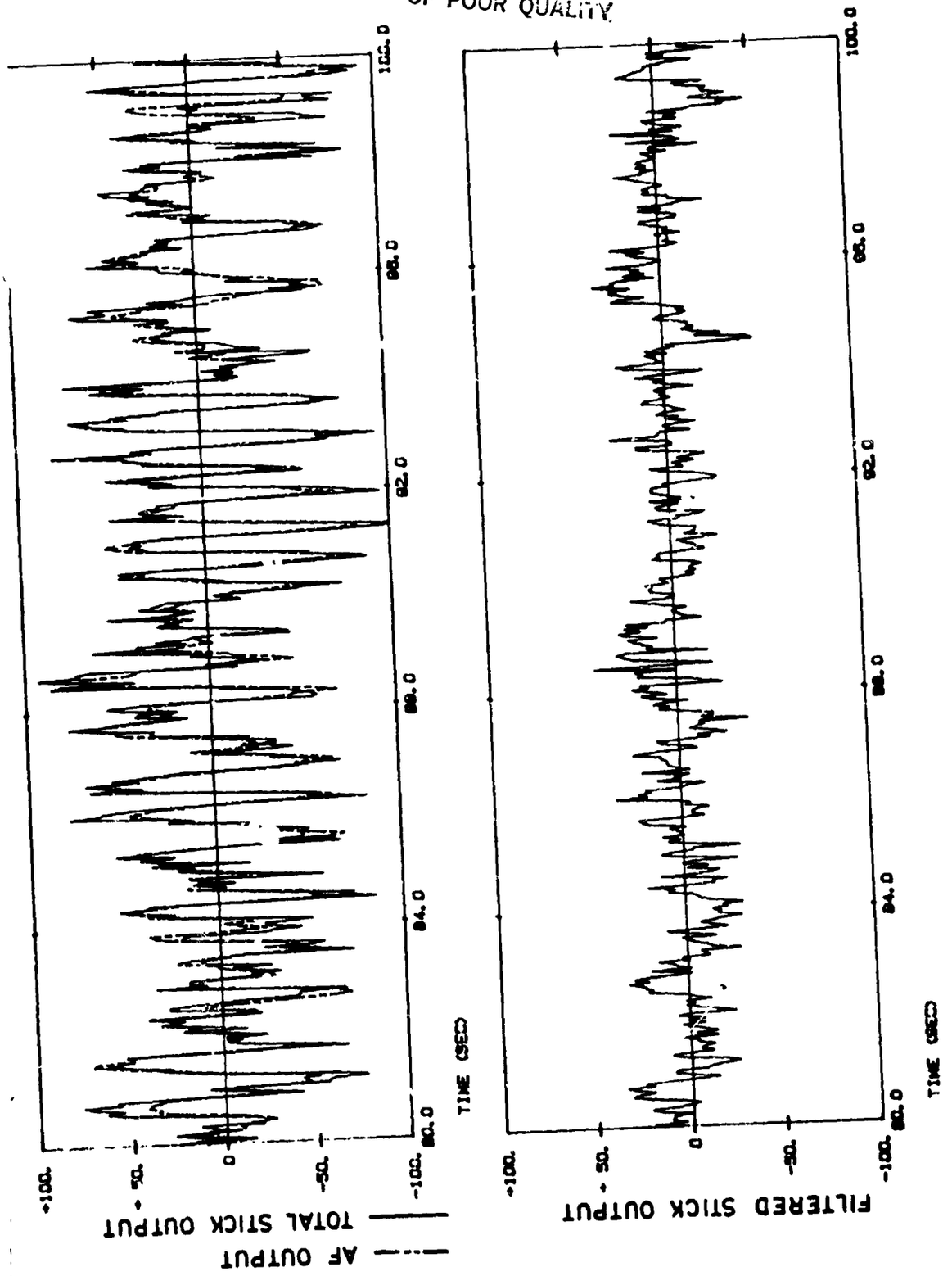

Figure 8. Time-Histories of Stick Output and Adaptive Filter Output in the Presence of Motion with $\sigma_{in}=0$; Subject A.

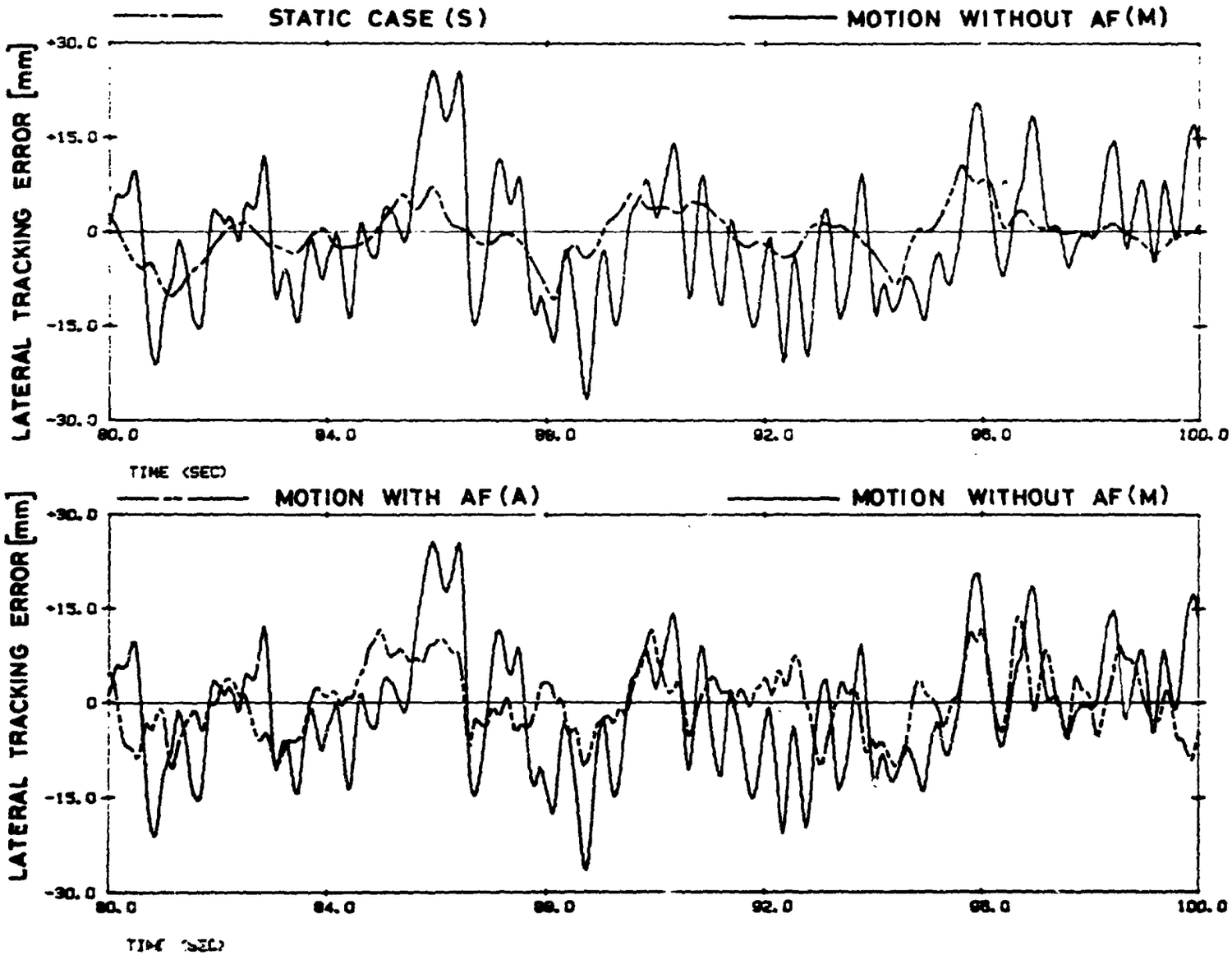

Figure 9. Time Histories of the Tracking Error for the Pursuit Task for Cases S,M and A with σ_{in}=15.5 mm; Subject A.

CONF	SYMBOL	σ_{in} [mm]	K_P
I	--▽--	7.8	0.022
II	--+--	15.5	0.022
III	—○—	31	0.022
IV	--✱--	15.5	0.2

COMPENSATORY TRACKING

SUBJECT A

S	STATIC
M	MOTION WITHOUT AF
A	MOTION WITH AF

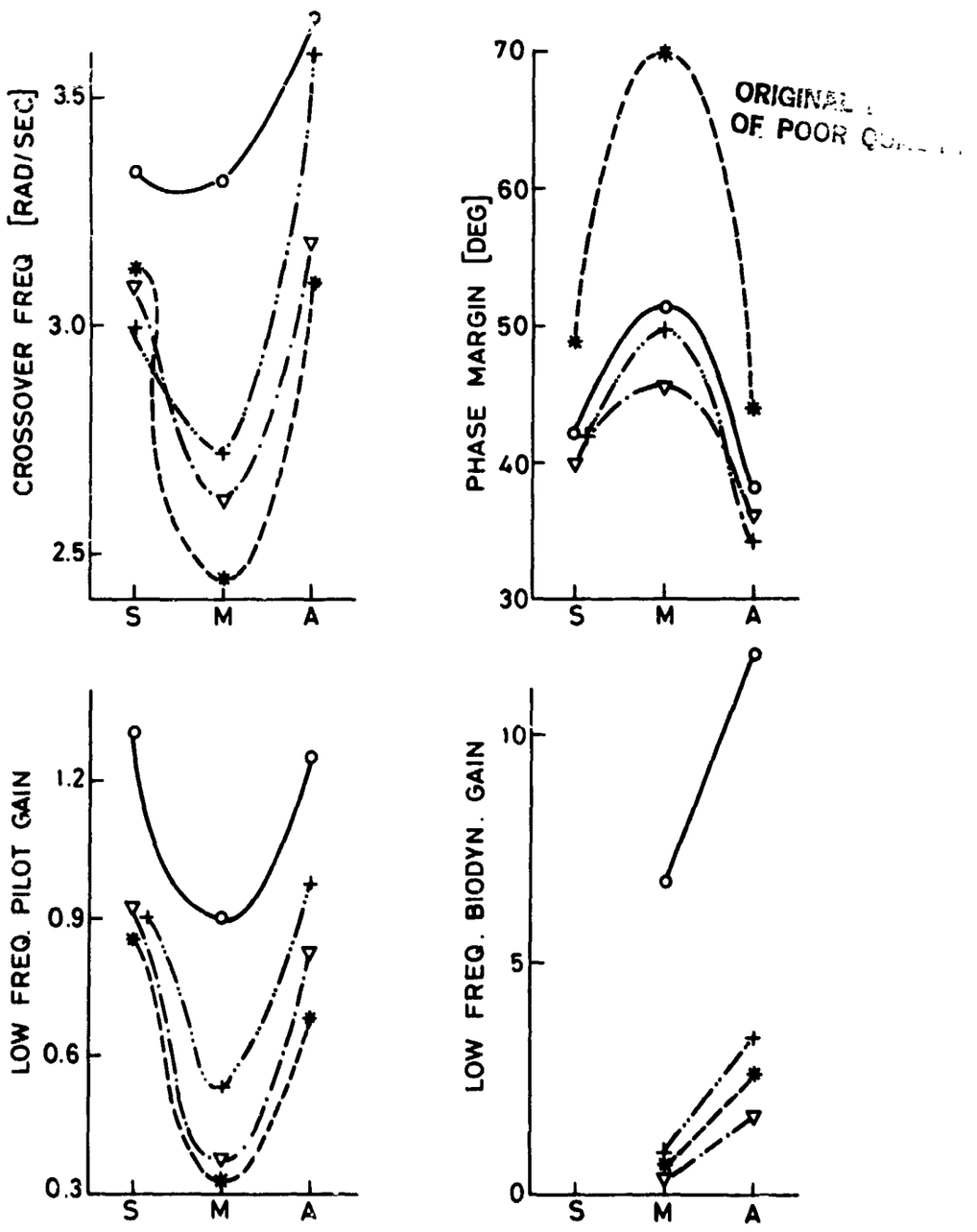

Figure 10. Visual Motor Dynamic Response Properties of the Pilot for the Compensatory Task; Subject A.

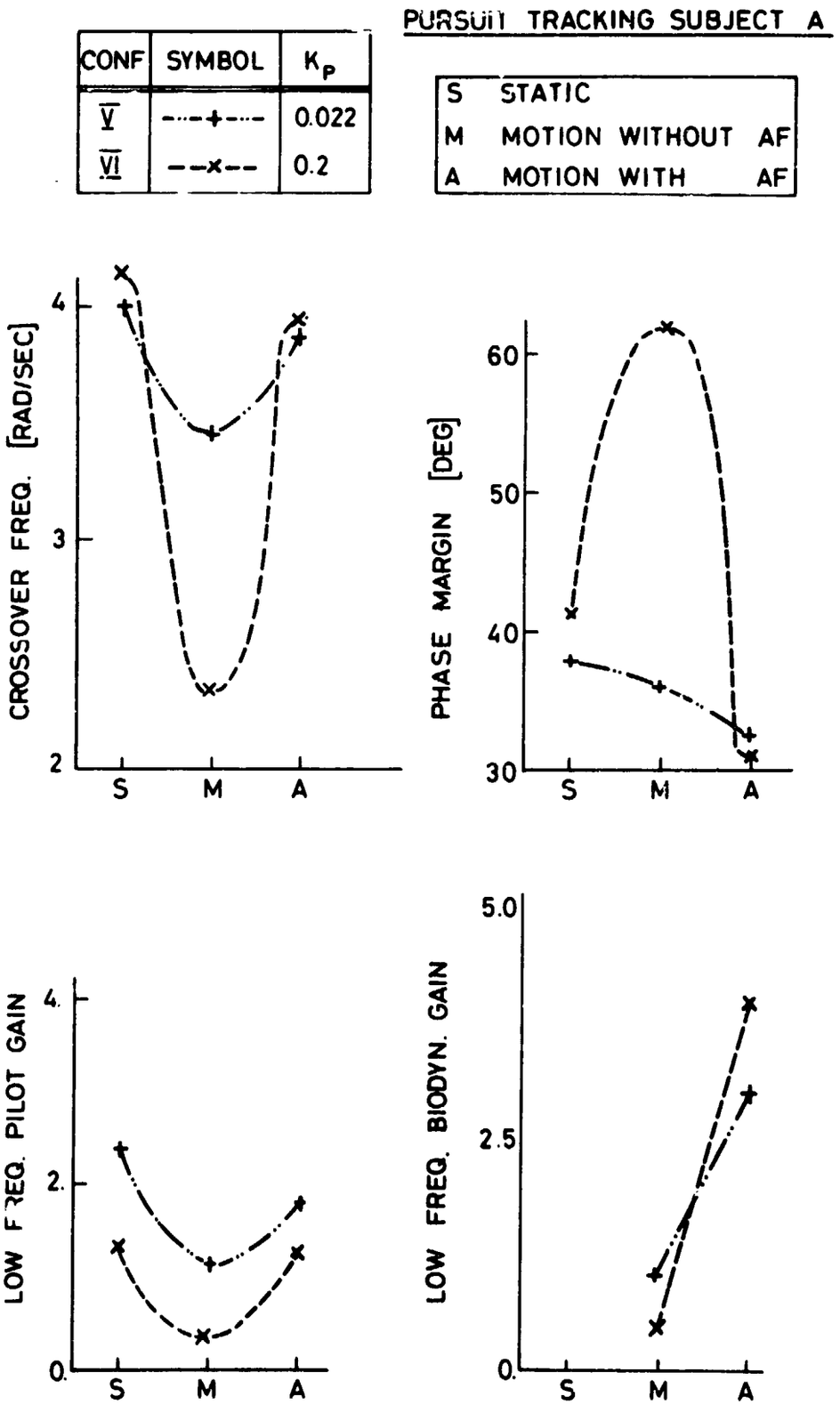

Figure 11. Visual Motor Dynamic Response Properties of the Pilot for the Pursuit Task; Subject A.

ACTIVE STICKS - A NEW DIMENSION IN CONTROLLER DESIGN

D. W. Repperger*, D. McCollor**

D44

N85 14531

* Air Force Aerospace Medical Research Laboratory, Wright Patterson Air Force Base, Ohio, 45433
** Raytheon Service Company

Abstract

In the design of a hand controller, one approach involves a stick with active characteristics. The term active used in this context refers to a control stick which actively exerts a force on the subject's hand so that it may aid in the tracking. Presently, with position type sticks, the human neuromotor bandwidth is limited to 10 radians/second as a consequence of the fact that two sets of muscles (antagonist and angonist) are used to perform neuromotor tracking. When a forearm movement is made in one direction (e.g. laterally) and then reversed, it is necessary to change from one set of active muscles to another set of muscle groups. The additional time to reverse control movements contributes to low levels of neuromotor bandwidth. One method to circumvent this problem and possibly aid in tracking would be to design a stick controller that will perform, partially, the function of some of the muscle groups during the tracking task.

At the Air Force Aerospace Medical Research Laboratory, Wright Patterson Air Force Base, a smart stick controller has been built which actively produces a force to interact with the subject's hand and to aid in tracking. When the human tracks in this situation, the man-machine system can be viewed as the combination of two closed loop feedback paths. The inner loop occurs as a result of a tactile information channel effecting the man-controller interaction through force movements of the stick on the human's hand. The outer feedback loop is a result of the visual display and visual signals. This paper reports the empirical results of tracking with this stick in the active mode (the stick generates a force) and the passive mode (the stick not generating a force). The most noteworthy observation is a significant increase in apparent neuromotor bandwidth and consequently better tracking performance.

Introduction

Much interest has arisen on the comparison of the effects of force versus displacement sticks on pilot tracking ability. Early F-16's were equipped with pure force sticks. Performance improvements occurred when the present limited motion stick replaced the force stick in the F-16. For this stick controller, approximately (1/4") displacement is allowed for a full commend input. In an effort to better understand why this occurred and the interaction between force and displacement feedback, a study was conducted a year ago [1] on the performance enhancement of an F-16 style force stick with limited

motion.

In this paper we use a position stick for both the passive (no force applied) and active (force applied to the pilot's hand from the stick) mode of operation. The position information from a stick displacement is sent to a computer. Dynamic restoring forces are sent back from the computer to the operator through the stick via computer control. Our observation that tracking performance improved with a lateral tracking task during lateral acceleration [1] forms the empirical basis to develop a position stick which moves giving force feedback to the operator. We hypothesized that a performance advantage would exist for a position stick which moves with force feedback to the operator in non acceleration environments. To test this hypothesis in a static environment (1Gz), we require (by computer control) the stick to push back on the wrist with a restoring force in a manner similar to the inertial force that would occur in the lateral G environment [1]. From this study it is observed that the unique combination of a visual feedback loop in parallel with a tactile (force feedback) loop figure (7) allows the human to operate the stick controller differently in the active mode as contrasted to the passive mode which only contains visual feedback. This paper reports some performance differences between the active and passive modes of operation. Finally, one additional parameter that was allowed to vary in this study was the electrical gain of the stick (volts output/degree of position of the stick). This variable was allowed to change to see how stick sensitivity effects the usefulness of the device.

The Electro-Mechanical Device

Figure (1) illustrates how the device is constructed. The mass, dashpot, and spring constant were fixed in this study. In general, we consider a device which may have the ability to change K_s, B_s, or M_s in figure (1) but, in addition, adds a biomechanical force directly to the pilot's hand through the control stick. In this sense the controller acts like an active device rather than a passive device. Figure (2) illustrates a system description of the electromechanical device which functions as the smart stick controller. Figure (12) illustrates the actual setup. In figure (2), the output from the computer algorithm drives two current sources I_1 and I_2. These current sources are inputs into two current-pressure transducers to produce pressures p_1 and p_2. The pressure difference $p_1 - p_2$ acting on the area A of the piston produces a force F on the rack and pinion. This force acts through the gear assembly deflecting the stick to the right or the left. The voltage-force characteristics of both of the current pressure transducers are illustrated in figure (3).

To understand the operation of the device, the electrical circuit used to control one current pressure transducer valve is illustrated in figure (4). In figure (4) the winding is inserted in the collector part of the circuit of the transistor using the common emitter configuration. This circuit design protects the windings of the current pressure transducer to a maximum current of (15v-.1)/510 ohms

= 29.2 ma under worst case conditions. The input signal V_{in} enters the base circuit from the computer and on positive swings drives the transistor from the active region into saturation. $V_{in\ max}$ = 10v. from the computer, hence $I_{b\ max}$ = 10v/51K ohms = .2 ma worst case. A clamping diode is inserted to cut off the transistor in the event v_{in} should swing negative and in the cutoff mode of operation I_c = 0. Thus the current-pressure transducer is protected by this current limited circuit arrangement. The common emitter configuration in figure (4) is actually operated in the active mode which is necessary as a result of the non-linear force-voltage input curves illustrated in figure (3). Since the left and right valve both have different characteristics and exhibit hysteresis and dead zone non-linearities, it was decided to bias the transducers about an operating point midway in the linear characteristics curve and to limit the input swings to only linear deviations on the curves in figure (3). To illustrate this point, for the value v_1 (movement right), a bias voltage of 5.3 + (1/2) (swing value) = 5.3 + (1/2)(3.2) = 6.9 volts was chosen as the nominal operating point. The swing voltage about this nominal value was chosen to be $\pm$ 1.6 volts peak to peak (95% of the time), thus ensuring linearity. For valve v_2, the bias value was chosen as 4.3 + (1/2) (1.2) = 4.9 volts with a swing voltage about the nominal of $\pm$ 1.2 volts peak to peak (95% of the time). In this manner both valves produce forces no greater than 3.5 pounds and appear linear within their operating region. Figure (5) illustrates the analog computer diagram relating the computer output of the biomechanical model to the input of the current-pressure transducers. The voltage signal from the computer (output of the biomechanical model) is put into amplifier A_1. The DC bias of 4.9 volts is added as an input to A_1 and goes to the left valve (input to the base circuit in figure (4)).

The Smart Algorithm

In the design of a controller with intelligence, the ability of the controller to perform is a function of the algorithm used in the design of the controller. The smart algorithm could possibly consist of a mathematical representation of an interaction in which improved biomechanical reactions would be obtained in the G acceleration fields. An alternative design would occur if some empirical evidence would support a particular design. In this paper we consider a design which produces inertial forces on the operator similar to those obtained in a previous experiment [1]. Figure (6) illustrates the biomechanical model which represents human response to sidewards accelerations (+Gy direction). The assumption is made that the human arm remains stationary at the elbow. The Gy force acts at the center of mass of the forearm and deflects the arm in the direction of the Gy force which adds a force component at the wrist-stick interface. In static equilibrium the sum of torques about point A in figure (6) is zero. Let F= the force required to compress the spring K_s and dashpot B_s:

Then $$F = K_s \theta_a L_a + B_s L_a \dot{\theta}_a \qquad (1)$$

where the small angle assumption $\theta_a \cong \sin \theta_a$ has been used, θ_a in

figure (5) represents the lateral angular movement of the forearm, and L_a is the length of the forearm. The sum of torques about A = 0 requires:

$$m_a Gy(La) / 2 - F L_a = 0 \quad (2)$$

or combining equations (1) and (2) we have:

$$m_a(1/2)\, G_y = K_s\, \theta_a + B_s\, \dot{\theta}_a \quad (3)$$

The transfer function between $\theta_a(s)$ and Gy(s) is given by:

$$\frac{\theta_a(s)}{m_a Gy(s)} = \frac{(1/2)}{K_s + B_s\, s} \quad (4)$$

Laplace transforming F from equation (1) yields:

$$F(s) = (K_s + B_s\, s)\; L_a\, \theta_a(s) \quad (5)$$

or

$$\frac{F(s)}{m_a\, Gy(s)} = \frac{1}{2} \quad (6)$$

"independent of La,Ks, and Bs". Thus the force necessary at the stick to counteract the G field force is just a constant proportional to the Gy accelerometer measurement. This simplification is derived here as a result of the static equilibrium model considered in this paper.

To complete the design of the smart controller, it is necessary to have some empirical basis by which the man-machine interaction can be improved. From an empirical study run [1] under Gy exposures, two types of biomechanical interaction were defined. Figure (8) illustrates these two types of interaction. Positive Biomechanical Feedthrough is defined such that a stick movement to the right gives rise to a G field in the same direction. This type of interaction accentuates spurious movements and is similar to a closed loop circuit with positive feedback and is undesireable or unstable. The second definition of the biomechanical interaction is what is termed "Negative Biomechanical Feedthrough". In this case the force induced by the G field is in a direction to oppose the original force. This is analogous to negative feedback in an electrical circuit and provides a stablizing influence on the man-machine interaction . Figure (10) illustrates results from [1] in which a comparison was made between static tracking and tracking under the influence of Negative Biomechanical Feedthrough. It was demonstrated that the influence of Negative Biomechanical Feedthrough on tracking performance is significant, especially for fast moving targets. This was the purpose of the design of the smart algorithm considered in this paper.

Implementation of The Device

Figure (7) illustrates the implementation of the device. As the subject makes a stick response (e.g. to the right), this position change is sensed via a circular potentiometer at the base of the stick which generates a voltage signal proportional to the number of degrees of deflection of the stick. This signal is added to a disturbance

input forcing function, which is composed of a sum of sine wave signals to simulate wind buffeting or other types of disturbance inputs into the system. The sum of the forcing function disturbance plus stick output becomes the input into an analog computer model of the centrifuge at AFAMRL/ Wright Patterson Air Force Base, Ohio. In this model, the roll dynamics of the cab of the centrifuge (located at the end of a 19 foot radius arm) is given by:

$$\frac{\theta_p(s)}{I(s)} = \frac{1.7}{s + 1.7} \qquad (7)$$

where s=1.7 radians/second is the break frequency of the dynamics of this electromechanical system, θ_p is the pointing vector of the cab, and I(s) is the input electrical signal into the cab circuit (output of the amplifier which sums the stick response with the disturbance input forcing function). From this analog model of the centrifuge, $\hat{\theta}_p$ is determined which estimates the postion vector of the cab on the centrifuge. Once $\hat{\theta}_p$ is determined, an estimate of Gy, denoted as $\hat{G}y$, can be obtained from the equations of motion. Using $\hat{G}y$, and the static equilibrium model illustrated in figure (6), the force at the center of gravity of the forearm can be determined. Translating this force to the wrist produces the biodynamic interaction on the forearm that would be similar to this G acceleration stress. The purpose of the experiment considered in this paper was to run subjects in the static mode of operation and to try to simulate forces similar to the biodynamic forces that appear on the forearm of the subject for the Negative Biomechanical Feedthrough case illustrated in figure (8b). If the simulation is accurate, then the performance scores when tracking in the static mode of operation with an active stick may improve tracking just as tracking in the dynamic mode (under Gy stress) has demonstrated for the Negative Biomechanical Feedthrough case in figure (10) with a passive stick.

Empirical Validation

A total of 6 subjects were run for the validation of this device. The subjects were all active duty USAF men between the ages of 23 to 35 years. They participated for two days of tracking. On day 1 they tracked for what was considered a training day which consisted of 6 runs with a passive stick (no force on the stick) and 6 runs with the stick active (a simulated Negative Biomechanical Feedthrough force acting on the wrist). Since 4 of the 6 subjects had previous experience with compensatory tracking tasks, the training level was defined as asymptote if we observed less than 5% change in performance scores between similar trials (replications). Three different electrical gain settings of the control stick output were used to assess if stick sensitivity could have had an influence on tracking performance. The choice of the electrical gains was determined [2] from the shape of the spectrum of the forcing function in the frequency domain. Figure (11) illustrates the empirical scores determined across the subjects. For a given controller gain, and for

two out of these three gains, the smart stick improved tracking performance not only significantly, but substantially by a factor of 2 or 3.

Explanation on How The Smart Stick Helps Tracking Performance

To investigate if perhaps some additional information may have been available during the runs of the smart stick and thus provided more information to a subject or perhaps investigate if the smart stick may automatically track the target itself, several tests were made. In Mode 1, the autopilot (an analog simulation) performed the tracking with a passive stick (no stick movement). Its characteristics were specified by:

$$G(s) = (1.7) / (s+1.7) \qquad (8)$$

which replaces the human operator in the loop in figure (7). Mode 2 is the autopilot tracking with the stick active. These results are displayed in Table I. Obviously no difference appears between these two cases. Mode 3 is the open loop mode (no hand on an active stick). Obviously no benefit is derived from lack of human inputs. Mode 4 occurs when the active stick is held at postion zero. Modes 5 and 6, respectively, are the e_{RMS} scores for the passive and active stick when averaged over the 6 subjects. From these runs there appears to be no advantage, information wise, in observing $\hat{\theta}_p$ which is related

Table I Runs To Examine Information in the Loop
(Values of Root Mean Square Error Signal (e_{RMS}))

	Gain 1	Gain 2	Gain 3
Mode 1(Autopilot, Passive Stick)	.019	.019	.019
Mode 2(Autopilot, Active Stick)	.019	.019	.019
Mode 3(Open Loop)	.164	.568	.605
Mode 4(Active Stick Held at Zero)	.034	.115	.318
Mode 5 (mean-Humans, Passive Stick)	.02475	.02463	.0445
(s.d.)	.00132	.00423	.01783
Mode 6 (mean-Humans, Active Stick)	.01725	.01075	.0325
(s.d.)	.00469	.00119	.0139

to the forcing function integrated through two simulations (figure (7)) to appear as the output $\hat{G}y$.
In summary, the subjects had no explicit knowledge of the forcing function disturbance other than implicit information obtained by observing $\hat{\theta}_p$ or $\hat{G}y$.

To better understand why a human tracks better with a smart stick is conjectured in figure (9). Using models akin to optimal control theory [3], typically neuromotor dynamics are modeled via a low pass filter with bandwidth $1/t_N$ and a noise $n(t)$ characterized by $E\{n(t)\} = 0$

and $E\{n(t)\, n^T(\gamma)\} = Q\, \delta(t-\gamma)$ where Q is a covariance matrix representation of human neuromotor noise or tremor. A Weber's law effect is known to occur in which Q scales with tension or force. For example, for twice the force output of the forearm, the noise covariance Q will scale proportionally.

Under the smart stick condition, however, an interesting physiological effect occurs. For normal tracking it is observed that hand movements must be made inward and outward, thus activating both antagonist and agonist muscles. With the smart stick, however, only one type of movement seems to be required. This is because the Negative Biomechanical Feedthrough like effect from our simulation replaces the second group of muscle movements, thus precluding the change in direction and delaying time in switching muscles. Preliminary analysis of these data indicates human operator neuromotor bandwidth increases a factor of 3 using a smart stick and lowers the value of the covariance Q in figure (9) of the noise output. This is the impact on the man-machine system with the use of a smart stick.

Summary and Conclusions

A smart stick has been developed. In tests with a simple lateral tracking task, subject scores were significantly better in the active stick mode than in the passive mode. In both modes, stick position provides the signal to the computer. In the active mode, the stick applies forces at the stick-hand interface that are dynamically similar to the inertial forces that would be generated by the inertia of the forearm if the tracking task were mounted in the AFAMRL human centrifuge. Thus, in the passive mode the subject receives visual target information only. In the active mode there is tactile information providing additional cues about vehicle motion. Serendipitously, the forces generated by the smart stick in the active mode tend to work against major muscle groups, allowing the subject to modulate his muscle force for fine control without the need to reverse direction. This contrasts with the need to continually shift muscle groups and force direction for fine control with a simple position stick in a passive mode of operation.

References

[1] Repperger, D.W., J. W. Frazier, and R. E. Van Patten, "Results From A Biomechanical Stick Study", Proceedings of The 1983 Aerospace Medical Association Meeting, May, 1983, Houston, Texas, pp. 192-193.

[2] Repperger, D.W., D.B. Rogers, J.W. Frazier, and K.E. Hudson, "A Task Difficulty-G Stress Experiment", Vol. 27, No. 2, pp.161-176, Ergonomics, 1984.

[3] Kleinman, D.L., Baron, S., and Levison, W.H., 1971, "A Control Theoretic Approach To Manned-Vehicle System Analysis", IEEE Transactions on Automatic Control, vol. AC-16, pp. 824-832.

List of Variables

I_1, I_2 - Electrical currents into windings (Fig 2)
P_1, P_2-Pressures in gas cylinder (Fig 2)
V_{in}- Voltage into transistor circuit (Fig 4)
I_b - Base Current into transistor (Fig 4)
I_c - Collector Current into transistor (Fig 4)
A_1 - Summing amplifier - (Figure 5)
Gy- Lateral G acceleration force (Fig 6)
F - Force (Fig 6)
K_s - Spring Constant (Fig 6)
θ_a - Angular Deflection of Arm (Fig 6)
L_a - Length of Forearm (Fig 6)
B_s - Dashpot constant (Fig 6)
M_a - Mass of Forearm
s - Laplace Transform Variable
θ_p - Pointing vector of the cab = Target position on display
$\wedge$ - estimate of a variable (e.g. $\hat{G}y$)
G(s) - Autopilot Transfer function
e_{RMS} - Root Mean Square error
A - Area of piston (Figure 2)
η - human neuromotor tremor
Q - Covariance of η
δ - Dirac delta function
γ - a time $\neq$ t

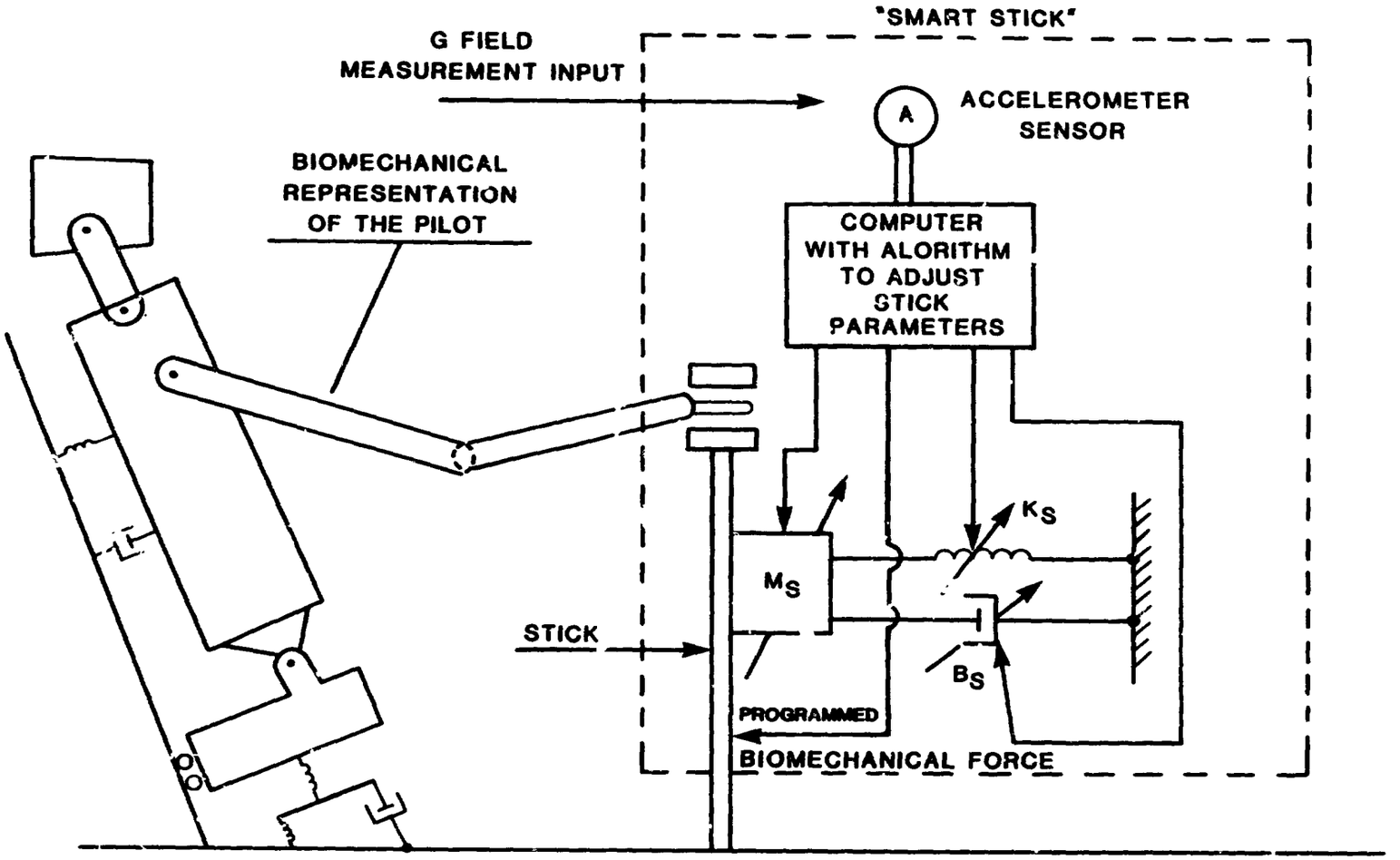

Figure (1) - THE "SMART STICK"

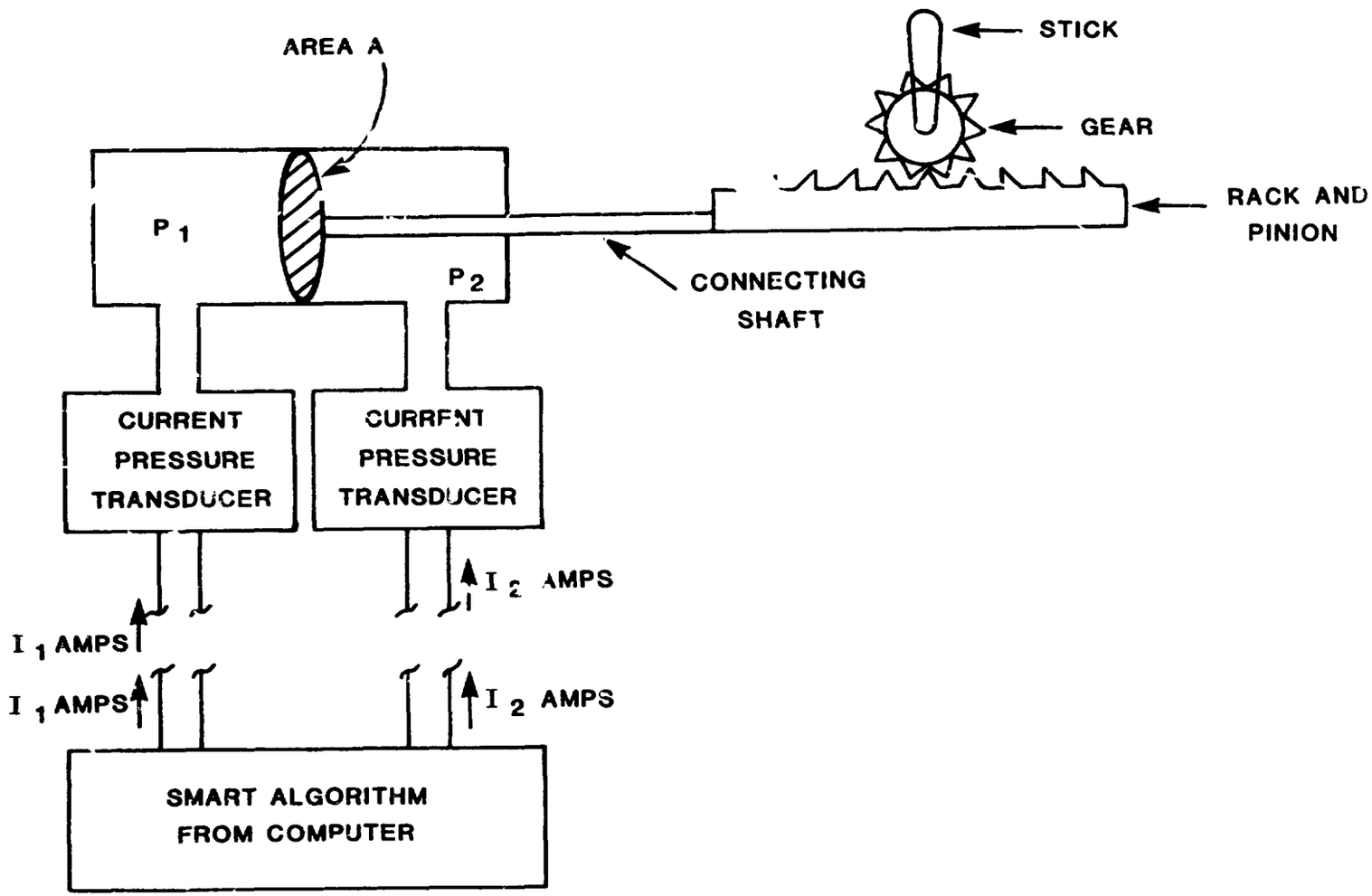

Figure (2) - THE ELECTROMECHANICAL DEVICE

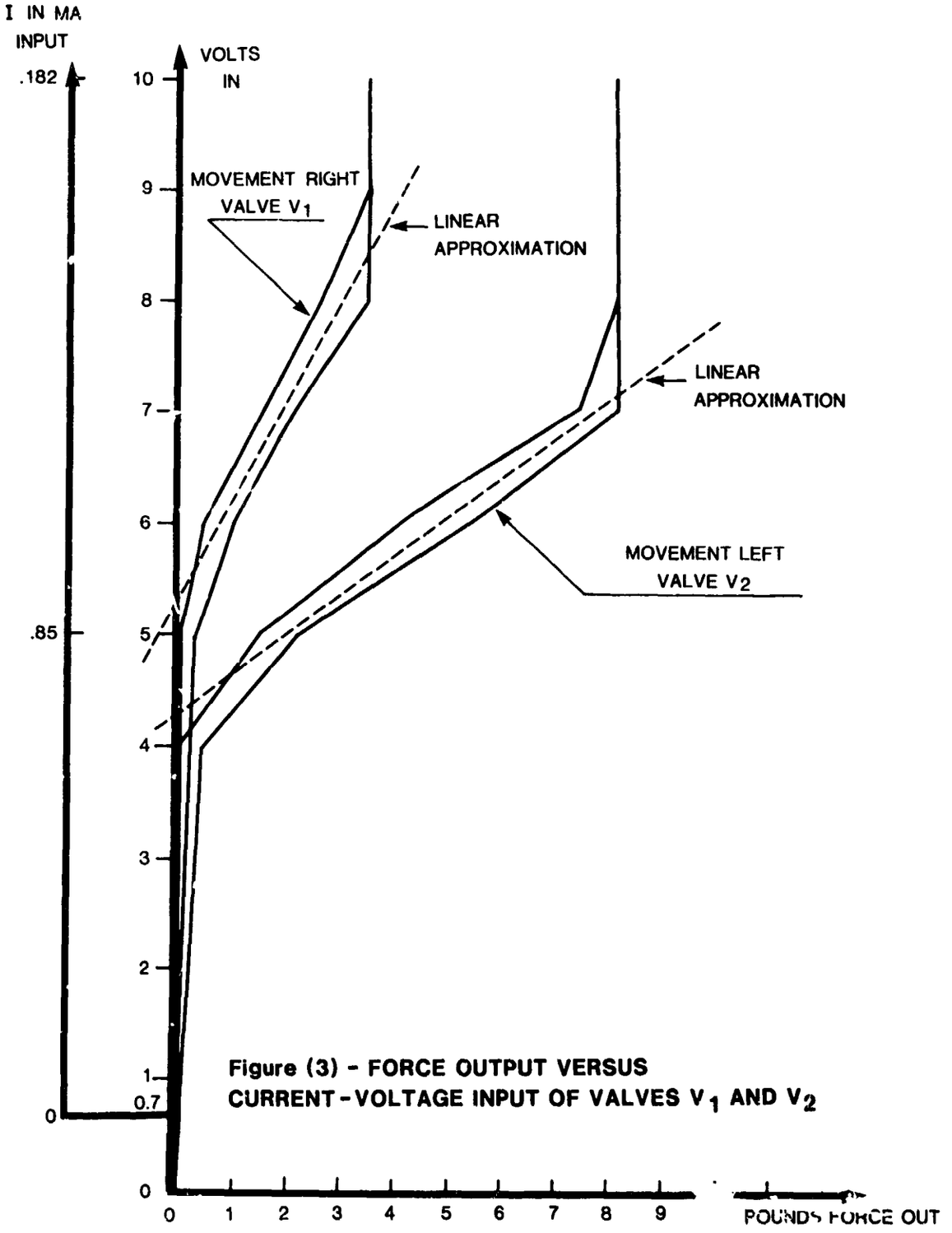

Figure (3) - FORCE OUTPUT VERSUS CURRENT-VOLTAGE INPUT OF VALVES V_1 AND V_2

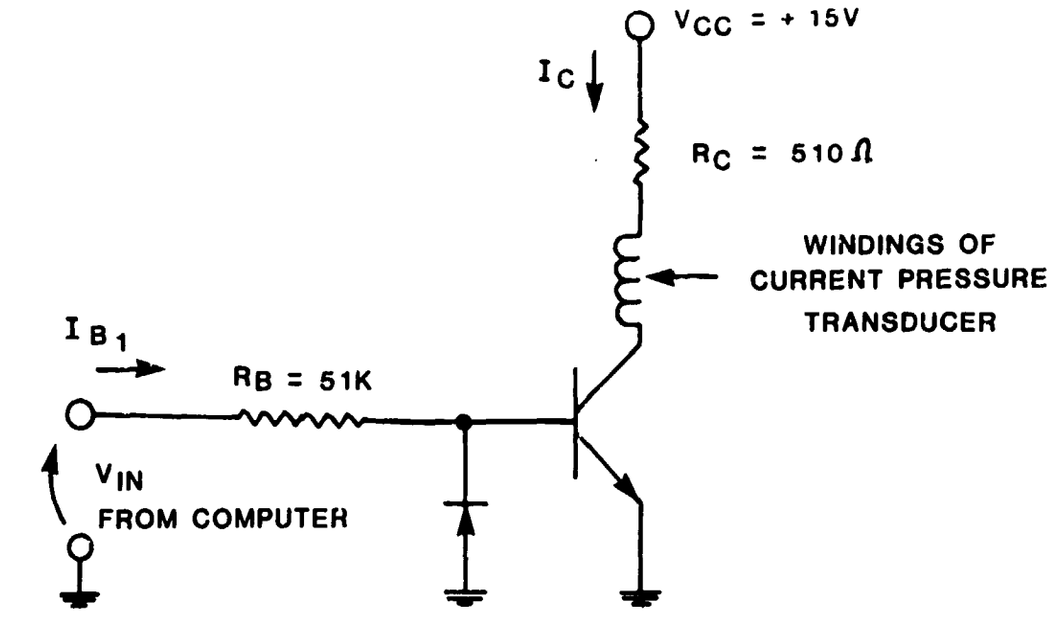

Figure (4) - THE CURRENT LIMITED ELECTRICAL CIRCUIT TO DRIVE THE CURRENT-FORCE TRANSDUCER

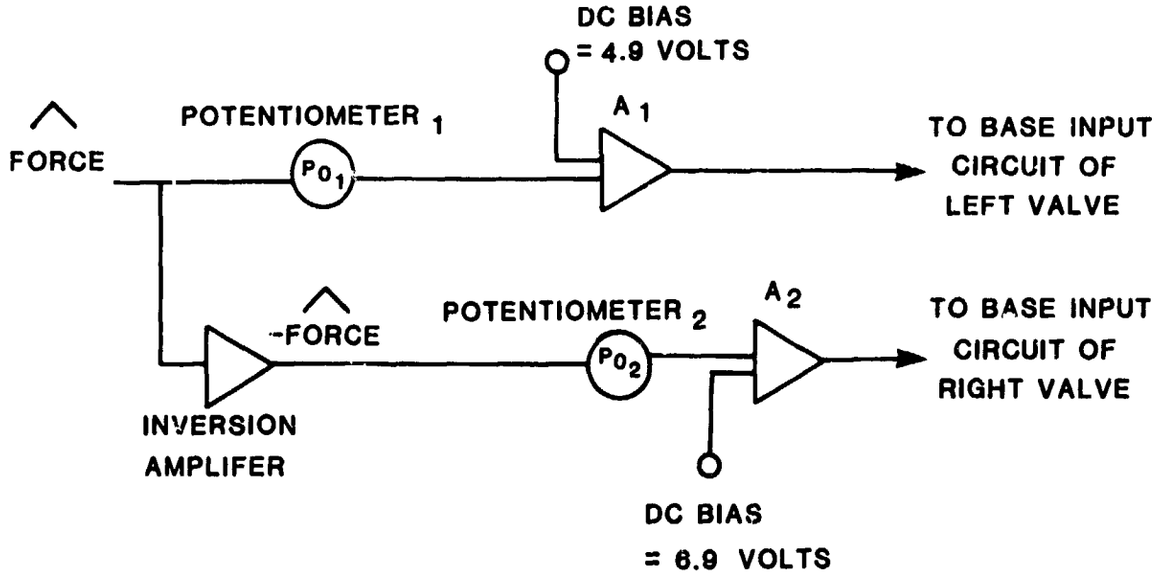

Figure (5) - THE ANALOG COMPUTER DIAGRAM

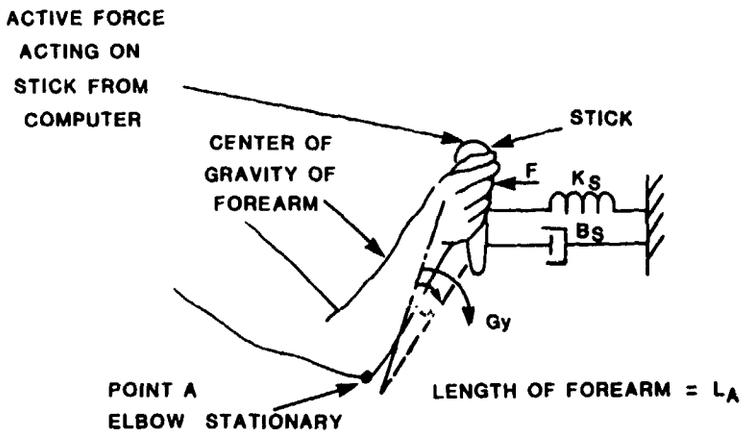

Figure (6) - THE BIOMECHANICAL MODEL

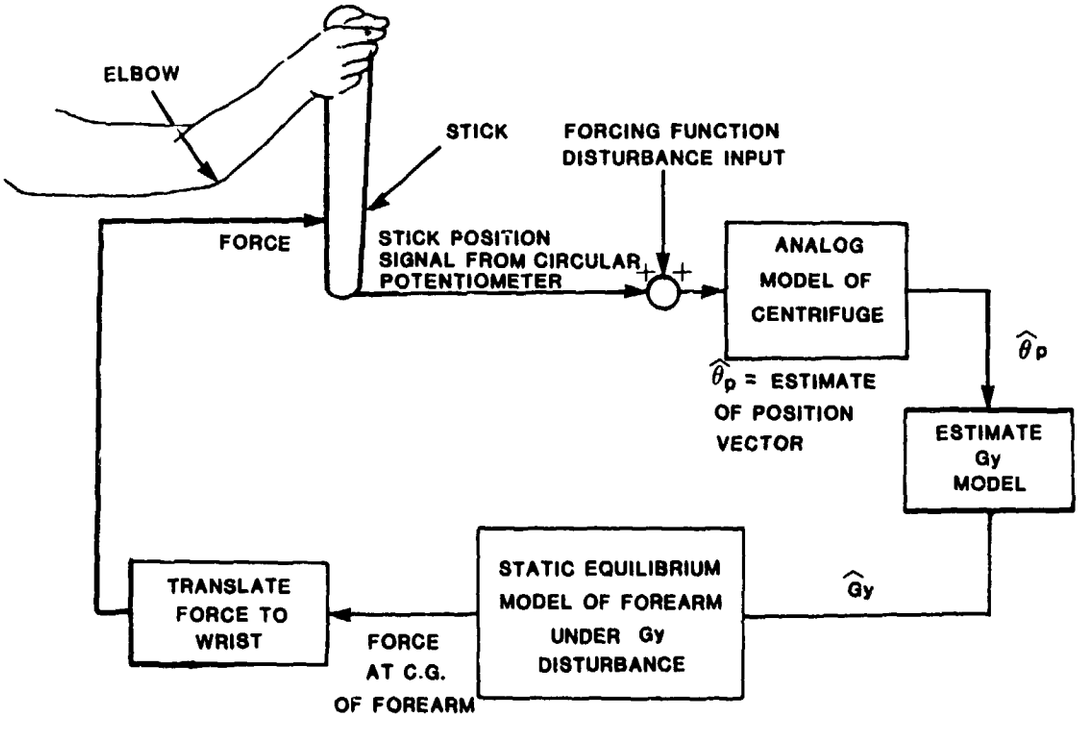

Figure (7) - IMPLEMENTATION OF SMART STICK

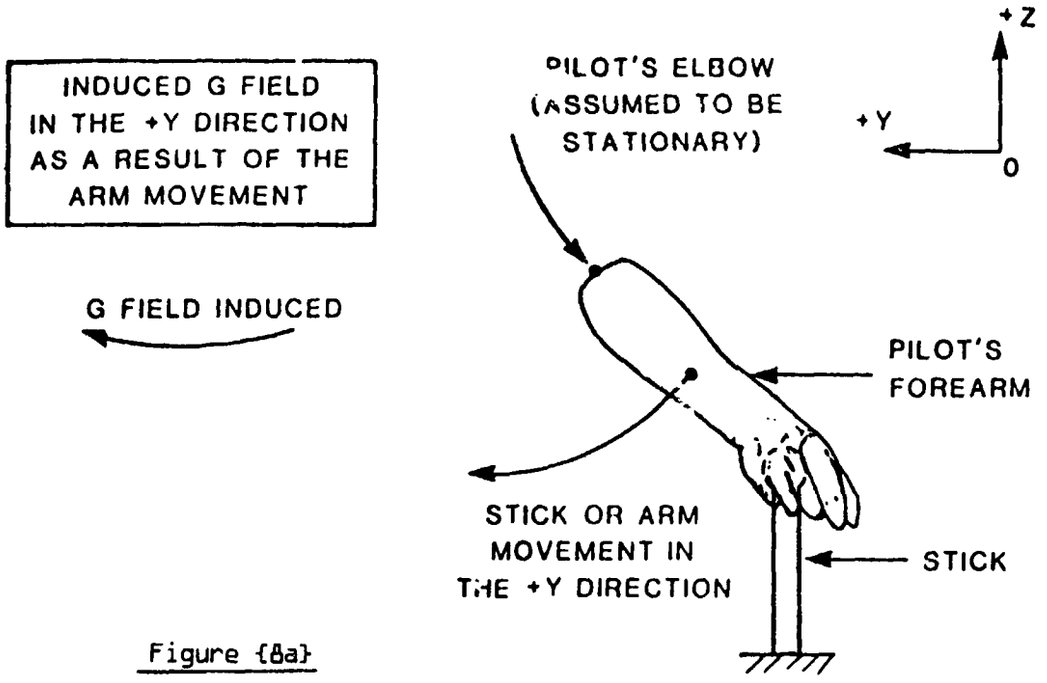

Figure {8a}

POSITIVE BIOMECHANICAL FEEDTHROUGH

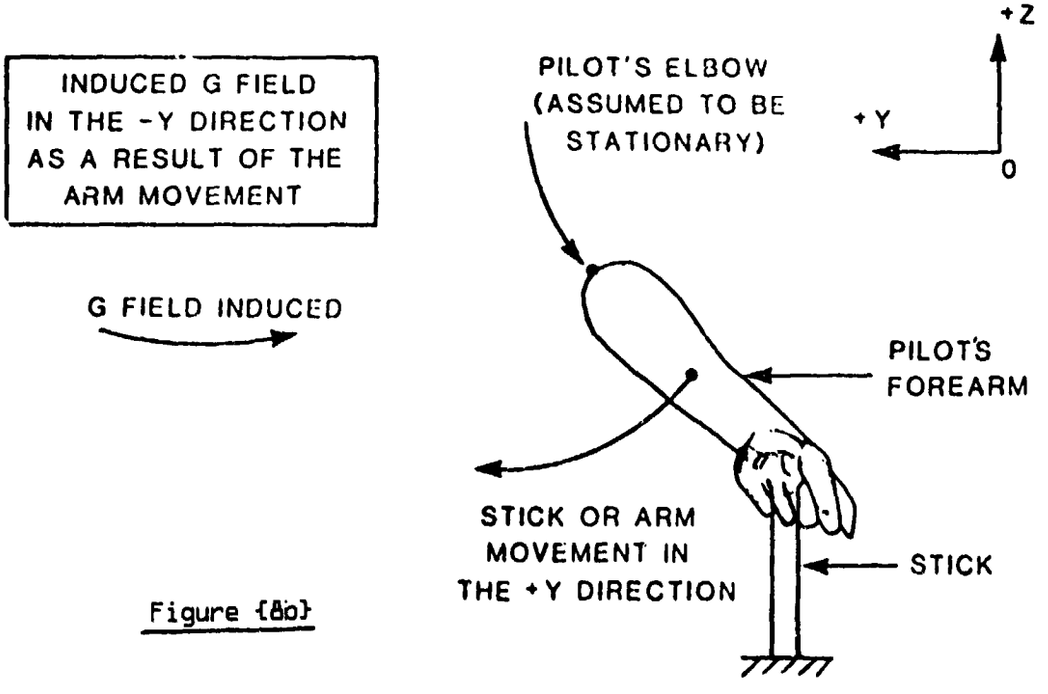

Figure {8b}

NEGATIVE BIOMECHANICAL FEEDTHROUGH

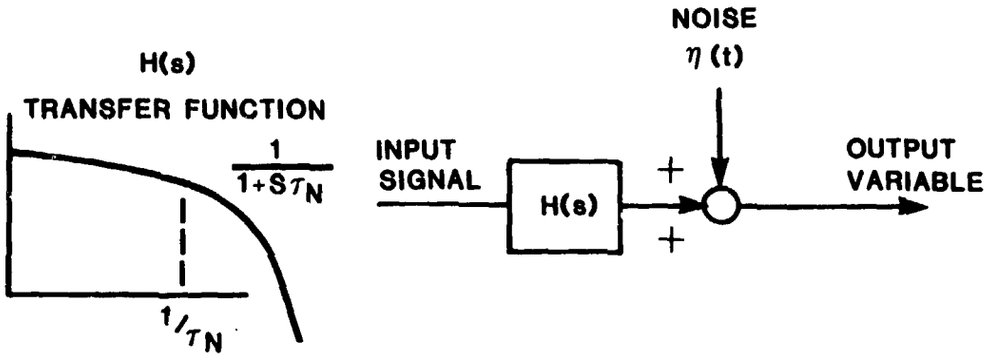

Figure (9) - AN INFORMATION CHANNEL REPRESENTATION OF NEUROMOTOR DYNAMICS

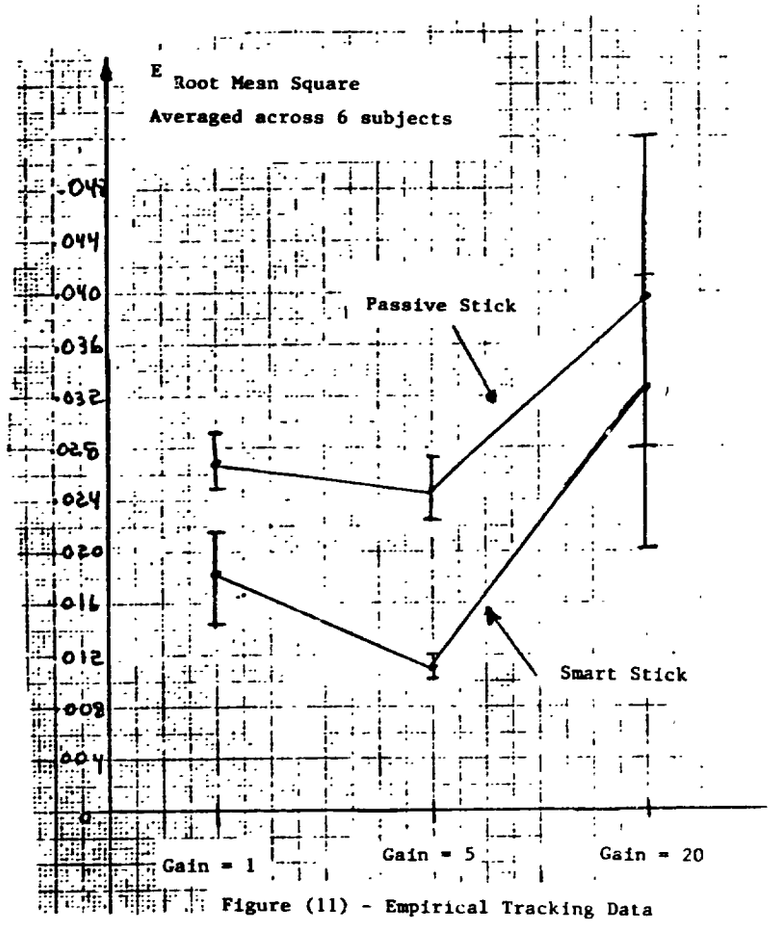

Figure (11) - Empirical Tracking Data

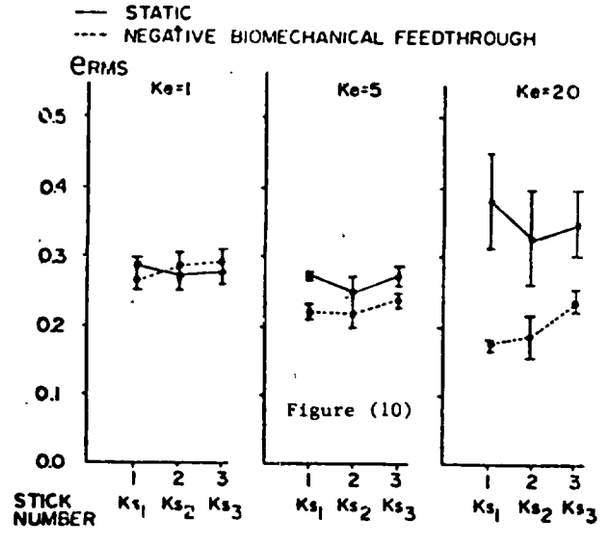

Figure (10)

ORIGINAL PAGE IS
OF POOR QUALITY

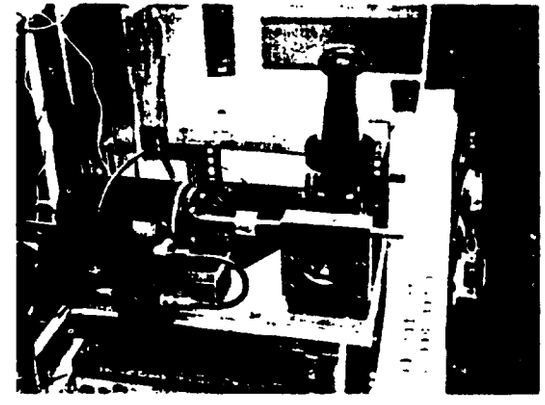

Figure (12) - The Device

D45

MODELS FOR THE EFFECTS OF G-SEAT CUING ON ROLL-AXIS TRACKING PERFORMANCE

N85 14532

William H. Levison
Bolt Beranek and Newman, Inc.
10 Moulton Street
Cambridge, MA 02238

Grant R. McMillan
Air Force Aerospace Medical Research Laboratory
Wright-Patterson AFB, Ohio 45433

Edward A. Martin
USAF Aeronautical Systems Division
Wright-Patterson AFB, Ohio 45433

submitted to the
20th Annual Conference on Manual Control
June 12-14, 1984, NASA-ARC, California

ABSTRACT

Including whole-body motion in a flight simulator improves performance for a variety of tasks requiring a pilot to compensate for the effects of unexpected disturbances. A possible mechanism for this improvement is that whole-body motion provides high derivative vehicle state information which allows the pilot to generate more lead in responding to the external disturbances. In developing new motion simulation algorithms for an advanced g-cuing system we were, therefore, surprised to discover that an algorithm based on aircraft roll acceleration produced little or no performance improvement. On the other hand, algorithms based on roll position or roll velocity produced performance equivalent to whole-body motion. This paper describes the analysis and modeling conducted at both the sensory system and manual control performance levels to explain the above results.

INTRODUCTION

The Air Force Aerospace Medical Research Laboratory and the Aeronautical Systems Division are jointly investigating motion and force cuing alternatives to whole-body motion. This paper summarizes the progress on an investigation of the capability of an advanced g-cuing system to provide rotational motion information to a pilot performing a flight control task. Human performance modeling is being conducted to explore hypotheses concerning the underlying sensory and performance mechanisms.

METHODS

Motion Cuing Devices

Two motion cuing devices were used: (1) the Advanced Low Cost G-Cuing System (ALCOGS), and (2) the Roll-Axis Tracking Simulator (RATS). The ALCOGS includes hydraulically-actuated seat pan, backrest, and seat belt elements mounted in an aircraft seat frame [1]. In the studies reported here, the one-piece seat pan was the only active cuing element. The RATS is a whole-body, roll-axis motion device. The axis of rotation is through the buttocks of the subject.

Drive Algorithm Development

Pressure Matching Algorithm. The initial approach was to develop a means of driving the ALCOGS seat pan such that the pressure produced on the human buttocks matched those one would experience in the RATS. Using small force-sensing strain gauges located under the ischial tuberosities of the buttocks, we measured the pressures produced by sinusoidal roll motion in the RATS. A multiple regression performed on data collected over a range of amplitudes and frequencies suggested that buttocks pressures were a function of RATS roll angle and roll acceleration:

$$PSI_{Buttocks} = -.064\ \phi_{RATS} + .0042\ \ddot{\phi}_{RATS} \quad (1)$$

where PSI = pressure in lbs/in^2, ϕ = roll angle in deg, and $\ddot{\phi}$ = roll acceleration in deg/sec^2. For data collected under a similar sinusoidal motion in the ALCOGS, buttocks pressures were a simple function of seat pan roll angle:

$$PSI_{Buttocks} = .081\ \phi_{ALCOGS} \quad (2)$$

Setting the equations equal to one another and solving for the ALCOGS seat pan angle (in deg) results in the following pressure matching algorithm:

$$\phi_{ALCOGS} = K(-.79\ \phi_{RATS} + .052\ \ddot{\phi}_{RATS}) \quad (3)$$

K values only up to 0.4 (40% of RATS pressures) were used to prevent the ALCOGS seat pan from striking its limits of travel.

The results obtained while testing this algorithm (see Primary Data Reduction Section), suggested that drive algorithms based on the separate derivatives of roll motion would be of

interest. Therefore, the following algorithms were also developed.

Single Derivative Algorithms. Pure position (Equation 4) and pure acceleration (Equation 5) algorithms were derived by setting either the acceleration or position coefficient of Equation 3 to zero. Since matching buttocks pressure was not a concern here, the equations are shown below in terms of the simulated aircraft motion parameters:

$$\phi_{ALCOGS} = .02\ \ddot{\phi}_{Simulated\ Aircraft} \quad (4)$$

$$\phi_{ALCOGS} = \pm .32\ \phi_{Simulated\ Aircraft} \quad (5)$$

where ϕ= roll angle in deg, and $\ddot{\phi}$= roll acceleration in deg/sec^2. As shown in Equation 5, both sign relationships were investigated with the position algorithm.

A velocity algorithm was also developed in which ALCOGS seat pan angle was made proportional to simulated aircraft roll velocity:

$$\phi_{ALCOGS} = \pm .23\ \dot{\phi}_{Simulated\ Aircraft} \quad (6)$$

where $\dot{\phi}$ = roll velocity in deg/sec. Both sign relationships were investigated with this algorithm, as well.

Drive Algorithm Testing

The utility of the algorithms was evaluated by comparing human performance on a roll-axis tracking task under static (visual cue only) and g-seat motion conditions (visual and g-seat cues). The visual display consisted of an aircraft symbol and a dotted reference line which subtended a 9 deg field-of-view. The task was to maintain zero roll angle (keep the symbol and reference aligned) in the presence of strong turbulence using a side-mounted, force-sensing control stick.

The roll dynamics were represented by the transfer function:

$$V(s) = 16 \cdot \frac{5}{s+5} \cdot \frac{20}{s+20} \cdot \frac{1}{s} e^{-.072} \quad (7)$$

At very low frequencies, a control input of one pound produced a simulated roll rate of 16 deg/sec. The lag at 5 rad/sec represents the roll response of a fighter-type aircraft; the lag at 20 rad/sec approximates the response of the moving-base

simulator; and the delay of 0.072 seconds represents the combined effects of digital frame time, sample-and-hold, antialiasing filters, plus the effective delay of the g-seat hydraulic and servo systems. (Regardless of whether a subject was performing the tracking task in the ALCOGS or RATS under static or visual plus motion conditions, the dynamics and delays were identical).

The external forcing function was generated as a sum of thirteen sine waves, with frequencies and amplitudes selected to approximate a random disturbance process having a power spectral density of the form:

$$\Phi_{ii} = \frac{K}{(s+2)^2} \qquad (8)$$

and an rms value of .88 pounds equivalent control force. The sinusoids were randomly phased with respect to each other, and from trial-to-trial, to minimize the predictability of the disturbance waveform. This forcing function added to the pilot's control input and thus served as a direct disturbance to vehicle roll angle.

Under g-seat motion conditions the seat pan of the ALCOGS was driven in roll using Equations 3-6. Because the research reported here consisted of a series of pilot studies, the "experimental design" included both within and between subject treatments and the number of subjects in each algorithm group was not the same. (See Table 1, below). With the exception of the acceleration algorithm, the data for each group represents asymptotic performance after 32 or more 3 minute training trials conducted over several days. In all cases, mean-squared or root-mean-squared (RMS) tracking error was provided to the subjects after each trial.

The tracking performance data collected under whole-body motion in the RATS also represented asymptotic performance. The task dynamics, visual display, control stick, etc. were identical to those used in the ALCOGS. The RATS drive algorithm, however, matched the roll angle of the simulated aircraft in a 1:1 fashion.

PRIMARY DATA REDUCTION

Formal analysis was performed on data obtained under the following cuing conditions:

a. "Static" (visual display of roll angle error; no ALCOGS motion)

b. "Position" (visual plus ALCOGS seat pan angle proportional to simulated aircraft roll angle)

c. "Velocity" (visual plus ALCOGS seat pan angle proportional to simulated aircraft roll velocity)

d. "Acceleration" (visual plus ALCOGS seat pan angle proportional to simulated aircraft roll acceleration)

e. "Combined" (visual plus ALCOGS seat pan angle proportional to a linear combination of simulated aircraft roll angle and roll acceleration).

Error standard deviation (SD) scores were computed for each data trial.* These scores were averaged across trials for each subject; the subject means were then averaged to yield group means for each experimental condition. Table 1a shows, for each cuing condition, the average tracking error SD score, the standard deviation of the subject means, and the number of subjects providing data. Note that the inter-subject variability was less than 20% of the group mean, even for the conditions with only two subjects.

The acceleration and combined algorithms yielded a modest reduction in the tracking error score (about 15%) compared to static performance. On the other hand, the position and velocity algorithms yielded reductions of about 50% and 65%, respectively, and were essentially equivalent to performance in the RATS (mean RMS error = 2.3 degrees).

Differences between pairs of group means were tested for statistical significance by means of a t-test appropriate to unequal sample sizes. Differences significant at an alpha level greater than 0.05 are considered "not significant" for this discussion. Table 1b shows that the mean error SD scores obtained for the position and velocity cuing conditions were significantly different from each other and from the scores obtained for the remaining cuing conditions. Differences among the static, acceleration, and combined conditions were generally not significant.

Effects of g-seat cuing on operator frequency response are shown in Figure 1; position and velocity cuing are compared with static in Figure 1a, whereas acceleration and combined cuing effects are shown in Figure 1b. A value of zero dB for the amplitude ratio ("gain") represents one pound of control force per degree of roll angle error; zero dB remnant signifies 1 pound^2 of control power per radian/second.

---

*Because the forcing function was a zero-mean process, the error SD score is approximately equal to the RMS tracking error.

TABLE 1. ANALYSIS OF THE TRACKING ERROR SD SCORES

a) Group Means

cuing	Mean	Std Dev	Subjects
Static	6.0	0.51	6
Position	3.0	0.50	6
Velocity	2.1	0.20	6
Acceleration	5.2	0.99	2
Combined	4.8	0.21	2

b) Alpha Level of Significance

	Posn.	Vel.	Accel.	Comb.
Static	.001	.001	--	.05
Position		.01	.01	.01
Velocity			.001	.001
Acceleration				--

-- Alpha > 0.05.
2 trials/subject.

a) Position and Velocity Algorithms

b) Acceleration and Combined Algorithms

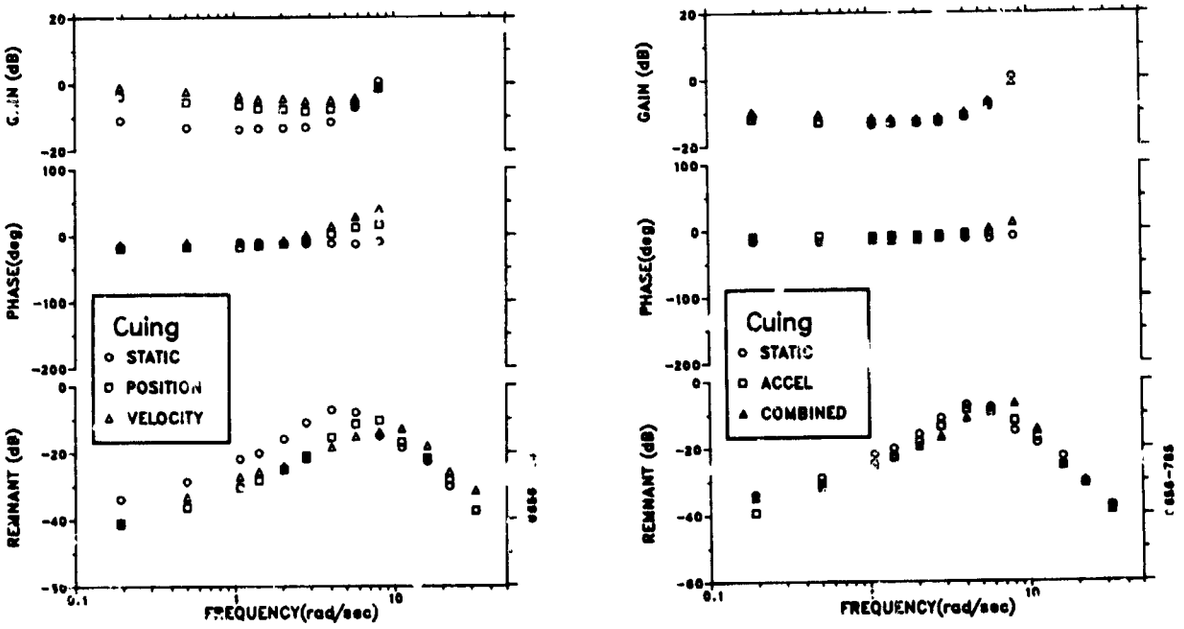

Figure 1. Effect of Cuing on Operator Frequency Response
Average of 2-6 subjects, 2 trials/subject

G-seat cuing with the position drive algorithm yielded larger operator gain at low frequencies, more phase lead at high frequencies, and less remnant at low frequencies. The velocity drive law yielded even larger gain and phase lead, and a remnant spectrum comparable to that of the position drive law. The acceleration and combined drive algorithms had much smaller effects on the frequency response. Overall, the frequency response trends shown in Figure 1 are consistent with the trends of the tracking error scores.

A follow-up experiment indicated that the subjects could perform the tracking task with positional ALCOGS cuing alone (i.e., no visual cues), and that error scores were nearly as low (mean RMS error = 3.7 degrees) as those obtained with concurrent ALCOGS and visual cuing.

In summary, the following experimental trends were revealed by the study on g-seat cuing:

1. A modest reduction in tracking error score with either the acceleration or the combined acceleration and position drive laws.

2. Substantially improved performance with the position and velocity g-seat drive laws.

3. Lower tracking error scores with velocity than with position cuing.

4. Ability to track almost as well with position g-cuing alone (i.e., no visual cuing) as with combined visual and position g-cuing.

MODEL ANALYSIS

Model analysis of the foregoing experimental results was conducted as part of the overall goal of developing a theoretical framework for predicting the pilot's use of combined visual and non-visual cues. A concurrent and more specific goal was to develop a model for the psycho-physiological mechanisms responsible for the observed relationship between g-seat cuing algorithm and tracking performance. The optimal control model (OCM) for pilot/vehicle systems was used for this analysis.

Model Description

The reader is assumed to be familiar with the general structure of the OCM. Figure 2 shows a block diagram of the task environment as modeled for this analysis. The first block contains the equations of motion of the simulated aircraft in the roll axis, plus the first-order approximation to the RATS dynamics. Six "outputs", (perceptual quantities) are considered:

C-9

tracking error and error rate for visual perception, and tracking error,error rate, error acceleration, and error acceleration rate for haptic cuing. The visual outputs are delayed by 0.072 seconds (approximated in the model formulation by a first-order Pade) to mimic the delays present in the laboratory simulation. The delayed outputs e_v and e_v represent the visual cues acted on by the pilot model.

The remaining four outputs of the dynamics block are processed by the g-seat drive algorithm, a second-order model of the g-seat dynamics, and a lead-lag model for mechanoreceptor transduction. To be consistent with our treatment of visual-cue processing, we assume that the pilot perceives both the primary receptor output "m" and its first derivative "m". We shall refer to these two cues as the "motion cues".

Relevant physiological and psychological literature was reviewed in order to derive a math model for transduction of haptic cues [2-19]. This literature covered a variety of receptor types, biological species, and experimental preparations. Consequently, the lead-lag model shown in Figure 2 does not reflect a particular sensory mechanism, but rather an average effect of (presumably) multiple mechanisms involved in the sensory process.

On the basis of largely qualitative information, we derived a lead-lag model for receptor response having a pole at 5 rad/sec (based on the minimum 0.2 second time constant found in the literature search) and a zero at 0.5 rad/sec (an educated guess based on published time histories). Lacking any meaningful data on bandwidth limitations, we did not associate any low-pass characteristics with this receptor model.

There is some psychophysical evidence to indicate that the human's reaction time to haptic stimuli are about 40 msec less than the reaction time to visual stimuli [18,19]. The formulation shown in Figure 2 accounted for this difference.

The only task-to-task variation relevant to the model of Figure 2 was the drive algorithm, which was changed to match the form of the experimental drive algorithm. The position, velocity, and acceleration drive algorithms were modeled as unity gains on either error, error rate, or error acceleration; and the combined algorithm was represented as an appropriately weighted sum of error and error acceleration. Since the experimental drive algorithms were considered sufficient to provide g-seat cuing well above sensory threshold levels, perceptual thresholds were not considered in this modeling exercise, and "display" scaling was therefore unimportant.*

*The OCM will scale its response strategy optimally with regard to display scaling.

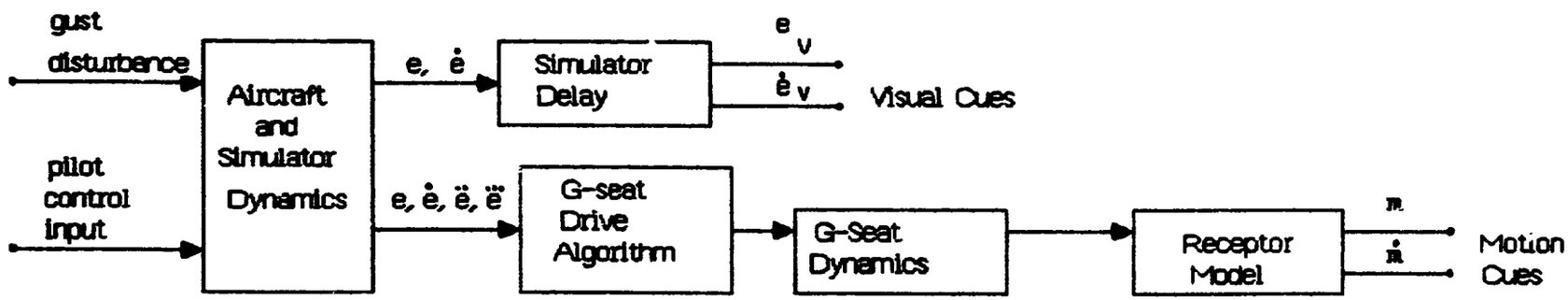

Simulator Delay: Pade Approximation to T=0.072 seconds

G-Seat Dynamics: $\dfrac{47.1^2}{S^2 + 1.414(47.1)S + (47.1)^2}$

Receptor Model: $\dfrac{S + 0.5}{S + 5}$

Figure 2. Model for System Dynamics and Displays

Independent model parameters relating to inherent limitations of the human operator were selected in a manner consistent with previous application of the OCM to laboratory tracking tasks. The following "nominal values" were assigned:

- o time delay for visual cues: Ø.2 seconds
- o motor time constant: Ø.1 second
- o observation noise/signal ratio for visual cues: -2Ø dB
- o motor noise/signal ratio: -5Ø dB

In addition, observation noise/signal ratios of -22.7 dB were assigned to the two motion cues to provide a good match to the tracking error score obtained with the position drive algorithm; this noise/signal ratio was maintained for analysis of the remaining cuing algorithms.

While Figure 2 may reflect a new way of treating g-seat cuing, it does not imply a change in the basic structure of the human operator model. That is, the relationships shown in Figure 2 were implemented within the existing OCM by appropriate definitions of systems dynamics and display variables -- no changes to the computer program were required.

We refer to the model of Figure 2 as the "receptor model" in the sense that it includes an explicit submodel for mechanoreceptor transduction. An alternative "noise model" was explored in which the receptor submodel was omitted and, instead, information provided by the g-seat was modeled directly. That is, the subject was assumed to perceive g-seat displacement and g-seat rate with associated observation noise/signal ratios of -15 dB and -25 dB, respectively.* As was the case with the receptor model, only the g-seat drive algorithm was changed from task-to-task; other independent parameters of the pilot model were held fixed for all experimental conditions.

The receptor and noise models are similar in that both present high-quality rate information related to g-seat motion and poor-quality displacement information. The receptor model accomplishes this quality differential by the way in which it linearly combines position and rate information. The noise model accomplishes a similar effect by assigning different perceptual noises to position and rate information. Because we assume that the subject perceives the first derivative of the receptor

---

*These noises where selected to provide a good match to the position-drive results.

output, the receptor model also provides g-seat acceleration information -- a quantity we have not included in the noise treatment.

Principal Model Results

Comparisons of model predictions with experimental tracking-error SD scores are shown in Figures 3a and 3b for the "receptor" and "noise" models, respectively. The solid symbols indicate the group means, and the vertical bars indicate the standard deviations of the subject means.

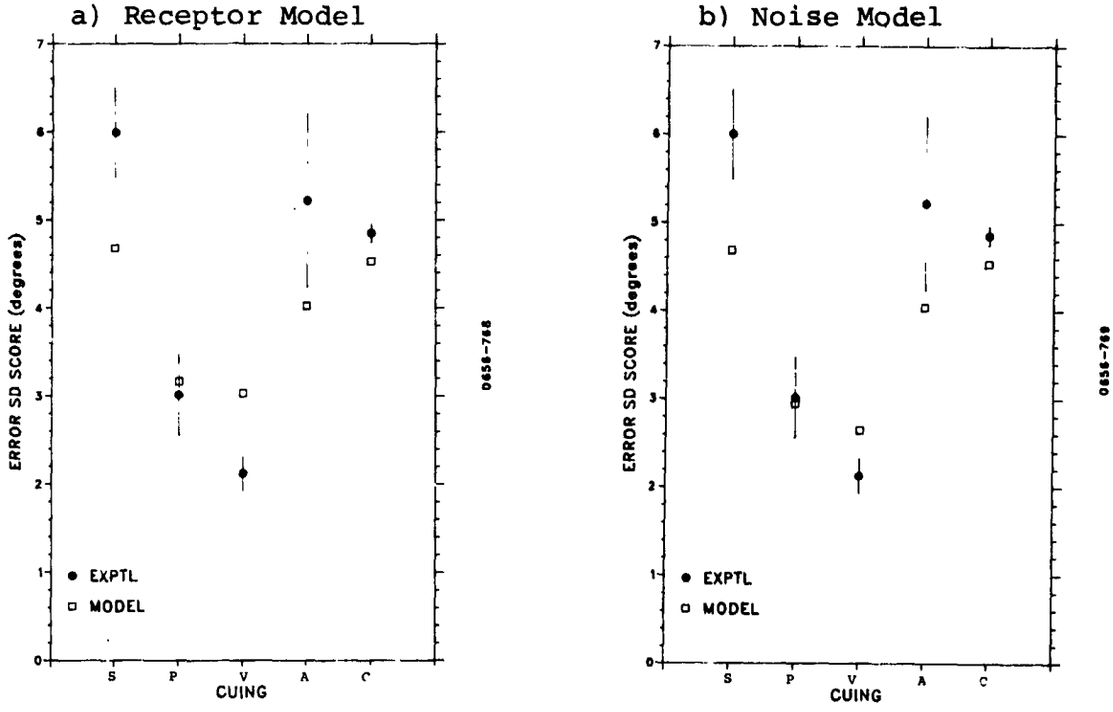

Figure 3. Effect of Cuing on Average Error SD Score
S = Static, P=Position, V=Velocity, A=Acceleration, C=Combined

The two model treatments yielded similar results, with the noise model providing slightly better matches to the position and velocity drive conditions. The model reproduced the major experimental trends: namely, that (1) position and velocity drive algorithms result in substantially improved performance compared to static tracking, and (2) the acceleration and combined algorithms result in only marginally improved performance relative to static.

Although not shown in Figure 3, the model also predicted that the subjects would be able to perform the task with position g-seat cuing alone (no visual cues), and that RMS error would be substantially lower than with visual cues only. This prediction agreed with the follow-up study.

There were some discrepancies between predicted and experimental results, however. Although the model predicted that the velocity algorithm would yield lower tracking errors than the position algorithm, the model underestimated the magnitude of this performance difference. The model also predicted that the acceleration algorithm would be superior to the combined algorithm, whereas the reverse trend was found experimentally.* Finally, the model underestimated tracking errors for the more difficult configurations.

Predicted and measured operator frequency response are shown in Figure 4. To minimize clutter, data from the position and velocity conditions are shown in one graph, whereas acceleration and combined conditions are represented in another. For convenience, static response is plotted in all graphs. Predictions obtained with the receptor model are shown in Figures 4a and 4b; results of the noise model are given in 4c and 4d.

The two models predicted the same overall performance trends. They correctly predicted that the position and velocity cuing algorithms would have a greater influence on operator frequency response, compared to visual-only cuing, than would the acceleration and combined response. Furthermore, the effects of position and velocity cuing on operator gain and phase shift were matched in some detail. The rank ordering of the remnant response across cuing conditions was also predicted.

DISCUSSION

Overall, the modeling philosophies explored here provided a good match to the important trends of the experimental results. Specifically, they accounted for the large effects of position and velocity g-seat cuing, and the relatively small effects of acceleration and combined g-seat cuing, with a consistent set of independent model parameters. Whether or not this modeling philosophy can be generalized to other cuing algorithms and other types of motion (e.g., z-axis translational motion) remains to be determined. Of the various modeling philosophies explored in this study, the approach described here seems to be the most promising.

Additional analyses revealed appreciable performance differences between groups trained with the plus and minus sign on the position or velocity drive algorithms. (Tracking scores were substantially lower than static cuing for either sign

---

*The acceleration group was not trained to asymptote. Training curves indicate that this group, trained to asymptote, would have performed about the same as the group trained with the pressure-matching algorithm.

a) Receptor Model,
Posn & Vel Algorithms

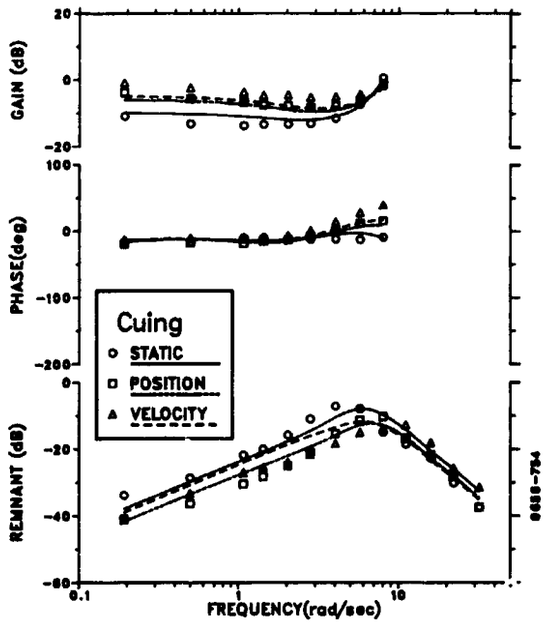

b) Receptor Model,
Accel & Comb Algorithms

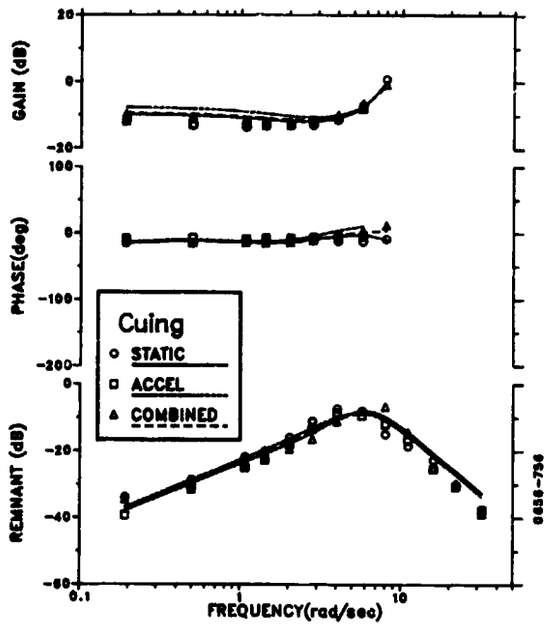

c) Noise Model,
Posn & Vel Algorithms

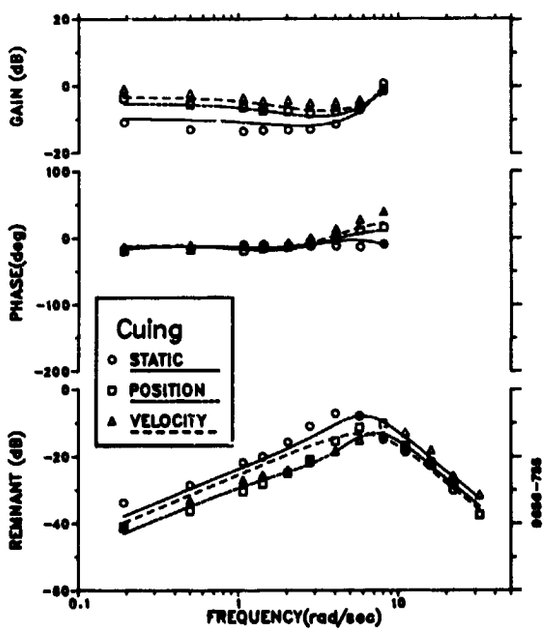

d) Noise Model,
Accel and Comb Algorithms

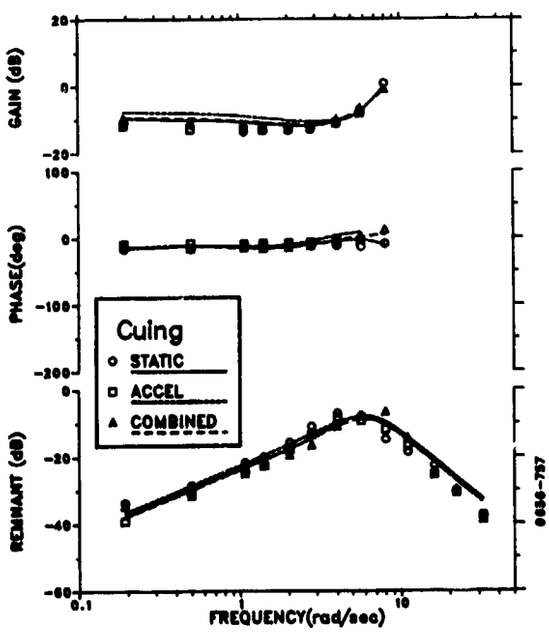

Figure 4. Effect of Cuing on Operator Frequency Response
Average of 2-6 Subjects, 2 trials/subject

convention, however.) Preliminary modeling suggested that these effects could be accounted for by appropriate modeling of biomechanical coupling between seat pan and control stick.

As we have noted, although gross trends were replicated, some of the finer details were not mimicked. To some extent, the performance compression seen in the model predictions may be due to the fact that, for this set of experiments, the model accounts for performance differences solely through task-related differences in perceptual cuing. Now, a recent review of a large body of experimental and model results suggests that, for systems having high-order response characteristics and/or significant delays, motion cuing may provide a double benefit [20]. First, the subject may be able to construct a more accurate "internal model" of system response dynamics than is possible with only visual cuing; and, second, motion-related cues allow more accurate state reconstruction because of high-derivative and/or low-noise information. Only the second factor has been considered in the model analysis presented here -- the current model analysis assumes a perfect internal model for all cuing conditions. Although the OCM is currently able to treat deficient internal models, further model development will be required if we are to predict how the operator's internal model is influenced by the cuing environment.

As mentioned earlier, because of the desire to explore training issues, different subject groups were used for the various experimental conditions. These groups did not all receive the same amount of training, and, in the case of the acceleration and combined-algorithm groups, there were only two subjects per group. Given these factors, it is not surprising that a precision match across all conditions cannot be obtained with a single set of independent model parameters.

The research reported here explored only the performance consequences of g-seat cuing and we have seen an approximate performance equivalence between haptic cuing (given the appropriate drive scheme) and whole-body motion cuing). Of considerable interest is the utility of the g-seat as a device for training the pilot to use whole-body motion cues. Transfer-of-training studies regarding these sensory modalities are being evaluated at ASD/AFAMRL.

SUMMARY

A study was performed to investigate the capability of an advanced g-cuing system to provide rotational cues in a laboratory roll-axis tracking task. Six cuing algorithms were explored:

1. "Static" (visual display of roll error, no g-seat cuing)

2. "Position" (visual plus seat pan angle proportional to simulated aircraft roll angle)

3. "Velocity" (visual plus seat pan angle proportional to simulated aircraft roll rate)

4. "Acceleration" (visual plus seat pan angle proportional to simulated aircraft roll acceleration)

5. "Combined" (visual plus seat pan angle proportional to a linear combination of simulated aircraft roll angle and roll acceleration)

6. Visual plus whole-body roll-axis motion cues.

The combined algorithm was designed to match the pressure pattern that would be felt in the whole-body moving-base Roll Axis Tracking Simulator (RATS).

Performance with either the position or velocity g-cuing algorithm yielded tracking error scores that compared favorably with performance in the RATS and were substantially lower than scores obtained in the static cuing conditions. To our initial surprise, the combined algorithm provided only marginal improvement in tracking performance relative to static cuing, as did g-cuing with the pure acceleration drive law. A follow-up study indicated that subjects could perform the task well in the absence of visual cues when the g-seat was driven by the position algorithm.

A review of the literature suggested that the various haptic sensor mechanisms could be represented mathematically by (1) a lead-lag network with a zero at 0.5 and a pole at 5 rad/sec, and (2) an effective time delay 40 msec less than that associated with visual cues. When this receptor model was incorporated into the framework of the optimal control pilot model, the model was able to replicate the major experimental trends, in terms of performance scores as well as operator frequency response, with a fixed set of values for independent operator-related model parameters. Similar results were obtained for a purely informational model receptor transduction.

ACKNOWLEDGEMENT

This research was supported by the Air Force Aerospace Medical Research Laboratory under contract F33615-81-C-0515 with John B. Sinacori Associates, Inc.

REFERENCES

1. Kleinwaks, J.M. (1980). Advanced Low Cost G-cuing System (AFHRL-TR-79-62). Brooks Air Force Base, TX, Air Force Human Resources Lab. (NTIS).

2. Borah, J., Young, L.R., Curry, R.E., Albery, W.B., "Multisensory Perception Model for Application to Aircraft Simulation", NTEC IH-306, November 14-16, 1978.

3. Chambers, M.R., Andres, K.H., V. Duering, M., Iggo, A., "The Structure and Function of the Slowly Adapting Type II Mechanoreceptor in Hairy Skin", Quarterly Journal of Experimental Physiology, (1973)73, pp. 417-445.

4. Chorzempa, A., "An Attempt to Determine the Structure of the Nervous System Serving Mechanoreceptors", Biol. Cybern., 42, pp. 51-56, (1981).

5. Freeman, A.W., Johnson, K.O., "A Model Accounting for Effects of Vibratory Amplitude on Responses of Cutaneous Mechanoreceptors in Macaque Monkey", J. Physiol., (1982)323, pp. 43-64.

6. Grandori, F., Pedotti, A., "Theoretical Analysis of Mechano-to-Neural Transduction in Pacinian Corpuscle", IEEE Trans. BME-27: pp. 559-565, October 1980.

7. Gum, D.R., "Modeling of the Human Force and Motion-Sensing Mechanisms", AFHRL-TR-72-54, June 1973.

8. Horch, K.W., Tuckett, R.P., Burgess, P.R., "A Key to the Classification of Cutaneous Mechanoreceptors", The Journal of Investigative Dermatology, Vol. 69, No. 1, pp. 75-82, 1977.

9. Iggo, A., Kornhuber, H., "A Quantitative Study of C-Mechanoreceptors in Hairy Skin of the Cat", J. Physiol., (1977)271, pp. 549-565.

10. Iggo, A., Muir, A.R., "The Structure and Function of a Slowly Adapting Touch Corpuscle in Hairy Skin", J. Physiol., (1969)200, pp. 763-796.

11. Iggo, A., Ogawa, H., "Correlative Physiological and Morphological Studies of Rapidly Adapting Mechanoreceptors in Cat's Glabrous Skin", J. Physiol., (1977)266, pp. 275-296.

12. Jarvilehto, T., Hamalainen, H., Soininen, K., "Peripheral Neural Basis of Tactile Sensations in Man: II. Characteristics of Human Mechanoreceptors in the Hairy Skin", Brain Research, 219(1981), pp. 13-27.

13. Jarvilehto, H., Hamalainen, H., Kekoni, J., "Mechanoreceptive Unit Activity in Human Skin Nerves Correlated with Touch and Vibratory Sensations", In Zotterman, Y., (ed), Proc. of the International

Symposium, held at the Winner-Gren Center, January 1976, pp. 215-230.

14. Johansson, R., "Skin Mechanoreceptors in the Human Hand: Receptive Field Characteristics", pp. 159-170.

15. Ogawa, H., Morimoto, K., Yamashita, Y., "Physiological Characteristics of Low Threshold Mechanoreceptor Afferent Units Innervating Frog Skin", Quarterly Journal of Experimental Physiology, (1981)66, pp. 105-116.

16. Pubols, B.H., "Factors Affecting Cutaneous Mechanoreceptor Response. I. Constant-Force Versus Constant-Displacement Stimulation", J. Neurophysiology, Vol. 47, No. 3, March 1982, pp. 515-529.

17. Vedel, J.P., Roll, J.P., "Response to Pressure and Vibration of Slowly Adapting Cutaneous Mechanoreceptors in the Human Foot", Neuroscience Letters, 34(1982), pp. 289-294.

18. Woodworth, R.S., and Schlosberg, H., Experimental Psychology, Revised, Holt, New York, 1956.

19. Boulter, L.R., "Attention and Reaction Times to Signals of Uncertain Modality", J. Expt. Psych: Human Perception and Performance, 3:379-388, August 1977.

20. Levison, W.H., "Development of a Model for Human Operator Learning in Continuous Estimation and Control Tasks", BBN Report No. 5331, Bolt Beranek and Newman, Inc., Cambridge, MA, September 1983.

D46

AN ANALYSIS OF KINETIC RESPONSE VARIABILITY

N85 14533

P.A. Hancock
Department of Safety Science and
Human Factors Department
Institute of Safety and Systems Management
University of Southern California
Los Angeles, California

and

L.G. Carlton and K.M. Newell
Motor Behavior Laboratory
Institute for Child Behavior and Development
University of Illinois
Champaign, Illinois

ABSTRACT

Studies evaluating variability of force as a function of absolute force generated are synthesized. Inconsistencies in reported estimates of this relationship are viewed as a function of experimental constraints imposed. Typically, within-subject force variability increases at a negatively accelerating rate with equal increments in force produced. Current pulse-step and impulse variability models are unable to accomodate this description, although the notion of efficiency is suggested as a useful construct to explain the description outlined.

INTRODUCTION

Understanding the nature of response variability has important practical and theoretical implications for manual control. In many movement tasks this variability has been recognized as the major limiting factor in performance. The relative scale of such variability may be used as a basis to distinguish between skilled and unskilled individuals. Theoretically, variability expressed in either kinetic or kinematic terms has been viewed as a reflection of the limitations in the neuromuscular system. These have been identified with time constraints of feedback in movement control (Crossman & Goodeve, 1983; Keele, 1968), noise in the neuromuscular system with respect to information transmission (Fitts, 1954) and inherent noise in the motor system itself (Schmidt, Zelaznik, Hawkins, Frank, & Quinn, 1979). A detailed analysis of kinetic response can consequently contribute insight into potential sources of limitation in the neuromuscular system and current models of movement control.

There have been a number of attempts to describe the relationship between force production and outcome variability through the use of a variety of motor tasks. The progression of research has been sporadic in terms of chronological development, with each era of activity occuring in seeming isolation with respect to previous efforts. In the following section we review a selection of these studies that have provided bases for the proposed variability functions, with a view to reconciling various inconsistencies that have emerged across experimental situations. We begin by considering force production in isometric

PRECEDING PAGE BLANK NOT FILMED

tasks, which are generally considered simpler than isotonic tasks in that changes in limb placement and resulting variation in muscle length do not occur. Force production in isotonic tasks are subsequently examined to provide a foundation for an overall force varibility function.

ISOMETRIC TASKS

Perhaps the earliest and certainly one of the most comprehensive studies of response variability is the treatise of Fullerton and Cattell (1892). Superficially, it appears to focus on the problems of perception in a traditional psychophysical analysis of the spatial, temporal and force characteristics related to movement control. However, examination of their experiments indicates that a primary method of measurement was through the use of average error. This procedure required participants to produce a number of responses that were directed at the replication of a criterion target and in essence represents the same procedure currently used to assess force variability. Fullerton and Cattell's results on force production indicated that variable error increased across the force production continuum but that this increase was not linear as would be predicted by a Weberian approach. They suggested that a square-root function was more appropriate in describing the function observed.

Although the work of Fullerton and Cattell represented an early step forward, analysis of the relation between force and force variability was not taken up again until the practical demands of the person-machine interface surface following the Second World War (cf., Fitts, 1947; Hick & Bates, 1950). The study of factors influencing the efficiency of machine controls helped promote an interest in force production. The primary focus of this research was to understand the relation of control dynamics to the accuracy with which movements could be generated particularly in the control of aircraft. In one study, Jenkins (1947) examined the accuracy of force production for stick, wheel and rudder controls. The forces generated ranged from 1 to 60lb and was in part dependent on the task in that less force was needed to move the stick compared to the other controls. The coefficient of variation for the three tasks, that is the standard deviation of force divided by the mean force decreased across the force range selected in the form of a descending exponential. The data for the standard deviation of response followed the general shape as observed earlier by Fullerton and Cattell, that being a progressive increase in variability but with the rate of gain in variability slowing with sequential increments in force produced.

The force variability function obtained by Jenkins appears to be of an exponential morphology, with the change in variability being greatest at low force values. This is demonstrated in both the coefficient of variation and standard deviation functions. The nonproportional relation between force level and force variability was subsequently found by Noble and Bahrick (1956) and Provins (1957), using comparable isometric force generation tasks. Collectively, the data of the immediate post-war period indicate that force variability increases at a decreasing rate with equal increments of force and affirms the general function originally observed by Fullerton and Cattell (1892).

Recently, Schmidt and his colleagues have regenerated interest in the description of force variability and in support of their motor-output variability model presented data indicating a linear relation between variability and absolute level of various movement parameters. In their experiments, subjects were asked to exert isometric forces to shoot a dot on an oscilloscope screen to a height proportional to the criterion peak force. The results exhibited a strong linear relation between the within-subject

variability in force and the amount of force produced. These data are inconsistent with a curvilinear relation that earlier studies might have led us to anticipate, given that the force range use by Schmidt and his co-workers covers the strong curvilinear component of the variability function as reported by Jenkins (1947).

As our synthesis has indicated, the majority of data sets are inconsistent with the finding of a linear and proportional relation between force and force variability. Sherwood and Schmidt (1980) subsequently modified the linear prediction derived from the motor-ouput variability model not on the basis of previous work, but in response to results from their additional experiment in which variability increased up to approximately 65% of maximum. However, at force levels above this value, variability decreased. The motor-output variability predictions were modified to account for the inverted-U shaped function that Schmidt and Sherwood also then found for movement accuracy.

Thus, the variability of force as a function of force has been claimed to be a square root function (Fullerton & Cattell, 1892), a nonproportional but increasing function (Jenkins, 1947), a linear function (Schmidt et al., 1979) and an inverted-U shaped function (Sherwood & Schmidt, 1980). There are a number of experimental factors that could influence estimates of force variability as s functio of force produced. Among these may be transfer effects (Poulton, 1973), insufficient force levels to adequately describe the function and insufficient data points at each force level to obtain a veridical estimate of variability (Fisher, 1915). One potential reason for the discrepancies reported may be that individual subjects varied the time with which they generated the force in a systematic manner. To test this assumption, Newell and Carlton (1984) tested subjects using an elbow flexion task. In absolute terms, force variability increased but at a decreasing rate in a manner similar to that reported by Fullerton and Cattell. However, it appeared that this was accomplished by increasing time to peak force as the required force level increased. This suggests that subjects are able to change rate of force production according to the criterion force required. Therefore future investigations of isometric force production tasks need to consider the individual freely chosen rate of production as an important variant.

ISOTONIC TASKS

In isotonic tasks the goal of the act is often based on spatial and temporal criteria. Investigations of isotonic contractions have focused on control parameters such as spring stiffness, viscous damping and inertia which affect the work required by the task and as has been presumed the kinasthetic feedback associated with response (Bahrick, 1957). In this work emphasis has been laid on the use of spring centered controls which allow for the simultaneous presentation of both distance and force cues. As force production is proportional to movement distance in these systems, force variability may be measured by distance variability and this has generally been the experimental tactic adopted. Although this confounding of distance and force parameters produces several interpretational problems, thes studies do provide useful insights into factors affecting output variability.

Although the early studies of Weiss (1954) suggested that force cues were not beneficial in dynamic responses, possibly as they provided only redundant information, a number of subsequent works have indicated the efficacy of such cues in improving spatial accuracy in positioning responses (Bahrick, Bennett, & Fitts, 1955; Gibbs, 1954; Howland & Noble, 1953). Bahrick, Bennett and Fitts (1955) is representative of this work. They examined the accuracy of positioning

responses under constant spring tension, where tension increased with change in position of the control stick. It was proposed that this protocol allowed for an evaluation of cues associated with amplitude, terminal torque and rate of change of torque with amplitude. The authors concluded that indeed each of these factors were important in governing positioning errors but that error was minimized when the ratio of relative torque change to displacement was maximized, particularly if this coincided with a large absolute change in torque with displacement. However, as Bahrick and his colleagues used absolute rather than variable error it is difficult to contrast their results directly with those for isometric force production.

With the advent of the motor-output variability model, there have been a variety of contemporary studies which have examined the force variability function in isotonic tasks. The basic tenet of the model is that there is a proportional relationship between the size of the impulse produced an it's variability. As support for this proposal, Schmidt and his colleagues produced data upon both discrete and reciprocal aiming movements and rapid timing responses. Their results indicated that the within-subject variability of impulse duration increased linearly with movement time. Also, there were no interactional effects between movement time and amplitude for the variability of impulse duration. As was indicated this affirmation leads to estimates of proportional relations between movement error and movement speed. Although Schmidt et al presented some data in support of such a position there is a substantial body of research that variable error increases at a negatively accelerating rate for constant increments of movement speed with a given movement amplitude (e.g., Fitts, 1954; Woodworth, 1899) and that variable timing error decreases at a negatively accelerating rate with constant increments of amplitude within a given movement time (Newell, 1980). The above represents only a short precis of a rather more complex picture of which much fuller details appear in Hancock and Newell (1984).

The prediction of the motor-output variability model that spatial errors increase proportionally with movement distance whereas movement timing error remains unaffected is based upon the assumption that absolute impulse varies with amplitude. For the case where double the amplitude is covered, double the impulse is required which doubles spatial error. However, because in this situation the movement is being generated twice as fast timing error is unaffected. Also, a proportional relation would require that the addition of mass to the movement system have no effect on spatial or temporal accuracy. This is because the addition of mass has two equal and opposing effects. First, it increases the variability of the motor system due to a larger impulse being produced but second, it increases the inertia of the system which provides resistence to variability in the movement. Therefore, if the relation between impulse and impulse variability were proportional, there should be no effect on timing accuracy when movement distance or when movement mass is varied. Recent studies by Newell and his colleagues have indicated that neither of these observations is born out in experimental data and therefore suggest that the force/force variability function is not a simple proportional relationship.

Taken collectively, the studies for isotonic tasks do not present as coherent a picture as those for isometric performance and this may be due to the variety of manipulations, e.g., spring centered controls, employed. However, in conditions which do not change throughout the force production continuum, a curvilinear function compatible with that observed in isometric tasks has been reported (e.g., Newell, Carlton, & Carlton, 1982). This overall function is also compatible with previous descriptions of kinematic variation (Hancock & Newell, 1984).

FORCE VARIABILITY AND MODELS OF RESPONSE PRODUCTION

The present synthesis of the relation between force and force variability in both isomteric and isotonic tasks suggests that a negatively accelerating rate of force variability is produced when equal increments of force are manipulated across the continuum available to the performer. This function is consistent with our space-time analysis of the movement speed accuracy relationship although we have yet to formalize a link between the kinematic and kinetic components of response variability (Hancock & Newell, 1984). Schmidt et al. (1979) made explicit and presented an attempt toward this link which has been implicit in movement studies since the earliest investigations (Fullerton & Cattell, 1892). However, certain predictions derived from the model of Schmidt and his colleagues have not been affirmed by experimental data and a full description of the kinematic-kinetic link awaits further development.

The current kinetic analysis of response variability reveals several limitations to extant models of force production. Subjects apparently minimize response variability by modulating the rate of force production for a given set of isometric or isotonic task constraints. In isometric tasks, subjects do not scale-up peak force by holding time tc peak force constant as postulated explicitly by pulse-step (Ghez & Vicario, 1978) and implicitly by motor-output variability (Schmidt et al., 1979) models. Rather, they systematically vary the time to peak force according to task constraints (Danoff, 1978; Newell et al., 1982). The basis for this variation is at present unclear, however, it appears consistent with principles of efficiency in muscular contraction, where efficiency is defined as the ratio of the work done to the energy expended.

In pioneering work, Hill (1922) investigated the speed of muscular contraction with respect to it's relationship to mechanical efficiency in human skeletal muscle. He suggested that the rate of contraction is the key parameter in determining this mechanical efficiency. Further, he observed a nonlinear relation between efficiency losses in muscular contraction and the deviation from the optimal contraction duration. Efficiency has since been invoked as an emergent property of the optimizing motor system (e.g., Sparrow, 1983). However, a formal link between notions of variability and efficiency has not yet been realized. It is conjectured that following practice, an individuals freely chosen rate of force production is optimal for the efficiency of muscular contraction.

Efficiency is an attractive avenue to pursue, not only because of it's theoretical appeal but because it can encapsulate arguments that may be advanced concerning the role of specific physiological mechanisms, such as motor unit recruitment, within the variability function (Hatze & Buys, 1977). Efficiency principles also suggest that the coordination and control of human movement cannot be understood from purely mechancical principles alone. Although this position has gained acceptance in research on biomechanical optimization, this perspective has yet to be fully developed by those seeking to understand processes of movement production. Efficiency of muscle mechanics is consistent with a peripheral hypothesis regarding response variability but central mechanisms may also affect force production. One premise of the motor-output variability model is that repeated responses enable the "same" motor program and thus minimizes centrally mediated response variability. However, and in accord with Schmidt and his colleagues, we would not suggest that this means no effect for supposed central processes. Indeed, our synthesis suggests that central mechanisms may well contribute to the force variability function. Whether central mechanisms can also be related to efficency in discrete responses as it can in gait (e.g., Bolis, Schmidt-Neilson, & Madrell, 1973) awaits development.

Efficiency could be a principle that specifies a priori a particular biokinematic organization of the organism and constrains the interaction of central and peripheral contributions in the coordination and control of movement (e.g., Sparrow, 1983). The implication of an efficiency orientation to motor control is that response variability will reflect the degree to which task and environmental constraints demand deviation from organismically optimal kinematics and kinetics.

REFERENCES

Bahrick, H.P. (1957). An analysis of stimulus variables influencing the proprioceptive control of movements. Psychological Review, 64, 324-328.

Bahrick, H.P., Bennett, W.F., & Fitts, P.M. (1955). Accuracy of positioning responses as a function of spring loading in a control. Journal of Experimental Psychology, 49, 437-444.

Bolis, L., Schmidt-Neilson, K., & Madrell, S.H.P. (1973). Comparative physiology. Amersterdam: North-Holland.

Crossman, E.R.F.W., & Goodeve, P.J. (1983). Feedback control of hand movements and Fitts' Law. Quarterly Journal of Experimental Psychology, 35A, 251-278.

Danoff, J.V. (1978). Power production by maximal velocity elbow flexion. Journal of Biomechanics, 11, 481-486.

Fisher, R.A. (1915). Frequency distribution of the values of the correlation coefficient in samples from an indefinitely large population. Biometrika, 10, 507-521.

Fitts, P.M. (1947). Psychological research on equipment design. Army Air Forces Aviation Psychology Program Research Reports No. 19, Washington, D.C.: U.S. Government Printing Office.

Fitts, P.M. (1954). The information capacity of the human motor system in controlling the amplitude of movement. Journal of Experimental Psychology, 47, 381-391.

Fullerton, G.S., & Cattell, J.McK. (1892). On the perception of small differences. University of Pennsylvania Philosophical Series, No 2.

Ghez, C., & Vicario, D. (1978). The control of limb movement in the cat: II. Scaling of isometric force adjustments. Experimental Brain Research, 33, 191-202.

Gibbs, C.B. (1954). The continuous regulation of skilled responses by kinaesthetic feedback. British Journal of Psychology, 45, 24-39.

Hancock, P.A., & Newell, K.M. (in press). The movement speed accuracy relationship in space-time. In H. Heuer, U. Kleinbeck, & K.H. Schmidt (Eds.), Motor Behavior: Programming, control and acquisition. Berlin: Springer.

Hatze, H., & Buys, J.D. (1977). Energy-optimal controls in the mammalian neuromuscular system. Cybernetics, 27, 9-20.